International Conference

ASIMMOD 2009

Proceedings

"Simulation for Unsolved Problems"

3rd International Conference on

Asian Simulation and Modeling 2009

January 22-23, 2009 Miracle Grand Convention Hotel

Bangkok, Thailand

Edited by ASIMMOD2009 Technical Committee

Supported by

Kasetsart University

Sripatum University

Royal Project Foundation

Modeling and Simulation Society of Thailand

Preface

This proceedings volume contains a set of full manuscripts accepted for presentations and publications at the third ASIMMOD 2009, an international conference held at Miracle Grand Convention Hotel, Bangkok, Thailand on January 22-23. As the chair of this conference, I would like to thank all participants who have contributed papers, all committee and other relative groups of interest who have directly and indirectly help organizing and setting up this meeting. My deeply sincere respect also goes to our technical committee for reviewing and editing this published workbook. It is my honor to write this preface on their behalves. This continued event would not have been possible without the initial leadership and continuous support from Professor Santas Rojanasunthorn, Royal Project Foundation of Thailand. Having set such a high standard on organizing the previous two meetings by Professors, Voratas Kachitvichyanukul from Asian Institute of Technology, Thailand and Benchaphun Ekasingh from Chiang Mai University, Thailand respectively should also be acknowledged. I also would like to acknowledge the support from our co-organizing partner, Sripatum Univesity led by President Rutchaneeporn Pookayaporn. Sripatum staffs have played a major role on resolving many jigsaw puzzles occurred during the last stage of organizing this conference. Last but not least, I would like to apologize for all mistakes if existed during the conference and we will use this experience of a better future and wish you all the best. Your continuous supports for the future ASIMMOD events will be expected and see you again on 2011.

Vudtechai Kapilakanchana,
President, Kasetsart University
President, Modeling and Simulation Society of Thailand (MSST)
ASIMMOD 2009, Organizing Chair

Organizing Committee

Vudtechai Kapilakanchana, Chancellor, Kasetsart University (Chairman) Rutchaneeporn Pookayaporn, Chancellor, Sripatum University (Vice-Chair)
Nontawat Junjareon, Dean of Engineering, Kasetsart University
Narong Yoothanom, Dean of Engineering, Sripratum University
Veerasak Udomchoke, Kasetsart University, Thailand
Kumut Sangkhasila, Kasetsart University, Thailand
Anan Mungwattana, Kasetsart University, Thailand

International Advisory Committee

Tony Jakeman, Australian National University, Australia
Kamlesh Mathur, Case Western Reserve University, USA
Vira Chankong, Case Western Reserve University, USA
Santas Rojanasunthorn, Royal Project Foundation, Thailand
Voratas Kachitvichyanukul, Asian Institute of Technology, Thailand
Benchaphun Ekasingh, Chiang Mai University, Thailand
Somjert Phatummin, Rubber Research Institute, Thailand

Technical Committee

Chidchanok Lursinsap, Chulalongkorn University, Thailand
Yongwimon Lenbury, Mahidol University, Thailand
Daniel Solow, Case Western Reserve University, USA
Thaweepat Buranathiti, King Mongkut's University of Technology Thonburi, Thailand
Sue Cuddy, CSIRO, Australia
Attachai Jintrawet , Chiang Mai University, Thailand
Putchong Utayopas, Kasetsart University, Thailand
Peerayuth Charnsethikul, Kasetsart University, Thailand
Juta Pichitlamken, Kasetsart University, Thailand
Asawin Wongwiwat, Sripratum University, Thailand
Chawalit Manisri, Sripratum University, Thailand

Assistant Technical Committee

Phensuda Homla, Kasetsart University, Thailand
Chanpen Udomchodpruch, Kasetsart University, Thailand

Sponsors

Contents Page

Session: Mathematical Theory, Modeling and Computing

A Numerical Method for Solving Linear Non-Autonomous Systems based on Genetic Algorithm 1
Hassan Kadkhodaei Khalafi and Omid Solaymani Fard

Variational Calculus for Random Field and Green's Functions Method 5
Pwint Phyu Moe

Mathematical Study of an Influenza Model with Seasonal Forcing in Transmission Rate 12
Settapat Chinviriyasit and Wirawan Chinviriyasit

A Numerical Solution for Optimal Control Problems based on Scatter Search 18
Omid Solaymani Fard and Hassan Kadkhodaie Khalfi

Relation between the Space with Reproducing Kernels and Rodrigues' Formula 21
Hnin Yu Mar

Generalized White Noise Functionals and Measures on Dirichlet Forms 29
Yu Yu Win San

A Role of The Lévy Laplacian Acting on The Space of Generalized White Noise Functionals 34
Moe Myint Swe

Stability of the ADI Schemes on the Application to Convection Diffusion Equations 39
Kay Thi Oo

Some Stability Results of the Douglas Splitting Method for an Advection – Reaction Equation 43
Yu Yu Swe

Traveling Wave Solutions of a Dental-Plaque Model with Non-linear Sorption 46
Patarawadee Prasertsang , Valipuram S. Manoranjan and Yongwimon Lenbury

Application of Singular Perturbation Technique to a Model Skeletal Muscle in Myotonia and Periodic Paralysis Incorporating Membrane Potential Dynamics 50
Kamonwan Kocharoen, Jonathan Bell and Yongwimon Lenbury

Application of Generalized Brownian Functionals to the Feynman Integral 56
May Thida Kyaw

Groundwater Contaminant Problem using an Operator Splitting Scheme 66
Kyawt Kyawt Khine

Stability of a Leapfrog Method for the Generalized FKPP Equation 72
Shwe Sin Win

Investigating Spatially Distributive Structures of Vegetation in Arid Environment by Modelling and Nonlinear Stability Analyses 80
Nichaphat Boonkorkuea , David J Wollkind, Francisco J Alvarado, and Yongwimon Lenbury

Contents Page

Simulation Tool for TOC Implementation 86
Chompoonoot Kasemset and Voratas Kachitvichyanukul

Assessment of the Impact of an Additional Intermodal Barge Terminal on a Waterway Network 99
An Caris, Gerrit K. Janssens, Katrien Ramaekers and Cathy Macharis

Profit as Criteria in Functioning a Supply Chain Management Problem 106
E.Y.T. Adesta, Hari H.Ramali, Satria Darsa, Suhendi Nur and Suwarto

A Simulation Modeling Approach for Analyzing Parking Space Availability in Parked Building of Sripatum University 110
Pattanapong Ariyasit

Study the Effect of Pretest-normality on Estimating Process Capability Indices via Monte Carlo Simulation 118
Siraprapa Manomat and Prapaisri Sudasna Na Ayudthya

Simulation of Elevators Queuing for Academic Building 123
Chawalit Manisri

Simulation of an Inventory System allowing Joint Replenishment from Secondary Supplier upon Depleted Stock 129
Warunee Sarika, *Yongwimon Lenbury and Chontita Rattanakul*

Modeling a sequencing problem for the mixed-model assembly line 136
Shusaku Hiraki, Hugejile and Zhuqi Xu

A Study on design of buffer for automobile assembly lines 141
Zhuqi Xu, Shusaku Hiraki, Yoshiaki Ishihara and Yuanming Su

Dynamic Multi-Product Multi-Level Capacitated Lot-Sizing Problems Using Heuristic Dynamics Programming 147
Songwut Prakaiwichien and Peerayuth Charnsethikul

Comparison of Total Inventory Cost between Estimated Demand by Normal Distribution and Fuzzy Set in the Case of Poor Data 152
Kawinthorn Saicharoen and Saowanee Lertworasirikul

Comparative Characterization of Various Initial-Cutting-Pattern Creations in One Dimensional Cutting Stock Problem 157
Sirirat Wongprakornkul

Using Network Flow Diagram for Creating Mathematical Model in Planning Process 163
Sirirat Wongprakornkul and Sirikul Chansawang

Production Rescheduling based on Stability under Uncertainty for Continuous Slab Casting 170
Kiatkajohn Worapradya and Thaweepat Buranathiti

A Genetic Algorithm for the Storage Location of Containers at a Seaport Terminal 179
José Maria A. Pangilinan and Gerrit K. Janssens

The Solution Space Reduction Using Frequency Domain of Simulated Annealing 185
Watha Minsan and Pornthep Anussornnitisarn

Contents Page

Comparing the solutions for a Vehicle Routing Problem with Uncertain Travel Times by Traffic Simulation 191
Tharinee Manisri and Anan Mungwattana

Determination of the Optimal Mixing Parameters for the Achievement of the Optimal Outcome among Input / Output Uncertainties in Sweet Production Case Study: Foi-thong Production 197
Somsak Chueakittisak, Rathaprom Promkam and Peerayuth Charnsethikul

Session: Modeling and Simulation in Chemistry

Monte Carlo Simulation of Mechanism of Water and Ions Transfer in Aquaporin Channel: as an approach for drug design 203
Majid Monajjemi

Molecular Simulation Approaches for Finding Amino Acids Interaction between Immobilization luciferase Enzyme on Liposome as a Hydrophobic Adsorbent 210
Sima Afsharnezhad, Elham Mousavi Nezhad, Saman Hosseinkhani Masoud Saleh Moghadam and Majid Monajjemi

Monte Carlo Simulation of Solvent Effects in Molecularly Imprinted Polymers Rational Design 215
Piyarat Nimmanpipug, Vannajan Sanghiran Lee, Mookda Pattarawarapan, Majid Monajjemi

Salt and temperature effects on nucleic acids solution: Molecular Dynamics Simulation and Normal Mode Analysis 219
Vannajan Sanghiran Lee, Piyarat Nimmanpipug, Chirlada Settakorn, Kanchanok Kodchakorn, and Majid Monajjemi

QM& MD Methods for Simulations of two liposome phospholipid layers structure 223
Mehrnoosh Khaleghian , Sima Afsharnezhad and Majid Monajjemi

Theoretical Investigation of Monte Carlo Simulation on DHA-Containing Phospholipids in Nerve Cell's Membrane 229
N .Khodayari, B .Honarparvar and Monajjemi.M

Session: Modeling and Simulation in Social Science

Corporate Cash Holdings: Evidence from Thailand 239
Suchada Manunphongpan

The Investigation of Target Leverage Role When Firms Make Financial Decision: Empirical Evidence In Australia Singapore And Thailand 250
Eakkachai Tangsageamvisai

Development of Successful Indicators Derived from Standards of the Distance Education via Satellite Management in Basic Education 255
Ameacha Pongpanpanu

Contents Page

Session: Agricultural/Environmental/Resources Modeling and Simulation

Simulation of Landform Evolution by Seepage Erosion 261
Adichai Pornprommin and Norihiro Izumi

A Neural Network Model for Prediction Puddling Index 267
Bandit Suksawat

Crop Monitoring Using Remote Sensing Data 273
Aye Mya Thein , Myint Myint Khaing and R.P Singh

Spatial Pattern Analysis of Land Degradation Using Satellite Remote Sensing Data and GIS in Mandalay Watershed, Central Myanmar 279
Kyaw Zaya Htun, Myint Myint Khaing, Swe Swe Aye and Lal Samarakoon

A Process-based model for methane emission from flooded rice production 289
Kruamas Smakgahn

Application of Geostatistical Analysis in Snow Depth and Density in Orazan Watershed 294
Mahdi Vafakhah Mohsen Mohseni Saravi Mohamad Mahdavi and Seyyed Kazem Alavipanah

Dynamic Mathematical Model for Site Specific N Fertilizer Recommendation 302
Kumut Sangkhasila, Sirisuda Butpetch, and Raweewan Chotiphan

Spatial Cd stock and flow analysis on Australian regional agricultural land 307
Napat Jakrawatana, Stephen Moore, Samsung Lim and Iain MacGill

Autonomous Security Hexapod Agent for Crop Production 322
Md. Masum Billah, Soheli Farhana and Md. Motasim Billah

Comparison of Thermal Time Calculated using Different Time Steps for Use in Crop Simulation Models 330
Afshin Soltani, Manouchehr Gholipoor and Benyamin Torabi

Material Flow Analysis of Nitrogen and Phosphorus for Rice Paddy in Bang Pakong Basin of Thailand 336
Wallapa Kupkanchanakul and Suphaphat Kwonpongsagoon

The Rainmaking Decision Model over River Basins of Thailand 342
Veerasak Udomchoke, Prasert Aungsuratana, Nitaya Lauhachninda, Unnop Homchan, Pongsakorn Jiwapornkupt and Krongjit Kesjinda

SCS-CN model: tool of head watershed management in Thailand. 355
P.Witthawatchutikul and P.Thitirojanawat

Application of Remote Sensing and GIS in Land Use Land Cover Change and Soil Erosion 361
Kyaw Zaya Htun, Swe Swe Aye and Lal Samarakoon

Participatory Agent-Based Modeling and Simulation of Rice Farming in the Rainfed Lowlands of Northeast Thailand 370
W. Naivinit, C. Le Page, M. Thongnoi, and G. Trébuil

Contents Page

Session: Modeling and Simulation in Engineering Science

Sand Dune Simulation of Nonuniform Sediment 380
Wandee Thaisiam and Yasuyuki Shimisu

Simulation of Turbulent Cavitating Flows around a Hydrofoil 386
Thaithacha Sudsuansee, Udomkiat Nonthakaew and Yodchai tiaple

Frequency of Coherent Vortices in Rigid Submerged Vegetation 391
Sandeep Patil, Enda Murphy, Vijay P. Singh and A. K. Rastogi

FEA Study on Parameters Affecting Springback of Forming of Advance High Strength Steel sheets (AHSS) 396
Watcharapong Sirigool, Nattawoot Depaiwa, Suwat Jirathearanat, Adachi Tadaharu

Applications of Ray Tracing Method in Illumination Design 403
Piyapong Premvaranon, Apichart Teralapsuwan, and Foifon Srisawat

A Study for Improvement of Production Efficiency in Hot Forging Processes Using the Finite Volume Method 410
Surasak Suranuntchai and Prarop Kritboonyarit

Effect of Co and Counter Flow to Transport Phenomena for Proton Exchange Membrane Fuel Cell by Numerical Simulation 417
Keerasut Suttanarak , Nirut Naksuk and Jarruwat Charoensuk

Monochromator Selection, Crystal Design & Replacement of X-ray Tubes 426
Md. Motasim Billah, Md. Masum Billah and Soheli Farhana

Comparative study of Low Phase Noise Oscillator 432
Soheli Farhana, AHM Zahirul Alam, Md. Masum Billah

Hexagonal Structure Hexapod Robot: Developing a Method for Omni-directional Navigation 435
Md. Masum Billah, Mohiuddin Ahmed, Md. Raisuddin Khan and Soheli Farhana

Turbulent Diffusion in Wave-Current-Vegetation Flow 441
Sandeep Patil

Design of Computer Experiment for Drawbead Design in Sheet Metal Restraint 449
Thaweepat Buranathiti and Anut Kositpipat

Spatial Pattern Analysis from High Resolution Data using Spatial and Spectral Properties 458
Thandar Htoon, Myint Myint Khaing, Minakshi Kumar

A Numerical Method for Solving Linear Non-Autonomous Systems based on Genetic Algorithm

Hassan Kadkhodaei Khalafi and Omid Solaymani Fard
School of Mathematics and Computer Science, Damghan University of Basic Sciences
Damghan, Iran

Abstract: In this paper, we present an effective approach to accommodate solution method for linear non-autonomous systems based on Genetic Algorithm(GA). In such method, we use the random candidate solutions to find out the desired solution. Indeed, we propose the method that offers performance enhancement and singularity. Beside, we show the accuracy of our method through simulation and analysis numerical examples.

Key words: Linear non-autonomous systems, Genetic Algorithm, Linear programming, Linearization.

INTRODUCTION

Working on solving differential equations have long story as solving differential calculus. With changing disciplines in non-autonomous linear systems, it is very applicable tools in most mathematics and physical topics. These tools can use in the method of finite differential for solving Partial Differential Equations (PDEs) or in some cases we are considering stability of solutions, in the theory of dynamic system.
This paper is going to find out the approximate solution of the following initial value problem:

$$\dot{X}(t) = A(t)X(t) + g(t), \qquad t \in [a,b] \qquad (1)$$
$$X(a) = X_a, \qquad (2)$$

where, $X = (X_1, X_2, \mathrm{K}, X_n)^T$ is a vector function with components in $C^1([a,b])$, and $X_a = (X_{a1}, \mathrm{K}, X_{an})^T$ is given. Here, $A(.)$ is an $n \times n$ matrix which its entries are continuous functions on $[a,b]$, and $g(.) = (g_1(.), \mathrm{K}, g_n(.))^T$ is an $n \times 1$ vector function with continuous components on $[a,b]$. There are many numerical methods to solve this problem and even nonlinear case. Some of these numerical methods are Euler, Range-Kutta, and Taylor series method (see [1]-[4]). By defining artificial controls, Alavi, et al [5] have converted this type of problems to an optimal control problem and then they have solved the modified problem by the method of [6]. Recently, Luis Lara in [7] and in [8], Mehne have considered the mentioned problem and they have presented new numerical method to solve the problem. Most numerical methods that we mentioned, have some advantages but they involve with some difficulty, too. For example, convergence of these methods for finding the real solution, cause that our method just is good for particular differentials equations and at the same time. In most cases these methods can not determine the error of their methods. The efficiency of our method is finding the exact solution as well as minimizing the error of the method. In summary, first we convert the initial value problem to a calculus of variation problem and then by using a special linearization method for changing the problem to a zero-one linear programming problem with linear or non-linear cost function. After that, we will able to produce some initial values that they are utilized by GA.

METAMORPHOSIS

In this part, it is convenient to change the initial value problem (1) and (2) to an optimization type problem. Hence, it is necessary to define the function $F : \Re^{2n} \to [0, \inf]$ as follows:

$$F(X(t), \dot{X}(t)) = \left\| \dot{X}(t) - A(t)X(t) - g(t) \right\|_p$$

where $\|.\|_p$ is the $L_p - norm$ defined as

$$\|x\|_p = \left(\sum_{i=1}^{n} |x_i|^p \right)^{\frac{1}{p}}, \qquad x = (x_1, \mathrm{K}, x_n) \in \Re^n .$$

Here, we consider the following calculus of variations problem:

Corresponding Author: Hassan Kadkhodaei Khalafi, School of Mathematics and Computer Science, Damghan University of Basic Science, Damghan, Iran , E-amil: h_kadkhodaei@dubs.ac.ir

$$\min \quad J(X(.),\dot{X}(.)) = \int_a^b F(X(t),\dot{X}(t))dt \qquad (3)$$

subject to:

$$X(.) \in C^1([a,b]), X(a) = X_a. \qquad (4)$$

We can easily show that $X(.)$ is the solution of (1) and (2) if only if $X(.)$ is the optimal solution of (3) and (4) with cost function $J(X(.),\dot{X}(.)) = 0$, (For more details you can see the proof of Theorem 1 in [8]).

Now, in order to modify the original problem (1)-(2) to an optimization problem, or equivalently a calculus of variation problem as (3)-(4), first we discretize the problem (1)-(2) as follows: Let N be a positive integer, $\Delta(N) = \frac{b-a}{N}$, and consider the following subsets of integer numbers:

$$J = \{1,2,\mathrm{K}\ ,N+1\},$$
$$J_1 = \{1,2,\mathrm{K}\ ,N\},$$
$$I = \{1,2,\mathrm{K}\ ,n\}.$$

Let $P(N) = \{t_1, t_2, \mathrm{K}\ , t_{N+1}\}$ be a partition of $[a,b]$, where $t_i = a + (j-1)\Delta(N), \quad \forall j \in J.$

For large value of N we have

$$\dot{X}_i(t_j) \approx \frac{X_i(t_j + \Delta(N)) - X_i(t_j)}{\Delta(N)} = \frac{X_i(t_{j+1}) - X_i(t_j)}{\Delta(N)}$$

Let define $X_{ij} = X_i(t_j)$ for all $i \in I$ and $j \in J_1$. Thus we have

$$\dot{X}_i(t_j) \approx \frac{X_{i,j+1} - X_{ij}}{\Delta(N)}, \quad \forall i \in I, \quad \forall j \in J_1.$$

We set

$$f_{ij} = \frac{X_{i,j+1} - X_{ij}}{\Delta(N)} - \sum_{k\in I} a_{ikj} X_{kj} - g_{ij}, \forall i \in I, \quad \forall j \in J_1$$

where

$$a_{ikj} = A_{ik}(t_j), \quad g_{ij} = g_i(t_j), \quad \forall i,k \in I, \forall j \in J_1,$$

Here, we may discretize problem (3)-(4) as problem (5)-(7).

$$\min\left(\sum_{i\in I}\sum_{j\in J_1} |f_{ij}|^p\right)^{\frac{1}{p}} \qquad (5)$$

subject to:

$$X_{i1} = X_{ia}, \qquad \forall i \in I, \qquad (6)$$
$$X_{ij} \quad free, \qquad \forall i \in I, \quad \forall j \in J_1. \qquad (7)$$

Problem (5)-(7) is a nonlinear programming problem with x_{ij} as decision variables. In the following, we just consider the case, $p = 1$. When $p = 1$, we can transform the problem to an LP.

CASE $p = 1$, LP FORMULATION

Let define

$$R_{ij} = \max\{f_{ij}, 0\}, \qquad S_{ij} = -\min\{f_{ij}, 0\}$$
$$for\ all \quad i \in I\ and\ j \in J_1.$$

Then we have

$$|f_{ij}| = R_{ij} + S_{ij}, \quad f_{ij} = R_{ij} - S_{ij}.$$

Now, we can linearize problem (5)-(7) by these new variables. Therefore we must solve the following LP,

$$\min \sum_{i\in I}\sum_{j\in J_1} (R_{ij} + S_{ij}) \qquad (8)$$

subject to:

$$R_{ij} - S_{ij} = f_{ij}, \qquad \forall i \in I, \ \forall j \in J_1, \qquad (9)$$
$$X_{i1} = X_{ia}, \qquad \forall i \in I, \qquad (10)$$
$$X_{ij} \quad free \qquad \forall i \in I, \ \forall j \in J, \qquad (11)$$
$$R_{ij}, S_{ij} \le 0, \qquad \forall i \in I, \ \forall j \in J_1, \qquad (12)$$

There are some methods to solve the above LP problem, for example Revised Simplex method, Interior Point methods, or Nelder-Mead Simplex method and so on. Furthermore, there are also many software for LP solving, a list of such solvers may be found easily thru an internet search engine. However in this paper we use GA toolbox of MatLab (the function gatool) to calculate and find out the exact solution of the LP problem (8)-(12),or indeed the approximate solution of (1)-(2) at points of $P(N)$.

However two essential questions have remained yet. The first one is , *does the above problem has a solution?*, and the second one is *dose the solution of this LP converge to the solution of (1)-(2)?*. In fact, both answers of the questions are positive. Since $A(.)$ has continuous entries, and the function $f(t, X) = A(t)X + g(t)$ is continuous and satisfies Lipschitz condition with respect to X, therefore the problem (1)-(2) has a solution. Furthermore, Mehneh in [8], has proved the following existence and uniqueness theorem which is the answer of the second question.

Theorem 3.1 The initial value problem (1)-(2) has a unique solution.

Proof. See [8].

EXAMPLE

In this section, we consider an example and solve it by the proposed method. First, we introduce a criterion for error estimation. Let define an Absolute error Function corresponding to N as follows:

$$AE(N) = \frac{1}{N}\sum_{j\in J}\left\|X(t_j) - X_j^N\right\|_\infty,$$

where, $X(t_j)$ denotes the exact solution at t_j, and X_j^N is the approximated value for $X(t_j)$ obtained by solving the corresponding LP problem for N. IF $\ddot{X}(.)$ be twice differentiable on $[a,b]$, from a theorem on error estimation of Euler method, it could be shown that

$$AE(N) \le (b-a)\frac{\exp((b-a)k)-1}{2KN}M_2,$$

where,

$$M_2 = \max_{t\in[a,b]}\left\|\ddot{X}(t)\right\|_\infty, \quad K = \max_{t\in[a,b]}\left\|A(t)\right\|_\infty$$

this shows that the Absolute error is a decreasing function of N (for more details see [8]).

Example 4.1 Consider the following linear non-autonomous system:

$$\dot{X}_1 = -X_2 + 3te^t - 5\cos t,$$
$$\dot{X}_2 = 2X_1 - 3X_2 + 10\sin t,$$
$$t \in [0,1]$$

with $X_1(0) = \frac{-7}{6}$ and $X_2(0) = \frac{-5}{5}$ as the initial conditions. The exact solution is (see [8])

$$X_1 = 2te^t - \frac{7}{6}e^t - 5\sin t,$$
$$X_2 = te^t - \frac{5}{6}e^t.$$

We solve the LP problem for six values of N. Table 1 shows the corresponding Absolute errors. The value of this table are used to draw the Absolute error as a function of N in Fig. 1. By this figure the decreasing behavior of Absolute error in terms of N is approved. Also, Approximate and exact solution with $N = 40$ have been compared in Fig. 2.

Table 1
Absolute errors for Example 4.1.

N	5	10	20	40	80	160
AE	0.2746	0.1429	0.0672	0.0296	0.0162	0.0074

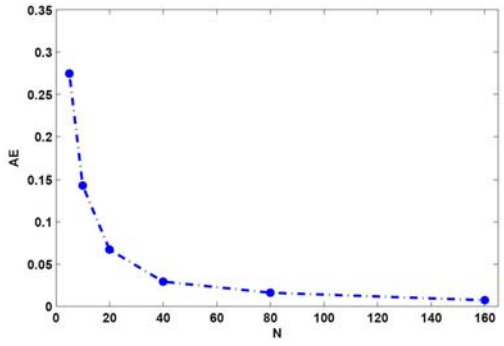

Figure 1: Absolute erro function.

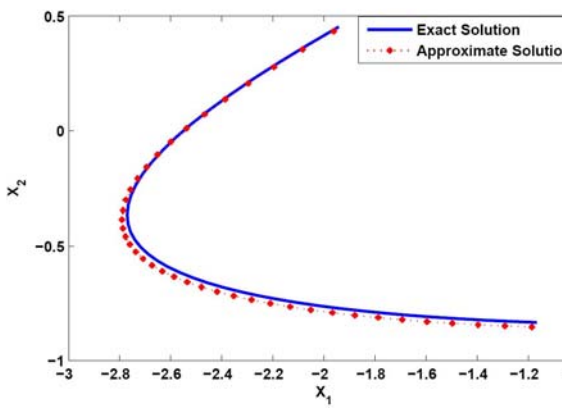

Figure 2: Exact and approximate solution.

CONCLUSIONS

In this article we have presented an approach to solving linear non-autonomous system based on genetic algorithm. Such a method would be useful, for example, to improve solving artificial control problems. Genetic algorithm has been used to analyze and obtain the initial values when exact solution is not available. Our methods improve stability of solutions and finding real solution as well. In our method we are trying to minimize the error of the method.

REFERENCES

1. D. J. Lambert, Numerical Methods for Ordinary Differential Systems: The initial Value Problem, John Wiley and Sons,1991.
2. T. S. Parker, L. O. Chua, Practical Numerical Algorithms for Chaotic Systems, Springer Verlag, New York Inc,1989.
3. S. Chapra, R. Canale, Numerical Methods for Engineers with Progamming and Software Applications, McGraw-Hill, London, 1999.
4. C. H. Edwards Jr., D. E. Penney, Elementary Differential Equations with Boundary Value Problems, Third Edition., Prentice Hall, New York, 1993.
5. S . A. Alavi, A. V. Kamyad, M. Gachpazan, Solving nonlinear ordinary differential equations as a control problem by using measure theory, Scientia Iranica Vol.7 , pp. 1-7, 2000.
6. J. E. Rubio, Control and Optimization: the Linear Treatment of Non-Linear Problems, Manchester University Press, Manchester,1986.
7. L. Lara, A numerical method for solving a system of non-autonomous linear ordinary differential equations, Applied Mathematics and Computation, 170, pp. 86-94, 2005.
8 H. H. Mehne , A numerical method for solving linear non-autonomous system , Applied Mathematics and Computation, 178, pp. 287-294, 2006.

Variational Calculus for Random Field and Green's Functions Method

Pwint Phyu Moe
Yangon Technological University, Myanmar
PwintPhyuMoeMyint@gmail.com.

Abstract : In this paper, we propose a new method of study of Gaussian random fields using the variational calculus . We get an idea on how to investigate a given stochastic process in an analytic manner from the Lévy infinitesimal equation for the ordinary stochastic processes. The variational calculus for Gaussian random fields will be proposed and developed in this paper that is one of the generalizations of the time variation of ordinary processes. The Hadamard equation or variational equations arising from electro-magnetic fields may be paraphrased in terms of white noise analysis.We discuss a multi-dimensional parameter generalization of a multiple Markov Gaussian process in the restricted sense. We establish a reasonably systematic development of the Green's function method.in second order differential operators.

1. INTRODUCTION

For ordinary stochastic processes, one can get an idea which is how to investigate a given stochastic processes in an analytic manner from the Lévy's infinitesimal equation and take time propagation into account. There, one can see a key role played by the innovation. Interesting results have been obtained in line with what was proposed by Lévy for ordinary stochastic process with one- dimensional time parameter.

The variational calculus for Gaussian random fields will be propos%d and developed in this paper that is one of the generalizations of the time variation of ordinary processes. By using this calculus, the way of dependency can be seen as the parameter of the field changes, and, in addit)/n in many favorable cases.

I. this paper a few concrete techniques for several particular cases will be prEsented iN what follows as the first step of our approach. They are

1) Fields depending on a plane circles which is wandering around in a two dimensional space $R^{\updownarrow}$.

The conformal group can be used to describe possible deformations of the circle which means that the possible change of the field can be seen according to the movement of the circle.

2) Use of the Green's function. If a given field is expressed as a white noise integral, then Laplacian applied to this field will take out the original white noise.

3) The Hadamard equation or variational equations arising from electromagnetic fields may be paraphrased in terms of white noise analysis.

2. BACKGROUND

One introduces white noise with parameter space R^d. Let a characteristic functional.

$$C(\xi) = \exp\left[-\frac{1}{2}\|\xi\|^2\right] \qquad (2.1)$$

be given on a space $E(\subset L^2(R^d))$ of test functions on R^d .Then by using the
Bochner – Minlos theorem ,a Gaussian measure μ can be introduced on the space E*(= the dual space of E)

Corresponding Author : Pwint Phyu Moe, Yangon Technological University, Myanmar
PwintPhyuMoeMyint@gmail.com.

of generalized functions on R^d in such a way that

$$C(\xi) = \int_{E^*} \exp[i < x, \xi >] \, d\mu(x)$$

This measure μ is called a white noise measure.

As soon as the measure space (E^*, μ) is given , a complex Hilbert space $(L^2) \equiv L^2(E^*, \mu)$ is formed. A member $\varphi(x)$ of (L^2) is called a white noise functional or a Brownian functional.

A good representation of white noise functionals may be obtained by the $\mathcal{S}$- transform:

$$(\mathcal{S}\varphi)(\xi) = \int_{E^*} \varphi(x + \xi) \, d\mu(x) \qquad (2.2)$$

$$\xi \in E, \quad \varphi \in (L^2)$$

Let $\mathcal{K}_1$ be the subspace of (L^2) spanned by the $< x, \xi >$, $\xi \in E$. Then the $\mathcal{S}$-transform establishes an isomorphism.

$$\mathcal{K}_1 \cong L^2(R^d), \qquad (2.3)$$

in such a way that

$$(\mathcal{S}\varphi)(\xi) = \int_{R^d} F(u) \xi(u) \, du, \qquad (2.4)$$

$$\varphi \in \mathcal{K}_1, \quad F \in L^2(R^d).$$

Using such a representation one can introduce a class $\mathcal{K}_1^{(-1)}$ of generalized white noise functionals extending the isomorphism (2.3) :

$$\mathcal{K}_1^{(-1)} \cong H^{-(d+\frac{1}{2})}(R^d), \qquad (2.5)$$

where $H^m(R^d)$ stands for the sobolev space of order m over R^d. Assume that the space of test functionals are taken to be the subspace $\mathcal{K}_1^{(1)} (\subset \mathcal{K}_1)$ which is isomophic to $H^{(d+1)/2}(R^d)$. Note that any member of the Sobolev space of order $(d+1)/2$ can be continuous and be evaluated at every point.

We have summarized just what we shall use in the following sections.

Proposition 2.1. Let M be an analytic manifold in R^d and let I_M be the indicator function of M. A functional

$$U(\xi) = \int_{R^d} I_M(u) f(u) \xi(u) d\sigma(u), \qquad (2.6)$$

$$\xi \in \mathcal{S}(R^d), \; f \in L^2(M, d\sigma),$$

$d\sigma$: volume element on M,

is the $\mathcal{S}$- transform of an $\mathcal{K}_1$ - functional φ if M is d-dimensional while U(ξ) is the $\mathcal{S}$ - transform of a generalized functional φ in $\mathcal{K}_1^{(-1)}$ if M is at most (d-1) dimensional.

A generalized white noise functional whose transform is given by (1.6) is often denoted by

$$\varphi(x) = \int_M f(u) x(u) d\sigma(u) \qquad (2.7)$$

The partial derivative of white noise x (u):

$$x_j(u) \equiv \frac{\partial x}{\partial u_j}(u), \qquad (2.8)$$

$$u = (u_1 ....., u_j, ..., u_d),$$

Which is defined by

$< x_j, \xi > = - < x, \xi_j >$, ξ_j (u) : partial derivative in u_j. For a smooth g(u) , the $\mathcal{S}$- transform of $< x_j, g>$ is given by

$$U(\xi) = - \int_{R^d} g_j(u) \xi(u) \, d\sigma(u).$$

(2.9)

With this fact in mind, the following proposition can be proved .

Proposition 2.2. Let M be a d- dimensional manifold and let g be such that $g_j \in L^2(M, d\sigma)$. Then a functional of the form

$$\varphi(x_j) = \int_M g(u) x_j(u) \, d\sigma(u)$$

(2.10)

is defined and its $\mathcal{S}$- transform is given by (2.9).

Remark. If g_j (u) is not in L^2 (M, dσ) , then φ (x_j) in (2.10) is a generalized white noise functional.

3. RESTRICTION OF PARAMETER

The parameter $\underline{u}$, running through R^d , of the white noise may be restricted to some lower dimensional manifold M, and one is , roughly given a white noise with time parameter set M.

In this paper, the way of restricting the parameter which is suggested by Proposition 2.1, in order to have consistent restrictions.

Take an analytic manifold M in R^d , and take a function F (u) in the Sobolev space H^m (R^d) with m = (d+1) /2 . Then there is a mapping P_M from $\mathcal{K}_1$ into itself

$$\int F(u)\,x(u)\,d\sigma(u) \to \int_M F(u)\,x(u)\,d\sigma(u) \tag{3.1}$$

If M is a closure of a d - dimensional domain, then P_M is extended to a projection down to a closed subspace of $\mathcal{K}_1$. However, if M is less than d - dimensional, one need to modify the mapping (3.1) and to give some interpretation. Let the mapping be represented by U- functionals so that integral of the image is well defined:

$$\int F(u)\,\xi(u)\,d\sigma(u) \longrightarrow \int_M F(u)\,\xi(u)\,d\sigma_M(u), \tag{3.2}$$

$$\xi \in E \subset L^2(R^d),$$

Where $d\sigma_M(u)$ is the measure over M induced by dσ (u) over R^d. Now the image under the mapping $\mathcal{S}$ $\mathbf{P_M}$ $\mathcal{S}^{-1}$ which is continuous on E (M), a nuclear space over M. One can , therefore, define a white noise measure μ_M with parameter set M, and

$$\int_M F(u)\,\xi(u)\,d\sigma_M(u)$$

is $\mathcal{S}$ - transform of Gaussian random function expressed as a linear functional of a white noise with parameter set M. This can be shown by using the fact that M is locally Educlidean (see [13]). Therefore (3.2) is paraphrased in terms of white noise :

$$\int F(u)\,x(u)\,d\sigma(u) \dashrightarrow \int_M F(u)\,x_M\,d\sigma_M(u) \tag{3.3}$$

The above mapping is also denoted by P_M.Summing up,therefore the following theorem.

Theorem 3.1 . The family of mappings

ρ = { P_M ; M closure of domain in R^d , ∂ M analytic }

Satisfies

i) P_M with d-dimensional M is a projection operator on $\mathcal{K}_1$, while P_M maps (L^2) - functionals into the space of generalized functionals , if the dimension of M is less than d .

ii) if M ⊃ N , then $P_M P_N$ is equal to P_N.

iii) ρ is a consistent family in the sense that for

M ⊃ N ⊃ K

$P_M P_N P_K = P_M P_K = P_K$

Proof of i) comes from Proposition 2.1 Other assertions are obvious.

4. RANDOM FIELDS DEPENDING ON A CIRCLE

Variational calculus for Gaussian random fields depending on a plane circle has been discussed in [8]. There circles vary under the action of the conformal group acting on R^2 . The technique of the $\mathcal{S}$ -transform has been used, by which random functions

can be represented in terms of functionals of C^{∞} - functions. One can therefore appeal to the classical theory of calculus of variations (cf. for example, P. Lévy [1], [2])

The basic idea for this particular case is that the set of all circles is topologized so as to be a 3-dimensional manifold, which is the parameter set of the Gaussian field. The conformal group acts on this parameter space as the symmetry group so that the irreducible representation of the conformal group can automatically be obtained (see Lee [12] mentioned above). By using this substantial property, one can prove the canonical property and even one can speak of a generalized notion of innovation.

5. GREEN'S FUNCTION METHOD

In this section, multi-dimensional parameter generalization of a multiple Markov Gaussian process which shall be discussed in the restricted sense. To establish a reasonably systematic development of the Green's function method, the case of second order differential operators is restricted in two- dimensional variable as well as their powers.

Given a general linear partial differential equation of second order over a domain D :

$$L\varphi = A\varphi_{11} + 2B\varphi_{12} + C\varphi_{22} + D\varphi_1 + E\varphi_2 + F\varphi = f \ , \tag{5.1}$$

Where A , ... F and f are given functions of $u = (u_1 , u_2)$, and where

$$\varphi_i = \partial\varphi / \partial_{u_i} \ \text{and} \ \varphi_{ij} = \partial\varphi^2 / \partial_{u_i} \partial_{u_j} \ .$$

The Green's function associated with the differential operator L will be denoted by G(u,v;C) where C stands for the boundary of the domain D on which (5.1) is defined. Assumed that L is formally self- djoint. The most important example in the approach is , of course, the Laplacian operator.

Let x (u) be white noise and define X (C) by

$$X(u, C) = \int_D G(u, v; C)\, X(v)\ d\sigma(v), \qquad u \in D \tag{5.2}$$

Then, applying the operator L , one obtains the white noise X :

$$(LX)(u, C) = X(u) \tag{5.3}$$

The white noise x(u), on which the X(u, C) is based , can be obtained by applying the operator L acting on X (u, C) itself. Thus obtained quantity x(u) may therefore be considered as the innovation for the field X(u, C) Proofs of these facts are given in terms of U-functionals by applying the $\mathscr{S}$ - transform .

Consider Green's functions of higher order. Let G(u,v) $u,v \in R^2$, be a symmetric kernel function , and let G^i (u,v) be defined inductively by

$G^O (u,v) \equiv 1, G^1 (u,v) = G (u,v)$,

$G^i(u,v) = \int_D G^{i-1}(u,s)\, G(s,v)\, d\sigma(s), \quad i = 1,2, \ldots$ The kernel $G^i (u,v)$ is, following V. Volterra, called the i-th power composition of the second kind of G (u,v). Obviously, the equation

$$LG^i (u,v) = G^{i-1} (u,v)$$

is obtained, where L is as an operator seting on functions of u.

Now set

$$Y(u,C) = \int_D G^N(u, v)\, x(v)\ d\sigma(v). \tag{5.4}$$

Then we have

$$L^N Y (u, C) = X (u) \tag{5.5}$$

Thus, the field Y (u,C) may be thought of as a generalization of N-ple Markov Gaussian process X(t) in the restricted sense which admits us to have an expression.

$$X(t) = \int_0^t (t-u)^{N-1} \dot{B}(u)\, du .$$

If it is viewed as a representation of Y (u, C), then it is a canonical representation of Y(u, C) in terms of the white noise x(u) in the following sense.

Propesition 5.1. We have

$\mathcal{B}_D$ (Y) = $\mathcal{B}_D$ (x), (5.6)

where $\mathcal{B}_D$ (·) denotes the σ – field generated by the random variables in the paranthesis with parameter running through D.

Proof. The property (5.6) comes from the equation (5.5).

Thus, we have seen an example of a canonical representation.

6. VARIATION OF FIELDS

One now returns to X(u, C) given by (5.2). The variable u is now fixed, while C is a variable. Let C be the class of plane curved introduced in R^2 and be topologized in a usual manner. Again the $\mathcal{S}$ - transform can be appealed to give a rigorous expression of the variation δX(u, C).

Theorem 6.1. Let { X(u, C) ; C ∈ $\mathcal{E}$ } be a Gaussian random field such that each X(u, C) is given by. (5.2). Then the variation δX(u,C) of X(u, C) when C varies in $\mathcal{E}$ is expressed in the form.

$$\delta X(u,C) = \int_D \delta G(u,v;C)\, x(v)\, d\delta(v) + \int_C G(u,S;C)\, x(s)\, \delta n(s)\, ds, \tag{6.1}$$

Where δG (. , ., ; C) denotes the variation of G (. , . , ; C) in C , and where s is the parameter on the curve C and ds is the line element.

Before the proof of the theorem, some interpretations are necessary so that the formula (6.1) can well be understood.

1) The exact expression of the variation δG(u, v ; C) is given by the so-called Hadamard equation (see [2] , [4, § 3]) :

$$\delta G(u,v;C) = -\frac{1}{2\pi} \int_C \frac{\partial}{\partial n} G(u,m;C)\, \frac{\partial}{\partial n} G(m,v;C)\, \delta n(s)\, ds, \tag{6.2}$$

Where m = m (s) runs through C and where δn = δn (s) denotes the normal displacement of the point m (s) when C changes to C + δC.

Remark 1. It is a great of the analysis that even a restriction of the parameter of white noise to a curve can be rigorously understood as is seen in the second term of (6.1).

Proof of the theorem. The $\mathcal{S}$ transform of X (u,C) is

$$(\mathcal{S}X)(u,C;\xi) = \int_D G(u,v;C)\, \xi(v)\, d\sigma(v),$$

$\xi \in \mathcal{S}(R^d)$ (6.3)

which will be denoted by U (u, C; ξ) . The Lèvy's variation technique is now ready to be applied, and one obtains

$$\delta U(u,C)(\xi) = \int_D G(u,v;C)\, \xi(v)\, d\delta(v) + \int_C G(u,s;C)\, \xi(s)\, \delta n(s)\, ds$$

Applying the $\mathcal{S}^{-1}$ to each term one has (6.1)

7. LOCAL OBSERVATION OF RANDOM FIELDS

Since the white noise analysis has extensively developed, we can consider x(t), $x \in E^*$, evaluated at $t \in R^d$ where x is a sample function of R^d -parameter white noise.

As in the case of R^1-parameter white noise, we can define the partial derivative $\frac{\partial}{\partial x(t)}$ in the variable x(t). Let it be denoted by ∂_t. Namely, let U(C) be the S-transform(see (1.2)) of a Gaussian random field X(C)=X(C, x) depending on a smooth manifold C. Our aim is to define $\partial_t X(C)$ by using the functional derivative U'(C,t).

So far, we discussed the variation δX(C) with the help of the S-transform and the variation is local.

S. Tomonaga [19] deformed δ(C) locally, and now we can consider a limit, that is, the case where delta δC tends to an infinitesimal movement of a point, say t of C. The corresponding random part can be done within the class of linear generalized white noise functional. In terms of X(C), we may consider $\frac{\partial X(C)}{\partial X(t)}$, t ∈ C.

We have thus proved

Theorem Let X(C) be a Gaussian random field expressed in the form

$$X(C) = \int_C F(s)\, X(s)\, ds$$

Then the local deformation of C enables us to define the partial derivative $\frac{\partial}{\partial X(s)} = \partial_s$ and we have $\partial_t X(C) = F(t)$, $t \in C$

Remark This method can be applied to an identification of a random system (e.g. in biology) that changes as C deforms.

8. CONCLUSION

(1) One shall be able to discuss the variation of X (C), C ∈ C, of the form

$$X(C) = \int_C F(s;C)\, x(s)\, ds \qquad (7.1)$$

we obtain

$$\delta X(C) = \int_C \{\delta F(s;C) - \kappa\, F(s;C)\, \delta n(s)\}\, x(s)\, ds + \int_C F(s;C) \frac{\partial}{\partial n} x(s)\, \delta n(s)\, ds \qquad (7.2)$$

If F is independent of C, one can think of transformations that carry C onto itself to determine the value of x (s).

(2) Canonical representation, can be considered for Lèvy's Brownian motion.

To fix the idea, one shall discuss a two dimensional parameter Lèvy Brownian motion {X (a) : a ∈ R^2}. Set X (a) = X (t , θ), a ∈ R^2, t ∈ R_+ , θ ∈ [0, 2π). Following H. P. McKean, one expands X (t, θ) in a Fourier series for each fixed t. Take a complete orthonormal basis is { φ_n (θ) : n ∈ N} and set

$$X_n(t) = \int_0^{2\pi} X(t,\theta)\varphi_n(\theta)\, d\theta, \qquad n \geq 0 . \qquad (7.3)$$

Then , one can prove the existence of the canonical representation of X_n (t) with one

dimensional parameter. Denote by B_n (t) the Brownian motion of the representation. The collection $\{\dot{B}_n(t) : n \in N,\ t \geq 0\}$ is equivalent of white noise.

REFERENCES

[1] P.Lévy, sur la variation de la distribution de l'électricité un conducteur dont la surface se déforme. Bull, société math. de France, 46 (1918), 35-68.

[2] _____, problèmes concrets d'analyse fonctionnelle. Gauthier villars, paris, 1951, Part. I. II.

[3] _____, A special problem of Brownian motion, and general theory of Gaussian functions. Proc. 3rd Berkeley Symp. vol.II (1965). 133-175.

[4] K.Aomoto, Formula variationelle d' Hadamard et modèle des variétés différentiables plongées. J.Functional Analysis 34 (1979), 493-523.

[5] T.Hida, Brownian motion (in Janese). Iwanami Pub. Co., Tokyo 1975; English Trans. Springer-Verlag, New York Heidelberg Berlin 1980.

[6] _____, Analysis of Brownian functions. Carleton Math. Lec Notes, no.13, Carleton Univ. Ottawa, 1975.

[7] _____, Stationary Stochastic Processes, Princeton University Press, Princeton, New Jersey.

[8] T. Hida, Hitsuda, M. 1976. Gaussian Processes. American Mathematical Society.

[9] T. Hida, H .-H Kuo, J. Potthoff and L. Streit :"White Noise : An Infinite Dimensional Calculus"; Kluwer Academic Publishers

[10] Accardi, L., Hitsuda, M., Kuo, H. H., Streit, L., Si Si and Saito, K. 1991. Selected papers of Takeyuki Hid. World Scientific Co., Ltd.

[11] J.L. Lions and E. Magenes, Non-homogeneous boundary value problems and applications, vol.I. Springer-Verlag, New York Heidelberg Berlin, 1972.

[12] Si Si, A note on Lévy's Brownian motion. Nagoya Math. J.108 (1987), 121-130.

[13] _____, Gaussian processes and conditional expectations. BiBos Notes 292/87. Univ. Bielefeld, 1987.

[14] Quantum information I, January 2001. Edited by T.Hida , K.Saitô

[15] Quantum information II, January 2002. Edited by T.Hida , K.Saitô

[16] Infinite Dimensional Analysis, Quantum Probability and Related Topics.VolumeIII , No(1), March 2007

[17] Infinite Dimensional Analysis, Quantum Probability and Related Topics. Volume V, No(2), June 2002

[18] Infinite Dimensional Analysis, Quantum Probability and Related Topics. Volume VII,No(1), March 2004

[19] Tomonasa, On a Relativistically Invariant Formulation of the Quantum Theory of Wave Fields. Progress of Theoretical Physics, 1(1946) 27-42

Mathematical Study of an Influenza Model with Seasonal Forcing in Transmission Rate

Settapat Chinviriyasit and Wirawan Chinviriyasit*
Department of Mathematics, King's Mongkut University of Technology Thonburi,
Pacha-U-tid Road, Bangmod, Bangkok, 10140, Thailand.

Abstract: A deterministic mathematical model is presented and used to investigate the epidemiological consequences of the drift mechanism for influenza A viruses. The model predicts that the prevalence of a virus is maximum for an intermediate value of R_0, the basic reproduction number. Although the equilibria of the model could not be expressed in closed form, their existence and threshold conditions for their stability are theoretically investigated. The model is shown to have a globally-asymptotically stable disease-free equilibrium (thus, influenza can be eradicated from the community) whenever a certain threshold, R_0, is less than unity. Furthermore, the model has a unique endemic equilibrium (leading to the persistence of influenza within the community) whenever this threshold exceeds unity. The effect of seasonality on the epidemiological regimes is investigated and leads to periodic and chaotic dynamics of epidemics which are present in the numerical simulations.

Key words: Basic reproductive number; Equilibria; Global stability, Chaos

INTRODUCTION

Influenza is caused by a virus that attacks mainly the upper respiratory tract, nose, throat and bronchi and rarely also the lungs. Most people recover within 1-2 weeks without requiring any medical treatment. In the very young, the elderly and people suffering from medical conditions such as lung diseases, diabetes, cancer, kidney orheart problems. Each year anaverage of 20,000 excess deaths are attributed to influenza and its complications making the disease one of the top ten causes of death [4].

Influenza is caused by a virus that can be of three different types (A, B and C, see [23]). Among these types, the virus A is epidemiologically the most important for humans, since it can recombine its genes with those of strains circulating in animal populations (birds, swine and horses). These relatively rare recombination's give rise every few decades to new viral subtypes via the so called antigenic shift mechanism [27]. Much evidence [7,18,19] shows that the antigenic distance between two different strains influences the degree of partial immunity, often called cross-immunity, conferred to a host already infected by one of the strains with respect to the other.

A number of mathematical models have been developed in the literature to gain insights into the transmission dynamics of influenza in a community (see, for instance, [2,3,9,10,15,16,20,24,25,27]). Andreasen et al. [2] and Lin et al. [20] developed epidemiological models to shown that multiple strains of influenza can persist in the human populations and that their prevalence can exhibit self-sustained oscillations through time. Pease [24] studied the emergence of new viral strains is that of introducing into the model a loss of immunity by the host. Gill and Murphy [10] and Potter et al. [25] showed that the probability of recovered individuals being reinfected by new circulating strains linearly increases with the time since last infection. Casagrandi [3] introduced a new compartment C in the population, which can be called cross-immune, to design an intermediate state between the fully susceptible state (S) and the fully protected one (R). Kermack and McKendrick [16] introduced epidemic models of temporary partial immunity – or variable susceptibility and have recently been studied in the context of influenza [15,27]. Most of these studies, however, not much have been done in terms of the mathematical modeling of human social behaviour. In particular, the authors are not aware of any mathematical study (talkless of the rigorous qualitative analyses of the models) for fully examining, and assessing, the impact of cross-immune individuals in the population.

The aim of this paper is to provide a qualitative study of the dynamics of influenza presented introduced by Casagrandi et al. [3]. The model presented here is called an SIRC model, which is improved over the classical SIR by including a fourth class (C) for the cross-immune individuals in the population, i.e., those that recovered after being infected by different strains of the same viral subtype in the past years. Further, the effect of seasonality (in the presence of cross-immunity) on influenza transmission dynamics is assessed via numerical simulations. The numerical simulations show that the simulated regimes are qualitatively and quantitatively consistent with reality for tropical countries such as Thailand and Singapore.

Corresponding Author: Settapat Chinviriyasit, Department of Mathematics, King's Mongkut University of Technology Thonburi, Pacha-U-tid Road, Bangmod, Bangkok, 10140, Thailand.

PRELIMINARIES

Model Formulation

The model presented in [3] for the spread influenza disease in the human population classifies the population in four classes: $S(t)$ is the proportion of susceptibles at time t (individuals that do not have the virus), $I(t)$ is the proportion of infected at time t (individuals that have the virus and can infect), $R(t)$ is the proportion of recovered at time t (individuals recovered from the virus and have a temporary immunity) and $C(t)$ is the proportion of cross-immune individuals at time t. One of the main assumptions of this model is that the per capita birth rate is a constant $\mu > 0$ and the birth rate is the same as death rate. The *SIRC* model is depicted in the compartment diagram of Fig. 1, and it is expressed as the initial-value initial-value problem:

$$\begin{aligned}
\frac{dS}{dt} &= \mu(1-S) + \gamma C - \beta SI, \quad S(0) = S_0 > 0 \\
\frac{dI}{dt} &= \beta SI + \sigma\beta CI - (\mu+\alpha)I, \quad I(0) = I_0 > 0 \\
\frac{dR}{dt} &= (1-\sigma)\beta CI + \alpha I - (\mu+\delta)R, \quad R(0) = R_0 > 0 \\
\frac{dC}{dt} &= \delta R - \beta CI - (\mu+\gamma)C, \quad C(0) = C_0 > 0.
\end{aligned} \tag{1}$$

The model assumes a population of constant size, *N*, so that $N = S + I + R + C$. Since, the model is normalized to unity, $S + I + R + C = 1$. Table 1 provides an interpretation of the model parameters.

Analysis of the Model

In this section, the model (1) will be qualitatively analyzed to investigate the existence and stability of its associated equilibria.

1. Disease-Free Equilibrium

In the absence of infection (that is, $I = 0$), the model has a disease-free equilibrium $P^0 = (1,\ 0,\ 0,\ 0)$

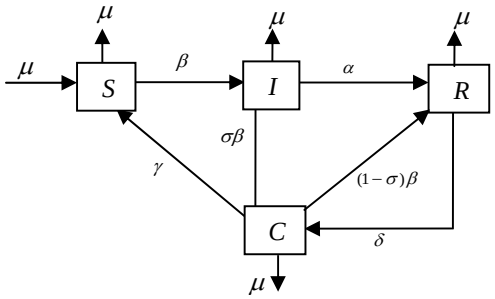

Fig. 1. Compartmental diagram for the *SIRC* model.

Table 1: Model parameters in (1)

Parameter	Definition	Values
μ	The mortality rate	0.02 y^{-1}
α	The infectious period	$365/3$ y^{-1}
δ	The total immune period	$1/1.6$ y^{-1}
γ	The cross-immune period	0.35 y^{-1}
σ	The recruitment rate of cross-immune into the infective	$0 \le \sigma \le 1$
β	Contact rate per year	1200
ε	Degree of seasonality	$0 \le \varepsilon \le 1$

which is obtained by setting the right-hand sides of (1) to zero. To establish the stability of this equilibrium, the Jacobian of (1) is computed and evaluated at P^0. The local stability of P^0 is then determined based on the signs of the eigenvalues of this Jacobian. The equilibrium P^0 is locally asymptotically stable if the real parts of these eigenvalues are all negative. The Jacobian of (1) at P^0 is

$$J(P^0) = \begin{bmatrix} -\mu & -\beta & 0 & \gamma \\ 0 & \beta-(\mu+\alpha) & 0 & 0 \\ 0 & \alpha & -(\mu+\delta) & 0 \\ 0 & 0 & \delta & -(\mu+\gamma) \end{bmatrix}$$

with eigenvalues $\lambda_1 = -\mu,\ \lambda_2 = -(\mu+\delta),$
$\lambda_3 = -(\mu+\gamma)$ and $\lambda_4 = \beta-(\mu+\alpha).$

Let $R_0 = \dfrac{\beta}{\mu+\alpha}$, thus $\lambda_4 < 0$ if and only if $R_0 < 1$. Since $\lambda_i,\ i = 1,2,3,4$ are negative (since all model parameters are assumed to be positive). Thus, we have established the following lemma.

Lemma 1. The disease-free equilibrium P^0 is locally asymptotically stable if $R^0 < 1$ and unstable if $R^0 > 1$.

The threshold quantity R_0 is called the basic reproductive number of infection [1]. In the context of epidemiological modeling (see [1]), it is generally known that if $R_0 < 1$, then the disease-free equilibrium is locally asymptotically stable (and the disease will be eradicated from the community if the initial sizes of the four state variables are within the vicinity of P^0). If the equilibrium P^0 is globally asymptotically stable, then the disease will be eradicated from the population irrespective of the initial sizes of the four state variables. Therefore, in the event of an epidemic, the theoretical determination of conditions that can make R_0 less than unity is of great public health interest.

Thus, it is imperative to show that the disease-free equilibrium, P^0, is globally-asymptotically stable (GAS). This is done below.

2. Global Stability of the Disease-Free Equilibrium

In order to investigate the global stability of P^0, we note, first of all, that the region

$$T = \left\{(S, I, R, C) \in R_+^4 : S + I + R + C \le 1\right\}$$

which is also positively invariant.

Theorem 1. If $R_0 \le 1$, the disease-free equilibrium P^0 is globally asymptotically stable in T.

Proof. Consider the following Lyapunov function:

$$V = I,$$

with Lyapunov derivative (where a dot represents differentiation with respect to *t*)

$$\begin{aligned} \dot{V} &= \dot{I} \\ &= \left\{\beta\left(S + \sigma C\right) - (\mu + \alpha)\right\} I, \\ &\le \left\{\beta - (\mu + \alpha)\right\} I, \quad \text{for } S + \sigma C \le 1 \\ &= (\mu + \alpha)\left\{\frac{\beta}{(\mu + \alpha)} - 1\right\} I \\ &= (\mu + \alpha)\left(R_0 - 1\right) I \quad \text{for } R_0 < 1. \end{aligned}$$

Since all the model parameters are non-negative, it follows that $\dot{V} < 0$ for $R_0 < 1$ with $\dot{V} = 0$ only if $I = 0$. Hence, V is a Lyapunov function on *T*. Therefore, by the LaSalle's Invariance Principle [12], every solution to the equations of the models (1), with initial conditions in *T*, approaches P^0 as $t \to \infty$.

3. Existence and Stability of Endemic Equilibrium

In the presence of infection ($I \neq 0$), model (1) has a unique endemic equilibrium given by

$P^* = (S^*, I^*, R^*, C^*)$ where

$$S^* = \frac{\mu + \alpha}{\beta} - \left[\frac{\delta\sigma\alpha I^*}{\beta(\mu + \sigma\delta) I^* + (\mu + \gamma)(\mu + \delta)}\right],$$

$$R^* = \frac{\alpha I(\beta I^* + \mu + \gamma)}{\beta(\mu + \sigma\delta) I^* + (\mu + \gamma)(\mu + \delta)},$$

$$C^* = \frac{\delta\alpha I^*}{\beta(\mu + \sigma\delta) I^* + (\mu + \gamma)(\mu + \delta)},$$

and I^* is the root of the equation

$$a(I^*)^2 + bI^* + c = 0 \qquad (2)$$

where $a = \beta^2(\mu + \alpha + \sigma\delta)$,

$b = (\mu + \alpha)(2\mu + \delta + \gamma) + \delta(\mu\sigma + \gamma) - \beta(\mu + \delta\sigma)$,

$c = (\mu + \gamma)(\mu + \delta)(\mu + \alpha)\left(1 - R_0\right)$. It is found that a is positive independently of the parameter values and c is negative if and only if $R_0 > 1$. Given these constraints, the positivity and uniqueness of P^* are guaranteed if and only if $R_0 > 1$.

In order to establish the local stability of P^*, we substitue $R = 1 - S - I - C$ to eliminate *R* from the equations in (1) leads to the following reduced three dimensional model:

$$\begin{aligned} \frac{dS}{dt} &= \mu(1 - S) + \gamma C - \beta SI, \\ \frac{dI}{dt} &= \beta SI + \sigma\beta CI - (\mu + \alpha) I, \\ \frac{dC}{dt} &= \delta(1 - S - I - C) - \beta CI - (\mu + \gamma) C. \end{aligned} \qquad (3)$$

Evaluating the Jacobian of (3) at P^* gives the characteristic polynomial:

$$f(\lambda) = \lambda^3 + a_1\lambda^2 + a_2\lambda + a_3 = 0$$

where $a_1 = 2\mu + \gamma + \delta + 2\beta I^*$,

$$a_2 = \beta I^*(\beta I^* + \alpha + 3\mu + \delta\sigma + \gamma + \delta) + (\mu + \delta)(\mu + \gamma),$$

$$a_3 = \frac{\beta I^*}{G^*}\left[D_1\beta^2\left(I^*\right)^2 + D_2\beta I^* + D_3\delta^2 + D_4\delta + D_5\right]$$

with $D_1 = (\delta\sigma + \mu)(\mu + \alpha + \delta\sigma)$,

$D_2 = 2(\mu + \delta)(\mu + \gamma)(\mu + \alpha + \delta\sigma)$,

$D_3 = ((1 - \sigma)\mu - \sigma + \gamma)\alpha + \gamma^2 + \mu^2 + 2\mu\gamma$,

$D_4 = (\mu + \gamma)(\alpha\gamma + 2\mu\gamma + 2\alpha\mu + 2\mu^2 - \sigma\alpha\mu)$,

$D_5 = \mu(\mu + \gamma)^2(\mu + \alpha)$.

Since $R_0 > 1$, it can be seen that $a_i > 0$, $i = 1, 2, 3$ and $a_1a_2 - a_3 > 0$, using the Routh–Hurwitz criterion [17], that the roots of $f(\lambda)$ have negative real parts. Thus, we have obtained the following result.

Lemma 2. If $R_0 > 1$, then the unique endemic equilibrium P^* is locally asymptotically stable.

A SIMULATION STUDY

To see the dynamical behavior of the model (1), the model (1) is integrated numerically by an unconditionally stable method (DSS1 method) (as developed in [6]) using the set of parameters values tabulated in Table 1 (unless otherwise stated) with the initial conditions $S(0) = 0.15$, $I(0) = 10^{-3}$, $C(0) = 0.44$, $R(0) = 1 - S(0) - I(0) - C(0)$, to illustrate the effect of cross-immunity on influenza transmission dynamics by varying the value of the cross-immunity parameter (σ). For instance, it is shown that when infection confers

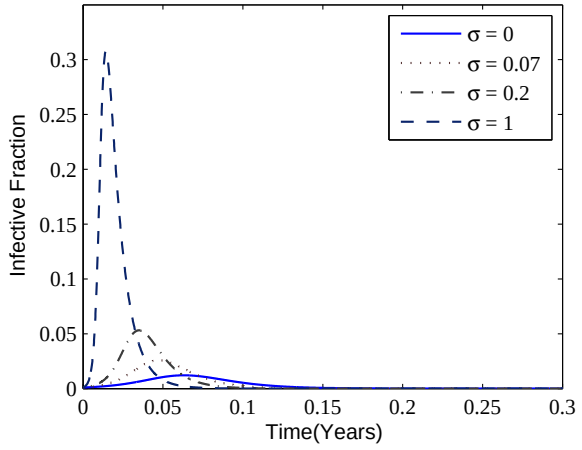

Fig. 2: Time series of infective fraction with $\beta = 1200$.

partial cross-immunity, the fraction of infective increases with increasing value of σ compared to the case in which complete cross-immunity (σ = 1) is offered (see Fig. 2).

The Effects of Seasonality

In this section, simulations are carried out to investigate the effect of seasonal variation in population on the transmission dynamics of Influenza. Such variation arise due to a number of factors such aspathogen appearance and disappearance via regular annual migration [14], variations in host susceptibility caused by physiological processes [8] and environmental changes [22].

As traditionally done for the study of childhood diseases since the early 70s [21,28], the seasonality can be introduced into the SIRC model by assuming that virus transmissibility varies periodically through time, with a yearly cycle. Thus, we can model the contact rate in the simplest form as a sinusoidal function of t [3], i.e.,

$$\beta(t) = \beta_0(1 + \varepsilon \cos 2\pi t)$$

where the two parameters β_0 and $0 \le \varepsilon \le 1$ represent the rate of transmission and the degree of seasonality, respectively. By substituting $\beta(t)$ into model (1) we obtain a periodically forced non-linear system

$$\begin{aligned}
\frac{dS}{dt} &= \mu(1-S) - \beta(t)SI + \gamma C \\
\frac{dI}{dt} &= \beta(t)SI + \sigma\beta(t)SI - (\mu+\alpha)I \\
\frac{dR}{dt} &= (1-\sigma)\beta(t)CI + \alpha I - (\mu+\delta)R \\
\frac{dC}{dt} &= \delta R - \beta(t)CI - (\mu+\delta)C
\end{aligned} \tag{4}$$

The behavior of system (4) is too complex to be investigated analytically. Since empirical estimates of are hard to be found in general [16] and particularly for influenza (see the caveat in [11]), it is important to understand how the behavior of the SIRC model changes under wide variations of the values attributed to the parameters ε and β_0 that fully describe the contact rate. The aim of these simulation is to investigate the effect of the degree of seasonality and cross-immunity in the presence of seasonal variation.

In this paper, the dynamic of model (4) will present in the numerical simulations with $\beta = 1200$ for different values of ε; $\varepsilon = 0.005$, $\varepsilon = 0.07$ and $\varepsilon = 0.3$. For all parameter values chosen in Table 1, the model is run for 250 years and show the results for the last 10 years (Fig. 3(a)–(b)) and 20 years (Fig. 3(c)). As ε increases, the solution passes from a period-one-year cycle (Fig. 3(a)) to a two-year cycle (Fig. 3(b)) and to chaotic behaviour (Fig. 3(c)). To compare the numerical solution of model (4) with the data in Tropical regimes such as Thailand and Singapore.

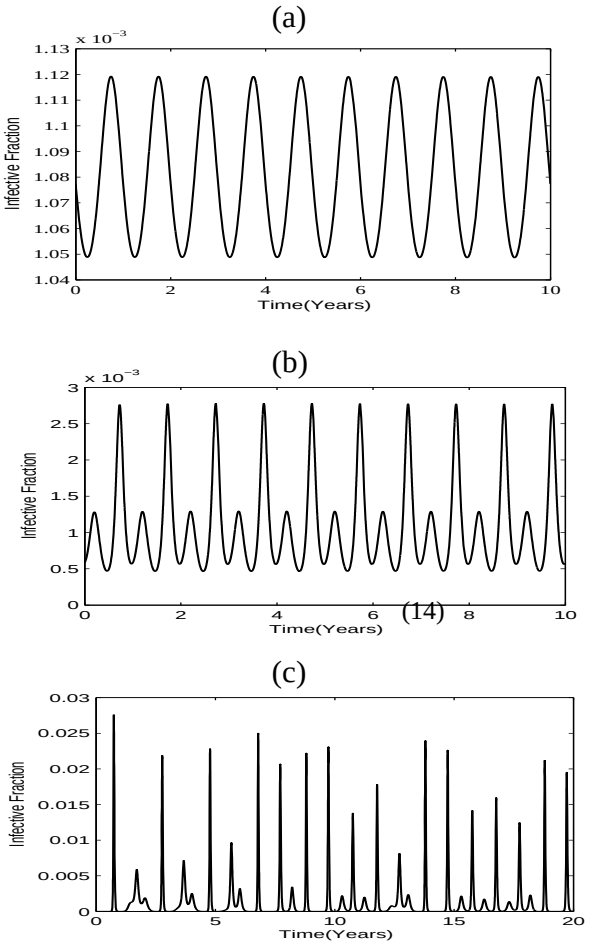

Fig. 3: Time series of infective fraction with $\beta = 1200$; (a) $\varepsilon = 0.005$, (b) $\varepsilon = 0.07$ and (c) $\varepsilon = 0.3$.

Fig. 3(b) shows a biannual epidemic cycle caused by the dominant strain with two peaks of activity which is a very general pattern for influenza in the Tropical regimes (see data in [3,13]). The exact timing of the two peaks and the difference in their amplitudes can vary from place to place. In Thailand, for example, the outbreaks can occur during spring and autumn months [26], while in Singapore [5,13] they occur in the summer and winter seasons.

CONCLUSIONS

The SIRC model is used to monitor the transmission dynamics of influenza. This model was extended to incorporate the seasonal forcing in transmission rate. The models were rigorously analysed to gain insight into their dynamical features. The study shows the following:

(i) the SIRC model considered in this study has a globally-stable disease-free equilibrium if a certain threshold quantity, known as the reproductive number, is less than unity; indicating that the number of infective in the community will be brought to zero if public health measures that make (and keep) the threshold to a value less than unity are carried out;

(ii) For the extended model by adding seasonal forcing in transmission rate, The effect of seasonality leads to periodic and chaotic dynamics of epidemics as the degree of seasonality, ε, increases.

(iii) The SIRC model with seasonal forcing can be used to predict the outbreaks of influenza in Tropical regimes such as Thailand and Singapore.

REFERENCES

1. Anderson, R. M. and R. M. May, 1991. Infectious diseases of humans: dynamics and control. New York: Oxford University Press.
2. Andreasen, V., J. Lin and S. Levin, 1997. The dynamics of cocirculating influenza strains conferring partial cross-immunity, J. Math. Biol., 35: 825-842.
3. Casagrandi, R., L. Bolzoni, S.A. Levin and V. Andreasen, 2006. The SIRC model and influenza A, Math. Biosci. 200 :152-169.
4. Centers for Disease Control and Prevention, 2000. Prevention and control of influenza from the Advisory Committee on immunization practices, Morbidity and Mortality Weekly Report, 1–38.
5. Chew, F., S. Doraisingham, A. Ling, G. Kumarasinghe and B. Lee, 1998. Seasonal trends of viral respiratory tract infections in the tropics, Epidemiol. Infect. 121(1):121-128.
6. Chinviriyasit, W., 2007. Numerical Modeling of the Transmission Dynamics of Influenza", Proceedings of the First International Symposium on Optimization and Systems Biology (OSB'07), August 8–10, , Beijing, China.
7. Davies, J., E. Grilli and A. Smith, 1984. Influenza A: infection and reinfection, J. Hyg., (Cambridge) 92: 125-127.
8. Dowell, S.F., 2001. Seasonal variation in host susceptibility and cycles of certain infectious diseases, Emerg. Infect. Diseases 7:369-374.
9. Earn, D., J. Dushoff and S. Levin, 2002. Ecology and evolution of the flu, Trends Ecol. Evol., 17:334-340.
10. Gill, P. and A. Murphy, 1977. Naturally acquired immunity to influenza type A: a further prospective study, Med. J. Austr., 2:761-765.
11. Gog, J.R., G.F. Rimmelzwaan, A.D.M.E. Osterhaus and B.T. Grenfell, 2003. Population dynamics of rapid fixation in cytotoxic T lymphocyte escape mutants of influenza A, Proc. Nat. Acad. Sci. USA, 100:11143-11147.
12. Hale, J.K., 1969. Ordinary Differential Equations, John Wiley and Sons, New York.
13. Hampson, A., 1999. Epidemiological data on influenza in Asian countries, Vaccine 17:S19-S23.
14. Hope-Simpson, R. and D., 1987, Golubev, A new concept of the epidemic process of influenza A virus, Epidemiol. Infect. 99(1):5-54.
15. Inaba, H., 2001. Kermack and McKendrick revisited: the variable susceptibility model for infectious diseases, Jpn. J. Indust. Appl. Math. 18:273-292.
16. Kermack, W.O. and A.G. McKendrick, 1991. Contributions to the mathematical theory of epidemics: II. The problem of endemicity, Proc. Roy. Soc. Lond. A 138:155, Reprinted in Bull. Math. Biol. 53:57–87.
17. Lambert, J. D.,1991. Numerical Methods for Ordinary Differential Systems: The Initial Value Problem, Wiley, Chichester, England .
18. Larson, H., D. Tyrrell, C. Bowker, C. Potter and G. Schild, 1978. Immunity to challenge in volunteers vaccinated with an inactivated current or earlier strain of influenza A(H3N2), J. Hyg., (Cambridge) 80: 243-248.
19. Levine, A., 1992. Viruses, W.H. Freeman & Co, New York, USA.
20. Lin, J. , V. Andreasen and S. Levin, 1999. Dynamics of influenza A drift: the linear three-strain model, Math. Biosci., 162:33-51.
21. London, W. and J. Yorke, 1973. Recurrent outbreaks of measles, chickenpox and mumps. I. Seasonal variation in contact rate, Am. J. Epidemiol. 98(6):458-468.

A Numerical Solution for Optimal Control Problems based on Scatter Search

Omid Solaymani Fard and Hassan Kadkhodaie Khalfi
School of Mathematics and Computer Science, Damghan University of Basic Sciences
Damghan, Iran

Abstract: In this paper we apply one of approaches in category of heuristic methods as Scatter Search for obtaining approximate solution of optimal control problems. First, we convert optimal control problem to a quasi Assignment Problem by defining some usual characters as defined in Scatter Search applications. Then we obtain approximate optimal control function as an piecewise constant function. Finally the numerical examples are given.

Key words: Optimal control, Integer programming, Scatter search, Discrete approximation, Linear programming

INTRODUCTION

In early decade Optimal Control Problem (OCP) as one of the most application issues has been taken into consideration. The analytical solution for OCP's are not always available. Thus, to find an approximate solution is the most logical way to solve the problems. Various approaches as, discretization, shooting method [2,3] , using concepts in measure theory [6], using Chebyshev polynomials [1], etc., have been proposed to obtain approximate solutions of OCP's. Some heuristic algorithm and their extensions are applied in topic of control problems. our aim is to apply Scatter Search to construct approximate optimal control function for OCP's. Scatter Search is a stochastic search technique inspired by the principles of natural selection and natural genetics which have revealed a number of characteristics particulary useful for application in optimization, engineering, computer science, among other fields. In this work, in order to apply Scatter Search to get an approximate solution for an OCP, we first convert The OCP to a quasi Assignment Problem (QASP) by a suitable linearizing. Then, we apply Scatter Search for the quasi assignment problem and we get an approximate solution as an piecewise constant function. Hence, the approximate solution obtained is a precise solution for the OCP.

STATEMENT OF THE OPTIMAL CONTROL PROBLEM

Consider a classical OCP as follows:

$$Minimize\ I(x(t),u(t)) = \int_0^{t_f} f_0(t,x(t),u(t))dt \qquad (1)$$

subject to:

$$\dot{x}(t) = g(t,x(t),u(t)) \qquad (2)$$

$$x(0) = x_0,\ x(t_f) = x_f. \qquad (3)$$

where t_f is known and $|u| \le K$. Our main aim is trajectory planning i.e. it is to find a control function $u(.)$ such that the corresponding state $x(.)$ satisfying (2)-(3) and minimize (1). In order to do this work, first, we discretize the interval $[0,t_f]$ to N subinterval $[t_{i-1},t_i]$, $i=1,2,...,N$. Since we tend to detect an approximate optimal control for problem (1)-(2), we focus on finding an optimal piecewise control function $u(.)$ for the problem. Corresponding each interval $[t_{i-1},t_i]$, $i=1,2,...,N$, we partition the interval $[-K,K]$ to m equal subinterval $[u_{j-1},u_j]$, $j=1,2,...,m$ where $u_0 = -K$ and $u_m = K$. Of course we need to find $m+1$ constants $u_0,u_1,...,u_m$. Thus we consider the space of time and control piecewise constant segments as it is shown in Fig 1.

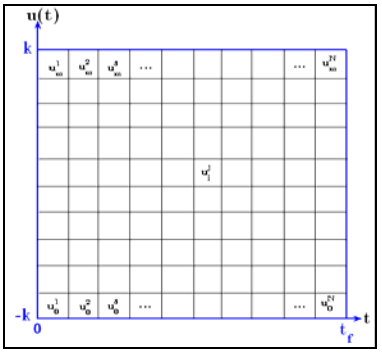

Figure 1.

Corresponding Author: Omid Solaymani Fard, School of Mathematics and Computer Science, Damghan University of Basic Science, Damghan, Iran

One of approach for finding the best selection among of all constants in each interval of $[t_{i-1}, t_i]$, $i = 1, 2, ..., N$, and finally to find the best approximate control is enumerate of all cases. But we will deal with an extreme hard computational complexity. Because we must check N^m piecewise constant functions.

Our aim is to use of Scatter Search approach for detecting the best approximate piecewise constant control function.

If $u(t) = \sum_{k=1}^{N} u_k \xi_{[t_{k-1}, t_k]}(t)$ be a piecewise constant function then by a numerical method as Euler method or Rung-Kutta, we can find trajectory corresponding $u(t)$ from (2) with initial condition $x(0) = x_0$. Thus, if (x, u) be a pair of the trajectory and the control which satisfy in (2) with initial condition $x(0) = x_0$ and for given a small number $\varepsilon > 0$, $\|x(t_f) - x(t_f)\| < \varepsilon$, then we can claim that, we have been found a good approximate pair for minimizing functional I in (1).

CONVERTING OCP TO QASP

To convert the OCP to QASP, we use a similar framework of solving QAP (Quadratic Assignment Problem) by ACO (Ant colony Optimization). In fact, we decide to assign a constant $u_k \in \{u_0, u_1, ..., u_m\}$ for every interval $[t_{i-1}, t_i]$, $i = 1, 2, ..., N$. These constants are selected by a Scatter Search programm written in Matlab. The process will be continued until the objective function gets its optimal value. In other word, after discretion of the OCP, the problem is converted to a QASP with an extra objective function, i.e. we add the term $\|x(t_f) - x(t_f)\|$ to the original objective function and then, we apply Scatter Search for this new criteria function.

Therefore, by applying the method above, the problem (1)-(2) with conditions (3) is converted to:

$$\text{Minimize} \quad I(x(t), u(t)) = \sum_{i=0}^{N} f_0(t_i, x(t_i), u(t_i)) + M \|x(t_f) - x(t_f)\| \tag{4}$$

Subject to:

$$x(t_{i+1}) = x(t_i) + g(t_i, x(t_i), u(t_i)), \; i = 0, 1, ..., N-1, \tag{5}$$

$$x(0) = x_0. \tag{6}$$

where, M is a very large positive number (like as BIG-M Method). To obtain a numerical solution for the problem (4)-(5) with initial condition (6) via Scatter Search, we focus just on the space time and control. Because, we use of equation (5) in definition of the objective function for Scatter Search. Now, we are ready to state the numerical algorithm to get the optimal control.

NUMERICAL EXAMPLES

In this section we propose our method to obtain approximate solutions of some OCP. Before proposing of examples we define an error function as $e(t_f) = x(t_f) - x_f$ on $[0, t_f]$, where x_f and $x(t_f)$ are the exact and the approximate solution obtained from using of Scatter Search for the example,respectively.
In all examples, we set $t_f = 1, M = 10^6, K = 1$, and we divide the closed interval $[0, t_f] = [0,1]$ into 16 partitions, i.e. the step size $\Delta t = 0.0625$. Also, we use Euler method to solve the condition corresponding to the differential equation of the problem.

Example 1: Consider the following OCP:

$$\text{Minimize} \qquad I = \int_0^1 u^2(t)dt$$

subject to:

$$\dot{x}(t) = x^2(t) + u(t)$$

$$x(0) = 0, \; x(t_f) = 0.5.$$

After solving the problem by the proposed method, we obtain the following results:

The final value $x(1) = 0.500054$, the optimal value $I^* = 0.4447$ and the error function $e(1) = 5.43 \times 10^{-5}$. The trajectory and control functions are shown in fig 2 and 3, respectively.

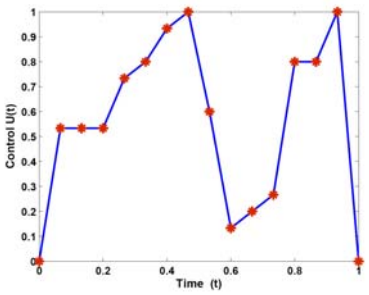

Figure 2.

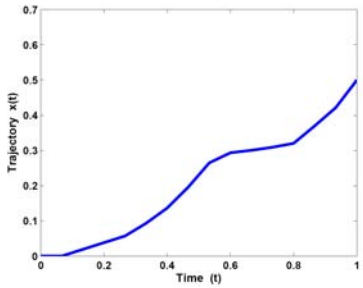

Figure 3.

Example 2: Consider the following OCP:

$$\textit{Minimize} \qquad I = \int_0^1 u^2(t)dt$$

subject to:

$$\dot{x}(t) = \frac{1}{2}x^2(t)\sin(x(t)) + u(t)$$

$$x(0) = 0, \;\; x(t_f) = 0.5.$$

After solving the problem by the proposed method, we obtain the following results:

The final value $x(1) = 0.500040$, the optimal value $I^* = 0.3526$ and the error function $e(1) = 4.095 \times 10^{-5}$. The trajectory and control functions are shown in fig 4 and 5, respectively.

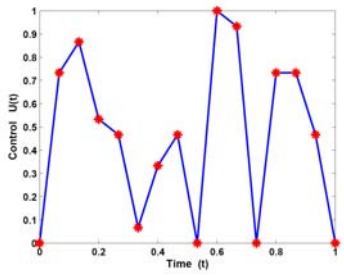

Figure 4.

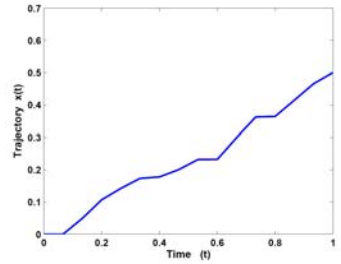

Figure 5.

REFERENCES

1. J. Vlassenbroeck, 1988. A chebyshev polynomial method for optimal control with bounded state constraints. Automatica. 24: 499-506.
2. H. Maurer and W. Gillessen, 1975. Application of multiple shooting to the numerical solution of optimal control with bounded state variables. Computing. 15: 105-126
3. G. Fraser Andrews, 1996. Shooting method for the numerical solution of optimal control problems with bounded state variable. Optimization Theory and Applications. 89: 351-372.
4. K. L. Teo, C. J. Goh, and K. H. Wong, 1991. A unified computational approach to optimal control problems. Longman Scientific and Technical.
5. L. C. Young, 1969. Calculus of Variation and Optimal Control Theory, Philadelphia: W.B. Saunders.
6. J. E. Rubio, 1986. Control and Optimization, The Linear Treatment of Nonlinear Problems., Manchester University Press, England.

Relation between the Space with Reproducing Kernels and Rodrigues' Formula

Hnin Yu Mar
Yangon Technological University, Myanmar
nninyumarsein@gmail.com.

Abstract: In this paper one studies the analysis on Hilbert space with reproducing Kernel arising from multiple Wiener integral which is given by using reproducing kernel Hilbest space theory. Stationary process and a transformation τ are introduced. The explicit correspondence is established between the Hilbert space L_2 and a unitary transformation $\mathcal{F}$. A group G(P) associated with a stationary process P which is introduced. The Hilbert space $\mathcal{F}$ arising from Poisson white noise which is discussed. It is the fundamental example of stationary processes. The collection G(P) includes not only shift transformations but also some other transformatios depending on the form of the characteristic functional.

Keywords: Hilbert Space, transformation, probability measure, measure space, characteristic functional.

1. INTRODUCTION

The multiple Wiener integral with respect to an additive process with stationary independent increments plays a fundamental role in the study of the flow derived from that additive process. The stationary processes whose sample functions are elements in E^* which is the dual of some nuclear pre-Hilbert function space E. For such processes, a definition of stationary process is introduced. It is a triple P = (E*, μ, $\{T_t\}$) , where μ is a probability measure on E^* and $\{T_t\}$ is a flow on the measure space (E^*,// u) derived from shift transformations whmch shift the arguments of the functioNs of E.

In ordEr tO fac litate the diScussion of the @ilbert space $L_2 = L_{\mathbb{}}$ (E^*, μ) , A transformation τ Is defindd by the Follow)ng fo2mula:

$$(\tau\varphi)(\xi) = \int_{E^*} e^{i<x,\xi>}\,\varphi(x)\,\mu(dx) \quad \text{for } \varphi \in L_2, \qquad (1.1)$$

where < . , . > deNotes the bilinEaR form of and $\xi \in E$. This transformation τ from L_2 to the space of functional on E is analogous to the ordinary Fourier transform, By formula (1.1) and a requirement that τ should be a unitary transformation,

$\mathcal{F} \equiv \tau(L_2(E^*, \mu))$ has to be a Hi,bert space with reproducing kernel $C(\xi - \eta)$, $(\xi, \eta) \in E \times E$, where C is the characteristic functional of the measure μ defined by

$$C(\xi) = \int_{E^*} e^{i(x,\xi)}\,\mu(dx), \qquad (1.2)$$

$\xi \in E$.

One study the explicit correspondence between L_2 and $\mathcal{F}$.

Another concept is a group G(P) associated with a stationary process P. Consider the set of all linear transformations $\{g\}$ on E satisfying the conditions that

(i) $C(g\xi) = C(\xi)$ for every $\xi \in E$, and (1.3)

Corresponding Author : Hnin Yu Mar, Yangon Technological University, Myanmar, nninyumarsein@gmail.com.

(ii) that g be a homeomorphism on E.

Obviously the collection G(P) of all such g's forms a group with respect to the operation $(g_1 g_2)\ \xi = g_1\ (g_2\ \xi)$. The collection **G(P)** includes not only shift transformations S_h, h real, defined by

$$(S_h\ \xi)\ (t) = \xi\ (t - h), \qquad (1.4)$$

but also some other transformations depending on the form of the characteristic functional.

An interesting subclass of stationary processes is the class of processes with independent values at every point. In these cases the independence at every point can be illustrated rather clearly in the space $\mathcal{F}$ by using a direct product decomposition. Furthermore, because of the particular form of the characteristic functional, one can get an infinite direct sum decomposition of $\mathcal{F}$:

$$\mathcal{F} = \sum_{n=0}^{\infty} \oplus\ \mathcal{F}_n. \qquad (1.5)$$

Each $\mathcal{F}_n$ appearing in the last expression is invariant under every V_g, g ∈ G(P) defined by

$$(V_g\ f)(\ \xi) = f(g\xi), \qquad f\ \in \mathcal{F}, \qquad (1.6)$$

that is, $V_g(\mathcal{F}_n)\ \subset \mathcal{F}_n$ for every $g\ \in$ G(P). With the aid of these two different kinds of decompositions, $\mathcal{F}$ is investigated.

2. PRELMINARIES

Before defining the term stationary process let us first introduce some notation. Let E be a real nuclear pre-Hilbert space. Denote the inner product by $< . , . >$; it determines the norm $\| . \|$. Let H be the completion of E in the norm $\| . \|$ and E^* be the dual of E. Then by the usual identification $H^* = H$ for Hilbert spaces, the following relation $E \subset H \subset E^*$.

Let $\mathcal{B} = \mathcal{B}(E^*)$ be the σ-algebra generated by all cylinder sets in E^*. If $C(\xi)$, $\xi \in E$, is a continuous positive definite functional with $C(0) = 1$, then there exists a unique probability measure μ on the measurable space $(E^*, \mathcal{B})$ such that

$$C(\xi) = \int_{E^*} \exp\ [i < x, \xi >]\ \mu\ (dx), \qquad \xi \in E \qquad (2.1)$$

Where E is a subset of R^T, R is the field of real numbers and T is the additive group of real numbers or one of its subgroups. Every element of E has a coordinate representation

$\xi = (\xi(t), t \in T)$. For every h, the point transformation S_h is defined by (1.4). Assume that E is invariant under all of the concerning with the S_h's. For each S_t, a transformation T_t is defined on E^* as follows:

$T_t : T_t\ x \in E^*,\ t \in T$ with $< T_t\ x, \xi> = <x,\ S_t\ \xi>$ for every ξ.

Obviously $\{T_t: t \in T\}$ forms a group satisfying

$$T_t\ T_s = T_s\ T_t = T_{t+s}, \quad s, t \in T,$$

$$T_0 = I \text{ (identity)}$$

The group $\{T_t\ ,\ t\ \in T\}$ can be considered as a transformation group acting on E^*.

Let $\mathcal{B}(T)$ be the topological Borel field of T.

Definition 2.1

The transformation group $\{T_t, t \in T\}$ is called a group of shift transformations if

$T_t\ x = f\ (x,t)$ is measurable with respect to $\mathcal{B} \times \mathcal{B}(T)$. The triple $P = (E^*, \mu, \{T_t\})$ is called a stationary process if μ is invariant under shift transformation T_t, $t \in T$.

Definition 2.2

The functional $C(\xi)$, $\xi \in E$, defined by (2.1) for a stationary process

P = $(E^*, \mu, \{T_t\})$, is called the characteristic functional of P.

For the measure space, $(E^*, \mathcal{B}, \mu)$, associated with a stationary process. Which the Hilbert space $L_2 = L_2(E^*, \mu)$ of all square summable complex-valued functions which can be formed with the inner product

$$\left\langle\left\langle \varphi, \psi \right\rangle\right\rangle = \int_{E^*} \varphi(x)\overline{\psi(x)}\, \mu(dx), \qquad \varphi, \psi \in L_2. \qquad (2.2)$$

Lemma 2.1

The closed linear subspace of L_2 spanned by $\{e^{i(x,\xi)}, \xi \in E\}$ coincides with the whole space L_2.

Lemma 2.2

For any stationary process P = (E^*, μ, $\{T_t\}$) there always exists a smallest Hilbert space $\mathcal{F} = \mathcal{F}(E, C)$ of functionals on E with reproducing kernel C (ξ - η), (ξ, η) ∈ $E \times E$, where C (ξ), ξ ∈ E, is the characteristic functional of P.

Let denote the inner product in $\mathcal{F}$ by (., .). Some of the properties of $\mathcal{F}$ is obtained.

(i) for any fixed ξ ∈ E, $C(. - \xi) \in \mathcal{F}$;

(ii) $(f(.), C(. - \xi)) = f(\xi)$ for any $f \in \mathcal{F}$;

(iii) F is spanned by $\{C(. - \xi), \xi \in E\}$.

From these properties and lemma 2.1, the following theorem can be proved.

Lemma 2.3

For any stationary process P = $(E^*, \mu. \{T_t\})$ there always exists a smallest Hilbert space of $\mathcal{F} = \mathcal{F}$ (E, C) of functionals on E with reproducing kernel C (ξ - η), (ξ , η) ∈ E × E, where C(ξ), $\xi \in E$, is the characteristic functional of P.

Theorem 2.1

The transformation τ defined by

$$\int_{E^*} \varphi(x) e^{i<x,\xi>}\, \mu(dx) \qquad (2.2)$$

is a unitary operator from L_2 onto $\mathcal{F}$.

In fact, the relation

$$\tau\left(\sum_{j=1}^{n} a_j e^{-i<x,\xi_j>}\right)(\cdot) = \sum_{j=1}^{n} a_j C(\cdot - \xi_j) \qquad (2.3)$$

shows that τ preserves norm since this relation can be extended to the entire space.

3. ORTHOGONAL POLYNOMIALS AND REPRODUCING KERNELS

One considers the decomposition of $L_2(E^*, u)$ and $\mathcal{F}(E, C)$ associated with a stationary process with independent values at every point. First one considers, the simple case where E is a finite dimensional space. One can find a relation between the space with reproducing kernel and Rodrigues' formula for a classical orthogonal polynomials. Such considerations will aid us in considering the case where E is an infinite dimensional nuclear space.

Let v be a probability measure (distribution) on R^1 and $\tilde{C}$ be its Fourier-Stieltijes transform (characteristic function); that is,

$$\tilde{C}(\lambda) = \int_{R^1} e^{i\lambda x}\, v(dx), \qquad \lambda \in R^1 \qquad (3.1)$$

Appealing to Aronszajn's results (1) stated in Lemma 2.2

One obtains the smallest Hilbert space $\tilde{\mathcal{F}} = \tilde{\mathcal{F}}(R^1, \tilde{C})$, the reproducing kernel of this space is $\tilde{C}(\lambda - \mu)$, $\lambda, \mu \in R^1$. By theorem 2.1, there exists an isomorphism $\tilde{\tau}$ which maps

$\tilde{L}_2 = L_2(v; R^1) = \{ f; \int_{R^1} | \int f(x) |^2 \, v(dx) \}$ onto $\tilde{F}$ in the following way:

$$(\tilde{\tau} f)(\lambda) = \int_{R^1} e^{i\lambda x} f(x) v(dx). \qquad (3.2)$$

One discusses the analysis on $\tilde{F}$ rather than on $\tilde{L}_2$, since, for one thing, the development of functions belonging to $\tilde{L}_2$ in terms of orthogonal polynomials turns out to be the power series expansion in $\tilde{F}$.

3.1 Gaussian Distribution.

Consider the case where

$$v(dx) = v(x; \sigma^2)\, dx = (2\pi\sigma^2)^{-1/2} \exp\left\{ -\frac{x^2}{2\sigma^2} \right\} dx, \qquad (3.3)$$

then

$$\tilde{C}(\lambda, \sigma^2) = \int_{R^1} e^{i\lambda x} v(x; \sigma^2)\, dx = \exp\left(-\frac{\sigma^2}{2} \lambda^2 \right). \qquad (3.4)$$

Choose Hermite polynomials

$$H_n(x; \sigma^2) = \frac{(-1)^n \sigma^{2n}}{n!} \frac{1}{v(x; \sigma^2)} \frac{d^n}{dx^n} v(x; \sigma^2), \quad n = 1, 2, \ldots \qquad (3.5)$$

(Rodrigues' formula), which form a complete orthonormal system in $\tilde{L}_2$. The isomorphism $\tilde{\tau}$ maps $H_n(x)$ to the n-th degree monomial of λ times $\tilde{C}$. In fact, we have

Proposition 1.1

$$(\tilde{\tau} H_n(\,.; \sigma^2))(\lambda) = \sigma_n \lambda^n \tilde{C}(\lambda : \sigma^2), \sigma_n = \frac{\sigma^{2n} i^n}{n!}. \qquad (3.6)$$

Proof

$$(\tilde{\tau} H_n(.; \sigma^2))(\lambda) \qquad (3.7)$$

$$= \frac{(-1)^n \sigma^{2n}}{n!} \int_{R^1} \exp(i\lambda x) \left\{ v(x; \sigma^2)^{-1} \frac{d^n}{dx^n} v(x; \sigma^2) \right\} v(x; \sigma^2) dx$$

$$= \frac{(-1)^n \sigma^{2n}}{n!} \int_{R^1} \{ \exp(i\lambda x) \left\{ \frac{d^n}{dx^n} v(x; \sigma^2) \right\} dx$$

$$= \frac{\sigma^{2n}}{n!} i^n \lambda^n \tilde{C}(\lambda; \sigma^2).$$

More generally, we have

$$\left\{ \tilde{\tau} \left(\sum_{n=0}^{\infty} a_n H_n(.; \sigma^2) \right) \right\} (\lambda) = \left(\sum_{n=0}^{\infty} a_n \sigma_n \lambda^n \right) \tilde{C}(\lambda : \sigma^2). \qquad (3.8)$$

3.2 Poisson Distribution.

Let $v(dx)$ be given by

$$v(dx) = v(x, c)\, \delta_{S_c}(dx) = \frac{e^{x+c}}{P(x+c+1)} e^{-c}, \quad x \in S_c, \qquad (3.9)$$

where, $S_c = \{ -c, 1-c, 2-c, \ldots.. \}$. One obtains orthogonal polynomials with respect to the measure $v(x, c)\, \delta s_c (dx)$, which are called generalized Charlier polynomials, by the following generalized Rodrigues' formula.

$$p_n(x, c) = (-c)^n (v(x, c))^{-1} \Delta_x^{"} v(x - n, c) = L_n^{s+c-n}(c) n!, \quad x \in S_c, \qquad (3.10)$$

where $\Delta_x^{"}$ denotes the n-th order difference operator acting on functions of x.

The relation

$$\tilde{C}(\lambda : c) = \int_{R^1} e^{i\lambda x} v(x; c) \delta_{S_c}(dx) = \sum_{x \in S_c} e^{i\lambda x} v(x, c)$$

$$= \exp \{ e^{i\lambda x} - 1 - i\lambda c \}$$

is easily obtained. Now put

$$Q_n(x,c)=\frac{1}{n!c^n}P_n(x,c); \qquad (3.12)$$

then one gets the orthogonality relation for Q_n:

$$\sum_{x\in Sc} Q_n(x,c)Q_m(x,c)v(x,c)=\delta_{n,m}, \quad n,m=1,2,..... \qquad (3.13)$$

Every $P_{n,}$ of course, belongs to L^2 (v, R^1), and it is transformed by $\tilde{\tau}$ into $(\tilde{\tau}\, P_n(\,.\,,\,c\,))\,(\lambda)$.

Then we have

Proposition 3.2

$$(\tilde{\tau}\, P_n(.,c))\,(\lambda)=c^n(e^{i\lambda}-1)^n\tilde{C}(\lambda:c). \quad (3.14)$$

Proof

$$(\tilde{\tau}\, P_n(\,.\,,\,c\,))\,(\lambda)=\int_{R^1} e^{\,i\lambda x}\,(-c)^n\,(v(x,c))^{-1}\,\Delta_x^n\,(v(x-n,c))v(x,c)\,\delta_{S_C}\,(dx)$$

$$=(-c)^n\,(-1)^n\sum_{x\in S_C}(\Delta_x^n\,e^{\,i\lambda x})v(x,c)$$

$$=c^n\sum_{x\in S}\sum_{m=0}^{n}(-)^{n-m}\binom{n}{m}e^{im\lambda}e^{ix\lambda}v(x,c)$$

$$=\ c^n\,(e^{\,i\,\lambda}-1)^{\,n}\ \tilde{C}\,(\lambda:c). \qquad (3.15)$$

Note that the last expression is of the monomial form of $(e^{i\,\lambda}-1)$ times $\tilde{C}$.

4. STATIONARY PROCESS WITH INDEPENDENT VALUES AT EVERY POINT

One studies the general theory for a certain class of stationary processes with independent values at every point.

Let P = $(E^*, \mu, \{T_t\})$ be a stationary process, where T is a set of real numbers and E is the function space $\mathcal{S}$. Let its characteristic function be given by

$$C(\xi) = \exp\int_{-\infty}^{\infty}\alpha(\xi(t))dt,$$

$\alpha(x) = (-\sigma^2x^2)/2 +$

$$\int_{-\infty}^{\infty}\left(e^{ixu}-1-\frac{ixu}{1+u^2}\right)\frac{1+u^2}{u^2}d\beta(u). \quad (4.1)$$

Here $0 \le \sigma^2 < \infty$ and $d\beta(u)$ is a bounded measure on $(-\infty, \infty)$ such that $d\beta(\{0\}) = 0$. Here P satisfies $C(\xi_1 + \xi_2) = C(\xi_1)\,C(\xi_2)$, whenever supp $(\xi_1) \cap$ supp $(\xi_2) = \phi$, that is, it is a stationary process with independent values at every point.

For the moment one studies from the flow $\{U_t,\ t$ real$\}$ to the direct sum decomposition of $\mathcal{F} = \mathcal{F}(\mathcal{S},\ C)$.

Define

$$K_0(\xi,\eta) = \exp\left(\int \alpha(\xi(t)\,dt)\exp\left(\int \alpha(-\eta(t)\,dt\right)\right.$$

$$= C(\xi)C(-\eta).$$

$$K_1(\xi,\eta) = \left(\int \alpha(\xi(t)-\eta(t))\,dt - \int \alpha(\xi(t)dt\right.$$

$$-.\int \alpha(-\eta(t))\,dt, \qquad (4.2)$$

$$K_p(\xi,\eta) = \frac{1}{p!}\,(K_1(\xi,\eta))^p,$$

$$p \ge 2,$$

$$k_p(\xi,\eta) = \frac{1}{p!}K_0(\xi,\eta),\,(K_1(\xi,\eta))^p, \qquad p \ge 0,$$

$\xi,\eta \in \mathcal{S}$.

Note that $C(\xi - \eta) = \sum_{p=0}^{\infty} k_p(\xi,\eta)$. By using the fact that $\alpha(x - y)$ is conditionally positive definite. One can prove the following lemma.

Lemma 4.1

The functionals $K_0(\xi,\eta)$, $K_p(\xi,\eta)$, and $k_p(\xi,\eta)$, p = 0,1, …., $(\xi,\eta) \in \mathcal{S} \times \mathcal{S}$, are all positive definite and continuous.

One obtains the Hibert spaces $\mathcal{F}$. $\tilde{\mathcal{F}}_p$ and $\mathcal{F}_p$, p = 0,1,2, …. with reproducing kernels C, K_p, and k_p respectively. Consider subspaces $\tilde{\mathcal{F}}_p$ and $\mathcal{F}_p$. One uses the symbol $\otimes^*$ to express the direct product of subspaces in the sense of Aronszjn [1]. Hereafter one uses subscripts to distinguish the various norms.

Lemma 4.2

The space $\tilde{\mathcal{F}}_p$ is the class of all restrictions of functionals belonging to

$$\tilde{\mathcal{F}}_1 \otimes^* \tilde{\mathcal{F}}_1 \otimes^* \cdots \otimes^* \tilde{\mathcal{F}}_1 \text{ (p times)}$$

to the diagonal set $\tilde{S}_p = \{(\xi, \ldots, \xi);\ \xi \in \mathcal{S}\}$. The norm $\|\cdot\|_{\tilde{\mathcal{F}}_p}$ in $\tilde{\mathcal{F}}_p$ can be expressed in the form

$$\|f\|_{\tilde{\mathcal{F}}_p} = \inf_{\substack{f' \in \tilde{\mathcal{F}}_1 \otimes^* \cdots \otimes^* \tilde{\mathcal{F}}_1 \\ f = f'/\tilde{S}_p}} \|f'\|_{\tilde{\mathcal{F}}_1} * \ldots \otimes^* \tilde{\mathcal{F}}_1 \quad (4.3)$$

where $f'/\tilde{S}_p$ denotes the restriction of f' to $\tilde{S}_p$

Lemma 4.3

The space $\mathcal{F}_p$ is the class of all restrictions of functionals belonging to $\tilde{\mathcal{F}}_p \otimes^* \tilde{\mathcal{F}}_p$ to the diagonal set $\tilde{S}_2 = \{(\xi, \xi);\ \xi \in \mathcal{S}\}$. The norm $\|\cdot\|_{\mathcal{F}_p}$ can be expressed in the form

$$\|f\|_{\mathcal{F}_p} = \inf_{\substack{f' \in \tilde{\mathcal{F}}_0 \otimes^* \\ \tilde{\mathcal{F}}f = f'/\tilde{S}_2}} \|f'\|_{\tilde{\mathcal{F}}_0 \otimes^* \tilde{\mathcal{F}}_p} \quad (4.4)$$

Lemma 4.4

The space $\mathcal{F}_p$, p = 1,2, …., are mutually orthogonal subspaces of $\mathcal{F}$.

Proof.

Put

$$K_{p.q}(\xi,\eta) = K_p(\xi,\eta) + K_q(\xi,\eta),\ p \neq q. \quad (4.5)$$

Then the Hilbert space $\tilde{\mathcal{F}}\,p.q$ with reproducing kernel $K_{p.q}(\xi,\eta)$ is expressible in the form

$$\tilde{\mathcal{F}}p,q = \tilde{F}_p + \tilde{\mathcal{F}}_q. \quad (4.6)$$

To prove this assertion we first show that

$$\tilde{\mathcal{F}}_p \cap \tilde{\mathcal{F}}_q = \{0\}. \quad (4.7)$$

Suppose $p > q$; then

$$K_p(\xi,\eta) = K_q(\xi,\eta)\,\frac{q!(p-q)!}{p!}K_{p-q}(\xi,\eta). \quad (4.8)$$

Consequently, $\tilde{\mathcal{F}}_p$ is the class of all restrictions of functionals belonging to $\tilde{\mathcal{F}}_q \otimes^* \tilde{\mathcal{F}}_{p-q}$ to the diagonal set $\tilde{S}_2$. Now suppose $f \in \tilde{\mathcal{F}}_p \cap \tilde{\mathcal{F}}_q$ and let $\left\{f_k^{(q)}\right\}$ be a complete orthonormal system in $\tilde{\mathcal{F}}_q$. Since $f \in \tilde{\mathcal{F}}_p$, it can be expressed in the form

$$f(\xi) = \sum_{k=1}^{\infty} g_k(\xi)\, f_k^{(q)}(\xi),\ g \in \tilde{\mathcal{F}}_{p-q} \quad (4.9)$$

But by assumption, f belongs to $\tilde{\mathcal{F}}_q$. Consequently, all the $g_{k's}$ must be zero, which implies $f = 0$.

By (4.7), if $f_p \in \tilde{\mathcal{F}}_p$, $f_q \in \tilde{\mathcal{F}}_q$, then

$$\|f_p + f_q\|^2_{\tilde{\mathcal{F}}_{p.q}} = \|f_p\|^2_{\tilde{\mathcal{F}}_p} + \|f_q\|^2_{\tilde{\mathcal{F}}_q}, \quad (4.10)$$

$$\|f_p - f_q\|^2_{\tilde{\mathcal{F}}_{p.q}} = \|f_p\|^2_{\tilde{\mathcal{F}}_p} + \|-f_q\|^2_{\tilde{\mathcal{F}}_q}, = \|f_p\|^2_{\tilde{\mathcal{F}}_p} + \|f_q\|^2_{\tilde{\mathcal{F}}_q},$$

Which imply Re (f_p, f_q) = 0. Similarly, one has Im (f_p, f_q) = 0. Thus one has (4.6) and the lemma.

By the proof of lemma 4.4, one can show the following.

Proposition 4.1

If $\mathcal{F}_{p.q}$ is reproducing kernel Hibert space with kernel $k_p(\xi, n) + k_q(\xi, \eta)$, then

$$\mathcal{F}_{p.q} = \mathcal{F}_p \oplus \mathcal{F}_a, \quad p \neq q,$$

and if $f \in \mathcal{F}_{p.q}$, then

$$(f(.), k_p(., \xi)) \equiv f_p(\xi)$$

is the projection of f on $\mathcal{F}_p$.

Lemma 4.5

The kernel $k_p(\xi, \eta)$, and $k_p(\xi, \eta)$, $p \geq 0$ are G(P) invariant; that is,

$$K_p(g\xi, g\eta) = K_p(\xi, \eta),$$

$k_p(g\xi, g\eta) = k_p(\xi, \eta)$ for every $g \in G(P)$.

Proof

It is sufficient to prove that K_o and K_1 are G(P) invariant. For K_o this is easily proved by (4.2) and the definition of G(P). Concerning K_1 we have

$$K_1(g\xi, g\eta) = \int_{-\infty}^{\infty} \alpha(g\xi)(t) - (g\eta)(t))\, dt - \int_{-\infty}^{\infty} \alpha((g\xi)(t))\, dt$$

$$- \int_{-\infty}^{\infty} \alpha(-(g\eta)(t))\, dt = \int_{-\infty}^{\infty} \alpha(g(\xi - \eta))(t))\, dt - \int_{-\infty}^{\infty} \alpha((g\xi)(t))\, dt$$

$$- \int \alpha(-(g\eta)(t))\, dt = K_1(\xi, \eta), \tag{4.11}$$

since every $g \in G(P)$ keeps the integral

$\int_{-\infty}^{\infty} \alpha(\xi(t))\, dt$ invariant.

Theorem 4.1

The space $\mathcal{F}$ has the direct sum decomposition

$$\mathcal{F} = \sum_{p=0}^{\infty} \oplus \mathcal{F}_p, \tag{4.12}$$

and it is G(P) invariant. The kernel $k_p(., \xi)$ is a projection operator in the following sense:

$$(f(.), k_p(.\xi)) \equiv f_p(\xi) \tag{4.13}$$

is the projection of f on $\mathcal{F}_p$.

Proof

By lemma 4.4,

$$\sum_{p=0}^{n} k_p(\xi,\eta), \quad (\xi, \eta) \in S \times S, \tag{4.14}$$

will be the reproducing kernel of the subspace $\sum_{p=0}^{n} \oplus \mathcal{F}_p$.

Noting that

$$C(\xi, \eta) = \sum_{p=0}^{\infty} k_p(\xi,\eta), \tag{4.15}$$

and

$$\left\| \sum_{p=0}^{\infty} k_p(.,\eta) \right\|_{\mathcal{F}}^2 = \sum_{p=n}^{m} k_p(\eta,\eta), \tag{4.16}$$

then

$$\mathcal{F} = \sum_{p=0}^{\infty} \oplus \mathcal{F}_p$$

The G(P)-invariantness of $\mathcal{F}_p$ comes from the definition of $\mathcal{F}_p$ and lemma 4.5. Coming back to L_2 space, one has the following decomposition:

$$L_2 = \sum_{p=0}^{\infty} \oplus L_2^{(p)} \text{ with } \quad \tau(L_2^{(p)}) = \mathcal{F}_p. \tag{4.17}$$

4. CONCLUSION

In this paper, the measure space, (E^*, B, μ), is associated with a stationary process, we can form the Hilbert space $L_2 = L_2(E^*, \mu)$ of all square summable complex-valued functions which can be formed with the inner product (2.2). In connection with G(P), a group $G^*(P)$ of linear transformations g^* acting on E^*. Another important concept relating to stationary processes is the purely non-deterministic properties. In

this paper, certain basic concepts relative to stationary process which are developed. We emphasized the importance of a stationary processes with independent values at every point. We are led to the analysis of the $L_2 (E^*, \mu)$ space arising from a stationary processes P with independent values at every point.

REFERENCES

[1] T.Hida "Analysis of Brownian Functionals", Carleton Mathematical Lecture notes No. 13 (1975)

[2] T.Hida: "Brownian Motion," Springer (1980)

[3] T. Hida, H.-H Kuo, J. Potthoff and L. Sreit: "White Noise: An Infinite Dimensional Calculus"; in preparation

[4] Quantum information I, January 2001. Edited by T.Hida, K. Saito

[5] Infinite Dimensional Analysis, Quantum Probability and Related Topics. Volume III, No(1), March 2007

[6] Quantum information II, March 2001. Edited by T.Hida, K. Saito

[7] Infinite Dimensional Analysis, Quantum Probability and Related Topics. Volume III, No(3), September 2007

[8] S. Albeverio, R. Hoegh-Krohn: "Dirichlet Forms and Diffusion Processes on Rigged HilbertSpaces"; Z. Wahrsch. 40 (1977).

[9] Y. Yokoi: "Positive Generalized Brownian Functional", in preparation

[10] Quantum information III, June 2001. Edited by T.Hida, K.Saito

[11] Infinite Diemensional Analysis, Quantum Probability and Related Topics, Volume III, No (2), June 2007

[12] Accardi, L., Hitsuda, M.,Kuo, H.H., Streit, L., Si Si and Saito, K. 1991. Selected papers of Takeyuki Hida. World Scientific Co., Ltd.

Generalized White Noise Functionals and Measures on Dirichlet Forms

Yu Yu Win San
yuyuwinsan@gmail.com
Yangon Technological University, Yangon, Myanmar

Abstract: In this paper some pertinent material from white noise analysis is assembled, in particular concerning positive white noise functionals and their representation by measures. As in the finite dimensional case the underlying nuclear rigging is far from unique and different alternatives should be explored, with a view towards different applications. Energy forms are also constructed from the positive generalized functionals of white noise and prove the closability of its criteria for the admissibility of these functionals, so that the forms correspond to positive-self adjoint operators.

Keywords: generalized white noise functionals, dirichlet forms, test functionals

1. INTRODUCTION

The generalized concept of white noise functionals is presented as a suitable framework of white noise analysis. It is convenient to embed the L^2-space over the white noise probability space in a Gel'fand triple

$$S^*(R) \supset L^2(R, dt) \supset S(R) \qquad (1.1)$$

of smooth, resp. generalized functionals which generates the probability space $(S^*(R), B, d\mu)$ of white noise with one dimensional time. The construction is far from unique .Such construction and its result also readily generated to any Gel'fand triple of function spaces of type (1.1).In section 2, we shall specialize to spaces which is constructed by using 'second quantization' and Fock space techniques. This leads and plays central roles in finite dimensional analysis. In section 3, the energy forms is constructed and also give the criteria of its closability. In the following a particular example of such a triple is constructed, the properties of which are convenient for our purpose.

Let $(S^*(R), B, d\mu)$ be the probability space of white noise and denote

$$(L^2) := L^2(S^*(R), B, d\mu) \qquad (1.2)$$

Recall the correspondence between white noise functionals F and sequences $(F_n, n \in N_0)$ of symmetric square integrable kernel functions $F_n \in L(R^n)$ $(F_0 \in \mathbb{R})$ given by

$$(L^2) \cong \bigoplus_{n \in N_0} L^2(R^n, n! d^n t) \qquad (1.3)$$

which is the standard isometry between (L^2) and the symmetric Fock space over $L^2(R, dt)$. In order to introduce the generalized white noise functionals, the further vital properties need to be explored.

2. GENERALIZED WHITE NOISE FUNCTIONALS AND PROPERTIES OF TEST FUNCTIONALS

The Fock space is an algebraic system (Hilbert space) used in quantum mechanics described quantum states with variable or unknown number of particles. Techanically, the Fock space is Hilbert space which is the direct sum o tensor products of single-particle Hilbert spaces. In the simplest, the Hilbert space (L^2) admits a direct sum decomposition: $(L^2) = \oplus H_n$, where H_n is a subspace spanned by the Fourier-Hermite polynomials . The decomposition established above is called a Fock space.

Introduce the useful transformation that is convenient to implement (1.3) by the following one:

$$(SF)(\xi) := \int F(x + \xi) d\mu(x) \qquad (2.1)$$

for $F \in (L^2)$ and $\xi \in S(R)$ .If $F \in (L^2)$ corresponds to (F_n) in the above sense, then

$$(SF)(\xi) = \sum_{n=0}^{\infty} \int_{R^n} F_n(t_1, ..., t_n)\xi(t_1)...\xi(t_n) d^n t \qquad (2.2)$$

Let A be a densely defined linear operator on $L^2(R, dt)$. Then its "second quantized" operator is given by

$$\Gamma(A) = \bigoplus_n A^{\otimes n} \qquad (2.3)$$

acting on the Fock space on the right hand side of (1.3) .The operator $S^{-1}\Gamma(A)S$ on (L^2) denoted by $\Gamma(A)$. Note that $\Gamma(A)$ is densely defined, linear and on appropriate domains- $\Gamma(A)^p = \Gamma(A^p)$, In particular, consider

$$A = 1 + t^2 - \frac{d^2}{dt^2} \qquad (2.4)$$

with Hermite eigen functions $e_k, k \in N_0$, where

Corresponding Author : Yu Yu Win San, Yangon Technological University, Yangon, Myanmar, yuyuwinsan@gmail.com

$e_n(t) = \left(2^n n!\sqrt{\pi}\right)^{-\frac{1}{2}} H_n(t)\exp(-\frac{1}{2}u^2), n \geq 0$. Hermite polynomial is $H_n(t) = \frac{1}{e^{-\alpha^2 t^2}} \frac{d}{dt^n}(-\alpha)^{-n} e^{-\alpha^2 t^2}; \alpha = 1$

Using the recurrence relation of Hermite polynomial $H_{n+1}(t) = 2tH_n(t) - 2nH_{n-1}(t)$, we have $Ae_k = (2k+2)e_k$. Denote $(S_p) := D(\Gamma(A^p)) \subset (L^2)$ (2.5)

A chain of continuously and densely embedded Hilbert spaces $(p \in N)$

$$\ldots \subset (S_{p+1}) \subset (S_p) \subset \ldots \subset (L^2) \subset \ldots \subset (S_{-p}) \subset (S_{-p-1}) \subset \ldots \quad (2.6)$$

which is obtained and their scalar products norms are denoted by $(\,.\,,\,.\,)_{2,p}$ and $\|\,.\,\|_{2,p}$.

The system $((\,.\,,\,.\,)_{2,p}; p \in \mathbb{Z})$ is compatible. One defines the space (S) of white noise test functionals as the projective limit of the chain (2.6),i.e.

$$(S) = \operatorname{I}_p (S_p) \quad (2.7)$$

and (S) is provided with the projective limit topology and (S) is the countable Hilbert. Therefore its dual $(S)^*$ is given by

$$(S)^* = \operatorname{U}_p (S_{-p}) \quad (2.8)$$

since $(S_p)^* = (S_{-p})$. By the choice of A, (S) is nuclear.

As usual $\varphi \in (S^*)$ has order p, if p is the minimal element in N_0 such that $\varphi \in (S_{-p})$.

Let $\xi \in S(R)$ and consider the $S^*(R)$ - functional

$$F(x) = e^{i<x,\xi>}, x \in S^*(R) \quad (2.9)$$

Then,

$$\Gamma(A^p)F(x) = e^{i<x,A^p\xi> + \frac{1}{2}(\xi,(A^p-1)\xi)} \quad (2.10)$$

Now, we are going to consider special situation of the one treated in the previous section. We found the properties of this test functional space which are the following lemmas.

Lemma 2.1: (S) is dense in (L^2) .

Lemma 2.2: (S) is an algebra.

Lemma 2.3: Each $F \in (S)$ has a version $\tilde{F}$ of the form

$$\tilde{F}(x) = \sum_n <: x^{\otimes n} :, F_n > \quad (2.11)$$

with F_n in $\hat{S}(R^n)$. Conversely any such $\tilde{F}$ is in (S) iff

$$\sum_n n! \left\| \Gamma(A^p)F_n \right\|_2^2 < \infty \quad (2.12)$$

for all $p \in N_0$.

Let $(S)_0$ denote the subspace of (S) consisting of those F which have only a finite number of nonvanishing F_n . Clearly $(S)_0$ is dense in all $(S_p), p \in \mathbb{Z}$. For all $F \in (S)_0$ and all $f \in L^2(R, dt)$ the Fre′chet derivatives D_f of SF (cf (2.2)) is well-defined. In fact, viewed as an operator on Fock space D_f is nothing but the annihilation operator of f. The closure of this operator in Fock space is denoted by the same symbol and we set

$$\partial_f := S^{-1} D_f S \quad (2.13)$$

If in particular $f = e_k, k \in N_0$ simply write ∂_k .

Lemma 2.4: For all $f \in L^2(R, dt)$

$$\partial_f : (S) \to (S) \quad (2.14)$$

Proof:

By elementary calculation on derives the bound

$$\left\| \partial_f F^{(n)} \right\|_{2,p} \leq n^{1/2} 2^{-n} \left\| A^{-1} f \right\|_2 \left\| F^{(n)} \right\|_{2,p+1} \quad (2.15)$$

for $F^{(n)}$ given by

$$F^{(n)}(x) = <: x^{\otimes n} :, F_n >, F_n \in \hat{S}(R^n).$$

Since $F \in (S)$ is given by a sum of such functionals satisfying (2.12), it is clear by lemma 2.3 that the estimate (2.15) proves the assertion.

Let us denote

$$(L^2) := (L^2) \otimes l^2 \quad (2.16)$$

l^2 being the Hilbert space of square summable sequences over N_0 and

$$\nabla : (L^2) \to (L^2) \quad (2.17) \text{ by}$$

$$\nabla F := (\partial_0 F, \partial_1 F, \ldots, \partial_k F, \ldots) \quad (2.18)$$

defined on $(S)_0$ .Obviously, ∇ is closable .Its closure is denoted by the same symbol.

Set

$$\left| \nabla F \right|^2 := \sum_{k \in N_0} \left| \partial_k F \right|^2 \quad (2.19)$$

to prove the following .

Lemma 2.5: $F \in (S)$ entails $\left| \nabla F \right|^2 \in (S)$.

Next we want to summarize results about positive generalized functionals and measures.

3. CONSTRUCTION OF DIRICHLET FORMS FROM POSITIVE GENERALIZED FUNCTIONALS

We introduce the cone of positive test functional as

$$(S)_+ := \{F \in (S) : F \geq 0 \ \mu - a.e.\} \qquad (3.1)$$

and call $\varphi \in (S)^*$ a positive generalized functional if it maps $(S)_+$ into the positive real numbers.

Theorem 3.1: For any positive generalized functional φ there is a unique positive finite measure ν on the Borel algebra over $S^*(R)$ such that for all $F \in (S)$

$$\langle \varphi, F \rangle = \int F d\upsilon \qquad (3.2)$$

φ plays as in finite dimensional analysis. Apply the notation $d\upsilon = \varphi d\mu$ and write $(L^2)_\upsilon$ for $L^2(\varphi d\upsilon)$, similarly $(L^2)_\upsilon$ .In order to prove this theorem we use the following lemma.

Lemma 3.2: Let $\varphi \in (S^*)$. Then the map $\xi \to T\varphi(\xi) := \langle \varphi, \exp[i\langle x, \xi \rangle] \rangle$ is continuous from S(R) into C.

Proof of theorem 3.1

Let $\varphi \in (S)^*_+$. Clearly this entails that φ is real $\overline{\varphi} = \varphi$. If $F \in \delta$ (algebra generated by exponential) then $\overline{F} \cdot F$ is positive and $\langle \varphi, \overline{F} \cdot F \rangle \geq 0$. This implies that $\xi \to T\varphi(\xi) := \langle \varphi, \exp[i\langle x, \xi \rangle] \rangle$ is positive definite. Due to above lemma we may apply Minlo's theorem, to the continuous S(R) functional $\xi \to T\varphi(\xi)$ and have the existence of a finite measure υ on B so that

$$\langle \varphi, \exp[i, \langle ., \xi \rangle] \rangle = \int_{S(R)} \exp[i, \langle x, \xi \rangle] \, d\upsilon$$

By linearity this extends to the dense subspace δ of (S): for all $F \in \delta$, we have (3.2).Now let $F \in (S)$. By using the fact that (S) is nuclear, there exists a sequence $\{F_n, n \in N\}$ in δ which converges to F in (S).Since multiplication is continuous in (S), this implies that also $\|F_n - F\|^2$ converges to zero in (S). But this shows that $\{F_n\}$ is Cauchy in $(L^2)_\varphi$, converging to an element ψ .Selecting a subsequence, we denote again by $\{F_n, n \in N\}$ we find that $F_n \to \psi, \upsilon$ almost everywhere. On the other hand, $F_n \to F$ pointwise. Thus $F = \psi, \upsilon$ almost everywhere and equation (3.2) holds for $F \in (S)$.

To focus on the study of "energy forms" generated by positive white noise functionals φ, the following forms will introduce

$$\mathcal{E}(F) \equiv \left\langle \phi, |\nabla F|^2 \right\rangle = \int |\nabla F|^2 \, d\upsilon \qquad (3.3)$$

Theorem 3.3: The energy form $\mathcal{E}$ arising from a positive generalized white noise functional φ, defined on (S), is a positive, densely defined, symmetric quadratic form on $(L^2)_\nu$.

Proof:

Note that by lemma 2.2 and theorem 3.1

$$\mathcal{D}(\mathcal{E}) = (S) \subset (L^2)_\upsilon \qquad (3.4)$$

Furthermore, the algebra generated by functionals of the forms (2.9) is dense in $(L^2)_\upsilon$ and is contained in (S), so that the embedding (3.4) is dense. The other assertions are obvious.

We now turn to the problem of closability of the quadratic form $\mathcal{E}$.

Definition 3.4: A positive generalized functional φ is called admissible if the corresponding energy form (3.3) is closable on $(L^2)_\upsilon$.

Theorem 3.5: Let φ be admissible. $\overline{\mathcal{E}}$ denotes the closure of $\mathcal{E}$, $\mathcal{D}(\overline{\mathcal{E}})$ its domain. Then there exists a unique positive self-adjoint operator H with $\mathcal{D}(H^{1/2}) = \mathcal{D}(\overline{\mathcal{E}})$ and such that $\mathcal{E}(F) = \left\| H^{1/2} F \right\|^2_{(L^2)_\upsilon}$.

Theorem 3.4: $\mathcal{E}$ is closable if

$$\nabla^* : (l^2)_\upsilon \to (L^2)_\upsilon \qquad (3.5)$$

is densely defined.

Example 3.5: $\varphi = 1$: in this case -H is the Laplace-Beltrami operator

$$H = \sum_k \partial_k^* \partial_k \qquad (3.6)$$

where ∂_k^* is the (L^2)-adjoint of ∂_k . H is of course the S-transform of the number operator on Fock space and generates the infinite-dimensional Orstein-Uhlenbeck process on $S^*(R)$ .In order to describe a convenient criterion in the case that υ is absolutely continuous with

respect to μ with positive density φ, one introduces the spaces $(L^{p,q})$, p=2,3,…, $q \in N_0$,which are the completions of the algebra E generated by functionals of the form (2.9) under the norms

$$\|F\|_{p,q} := \|(1+H)^q F\|_p \qquad (3.7)$$

where H is the number operator (3.6).

Note that $(S) \subset (L^{p+q}) \subset (L^2)$ for all p=2,3,…, $q \in N_0$ and that these embeddings are dense and continuous.

Theorem 3.6: Assume that $\varphi > 0(\mu - a.e)$ and $\varphi^{1/2} \in (L^{4,1})$.Then φ is admissible.

Lemma 3.7: Under the hypothesis of theorem (3.6)

$$\partial_k \varphi^{1/2} = \frac{1}{2}\varphi^{1/2}\partial_k \varphi \qquad (3.8)$$

for all $k \in N_0$ in (L^2) sense.

Proof:

From the assumption it follows that there is a sequence $(f_n : n \in N_0)$ in E, so that $f_n \to \varphi^{1/2} in (L^{4,1})$ and $f_n^2 \to \varphi$ in (L^2) it is easy to check that for every $k \in N_0$; ∂_k is a derivation on E , so that for every $k \in N_0$; $\partial_k f_n^2$ is Cauchy in (L^2). Moreover $\partial_k \varphi$ is in (L^2), which can be seen as follows

$$\begin{aligned}\|\partial_k \varphi\|_2 &\le \|\nabla \varphi\|_2 \\ &= \|H^{1/2}\varphi\|_2 \\ &\le \|H\varphi\|_2 \\ &\le \text{const.}\|H^{1/2}\varphi\|_4^2\end{aligned}$$

where the last inequality followed from Meyer's equivalence. Thus the closed graph theorem implies that

$$\begin{aligned}\partial_k \varphi = \partial_k(\varphi^{1/2})^2 &= \lim_n \partial_k f_n^2 \\ &= 2\lim_n f_n \partial_k f_n = 2\varphi^{1/2}\partial_k \varphi^{1/2}\end{aligned}$$

where the limits are taken in (L^2).

Proof of theorem 3.6:

Let $(F_k ; k \in N_0)$ be a sequence with $F_k = 0$ for almost all $k \in N_0$ and $F_k \in E$ for all $k \in N_0$. Then $\underline{F} \equiv (F_k) \in (l^2)_\upsilon$ and

$$\nabla^* \underline{F} = \sum_k (-\partial_k + x_k - (\varphi^{-1}\partial_k \varphi))F_k \qquad (3.9)$$

where x_k is the multiplication operator $(x_k F)(x) = < x, e_k > F(x)$.

Thus

$$\begin{aligned}\|\nabla^* \underline{F}\|^2_{(L^2)_\upsilon} \le 2\{ &\int d\mu(x)\varphi(x)\left|\sum_k (-\partial_k + x_k)F_k(x)\right|^2 \\ &+ \int d\mu(x)\varphi(x)\left|\sum_k (\varphi^{-1}\partial_k \varphi)F_k(x)\right|^2 \}\end{aligned}$$

Since $(F_k \in E)$ and $\varphi \in (L^2)$ it is a trivial application of Schwartz' inequality to show that the first of the last two terms is bounded. For the second term note that each F_k is bounded and that the sum has only a finite number of terms. Thus it suffices to show that

$$\sum_k \int d\mu(x)\varphi(x)(\varphi^{-1}\partial_k \varphi)^2(x)$$

is bounded. By lemma 3.7 this expression equals

$$4\int d\mu(x)\left|\nabla \varphi^{1/2}\right|^2(x) = 4\|H^{1/2}\varphi^{1/2}\|_2^2$$

which is finite by the assumption. In the case that φ is a genuine generalized functional, i.e υ not absolutely continuous with respect to μ.

4. CONCLUSION

In this paper, the fruitful properties of test functionals give us many interesting ideas. The admissibility of the energy form $\mathcal{E}$ plays an important role in white noise analysis.

REFERENCES

[1] T.Hida, H.-H. Kuo, J. Potthoff and L. Streit: " While Noise: An Infinite Dimensional Calculus"; in preparation

[2] T.Hida: "Analysis of Brownian Functionals"; Carleton Mathematical Lecture Notes No. 13 (1975)

[3] M. Fukushima : "Dirichlet Forms and Markov Processes"; in " Mathematics + Physics. Lectures on Recent Results", vol. 1; (L. Streit, ed.) World Scientific (1985)

[4] T. Hida: "Brownian Motion", Springer (1980)

[5] S. Albeverio, R. Hoegh-krohn: "Dirichlet Forms and Diffusion Processes on Hilbert Spaces "; Z . Wahrsch. 40 (1977), 1

[6] Infinite Dimensional Analysis, Quantum Probability and Related Topics. VolumeIII,No(1),March 2000

[7] Infinite Dimensional Analysis, Quantum Probability and Related Topics. VolumeIV,No(2), June 2001

[8] Accardi, L., Hitsuda,M., Kuo, H. H., Streit, L., Si Si and Saito, K. 1991. Selected papers of Takeyuki Hida. World Scientific Co., Ltd.

[9] M. Fukushima: "Dirichlet Forms and Markov Processes"; Kodansha and North Holland (1980)

[10] T. Hida: “Stationary Stochastic Processes” Princeton University Press and the University of Tokyo Press, Princeton, nwe Jersey, 1970.

[11] J. Potthoff: “ On Meyer’s Equivalence”, TUB preprint (1986)

A Role of the Lévy Laplacian Acting on the Space of Generalized White Noise Functionals

Moe Myint Swe
Yangon Technological University, Myanmar
moe2moegyi@gmail.com

Abstract: In this paper, we discuss the Lévy Laplacian which is just fitting for purpose of carry out the differential and integral calculus of generalized Brownian functionals. Starting from a quick review of background of white noise analysis we come to state characteristic properties of the Lévy Laplacian. Unlike finite dimensional Laplacian we can see interesting properties of the Laplacian like its domain, eigenfunctionals and so forth.

Keyword: Lévy Laplacian, white noise, generalized white noise functional, infinite dimensional rotation group.

I. INTRODUCTION

The white noise analysis which discusses the analysis of Brownian functionals has an aspect of the harmonic analysis arising from the infinite dimensional rotation group. T.Hida introduced a "generalized" Brownian functionals, which are called nowadays generalized white noise functionals (or often called "Hida distributions"). The Laplacian plays a key role as it does in the finite dimensional analysis.

P. Lévy proposed a Laplacian in the study of functionals defined on a Hilbert space $H = L^2([0,1])$ and showed that its properties are useful for the calculus of functionals on H .

There are many operators that may be viewed as infinite dimensional analogue of the ordinary Laplacian. Among them, the Lévy Laplacian is fitting to carry out the differential and integral calculus of generalized Brownian functionals.

One can find intimate relation between the Lévy Laplacian and the Lévy group g that comes from the permutation of the coordinate axes. One can see a strong relationship between harmonic analysis (in particular, the theory of the rotation group and the Laplacian operator) and the theory of causal calculus. Δ_L commutes with the group g and it is a quadratic form of the differential operators. One can even observe that Δ_L is like an operator obtained by taking the limit of

$$\frac{1}{N}\sum_{1}^{N}\frac{\partial^2}{\partial\xi_n^2} \qquad \text{as} \qquad N\to\infty .$$

One can prove that the group g would characterize the operator Δ_L .

In this paper, the Lévy Laplacian is discussed within the framework of the theory of white noise analysis. So, one will give a short review of white noise analysis. Then one proceeds to the topic which deals with functional differential equations involving the Lévy Laplacian.

II. BACKGROUND

Let the time parameter set T be taken to be the unit interval [0, 1], and let H be the Hilbert space involving real, square integrable functions on T . One starts with a Gel'fand triple

$$E \subset H \subset E^* ,$$

where E is a nuclear space and E^* is the dual space of E .

Let μ be a white noise measure introduced on the space E^* of generalized functionals on R . It is given by the characteristic functional $C(\xi)$ of the form

$$C(\xi) = \exp[-\frac{1}{2}\|\xi\|^2]$$

$$C(\xi) = \int_{E^*} \exp[i < x,\xi >]d\mu(x), \xi \in E.$$

Then, a complex Hilbert space $(L^2) = L^2(E^*,\mu)$ is formed. A member of (L^2) is a Brownian functional or a white noise functional. The Wiener-Itô decomposition is given as follows:

$$(L^2) = \hat{\oplus}_{0}^{\infty} H_n \qquad \text{(Fock space)} \qquad (1)$$

Corresponding Author: Moe Myint Swe, Yangon Technological University, Myanmar, moe2moegyi@gmail.com

The S –transform of a white noise functional $\varphi(x)$ is defined

$$(S\varphi)(\xi) = \int \varphi(x+\xi)d\mu(x) \qquad (2)$$

$$= \exp[-\frac{1}{2}\|\xi\|^2] \int \exp[< x,\xi >]\varphi(x)d\mu(x).$$

The S –transform is often denoted by $U(\xi)$ and is called the U -functional associated with $\varphi(x)$. The S – transform gives an injective map from (L^2) to a space of continuous functionals of ξ.

The integral representation of a Brownian functional is obtained by the T –transform:

$$(T\varphi)(\xi) = \int \exp(i < x,\xi >)\varphi(x)d\mu(x), \quad \varphi \in (L^2). \qquad (3)$$

If φ is restricted to the subspace H_n, then we have

$$(T\varphi)(\xi) = i^n C(\xi)U(\xi)$$
$$U(\xi) = \int_{T^n} F(u_1,...,u_n)\xi(u_1)...\xi(u_n)du^n. \qquad (4)$$

and establish an isomorphism:

$$\varphi \to F \in \hat{L}^2(T^n)(=\text{symmetric}\, L^2(T^n)\,\text{space}),$$
$$\|\varphi\|_{(L^2)} = \sqrt{n!}\|F\|_{L^2(T^n)} \qquad (5)$$

The function F is called the kernel of the representation of φ.

In order to carry out the causal calculus, a class of generalized Brownian functionals is introduced. The space $H_n^{(n)}(\subset H_n)$ of test functionals is defined as:

$$H_n^{(n)} = \{\varphi \in H_n; \text{kernel of } \varphi \text{ is in } \hat{H}^{(n+1)/2}(T^n) \cap \hat{L}^2(T^n)\}. \qquad (6)$$

where $\hat{H}^{(n+1)/2}(T^n)$ is a Sobolev space over (T^n) of order $(n+1)/2$.

$\|\varphi\|_n = \sqrt{n!}.H^{(n+1)/2}(T^n)$ - norm of the kernel.

The space $H_n^{(-n)}$ is defined to be the dual space of $H_n^{(n)}$. Thus a triple:

$$H_n^{(n)} \subset H_n \subset H_n^{(-n)}.$$

A member in $H_n^{(-n)}$ is called a generalized Brownian functional or generalized white noise functional of order n.

The T -transform is extended to the space $H_n^{(-n)}$ and U –functional of a generalized Brownian functional is defined by the S –transform.

A typical example of a generalized Brownian functional φ is given by the following U -functional

$$U(\xi) = \int_{T^k} G(u_1,...,u_k)\xi(u_1)^{n_1}...\xi(u_k)^{n_k}du^k,$$
$$G \in L^2(T^k). \qquad (7)$$

Applying the transform S^{-1} to this U we get a generalized Brownian functional expressed in the form

$$(S^{-1}U)(x) = \int_{T^k} G(u_1,...,u_k) : x(u_1)^{n_1}...x(u_k)^{n_k} : du^k, \qquad (8)$$

where **:** **:** means the renormalization.

Note that the functional is a realization of a polynomial, indeed, a Hermite polynomial in $\dot{B}(t)$'s.

A weighted sum $(L^2)^- \equiv (L^2)^-_{\{c_n\}}$ is defined as the dual space of the space $(L^2)^+ \equiv (L^2)^+_{\{c_n\}}$ of test functionals:

$$(L^2)^+_{\{c_n\}} = \{\varphi = \sum \varphi_n; \varphi_n \in H_n^{(n)}, \sum c_n\|\varphi\|_n^2 < \infty\},$$

where $\| \|_n$ is the $H_n^{(n)}$-norm, and $0 < c_n$.

Example

An exponential function of the form

$$\varphi(x) =: \exp(c \int x(t)^2 dt) :, \quad c < \frac{1}{2}, \qquad (9)$$

is a generalized functional living in $(L^2)^-$, the U -functional of which is given by

$$\exp(c' \int \xi(t)^2 dt), \quad c' = \frac{c}{(1-2c)}.$$

The renormalization in (9) is multiplicative, since the functional is exponential.

A differential operator ∂_t is the partial differential operator with respect to the variable $x(t)$, or to the $\dot{B}(t)$.

Definition

Let $U(\xi)$ be the U -functional associated with an (L^2)-functional φ. If $U(\xi)$ is Fréchet differentiable and if the derivative $\frac{\partial U}{\partial \xi(t)}$ is a U -functional associated with some φ_t' in the space $(L^2)^-$, then φ is said to be ∂_t -differentiable and define

$$\varphi_t' = \partial_t \varphi$$
$$= (S)^{-1}\{\frac{\delta}{\delta\xi(t)}(S\varphi)(\xi)\}, \quad (10)$$

where $\frac{\delta}{\delta\xi(t)}$ is the Fréchet derivative.

The domain of the operator ∂_t is rich enough in (L^2). One can therefore determine the adjoint operator ∂_t^* of ∂_t:

$$< \partial_t\varphi, \psi >=< \varphi, \partial_t^*\psi >_\mu ,$$

where $< , >_\mu$ is the inner product in (L^2).

The operator ∂_t is, in terms of quantum dynamics, the annihilation operator, while the ∂_t^* is the creation operator. Multiplication by $x(t)$, called multiplication operator and denoted by m_t, is given by the formula

$$m_t = \partial_t^* + \partial_t \quad (11)$$

The index t may be thought of as the time parameter, so that ∂_t and ∂_t^* as well as m_t are fitting to carry on the calculus of white noise functionals that describe random phenomena changing as time t goes by. Such a calculus is called the causal calculus because the time development can explicitly be described by using those operators.

In order to develop the causal calculus, it is necessary to introduce a larger class of white noise functionals, namely a class of generalized white noise functionals. Like the Schwartz space S of test functionals on R, one can introduce a nuclear space (S), and its dual space $(S)^*$ so that one has a Gel'fand triple:

$$(S) \subset (L^2) \subset (S)^* .$$

The space (S) is an algebra consisting of test functionals.

III. THE LÉVY LAPLACIAN

One is interested in an infinite dimensional analogue of the finite dimensional Laplacian. Such an operator would be a quadratic form of the differential operators $\partial_t, t \in T$.

Before the definition of the Lévy Laplacian, the definition of the second order Fréchet derivative will be given.

Let $U(\xi)$ be a functional on E, and let $U'(t)$ be the Fréchet derivative of U. If the variation $\delta U'(t)$ is expressed in the form

$$\delta U'(t) = U''_{\xi\xi}(t)\delta\xi(t) + \int U''_{\xi\eta}(t,s)\delta\xi(s)ds \quad (12)$$

then $U''_{\xi\xi}$ and $U''_{\xi\eta}$ are called the second order Fréchet derivatives.

Let φ be an (L^2)-functional with U-functional $U(\xi)$. Assume that $U''_{\xi\xi}(t)$ is a U-functional associated with some generalized fuctional φ_t''. Then the Lévy Laplacian Δ_L is defined to be an operator acting in the form

$$\Delta_L = \int \varphi_t'' \, dt . \quad (13)$$

Now the domain of the Laplacian will be discussed. Let $\mathcal{D}$ be the vector space spanned by the normal functions. Significant example is a quadratic normal functional of the form $\int f(u) : \dot{B}(u)^2 : du$ where f is integrable.

Proposition 1

The functional $\int f(u) : \dot{B}(u)^2 : du$ is viewed as the renormalized limit of a quadratic form $Q_1 = \sum_{i=1}^{n} a_i \xi_i^2$, where ξ_i's are independent standard Gaussian random variables. General quadratic form is expressed as $Q = \sum a_{ij}$ and Q_1 is is a part of Q involving non-harmonic terms. The limit of Q_1, as $n \to \infty$ is in $H_2^{(-2)}$ and creates singularity of order 1.

A norm $\| \ \|_e$ is introduced to $\mathcal{D}$:

$$\|\varphi\|_e^2 = \|\varphi\|_-^2 + \int \| \partial_t \varphi \|_-^2 dt + \int \| \partial_t^2 \varphi dt \|_-^2 dt, \quad (14)$$

$\| \ \|_- : (L^2)^-$ - norm.

Obviously $\| \ \|_e < \infty$ for any $\varphi \in \mathcal{D}$. The completion of $\mathcal{D}$ with respect to the norm $\| \ \|_e$ will be denoted by Δ and is taken to be the domain of the Lévy Laplacian.

Obviously, we have

Proposition 2

For φ in Δ

$$\|\Delta_L \varphi\|_- \le \|\varphi\|_e .$$

If there is any connection between the Lévy Laplacian and the limit

$$\lim \frac{1}{N} \sum_1^N \frac{\partial^2}{\partial \xi^2} \equiv \tilde{\Delta}$$

which was the motivation of the Lévy's work. It is given as an interpretation in the following manner.

Let ξ_n be a complete orthonormal system in H which is "equally dense", that $\frac{1}{N}\sum_{1}^{N}\xi_n(t)^2 \to 1$ in $L^2(T)$, as $N \to \infty$.

Then, if $U(\xi)$ is the U - functional associated with a functional in Δ, then

$$\int U''_{\xi\xi}(t)dt = \tilde{\Delta}U,$$

as is expected.

There is an interesting observation on the Lévy Laplacian.

$$\Delta_L = \int \partial_t^2 (dt)^2 . \qquad (15)$$

Although the above integral has only formal meaning, plausible interpretation can be given to (15) with a note that one dt is used to cancel the singularity of the operand.

Proposition 3

Exponential functionals given by (9) are all eigen-functionals of the operator Δ_L with eigenvalues $2c'$.

IV. EIGENFUNCTIONALS OF Δ_L

From this section onward, the time variable t is assumed to run over the unit interval [0, 1], and hence the basic Hilbert space is $L^2([0,1])$.

Start with the eigenvalue problem for Δ_L. Namely, one shall consider the following equation

$$\Delta_L \varphi_\lambda = -\lambda\varphi_\lambda, \varphi_\lambda \in (S)^*, \lambda \in R. \qquad (16)$$

Before the actual computation, some notation shall be introduced. Set

$$\mathfrak{D}_L = S\Delta_L = \int_0^1 \frac{\delta^2}{\delta\xi(t)^2}dt . \qquad (17)$$

It is the operator acting on the U-functional of the test function ξ. Then we have

Proposition 4

The equation (16) has a solution in $(S)^*$, which is expressed in the form

$$\varphi_\lambda(x) = \psi(x) \Diamond : \exp[-\frac{1}{2}\lambda r(x)^2] : , \qquad (18)$$

where ψ is harmonic in the sense that $\Delta_L\psi = 0$, and where r^2 is the generalized white noise functional, the S-transform of which is $\|\xi\|^2$.

Remark: ":" in (18) means the renormalized functional.

Proof:

Let $U_\lambda(\xi)$ be the U-functional associated with $\varphi_\lambda(x)$. Then, the equation (16) is equivalent to

$$\mathfrak{D}_L U_\lambda(\xi) = -\lambda U_\lambda(\xi) . \qquad (16')$$

Since the equation (16') is linear and Δ_L has a property like a first order differential operator, a special solution to the equation (16') is easily obtained:

$$U_{\lambda 0}(\xi) = A.\exp[-\frac{1}{2}\lambda\|\xi\|^2], A \text{ constant.}$$

Suppose there are two solutions $U_{\lambda 1}$ and $U_{\lambda 2}$ to (16'). Then,

$$\mathfrak{D}_L\{\frac{U_{\lambda 1}}{U_{\lambda 2}}\} = \mathfrak{D}_L U_{\lambda 1}.U_{\lambda 2}^{-1} + U_{\lambda 1}.\mathfrak{D}_L U_{\lambda 2}^{-1}$$

$$= \lambda U_{\lambda 1}.U_{\lambda 2}^{-1} + U_{\lambda 1}.[\lambda U_{\lambda 2}.U_{\lambda 2}^{-2}] = 0 .$$

This shows that any solution to (16') is expressible as a product of $U_{\lambda 0}$ given above and a $\mathfrak{D}_L$-harmonic functional $H(\xi)$. This $H(\xi)$ has to be a U-functional satisfying the condition given by [13], because the $U_{\lambda 0}$ is of the following particular type

const. exp [quadratic function of ξ].

Set $(S^{-1}H)(x) = \psi(x)$, then $\psi(x)$ is Δ_L-harmonic. This completes the proof.

V. CONCLUSION

Our new result, stated in Proposition 1, can be used to obtain the functional in the domain of Δ_L as a generalization of φ_λ, expressed in (18).

REFERENCES

[1] Accardi, L., Hitsuda, M., Kuo, H.H., Streit, L., Si Si and Saito, K. 1991. Selected papers oæ Takeyuki Iita. World Sciuntific Co., Ltd.

[2] P.Lévy, Problems concrmts d'analyse fonctionnelle, Gauthier-Villars, 1951.

[3] T.Hida, Brownian motion (English translatioo), Springer-Verlag, New York,
2 $ 1980.

[4] I.Kubo and S.Takenaka, Calculus of Gáussian white noise, Proc. Japan Acad. 56A: 3 76-380, 411-416; 57A: 433-437; 58A:186-189, 1980, 1981, 1982.

[5] H.-H.Kuo, Brownian functionals and applications, Acta Applicandae Mathematicas 1, 175-188, 1983

[6] H.-H.Kuo, On Fourier transform of generalized functionals. J.of Multivariate Analysis,12, 415-432, 1982.

[7] N.Obata, A note on certain permutation groups in the infinite dimensional rotation group to appear.

[8] G.Kallianpur and R.L.Karandikar, White Noise Theory of prediction, filtering and smoothing. Stochastic Monographs vol.3,1988, Gordon and Breach Science Pub.

[9] T.Hida, Brownian motion. Applications of Mathematics vol.11,1980, Springer-Verlag.

[10] T.Hida, H.-H.Kuo, J.Potthoff and L.Streit, White Noise - An infinite dimensional calculus. Monograph to appear.

[11] T.Hida, J.Pothoff and L.Streit, white noise analysis and applications. Mathematics + Physics vol.3, ed. L.Streit,1998, World Scientific, 143-178.

[12] T.Hida, N.Obata and K.Saitô, Infinite dimensional rotations and Laplacians in terms of white noise calculus. preprint.

[13] J.Potthoff and L.Streit, A characterization of Hida. distributions. J.Funct. Anal. 101(1991),212-229.

Stability of the ADI Schemes on the Application to Convection Diffusion Equations.

Kay Thi Oo
Department of Engineering Mathematics
Yangon Technological University
Yangon, Myanmar.

Abstract: In solving many convection-diffusion equations, the Alternative Direction Implicit (ADI) schemes are very useful. In this paper, the stability of three A.D.I schemes (the Douglas Scheme; the Craig and Sneyd Scheme and the Hundsdorfer) is presented.

Keywords: Initial-boundary value problems: Convection-diffusion equations: ADI splitting schemes: Von Neumann stability analysis.

Introduction

Research work is based on alternating Direction Implicit Schemes which is used to find the numerical solution of initial-boundary value problems for convection diffusion equations with cross derivative terms.

Three Alternating Direction Implicit Schemes

In this paper, the large system of ordinary differential equations (ODEs)

$$U'(t) = F(t, U(t)) \ (t \geq 0), \qquad (1)$$

with given function F and initial value $U(0) = U_0$, arising from the semi-discretization of an initial-boundary value problem for a multi-dimensional convection-diffusion equation is considered. In splitting methods for the numerical solution of (1), the function F is decomposed into a sum

$$F(t,v) = F_0(t,v) + F_1(t,v) + \ldots + F_k(t,v), \qquad (2)$$

where the terms F_j are simpler to handle than F itself. Assume that F_0 is treated explicitly in time- integration schemes, whereas F_1, F_2,...,F_k represent stiff, unidirectional contributions in F that are treated implicitly.

The analysis to be presented in this paper is mostly relevant to ODE systems (1) originating from convection-diffusion problems in two spatial variables. For the formulation of the splitting schemes below, however, the particular spatial dimension of the problem is not yet important.

Let time step $\Delta t > 0$. The Douglas scheme defines an approximation $U_n \approx U(t_n)$, with $t_n = n\Delta t$, successively for n=1, 2, 3, . . . by

$$\begin{cases} Y_0 = U_{n-1} + \Delta t\, F(t_{n-1}, U_{n-1}), \\ Y_j = Y_{j-1} + \theta\Delta t\,(F_j(t_n, Y_j) - F_j(t_{n-1}, U_{n-1})), \\ \qquad\qquad j = 1,2, \ldots, k, \\ U_n = Y_k, \end{cases} \qquad (3)$$

Here $\theta > 0$ denotes a real parameter, which specifies the scheme. In (3) the forward Euler predictor step is followed by k implicit but unidirectional corrector steps, whose purpose is to stabilize the predictor step.

It can be verified that the classical order[1] of the scheme (3) is equal to 2 whenever $F_0 = 0$ and $\theta = 1/2$, and it is of order 1 otherwise. In application always $F_0 \neq 0$ and, consequently, the order of the Douglas scheme (3) reduces to just 1, for any given θ . In the following we formulate two ADI schemes are formulated that attain order 2 also if $F_0 \neq 0$.

The subsequent scheme can be regarded as an extension of (3);

$$\begin{cases} Y_0 = U_{n-1} + \Delta t\, F(t_{n-1}, U_{n-1}), \\ Y_j = Y_{j-1} + \theta\Delta t\,(F_j(t_n, Y_j) - F_j(t_{n-1}, U_{n-1})), \\ \qquad\qquad j = 1,2, \ldots, k, \\ \tilde{Y}_0 = Y_0 + \sigma\Delta t\,(F_0(t_n, Y_k) - F_0(t_{n-1}, U_{n-1})), \\ \tilde{Y}_j = \tilde{Y}_{j-1} + \theta\Delta t\,(F_j(t_n, \tilde{Y}_j) - F_j(t_{n-1}, U_{n-1})), \\ \qquad\qquad j = 1, 2, \ldots, k, \\ U_n = \tilde{Y}_k, \end{cases} \qquad (4)$$

Here $\sigma > 0$ denotes a second real parameter. If $F_0 = 0$, then (4) reduces to the Douglas scheme (3). Clearly, (3) uses the (stable) approximation Y_k to $U(t_n)$ obtained from the Douglas method so as to introduce a correction with respect to the F_0 part as well. The scheme (4) is of classical order 2 whenever

Corresponding Author : Kay Thi Oo, Department of Engineering Mathematics Yangon Technological University Yangon, Myanmar.

{F_0= 0 and θ = ½ } or {θ = σ = ½}, and it has order1 otherwise. Hence, contrary to (3), with the scheme (4) order 2 can be attained independently of F_0-upon taking θ = σ = ½.

[1] i.e., the order for fixed non-stiff ODEs.

The so-called "iterated scheme" that was proposed by Craig and Sneyd [1] can be reformulated as (4). Correspondingly, (4) shall be referred as the Craig & Sneyd scheme. These authors studied the scheme (4) in the application to

pure diffusion problems where mixed spatial derivative terms are present. Note that a version of the Douglas scheme(3) was considered in [1] as well, where it was called the "simple scheme". It is interesting to remark that a variant of (4) is used in financial option pricing. When applied to linear autonomous problems (1), this variant is readily seen to reduce to (4)) with k =2 and θ = σ = ½ .

The following scheme can be regarded as a second, different extension of the Douglas scheme:

$$\begin{cases} Y_0 = U_{n-1} + \Delta t\, F(t_{n-1}, U_{n-1}), \\ Y_j = Y_{j-1} + \theta\Delta t\,(F_j(t_n, Y_j) - F_j(t_{n-1}, U_{n-1})), \\ \qquad\qquad j = 1,2,\ldots,k, \\ \tilde{Y}_0 = Y_0 + \sigma\Delta t\,(F_0(t_n, Y_k) - F(t_{n-1}, U_{n-1})), \\ \tilde{Y}_j = \tilde{Y}_{j-1} + \theta\Delta t\,(F_j(t_n, \tilde{Y}_j) - F_j(t_n, Y_k)), \\ \qquad\qquad j = 1, 2, \ldots, k, \\ U_n = \tilde{Y}_k, \end{cases} \qquad (5)$$

If σ = ½ the scheme (5) is identical to a scheme formulated by Hundsdorfer [5,p. 222]. Furthermore, in the case of linera autonomous problems (1) it is equivalent to a Rosenbrock type method discussed e.g in Hundsdorfer and Verwer[6,p.400]. In view of (5) shall referred as the Hundsdorfer & Verwer scheme. This scheme has been considered in [5,6] for the application to convection-diffusion-reaction problems without mixed derivative terms.

For any given θ, the scheme (5) is of classical order 2 if σ = ½ and of order 1 otherwise, independently of F_0. Compared to (4) note e.g that (5) uses the full right-hand side function F from (1) for the update $\tilde{Y}_0$, instead of just F_0 alone.

All three schemes (3) - (5) above are called Approximate Matrix Factorization methods.

When applied to the linear scalar test equation

$$U'(t) = (\lambda_0 + \lambda_1 + \ldots + \lambda_\kappa)\, U(t), \qquad (6)$$

with complex constants λ_j ($0 \le j \le k$), the Douglas scheme (1.3) reduces to

$$U_n = R(z_0, z_1, \ldots, z_k)\, U_{n-1} \qquad (7)$$

with $z_j = \lambda_j \Delta t$ ($0 \le j \le k$) and

$$R(z_0, z_1, \ldots, z_k) = 1 + \frac{z_o + z}{p} \qquad (8)$$

Here, and throughout this paper, we adopt the notation

$$z = z_1 + z_2 + \ldots + z_k$$

and

$$p = (1 - \theta z_1)(1 - \theta z_2)\ldots(1 - \theta z_k) \qquad (9)$$

The Craig & Sneyd scheme (2.4) reduces in the case of (2.6) to

$$U_n = S(z_0, z_1, \ldots, z_k) U_{n-1} \qquad (10)$$

with

$$S(z_0, z_1, \ldots, z_k) = 1 + \frac{z_o + z}{p} + \sigma\frac{z_0(z_0 + z)}{p^2} \qquad (11)$$

Finally, the Hundsdorfer & Verwer scheme (2.5) reduces, in the case of (2.6) to

$$U_n = T(z_0, z_1, \ldots, z_k)\, U_{n-1} \qquad (12)$$

with

$$T(z_0, z_1, \ldots, z_k) = 1 + 2\frac{z_0 + z}{p} - \frac{z_0 + z}{p^2} + \sigma\frac{z_0(z_0 + z)^2}{p^2} \qquad (13)$$

The iterations (2.7), (2.10), (2.12) are stable if

$$|R(z_0, z_1, \ldots, z_k)| \le 1 \qquad (14)$$

$$|S(z_0, z_1, \ldots, z_k)| \le 1 \qquad (15)$$

and

$$|T(z_0, z_1, \ldots, z_k)| \le 1 \qquad (16)$$

respectively.

Stability Of The Three ADI Schemes In The Application To Multi-Dimensional Convection-Diffusion Equations

In this section, the stability of the three schemes (3) - (5) when applied to the semi-discretized k-dimensional convection-diffusion equation

$$\frac{\partial u}{\partial t} = c \cdot \nabla u + \nabla \cdot (D \nabla u) \qquad (17)$$

is considered on a rectangular domain, suppleme-nted with initial and boundary conditions. Here c denotes a given convection vector and D is a given diffusion matrix, which is always assumed to be positive semi-definite. If D is positive definite, then (17) is parabolic. The main interest is in the general equation (17), where D is a full (non-diagonal) matrix and c is non-zero. Thus, both mixed derivative and convection terms which are presented (17). Multi-dimensional convection-diffusion equations of this kind arise in many applied areas, such as mathematical biology and financial mathematics. Also note that full matrices D arise when converting, by coordinate transformation, from convection-diffusion equations with diagonal

matrices D on non-rectangular domains to equations on rectangular domains.

The stability results derived in the paper for the three schemes (3)-(5) are primarily relevant to the two-dimensional case of (17), i.e., k = 2. These results for k = 2 however do represent a substantial improvement over known results existing in literature. Moreover, analysis covers the above three ADI schemes together with a large variety of spatial discretizations under one single umbrella.

The stability of (3) - (5) in the application to semi-discrete versions of (17) using the wellknown von Neumann method (Fourier transformation)shall be analysis and the usual assumption that c and D are constant and that the boundary condition for (17) is periodic are adopted. This leads to the conditions (14), (15) and (16), respectively, where each $z_j = \lambda_j \Delta t$ with λ_j an eigenvalue of the linear operator F_j that is obtained after semi-discretization.

The main interest in this paper is in unconditional stability, i.e., stability without any restriction on the time step $\Delta t > 0$. Inline with the von Neumann method, stability is always understood here to be with respect to the l_2-norm.

At present only few, partial results appear to be known in the literature concerning the application and the stability on the schemes (3)-(5) relevant to general convection-diffusion problems with mixed

Craig and Sneyd [1] performed a von Neumann stability analysis of the two schemes (3), (4) relevant to Eqs. (17) with c=0 and D a full matrix, i.e., no convection, only diffusion. The semi-discretization was done using standard, centered finite differencing and a splitting (2) was considered where F_0 contains all the discretized corss derivative terms and Fj , for $1 \le j \le k$ represents the discretized diffusion operator in the jth spatial direction. With these choices, it was proved in [1] that the Douglas scheme (3) is unconditionally stable whenever the parameter θ is sufficiently large, with a lower bound on θ that only depends on k, In particular, for k = 2 , unconditional stability of (3) was obtained whenever $\theta \ge ½$ (see also McKee and Mitchell [7] if $\theta = ½$). For the scheme (4), Craig and Sneyd [1] arrived at a similar result, under an additional condition on the parameter σ .In particular, for k =2, they showed that (4) is unconditionally stable whenever $\theta \ge \sigma \ge ½$.

The above, favorable, stability results are surprising in view of the fact that the F_0 part is integrated explicitly, whereas its scaled eigenvalues z_0, which lie on the real axis, range from large negative to large positive values .

McKee et al. (1970) examined the unconditio-nal stability of an equivalent version of the Douglas scheme (3) when applied to a standard finite difference discretization of (17) in the two-dimensional case (k = 2) with convection ($c \ne 0$) and a cross derivative term (D non-diagonal). The F_0 part in their case represents again the discretized cross derivate term. Next, F_j, for j = 1,2, contains the discretized first-and second-order derivatives in the jth spatial direction. The positive result was proved by McKee et al. that, in the presence of convection, unconditional stability of the Douglas scheme (3) is maintained whenever k = 2 and $\theta = ½$.

Hundsdorfer [4] considered general, necess-ary and sufficient, conditions on the z_j ($0 \le j \le k$) with regard to the stability requirement (14). It was proved in [4] that if $k \ge 2$, $\theta \ge ½$ and $z_0 = 0$, then (14) holds for all z_j ($1 \le j \le k$) lying in a wedge $\{ \zeta \in \mathbb{C} : |\arg(-\zeta)| \le \alpha \}$ if and only if the angle $\alpha \le \frac{1}{k-1}\frac{\pi}{2}$. In particular, if k= 2 and $\theta \ge ½$, the condition (14) is thus fulfilled whenever $\Re z_1, \Re z_2 \le 0$ and $z_0 = 0$, all conclusions about (14) are directly valid for the requirement (15) as well. Additional results on (14) under the assumption that z_0 belongs to the stability region of the forward Euler method, i.e $|1+z_0| \le 1$, were also derived in [4].

The above stability bound on the angle α was proved by Hundsdorfer [5] for a very general type of rational functions, including also (2.13) withe $z_0 = 0$. Correspondingly, it is not clear at present whether useful ADI splitting schemes exist that are unconditionally stable when applied to general (semi-discrete) convection-diffusion problems in dimension $k \ge 3$. We remark that in the case of pure diffusion problems, without convection, there is no such limitation on the dimension, cf. [1,3]. In the latter case all eigenvalues $z_0, z_1, ..., z_k$ are real.

The requirement (16) with $\sigma = ½$ was investigated numerically in Hundsdorfer [5]. The numerical experiments in [5] suggested that if k=2, $z_0=0$ and θ is larger than a certain threshold value, then (16) is fulfilled whenever $\Re z_1, \Re z_2 \le 0$. This conjecture was proved by Lanser et al (2001), with threshold value $\theta = \frac{1}{2} + \frac{1}{6}\sqrt{3}$. Additional numerical results regarding (16) were presented in [5] under the assumption that z_0 belongs to the stability region of the explicit improved Euler method, i.e., $|1 + z_0 + ½ z_0^2| \le 1$. In our application, however, z_0 represents the eigenvalues of the discretized cross derivative terms, which may lie anywhere along the real axis, and we shall need a different kind of condition on z_0 than $|1 + z_0 + ½ z_0^2| \le 1$, or $|1+z_0| \le 1$, to assess the stability of the three ADI schemes.

Conclusion

From now on our research work is continuing study for solving complicated engineering problems, namely chemical engineering problems because of the one read of our developing country.

References

[1] I.J.D.Craig, A.D. Sneyd, An alternating-direction implicit scheme for parabolic equations with mixed derivatives, Comput, Math. Appl. 16 (1988) 341-350

[2] J.Douglas, Alternating direction methods for three space variables, Numer. Math. 4(1962) 41-63.

[3] K.J. in't Hout, B.D. Welfert, Unconditional stability of ADI schemes applied to multi-dimensional diffusion equations with mixed derivative terms, in preparation.

[4] W.Hundsdorfer, Stability of approximate factorization with θ - methods, BIT 39(1999) 473-483.

[5] W. Hundsdorfer, Accuracy and stability of splitting with Stabilizing Corrections, Appl. Numer Math, 42 (2002) 213-233.

[6] W. Hundsdorfer, J.G Verwer, Numerical Solution of Time-Dependent Advection-Diffusion-Reaction Equations, Springer Ser. Comput. Math., vol. 33, Springer, Berlin, 2003.

[7] S. McKee, A. R. Mitchell, Alternating direction methods for parabolic equations in two space dimensions with a mixed derivative, Comput. J. 13 (1970) 81-86.

[8] A.R. Mitchell, D.F. Griffiths. The Finite Difference Method in Partial Differential Equations, Wiley, NewYork, 1980.

Some Stability Results of the Douglas Splitting Method for an Advection - Reaction Equation

Yu Yu Swe
Department of Engineering Mathematics,
Yangon Technological University
Yangon, Myanmar.

Abstract: In this paper, some stability results of the Douglas Splitting Method, which are useful in solving an advection- reaction equation, are presented.

Keywords: Numerical analysis, initial - boundary value problems, splitting methods, growth factor.

Introduction

The initial value problem for a system of ordinary differential equations

$$u'(t) = F(t, u(t)) \quad (1)$$

with $0 \le t \le T$ and given initial value $u(0)$ and then numerical schemes with step size h yielding approximations u_n to the exact solution $u(t_n)$ at time levels $t_n = nh$ for $n = 0,1,2, \ldots$, starting with $u_0 = u(0)$ are considered.

For problems that arise by spatial discretization of multi-dimensional partial differential equations it is often possible to decompose the function F into a number of simpler component functions,

$$F(t,\omega) = F_1(t,\omega) + F_2(t,\omega) + \ldots + F_s(t,\omega). \quad (2)$$

Splitting methods use this decomposition by treating in each stage at most one of the components implicitly. The best known method of this type is the ADI-Peaceman-Rachford method, but this method can only deal with 2-component splittings. In this paper the related second-order method of Douglas [1], known as the method of Stabilizing Corrections:

$$\begin{aligned} v_0 &= u_n + hF(t_n, u_n), \\ v_i &= v_{i-1} + \tfrac{1}{2}h\,(F_i(t_{n+1}, v_i) - F_i(t_n, u_n)) \\ &(i = 1, 2, \ldots, s), \\ u_{n+1} &= v_s, \end{aligned} \quad (3)$$

with internal vectors v_i is considered.

A big advantage of (3) over many other splitting methods[1,2] is that all internal vectors v_i are consistent approximations to the exact solution, namely at time t_{n+1}. Consequently a steady state $F(u) = 0$, with F independent of t, is a stationary point of the scheme (3).

Some stability results for the scalar complex test equation is presented where

$$Fj(t,\omega) = \lambda_j \omega \quad (4)$$

with $\lambda_j \in \mathbb{C}$. In applications for partial differential equations the λ_j will represent eigenvalues for the various components, found by inserting Fourier modes. Let $z_j = h\lambda_j$. For the test equation the method reduces to

$$u_{n+1} = Ru_n \quad (5)$$

with growth factor

$$R = 1 + \Big(\prod_{j=1}^{s}(1-\frac{1}{2}z_j)\Big)^{-1}\sum_{j=1}^{s} z_j. \quad (6)$$

And this R corresponds to the stability function for standard one-step methods. Ideally, one would have $|R| \le 1$ for arbitrary λ_j in the left half-plane $\mathbb{C}^-$ without restriction on the time step. For R given by (6), this is not true if $s \ge 3$. $|R| \le 1$ when all z_j are real and negative (unconditional stability for purely parabolic equations) [3]. On the other hand, if $s \ge 3$ and all $z_j = iy$ then $|R| > 1$ for any $y \ne 0$ (unconditional instability for purely hyperbolic equations) [5]. In this paper one of the theorems for some stability results which are applicable to advection-diffusion and advection-reaction equations are presented.

Theorem

Let $R = 1 + \Big(\prod_{j=1}^{s}(1-\frac{1}{2}z_j)\Big)^{-1}\sum_{j=1}^{s} z_j$ be the growth factor with $s \ge 2$. Then

$$|R| \le 1 \text{ for all } z_j \in W_\alpha \Leftrightarrow \alpha \le \frac{1}{s-1}\frac{\pi}{2},$$

where the wedge ay

$$W_\alpha = \{\zeta \in \mathbb{C} : |\arg(-\zeta)| \le \alpha\}$$

in the left half-plane.

Proof of Theorem

Let $\xi = R-1$ and $\eta = -\Big|\sum_j z_j\Big|^2 (\frac{1}{\xi} + \frac{1}{2})$.

Where all summations will be from 1 to s, unless indicated otherwise.

Correponding Author : Yu Yu Swe Ph.D candidate, Engineering Maths 11th batch, Department of Engineering Mathematics, Yangon Technological University, Yangon, Myanmar.

Clearly $|R| \le 1$ is equivalent with the following

$$|1+\xi| \le 1 \Leftrightarrow \mathrm{Re}\,\frac{1}{\xi} \le -\frac{1}{2} \Leftrightarrow \mathrm{Re}\,\eta \ge 0.$$

By some calculations it is seen that

$$\eta = -(\sum_j \bar{z}_j)(1+(-\frac{1}{2})^2 \sum_{j<k} z_j z_k + (-\frac{1}{2})^3 \sum_{j<k<l} z_j z_k z_l + \ldots + (-\frac{1}{2})^s z_1 z_2 \ldots z_s). \quad (7)$$

By considering z_j on the boundary of W_α the statement of the theorem can be verified as follows.

Let $t_j \ge 0$ be arbitrary, $0 \le q \le \frac{1}{2}s$ and

$z_j = -e^{i\alpha} t_j$ $(1 \le j \le s - q)$,
$z_j = -e^{-i\alpha} t_j$ $(s - q < j \le s)$.
If q = 0,

$$\eta = (e^{-i\alpha} \sum_j t_j)(1 + (\frac{1}{2})^2 e^{2i\alpha} \sum_{j<k} t_j t_k + \ldots + (\frac{1}{2})^s e^{si\alpha} t_1 t_2 \ldots t_s)$$

and

$$\mathrm{Re}\ \eta = (\sum_j t_j)(\cos(\alpha) + (\frac{1}{2})^2 \cos(\alpha) \sum_{j<k} t_j t_k + \ldots + (\frac{1}{2})^s \cos((s-1)\alpha) t_1 t_2 \ldots t_s).$$

It follows that Re $\eta \ge 0$ for all $t_j \ge 0$ if and only if $\cos(k\alpha) \ge 0$ $(k = 1, 2, \ldots, s-1)$, that is,

$$(s-1)\,\alpha \le \frac{\pi}{2} \quad (8)$$

Next, suppose that q = 1. Then from Equation (7)

$$\eta = (\sum_{j<s} e^{-i\alpha} t_j + e^{i\alpha} t_s)(\sum_{k=0}^{s=1} p_k e^{ik\alpha}).$$

with $p_k \ge 0$ depending on the t_j. The actual expressions easily follow from (7). In particular

$$p_{s-1} = (\frac{1}{2})^{s-1} t_1 t_2 \ldots t_{s-1},$$

$$p_{s-3} \ge (\frac{1}{2})^{s-1} t_1 t_2 \ldots t_{s-1}, (\frac{1}{t_1} + \frac{1}{t_2} + \ldots + \frac{1}{t_{s-1}}) t_s .$$

Assuming (8), it follows that

$$\mathrm{Re}\ \eta \ge (\frac{1}{2})^{s-1} \cos(s\alpha) t_1 t_2 \ldots t_s + (\frac{1}{2})^{s-1} (s-1) \cos((s-4)\alpha) t_1 t_2 \ldots t_s.$$

Further more, equation (8) implies cos (sα) + (s-1) cos ((s-4) α) ≥ 0. Hence, also for this case q = 1, it can be seen that Equation (8) implies $|R| \le 1$.

Finally, suppose that q ≥ 2. Then

$$\eta = (\sum_{j \le s-q} e^{-i\alpha} t_j + \sum_{j>s-q} e^{i\alpha} t_j)(\sum_{k=-q}^{s-q} q_k e^{ik\alpha})$$

with $q_k \ge 0$. Therefore, Re η is a sum of cos (kα) terms with $-(q+1) \le k \le s-q+1$ and nonnegative coefficients, and again it follows that Equation (8) is sufficient to have $|R| \le 1$.

Remark

If s = 3 and z_j = iy for j = 1, 2, 3, then Re $\eta = -\frac{3}{8} y^4 < 0$ for any y ≠ 0. Hence, for any C > 0, max $\{|R| : z_j = iy_j,\ |y_j| \le C\} > 1$. This instability results was already obtained by Warming and Beam [5] for a class of multistep spitting methods, containing the Douglas method as a special case.

Theorem

Let $R = 1 + (\prod_{j=1}^{s} (1 - \frac{1}{2} z_j))^{-1} \sum_{j=1}^{s} z_j$, and let $1 \le r \le s-1$. Then $|R| \le 1$ for arbitrary $z_1, \ldots, z_{s-\Upsilon} \in W_\beta, z_{s-\gamma+1}, \ldots, z_s < 0 \Leftrightarrow \beta \le \frac{1}{s-r}\frac{\pi}{2}$.

Proof of Theorem

First, one of the case is considered where one of the z_k is real and negative, say $z_s < 0$. The other z_j are assumed to lie in the wedge W_β. It will be shown that

$$(s-1)\beta \le \frac{\pi}{2} \quad (9)$$

is necessary to guarantee that $|R| \le 1$ if $z_s \to -\infty$. By Theorem from section 2, it can already be known is a sufficient condition for arbitrary $z_s < 0$.

In the limit $z_s \to -\infty$ we have $R \to S$ with

$$S = 1 - 2(\prod_{j<s} (1 - \frac{1}{2} z_j))^{-1}.$$

It is easily seen that $|S| \le 1$ is equivalent with

$$\mathrm{Re} \prod_{j<s} (1 - \frac{1}{2} z_j) \ge 1.$$

Take $z_j = -e^{i\beta} t_j \ (1 \le j \le s-1)$ with $t_j > 0$. Then

$$\text{Re} \prod_{j<s} (1-\frac{1}{2} z_j) =$$

$$\text{Re}\ (1+(-\frac{1}{2})\sum_{j<s} z_j + (-\frac{1}{2})^2 \sum_{j<k<s} z_j z_k + \ldots + (-\frac{1}{2})^{s-1} z_1 z_2 \ldots z_{s-1}) =$$

$$= 1 + \frac{1}{2}\cos(\beta) \sum_{j<s} t_j + (\frac{1}{2})^2 \cos(2\beta)$$

$$\sum_{j<k<s} t_j t_k + \ldots + (\frac{1}{2})^{s-1} \cos((s-1)\beta) t_1 t_2 \ldots t_{s-1}.$$

Thus it can be seen that (9) is necessary if $t_1, \ldots, t_{s-1}$ are sufficiently large.

Next the general situation $z_1, \ldots, z_{s-\Upsilon} \in w_\beta, z_{s-r+1}, \ldots, z_s < 0$ with $1 \le r \le s-1$ is considered. Then the result

$$(s-r)\beta \le \frac{\pi}{2} \qquad (10)$$

is a necessary and sufficient condition for $|R| \le 1$ must be shown.

Note that R is fractional linear in all z_j with denominator $1-\frac{1}{2} z_j$. Considering fixed $z_1, \ldots, z_{s-\Upsilon}$, it follows that

$$|R| \le 1 \text{ for all } z_{s-\Upsilon+1}, \ldots z_s < 0$$

if this holds for $z_{s-\Upsilon+1}, \ldots, z_s$ equal to 0 or ∞. This amounts to verification of the two inequalities

$$\left| 1 + \left(\prod_{j \le s-\Upsilon} (1-\frac{1}{2} z_j) \right)^{-1} \sum_{j \le s-\Upsilon} z_j \right| \le 1,$$

$$\left| 1 - 2 \left(\prod_{j \le s-\Upsilon} (1-\frac{1}{2} z_j) \right)^{-1} \right| \le 1.$$

From the above results, with $s-r$ replacing s and s-1, respectively, it follows that this will be satisfied for arbitrary $z_z, \ldots, z_{s-\Upsilon} \in w_\beta$ if and only if (10) holds.

Conclusion

We are now studying to compare the trapezoidal rule and implicit midpoint rule with the splitting methods which make of the method of fractional steps of Yanenko (the late famous Russian professor) and then we will continuous our research work using these methods of splitting, to solve the non-linear for convection-diffusion problems.

REFERENCES

[1] A.R.Mitchell, D.F.Griffiths , The Finite Difference Method in Partial Differential Equations. John Wiley & Sons, Chichester, 1980.

[2] G.I.Marchuk, Splitting and alternating direction methods. Handbook of Numerical Analysis 2(P.G.Ciarlet.J.L.Lioms,eds.), North-Holland, Amsterdam, pp.197-462, 1990.

[3] J. Douglas, Alternating direction Method for three space variables. Numer. Math. 4, pp. 41-63 (1962).

[4] N.N.Yanenko, The Method of Fractional steps. Springer verlag, Berlin, 1971.

[5] R.F. Warming, R.M. Beam, An extension of A-stability to alternating direction methods. BIT 19, pp-395-417 (1979).

[6] W.Hundsdorfer, Trapezoida and midpoint splittings for initial-boundary value problems. CWI Report, 1996.

Traveling Wave Solutions of a Dental-Plaque Model with Nonlinear Sorption

Patarawadee Prasertsang[1] , Valipuram S. Manoranjan[2] and Yongwimon Lenbury[1]

[1] Department of Mathematics, Faculty of Science, Mahidol University, Bangkok, 10400.

[2] Department of Pure and applied Mathematics, Washington State University, Pullman, WA 99167-3133, U.S.A.

Email: kai_patty@hotmail.com

Abstract: We investigate the diffusion behavior of substrate on teeth leading to dental plaques. The sorption of any substrate concentration on teeth, which we model as a nonlinear process, activates the plague formation. Specifically, the extent of dental plaque depends on individual features of a tooth. We have been able to show that it is possible to obtain the exact solution of this model by using travelling wave coordinate where the wave is assumed to be moving at a constant speed.

1. Introduction

In this study, we focus on the extent of the dental plaque where biofilm behaves as a porous system while the bacteria act as reactors and the sorption of the substrate concentration on teeth is activated independent of the types of substrate. Moreover, we show that under certain conditions, it is possible to obtain the exact closed form travelling wave solutions of a nonlinear dental plaque model.

2. Mathematical Model

We consider the following dental plaque model which we have modified from that in [1]:

$$\frac{\partial C_m}{\partial t} = D\frac{\partial^2 C_m}{\partial x^2} - \alpha\frac{\partial C_i}{\partial t} - \delta\frac{\partial C_m}{\partial x} \tag{1}$$

$$\frac{\partial C_i}{\partial t} = \beta C m^{1/2} - \gamma C_i, \tag{2}$$

where C_m and C_i are the mobile and immobile concentrations of the solute in the aqueous phase and absorbed phase, respectively. Further, D is the diffusion constant, α is a constant related to rate of change of C_i in time, δ is convection coefficient such that $\delta \geq 6\times 10^{-5}$, β is reaction rate constant, and is a constant related to C_i.

We study this model which is given by (1) and (2) on the real line for $t > 0$ when zero asymptotic condition is assumed to eliminate the constant of integration.

If the rate of change of C_i is very small when *t* tends to infinity (i.e, $\frac{\partial C_i}{\partial t} = 0$), (2) yields $C_i = \frac{\beta}{\gamma} C_m^{\frac{1}{2}}$. Then, we can reduce (1) as in [2].

Before proceeding further, we transform [3] Eqs. (1) and (2) to the following form:

$$\frac{\partial C_m}{\partial t} = \frac{\partial^2 C_m}{\partial \bar{x}^2} - \frac{\partial \bar{C}_i}{\partial t} - \delta_2\frac{\partial C_m}{\partial \bar{x}}$$

$$\frac{\partial \bar{C}_i}{\partial t} = \beta_2 C m^{1/2} - \bar{C}_i$$

by appropriate changes of variables. We then introduce the traveling wave coordinate $z = \bar{x} - vt$ [4,5] , the wave being assumed to be moving at a constant speed. Then, we have a single second-order differential equation in C_m ,

$$vC_m'' + (v^2 - \delta_2 v - 1)C_m' + (\delta_2 - v)C_m - \beta_2 v C_m^{\frac{1}{2}} = 0 \tag{3}$$

We then solve this equation to obtain the exact solution to this model by letting $C_m' = aC_m + bC_m^{\frac{3}{4}}$ be the solution of (3), where *a* and *b* are not equal to zero and *n* is a positive integer.

Corresponding Author: Patarawadee Prasertsang , Department of Mathematics, Faculty of Science, Mahidol University, Bangkok, 10400

3. Results

We obtain the exact solution for this model system as,

$$C_m(x,t)=\left(\frac{b}{a}\right)^4\left(e^{\frac{a}{4}\left(\sqrt{\frac{\gamma}{D}}x-\gamma vt\right)}-1\right)^4 \tag{4}$$

$$C_i(x,t)=-\frac{\beta b^2}{\gamma v a^2}\left[\frac{2v}{av-2}e^{\frac{a}{2}\left(\sqrt{\frac{\gamma}{D}}x-\gamma vt\right)}-\frac{8v}{av-4}e^{\frac{a}{4}\left(\sqrt{\frac{\gamma}{D}}x-\gamma vt\right)}-v\right]-\frac{\beta b^2 v^2}{\gamma(av-2)(av-4)}e^{\frac{1}{v}\left(\sqrt{\frac{\gamma}{D}}x-\gamma vt\right)} \tag{5}$$

Here, for i = 1,2,3,4,

$$v_i=\frac{\delta}{2\sqrt{\gamma D}}\pm\sqrt{\frac{\delta^2}{4\gamma D}-\frac{3}{4}},\frac{\delta}{2\sqrt{\gamma D}}\pm\sqrt{\frac{\delta^2}{4\gamma D}-\frac{4}{3}}$$

$$a_i=-\frac{4}{7v_i}\left(v_i^2-\frac{\delta}{\sqrt{\gamma D}}v_i-1\right) \tag{6}$$

$$b=\pm\sqrt{\frac{4\alpha\beta}{3\gamma}}$$

In figures 1-2, we show the plots of the mobile and immobile concentrations with $\alpha=\gamma=1,\ D=6\times10^{-10},\delta=6\times10^{-5},\beta=10^{-7}$, and v = 2.09077, as functions of $\bar{x}$ as t changes from 0 to 20.

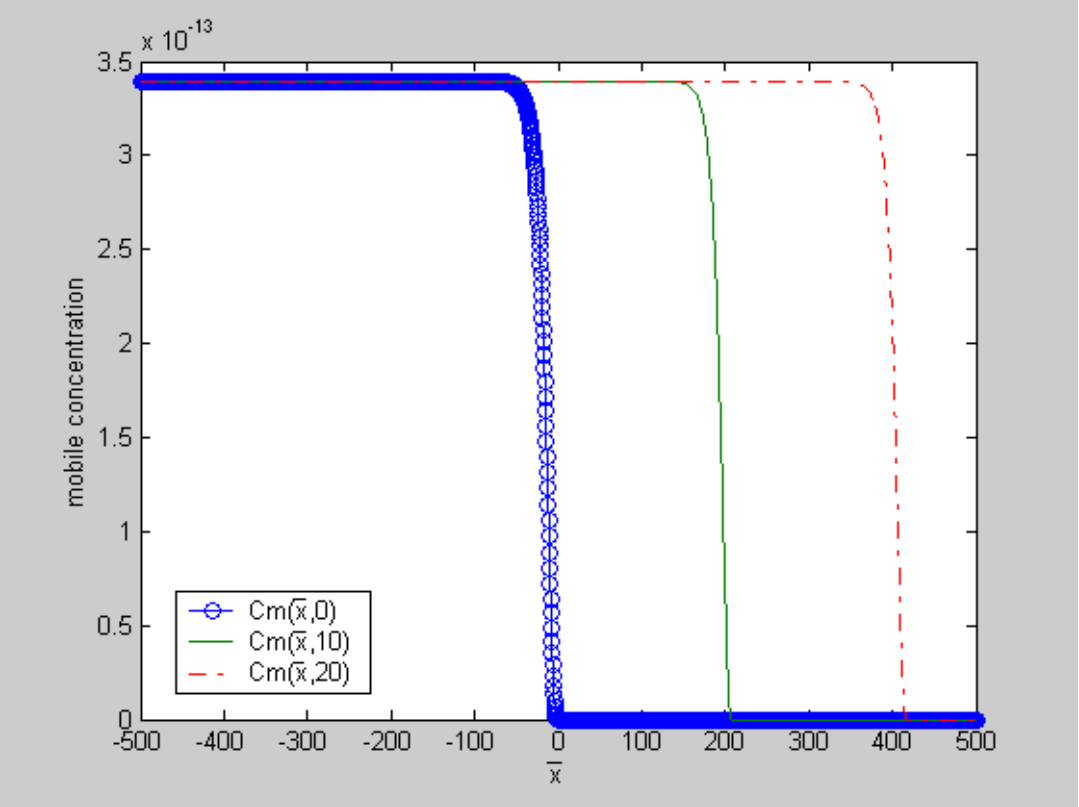

Figure 1. The mobile concentration waves at time $t = 0$ (left most), $t = 10$ and $t = 20$ (right most) at a constant speed is 2.09077.

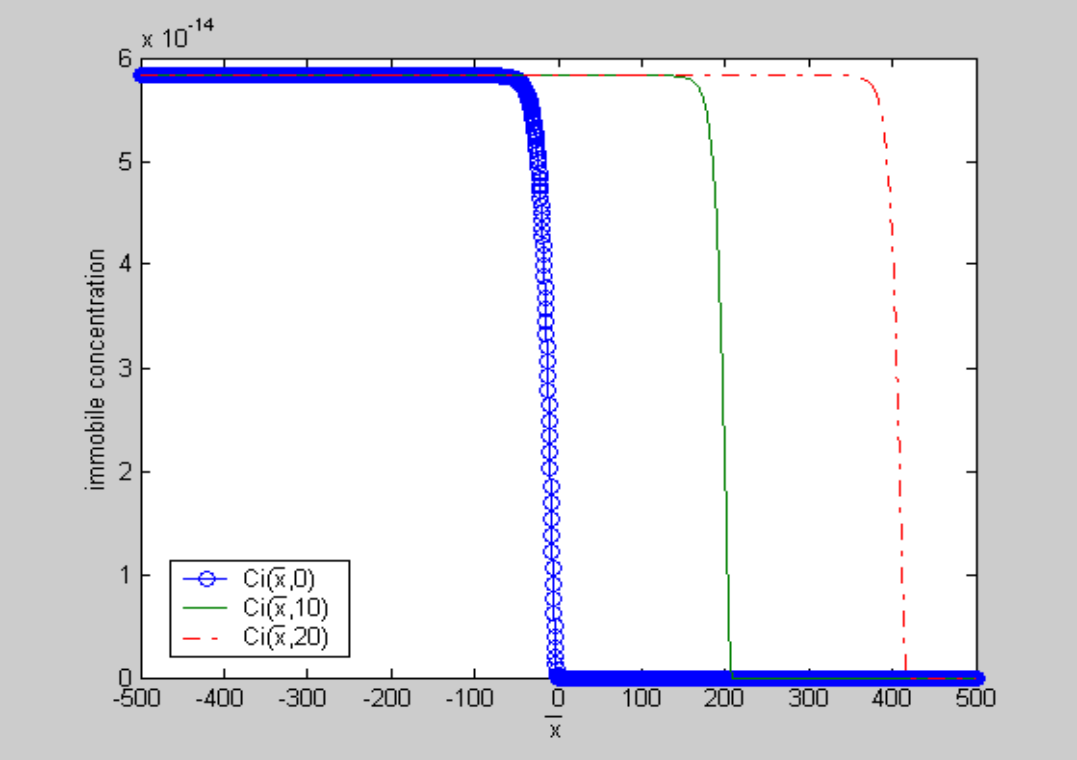

Figure 2. The immobile concentration waves at time $t = 0$ (left most) , $t = 10$ and $t = 20$ (right most) at a constant speed is 2.09077.

4. Conclusion

In this work, we have shown that the exact solution can be found for a dental plaque model with appropriate nonlinear sorption term and in figures 1-2 , we can see that the dental plaque is increasing (as t tends to infinity) while the wave of the solute concentration is moving at a constant speed.

Acknowledgements: Appreciations are extended toward the Commission on Higher Education , Department of Mathematics, Mahidol University, Department of Pure and Applied Mathematics, Washington State University, USA, and the National Center for Genetic Engineering and Biotechnology.

References

[1] Lewandowska, K.D. and Kosztolowicz, T., Perturbation method to model enamel caries progress, cond-mat., pp.1-8,(2007).

[2] Dibdin, G.H., Mathematical modeling of biofilms, Adv. Dent. Res., 11(1),127-132,(1997).

[3] Manoranjan,V.S. and Stauffer, T.B., Exact solution for contraminant transport with kinetic Langmuir sorption, 32 No. 3, 749-752.

[4] Chang,C.M. and Manoranjan,V.S., Travelling wave solutions of contraminant transport model with nonlinear sorption, Mathl. Comput. Modelling, 28 No.9, pp.1-10,(1998).

[5] Gomez,M.O., Chang,C.M. and Manoranjan,V.S., Exact solution for contraminant transport model with nonlinear sorption, Appl. Math. Lett., 9(1),83-87,(1996).

Application of Singular Perturbation Technique to a Model Skeletal Muscle in Myotonia and Periodic Paralysis Incorporating Membrane Potential Dynamics

Kamonwan Kocharoen[1], Jonathan Bell[2] And Yongwimon Lenbury[1]
[1]Department of Mathematics, Faculty of Science, Mahidol University,Rama 6 Rd., Bangkok, Thailand
[2]Department of Mathematics and Statistics, University of Maryland, Baltimore County, USA

Abstract: It has been discovered that malfunction in the voltage-gated sodium channels can cause abnormalities of skeletal muscle in the form of myotonia and periodic paralysis. This research considers the channel behavior in terms of the dynamics of membrane potentials. We have modified the Hodgkin Huxley model (Hodgkin and Huxley, 1952) by reformulation of the sodium current term. A stability analysis of the model system consisting of rate equations on the membrane potentials and the probability of gates activation is carried out. Using the singular perturbation method, the existence of limit cycles will be examined. We also derive conditions on the system parameters under which the model exhibits various dynamic behavior found in clinical observations.

Key words: Skeletal muscle model, slow-fast oscillations, myotonia, periodic paralysis

INTRODUCTION

This research investigates the qualitative behavior of a model for skeletal muscles to understand the mechanism whereby the alterations in the voltage-gated non-inactivating sodium channels cause myotonia and periodic paralysis. The Hodgkin Huxley model [3] is reformulated by changing of the sodium current term. The surface membrane potential has been observed to have very fast dynamics while the T-tubule membrane potential has the slowest dynamics. The probability of activation gates of the surface membrane potassium channels to be open is assumed to have intermediate dynamics. In such a situation of highly diversified dynamics, the model may be analyzed by the singular perturbation technique. The conditions under which of the model exhibits different dynamic behavior that resembles clinical observations are derived by considering the paths of solution trajectories on the system's equilibrium manifolds in various shapes and locations

A SKELETAL MUSCLE MODEL

The model proposed by Cannon and co-workers in [2] consists of surface and T-tubule membrane compartments. They assumed that the fiber is space-clamped such that all points of the surface membrane and T-tubule membrane are at the same potential. This property means that the entire T-tubule is attached to a unit area of the surface membrane. Disorder can arise from a loss of function in the inactivation of the sodium channels. They modified the model by changing

$$C_M \frac{dv}{dt} = I_m - g_l(v-E_l) - \bar{g}_{Na} m_\infty^3(v) f_{cd}(v-E_{Na}) - \bar{g}_K n^4(v-E_K) - g_a(v-w) \quad (1)$$

$$\frac{dn}{dt} = \alpha_n(v)(1-n) - \beta_n(v)n \quad (2)$$

$$C_M \frac{dw}{dt} = g_b(v-w) - \eta_K \bar{g}_K r_\infty^4(w)(w-E_K) - \eta_l g_l(w-E_l) - \eta_{Na} \bar{g}_{Na} m_\infty^3(w) f_{cd}(w-E_{Na}) \quad (3)$$

the sodium current term. Letting f_{cd}, $0 \le f_{cd} \le 1$, be the fractional proportion of non-inactivating sodium channels, the full model is the eight-dimensional system of ordinary differential equations [2]. Under the observations made by Cannon et al. in [1], the system reduces to

where v is the surface membrane potential (mV), w is the T-tubular membrane potential (mV), n is the probability of activation gates of surface membrane potassium channels to be open, C_M is the capacitance ($\mu F/cm^2$), $\bar{g}_{Na}$ is the maximal sodium conductance (mS/cm^2), $\bar{g}_K$ is the maximal potassium conductance (mS/cm^2), g_l is the leak conductance (mS/cm^2), E_l, E_{Na} and E_K are the reverse potentials of the surface membrane (mV), E_l, E_{Na} and E_K are the reverse

Corresponding Author: Yongwimon Lenbury, Department of Mathematics, Faculty of Science, Mahidol University, Rama 6 Rd., Bangkok, Thailand

potentials in T-tubular membrane (mV), I_m is the external applied current ($\mu A/cm^2$), $g_a = \frac{1000}{R_a}$, and $g_b = \frac{g_a}{\gamma}$. R_a is an access resistance at the vestibule of the tubule (Ωcm^2), $\eta_l = 0.5$, $\eta_{Na} = 0.1$ and $\eta_K = 0.4$ are the ratios of T-tubular to surface membrane channels, $\gamma = 4.8$ is the ratio of the T-tubular membrane area/unit area of surface membrane,

$$m_\infty(x) = \frac{\alpha_m(x)}{\alpha_m(x)+\beta_m(x)};\ x = v,w$$

$$\alpha_m(x) = \frac{\bar{\alpha}_m(x-\bar{V}_m)}{1-e^{-(x-\bar{V}_m)/K_{\alpha_m}}},\ \beta_m(x) = \bar{\beta}_m e^{-(x-\bar{V}_m)/K_{\beta_m}},,$$

$$\alpha_n(v) = \frac{\bar{\alpha}_n(v-\bar{V}_n)}{1-e^{-(v-\bar{V}_n)/K_{\alpha_n}}}, \beta_n(v) = \bar{\beta}_n e^{-(v-\bar{V}_n)/K_{\beta_n}},.$$

$$r_\infty(w) = \frac{\alpha_n(w)}{\alpha_n(w)+\beta_n(w)},$$

$$\alpha_n(w) = \frac{\bar{\alpha}_n(w-\bar{V}_n)}{1-e^{-(w-\bar{V}_n)/K_{\alpha_n}}},\ \beta_n(w) = \bar{\beta}_n e^{-(w-\bar{V}_n)/K_{\beta_n}}.$$

The values of the parameters in these expressions, representative of mammalian muscles, either of rats or human, were reported by Cannon *et al.* in 1993 [1].

SINGULAR PERTURBATION ANALYSIS

In order to carry out a singular perturbation analysis on (1) – (3), we introduce small scaling factors ε and δ by letting $\alpha_n = \frac{\alpha_n}{\varepsilon}$, $\beta_n = \frac{\beta_n}{\varepsilon}$, $g_b = \varepsilon\delta g_b$, $\eta_l = \varepsilon\delta\eta_l$, $\eta_{Na} = \varepsilon\delta\eta_{Na}$, and $\eta_K = \varepsilon\delta\eta_K$. The model system (1) – (3) can then be written as

$$\frac{dv}{dt} = F(v,n,w) \tag{4}$$

$$\frac{dn}{dt} = \varepsilon G(v,n,w) \tag{5}$$

$$\frac{dw}{dt} = \varepsilon\delta H(v,n,w) \tag{6}$$

where

$$F(v,n,w) = \frac{1}{C_M}\{I_m - g_l(v-E_l) - \bar{g}_{Na}m_\infty^3(v)f_{cd}(v-E_{Na}) - \bar{g}_K n^4(v-E_K) - g_a(v-w)\}$$

$$G(v,n,w) = \alpha_n(v)(1-n) - \beta_n(v)n$$

$$H(v,n,w) = \frac{-1}{C_M}\{\eta_l g_l(w-\bar{E}_l) + \eta_{Na}\bar{g}_{Na}m_\infty^3(w)f_{cd}(w-\bar{E}_{Na}) \eta_K\bar{g}_K r_\infty^4(w)(w-\bar{E}_K) + g_b(w-v)\}$$

Thus, when f_1, f_2, and f_3 are finite and nonzero, $\left|\frac{dv}{dt}\right| = O(1)$, $\left|\frac{dn}{dt}\right| = O(\varepsilon)$, and $\left|\frac{dw}{dt}\right| = \varepsilon\delta$ so that, for small ε and δ, v has the fastest dynamics, n the intermediate, and w the slowest amongst the three state variables, as has been observed in [1].

Then, for sufficiently small values of ε and δ, the solution of the system can be approximated by a sequence of simple dynamic transitions occurring at different speeds. First, for appropriate parametric values, the fast manifold

$$F(v,n,w) = 0 \tag{7}$$

is shaped as shown in Fig. 2. Solving equation (7), the fast system has an equilibrium manifold where $\frac{dv}{dt} = 0$ given by

$$n = \left\{\frac{I_m - g_l(v-E_l) - \bar{g}_{Na}m_\infty^3(v)f_{cd}(v-E_{Na}) - g_a(v-w)}{\bar{g}_K(v-E_K)}\right\}^{\frac{1}{4}} \equiv n_1(v,w) \tag{8}$$

The intermediate manifold

$$G(v,n) = 0 \tag{9}$$

yields

$$n = \frac{\alpha_n(v)}{\alpha_n(v)+\beta_n(v)} \equiv n_2(v) \tag{10}$$

The slow manifold

$$H(v,n) = 0 \tag{11}$$

or equivalently

$$v = n_3(w) \equiv w - \frac{-1}{g_b C_M}\{\eta_{Na}\bar{g}_{Na}m_\infty^3(w_s)f_{cd}(w_s-E_{Na}) + \eta_K\bar{g}_K r_\infty^4(w_s)(w_s-\bar{E}_K) + \eta_l g_l(w_s-\bar{E}_l)\},$$

intersects the curve $F(v,n_2(v),w) = 0$ at the equilibrium point (v_s, n_s, w_s). That is, we have

$$F(v_s,n_s,w_s) = 0 \tag{12}$$

$$G(v_s,n_s) = 0 \tag{13}$$

$$H(v_s,w_s) = 0 \tag{14}$$

To ensure that the line where $G = 0$ intersects the (n, w)-plane lies entirely above the relative maxima on the surface $F = 0$, or $n = n_1(v,w)$, we also assume that

$$n_2(0) > n_1(v_M, 0) \tag{15}$$

where v_M is the value of v at the relative maximum point of $n = n_1(v,0)$, $n_1(v,0)$ being increasing with w.

There are then three cases of interest, the equilibrium manifolds and solution trajectories in each of which are shown in Figure 1.

Case I : The curve $F = G = 0$ lies in the region where the manifold $F = 0$ is stable for all w in the region of interest. Since $w < 0$ in the entire region of interest, considering $n_1(v,w)$ in (8), we see that $n_1(v,0) > n_1(v,w)$ forall $w < 0$. The shapes and relative positions of the equilibrium manifolds will therefore be as depicted in Fig. 1a) if the following inequalities hold:

$$n_2(v_m) > n_1(v_m,0), \tag{16}$$

$$n_2(v_M) > n_1(v_M,0), \tag{17}$$

$$\frac{\partial n_1(v_s,w_s)}{\partial v} < 0, \tag{18}$$

and

$$\frac{\partial^2 n_1(v_s,w_s)}{\partial v^2} > 0 \tag{19}$$

where v_m and v_M are, respectively, the values of v at the relative minimum and relative maximum points of $n = n_1(v,0)$ as seen in Fig. 1.

Case II : The curve $F = G = 0$ lies in the region where the manifold $F = 0$ is unstable for all w in an open interval $I = (w_s - \delta, w_s + \delta)$ for some $\delta > 0$. The shapes and relative positions of the equilibrium manifolds will be as depicted in Fig. 1b) if the following inequalities (18), (20) are satisfied, and

$$\frac{\partial n_1(v_s,w_s)}{\partial v} > 0. \tag{20}$$

Case III : The curve $F = G = 0$ lies in the region where the manifold $F = 0$ is unstable for $w < \underline{w}$ and passes to the region where the manifold $F = 0$ is stable for $w > \underline{w}$, for some $\underline{w} < w_s < 0$. The shapes and relative positions of the equilibrium manifolds will be as depicted in Fig. 1c) if (15), (17)-(19) hold and

$$n_2(v_m) < n_1(v_m,0). \tag{21}$$

RESULTS AND DISCUSSION

Computer simulations of the model system with parametric values chosen to satisfy the conditions that characterize each of the three cases discussed in the previous section are shown in Figure 2. As theoretically predicted, the trajectory approaches the stable steady state as time passes in Fig. 2a) which corresponds to Case I. It tends to a limit cycle in Fig. 2b) which corresponds to Case II, and a damped oscillation is seen in Case III in Fig 2c). The common parametric values utilized here are those reported in [2], except for those parameters that elicit different dynamic behavior from the model, such as f_{cd}, and E_l, or I_m. In all computer simulations discussed here, $\gamma = 4.8$, $g_a = 6.7$, $g_l = 0.75$, $\bar{g}_{Na} = 150$, $\bar{g}_K = 21.6$, $\eta_l = 0.5$, $\eta_{Na} = 0.1$, $\eta_K = 0.42$, $E_l = -85.032$, $E_{Na} = 46.5839$, $E_K = -93.127$, $\bar{E}_{Na} = 46.5839$, $\bar{E}_K = -93.127$, $\bar{E}_l = -76.3144$, $\alpha_m = 0.288$, $\alpha_h = 0.0081$, $\alpha_n = 0.0131$, $\beta_m = 1.38$, $\beta_h = 4.38$, $\beta_n = 0.067$, $\bar{V}_m = -46$, $\bar{V}_h = -45$, $\bar{V}_n = -40$, $K_{\alpha m} = 10$, $K_{\alpha h} = 14.7$, $K_{\alpha n} = 9$ $K_{\beta m} = 18$, $K_{\beta h} = 9$, and $K_{\beta n} = 40$. Here, $\varepsilon = \delta = 1.0$, which means that the traced transitions give good approximation to the exact solution trajectory even when ε and δ need not be so small.

CONCLUSION

The dynamical behavior of a skeletal muscles model, composed of the membrane potentials and the probability function connected to the opening of the potassium channels activation gates, are discussed in this study. The analysis of system is carried out using the singular perturbation technique. The conditions under which were classified on three state variables the solution trajectories exhibit different dynamic behavior have been derived, which can potentially be linked to various as pathological situations of interest.

ACKNOWLEDGEMENT

This research work is partially supported by the National Center for Genetic Engineering and Biotechnology, the Faculty of Graduate Studies, Mahidol University and the Staff Development Project of the Commission on Higher Education.

REFERENCES

1. Cannon, S.C., 1996. Ion-channel defects and aberrant excitability in myotonia and periodic paralysis, Trends Neurosci. 19:3-10.
2. Cannon, S.C., Brown R.H., Corey D.P., 1993. Theoretical Reconstruction of Myotonia and Paralysis Caused by Incomplete Inactivation of Sodium Channels, Biophys.J. 65:270-288.
3. Hodgkin, A.L., Huxley, A. F., 1952. A Quantitative description of membrane current and its application to conduction and excitation in nerve, J. Physiol. 117:500-544.

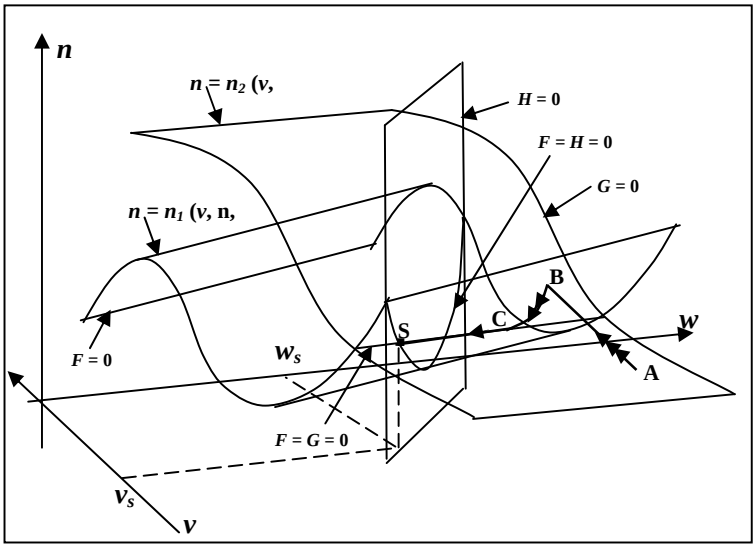
n
n = n2 (v,
H = 0
F = H = 0
G = 0
n = n1 (v, n,
B
C
S
w
F = 0
ws
A
F = G = 0
vs
v

1a)

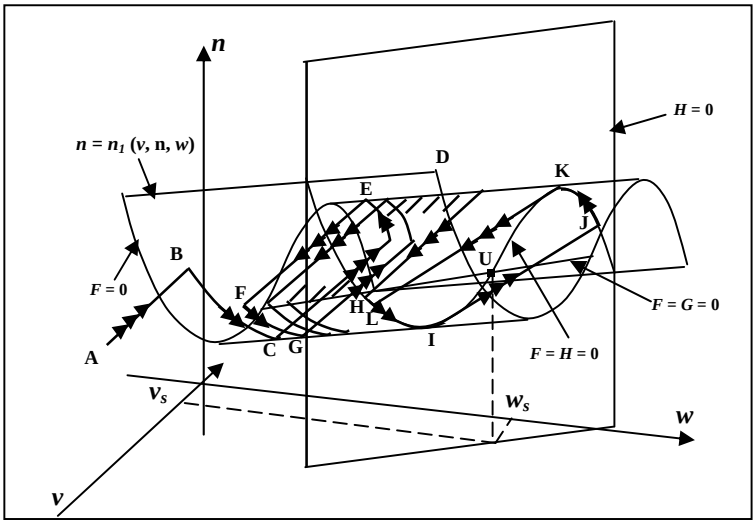
n
H = 0
n = n1 (v, n, w)
D
K
E
J
B
U
F = 0
F
H
F = G = 0
L
C
G
I
A
F = H = 0
vs
ws
w
v

1b)

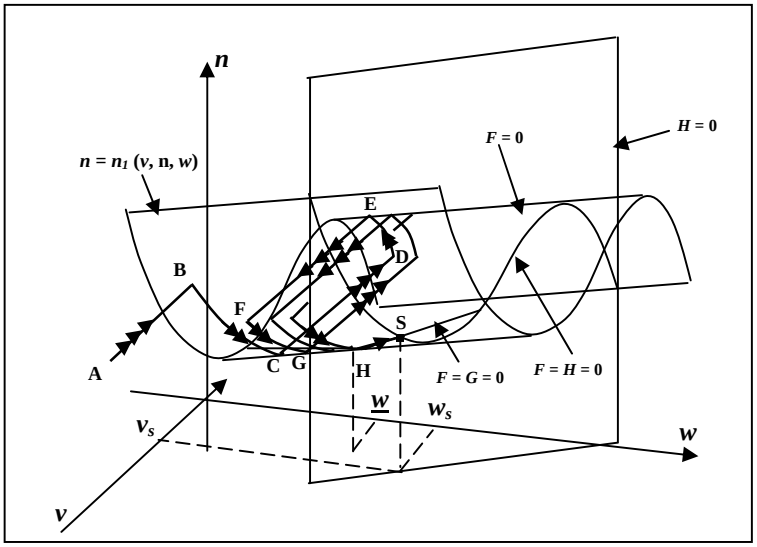

1c)

FIGURE 1.

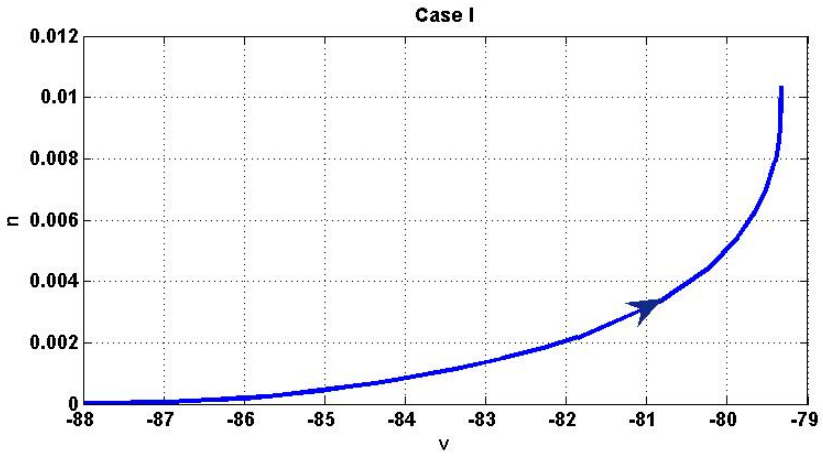

2 a)

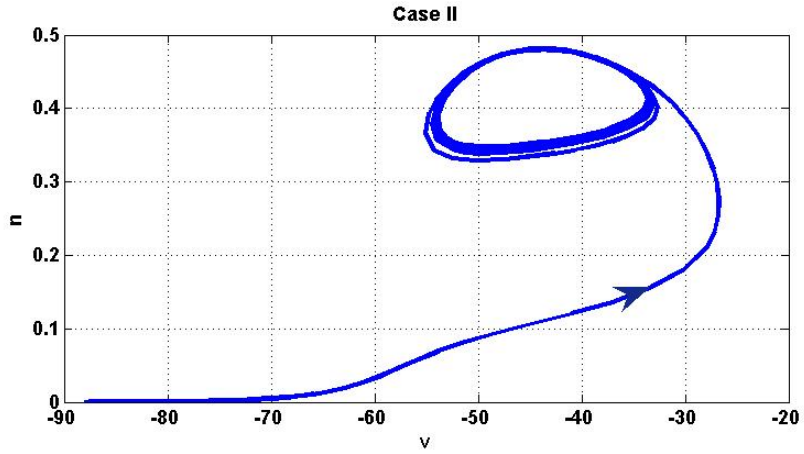

2 b)

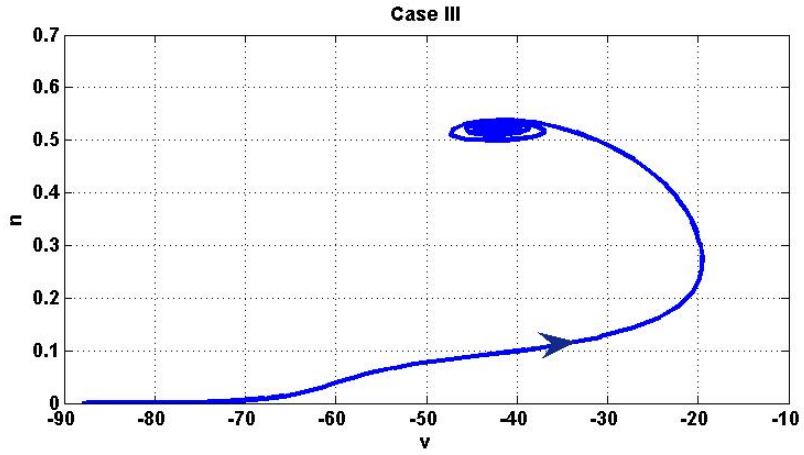

2 c)

FIGURE 2.

Application of Generalized Brownian Functionals to the Feynman Integral

May Thida Kyaw
Yangon Technological University, Myanmar
maythidakyaw@gmail.com.

Abstract : In this paper, we give an interpretation to classes of generalized Brownian functionals from the viewpoint of functional analysis. We discuss the application of this theory to the so-called Feynman integral. We reformulate the path integral for the propagator in terms of Brownian functionals where the averaging over paths is understood as an expectation over fluctuating paths generated by Brownian motion. In order to evaluate the propagators are interested in Lagrangians with local potentials which grow at most questionably.

We mean a nonlinear functional of a Brownian motion [B(t)]: f(B(t), t ∈ T) by a Brownian functional. Finally we step towards an application to the Feynman path integral.

INTRODUCTION

The purpose of this paper is to give an interpretation, from the viewpoint of functional analysis, to classes of generalized Brownian functionals, in particular to exponentials of quadratic (generalized) functionals and to discuss the application of this theory to the so-called Feynman integral. As an example one reformulates the path integral for the propagator in terms of Brownian functionals, where the averaging over paths is understood as an expectation over fluctuating paths generated by Brownian motion. In order to evaluate the propagators one has attention mainly to Lagrangians with local potentials which grow at most quadratically.

Before one comes to our main topics the theory of Brownian functionals are expressed in section 1. By a Brownian functional one means a functional *f*, nonlinear in general, of a Brownian motion {B (t)} : *f* (B) (t), t ∈ T). then in section 2, one is led to introduce generalized Brownian functionals, which will allow in particular the formulation of (nonlinear) functionals of white noise B(t) = (d/dt) B(t). One discusses various examples, with some remarks on possible generalization.

The analysis one steps forwards towards an application to the Feynman path integral in Section 3, the second subject to be discussed in this paper.

1. BROWNIAN FUNCTIONALS

For simplicity the time parameter space T is taken to be R^1. (Applications in quantum field theory will require generalizations to R^{s+1}. A Brownian functional can be expressed as a functional of white noise $\{\dot{B}(t), t \in \cap^{1}\}$. A realization of such functionals may be given by introducing the Hibert space $(L^2) \equiv L^2(S^*, \mu)$, where S^* is the dual of the Schwartz space $S(R^1)$ and where μ on S^* is the probability distribution of $\{\dot{B}(t), t \in R^1\}$ with the characteristic functional $C(\xi)$:

$$C(\xi) = E(e^{i\dot{B}(\xi)}) = \int_{S^*} e^{i(x,\xi)}\, d\mu(x). \qquad (1.1)$$

Corresponding Author : May Thida Kyaw, Yangon Technological University, Myanmar, maythidakyaw@gmail.com.

With this μ, almost every x ∈ S * is viewed as a sample function of $\mathcal{B}^{\natural}$(t), and hence any element φ(x) in (L^2) can be thought of as a realization of a

Brownian functional with finite variance.

The structure of Brownian functional can be learned by introducing as isomorphism T as follows:

$$('\mathsf{T}\varphi)(\xi)=\int_{S^*} e^{i(x,\xi)}\varphi(x)d\mu(x). \qquad (1.2)$$

The collection $\mathcal{F}$ = { $\mathcal{T}$φ; φ ∈ (L^2)} forms a reproducing kernel Hilbert space with kernel C (ξ - η), ξ, η ∈ S, and T gives the isomorphism

$$(L^2)\cong\mathcal{F}. \qquad (1.3)$$

Another basic tool of our analysis is the Wiener-It ô decomposition of (L^2):

$$(L^2)=\sum_{n=0}^{\infty}\oplus\mathcal{H}_{n,} \qquad (1.4)$$

where $\mathcal{H}_n$ is the space of multiple Wiener integrals of degree n spanned by the Fourier-Hermite polynomials in *x* of degree *n*.

Now one states the theorem on the integral representation of Brownian functionals.

Theorem

Associated with φ ∈ $\mathcal{H}_n$ is a symmetric L^2 (R^{2n}) – function *F* such that

$$(\mathsf{T}\varphi)(\xi)=i^n C(\xi)U(\xi), \qquad (1.5)$$

$$U(\xi)=\int_{\mathfrak{n}^n} F(t_1,.....t_n)\xi(t_1).....\xi(t_n)d^n t,$$

and such that

$$\|\varphi\|^2_{(L^2)}=n!\|F\|^2_{L^2(\mathfrak{n}^n).} \qquad (1.6)$$

So one has actually two representations of such φ: through U(ξ) with i^n *C(ξ) U(ξ)* ∈ $\mathcal{F}$, or through symmetric square integrable functions *F* in L^2 (∩ ^{n})^, which is the subspace of L^2 (∩ ^{n}) consisting of symmetric functions. Namely, the above integral gives rise to the isomorphism

$$\sum_n\oplus\mathcal{F}_n\overset{\mathcal{T}}{\cong}\sum_n\oplus\mathcal{H}_n\overset{\mathcal{K}}{\cong}\sum_n\oplus\sqrt{n!}\,L^2(\mathfrak{n}^n\hat{})$$

(1.7)

where $\mathcal{F}_n$ is the image of the subspace $\mathcal{H}_n$ under T.

The projection P_n : $\mathcal{F}\rightarrow\mathcal{F}_n$ acts on vectors *f* ∈ $\mathcal{F}$ as follows:

$$(P_n f)(\xi)=\frac{1}{n!}C(\xi)\frac{d^n}{d\lambda^n}\frac{f(\lambda\xi)}{C(\lambda\xi)}\Big|_{\lambda=0} \qquad (1.8)$$

Example 1.1

Let {e_n ∈ λ } be orthogonal and {an} ∈ l_1, and consider the trace class operator *K* = $\sum_n a_n P_n$ ∈ $\mathcal{B}_1$ (L^2 (R^1)), where P_n denotes the projection operator to the one dimensional subspace spanned by e_n. Then one finds for φ ($\mathcal{B}^{\natural}$) = $\sum_n a_n$ $\mathcal{B}^{\natural}$ $(e_n)^2$ ≡ ($\mathcal{B}^{\natural}$, *K* $\mathcal{B}^{\natural}$).

$$\mathcal{T}(\mathcal{B}^{\natural},K\mathcal{B}^{\natural})(\xi)=C(\xi)\{-(\xi,K\xi)+Tr\,K\}$$

. (1.9)

From this one sees that the Hermite polynomial ('normal ordered' or 'Wick ordered' polynomial) ($\mathcal{B}^{\natural}$, *K* $\mathcal{B}^{\natural}$) – *Tr K*, for short : ($\mathcal{B}^{\natural}$, *K* $\mathcal{B}^{\natural}$) :, is in $\mathcal{H}_2$ with

$$\mathcal{T}(:(\mathcal{B}^{\natural},K\mathcal{B}^{\natural}):)(\xi)=-C(\xi)(\xi,K\xi)_{L^2(\mathfrak{n}^1),} \qquad (1.10a)$$

$$\aleph\quad(:(\mathcal{B}^{\natural},K\mathcal{B}^{\natural}):)=+\sum_n a_n e_n(t_1)e_n(t_2)\equiv K(t_1,t_2)$$

(1.10b)

With regard to the above example (2.5) one we considers only : ($\mathcal{B}^{\natural}$, *K* $\mathcal{B}^{\natural}$):, one may drop the condition that *K* be in trace class. One shall deal with a Brownian functional, an element of (L^2), as long as

$$\aleph\ (:(\mathcal{B}^{\natural},K\mathcal{B}^{\natural}):)=(t_1,t_2)=K(t_1,t_2)$$

is square integrable, i.e. as long as *K* is a Hilbert-Schmidt operator. If *K* is not in trace class the (additive) renormalization in the definition of $:(B^{\diamond}, KB^{\diamond}):$ is necessary, and in fact, $(B^{\diamond}, KB^{\diamond})$ itself becomes infinite i.e. the latter expression ceases to be a well-defined random variable.

Example 1.2

Let *K* furthermore be such that *M* = *K* (*1+K*) $^{-1}$ has Hilbert-Schmidt norm less than one, in other words, for

$$M(t_1,t_2) = \aleph\ (:(B^{\diamond}, MB^{\diamond}):)(t_1,t_2),$$

$$||M||^2_{HS} = \int\int |M(t_1,t_2)|^2\, dt_1\, dt_2 = \sum_v \left|\frac{a_v}{1+a_v}\right|^2 < 1 \qquad (1.12)$$

holds, and consider the Brownian functional

$$\varphi(B^{\diamond}) = \exp[-\tfrac{1}{2}(B^{\diamond}, KB^{\diamond})]\ . \qquad (1.13)$$

Then one readily computes

(T φ) (ξ) = (det (1 + K))$^{-1/2}$ exp [½ (ξ, K (1+K)$^{-1}$ ξ)] (1.14)

and

$$P_{2n}(T\varphi)(\xi) = C(\xi)\frac{(\det(1+K))^{-1/2}}{2^n n!}(\xi, M\xi)^n,\ P_{2n+1}(T\varphi)=0 \qquad (1.15)$$

As a result, the L^2 (R^n)^ -functions corresponding to φ under the isomorphism Σ are given by

Σ : φ ↔ ((2n) !) F_{2n} , n = 0, 1, 2,……,

with

$$F_{2n}(t_1,.....,t_{2n}) = \frac{(-1)^n}{2^n n!}(\det(1+K))^{-1/2}\left(\prod_{v=1}^{n} M(t_v, t_{n+v})\right) \qquad (1.16)$$

so that

$$(2n)!||F_{2n}||^2 = \frac{(2n)!}{(2^n n!)^2}(\det(1+K))^{-1/2}||M||^{2n}_{HS} \qquad (1.17)$$

which is summable under the stated conditions, so that φ is as a Brownian functional.

Similarly, in Example 1.1, a multiplicative renormalization

Exp [-½ ($B^{\diamond}$, K $B^{\diamond}$)] → exp [-½ (($B^{\diamond}$, K $B^{\diamond}$) – E ($B^{\diamond}$, K $B^{\diamond}$))] (1.18)

yields a functional as in (1.13) – (1.17) except for the replacement of the Fredholm determinant.

det (1 + K) = exp [Tr 1n (1 + K)] (1.19)

by the modified one: *Exp [Tr (1n (1 + K) – K)]*. (1.20)

The latter however requires only Hilbert-Schmidt properties of K to be finite, and to make the renormalized φ a Brownian functional. Here the renormalization is multiplicative and as before the unrenormalized functional ceases to be well-defined when K leaves the trace class.

Considering the $\mathcal{T}$ and ℵ transforms of the quadratic and exponential-of-quadratic functionals which one has discussed in the two examples. One sees that a further generalization to K resp. M not Hilbert-Schmidt would have two features:

(a) the square integrability of $F_n \in L^2$ (∩ ^{n})^ and /or the summability of $\{\sqrt{n!}||F_n||\} \in l^2$ would be violated;

(b) on the other hand, many such generalizations leave the $\mathcal{T}$ transforms well defined.

It is on these two observations that one bases the discussion of generalized Brownian functionals in the following section.

2. GENERALIZED BROWNIAN FUNCTIONALS

One can, think of many generalizations of the concept of Brownian functionals as developed

above, and one shall come to specific examples after some words about the general framework for such

generalizations. For some motivation it may suffice at this point to observe that the quadratic functinals discussed up to now are not local, i.e. they are not additive under arbitrary decompositions of the 'time' parameter set T. One would like to consider additive

$$\varphi = \varphi_1 + \phi_2, \qquad (2.1)$$

or multiplicative

$$\varphi = \varphi_1 . \phi_2 \qquad (2.2)$$

local functionals where, for any decomposition of T,

$T = T_1 \cup T_2$, T_1, T_2 disjoint Borel subsets of T,

the φ_i can be found in such a way that they are functions only of $\{\dot{B}(t), t \in T_i\}$, I = 1, 2. Formally, expressions such as $\int \dot{B}(\tau)^2 \rho(\tau)\, d\tau$, resp. their exponentials, would have this property, but the corresponding operator $K : f \to \rho f$ is of course not of Hilbert-Schmidt type. To discuss such (generalized) functionals the mappings T and $\aleph$ are used. As mentioned before, $\mathsf{T}\varphi$ allows a straightforward extension to a wide class of kernels K. Hence one proposes to study the kernels as generalized functions, i.e. elements of G_n' in the space triplet

$$G_n \subset L^2(R^n)\hat{} \subset G_n'. \qquad (2.3)$$

Correspondingly, by the isomorphism $\aleph$, the multiple Wiener integral of degree *n* is embedded in a triplet.

$$\mathsf{G}_n \subset \mathcal{H}_n \subset \mathsf{G}_n^* \qquad (2.4)$$

where Brownian functionals $\varphi \in \mathsf{S}_n$ play the role of 'smooth' or 'test' functionals with the generalized functionals in S_n^* as their dual. One leaves details to separate investigations. Here one only wants to emphasize the usefulness of relaxing not only square integrability, but also square summability in *n*, as suggested by Example 1.2 and others to be discussed below. For the present purpose it will be simpler to characterize the smoothness and summability properties of test functionals indirectly, by considering the algebra of functionals generated by the f with the properties that

(a) f is continuous on $S(\mathbf{R}^n)$,

(b) $f(\lambda\xi)$ for any ξ is entire in λ, with $(d/d\lambda)^n f(\lambda\xi)$ continuous in ξ.

Under these conditions the operator P_n of (1.8) extends to the functionals f in such a way that

$$(P_n f)(\xi) = i^n C(\xi) U_n(\xi), \qquad (2.5)$$

where U_n is the restriction of an n-linear continuous functional $\tilde{U}_n$. By the kernel theorem on a generalized function there is an index $m \in N^k$ and a continuous function F_k of at most polynomial growth in $\sum_i t_1^2$ such that

$$\tilde{U}_n(\xi_1 \otimes \ldots \otimes \xi_n) = \int F_n(t_1, \ldots t_n)\, \xi_1^{(m_1)}(t_1) \ldots \xi_n^{(m_n)}(t_n)\, d^n t, \quad m = (m_1, \ldots, m_n), \qquad (2.6)$$

and

$$\tilde{U}_n(\xi \otimes \ldots \otimes \xi) = U_n(\xi).$$

This is a generalization of the representation (1.5). Accordingly one shall associate with any such F a generalized functional $\varphi \in S^*$ defined on the algebra of powers and exponentials of the $\dot{B}(\xi_i), \xi_i \in S(R^1)$, and characterized by

$$E(\varphi \exp[i\dot{B}(\xi)]) = f(\xi). \qquad (2.7)$$

(As a matter of notation one extends the concept of expectation to include the bilinear forms on $G^* \times G$. If φ is in $\mathcal{H}_n \subset G^*$, this of course reduces to the usual T transform.)

Let us now illustrate this framework by some examples.

Example 2.1

Let K be an operator on $L^2(\mathbf{R}^1)$ such that $(\xi_1, K\xi_2)$ is a continuous bilinear form on $S(\mathbf{R}^1) \times S(\mathbf{R}^1)$. Then set

$$: (\dot{B}, K\dot{B}): = T^{-1}(-C(\xi)(\xi, K\xi)). \quad (2.8)$$

This gives rise to a kernel function $K(t_1, t_2) \in S^*(\mathbf{R}^{2)\wedge}$, It includes Example 1.1, if $K(t_1, t_2) \in L^2(R^2)\wedge$, and is local if

$$K(t_1, t_2) = \delta(t_1 - t_2)\, k(t_1) \quad (2.9)$$

with k integrable and of no more than polynomial growth.

Note that generalized Brownian functionals are defined as linear forms. As with generalized functions, there is no obvious way to exponentiate them. Hence the next example is of particular interest.

Example 2.2.

Let K be an operator on $L^2(\mathbf{R}^1)$ such that $M \equiv K(1+K)^1$ defines a continuous bilinear form on $S(R^1) \times S(\mathbf{R}^1)$. Then set

$$N \exp\left[-\frac{1}{2}(\dot{B}, K\dot{B})\right] \equiv T^{-1}\left(C(\xi) \exp\left[\frac{1}{2}(\xi, M\xi)\right]\right). \quad (2.10)$$

The kernel functions are computed, as in Example 1.2, to be

$$F_{2n}(t_1, \ldots, t_{2n}) = \frac{(-1)^n}{2^n n!}\left(\prod_{i=1}^{n} M(t_i, t_{n+i})\right)\wedge. \quad (2.11)$$

If K is a Hilbert-Schmidt operator, then the functional N exp [.] in (2.10) differs from the renormalized one of the formula (1.18) by a finite factor, the modified Fredholm determinant. In this case as well as in the more general situation considered here, the functional N exp is formally related to exp by an (infinite) renormalization, and the

former is well defined as a (generalized) Brownian functional. As a matter of notation the definition of N exp is extended to include linear and sure terms in the argument as follows: for

$f \in L^2(\mathbf{R}^1)$ and $a \in$ ש , set

$$N \exp[-\tfrac{1}{2}(\dot{B}, K\dot{B}) + \dot{B}(f) + a] = \exp[\dot{B}(f) + a]$$

$$N \exp[-\tfrac{1}{2}(\dot{B}, K\dot{B})]. \quad (2.12)$$

With a view to applications later on one also calculates the following example.

Example 2.3

We have

$$T(N \exp[-\tfrac{1}{2}(\dot{B}, K\dot{B})] \exp[-\tfrac{1}{2}(\dot{B}, L\dot{B})](\xi)$$
$$= \exp[-\tfrac{1}{2} \mathrm{Tr} \ln(1 + L(1+K)^{-1}] \exp[-\tfrac{1}{2}(\xi, (1+K+L)^{-1}\xi)]. \quad (2.13)$$

For, e.g. K, L of trace norm smaller than one this is a matter of direct calculation, but the right hand side extends as an admissible functional as long as the trace is finite and $(1+K+L)^{-1}$ is a continuous bilinear form on $S(R^1) \times S(R^1)$.

Examples 2.2. and 2.3 provide an illustration that Brownian functionals may be generalized ones although their symmetric kernel functions are square integrable for all n. If the operators $K(1+K)^{-1}$ resp. $(K+L)(1+K+L)^{-1}$ are of Hilbert-Schmidt type, then

$$\sqrt{n!}\, \| F_n \|_{L^2(\mathrm{n}\ n)} < \infty, \quad (2.14)$$

but if they are large, this sequence of norms will not be square summable in n. A case in point is the following.

Example 2.4

For t, $\varepsilon > 0$ and $y \in R^1$, set

$$\delta_{\in} = \delta_{\in}(B(t)-y) \equiv (\pi\varepsilon)^{-1/2} \exp\left[-\frac{1}{\varepsilon}(B(t)-y)^2\right]. \tag{2.15}$$

This is a slight generalization of Example 1.2. The formula (2.15) gives

$\delta_{\in} = (\pi\varepsilon)^{-1/2} \exp[-y^2/\varepsilon] \exp[-\frac{1}{2}(B, K_{\varepsilon} B) + B(f_{\varepsilon})]$, where

$K_{\varepsilon}(t_1, t_2) = (2/\varepsilon)_{X[0,1]}(t_1)_{X[0,1]}(t_2)$ and $f_{\varepsilon} = (2/\varepsilon)_{yX[0,1]}$

The operator K_{ε} is given by $(2t/\varepsilon)$P with P projection onto multiples of $e \equiv t^{-1/2} X_{[0,1]}$ and is of course in the trace class, its only nonzero eigenvalue $2t/\varepsilon$ being simple, and the Hilbert-Schmidt norm of $M_{\varepsilon} = K_{\varepsilon}(1+K_{\varepsilon})^{-1}$ is thus $2t/(2t+\varepsilon)$, i.e. smaller than one as long as ε and t are positive. The T transform can be given explicitly:

$$(T\delta_{\varepsilon})(\xi) = (\pi(2t+\varepsilon))^{-1/2} C(\xi) \times \exp\left[\frac{1}{2t+\varepsilon}\left(\int_0^t \xi(s)\,ds\right)^2 + \frac{2iy}{2t+\varepsilon}\int_0^t \xi(s)\,ds - \frac{y^2}{2t+\varepsilon}\right]. \tag{2.16}$$

Note that the limit of this expression, as $\in \to +0$, produces an admissible functional:

$$\delta(B(t)-y) = T^{-1}\left\{(2\pi t)^{-1/2} \exp\left[-\frac{1}{2t}\left(y - i\int_0^t \xi(s)\,dqs\right)^2\right] C(\xi)\right\} \tag{2.17}$$

is a generalized Brownian functional. Of course, so is

$$\frac{(T\delta)(\xi)}{(T\delta)(0)} = \frac{E(\delta(B(t)-y\exp[iB(\xi)])}{E(\delta(B(t)-y))}$$

$$= C(\xi)\exp\left[\frac{iy}{t}\int_0^t \xi(s) + \frac{1}{2t}\left(\int_0^t \xi(s)\,ds\right)^2\right], \tag{2.18}$$

Which one recognizes, consistently, as the conditional expectation

$$E(\exp[iB(\xi)] \mid B(t) = y). \tag{2.19}$$

More generally, again, one may consider a combination of the previous types with the previous examples as special cases, and given in the following example.

Example 2.5

Let L be in the trace class and K be such that $1 + K$ and $N = 1 + K + L$ have a bounded inverse. Denote by e the unit vector $t^{-1/2} X_{(0,r)} \in L^2(\mathbb{R}^1)$. Then one can define

$$N \exp[-\tfrac{1}{2}(B, KB)] \exp[-\tfrac{1}{2}(B, LB) + iB(g)]\,\delta(B(t)-y)$$

$$= T^{-1}([2\pi t\,(e, N^{-1}e) \det\{1 + L(1+K)^{-1}\}]^{-1/2} \times \exp\left[-\tfrac{1}{2}(\xi+g, N^{-1}(\xi+g)) - \frac{1}{2}\frac{1}{(e, N^{-1}e)}\left(\frac{y}{\sqrt{t}} - i(\xi+g, N^{-1}e)\right)\right.$$

$$\left. \times\left(\frac{y}{\sqrt{t}} - i(e, N^{-1}(\xi+g))\right)\right]. \tag{2.20}$$

To conclude this section one wishes to remark that characteristic functionals C of finite measures on a space of generalized functions are admissible functionals if $C(\lambda\xi)$ is analyticity in λ near zero. Continuity of S is implied by their definition [7], and the analyticity requirement amounts to the existence of the covariance functionals. The corresponding 'positive' generalized Brownian functionals can thus be viewed as generalized Radon-Nikodym derivatives, with respect to the white noise measure. This points towards possible future applications in quantum field theory [13], since the Schwinger functions of Euclidean quantum field theory models are indeed generated by such characteristic functionals. This point of view is emphasized particularly in [5,6].

Finally, we want to point out that it would be very interesting to relax the ray analyticity requirement for the T transforms of generalized Brownian functionals to include examples where some weaker (such as Borel) summability holds with a view toward extending the Feynman integral (discussed in the next section) to larger classes of potentials for which only such weaker summability properties hold.

3. THE FEYNMAN INTEGRAL

As proposed by Feynman [4], quantum mechanical transition amplitudes may be thought of as a kind of averaging over fluctuating paths, with oscillatory weight functions given in terms of the classical action

$$s[x]=\int_{t_1}^{t_2} d\tau L\left(x,\dot{x}\right)(\tau). \qquad (3.1)$$

Typically, the Lagrangian *L* will be a sum of two terms such as e.g.

$$L\left(\dot{x},x\right)=L_0\left(\dot{x}\right)+L_1\left(x\right)=\frac{1}{2}m\dot{x}^2-V\left(x\right) \quad (3.2)$$

for a particle of mass *m* moving in the force field of a potential *V*. And accordingly

$$S[x]=S_0[x]-\int V d\tau.$$

In a popular intuitive notation the Feynman path integral is then expressed as

$$I\left(\phi\right)=N\int \exp\left[\left(i/\hbar\right)S[x]\right]\phi\left(x\right)\prod_{t_1<\tau<t_2} dx(\tau), \qquad (3.3)$$

$\hbar=h/2\pi$, *h* Planck's constant.

If in particular ϕ is taken to be 1 and if the integral is thought of as being over paths with $x\left(t_1\right)=y_1,\ x\left(t_2\right)=y_2,$ then the above expression gives the quantum mechanical propagator.

One observes that the Feynman integral can be viewed as the expectation of a generalized Brownian functional.

One introduces trajectories x consisting of a sure path y plus Brownian fluctuation:

$$x(\tau)=y(\tau)+\left(\hbar/m\right)^{1/2}B(\tau),\ 0\le\tau\le t. \qquad (3.4)$$

To describe the propagator $G\left(y_1,y_2,t\right)$, set $y\left(0\right)=y_1,$ and claim then that for well-behaved potential *V* one has

$$G(y_1,y_2,t)=E\left\{N\exp\left[\frac{i}{\hbar}\frac{m}{2}\int_0^t\dot{x}(\tau)^2d\tau+\frac{1}{2}\int_0^t B(\tau)^2d\tau\right]\exp\left[-\frac{i}{\hbar}\int_0^t V\left(x(\tau)\right)d\tau\right]\delta\left(x(t)-y_2\right)\right\}. \qquad (3.5)$$

In this expression the sum of the first and the third integral is the action $S[x]$, and the Dirac delta function serves to pin trajectories to y_2 at time t. The necessity of the second integral in the exponent can be made plausible by recalling that the white noise measure is Gaussian, while the Feynman integration should be with respect to a 'flat' measure. 47

One considers trajectories as in (3.4) with the strength of fluctuation $\left(\hbar/m\right)^{1/2}$ replaced by an arbitrary α, and find, consistently with the above remarks, that the quantum mechanical propagator results for $\alpha\to\infty$.

Example 3.1

To verify the equation (3.5) for the propagator one first consider a 'free particle', i.e. $V=0.$ Then the evaluation of the right-hand side of (3.5) is an application of example (2.5) Note that

$$\frac{i}{\hbar}\frac{m}{2}\int_2^t\dot{x}^2d\tau=\frac{i}{2}\frac{m}{\hbar}\int_0^t\dot{y}^2d\tau+i\left(\frac{m}{\hbar}\right)^{1/2}\int_0^t\dot{y}\dot{B}d\tau+\frac{i}{2}\int_0^t\dot{B}^2d\tau \qquad (3.6)$$

to have the expectation of the so-called *Feynman functional*

$$E\left(I\right)\equiv E(N\exp\left[\frac{i}{2}\frac{m}{\hbar}\int_0^t\dot{x}^2d\tau+\frac{1}{2}\int_0^t\dot{B}^2d\tau\right]\delta(x(t)-y_2))$$

$$=E\left(N\exp\left[\frac{1+i}{2}\int_0^t\dot{B}^2d\tau\right]\right)$$

$$\times \exp\left[i\left(\frac{m}{\hbar}\right)^{1/2} \int_0^t y\,dB \right] \delta(x(t)-y_2)) \exp\left[\frac{i}{2}\frac{m}{\hbar}\int_0^t y^2 d\tau \right], \tag{3.7}$$

so that in the notation of example (2.5) one takes

$$K = -(1+i)_{\chi^2[0,t]}, \qquad L \equiv 0,$$

$$g = i\left(\frac{m}{\hbar}\right)^{1/2} y \tag{3.8}$$

($\chi^2[0,t]$ denotes an operator such that $\iint \chi^2[0,t](u,\upsilon)F(u,\upsilon)du\ d\upsilon = \int_0^t F(u,\upsilon)du)$ and $\delta(B(t)-y)$ is replaced by

$$\delta(x(t)-y_2) = \left(\frac{m}{\hbar}\right)^{1/2} \delta\left(B(t) - \left(\frac{m}{\hbar}\right)^{1/2} (y_2 - y(t)) \right), \tag{3.9}$$

that is, y in (2.20) is replaced by

$$\left(\frac{m}{\hbar}\right)^{1/2} (y_2 - y(t)).$$

The equation (2.20) therefore gives us for $\xi = 0$

$$E(I) = \left(\frac{m}{2\pi i\hbar\, t}\right)^{1/2} \exp\left[-\frac{i}{2}\frac{m}{\hbar}\int_0^t y^2 d\tau - \frac{1}{2i}\left(\left(\frac{m}{\hbar t}\right)^{1/2} (y_2 - y(t)) \right.\right.$$

$$= \left(\frac{m}{2\pi i\hbar\, t}\right)^{1/2} \exp\left[\frac{im}{2\hbar\, t}(y_2 - y_1)^2 \right] \equiv G_0(y_1, y_2, t), \tag{3.10}$$

which is the propagator for an isolated quantum mechanical particle.

Note that the result is independent of the 'sure' part of the trajectory. One exemplifies this by evaluating

$$\mathcal{F}\left(N \exp\left[\frac{im}{2\hbar}\int_0^t x^2 d\tau + \frac{1}{2}\int_0^t B^2 d\tau \right] \delta(x(t)-y_2) \exp\left[i\int f(\tau)x(\tau)d\tau \right] \right)(\xi)$$

$$= \left(\frac{m}{2\pi\hbar i}\right)^{1/2} \exp\left[-\frac{1}{2}\| \xi \|^2 - \frac{i}{2}\frac{\hbar}{m}\| F \|^2 - i\left(\frac{m}{\hbar}\right)^{1/2} (\xi, y) - i\left(\frac{\hbar}{m}\right)^{1/2} (\xi, F) \right.$$

$$+ iy_1 F(t) - \frac{1}{2i}\left(\left(\frac{m}{\hbar\,\tau}\right)^{1/2} (y_2 - y_1) \right.$$

$$+ t^{-1/2}\int_0^t \xi(s)ds + \left(\frac{\hbar}{m}\right)^{1/2} \left.\left.\int_0^t F(s)\,ds \right)^2 \right], \tag{3.11}$$

where $F(t) = \int_0^t f(\tau)d\tau.$

Then one sees that the expectation (i.e. (1.11) evaluated at $\xi = 0$) is independent of $y(\cdot)$. As an example one observes a special case where $f = \sum_\nu \alpha_\nu \delta(\tau - \tau_\nu).$ Denoting the left-hand side of (1.11) by $\mathcal{F}\left(I \exp\left[i\int f(\tau)x(\tau)d\tau \right] \right)(\xi)$, the expectation in question is given by

$$E\left(I \exp\left[i\sum \alpha_\nu x(\tau_\nu) \right] \right)$$

$$= G_0 \exp\left[-\frac{i\hbar}{2m}\sum \alpha_\mu \alpha_\nu (\tau_\mu \wedge \tau_\nu - \frac{\tau_\mu \tau_\nu}{t}) + \frac{i(y_2 - y_1)}{t}\sum \alpha_\nu \tau_\nu + iy_1 \sum \alpha_\nu \right]. \tag{3.12}$$

Such a property to be independent of $y(\cdot)$ is plausible if one realizes that a change of $y(\cdot)$ is a translation in the sample space and that Feynman expectation is constructed so as to resemble a translation invariant integral.

Example 4.2.

The formula (3.11) further tells us that one may extend

$$\mathcal{T}(I)(\xi) = E\left(I \exp\left[iB(\xi) \right] \right)$$

$$G_0(y_1, y_2, t) \exp\left[-\frac{i}{2}\int_{-\infty}^{\infty} \xi(\tau)^2 d\tau + \frac{i}{2t}\left(\int_0^t \xi(\tau)d\tau \right)^2 \right.$$

$$\left. -i\left(\frac{m}{\hbar}\right)^{1/2} \int_0^t \xi(\tau)(y - \frac{y_2 - y_1}{t})\, d\tau \right] \tag{3.13}$$

to $\xi \in L^2(\mathbf{R}^1)$ In particular one may view $E(I \exp\left[i\sum_\nu \alpha_\nu x(\tau_\nu) \right])$ as the action of I on a test functional. By the results of Albeverio and H $\varnothing$ egh-Krohn, I further extends to

$\exp\left[-(i/\hbar)\int V(x(\tau))d\tau\right]$ if V is the Fourier transform of a bounded measure:

$$V(x)=\int \exp\left[i\alpha x\right]dm(\alpha).$$

From (3.11) and the expansion

$$\exp\left[-\frac{i}{\hbar}\int V(x(\tau))d\tau\right]=\sum_{n=0}^{\infty}\frac{(-1)^n}{n!}\int d^n\tau\int\exp\left[i\sum_{v}\alpha_v x(\tau_v)\right]dm(\alpha_v)$$

one is given the Dyson series for the propagator G of a particle in the field of the potential V:

$$E\left(I\exp\left[-\left(\frac{i}{\hbar}\right)\int Vd\tau\right]\right)\equiv G(y_1,y_2,t)$$

$$=G_0(y_1,y_2,t)\sum_{n=0}^{\infty}\frac{(-i/\hbar)^n}{n!}\prod_{v=0}^{n}\int_0^t d\tau_v\int dm(\alpha_v)$$

$$\times\exp\left[-\frac{i\hbar}{2m}\sum\alpha_t\alpha_\mu\left(\tau_v\wedge\tau_\mu-\frac{\tau_v\mu_\mu}{t}\right)+i\frac{(y_2-y_1)}{t}\sum\alpha_v\tau_v+iy_1\sum\alpha_v\right].$$

(3.14)

5. THE RELATION BETWEEN BROWNIAN BRIDGE AND THE FORMULA (3.4) PLUS DELTA FUNCTION

Concerning the expression of the quantum mechanical paths, we proposed the sum of the classical paths and Brownian bridge. But actual computation uses the sum of classical paths and an ordinary Brownian motion, and in addition a delta function.This trick is quite reasonable. However, for actual computation we use the expression of quantum mechanical trajectories by the formula (3.4). And use the delta function of the form $\delta(x(t)-y_2)$

Hence the problem is that"What is the relation between brownian bridge and the formula (3.4) + delta function.

Let B(t) be a Brownioan motion. A brownian bridge) $B_t(\tau)$, $0<\tau<t$, is expressed in the form

$$B_t(\tau)=B(\tau)-\frac{\tau}{t}B(t)\ ,\quad \text{(I)}$$

On the other hand, $B_t(\tau)$ has the canonical representation of the form

$$B_t(\tau)\ =(t-\tau)\int_0^t\frac{1}{t-\tau}\,dB_1(\tau)\ ,\quad \text{(II)}$$

where B_1 is a Brownian motion which gives the canonical representation of $B_t(\tau)$. One may ask what is the difference between

$$B(\tau)\quad and\quad B_t(\tau).$$

Before we state the answer, we say the following

i) Our proposal of using the brownina bridge has been motivated motivated by Dirac's idea section 32 in the 14(in the book P.A.M. Dirac, Principles of quantum mechanics. 1930 Oxford, Section 32. Action principle). We wish to use a Brownian bridge.

ii) For computation , we have used free Brownian motion and the delta function $\delta(x(t)-y_2)$ in order to get pinning effect at time t.

Now we can say

Theorem.

Using free Brownian motion and the delta function $\delta(x(t)-y_2)$ in order to get pinning effect at time t. is reasonable and is in agreement of the idea of using Brownian bridge.

Proof.

A Brownian bridge $B_t(\tau)$, $0<\tau<t$, has the canonical representation of the form (II). Namely $B_t(\tau)$ has less information than the original $B(\tau)$. In fact, let Y be a function of B(u) expressed in the form

$$Y=\int_0^t f(u)\,dB(u)$$

Y express the amount of the information less than the free Brownina motion. Y is independent of { B(u), $0 < u < t$ if and only if $E(Y B_t(\tau))$ = 0, for every τ

That i

$$E(\int_0^t f(u)\, dB(u) \dot{c}[\, B(\tau) - \frac{\tau}{t} B(t)] = 0$$

for every u < t. Since $B(\tau) = \int_0^\tau 1 dB(u)$, the above equation becomes

the equation $\int_0^t f(u)\, (I_{[0,\tau]} - \frac{\tau}{t} 1)\, du = 0$,

where I_A is the indicator function of the set A. Hence

$$\int_0^\tau f(u)\, du = \frac{\tau}{t} \int_0^t f(u) du \ .$$

Namely, applying $\frac{d}{d\tau}$, we have

f(\tau) = \frac{1}{t} \int_0^t f(u)du.

$$f(\tau) = \frac{1}{t} \int_0^t f(u)\, du \ .$$

Thus we conclude that f is a constant (depending only on t). This result concludes that B_t has less information as much as Y has. And we know Y = const B(t). In other word, the less amount of information can be realized by letting B(t) be constant, that is the pinning effect by $\delta(B(t) - y_2)$.

References

[1] S. Albeverio and R.H∅egh-Krohn, Mathematical Theory of Feynman Path Integrals, Lecture Notes in Mathematic 523 (Spring, Berlin, 1976).

[2] S. Albeverio et al., eds., Feynman Path Integrals, Proceedings, Marseille 1978, Lecture Notes in Physics 106 (Springer, Berlin, 1979).

[3] J.-P. Antone and E. Tirapegui, eds., Functional Integration: Theory and Applications, Proceedings, Louvain-la-Neuve, Belgium 1979 (Plenum, New York 1980).

[4] R.P. Feynman, Space-time approach to non-relativistic quantium mechanics, Review of Modern Physics 20 (1948) 367-387.

[5] J. Frohlich, Schwinger functions and their generating functions 1, Helv, Phys, Acta 47 (1974) 265-306.

[6] Frohlich, Schwinger functions and their generating functions II: Markovian and generalized path space measures on S ' , Adv, in Math. 23 (1977) 119-180.

[7] I.M. Gel'fand and N.Ya. Vilenkin, Generalized functions, Vol. 4 (Academic Press, New Yoirk 1964).

[8] T. Hida, Analysis of Brownian functinals, Carleton Mathematical Lecture Notes 13 (Carleton Univ. Press, 2nd ed. 1978)

[9] T. Hida, Causal anaysis in terms of white noise, in: L. Streit, ed., Quantum Fileds, Algebras, Processes (Springer, Berlin, 1980) 1-19

[10] T. Hida, Brownian motion, in: Application of Mathematics 11 (Springer, Berlin, 1980)) (English translation).

[11] I. Kubo and S. Takenaka, Calculus of Gaussian white noise I, Proc. Japan Acad. Ser. A 56 (1980) 376-380.

[12] I. Kubo and S. Takenaka, Calculus of Gaussian white noise II, Proc, Japan Acad. Ser. A 56 (1980) 411-146.

[13] L. Streit, Dynamics in terms of energy forms, Lectures at Primorsko (Bulgaria) Summer School 1980 (to be published as Springer Lecture Notes in Mathematics).

Groundwater Contaminant Problem using an Operator Splitting Scheme

Kyawt Kyawt Khine
Department of Engineering Mathematics, Yangon Technological University,
Yangon, Myanmar.

Abstract: For solving two-dimensional convection-dispersion-adsorption problems, one efficient numerical method is needed. In this paper, an efficient method for solving Groundwater contamination which is one of the most typical hydrogeological problems, namely Groundwater contamination is presented with corresponding Operator Splitting Scheme. A general mathematical model which includes contaminant transport, mechanical dispersion, molecular diffusion and adsorption in both equilibrium and non-equilibrium modes is presented. First, the original half-plane domain is transformed to a rectangle using a bipolar orthogonal transformation. Then in each time step we solve separately the transport, dispersion and adsorption parts.

Key words: Convection-diffusion problem; Contaminant transport; Operator splitting.

1. Introduction

One of the most typical hydrogeological problems is Groundwater contamination in this paper how to construct a mathematical model for Groundwater contamination is discussed. Also a numerical method , namely Operator Splitting Scheme to solve the problem is presented.

2. Mathematical model

In figure (2.1) two monitor wells are situated at points (-d , 0) and (d, 0) with given radii r_1, r_2 respective ly.Let us assume that for the pumping rate Q_1 of the injection well and the discharge Q_2 in the extraction well, $Q_2 = -Q = Q$. Then the flow potential for the steady-state flow in the outer domain can be obtained by superposition of flow potentials of both wells

$$\Phi(x,y) = \frac{Q}{4\pi}\ln\frac{(x+d)^2+y^2}{(x-d)^2+y^2} + \Phi_0 \ , \qquad (2.1)$$

Where Φ_0 is determined from the boundary conditions.

The relation between flow potential and piezometric head h (x,y) is given

$$\Phi(x,y) = khH - \tfrac{1}{2}kH^2 \qquad (2.2)$$

for the saturated region, where H is the height of the acquifer and k is the hydraulic conductivity. For the unsaturated region,

$\Phi(x,y) = \tfrac{1}{2}kh^2$ is obtained.

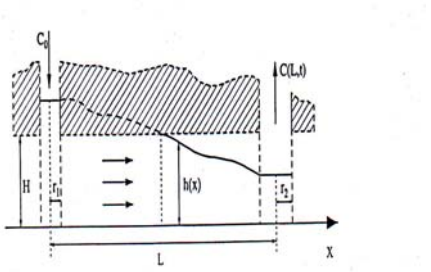

Fig. 2.1 System of two monitor wells. The dotted line represents the border between saturated and unsaturated region.

Then the velocity field for the flow.

$$V = -\frac{1}{h_{eff}\theta_0}\nabla\Phi \ , \qquad (2.3)$$

can be determined where $h_{eff} = H$ for saturated region and $h_{eff} = h(x,y)$ for unsaturated region. θ_0 is the porosity.

The contaminant transport problem with dispersion and adsorption (reaction) in a homogeneous porous media is represented by the following system of differential equations:

Corresponding Author : Kyawt Kyawt Khine Ph. D Candidate, Engineering Maths. 11th batch, Department of Engineering Mathematics, Yangon Technological University. Yangon, Myanmar.
kyawtkyawtkhine.myanmar@gmail.com . Ph – 09517278

$h_{eff}\,\partial_t (C + \psi_e(c)) - \mathrm{div}\,(Dh_{eff}\nabla C) - \mathrm{div}\,(h_{eff} vc) + h_{eff}\partial_t S = 0$ (2.4)

$\partial_t S = k(\psi_n(c) - S)$, (2.5)

where C(x,y,t) represents the contaminant concentration and S(x,y,t) is the concentration of adsorbed pollution. The adsorption in both equilibrium mode represented by sorption isotherm $\psi_e(C)$ and non-equilibrium mode represented by $\psi_n(C)$ are considered. In this case both isotherms are of Freundlich type,

$\psi(C) = AC^p$, $A > 0$, $0 < p < 1$.

Here D is the dispersivity tensor

$$D_{ij} = \{(D_0 + \alpha_T |v|)\,\delta_{ij} + \frac{v_i v_j}{|v|}(\alpha_L - \alpha_T)\},$$

where D_0 is the molecular diffusion coefficient and δ_{ij} the Kronecker symbol. α_L and α_T are longitudinal and transversal dispersivities.

As the original two-dimensional domain Ω is symmetric along x-axis, it can be restricted only to one of its half-planes. Using a bipolar transformation, this domain can be transformed to a rectangle $\Omega_R = (0,\pi) \times (v^{(1)}, v^{(2)})$ (sides $v = v^{(1)}$, $v = v^{(2)}$ corresponding to well borders). where the equipotential curves and streamlines of the flow are parallel to coordinate axes and orthogonal to each other (see Fig. 2.2). In this new domain, the groundwater flow is parallel to the v-axis and the contaminant is transported only in this direction. The bipolar coordinates (u,v) are defined by

$$x = \frac{\delta}{2}\frac{\sinh v}{\cosh v - \cos u}, \qquad y = \frac{\delta}{2}\frac{\sin u}{\cosh v - \cos u},$$

$$\sqrt{r_1^2 + 1/4\delta^2} + \sqrt{r_2^2 + 1/4\delta^2} = 2d. \quad (2.6)$$

where

$$d = \frac{1}{2}\sqrt{\frac{2r_1^2 D^2 + r_1^4 - 2r_1^2 r_2^2 + r_2^4 - 2r_2^2 D^2 + D^4}{D^2}}$$

$$\delta = 2\sqrt{d^2 - r_1^2}$$

$$c = D - 2d$$

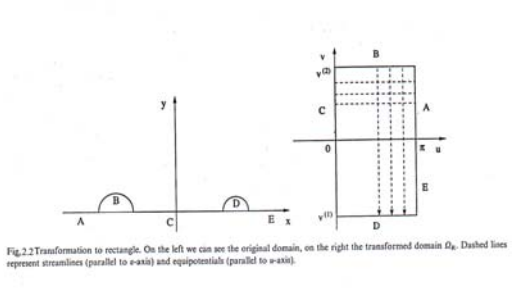

Fig. 2.2 Transformation to rectangle. On the left we can see the original domain, on the right the transformed domain Ω_R. Dashed lines represent streamlines (parallel to v-axis) and equipotentials (parallel to u-axis).

The values $v^{(1)}$, $v^{(2)}$ are obtained from

$$\sinh v^{(1)} = -\frac{\delta}{2r_1}, \quad \sinh v^{(2)} = \frac{\delta}{2r_2}. \quad (2.7)$$

As for the flow potential, it depends now only on the variable υ and can be expressed as

$$\bar{\Phi}(v) = Av + B, \quad (2.8)$$

The coefficients A, B can be determined from the boundary conditions

$Av^{(1)} + B = \Phi_1$, $Av^{(2)} + B = \Phi_2$,

where Φ_1, Φ_2 are given values (potentials at the well borders).

Then the pressure -head with the water level can be identified. In the injection well the water level $h_2 > H$. Other possibilities, e.g. $H < h_1 < h_2$; $h_1 < h_2 < H$, can also be included.

(i) for $h > H$

$$\partial_t C = \frac{4\lambda^2}{\delta^3\theta_0 H}\{\partial_u[(D_0\theta_0 H\delta + 2\alpha_T\lambda(\partial_v\tilde{\phi}(v)))\partial_u C] + \partial_v[(D_0\theta_0 H\delta + 2\alpha_L\lambda(\partial_v\tilde{\phi}(v)))\partial_v C - \delta(\partial_v\tilde{\phi}(v))C]\},$$

(ii) for $h < H$,

$$\partial_t C = \frac{4\lambda^2}{\delta^3\theta_0 h(v)}\{\partial_u[(D_0\theta_0 h(v)\delta + 2\alpha_T\lambda(\partial_v\tilde{\phi}(v)))\partial_u C] + \partial_v[(D_0\theta_0 h(v)\delta + 2\alpha_L\lambda(\partial_v\tilde{\phi}(v)))\partial_v C - \delta(\partial_v\tilde{\phi}(v))C]\},$$

where $\lambda = \cosh v - \cos u$ and $\partial_v\tilde{\phi}(v) = A$.

Applying the transformation described above to the equations in (x,y) coordinates, we obtain the following convection-diffusion-adsorption problem in (u,υ) coordinates:

$\partial_t (C + \psi_e (c)) - F\partial_v C - g(\partial_u (a\partial_u C) + \partial_v (b\partial_v C) +$
$+ \partial_t S = 0$ (2.9)
$\partial_t S = K(\psi_n (C) - S)$ (2.10)
for $(u, v) \in \Omega_R$, $t \in (0, T)$. Here
$a(u,v)=(D_0\theta_0 h_{eff}\delta + 2\alpha_T(\cosh v - \cos u)(\partial_v \Phi(v))$
$b(u,v)=(D_0\theta_0 h_{eff}\delta + 2\alpha_T(\cosh v - \cos u)(\partial_v \Phi(v))$

$$g(u,v) = \frac{4(\cosh v - \cos u)^2}{\delta^3 \theta_0 h_{eff}}$$

$F(u, v) = g(u, v)(\delta \partial_v \Phi(v))$,
and $\Phi(v)$ is obtained from (2.8).
We consider the boundary conditions
$C = C_0(t)$ on Γ_1, $\partial_u C = 0$ on $\Gamma_2 \cup \Gamma_4$, $\partial_v C = 0$ on Γ_3, (2.11)
where $\Gamma_1 = (0, \pi) \times \{v = v^{(2)}\}$, $\Gamma_2 = (0) \times \{v^{(1)} = v^{(2)}\}$,
$\Gamma_3 = (0, \pi) \times \{v = v^{(1)}\}$, $\Gamma_4 = (\pi) \times \{v^{(1)} = v^{(2)}\}$.
The initial conditions are
$C((u, v), 0) = 0$, (2.12)
$S((u, v), 0) = 0$, (2.13)

3. Operator splitting scheme

The method of solution of (2.9)-(2.13) is based on time stepping and operator splitting approach. First we discretized the time interval [0,T], $0 = t_0, t_1, \ldots, t_{n-1}, t_n = T$. Then in each time step we separately solve three parts of the problem-transport, dispersion and non-equilibrium adsorption problem.

The basic principle of the operator splitting method is as follows. First step is to solve the transport part that presents a hyperbolic problem of the form
$\partial_t(\phi + \psi_e(\phi)) - F\partial_v \phi = 0$, $t \in (t_{k-1}, t_k)$, $k = 1 \ldots n$ (3.1)
with boundary conditions of the form(2.11) and initial condition
$\phi(u, v, t_{k-1}) = C_{k-1} = C(u, v, t_{k-1})$.
By $C_k^{1/3}$ we denote the obtained solution, i.e.

$$C_k^{1/3} := \phi(u, v, t_k).$$

The second step is to solve the problem (the diffusion part)
$\partial_t(\phi + \psi_e(\phi)) - g(\partial_u(a\partial_u\phi) + \partial_v(b\partial_v\phi)) = 0, t \in (t_{k-1}, t_k)$ (3.2)
with the same boundary conditions and initial condition $\phi(u, v, t_{k-1}) = C_k^{1/3}$. The obtained solution will be denoted $C_k^{2/3}$.
And the last part of the procedure is solving the reaction part represented by the system
$\partial_t(\phi + \psi_e(\phi)) + \partial_t s = 0$, (3.3)
$\partial_t s = K(\psi_n(\phi) - S)$ (3.4)
with the initial conditions $\phi(u, v, t_{k-1}) = C_k^{2/3}$,
$S(u, v, t_{k-1}) = S_{k-1}$.
Finally, we put
$C_k := \phi(u, v, t_k)$, $S_k := S(u, v, t_k)$,
where $\phi(u, v, t_k)$, $S(u, v, t_k)$ represent the solution of (3.3) (3.4).

4. The Transport Part of the Problem

Due to the transformation described in chapter 3, the contaminant transport in domain Ω_R is realized only in v-direction. Therefore by using space discretization in u-direction, $u_{-1/2} = 0$, $u_{1/2}, \ldots, u_{m-1/2}, u_{m+1/2} = \pi$, the original two-dimensional transport problem is reduced to a set of one dimensional problems solved in each strip $\Pi_i = (u_{i-1/2}, u_{i+1/2}) \times (v^{(1)}, v^{(2)})$, $i = 0 \ldots m$.

One of these strips with discretization in v-direction, $v_0 = v^{(2)}, v_{3/2}, v_{5/2}, \ldots, v_{l-1/2}, v_l = v^{(1)}$ is consider and assume that the solution C_{k-1} already exist and moreover let this solution have a piecewise constant profile on Π_i, with shocks in $v_{j+1/2}$, $j = 1 \ldots l$-1. Under these conditions, it is possible to find the solution of transport problem in analytical form.

In general, F in equation (2.14) is not a constant but depends on v. Therefore by using the transformation

$$z = G(v) = z_0 - \int_{v^{(1)}}^{v} \frac{ds}{F(s)} \qquad (4.1)$$

where $z_0 = \int_{v^{(1)}}^{v^{(2)}} \frac{ds}{F(s)}$ and the transport problem in new coordinates is obtained as follows:
$\partial_t(\phi + \psi_e(\phi)) + \partial_z \phi = 0$, $\phi(z,0) = \phi_0(z) = C_{k-1}(G^{-1}(z))$. (4.2)
Considering the saturated region, it is possible to express G(v) in analytical form. Namely,
$G(v) = H\,\delta^2\theta_0(\bar{G}(v) - \bar{G}(v^{(1)}))/(4A)$
where

$$\bar{G}(v) = \frac{2ps-2}{(1-p^2)(s^2-2ps+1)} + \frac{2p}{(1-p^2)^{3/2}} \tan^{-1}\frac{s-p}{\sqrt{1-p^2}}$$

and $s = e^v$, $p = \cos u_i$ in strip Π_i. Constant A comes from the boundary conditions for potential $\bar{\Phi}(v)$. In the unsaturated region, G(v) must be computed numerically.

4.1 Transport Problems

4.1.1 Linear transport problem

Firstly, the simple case when $\psi_e(\phi) \equiv 0$ is considered. For example, no equilibrium adsorption is present. Then the problem is reduced to linear transport problem

$$\partial_t \bar{\phi} + \partial_z \bar{\phi} = 0$$

that can be solved easily by shifting the initial profile, i.e.

$$\bar{\phi}(z,t) = \bar{\phi}(z-t,0) = \bar{\phi}_0(z-t).$$

4.1.2 Non-linear transport problem

In this section principle of solving non-linear transport problems will be roughly presented. The detailed description of the method can be found in . Theoretical results that guarantee existence and uniqueness of the solution can be found in.

Firstly, by taking $\xi = \bar{\phi} + \psi_e(\bar{\phi}) =: \varphi(\bar{\phi})$ (which implies $\bar{\phi} = f(\xi)$, f is the inverse function of φ) and transforming equation (2.14) into the form

$$\partial_t \xi + \partial_z f(\xi) = 0, \quad \xi^0(z) = \varphi(\bar{\phi}_0(z)). \quad (4.3)$$

Now a hyperbolic equation is obtained. If the piecewise constant initial profile is considered, as a multiple Riemann problem. The way of obtaining the analytical solution will be briefly described as follows.

A piecewise constant profile consists of shocks that can be acceptable or not acceptable. The shock for a concave function φ in $\xi^0(z)$ at $z = z^*$ is called acceptable if

$$\xi^0(z_-^*) = \lim_{z \to z_-^*} \xi^0(z) > \xi^0(z_+^*) = \lim_{z \to z_+^*} \xi^0(z).$$

This shock will move in z-direction with Rankine-Hugoniot speed

$$v = \frac{f(\xi^0(z_-^*)) - f(\xi^0(z_+^*))}{\xi^0(z_-^*) - \xi^0(z_+^*)}.$$

If $\xi^0(z_-^*) < \xi^0(z_+^*)$ then the shock is not acceptable. Such a shock is replaced in time by a rarefaction wave which is a smooth function of the form $\xi^*(z - z^*) \equiv \xi^*\left(\frac{z - z^*}{t}\right) = \left[f'\right]^{-1}\left(\frac{z - z^*}{t}\right)$ for $0 < t < t_1^*$,

$z^* + f'(\xi^0(z_-^*))t < z < z^* + f'(\xi^0(z_+^*))t$.

The time t_1^* is the time of collision of the rarefaction wave and an acceptable shock in front. For a convex function φ, the roles of acceptable and not acceptable shocks would be exchanged.

The result of this is that solution of a multiple Riemann problem consists of constants and rarefaction waves. Both shocks and rarefactions are moving ahead in
z-direction, each one at its own velocity, and collisions between them may occur as well. The complete process of constructing the solution consists of tracing the moving shocks and waves and treating their collisions. Essentially, in case only convex or concave function φ is considered and it can be summarized it like this.

- Two neighboring rarefaction waves never meet.
- If two neighboring acceptable shocks collide (the faster one meets the slower one), the slower shock disappears and the shock that remains will now move with a new velocity.
- When a rarefaction wave meets the shock in front, its propagation is from this moment governed by a first order ordinary differential equation that depends on the type of isotherm.

In most cases this ordinary differential equation has to be solved numerically.
The last step of the solution will be a again projection to the original grid. A new piecewise is obtain constant profile is obtained that can be used as the initial condition for the next (dispersion) part of the operator splitting procedure.

4.2 Solution of dispersion problem

In this section how to solve the dispersion problem of the form

$$\partial_t \varphi(\phi) - g(\partial_u(a\partial_u\phi) + \partial_v(b\partial_v\phi)) = 0, t \in (t_{k-1}, t_k) \quad (4.4)$$

with boundary conditions of the form (2.11) and initial condition $\phi(u, v, t_{k-1}) = C_k^{1/3}$ is considered as follows.

A standard finite volume method can be used for this purpose.In this purpose V_{ij} stand for the volume
$(u_{k-1/2}, u_{i+1/2}) \times (v_{j-1/2}, v_{k+1/2})$for i=0 . . . m,v=1 . . . λ,
$V_{i0} = (u_{i-1/2}, u_{i+1/2}) \times (v_0, v_{3/2})$. By integrating (4.4) over $\Delta t = (t_{k-1}, t_k)$ and V_{ij} and assuming that values $\phi_{ij} = \phi(u_i, v_j)$ and $g_{ij} = g(u_i, v_j)$ are dominant over V_{ij},

$$V_{ij} \int_{\Delta t} \partial_t \varphi(\phi_{ij}) dt = g_{ij} \int_{\Delta t} \int_{V_{ij}} (\partial_u(a(u,v)\partial_u\phi) + \partial_v(b(u,v)\partial_v\phi)) \, du \, dv \, dt. \quad (4.5)$$

is obtained.
For convenience, the following notations are used:

$$\phi^E = \phi_{i+1j}, \quad \phi^W = \phi_{i-1j}, \quad \phi^N = \phi_{ij+1}, \quad \phi^S = \phi_{ij-1}$$

and

$a^E = a_{i+1/2j}$, $a^W = a_{i-1/2j}$, $a^N = a_{ij+1/2}$, $a^S = a_{ij-1/2}$

and analogously for b^W, b^E, b^N, b^S .

Further Δ u =

$u_{i+1/2} - u_{i-1/2}$, $\Delta v = v_{j-1/2} - v_{j+1/2}$, $\Delta u_+ = u_{i+1} - u_i$,

$\Delta u_- = u_i - u_{i-1}$ and similar for Δv_+ , Δv_- .

Approximate the derivatives $\partial_u \phi$ on edges$\{u_{i+1/2}\}$ x $(v_{j-1/2}, v_{j+1/2})$, { } x $(v_{j-1/2}, v_{j+1/2})$ by $(\phi^E - \phi_{ij})/\Delta u_+$ respectively.

$(\phi_{ij} - \phi^W)/\Delta u_-$ and similar for $\partial_v \phi$ on edges $\{v_{j+1/2}\}$ x $(u_{j-1/2}, u_{j+1/2})$,

$\{v_{j-1/2}\}$ x $(u_{j-1/2}, u_{j+1/2})$.

Finally by taking $\partial_t \varphi(\phi_{ij}) \approx (\varphi(\phi_{ij}) - \varphi(\phi_{ij}^{k-1}))/\Delta t)$, the following numerical scheme is obtained;

$$\frac{|V_{ij}|}{g_{ij}}\varphi(\phi_{ij}) + \left(a^E\frac{\Delta v}{\Delta u_+} + a^W\frac{\Delta v}{\Delta u_-} + b^N\frac{\Delta u}{\Delta v_+} + b^S\frac{\Delta u}{\Delta v_-}\right)\Delta t\phi_{ij} =$$

$$\Delta t\left(a^E\frac{\Delta v}{\Delta u_+}\phi^E + a^W\frac{\Delta v}{\Delta u_-}\phi^W + b^N\frac{\Delta u}{\Delta v_+}\phi^N + b^S\frac{\Delta u}{\Delta v_-}\phi^S\right) + \frac{|V_{ij}|}{g_{ij}}\varphi(\phi_{ij}^{k-1}) . \quad (4.6)$$

According to the boundary conditions, put $a^W = 0$ for points $\{u_0, v_j\}$, $a^E = 0$ for $\{u_m, v_j\}$, j=1. . . λ. Similarly $b^S = 0$ for points $\{u_i, v_l\}$, i = 0 . . . m

Equation (4.6) represents a non-linear algebraic system that can be solved using standard Newton-Kantorovich method. The linear system that arises in each Newton iteration is tridiagonal if $\alpha_T = 0, D_0 = 0$, otherwise it has not more than five non-zero elements in each row.

4.3 Non-equilibrium adsorption problem

The non-equilibrium adsorption problem is problem is represented by the following ODE system;

$$\partial_t \varphi(\phi) + \partial_t S = 0 , \quad (4.7)$$

$$\partial_t S = K(\psi_n(\phi) - S) \quad (4.8)$$

with initial conditions

$$\phi(u, v, t_{k-1}) = \phi_0(u,v) = C_k^{2/3} \quad (4.9)$$

$$S(u, v, t_{k-1}) = S_0(u, v) = S_{k-1} \quad (4.10)$$

for t$\in (t_{k-1}, t_k)$.

Firstly a shift $t_{k-1} \to 0$ is made, and so the time interval becomes $(0, t_k - t_{k-1})$. It can be expressed S(t) for which (4.8) can be solve in S as follows:

$$S(t) = S_0 e^{-Kt} + K\int_0^t e^{-K(t-z)}\psi_n(\phi(z))dz . \quad (4.11)$$

Now integrating (4.7) in t,

$$\varphi(\phi(t)) + S(t) = c$$

is obtained and using the initial conditions (4.9) and (4.10), c becomes as c = $\varphi(\phi_0) + S_0$ which implies

$$\varphi(\phi(t)) + S(t) = \varphi(\phi_0) + S_0 . \quad (4.12)$$

Finally, putting (4.11) into (4.12) an integral equation of the form

$$\varphi(\phi(t)) + S_0 e^{-Kt} + K\int_0^t e^{-K(t-z)}\psi_n(\phi(z))dz = \varphi(\phi_0) + S_0$$

(4.13) is obtained.

Next, the procedure is continued as follows. First marking equidistantly discretize the time interval (t_{k-1}, t_k), s+1 time levels $t_{k-1} = \bar{t}_0, \bar{t}_1, \ldots, \bar{t}_{s-1}, \bar{t}_s = t_k$ will be obtained , where $\bar{t}_i = i\tau$, τ is the time step.

And then for any i = 0. . . s

$$I_i := \int_0^{\bar{t}_i} e^{-K(\bar{t}_i - z)}\psi_n(\phi(z))\,dz = \sum_{j=1}^{i}\int_{\bar{t}_{j-1}}^{\bar{t}_j} e^{-K(\bar{t}_i - z)}\psi_n(\phi(z))\,dz \quad (4.14)$$

Next the following approximations are considered as:

$\phi(t) \approx \phi_j$, $\psi_j = \psi_n(\phi_j)$ $\forall t \in (\bar{t}_{j-1}, \bar{t}_j)$,

$$\psi_n(t) \approx \psi_{j-1} + \frac{t - \bar{t}_{j-1}}{\tau}(\psi_j - \psi_{j-1}) = \psi_{j-1}\left(1 - \frac{t - \bar{t}_{j-1}}{\tau}\right) + \psi_j\frac{t - \bar{t}_{j-1}}{\tau} \quad (4.15)$$

Using linear approximation (4.15) , approximation of I_i may be expressed as

$$I_i \approx \sum_{j=1}^{i}\int_{\bar{t}_{j-1}}^{\bar{t}_j} e^{-K(t_i - z)}\left(\left(1 - \frac{z - \bar{t}_{j-1}}{\tau}\right)\psi_{j-1} + \frac{z - \bar{t}_{j-1}}{\tau}\psi_j\right)dz$$

$$= \sum_{j=0}^{i}\alpha_{ij}\psi_j =: \bar{I}_i$$

As for the coefficients α_{ij} ,

$$\alpha_{ij} = \frac{1}{K^2\tau}e^{-K(\bar{t}i - \bar{t}j)}(-2 + e^{K\tau} + e^{-Kt}) \text{ for j=1,...,i-1,}$$

$$\alpha_{i,0} = \frac{1}{K\tau}e^{-K\bar{t}_i}\left(-\tau - \frac{1}{K} + \frac{1}{K}e^{K\tau}\right) ,$$

$$\alpha_{i,i} = \frac{1}{K\tau}\left(\tau - \frac{1}{K} + \frac{1}{K}e^{-K\tau}\right) .$$

Now, for $\alpha_{i+1,j}$ it holds

$$\alpha_{i+1,j} = \frac{1}{K^2\tau}e^{-K(\bar{t}i+1 - \bar{t}j)}(-2 + e^{K\tau} + e^{-K\tau}) = e^{-K\tau}\alpha_{ij} \quad \forall j = 0,\ldots,i-1$$

which can be used for deriving the following recursion formula:

$$\bar{I}_1 = \sum_{j=0}^{i} \alpha_{i+1\,j}\psi_j = \sum_{j=0}^{i-1} \alpha_{i+1\,j}\psi_j + \alpha_{i+1,i}\psi_i$$

$$= e^{-K\tau} \sum_{j=0}^{i=1} \alpha_{ij}\psi_j + \frac{1}{K^2\tau} e^{-Kt}(-2 + e^{Kt} + e^{-Kt})\psi_i$$

$$= e^{-K\tau} \bar{I}_i^{*} + \frac{1}{K^2\tau}(e^{-Kt} - 1)^2 \psi_i \qquad (4.16)$$

for i =1... n-1,while $\bar{I}_1^{*} = -\frac{(K\tau e^{-K\tau} + e^{-K\tau} - 1)}{K^2\tau}\psi_0$.

Now a numerical scheme for solving (4.13) can be introduced. First, using the transformation

$\zeta = \psi_n(\phi)$, and (4.14) can be rewritten into the form

$$\varphi(\psi_n^{-1}(\zeta)) =: f(\zeta) = \varphi(\phi_0) + S_0 - S_0 e^{-Kt} - K\int_0^t e^{-K(t-z)}\zeta(z)dz ,$$

and using the time discretization

$f_i = \varphi(\phi_0) + S_0 - S_0 e^{-Kt_i} - KI_i$ for i = 0, 1, . . . ,s

respectively.

$$f_{i+1} = \varphi(\phi_0) + S_0 - S_0 e^{-Kt_{i+1}} - KI_{i+1} \approx \varphi(\phi_0) + S_0 - S_0 e^{-Kt_{i+1}} - K\bar{I}_{i+1}^{*} - K\alpha_{i+1,i+1}\zeta_{i+1}$$

using now ζ_j instead of ψ_j in terms I_{i+1}, $\bar{I}_{i+1}^{*}$.

This represents the following implicit scheme for finding ζ_{i+1} , with m being the iterative index:

$$f_{i+1}^{(m+1)} = \varphi(\phi_0) + S_0 - S_0 e^{-Kt_{i+1}} - K\bar{I}_{i+1}^{*} - K\alpha_{i+1.o+i}\zeta_{i+1}^{(m)} \qquad m = 0,1,\ldots, \qquad (4.17)$$

$\zeta_{i+1}^{(0)} = \zeta_i$. The value $\zeta_{i+1}^{(m+1)}$ is needed, in each step of the implicit process a non linear equation of the form $f(\zeta_{i+1}^{(m+1)}) = f_{i+1}^{(m+1)}$ must be solved.

For this purpose the standard Newton method can be used. To evaluate the term $\bar{I}_{i+1}^{*}$ recursion formula is used(4.20), by substituting ψ_j with ζ_j

.

4. Conclusion

This paper described how to construct a mathematical model for Groundwater contaminantion and the Operator-splitting Scheme. Using these our research will be continued for solving environmental problems in delta area in our country.

References

[1] D. Constales, J.Kacur, B. Malengier, A precise numerical scheme for contaminant transport in dual-well flow, Water Resour, Resour. Res. 39 (30) (2003) 1303.

[2] M.G. Crandall, A. Majda, The method of fractional steps for conservation laws, Numer. Math.34 (1980)285-314.

[3] H.M. Hajdjema, Analytical Modeling of Groundwater Flow, Academic Press, New York, 1995.

[4] H.Holden, K.H. Karlsen, K.A. Lie, Operator splitting methods for degenerate convection-diffusion equation I: Convergence and entropy estimates, stochastic processes, physics and geometry: new interplays, II(Leipzig, 1999), in: CMS Conf. Proc., vol.29, Amer. Math. Soc., Providence, RI, 2000, pp.293-316.

[5] SM. Kruzkov, First order quasi linear equations in several independent variables, Math. USSR Sbornik 10(2) (1970) 217-243.

Stability of Leapfrog Method for the Generalized FKPP Equation

Shwe Sin Win,
Department of Engineering Mathematics,Yangon Technological University,
Yangon, Myanmar.

Abstract: In this paper we study stability of leapfrog method for solving the generalized Fisher-Kolmogorov-Petrovskii-Piskunov (FKPP) equation numerically. The method is obtained by considering the Method of Lines (MOL) approach and using three time-levels. We investigate the stability of Richardson method and modify it to get the leapfrog method. Some examples are presented to support our study.

Keywords: Fisher equation**,** FKPP equation, Method of lines, Finite differences, Richardson method, Leapfrog method, Stability.

1. Introduction

We consider the generalized Fisher-Kolmogorov-Petrovskii-Piskunov (FKPP) equation

$$\frac{\partial U}{\partial t}(x,t) = \frac{D}{\tau}\int_0^t e^{-\frac{t-s}{\tau}} \frac{\partial^2 U}{\partial x^2}(x,s)\ ds + f(U(x,t)),\quad x\in(a,b),\ t>0, \tag{1.1}$$

where $D \geq 0$ and $\tau > 0$ are known constants and f is a given function.

We let the initial condition be

$$U(x,0) = U^o(x),\quad x\in(a,b), \tag{1.2}$$

and the boundary conditions

$$U(a,t) = U_a(t),\ U(b,t) = U_b(t),\ t>0. \tag{1.3}$$

When the relaxation parameter τ tends to zero, the FKPP equation becomes the Fisher equation

$$\frac{\partial U}{\partial t}(x,t) = D\frac{\partial^2 U}{\partial x^2}(x,t) + f(U(x,t)). \tag{1.4}$$

The existence and the properties of solutions of (1.1) for $(a,b)=(0,1)$ with $f(U) = \acute{U}U(1-U)$, constant $\acute{U} > 0$, and a Heaviside initial condition, are studied in [5]. In [2], the authors discuss the qualitative properties of numerical solutions of the same problem. Some numerical schemes obtained by the method of lines approach are investigated in [3]. The stability and convergence properties of time discretization of a general form of this type with $f = f(t)$ are examined in [9]. In [1], the authors consider the equation (1.1) with $f(U(x,t)) = \alpha\frac{\partial^2 U}{\partial x^2}(x,t), \alpha \geq 0$, which is also known as the Jeffrey's equation, and homogenerous Dirichlet boundary conditions.

In this paper we will consider the stability of leap-frog method that approximate (1.1). The integral term is approximated by simple rectangular rule.

Methods using trapezoidal rule and quadrature rule can also be possible.

Corresponding Author : Shwe Sin Win, Department of Engineering Mathematics,Yangon Technological University, Yangon, Myanmar.shwezinwin22@gmail.com

2. Discretization of the Problem

We consider the problem (1.1)-(1.3) in $(a,b)\times(0,T)$, and the space grid $\{x_j \mid x_j = a + jh,\ \ j = 0,1,2,...,J\ \}$ with $h = \frac{b-a}{J}$. Let us also consider the time grid $\{t_n \mid t_n = nk, n = 0,1,2,...,N\}$ with $k = \frac{T}{N}$.

We will denote approximation of $U(x,t)$ by $u(x,t)$, and write $U(x_j,t) = U_j(t)$, $u(x_j,t) = u_j(t)$, $U(x_j,t_n) = U_j^n$ and $u(x_j,t_n) = u_j^n$.

We discretize the partial derivatives with respect to *x* as

$$D_2u_j(t) = \frac{1}{h^2}\left(u_{j-1}(t) - 2u_j(t) + u_{j+1}(t)\right),$$

$$D_2u_j^n = \frac{1}{h^2}\left(u_{j-1}^n - 2u_j^n + u_{j+1}^n\right),$$

$$D_2^*u_j(t) = \frac{1}{h^2}[u_{j-1}(t) - \{u_j(t-k) + u_j(t+k)\} + u_{j+1}(t)],$$

$$D_2^*u_j^n = \frac{1}{h^2}\left\{u_{j-1}^n - \left(u_j^{n-1} + u_j^{n+1}\right) + u_{j+1}^n\right\},$$

and, with respect to *t*, as

$$D_+^tu_j^n = \frac{1}{k}\left(u_j^{n+1} - u_j^n\right),$$

$$D_-^tu_j^n = \frac{1}{k}\left(u_j^n - u_j^{n-1}\right),$$

$$D_0^tu_j^n = \frac{1}{2k}\left(u_j^{n+1} - u_j^{n-1}\right),$$

respectively.

The initial condition is discretized as

$U_j^0 = U(x_j,0) = U^o(x_j)$, $j = 0,1,2,...,J$,

and the boundary conditions as

$U_0^n = U(a,t_n) = U_a(t_n)$ and

$U_J^n = U(b,t_n) = U_b(t_n)$, $n = 1,2,3,...,N$.

We will approximate $\frac{\partial^2U}{\partial x^2}(x_j,t)$ by $D_2u_j(t)$ and $\frac{\partial^2U}{\partial x^2}(x_j,t_n)$ by $D_2u_j^n$.

For the approximate solution, the initial and boundary conditions will be taken as $u_j^0 = U^o(x_j)$, $j = 0,1,2,...,J$, $u_0^n = U_a(t_n)$ and $u_J^n = U_b(t_n)$, $n = 1,2,3,...,N$.

3. Method of Lines

At first we consider the method of lines (MOL) approach to obtain a semi-discrete numerical approximation $u_j(t)$ to the solution $U\ (x,t)$ of (1.1) - (1.3). At $x = x_j$, (1.1) becomes ordinary differential equation

$$\frac{dU}{dt}(x_j,t) = \frac{D}{\tau}\int_0^t e^{-\frac{t-s}{\tau}}\frac{\partial^2U}{\partial x^2}(x_j,s)ds + f\left(U(x_j,t)\right). \qquad (3.1)$$

We discretize $\frac{\partial^2U}{\partial x^2}(x_j,s)$ in (3.1) by $D_2u_j(s)$ to get the system of ordinary differential equations

$$\frac{du_j(t)}{dt} = \frac{D}{\tau}\int_0^t e^{-\frac{t-s}{\tau}}D_2u_j(s)\ \ ds + f\left(u_j(t)\right), \quad j = 1,2,3,...,J-1. \qquad (3.2)$$

We will use rectangular rule to compute the integral numerically. When $t = t_{n+1}$, we can approximate the right hand side of (3.2) in the following ways:

(i)Explicit scheme

$$\left.\frac{du_j(t)}{dt}\right|_{t=t_{n+1}} = \frac{D}{\tau}k\sum_{m=0}^{n} e^{-\frac{t_{n+1}-t_m}{\tau}} D_2 u_j^m + f(u_j^n). \qquad (3.3)$$

(ii)Implicit scheme

$$\left.\frac{du_j(t)}{dt}\right|_{t=t_{n+1}} = \frac{D}{\tau}k\sum_{m=0}^{n} e^{-\frac{t_{n+1}-t_{m+1}}{\tau}} D_2 u_j^{m+1} + f(u_j^{n+1}). \qquad (3.4)$$

(iii)Implicit -Explicit scheme

$$\left.\frac{du_j(t)}{dt}\right|_{t=t_{n+1}} = \frac{D}{\tau}k\sum_{m=0}^{n} e^{-\frac{t_{n+1}-t_{m+1}}{\tau}} D_2 u_j^{m+1} + f(u_j^n). \qquad (3.5)$$

We can apply trapezoidal rule to get more accurate numerical solution. From (3.3) or (3.4) or (3.5), we will have fully discrete approximation.

For the first time step, we need to use backward finite difference and so we approximate

$\left.\frac{du_j(t)}{dt}\right|_{t=t_1}$ by $D_-^t u_j^1$.

4. Unstable Richardson Method

In Richardson approximation, time-derivatives $\left.\frac{du_j(t)}{dt}\right|_{t=t_{n+1}}$ are approximated by

$D_0^t u_j^n$ for $n \geq 1$. Thus we have the followings:

(i) Explicit scheme

For $n = 0$,

$$\frac{u_j^1 - u_j^0}{k} = \frac{D}{\tau}ke^{-\frac{t_1-t_0}{\tau}}\frac{u_{j-1}^0 - 2u_j^0 + u_{j+1}^0}{h^2} + f(u_j^0)$$

$$u_j^1 = u_j^0 + \frac{D}{\tau}\frac{k^2}{h^2}e^{-\frac{t_1}{\tau}}(u_{j-1}^0 - 2u_j^0 + u_{j+1}^0) + k\ f(u_j^0), \quad j = 1,2,...,J-1. \qquad (4.1)$$

For $n \geq 1$,

$$\frac{u_j^{n+1} - u_j^{n-1}}{2k} = \frac{D}{\tau}k\sum_{m=0}^{n} e^{-\frac{t_{n+1}-t_m}{\tau}}\frac{u_{j-1}^m - 2u_j^m + u_{j+1}^m}{h^2} + f(u_j^n)$$

$$u_j^{n+1} = u_j^{n-1} + \frac{D}{\tau}\frac{2k^2}{h^2}e^{-\frac{t_{n+1}}{\tau}}\sum_{m=0}^{n} e^{\frac{t_m}{\tau}}\left(u_{j-1}^m - 2u_j^m + u_{j+1}^m\right) + 2k\ f(u_j^n), \quad j = 1,2,...,J-1. \qquad (4.2)$$

(ii)Implicit scheme

For $n = 0$,

$$\frac{u_j^1 - u_j^0}{k} = \frac{D}{\tau}ke^{-\frac{t_1-t_1}{\tau}}\frac{u_{j-1}^1 - 2u_j^1 + u_{j+1}^1}{h^2} + f(u_j^1)$$

$$u_j^1 - u_j^0 = \frac{D}{\tau}\frac{k^2}{h^2}(u_{j-1}^1 - 2u_j^1 + u_{j+1}^1) + k\ f(u_j^1), \quad j = 1,2,...,J-1. \qquad (4.3)$$

For $n \geq 1$,

$$\frac{u_j^{n+1}-u_j^{n-1}}{2k} =$$

$$\frac{D}{\tau}k\sum_{m=0}^{n} e^{-\frac{t_{n+1}-t_{m+1}}{\tau}} \frac{u_{j-1}^{m+1}-2u_j^{m+1}+u_{j+1}^{m+1}}{h^2} + f(u_j^{n+1}).$$

$$u_j^{n+1}-u_j^{n-1} =$$

$$\frac{D}{\tau}\frac{2k^2}{h^2}e^{-\frac{t_{n+1}}{\tau}}\sum_{m=0}^{n} e^{\frac{t_{m+1}}{\tau}}\left(u_{j-1}^{m+1}-2u_j^{m+1}+u_{j+1}^{m+1}\right)+2k$$

$$f(u_j^{n+1}), \quad j=1,2,...,J-1. \qquad (4.4)$$

(iii)Implicit -Explicit scheme

For $n=0$,

$$\frac{u_j^1-u_j^0}{k} = \frac{D}{\tau}ke^{-\frac{t_1-t_1}{\tau}}\frac{u_{j-1}^1-2u_j^1+u_{j+1}^1}{h^2} + f(u_j^0)$$

$$u_j^1-u_j^0=\frac{D}{\tau}\frac{k^2}{h^2}(u_{j-1}^1-2u_j^1+u_{j+1}^1)+ k\ f(u_j^0),\ j=1,2,...,J-1. \qquad (4.5)$$

For $n\geq 1$,

$$\frac{u_j^{n+1}-u_j^{n-1}}{2k} =$$

$$\frac{D}{\tau}k\sum_{m=0}^{n} e^{-\frac{t_{n+1}-t_{m+1}}{\tau}} \frac{u_{j-1}^{m+1}-2u_j^{m+1}+u_{j+1}^{m+1}}{h^2} + f(u_j^{n}).$$

$$u_j^{n+1}-u_j^{n-1} =$$

$$\frac{D}{\tau}\frac{2k^2}{h^2}e^{-\frac{t_{n+1}}{\tau}}\sum_{m=0}^{n} e^{\frac{t_{m+1}}{\tau}}\left(u_{j-1}^{m+1}-2u_j^{m+1}+u_{j+1}^{m+1}\right)+2k$$

$$f(u_j^{n}), \quad j=1,2,...,J-1. \qquad (4.6)$$

Now we will present an example to show unstability of Richardson method.

5. An Example Showing Unstability

To illustrate the method we will use the following data:

$a=0,\ b=1,\ T=0.2,\ D=0.2,\ \tau=0.1,$

$f(U)=\acute{U}U(1-U)$ with $\acute{U}=1$,

$$U^o(x) = \begin{cases} 1, x\in[a,\frac{1}{2}(a+b)], \\ 0, x\in(\frac{1}{2}(a+b),b], \end{cases}$$

$U_a(t)=1,\ U_b(t)=0.$

Let us take $J=80$ and $N=180$ .Then

$h=\frac{1}{80}=0.0125,\ k=\frac{0.2}{180}=\frac{1}{900}$ and

$r=\frac{k}{h^2}=\frac{64}{9}$.

We will apply Richardson's explicit scheme (4.1) - (4.2) for calculation to be as simple as possible. The numerical result is shown in the following figure. It shows that the scheme is unstable.

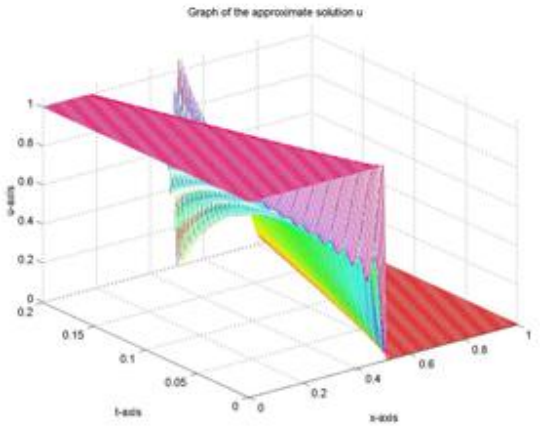

Figure 5.1

6. Modification of the Method

Richardson method is unstable because $\frac{\partial^2 U}{\partial x^2}(x_j, s)$ is approximated by $D_2 u_j(s)$. So we need to modify it.

Now we will discretize $\frac{\partial^2 U}{\partial x^2}(x_j, s)$ by $D_2^* u_j(s)$.

Then (3.1) becomes

$$\frac{du_j(t)}{dt} = \frac{D}{\tau}\int_0^t e^{-\frac{t-s}{\tau}} D_2^* u_j(s)\, ds + f(u_j(t)). \quad (6.1)$$

When $t = t_{n+1}$, $n \geq 1$,we approximate the right hand side of (7.1) as in section 3,and get the following schemes:

(i)Explicit scheme

$$\frac{du_j(t)}{dt}\Big|_{t=t_{n+1}} = \frac{D}{\tau} k \sum_{m=0}^{n} e^{-\frac{t_{n+1}-t_m}{\tau}} D_2^* u_j^m + f(u_j^n). \quad (6.2)$$

(ii)Implicit scheme

$$\frac{du_j(t)}{dt}\Big|_{t=t_{n+1}} = \frac{D}{\tau} k \sum_{m=0}^{n} e^{-\frac{t_{n+1}-t_{m+1}}{\tau}} D_2^* u_j^{m+1} + f(u_j^{n+1}). \quad (6.3)$$

(iii)Implicit -Explicit scheme

$$\frac{du_j(t)}{dt}\Big|_{t=t_{n+1}} = \frac{D}{\tau} k \sum_{m=0}^{n} e^{-\frac{t_{n+1}-t_{m+1}}{\tau}} D_2^* u_j^{m+1} + f(u_j^n). \quad (6.4)$$

If we discretize the left hand sides of the above equations, we will get fully discrete approximations.

7. Stable Leapfrog Method

As before time-derivatives $\frac{du_j(t)}{dt}\Big|_{t=t_{n+1}}$ are approximated by $D_-^t u_j^1$ for $n = 0$, and by $D_0^t u_j^n$ for $n \geq 1$ .Now, the schemes are as follows:

(i)Explicit scheme

For $n = 0$,

$$\frac{u_j^1 - u_j^0}{k} = \frac{D}{\tau} k e^{-\frac{t_1 - t_0}{\tau}} \frac{u_{j-1}^0 - (u_j^0 + u_j^1) + u_{j+1}^0}{h^2} + f(u_j^0)$$

$$u_j^1 = u_j^0 + \frac{D}{\tau}\frac{k^2}{h^2} e^{-\frac{t_1}{\tau}} \left\{u_{j-1}^0 - (u_j^0 + u_j^1) + u_{j+1}^0\right\} + k\ f(u_j^0)$$

$$\left(1 + \frac{D}{\tau}\frac{k^2}{h^2} e^{-\frac{t_1}{\tau}}\right) u_j^1 = u_j^0 + \frac{D}{\tau}\frac{k^2}{h^2} e^{-\frac{t_1}{\tau}} \left(u_{j-1}^0 - u_j^0 + u_{j+1}^0\right) + k\ f(u_j^0),$$

$$j = 1, 2, ..., J-1. \quad (7.1)$$

For $n = 1$,

$$\frac{u_j^2 - u_j^0}{2k} = \frac{D}{\tau}\ k\ e^{-\frac{t_2}{\tau}} \left[e^{\frac{t_0}{\tau}} \frac{u_{j-1}^0 - (u_j^0 + u_j^1) + u_{j+1}^0}{h^2} + e^{\frac{t_1}{\tau}} \frac{u_{j-1}^1 - (u_j^0 + u_j^2) + u_{j+1}^1}{h^2} \right] + f(u_j^1)$$

$$\left(1 + \frac{D}{\tau}\frac{2k^2}{h^2} e^{-\frac{k}{\tau}}\right)\ u_j^2$$

$$= u_j^0 + \frac{D}{\tau}\frac{2k^2}{h^2} e^{-\frac{t_2}{\tau}} \left[\left\{ u_{j-1}^0 - (u_j^0 + u_j^1) + u_{j+1}^0 \right\} + e^{\frac{t_1}{\tau}} \left\{ u_{j-1}^1 - u_j^0 + u_{j+1}^1 \right\} \right] + 2k \quad f(u_j^1). \quad (7.2)$$

For $n \geq 2$,

$$\frac{u_j^{n+1} - u_j^{n-1}}{2k}$$

$$= \frac{D}{\tau} k \quad e^{-\frac{t_{n+1}}{\tau}} \left[e^{\frac{t_0}{\tau}} \frac{u_{j-1}^0 - (u_j^0 + u_j^1) + u_{j+1}^0}{h^2} + \sum_{m=1}^{n} e^{\frac{t_m}{\tau}} \frac{u_{j-1}^m - (u_j^{m-1} + u_j^{m+1}) + u_{j+1}^m}{h^2} \right] + f(u_j^n)$$

$$u_j^{n+1} = u_j^{n-1} + \frac{D}{\tau}\frac{2k^2}{h^2} e^{-\frac{t_{n+1}}{\tau}} \left[\left\{ u_{j-1}^0 - (u_j^0 + u_j^1) + u_{j+1}^0 \right\} + \sum_{m}^{n-1} \quad e^{\frac{t_m}{\tau}} \left\{ u_{j-1}^m - (u_j^{m-1} + u_j^{m+1}) + u_{j+1}^m \right\} + e^{\frac{t_n}{\tau}} \left\{ u_{j-1}^n - (u_j^{n-1} + u_j^{n+1}) + u_{j+1}^n \right\} \right] + 2k \quad f(u_j^n)$$

$$\left(1 + \frac{D}{\tau}\frac{2k^2}{h^2} e^{-\frac{k}{\tau}}\right) u_j^{n+1} = u_j^{n-1} + \frac{D}{\tau}\frac{2k^2}{h^2} e^{-\frac{t_{n+1}}{\tau}} \left[\left\{ u_{j-1}^0 - (u_j^0 + u_j^1) + u_{j+1}^0 \right\} + \sum_{m=1}^{n-1} \quad e^{\frac{t_m}{\tau}} \left\{ u_{j-1}^m - (u_j^{m-1} + u_j^{m+1}) + u_{j+1}^m \right\} + e^{\frac{t_n}{\tau}} \left\{ u_{j-1}^n - u_j^{n-1} + u_{j+1}^n \right\} \right] + 2k \quad f(u_j^n),$$

$$j = 1, 2, ..., J-1. \quad (7.3)$$

(ii)Implicit scheme

For $n = 0$,

$$\frac{u_j^1 - u_j^0}{k} = \frac{D}{\tau} k e^{-\frac{t_1 - t_1}{\tau}} \quad \frac{u_{j-1}^1 - (u_j^0 + u_j^1) + u_{j+1}^1}{h^2} + f(u_j^1)$$

$$u_j^1 - u_j^0 = \frac{D}{\tau}\frac{k^2}{h^2} \quad \left\{ u_{j-1}^1 - (u_j^0 + u_j^1) + u_{j+1}^1 \right\} + k \quad f(u_j^1), \quad j = 1, 2, ..., J-1. \quad (7.4)$$

For $n \geq 1$,

$$\frac{u_j^{n+1} - u_j^{n-1}}{2k} =$$

$$\frac{D}{\tau} k \sum_{m=0}^{n-1} \quad e^{-\frac{t_{n+1} - t_{m+1}}{\tau}} \quad \frac{u_{j-1}^{m+1} - (u_j^m + u_j^{m+2}) + u_{j+1}^{m+1}}{h^2} + \frac{D}{\tau} k \; e^{-\frac{t_{n+1} - t_{n+1}}{\tau}} \quad \frac{u_{j-1}^{n+1} - (u_j^n + u_j^{n+1}) + u_{j+1}^{n+1}}{h^2} + f(u_j^{n+1})$$

$$u_j^{n+1} - u_j^{n-1} = \frac{D}{\tau}\frac{2k^2}{h^2} e^{-\frac{t_{n+1}}{\tau}} \sum_{m=0}^{n-1} \quad e^{-\frac{t_{n-1}}{\tau}} \left\{ u_{j-1}^{m+1} - (u_j^m + u_j^{m+2}) + u_{j-1}^{m+1} \right\} + \frac{D}{\tau}\frac{2k^2}{h^2} \left\{ u_{j-1}^{n+1} - (u_j^n + u_j^{n+1}) + u_{j+1}^{n+1} \right\} + 2k \quad f(u_j^{n+1}),$$

$$j = 1, 2, ..., J-1. \quad (7.5)$$

We will not present implicit-explicit scheme here since it can be obtained from (7.4) and (7.5) by replacing $f(u_j^1)$ and $f(u_j^{n+1})$ with $f(u_j^0)$ and $f(u_j^n)$,respectively.

8. Some Examples Showing Stability

We will try the same example in section 5, with various data, again by applying leapfrog explicit scheme (7.1)-(7.3).We plot the numerical solutions as shown in the figures.It can be seen that the scheme is stable.

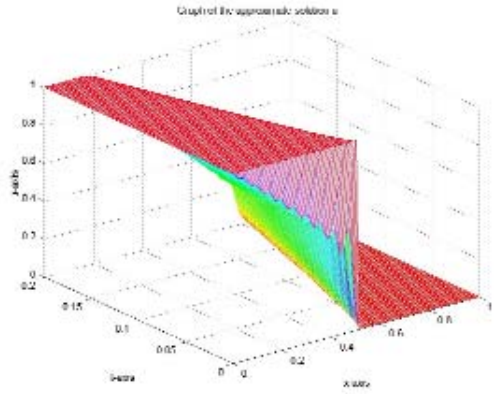

Figure 8.1

T=0.2, J=80,N=180,h= $\frac{1}{80}$,k= $\frac{0.2}{180} = \frac{1}{900}$

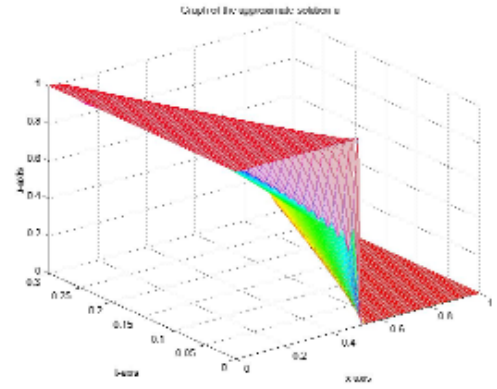

Figure 8.2

T=0.3, J=80,N=180,h= $\frac{1}{80}$,k= $\frac{0.2}{180} = \frac{1}{900}$

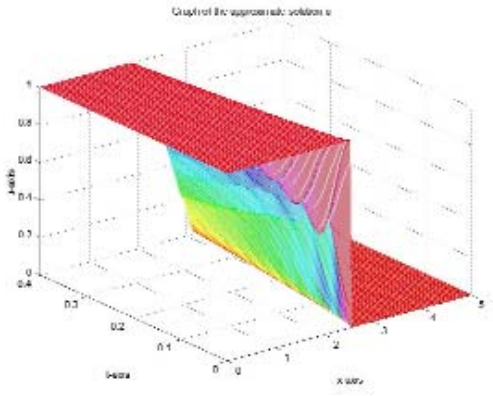

Figure 8.3

J=100,N=200,h= $\frac{5}{100} = \frac{1}{20}$,k= $\frac{0.4}{200} = \frac{1}{500}$

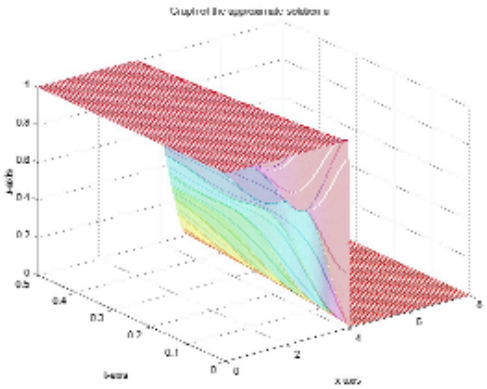

Figure 8.4

J=80,N=100,h= $\frac{8}{80} = \frac{1}{10}$,k= $\frac{0.5}{100} = \frac{1}{200}$

The stability of the leapfrog method can be shown analytically by applying Von Neumann analysis.

References

[1] Arauso , A., Branco, J.R. and Ferreira, J.A., “On the stability of a class of splitting methods for integro-differential equations”, Preprint Number 06-55, Universidade de Coimbra, (2006).

[2] Araujo,A.,Ferreira,J.A. and Oliveira,P.,"Qualitative behaviour of numerical traveling solutions for reaction diffusion equations with memory," Preprint Number 04-23,Universidade de Coimbra,(2004).

[3] Branco,J.R.,Ferreira, J.A. and Oliveira,P.,"Numerical methods for the generalized Fisher-Kolmogorov-Petrovskii-Piskunov equation",Appl Number Math 57, 89-102,(2007).

[4] Cooper,J.,"Introduction to partial differential equations with MATLAB", Birkhäuser,(1998).

[5] Fedotov,S.,"Travelling waves in a reaction-diffusion system:Diffusion with finite velocity and Kolmogorov-Petrovskii-Piskunov kinetics," Phys Rev E58, 5143-5145, (1998).

[6] Haberman,R.,"Applied partial differential equations". Fourth edition,Pearson Prentice Hall,(2004).

[7] Hubdsdorfer ,W. and Verwer,J.,"Numerical solution of time-dependent advection-diffusion-reaction equations", Springer,(2003).

[8] Mitchell,A.R. and Driffiths,D.F.,"The finite difference method in partial differential equations", John Wiley & Sons,(1980).

[9] Sloan,I.H. and Thomée,V.."Time discretization of an integro-differential equation of parabolic type",SIAM J. Numer Anal Vol23,No.5,(1986).

[10] Smith ,G.D.,"Numerical solution of partial differential equations: Finite difference methods", Third edition , Clarendon Press, Oxford,(1985).

[11] Strikwerda,J,C,,"Finite difference schemes and partial differential equation", Wadsworth & Brooks/Cloe, Advanced Books & Software,(1989).

[12] Thomas,J.W.,"Numerical partial differential equations:Finite difference methods",Springer-Verlag,NewYork,Inc.,(1995).

Investigating Spatially Distributive Structures of Vegetation in Arid Environment by Modelling and Nonlinear Stability Analyses

Nichaphat Boonkorkuea [1], David J Wollkind [2], Francisco J Alvarado[3], and Yongwimon Lenbury [1]

[1]Department of Mathematics, Faculty of Science, Mahidol University,
Rama 6Road Bangkok 10400, Thailand

[2]Department of Mathematics, Washington State, University Pullman, WA 99164-3133, U.S.A.

[3] Departmento de Ciencias Basicas, Technologico de Monterrey, Campus Guadalajara, Zapopan, Jalisco C.P. 45201, Mexico

Email: nichapat_saw@hotmail.com

Abstract: We investigate spontaneous pattern formation induced by facilitative and competitive interactions of plant community in arid environment. Rhombic platform weakly nonlinear stability analysis is performed on relevant model equation in order to identify regions in a two dimensional parameter space in which various spatial patterns may occur. As a result, we can deduce quantitative relationship between system parameters and stable patterns which are stripes and rhombic arrays of rectangles.

Introduction

Nonlinear systems subjected to disturbances to an equilibrium state have been often analyzed by the linear theory which discards the nonlinear terms in the perturbation quantities [5]. Basically, the critical boundary conditions for stability in linear theory can be derived from the initially infinitesimal disturbances and the wavelength associated with those disturbances which are most likely to grow first. However, if the long-term behavior of growing disturbances is to be ascertained, or if the spatial pattern of the growing disturbance is to be predicted, the nonlinear effects must be taken into account which is not admitted by linear theory.

We akly nonlinear stability analysis is the method traditionally used to study such pattern formation that is the result of nonlinear diffusion processes of the relevant system. This method pivots a perturbation procedure about the critical point of the linear stability theory, making use of Landau equations [16]. Such an approach allows one to deduce the quantitative relationship between system parameters and stable patterns that are valuable for planning and designing purposes which is difficult to accomplish by using simulation alone [10].

In this paper, we examine the nonlinear phenomenon of spontaneous pattern formation discovered in plant communities by performing rhombic planform weakly nonlinear stability analysis on the governing spatio-temporal evolution equation.

Corresponding Author: Nichaphat Boonkorkuea, Department of Mathematics, Faculty of Science, Mahidol University, Rama 6Road Bangkok 10400, Thailand

Mathematical Model

The characteristic features of vegetation which describe different modes of patterning have been observed in arid regions in Africa, America and Australia [8]. Specifically, arid environment refers to an environment characterized by an extended dry season, and water availability is a limiting factor of plant growth [8, 11]. The nondimensional space-time organization of vegetation describes the deviation of the interface from its mean planar position and defined on an unbounded two-dimensional spatial domain is given by [9]

$$\frac{\partial \rho(x,y,t)}{\partial t} = (1-\mu)\rho + (\Lambda - 1)\rho^2 - \rho^3 + \frac{1}{2}(L^2 - \rho)\nabla^2\rho - \frac{1}{8}\rho\nabla^4\rho \quad (1)$$

where the single variable, ρ, is defined as total phytomass density appropriately adimensionalized to be defined on the interval [0,1], t is time, and ∇ is the two-dimensional gradient operator. Three positive parameters controlling the dynamics are: μ, the mortality-to-growth rate ratio which increases with the aridity, Λ the facilitation-to- competition susceptibility ratio , and L is the of the spatial ranges over which the facilitative and competitive interactions operate.

Results and Discussion

We are interested in the nonzero uniform plant distributions of vegetation that is real, positive, and linearly stable. The only nonzero homogeneous steady state that we need to consider is given by

$$\alpha = \rho_0^+ = \frac{\Lambda - 1 + \sqrt{(\Lambda - 1)^2 + 4\Lambda(1-\mu)}}{2\Lambda}. \quad (2)$$

The linear stability analysis yields the secular equation

$$\sigma = \alpha(\Lambda - 1 - 2\alpha) + \frac{1}{2}(L^2 - \alpha)q^2 - \frac{1}{8}\alpha q^4. \quad (3)$$

In what follows, we set

$$L^2 = \beta, \quad (4)$$

$$q^2 = q_c^2(\alpha,\beta) = 2(1-\beta/\alpha) > 0,\ \sigma = \sigma_c(\alpha,\beta) = \frac{2}{\alpha}\left[\frac{(\alpha-\beta)^2}{2} - \frac{\alpha^2(2\alpha+1-\Lambda)}{2}\right] \quad (5)$$

where (q_c^2, σ_c) is the maximum value of the parabola in the (q^2, σ) plane. Since $\sigma_c(\alpha, \beta_c) = 0$ where $\beta_c = \alpha - \sqrt{2\alpha^2(2\alpha + 1 - \Lambda)}$, the homogeneous solution is linearly stable for $\beta > \beta_c(\alpha)$, neutrally stable for $\beta = \beta_c(\alpha)$, and unstable for $0 < \beta < \beta_c(\alpha)$.

We next perform the weakly nonlinear stability to two-dimensional rhombic planform solutions as follows:

Two-Dimensional Pattern: A Rhombic Planform Analysis

We shall consider a rhombic planform solution and Landau equations of the form [10]

$$\rho(x,y,t) \sim \alpha + R(x,y,t) \quad (6)$$

Where

$$
\begin{aligned}
R(x, y, t) = {} & A(t)\cos(q_c x) + B(t)\cos(q_c z) \\
& + A^2(t)\left[R_{2000} + R_{2020}\cos(2 q_c x)\right] \\
& + A(t)B(t)\left[R_{1111}\cos\left[q_c(x+z)\right] + R_{111(-1)}\cos\left[q_c(x-z)\right]\right] \\
& + B^2(t)\left[R_{0200} + R_{0202}\cos(2 q_c z)\right] \\
& + A^3(t)\left[R_{3010}\cos(q_c x) + R_{3030}\cos(3 q_c x)\right] \\
& + A^2(t)B(t)\left[R_{2101}\cos(q_c z) + R_{2121}\cos\left[q_c(2x+z)\right] + R_{212(-1)}\cos\left[q_c(2x-z)\right]\right] \\
& + A(t)B^2(t)\left[R_{1210}\cos(q_c x) + R_{1212}\cos\left[q_c(x+2z)\right] + R_{121(-2)}\cos\left[q_c(x-2z)\right]\right] \\
& + B^3(t)\left[R_{0301}\cos(q_c z) + R_{0303}\cos(3 q_c z)\right]
\end{aligned}
\tag{7}
$$

with

$$z = x\cos(\phi) + y\sin(\phi) \tag{8}$$

and

$$
\begin{aligned}
\frac{dA(t)}{dt} &\sim \sigma A(t) - A(t)\left[aA^2(t) + bB^2(t)\right], \\
\frac{dB(t)}{dt} &\sim \sigma B(t) - B(t)\left[aB^2(t) + bA^2(t)\right].
\end{aligned}
\tag{9}
$$

After substituting (6)-(9) into (1), we obtain

$$\sigma = \sigma(\alpha, \beta), \tag{10}$$

$$a = \frac{1}{36\alpha^2(1+2\alpha-\Lambda)}\left[\begin{array}{c} -866\alpha^3 - 119(\Lambda-1)\sqrt{2\alpha^2(1+2\alpha-\Lambda)} + \alpha^2(-798+706\Lambda) \\ +\alpha\left(-192+299\sqrt{2\alpha^2(1+2\alpha-\Lambda)} + 338\Lambda - 146\Lambda^2\right) \end{array}\right] \tag{11}$$

$$
b = \frac{1}{2\alpha^2(-1-2\alpha+\Lambda)\left(1-8\cos^2(\phi)+16\cos^4(\phi)\right)}\cdot
$$

$$
\left\{\begin{array}{l}
\left[31(\Lambda-1)\sqrt{2\alpha^2(2\alpha+1-\Lambda)} + \left(-75\sqrt{2\alpha^2(2\alpha+1-\Lambda)} + 48 - 82\Lambda + 34\Lambda^2\right)\alpha + (190-162\Lambda)\alpha^2 + 194\alpha^3\right] \\
+\left[-24(\Lambda-1)\sqrt{2\alpha^2(2\alpha+1-\Lambda)} + \left(48\sqrt{2\alpha^2(2\alpha+1-\Lambda)} - 48 + 96\Lambda - 48\Lambda^2\right)\alpha + (-192+192\Lambda)\alpha^2 - 192\alpha^3\right]\cos^2(\phi) \\
+\left[112(\Lambda-1)\sqrt{2\alpha^2(2\alpha+1-\Lambda)} + \left(-272\sqrt{2\alpha^2(2\alpha+1-\Lambda)} + 192 - 352\Lambda + 160\Lambda^2\right)\alpha + (800-736\Lambda)\alpha^2 + 864\alpha^3\right]\cos^4(\phi)
\end{array}\right\}
\tag{12}
$$

The equivalence class of critical points (A_0, B_0) of (9) are I: $A_0 = B_0 = 0$ which is stable for $\sigma < 0$ and correspond to the uniform planform interface, II: $A_0^2 = \frac{\sigma}{a}$, $B_0 = 0$ which is stable for $\sigma > 0$ and $b > a$ and correspond to stripe pattern, and III : $A_0 = B_0$ with $A_0^2 = \frac{\sigma}{a+b}$ which is stable for $\sigma > 0$ and $a > b$ and corresponds to rhombic pattern.

The following figures are the contour plots of (6) corresponding to the critical points II and III respectively.

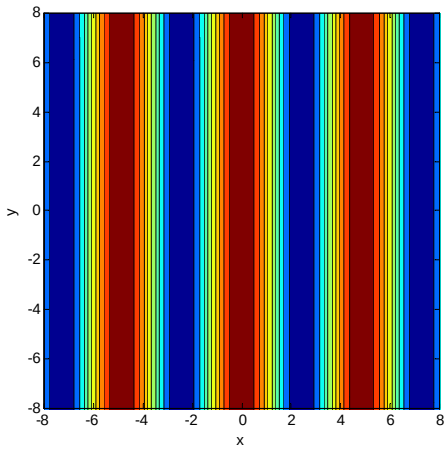

Figure 1. Contour plot of (7) for critical point II with $\Lambda = 1, \alpha = 0.12, \beta = 0.02$.

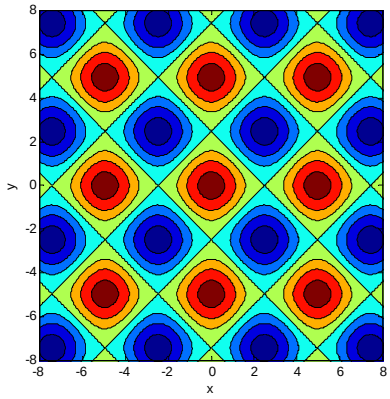

Figure 2. Contour plot of (7) for critical point III with $\Lambda = 1, \alpha = 0.1, \beta = 0.02, \phi = \pi/2$.

Conclusion

We have performed systematic stripe- and rhombic-planform weakly nonlinear stability analyses on an evolution vegetation equation describing the deviation of the interface from its mean planar position over an unbounded one and two-dimensional domains. The patterns consist of ripples, and rhombic arrays of rectangles. The stability behavior of the structures depends on two relevant positive parameters α, β. This interaction-redistribution problem of vegetation dynamics, described by a single evolution equation, is useful for ecological management and landscape design purposes.

Acknowledgments

This research has been financially supported from The Ministry Staff Development Project on Ministry of Education, and King Mongkut's University of Technology North Bangkok. The authors also wish to thank The National Center for Genetic Engineering and Biotechnology for its financial support.

References

[1] de Bruyn, J. R., Eberhard, B., Stephen, W. M., Steven, P. T., Yuchou, H., David, S. C., and Guenter, A.,Apparatus for the Study of Rayleigh-Benard Convection in Gases under Pressure, American Institute of Physics 2043-2067 (1996).

[2] HilleRisLambers, R., Rietkerk, M., van den Bosch, F., Prins, H. H. T., and de Kroon, H., Vegetation Pattern Formation in Semi-Arid Grazing Systems, Ecological Society of America 82, 50-61 (2001).

[3] Klausmeire, C. A.,Regular and Irregular Patterns in Semiarid Vegetation, Science 284, 1826-1828 (1999).

[4] Kozyreff, G., and Tlidi, M., Optical patterns with differnt wavelengths, Physical Review E 69, (2004).

[5] Laura, E. S., and Wollkind, D. J.,Weakly nonlinear stability analyses of one-dimensionalTuring pattern formation in activator-inhibitor/immobilizer model systems,Math. Biol. 33, 771-815 (1995).

[6] Lefever, R., and Lejeune, O.,On the Origin of Tiger Bush,Bulletin of Mathematical Biology 59, 263-294 (1997).

[7] Lejeune, O., and Tlidi, M., Localized vegetation patches: A self-organized response to resource scarcity,Physical Review E 66, (2002).

[8] Lejeune, O., Tlidi, M., and Lefever, R.,Vegetation Spots and Stripes: Dissipative Structures in Arid Landscapes,International Journal of Quantum Chemistry 98, 261-271 (2004).

[9] Maini, P. K., and Othmer, H.,Mathematical Models for Biological Pattern Formation,Willard Miller, Jr. (Ed.),Springer, Verlag, New York.81-112 (2001).

[10] Pansuwan, A., Rattanakul, C., Lenbury,Y., Wollkind, D.J., Harrison, L., Rajapakse, I., and Cooper, K.,Nonlinear stability analyses of pattern formation on solid surfaces, Mathematical and Computer Modeling 41, 939-964 (2005).

[11] Rietkerk, M., Boerlijst, M. C., van Langevelde, F., HilleRisLambers, R., van de Koppel, J., Kumar, L., Prins, H. H. T., and de Roos, A. M.,Notes and Comments Self-Organization of Vegetaion in Arid Ecosystems,The Ameican Nauralist 160, 524-530 (2002).

[12] Rietkerk, M., Dekker, S. C., de Ruiter, P. C., and van de Koppel, J.,Self-Organized Patchiness and Catastrophic Shift in Ecosystems,Science 305, 1926-1929 (2004).

[13] Sherratt, J. A.,An Analysis of Vegetation Stripe Formation in Semi-Arid Landscape,J. Math. Biol. 51, 183-197 (2004).

[14] von Hardenberg, J., Meron, E., Shachak, M., and Zarmi, Y.,Diversity of Vegetation Patterns and Desertification,J. Phys. Rev. Letts. 87, 198101-1-198101-4 (2001).

[15] Walgraef, D.,Spatio-Temporal Pattern Formation With Examples from Physics, Chemistry, and Mateials Science,L.Lam (Ed.),Springer, (1996).

[16] Wollkind, D. J.,Rhombic and hexagonal weakly nonlinear stability analyses: Theory and application,Nonlinear Instability Analyses IIL.Debnath (Ed.),Springer, Southhampton, England. 221-272 (2001).

[17] Wollkind, D. J., Manoranjan, V.S., and Zhang, L.,Weakly Nonlinear Stability Analyses of

Prototype Reacton-Diffusion Model,SIAM Review 36, 176-214 (1994).

[18] Wollkind, D. J., and Stephenson, L.E.,Chemical Turing pattern formation analysis: Comparison of theory with experiment, SIAM J. Appl. 61, 387-431 (2000).

Simulation Tool for TOC Implementation

Chompoonoot Kasemset and Voratas Kachitvichyanukul
Industrial Engineering and Management, School of Engineering and Technology
Asian Institute of Technology, P.O. Box4 Klong Luang, Pathumthani, 12120, Thailand
Tel: (66 2) 0-2524-5675; Fax: (66 2) 0-2524-5697; Email: {st104182, voratas}@ait.ac.th

Abstract: This paper describes the development of a simulation model to facilitate TOC implementation. The simulation tool is built with ARENA and it is divided into two parts; the first part is for the evaluation of current system and the second part is for new system (with TOC) deployment. Both parts are linked and the user can define how he/she wants to use the model. For the first part of the model, this tool is built to collect statistics in order to identify the system bottleneck. The second part of the model is used when TOC is applied to improve the system. It includes two module types, Logic Module and Data Module. The Logic Module is used to display the physical flow and the Data Module is used to provide support data for the physical flow. Moreover, the way to construct this model allows this model to be flexibly applied with any job shop configuration. The details of the model construction are discussed.

Key words: TOC, Simulation, Logic Module, Data Module, Physical Flow

INTRODUCTION

The objective of manufacturing system is to earn money by producing goods. Manufacturing systems deal with Processes (direct and indirect manufacturing process) and Entities. The entities that flow through the processes include not only the parts or materials but also the information that supports the system control. Management of materials and information flow is the major activity that the managers must focus on.

Simulation is a useful tool to study the behaviors of any process. A suitable simulation model can provide an effective way to evaluate a process. It can show how the real process is affected by changes in policy. Moreover, the simulation can be used to evaluate the effectiveness of factors in the system without disturbing the real system.

Theory of Constraints (TOC) is an operation management policy developed by Eliyahu M. Goldratt. The goal of this policy is quite different from those of JIT and MRP. Goldratt and Cox[1] addressed that TOC main approach is to manage a few machines or workstations that restrict the process capability because their capacities are less than or equal to the demand rate. These machines are called Bottleneck machines or Capacity Constraint Resources (CCR).

In order to implement TOC policy, many operation configurations must be set and simulation is one tool that can be used to handle this task.

TOC CONCEPT ADOPTED IN DEVELOPING THIS TOOL

The definite difference between TOC and traditional system is that the TOC utilizes dynamic information and attempts to improve the performance of the bottleneck station. For a given production volume, the bottleneck resource is identified. This is quite different from the traditional push system where it did not concern with the bottleneck concept.

In TOC, there is a control mechanism called DBR, Drum, Buffer and Rope. *Drum* is the signal to inform the process preceding the bottleneck to slow down when the bottleneck is busy and has excess inventory. *Rope* is the tool to synchronize the whole process. *Buffers* are the stored parts to cover the statistical fluctuation and to keep the bottleneck busy all the time.

The DBR control mechanism is effective when it is applied in TOC system. Duclos and Spencer [2] conducted the simulation study to compare the performance of the three different manufacturing environments, MRP (as a push system), DBR (with TOC system) and the buffer modified MRP. The result from this study shows that the DBR in TOC system is the best policy among the three cases.

Chakravoty [3] has also evaluated the DBR control mechanism in job shop environment. The result showed that the DBR control mechanism performs well in a job shop environment.

Corresponding Author : Chompoonoot Kasemset, Industrial Engineering and Management , School of Engineering and Technology, Asian Institute of Technology, Thailand,
Email: st104182@ait.ac.th

Under TOC system, this tool is designed to employ DBR system for users to easily and effectively control the physical flow in the system. Users can set the value of each parameter (the location of bottleneck, buffer size and the location of rope) or apply this tool to find the optimal value for each parameter.

Other concept to exploit the system bottleneck capacity is the lot splitting concept. Applying different lot size when transferring between each process, called transfer lot size, can help in reducing the waiting time on bottleneck machines. In this simulation tool, users can separately define the size of production lot and the size of transfer lot.

The simulation tool development is described in detail in the next section.

SIMULATION TOOL DEVELOPMENT

ARENA Simulation Software provides two basic modules; (1) Logic Module and (2) Data Module. Logic Module is used to display the physical flow and Data Module is used to store support data for the physical flow.

In this research, the simulation tool is developed in order to study the system performance when the operation policy is changed from push policy to TOC.

The proposed simulation tool is composed of four sub models:

1. Order Release Sub Model
2. Production Sub Model
3. Initial Buffer Sub Model
4. Product Exit Sub Model

In each sub model, (1) the physical flow generic model and (2) the information generic model are connected by (3) the connecter to work together under TOC policy. The detail in each sub model is explained as follows.

The physical flow generic model is used when simulating the existing system (push system).When TOC is adopted the information flow generic model is activated and work together with the physical model.

The sub-models are explained in the subsequent sections.

1. Order Release Sub Model

The Order Release Sub Model simulates the releases of material into the system at the beginning of the production. In this sub model, the physical model is connected with the information model. The *Decide Logic Module* of ARENA is used as a connecter. The detail of the physical model, the information model and the connecter are illustrated in the next section.

1.1 Physical Generic Model in Order Release Sub Model

This section describes the work flow of the order release submodel as shown in Figure 1.1.
First, the entities are created in the *Create Module*. After that they enter the *Assign Module*. In this module, the important system parameters such as Product Mixed, Product Type, and Production Sequences, Implement Step are assigned. These items are the basic parts of the entity attribute used in the generic model.

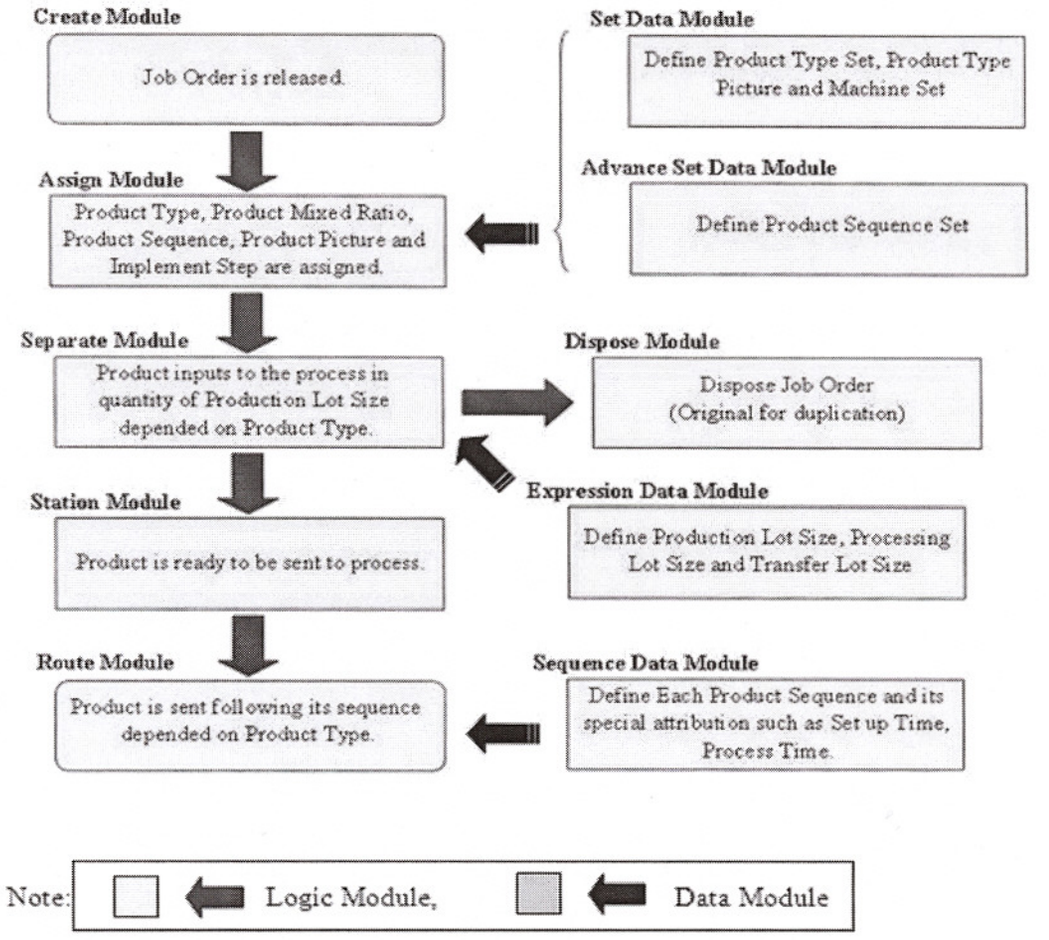

Fig. 1.1: Work flow of physical model in order release sub-model

Subsequently, the assigned entities pass to a *Separate Module* to duplicate entities following the expression "Production Lot Size". The number of each production lot size of each product can be the same or different depending of the "Production Lot Size" expression defined in the *Expression Data Module*. The construction of this part makes the model generic and the production lot size of each product can be separately defined by the users.

Then, the entities are separated from the original job order via a Separate Module. The original job order is sent to *Dispose Module* and exit the system.

The cloned entities from the separate module go to *Station Module* and *Route Module*. The Route Module is the starting point of product sequence that is defined specifically for each product in the *Sequence Data Module*. This part allows user to define various manufacturing configurations by simply chaining input data on product sequences that can be the same or different for all products. This model part is generic and can be employed with either Job-shop or Flow-shop system.

1.2 Connecting Point between the Physical Model and Information Model in Order Release Sub Model

The physical model and the information model is connected via a *Decide Module* of ARENA as shown in Figure 1.2. First the Implement Step is assigned at *Assign Module* in the Order Release Sub model. *Implement Step 1* deactivates the information control. This assigned value is used when manufacturing system under the push policy is analyzed in the first run. *Implement Step 2* activates the information control when the system is managed under TOC policy. This control point make the model generic and can be applied with both systems.

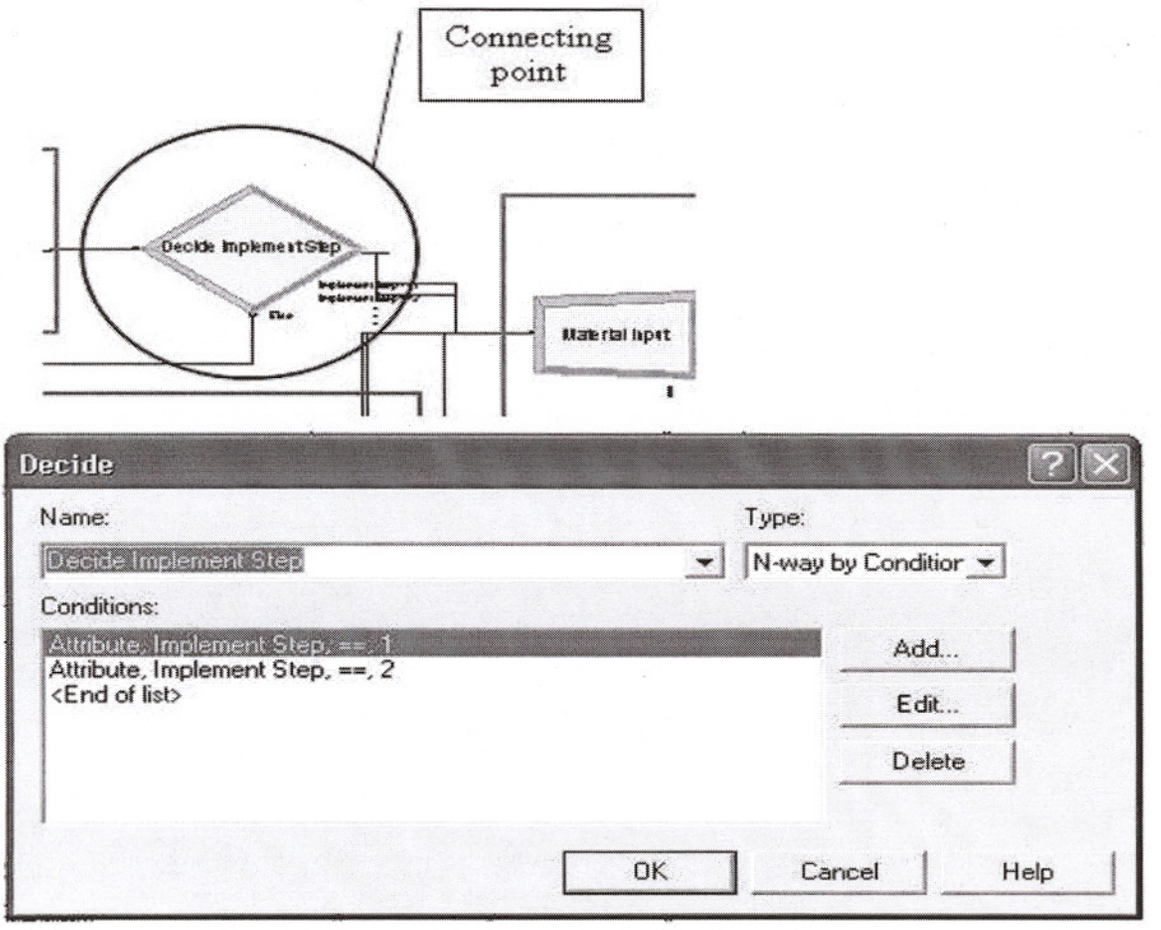

Fig. 1.2: Decide module as a connecter

1.3 Generic Information Model in Order Release Sub Model

When *Implement step 2* is assigned, the generic information control model is activated to control the physical flow. The work flow is shown in Figure 1.3. When entities pass the *Decide Module*, they are held if the required quantity of each product has been produced. If the entity passes the *Decide Module*, it will be sent to another *Decide Module* to check the number in the bottleneck queue . If the number in queue of bottleneck station exceeds the allowed buffer size, the entities will be held until a product of the same type is completed at the bottleneck station. These two control points help in controlling work in process in the system following the concept of subordinating the system constraint in TOC.

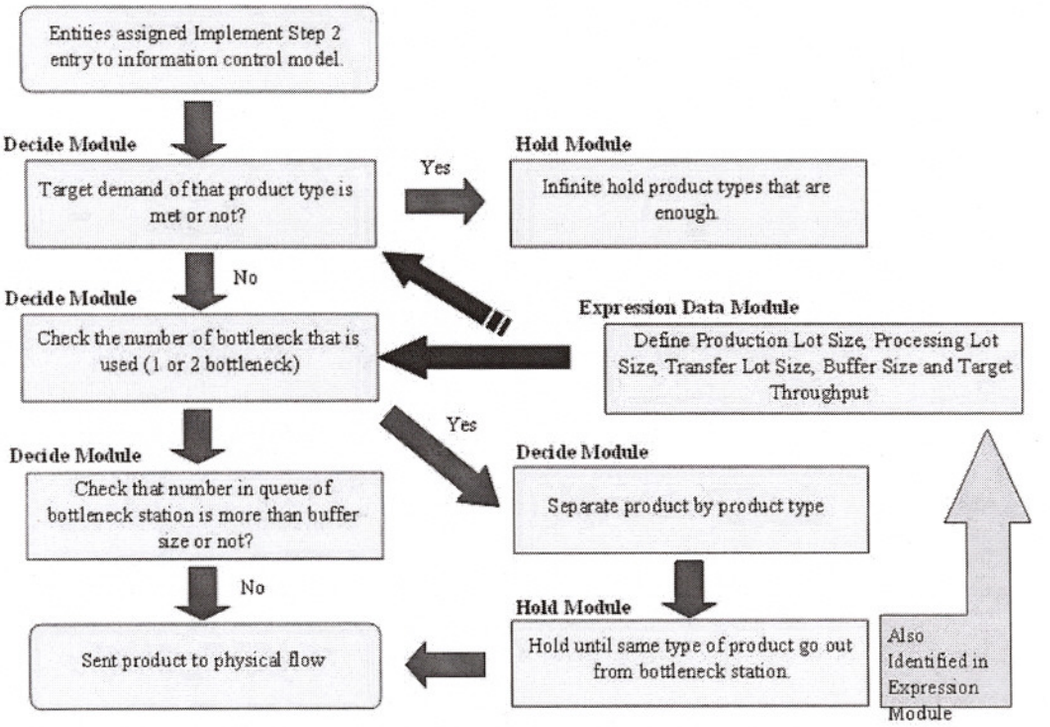

Fig. 1.3: Information Control Order Release Sub Model

2. Production Sub Model

The production sub model simulates the actual processing of a part at a processing station.

2.1 Generic Physical Model in Production Sub Model

Station, Batch, Record, Seize, Assign, Decide, Delay, Process, Separate and Route Logic Modules are used to build the model of the production area.

In this part, *Batch* and *Separate Logic Modules* are placed to make this part flexible for handling any process with various production and transfer lot sizes. This production sub-model is designed to support the TOC policy.

The function of each module in Production Sub Model is shown in Figure 2.1.

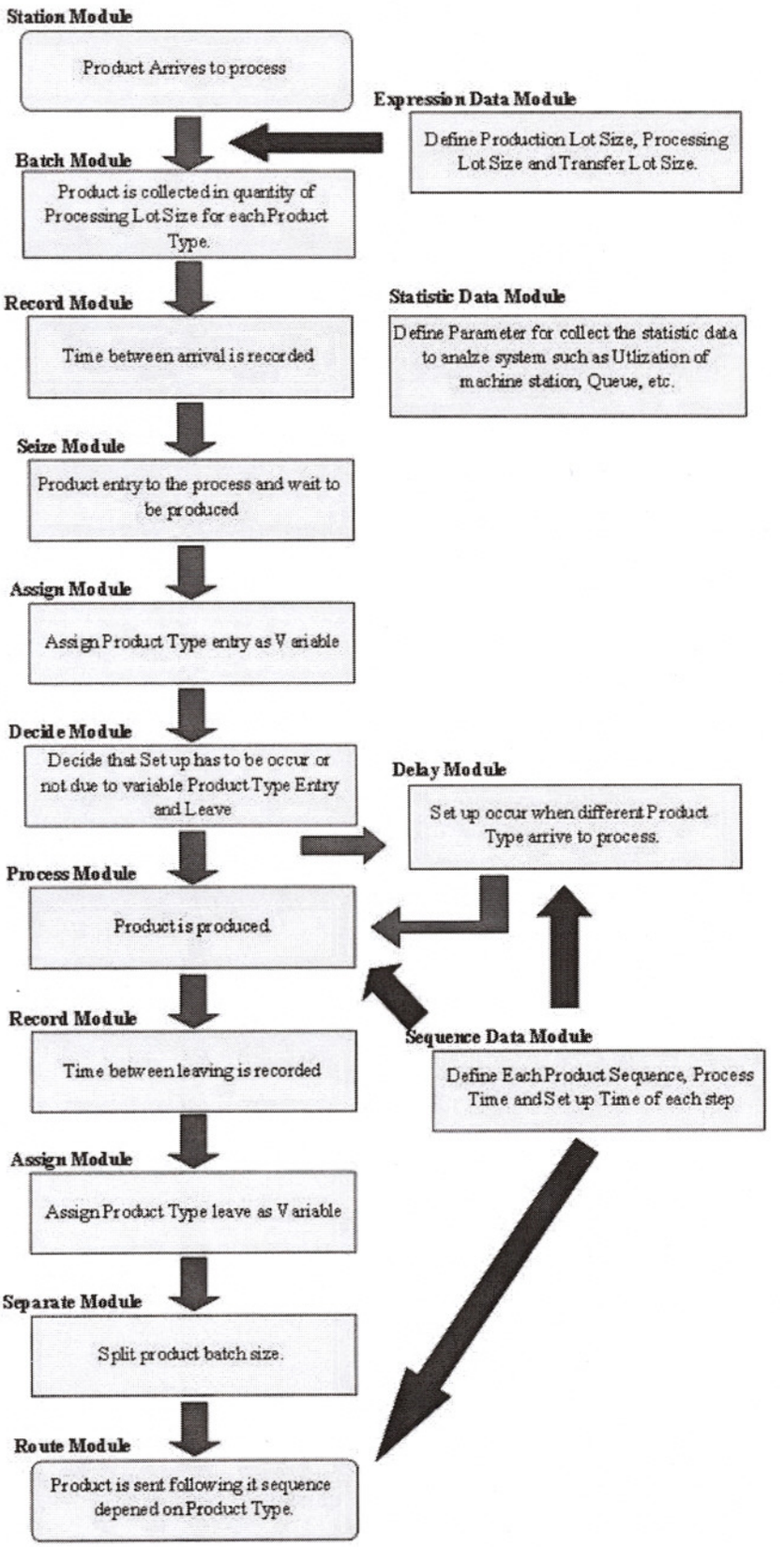

Fig. 2.1: Production Sub Model Flow

When entities pass *Station Module*, they are collected into proper batch sizes by *Batch Module* and sent to *Record Module* to record time between arrivals before they pass to the *Seize Module*. Before entering to the process, *Assign Module* will be used to assign the variable "Product Entry" to product. The entities then go to *Decide Module* to decide whether set up is necessary. If Product Entry and Product Leave (Variable Parameter) are not the same as Product Type, the set up must occur at *Delay Module* before entities are produced via a *Process Module*. This part is built to support products that have a setup time.

The *Record Module* records time between departures. The recorded time is collected to use as one parameter to identify system bottlenecks. After that entities are sent to *Separate Module* to be splitted as the same number as transfer lot to prepare to be sent tothe next processby passing *Route Module* to follow their sequences.

2.2 Connecting Point between the Physical Model and Information Model in Production Sub Model

Similar to the first submodel, *Decide Module* is used as the connecter between Physical and Information Model. For Implement Step 2 the information is route to the information control model when this tool is used to study the system under TOC policy.

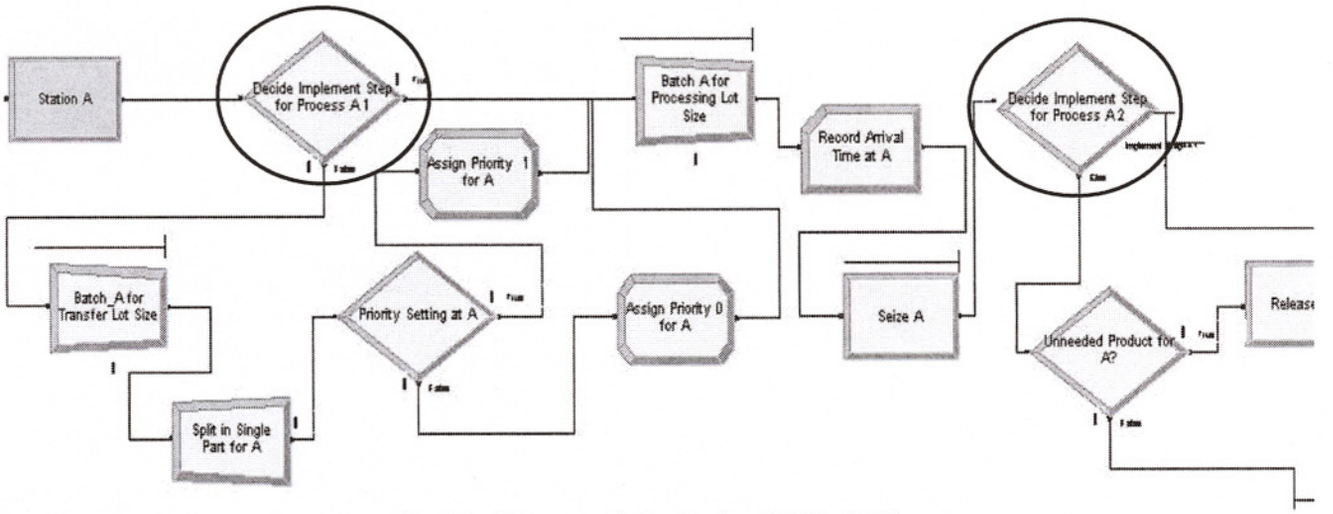

Fig. 2.2: Connecters in Production Sub Model Flow

2.3 Information Generic Model in Production Sub Model

There are two information control systems in this sub model. The first part is an information model that controls the use of transfer lot size and assign priority to product for sequencing with Priority Rule. The second part controls the release of material in order not to process unneeded parts.

In the first information control system, not only Transfer Lot Size concept can be used but Priority can also be set for entities. High Priority is set when same type of processing part is waiting in queue, otherwise is set as Low Priority. This Information
Control Model are shown in Figures 2.3.1 and 2.3.2.

Entities assigned Implement Step 2 will enter the *Batch Module* to be accumulated in quantity of Transfer Lot Size and pass to *Separate Module* to be splitted into single part. They are then passed to the *Decide Module* to be separated for assigning priority at *Assign Module* and sent to the physical model.

The second information control model is used to prevent the production of unneeded part. The product type that already met the production target is not allowed to enter the system in order to protect the constraint from wasting the capacity.

Entities enter to *Decide Module*. By each type of product, if their target demands are met, entities are sent to *Hold Module* to be held infinitely; otherwise they are sent to follow the physical flow.

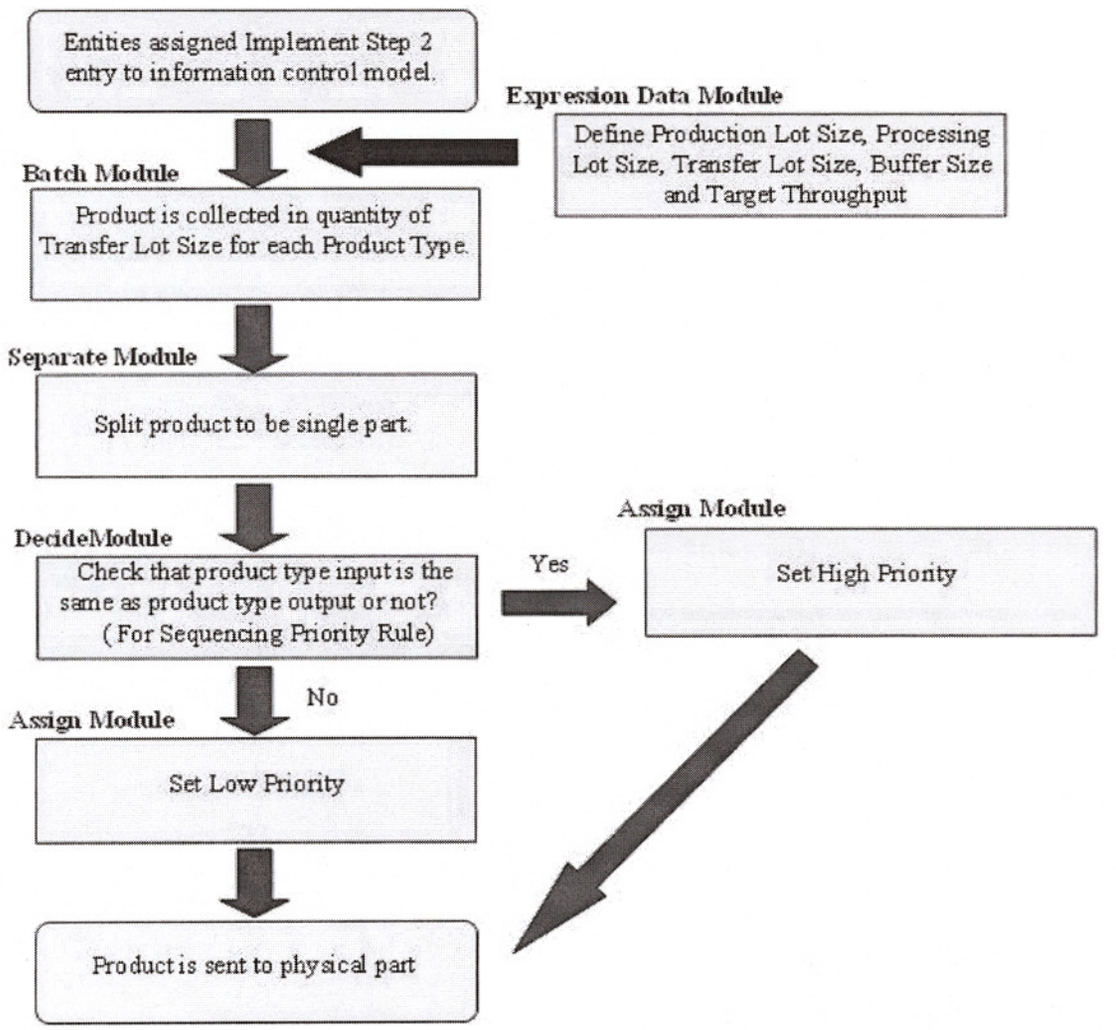

Fig. 2.3.1: First Information Control in Production Sub Model Work Flow

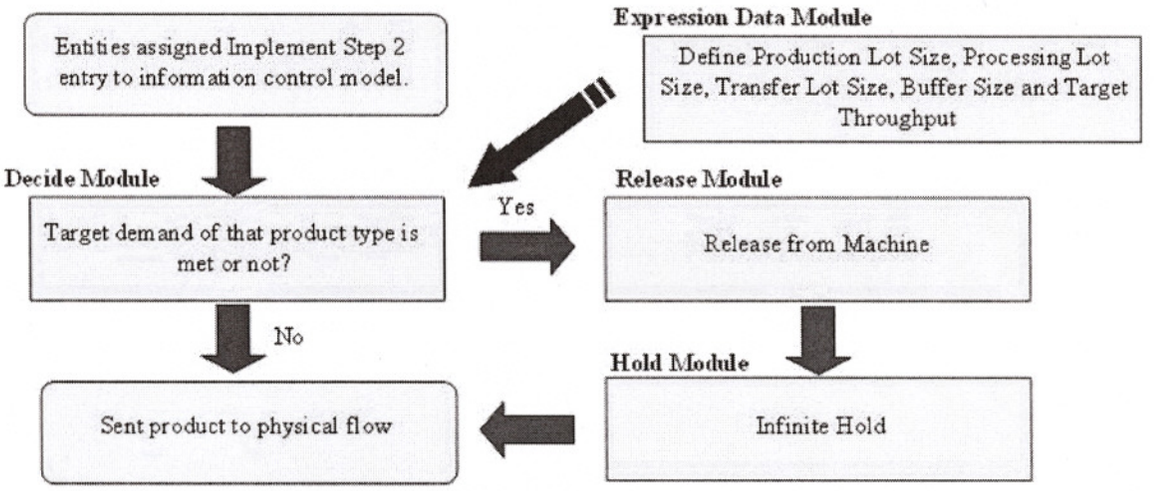

Fig. 2.3.2: Second Information Control in Production Sub Model Work Flow

3. Initial Buffer Sub Model

This sub model generates initial buffers when start running simulation model. The size of buffer is defined in *Expression Module*.

In this simulation tool, there are two initial buffers sub model. Constraint Buffer for Bottleneck1 and Constraint Buffer for Bottleneck 2, are provided to handle both single and double bottleneck cases. These sub models are used only in Implement step 2 when the information control is applied. These sub models create the initial buffer when simulation begins. The work flow of these sub models is shown in Figure 3.

Buffer Units are created via the *Create Module*. Similar to the Order Release Sub Model, all entity attributes are assigned at *Assign Module*. They are then separated by product type to be assigned job step attribute and held. When there is no more work at the bottleneck process entities are duplicated at Separate Module and sent to the bottleneck process.

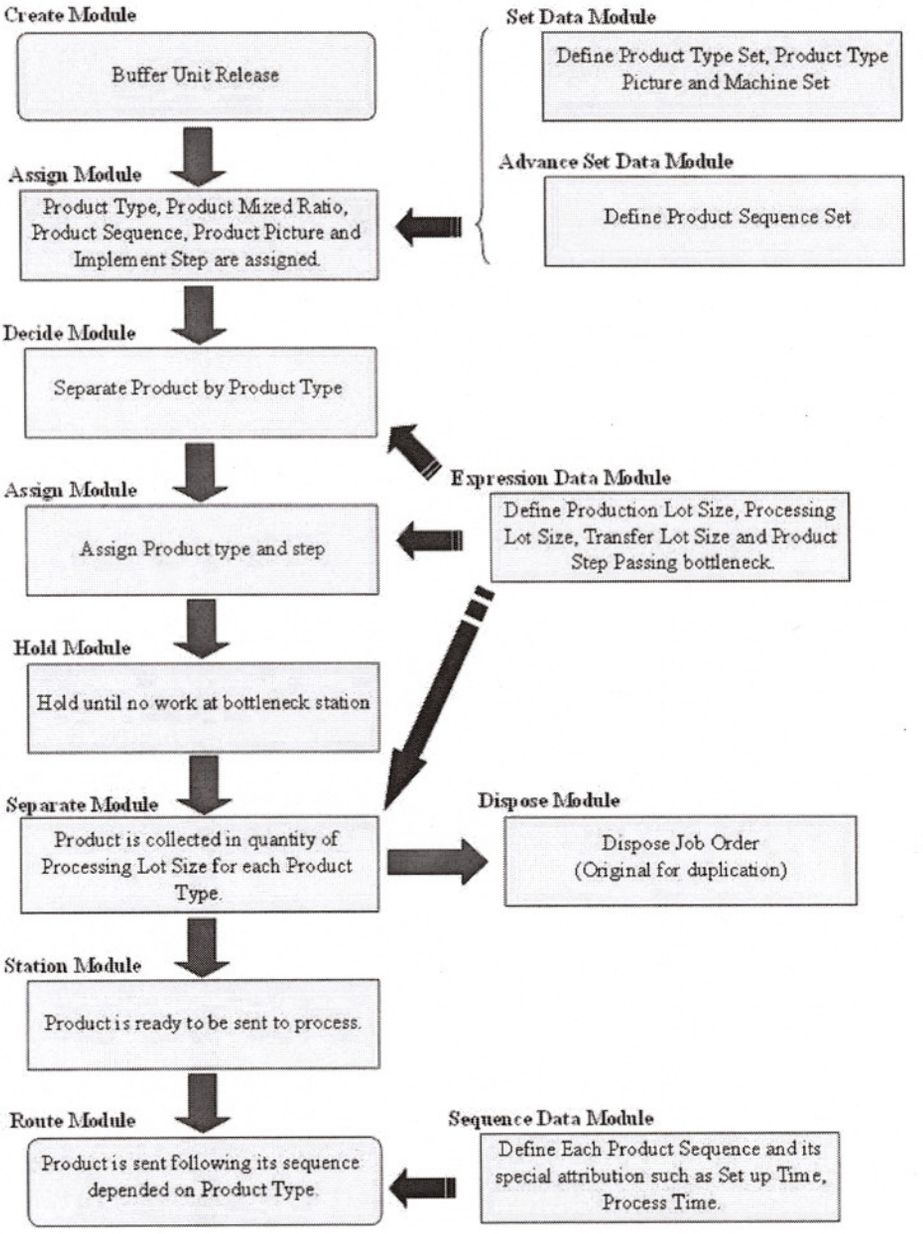

Fig. 3: Initial Buffer Sub Model Work Flow

4. Product Exit Sub model

Product Exit Sub model is the end of the simulation model. The Exit System Station is indicated as the last job step in every product sequence. Relevant statistics are collected prior to the termination of the entities.

Station and *Dispose Logic Module* are used to build the Product Exit sub model.

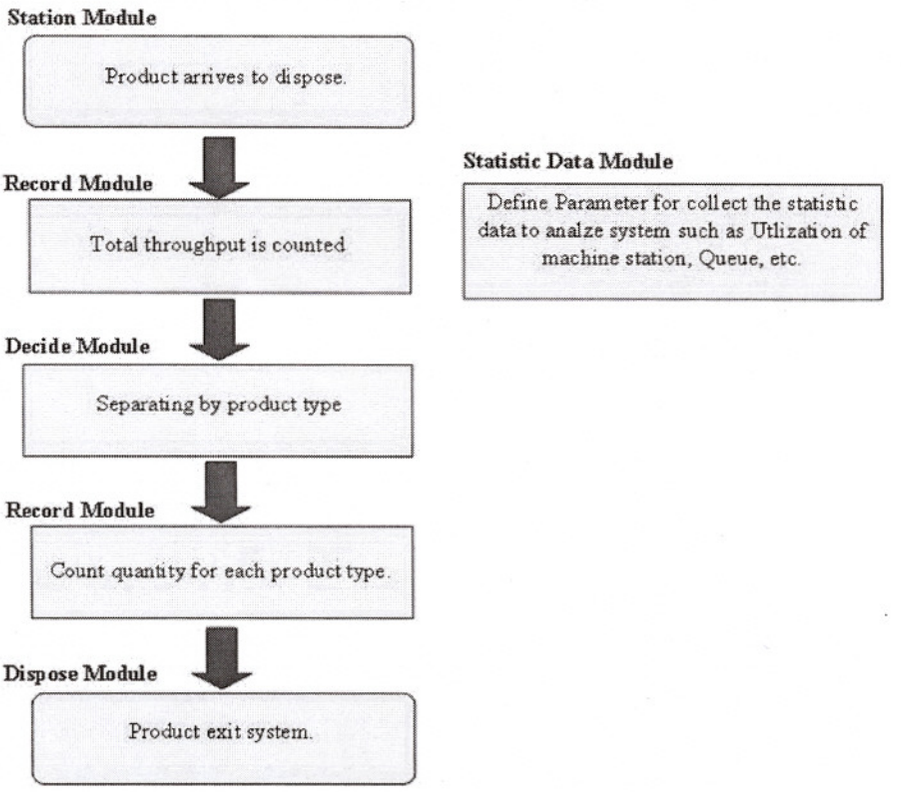

Fig. 4: Product Exit Sub Model WorkFlow

STATISTIC DATA COLLECTION

In both the Production and Product Exit Sub Models, Statistic Data Module is used to collect the statistic data that are used in TOC Implementation. The relevant statistics collected by the simulation include:

Utilization: The measurement of process utilization is defined in Statistic Data Module. The process utilization is equal to the average value of the machine utilization in machine set. The formula of the average value of the machine utilization in machine set can be defined directly in this module or by using Expression module. This statistic is defined as output type and they are shown in a report after the simulation finished.

Total Output and Each Product Output: These data are indicated as output type in this module and can be collect in .DAT file for analyzing the mean confident interval in the Output Analyzer.

Average Arrival and Departure Rate of Entities at the Bottleneck Station: These data are used to calculate buffer size for each bottleneck station. The formulas of these items are defined in Expression Module and work with this module. This item is defined as output type.

In addition to all of these items, other statistics can be defined based on the requirement of users.

GUIDELINE FOR USING THE SIMULATION-BASED TOOL IN TOC IMPLEMENTATION

Tool Assumption:

1. Demand is assumed to be strong enough so such outside manufacturing constraint as Market Constraint is not considered.
2. There are sufficient raw materials.
3. Each production stage has its own inventory in front of the stage for storing the waiting items. The first stage has initial inventories to store the raw material.
4. Buffer, Inventory and Queue is considered as mixed type of product for each stage.
5. The number of bottleneck stations can be more than one station to up to the limitation of the tool.
6. The target demand/throughput per unit time period is used as a system performance measure.
7. Information system control is considered and applied depended on each product type.

Scope and Tool Limitation:

1. The hypothetical systems are modeled to illustrate a real world manufacturing system based on ARENA simulation software
2. The operation configurations that come from the simulation model are based on the existed input data. The input data include the demand (customer demand/order or forecasting demand) at the specific time period, the production capacity and the processing time.
3. This tool can be used to implement TOC policy in a manufacturing system by changing from the push traditional policy.
4. This tool can be used to analyze the common classification production process (Job shops and Flow shops) and in both make to stock and make to order environmental.
5. This tool can be used for both single and mixed product type. Based simulation model in this study is developed to use with maximum of five product types, seven processes and two bottlenecks.
6. Transfer lot size, processing lot size for batch process can be different from production lot size and can be applied with this tool.
7. The transportation process is omitted in this thesis.
8. Transfer time between processes can be applied.
9. Schedule and Failure Probability can be applied based on ARENA simulation software.
10. The shipping buffer is one of the factors in TOC to absorb the uncertainty of the overall processes but in this study the shipping buffer size is not the result from the simulation model because it concerned about the company inventory policy.

THE PROPOSED SIMULATION TOOL APPLICATION

The application of this tool can be found in [4, 5 and 7] that applied this tool to implement TOC system with single and multiple bottleneck cases. Another application is address in [6] that applied this tool as one part of system bottleneck identification approach.

CONCLUSION AND RECOMMENDATION

This study presented the development of the generic simulation model to support TOC implementation. In order to employ TOC to job shop system that was previously operated with push policy, the simulation tool is created to support both systems in the same model. The way to model this is to separate the model into two parts, generic physical flow and information flow model, and connect them together via the connecter. The connecter reacts like a switch to change between push and TOC policy. Users can indicate which policy they want to use.

Moreover, the system performance is simply to measure and compare between two different systems. Changing in any factor of system configuration can be easily evaluated by applying this tool.

For recommendation and further study, this generic tool can be applied with Pull System under information system control of the pull system with some changes in simulation model. The generic model from this study can be used as a basis for simulation template development. Moreover, users who have background in programming can create decision support tool based on this procedure as well.

REFERENCES

1. Goldratt, E.M., and CoX, J., 1986, The Goal: A Process of Ongoing Improvement, Revised Edition, North River Press.
2. Duclos, L.K., and Spencer, M.S., 1995, The impact of s constraint buffer in a flow shop, International Journal Production Economics, Vol.42, pp. 175-185
3. Chakravorty, S.S., 2001, An evaluation of the DBR control mechanism in a job shop environment, Omega, Vol. 29, pp. 335-342
4. Kasemset, C., 2005, Simulation-based Tool for Theory of Constraints (TOC) Implementation, Master's Thesis, Asian Institute of Technology, Bangkok, Thailand.
5. Kasemset, C., Kachitvichyanukul, V., 2005, Simulation-based Tool for Implementing Theory of Constraints, Proceeding of The 6th APIEMS Conference, Manila, Philippines
6. Kasemset, C., Kachitvichyanukul, V., 2007, Simulation-Based Procedure for Bottleneck Identification, Proceeding of AsiaSim 2007, Asia Simulation Conference 2007, Seoul, Korea
7. Kasemset, C., Kachitvichyanukul, V., 2008, Simulation-based Procedure for Implementing Theory of Constraints: Extension for Cases with Multiple Bottlenecks, Proceeding of The 9th APIEMS Conference, Bali, Indonesia

AUTHOR BIOGRAPHIES

Chompoonoot Kasemset is a doctoral student in Industrial Engineering and Management, School of Engineering and Technology, Asian Institute of Technology, Thailand. Her research interests include operation management and simulation and applied operation research. Her email address is <st104182@ait.ac.th>

Voratas Kachitvichyanukul is an Associate Professor in Industrial Engineering & Management, School of Engineering and Technology, Asian Institute of Technology, Thailand. He received a Ph. D. from the

School of Industrial Engineering at Purdue University in 1982. He has extensive experiences in modeling of manufacturing systems. He had worked for FORTUNE 500 Companies such as Compaq Computer Corporation and Motorola Incorporated. He had also worked for SEMATECH as technical coordinator of the future factory program. His teaching and research interests include evolutionary algorithms for combinatorial optimization, planning and scheduling, supply chain and logistics, high performance computing and applied operations research with special emphasis on industrial systems. His email address is <voratas@ait.ac.th>

Assessment of the Impact of an Additional Intermodal Barge Terminal on a Waterway Network

[1]An Caris, [1]Gerrit K. Janssens, [1]Katrien Ramaekers and [2]Cathy Macharis
[1]Transportation Research Institute, Hasselt University – campus Diepenbeek, Wetenschapspark – Building 5, 3590 Diepenbeek, Belgium
[2]Department MOSI – Transport and Logistics, Vrije Universiteit Brussel – Management school Solvay, Pleinlaan 2, 1050 Brussel, Belgium

Abstract: In this paper a discrete event simulation model for intermodal barge transport (SIMBA) is presented. The intermodal context in Belgium is described. The simulation model covers the hinterland waterway network of a major port in Western-Europe. The simulation modeling approach is elaborated. The SIMBA model is part of a larger decision support system for intermodal transport policy making (DSSITP). The simulation model is applied to analyze potential impacts of adding a new intermodal barge terminal to a hinterland network.
Keywords: Discrete event simulation, intermodal freight transport, ex-ante analysis, decision support system, policy making

INTRODUCTION

Emerging freight transport trends, such as a geographical expansion of distribution networks and continuing growth rates in freight transport, demonstrate the importance and necessity of intermodal freight transport systems. European, national and regional governments intend to stimulate a modal shift towards more environment-friendly transport modes, such as rail and barge transport. Intermodal transport has grown into a dynamic transportation research field. Many new intermodal research projects have emerged. Intermodal transport integrates at least two modes of transport in a single transport chain, without a change of container for the goods, with most of the route traveled by rail, inland waterway or ocean-going vessel and with the shortest possible initial and final journeys by road (Macharis and Bontekoning[1]). An overview of planning issues in intermodal transport is given by Caris, Macharis and Janssens[2].

This paper describes a discrete event Simulation Model for InterModal BArge transport (SIMBA), which is developed as part of a Decision Support System for supporting Intermodal Transport Policy making in Belgium (DSSITP). Intermodal planning problems are complex due to the inclusion of multiple transport modes, multiple decision makers and multiple types of load units. Because of this increased complexity and the required level of detail, discrete event simulation is the appropriate tool of analysis. The SIMBA simulation model is created to support decisions in intermodal transport at the strategic level. Simulation models have been widely used to optimize the design of intermodal terminals. For example, Rizzoli, Fornara, and Gambardella[3] present a simulation tool for the combined rail/road transport in intermodal terminals. Parola and Sciomachen[4] describe a strategic discrete event simulation model to analyze the impact of a possible future growth in sea traffic on land infrastructure in the north-western Italian port system.

The SIMBA simulation model covers the hinterland waterway network of a major port in Western-Europe. In the following section, the intermodal context in Belgium is presented. Next, the discrete event simulation model is discussed. The SIMBA model is part of a larger decision support system for intermodal transport policy making. The DSSITP framework is briefly introduced. In the final section the SIMBA model is demonstrated by analyzing the impact of an additional barge terminal in the hinterland waterway network.

INTERMODAL CONTEXT IN BELGIUM

In the intermodal context in Belgium, the importance of inland navigation is increasing. A key element in the competitiveness of seaports consists of their hinterland

Corresponding Author: Gerrit K. Janssens, Transportation Research Institute, Hasselt University – campus Diepenbeek, Wetenschapspark – Building 5, 3590 Diepenbeek, Belgium, E-mail: gerrit.janssens@uhasselt.be

access. Ports have become a part of intermodal networks and competition takes place amongst transport chains instead of between ports. The intermodal hinterland network of the port of Antwerp serves as the real-world application in our study. In the port of Antwerp a modal shift towards inland navigation is observed in recent years. The share of barge container transport in the modal split of the port of Antwerp amounted to 32% in 2004. As transport volumes are expected to further increase, inland navigation is often seen as a promising solution to ensure an effective hinterland access. The quality of the hinterland access of a port depends on multiple actors in the transport flow, such as truck companies, terminal operators, barge operators, freight forwarders, carriers and port authorities. De Langen and Chouly[5] think of the improvement of hinterland access as a collective action problem, which requires coordination between actors. Inter-organizational coalitions are necessary to invest in hinterland transport services.

SIMULATION MODEL FOR INTERMODAL BARGE TRANSPORT

This section gives an overview of the methodology of the SIMBA model. The simulation model covers the hinterland waterway network of a major port in Western-Europe. First, the intermodal transport network is presented. Next, the conceptual model of the current network is discussed. A number of assumptions are made to implement the conceptual model into a computer simulation model. Finally, an overview is given of the inputs and outputs of the discrete event simulation model.

Intermodal Transport Network

In Belgium three regions of origin can be identified in the hinterland network of the port of Antwerp. The first group of container terminals is situated along the Albert Canal towards the eastern part of Belgium. A second region of origin is located in the central part of the country, connected to the port of Antwerp by the Brussels - Scheldt Sea Canal. The third group of intermodal container flows originates in the basin of the Upper Scheldt and the river Leie. All intermodal container terminals organize shuttle services either to the port of Antwerp or to the ports of Rotterdam and Amsterdam. Two clusters of sea terminals can be identified in the port area of Antwerp. Until recently the main center of activity was situated on the right river bank. With the construction of a new dock (Deurganckdok) in the port of Antwerp, a second cluster of sea terminals emerged on the left river bank. Barges sail through the Scheldt-Rhine connection to Rotterdam and Amsterdam. A last destination is the port of Zeebrugge, which can be reached via Antwerp and navigation on the river Scheldt. Shuttle services transport containers from inland terminals to sea terminals in the port area and carry containers from sea terminals to inland destinations in a round trip.

Conceptual Model

Three major components can be identified in the intermodal hinterland network, as depicted in figure 1. The first component in the intermodal freight transport network is the inland waterway network. The inland waterway network is made up of terminals, waterway connections and container flows. Entities are defined as barges which originate from the different inland terminals and carry containers in round trips to the various ports. A second component is the port area of Antwerp. Barges may visit sea terminals on the left river bank and right river bank in the same round trip, go to Rotterdam or Amsterdam via the Scheldt-Rhine connection or sail to Zeebrugge via the Scheldt estuary. On the right and left river bank, barges queue for handling at the sea terminals. Barges moor as soon as enough quay length is available. The handling time at the sea terminal depends on the number of containers that need to be unloaded from or loaded into the inland vessel. In the inland waterway network as well as in the port area multiple locks are present. Therefore, lock planning constitutes a third major component.

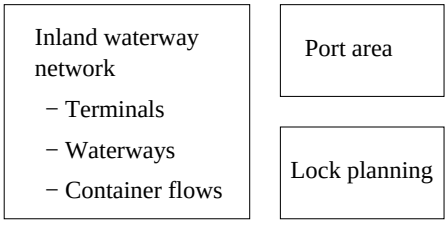

Fig. 1: Components

The operations of locks strongly affect waiting times of barges for lockage. A number of decision rules are defined to make the operations of the locks in the simulation model reasonably realistic. A first group of decision rules relates to the assignment of barges to lock chambers. Barges are assigned to a lock chamber only if its size is within the allowed dimensions. Secondly, barges are assigned to the smallest lock chamber that is open. A third decision rule is applied

when no lock chamber is open in the sailing direction of the barge. In this situation the barge is assigned to the lock chamber which is the first available.

A second group of decision rules is introduced to determine when a lock chamber is closed. A lock chamber is closed when there is not enough remaining space for the next barge in queue or when no additional barges arrive within a predefined number of time units. From interviews with waterway administrators it appears that the operations of locks are entrusted to a lockkeeper, without fixed rules. Future research could introduce more complex decision rules in the simulation model.

The conceptual model of the current container flow is depicted in figure 2. At present all barges enter the port area and visit one or multiple sea terminals.

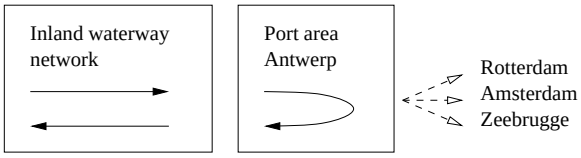

Fig. 2: Conceptual model of the current situation

Assumptions

A number of assumptions are made to translate the actual intermodal network into a discrete event simulation model. The emphasis lays on inland waterway transport. Rail connections in the hinterland network are not taken into account. The model further assumes a homogeneous container type and equal handling time for each container. All main waterway connections between inland terminals and the port area are incorporated in the simulation model. Small waterways without inland terminals are not included in the simulation model of the current situation. Sailing times are assumed to be stochastic and follow a probability distribution. A probability distribution is also used to model the stochastic lockage times and handling times in the port area.

Inputs

The intermodal terminals in the inland waterway network were requested for information to identify the container flows. Real data on shuttle services is used as input for the simulation model, constructed in the simulation software Arena. For each shuttle service the following information is required: which type of barge is used, which destinations are visited and what is the average number of import and export containers for each destination.

Container transport interacts with other freight flows. Therefore, the flow of non-containerized goods on the inland waterway network is introduced as input in the simulation model. These flows affect the waiting times at locks. The waterway administrators provided information on the network connections. In the port area of Antwerp three clusters of locks connect the inner port area with the sea side. Data is required on the choice of locks when sailing in the port area. The average quay length available for handling inland navigation at sea terminals gives an indication of the service capacity in the port area of Antwerp. Finally, an enquiry is made into the turnaround times of vessels and average waiting times at locks in order to verify and validate the model.

Outputs

Table 1 gives an overview of performance measures generated by the simulation model. The turnaround time of shuttles is defined as the total time necessary for a barge to sail from an inland container terminal to the port area, visit all sea terminals and return to the inland terminal. The turnaround time depends on the waiting times at locks and in the port area. Outputs measured at locks are the percentage of barges that have to wait, the number of barges that have to queue and the waiting time of barges in the queue. In the port area the waiting time before handling is measured, as well as the number of vessels queueing for service. A final set of performance measures concerns the capacity utilization. In the port area this is expressed as the average percentage of quay length occupied. In the hinterland network the average and maximum number of barges on each network connection is recorded.

Table 1: Performance measures

Shuttles	Turnaround time
Locks	Total number waiting
	Number waiting in queue
	Waiting time in queue
Port area	Waiting time in queue
	Number waiting in queue
Capacity utilization	Quay length
	Network connections

EVALUATION OF POLICY MEASURES

The SIMBA model is part of a decision support system for evaluating policy measures intended to stimulate intermodal transport. The DSSITP framework is depicted in figure 3 [6]. Due to the combination of three models, the analysis of policy measures is performed on multiple levels of aggregation over multiple transport modes. Each model has its specific purpose and outputs. The multimodal freight model NODUS is situated on the highest level of aggregation and constitutes the first step in the analysis of a potential policy measure. NODUS implements the virtual networks methodology as defined by Jourquin and Beuthe[7]. The NODUS model provides traffic prognoses and optimal locations which serve as inputs for the LAMBIT model and SIMBA model. The NODUS model produces aggregated outputs of the various transport modes, such as their accessibility, environmental impact, share in modal split and total costs of an intermodal service. The LAMBIT model is scaled on the Belgian intermodal network. The model analyzes the potential market area of a new terminal and assesses the impacts on existing terminals. It further produces cost indicators and potential modal shifts. The SIMBA model is situated on the lowest level of aggregation and produces detailed output related to the reliability, speed and capacity utilization of the waterway network. The operations of the inland navigation network are modeled in detail. This enables an ex-ante examination of potential policy measures to stimulate intermodal transport by barge. With the SIMBA model, the impact of volume increases in the network or the introduction of new intermodal barge terminals can be simulated. Also alternative consolidation strategies may be compared.

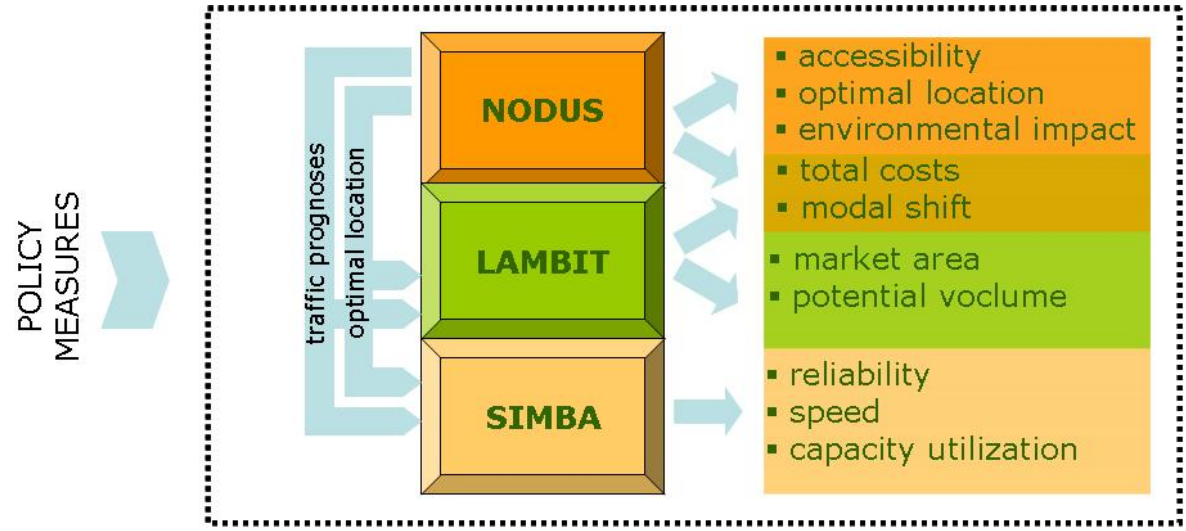

Fig. 3: DSSITP assessment framework [6]

Three categories of policy measures may be identified. The first group of policy measures affects intermodal transport costs. Both federal and regional governments in Belgium establish subsidy schemes to promote the growth of intermodal transport. Second, transport policies may affect investments costs necessary to provide intermodal transport infrastructure. Infrastructure related policy measures include the construction of new terminals and intermodal network extensions. A third group of policy measures is intended to improve intermodal transport services. An example of service related policy measures is given by Caris, Macharis and Janssens[8] who study the effect of alternative consolidation strategies in intermodal barge transport.

In this paper the SIMBA model is applied to analyze the impact of a new intermodal barge terminal on the waterway network. The impact on network characteristics such as average and maximum waiting times at locks and in the port area is measured. Potential bottlenecks and necessary capacity investments may also be deducted. As depicted in figure 3, the location and volume of a new intermodal barge terminal is received from the NODUS model. The market area may also be analyzed with LAMBIT. A new location is identified in the southern part of the country, at Roucourt on the Nimy-Blaton-Péronnes canal. A potential volume of 7,000 containers per year with the port of Antwerp as origin or destination is assumed. Vessels will sail via the Upper Scheldt to the port area in Antwerp. The Nimy-Blaton-Péronnes canal is navigable for vessels up to 1350 tons. As the terminal currently does not exist, assumptions have to be made regarding the service schedule offered to customers. Vessels of size 32 TEU and 66 TEU sail in a roundtrip to the port area. Three departures are equally distributed in a weekly schedule. Vessels may visit both clusters of sea terminals on the right and left river bank in a single roundtrip. As the new terminal is situated in the southern part of Belgium, it takes almost a day to sail from the hinterland to the port of Antwerp. Barges depart in the morning of day 1 in Roucourt and arrive at sea terminals in the morning of day 2. No changes are made to the schedules of the existing inland terminals. A separate random-number stream is dedicated to each source of randomness in the model in order to synchronize the current and new situation as much as possible.

Performance measures relevant for the comparison of the current and new situation are discussed next. Ten simulation runs of 672 hours are performed. Table 2 gives the average turnaround times of all inland terminals, expressed in hours in the current and future situation. Inland vessels may only sail to Antwerp (Antw) or they can make a combined trip to Antwerp and Rotterdam (Rdam) or Amsterdam (Adam). The standard deviation is mentioned between brackets below the average turnaround time. From table 2 may be concluded that the introduction of a new terminal has no influence on the turnaround times of existing terminals. Shuttle services offered by the terminal in Roucourt incur a turnaround time of 63.31 hours.

Table 2: Average turnaround times current situation and after introduction new terminal

Shuttle services	**Current**	**New terminal**
	Avg	**Avg**
Gosselin Deurne - Apen	15.10	15.20
	(0.32)	(0.41)
Gosselin Deurne - Rdam	21.21	21.26
	(0.09)	(0.07)
Gosselin Deurne - Apen + Rdam	22.44	21.64
	(0.46)	(0.88)
WCT Meerhout - Apen	29.09	28.84
	(0.46)	(0.41)
WCT Meerhout - Rdam / Adam	38.20	38.30
	(1.07)	(0.46)
WCT Meerhout - Apen + Rdam / Adam	41.59	41.75
	(0.42)	(0.56)
Haven van Genk - Apen	38.70	38.84
	(0.53)	(0.66)
Haven van Genk - Rdam	45.07	45.03
	(0.46)	(0.54)
Haven van Genk - Apen + Rdam	50.30	49.87
	(0.95)	(1.05)
Renory Luik - Apen	46.47	46.28
	(0.31)	(0.38)
IPG Gent - Apen	20.24	20.55
	(0.53)	(0.69)
IPG Gent - Rdam	35.43	35.28
	(0.49)	(0.32)
RTW Wielsbeke - Apen	38.63	38.77
	(0.51)	(0.36)
RTW Wielsbeke - Rdam	49.29	49.04
	(0.91)	(1.10)
AVCT Avelgem - Apen	41.98	42.09
	(2.13)	(1.99)
AVCT Avelgem - Rdam	57.53	58.21
	(0.90)	(1.16)

Shuttle services	Current	New terminal
	Avg	Avg
AVCT Avelgem - Apen + Rdam	62.82	62.57
	(0.48)	(0.41)
TCT Willebroek - Apen	14.74	14.79
	(0.19)	(0.13)
TCT Willebroek - Apen+Rdam	35.47	35.36
	(0.36)	(0.36)
Cargovil Grimbergen - Apen	20.91	21.07
	(0.17)	(0.38)
Cargovil Grimbergen - Rdam	38.17	38.24
	(0.38)	(0.11)
BTI Brussel - Apen	21.74	21.76
	(0.29)	(0.29)
BTI Brussel - Rdam	40.61	40.84
	(0.83)	(0.99)
BTI Brussel - Apen + Rdam	40.63	40.78
	(0.36)	(0.45)
Batop Herent - Apen	21.98	21.80
	(0.27)	(0.14)
Roucourt - Apen	/	63.31
	/	(0.70)

Table 3 summarizes performance measures in the port area. The average and maximum waiting time before handling, expressed in hours, are given for the sea terminals on the right and left river bank. Next, the average and maximum utilization of the quays on the right and left river bank and at the hub are measured.

Table 3: Performance measures in port area

	Current		New terminal	
	Avg	Stdev	Avg	Stdev
Avg Waiting time port area				
RO	0.06	0.02	0.08	0.02
LO	0.05	0.02	0.05	0.02
Max Waiting time port area				
RO	4.37		7.72	
LO	3.98		3.97	
Avg Capacity utilisation				
RO	0.1666	0.0017	0.1715	0.0015
LO	0.1742	0.0017	0.1786	0.0019
Max Capacity utilisation				
RO	0.9834		0.9834	
LO	0.9850		0.9850	

Following Law[9], paired-*t* confidence intervals are constructed to compare the results. Table 4 presents the 95% confidence intervals for which the difference between the introduction of a new terminal in Roucourt and the current situation is significant. The average handling time in both clusters of sea terminals on the left and right river bank increases slightly due to the introduction of a new terminal in the waterway network. An increase of 0.5% is only a minor effect. No large impact was to be expected in light of the small market area of the new inland terminal. However, the analysis clearly demonstrates the possibilities of the SIMBA model and the DSSITP framework. The framework is able to quantify ex-ante the impact of future policy measures.

Table 4: Comparison current and new situation

Avg Capacity utilisation	95% Confidence interval
Quay RO	0.0005; 0.0094
Quay LO	0.0002; 0.0084

CONCLUSIONS

A discrete event simulation model is set up to analyze potential impacts of policy measures intended to stimulate intermodal barge transport. The operations in the hinterland network of the port of Antwerp are modeled in detail to assess the impact on the network infrastructure and operational characteristics. The model is applied to estimate the influence of a new intermodal barge terminal in Roucourt. The shuttle services offered by the new terminal cause a slight increase in average handling time in both clusters of sea terminals on the left and right river bank. Impacts are only minor or non-existent due to the fact that this new terminal is not able to attract large volumes. The analysis clearly shows the possibilities of the simulation model and the DSSITP framework.

ACKNOWLEDGEMENTS

We thank the Belgian Science Policy (BELSPO) for their support on our research project DSSITP (Decision Support Systems for Intermodal Transport Policy) in the research programme "Science for a Sustainable Development - call 2", under contract number SD/TM/08A.

REFERENCES

1. Macharis, C. and Y. M. Bontekoning (2004). Opportunities for OR in intermodal freight transport research: A review. European Journal of Operational Research 153, pp. 400-416.

2. Caris, A., Macharis, C. and Janssens, G.K., (2008). Planning Problems in Intermodal Freight Transport: Accomplishments and Prospects, Transportation Planning and Technology 31 (3), pp. 277-302.
3. Rizzoli, A. E., N. Fornara, and L. M. Gambardella (2002). A simulation tool for combined rail/road transport in intermodal terminals. Mathematics and Computers in Simulation 59, pp. 57-71.
4. Parola, F. and A. Sciomachen (2005). Intermodal container flows in a port system network: Analysis of possible growths via simulation models. International Journal of Production Economics 97, pp. 75-88.
5. De Langen, P.W. and A. Chouly (2004). Hinterland access regimes in seaports. European Journal of Transport and Infrastructure Research 4 (4), pp. 361-380.
6. Pekin, E., Caris, A., Crépin, T., Macharis, C., Jourquin, B. and G.K. Janssens, (2008). Integrated decision support tool for intermodal freight transport. Nectar Logistics and Freight Cluster Meeting, Delft, the Netherlands.
7. Jourquin, B. and M. Beuthe, (1996). Transportation Policy Analysis with a GIS: The virtual Network of Freight Transportation in Europe. Transportation Research Part C 4 (6), pp. 359-371.
8. Caris, A., Macharis, C. and G.K. Janssens, (2008). Network Analysis of Container Barge Transport in the Port of Antwerp by means of Simulation, Nectar Logistics and Freight Cluster Meeting, Delft, the Netherlands.
9. Law, A.M. (2007). Simulation modeling & analysis (Fourth ed.). McGraw Hill.

BIOGRAPHY

An Caris graduated as Master of Business Economics with a major in Operations Management and Logistics at the Limburg University Centre (LUC), Belgium, in 2003. After one year of practical experience in inventory management at Reynaers Aluminium, she started as a teaching assistant in operations research at the Hasselt University (UHasselt), Belgium. In addition she is preparing a Ph.D. in Applied Economic Sciences. She is a member of the research group Data Analysis and Modelling and the Transportation Research Institute (IMOB) of the Hasselt University. She takes a research interest in modelling intermodal freight transport networks with a focus on inland navigation.

Gerrit K. Janssens received degrees of M.Sc. in Engineering with Economy from the University of Antwerp (RUCA), Belgium, M.Sc. in Computer Science from the University of Ghent (RUG), Belgium, and Ph.D. from the Free University of Brussels (VUB), Belgium. After some years of work at General Motors Continental, he joined the University of Antwerp until the year 2000. Currently he is Professor of Operations Management and Logistics at Hasselt University within the Faculty of Business Administration. He holds the CPIM certificate of the American Production and Inventory Control Society (APICS). During the last fifteen years he has repeatedly been visiting faculty member of universities in Thailand, Vietnam, Philippines, Cambodia and Zimbabwe. His research interests include the development and application of operations research models in production and distribution logistics.

Katrien Ramaekers graduated as Master of Business Economics at the Limburg University Centre in 2002. In October 2007, she obtained her Ph.D. in Applied Economic Sciences at Hasselt University. Her Ph.D. research is on the integration of simulation and optimisation, especially as a support for complex logistics decision-making and for decision support with limited information in supply and demand. Currently, she is a post-doctoral researcher at Hasselt University and is working on the modelling of freight transport. She is a member of the research group Data Analysis and Modelling and the Transportation Research Institute of Hasselt University.

Cathy Macharis received her Master of Business Economics and Ph.D. degrees from the Solvay Business School, Free University of Brussels (VUB), Belgium. Currently she is professor at the Free University of Brussels (VUB), Faculty of Economics, Social and Political Sciences and Solvay Business School. She teaches courses in operations and logistics management, transport and business economics. Her research focuses on establishing linkages between advanced operations research methodologies and practical logistics challenges faced by senior management in firms and public agencies. She has been involved in several national and European research projects dealing with topics such as location selection, intermodal transport optimization, road safety enhancement through telematics applications, public transport and inland navigation.

Profit as Criteria in Functioning a Supply Chain Management Problem

E.Y.T. Adesta, Hari H.Ramali, Satria Darsa, Suhendi Nur, Suwarto
Industrial Colleagues
Kotakpos 1389, Bandung 40013, Indonesia
e-mail: industrial_club@yahoo.com

Abstract: Simulation and modeling of a suppy chain management system has been the subject of many discussions in numerous papers. Theoretical solutions have been found however difficulties arise at the application stage due to the fact that real world set-up is not in conformity with the model. Usually the chain consists of producer/supplier of parts--components--modules--final products assembler. Cost is selected as criteria for optimization, while in practice profit is used. Modeling of supply chain and simulation to find an optimum profit should therefore give a more practical solution.

Keywords: Modeling, simulation, supply chain, profit/cost.

INTRODUCTION

Most theoretical models are concerned with one supplier and one manufacturer system. There is no difference between "producer & supplier" and "pure supplier." A pure supplier buys goods from producers and then sells them to manufacturer. Supplier has its own stock or inventory. Producer & supplier has production facility and warehouse of its owns and sells its products to supplier/manufacturer. If a supplier doesn't have stock/inventory and it bridges producer & supplier and manufacture, then it becomes only an agent of distribution. The problem in practice is complex. Representing a real situation by elaboration (start simple), analoging (use similarity), and iteration (refine it again and again), which covers many variables in the model to be, is not always possible though. The number of suppliers, manufacturers, goods, prices, tender contract, speeds, etc. should be included in the model.

REAL SET UP OF A SUPPLY CHAIN

Take a big airplane as an example. It might consist of more than eighty-thousands parts to be assembled into components, modules and a final product. There are many aircraft manufacturers and parts producers. Other examples are automotive and electronic industries around the world. They have choices, for example to produce and assemble all parts in one roof, or to let some manufacturers do some jobs of producing and assembling in different places.

The situation might be described in the following ways:

1. One supplier (S), one part (P), one manufacturer (M)
2. One S, more than one P, one M
3. More than one S, one P, one M
4. More than one S, more than one P, and one M
5. One S, one P, more than one M
6. One S, more than one P, more than one M
7. More than one S, one P, more than one M
8. More than one S, more than one P, and more than one M

There are independent and dependent suplliers (groups). There are manufactures groups too.

COST AND/OR PROFIT

Figure 1 shows two cost curves. Supplier buys part from producer. The first curve shows the cost as a function of lot size. The economic lot size is pointed by Axy. Manufacturer buys part from supplier. The economic lot size is pointed by Bxy. In most cases, Axy is not the same as Bxy. In this example, curves cross each other in two points, Cxy and Dxy. These points could be named joint cost, which means that supplier and manufacturer have the same total cost and the same amount of part bought. Both are not the optimum cost for seller nor buyer.

Line y = Y represents the price paid by manufacturer which buys part from supplier. Simulation can be conducted within the range of X minimum and X maximum. The range is negotiable beside the price, which are stated in a sell and buy contract between supplier and manufacturer. The profit is the difference between price and cost. Simulation is done to find optimum profit for supplier or seller.

Supplier can use their own working capital, or borrow it from a bank. Its return should be higher than the interest rate, which varies from one country to others. Payback periods should be in accordance with the terms of borrowed working capital.

Corresponding Author: E.Y.T. Adesta, Industrial Colleagues Kotakpos 1389, Bandung 40013, Indonesia
e-mail: industrial_club@yahoo.com

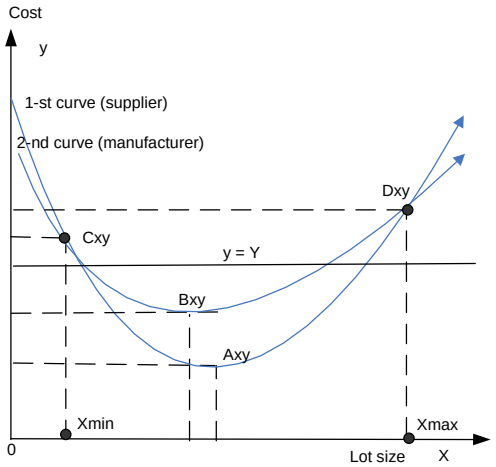

Figure 1. Cost curves (sample)

MULTI PARTS AND SOURCES

Producer & supplier or simply supplier can sell parts/goods to a "free market." They can also sell to a certain manufacturer. They are not allowed to sell them to other manufacturers. Transactions can also happen between or among suppliers.

Usually, manufacturer buys parts /components /modules from various sources. There are many problems to be solved, for example manufacturer has to wait four years to have a complete module in his assembly line. An aircraft consists of several modules, for example, cockpit, body, tail, engine, wing, etc. Problems arise when all modules don't arrived in the plant on time. The causes of the problems can be traced from producer & supplier of parts, components, modules, and in the final assembly it self. In short, scheduling is of prime importance in a supply chain management system.

SUPPLY CHAIN SYSTEM PERFORMANCE

There are several measures in this respect, namely:

1. Maximum completion time
2. Total time spent on all jobs
3. Summed lateness of all jobs
4. Summed tardiness of all jobs
5. Summed earlyness of all jobs
6. Lateness of the lastest job
7. Tardiness of the tardiest

The first measure, makespan model consists of processing time and sequence (from three Sources) as follows:

Source(S)	S1	S2	S3	
Part, P	4	3	2	months
Component, C	1	4	4	
Module, M	3	2	3	
(Assembly, A	3	3	1)	
Sequence	P	C	M	
	C	P	M	
	M	C	P	
	C	M	P	

Makespan = 16 months, maximum completion time

(Lateness, tardiness, earlyness, lateness of the latest job, the tardiest, and total time spent on all jobs, are not presented)

THE DYNAMIC NATURE OF PROFIT/COST

It is shown in Figure 1 that price line y =Y is above Axy and Bxy. It means that supplier and manufacturer obtain profit. If the line is under Axy, then supplier and manufacturer are at lost. If the line is between Axy and Bxy, then manufacturer is at lost, but supplier obtains profit. If the line crosses Cxy or Dxy, then supplier and manufacture obtain nothihg, but at a different lot size. Between these two lot sizes, supplier and manufacturer obtain profit.

Price is a subject for negotiation. Supplier and manufacturer have their own strategies to serve both interests. If supplier is a subsidiary of manufacturer, then the process of negotiation become a "family matter." If several suppliers agree to become a group, then they have a stronger bargaining position. The same situation happens when several manufacturers agree to become a group.

Table I and II show samples of supplier financial performances. The percentage of profit/cost should be higher than the central bank rate. In other words, the internal rate of return should be high enough to cover borrowed working capital, taxes, divident, etc. The "values" of shares of the suppliers are affected by their financial performances. Supply-chain management systems are very dynamic when they borrow money from various capital markets.

THE DYNAMIC NATURE OF SCHEDULING

There are more than one manufacture and one supplier of any kind of products, engineering, durable, or consumer ones. If there is a well structured and organized manufacturers and suppliers, then scheduling problems might be easier to be formulated and solved mathematically. In practice, it is not always clear the

interrelations between/within manufacturers and suppliers, and therefore simulation techniques "come into scheduling picture." Time value of money is related to the makespan and delivery date.

Gantt-chart, critical path method, and program evaluation and preview technique, are means to schedule activities in the early period of the scientific management. Nowadays, in the age of information and computer technology, sophisticated scheduling methods/techniques appear almost every month in the journals. In the job-shop scheduling alone, more than 1000 articles have been published in various media.

There are active, semi-active, non delay, and optimum schedules. An exact optimum solution is expected to come out from a mathematical programming method, for example linear programming. A near optimum solution is expected to come out from a non mathemathical programming method, for example heuristic and/or "meta-heuristic" methods.

There are 3 groups of heuristic:

1. Biological based, Generic algorithm, Ant colonies, Artificial neural network, and Artificial immune systems
2. Physical based, for example simulated annealing
3. Social based, for example tabu reasearches.

In the Artificial Immune System, four steps should be taken, encoding, similarity, selection, and mutation. There are four basic immune system models and algorithms, Bone Marrow, negative selection, cloning selection algorithm, and somantic hypermutation. Flowcharts are developed for artificial immune system schedule, conventional makespan, invers mutation, pairwise mutation, and receptor editing.

Closing Notes. It is impossible to present the whole data and information processing in this paper. The original makespan of 15 months could be improved to become 14.20 months after 1500 iterations. It still could be improved further though.

Reading Materials/References.

1. Engin 0; Artificial Imune System and Application in Industrial Problems, Konya, Turkey, 2004.

2. Grant, E.L; Ireson, W.G; Principles of Engineering Economy, The Ronald Press Coy; 4-th Edition, NY, USA

TABEL I

PERFORMANCES OF 20 SUPPLIES IN JANUARY 2007 (PARTS)

Suppfier /Number	Date of Order	Production Cost (USD)	Finishing Date	Profit (USD)	Payment Receiving Date	Profit/Cost (Percent)
1	07/01/2007	31231000	08/01/2007	4355000	17/01/2007	13,94
2	08/01/2007	30033593	13/01/2007	4047000	22/01/2007	13,47
3	08/01/2007	30069185	13/01/2007	4085000	19/01/2007	13,58
4	08/01/2007	15638000	12/01/2007	2203000	17/01/2007	14,08
5	08/01/2007	23012126	11/01/2007	2817500	23/01/2007	12,24
6	08/01/2007	36969004	11/01/2007	4669500	25/01/2007	12,68
7	12/01/2007	20723998	17/01/2007	2807000	23/01/2007	13,54
8	14/01/2007	6972505	17/01/2007	708000	01/01/2007	10,15
9	21/01/2007	15630275	25/01/2007	2290000	09/01/2007	14,07
10	21/01/2007	18614000	27/01/2007	2477000	29/01/2007	13,30
13	22/01/2007	11410070	29/01/2007	1152000	05/01/2007	10,09
14	22/01/2007	15534000	29/01/2007	3228634	05/01/2007	20,78
11	25/01/2007	9344803	31/01/2007	1280000	31/01/2007	13,69
12	25/01/2007	12762233	31/01/2007	2039000	31/01/2007	15,97
15	28/01/2007	1650000	05/02/2007	165000	28/02/2007	10,00
16	28/01/2007	670034	05/02/2007	67010	05/02/2007	10,99
17	28/01/2007	48376129	02/02/2007	4848000	14/02/2007	9,26
18	28/01/2007	4580801	02/02/2007	469000	12/02/2007	10,23
19	28/01/2007	4645240	02/02/2007	475000	12/02/2007	10,22
20	28/01/2007	12499461	02/02/2007	1710000	07/02/2007	13,68

TABEL II
PERFORMANCE OF ONE SUPLIER IN THE YEAR 2007 (PART)

Date of Order	Production Cost (USD)	Finishing Date	Profit (USD)	Payment Receiving Date	Profit/Cost (Percent)
25/01/2007	9344803	31/01/2007	1280000	31/01/2007	13,69
25/02/2007	9313834	03/03/2007	1246000	05/03/2007	13,37
25/03/2007	9287763	02/04/2007	1217000	09/04/2007	13,10
25/04/2007	9172742	01/05/2007	1150000	30/04/2007	12,53
25/05/2007	9775945	30/06/2007	1754000	29/05/2007	17,94
25/06/2007	8865413	30/06/2007	1341000	04/07/2007	15,12
25/07/2007	9056600	01/08/2007	1200000	31/07/2007	13,25
26/08/2007	9317289	01/09/2007	1250000	04/09/2007	13,41
25/09/2007	9676931	02/10/2007	1645000	02/10/2007	16,99
25/10/2007	9276566	30/10/2007	1205000	01/11/2007	12,98
25/11/2007	9323886	01/12/2007	1300000	26/11/2007	13,94
25/12/2007	9787937	29/12/2007	1767000	02/01/2008	12,05

About the authors.

1. Andesta hold a PhD degree from the U.K. He is Chairman of the Institute for Research at Untar Jakarta
2. Ramali was graduated from ITB, Bandung. He is Director of a Glue/Adhesive Distribution Company
3. Darsa is Professional Industrial Engineer. He is President of IIE 240 Indonesia.
4. Suhendi Nur was graduated from ITB, Bandung. He is now Director at the Mandiri Bank in Jakarta.
5. Suwarto hold the Degree of MSc in Industrial Management. He is Director of the Jakarta Hospital Management system.

(A complete readings materials/references, can be obtained by writing to industrial_club@yahoo.com)

A Simulation Modelling Approach for Analyzing Parking Space Availability in Parked Building of Sripatum University

Pattanapong Ariyasit
Department of Industrial Engineering, Faculty of Engineering, Sripatum University,
Bangkok 10900
E-mail: pattanapong.ar@spu.ac.th

Abstract: This Simulation presents as evaluation of parking space availability current Parking Spot for efficiency and energy conservation in parking building of Sripatum University. By using simulation, as Not choose parking spot before drive in the park building and choose parking spot before drive in the park building. Result of both model less than real time but all activities can check in the model. In condition not choose same use selection card and another condition same the present of parking building. Condition of choose is spread in all floors and use securities to work more than condition of not choose but check free park spot decision.

Keywords: Arena, Car Parking, Park Building, Energy Conservation, Efficiency

1. Introduction

The parking area in Sripatum University have 7 zones not include motorbike. Some area assign only professor in university but parking building number 9 every person can park and this building be close system when car drive in and out by only one way. For any floor have security deposited to check and record detail of car.

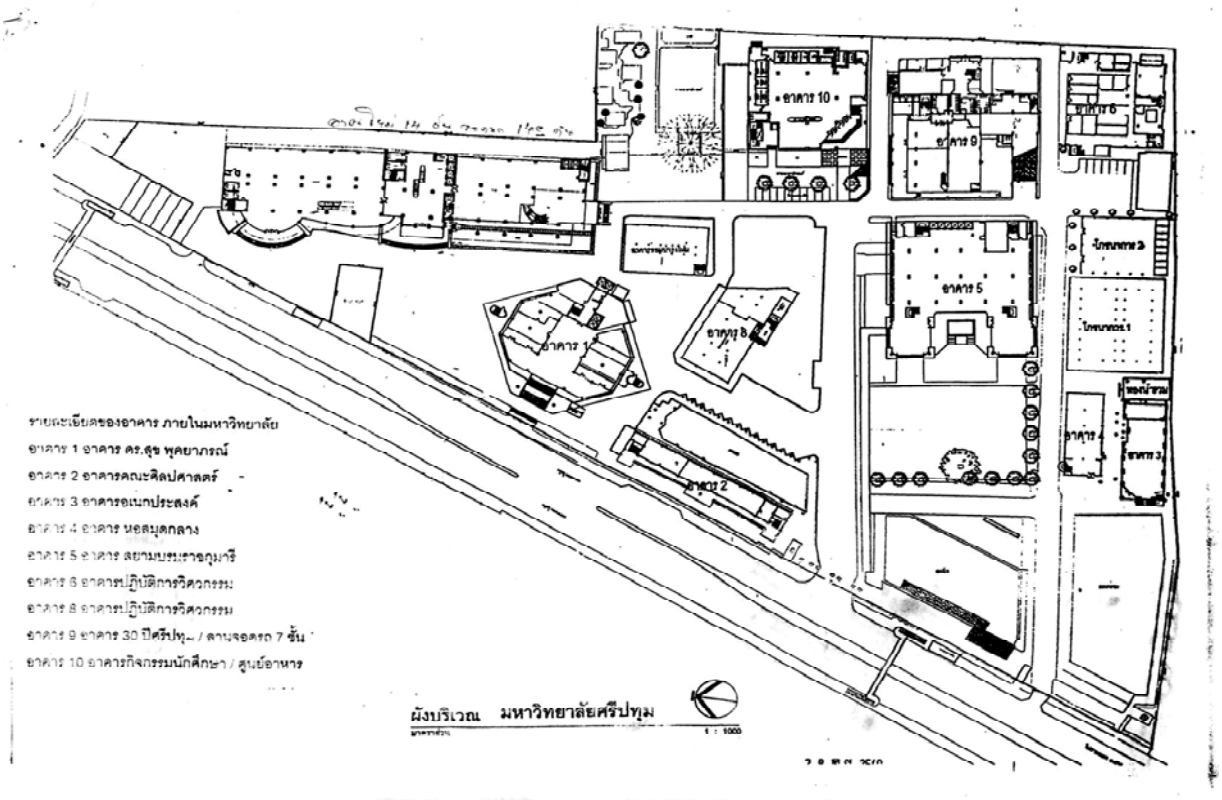

Figure 1. Layout of Sripatum University

Corresponding Author : Pattanapong Ariyasit Department of Industrial Engineering, Faculty of Engineering, Sripatum University, Bangkok 10900 E-mail: pattanapong.ar@spu.ac.th

Parking System of parking building Number 9 is Car drive in the building move to the first floor by 20 second and check parking spot if have idle park spot be parked in the spot. Security record detail ID Car color and number of park spot, these detail record for only security. Number of floor have 13 floor 258 park spots

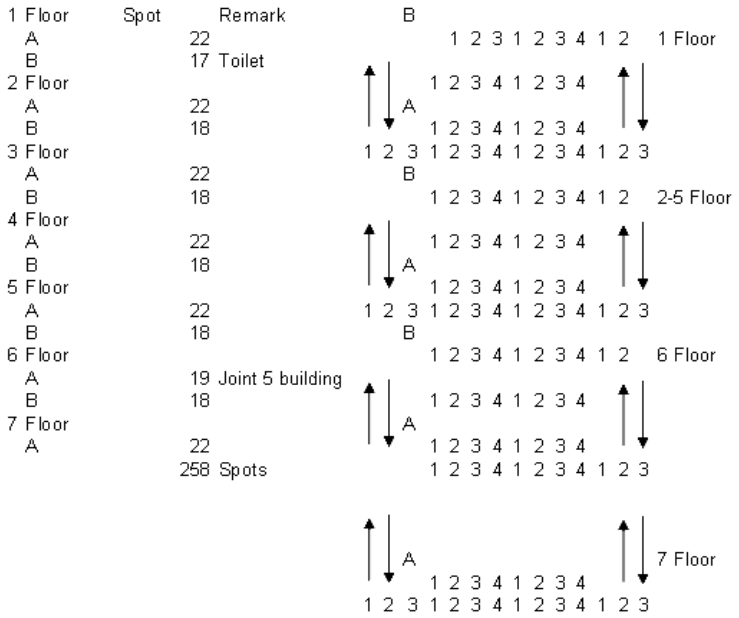

Figure 2. Park spot number and position of Park building number 9

Data Collection Distribution of cars drive in the university for 3 hours in the morning -0.001 + EXPO(0.229), this rate be reduced in any of parking area at the park building, distribution before car drive in be -0.5 + LOGN(1.93, 2.3). Distribution in any floors of the park building show below in the table 1.

Table 1. Parking in 3 hours*

Floor number	Distribution
1A	TRIA(5, 356, 1.16e+003)
1B	UNIF(255, 737)
2A	11 + WEIB(221, 1)
2B	30 + 595 * BETA(0.354, 0.739)
3A	90 + 510 * BETA(0.505, 0.22)
3B	32 + EXPO(274)
4A	NORM(368, 165)
4B	105 + 435 * BETA(1.26, 0.722)
5A	49 + EXPO(240)
5B	5 + WEIB(194, 1.05)
6A	TRIA(3, 93.9, 687)
6B	73 + EXPO(112)
7A	61 + 299 * BETA(1.18, 1.23)

* These result calculate from by input analyzer 8.01

2. Model Description

From data collection show the parking system of building is close system as gate in and out is only one way, every property is assigned from security at gate in by radio communication from 7 securities. And time to move between floors is 20 second and cumulative is 260 second of 13 floors. From data collection have two decisions is the first is Not choose parking spot before drive in the park building and another Choose parking spot before drive in the park building

2.1 Not choose parking spot before drive in the park building

When car drive in the park building before choose park spot. The car has two ways for parking as between the first floor and the second floor. This case will use decide to choose two ways by current number in queue equal zero condition. If car park at the first floor as finish choose but the car have not park at the first floor that car will have two condition same the first floor for choose between the second floor with the third floor. The park building has 13 floors when drive into the top will drive back down and choose two ways same driving up.

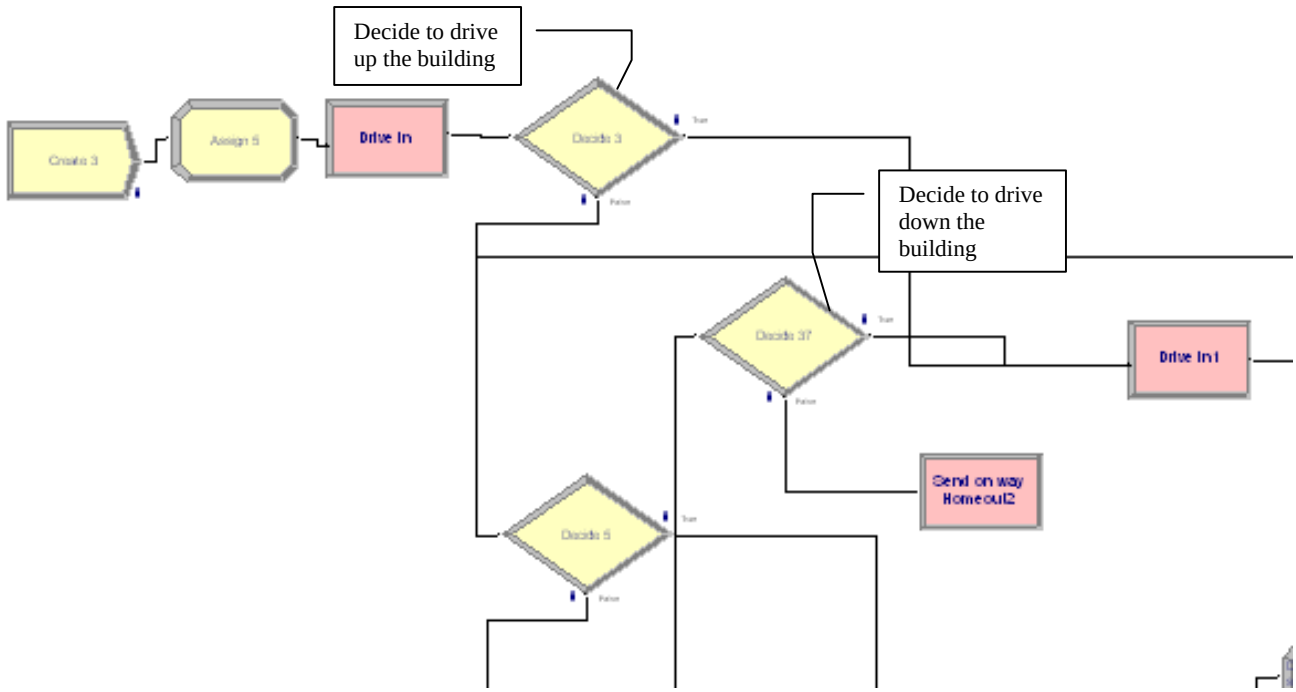

Figure 3. Decide module to choose park for drive up and drive down from building.

After have park spot will be get parking spot by seize module by construct set of parking spot 13 rows in set spreadsheet for 13 floors of park building.

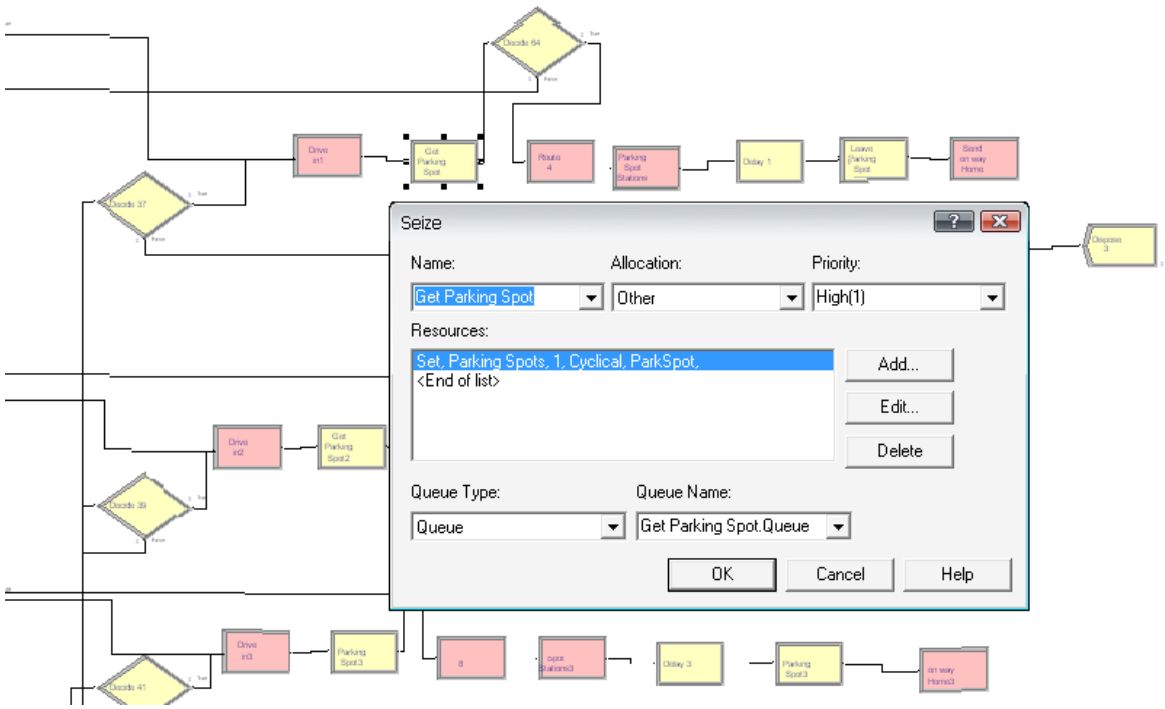

Figure 4. Seize module properties.

Decide for status in the system by current number in queue equal zero condition again. Route module expression by Member(ParkingSet.Station, ParkSpot) and route time is every 20 seconds in any floors.

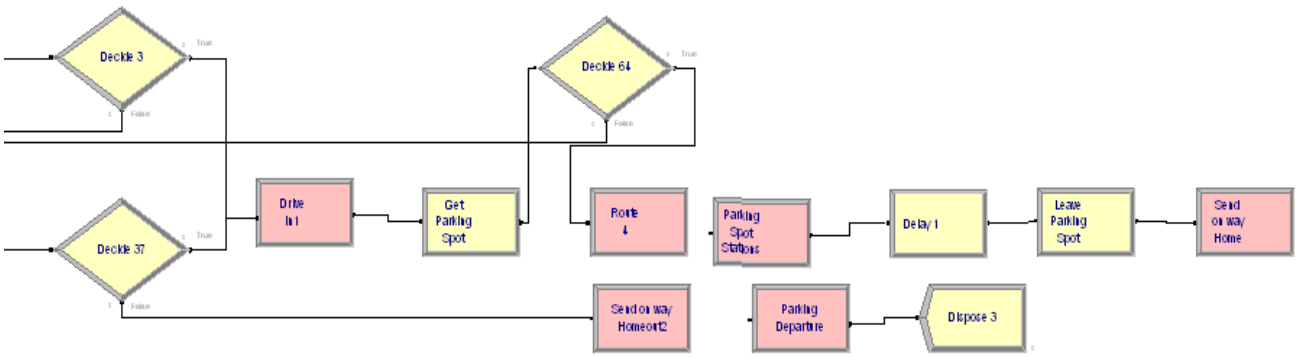

Figure 5. Module of the system.

Route continue to Parking Spot Stations module choose type is set of parking spot. Assign minute of process time in delay module and release module, route module. Station of Parking Departure from station name is ParkLeave.

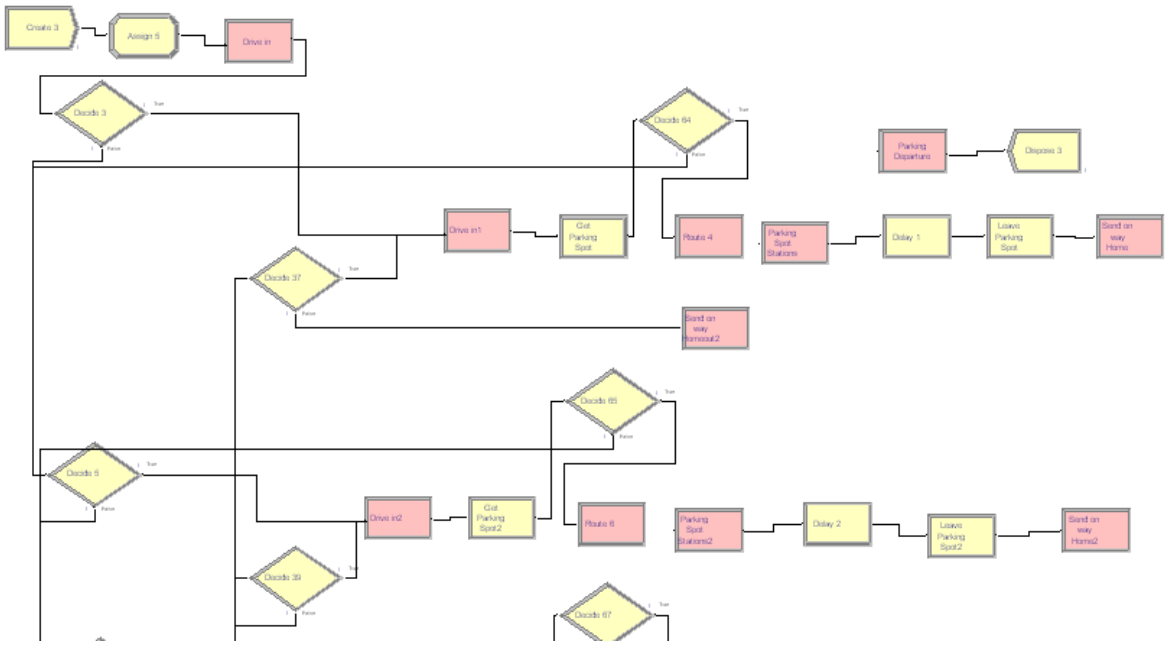

Figure 6. model of not choose parking spot before drive in the park building

2.2 Choose parking spot before drive in the park building

Module in the condition be same of not choose but have decide module of drive in assign percent of any floor at the first floor. From data collection show that the first three floor of park building have more priority 10 % Decide assigned and same percent of 10 to 12 floors because junction gate to classroom.

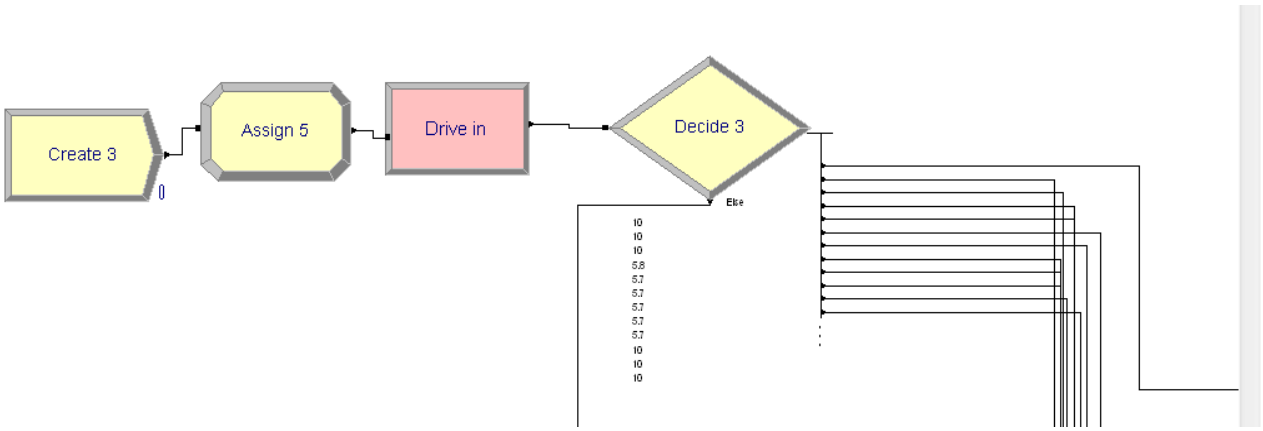

Figure 7. Assign percent in Decide module of the system.

Percent of choose way to park of drive down from the top is same not choose parking.

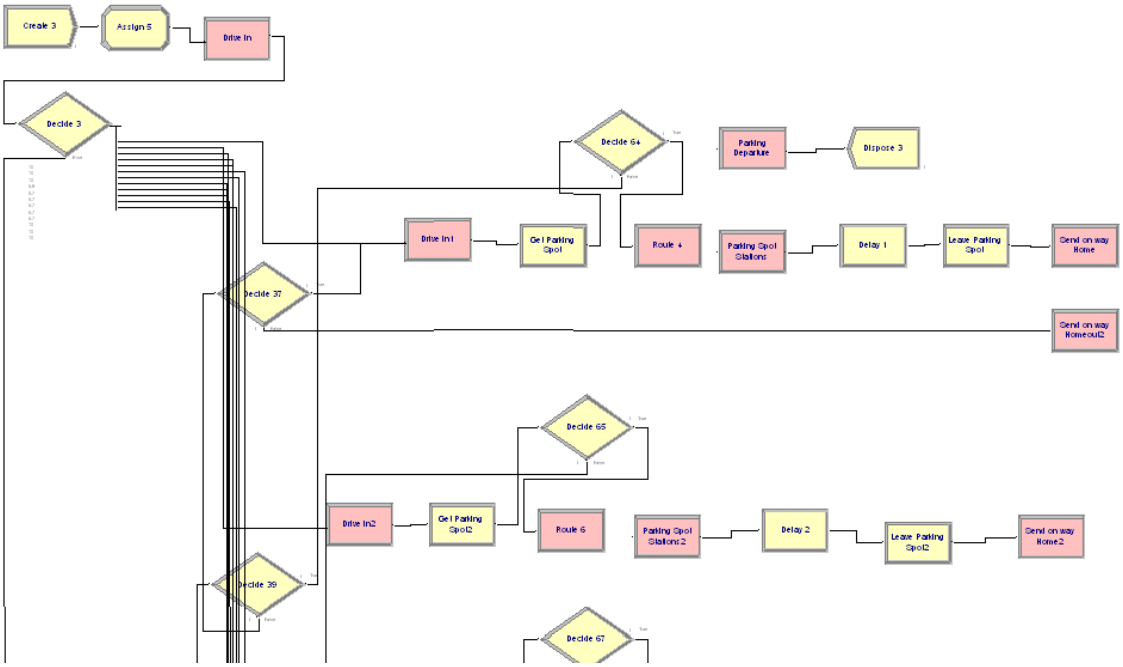

Figure 8. model of not choose parking spot before drive in the park building

3. Parking methodology in the park building

Circumstance of energy cost by park at lower parking spot before any parking spot**.**

3.1 Model condition

Assign condition of the seize module is preferred order.

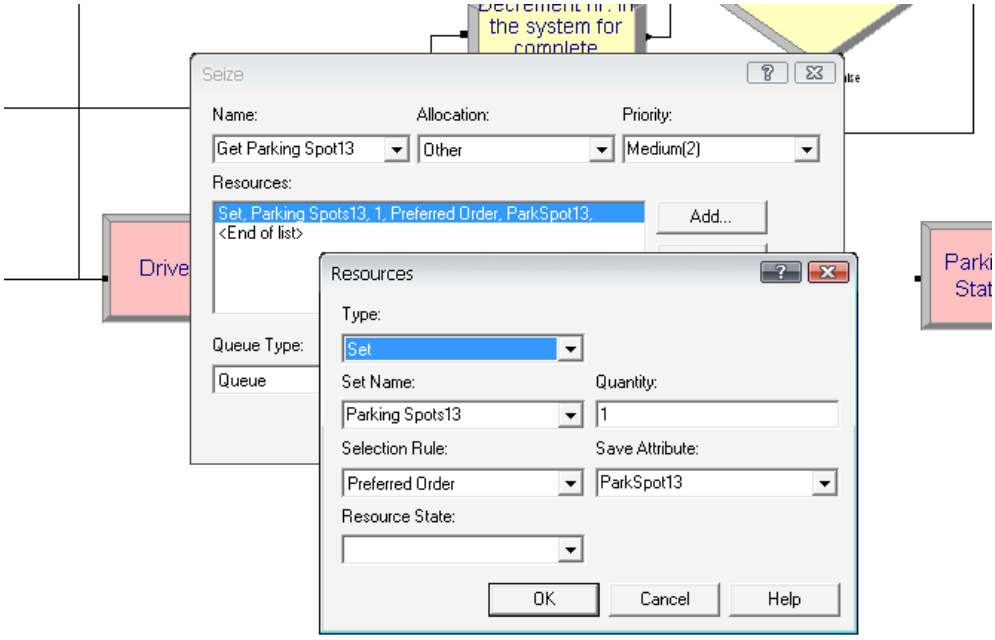

Figure 9. Assign selection rule of seize module.

3.2 Applied parking with card selection

From energy conservation be assigned card selection to give driver before drive up to the park building by difference color and size card in any floor. At gate in security give largest of selection card with driver to park at lower parking spot before any parking spot**.**

Figure 10. Difference Size and Color Card selection for 13 floors

After car left out of building return selection card and security will choose large size for next car drive in and color assign for parallel control.

4. Experimentation

4.1 Model condition

Table 2. Parking in 3 hours

Time (am.)	Number of Car	
	Choose	Not choose
9:00	44	37
10:00	36	27
11:00	35	26
Total	115	90

Table 3. Space utilization of parking at 9 am.

Floor no.	Number of Car		Space utilization (%)	
	Choose	Not choose	Choose	Not choose
1A , 1B	7	37	18	95
2A , 2B	4	0	10	0
3A , 3B	7	0	18	0
4A , 4B	4	0	10	0
5A , 5B	7	0	18	0
6A , 6B	11	0	30	0
7A	4	0	18	0
Total/Avg.	44	37	18	95

Table 4. Space utilization of parking at 10 am.

Floor no.	Number of Car		Space utilization (%)	
	Choose	Not choose	Choose	Not choose
1A , 1B	17	39	44	100
2A , 2B	8	25	20	63
3A , 3B	13	0	33	0
4A , 4B	6	0	15	0
5A , 5B	13	0	33	0
6A , 6B	18	0	49	0
7A	5	0	23	0
Total/Avg.	80	64	31	82

Table 5. Space utilization of parking at 11 am.

Floor no.	Number of Car		Space utilization (%)	
	Choose	Not choose	Choose	Not choose
1A , 1B	23	39	59	100
2A , 2B	16	39	40	98
3A , 3B	14	12	35	30
4A , 4B	8	0	20	0
5A , 5B	21	0	23	0
6A , 6B	26	0	70	0
7A	7	0	32	0
Total	115	90	40	76

4.2 Applied parking with card selection

Table 6. Parking in 3 hours

Time (am.)	Number of Car	
	No card	Card
9:00	61	65
10:00	69	75
11:00	58	55
Total	188	195

Table 7. Space utilization of parking at 9 am.

Floor no.	Number of Car		Space utilization (%)	
	No card	Card	No card	Card
1A , 1B	48	52	92	100
2A , 2B	13	13	25	25
3A , 3B	0	0	0	0
4A , 4B	0	0	0	0
5A , 5B	0	0	0	0
6A , 6B	0	0	0	0
7A	0	0	0	0
Total/Avg.	61	65	59	63

Table 8. Space utilization of parking at 10 am.

Floor no.	Number of Car		Space utilization (%)	
	No card	Card	No card	Card
1A , 1B	50	52	96	100
2A , 2B	49	52	94	100
3A , 3B	31	36	59	69
4A , 4B	0	0	0	0
5A , 5B	0	0	0	0
6A , 6B	0	0	0	0
7A	0	0	0	0
Total/Avg.	130	140	83	90

Table 9. Space utilization of parking at 11 am.

Floor no.	Number of Car		Space utilization (%)	
	No card	Card	No card	Card
1A , 1B	51	52	98	100
2A , 2B	48	52	92	100
3A , 3B	50	52	96	100
4A , 4B	39	39	73	75
5A , 5B	1	0	2	0
6A , 6B	0	0	0	0
7A	0	0	0	0
Total/Avg.	188	195	72	94

5. Conclusions and Recommendation

The simulation resulted of Space Utilization less than real time but not difference in methodology can check activity happened in the park building. And trend of happening in the park building are same. From the distribution show that in the below of the car building is Uniform distribution as all people park all day or these is person of university maybe prepare park spot suited number of these distribution. Interarrival time distribution of cars drive in the

university created in the model of park building, it can support all cars for 1 hour. No choose park spot construction condition same like Selection Card that implement with real circumstantial This paper set for 3 hours in the morning because this interval time is more traffic. Any interval will be slowly to increate and decrease. From animation show that park spread all 13 floors when set condition as choose parking spot before drive in the park building. If use another condition in three hours morning will use security to manage 3 to 4 persons but another one every one works same time all day.

Acknowledgments

Upon the completion of this study, I would like to express gratitude and sincere appreciation to all of Dr.Chanin Srisuwanapa and for their valuable suggestions and all data from Security of park building , throughout the completion of the simulation.

I am grateful to Sripatum University regards their fully data support throughout financial support of this simulation.

Special thank are also extended to my dear family to supports, always powerful and encouragement during the studying.

References

[1] W.David kelton Randall P. Sadowski Deborah A. Sadowski SIMULATION WITH AREANA McGraw-hill International Editiona Industrial engineering Series1998

[2] John M. Harris and Yasser Dessouky, , A SIMULATION APPROACH FOR ANALYZING PARKING SPACE AVAILABILITY AT A MAJOR UNIVERSITY

[3] John M. Harris and Yasser Dessouky, , A SIMULATION APPROACH FOR ANALYZING PARKING SPACE AVAILABILITY AT A MAJOR UNIVERSITY

[4] Hensher, D.A., and King, J. " PARKING DEMAND RESPONSIVENESS TO SUPPLY, PRICING AND LOCATION IN SYDNEY CENTRAL BUSINESS DISTRICT. " Transportation Research Part A 2001

[5] Hensher, D.A., Button, K., " HANDBOOK OF TRANSPORT MODELLING. " Pergamon 2000 Hensher, D.A., Louviere, J., and Swait, J., " STATED CHOICE METHODS ANALYSIS ANDAPPLICATIONS. " Cambridge 2000

Study the Effect of Pretest-normality on Estimating Process Capability Indices via Monte Carlo Simulation

Siraprapa Manomat and Prapaisri Sudasna Na Ayudthya
Department of Industrial Engineering, Kasetsart University
Bangkok, Thailand

Abstract: The aim of this study was to investigate the effect of preliminary test for normality before using process capability indices (PCIs) estimators when the investigator was uncertain that the process followed a normal distribution. Monte Carlo simulation with 1,000 runs under normal, lognormal and Weibull distribution was conducted to investigate the PCIs estimators. The study applied Shapiro-Wilk method as the preliminary test for normality. Besides the general method, the unbiased method and the first four moments method are applied for determining PCIs estimators. In case of normal distributed process, the results showed that PCIs estimators were similarly in every method and sample size. For the non-normal distributed process, the non-preliminary test for normality which using the first four moments method gave the best result when sample sizes of 10 and 30. However, the sample sizes of 50, 100 and 150 indicated that the preliminary and non-preliminary test for normality which using the first four moments method gave nearly the same results, but these both methods were better than the assumed normal methods.

Key words: Test for normality , Shapiro-Wilk's test , Process Capability Indices

INTRODUCTION

Process capability analysis is the statistical techniques for measuring inherent variation of the production process and analysis process variation under the product requirement or specification. The process capability indices (PCIs) are the tool for comparing the specification with the actual performance of a manufacturing process. The most common indices such as potential capability index (Cp) and actual capability index (Cpk) are usually under the assumption that the process follows a normal distribution.

Unfortunately, many data from practical processes are not normally distributed. Several authors develop PCIs under non-normality[1,2,3]. Tang and Than[4] compared PCIs estimator of non-normal data and indicated that the transformation methods, Box-Cox transformation and Johnson transformation, are superior to the other method. However, the transformation methods are difficult in calculating and translating result. Ding[5] suggested a method to estimate the process capability index for non-normal data from its first four moments, namely mean, standard deviation, skewness and kurtosis. The first four moments method is compared with some other existing methods following the approach of Tang and Than[4]. This method gives more accurate, less sensitivity to sample size and not depend on normality or non-normality of the process.

In practice, the process distribution is not easy to define. When the investigator is uncertain that the process followed a normal or non-normal distribution, a test of normality may be used. Han [6] studied the effect of the preliminary test for normality on PCIs estimators when the process follows a normal distribution and found that the biases and MSEs decreased when the level of significance of the preliminary test was increased.

In this study, the effects of pretest-normality on PCIs estimators when the process follows normal and non-normal distributions are investigated. Next section, methods for estimating PCIs based on normal and non-normal distributed processes are provided. Monte Carlo simulation section gives the details of simulation.

METHODOLOGY

PCIs AND THEIR ESTIMATORS

PCIs are used to compare the specification tolerance range with the actual production tolerance range. The most common indices Cp and Cpk are defined by

$$Cp = \frac{\text{specification width}}{\text{process width}} = \frac{USL - LSL}{6\sigma}$$

$$Cpu = \frac{USL - \mu}{3\sigma}, \quad Cpl = \frac{\mu - LSL}{3\sigma} \qquad (1)$$

$$Cpk = \min[Cpu, Cpl]$$

where USL and LSL are the upper and lower specification limits of the process, μ is the process mean and σ is the process standard deviation.

Corresponding Author: Siraprapa Manomat, Department of Industrial Engineering, Kasetsart University, Bangkok, Thailand, Email : srm@kmutnb.ac.th

Under the assumption that the process follows a normal distribution and the process mean is at the midpoint (m) of USL and LSL, m = (USL+LSL)/2, Cp and Cpk equal to 1. It implies that 99.73% of data fall within the specification or about 0.27% of data out of the specification. In general, sample data will be collected from the process. The process mean (μ) and standard deviation (σ) are usually unknown, so the estimator of μ and σ are used.

Let $X_1, X_2, \ldots, X_n$ be the random sample with sample size n. The estimator of μ and σ are:

$$\overline{X} = \frac{\sum_{i=1}^{n} X_i}{n}$$

$$S = \sqrt{\frac{\sum_{i=1}^{n} (X_i - \overline{X})^2}{n-1}}$$

Thus, the natural estimators to estimate the indices Cp and Cpk are defined by

$$\hat{C}p = \frac{USL - LSL}{6S}$$

$$\hat{C}pu = \frac{USL - \overline{X}}{3S}, \quad \hat{C}pl = \frac{\overline{X} - LSL}{3S} \qquad (2)$$

$$\hat{C}pk = \min[\hat{C}pu, \hat{C}pl]$$

These equations are called "general PCIs estimators"

However, Pearn[7] showed that $\hat{C}p$ is the biased estimator and Pearn[8] showed that $\hat{C}pk$ is the biased estimator. The correction faction is

$$b_{n-1} = \sqrt{\frac{2}{(n-1)}} \times \frac{\Gamma[(n-1)/2]}{\Gamma[(n-2)/2]}$$

so, the unbiased estimators to estimate the indices Cp and Cpk are defined by

$$\tilde{C}p = b_{n-1}\hat{C}p$$

$$\tilde{C}pu = b_{n-1}\hat{C}pu, \quad \tilde{C}pl = b_{n-1}\hat{C}pl \qquad (3)$$

$$\tilde{C}pk = \min[\tilde{C}pu, \tilde{C}pl]$$

THE FIRST FOUR MOMENTS METHOD

The first four moments method is a method to estimate the process capability index for a set of non-normal data from its first four moments. Ding[5] uses ten order of Chebyshev-Hermite polynomials from first four moments of data such as mean, standard deviation, skewness and kurtosis to develop PCIs estimators.

If a set of data from a process follows a normal distribution with zero mean, Cp equal to 1. It implies that 99.73% of data fall within ±3σ range. However, if a set of data from a process is not satisfied normal distribution, numbers of data fall within specification should not be valid for 99.73%.

So, the effective range, Er, is defined such that a pre-determined percentage of data falls within ±Er. If 99.73% of data are within the effective range, PCI and Er will be defined by

$$C_{p-Er} = \frac{USL - LSL}{2Er} = \frac{USL}{Er} \qquad (4)$$

$$Er = \left\{ 2.78248 + 0.21752 \exp\left[-\left(\frac{|\mu|}{0.18418\sigma} \right)^{1.1402} \right] + (\pm 1.1229|\gamma_1| - 0.6263\gamma_1^2)\left[1 - \exp\left(-50\left(\frac{\mu}{\sigma} \right)^2 \right) \right] + 0.6063\gamma_2 \right\} \sigma + |\mu|$$

where the plus sign is used when both μ and γ_1 have the same sign, otherwise the minus sign is used, μ is the mean, σ is standard deviation, γ_1 and γ_2 are skewness and kurtosis respectively.

To estimate the PCI from the first four moments method, μ is replaced with $\overline{X}$, σ is replaced with S, γ_1 and γ_2 are replaced with $\hat{\gamma}_1$ and $\hat{\gamma}_2$ where

$$\hat{\gamma}_1 = \frac{n}{(n-1)(n-2)} \sum_{i=1}^{n} \left(\frac{X_i - \overline{X}}{S} \right)^3$$

$$\hat{\gamma}_2 = \frac{n(n+1)}{(n-1)(n-2)(n-3)} \sum_{i=1}^{n} \left(\frac{X_i - \overline{X}}{S} \right)^4 - \frac{3(n-1)^2}{(n-2)(n-3)}$$

MONTE CARLO SIMULATION

In practice, mean, standard deviation and the distribution of the process are usually unknown. The simulation is the best way to investigate the effect of pretest-normality before using PCIs estimators.

The assumption still hold that the process mean is at the midpoint of USL and LSL. The simulation study is conducted to generate simulation data from normal, lognormal and Weibull distribution where sample size n = 10, 30, 50, 100 and 150 and with target Cpu values of 1, 1.5 and 1.667. Under normal distributed process, the fraction of non-conforming (FNC; ppm.) is computed by using

$$FNC = 1 - \Phi(3Cpu)$$

For normal(0,1), when target value of Cpu = 1, it implies that USL = 3 and FNC will be 1349.667 ppm. If target value of Cpu = 1.5, it implies that USL = 4.5 and FNC will be 3.401 ppm. When target value of

Cpu = 1.667, it implies that USL =5 and FNC will be 0.287 ppm.

For non-normal distributed process, Tang and Than[4] gave the USL value for lognormal and Weibull distributions with the same fraction non-conforming. The USL values for lognormal and Weibull distributions that used in calculation are shown in Table 1.

Table 1: USL values for lognormal and Weibull distribution used in calculation

USL for	Target Cpu		
	1 FNC=1349.667 ppm.	1.5 FNC=3.401ppm.	1.667 FNC=0.287ppm.
Lognormal(0,0.3)	5.175	11.7606	15.4021
Lognormal(0,0.5)	8.3421	24.0947	34.1217
Weibull(1,1)	6.6077	12.5915	15.6635
Weibull(2,1)	2.5705	3.5485	3.8812

In each simulation, Cpu estimators are calculated for five cases to study the effect of pretest-normality on estimating PCIs. The first three cases are non-preliminary test for normality and last two cases are pretest-normality by using Shapiro-Wilk test with $\alpha = 0.05$ under null hypothesis, Ho: the process follows a normal distribution. The five cases are specified as follows:

Case I : *Non-preliminary test for normality* and *assumed normal distributed process*

Cpu estimators are calculated by general method (equation (2))

Case II : *Non-preliminary test for normality* and *assumed normal distributed process*

Cpu estimators are calculated by unbiased method (equation (3))

Case III : *Non-preliminary test for normality* and *do not consider distributed process*

Cpu estimators are calculated by the first four moments method (equation (4))

Case IV : *Preliminary test for normality*

If the test rejects the null hypothesis, Cpu estimators will be calculated by the first four moments method (equation (4)).

Else general method (equation (2)) will be used.

Case V : *Preliminary test for normality*

If the test rejects the null hypothesis, Cpu estimators will be calculated by the first four moments method (equation (4)).

Else unbiased method (equation (3)) will be used.

For each of the different distribution and sample size, Monte Carlo simulation is conducted 1,000 times to obtain the average of Cpu estimators under the five cases above. The result is shown in the next section.

SIMULATION RESULTS

The simulation results from investigation for normal, lognormal and Weibull distribution with target Cpu = 1 are shown in Fig. 1. Results for target Cpu = 1.5 and 1.667 are not shown because patterns of these results are similarly, but Cpu estimators for target Cpu = 1 are closed to the target value.

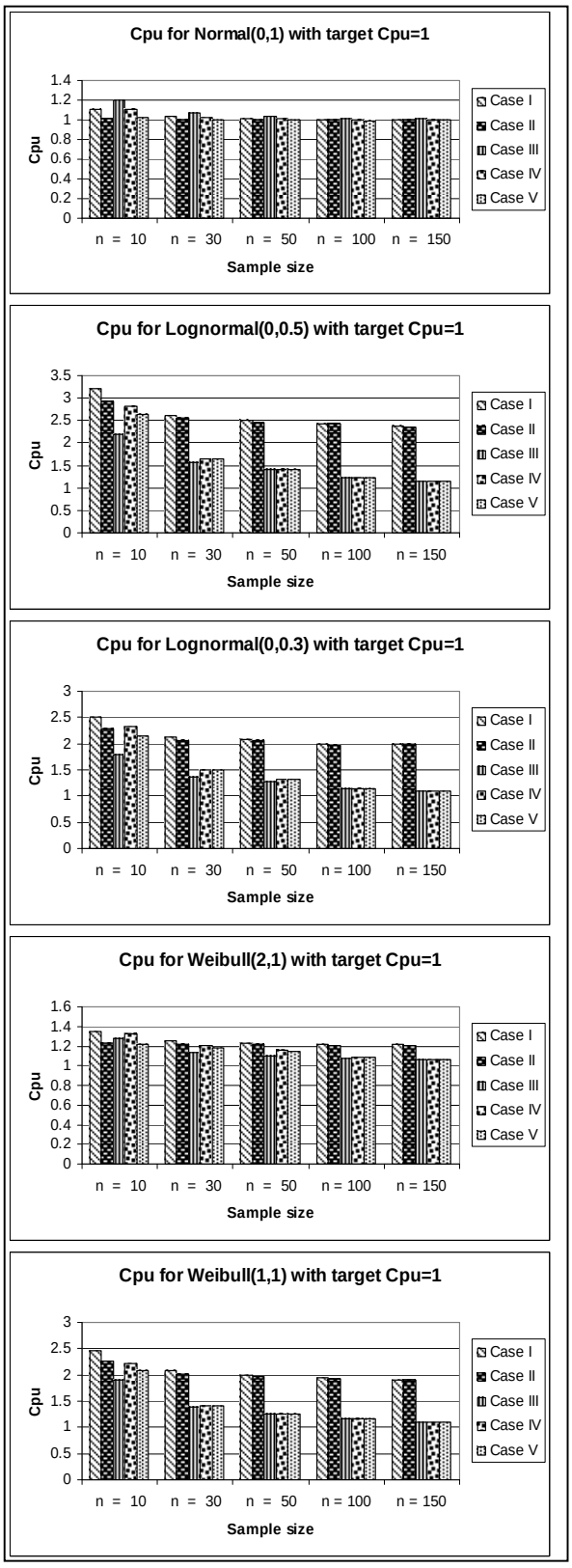

Fig. 1: The average Cpu for normal and non-normal distributed processes.

For normal distribution, non-preliminary test for normality and using unbiased method (case II) is the best for every sample size. However, every case is nearly the same result.

For non-normal distribution, lognormal and Weibull distribution, non-preliminary test for normality with using the first four moments method (case III) is the best for sample size of 10 and 30. However, when the sample sizes are 50, 100 and 150, preliminary test (case IV and case V) and non-preliminary test for normality with using the first four moments method (case III) are nearly the same result. Moreover, the last three cases are better than case I and case II (assumed normal distribution) for every sample size.

To obtain the mean square errors(MSEs) and biases of the Cpu estimators, let $\hat{Cpu}_j$ be the estimator of Cpu for j^{th} run. The bias and MSE of the simulations are

$$MSE = \frac{\sum_{j=1}^{1,000} [\hat{Cpu}_j - Cpu]^2}{1{,}000}$$

$$Bias = \frac{\sum_{j=1}^{1,000} \hat{Cpu}}{1{,}000} - Cpu$$

The MSEs and biases of the Cpu estimators for normal(0,1), lognormal (0,0.3)and Weibull(1,1) when the sample size equal to 10, 30, 50,100 and 150 are shown in Fig. 2.

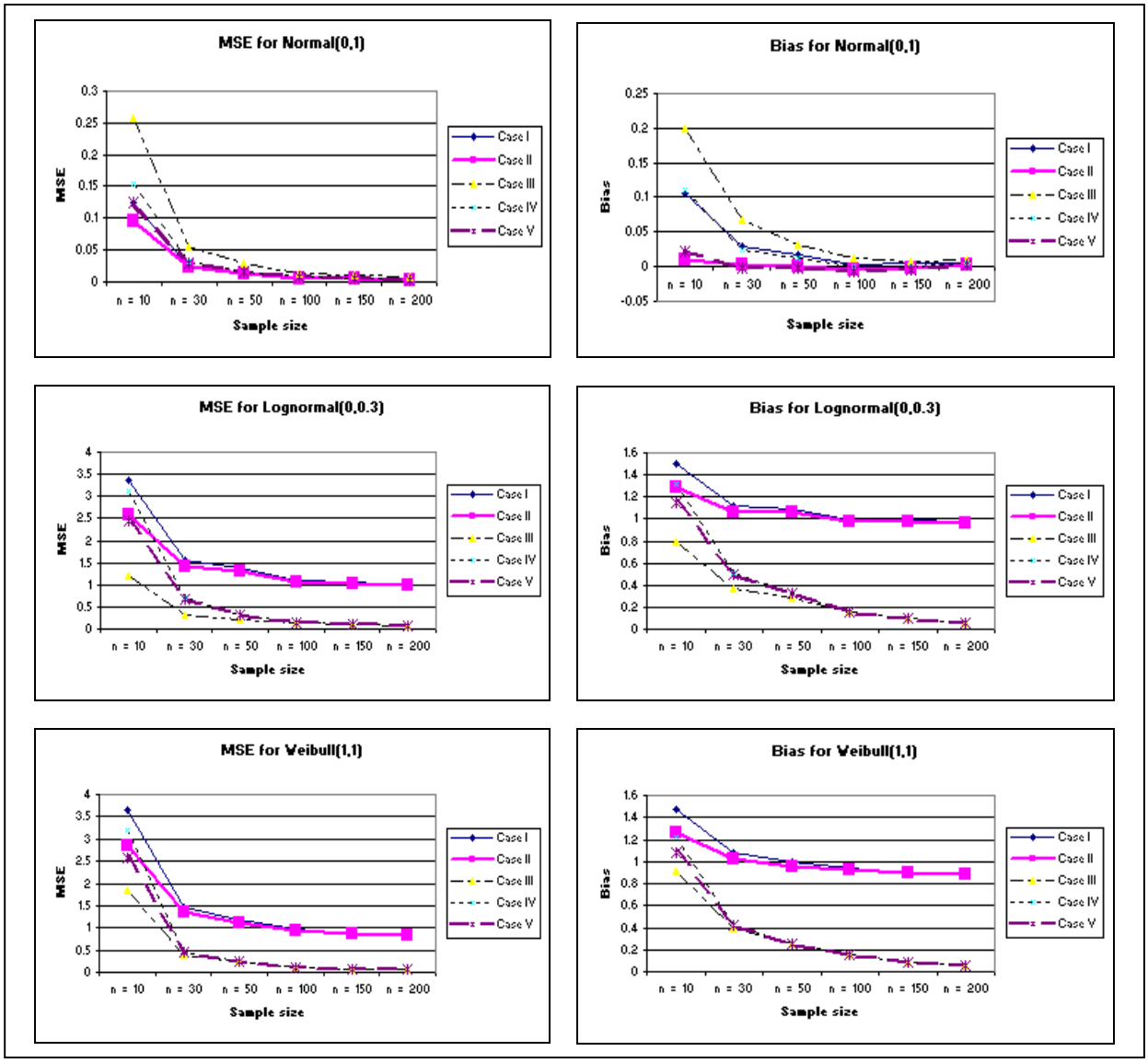

Fig.2 : MSEs and Biases of Cpu estimator for normal(0,1), lognormal(0,0.3) and Weibull(1,1) distribution

For normal distributed process, the values of MSEs and biases in case III are the highest when the sample size is 10. It will be decreased rapidly when the sample size goes up to 30. However, when the sample size is more than 50, every case yields nearly the same result. All of them have flattened out.

For non-normal distributed processes, the values of MSEs and biases in case I are the highest when the sample size is 10 and they go down quickly when the sample size is changed to 30. However, when the sample sizes are more than 50, MSEs and biases remain stable and show that the MSEs and biases in case I and case II are higher than the last three cases.

CONCLUSION

Pretest-normality is used to check the normality of process when the investigator is uncertain about process distribution that followed the normal assumption. Shapiro-Wilk test is a good test for normality. In some process that can not use the large sample size, non-preliminary test for normality and the use of the first four moments method should be suggested. Since the method is considered to be the best one. For large sample size, non-preliminary test for normality and the use of the first four moments method is similarly to the preliminary test for normality. However, when the investigator convinces that the process distribution is normal or non-normal, the investigator should select the appropriate method, i.e. if the investigator convinces that the process is normally distributed, the unbiased method should be applied. If the investigator convinces that the process is non-normally distributed, the first four moments method should be applied.

REFERENCES

1. Clement,J.A., 1989. Process capability indices for non-normal calculations. Quality Progress, 22:49-55.
2. Pearn,W.L. and S. Kotz, 1994. Application of Clements' method for calculating second and third generation process capability indices for nonnormal Pearsonian populations. Quality Engineering, 7:139-145.
3. Rivera,L.A.R., N.F. Hubele and F.D.Lawrence, 1995. Cpk index estimation using data transformation. Computers and Industrial Engineering, 29:55-58.
4. Tang,L.C. and S.E. Than, 1999. Computing process capability indices for non-normal data: a review and comparative study. Quality and Reliability Engineering International, 15:339-353.
5. Ding,J., 2004. A method of estimating the process capability index from the first four moments of non-normal data. Quality and Reliability Engineering International, 20:787-805.
6. Han,C.P., 2006. Effect of testing normality on estimating process capability indices. Quality Engineering, 18:391-395.
7. Pearn,W.L., G.H. Lin and K.S. Chen, 1998. Distributional and inferential properties of the process accuracy and process precision indices. Communications in Statistics: Theory and Methods, 27:985-1000.
8. Pearn,W.L., S. Kotz and N.L. Johnson, 1992. Distributional and inferential properties of process capability indices. Journal of Quality Technology, 24:216-231.

Simulation of Elevators Queuing for Academic Building

Chawalit Manisri
Department of Industrial Engineering, Sripatum University,
61 Phahon Yothin Rd. Chatuchak Bangkok 10900, Thailand

Abstract: This paper presents a simulation modeling of elevators queuing in an academic building. The cause of the study is a large number of students who waste their time to wait for elevators to go to class. This directly affects to a teaching-learning system. The main objective of the study, therefore, is to investigate the best destination floor of each elevator in the high building. However, it is found that the problem becomes more complex when there is a difference of numbers of students with different destination floor in specific time according to a course schedule. Thus, the simulation modeling of the 15-storey academic building with six elevators is developed by applying ARENA software. This study introduces alternatives to reduce the waiting time and numbers of students in queues. Decisions will consider about waiting time, queues and distance to class. The results clearly reveals that the average waiting time decreases from 1.14 minutes to 0.88 minutes, and the average number in queues decreases from 12.11 persons to 10.13 persons.

Key words: Simulation modeling and analysis, elevators simulation, waiting time, number in queues

INTRODUCTION

Academic buildings of universities in a city which high density of population tend to be constructed as high buildings because of limited land and an increase number of students. Therefore, elevators are generally used to facilitate students to go to class. However, there is a limitation of elevators because they can carry passengers only 8-24 persons a ride. Consequently, crowds of students and their waiting time increase. As a result, the students are late to class, and this causes students to lose their lesson concentration. Eventually, their learning efficiency drops. At present Sripatum University, one of universities in Bangkok, Thailand covering approximately 24 Rai with four buildings higher than 12-storey has also experienced the mentioned problem. In the near future, a new building with 15-storey will be built. There will approximately be 1,500 elevator passengers during each period.

The simulation modeling of elevators queuing is, therefore, developed to solve this problem by figuring out the best destination floor. There are a lot of advantages of the simulation modeling. First, it is compatible with a complex system. Next, it does not affect to real situations, so we can try different alternatives. ARENA 8.00.01 is used to speed up this simulation modeling and respond to complicated needs. Finally, this provides a model of elevator service management for each semester.

SIMULATION METHODS

This section explains the simulation methods for the elevator system of the academic building as follows:

1. Study the system and analyze input:
   - Elevator rules for the best destination floor
   - Peak hours of elevator taking
   - Performance of elevators such as speed to go up-down and open-close doors, along with maximum load
   - Amount of students in each period according to a class schedule
   - Amount of storey
   - Amount of elevators
   - Distance to class
   - Behaviors of the system such as numbers of balked students
2. Formulate the model and check for its accuracy
3. Test the model
4. Introduce alternatives and process to compare the results
5. Summarize

EXPERIMENTATION

It is found that the elevator system of academic buildings in many universities is similar to each other, but there is a difference in details. The 15-storey Building #5 with six elevators is chosen to study (In the elevators, the number of storey is run from 1 – 16 by skipping 13 because of belief).

1. Elevators #1-2 Stop on floor 1, 6, 9, 12, and 14
2. Elevators #3-4 Stop on floor 1, 7, 11, 14, and 16
3. Elevator #5 Stop on floor 1, 4, 8, 11, and 16
4. Elevator #6 Stop on every floors

Corresponding Author: Chawalit Manisri, Department of Industrial Engineering, Sripatum University, 61 Phaholyothin Rd. Chatuchak Bangkok 10900, Thailand

Normally, peak time of elevator taking is around 15 minutes before class with approximately 1,500 passengers. The above data is applied to investigate a probability to choose the right floor to stop depending on specific time as shown in appendix, Table 1 to 4. In this study, teaching – learning is scheduled into two sets of time:

- The 3-hour periods: at 8:30-11:20, 11:40-14:30, 14:50-17:40, and 18:00-20:50
- The 2-hour periods: at 08:30-10:20, 10:30-12:20, 12:30-14:20, 14:30-16:20, 16:30-18:20, and 18:30-20:20

Performance of elevators:

- Time to open or close doors which distribution TRIA(1.74, 1.86, 1.98) seconds
- Speed to go up-down: 2.59 m/s
- Maximum load: 17 persons or 1,150 kg

Passenger behaviors

- Time of walk into or out from elevators which distribution TRIA(1.74, 1.86, 1.98) seconds per person
- Queue balking: two students once; they leave the longest queue to be in a queue that elevators have just gone up from the first floor.

Limitations of the study

- Consider only queues to six elevators on the first floor. It is understood that students take a ride with a shortest queue.
- Do not consider students from other floors to the first floor.
- This simulation is developed based on data of this current academic year only, but this can be modified for the next semester
- This article emphasizes on 10-storey buildings and the higher
- Students not walk exceed 2 floors. Average distance to class about 16 m and 32 m for 1 floor and 2 floors.

According to Figure 1, it shows that students who study in different time in Building #5 choose to queue in the shortest queue to take elevators. After they reach to the destination floor or the nearest, they leave them. Figure 2 shows a modeling that students approach the system including details to destination floors according to the probability in Table 3. After students have known their conditions, they will choose the shortest queue. The elevator will take these students to the floor due to their conditions with time weight on the numbers of student who stops each floor. After the complete computing, the averages of waiting time and amounts of students in queue as appeared in Table 4 are used to analyze for a good alternative.

RESULTS

From the results, there are three alternatives of the improving models to set the destination floors of the elevators to reduce numbers of queues and waiting time. However, elevator #6 still runs as usual since it is used in a case of emergency.

Alternative #1, the destination floor is considered based on numbers of students in each floor. The elevators #1-4 stop only on floor 1, 6, 9, 12, and 15 while the elevator #5 stops only on floor 1, 4, 7, 10, and 14. The service assumptions of elevators number 1-4 in this alternative as following:

- Stopping on 6^{th} floor services for floor 5, 6, and 7.
- Stopping on 9^{th} floor services for 8, 9, and 10.
- Stopping on 12^{th} floor services for 11, 12, and 14.
- Stopping on 15^{th} floor services for 15 and 16

And the other is

- Stopping on 4^{th} floor services for floor 3, 4, and 5.
- Stopping on 7^{th} floor services for 6, 7, and 8..
- Stopping on 10^{th} floor services for 9, 10, and 11.
- Stopping on 14^{th} floor services for 12, 14, and 16

Alternative #2, the destination floor is considered as equal distribution. All elevators #1-5 stop on floor 1, 6, 9, 12, and 15. The service assumptions of elevators number 1-5 in this alternative as following:

- Stopping on 6^{th} floor services for floor 5, 6, and 7.
- Stopping on 9^{th} floor services for 8, 9, and 10.
- Stopping on 12^{th} floor services for 11, 12, and 14.
- Stopping on 15^{th} floor services for 15 and 16

Alternative #3, the destination floor is considered based on the least number of elevator stop on specific floors, so the elevators can go back to the first floor to serve passengers faster. Thus, all five elevators stop on floor 1, 6, 10, and 14. However, passengers have to walk longer to class. The service assumptions of elevators number 1-5 in this alternative as following:

- Stopping on 6^{th} floor services for floor 4, 5, 6, and 7.

- Stopping on 10th floor services for 8, 9, 10, and 11.
- Stopping on 14th floor services for 12, 14, 15, and 16.

After processing according to three alternatives, the results are shown in Table 5. Table 5 clearly reveals that all three alternatives provide more efficiency than the existing system. The waiting time and the number of students in queue decrease. In this case, alternative #3 seems to be the best solution because it provides the shortest waiting time and the least number of students in queue. Alternative #1 also reduces waiting time and numbers of students in queue as nearly well as alternative #3. However, it is found that students following alternative #3 have to walk to class longest, and this causes them tired and to lose concentration in class

Referring to overall advantages, alternative #1 provides more efficiency than alternative #3. This decline numbers of students in queue with shortest walking distance to class.

CONCLUSION AND FURTHER WORK

The simulation modeling is one kind of problem solving, especially to a complicated problem affecting the elevator system in the academic building. This system is very complex and dynamic in every semester. Referring to the findings, the first alternative is an appropriate one, but it is not the best alternative due to passenger behaviors. However, the simulation modeling can be applied further.

REFERENCES

1. Bard S. Crawford, 1987. Building an elevator simulation in Ada using a process oriented methodology and support tool**,** Proceedings of the Joint Ada conference fifth national conference on Ada technology and fourth Washington Ada Symposium**,** pp: 223 – 230.
2. Henri Hakonen, 2003. Simulation of Building Traffic and Evacuation by Elevators, Licentiate Thesis, Helsinki University of Technology.
3. John M. Harris and Yasser Dessouky, 1997. A Simulation Approach for Analyzing Parking Space Availability at a Major University, Proceeding of the 1997 Winter Simulation Conference, pp: 1195 – 1198.
4. Yaniv Lisha and Boris Frenkel, 2003. Simulation Approach to Optimization of Two Stored Building Elevator, Proceedings of Student Research Works, Issue 4, pp: 32 – 35.
5. Thomas Bartz–Beielstein, Mike Preuss, and Sandor Markon, 2004. Validation and Optimization of an Elevator Simulation Model with Modern Search Heuristics, University of Dortmund, pp: 1 – 18.
6. Simone Appelt, Rajan Batta, Li Lin, and Colin Drury, 2007. Simulation of Passenger Check-in at a Medium-sized US Airport**,** Proceeding of the 1997 Winter Simulation Conference, pp: 1252 – 1260.
7. David W. Kelton, Randall P. Sadowski and Deborah A. Sadowski, 2006. Simulation with Arena, 4 edition, McGraw-Hill Series in Industrial Engineering and Management.

APPENDIX

Table1: Numbers of students in the 3-hour periods

Time / Day	08:30-11:20	11:40-14:30	14:50-17:40	18:00-20:50
Monday	1275	1315	1565	530
Tuesday	1885	1840	1887	1130
Wednesday	2227	2270	1700	1021
Thursday	1785	1825	2017	542
Friday	2056	1810	1990	570
Saturday	670	80	80	0
Sunday	1365	1346	1000	0
TOTAL	11263	10486	10239	3793

Table 2: Numbers of students in the 2-hour periods

Time / Day	08:30-10:20	10:30-12:20	12:30-14:20	14:30-16:20	16:30-18:20	18:30-20:20
Monday	640	720	550	740	280	360
Tuesday	568	320	360	240	288	340
Wednesday	380	400	660	705	240	330
Thursday	312	440	320	600	120	320
Friday	280	40	220	90	320	240
Saturday	80	80	80	35	0	0
Sunday	180	444	740	420	0	0
TOTAL	2440	2444	2930	2830	1248	1590

Table 3: A probability to choose the right floor to stop (on Monday)

Time / Floor	8:30	10:30	11:40	12:30	14:30	14:50	16:30	18:00	18:30
2	0	0	0	0	0	0	0	0	0
3	0	0	0	0	0	0	0	0	0
4	0	0	0.126246	0	0	0.11831	0	0	0
5	0.083551	0	0.053156	0.072727	0	0.028169	0	0	0
6	0.250653	0	0.318937	0	0.243243	0.360563	0.857143	0.792453	0.5
7	0.365535	0.777778	0.212625	0.581818	0.756757	0.225352	0	0.150943	0.5
8	0	0	0	0	0	0	0	0	0
9	0.023499	0	0.069767	0	0	0.076056	0	0.056604	0
10	0.020888	0.222222	0	0.218182	0	0	0.142857	0	0
11	0.020888	0	0	0.127273	0	0.016901	0	0	0
12	0.083551	0	0.126246	0	0	0.033803	0	0	0
14	0	0	0.053156	0	0	0.078873	0	0	0
15	0.099217	0	0	0	0	0.061972	0	0	0
16	0.052219	0	0.039867	0	0	0	0	0	0

Table 4 The simulation results

Performance Measures	Results
Average waiting time	1.14 mins
Average number of students in queue	12.11 persons

Table 5: Elevators performance from three alternatives

Performance measures	Alternative#1	Alternative#2	Alternative#3
Average waiting time	0.88 min	0.94 min	0.85 min
Average number of students in queue	10.13 persons	10.32 persons	10.57 persons

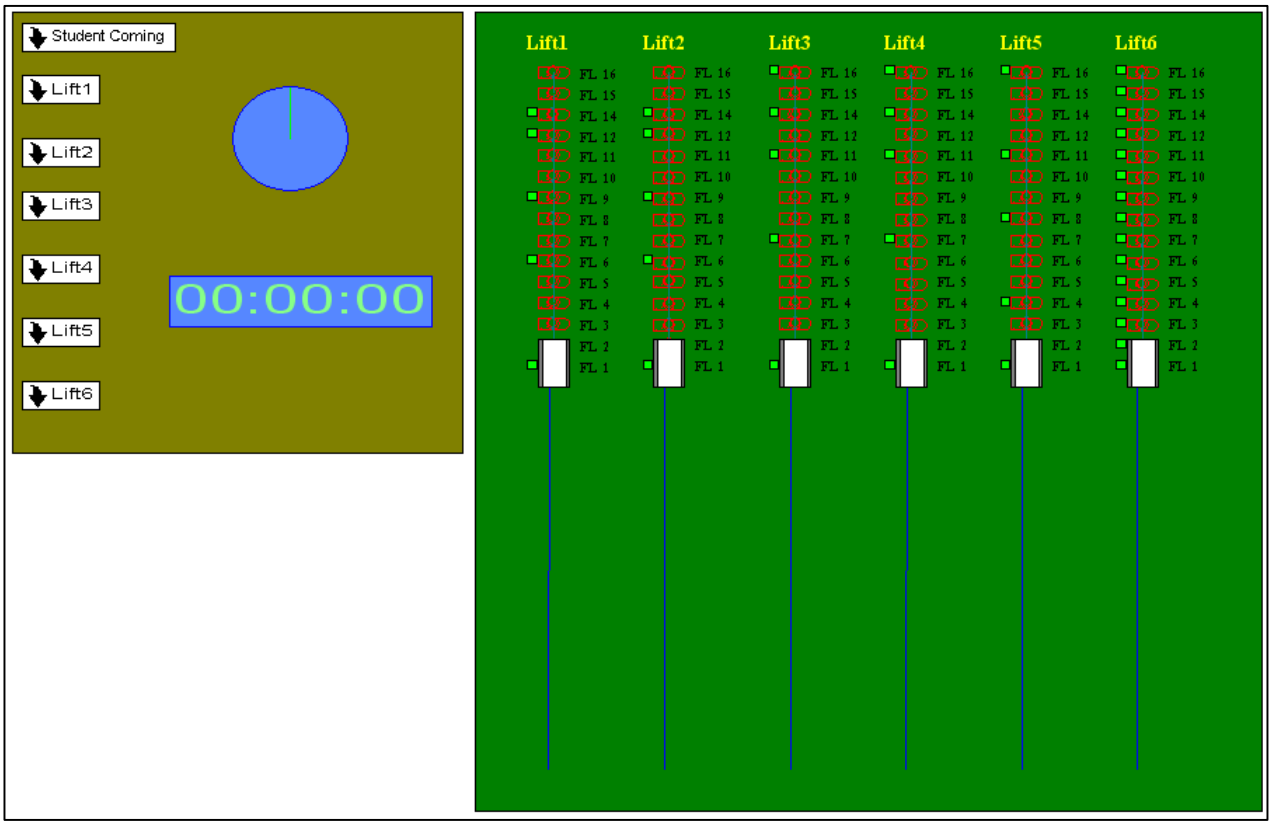

Figure 1: Overview of the simulation modeling

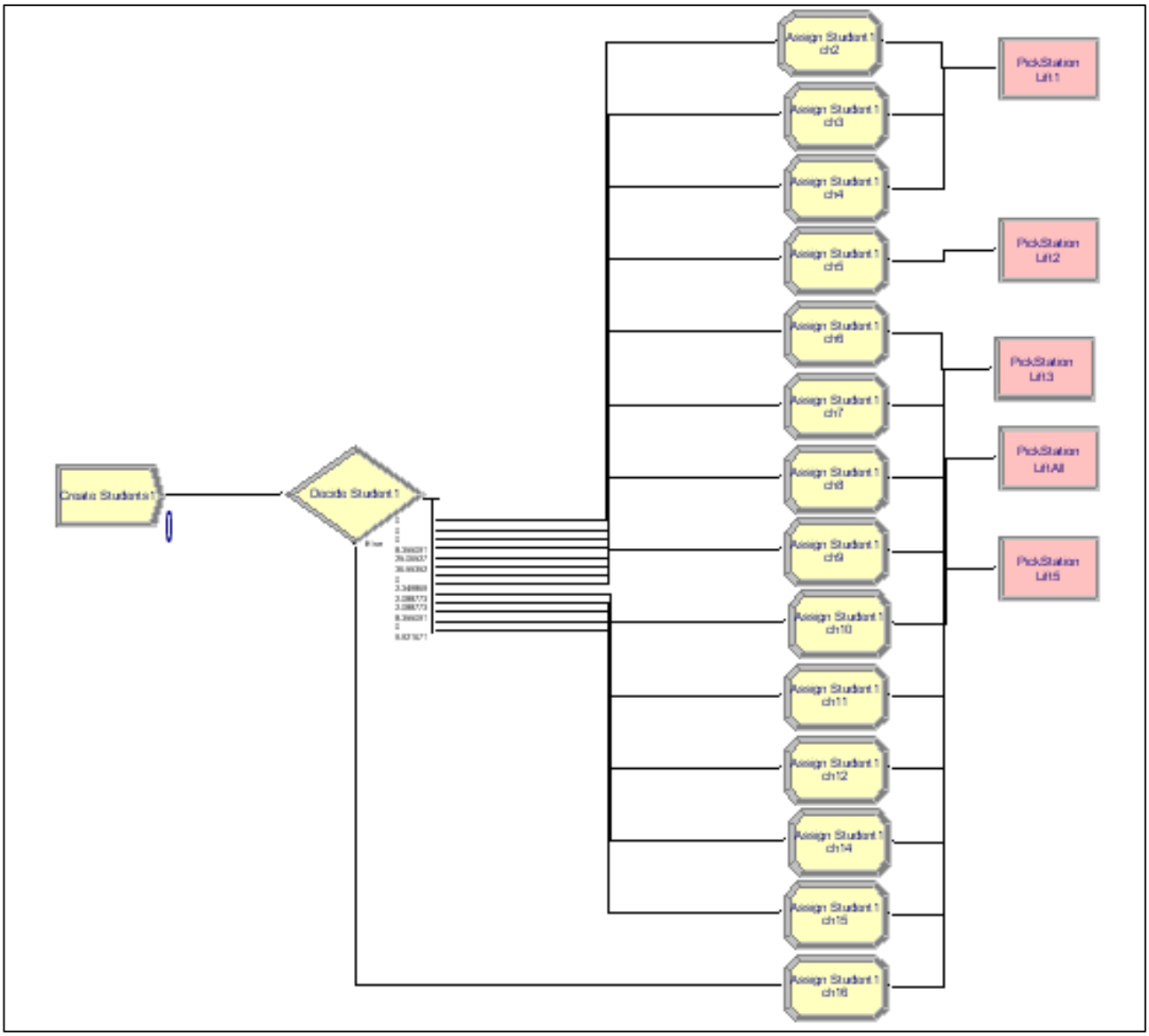

Figure 2 Rules of the system approach and students' destination floor

Simulation of an Inventory System allowing Joint Replenishment from Secondary Supplier upon Depleted Stock

Warunee Sarika, Yongwimon Lenbury*, Chontita Rattanakul
Dept of Mathematics, Faculty of Science, Mahidol University
Centre of Excellence in Mathematics, Postgraduate Education and Research Development Office
Bangkok, Thailand.

Abstract: This paper applies the simulation technique to compare the outcome of different replenishment and inventory strategies upon uncertain demand and lead time, at different levels of safety stocks and holding costs. The order quantity varies with different strategies so that the frequencies of replenishment in different strategies are approximately equal to that assigned by the main distributor. The strategy which keeps a relatively low safety stock but allows joint replenishment from an alternative supplier if the stock is depleted, is shown to be optimal in terms of the total expected inventory cost with the assumption that the profit reduction and average delivery cost are relatively small.

Keywords: Inventory system, uncertain demand, joint replenishment.

Introduction

A supply chain is a network of facilities that perform a series of activities: procuring raw material, transformation of raw material into products or services, stocking finished goods and distributing products to customers [1]. Inventory control plays an important role in supply chain management because it can increase profitability through improved inventory management, predict the impact of policies on inventory levels and minimize the total cost of logistics activities which meets the customer service requirements [2]. Moreover, the efficiency and efficacy of inventory planning can also decrease the total cost of logistics. Thus, the efficiency in inventory management is essential.

Inventory control is a common problem to all organizations such as hospitals, wholesalers, retailers, manufactures, warehouses and so on. Inventory is also relevant to the household unit in food, clothing, medicines, and so forth [3]. Due to uncertainties from many factors (e.g. customer's demand, lead times, economic situations and so on), it is essential to implement appropriate inventory control. Efficient operations in inventory management will prevent a stock out or shortage or an excess of raw materials. These events may lead to increased expenses for holding cost in case of excessive inventories, or to disturbance of normal operations in case of inventory shortage and also to reduction of the profit.

In this paper, simulation technique is applied to compare the outcome of 2 different inventory policies, based on real word practices upon uncertain demand and lead time. In the first strtegy, the safety stock is set at a fixed high level while the holding cost is relatively low, and joint replenishment from an alternative supplier is not allowed. In comparison, the other strategy, often found to be practiced by small retailer stores, allows the use of an alternative supplier when the uncertain demand depletes the stock before stock replenishment from the main supplier can be accomplished upon uncertain lead time. The total costs of the two policies are compared for different safety stock levels and holding costs.

Inventory Strategies for Practical Control

In practical situations, many factors cannot be controlled. Even if we know that certain conditions will lead us to the minimum operation cost, such conditions may not be attainable since in real business dealings we are restricted to operate under pre-assigned conditions which cannot be changed at will. For example, the frequency of replenishment may not be entirely up to the store's owner but the main supplier of the ordered item. In such a situation, the order amount is also not entirely under our control. For example, if it is required that we should re-order no often than once a month, then the amount of order could be perhaps the average demand or maximum demand times the lead time plus 30 days. A retailer operating under such restrictions may adopt one of the following strategies.

Strategy I:The store may keep the safety stock (ss_1) at the level

$$ss_1 = \text{maximum daily demand} \times \text{lead time}$$

Once the demand renders the inventory level (i) to fall

Corresponding Author: Yongwimon Lenbury, Dept of Mathematics, Faculty of Science, Mahidol University Centre of Excellence in Mathematics, Postgraduate Education and Research Development Office Bangkok, Thailand

below ss_1, then the item is ordered from the main supplier, so that the next order should be approximately *T* days ahead, at the amount *O*:

$$O = (ss_1 - i) + \text{ average daily demand} \times T$$

where the average demand is found from the actual number of tires sold during the past *T* days. If the daily demand depletes the stock then replenishment from an alternate supplier is not allowed, and the shortage cost c_s is incurred. The total inventory cost C_t is then the total sum of delivery cost, holding cost, shortage cost, and unsold product cost.

Strategy II: The store may choose not to keep a safety stock $(ss_2 = 0)$ and re-order every *T* days, whether the stock is depleted or not, at the amount

$$O = (T + \text{leadtime}) \times \text{ average daily demand}$$

As in Strategy I, if the stock is depleted before *T* days have past, replenishment from an alternative supplier is not allowed, sale opportunity is lost, and the shortage cost c_s in incurred. C_t is then the total sum of delivery cost, holding cost, shortage cost, and unsold product cost.

Strategy III: Again, stock replenishment is done from the main supplier every *T* days and no safety stock is kept $(ss_3 = 0)$. The order amount is

$$O = (T + \text{leadtime}) \times \text{ average daily demand}$$

However, if the stock is depleted when there is a demand then the item is acquired from a neighboring store (alternative supplier) at a higher cost. Therefore a profit reduction r_p is incurred. C_t in this case is then the total sum of delivery cost, holding cost, r_p, and unsold product cost.

Strategy IV: The safety stock is set at some appropriate level ss_4. Once the inventory falls below ss_4, then the item is ordered from the main supplier as

$$O = (ss_1 - i) + \text{ average daily demand} \times T$$

so that the stock should last approximately *T* days before a re-order is necessary. However, since the order amount *O* does not take into account the lead time, the stock may run out before replenishment from the main supplier is delivered. The item is then acquired from a neighboring store (alternate supplier) at the amount equal to the demand to satisfy the customer but a profit reduction r_p is incurred. C_t is then the total sum of delivery cost, holding cost, r_p, and unsold product cost.

Simulation Results and Discussion

We carried out Monte Carlo simulations on a case study of an automobile tire store. Real data on customer daily demand of a particular brand of tires have been obtained from the store's registry over the 6 months from January to June of the year 2008. From the number of automobile tires sold during these months, we found the average demand to be 3 tires per day. This is then the initial input value for the average daily demand to start the simulations. The average daily demand is then updated each time there is an order by using the demand up to the time of the order.

The computer code for this simulation program may be found on www.sc.mahidol.ac.th/scma/faculty/Lenbury_Y.html. The values used in the simulations are delivery cost $= 500$ baht for each delivery, $c_s = 127.6675$ baht per unit, $T = 30$ days, $r_p = 39.8$ baht per unit, unit cost $C_u = 1,850$ baht.

The daily demand is randomized based on the probability distribution computed from the real data of tires sold by the store during the above mentioned period. The lead time, on the other hand, was first set equal to 3 days. The simulation result is shown in Figures 1 and 2. Then, the lead time is taken to be uncertain, ranging 2-5 days and assumed to have a normal probability distribution. The simulation result upon uncertain demand and lead time is shown in Figures 3 and 4.

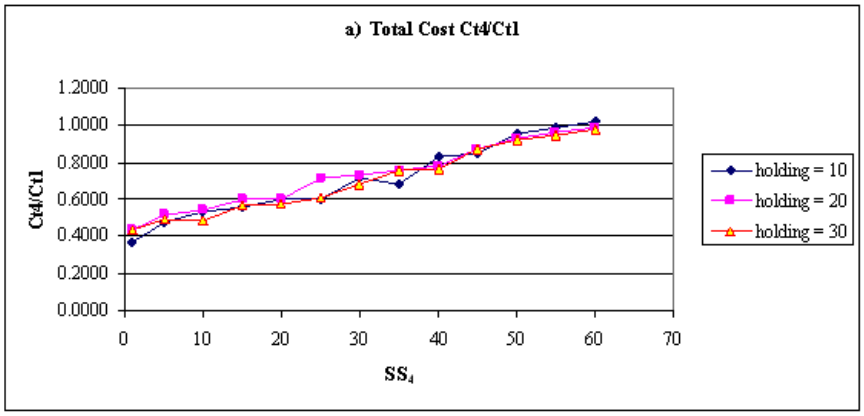

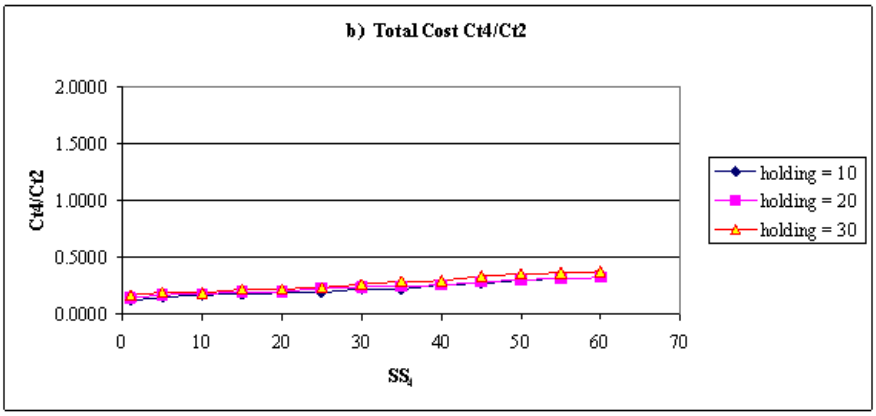

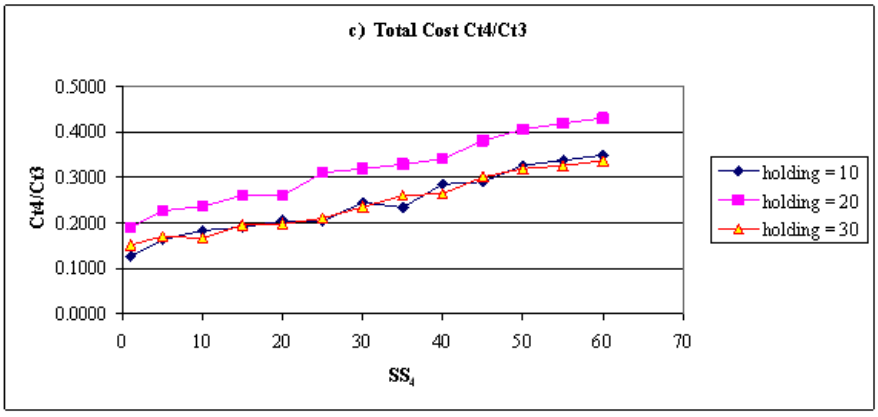

Figure 1: Total cost C_t of Strategy IV, Ct4, compared to those of Strategies I-III, Ct1-Ct3 respectively, for different holding costs per unit, and different ss_4, upon uncertain demand but constant lead time $= 3$ days.

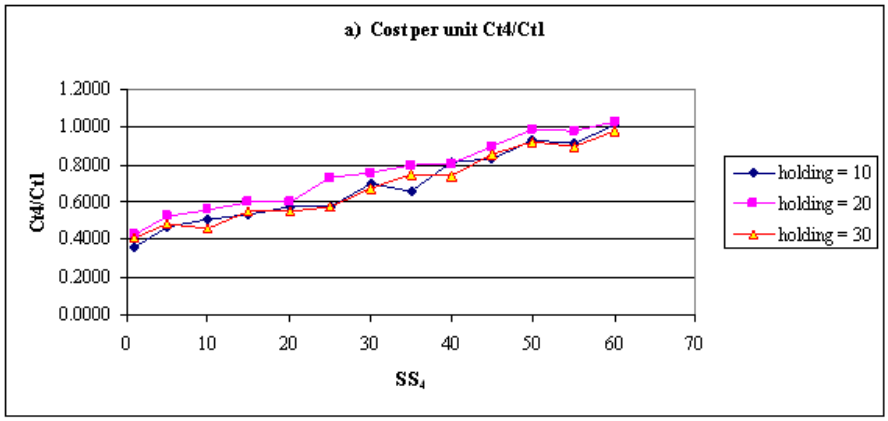

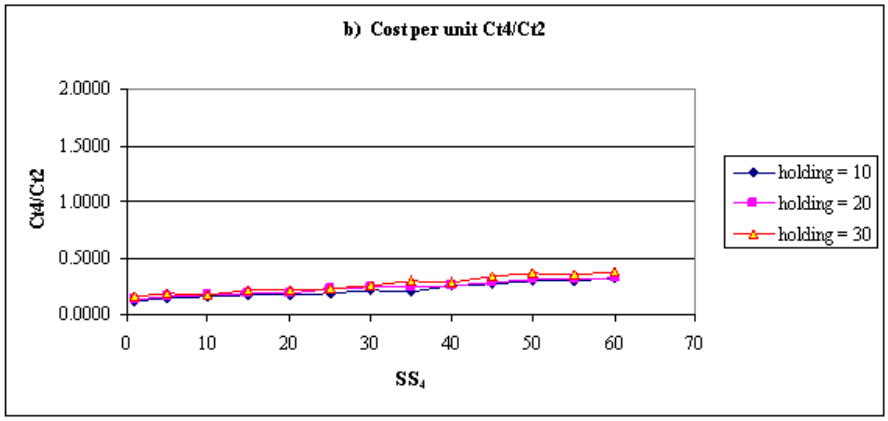

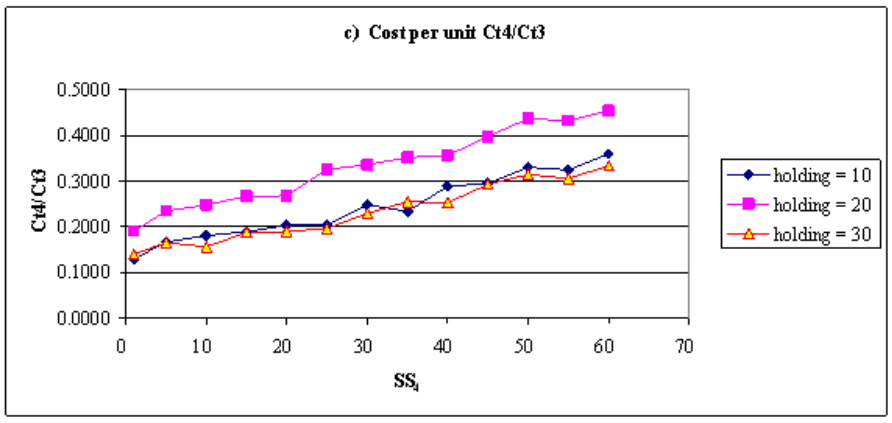

Figure 2: Cost per unit of Strategy IV, C4, compared to those of Strategies I-III, C1-C3, respectively, for different holding costs per unit, and different ss_4, upon uncertain demand but constant lead time $= 3$ days.

In all Figures, Strategy I uses safety stock $= 60$ units, while ss_4 in Strategy IV is varied from 1 to 60. Figures 1 and 2 show C_t against ss_4, while Figures 2 and 4 show the total cost per unit. On considering Figures 1 and 2, we see that Strategy IV proves to incur the least cost when compared to the other 3 strategies for all ss_4, whether the holding cost is 10, 20, or 30 baht per unit. However, Strategies I and III work better at a holding cost of 20 baht per unit, compared to Strategy IV, than at the holding cost of 10 or 30 baht per unit.

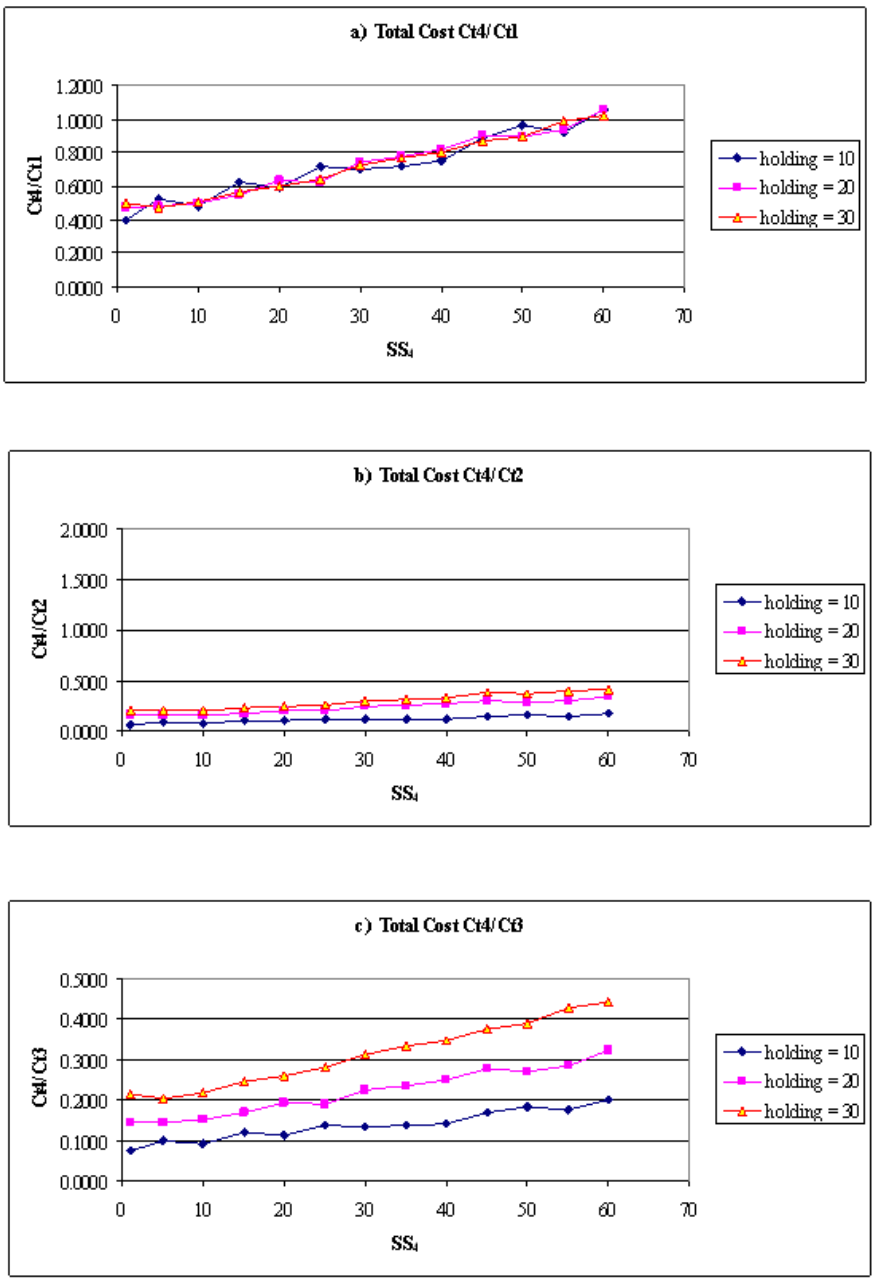

Figure 3: Total cost C_t of Strategy IV, Ct4, compared to those of Strategies I-III, Ct1-Ct3 respectively, for different holding costs per unit, and different ss_4, upon uncertain demand and uncertain lead time.

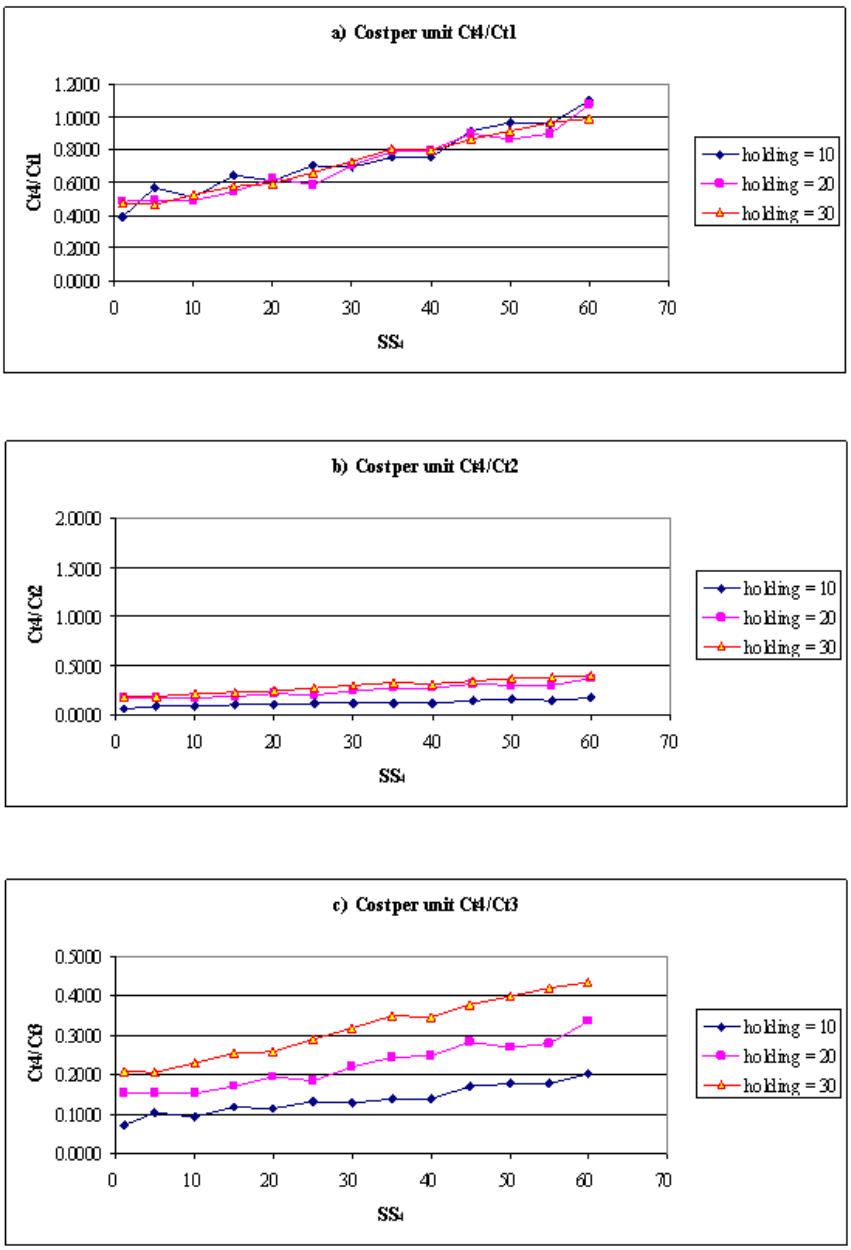

Figure 4: Cost per unit of Strategy IV, C4, compared to those of Strategies I-III, C1-C3 respectively, for different holding costs per unit, and different ss_4, upon uncertain demand and uncertain lead time.

If we consider Figures 3 and 4, however, where the simulations have been done with uncertain lead time as well as demand, we clearly see the advantage that Strategy IV has over Strategy III decreases monotonically as the holding cost per unit increases. The advantage that Strategy IV has over Strategy I (Figure 3 a) and 4 a)) does not appear to depend on the holding cost, at least in this range of relatively low holding costs under consideration. The advantage decreases as ss_4 increases to 60 since C4T/CT1 and C4/C1 both tend to 1 as $ss_4 \to 60$, which is to be expected since Strategy I keeps a constant safety stock of 60 units. However, Strategies II and III are worst off than Strategy I, in the range of unit holding cost under consideration.

Conclusion

It has been shown by a simulation technique that an inventory policy that allows joint replenishment from a main supplier and an alternative secondary supplier when inventory falls below a safety stock level, which could be quite low, can be the better choice for inventory control, provided that the profit reduction is low relative to the shortage cost. Further simulations may be carried out to investigate the effect of variations in the delivery cost, profit reduction, or shortage cost, in order to select the optimal policy which accommodated the conditions or constraints imposed by the market environment or business partners in practical situations.

Acknowledgements

This work is supported by the National Center for Genetic Engineering and Biotechnology and the Centre of Excellence in Mathematics, Postgraduate Education and Research Development Office, Commission on Higher Education, Thailand.

References

[1] Lee, H.L., Billington, C., 1993. Material Management in Decentralized Supply Chains. Operations Research, 41(5), 835-847.

[2] Douglas, M.L., James, R.S., Lisa, M.E., 1998. Fundamental of Logistics Management. Irwin/McGraw-Hill, 120.

[3] Tersine, R.J., 1988. Principle of Inventory and Materials Management 3rd edition. Elsevier Science Publishing Co., Inc. New York, U.S.A., 3.

[4] Harris, F.W., 1915. Operation and Cost. In Factory Management Series. A.W. Shaw Co. Chicago, U.S.A., 45-52.

[5] Wagner, H.M., Whitin, T.M., 1958. Dynamic Version of the Economic Lot Size Model. Management Science. 6, 89-96.

[6] Johnson, L.A., Montgomery, D.C., 1974. Operations Research in Production, Scheduling and Inventory Control. John Wiley, New York, U.S.A., 296.

[7] Song, J.S., Zipkin, P., 1993. Inventory Control in a Fluctuation Demand Environment. Operations Research. 41(2), 351-370.

[8] Lau, H.S., Zhoa, L.G., 1993. Optimal Ordering Policies with Two Suppliers when Lead Times and Demand are all Stochastic. European Journal of Operational Research. 68, 120-133.

[9] Song, J.S., 1994. The Effect of Lead Time Uncertainty in a Simple Stochastic Inventory Model. Management Science. 40(5), 603-613.

[10] Winston, W.L., 1994. Operation Research: Application and Algorithms. 3rd edition. Duxbury Press. Belmont. California, U.S.A., 1318.

[11] Brill, P.H., Chaouch, B.A., 1995. An EOQ Model with Random Variations in Demand. Management Science. 41(3), 927-936.

[12] Axsater, S., 1996. Using the Deterministic EOQ Formula in Stochastic Inventory Control. Management Science. 42(6), 830-834.

[13] Dutta, R.K., 1997. Stochastic Inventory Modeling and Simulation for Materials Requirement Planning: A Case Study. IE Journal. 26(5), 6-10.

[14] Sobel, M.L., Zhang, R.Q. 2001. Inventory Policies for System with Stochastic and Deterministic Demand. Operations Research. 49(1), 157-162.

[15] Shu, F.T., 1971. Economic Ordering Frequency for Two Items Jointly Replenished. Management Science. 17(6), B406-B410.

[16] Nocturne, D.C., 1973. Economic Ordering Frequency for Several Items Jointly Replenished. Management Science. 19(9), 1093-1096.

[17] Goyal, S.K., 1973. Determination of Economic Frequency for Items Jointly Replenished. Management Science. 20(3), 232-235.

[18] Silver, E.A., 1976. A Simple Method of Determining Order Quantities in Joint Replenishment under Deterministic Demand. Management Science. 22(12),1351-1361.

[19] Goyal, S.K., Stair, A.T., 1989. Joint Replenishment Inventory Control: Deterministic and Stochastic Model. European Journal of Operation Research. 38, 2-13.

[20] Chansri, N., 2001. The Design of Inventory Model under Uncertain Demand. M.S. Thesis. Kasetsart University, Bangkok, Thailand.

[21] Fogarty, D.W., Blackstone, J.H., Hoffman, T.R., 1991. Production and Inventory Management. 2nd Edition. South-West Publishing Co. Cincinnati, Ohio, U.S.A., 870.

Modeling a sequencing problem for the mixed-model assembly line

[1]Shusaku Hiraki, [1]Hugejile and [2]Zhuqi XU
[1]Faculty of Economic Sciences, Hiroshima Shudo University, 1-1-1,
Ozukahigashi, Asaminami-ku, Hiroshima 731-3195 Japan.
[2]Faculty of Law and Letters, Ehime University, Ohkubo, 3-Ban,
Bunkyou-cho, Matsuyama, Ehime 790-8577 Japan.

Abstract: This paper deals with the problem of sequencing products for a mixed-model assembly line in just-in-time production systems. From the standpoint of the supply chain management, we propose a new sequencing method that considers not only (1) keeping a constant rate of production of every part in preceding processes and (2) minimizing the maximal work congestion in the assembly line, but also (3) keeping the due date of delivery time to the dealers when the final products are delivered by the car carrier vehicles. In order to simultaneously satisfy these three goals, we introduce a two-stage approach. At first, by dividing the production period into some shorter periods, we determine the production volume of each product for each divided period in order to keep a constant rate of parts usage and the due date of delivery time. Next, we determine the production schedule of each divided period that realizes the smoothed production in the assembly line. Finally, we will show a numerical example to explain and clarify the effectiveness of the sequencing procedure proposed.

Key words: Mixed-model assembly line, Sequencing problem, Smoothed production, Delivery time

INTRODUCTION

When we determine the sequence of the mixed-model assembly line, we usually considere the following two goals: (1) Leveling the load (total assembly time) on each process within the line. (2) Keeping a constant speed in consuming each part on the line. Concerning goal one, we determine the sequence that minimizes the maximum work congestion[1,2,3]. Concerning goal two, we determine the sequence that the quantity used per hour (i.e. consumption speed) for each part in the mixed-model assembly line must be kept as constant as possible[4,5,6]. Also, some papers consider these two goals simultaneously[7,8,9]. In this paper, from the standpoint of the supply chain management, we propose a new sequencing method that considers not only the traditional two goals mentioned above, but also the third goal, i.e., shortening the delivery time to the dealer when the final products are delivered by the car carrier vehicles. In order to simultaneously satisfy these three goals, we introduce a two-stage approach. At first, by dividing the production period into some shorter one, we determine the production volume of each product for each divided period in order to keep a constant rate of parts usage and the due date of delivery time in stage-one. Next, we determine the production schedule of each dividedperiod that realizes the smoothed production in the assembly line in stage-two. We also show a numerical example to explain and clarify the effectiveness of the sequencing procedure proposed.

ASSMPTIONS AND NOTATION

Assumptions

In this paper, we assume the following conditions.

(1) The conveyer speed is constant, that is, the cycle time of the conveyer line is fixed.
(2) Line balancing of the conveyer line is being performed appropriately.
(3) Parts withdrawals are performed at fixed interval.
(4) Final products are delivered to the dealers by the car carrier vehicles.
(5) The due date of delivery time to the dealer is pre-determined, that is, the starting time of each car carrier vehicle is given.

Notation

Let us define notation as follows;

m : the number of product types. $I = \{1, \Lambda\ , m\}$

n : the number of part types. $J = \{1, \Lambda\ , n\}$

d_i : total production quantity of product i.

a_{ij} : necessary quantity of part j to be utilized for producing product i.

n_j : total necessary quantity of part j to be consumed for producing all products.

Corresponding Author: Shusaku Hiraki, Faculty of Economic Sciences, Hiroshima Shudo University, 1-1-1, Otsukahigashi, Asaminami-ku, Hiroshima 731-3195 Japan

$n_j = \sum_{i \in I} a_{ij} * d_i \quad (j \in J)$

p : total production quantity of all products.

$p = \sum_{i \in I} d_i$

$K = \{1, \Lambda\ , p\}$

k : position of a unit in the sequence.

r_j : average necessary quantity of part j per unit product.

$r_j = n_j / p$ (j ∈ J)

Z_{jk} : it takes one when j is withdrawal in position k , otherwise it takes zero.

Q : the set of k that one or more types of part are withdrawn in position k .

$Q = \{k \mid Z_{jk} = 1$ (j ∈ J; k ∈ K)}

$q = |Q|$

We divide the production period into k shorter period.

Q' : ordered set of Q .

X_{ik} : cumulative production volume of product i sequenced from position one to $k \in Q$.

Y_{jk} : total volume of part j required to assemble the products sequenced from position one to $k \in Q$.

M_k : the set of part j withdrawn in position k .

$M_k = \{ j \mid Z_{jk} = 1$ (j ∈ J)} $(k \in Q)$

V_k : the set of car carrier vehicles that has to start when the products sequenced from position one to k are loaded.

v_{hik} : the number of product i to be carried by the vehicle $h \in V_k$.

s_{ik} : the number of product i to be sequenced before the product positioned k is possible to carry.

$s_{ik} = \sum_{h \in V_k} v_{hik} \quad (i \in I; k \in Q)$

FORMULATION

We propose a sequencing method so called two-stage approach.

Stage-one

In stage-one, we will attempt to determine the production volume of each product in each divided period in order to keep both a constant rate of parts usage and the due date of delivery time to the dealers by solving a mathematical programming problem. We have following constraints.

$$X_{ik} \le X_{ik'} \quad (i \in I; k, k' \in Q', k \ne q) \qquad (1)$$

Where, k' is the next element of k in the ordered set Q'.

$$X_{ip} = d_i \quad (i \in I) \qquad (2)$$

$$\sum_{i \in I} X_{ik} = k \quad (k \in Q) \qquad (3)$$

$$Y_{jk} = \sum_{i=1,\Lambda\ ,I} a_{ij} * X_{ik} \quad (j \in M_k; k \in Q) \qquad (4)$$

$$X_{ik} \ge (1 - \alpha_k) * s_{ik} \quad (i \in I; k \in Q) \qquad (5)$$

Where, α_k is a parameter that satisfies $1 \ge \alpha_k \ge 0$.

X_{ik}, Y_{jk} (i ∈ I; j ∈ J; k ∈ Q) non-negative integer (6)

Constraint (1) ensures that it is not possible that the cumulative production volume of product i in the withdrawal position k is less than the one just after position k'. Constraint (2) ensures that the cumulative production volume of product i in the last position is equal to the total production quantity of product i to be assembled. Constraint (3) ensures that exactly k products are scheduled from position one to k . Constraint (4) calculates the total volume of part j required to assemble the products sequenced from position one to k utilizing the bill of materials. Constraint (5) ensures that the car carrier vehicles keep the predetermined starting time.

Under these constraints, we consider to minimize the objective function (7) which implies the sum of the absolute value of the difference between the average nessesary quantity and the withdrawal quantity of all parts in each withdrawal position.

$$f_1 = \sum_{k \in Q} \sum_{j \in V_k} \left| k * r_j - Y_{jk} \right| \qquad (7)$$

As the function (7) is non-linear, let us introduce the following two variables in order to transform the objective function (7) into the linear function.

$$b_{jk}^{+} = (1/2) * \{ \left| k * r_j - Y_{jk} \right| + (k * r_j - Y_{jk}) \}$$

$$b_{jk}^{-} = (1/2) * \{ \left| k * r_j - Y_{jk} \right| - (k * r_j - Y_{jk}) \}$$

Then, we can transform (7) into the following linear function (8) under the additional constraint (9).

$$f_1^{'} = \sum_{k \in Q} \sum_{j \in V_k} (b_{jk}^{+} - b_{jk}^{-}) \quad (8)$$

$$Y_{jk} + b_{jk}^{+} - b_{jk}^{-} = k * r_j \quad (9)$$

We call the mathematical programming problem that minimizes the objective function (8) under the constraints (1)-(6) and (9) stage-one.

Stage-two

After solving stage-one, we determine the production schedule that realizes the smoothed production in the assembly line for each divided period in stage-two. There are many studies with respect to this subject. In this paper, we utilize the cycle launching system by reciprocal ratio[10] because of its simplicity.

NUMERICAL EXAMPLE

Let us introduce a numerical example. We utilize the Mathematical Program Software Xpress-MP for the calculation in stage-one.

Input Data

(1) The number of product types: *m=4*.
(2) The number of part types: *n=6*.
(3) Production quantity of products: d_i

$d_1 = 30$, $d_2 = 40$, $d_3 = 30$, $d_4 = 20$,

(4) Necessary quantity of parts (Bill of materials): a_{ij}

Table 1: Bill of materials

i / j	(30) 1	(40) 2	(30) 3	(20) 4	n_j
1	1	0	1	3	120
2	0	1	1	1	90
3	1	2	1	0	140
4	1	3	2	1	230
5	2	1	0	1	120
6	2	1	1	3	190

(5) Total necessary quantity of parts: n_j

We show the total necessary quantity of part j in right hand column of Table 1.

(6) Total production quantity of all products: $p = 120$

(7) Average necessary quantity of parts: r_j

$r_1 = 1$, $r_2 = 0.75$, $r_3 = 7/6$, $r_4 = 23/12$,
$r_5 = 1$, $r_6 = 19/12$

(8) The set of position that one or more types of part are withdrawn: $Q = \{40,60,80,120\}$

(9) The set of parts withdrawn in position $k \in Q$:

$M_{40} = \{1,2\}$, $M_{60} = \{3,4,5\}$, $M_{80} = \{1,2\}$,
$M_{120} = \{1,2,3,4,5,6\}$

(10) The set of car carrier vehicles that has to start before the products sequenced from position one to $k \in Q$ are loaded: V_k

$V_{40} = \{1,2,3,4,5,6,7,8\}$,
$V_{60} = \{1,2,3,4,5,6,7,8,9,10,11,12\}$,
$V_{80} = \{1,2,3,4,5,6,7,8,9,10,11,12,13,14,15,16\}$,
$V_{120} = \{1,2,3,4,5,6,7,8,9,10,11,12,13,14,15,16,$
$17,18,19,20,21,22,23,24\}$

(11) The number of products to be carried by the car carrier vehicles: v_{hik}

Table 2: The number of products to be carried

position						
Vehicle no. / Product type	1	2	3	4	5	6
1	1	2	3	0	0	2
2	1	0	1	1	1	2
3	2	0	1	2	1	0
4	1	3	0	2	3	1

(continue)

position		40				60
Vehicle no. / Product type	7	8	9	10	11	12
1	1	3	1	2	3	0
2	1	0	1	0	1	2
3	1	1	2	2	1	3
4	2	1	1	1	0	0

(continue)

position				80		
Vehicle no. / Product type	13	14	15	16	17	18
1	0	2	1	3	1	1
2	3	2	2	0	2	2
3	1	0	2	1	2	2
4	1	1	0	1	0	0

(continue)

position						120
Vehicle no. / Product type	19	20	21	22	23	24
1	1	0	0	1	1	1

2	3	3	2	4	3	3
3	1	2	1	0	1	1
4	0	0	2	0	0	0

(12) The number of product i to be sequenced before the product positioned k is possible to carry: s_{ik}

Table 3: The number of products to be sequenced

k Q / i	40	60	80	120
1	12	18	24	30
2	7	11	18	40
3	8	16	20	30
4	13	15	18	20

Output results

Solving stage-one, we have following results. When we set α_k =0.5 and 0.1, cumulative production volume of product i sequenced from position one to k is determined as shown in Table 4.

Table4: Cumulative production volume of products

(α_k =0.5)

k Q / i	40	60	80	120
1	10	5	5	10
2	16	4	0	20
3	6	9	15	0
4	8	2	0	10

(α_k =0.1)

k Q / i	40	60	80	120
1	11	6	5	8
2	9	5	9	17
3	8	7	3	12
4	12	2	3	3

Solving stage-two, we have following production schedule for each divided period. For the convenience of understanding, we denote the products i $(i = 1,2,3,4)$ as A, B, C, D, respectively.

(1) α_k =0.5

a) 1-st divided period: (40 units)
BABDCBABDABCBDABABCDBABDCBABD
ABCBDABABCD
b) 2-nd divided period: (20 units)
CACDCACBDCACBCACABCD
c) 3-rd divided period: (20 units)
CCACCCACCCACCCACCCAC
d) 4-th divided period: (40 units)
BABDBABDBABDBABDBABDBABDBABDB
ABDBABDBABD

(2) α_k =0.1

a) 1-st divided period: (40 units)
DABCDABCDABDCADBACDABDCABCDAB
DADCBADABCD
b) 2-nd divided period: (20 units)
CABCABCADCBACBACABCD
c) 3-rd divided period: (20 units)
BABABCDBBABCDBABABCD
d) 4-th divided period: (40 units)
BCBACBBACBCDBABCBACBCABBCDBACB
BCABCBABCD

CONCLUSION

In this paper, we proposed a new sequencing method that considers not only (1) keeping a constant rate of production of every part in preceding processes and (2) minimizing the maximal work congestion in the assembly line, but also (3) keeping the due date of delivery time to the dealers when the final products are delivered by the car carrier vehicles and showed a numerical example to explain the effectiveness of the sequencing procedure proposed.

Acknowledgments

This research was partly supported by the Grant-in-Aid for Scientific Research of the Japanese Ministry of Education, Science and Culture under the Contract No. (C) 18510141 (2008).

REFERENCES

1. Thomopoulos,N.T., 1967. Line Balancing-Sequencing for Mixed-Model Assembly, Manage. Sci., Vol.14, No.2, pp.59-75.
2. Mitsumori,S., 1969. Optimal Schedule Control of Conveyer Line, IEEE Translations, Vol.AC-14, No.6, pp.633-639.
3. Tsai, L. H., 1995. Mixed-model sequencing to minimize work and the risk of conveyor stoppage, Manage. Sci., Vol.41, No.3, pp.485-495.
4. Miltenburg, J., 1989. Level Schedules for Mixed-model Assembly Lines in just-in-time production systems, Manage. Sci., Vol.35, No.2, pp.192-207.
5. Cakir,A.R. and Inman,R.R. 1993. Modified goal chasing for products with non-zero/one bills of material, Int. J. Prod. Res., Vol.31, No.1, pp.107-115.
6. Monden, Y., 1998. Toyota Production System (3rd Ed.) Chapman & Hall.
7. Miltenburg, J. and Goldstein, T., 1991. Developing production schedules which balance part usage and smooth production loads for just-in-time production systems, Nav. Res. Log., Vol.38, No.6, pp..893-910.
8. Bard, J. F., Shtub, A. and Joshi, S. B., 1994. Sequencing mixed-model assembly lines to level parts usage and minimize line length, Int. J. Prod. Res., Vol.32, No.10, pp.2431-2454.
9. Zeramdini, W., Aigbedo, H. and Monden, Y., 2000. Bicriteria sequencing for just-in-time mixed-model

assembly lines, Int. J. Prod. Res., Vol.38, No.15, pp.3451-3470.

10. Muramatsu, R., 1977. Production Planning and Control (Revised Ed.) (in Japanese) Asakura-Shoten.

A Study on design of buffer for automobile assembly lines

[1]Zhuqi Xu, [2]Shusaku Hiraki, [3]Yoshiaki Ishihara, [4]Yuanming Su
[1] Ehime University, [2] Hiroshima Shudo University,
[3]Oshima National College of Maritime Technology, [4]Hiroshima University
[1] Faculty of Law and Letters, Ehime University
Bunkyou-cho, Matsuyama City, Ehime 790-8577 Japan

Abstract: This paper deals with the problem of design of buffer for thoes automobile assembly lines like self-completion assembly lines. We formulate the sequencing problem of determining the sequences for the lines, and we develop an approximate method to desing buffer in order to shortening of the total length of the lines. Finally, we numerically analyze the effects that working delay and line stop could be absorbed by the introduction of the auxiliary workers and the buffer product between the lines.

Key words: Self-completion Lines, JIT, Scheduling and sequencing, Buffer

1.INTRODUCTION

As strick competition situations and Green Economic have been kept going, the economic environment has made automobile industry to reform their production systems not only in Japan but also in the world. Some points have been shown as the characteristics concerned with the design, management of the car production system.

(1) It proceeds that the automobile industry becomes global, and international competitions are violent all the more. An enterprise must provide the product of the high quality for the market rapidly by the low price.
(2) It becomes shortening on the life cycle of the goods, and they become multiple kinds all the more on the product. The development of the new goods connected with the decrease of the environment load proceeds, and shortening of the development, production preparation period of the new goods is being requested.
(3) It is asked to improve productivity by excluding the useless element as much as possible and reducing the production cost.
(4) Shortening of the time limit of delivery of the product which a consumer ordered is being asked. The flexibility of the production system is looked for to provide the product of the multiple kinds in the market needs rapidly.
(5)Each car manufacturer must change a usual system with an increase in the production ability and altitude to the flexible production system which can be adapted to the above-mentioned change in the economic environment, in order to secure high quality and a high profit by the low cost.

2. SELF-COMPLETION LINES

The production system must be considered synthetically to design a production method which is adapted to the production system. The production method of each production factory may have each characteristic. As for the Japanese automobile industry, the final assembly plant of the car does assembling by using the mixed-model line which would mix some kinds of the different cars on one line. The various parts are assembled into the painted body and one car is assembled from these parts which usually reach 2000-3000 items.

Ohta[1] points out the next four points as a concept of the design of the future new mixed line to cope with a change in an economic environment to surround the automobile industry.

(1) To raise a worker's incentive to work harder.
(2) To design a gentle assembly line to the worker in the decrease and rationalization of working
(3) To take into the consideration of automation connected with will that equipment coexists with the worker
(4) To build a working environment in the form corresponding to the improvement in the social abundance

The self-completion assembly lines have been introduced as an improvement of the usual mixed-model assembly line and an expansion in such conditions since the beginning in the 1990's at some final assembly plant. The self-completion line is a form that the usual line which all working processes are connected with on one conveyer line is divided into some shorter lines by function of the car and which

Corresponding Author: Zhuqi Xu, Faculty of Law and Letters, Ehime University, Bunkyou-cho, Matsuyama City, Ehime 790-8577 Japan Email: joxu@LL.ehime-u.ac.jp

several kinds of products are mixed with and to produce continuously(Fig.1)

3. MATHEMATICAL MODEL

The cycle time of the line production including the self-completion lines could be calculated that the amount of production is divided by the plan period. But, in fact when it is managed, the fine tuning of the cycle time is recognized in the reality for the self-completion lines.

A self-completion lines system is composed by some shorter lines, and several kinds of products are mixed, and it does assembling work. Each shorter line is formed by the plural working processes connected by conveyor and so on.

Each working process is settled physically and the line stop will occur when the worker in the line fails to complete operations within his work zone. The work load of each product in each working process is different in every kind. When products with a heavy work load would have been assembled continuity, a worker's position may be in rear of his work zone. A line stop occurs when assembling work can't be finished even if a product reaches the last tail of the work zone. In fact, the amount of production of each product changes every day. The total production time required grows longer when line stops are easy to cause, if the amounts of production with an especially heavy work load increase.

It is necessary to make working delay as small as possible to restrain the occurrence of the line stop, and the following factors are taken into consideration for that.

(1)A work load in each working process is changed by the sequence of products. The appropriate sequence is necessary to level work load in order to make working delay as small as possible. In this paper, we use a goal-adjustment method to decide the sequence of products.

(2) If the assembly line has a longer cycle time, it is no wonder that working delay and line stop would decrease. But it is connected with the increase in the total production time required. Therefore, the decision of the appropriate cycle time is necessary.

(3) Using an auxiliary worker assisting in the operation different from the utility worker, it is possibly to shorten the time of line stops.

(4) The buffer products between the self-completion lines are installed to prevent the influence of the line stop, and the buffer products increase, and the total production time required gets longer. Therefore, the proper arrangement of the buffer products is necessary.

In this paper, a mathematical model to attempt shortening of the length of self-completion lines is considered and a numerical experiment showing the way of designing the cycle time has been given. The setup of the buffer products between the lines is shown in the Figure 2.

A precondition is as the following.

(1) The cycle time of the whole line is the same.
(2) An auxiliary worker could move to the working process when a line stop occurred at once, and the auxiliary worker does assembling work with the worker of that working process. But, there is one and only one auxiliary worker in each line. An auxiliary worker will be arranged preferentially in the working process whose necessary time of the line stop is longest when a line stop occurred in more than one working process at the same time. A worker can't enter the work zone of other working processes.
(3) The length of the work zone of all the working processes is the same.
(4) The movement time of workers in working processes are so short that it can be ignored.

The example of the worker's movement path in the line is shown in the Figure 3.

Notation:

i :The number of the product

d_i :The amount of production of the product i

K :The amount of total production

S : The amount of total work processes

s :The number of the working process $(s = 1,2,...S)$

c : The cycle time

t_{is} : The assembly time of product i at working process s

k :The order of production

l_1 : The length between two products in the line

$l^s{}_2$: The length of buffer area at working process s

v : The speed of the line $v = \dfrac{l_1}{c}$

j_{ks} :The product in the order k at working process s

Y_{ks} : The assembly time of the product in order k at working process s

L^s :The length of working process s $L^s = l_1 + l^s{}_2$

t :The time unit

n_{ts} : The product of working process s at the time t

$Un_{ts}s$: The accumulative assembly time of the applicable product of working process s at the time t

m_{ts} : The location of the worker of working process s at the time t

P_t : The 0-1 variable which shows line stop condition.
VTP :Total allowable working time

Formulation:

We formulate a mathematical model of designing buffer area which attempts shorting the length of the line.
Objective function:

$$\min . \sum_{s=1}^{S} l^s{}_2 \quad (1)$$

S.t.

$$n_{ts} = n_{t-1s} + 1 \quad (Un_{t-1s}s \geq Yn_{t-1s}s, m_{ts} \geq L^s) \quad (2\text{-}1)$$

$$n_{ts} = n_{t-1s} \quad (Un_{t-1s}s \; \pi \; Yn_{t-1s}s \; or \; m_{ts} \; \pi \; L^s) \quad (2\text{-}2)$$

$$m_{ts} = m_{t-1s} + v \quad (Un_{t-1s}s \; \pi \; Yn_{t-1s}s, P_t = 0) \quad (3\text{-}1)$$

$$m_{ts} = m_{t-1s} \quad (Un_{t-1s}s \; \pi \; Yn_{t-1s}s, P_t = 1) \quad (3\text{-}2)$$

$$m_{ts} = m_{t-1s} - l_1 \quad (Un_{t-1s}s \geq Yn_{t-1s}s, m_{t-1s} \geq L^s) \quad (3\text{-}3)$$

$$m_{ts} = m_{t-1s} \; (Un_{t-1s}s \geq Yn_{t-1s}s, P_t = 1, m_{t-1s} \; \pi \; L^s) \quad (3\text{-}4)$$

$$m_{ts} = m_{t-1s} + v \quad (Un_{t-1s}s \geq Yn_{t-1s}s, P_t = 0, m_{t-1s} \; \pi \; L^s) \quad (3\text{-}5)$$

$$Un_{ts}s = Un_{t-1s}s + 1 \quad (n_{ts} = n_{t-1s}, n_{ts} \neq e_t) \quad (4\text{-}1)$$

$$Un_{ts}s = 1 \quad (n_{ts} = n_{t-1s}, n_{ts} \neq e_t) \quad (4\text{-}2)$$

$$Un_{ts}s = Un_{t-1s}s + 2 \quad (n_{ts} = e_t) \quad (4\text{-}3)$$

$$Et = \{s \mid m_{t-1s} > l_1 + l_2\} \quad (5\text{-}1)$$

$$e_t = s^*, (Y_{t-1s^*} - U_{t-1s^*} \geq Y_{t-1s} - U_{t-1s}, \; s, s^* \in Et, s \neq s^*) \quad (5\text{-}2)$$

$$P_t = 1 \quad (E_{t-1} \neq \Phi) \quad (6\text{-}1)$$

$$P_t = 0 \quad (Et = \Phi) \quad (6\text{-}2)$$

$$TP = \sum_{t=1}^{T} P_t \quad (7\text{-}1)$$

$$VTP \geq c * K + TP \quad (7\text{-}2)$$

4. NUMERICAL EXPERIMENT

A numerical value experiment is done on the following initial condition.
The amount of production of the products: Table 1
The amount of working processes: 9
The assembly time of the products at each working process: Table 2

Tab.1 The amount of production

amount	450	Mixed rate
product1	50	1
product2	100	2
product3	50	1
product4	150	3
product5	100	2

The sequence of products: Table 3
The beginning position of each worker: Table 4
The result of the numerical experiment is shown in the table 5.

5.SIMULATION RESULTS

We can get the optimum solution of desiging buffer for the lines shown before under the condition that the amout of products follew the Table.1. And certainly, the difference of mixed-rates make the different buffers for the lines. We range the mixed rates of pruduct1,2…,5 from 1 to 5 by uniform random number. The results show that Table 5 can satisfy the about 90% cases.

6. CONCLUSION

In this paper, a mathematical model to attempt shortening of the total length of the self-completion lines had been considered and a numerical experiment showing the way of designing the length of buffer area had been given. Moreover, we had confirmed that working delay and line stop could be absorbed by the introduction of the auxiliary workers and the buffer product between the lines.

REFERENCES

[1] I.Ohta: “A new production system of assembly lines, Journal of the Society of Plant Engineers Japan,Vol.7， No.3， pp.198-205(1995) (in Japanese)
[2] A.Niimi:” The establishment of the completion process at the car assembly line”, *TOYOTA Technical Review*， Vol.44， No.2， pp.86-91(1994) (in Japanese)
[3] Yasuhiro, MONDEN: ”Toyota Production System, Industrial Engineering & Management Press (1991)(in Japanese)

[4] Yano,C.A. & Rachamadugu,R.: "Sequencing to Minimize Work Overload in Assembly Lines with Product Options", *International Journal of Production Research*, Vol.46,No.3(1991)

[5] Zhuqi XU, Shusaku HIRAKI, Yoshiaki ISHIHARA, Yuanming SU, "A Study on Designing Buffer Area for Self-Completion Lines",the 8th ICIM,(2006)

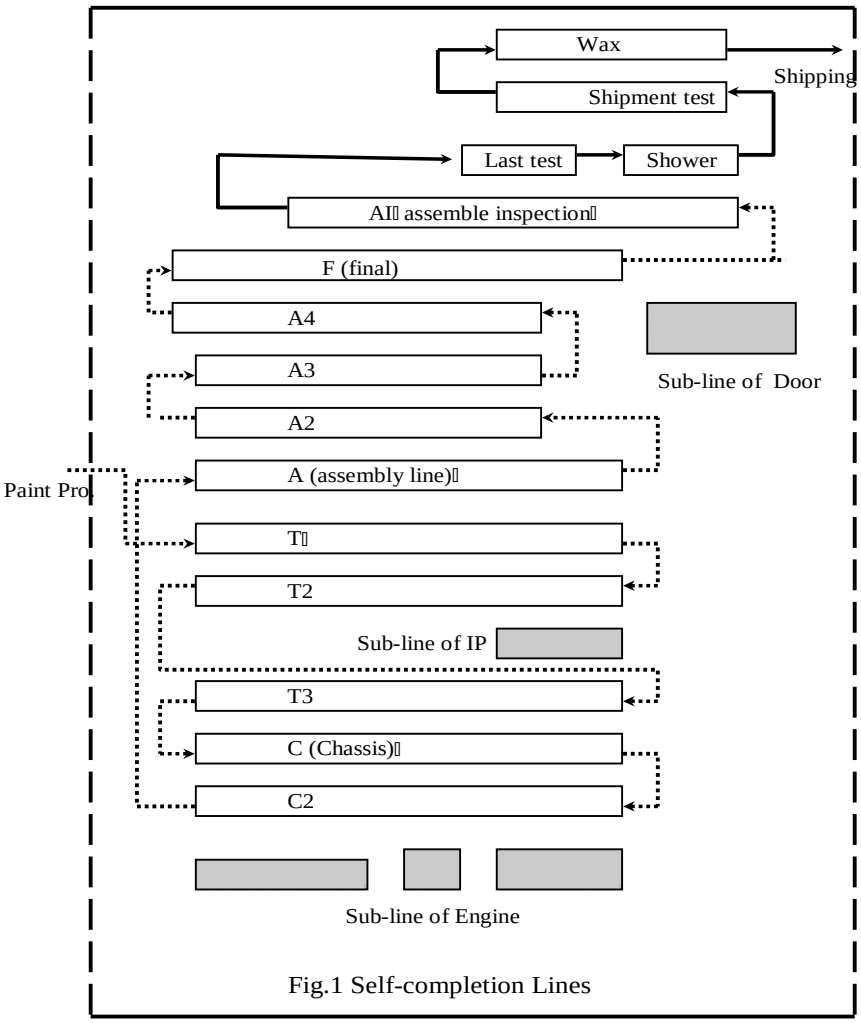

Fig.1 Self-completion Lines

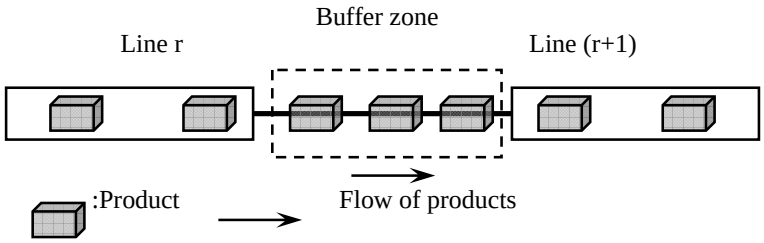

Fig.2 Buffer products between the lines

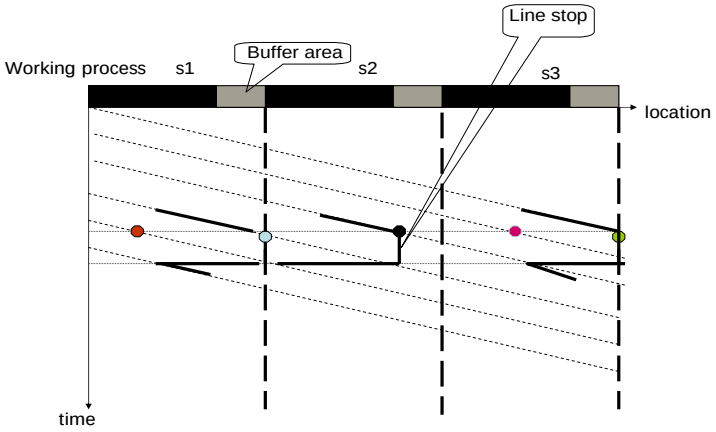

Fig.3 the worker's movement path

Tab.2 The assembly time of the products at each working process

	S=□	S=□	S=□	S=□	S=□	S=□	S=□	S=□	S=□	Aver.
□ =1	58	53	62	68	58	58	53	58	55	57.6
□ =2	69	60	59	51	62	55	58	67	65	61.3
□ =3	63	69	53	59	62	62	67	57	56	59.8
□ =4	50	62	61	66	58	66	55	59	63	60.3
□ =5	62	55	59	56	61	56	69	57	55	58.4
Average	60.4	59.8	58.8	60	60.2	59.4	60.4	59.6	58.8	
weighted average	59.2	59.8	59.3	59.9	60.0	60.0	59.9	60.0	60.0	

Tab.3 The sequence of product

order 1	order 2	order 3	order 4	order 5	order 6	order 7	order 8	order 9
□ =□	i=□	i=□	i=□	i=□	i=□	i=□	i=□	i=□

Tab.4 The beginning position of each worke

K	position	position	order	s	condition
1	0	0	13	1	being done
2	6	6	12	1	finished
3	12	12	11	2	being done
4	18	18	10	3	being done
5	24	24	9	4	being done
6	30	30	8	4	finished
7	36	36	7	5	being done
8	42	42	6	6	being done
9	48	48	5	7	being done
10	54	54	4	7	finished
11	60	60	3	8	being done
12	66	66	2	9	being done
13	72	72	1	10	being done
14	78				

Tab.5 The optimum solution

c(s)	60	stop time(s)	40
auxiliary worker	1	K(s)	1080
v(m/s)	0.1	VTP	1120
l_1 (m)	6.0	$l^s{}_2$ (m)	2.0
L^s (m)	8.0	total length of buffer area	18

Dynamic Multi-Product Multi-Level Capacitated Lot-Sizing Problems Using Heuristic Dynamics Programming

Songwut Prakaiwichien and Peerayuth Charnsethikul
Department of Industrial Engineering
Faculty of Engineering Kasetsart University, Bangkok, Thailand

Abstract: To solve Dynamic Multi-Product Multi-Level Capacitated Lot-Sizing problems by using the dynamic programming approach will consume a lot of time because this method will search all alternatives occurred in every period. Therefore, this research propose to use Heuristic method to find the initial solution and then use the Dynamic Programming to find the best solution. This algorithm can reduce the alternatives occurred by eliminating alternatives which cost more than initial solution at the same stage. This method will cause reduction in processing time to find the next step solution. The result confirms that the best solution of the proposed technique in comparing with the optimum solution by Lingo Software does not exceed than 5%. The processing time is nearly the same as LINGO when run large scale problems.

Keywords: Dynamic Multi-Product Multi-Level Capacitated Lot-Sizing, Dynamic Programming, Heuristic method

INTRODUCTION

Material requirement planning (MRP) is a system commonly used by multi level product industry in order to provide components both type and quantity in all level of production which results in sufficient material in time. Dynamic Multi-Product Multi-Level Capacitated Lot-Sizing problems are important problems occurred in lot sizing procedure. Since MRP must concern about 2 important issues ie the limitations of the production resources and take into account of Total cost which compose of holding cost and setup cost . However, the MRP system is not concern about the above – mentioned issues. As a result, MRP system does not provide an optimal production plan in the aspect of total cost.

To lot sizing problems in assembly production systems by using dynamic programming algorithms and a branch and bound algorithms to obtain the optimal solution, Crowston and Wagner (1973) . Tempelmerier and Derstroff(1996) develop a Lagrangean heuristic. They also started with a Wagner-Within solution and then used a smoothing procedure to try to find a feasible solution. Ozdamar and Barbarosoglu(2000) presented another heuristic using Lagrangean Relaxation and Simulated Annealing. Dellaert , Jeunet and Jonard (2000) propose A genetic algorithms to solve the general multi-level lot-sizing problem with time-varying costs by develop a binary encoding genetic algorithm and design five specific genetic operators to ensure that exploration takes place within the set of feasible solutions. Dellaert and Jeunet (2003) proposed A randomized multi-level lot sizing heuristic for general product structures.

The objective of this paper is to minimize total cost for Dynamic Multi-Product Multi-Level Capacitated Lot-Sizing problems under assembly production systems while no backlogging is allowed by use Heuristic method to find the initial solution and then use the Dynamic Programming to find the best solution.

METHODS

Model formulation

The dynamics multi level capacitated lot sizing problem is aimed at minimizing variable production costs over a finite planning interval. The variable production costs which are considered comprise of holding costs and setup costs. The planning interval is divided into several periods and limited by the planning horizon T.

For each period in the planning interval, the end item demand is assumed to be known and has to be fulfilled without backlogging. Inventory holding

Corresponding Author: Songwut Prakaiwichien, Department of Industrial Engineering Faculty of Engineering Kasetsart University, Bangkok, Thailand

costs are calculated based on the end of period inventory. Setup costs and setup times accrue for an item in each period of production.

Minimize

$$\sum_{j=1}^{j}\sum_{t=1}^{T}(sc_j Y_{jt} + h_j I_{jt} + oc_j O_{jt}) \qquad (1)$$

Subject to

$$I_{j(t-1)} + X_{jt} = D_{jt} + \sum_{k\in S_j} r_{jk} X_{kt} + I_{jt} \;,$$
$$j = 1,\ldots,J;\ t = 1,\ldots,T \qquad (2)$$

$$\sum_{j=1}^{J} a_{mj} X_{jt} \le C_{mt} + O_{jt} \;,$$
$$m = 1,\ldots,M;\ t = 1,\ldots,T \qquad (3)$$

$$X_{jt} \le B_{jt} Y_{jt} \;, j = 1,\ldots,J;\ t = 1,\ldots,T \qquad (4)$$

$$I_{jt}, O_{jt}, X_{jt} \ge 0 \;, j = 1,\ldots,J;\ t = 1,\ldots,T \qquad (5)$$

$$Y_{jt} \in \{0,1\} \;, j = 1,\ldots,J;\ t = 1,\ldots,T \qquad (6)$$

Indices and index sets:

j	Items or operations , j=1, ..., J
m	Resources , m=1, ..., M
t	Periods, t=1, ..., T
S_j	Set of immediate successors of item j in the bill of material

Where the known parameters are

a_{mj}	Capacity needed on a resource m for one unit of item j
B_{jt}	Large number, not limiting feasible lot-sizes of item j in period t
C_{mt}	Available capacity of resource m in period t
h_j	Holding cost for one unit of item j in a period
oc_{jt}	Overtime cost for one unit of item j in period t
D_{jt}	External demand for item j in period t
r_{jk}	Number of units of item j required to produce one unit of the immediate successor item k
s_{cj}	Setup cost for a lot of item j

and the decision variables are

I_{jt}	Inventory of item j at the end of period t
O_{jt}	Amount of overtime of item j used in period t
X_{jt}	Amount of item j produced in period t
Y_{jt}	Binary variable indicating where production is allowed for item j in period t (=1, if item j is produced in period t, 0 otherwise)

The objective (1) is to minimize the sum of holding, setup and overtime costs. Equations (2) are the inventory balances to make sure that no backlogging will occur. For multi-level production, a lot-size of item k will result in a dependent demand for its immediate predecessor items j. Required capacities for lot-size production must not exceed available normal capacities (possibly extended by overtime; (3). Capacity requirements result from both production time per item times the amounts produced as well as setup times incurred with each lot. Setup constraints (4) enforce binary variables Yjt to unity, in case a lot of item j is produced in a period t. All variables are restricted to non-negative or binary values, respectively (5),(6).

Method of solving problems

Method of solving problems can be divided into 2 following steps:

Step I use the Heuristic Method in finding the initial solution (IS) which consists of the number of production, inventory and total cost of each item in each stage.

Step II use Forward Dynamics Programming to find the alternatives step by step and compare with the initial solution at the same period. The alternatives in each stage are the amount of inventory at the end period of all items and cumulative total cost. The mentioned alternative will be limited by 2 conditions.

1. The production must not exceed the capacity in each stage except for the necessary case which resources have limited capacities per period and may be extended by overtime in order not to let the backlogging.
2. After the alternatives according to the first condition are generated, they will be reduced by cutting off the alternatives which have cumulative total cost (CTC) higher than the initial solution (IS) in the same period plus allowance value (AV) which have been defined.

$$CTC \ge IS + AV$$

The remain alternatives will send the number of inventory at the end period and cumulative total cost of each item to the next stage.

Heuristic Method

1. Start at period 1

To choose the item for determining the lot size according the structure of bill of material structure (BOM) from the highest to the lowest level. First item is finish products. Next item is from the next level which is subassembly of the first item. Do the same process until all items are chosen.

According to the BOM, in order to determine lot size items are divided into 2 groups:

Group 1 Finished product and subassembly

Finished product and subassembly which are immediate successor will influence the number of items which are the predecessors. This group will produce in lot for lot according to the demand in that period.

Group 2 Part and Raw material which have not any parts to be made before

To choose the item for determining lot size according to the holding cost per unit, start from the highest to the lowest holding cost per unit. Lot sizing will be Lot for Lot except for the last item which will be produced equal to the remaining capacity. If the inventory in the prior period is higher than present demand, the production will be 0 and reduce the quantity of production in the prior period. That means production (t-1) = production (t-1)-(inventory (t-1) – Demand(t)) in order to make the inventory(t) = 0 .
Then consider part or raw material in the previous order that use common resources and is not a successor. The production should be produced as much as possible but not exceed capacity and cumulative total quantity demand from now to the last period.

To calculate cumulative total cost at this stage as follows:
Cumulative total cost (t) = Cumulative total cost (t-1) + Total cost (t)

Step 2 Do the same process until the last period.

Forward Dynamics Programming Method

1. To start stage 1 in period 1
2. To determine the pattern of lot size of all items which can be possible provided that the lot size will not exceed capacity as following equation (3)

$$\sum_{j=1}^{J} a_{mj} X_{jt} \le C_{mt} + O_{jt} \quad , \; m = 1,\ldots,M \; ; \; t = 1,\ldots,T$$

In accordance with the conditions which demand of each item depend on immediate successor as following equation (2)

$$I_{j(t-1)} + X_{jt} = D_{jt} + \sum_{k \in S_j} r_{jk} X_{kt} + I_{jt} \; ,$$
$$j = 1,\ldots,J \; ; \; t = 1,\ldots,T$$

3. To calculate cumulative total cost of each pattern , according to equation **(1)**

$$\text{Total Cost} = \sum_{j=1}^{j} \sum_{t=1}^{T} (sc_j Y_{jt} + h_j I_{jt} + oc_j O_{jt})$$

4. To compare cumulative total cost in each pattern with solutions from Heuristic method. After the alternatives are generated, they will be reduced by cutting off the alternatives which have cumulative total cost (CTC) higher than the initial solution (IS) in the same period plus allowance value (AV) which have been defined.

$$CTC \ge IS + AV$$

5. To do the same process until the last stage.
6. To find the solution, start from the last stage. Choose the alternative with the lowest cumulative total cost. Use inventory (t-1) in this alternative for considering the value of cumulative (t-2), inventory (t-2) and pattern of lot sizing (t-1) in the previous stage. To do the same process until the first stage, the solution will be all x(i,t) and all cumulative total cost (t)

RESULTS AND DISCUSSION

The performance of the Heuristics dynamics algorithm described in the previous section was evaluated on a set of testing problems. The algorithm was programmed with Matlab (Version 7.0) running under Windows XP on a compatible personal computer (Model Intel(R) CORE(TM)2 Duo CPU T5250@ 1.50 GHz) . The experiments revealed that Heuristics dynamics algorithm could obtain good approximation solution of Dynamic Multi-Product Multi-Level Capacitated Lot-Sizing Problems in reasonable

computation time. Following are the examples of the experiments.

Example: (Assembly System) For assembly product structures shown in Fig.1 (4 items) constrained by two resources (A , B). The test instance data of each test set is shown in Table 1 and 2.

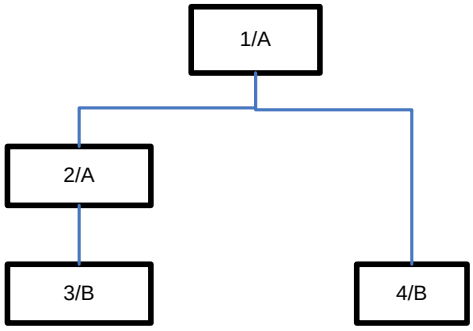

Fig.1 The Product structure for Example

Table 1. The test instance data for all Test set

	Item 1	2	3	4
Holding cost/unit/period	6	3	2	1
Setup cost for item	200			
Overtime cost/unit/period	100			
Capacity A (all period)	30			
B (all period)	32			

Table 2. The External Demand for each test set

Test set No.	External Demand for item 1
1	15,15,16,13,17,14
2	14,15,16,13,17,14
3	13,15,16,13,17,14
4	12,15,16,13,17,14
5	11,15,16,13,17,14
6	10,15,16,13,17,14
7	9,15,16,13,17,14
8	8,15,16,13,17,14
9	7,15,16,13,17,14
10	16,15,16,13,17,14
11	17,15,16,13,17,14
12	18,15,16,13,17,14
13	19,15,16,13,17,14
14	20,15,16,13,17,14
15	15,15,20,13,17,14
16	15,15,21,13,17,14
17	15,15,22,13,17,14
18	15,15,23,13,17,14
19	15,15,24,13,17,14
20	12,15,14,13,17,14,12,11
21	12,15,14,13,17,14,12,11,14
22	12,15,14,13,17,14,12,11,14,12
23	12,15,14,13,17,14,12,11,14,12,13
24	12,15,14,13,17,14,12,11,14,12,13,12
25	12,15,14,13,17,14,12,11,14,12,13,12,13
26	12,15,14,13,17,14,12,11,14,12,13,12,13,14

Table 3. Results of the Numerical Experiments

Test set No.	Best Solution found by		Difference of Solution	Times(sec)	
	HDP	Lingo6		HDP	Lingo6
1	2812	2812	0%	0.39	<1.0
2	2424	2424	0%	0.53	<1.0
3	2424	2424	0%	1.01	<1.0
4	2374	2374	0%	1.96	<1.0
5	2291	2291	0%	4.85	<1.0
6	2197	2197	0%	2.65	<1.0
7	2117	2117	0%	24.8	<1.0
8	2019	2019	0%	25.17	<1.0
9	1954	1954	0%	24.29	<1.0
10	3212	3212	0%	0.502	<1.0
11	4012	4012	0%	0.353	<1.0
12	4812	4812	0%	0.348	<1.0
13	5612	5612	0%	0.356	<1.0
14	6412	6412	0%	0.352	<1.0
15	5218	5218	0%	0.27	<1.1
16	6018	6018	0%	0.27	<1.2
17	6818	6818	0%	0.27	<1.3
18	7618	7618	0%	0.27	<1.4
19	8418	8418	0%	0.29	<1.5
20	2816	2816	0.0%	1.73	1
21	3079	3079	0.0%	11.4	3
22	3345	3345	0.0%	88.07	5
23	3657	3634	0.6%	199.6	19
24	3927	3927	0.0%	164.5	58
25	4235	4235	0.0%	355.94	414
26	4576	4500	1.7%	1375	1440

CONCLUSION

In the development of heuristic Dynamics Programming in solving Dynamic Multi-Product Multi-Level Capacitated Lot-Sizing Problems, the result shows that to use the Heuristic Method in finding

initial solution in order to reduce alternatives occur in each stage will reduce a lot of processing time by using Dynamic Programming in the next step. The experiment reveals that the solution has been improved while comparing to the solution calculated by Lingo6 software does not exceed than 2 %.

In the case of small scale problem without overtime, the processing time calculated by proposed method will exceed the processing time calculated by Lingo6 software but can be acceptable. However, if there are with overtime, the processing time is nearly the same because alternatives in each stage were reduced evidently. In the case of large scale problem, the processing time will be slightly different to Lingo6.

For further research, more numerical experiments can be made and to develop the method in solving problems by using the results from Heuristic Dynamic Programming. This method considering only the alternative which has potential to improve the solution and reduce processing time.

ACKNOWLEDGEMENTS

I would like to acknowledge and extend my heartfelt gratitude to Assoc. Prof. Peerayuth Chansethikul, Ph.D. for his useful comments and suggestions which have made the completion of this paper possible.

REFERENCES

1. Crowston W.B., M. W. Wegner, 1973. Dynamic Lot Size Models for Multi stage Assembly Systems, Manegement Science 20(1),14-21.
2. Dellaert, N. , Jeunet, J. and Jonard, N., 2000. A genetic algorithms to solve the general multi-level lot-sizing problem with time-varying costs. International Journal of production economics 68, 241-257
3. Dellaert, N.P. and Jeunet, J., 2003. Randomized multi-level lot sizing heuristic for general product structures. European Journal of Operational Research 148, 211-228
4. Ozdamar, L., Barbarosoglu, G., 2000. An integrated lagrangean relaxation simulated annealing approach to multi-level multi-item capacitated lot sizing problem. International Journal of Production Economics 68,319-331
5. Tempelmeier, H., Derstroff, M., 1996. A Lagrangean-based heuristic for dynamic multi-level multi-item constrained lotsizing with setup times. Management Science 42(5),738-757.

Comparison of Total Inventory Cost between Estimated Demand by Normal Distribution and Fuzzy Set in the Case of Poor Data

[1]Kawinthorn Saicharoen and [2]Saowanee Lertworasirikul
[1]Department of Industrial Engineering and [2]Department of Product Development
Kasetsart University, Bangkok, Thailand

Abstract: When we calculate Economic Order Quantity (EOQ.), Re-Order point (ROP) and safety stock in a continuous-review inventory model with safety stock (SS model), we usually use annual demand that comes from uncertain demand estimated by normal distribution. However, when lacking of enough demand data, a fuzzy set is an alternative option for estimating uncertain demand data. Therefore, in this paper we propose a fuzzy set for estimating demand data when there is no enough demand data to use normal distribution. This paper compares total inventory costs between annual demand data that estimated by fuzzy set and normal distribution in the SS inventory model. The results show that when lead time is long, the total inventory costs with fuzzy set demand are significantly lower than those with demand estimated by normal distribution.

Keywords: Inventory , EOQ , Fuzzy set ,Normal Distribution , Poor data

Introduction

Over the past 40 years, fuzzy set theory has been studied and used to estimate uncertain data. Uncertain data in inventory management may include annual demand, holding cost, ordering cost, and shelf-life time. Normally to calculate EOQ and ROP with uncertain demand, the demand is estimated by normal distribution. However, normal distribution is generally used when there are more than 25 randomly and independent data points. For new products or new businesses, usually there are no historical data or there may be lack of some data to be represented by normal distribution.

In the past few years, researchers applied fuzzy set theory to solve inventory models with fuzzy demand. For example, in 1987 Park used an extension principle to calculate EOQ in the inventory cost model with trapezoidal fuzzy set demand.

In 2002, Kao and Hsu proposed a lot size-reorder point inventory model with fuzzy demand. They used Yager's ranking method to estimate fuzzy demand. In this paper, the (Q, r) inventory model with backorder cost, which was charged in terms of a shortage cost, was studied. The solutions developed in this paper provided an optimal solution.

In 2006, Yang proposed a two-echelon inventory model with fuzzy annual demand in a supply chain. The consideration was based on total inventory cost optimization. He derived an optimal number of lots and buyer's order quantity. He suggested a signed distance to estimate fuzzy annual demand.

However, from the past research, the effect of different demand estimations, i.e., demand estimated by fuzzy set and normal distribution, on total inventory costs has not been studied. Therefore, in this paper focuses on the inventory model with uncertain demand. The uncertain demand is defined by a fuzzy set and normal distribution. Then the models are compared base on total inventory cost.

The rest of the paper is organized as follows. In Section 2, notations and assumptions of the inventory model in this study are given. Section 3 presents fuzzy demand estimation and calculation of total inventory cost. In Section 4, experimental results and discussion are given. Finally in Section 5, conclusions and future research are presented.

Notations and assumptions

Notations:

The following notations are used throughout this paper.

TC	:	total inventory cost
D	:	average annual demand
Q	:	order quantity
A	:	ordering cost
ss	:	safety stock
H	:	holding cost

Corresponding Author: Kawinthorn Saicharoen, Industrial Engineering Department Kasetsart University, 50 Phahon Yothin Rd, Chatuchak Bangkok 10900, Thailand, E-mail kawinpun@hotmail.com, Tel. +6684 707 0550

C : purchasing price per unit
ROP : re-order point
d : daily demand
k : customer service level
σ : Standard deviation of demand
L : Lead time
I_i : Inventory stock level at day i
Γ_i : Inventory stock level that lower than 0 at day i
C_L : Penalty cost for lost sale

The SS inventory model in this study is composed of the following equations:

$$TC = \frac{D}{Q}A + (\frac{Q}{2} + ss)H + CD \quad (1)$$

$$ROP = (d \times L) + ss \quad (2)$$

$$ss = k\sigma\sqrt{L}. \quad (3)$$

Assumptions of the inventory model

For the SS inventory model, we need to calculate Economic Order Quantity (EOQ), Re-order point (ROP), and safety stock (ss). Then total optimal inventory costs are calculated by using the optimal purchase quantity (EOQ) and ROP. The SS model in this study is based on the following assumptions.

1. Demand data for one year are generated from Exponential distribution. Then 30 demand data out of 364 generated demand data are randomly selected to be an initial data set in this experiment, i.e., assuming that we know only daily demand for 30 days in a year.
2. ROP is calculated from demand during lead time and safety stock by assuming that ROP can satisfy demand during lead time period for at least 99%.
3. An inventory level is reviewed at the end of each day and replenishment is done whenever the inventory level is lower or equal to ROP.
4. When stock out is occurred, the inventory level is set to zero and a penalty cost is charged in that day.
5. Inventory costs are calculated daily and then sum up for one year for comparing total cost that estimated demand by normal distribution and fuzzy set.

Estimation of annual demand and calculation of total inventory cost

The classical inventory models assume deterministic characteristics, continuous review, and no lead time. The order quantity that minimizes total inventory cost is called EOQ and usually calculated by following this formula.

$$EOQ = Q^* = \sqrt{\frac{2DA}{H}} \quad (4)$$

In the case of uncertain demand, we first estimate the representative demand and then calculate EOQ using Equation (4) based on the estimated demand. In this paper, there are two methods for estimating representative demand. The first method is using normal distribution principle and the other is based on a fuzzy set principle.

Normal distribution method is used to calculate mean and variance of daily demand. The annual demand is calculated by multiplying daily demand with 364. ROP can be calculated by Equation (2) and SS can be calculated by Equation (3).

Before presenting a fuzzy set principle to estimate demand, we present some definitions and properties of fuzzy sets with relevant operations [8].

Definition 1 If X is a collection of x, then a fuzzy set $\widetilde{A}$ in X is a set of ordered pairs:

$$\widetilde{A} = \{(x, \mu_{\widetilde{A}}(x)) / x \in X\}.$$

When $\mu_{\widetilde{A}}(x)$ is called membership function x in $\widetilde{A}$ and membership function is a member of nonnegative real number.

Definition 2 Let $0 \le \alpha \le 1$, the membership degree of fuzzy set $\widetilde{A}$ is called alpha-cut (α-cut) or alpha-level of set A

$$A_\alpha = \{x \in X / \mu_{\widetilde{A}}(x) \ge \alpha\}.$$

Definition 3 For $\widetilde{A}$ = (a, b, c), where b < a < c, $\widetilde{A}$ will be called triangular fuzzy set, if a membership function of $\widetilde{A}$ is given by (5).

$$\mu_{\tilde{A}}(x)=\begin{cases}\dfrac{(x-b)}{(a-b)};b\le x\le a\\ \dfrac{(c-x)}{(c-a)};a\le x\le c\\ 0;otherwise\end{cases} \quad (5)$$

When demand is represented by a fuzzy set, we produce a fuzzy demand set from raw data using the following procedure. The fuzzy demand in this paper is assumed to be a triangular fuzzy number.

1. Draw a daily demand histogram with 7 intervals.
2. Determine a middle value of each interval in the histogram and use it as a representative for each level.
3. Set the membership function values of minimum and maximum points of daily demand to be zero.
4. Find a middle value of the interval that has the highest frequency. At the middle value, set a membership function value to be 1 (a top of triangular fuzzy set). This middle value is then used as an estimated daily demand (d).
5. Multiply d with 364 to become an annual demand ($\widetilde{D}$).

Based on daily and annual fuzzy demand sets, we calculate EOQ by using Equation (4) but replacing D with $\widetilde{D}$. ROP and SS are determined by Equations (6) and (7). In general, ROP is calculated such that 99% of customer demand during a lead time period is satisfied. However, when demands are fuzzy numbers, ROP and ss are calculated as follows

ROP = Max(d) x Lead time (6)

ss = (Max d - d) x Lead time (7)

From Equation (6) that ROP is calculated by using a maximum daily demand multiplied with the lead time. Therefore, the ROP is a maximum demand that might be arriving during the lead time.

The objective of this experiment is to compare the total inventory cost when demand data are estimated by a normal distribution and a fuzzy set. Therefore, we use the same demand data by simulating from Exponential distribution, and observe the inventory stock levels and total inventory costs. In every experiment, an inventory level in some days might be lower than zero. In this case, we add lost-sale cost as a penalty cost in calculating inventory cost on that day. Total inventory cost per year is calculated by adding up daily inventory costs. The details of the experiment are given in the following procedure.

1. From initial demand, calculate mean and standard deviation of fuzzy daily demand.
2. Calculate annually demand, EOQ, ROP, and ss for both the case of demand estimated with normal distribution and fuzzy set.
3. For this experiment fulfillment, let a lot of purchase is at least 10 units and each order quantity is divisible by 10.
4. Generate 364 random data demand.
5. Initial inventory stock is EOQ + ss
6. Calculate an inventory level of each day from Equation (8) and calculate a holding cost (HC) from Equation (9). If I_{i-L} has a purchase order, then Q = EOQ. Otherwise, Q = 0

   $I_i = I_{i-1} + Q - d$ (8)

   $HC = I_i \times H$ (9)
7. If $I_i \le ROP$, then buy items and calculate ordering cost.
8. If $I_i \le 0$, then set I_i as 0 and calculate a lost sale cost.

   Lost sale cost = $I_i^- \times C_L$ (10)
9. The total yearly inventory cost is a summation of daily inventory cost.
10. Compare total inventory cost for 10 cases.

In this paper, we compare total inventory costs when demand data are estimated by normal distribution and fuzzy set and lead times are set as 1 day and 7 days.

Experimental results and discussion

In this experiment, we consider the inventory system with the following data: Ordering cost (A) = 25/order, Holding cost (H) = 5/unit /year, Penalty cost for lost sale (C_L) = 10/unit/year, Purchasing price (C) = 25/unit, Customer service level (k) ≥ 99%. We perform 10 experimental cases. The results of this experiment are shown in Figures 2 and 3.

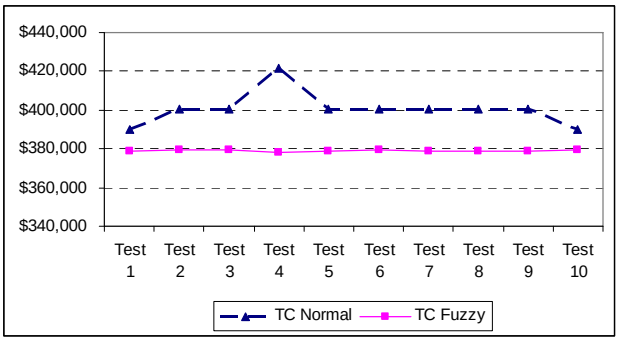

Figure 2 the result of total inventory cost with 7 days lead time

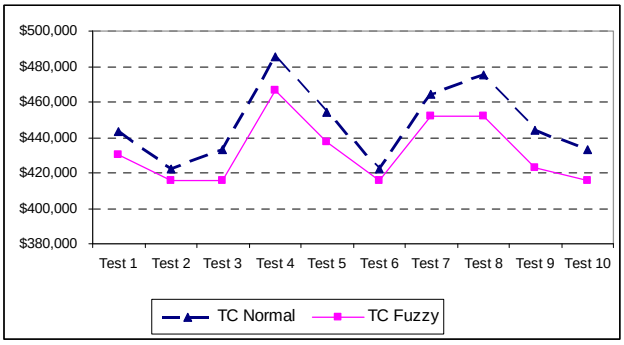

Figure 3 the result of total inventory cost with 1 days lead time

Figure 2 and figure 3 show graphs presenting the difference of total inventory costs between the case of inventory with 7 days of lead time and 1 day of lead time, respectively. In Figure 2, all of 10 total inventory costs from the normal distribution method are higher than total inventory costs from the fuzzy set method. However, the inventory holding cost, the penalty cost, and the set up cost of the normal distribution method are not significant higher than the fuzzy set method except the purchase cost, which is significantly higher than the fuzzy set method. In Figure 3, the results are similar to the results from Figure 2 but total inventory costs from the normal distribution method and the fuzzy set method in Figure 3 are not significantly different as in Figure 2. This experiment shows that a purchasing cost has a major effect on the total inventory cost. Also, when demand is uncertain and is approximated by a fuzzy set, the inventory model gives a small EOQ but a large ROP. On the other hand, when uncertain demand is approximated by a normal distribution, the inventory model gives a large EOQ but a small ROP. Therefore, using the normal distribution method, the number of items purchasing each time is larger than those from the fuzzy set method.

However, when we have adequate demand data, total inventory costs are relatively close no matter what method we use to estimate demand. This might be because of the way that a membership function is constructed. In this paper, a membership function of fuzzy sets is defined by a graphical method based on histogram. Thus, a membership function of fuzzy sets has a similar shape to a normal distribution. However, having inadequate data or qualitative data, a fuzzy set method is a powerful method to use for demand estimation in the inventory model.

Conclusions and future research

In this paper, we compare total inventory costs when demand data are estimated by a normal distribution and a fuzzy set. Long lead time of 7 days and short lead time of 1 day are used to compare the total inventory costs. From the results, when lead time is long (7 days), the total inventory costs with fuzzy set demand are 95% significantly lower than those with normal distributed demand. However, when lead time is short (1 day), the total inventory costs with fuzzy set demand are not significantly lower than those with normal distributed demand.

In summary, normal distribution is a good approximation when data are rich, while a fuzzy set is a promising method to represent demand data when it is not easily approximated by normal distribution.

So far there are many researchers interested in the EOQ model with fuzzy set data. From the literature, mostly fuzzy inventory is solved by using fuzzy set theory. Fuzzy logic is another promising way to deal with fuzzy inventory. Therefore, in future research, we will study behaviors of inventory level based on fuzzy logic.

References

1. A. L. Guiffrida and R. Nagi. Fuzzy set theory applications in production management research: a literature survey. Journal of Intelligent Manufacturing, Volume 9, 1998, Pages 39-56.
2. H. Chang, An application of fuzzy sets theory to the EOQ model with imperfect Quality items, computer and operation research, Volume 31, 2004, Pages 2079-2092.

3. K. S. Park, Fuzzy-set theoretic interpretation of economic order quantity, IEEE Transaction on system, Man and Cybernetics, Volume SMC-17, 1987, Pages 1082-1084.
4. M. Vojosevic, D. Petrovic, R. Petrovic, EOQ formula when inventory cost is fuzzy, International Journal of Production Economics, Volume 45, 1996, Pages 499-504.
5. M. Yang, A two-echelon inventory model with fuzzy annual demand in a supply chain, Journal of Information and Optimization Sciences, Volume 27, Issue 3, 2006, Pages 537-550.
6. S. Chen, Back order fuzzy inventory model under function principle, Information Sciences, Volume 95, 1996, Pages 71-79.
7. G. Klir, U. St. Clair, B. Yuan, Fuzzy Set Theory Foundation and Applications, Printice Hall International, Inc., 1997.
8. H. J. Zimmermann, Fuzzy Set Theory and Its Application, 3rd edition, Kluwer Academic publishers, Boston/Dordrecht/London, 1996.

Comparative Characterization of Various Initial-Cutting-Pattern Creations in One Dimensional Cutting Stock Problem

Sirirat Wongprakornkul
Department of Statistics, Faculty of Science, Khon Kaen University,
Khon Kaen, Thailand. 40002.

Abstract: The One-dimensional cutting stock problem (1D-CSP) is an integer linear programming. This problem arises from many applications in industry. It has been called a classical NP-hard problem which cannot be solved within polynomial computation time. The finite number of cutting patterns may be very large. Gilmore and Gomory (1963) claimed that if the stock to be cut has length l = 200 inches and there are demands for 40 different lengths from 20 to 80 inches, the number of possible patterns could be exceed 10 to 100 million. The more cutting patterns these are, the more columns of constraints are involved. The most powerful algorithm for solving linear programming with many columns is Column-Generation Procedures. By the way, initial cutting patterns are necessary to create at first step before using the Column-Generation Technique to create other essential cutting patterns.

In this paper, 3,000 instances of one-dimensional cutting stock problems with multiple retail sizes were investigated. These instances were separated into six sets of CSP[L; l_1, l_2, …, l_m] consist of CSP[17; 3, 5, 9], CSP[273; 18, 91, 21, 136, 51], CSP[490; 18, 91, 21, 136, 51, 80, 100, 127, 190, 201], CSP[150; 6, 10, 15, 22, 25, 28, 31, 34, 37, 40, 44, 47, 50, 52, 55, 58, 62, 65, 68, 72], CSP[250; 6, 10, 15, 22, 25, 28, 31, 34, 37, 40, 44, 47, 50, 52, 55, 58, 62, 65, 68, 72], and CSP[300; 5, 10, 15, 20, 25, 30, 35, 40, 45, 50, 55, 60, 65, 70, 75, 80, 85, 90, 95, 100, 105, 110, 115, 120, 125, 130, 135, 140, 145, 150, 155, 160, 165, 170, 175, 180, 185, 190, 195, 200]. Each set was generated into 500 instances varying demands. Four initial-cutting-pattern creations, named A, B, C, and D, were raised for forming also four various mathematical models. The studied characteristics were minimum, maximum, and average of iterations and number of solvable instances. We found that although A, B, and C could solve more problems than D, but the average iteration of D was the lowest.

Key words: Initial-cutting-pattern creation, Column-Generation Technique, One-dimensional cutting problem

INTRODUCTION

A one-dimensional cutting stock problem (1D-CSP) is an integer linear programming problem. It arises from many applications in industry for example paper, film, leather, steel, etc. This problem has an important practical generalization when a cutting process is distributed over several successive stages. The products are cut to produce smaller sizes. The intermediate products are both output and input during the cutting process. This problem is a classical combinatorial problem, which is solvable in non-polynomial time, also known as an NP-hard problem. More than four decades ago, mathematicians studied ways to solve large scale problems. Dantzig and Wolfe[1] initiated the extensive work on large-scale mathematical programming. The most efficient technique when applied to linear programs is the Column-Generation Technique. It is applied for solving problems with few rows and much more columns. There are wide varieties of problems, which can be solved by this approach.

The 1D-CSP can be addressed by finding the best process with the minimum cost to cut intermediate products (stocks) to meet the demand for finished sizes (retail sizes) of prescribed dimensions. This problem is very difficult; since all variables must be integers and the number of columns can be very large. For example, if the stock to be cut has length 200 inches and the required demands for 40 different lengths from 20-80 inches, the number of possible patterns could easily exceed from 10 to 100 million[3]. However, some patterns are not needed to solve the problems. Hence, the important concept for solving the problems faster is to find out the technique to originate the effective patterns. That technique is the column-generation technique. This technique is successful for solving the large number of variables in the linear programming formulation of the problem[2, 3]. In addition, the 1D-CSP is broadly applied in industries such as in the aluminum industry[7] and the clothing industry[4]. Typical cutting stock problems implicitly assume that the stocks are cut at a single facility. Holthaus[5] raised decomposition approaches based on the Column-Generation Technique

Corresponding Author: Sirirat Wongprakornkul, Department of Statistics, Faculty of Science, Khon Kaen University, Khon Kaen, 40002, Thailand, Tel/Fax:+(66)43-202375, Email: sirwon@kku.ac.th

for solving the 1D-CSP with different types of standard lengths or multiple cutting facilities. Wongprakornkul[8] raised a heuristic method for solving One-Dimensional cutting stock problem to reach integer solution.

To apply the Column-Generation technique, initial cutting patterns are necessary to create. In this study, four initial-cutting-pattern creations, named A, B, C and D, were analyzed to compare their effects on the Column-Generation procedure.

OBJECTIVES

1) To study approaches for creating initial cutting patterns.

2) To compare the effects on the Column-Generation procedure within different initial-cutting-pattern creations

LITERATURE REVIEWS

There are many papers working on the 1D-CSP. In this paper may express some of them as follows:

The Delayed Column-Generation Technique

The first attempt to solve this problem has been found since 1961 by the Delayed Column-Generation Technique[2]. Let D_m be the required number of retail items l_m where m$\in\{1,..,M\}$ to be cut from stock length L_k where k $\in\{1,..,K\}$ and the number of stock k is unlimited, c_k be the cost per unit of the stock length k, x_{kp} be the number of times at stock k and pattern p where p $\in\{1,..,P\}$. For a stock size k with length L_k a cutting pattern p indicates how often each order length l_m has to be cut off from this stock size. Any feasible cutting pattern p for stock size k can be represented by M-dimensional non-negative integer vector $a_{.kp} = \left(a_{1kp},\text{K},a_{Mkp}\right)^T$, fulfilling $\sum_{m=1}^{M} l_m a_{mkp} \le L_k$. This model can be formulated as Integer Linear Programming (ILP) model with the objective that minimizes the total cost of all stock lengths as follows:

$$\text{Minimize} \quad \sum_{p=1}^{P}\sum_{k=1}^{K} c_k x_{kp} \ , \tag{1}$$

Subject to

$$\sum_{p=1}^{P}\sum_{k=1}^{K} a_{mkp} x_{kp} \ge D_m \ , \text{m=1,…, M,} \tag{2}$$

$$x_{kp} \ge 0 \ , \text{k=1,…, K, p=1,…, P} \tag{3}$$

From equation (2), if the demand and different sizes of retail items are large, the overall patterns to be generated are not practical. Therefore, the duality theorem can be used to relax this model by starting basis columns with a minimum number of patterns that can solve (1) – (3). These columns are referred as the initial patterns. From the weak duality theorem, any pattern, this is not to be a basis column, if $\sum_{m=1}^{M} u_m D_m \le c_k$, $\forall$k where u_m be dual variables, Otherwise, one pattern that $\sum_{m=1}^{M} u_m D_m > c_k$, $\exists$k can be entered as a basis column. The sub-problem to be determined for the basis column is called the unbounded knapsack problem (UKP) with a mathematical model as follows:

$$\text{Maximize} \quad \sum_{m=1}^{M} u_m a_{mk(P+1)} \ , \tag{4}$$

Subject to

$$\sum_{m=1}^{M} l_m a_{mk(P+1)} \le L_k \ , \tag{5}$$

$$a_{mk(P+1)} \in I^+ , \forall \text{m.} \tag{6}$$

The UKP can be solved as a branch-and-bound procedure because of the restriction of $a_{mk(P+1)}$ to be integer variables of (6) or an algorithm based on dynamic programming as such

$$F_m(l) \ge \max\{F_m(l-l_m)+u_m, F_{m-1}(x)\} \quad \text{for m} > 1 \tag{7}$$

where $\text{L} \ge 1 > \sum_{m=1}^{M} l_m a_{mk(P+1)}$.

The UKP is to be solved for each different stock size by the single dynamic programming as described earlier. When the constraints, $\sum_{m=1}^{M} u_m D_m > c_k$, could not be detected, an optimal solution is verified.

A branch-and-bound procedure for solving the 1D-CSP exactly with single stock length

One possible method for solving the 1D-CSP if all patterns have been known under a single stock length is a branch-and-bound method[6]. Consider at each stock length k, three lower bounds can be computed for each branching nodes after solving the continuous relaxation of the 1D-CSP as follows:

$$\text{Lowerbound}_1 = \quad Z \ + \left\lceil \frac{(l)^T d_m^r}{L_k} \right\rceil \tag{8}$$

where $Z = \sum_{p=1}^{P} c_k \lfloor x_{kp} \rfloor$,

$$d_m^r = D_m - \sum_{p=1}^{P} a_{mkp} \lfloor x_{kp} \rfloor .$$

The second lower bound will be suggested as followed:

$$Z_c = \text{Minimize} \sum_{p=1}^{P} c_k x_{kp} , \quad (9)$$

Subject to

$$\sum_{p=1}^{P} a_{mkp} x_{kp} \geq d_m^r , \forall \text{m}, \quad (10)$$

$$x_p = 0 , \text{if } a_{mkp} > D_m , \forall \text{m}. \quad (11)$$

From equations (9)–(11) the obtained lower bound is

$$\text{Lowerbound}_2 = Z + Z_c \quad (12)$$

The third lower bound is obtained from the solution of a knapsack problem with weight $q_{km} = \lfloor L_k / l_m \rfloor$ and suggested as follows:

$$\mu = \text{maximize} \sum_{m=1}^{M} \frac{a_{mk(P+1)}}{q_{km}} , \quad (13)$$

Subject to

$$\sum_{m=1}^{M} l_m a_{mk(P+1)} \leq L_k , \quad (14)$$

$$a_{mk(P+1)} \leq d_m^r , \forall \text{m} \quad (15)$$

$$a_{mk(P+1)} \in \text{I}^+ , \forall \text{m} \quad (16)$$

From equations (13) – (16) the obtained lower bound is

$$\text{Lowerbound}_3 = Z + \left\lceil \frac{1}{\mu} \sum_{m=1}^{M} \frac{d_m^r}{q_{km}} \right\rceil \quad (17)$$

The branch-and-bound procedure uses these three lower bounds to decide when to exclude or include a_{mkp} for each branching nodes. The number of x_{kp} variables will be increased by one.

Column-Generation Technique

Consider the procedure to apply the Column-Generation Technique to the 1D-CSP with single stock length so that at least x_k pieces of standard length L are furnished. First, the problem is relaxed in order to provide the simplex multipliers. The rules for converting PRIMAL problem to DUAL problem are shown in Table1.

Table 1: Rules for converting PRIMAL to DUAL

PRIMAL MINIMIZATION PROBLEM			
If the primal variables are	Then the dual constraints are	If the primal constraints are	Then the dual variables are
≥	≤	≥	≥
≤	≥	≤	≤
Unrestricted	=	=	Unrestricted

Table 1: Rules for converting PRIMAL to DUAL (cont'd)

PRIMAL MAXIMIZATION PROBLEM			
If the primal variables are	Then the dual constraints are	If the primal constraints are	Then the dual variables are
≥	≥	≥	≤
≤	≤	≤	≥
Unrestricted	=	=	Unrestricted

After that, the problem is decomposed into I sub-problems, called [new pattern procedure or NPP]: a new-pattern generated sub-problem. These sub-problems applied the Column-Generation Technique to search the essential cutting patterns for the problem.

The ID-CSP model is written in the relaxed form (see also equations (18)-(21)) as the PRIMAL model. Following the rules in Table 1, the DUAL model is written in equations (22)-(25).

k = index for patterns (k = 1, …, K),
m = index for retail items (m = 1, …, M),
L = the length of stock,
l_m = the length of item m; m = 1, …, M,
g = the cost of stock,
R = amount of stock available,
a_{mk} = the number of strips of item m cut in pattern k , fulfilling $\sum_{m=1}^{M} l_m a_{mk} \leq L$,
D_m = the demands of item m, and
x_k = decision variables that represent the number of times pattern p of stock k is used.

[PRIMAL]:

$$\text{Minimize} \sum_{k=1}^{K} g x_k \quad (18)$$

Subject to

$$-\sum_{k=1}^{K} x_k \geq -R , \quad (19)$$

$$\sum_{k=1}^{K} a_{mk} x_k \geq D_m , \forall \text{m}, \quad (20)$$

$$x_k \geq 0 , \forall \text{k}. \quad (21)$$

To develop the DUAL model, the simplex multipliers used throughout this paper are defined as follows:

e = the simplex multipliers of the used stock from constraints (19),

r_m = the simplex multipliers of the item m from constraints (20).

[DUAL]:

$$\text{Maximize } e(-R)+\sum_{m=1}^{M} r_m D_m, \qquad (22)$$

Subject to

$$-e+\sum_{m=1}^{M} r_m a_{mk} \le g \text{ , } \forall \text{k}, \qquad (23)$$

$$e \ge 0, \qquad (24)$$

$$r_m \ge 0 \text{ , } \forall \text{m}, \qquad (25)$$

The simplex multipliers of [DUAL] are used to search a new legitimate cutting pattern. The multi-sub-problems are decomposed by the Column-Generation Technique to find out the effective cutting patterns. The [NPP] can be modeled as:

[NPP]:

$$\text{Maximize } V_{k^*}=\sum_{m=1}^{M} r_m a_{mk^*p^*} - g_{k^*} - e_{k^*}, \qquad (26)$$

Subject to

$$\sum_{m=1}^{M} l_m a_{mk^*} \le L, \qquad (27)$$

$$\sum_{k=1}^{K} q_k = 1, \qquad (28)$$

$$a_{mk^*} \ge 0 \text{ and integer, m = 1, ..., M,} \qquad (29)$$

where

e_{k^*} = the simplex multipliers of the used stock k* for cutting a new pattern from constraints (19),

a_{mk^*} = the number of strips of item m cut in the new pattern k*,

Every supplier is solved to obtain the effective patterns. If $V_{k^*} = \max \{V_k | \text{ k=1,..., K }\} > 0$ then the new column $a_{mk^*} = (a_{1k^*}, \ldots, a_{Mk^*})^T$ is introduced into model (18)-(21) as a new basis column. If $V_{k^*} \le 0$, the current column is proven to be globally optimal. For a profound description of the column-generation procedure for cutting stock problems.

METHODS

In this study, four initial-cutting-pattern creations were proposed, named A, B, C, and D.

Approach A, the matrix of l_m x P_k is as below:

$$\begin{bmatrix} 1 & 0 & \Lambda & 0 \\ 0 & 1 & \Lambda & 0 \\ \text{M} & \text{M} & \text{O} & \text{M} \\ 0 & 0 & \Lambda & 1 \end{bmatrix}_{M\times K}$$

This method defines only one strip in a pattern of each retail item. Therefore, the matrix of patterns is an Identity matrix.

Approach B, the matrix of l_m x P_k is as below:

$$\begin{bmatrix} \max & 0 & \Lambda & 0 \\ 0 & \max & \Lambda & 0 \\ \text{M} & \text{M} & \text{O} & \text{M} \\ 0 & 0 & \Lambda & \max \end{bmatrix}_{M\times K}$$

This method defines the maximum of strips that retail item could cut in a pattern of each retail item or $\left\lfloor \frac{L}{l_m} \right\rfloor; m = 1,2,\text{K}, M$. Therefore, the matrix of patterns is a diagonal matrix.

Approach C, the matrix of l_m x P_k is as below:

$$\begin{bmatrix} \textit{Random} & 0 & \Lambda & 0 \\ (1\ldots\max) & & & \\ 0 & \textit{Random} & \Lambda & 0 \\ & (1\ldots\max) & & \\ \text{M} & \text{M} & \text{O} & \text{M} \\ 0 & 0 & \Lambda & \textit{Random} \\ & & & (1\ldots\max) \end{bmatrix}_{M\times K}$$

This method picks a random number of strips between 1 to the maximum of strips that each retail item could cut or $\left\lfloor \frac{L}{l_m} \right\rfloor; m = 1,2,\text{K}, M$. Therefore, the matrix of patterns is also a diagonal matrix.

Approach D, the matrix of l_m x P_k is as below:

$$\begin{bmatrix} a_{11} & a_{12} & \Lambda & a_{1K} \\ a_{21} & a_{22} & \Lambda & a_{2K} \\ \text{M} & \text{M} & \text{O} & \text{M} \\ a_{M1} & a_{M2} & \Lambda & a_{MK} \end{bmatrix}_{M\times K}$$

This method defines that the scrap of each pattern is less than the shortest retail item. And the number of

strips of item m cut in pattern k has to accomplish $\sum_{m=1}^{M} l_m a_{mk} \le L$.

For doing the experiments, there were six sets of CSP[L; l_1, l_2, …, l_m] consist of CSP1[17; 3, 5, 9], CSP2[273; 18, 91, 21, 136, 51], CSP3[490; 18, 91, 21, 136, 51, 80, 100, 127, 190, 201], CSP4[150; 6, 10, 15, 22, 25, 28, 31, 34, 37, 40, 44, 47, 50, 52, 55, 58, 62, 65, 68, 72], CSP5[250; 6, 10, 15, 22, 25, 28, 31, 34, 37, 40, 44, 47, 50, 52, 55, 58, 62, 65, 68, 72], and CSP6[300; 5, 10, 15, 20, 25, 30, 35, 40, 45, 50, 55, 60, 65, 70, 75, 80, 85, 90, 95, 100, 105, 110, 115, 120, 125, 130, 135, 140, 145, 150, 155, 160, 165, 170, 175, 180, 185, 190, 195, 200]. In each set, a random number in range 5 to 5,000 were chosen as a demand of each retail item. Furthermore, 500 instances of each set were generated by varying demands. After that, four initial-cutting-pattern creations were proposed (A, B, C, and D) for forming mathematical models. To do this research, the Revised Simplex and the Dynamic Programming were developed in case of performing the Column-Generation technique. Finally, some characteristics such as minimum, maximum, and average of iterations and number of solvable instances were investigated.

EXPERIMENT RESULTS

The six sets of CSP[L; l_1, l_2, …, l_m] were generated with 500 instances per each. The results were shown in Table 1-6. Four characteristics were investigated such as solubility, the minimum, the maximum, and the average of iterations. The cause of unsolvable was occurring degeneracy problem.

Table 1: CSP1[17; 3, 5, 9]

Approach	Solubility	Iterations		
		Min	Average	Max
A	500	4	4.00	4
B	500	2	2.00	2
C	500	2	3.46	5
D	249	2	2.00	2

Table 2: CSP2[273; 18, 91, 21, 136, 51]

Approach	Solubility	Iterations		
		Min	Average	Max
A	500	6	6.00	6
B	500	2	2.00	2
C	500	3	5.00	7
D	500	1	1.00	1

Table 3: CSP3[490; 18, 91, 21, 136, 51, 80, 100, 127, 190, 201]

Approach	Solubility	Iterations		
		Min	Average	Max
A	500	20	25.89	43
B	499	15	21.95	36
C	500	14	24.36	40
D	129	14	18.53	30

Table 4: CSP4[150; 6, 10, 15, 22, 25, 28, 31, 34, 37, 40, 44, 47, 50, 52, 55, 58, 62, 65, 68, 72]

Approach	Solubility	Iterations		
		Min	Average	Max
A	497	26	85.41	601
B	498	22	73.45	601
C	499	22	72.57	601
D	31	16	25.48	49

Table5: CSP5[250; 6, 10, 15, 22, 25, 28, 31, 34, 37, 40, 44, 47, 50, 52, 55, 58, 62, 65, 68, 72]

Approach	Solubility	Iterations		
		Min	Average	Max
A	499	32	66.97	601
B	499	31	55.32	601
C	497	34	63.79	601
D	111	20	41.16	601

Table 6: CSP6[300; 5, 10, 15, 20, 25, 30, 35, 40, 45, 50, 55, 60, 65, 70, 75, 80, 85, 90, 95, 100, 105, 110, 115, 120, 125, 130, 135, 140, 145, 150, 155, 160, 165, 170, 185, 180, 185, 190, 195, 200]

Approach	Solubility	Iterations		
		Min	Average	Max
A	495	77	157.18	601
B	491	51	117.50	601
C	496	48	138.96	601
D	-	-	-	-

According to the results of the six sets of CSP[L; l_1, l_2, …, l_m], the average iterations and the number of solvable instances were compared with four initial-cutting-pattern creations as shown in Fig. 2-3.

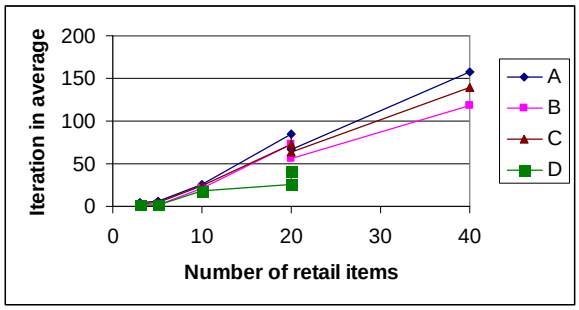

Fig. 2: Comparative the average iterations of initial-cutting-pattern creations

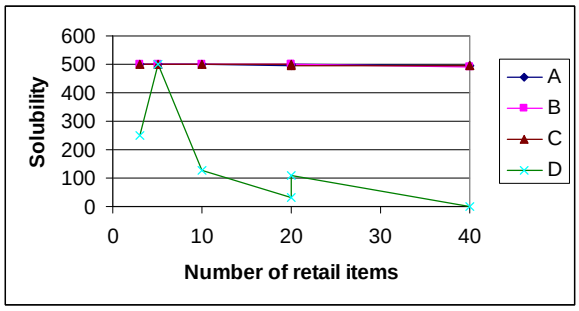

Fig. 3: Comparative the solubility of initial-cutting-pattern creations

CONCLUSION

This paper presents four initial-cutting-pattern creations (A, B, C and D) to compare the average iterations and the number of solvable instances. Consideration average iterations, the trends of A, B, and C went faster than D when the number of retail items grew larger. D could solve with the lowest average iterations. Consideration solubility, the efficiency of A, B and C seems better than D. The solubility of D was fluctuated and could not solve any instance in the CSP6.

REFERENCES

1. Dantzig, G. B. and Wolfe, P. 1961. The decomposition algorithm for linear programming. Econometrica, 29:767-778.
2. Gilmore, P. C. and Gomory, R. E. 1961. A linear programming approach to the cutting stock problem. Operations Research, 9: 849-859.
3. Gilmore, P. C. and Gomory, R. E. 1963. A linear programming approach to the cutting stock problem - Part II. Operations Research, 11: 863-888.
4. Gradišar, M., Jesenko, J., and Resinovič, G. 1997. Optimization of roll clothing in clothing industry. Computer and Operations Research, 24: 945-953.
5. Holthaus, O. 2002. Decomposition approaches for solving the integer one-dimensional cutting stock problem with different types of standard lengths. European Journal of Operation Research, 141: 295-312.
6. Scheithauer, G., Terno, J. 1995. A branch-and-bound algorithm for solving one-dimensional cutting stock problems exactly. Applications Mathematica, 23(2):151-167.
7. Stadtler, H. 1990. A one-dimensional cutting stock problem in the aluminum industry and its solution. European Journal of Operation Research, 44: 209-223.
8. Wongprakornkul, S. (2006). Heuristic Method for Solving One-Dimensional Cutting Stock Problem. TISD2006: The Technology and Innovation for Sustainable Development Conference 2006. 25-27 January, KKU, Conference Faculty of Engineering, Khon Kaen University, Khon Kaen, Thailand: 140.

Using Network Flow Diagram for Creating Mathematical Model in Planning Process

[1]Sirirat Wongprakornkul and [2]Sirikul Chansawang
[1]Department of Statistics, Faculty of Science, Khon Kaen University, 40002. THAILAND
[2]Department of Chemical and Material Engineering, Faculty of Emgineering,
Rangsit University, 12000. THAILAND

Abstract: Planning is one of four activities in continuous improvement process consist of Plan, Do, Check, and Act. For planning, there are many approaches in both quality processes and quantity processes. In this study, network flow diagram and mathematical model were raised for helping planning under the optimum situation. The objectives of this study were to present methods by using network flow analysis and mathematical model for solving the optimum solution to meet the minimum cost of table-mat-and-napkin planning and to perform the action plan of table-mat-and-napkin planning problem. For generating the mathematical model of the problem, network flow diagram was applied to display all relationships occurred in each day for planning, which eases to formulate an Integer Linear Programming Model. Although, all decision variables are integers, but the model takes an advantage for solving with relaxations as a linear programming problem. The objective function of this model was to find out the minimum cost for table-mat-and-napkin management within constrains under known demands. Excel Solver was used for the final execution. An example was generated. We found that the minimum cost was 68,178 baht per week. The total number of purchased table mats was 375 pieces and the total number of purchased napkins was 323 pieces. For laundry, the total numbers of table mats and napkins in fast cleaning were 467 and 490 pieces, respectively and the total numbers of table mats and napkins in normal cleaning were 782 and 821 pieces, respectively.

Keywords: Network Flow Analysis, Integer linear Programming, Napkin Planning

INTRODUCTION

System perspective is one of critical values to be high performance organizations. The systematic operating begins with action planning for performing efficiently and effectively. Linear programming and Integer programming are well known techniques lead into mathematical model formulation of real world problems; such as production planning problem, network flow problem, transportation problem, assignment problem, plant layout problem and etc. These techniques could solve problems within limited resources or constraints like raw materials, men, labors, machines, times, and/or energy. The quest for optimal solution, mathematical model is created with all relations constraints and objective function.

This paper raised mathematical tools; Network flow diagram and Integer linear programming, which were applied to do action planning of table-mat-and-napkin planning problem. The purposes of this action plan were to reach the minimum cost of the table-mat-and-napkin management, to meet requirements, and to know the plan to manage table-mat-and-napkin for laundry. There were four steps for solving the problem as mentioned before. First, network flow diagram was created. This step was useful to understand how napkins move in each day. Second, the mathematical model was presented by imitating the network flow diagram in step 1. Third, the model was solved for the optimal solution. And the last one, the solution was managed the napkin plan.

OBJECTIVES

1) To present methods by using network flow analysis and mathematical model for solving the optimum solution to meet the minimum cost of table-mat-and-napkin planning.

2) To perform the action plan of table-mat-and-napkin planning problem.

LITERATURE REVIEWS

Nonlinear programming problems with linear constraints [1] were formulated for planning an advertising campaign of goods and services. In this paper said that a generalization of the mathematical model and operations research problems were presented as the framework of an approach for planning.

A multi-commodity circulation minimum cost network flow model with side constraints [2] was claimed to increase productivity. It has long been recognized that productivity in manufacturing plants can often be increased by producing similar products in cells. This involves (i) assigning parts to individual machines, and (ii) forming machines into cells. These two activities have traditionally been carried out separately. However, most solution procedures for (i) above utilize a solution to (ii), and vice versa. Here we present a unified approach that deals with (i) and (ii) simultaneously.

[1]**Coressponding Author:** Sirirat Wongprakornkul, Department of Statistics, Faculty of Science, Khon Kaen University, Khon Kaen, 40002, Thailand, Tel/Fax:+(66)43-202375, Email: sirwon@kku.ac.th

Dynamic programming techniques [3] were proposed that problems of efficiently responding to a situation in a Command, Control, Communications, and Intelligence (C31) network can be investigated. An initial mode1 in the form of an integer linear program was decomposed to reveal a recurrence relation, which could then be solved using a method of successive approximations. Because the recurrence relation could not be directly realized as an algorithm, a modified problem was proposed that considers only those candidate solutions having at most some prescribed number of transmission and transform operations. Solving this for successively increasing numbers of acceptable transforms eventually yields the optimum for the original model. With the understanding that the set of all possible allocations of information to nodes of the network may be infinite, some way of ensuring eventual termination of the algorithm is required. Two possibilities for limiting the state space were explored in this paper; the modified problem can be solved for some suitably large maximal number of operations, or a known upper bound on the optimal cost can be assumed.

Mathematical modeling [4] was presented as a theoretical investigation of the influence of blood flow through a tumour-induced capillary network, whereby the vascular architecture adapts as it grows to the associated haemodynamic forces resulting in what we describe as adaptive tumour-induced angiogenesis (ATIA). The network is generated in response to tumour angiogenic factors (TAFs), which are released from hypoxic cells within a solid tumour. First, a refined model was described for tumour-induced angiogenesis, which aims to describe the capillary growth process at the cellular level by explicitly taking into account the effects of matrix degrading enzymes and the local properties of the host tissue during endothelial cell migration. Then, blood rheological properties were incorporated into the formulation and investigate the influence of wall shear stress induced by the blood flow during dynamic vascular growth. After that a number of feedback mechanisms affecting vascular resistance and network architecture were gone on to examine. The results clearly demonstrate that the combined effects of network architecture and vessel compliance should be included in future models of angiogenesis if therapy protocols and treatment efficacy are to be adequately assessed.

The optimization based heuristic approaches [5] that suggested for solving an integrated one-dimensional cutting stock-transportation problem (1DCSP&TP) was computed by decomposition principle. A 1DCSP&TP was formed into a mathematical model. Due to a One-dimensional cutting stock problem is a classical NP-hard problem which cannot be solved with the polynomial computation time. Therefore, 1DCSP&TP is an application of large scale problem. Column-Generation Technique and Bender decomposition were applied for creating all possible essential cutting patterns. After that, the proposed heuristic method was raised to solve the problem. The solution of 1D-CSP&TP is necessary for planning production and transportation strategies in the lowest cost.

METHODS

The network flow diagram of table-mat-and-napkin planning was conducted for easy generating the integer linear programming model. In this paper, this flow was performed for a week as shown in figure 1. There were two cloth types such as table mats and napkins (see also figure 2). If the numbers of existing clothes are not enough requirements, new pieces were purchased for fulfilling. In addition, existing clothes could be reused by laundry. There were two ways for laundry such as fast cleaning and normal cleaning.

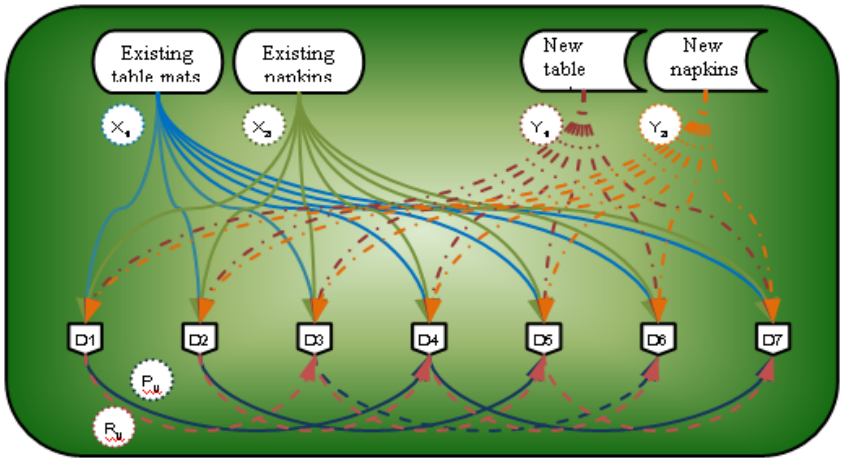

Figure 1. Network flow diagram of table-mat-and-napkin planning

Figure 2. Table mat and napkin

The diagram has been shown the movements of table mats and napkins in each day which is very useful to perform Integer linear programming. Those relationships were analyzed for forming mathematical model. The notations are categorized into 4 groups as following:

1. Specify decision variables:
   X_{ij} = Number of the existing cloth type i used in day j; where i=1 means Table Mat and i=2 means Napkin, j=1,2,…,7
   Y_{ij} = Number of purchased cloth type i used in day j
   R_{ij} = Number of fast cleaning cloth type i (within one day return) used in day j
   P_{ij} = Number of normal cleaning cloth type i (within two day return) used in day j
2. Establish objective function:
   Z = Cost of napkin management (Baht per week)
3. Constraints:
   D_{ij} = Demands of cloth type i in day j
   N_i = Total number of existing cloth type i
4. Coefficients of decision variables:
   a_i = Fast cleaning cost (baht/piece) of cloth type i
   b_i = Normal cleaning cost (baht/piece)
   c_i = Price of cloth type i (baht/piece)

The mathematical model of table-mat-and-napkin planning is as follow:

$$Min\ Z = 0\sum_i\sum_j X_{ij} + c_i\sum_i\sum_j Y_{ij} + a_i\sum_i\sum_j R_{ij} + b_i\sum_i\sum_j P_{ij}$$

Subject to

$$X_{ij} + Y_{ij} + R_{i(j-2)} + P_{i(j-1)} \geq D_{ij}, \forall i, j$$

$$X_{ij} + Y_{ij} + R_{i(j-2)} + P_{i(j-1)} - R_{ij} - P_{ij} \geq 0, \forall i, j$$

$$\sum_j X_{ij} \leq N_i, \forall i$$

$$X_{ij}, Y_{ij}, R_{ij}, P_{ij} \geq 0, \forall i, j$$

RESULTS

In this paper, all data including demands were generated as shown in figure 3. Suppose, the number of napkins was greater than the number of table mats about 5%.

DEMANDS

Table Mat : Napkin

Day 1	276	290	pieces
Day 2	204	214	pieces
Day 3	181	190	pieces
Day 4	302	317	pieces
Day 5	286	300	pieces
Day 6	568	596	pieces
Day 7	407	427	pieces

DATA

Table Mat : Napkin

Existing	600	700	pieces
Price	100	55	baht/piece
Fast cleaning	7	5	baht/piece
Normal cleaning	5	4	baht/piece

Figure 3. Data and demands for computing

All data were formed in mathematical model of this particular problem as shown in the following:

$$Min\ Z = 0\sum_i\sum_j X_{ij} + 100\sum_j Y_{1j} + 55\sum_j Y_{2j} + 7\sum_j R_{1j} + 5\sum_j R_{2j} + 5\sum_j P_{1j} + 4\sum_j P_{2j}$$

Subject to

$$X_{11} + Y_{11} \geq 276$$
$$X_{12} + Y_{12} \geq 204$$
$$X_{13} + Y_{13} + R_{11} \geq 181$$
$$X_{14} + Y_{14} + R_{12} + P_{11} \geq 302$$
$$X_{15} + Y_{15} + R_{13} + P_{12} \geq 286$$
$$X_{16} + Y_{16} + R_{14} + P_{13} \geq 568$$
$$X_{17} + Y_{17} + R_{15} + P_{14} \geq 407$$
$$\sum_j X_{1j} \leq 600$$
$$X_{11} + Y_{11} - R_{11} - P_{11} \geq 0$$
$$X_{12} + Y_{12} - R_{12} - P_{12} \geq 0$$
$$X_{13} + Y_{13} + R_{11} - R_{13} - P_{13} \geq 0$$
$$X_{14} + Y_{14} + R_{12} + P_{11} - R_{14} - P_{14} \geq 0$$
$$X_{15} + Y_{15} + R_{13} + P_{12} - R_{15} \geq 0$$
$$X_{21} + Y_{21} \geq 290$$
$$X_{22} + Y_{22} \geq 214$$
$$X_{23} + Y_{23} + R_{21} \geq 190$$
$$X_{24} + Y_{24} + R_{22} + P_{21} \geq 317$$
$$X_{25} + Y_{25} + R_{23} + P_{22} \geq 300$$
$$X_{26} + Y_{26} + R_{24} + P_{23} \geq 596$$
$$X_{27} + Y_{27} + R_{25} + P_{24} \geq 427$$
$$\sum_j X_{2j} \leq 700$$
$$X_{21} + Y_{21} - R_{21} - P_{21} \geq 0$$
$$X_{22} + Y_{22} - R_{22} - P_{22} \geq 0$$
$$X_{23} + Y_{23} + R_{21} - R_{23} - P_{23} \geq 0$$
$$X_{24} + Y_{24} + R_{22} + P_{21} - R_{24} - P_{24} \geq 0$$
$$X_{25} + Y_{25} + R_{23} + P_{22} - R_{25} \geq 0$$
$$X_{ij}, Y_{ij}, R_{ij}, P_{ij} \geq 0, \forall i, j$$

By Excel Solver of Microsoft Excel, data for assessing were prepared as shown in figure 4.

Table Mat and Napkin Planning

DEMANDS

	Table Mat	: Napkin	
Day 1	276	290	pieces
Day 2	204	214	pieces
Day 3	181	190	pieces
Day 4	302	317	pieces
Day 5	286	300	pieces
Day 6	568	596	pieces
Day 7	407	427	pieces

	Table Mat	: Napkin	
Existing	600	700	pieces
Price	100	55	baht/piece
Fast cleaning	7	5	baht/piece
Normal cleaning	5	4	baht/piece

	Table Mat	: Napkin	
Expense	44679	23499	baht

Min. Expenses= **68178** baht

Constrains

1	276	>=	276
2	204	>=	204
3	181	>=	181
4	302	>=	302
5	286	>=	286
6	568	>=	568
7	407	>=	407
8	0	>=	0
9	0	>=	0
10	0	>=	0
11	0	>=	0
12	0	>=	0
13	600	<=	600
1	290	>=	290
2	214	>=	214
3	190	>=	190
4	317	>=	317
5	300	>=	300
6	596	>=	596
7	427	>=	427
8	0	>=	0
9	0	>=	0
10	0	>=	0
11	0	>=	0
12	0	>=	0
13	700	<=	700

Existing pieces

	Table Mat	: Napkin	
Day 1	276	290	pieces
Day 2	10	81	pieces
Day 3	0	0	pieces
Day 4	26	27	pieces
Day 5	82	86	pieces
Day 6	206	216	pieces
Day 7	0	0	pieces
Total	600	700	pieces

Fast cleaning

	Table Mat	: Napkin	
Day 1	0	0	pieces
Day 2	0	0	pieces
Day 3	0	0	pieces
Day 4	181	190	pieces
Day 5	286	300	pieces
Day 6	0	0	pieces
Day 7	0	0	pieces
Total	467	490	pieces

New pieces

	Table Mat	: Napkin	
Day 1	0	0	pieces
Day 2	194	133	pieces
Day 3	181	190	pieces
Day 4	0	0	pieces
Day 5	0	0	pieces
Day 6	0	0	pieces
Day 7	0	0	pieces
Total	375	323	pieces

Normal cleaning

	Table Mat	: Napkin	
Day 1	276	290	pieces
Day 2	204	214	pieces
Day 3	181	190	pieces
Day 4	121	127	pieces
Day 5	0	0	pieces
Day 6	0	0	pieces
Day 7	0	0	pieces
Total	782	821	pieces

Figure 4. Input data window for processing

The lowest cost was 68,178 baht per week as shown in figure 4 and its network flow diagram was demonstrated in figure 5.

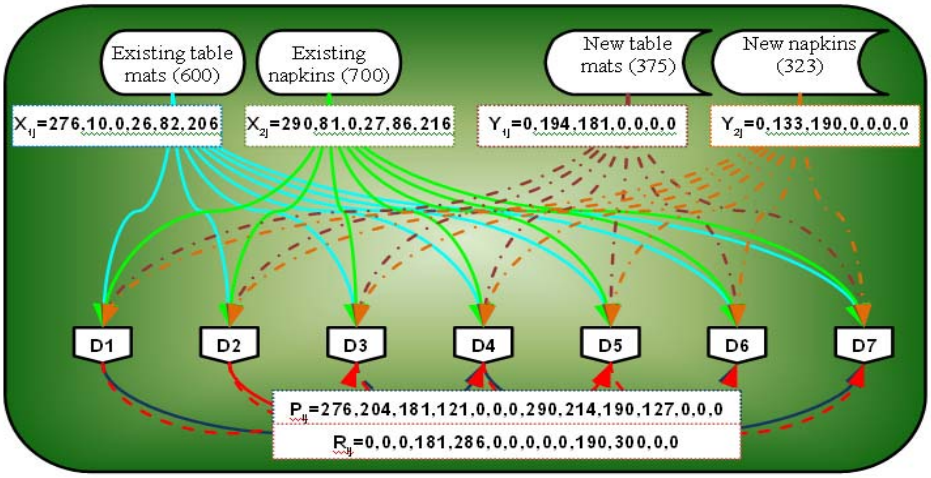

Figure 5. Network flow diagram

After the model was computed, results could clearly interpret to table-mat-and-napkin plan for one week. The total number of purchased table mats was 375 pieces and the total number of purchased napkins was 323 pieces. For laundry, the total numbers of table mats and napkins in fast cleaning were 467 and 490 pieces, respectively and the total numbers of table mats and napkins in normal cleaning were 782 and 821 pieces, respectively. For the details of how manage all table mats and napkins in each day were shown in table 1.

Table 1. Results of Integer linear programming for napkin planning in restaurant with Minimum cost = 68,178 baht

	Day	Table Mat (Pieces)	Napkin (Pieces)		Day	Table Mat (Pieces)	Napkin (Pieces)
Existing pieces (Xij)	1	276	290	Fast cleaning (Rij)	1	0	0
	2	10	81		2	0	0
	3	0	0		3	0	0
	4	26	27		4	181	190
	5	82	86		5	286	300
	6	206	216		6	0	0
	7	0	0		7	0	0
New pieces (Y_{ij})	1	0	0	Normal cleaning (Pij)	1	276	290
	2	194	133		2	204	214
	3	181	190		3	181	190
	4	0	0		4	121	127
	5	0	0		5	0	0
	6	0	0		6	0	0
	7	0	0		7	0	0

CONCLUSION

This study could find out the optimum of table-mat-and-napkin planning by creating network flow diagram to facilitate generating linear programming model. Excel Solver was then used for the optimum execution. This approach could be applied in general term. Although, this problem is an integer linear programming, it could solve as a linear programming by relaxing all variables.

REFERENCES

[1] Belenky , A. S. and Belenkii , I. 2002. Optimization of planning an advertising campaign of goods and services. **Mathematical and Computer Modeling,** Volume 35, Issue 13, pp. 1391-1403.

[2] Foulds, L. R. and Neumann, K. 2003. A network flow model of group technology. **Mathematical and Computer Modeling.** Volume38, Issues 5-6, pp. 96-123.

[3] Reid, D. J. 1999. Optimising the Flow of Information within a C31 Network. **Mathematical and Computer Modelling.** Volume30, Issues 5-6, pp. 225-243.

[4] Stéphanou, A., McDougall, S.R., Anderson, A.R.A., and Chaplain, M.A.J. 2006. Mathematical modelling of the influence of blood rheological properties upon adaptative tumour-induced angiogenesis. **Mathematical and Computer Modelling.** Volume 44, Issues 1-2, pp. 96-123.

[5] Wongprakornkul, S. and P. Charnsethikul. 2007. Optimization Based Heuristic Approaches for Solving an Integrated One-dimensional Cutting Stock-Transportation Problem. **Journal of Mathematics and Statistics** 3 (3): 142-150.

Production Rescheduling based on Stability under Uncertainty for Continuous Slab Casting

Kiatkajohn Worapradya and Thaweepat Buranathiti *
Integrated Product Design and Manufacturing Program,
School of Energy, Environment and Materials,
King Mongkut's University of Technology Thonburi, Bangkok 10140, Thailand

Abstract: Production scheduling in a multi-strand continuous casting process is complex while the need of production rescheduling frequently appears. This paper presents a production rescheduling system for a continuous slab casting process. The continuous casting process is a flexible flow shop and a bottleneck of steel production. In addition to have the job sequencing and resource allocation properly defined, the production stability due to the new schedule is also taken into account in this paper. A performance criterion and a rescheduling strategy are developed to fit the rescheduling process in a case of disruptions. Due to uncertainty in the casting process time, validated uncertainty process model and genetic algorithm (GA) are used as tools to optimize the new schedule. Optimization and simulation results indicate that under an uncertainty environment an effective schedule can be achieved by the objective function based on stability.

Keywords: Rescheduling, Robust Optimization, Continuous Casting

INTRODUCTION

Iron and steel sector is one of the most important industries due to being the upstream for manufacturing chain. Since it is capital intensive and the current production is on the mass customization focus, the productivity improvement through increasing some production lines is necessary, especially, on the continuous casting lines, which are the bottleneck. This requirement will not only raise the complexity of the production scheduling, but also that of the rescheduling. Thus, the development of the effective rescheduling methods is important.

For rescheduling, the previous researches proposed the objective function that takes the efficiency and stability into account such as Cowling *et al.*[1], which applied it for the single machine rescheduling case. Rangsaritratsamee *et al.*[2] and Pfeiffer *et al.*[3] applied it to the job shop production. Recently, this concept was also applied on the steel making-continuous casting, which is the flexible flow shop. For instances, Yan-hai *et al.* [4] proposed the rescheduling based on stability in case of rush order and Guo *et al.*[5] applied the objective function based on stability on the rescheduling of a 2 line continuous casting. However, most of above researches defined the efficiency assessment in the objective function by the tardiness or makespan, which are not enough for the scheduling in the steel making-continuous casting production as described in Tang *et al.*[6]. In addition, practically, since the uncertainty occurs on the steel making-continuous casting time, the rescheduling under uncertainty must therefore be developed.

This paper presents a production rescheduling system for a continuous slab casting process under uncertainty on the processing time. Characteristics of the process and rescheduling system will be described on the first two sections, respectively. Then the appropriate objective functions and uncertainty model will be defined. Finally, the optimal rescheduling examples will be shown in each case.

CONTINUOUS SLAB CASTING

The steel production normally consists of 3 stages: melting, refining, and continuous casting as shown in Figure 1. In the melting stage, carbon, sulphur, silicon, and other impurity contents of molten iron are reduced to desirable levels by burning with oxygen in Electric Arc Furnace (EAF). The output from this stage is molten steel with the main alloy elements is transported to a refining furnace (RF) for refining. The operation at this stage further refines the chemicals and eliminates impurities in the molten steel or adds the required alloy ingredients. After that, refined molten steel is delivered to the caster and is poured into a tundish (buffer) for casting. At mould, the molten steel continuously

Corresponding Author: Thaweepat Buranathiti, School of Energy, Environment and Materials,
King Mongkut's University of Technology Thonburi E-mail: thaweepat.bur@kmutt.ac.th

solidifies into strand at the bottom of the caster. The strand is straightened and directed toward the shear machines for cutting into steel slabs.

Normally, a furnace-load of steel is called *Heat* and a unit of production that consists of a sequence of operations on a heat is called *Charge*. A set of charges that continually casts on the same continuous caster and has a similar chemical composition is called *Cast*.

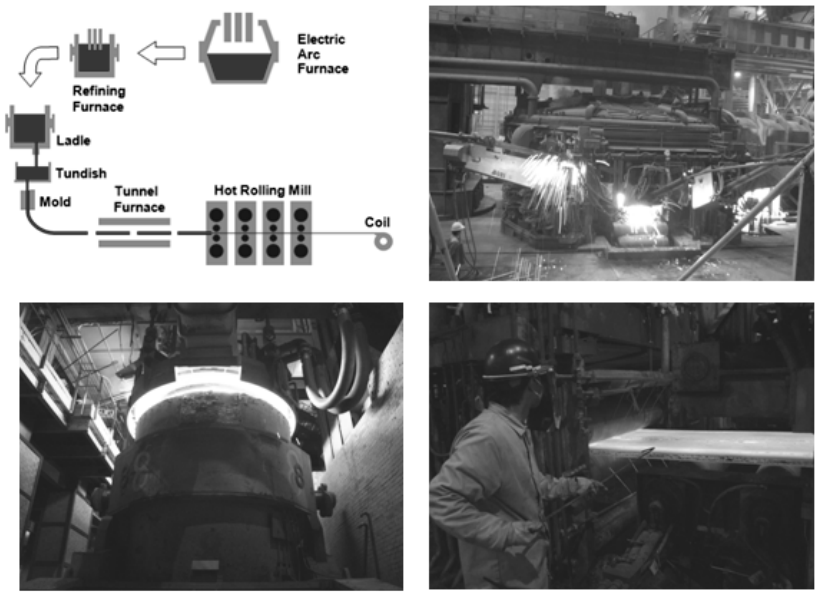

Fig. 1: Steel making and continuous casting

RESCHEDULING SYSTEM

Many manufacturing environments, including steel making industry, use an enterprise resource planning (ERP) or manufacturing execution system (MES) for medium and short term planning. With MES, real time information from the shop floor is feedback to improve the schedule as the rescheduling system in Fig 2. The optimal rescheduling decision is made based on the disruption events (such as the machine failure or rush order drive) and planned strategies. To predict the results of the designed schedule, the simulation unit, which is updated by the shop floor information, is integrated to the system.

To achieve the optimal rescheduling, 2 performance indicators; efficiency and stability, are proposed in this paper.

Efficiency Criterion

Typically, efficiency criterion for a production scheduling problem is often measured by makespan and tardiness[3], However, the efficiency criterion for the continuous slab casting mostly takes the job/group sequencing of the production order, and allocation of production and utilization of manufacturing unit into account [6]. Therefore, this work defines the efficiency criterion, which is developed from objective functions in Xue *et al*.[7] and Tang *et al*.[6] in term of the production cost as follows:

1. The loss of steel grade difference between each arranged charge. The mixed slab will be defined to the second grade product, therefore the steel grade must be the same or to be near.
2. The loss of width and thickness change. During the continuous casting, steel slab, which is out of specification from the thickness or width change, must be disposed.
3. The loss of consignment date, late of delivery leads to cost, e.g. for inventory and compensation to customers and shipping.
4. The loss of casting break and waiting time, when the casting is broken (idled), the remaining of molten steel must be re-heated or drained out. The proposed efficiency criterion is shown on Eqs. (1), (2), (3) and (4).

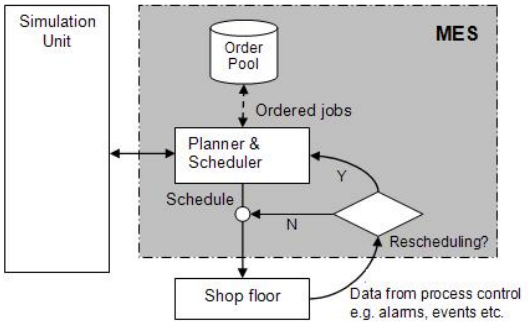

Fig. 2: Rescheduling system based on simulation

$$E = \sum_{m=1}^{M} \sum_{k \in P_m} X_k^{\,T} Q X_k \qquad (1)$$

$$Q = \begin{bmatrix} q_{11} & \Lambda & q_{1N} \\ \mathrm{M} & \mathrm{O} & \mathrm{M} \\ q_{N1} & \Lambda & q_{NN} \end{bmatrix}, \quad X_k = \begin{bmatrix} x_{1k} \\ \mathrm{M} \\ x_{Nk} \end{bmatrix}$$

$$q_{ij} = c_{ij}^{g} + c_{ij}^{w} + c_{ij}^{th} + c_{ij}^{d} + c_{ij}^{q}$$

Subjected to:

$$\sum_{j=1}^{P} x_{ij} = 1, \quad i = 1, \Lambda\ , N \qquad (2)$$

$$2 \le \sum_{i=1}^{N} x_{ij} \le L, \quad j = 1, \Lambda\ , P \qquad (3)$$

$$x_{ij} \in \{0, 1\}, i = 1, \Lambda\ , N \quad j = 1, \Lambda\ , P \qquad (4)$$

where

- M the total number of machines
- P the total number of casts
- P_m the set of casts which are processed on machine m
- N the total number of charges to be arranged
- L the maximum number of charges for a cast
- X_k decision vector of k^{th} cast, each element is the binary decision variable x_{ij} where equals 1 if charge j belongs cast i and is processed on machine m
- q_{ij} production cost matrix between charge i and j, which contains the losses as follows:
- c_{ij}^{g} loss of steel grade difference
- c_{ij}^{th} loss of thickness change
- c_{ij}^{wd} loss of width change
- c_{ij}^{cd} loss of consignment date
- c_{ij}^{cb} loss of cast break and waiting time.

All of the loss functions can be shown as follows:

$$c_{ij}^{g} = \begin{cases} 0 & \text{steel grade of charge } i \text{ and } j \text{ are equal} \\ f_1 & \text{charge } i \text{ and } j \text{ belong to the same steel grade serial} \\ \infty & \text{charge } i \text{ and } j \text{ is the difference steel grade serial} \end{cases}$$

$$c_{ij}^{wd} = \begin{cases} 0 & d_i = d_j \\ f_2 * \left| d_i - d_j \right| & \left| d_i - d_j \right| \ge \Delta D_{\max} \end{cases}$$

$$c_{ij}^{th} = \begin{cases} 0 & h_i = h_j \\ f_3 * \left| h_i - h_j \right| & \left| h_i - h_j \right| \ge 0 \end{cases}$$

$$c_{ij}^{cd} = \begin{cases} f_4 * (c_i - c_j) & c_i - c_j \ge 0 \\ f_5 * (c_j - c_i) & c_j - c_i < 0 \end{cases}$$

$$c_{ij}^{cb} = \begin{cases} f_{6\,*\,(t_i - a_i)} & t_i - a_i \ge TW_{\max} \\ \infty & t_i - a_i < 0 \end{cases}$$

- $f_1, \Lambda\ , f_6$ penalty factors
- d_i ordered slab width of charge i
- h_i ordered slab thickness of charge i
- $\Delta D_{\max}$ maximum width
- $TW_{\max}$ maximum waiting time
- c_i consignment date of charge i
- t_i start time of charge i
- T_i processing time of charge i
- a_i arrived time of caster of charge

Stability Criterion

When a new production schedule of an area is complied, the job sequence that is changed has an effect to upstream line through downstream line such as machine re-setup, rescheduling in other areas. Mostly, the effect is measured in term of stability, which is expressed by the deviation of start and/or completion of production, as explained in the works of Cowling *et al*[1], Rangsaritratsamee *et al.*[2], and Pfeiffer *et al.*[3]. To reduce the effect on upstream, this paper assume that there is available time for re-schedule of the downstream. In other words, the study on starting time deviation is used for measuring the schedule stability as expression (5); not considering on downstream line.

$$ST = \sum_{m=1}^{M} \sum_{i \in N_m} \alpha \left| t_{i,m} - t'_{i,m} \right| \quad (5)$$

where $t_{i,m}$ and $t'_{i,m}$ are the start casting process time of charge i on machine m of the old and revised schedules, respectively. α is the weighting factor and N_m is the total charges which are cast on machine m.

From above, the performance criteria for the optimal rescheduling can be defined by combining (1) and (5) as shown in (6). By using the stability factor (β), the compromise between the efficiency and stability can be performed.

$$z = \beta E + (1-\beta) ST \quad (6)$$

Rescheduling Strategies

The rescheduling strategy is to control the decision based on the disruptions for handle the remaining jobs such as decision to do nothing or reschedule, including to appropriately define the objective function parameters (in case of rescheduling is decided). Normally, the rescheduling can occur for a variety of reasons (Lee *et al.* [7]).

- A manufacturing unit goes down.
- Excessive defects occur during an operation.
- A new, high-priority order is introduced.
- An order is canceled.

However, most papers mainly focus on 2 disruptions; rush order case such as Guo and Li[5], and machine failure case, which includes shutting down to maintenance such as Guo *et al.*[8] and extending the processing time such as Akturk and Gorgulu[9]. This paper deals with both cases. The definition of the strategy is discussed later.

SIMULATION MODEL AND UNCERTAINTY

Since the stability is defined according to the upstream line, the parallel production, as shown in Figure 3, which contains the melting and refining processes, is studied by simulation. The real data from a factory, which is a single line, is used to complete the parallel line model. In this model, the uncertainty of the processing time of each process is considered as follows.

Uncertainty Analysis

- *Melting time*: Typically, the uncertainty of the processing time depended on the operator's experience and skill such as to manually control of electric input and chemical elements, and slag forming. By the actual production data of a steel factory, 1000 samples of the processing time are represented via a probability density function (PDF) as shown in Table 1
- *Refining time*: Normally, the melting and refining processes are deterministically defined with the same processing time as the melting (Bellabdaoui and Tegham[10]). However, for the uncertainty, it is similar with melting case; the experience and skill are the main reason. By the same number of data, the processing time are expressed as shown in Table 1.
- *Casting time*: Since the processing time of the continuous casting process depends on the variety factors such as slab dimension, casting speed and steel weight in ladle, it provides the different processing time at each charge as shown on equation (7). The uncertainty occurs on the steel weight, which is different in each ladle that depended on the amount of the added element during the refining process. By the same number of data, the steel weight is expressed as shown in Table 1.

$$p_i = \frac{W_{steel}}{v_i d_i h_i \rho_{steel}} \quad (7)$$

where W_{steel} is steel weight in ladle, ρ_{steel} is steel specific weight, d_i and h_i are slab width and thickness of charge i, respectively, and v_i is casting speed, which depends on steel grade and mould dimension.

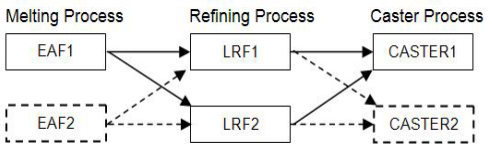

Fig. 3: An actual production line from a factory (solid line)

Table 1: Expression of the process time

Parameter	Range	Expression
Melting time	40.5-79.5	42.5 + Gamma (2.03, 10.6)
Refining time	50.5-99.5	50.5 + 49*Beta (1.4, 1.01)
Ladle weight	170-206	Norm (188, 6.18)

Validation

To validate the process model, confidence interval approach, which is described by Sagent *et al.*[11] and Buranathiti *et al.*[12], is applied. By this approach, if all corresponding experiment results are found in

confidence intervals created on PDF of the model, the model will be not considered to be invalid at the design space tested with that confidence interval. In other words, there is not enough statistical evidence to reject the null hypothesis (accepted H_0 with type I error).

To achieve the approach, Monte Carlo simulation (MCS) using the processing time in Table 1 and comparison of PDF between the simulation results and actual data. The simulation model is created on MATLAB/Simulink and 240 replications are run. The competition time is recorded and calculated confidence intervals are shown in Table 2. The results point that confidence intervals of the actual data are in 95% confidence intervals from the simulation results, thus designed model is good enough to represent the actual production.

Table 2: Monte Carlo simulation results

Data source	No. of Data	Normal distribution		Confidence interval (95%)
		$\overline{X}$	σ_x	
Melting				
Act. production	240	64.42	10.40	[44.03, 88.04]
Simulation	240	63.76	16.25	[31.91, 95.61]
Refining				
Act. production	240	128.84	23.59	[82.55, 175.10]
Simulation	240	129.05	36.05	[58.38, 199.72]
Casting				
Act. production	240	74.53	7.14	[60.51, 88.54]
Simulation	240	73.86	8.50	[57.23, 90.51]

OPTIMIZATION

Minimax Formulation

To deal with the uncertainty, the robust discrete optimization is applied in this paper. In general, it can be formulated as follows: Let X is the set of all solutions and S is the set of all possible scenarios. And $z(x,s)$ is an objective function of solution $x \in X$ in scenario $s \in S$. The problem is to find the best solution on the worst-case scenario, in other words, it is the same as minimizing (overall solutions) the maximum (overall scenarios) cost:

$$\min_{x \in X} \max_{s \in S} z(x,s) \qquad (8)$$

Genetic Algorithm

Genetic algorithm (GA) is applied for searching the robust schedule in this paper because it is widely-used and suitable for the flow shop production [13]. By the minimax problem, two loops of GA; for searching the optimal schedule structure (outer loop) and the worst scenario (inner loop), have to be performed. The result of the inner loop will be used as the fitness value of the outer loop.

For chromosome coding for rescheduling problem in this paper, the feasible solutions and scenarios are coded into the binary chromosomes in a form of $x = (X_1, \Lambda\ , X_P)$ and $s = (W_1, \Lambda\ , W_M)$, where X_i is the decision vector in equation (1) and W_i is the steel weight for casting on each machine in equation (7). By this coding, the charge grouping/sequencing is pointed by the amount and position of elements of X_i that is set to 1. Other parameters of GA and objective function, which are defined based on the actual casting cost from a factory, are shown in Table 3.

Table 3: Objective function and GA parameters

Objective function		Genetic Algorithms	
Parameters	Value	Parameters	Value
$f_1, f_2,$	600, 7.36,	Representation	Binary
$f_3, f_4,$	1612, 300,	Population size	30
f_5, f_6	300, 6.7	Max. iteration	40
N, P, L	12, 2, 4	Crossover	Single point (rate 0.8)
∞	14400	Selection	Stochastic uniform
$\Delta W_{\max}$	4 mm	Mutation	Random (rate 0.01)

RESCHEDULING

In this section, the case study of 12 charges of continuous casting is rescheduled with machine failures and rush order disruptions.

Definition of Rescheduling Strategy

To define the rescheduling strategy, the behavior of the objective function through varying the stability factor is firstly studied. For the case study in this paper, 5 replications of simulation using the mean processing time are performed and the average queue time, cast break (idle) time, efficiency, and stability are observed.

The results are normalized and shown on Figure 4. It is noted that in addition to the stability-oriented cases (low β) providing a bad efficiency, the cast break is also bad while the stability and queue time trend are decreased. By the factor trends, the strategy can be defined as follows:

- *Machine failure case*: In this situation, the processing time on some machines is extended or shut down for maintenance. In case of unchanging the schedule at the upstream line, reducing the effect to upstream line by the low stability factor is necessary. Therefore, β = 0.4, which is the compromise point between the total cast break and queue, is proper for this case study.
- *Rush order case*: In this situation, some products (charges) must be replaced by the rush orders. Since the rescheduling have to be done through the production line, the efficiency should be therefore emphasized by choosing the high stability factor. Thus, $\beta = 0.8$ is used for this case study.

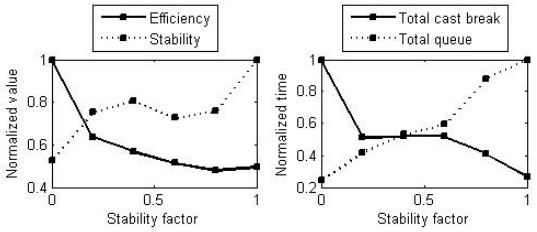

Fig. 4: Relation of the variety factors by varying β

Rescheduling: Machine failure case

Regarding the defined strategy, objective function, and parameters in Table 3, rescheduling occurs under the following conditions:

- An initial production schedule is on Table 6.
- The machine failure disruption on the caster 1 occurs while the 2nd charge is casting (and 5th change is on the caster 2). The caster 1 has to be maintained for 20 minutes, thus 3rd and 6th-12th charges will be rescheduled.
- The strategy with β=0.4 is used. The revised schedule will be compared with the revised schedule that the stability is not taken into account (β=1.0).

Results are shown on Table 4. They indicate the best worst case performance at \$17226.34 for β=0.4 and \$27772.21 for β=1.0. The revised schedules of both cases are shown in Table 7 and 8, respectively. By unchanging the charge sequence on upstream production line, the revised schedule based on stability (β=0.4) will provide less queue time because it is close to the old schedule.

After running the Monte Carlo simulation using the best worst case schedule with 200 replications, shown in Figure 6; it shows that more than 95% of the objective values are under the best worst case obtained.

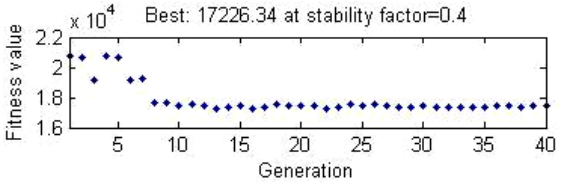

Fig. 5: Best objective value in each generation (β=0.4)

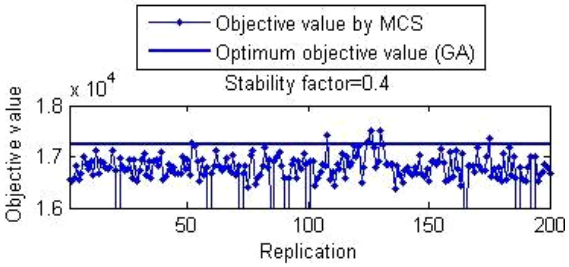

Fig. 6: Comparison of the objective value with uncertainty by MCS and the optimal objective value (β=0.4).

Table 4: Optimization results

β	Parameters				
	Queue (min)	Cast break (min)	Efficiency (\$)	Stability (\$)	z (\$)
Machine failure case					
1	246.4	118.2	27772	5309.4	27772
0.4	125.2	57.4	36220	4563.8	17226
Rush order case					
0.8	158.1	112.8	11768	4503	26297

Rescheduling: Rush order case

Under the same circumstance of the machine failure case, a planner receives a rush order disruption for a charge as shown in Table 5. Thus, the 3rd and 6th to 12th charges have to be re-arranged using the strategy *rush order case* (β =0.8). In this case, the replaced charge and optimal schedule have to be searched.

Table 5: Rush order

Consign-ment date	Grade Serial	Steel grade	Width (mm)	Thickn. (mm)	Weight (ton)
14/12/07	D011	1008MnDK-M1	1230	60	16000

The results shown in Tables 4 and Figure7 indicate that the best worst case performance is at \$26297 by replacing the 7th charge and the revised schedule is shown in Table 9. The comparison of the cost between the revised schedule and the old schedule at the worst scenario, which is \$26750 as shown in Figure 8, clearly shows that the rescheduling is a better solution (higher robustness).

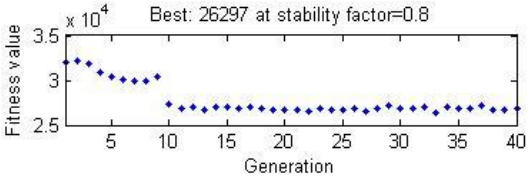

Fig. 7: Best objective value in each generation (β =0.8)

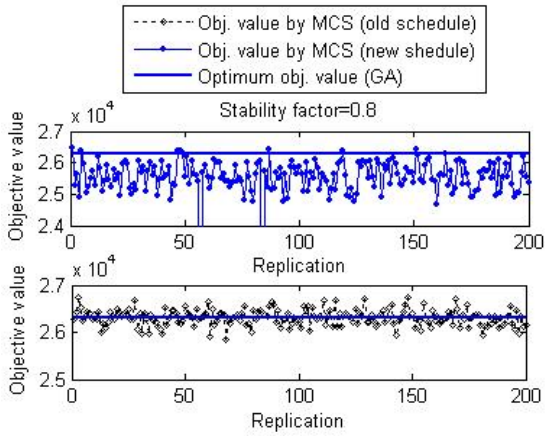

Fig.8 : Comparison of the objective values by MCS and the optimal objective value (β =0.8).

.

CONCLUSION

Suitable rescheduling for continuous slab casting can be achieved by the proposed rescheduling system and performance criterion based on stability. To perform this approach, uncertainty of the processing time was analyzed and modeled. The strategy, which is the compromise between the efficiency and stability, was defined for 2 case studies; (1) the Machine failure and (2) rush order disruptions. The problem was formulated to the minimax optimization and solved by GA with simulation. The results show that the new schedules of both cases are the best worst cases that are enough robust to the uncertainty and can provide an acceptable performance.

REFERENCES

1. Cowling, P., Johansson, M., 2002. Using real time information for effective dynamic scheduling. European Journal of Operational Research, 139: 230–244.
2. Rangsaritratsamee, R., Ferrell, W. G., Kurz, M. B., 2004. Dynamic rescheduling that simultaneously considers efficiency and stability. Computers & Industrial Engineering, 46: 1–15.
3. Pfeiffer, A, Kadar, K., Monostori, L., 2007. Stability-oriented evaluation of rescheduling strategies by using simulation. Computers in Industry, 58: 630–643.
4. Yan-hai, H., Junqi, Y., Fei-fan, Y., Jun-he, Y., 2005. Flow shop rescheduling problem under rush order. Journal of Zheiang University SCIENCE, 10: 1040-1046.
5. Guo, D., Li, T., 2007. Rescheduling algorithm for steelmaking- continuous casting. Proceeding of 2nd IEEE Conference on Industrial Electronics and Applications: 1421-1425.
6. Tang, L. X., Luh, P. B., Liu, J., Fang, L., 2000. A mathematical programming model for scheduling steel-making-continuous casting production. European Journal of Operation Research 120: 55-70.
7. Lee, H. S., Murthy, S. S., Haider, S. W., Morse, D. V., 1996. Primary production scheduling at steelmaking industries. IBM Journal of Research Development, 40: 231-352.
8. Guo, B., Nonaka, Y., 1993. Rescheduling and optimization of scheduling considering machine failures. Int. Journal of Production Economics, 60: 503-513.
9. Akturk, M. S., Gorgulu, E., 1999. Match-up scheduling under a machine breakdown. European Journal of Operation Research, 122: 81-97.
10. Bellabdaoui, A., Teghem, J., 2006. A mixed-integer linear programming model for the continuous casting planning. International Journal Production Economics, 104: 260-270.

11. Sargent, R. G., 1998. Verification and validation of simulation models. Proceeding of the Winter Simulation Conference: 121-130.
12. Buranathiti, T., Cao, J., Chen, W., Baghdasaryan, L., Xia, Z. C., 2006. Approach for model validation: methodology and illustration on a sheet metal flanging process. Journal of Manufacturing Science and Engineering 128: 588-597.
13. Reeves, C. A., 1995. A genetic algorithm for flow shop scheduling. Computers and Operation Research 22: 5-13.

Table 6: Original schedule

Cast No.	Charge No	Consign-ment date	Grade Serial	Steel grade	Width (mm)	Thickness (mm)	Weight (ton)	Caster 1	Caster 2
	1	16/12/07	D020	1008MnDK2	1272	60	14300	×	
1	2	16/12/07	D020	1008MnDK2	1258	60	14300	×	
	3	16/12/07	D020	1008MnDK2	1252	50	14300	×	
	4	16/12/07	D011	1008MnDK-M1	1230	60	16000		×
2	5	16/12/07	D011	1008MnDK-M1	1230	60	16000		×
	6	16/12/07	D013	1008MnDK-M3	1272	60	24500		×
	7	16/12/07	D013	1008MnDK-M3	1552	50	14300	×	
3	8	16/12/07	D013	1008MnDK-M3	1245	50	16000	×	
	9	16/12/07	D021	1008MnDK2	1240	60	16000	×	
	10	16/12/07	G001	1007DKGXA-00	1272	60	14300		×
4	11	16/12/07	G001	1007DKGXA-00	1255	60	19500		×
	12	16/12/07	G001	1007DKGXA-00	1275	50	24500		×

Table 7: New schedule in case of β = 0.4 (Machine failure case)

Cast No.	Charge No	Consign-ment date	Grade Serial	Steel grade	Width (mm)	Thickness (mm)	Weight (ton)	Caster 1	Caster 2
	1	16/12/07	D020	1008MnDK2	1272	60	14300	×	
1	2	16/12/07	D020	1008MnDK2	1258	60	14300	×	
	4	16/12/07	D011	1008MnDK-M1	1230	60	16000		×
2	5	16/12/07	D011	1008MnDK-M1	1230	60	16000		×
	3	16/12/07	D020	1008MnDK2	1252	50	14300	×	
3	10	16/12/07	G001	1007DKGXA-00	1272	60	14300	×	
	11	16/12/07	G001	1007DKGXA-00	1255	60	19500	×	
	6	16/12/07	D013	1008MnDK-M3	1272	60	24500		×
	7	16/12/07	D013	1008MnDK-M3	1552	50	14300		×
4	8	16/12/07	D013	1008MnDK-M3	1245	50	16000		×
	9	16/12/07	D021	1008MnDK2	1240	60	16000		×
	12	16/12/07	G001	1007DKGXA-00	1275	50	24500		×

Table 8: New schedule in case of β = 1.0 (Machine failure case)

Cast No.	Charge No	Consign-ment date	Grade Serial	Steel grade	Width (mm)	Thickness (mm)	Weight (ton)	Caster 1	Caster 2
	1	16/12/07	D020	1008MnDK2	1272	60	14300	×	
1	2	16/12/07	D020	1008MnDK2	1258	60	14300	×	
	4	16/12/07	D011	1008MnDK-M1	1230	60	16000		×
2	5	16/12/07	D011	1008MnDK-M1	1230	60	16000		×
	3	16/12/07	D020	1008MnDK2	1252	50	14300	×	
	6	16/12/07	D013	1008MnDK-M3	1272	60	24500	×	
	7	16/12/07	D013	1008MnDK-M3	1552	50	14300	×	
3	8	16/12/07	D013	1008MnDK-M3	1245	50	16000	×	
	9	16/12/07	D021	1008MnDK2	1240	60	16000	×	
4	10	16/12/07	G001	1007DKGXA-00	1272	60	14300		×
	11	16/12/07	G001	1007DKGXA-00	1255	60	19500		×
	12	16/12/07	G001	1007DKGXA-00	1275	50	24500		×

Table 9: New schedule in case of rush order

Cast No.	Charge No	Consign-ment date	Grade Serial	Steel grade	Width (mm)	Thickness (mm)	Weight (ton)	Caster 1	Caster 2
	1	16/12/07	D020	1008MnDK2	1272	60	14300	×	
1	2	16/12/07	D020	1008MnDK2	1258	60	14300	×	
	4	16/12/07	D011	1008MnDK-M1	1230	60	16000		×
2	5	16/12/07	D011	1008MnDK-M1	1230	60	16000		×
	3	16/12/07	D020	1008MnDK2	1252	50	14300	×	
3	6	16/12/07	D013	1008MnDK-M3	1272	60z	24500	×	
	8	16/12/07	D013	1008MnDK-M3	1245	50	16000	×	
	9	16/12/07	D021	1008MnDK2	1240	60	16000	×	
	7	14/12/07	D011	1008MnDK-M1	1230	60	16000		×
4	10	16/12/07	G001	1007DKGXA-00	1272	60	14300		×
	11	16/12/07	G001	1007DKGXA-00	1255	60	19500		×
	12	16/12/07	G001	1007DKGXA-00	1275	50	24500		×

A Genetic Algorithm for the Storage Location of Containers at a Seaport Terminal

[1]José Maria A. Pangilinan and [2]Gerrit K. Janssens
[1]Saint Louis University, Baguio City, Philippines
[2]Hasselt University, Diepenbeek, Belgium

Abstract: This research focuses on an improved use of the storage area by reducing the time for the yard cranes to transfer containers from the storage area to the marshalling area for loading onto the vessels. Minimizing the handling time of containers in the storage yard reduces to the problem of finding an efficient stacking strategy and a loading schedule that avoids unnecessary moves of containers in the storage yard. Two loading strategies are examined, namely LCFS and FCFS in terms of handling time in the storage area. Results show that an LCFS loading schedule is far more efficient than an FCFS schedule. A genetic algorithm (GA) is used to optimize both loading schemes. The effect of the genetic operators on the solutions are analyzed and results show that a GA with mutation as operator only is best in finding efficient solutions.

Keywords: Containers, storage location, genetic algorithm

INTRODUCTION

A container terminal serves as an interface connecting container vessels on sea with trucks on land. It provides loading and unloading services for the container carriers. On top, the terminal serves as a temporary storage space for containers between two journeys on carriers. Due to increasing container traffic, sometimes thousands of trucks pass the gates of the terminal, of which probably the surface area is relatively small. This combination requires for highly efficient handling of the operations. Efficient methods are required for assigning containers to storage areas before export, in order to reduce berthing times.

Quay cranes discharge inbound and transit containers from vessels and load outbound and transit containers to vessels. The storage yard is made up of blocks of containers. In a block, containers are stored, usually in six lanes side by side, with each lane including 20 or more container stacks. The level at which a container is stacked is called a tier. Container stacks typically have four or five tiers.

Performance indicators of a container terminal have been defined, measuring productivity, resource utilization and customer satisfaction. Two examples of performance indicators taken as objectives are: (1) to minimize the vessel berthing time, which is a service measure of the terminal, or (2) to maximize the throughput of the quay cranes, which is a productivity measure of the terminal.

The berthing time of a vessel consists of several components like waiting, berthing, unloading, loading and departing. The times spent in each of those components are related to availability of required resources. Quay cranes discharge and load the containers. Internal trucks provide transportation of containers between the quay cranes and the storage blocks. External trucks bring outbound containers into the yard and pick up inbound containers from the yard. Yard cranes handle the containers in the storage blocks. They load containers from trucks and stack them onto blocks, and retrieve containers from blocks and load them onto trucks. Decisions about the storage of containers in the yard directly affect the workload of yard cranes and the travelling distances of the internal trucks and indirectly affect the efficiency of the quay cranes.

An overall optimization model of the operational decisions in a container terminal is not easy, and maybe not feasible, because of the complexity and the multi-criteria nature of the problem. In fact, decisions are required on berth allocation, schedule and stowage plan of the vessels, quay crane allocation, storage space allocation, location assignment of containers in blocks, etc. It looks more feasible to split the overall problem into several sub-problems. This paper concentrates on the storage location of outbound containers in the yard.

This research focuses on an improved use of the storage area by reducing the time for the yard cranes to transfer containers from the storage area to the

Corresponding Author: Gerrit K. Janssens, Faculty of Applied Economics, Hasselt University, Diepenbeek, Belgium.
E-mail: gerrit.janssens@uhasselt.be

marshalling area for loading onto the vessels. The objective is to minimise the time the vessels spend at the berth. To obtain this objective the time spent transferring containers from a storage area to the vessel (i.e. the sum of set up times and travel times for all containers) needs to be minimised.

While the model may be formulated as a mixed integer linear program, its computational complexity increases exponentially with the number of containers in the schedule. A genetic algorithm is formulated as a tool to generate good solutions.

According to Dekker et al.[1], the main objectives of a stacking strategy are a) efficient use of storage space, b) efficient and timely transportation from quay to stack and further destination and vice versa, and c) avoidance of unproductive moves. The second objective can be achieved by stacking export containers close to the destination ship so that the handling time will be short. The first and third objectives contradict each other since the ideal arrangement of containers which avoids unproductive moves is to have a stack with a maximum height of one container which leads to an inefficient use of storage space.

Other issues include the manner of stacking export containers which may be according to container information such as size, weight, departure time, and destination ship among others.. In category stacking, containers of the same category are stacked together in the same yard bay or in contiguous yard bays. In the residence time strategy, a container is stacked relative to its departure time i.e. containers which leave earlier are stacked on top of containers that leave at a later time. Steenken et al.[2] present two methods, a) storage planning wherein storage space is allocated before the ship's arrival and b) scattered stacking wherein containers are assigned to a berthing place before a ship's arrival. Dekker et al.[1] states that scattered stacking results in higher yard utilization and offers a significant reduction in the number of reshuffles (unproductive moves).

A description of unproductive moves in port terminals is provided by Chen et al.[3] while Murty[4] defines an objective function of minimizing reshuffles and maps a solution which is analogous to a bin packing problem. In category stacking, weight is a useful criterion as heavy containers are usually stored deep in a ship. Kim et al.[5] derived decision rules using weight groups for determining the storage slots of arriving containers through dynamic programming. Kim and Kim[6] relate the efficiency of loading operations to a loading sequence derived from a routing solution of transfer cranes. Kim and Bae[7] describe an approach to move containers efficiently from a current layout to an ideal layout by decomposing the container problem into two stages – a bay matching problem and a sequencing problem. They propose that heuristic techniques should be developed for more efficient calculations. Kozan and Preston[8] describe the effects of loading schedules and storage utilization in minimizing turn-around time of container ships through genetic algorithms. Kim et al.[9] define a beam search algorithm to minimize handling time of transfer cranes and quay cranes for export containers. Other studies show the importance of improving space allocation methods of export containers in the management of port terminals[10,11,12].

CONTAINER LOCATION MODEL

In practice wherever possible, storage yards are grouped into two categories, import and export yard blocks. Import containers are unloaded from container ships from overseas and continue through inland transport while export containers are loaded on ships for overseas. Arrival of import containers is foreseeable but their departure is unpredictable. Because of the randomness in their departure, import containers are not stacked so high. Departure of export containers is usually connected to a ship and can be stacked more efficiently. This paper mainly addresses the problem of stacking export containers and show how loading schedules affect handling time in seaport terminals.

According to Kozan and Preston[8], the objective of the container location model (CLM) is to determine the optimal storage strategy for various handling schedules such that the containers must be stored in a manner that minimizes the amount of handling time.

Making use of the following definitions:
travelling_time is the time required to transport container *i* between the storage area, marshalling area, track area and inter-modal terminal and is defined as

$$lock + \frac{x_i RW + y_i CW}{V} + lock$$

setup_time is the time required to access the desired container i at the storage area and defined as

$$\begin{Bmatrix} z_i(4lock + 2move) + 2lock + move \\ 0 \end{Bmatrix}$$

move is the time required to move containers to an adjoining position to access containers below
CW is the length of a column of the storage area
lock is the timetime needed for the yard machinery to lock-on to a container before picking it up. This is also

assumed to be the time to unlock a container after moving it.
RW is the width of a row of the storage area
x_i is the row where container *i* is stored
y_i is column in the storage area where container *i* is stored
$z_{i,t}$ is the vertical storage position of container *i*
V is the velocity of the yard machine

They define the optimization problem as,

Minimize Max $\sum(travelling\ \_time_i + setup\ \_time_i)$
Subject to the **Constraints**

1. Only one container can be stored in a given storage position
2. A yard machine is scheduled to handle one container at a given time.
3. A container arriving at time *t*' cannot be stored under a container arriving at time *t* such that $t < t'$.

SOLUTION METHOD

Evolutionary algorithms are adaptive heuristic search algorithms based on the evolutionary ideas of natural selection and genetics. As such they represent an intelligent exploitation of a random search used to solve optimization problems. Although randomized, EAs are by no means random instead they exploit historical information to direct the search into the region of better performance within the search space. At each generation, a new set of approximations is created by the process of selecting individuals according to their level of fitness in the problem domain and breeding them together using operators borrowed from natural genetics. This process leads to the evolution of populations of individuals that are better suited to their environment than their ancestors, just as in natural adaptation.

A number of multiobjective evolutionary algorithms (MOEA) exist and Zitzler's et al. SPEA2[13] is regarded as one of the better elitist algorithms. It has three favorable characteristics. First, SPEA2 features an excellent fitness assignment strategy that accounts for an individual's strength in terms of the individuals that it dominates and the strength of its dominators. Second, SPEA2 incorporates a density estimation technique which discriminates individuals efficiently, and third, it has an archive truncation method that prevents boundary solutions from elimination. Zitzler et al.[14] provided a ready-to-use package which implements SPEA2 for multiobjective optimization problems. The public-domain package, Platform and Programming Language Independent Interface for Search Algorithms (PISA) is used to generate solutions to the container location problem.

Genetic Representation and Operators for the CLM

A chromosome or an individual consists of integer-valued elements that form a string which contains the location of a container in the storage yard. The index of each element in the string represents the ID of each container. The length of the chromosome is variable and may not be greater than the number of containers, *n*. A chromosome is randomly generated and an integer with a value less than the maximum size of the storage block is assigned to each position of the chromosome. The assignment of storage locations ensures that CLM constraints are met, e.g. a container which arrives at time *t* cannot be stacked on top of a container which arrives at time *t*+1. The fitness of an individual is computed based on handling time of containers, i.e. the sum of the *travelling_time* and *setup_time* in loading the necessary containers on a container ship. The individual which has a smaller fitness value is the better the solution. The crossover operator is an adaptation of the one-point crossover. For each pair of individuals, a locus is randomly selected from one of the chromosomes and the value of the locus is interchanged with the value of the locus in the other chromosome. Repairs are done to ensure that only one container is assigned to a single storage space and that a container does not occupy a location that is not positioned on the ground or on top of another container. In the mutation operator, a locus is randomly selected from the chromosome and the value of the locus is replaced by a new value whenever there is a vacant position in the storage block.

Fitness Evaluation and Selection

The fitness function is evaluated using SPEA2. SPEA2 first assigns a strength value $S(p)$, to each individual p from the archive ($\overline{N}$) and population (N) representing the number of solutions p dominates. Then the raw fitness $R(p)$ of each individual p is calculated which measures the strength of p's dominators. The raw fitness acts as a niching mechanism but poorly performs when most solutions in $M=N+\overline{N}$ are non-dominated, i.e. the population forms new solutions in only a few clusters, in effect compromising exploration of the search space. This phenomenon is called genetic drift.

SPEA2 introduces a density estimator, a fitness sharing mechanism to avoid genetic drift. The density

estimator is defined as the inverse of the distance of an individual in objective space to the *k*-th nearest neighbor. The density value is then added to the raw fitness value to give the final fitness function.

The selection operator in SPEA2 offers two selection procedures, environmental and mating selection. The environmental selection is concerned with choosing individuals that will have to move on to the next generation archive $\overline{P}_{t+1}$ from the current archive $\overline{P}_t$ and population P_t. SPEA2 maintains an archive $\overline{P}_t$ in each generation and is composed of the "best" individuals of a fixed size $\overline{N}$ which is equal to the population size *N*. Two usual situations may occur in selection. First, the number of non-dominated solutions in $\overline{P}_{t+1}$ is less than $\overline{N}$. SPEA2 resolves this by adding the "best" dominated individuals from $\overline{P}_t + P_t$ to $\overline{P}_{t+1}$. Second, the number of non-dominated solutions for the next generation is greater than $\overline{N}$. SPEA2 uses a truncation procedure whereby the individual with the minimum distance to another individual is truncated until $|\overline{P}_{t+1}| = \overline{N}$. SPEA2 implements binary tournament selection with replacement to fill in the mating pool. This type of mating selects two solutions at a time in each tournament. Their fitness values are evaluated and the better solution is placed in the mating pool.

RESULTS AND DISCUSSION

The experiment intends to show by comparison, the performance based on handling time of two export container loading schemes namely, LCFS and FCFS. The study also intends to evaluate the viability of a genetic algorithm in optimizing solutions generated from the standard LCFS and FCFS schedules and evaluate the effect of the genetic operators on the output such as crossover and mutation.

The experiment has the following assumptions:

1. A single yard machine is considered.
2. All containers for loading are located in one block and near the departure ship.
3. One block is composed of 5 yard bays. One yard bay contains 6 rows and is 4 tiers high.
4. All containers are loaded in only one departure ship and a maximum of 120 containers can be loaded.
5. *V*=.33 m/s, *RW*=2.4 m, *CW*=6.1 m, *lock*=60 sec, and *move*=60 sec.

Ten configurations for the storage utilization are defined, i.e. from 10% to 100% usage. For each usage configuration. Hundred instances of container arrangements are randomly generated.

Fig. 1 shows a comparison of the average handling time of both the FCFS and the LCFS loading schedule with regard to storage use from 10% to 100%. The LCFS schedule shows a linear behavior and its slope is small whereas the FCFS schedule produces a curve wherein the handling time increases dramatically as the storage use increases. The performance of the LCFS loading becomes obviously better whereas the FCFS schedule becomes worse as the utilization of the storage yard increases. This is due to the fact that the storage yard emulates a stacking structure.

The storage block in this experiment contains 120 storage spaces, i.e. six rows, 5 columns, and 4 tiers which means that one tier can accommodate 30 containers. In this context, the performance of FCFS is ideal only if the containers are placed in one tier but if the number of containers to be stored is more than 25% of the storage block capacity then the LCFS loading scheme will always perform better than the FCFS.

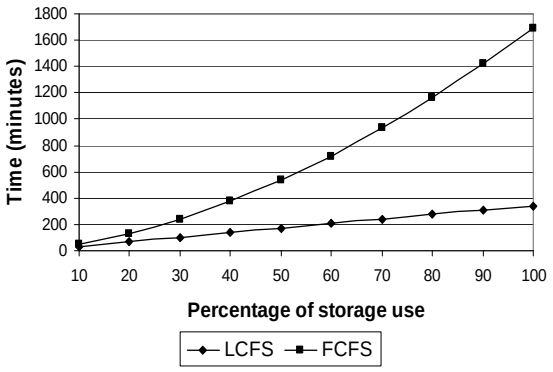

Fig. 1: Handling time. LCFS vs. FCFS

With regard to the GA, three configurations are used, a) GA with crossover only, b) GA with mutation only, and c) GA with both mutation and crossover. Each configuration is tested on both the FCFS and LCFS loading schemes. An initial population of 100 individuals was generated and run for 25 generations. Initial tests show that a generation count exceeding 25 did produce significant improvements in the solutions.

Table 1: Best solutions in an FCFS and GA-FCFS-mutation only

Storage Use (%)	FCFS (minutes)	GA-FCFS (minutes)	Difference (minutes)
10	30.44	30.44	0.00
20	84.46	83.60	0.86
30	200.2	182.19	18.01
40	326.21	318.92	7.29
50	488.66	486.94	1.72
60	676.82	670.38	6.44
70	887.26	880.40	6.86
80	1131.57	1128.13	3.44
90	1402.43	1400.72	1.71
100	1693.03	1693.03	0.00

Table 2: Best solutions in an FCFS and GA-FCFS mutation only

Storage Use (%)	LCFS (minutes)	GA-LCFS (minutes)	Difference (minutes)
10	28.29	24.43	3.86
20	62.17	56.16	6.01
30	95.61	87.88	7.73
40	130.77	120.9	9.87
50	163.79	155.63	8.16
60	198.09	188.22	9.87
70	232.39	224.24	8.15
80	267.13	260.26	6.87
90	304.43	300.14	4.29
100	343.03	343.03	0.00

Table 1 presents a comparison of the best solutions in the standard FCFS schedule and the GA-mutation-only (GA-FCFS). The mutation probability = 1.0. Table 1 shows that the GA-FCFS solutions have shorter handling times for each storage utilization configuration as compared to the results of the standard FCFS. The difference in container handling time between the FCFS and the GA-FCFS is shown in the rightmost column. There does not exist any pattern in their differences but an improvement in handling time for each configuration is obvious, particularly when the storage utilization is 30% (18 minutes improvement).

Table 2 presents a comparison of the best solutions in the standard LCFS schedule and the GA-mutation-only (GA-LCFS). Table 2 shows that the GA-LCFS solutions have shorter handling times for each storage utilization configuration as compared to the results of the standard LCFS. The difference in container handling time between the FCFS and the GA-FCFS is shown in the rightmost column. There exists similarities among the improvement of handling times from 20% utilization and 80% utilization and there is no single configuration wherein the improvement is significantly higher than the rest.

The improvements in the solutions by the GA-mutation-only mean that the mutation operator is able to explore better solutions in the search and at the same time exploit the good solutions that have been identified in previous generations.

Results (not shown) for the GA-crossover-only show no improvement in the handling time of the best solutions resulting from the standard LCFS and FCFS schemes. The GA-crossover-only generated the same solutions as the standard scheduling schemes results. This means that the crossover operator does not explore the search space and quickly converges to known solutions in the search space. In the case where the GA used both crossover and mutation, the mutation operator dictated the results in the final generation. This implies that the crossover operator has almost no effect in finding new solutions in the search space for both the FCFS and LCFS loading schemes.

CONCLUSION

This paper presents the differences in the performance of an LCFS and an FCFS loading schedule according to the duration of their container handling time and storage yard utilization. Results show that an LCFS loading schedule is superior to an FCFS loading schedule particularly when the storage utilization is higher than 25%. The employment of a GA in both FCFS and LCFS schedules show improvement in their handling times but the GA-based solutions are not necessarily optimal solutions. The crossover operator quickly converges to known solutions and has almost no effect in generating new solutions. The mutation operator on the other hand greatly affects the exploration and exploitation of new and better solutions in the search space with regard to finding shorter handling times for the container location model.

REFERENCES

1. Dekker, R., P.Voogd, and E. van Asperen, 2006. Advanced methods in container stacking. OR Spectrum, 28:563-586.
2. Steenken, D., S. Vob, and R. Stahlbock , 2004. Container terminal operation and operations research – a classification and literature review. OR Spectrum, 26:3-49.
3. Chen, T., 1999. Yard operations in the container terminal-a study in the 'unproductive moves'. Maritime Policy and Management, 26:27-38.
4. Murty, K. G., J. Liu, Y. Wan, and R. Linn, 2005. A decision support system for operations in a container terminal. Decision Support Systems, 39:309-332.
5. Kim, K.H., Y.M. Park, and K.R. Ryu, 2000. Deriving decision rules to locate export containers in container yards. European Journal of Operational Research 124:89-101.
6. Kim, K.H., and K.Y. Kim, 1999. An optimal routing algorithm for a transfer crane in port container terminals. Transportation Science, 33:17-33.
7. Kim, K.H., and J.W. Bae, 1998. Re-marshalling export containers in port container terminals. Computers and Industrial Engineering, 35:665-658.
8. Kozan, E. and P. Preston, 2001. An approach to determine storage locations of containers at seaport terminals. Computers & Operations Research, 28:983-995.
9. Kim, K.H., J.S. Kang, and K.R. Ryu, 2004. A beam search algorithm for the load sequencing of outbound containers in port container terminals. OR Spectrum 26:93-116
10. Kim, K.H. and K. Park, 2003. A note on a dynamic space-allocation method for outbound containers. European Journal of Operational Research, 148:92-101.
11. Zhang, C., J. Liu, Y. Wan, K. Murty, and R. Linn, 2003. Storage space allocation in container terminals. Transportation Research Part B, 37:883-903
12. Chen, P., Z. Fu, A. Lim, and B. Rodrigues, 2004. Port yard storage optimization. IEEE Transactions on Automated Science and Engineering, 1:26-37.
13. Zitzler , E., M. Laumanns, and L. Thiele, 2002. SPEA2: improving the strength Pareto evolutionary algorithm for multiobjective optimization. Evolutionary Methods for Design, Optimization and Control, CIMNE, Barcelona. pp. 19-26.
14. Zitzler , E., S. Bleuler, M. Laumanns, and L. Thiele, 2003. PISA-a platform and programming language independent interface for search algorithms. Swiss Federal Institute of Technology, Tech Rep. TIK No. 154.

The Solution Space Reduction Using Frequency Domain of Simulated Annealing

Watha Minsan and Pornthep Anussornnitisarn*
Department of Industrial Engineering
Faculty of Engineering Kasetsart University, Thailand
*E-Mail: fengpta@ku.ac.th

Abstract: The objective of this research is used frequency domain for factor screening while simulated annealing method searches for an optimum. Each iteration of simulated annealing, we consider as two problems, primal and shadow problem. Primal problem runs the conventional simulated annealing. On the other hand, a model using input variables that oscillate at different frequencies during a run which called "Shadow Problem". It is indicated by the frequency spectrum of the output variable where run lenght (denoted by) is large enough. For shadow problem, If the output variable is sensitive to changes in a particular input variable, then oscillating of this input variable induces oscillations in the output variable. The after factor screening, the only remaining important input variables will run continuously on the simulated annealing for solving the primal problem. However, the unimportant input variables are assigned to be constant values from the best values of the simulated annealing of the primal problem. We found that the frequency domain of simulated annealing requires quite fewer iterations than conventional simulated annealing. We describe the method, illustrate a nonlinear problem effectiveness at identifying important main effects, two-way interaction, and quadratic term of known model.

Key words: Simulation Optimization, Frequency Domain Experiment, Factor Screening

INTRODUCTION

The Simulated Annealing (SA) is designed to enhance the likelihood of avoiding local minima en route to global minimum of problem. This technique uses magnitudes of random perturbations as reduced-annealed in a controlled manner. Wherever the injected randomness helps prevent convergence to a local minimum by providing a greater "jumpiness" to the algorithm[1]. However, the interpretation of large amounts of input factors can become an intimidating task.

Factor screening is useful when there are many input factors that affect potentially a simulation output or an output variable. However, we believes that relatively less factors and/or interactions provide an adequate function of the system's behavior. An experiment run the model several times. For example, 2^k (or more) prospective configurations as called 2^k factorial design, where k is amount of input factors in problem function.

For quantitative factors, response surface metamodel is applied and analyzed by regression techniques. The techniques just described all have a run-oriented approach. Run-oriented approaches work well for few input-factors problem. For example, a full factorial experiment involving 5 factors requires 32 runs[2]. As we interest in 20 input-factors, then a factorial experiment involving all these factors would requires 1,048,576 runs. For more precise experiment, 3^k factorial is used, it requires over 3,486,784,401 runs. Unfortunately, response surface methodology requires a large number of simulation runs and is supported by very restrictive assumptions on system's behavior[3]. It is not a good technique for factor screening before run the simulated annealing to optimize a large problem as we interest.

An alternative simulation factor screening method, Schruben and Cogliano (1987) introduced Frequency Domain Methodology for screening many factors only few computer runs[4]. A frequency domain method for factor screening is a simulation model. It is a run with input factors that are varied during a run according to sinusoidal oscillations. Different frequencies during a run are assigned for each factor. Whenever the simulation response is sensitive to changes in a particular factor, then oscillating of this factor induces oscillations in the response. The frequency domain experiment permits one to identify an appropriate polynomial model for simulation output. The frequency domain simulation experiments typically will require 2-3 runs for factor screening.

In this paper, we demonstrate how the methodology called Frequency Domain Experimentation (FDE) can screen input factors during the SA run. The proposed technique will reduce a solution space and number iterations of SA.

Corresponding Author: Watha Minsan Department of Industrial Engineering Faculty of Engineering Kasetsart University, Thailand

METHODS

Simulated Annealing Algorithm:

The SA algorithm is based on the analogy between the simulation of the annealing of solids and the problem of solving large combinatorial optimization problems. For this reason the algorithm became known as "Simulated Annealing"[5]. Its algorithm is shown as below

Line 1: Start
Line 2: Select an initial solution X_i;
Line 3: Select an initial temperature $t_0 > 0$;
Line 4: Select a temperature reduction function α;
Line 5: Repeat
Line 6: Repeat
Line 7: Randomly select $X \in N(X_0)$;
Line 8: $\Delta = f(X) - f(X_0)$;
Line 8: If $\Delta < 0$ then $X_0 = X$;
Line 9: Else
Line 10: Generate random r uniformly in range (0, 1);
Line 11: If $r < P_{accept}$ then $X_0 = X$;
Line 12: Endif
Line 13: Endif
Line 14: Until iteration_count = n_repeat;
Line 15: Set $t = \alpha(t)$;
Line 16: Until stopping condition = true
Line 17: End.

Where

X is set of input factors

P_{accept} is probability to accept for energy change

n_repeat is cooling schedule

$\alpha(t)$ is temperature reduction function.

Frequency Domain Experiment Algorithm:

Frequency domain experiment assumes the expected output of a simulation model, which is modeled over an experimental region by a p-order polynomial given by

$$E(Y) = \beta_0 + \beta_1\tau_1 + \beta_2\tau_2 + ... + \beta_q\tau_q, \quad (1)$$

Where

$E(Y)$ is the expected output

τ_j is a term in the p-order polynomial and is a particular product of the nonnegative integer powers of the input factors $X_j, j \in (1, 2, ..., K)$ where the sum of the exponents is not greater than p (e.g., if $p = 5$, $X_1^2X_2^4$ is not a term)

β is the coefficient of the τ term

q is the number of potential terms; and

X is input factors $X_1, X_2, ..., X_k$.

The equation (1) describes a static relationship between the expected output and configuration of input factors. For frequency domain experiment, this relationship is obtained through static experiments. For each static experiment, the input factors are varied at specific values in the region of each input factors and $E(Y)$ is estimated. This process is not repeated unnecessarily in the experiment.

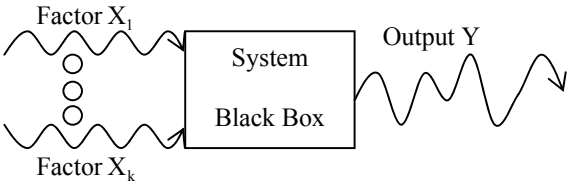

Fig. 1 Frequency Domain Experiment in the Black Box.

Fig. 1, if we view the inputs and outputs of the simulation runs as time series (t) rather than constant values, we can then oscillate the input factors during the simulation run. For each input factor affects the system performance, then the output time series will oscillate at a related driving frequency. Alternatively, for each input factor does not affect performance, then the 'black box' will not transmit the oscillation at a related driving frequency through to the output time series[2].

For the frequency domain factor screening technique, the input factor level setting for each factor $X_j, j \in (1, 2, ..., K)$, (and k is the number of input factors), is varied according to:

$$X_j(t) = X_j(0) + a_j \cos(2\pi\omega_j t). \quad (2)$$

Here,

$t = 0, 1, ..., N-1$, where N is the total number of observations generated by the simulation runs, which is based on time series.

$X_j(0)$ is $0.5(U_j + L_j)$ are the nominal value of factor X_j in time 0, U_j is upper bound of factor X_j and L_j is lower bound of factor X_j

a_j is $0.5(U_j - L_j)$ are the amplitude of the factor X_j

ω_j is the unique driving frequency for factor X_j [6].

It is important to note that equation (2) describes an input factor that oscillates at different frequencies during a run.

After run experiment, we analyze the output $Y(t)$ by using spectral analysis.

Frequency Domain of Simulated Annealing:

We have developed a new technique based on a conventional SA method which is applied a frequency domain experiment for reducing a solution space during the SA run for optimization. This technique is a simulated annealing-based simulation optimization method developed to improve the performance of simulated annealing for continuous variable simulation optimization.

We adapte a simulated annealing algorithm by adding a few commands to collect observations of $Y(t)$ for transforming the time domain into frequency domain and then analyze its spectral frequency. The command are given by

$$X_0^{shadow} = X_0 + a\cos(2\pi\omega_j t), \qquad (3)$$

Where

X_0 is set of new input factor values from SA

$a\cos(2\pi\omega_j t)$ is set of term of frequency domain experiment method

And

$$Y^{shadow}(t) = f(X_0^{shadow}), \qquad (4)$$

Where

$f(X_0^{shadow})$ is the output response of function assign to $Y^{shadow}(t)$

t is a iteration_count.

Equation (3) and (4) is added to SA algorithm before line 14, respectively. For equation (4), it is called is "Shadow Problem". Whenever we run lengths of simulation run (denoted by n) large enough to include at least 10 full cycles of the lowest term indicator frequency. The larger the value of n, the smaller the variance of the spectral estimators[4]. The run lengths of SA can be made typically large iterations, but experimental cost for run increase very little margin. For example, we run lengths 2^{15} observations of $Y(t)$.

Last added command is a command to analyze spectral frequency of shadow problem. There is given by

```
If iteration_count = n_check then
    f(ω) = fft(Y^shadow);
    Check Y′
    If X are unimportant inputs then reduce set of X
    Endif
Endif
```

Were

n_check is the maximum run lengths (n)

fft is the fast Fourier transform

$f(\varpi)$ is the spectral term of Y^{shadow}.

The previous command is added after the equation (4). Shadow problem is indicated by the frequency spectrum of $Y^{shadow}(t)$, if the output variable is sensitive to changes in a particular input variable, then oscillating of this input variable induces oscillations in the output variable. The only remaining important input variables will run continuously on the SA and unimportant input variables are assigned to be constant from the best values of the simulated annealing of the primal problem. Then we obtain a smaller set of input variables for solving the SA of the primal problem next.

EXPERIMENT

Suppose that we interest in twenty input factors. A black box system is given as follow

$$\begin{aligned} Y(t) = &-4X_1^2 + 25X_2^2 + 50X_3^2 + 100X_4 + 75X_5 \\ &- 50X_6 - 25X_7 + X_8 + X_9 + X_{10} + X_{11} \\ &+ X_{12} + X_{13} + X_{14} + X_{15} + X_{16} + X_{17} \\ &+ X_{18} - X_{19} - X_{20}. \end{aligned}$$

The following steps summarize the frequency domain of SA procedure

Step 1: Our performance measure is the simulation out put, Y.

Step 2: Twenty input factors will be oscillated during the SA runs to assess their impact on Y.

Step 3: The twenty input factors were oscillated at unique frequencies of $310/2^{15}$, $598/2^{15}$, $763/2^{15}$, $825/2^{15}$, $846/2^{15}$, $949/2^{15}$, $1321/2^{15}$, $2063/2^{15}$, $3054/2^{15}$, $3446/2^{15}$, $4024/2^{15}$, $5303/2^{15}$, $6005/2^{15}$, $6789/2^{15}$, $7882/2^{15}$, $9223/2^{15}$, $11039/2^{15}$, $12546/2^{15}$, $14547/2^{15}$ and $14588/2^{15}$ cycles per time unit, respectively. Results of primary indicator frequencies are the driving frequencies for main effects. Indicator frequencies for quadratic effects are $620/2^{15}$, $1196/2^{15}$, $1526/2^{15}$, $1650/2^{15}$, $1692/2^{15}$, $1898/2^{15}$, $2642/2^{15}$, $4126/2^{15}$, $6108/2^{15}$, $6892/2^{15}$, $8048/2^{15}$, $10606/2^{15}$, $12010/2^{15}$, $13578/2^{15}$, $15764/2^{15}$, $14322/2^{15}$, $10690/2^{15}$, $7676/2^{15}$, $3674/2^{15}$ and $3592/2^{15}$ cycles per time unit, respectively[6].

Step 4: The run length is 2^{15}.

Step 5: We use MATLAB program to compute this experiment.

Figure 2 illustrated the total spectrum of main effect and quadratic effect altogether in each input factors to analyze the whole picture of each factors. We found that input factor X_3 had the highest influence followed by X_1, X_2, X_4, X_5, X_6 and X_7 respectively.

These factors had high influence towards the response variable $Y(t)$, when considered with indicated our problem which correlated. This meant that this factor screening method was work well.

RESULTS AND DISCUSSION

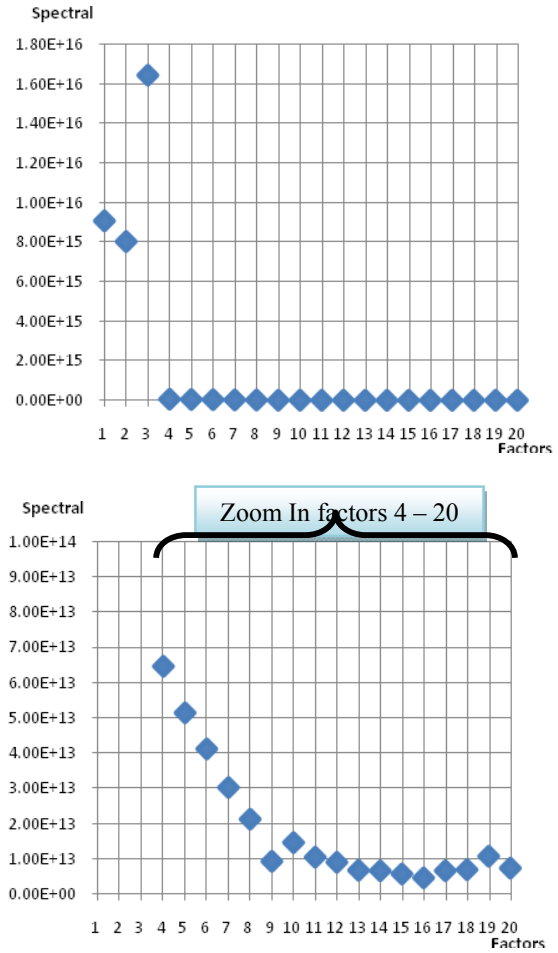

Fig 2. Spectral term of 20 factors with $n = 2^{15}$

We could organize the order of the input factors which had influence towards the response variable $Y(t)$ according to the experiment as follows;

$X_3, X_1, X_2, X_4, X_5, X_6, X_7, X_8, X_{10}, X_{19}, X_{11}, X_9, X_{12}$ $X_{20}, X_{18}, X_{13}, X_{17}, X_{14}, X_{15}$, and X_{16} respectively.

From table 1, we determined the reduction of input factors by creating policies. The identified policies were 10 policies altogether. The first policy did not require decreasing in the numbers of input factors. The second policy would like to decrease in the numbers of input factors used in the system by 10%. The third policy to the tenth policy would like to decrease in the number of input factors used in the system by 20% to until 90% respectively. Therefore, creating policies for input factors was convenient to solve a problem in operation management. The fewer input factors would also result in less confusion.

From the result, SA took 8,743,314 iterations to find the solution when compared with frequency domain of SA with each policy; we found that the numbers of iterations spent were fewer. When we determined to find the answer from input factors 90% (the number of input factor 10% were not applied) we received 2 variables that would not be used which were X_{15} and X_{16} respectively (considered from input factors ordering). This policy applied the numbers of iterations in searching the answers 7,554,054 iterations which were decreased about 1 million iterations from the previous one. When we determined to decrease the numbers of input factors continuously, it was found that the numbers of iterations were also decreased. At the 10th policy, the numbers of input factors were at 10% (the number of input factor 90% were not applied), the numbers of iterations spent were only 38,900 rounds.

From the indicated statement problem, although the decrease in number of the variables, the effects to the answer when compare to global optimization there was only a few percentage different. From table 1, you will see that although we reduced the number of input factors down to 10%. The answer was different from global optimization only around 18%. However, the effects towards the answer would vary amongst each problem statements, a researcher should consider carefully the number of input factors to be decreased by considering spectrum graph of frequency domain according to figure 2.

From figure 4, we test running on 4 computers with different CPU applying the same seed. We found that computers with many cores were faster than one core computers. However, no matter types of computer used for input factors of 20 variables would spend so much time. The best computer still took more than 1 hour for computing the answer of this statement problem, but if the numbers of input factors were reduced to 10%, it would take only less than 1 minute.

CONCLUSION

We have shown that heuristic and factor screening could be able to implement at the same time by not taking more time in processing process. Our aim was to encourage researchers and practitioners applied this technique in operation management or other related fields. For example, in an industrial plant, the numbers of relevant factors might be high so it might be difficult to find a suitable set up for the mechanic. The decrease in variables would be benefit and convenient.

However, frequency domain experiment was not widely used as most of researchers and practitioners could not foresee a benefit of changing from time domain to frequency domain which normally would be complicated. We would like to show that frequency domain was not that complicated and at present there

were a lot of equipment to help transform to frequency domain. In this research, we used MATLAB to transform with function Fast Fourier Transform (fft) which the numbers of data 2^{15} took only 2 seconds.

Our next research will be an experiment on factor screening by other methods such as Genetic Algorithm or Tabu Search considering discrete event input factors in the problem statement as well.

Table 1 Optimization results: identification of policy

Policy	Minimum Objective value	Difference from Global Optimum solution		Number of Iterations
		% Diff.	Value Diff.	
Simulated Annealing	-4,000,263,000,000.00	1.000000E+02	-609.22	8,743,314.00
Policy 1 (not reduced)	-4,000,262,999,390.78	1.000000E+02	-609.22	8,005,826.00
Policy 2 (18 Vars.)	-4,000,262,999,390.78	9.999995E+01	-1,897,417.57	7,544,054.00
Policy 3 (16 Vars.)	-4,000,261,102,582.43	9.999989E+01	-4,271,096.99	5,287,136.00
Policy 4 (14 Vars.)	-4,000,258,728,903.01	9.999984E+01	-6,313,741.32	5,271,654.00
Policy 5 (12 Vars.)	-4,000,256,686,258.68	9.999979E+01	-8,422,887.43	5,191,734.00
Policy 6 (10 Vars.)	-4,000,254,577,112.57	9.999973E+01	-10,746,468.91	3,229,100.00
Policy 7 (8 Vars.)	-4,000,252,253,531.09	9.999969E+01	-12,561,330.94	1,979,650.00
Policy 8 (6 Vars.)	-4,000,250,438,669.06	9.999942E+01	-23,059,832.47	3,534,780.00
Policy 9 (4 Vars.)	-4,000,239,940,167.53	9.999570E+01	-171,888,932.31	1,034,363.00
Policy 10 (2 Vars.)	-4,000,091,111,067.69	8.263402E+01	-694,685,069,336.95	38,900.00

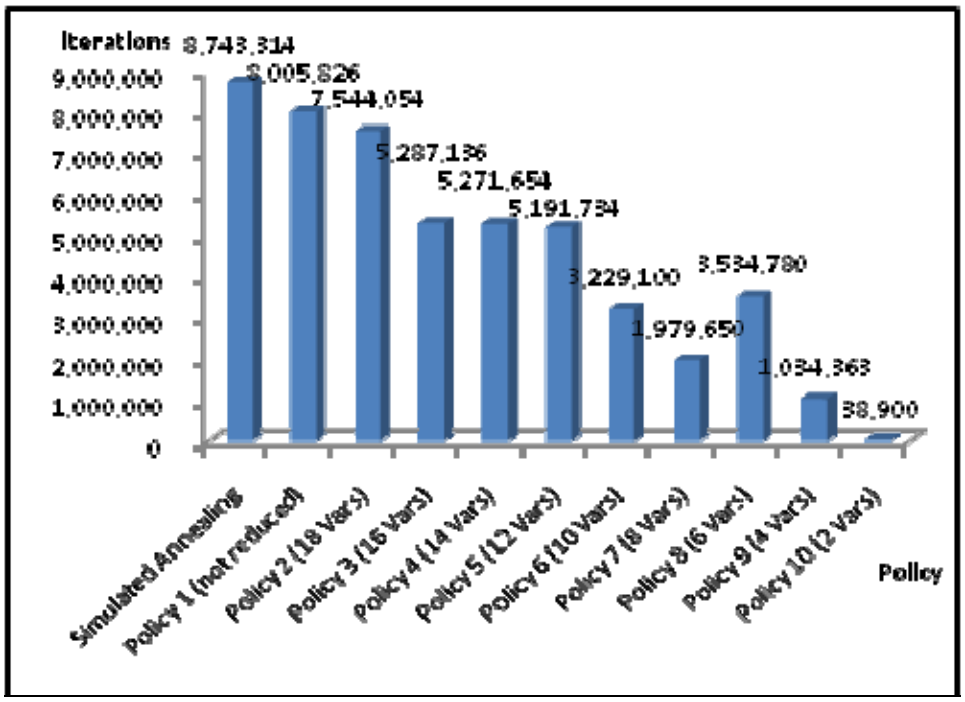

Fig 3. Iteration results: identification of policy

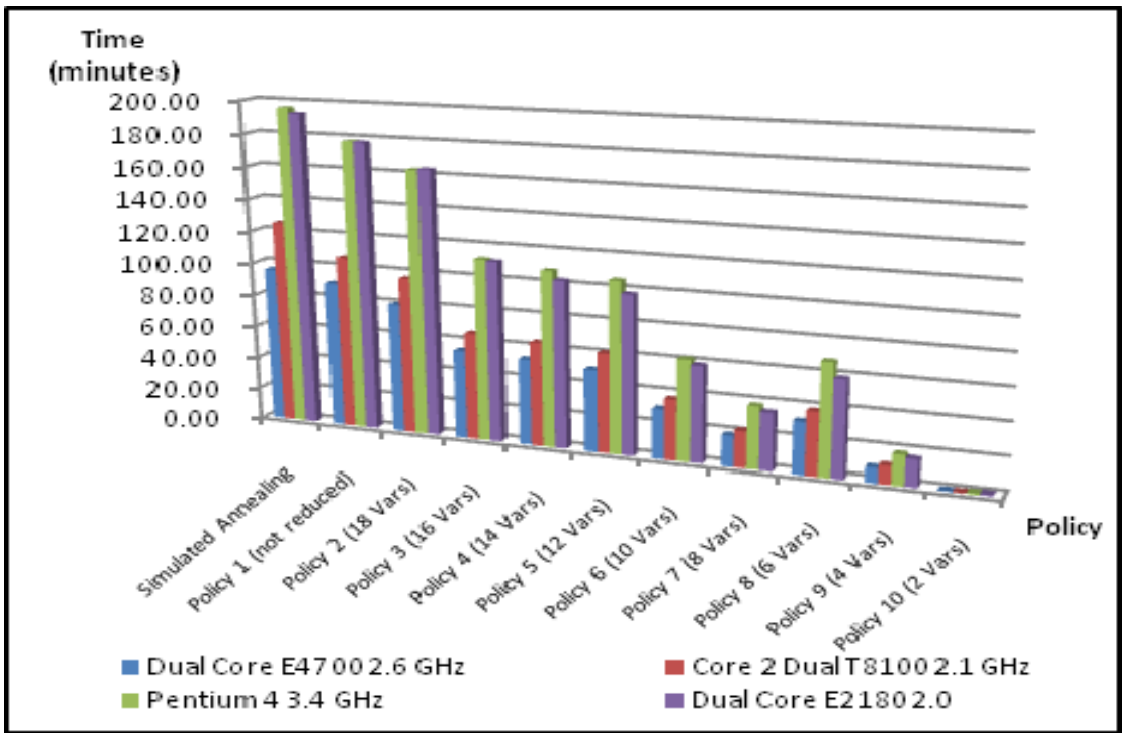

Fig 4. Time to run optimization by same seed: CPU benchmarks

REFERENCES

1. James C. Spall (2003). *Introduction to stochastic search and optimization: estimation, simulation, and control.* Wiley, New Jersey.
2. Susan M. Sanchez , Farhad Moeeni and Paul J. Sanchez (2006)., *So many factors, so little time… Simulation experiments in the frequency domain*, Science Direct , Int. J. Production Economics 103, 149-165.
3. Douglas J. Morrice (1989). *Simulation sensitivity analysis using frequency domain experiments.* Proceedings of the 1989 Winter Simulation Conference.
4. Schruben, L. W. And V. J. Cogliano (1987). *An Experimental Procedure for Simulation Response Surface Model Identification. Commu. Association for Computing Machinery, 30, 716-730.*
5. P. J. M. van Laarhoven and E. H. L. Aarts (1987). *Simulated Annealing Theory and Applications*. Springer.
6. Jacobson, S., A. Buss and L. Schruben (1991). *Driving Frequency Selection for Frequency Domain Simulation Experiments.* Operations Research, 39(6), 917-924.

Comparing the Solutions for a Vehicle Routing Problem with Uncertain Travel Times by Traffic Simulation

Tharinee Manisri and Anan Mungwattana
Department of Industrial Engineering, Kasetsart University,
50 Phahon Yothin Rd. Chatuchak Bangkok 10900, Thailand

Abstract: The main objective of this paper is to find a robust solution of a vehicle routing problem (VRP) that minimizes (over all solutions) the maximum (over all scenarios) of a performance measure. This VRP model reflects the intrinsic difficulties to estimate travel times exactly in reality such as traffic conditions, accidents, traffic jams or weather conditions. Accordingly, the critical element of this paper is the uncertainty model. Traffic simulation has been chosen as a tool to study the system behavior and used to evaluate the effectiveness of the VRP solution. We use the hybrid algorithm to find the robust solution with a scenario-based approach. 16 instances occur in the experiments. Each set of problem instances can be denote by the percentage of uncertainty, β equals 0.2, 0.4, 0.6 and 1.0 of the based-case travel times. The number of scenarios generate randomly by uniform distribution of interval travel times, thus equal to 10, 20, 40 and 80 instances for each problem set. The simulation compares three approaches: the scenario-based approach, the worst-case performance approach and the expected-value approach in the relative ratio performance measure. The results clearly show that the scenario-based approach is potential and strongly against perturbation of traffic conditions.

Key words: Vehicle routing problem, robust approach, traffic simulation, uncertainty

INTRODUCTION

The vehicle routing problem (VRP) is defined as the problem of routing a fleet of vehicles from a depot to service a set of customers that are geographically dispersed. This type of problem becomes complex when travel times are uncertain. Therefore, there is a need to develop routing and scheduling tools that account directly for the uncertainty. Recently, researchers have begun to study such problems and to develop approaches for finding robust solutions which have the best worst-case performance over a set of possible scenarios. Kouvelis and Yu [1] discuss approaches for handling uncertainty and they review robust discrete optimization problems and a wide variety of their applications.

This paper proposes a hybrid algorithm including a modified push-forward insertion heuristic (MPFIH) and a λ-interchange local search descent method (λ-LSD) by using tabu search (TS). This algorithm is a meta-heuristic technique for solving "the minimax optimization problems", which is the same as minimizing (over all solutions) the maximum (over all scenarios) performance. It's objective is to find a robust route that minimizes the worst-case value over all data sets of uncertainty. The traditional approaches for handling uncertainty in decision making have been divided conventionally into three categories: the deterministic optimization approach, the stochastic optimization approach and the robust optimization approach. A major weakness of the deterministic approach is its inability to recognize the presence of plausible data instances other than the "most likely" one used to generate the "optimal" decision. The stochastic optimization approach does recognize the presence of multiple data instances that might be potentially realized in the future. However, the failure of either stochastic or deterministic optimization approaches is their inability to recognize every decision. It is a whole distribution of outcomes depending on which data scenario is actually realized. Thus any approach that evaluates decisions using only a single data scenario, either the best solution has been selected in the expected outcome.

In our aspect, decision makers in a decision environment with significant uncertainty, want a robust decision, one that performs well across all scenarios. It hedges against the worst of all possible scenarios while the probability of data is unknown exactly. We use a scenario-based approach, structuring uncertainty that it is part of the robust approach, requiring executives to participate in the generation and evaluation processes for all scenarios.

In a transportation network, the feasible connecting routes from one point in the city to another might not change over a short term planning horizon. However, in determining a robust vehicle routing with significant uncertainty in traffic conditions, the decision maker has to deal with uncertainty in the travel times that are assigned to each arc of the network. Thus, the scenario construction includes the objective function coefficient, but it does not affect the constraint set. Experimental

Corresponding Author: Tharinee Manisri, Department of Industrial Engineering, Kasetsart University, 50 Phahol Yothin Rd. Chatuchak Bangkok 10900, Thailand

results show that the hybrid algorithm with the scenario-based approach can provide robust solutions. Then the traffic simulation is utilized to evaluate the effectiveness of the proposes. We simulate an instance of a travel time by generating random elements from a uniform distribution and use them to evaluate the solutions under the relative robust criteria. This relative performance measure is compared the scenario-based approach, worst-case scenario approach and the expected-value approach.

The rest of this paper is organized as follows: The literature review focuses on literature which is relevant to the vehicle routing problem with uncertain travel times. The problem formulation and the method section explain how the problem is formulated and solved. The simulation study section presents the results and discussion from the experimental results. Finally, conclusions and future work are explained in the last section.

LITERATURE REVIEW

In this section, we review well-known problems in the literature which are relevant to our problem at hand. The first paragraph introduces the general VRP problem and the next one introduces briefly the approaches for handling the uncertainty. Finally, we review the applications of the robust discrete optimization problem.

The VRP arises in a retail distribution such as a school bus routing, a mail and newspaper delivery, a municipal waste collection, a fuel oil delivery, a dial-a-ride service, an airline and railway fleet routing and a scheduling. The VRP is defined on a given graph $G = (V, A)$, where $V = \{\upsilon_1, \upsilon_2, ..., \upsilon_n\}$ is a set of vertices and $A \subseteq \{(\upsilon_i, \upsilon_j) : i \neq j, \upsilon_i, \upsilon_j \in V\}$ is the arcs set. An optimal set of routes is composed by cyclic linkage of arcs. The routes have provided to start and end at a depot that can serve a demand for a given set of customers at each vertex[2]. The classical VRP is described in Osman [3], Laporte[4], Fisher[5], and Bodin et al.[6] for more details. The VRP represents a hard combinatorial problem which, in practice, in usually solved by heuristic and meta-heuristic methods.

Since the VRP is NP-hard, which is a problem becomes even more complex when uncertainty occurs. It is hard to find an algorithm which would work satisfactorily for a wide range of problems. A field of decision-making under uncertainty was pioneered in the 1950s by Dantzig[7] along with Charnes and Cooper[8], who set the foundation stochastic programming and optimization under probabilistic constraints. Nowadays, stochastic programming has established for solving a problem which consists of uncertainty, called random elements, efficiently. In many real-life applications, an accurate probabilistic description of the randomness is unknown (Montemanni, Barta and Gambardella[9]). The uncertainty can be presented in different parts of VRP. This research focuses on the uncertain travel times because of their existances in a large city which high density traffic. The estimation of travel times is typically a difficult task, since they depend on many factors which are difficult to predict such as traffic conditions, accidents, traffic jams or weather conditions. Kao[10] first proposed heuristics method based on dynamic programming and implicit enumeration for the TSP with stochastic travel times. Laporte, Louveaux and Mercure [11] performed systematic research on the VRP with stochastic service and travel times (VRPSSTT). They proposed three models for the VRPSSTT: chance constrained model, 3-index recourse model, and 2-index recourse model, using general branch-and-cut algorithms. Most of literature in a field of uncertainty proposed stochastic optimization approach. However, before feeding the data instances to the decision model, one has to ask the decision-maker for explicit information on the probability value with which these instances might be realized. The solution of stochastic programming model will attempt to generate a solution that maximizes (or minimizes) an expected performance measure. In a real application, the expected outcome is not necessary as much as the robust decision. Then the route planning in the worst-case made the business to avoid the risk for unsatisfied services because that planning covers all perturbations of traffic conditions.

Recently, the researchers are more interested in a robust optimization approach. The structuring of data uncertainty is a part of critical elements in the applications of the robust approach but its probability density function is insignificantly important. Therefore, the decision makers have to create the scenarios that is likely to be occured to be used in the model of the robust discrete optimization.

In the mid-1990s, research teams led by Ben-Tal and Nemirovski[12][13][14] and El-Ghaoui and Lebret[15] addressed the uncertain parameters belonging to ellipsoidal sets, which remove the most unlikely outcomes of consideration and yield tractable mathematical programming problems. In line with the authors' terminology, optimization for the worst-case value of parameters within a set becomes known as “robust discrete optimization”. The robust decision under the worst-case performance is the best solution under the robust approach but it leads to overly conservative and highly cost. The scenario-based approach is an alternative method to avoid the overly conservative solution. The scenario-planning process is challenging when implemented in large organizations. Herrmann[16] applies the scenario-based approach to model the uncertainty and uses a two-space genetic algorithm to find the optimal makespan for the robust parallel machine scheduling problem. Montemanni,

Barta and Gambardella[9] present a new extension to the traveling salesman problem (TSP), where the travel times are specified as range of possible values. They applies the robust deviation criterion and the exact methods to solve optimization. These exact methods are available for small scale problems but they might not be feasible for the large scale problems.

This paper proposes the scenario-based approach to model the uncertainty of travel times. The minimax optimization problem is the main objective of this paper. It finds a robust solution under the relative robust criteria by using the hybrid heuristic algorithm. In next section, we describe the method to solve the VRP with uncertain travel times where a travel time is defined as a finite interval.

METHODS

In this paper, we develop a hybrid algorithm based on the robust approach and the heuristic methods to solve the VRP solutions under interval uncertainty of travel times. The scenario-based approach represents the uncertainty through a finite set of uncertainty. A scenario model can be seen as a snapshot representing the transportation network situation as a path of any possible edge cost configuration.

A robust discrete optimization problem can be formulated as follows. Let X be the set of all solutions. Let S be the set of all possible scenarios. The performance of the solution is $x \in X$ and the scenario, $s \in S$ is $F(x,s)$. The problem is to find the solution that has the best worst-case performance, which is the same as minimizing (over all solutions) the maximum (over all scenarios) performance.

$$\min_{x \in X} \max_{s \in S} F(x,s) \qquad (1)$$

The objective function (1) is the general form of the robust discrete optimization. Three main notions of robustness are considered by Kouvelis and Yu[1], each of them defining a different robust optimization problem. The first is an absolute robustness criteria, the second is a robust deviation criteria and the third is a relative robust criteria. In this paper we present the last one of robustness criterion: the relative robust criteria. In order to describe formally all definitions for this problem, we define as follows:

Definition 1: A scenario S is realization of the arc travel times, i.e. t_{ij} is the travel times for each pair of customers i to j. An interval of the travel times is defined as $[l_{ij}, u_{ij}]$ where l_{ij} is minimum travel times and u_{ij} is maximum travel times. In a base case scenario s is randomly generated from a $[l_{ij}, u_{ij}]$. There construct a matrice of the travel times cost.

Definition 2: The relative robust criteria, Z_R measures a percentage deviation of the best worst-case from optima among all feasible decisions over all realizable input data scenarios.

$$Z_R = \min_{x \in X} \max_{s \in S} \frac{f(x_R, t^s) - f(x_s^*, t^s)}{f(x_s^*, t^s)} \qquad (2)$$

The objective function in equation (1) is made explicit as equation (2). The x_s^* is an optimum solution and t^s is a travel times which realized for the scenario s. The constraints of this problem are same as the original VRP for deterministic optimization. The mathematical formulation of the VRP defines x_{ijk} as a decision variables where $x_{ijk} = 1$ if there exists arc $\{i, j\}$ for vehicle number k is on the route and 0 else.

The hybrid algorithm for this problem includes MPFIH and λ-LSD with TS. The MPFIH is a heuristic method for inserting customer into a route based on push-forward insertion method of Solomon [17] and Thangiah[18]. It is an efficient method for computing the inserting a new customer into the route. The λ-LSD, using the TS, is a type of neighborhood search that the set of all neighbors generate by the LSD for a given integer λ. It is a sequential search selects all possible combination of different pair of routes. Then the TS is used as a diversification method that prevents the algorithm fall in a local optima. The TS is often refer to as "meta-heuristic". The TS is used to swap node or re-arranges a sequence of customers for each route. The TS is a memory-based search strategy which guides the local search descent method (LSD) to continue their search beyond local optimum (Glover[19] [20]). When a local optimum is encountered, a move to the best neighbor is made to explore the solution space, even thought there may cause of a deterioration in the objective function value. The TS seeks the best available move that can be determined in a reasonable amount of time. If the set of neighborhood is large or their elements are expensive to evaluate, candidate list strategies are used to help restrict the number of solutions examined on a given iteration.

This hybrid algorithm for the robust discrete optimization can be summarized as follow:

1. Construct a base case scenario s_o from uniform distributed, $t^o \in [l_{ij}, u_{ij}]$.
2. Generate for all possible scenarios by percentage of uncertainty β,
   i.e. $t^s \in [(1-\beta)l_{ij}, (1+\beta)u_{ij}]$.
3. Construct the initial solution x_0 by MPFIH method.

4. For each individual s, evaluate the minimum solution, $g(s) = \min\{F(x,t^s) : x \in X\}$ by using the λ-LSD and TS algorithm.
5. For each individual x, evaluate the maximum solution among all possible scenarios s, $h(x) = \max\{F(x,t^s) : s \in S\}$
6. Find x_R that is the robust solution belong to equation (2).

A SIMULATION STUDY AND RESULTS

To implement the hybrid algorithm, we created the source code on MATLAB computing software. We tested the algorithm on randomly generated problem instances. All instances have 25 customer nodes and a single depot node. The total demand and vehical capacity are 430 and 100 units, respectively . The perturbation parameter, β, control percentage of uncertainty in travel times. When the traffic appears smoothly, thus β is low. Its value increases when the traffic jam, accident or the badly weather occurs. The minimum travel times l_{ij} is selected from a uniform distribution with the range [1, 2]. The delay time, d_{ij} for each route is selected from a uniform distribution with range [1, (1+ β)2] where β equals 0.2, 0.4, 0.6 and 1.0, respectively. The maximum travel times which is taken into a term of the delay time becomes $u_{ij} = l_{ij} + d_{ij}$.

Number of scenarios, |S|= 10, 20, 40 and 80 are considered in our simulation experiments. For each experiment, the realizations of scenarios are computed to evaluate the quality of the routes, generated by the scenario-based approach, the worst-case performance approach and the expected-value approach. We observed how each type of route performs under random generated travel times situations. The performance measure, the ratio *R*, quantifies the relative extra travel times of the robust solution with respect to the optimum travel times for each scenario. It is calculated by $R = \dfrac{Z_r - Z_s}{Z_s}$ where Z_r is the optimal objective value of the robust counterpart and Z_s is the optimal objective function value of each scenario belonging to the deterministic VRP. This ratio gives information on how much extra travel times that will be incurred if we implement the robust route to protect against all possible realizations of the traffic simulation. When R is close to zero, it indicated that obtains a high performance solution. We compared the solutions by the average relative ratio, $\overline{R}$, for example; where |S|=10 then $\overline{R} = \dfrac{1}{10}\sum_{s=1}^{10} \dfrac{Z_r - Z_s}{Z_s}$. The corresponding results are shown in Table 1.

Table 1: Simulated average relative ratio of solutions for n = 25

|S|	β	Solutions		
		Scenario-based	Worst-case	Expected-value
10	0.2	0.24	0.13	0.23
10	0.4	0.38	0.31	0.30
10	0.6	0.26	0.29	0.28
10	1.0	0.30	0.58	0.86
20	0.2	0.24	0.15	0.21
20	0.4	0.36	0.29	0.28
20	0.6	0.30	0.30	0.32
20	1.0	0.34	0.57	0.77
40	0.2	0.28	0.16	0.26
40	0.4	0.37	0.29	0.26
40	0.6	0.39	0.33	0.32
40	1.0	0.39	0.59	0.66
80	0.2	0.27	0.15	0.27
80	0.4	0.23	0.29	0.28
80	0.6	0.41	0.34	0.32
80	1.0	0.37	0.60	0.65

Table 1 shows that the performance of scenario-based approach is stable with changing level of uncertainty. Fig.1 clearly, shows results of the simulation comparison for S=10, 20, 40 and 80, respectively. Another two approaches, the worst-case performance and the expected-value are analogous direction. They show good performance in case of lower percentage of uncertainty and increase raplidly where is over 60%. Moreover, the results show that the scenario-based approach is the best for any percentage of uncertainty. For each set of problems, the number of scenarios are not significant effect to the performance of solutions.

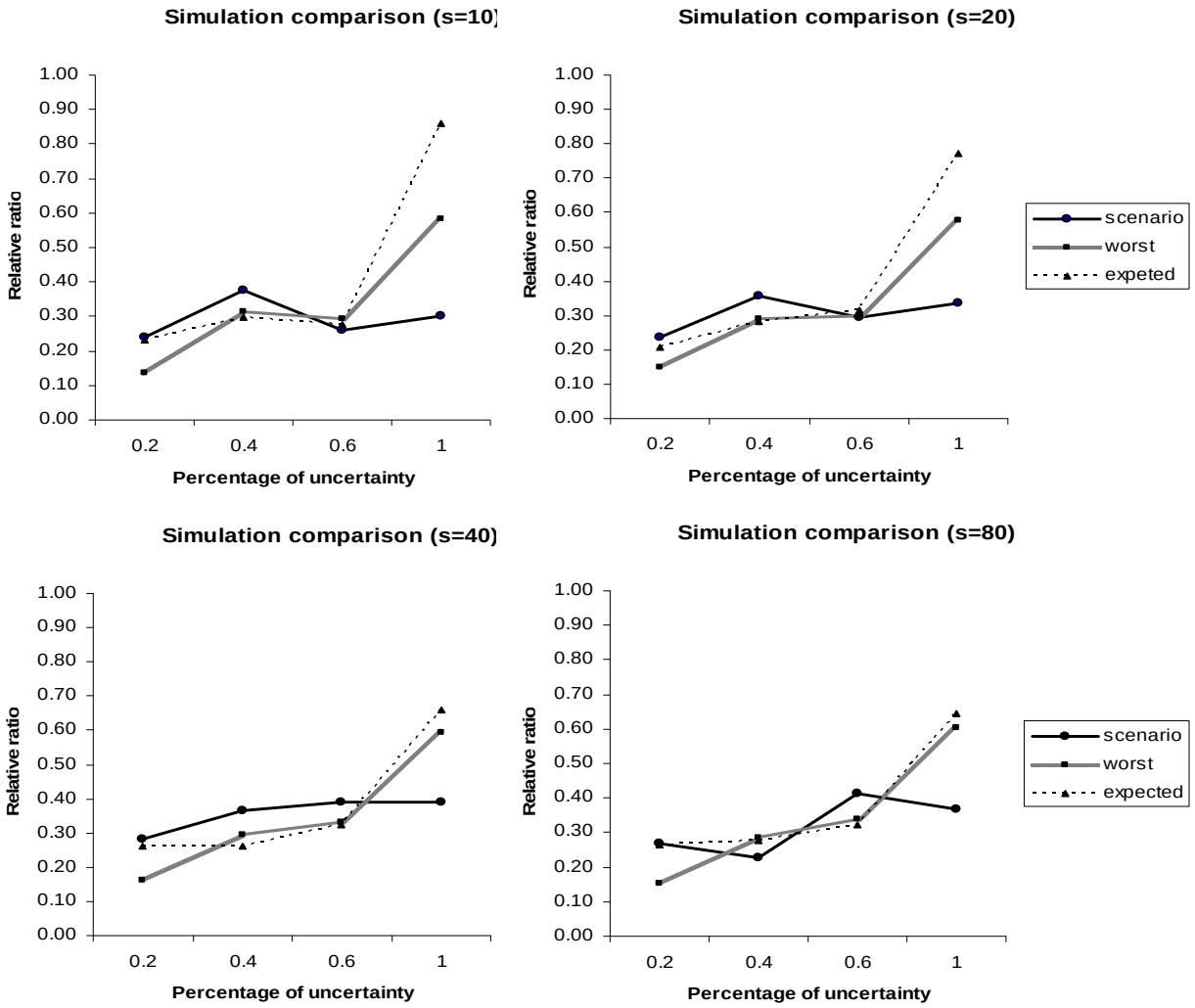

Fig. 1: The simulation comparison for S=10,20,40,80

CONCLUSIONS AND FUTURE WORK

The modeling of VRP with uncertain travel times aims to minimax robust discrete optimization by using the relative robust criteria. The results are compared between the three well known approaches in the field of uncertainty. The simulation experitments clearly show that the robust solution from the scenario-based approach is potential and strong for the perturbation of traffic conditions and the change in uncertainty. The worst-case performance and the expected-value approaches can recognize uncertainty but their efficiency decreases when increases the level of uncertainty. Obviously, they are overly conservative. For future work, we will use the hybrid algorithm with scenario-based approach for the large scale VRP, i.e. n = 50, 100, 200, 1000 to illustrate its performance when the number of customers increases. However, the algorithm may require adjustments for solving the large scale problem when this condition does not hold or run-times are over.

ACKNOWLEDGMENTS

The authors wish to thank Gerrit K. Janssens and N. Tippayawannakorn for review this paper. This material is based upon work partly supported by the graduate school Kasetsart University.

REFERENCES

1. Kouvelis, P. and G. Yu, 1977. Robust discrete optimization and its applications. Kluwer Academic Publishers, Netherlands.
2. Shen, Z., F. Ordonez and M. Dessouky, 2006. The minimum unmet demand stochastic vehicle routing problem. USC ISE Working paper #2006-07.
3. Osman, I. H., 1993. Vehicle routing and scheduling: Applications, algorithms and developments. Proceedings of the International Conference on Industrial Logistics, Université de Rennes, France, paper 2.3, pp. 1-37.
4. Laporte, G., 1992. The vehicle routing problem: An overview of exact and approximate algorithms. European Journal of Operational Research, 59, 345-358.
5. Fisher, M., 1993. Vehicle routing, In: Ball, M.O., Magnanti, T.L., Monma, C.L., Nemhauser, G.L., (Eds.). Handbooks in Operations Research and Management Science. Elsevier Science B.V., 1-33.
6. Bodin, L., B. Golden, A. Assad and M. Ball, 1983. The state of the art in the routing and scheduling of vehicles and crews. Computers and Operations Research, 10 (2), 63-211.
7. Dantzig, G., 1955. Linear programming under uncertainty. Management Science, 1(3-4), 197-206.
8. Charnes, A. And W. Cooper, 1959. Chance-constrained programming. Management Science, 6(1), 73-79.
9. Montemanni, R., J. Barta, M. Mastrollili and L.M. Gambardella, 2007. The robust traveling salesman problem with interval data, Transportation Science, 41(3), 366-381.
10. Kao, E., 1978. A preference order dynamic program for a stochastic travelling salesman problem. Operations Research, 26:1033-1045.
11. Laporte, G., F. Louveaux and H. Mercure, 1992. The vehicle routing problem with stochastic travel time. Transportation Science, 26(3).
12. Ben-Tal, A. and A. Nemirovski, 1998. Robust convex optimization. Mathematics of Operations Research, 23(4), 769-805.
13. Ben-Tal, A. and A. Nemirovski, 1999. Robust solutions to uncertain programs. Operations Research Letters, 25, 1-13.
14. Ben-Tal, A. and A. Nemirovski, 2000. Robust solutions of linear programming problem contaminated with uncertain data. Mathematical Programming, 88, 411-424.
15. El-Ghaoui, L. and H. Lebret, 1997. Robust solutions to least-square problems to uncertain data matrices. SIAM Journal on Matrix Analysis and Applications, 18, 1035-1064.
16. Herrmann, J.W., 1999. A genetic algorithm for minimax optimization problems. In: Angeline, P.J., Michalewicz, Z., Schoenauer , M., Yao, X., Zalzala, A., (Eds.). The 1999 Congress on Evolutionary Computation, Washington DC, IEEE Press, 1099-1103.
17. Solomon, Marius M., 1987. Algorithms for the vehicle routing and scheduling problems with time window constraints. Operations Research, 35 (2), 254-265.
18. Thangiah, Sam R., 1993. Vehicle routing with time windows using genetic algorithms. Submitted to the International Journal on Computers and Operations Research.
19. Glover, Fred, 1989. Tabu Search-Part I. ORSA Journal on Computing, 1(3), 190-206.
20. Glover, Fred, 1990. Tabu Search-Part II. ORSA Journal on Computing, 2(1), 4-32.

Determination of the Optimal Mixing Parameters for the Achievement of the Optimal Outcome among Input / Output Uncertainties in Sweet Production Case Study: Foi-thong Production

[1]Somsak Chueakittisak, [2]Rathaprom Promkam, and [3]Peerayuth Charnsethikul
[1] Industrial Engineering Department, Faculty of Engineering, [2]Mathematics and Statistics Department, Faculty of Science and Technology,
Thammasat University, Klonnueng, Klongluang, Pathumtanee, 12121, Thailand.
[3]Industrial Engineering Department, Faculty of Engineering, Kasetsart University, Bangkhen, Bangkok, 10220, Thailand.
E-mail: [1]csomsak@engr.tu.ac.th, [2]epsilonxe@hotmail.com, [3] fengprc@ku.ac.th,

Abstract: The objective of this research work was to determine the most appropriate mixing ratio of raw materials which generates the minimum cost and contains the required nutritional value for the case of Foi-thong production in which the main ingredient is the egg-yolk emulsion mixture between duck-egg yolks and hen-egg yolks. The authors applied the stochastic linear programming, two-stage model under uncertainties of both the input ingredients and the finished output by calculating through the objective function and subjecting to the entire requirement constraints. The primary result, the trial solution, was that 1 gram of egg-yolk emulsion should contain duck-egg yolk and hen-egg yolk in the intervals of [0.9199, 0.9457] and [0.0611, 0.0807] gram respectively with the minimum cost of [1.3748, 1.4876] baht / gram. The second-stage information was passed to the calculation program again to determine more exact values which approached to the target. The weight of duck-egg and hen-egg yolk mentioned above was stated as fixed parameters, and then calculation was started from the lower bound to the upper bound with gradual steps of 0.0001resolution. Thus, the final result achieved was that 1 gram of egg-yolk emulsion should compose of 0.9259 gram of duck-egg yolk and 0.0741 gram of hen-egg yolk with the minimum cost per gram of 1.3951 baht.

Keywords: Input / Output Uncertainties, Foi-thong Machine, Foi-thong Production, Product Design, Two - stage Linear Stochastic Programs.

INTRODUCTION

In general, an exact nutrient value in the raw materials (ingredient) fed into the food mixing process cannot be expected. Because raw materials are different in quality from place to place, therefore, the nutrient value can be very variable. Such variation has a big effect directly on the output of the process, especially, as the nutrient values required by the market are the conditions which have to be fulfilled. The primitive mixing process is a compromised process, with an element of trial and error. Depending on the quality of the output, the amount of raw material put into the process would be adjusted to compensate. For example, the traditional mixing ratio between duck and hen egg-yolk in making Foi-thong is generally 80:20; 50:50; 70:30 or by trial and error according to the maker's experience **[2][3].** It is therefore difficult to solve for the best result of mixing under uncertainties. The input parameters are in intervals and build up a lot of possible alternatives. Each mixing alternative must be under the expected condition for the controlled nutrient value of the output. Therefore, there are a lot of alternative equations containing variables which have to be solved. For this purpose, the linear stochastic programming / two-stage model is applicable. But, it is a rather time-consuming calculation. So, this study applied the linear stochastic programming by randomizing the variables to reduce the calculation time.

RESEARCH METHODOLOGY

The stochastic programming model is a mathematic programming that can be a linear, non-linear, integer or mix programming. The input data is randomized, meaning that the exact coefficients of the variables are not determined, only their statistical distributions are known.

Stochastic Linear programming is therefore involved with scenarios under uncertainties **[5][6][7].**

Corresponding Author: Somsak Chueakittisak Industrial Engineering Department, Faculty of Engineering, Thammasat University, Klonnueng, Klongluang, Pathumtanee, 12121, Thailand.

This research work concerns the study of the linear stochastic programming through simulation.
This following problem is composed of an objective function, and the function for determination of the minimum cost of one gram of egg-yolk emulsion which is the mixture between duck-egg yolk and hen egg yolk under all controlled conditions. For this case study, only energy, protein and fat are considered.

Symbols

- n Type of raw materials
- m Total scenario numbers
- k Number of constraints under uncertainty
- ρ Sum of all variables (main, slack, surplus, and pseudo variables)
- p_e Probability at scenario e
- c_j Cost of material at type j
- x_j Quantity of material at type j
- g_t Compensation cost for the lacking nutrient at type t
- h_t Compensation cost for the exceeding nutrient at type t
- a_{tje} Nutrient value at type i raw material at type j under scenario e
- b_{te} Nutrient value at type i required in finished mixture under scenario e
- u_{ie} Nutrient value at type i lacking in scenario e
- o_{ie} Nutrient value at type i exceeding in scenario e
- g_{te} Mean unit cost for compensation of lacking nutrient value at type t under scenario e equal to $g_t \times p_e$
- h_{te} Mean unit cost for compensation of exceeding nutrient value at type t under scenario e equal to $h_t \times p_e$

Objective function

$$Min \sum_{j=1}^{n} c_j x_j + \sum_{e=1}^{m}\sum_{t=1}^{k}(g_{te}u_{te} + h_{te}o_{te})$$

Subject to

$$\sum_{j=1}^{n} a_{tje}x_j + u_{te} - o_{te} = b_{te}$$

$$f_i(x_1, x_2, \dots, x_n, \dots, x_{n+\rho}) = d_i$$

$$\forall x_j, u_{te}, o_{ie} \geq 0$$

$$i = 1,2,\dots,k, e = 1,2,\dots,m$$

$$\rho \in \mathbb{Z}^+ \cup \{0\}, i = 1,2,\dots,y$$

Where f_i is a linear function that is independent to the uncertainty which can be written in matrix form $Ax = b$ such that

$$X = \begin{bmatrix} x_1 \\ \vdots \\ x_n \\ u_{11} \\ \vdots \\ u_{1m} \\ \vdots \\ u_{k1} \\ \vdots \\ u_{km} \\ o_{11} \\ \vdots \\ o_{1m} \\ \vdots \\ o_{k1} \\ \vdots \\ o_{km} \\ \vdots \\ \vdots \\ x_{n+\rho} \end{bmatrix}_{(n+2km+\rho)\times 1}, b = \begin{bmatrix} b_{11} \\ \vdots \\ b_{k1} \\ b_{12} \\ \vdots \\ b_{k2} \\ \vdots \\ b_{1m} \\ \vdots \\ b_{km} \\ d_1 \\ \vdots \\ d_y \end{bmatrix}_{(km+y)\times 1}$$

$$b_{i1} = b_{i2} = \cdots = b_{im} \quad \forall i = 1,2,\dots,k$$

$$A = \begin{bmatrix} \xi & \eta & Z_1 \\ Y & Z_2 & D \end{bmatrix}_{(km+y)\times(n+2km+\rho)}$$

$$\xi = \begin{bmatrix} \xi_1 \\ \vdots \\ \xi_m \end{bmatrix}_{km\times n}$$

$$\xi_e = \begin{bmatrix} a_{11e} & a_{12e} & \cdots & a_{1ne} \\ a_{21e} & a_{22e} & \cdots & a_{2ne} \\ \vdots & \vdots & \vdots & \vdots \\ a_{k1e} & a_{k2e} & \cdots & a_{kne} \end{bmatrix}_{k\times n}$$

$; e = 1,2,\dots,m$

$$\eta = [\eta_u \quad \eta_o]_{km\times 2km}$$

$$\eta_u = I_{km\times km}$$

$\eta_o = -\eta_u$; I is Identity matrix

Y Coefficient matrix corresponding to f_i

Excluding pseudo, slack and surplus variables $;l = 1,2,\dots,y$

D Coefficient matrix of pseudo, slack and surplus variables corresponding to Y

Z_1 Zero matrix size $km \times \rho$

Z_2 Zero matrix size $y \times 2km$

Assumptions

1. The quantity of each nutrient value in each type of raw material is a continuous event. The values are uncertain but the values interval can be known in the form of a uniform distribution and they are independent of each other.
2. The data by all scenarios are uniformly distributed and independent of each other.

Problem Statement

By mixing problem, the minimum cost of production (under uncertainties) will disclose when the quantity of nutrient value **[8]** contained in each type of raw material is under uncertainty and known in an interval with a uniform distribution. The finished-mixture product could have less or more nutrient value than expected. This always varies and differs from raw material to raw material. Such variation can cause a higher cost for solving the problem. To determine the mixture of egg yolk, **Table 1**. is referred to.

Table1. Costs and nutrient values of egg yolk:

Material	Cost (Baht)	Energy (Calorie)	Protein (Gram)	Fat (Gram)
Duck egg-yolk (1 g.)	0.1648	1850 ± 15	0.1281 ± 0.0004	0.1377 ± 0.0060
Hen egg-yolk (1 g.)	0.1440	1500 ± 10	0.1249 ± 0.0001	0.1061 ± 0.0059

The cost of mixture compensation (lacking or exceeding) is as shown in Table 2.

Table2. Costs for nutrient values compensation:

Compensation cost	Energy (Baht/g.)	Protein (Baht/g.)	Fat (baht/g.)
Nutrient value: Lacking	0.1	0.05	0.08
Exceeding	0.033	0.018	0.026

By each gram of the finished-mixture product, the nutrient values are containing as shown in Table 3.

Table 3. Required nutrient values per 1 unit weight of product:

	Energy (Calorie)	Protein (Gram)	Fat (Gram)
Required nutrition value	1800 ± 50	0.2 ± .01	0.1 ± .01

By consideration of mixing behavior, the problem model can be formulated:

Objective function

$$Min\ 0.1648x_1 + 0.1440x_2 + \sum_{s=1}^{tt}\left((0.1u_{1s} + 0.033o_{1s}) + (0.05u_{2s} + 0.018o_{2s}) + (0.08u_{3s} + 0.026o_{3s})\right)$$

Subject to

$$[1835,1865]x_1 + [1490,1510]x_2 + u_{1s} - o_{1s} = 1750\,,\,1850$$

$$[.1277,.1285]x_1 + [.1248,.1250]x_2 + u_{2s} - o_{2s} = 0.19\,,\,0.21$$

$$[.1317,.1437]x_1 + [.1002,.1120]x_2 + u_{3s} - o_{3s} = 0.09\,,\,0.11$$

$$x_1 + x_2 = 1$$

$$\forall_{x_j}\,,\,u_{is}\,,\,o_{is} \geq 0$$

Steps of Research

The algorithm for solving this problem, the Linear Stochastic Programming problem, was formulated in MATLAB Programming format. This is a program for solving the objective function under all relevant constraints by random selection of samples (the quantity of the nutrient values in raw material of each scenario). Because the quantity of nutrient values is continuous data, they have to be converted into the form of discrete data by selecting a $StgNum$ (Significant number). *E.g.* for $StgNum$ = 3 the resolution of the data would be $\delta = 10^{-StgNum} = 10^{-3} = 0.001$ and thus, the continuous data which is defined in closed interval $[a_1\,,a_N\,]$ after conversion into discrete values, could be written in a mathematic formulation as follows:

$$a_1, a_1 + \delta, a_1 + 2\delta, \ldots, a_n, \ldots, a_N$$

This is an arithmetic Sequence which could be reformulated in general form like this:

$$a_n = a_1 + (n-1)\delta \;;\quad n = 1,2,\ldots$$

It is clearly to see $\lim_{StgNum \to \infty} \delta = 0$.

The higher the significant number is, the more the accuracy of δ will approach zero. By this arithmetic conversion, the discrete and continuous data, with point by point comparison, can be approximately the same. Therefore, this algorithm has been applied for solving this mixing problem.

Solving the Stochastic Programming Problem by Randomizing the Nutrient Values.

The model in this research is the objective function and the function of all constraints by randomizing the input nutrient value contained in each type of raw material in all calculation scenarios. These following steps of specifications were set up in the form of the M-Files in MATLAB Formatting:

1. Specify $StgNum$ as integer $0,1,2,\ldots$
2. Specify m as positive integer respective to all scenario.
3. The matrix val is cost of each type of material
4. The matrix R is cost for compensation of each lacking material
5. The matrix S is cost for compensation of each exceeded material
6. The matrix $coef$ is each nutrient value quantity in each type of material under uncertainty
7. The matrix $coef\_tol$ is the uncertainty of the matrix $coef$
8. The matrix Y is each nutrient value quantity of each material type
9. The matrix b is each nutrient value quantity required in finished product under uncertainty and dependent to $coef$
10. The matrix b_tol is the uncertainty of the matrix b
11. The matrix d the other conditions dependent to the matrix Y
12. Substitution of all above parameters in the mathematic model in the MATLAB Formatting
13. Solving the MATLAB Formatting by MATLAB Programming Software.
14. Repeating the operation steps from 11-13 with the iteration number of N
15. Comparison the result of each iteration from step 14

RESULTS AND DISCUSSION

This research used a personal computer with technical specification CPU: Core 2 Duo T7250 @ 2.0 GHz, RAM: 2 GB, HDD: SATA (5400 rpm) 160 GB, MATLAB software on Windows Vista (x86) operating system. The results are shown below in tables 4 to 6.

In Table 4 by calculation of 10 batches and 500 scenarios with selecting of $StgNum$ 0, 1, 2 and 3, it can be noticed that the significant number or resolution number has no effect on the calculation time.

Table 4. Research results for mixing ratio and production cost where $m = 500, N = 10$

$StgNum$	t_set	t_sol	var	z	x_1	x_2
0	5.6488	8.6625	3002	[1.4194, 1.5108]	[0.9193, 0.9356]	[0.0644, 0.0807]
1	5.5343	8.5065	3002	[1.3748, 1.5315]	[0.9200, 0.9380]	[0.0620, 0.0800]
2	5.5379	8.3973	3002	[1.3515, 1.5412]	[0.9228, 0.9317]	[0.0683, 0.0772]
3	5.6721	8.1549	3002	[1.4194, 1.4885]	[0.9210, 0.9336]	[0.0664, 0.0790]

Table 5. Research results for mixing ratio and production cost where $N = 1, StgNum = 4$

m	t_set	t_sol	var	z	x_1	x_2
100	0.1262	0.4161	602	1.4002	0.9457	0.0543
300	0.3293	0.3446	1802	1.4876	0.9340	0.0660
500	0.5824	0.7822	3002	1.4152	0.9323	0.0677
700	0.9895	1.7324	4202	1.4040	0.9331	0.0669
1000	1.7423	3.9574	6002	1.4320	1.9237	1.0763

Table 6. Research results for mixing ratio and production where $m = 1000, StgNum = 4$

N	t_set	t_sol	var	z	x_1	x_2
1	1.7423	3.9574	6002	1.4320	0.9237	0.0763
5	7.7364	17.4036	6002	[1.3905, 1.5194]	[0.9212, 0.9316]	[0.0684, 0.0788]
10	15.4128	35.3373	6002	[1.4263, 1.5179]	[0.9216, 0.9363]	[0.0637, 0.5784]
20	30.2164	69.3962	6002	[1.3972, 1.4857]	[0.9207, 0.9366]	[0.0634, 0.0793]
30	45.2439	105.4856	6002	[1.4266, 1.5203]	[0.9099, 0.9389]	[0.0611, 0.0801]

Where each result is

t_set	Setting up time for model building (sec.)
t_sol	Solution time (sec.)
var	Number of variables
z	Production cost (Baht/gram)
x_1	Quantity of duck egg-yolk in product (gram)
x_2	Quantity of hen egg-yolk in product (gram)

The results in **Table 5** and **Table 6** report the interval values of the quantity of the duck egg-yolk and the quantity of the hen egg-yolk as [0.9199, 0.9457] and [0.0611, 0.0807] respectively. The production costs by those mixture quantities are in [1.3748, 1.4876] Baht/gram. Therefore, the optimal quantity of duck egg-yolk should be in the interval 0.9100 – 0.9500 gram and the quantity of hen egg-yolk should be 0.0500 – 0.0900 gram

Hence, in order to calculate the best minimum production cost, let us run the simulation by replacing the previous quantities with the above values of duck egg-yolk [0.9100, 0.9500] gram and hen egg-yolk [0.0500, 0.0900] and $StgNum = 4$.

Fig.1 shows the simulation result.

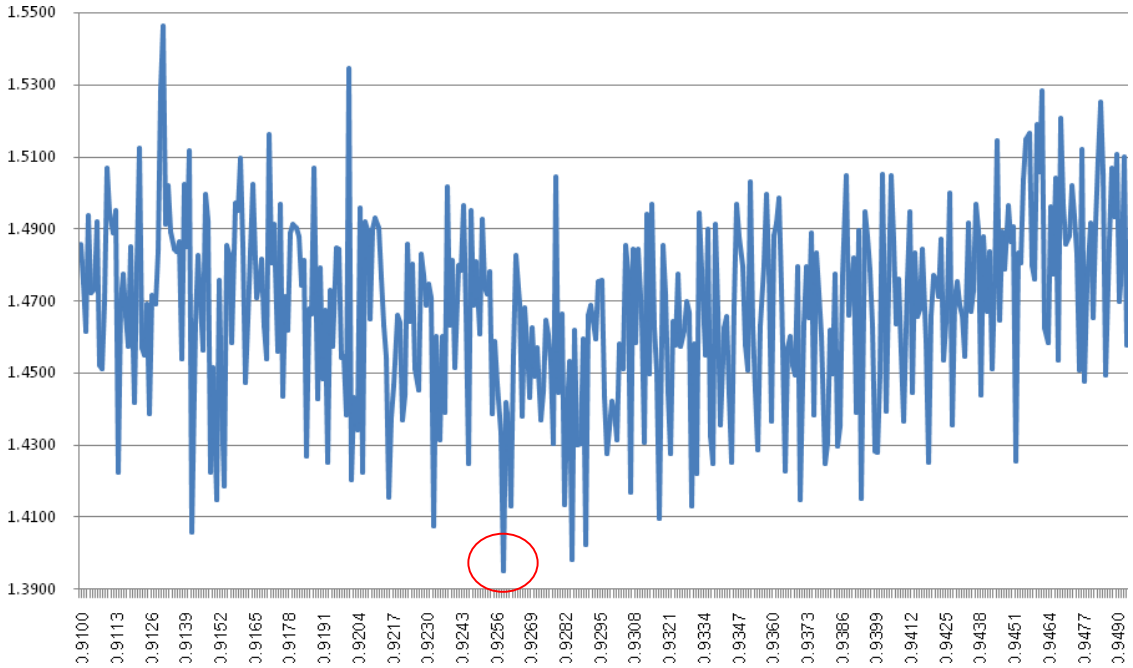

Fig. 1 Simulation result by replacing the previous input data with the (new) duck egg-yolk 0.8700 – 0.8800 gram.

The above simulation result in **Fig.1** represents the relation of the duck egg-yolk quantity and the minimum production cost. The duck egg-yolk is **0.9259** gram whereas the hen egg-yolk is **0.0741** gram and the minimum production cost per gram is **1.3951** Baht.

CONCLUSION

This research problem was solved by mean of the stochastic linear programming, two- stage model under uncertainties of both the input ingredients and the required finished product. The assumptions were that the nutrition values of input in each scenario have uniform distribution and are independent to each other. The primary result of egg-yolk emulsion containing duck egg-yolk and hen egg-yolk, and the minimum cost of production have just been roughly estimated. To determine more exact values which approach to the target, the primary result, the weight of duck egg-yolk and hen egg-yolk have been fixed as constant parameters. After the second calculation run, the final results have been achieved new values as follows. The weight of one gram egg-yolk emulsion would be composed of **0.9259** gram **(92.59 %)** duck egg-yolk and **0.0741** gram **(7.41%)** hen egg-yolk, and the minimum cost would be **1.3951** Baht/gram. It can be noticed that by the duck egg-yolk increasing, the hen egg-yolk decreases and the cost of production consequently rises up.

This mixing method should be better suited for the market need with nutrient value tolerances (in the values intervals) of the finished goods. The cost has increased because of the compensation of the nutrient values in raw material input. To satisfy the customer needs a compromise should be made. It means to commit to the nutrient values of the finished goods in fixed conditions. So, such a case will be matching to the case of one-sided uncertainty referred to in the research result **[10].**

It would be very interesting for the next research problem to consider the input data, the raw material ingredients, set up with some other distribution patterns and the necessary nutrition values such as various types of vitamins.

ACKNOWNLEDGMENTS

For this research work conducted to support the design and setting up of a 250 gm. Foi-thong apparatus [**9]** we would like to acknowledge:

5.1 Thammasat University, Klongluang Pathumtani for providing a research grant during the fiscal year 2006 – 2008.

5.2 Industrial Engineering Department, Faculty of Engineering, Thammasat University, Klongluang Pathumtani for providing the production laboratory in the workshop.

REFERENCES

[1] Sompong Jesadathamstit. 2541. A Decision Support System for Ration Formulation, Master thesis, Industrial Engineering Dept., Kasetsart University, Bangkhen, Bangkok,

[2] Kimlaung. 1990. Sweet Production, in the Province Petchaburee, Phone: (081)8567598

[3] Kimlai. 1990. Sweet Production, Petchaburee Province, Tel. (032)425618

[4] Pisit Sang-Xuto, Pisnu Thongkhao, Somsak Chueakittisak, Peerayuth Charnsethikul 2008. Aggregate Planning under Uncertain Demands by Stochastic Programming Technique. Chaophya Park, Rachadapisek Rd, Dindaeng, Bangkok, Thailand. 24-25 July, 2008

[5] Charnsethikul, P. 2005. Teaching manuscript 206691 / 206697: Calculation of the Effect from Uncertainty of Nutrient Value for Determination of the input raw material by Stochastic Programming. At Industrial Eng. Dept., Faculty of Engineering, Kasetsart Univ., Bangkhen, Bangkok, Thailand.

[6] Charnsethikul, P. 2000. Linear Programming with Constraint Coefficient Tolerances. IE Department, Kasetsart University, Bangkhen Bangkok, Thailand.

[7] Gerd Infanger. 1993. Planning under uncer- tainty solving large scale stochastic linear programs, pp. 15-22.

[8] USDA .1989. Supplement-Agriculture Handbook No. 8, Human Nutrition Information Service, 1979 Poultry Science 58:131-134

[9] Somsak Chueakittisak 2005. Design and Set up of 250 gram Foi-Thong Pouring Prototype Machine, Industrial Engineering Network Conference, 3 - 5 October, Chulalongkorn University, Bangkok, Thailand.

[10] Somsak Chueakittisak, Rathaprom Promkham, Peerayut Charnsethikul, 2008. Stochastic Linear Programming supporting a Decision making for the Determination of Mixing Parameters of 250 gram Foi-thong Machine, Industrial Engineering Network Conference, Simira Hotel, Songkhla University, Songkhla, Thailand. 21-23 October, 2008

Monte Carlo Simulation of Mechanism of Water And Ions Transfer in Aquaporins Channel: as an Approach for Drug Design

Majid Monajjemi
Department of Physical Chemistry, Science & Research Branch, Islamic Azad University, Tehran. IRAN

Abstract: Aquaporins are membrane water channels that play critical role in controlling the water contents of cells. Therefore, the generation of Aquaporin structure models is useful for solving mechanistic questions on the channel selectivity and especially for virtual drug design. For achieving to this purpose, in this study, we have used Hybrid Monte Carlo (HMC) method which is a Monte Calro (MC) algorithm utilizing Molecular Dynamics (MD) to generate a trial move of system atoms to solve a biological mystery: how water molecules can pass through a protein pore in a cell membrane as rapidly as they do without ferrying extra protons across with them. Water permeation and electrostatic interactions between water and channel are investigated in the Aqp4, a member of the Aquaporin water channel family, by CHARMm software. Renal collecting Aquaporins are the main sites for regulation of whole body potassium balance. Changes in dietary intake of potassium induce pleiotropic adaptations of collecting duct cells, which include alterations of ion and water transport properties along with a hypertrophic response. For improve undressing of water and K+ permission in membrane water channels. We have also used a single subunit of De Young–Keizer (DYK) model was simulated using Gillespie algorithm. the conditions which affect K+ and Water concentrations on stochastic fluctuations were investigated. In our study, HMC method shows detailed mechanism of action of AQP4 was considered at DMPC membrane. Water molecules passing the channel are forced, by the protein's electrostatic and vdW forces, to flip at the center of the channel. Therefore, breaking the alternative donor-acceptor arrangement is necessary for proton translocation. We also found out that decreasing open probability is a function of K+ concentration in fast time domain by Gillespie algorithm.
These results are show that in comparison with the chemical master equation, Gillespie algorithm is also provides a wide area for studying biological systems from other points of view.

Keywords: Aquaporin, Monte Carlo, Molecular Dynamics, DMPC membrane, Gillespie algorithm .

1. Introduction

The regulation of water balance in the brain is crucial. A disruption in this equilibrium causes an increase in brain water content that significantly contributes to the pathophysiology of traumatic brain injury, hydrocephalus, and a variety of neurological disorders [1]. Aquaporin-4 (AQP4) is the primary cellular water channel in the brain, localized to astrocytic foot processes along the blood–brain barrier and brain–cerebrospinal fluid interface [2]. AQP4 may play a key role in modulating brain water transport (Figure 1) and raised the possibility that AQP4 inhibition could provide a new therapeutic option for reducing brain edema in a wide variety of cerebral disorders [3].

Corresponding Author: Majid Monajjemi, Department of Physical Chemistry & Research Branch, Islamic Azad University, Tehran, IRAN

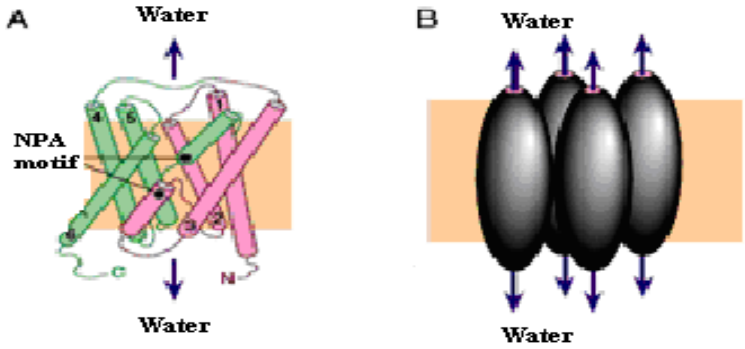

Figure 1; A) AQP4 structure, B) permeation of water through AQP4

The open probability of the some AQP4s depends on the K+ concentratin on the cytosolic side of the channel and the H2O concentration. The AQP4 channel consists of one subunit.

All of them share basically the same response with respect to the water concentration AQP4 channels open and close randomly. The stochastic gating of the water channels have been studied in different ways. The previous works included Monte Carlo simulations with using the master equation approach [3] or some derivations of the models with the stochasticity approach [4].In the present work, the single subunit dynamics was studied as a stochastic realization of the De Young–Keizer model.

The model has been introduced as a deterministic model by its authors at first and was later on used as a stochastic scheme by Falcke et al. [4].

We used a Monte Carlo based exact simulation algorithm (Gillespie algorithm) for simulating the set of reactions in this model, without any simplifications of the model.

Furthermore, in this study, we have used Hybrid Monte Carlo (HMC) method [5] is a Monte Calro (MC) algorithm utilizing molecular dynamics (MD) to generate a trial move of system atoms. The Monte Carlo methods in CHARMm have been designed to allow providing a pre-defined set of move types which can be combined to specify the allowed movements of an arbitrary CHARMm molecule [6]. The basis of the models and the description of the algorithm are described in the next section.

2. Computational Method

2.1 MD simulation

All the simulations were carried out with the MD program using the CHARMm22 [7] for proteins, for lipids, and TIP3P [8] for water. The crystal structure of AQP4 protein was obtained from the Research Collaboratory for Structural Bioinformatics Data Bank (PDB), (PDB entry code 2d57).

The microscopic system consist of one AQP4, 84 DPPC (41 in the upper layer and 43 in the lower layer), and 1888 water molecules. Dimensions of system were chosen as: 72×58×200 A°. The membrane plane was in the xy plane, and the An optimal position, where equal distances from the lipid headgroups to the above residues resulted, was obtained by separately adjusting the two monolayers relative to the protein. The system was then fully hydrated by overlaying preequilibrated water box of appropriate dimention X and Y. Before every dynamic step, the system was minimized for removing all of bad contacts. After that, 6000 Ps was done to reach the system in equilibrium, then this system was energy minimized and equilibrated for 3 ns at 298 K and 1 atm. The system equilibrium was checked by monitoring potential energy and volume over the course of the simulation. The standard deviation of potential energy from the mean was (-210 kcal/mol), that suggests that the system is in equilibrium. A hydrostatic pressure gradient was established across the membrane by applying extra force to a layer of solvent molecules parallel to the membrane interface. Applied time MD simulations of different time length were performed at 5, 8 and 20 ns for AQP4/H2O

system. Electrostatic calculations were performed without a cutoff operation using the particle mesh Ewald method with periodic boundary conditions [9].

2.2 MC simulation

For AQP4, we imaging that it consists of three binding sites: an activating and an inhibitory K+ binding site (the second K+ which produced an inhibited state of the subunit) and an activating H2O binding site. Therefore the state of a subunit can be specified by a triplet index of *ijk*. The index *i* stand for the H2O site, *j* for the activating K+ site, and *k* for the inhibiting K+ binding site. An index equals 1 when a site is occupied and 0 otherwise. Hence the state 1 1 0 refers to H2O and K+ bound to the activating sites, respectively, and no K+ attached to the inhibiting binding site. The resulting eight states of a subunit are shown in Fig.2. The binding rate constants for H2O activation are given by $a1$ and $a3$, where as $a2$ and $a4$ refer to K+ inhibition. K+ activation is controlled by $a5$ [10].

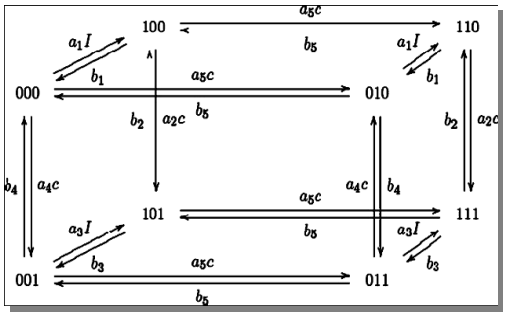

Figure 2; Transition scheme of the De Young–Keizer model.

2.2.1. Stochastic algorithms: Gillespie algorithm

The time behavior of a spatially homogeneous chemical system can be mathematically described in two formalism: the deterministic approach regards the time evolution as a continuous, wholly predictable process which is governed by a set of coupled, ordinary differential equations (the "reaction-rate equations"); the stochastic approach regards the time evolution as a kind of random-walk process which is governed by a single differential-difference equation (chemical master equation or simply master equation).

Unfortunately the stochastic master equation is often mathematically intractable, because it tries to write a set of (differential) equations and solve them simultaneously for all possible states. So this approach can be used just for very simple systems.

The problem is solving by use of an exact numerical calculations within the framework of the stochastic formulation without having to deal with the master equation directly. It is a relatively simple digital computer algorithm which uses a strictly derived Monte Carlo procedure to numerically simulate the time evolution of the given chemical system. This stochastic simulation algorithm (SSA) correctly accounts for the inherent fluctuations and correlations that are necessarily ignored in the deterministic formulation, as well as the master equation Gillespie developed two exact stochastic simulation algorithms, direct method and first reaction method (FRM). Both of the two Gillespie algorithms, we can use random numbers to select the transitions. The direct method, exactly calculates which reaction occur next (that is shown by random number of μ) and when it occurs (which is shown by random number of τ). In other words, the aim is to generate a random couple of (τ, μ) in correspondence with the suitable probability density. The latter method generates for each reaction μ, a putative time $\tau\mu$ at which reaction occurs. Then select the first reaction with the smallest $\tau*\mu$ and execute it in time $\tau*\mu$. At first look, it may seem that these two algorithms have a great difference with each other, but it can be proved that they are the same [11]. Although, this algorithm solves the master equation. But it needs a large amount of computational effort for simulating of a complex system. Gibson made an improvement of Gillespie algorithm by his "next reaction method". Gillespie algorithm has been applied in many in recent simulations Jason Kastner and Farser [12], Kierzek et al. [13], McAdams and Arkin [14]. The AQP4 channel was simulated by using the Gillespie algorithm (direct method). A FORTRAN program was written for the interested system. An initial value of 10,000 molecules in the initial

state of the model (X0 0 0) has been used in all runs. The rpd (reaction per dot) notation has been used for all resulted graphs. It shows the number of reaction that occurs between each point that appears on a simulation output graph [11]. All the plots are 100 rpd plots. Because of having no truly cutoff range for the complex reactions, Time evolution in range of several minutes has not much effect on the system. This behavior was checked for different selections of H2O and K+ concentrations. So, the simulations have been considered for the first 5 min.

3. Result and Discussion

3.1. Numerous molecular dynamics (MD) simulations provide further insight into how waters across from AQP channels work.

We have used AQP4 as a model. This protein is made up of six transmembrane α-helices arranged in a right-handed bundle, with the amino and the carboxyl termini located on the cytoplasmic surface of the membrane. Contrary to earlier speculations, the MD results of Kong and Ma [15] indicated that asparagines residues of the Asn-Pro-Ala (NPA) motifs in AQP1 are essential for maintaining the water connectivity.

NPA motif has overlapped the middle of the lipid bilayer of the membrane forming a In our model simulation we also find a single file of seven water molecules in all MC runs. Both cytoplasmic and pericytopelasmic vestibules contain many waters. It is oriented perpendicular to the channel axis and is four (or possibly even five) coordinate. Water 4 (at the NPA site) accepts an H-bond from Asparagine residues of the NPA (Asn-Pro-Ala) motifs and donates both H atoms to two adjacent waters. Other waters either donate or accept hydrogen from adjacent waters or donate hydrogen to of the channel protein (Fig 3).

3-D 'hourglass' structure where the water flows through.

This overlap forms one of the two well-known channel constriction sites in the peptide, the NPA motif and a second and usually narrower constriction known as 'selectivity filter' (SF) or ar/R selectivity filter.

This region is usually found towards the extracellular vestibule, approximately 8Å above the NPA motif and is often the narrowest part of the pore.

The results of equilibrium MD simulation, was shown NPA motif and SF region have the most potential energy (Figure 3) and always maintained H-bonds with protein hydrogens in the SF and NPA regions.

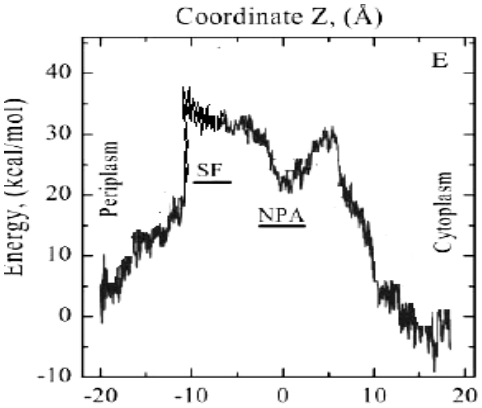

Figure 3; Nonbonded (electrostatic and vdW) interaction energies [2].

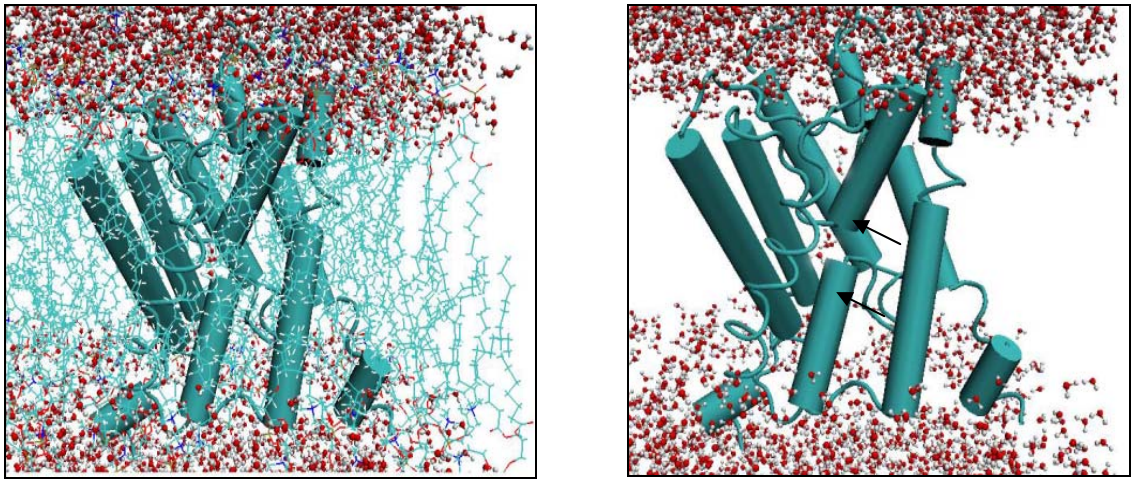

(A) **(B)**

Figure4; A) Part of simulated bilayer membrane and AQP4 protein was placed in it with that obtained at 5 ns applied hydrostatic pressure. **B**) Delete of DMPC molecules for better observing.
NPA motif has shown in flash, water molecules have also shown with CPK drawing method. All of the molecular figures were generated in VMD.

Table 1, Results of Applied Time MD simulations for H_2O

Time	No of H_2O permeation	kcal/mol
ns		
5	7	0.0053
8	12	0.0098
20	100	0.0486

Our result also shows that when time simulation was applied, the concentration of water became slightly higher on the left side and lower on the right side of the membrane due to the compressibility of water (Figure 4). The orientations of the water dipole in our simulations (Figure 3B), which are unique properties of the AQPs family, are correctly reproduced with previous studies like Tajkhorshid et al., [16]. However, in this study we have performed a quantitative permeability measurement using different time simulation on AQP4 model simulation. Results of our time simulations effect are reported in Table 1 and Fig. 4A

3.2. Monte Carlo (MC) simulations provide further insight into how an AQP channel depends on the K+ concentration and the H2O concentration.

We performed 3 simulations for each group selection of water and K+ concentrations by using the direct method of Gillespie. The results have been reported in three times domains: fast (small *t*: 10−4 s), medium (*t*: 10−3 s) and slow domains (large *t*: 10−2 and in some cases 10−1 s) (see Table 2).

Table2, Number of AQP4 states for different concentration of K+ and Water, in different time domain**

Concentrations*	Time	Number							
		X000	X100	X110	X010	X001	X101	X111	X011
K+= 0.15, H2O=0.15	4.6E-04	5289.194	344.0901	0.263	26.11128	0.3396	0	0	0
	4.49E-03	2739.23	1577.903	42.36	120.1443	32.21955	4.18557	0.098	0.055468
	4.7E-02	25.28379	233.754	149.70	143.4312	110.6819	17.57656	5.7	3.2262
K+=0.3, H2O=0.2	4.73E-04	4991.532	644.8834	2.494	20.31261	0.754478	0.020942	0	0
	4.15E-03	1809.355	1988.014	50.90	69.82742	36.70057	9.95877	0.337	0.190742
	1.52E-02	67.01214	767.0794	153.94	86.48027	115.9977	34.72863	1.698	0.961068
K+=0.6, H2O=0.3	4..5E-04	4488.121	1144.698	2.522	19.84509	2.90358	0.208854	0	0
	4.53E-03	836.7303	2296.893	96.84	56.45227	60.89198	29.19598	0.927	0.524682
	1.57E-02	33.74832	825.8993	221.7	66.75744	135.9985	83.49632	7.48	4.23368

** The results are averages in 100 rpd (run per dot).
* Concentrations are given in _M.

The populations of each state in different time domains have been used to describing the results. Table 2 shows that the whole reactions have stochastic nature and the reactants in different states are dependent to each other. They show a non-linear behavior (for instance, see Fig.5).

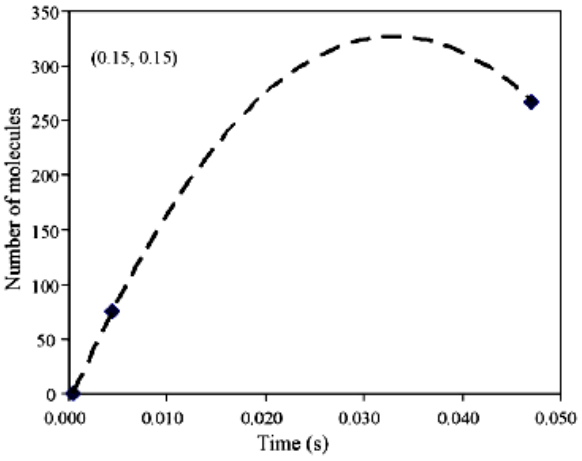

Figure 5; The number of molecule in the X110 state vs. time. Concentrations are 0.15 and 0.15 μM for H2O and K+, respectively

It has a Gaussian form (bell-shaped) dependency to [K+] on the fast time domain. On the other hand, in fast time domain is dependent to [K+] and in small time domain is dependent to [H2O]. Using the results given in Table 2, we can see a distribution of population. This distribution makes a basis for a kinetically reaction pattern which is independent from the concentrations of K+. It shows that reaction paths are strongly time dependent and it is not just [K+] or [H2O] dependent. Of course this pattern may not totally in accordance with experimental or other theoretical results, but such patterns may help to a better understanding of the base unit in any model for extracting the reaction paths and the effective factors on these paths to give more correlation between the theoretical models with experiment. The distribution of population in the states may be used to determine a reaction pattern. This pattern can be seen completely in fast time domain. It still may see, more or less, in medium time domain. So, the reaction path is strongly time dependent. These results indicate that Gillespie algorithm can be a better choice than chemical master equation in biological systems.

In conclusion, it is suggested that the type of studies presented here may give useful information in connection with Molecular modeling could accurately predict the permeability of H2O and K+ in AQP4 in advance of experimental measurements. This study will be helpful for designing MD simulations to study permeation of solutes through AQP4 that are not easily amenable to experiments such as carbon dioxide, oxygen and some drugs. MC simulations make a basis for a kinetically reaction pattern ions across the AQP4 channels.

References

[1] de Groot, B. L., A. Engel, and H. Grubmu¨ ller. 2001. A refined structure of human aquaporin. FEBS Lett. 504:206–211.

[2] Amizoguchi, Y .Fujiyoshi. 2005. Implications of the Aquaporin-4 structure on array. J.MOL.BIOL.355:628-637

[3] Mazzag, B., Tignanelli, C.J., Smith, G.D., 2005. The effect of residual Ca2+ on the stochastic gating of Ca2+-regulated Ca2+ channel models. J. Theor. Biol. 235, 121–150.

[4] Falcke, M., 2003b. Buffers and oscillations in intracellular Ca2+ dynamics. Biophys. J. 84, 28–41.

[5] Owicki, J. C., and H. A. Scheraga. 1977. Preferential sampling near solutes in Monte Carlo calculations on dilute solutions. Chem. Phys. Lett. 47:600–602.

[6] Hu, J., Ma, A. and Dinner, A. R. 2006 Monte Carlo simulations of biomolecules: The MC module in CHARMM. J. Comp. Chem. 27, 203-216.

[7] Roux, M. Schlenkrich, J. C. Smith, R. Stote, J. Straub, M. Watanabe, J. Wiorkiewicz-Kuczera, D. Yin, and M. Karplus. 1998. All-atom empirical potential for molecular modeling and dynamics studies of proteins. J. Phys. Chem. B 102:3586-3616.

[8] Jorgensen, W. L., J. Chandrasekhar, J. D. Madura, R. W. Impey, and M. L. Klein. 1983. Comparison of simple potential functions for simulationg liquid water. J. Chem. Phys.

[9] Essmann, U., L. Perera, M. L. Berkowitz, T. Darden, H. Lee, and L. G. Pedersen. 1995. A smooth particle mesh Ewald method. J. Chem. Phys. 103:8577-8593.

[10] H.H. Haeri, M. Monajjemi. 2007. A kinetic Monte Carlo simulation study of inositol 1,4,5-trisphosphate receptor (IP3R) calcium release channel. Computational Biology and Chemistry 31 (2007) 99–109.

[11] Gillespie, D.T., 1977. Exact stochastic simulation of coupled chemical reactions. J. Phys. Chem. 8 (1), 25.2340–25.2361.

[12] Finch, E.A., Turner, T.J., Goldin, S.M., 1991. Calcium as coagonist of inositol 1,4,5-trisphosphate-induced calcium release. Science 252, 443–446.

[13] Keizer, J., Smith, G.D., 1998. Spark-to-wave ransition: salutatory transmission of calcium waves in cardiac myocytes. Biophys. Chem. 72, 87–100.

[14] Mak, D.D., McBride, S., Raghuram, V., Yue, Y., Joseph, S.K., Foskett, J.K., 2000. Single-channel properties in endoplasmic reticulum membrane of recombinant type 3 inositol trisphosphate receptor. J. Gen. Physiol. 115, 241–255.

[15] Kong, Y., and J. Ma. 2001. Dynamic mechanisms of the membrane water channel aquaporin-1 (AQP1). Proc. Natl. Acad. Sci. USA. 98:14345–14349.

[16] Ilan, B., E. Tajkhorshid, K. Schulten, and G. A. Voth. 2004. The mechanism of proton exclusion in aquaporin channels. Proteins. 55:223–228.

Molecular Simulation Approaches for Finding Amino Acids Interaction between Immobilization luciferase Enzyme on Liposome as a Hydrophobic Adsorbent

Sima Afsharnezhad[*1], Elham Mousavi Nezhad [2], Saman Hosseinkhani[3]
Masoud Saleh Moghadam[2], Majid Monajjemi[4]
sanegad@yaho.com

[1]Department of Biochemistry, Mashhad Islamic Azad University Branch, Mashhad. IRAN.
[2]Department of Biochemistry, Payame Nour University, Mashhad. IRAN.
[3]Department of Biochemistry, Tarbiat Modarres University, Tehran,IRAN
[4] Department of Physical Chemistry, Science & Research Branch ,Islamic Azad University, Tehran. IRAN

Abstract: Bio- Luminescence is an attractive phenomenon in which an organism converts chemical energy into light. This reaction is catalyzed by enzymes generally called luciferase. They catalyze the oxygenation of compounds which generally called luciferin. On of the problems for working with luciferase enzyme is that this enzyme loses its activity and resistance. Reform of enzymes functional characteristics (such as energy and resistance) by fixing them on solid matrix is considered as operational approaches in enzyme technology.

This approach causes easy use of enzyme, flexiblity in the reactor designing, less enzyme consumption, and no product pollution with enzyme, etc. This research goal is to entrap luciferase protein in liposome as a hydrophobe bed and to determine the involved areas and amino acids of this protein with the hydrophobe bed. Finding of these involved amino acids with liposome membrane can be effective to fix the enzyme better by using protein engineering method such as side direct mutagenesis.

Keywords: Luciferase, DPPC, liposme, Molecular Dynamic simulation.

1- Introduction

Luciferase is a generic name for enzymes commonly used in nature forbioluminescence. The most famous one is firefly luciferse from the firefly *Photinus pyralis* [1].

In luminescent reactions, light is produced by the oxidation of a luciferin (a pigment), sometimes involving Adenosine triphosphate (ATP).

The rates of this reaction between luciferin and oxygene are extremely slow until they are catalyzed by luciferase. The reaction takes place in two steps [2]:

luciferin + ATP→ luciferyl adenylate + ppi

luciferyl adenylate + O_2→ oxyluciferin + AMP+ light

In first phase, luciferase with carboxyle- luciferin group adonilation in the presence of MgATP activates this subestrate.

In second phase, luciferase acts as a mono- oxygenase and by effect on luciferile- adonilate as well as making products, produces light- ray.

Firefly luciferase is a 62 kDa protein [3] and is a single chain polypeptide with 550 amino acids. The protein is folded into two compact domains. The large N-terminal domain consists of a b-barrel and two b-sheets. The sheets are flanked by a-helices to form a αβαβαfive-layered structure [4].

Corresponding Author: Sima Afsharnezhad**,** [1]Department of Biochemistry, Mashhad Islamic Azad University Branch, Mashhad. IRAN.

Figure 1: Luciferase structure

Firefly luciferase has been extensively used in molecular and cell biology, in particular for the efficient detection and quantification of ATP and as a reporter of genetic function [5]. Luciferase has also been studied as a model for possible protein–anaesthetic interactions, being one of the few soluble proteins sensitive to a wide range of general anaesthetics[6].

The bioluminescent reaction has applications in a wide range of analytical techniques [7-9]. The scope of its applications include: the ultra-sensitive detection of ATP [10,11]; the detection of phosphatase activity [12]; use as a reporter gene in molecular biology [7]; use in DNA sequencing [13]; as a tool for monitoring in vivo protein folding and chaperonin activity [14].

The ultra-sensitive detection of ATP forms the basis of its use in the detection of microorganisms [15].

One of the most interesting luciferase application is to measure ATP in various systems therefore, in this purpose luciferase immoblization is always considered. Today, liposomes are used as a matrix for enzymes fixation [16]. Since one of the most successful enzyme immoblizatin methods is to enclose them in the liposome, hence, dynamic molecullar simulation of liposome proteins helps in understanding more about their function and interaction with their surrounding environment.

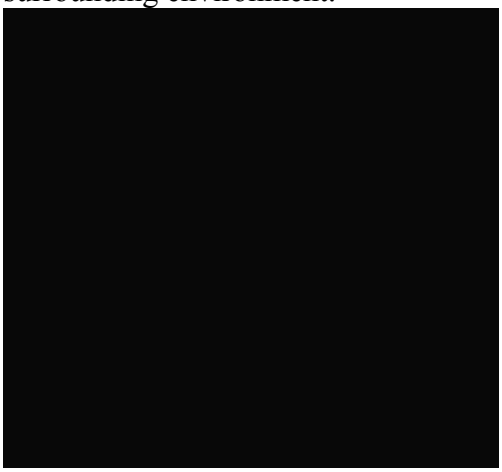

Figure2: liposome structure

Two basic methods are used to add protein to the liposome system. First, protein radius is estimated, then lipid structures add to a protein and two lipid layers are formed around protein. Finally, through intellectual optimizing stage worst connections are eliminated and an appropriate structure including protein- liposome is obtained (CHARMm) program uses this method, so in this research, modeling of luciferase liposome system is performed by this method.

2- Methods and Matrials

2-1 Luciferase simulation in the membrane

Accordingly, PDB file of related protein with 1BA3 code was obtained from protein data bank. Luciferase protein containing amino acid is 1BA3 structure of obtaind information from solid crystalography for the mentioned protein. Then, protein is rotated around the X- axis in a way that it is along with Z- axis.

In the next stage by using the simulated DPPC of the previous stage, a two layer phospholipid is made, there by 83 DPPC molecules in the upper layer and 81 DPPC moleculse with H_2O in lower layer are placed.

After making the liposome protein system, the moderation stages of dynamic molecules were carried out by two dynamic methods of NRT (instant volume and temperature) and NPAT (instant potential, area, and temperature) for two DPPC layers in 323^{o}k. Finally, system in 2ns period by using dynamic molecullar method was moderated. Last stage of simulated model in term of amino acids involved in luciferase protein interaction with DPPC lipid two- layer membrance is analyzed by VMD software as a part of two- layer lipid liposome.

3- Results and Discussion

Finally, after considering all the aspects such as the number and distance of H_2O molecules around phospholipid, part of simulated membrane and luciferase protein was placed in it by dynamic molecular method and finally amino acids involved in liposme membrane were determined by VMD graphic software.

Table. 1; Amino acids which have interaction with bilayer lipid of liposome.

TYR-179	LYS-180	ASP-181	ARG-182	GLN-183
	68	69	70	71
	PHE-167	VAL-168	THR-169	SER-170
HIS-171	LEU-172	PRO-173	PRO-174	
GLY-175	PHE-176	ASN-177	GLU-178	

As it was shown, these amino acid are often aromatic (esp: Phe 181- Phe176, Glu178 and Asp 180) and interact with polar heads of DPPC phospholipid.

These amino acids are located in some part of helix number 6 and 2 (see Figure 3) of luciferase are placed in liposome and smallenss of this involved area can be the rationale for the lowpercent of luciferase entrapment. This helixes are far from active site of luciferase, so, intrapping dose not effect to activity of luciferase.

In conclusion, it is suggested that the type of studies presented here may give useful information in connection with Molecular modeling and site-directed mutagenesis to engineer, Luciferase for special purposes. Furthermore, MD simulation provides insight into the mechanism of Luciferase immobilization on hydrophobic adsorption, like liposome.

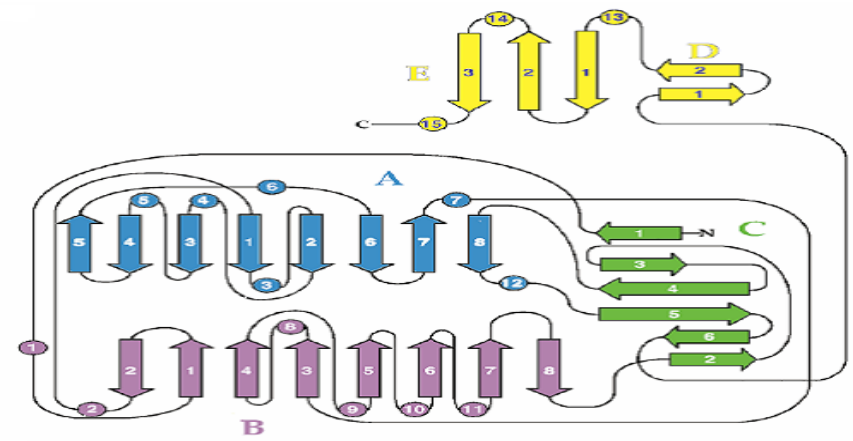

Figure 3: Overall topology of the firefly luciferase enzyme, Topological diagram illustrating the secondary structure elements coloured by subdomains. The circles represent a-helices, which have been numbered sequentially, and the arrows represent b-strands, which have been numbered sequentially for each of the five b-sheets, A–E. The secondary structure elements have been assigned using the program DSSP [4].

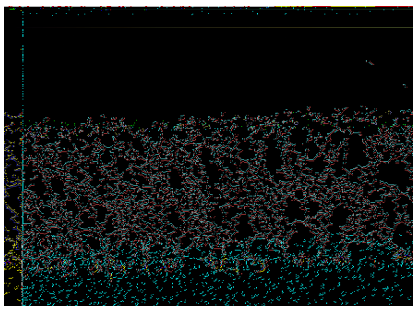

Figure4: the figure of DPPC with H2O.

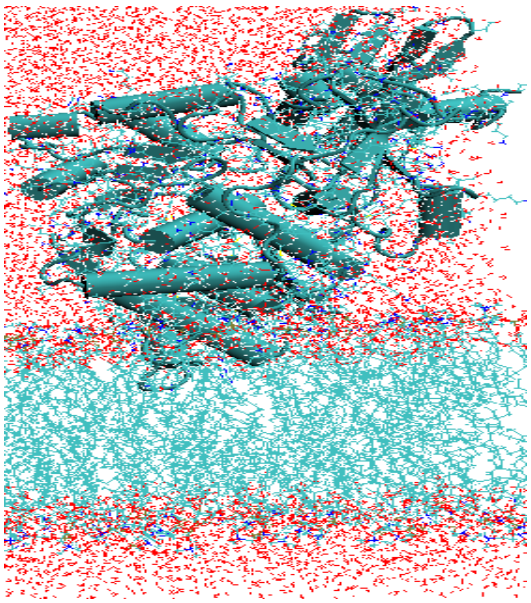

Figure5: A Part of simulated membrane and luciferase protein was placed in it by molecular dynamic method.

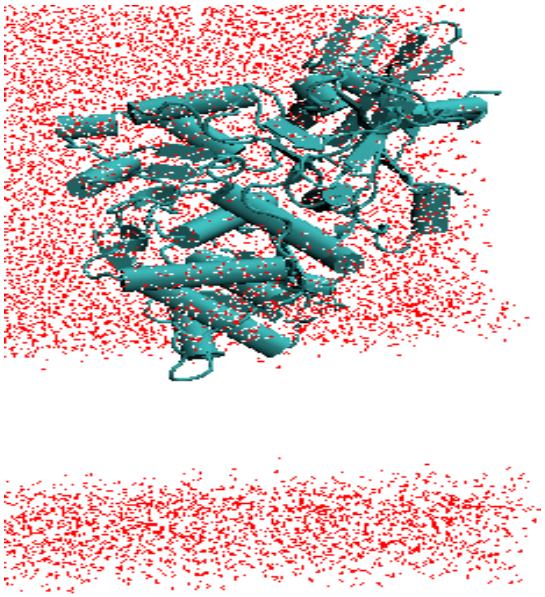

Figure6: A Part of simulated membrane and luciferase protein, but DPPC molcules were deleted for better observation.

References

[1] Cormier, M.J., Hori, K. and Anderson, J.M. 1975. Bioluminescence in coelenterates. Biochim.Biophys. Acta 14 : 2371-2376.

[2] Bruce R. Branchini, Rachelle A. 1997. Identification of a Firefly Luciferase Active Site Peptide Using a Benzophenone-based Photooxidation Reagent, BBA. 272:19359-19364

[3] De Wet, J.R., Wood, K.V., Helinski, D.R. & DeLuca, M. 1985. Cloning of firefly luciferase cDNA and the expression of active luciferase in Escherichia coli. Proc. Natl. Acad. Sci. USA 82: 7870–7873.

[4] Elena Conti, Nick P Franks and Peter Brick, 1996. Crystal structure of firefly luciferase throws light on a superfamily of adenylate-forming enzymes, Biophysics Section, Current Biology 4:287–298.

[5] Gould, S.J. & Subramani, S. 1988. Firefly luciferase as a tool in molecular and cell biology. Anal. Biochem. 175: 5–13.

[6] Franks, N.P. & Lieb, W.R. 1984. Do general anaesthetics act by competitive binding to specific receptors? Nature 310: 599–601.

[7] Gould S.J., Subramani S., 1988 Anal. Biochem. 175- 5.

[8] K.V. Wood, Y.A. Lam, W.D. McElroy, 1989 J. Biolumin Chemilumin. 289-294.

[9] Price R.P., Squirrel D.J., Murphy. M, J. 1998. Clinical Ligand Assay 21: 349-354.

[10] Brovko L., Romanova N.A., Ugarova N., 1994. Anal. Biochem 220- 410.

[11] Spielmann H., Jacob-Muller U., P. Schulz, 1981. Anal. Biochem 113: 172.

[12] Miska W., Geiger R., 1988. Biol. Chem. Acta, 369- 407.

[13] Ronaghi M., Karamohamed S., B. Pettersson, M. Uhlen, P. Nyren, 1996. Anal. Biochem. 242- 84.

[14] Holm, L. & Sander, C. 1993. Protein structure comparison by alignment of distance matrices. J. Mol. Biol. 233:123-138.

[15] Ludin A., in: M. DeLuca, W.D. McElroy (Eds.), Bioluminescenc and Chemiluminescence, Academic Press, New York 1981, p. 187.

[16] Khaleque A., Okumura Y., M. Mitani**,** 2006. Liposome Immobilization on Cross- linked Polymer Gel by In Situ Formation of Cleavable Covalent Bonds Journal of Bioactive and Compatible Polymers,. 21:539-555.

Monte Carlo Simulation of Solvent Effects in Molecularly Imprinted Polymers Rational Design

[1]Piyarat Nimmanpipug, [1]Vannajan Sanghiran Lee, [1]Mookda Pattarawarapan, [2]Majid Monajjemi
[1]Department of Chemistry, Faculty of Science, Chiang Mai University, Chiang Mai, Thailand,
[2]Department of Chemistry, Science and Research Campus, Islamic Azad University, Tehran, Iran

Abstract: Monte Carlo simulation and Quantum Calculations for the design of molecularly imprinted polymers (MIPs) are studied. Molecular template using the rational choice of suitable monomer set used in MIP was designed. Monte Carlo simulations were performed at various temperatures in different solvent and dielectrics effects. The prepolymerization adducts between the template at different functional monomers will be discovered in this study.

Keywords: MIP, Monte Carlo, Quantum Calculations

INTRODUCTION

Molecularly imprinted polymers (MIPs) have been interested in analytical science and technology. Such polymers have many potential applications ranging from solid phase extraction (SPE) materials, antibody-like sorbent assays, and selective recognition layers in sensing devices from their chemical and mechanical stability together with high selectivity for specific template.

As molecular recognition of biologically relevant molecules governs essential biological interactions, the creation of synthetic selective receptor-like macromolecule capable of recognizing molecular targets of interest with high affinity and selectivity have been one of long-term goals for chemical, biological and pharmaceutical research scientists. To obtain specific nano-pore structure, synthesis conditions in term of monomer structure and solvent are needed to be designed.

To understand MIP from chemical and physical basic, the molecular interactions involving in the templating process in self-assembly will be clarified. In this study, a combination of Monte Carlo (MC) simulation and quantum calculations for the design of MIPs is studied. Molecular template using the rational choice of suitable monomer set used in MIP was designed using the methods. MC simulations were performed at various temperatures in different solvent effects and dielectrics. The prepolymerization adducts between the template at different functional monomers will be gotten for indinavir (IDV) template.

MATERIALS AND METHODS

Totally 20 different monomers: acrolein, acrylamide, acrylamido-2-methyl-1-propanesufonic acid, acrylic acid, acrylonitrile, allylamine, *m*-divinyl benzene, *p*-divinylbenzene, *N,N'*-diethylamino ethyl methacrylate, ethylene glycol dimethacrylate, 2-hydroxyethyl methacrylate, itaconic acid, methacrylic acid, *N,N'*-methylene bisacrylamide, urocanic acid ethyl ester, vinyl benzene, 1-vinyl imidazole, 2-vinyl imidazole, and 4-vinyl imidazole, was generated for investigate molecular recognition properties. Five selected monomers were docked on IDV template. The template structure was minimized using density functional theory B3LYP 6-31G* method of Gaussian 03 program. Configurational and conformational searches of monomer-IDV complexes were carried out with a Monte Carlo simulation technique with COMPASS forcefield. The docked bimolecular complexes were set by a random rotation around all three axes at its center of mass and translational movement in three-dimensional space. Each monomer was allowed to be flexible and rotate randomly toward IDV using Materials studio 4.2 suite of program. To investigate the solvent effect, IDV molecule was solvated with pure water (Figure 1), 50% MeOH, and pure MeOH in box size of 15 x 15 x 25 angstrom in HyperChem 7.0 for MC simulation at 300, 320, and 340 K. The lowest energy structure from MC search was collected and optimized to calculate IR frequency using HF 6-31G* in Gaussian program.

Corresponding Author: Piyarat Nimmanpipug, Department of Chemistry, Chiang Mai University, Chiang Mai,Thailand , Tel: +66-53-943341-5 ext. 136, Fax: +66-53-892277, E-mail:piyaratn@gmail.com
Majid Monajjemi, Department of Chemistry, Islamic Azad University, Science and Research Branch, P. O. Box 14155-775, Tehran, Iran, E-mail: m_monajjemi@yahoo.com

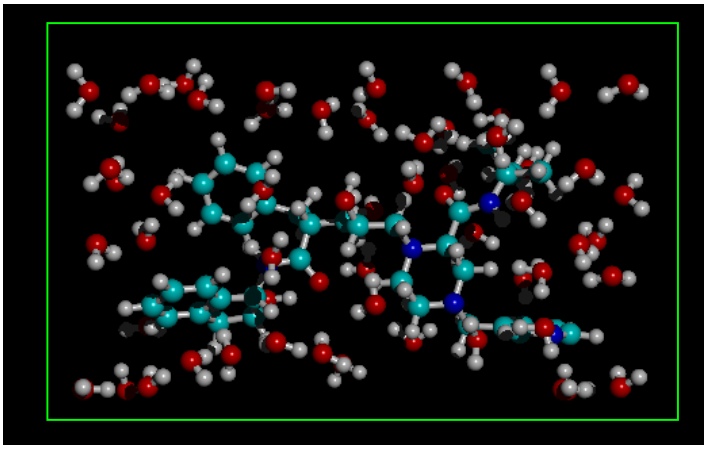

Fig. 1: IDV molecule solvated with water for MC simulation in HyperChem program

MC simulations: The Metropolis Monte Carlo method is used in Materials studio 4.2 suite of program. The MC method samples the configurations in an ensemble by generating a set of configurations, m, n, ..., where the probability of transition from m to n is π_{mn}. In case that configuration m is sampled with a frequency ρ_m, by mean, $\rho_m\pi_{mn}$ of them are transformed to n. In the same way, configurations n are transformed to m with probability of $\rho_n\pi_{nm}$. The flux density of the flow, ρ, will be, then, preserved. The balance condition for equilibrium is as following:

$$\rho_m\pi_{mn} = \rho_n\pi_{nm}$$

In the MC method, the transforms configuration m to n is a two-stage process. Starting with sampling a configuration with probability α_{mn}. Then, transition probability, π_{mn}, can be calculated using the equation:

$$\pi_{mn} = \alpha_{mn}P_{mn}$$

transitions of a configuration m to a higher probability ($\rho_n > \rho_m$) will be accepted, on the other hand, transitions to configurations with a lower favorable ($\rho_n < \rho_m$) are less likely to be accepted.

RESULTS AND DISCUSSION

Monomer library and prepolymerization adducts: The lowest binding energy per monomer of each compound was gotten from MC simulation. Among variety functional monomer, *N,N'*-methylene bisacrylamide shows the lowest binding energy stabilized from H-bonding and *van der Waals* interactions. Figure 2 shows the *N,N'*-methylene bisacrylamide-IDV binding structure. The H-bond was formed both between monomers and monomer-template indicating recognition properties of noncovalent MIPs to maintain the complexe during and after the polymerization.

Solvent effect: Solvating with various solvent systems (water, 50% MeOH, and MeOH), IDV was found to show different IR spectrum. As shown in Figure 3, IR intensity is decreased at 3,490 and 1,450 cm^{-1} at 300K. In addition, we found that the profile is changed in far-IR region. The spectrum in range 200-400 cm^{-1} was changed from replacing water with MeOH. These phenomena are the result of changing of molecular bond torsion of amide group next to i-butyl group from solvent effect. The dielectrics change influences on molecular vibration and attributed to bending, torsional, and elastic motions associated with the local structure of solvent.

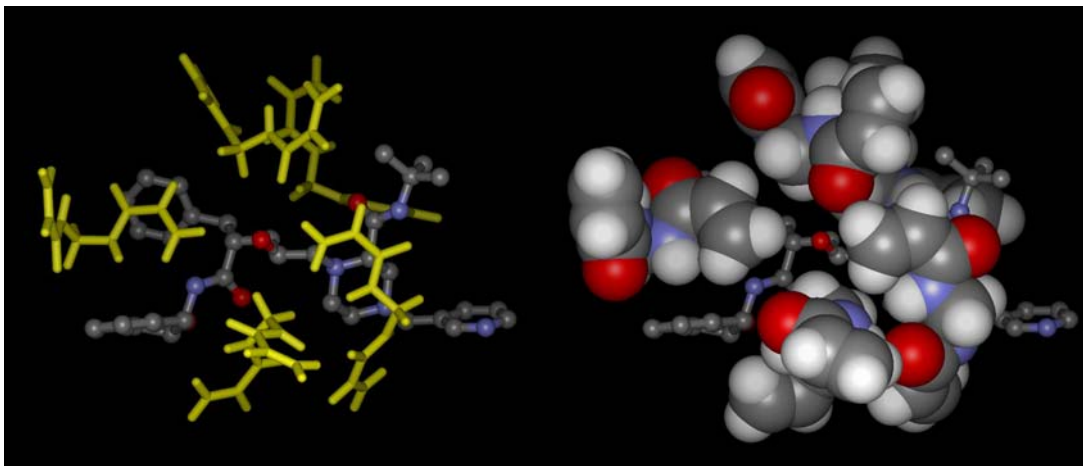

Fig. 2: *N,N'*-methylene bisacrylamide-IDV binding structure from MC simulation

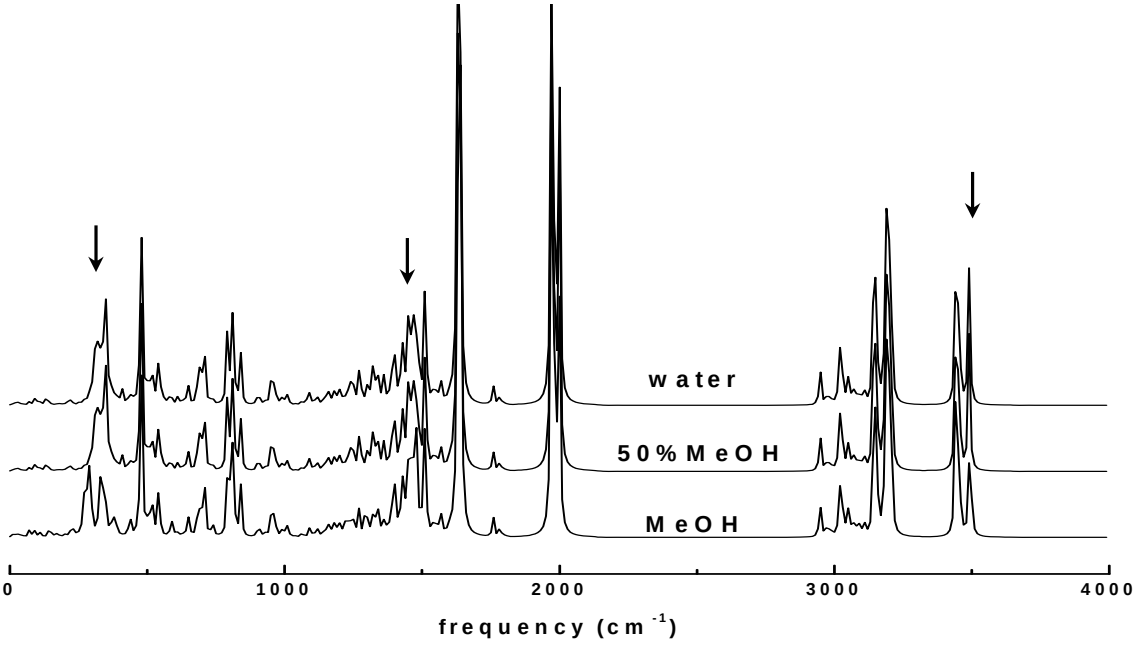

Fig. 3: Infrared Spectrum calculated by semi-empirical AM1 method with 6-31G* basis set of IDV structure from three solvation MC simulation systems at 300K

CONCLUSION

By means of MC simulation and quantum calculations, monomers with different functional group complexed with an anti-HIV drug, IDV, were generated. In this screening, *N,N'*-methylene bisacrylamide shows the lowest binding energy structure. Replacing water with MeOH solvation,

changing of molecular bond torsion of amide group next to i-butyl group was observed. This study shows that dielectrics change influences on molecular vibration and attributed to bending, torsional, and elastic motions.

ACKNOWLEDGEMENTS

We would like to acknowledge Computational Nanoscience Consortium (CNC) Nanotechnology (NANOTEC), Thailand for the access to Material Studio Version 4.2 program package, Computational Simulation and Modeling (CSML), Department of Chemistry, Chiang Mai University, Chiang Mai, Thailand, the Center for Innovation in Chemistry: Postgraduate and Research Program in Chemistry (PERCH-CIC), and the Commission on Higher Education and Thailand Research Fund (TRF), Thailand for the contribution and for providing the grant to support this project.

REFERENCES

1. Wulff, G.; Sarhan, A. *Angew*. *Chem., Int. Ed. Engl.* 1972, *11*, 341-344.
2. Vlatakis, G.; Andersson, L. I.; Müller, R.; Mosbach, K. *Nature (London)* 1993, *361*, 645-657.
3. Andersson, L. I. *Anal. Chem.* 1996, *68*, 111-117.
4. Frisch, M. J.; Trucks, G. W.; Schlegel, H. B.; Scuseria, G. E.; Robb, M. A.; Cheeseman, J. R.; Montgomery, Jr., J. A.; Vreven, T.; Kudin, K. N.; Burant, J. C.; Millam, J. M.; Iyengar, S. S.; Tomasi, J.; Barone, V.; Mennucci, B.; Cossi, M.; Scalmani, G.; Rega, N.; Petersson, G. A.; Nakatsuji, H.; Hada, M.; Ehara, M.; Toyota, K.; Fukuda, R.; Hasegawa, J.; Ishida, M.; Nakajima, T.; Honda, Y.; Kitao, O.; Nakai, H.; Klene, M.; Li, X.; Knox, J. E.; Hratchian, H. P.; Cross, J. B.; Bakken, V.; Adamo, C.; Jaramillo, J.; Gomperts, R.; Stratmann, R. E.; Yazyev, O.; Austin, A. J.; Cammi, R.; Pomelli, C.; Ochterski, J. W.; Ayala, P. Y.; Morokuma, K.; Voth, G. A.; Salvador, P.; Dannenberg, J. J.; Zakrzewski, V. G.; Dapprich, S.; Daniels, A. D.; Strain, M. C.; Farkas, O.; Malick, D. K.; Rabuck, A. D.; Raghavachari, K.; Foresman, J. B.; Ortiz, J. V.; Cui, Q.; Baboul, A. G.; Clifford, S.; Cioslowski, J.; Stefanov, B. B.; Liu, G.; Liashenko, A.; Piskorz, P.; Komaromi, I.; Martin, R. L.; Fox, D. J.; Keith, T.; Al-Laham, M. A.; Peng, C. Y.; Nanayakkara, A.; Challacombe, M.; Gill, P. M. W.; Johnson, B.; Chen, W.; Wong, M. W.; Gonzalez, C.; and Pople, J. A.; Gaussian, Inc., Wallingford CT, 2004.

Salt and temperature effects on nucleic acids solution: Molecular Dynamics Simulation and Normal Mode Analysis

[1] Vannajan Sanghiran Lee, [1] Piyarat Nimmanpipug, [2] Chirlada Settakorn, [3] Kanchanok Kodchakorn, and [4] Majid Monajjemi
[1] Department of Chemistry, [2] Department of Physics, Faculty of Science, Chiang Mai University, Chiang Mai, Thailand, [3] Department of Biochemistry, Faculty of Medicine, Chiang Mai University, Chiang Mai, Thailand, [4] Department of Chemistry, Islamic Azad University, Science and Research Branch, P. O. Box 14155-775, Tehran, Iran

Abstract: Major factors in determining the stability and the binding behavior of nucleic acids are depend on the salt concentration and temperature. This study has been focused on the calculation of the absorption spectra of DNA in B-form. Monte dynamics simulation has been performed to obtain the optimum structure of DNA in water and various salts concentrations with the temperature range of 300-315K using AMBER 9. The potential energy of nucleic acids is minimized and the normal mode analysis is performed using Materials Studio 4.3 program package. The calculated absorption spectra are compared to experimental data. The results are correspondence well with the experimental data.

Keywords: DNA conformation transition, Molecular dynamics simulation, Salt effect, Temperature effect, normal mode analysis, FIR spectra

INTRODUCTION

The main DNA conformations (A and B forms, shown in Fig. 1) depend on the sequence, ionic environment, and hydration conditions. Ions play an important role in DNA structure by shielding the phosphate charges in the DNA backbone and affecting water activity around DNA[1-5]. Increased salt concentrations over 1 M salt favor the formation of A-DNA and Z-DNA over B-DNA[6,7] and salt effects constitute major electrostatic contributions in the binding of ligands to nucleic acids[8]. There has been an increasing interest in the application of terahertz (THz) radiation to the spectroscopic sensing of DNA materials and related biological materials[9-13]. This involves the fundamental measurements of absorption signatures of biological materials and the theoretical interpretation of the physical origin of these signatures. The calculated absorption spectra of DNA reproduce many essential features of the experimental THz signatures in 10-25 cm^{-1} range. Many experimental biophysical techniques are available for the study of nucleic acid structural properties. However, no experimental technique is capable to detect the structural evolution of DNA and to generate a complete description of the dynamic structure in solution environment.

In this paper, we are interested in how salt concentration affects in the dynamic process of the B-DNA to A-DNA transition in two different temperatures using Molecular Dynamics (MD) simulation and to observe the change in the normal modes of the very far IR absorption spectra. Such theoretical technique can provide a complete description of the structures, structural evolution, and information about the spectral characteristics of the vibrational spectra, which is one of fundamental importance for the solution of many applied and scientific problems.

MATERIALS AND METHODS

Two models of 12 base pairs poly(A)-poly(T) DNA in a canonical double-strand A-form (model A) and B-form (model B) in Figure 1 generated from Discovery Studio 1.7[14] have been investigated using MD simulations.

Corresponding Author: Vannajan Sanghiran Lee, Department of Chemistry, Chiang Mai University, Chiang Mai,Thailand , Tel: +66-53-943341-5 ext. 117, Fax: +66-53-892277, E-mail: vannajan@gmail.com
Majid Monajjemi, Department of Chemistry, Islamic Azad University, Science and Research Branch, P. O. Box 14155-775, Tehran, Iran, E-mail: m_monajjemi@yahoo.com

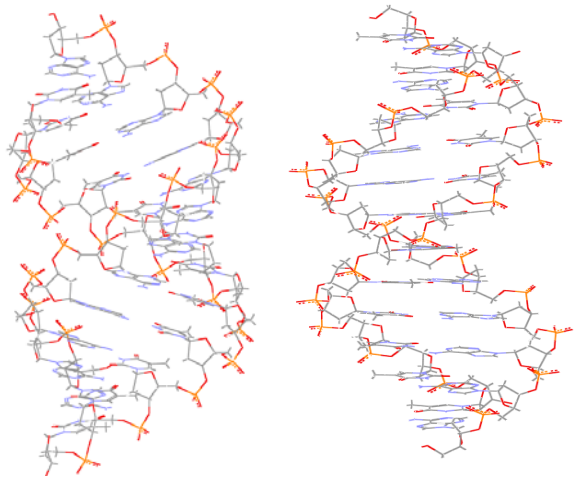

Fig. 1: A-DNA (left) and B-DNA (right)

Two different salt concentrations and two different temperatures were simulated. In aqueous solution, the neutralized poly(A)-poly(T) was solvated by a cubic box of SPC waters which extended at 6 Å from DNA while in salt condition, NaCl salts were added in extended at 6 Å to the neutralized poly(A)-poly(T) without water. Each models were simulated at 300 and 315 K using force filed ff03 in the AMBER9 package[15] for a total time scale of 1 ns. The systems were identified as

A1) minimized A-DNA in gas phase at 300 K
A2) A-DNA in water at 300 K
B1) minimized B-DNA in gas phase at 300 K
B2) B-DNA in water at 300 K
B3) B-DNA in water at 315 K
B4) B-DNA in salts at 300 K
B5) B-DNA in salts at 315 K.

Then, simple protocols were adopted: first, a short minimization was performed with 500 cycles of steepest descent followed by 500 cycles of conjugated gradient during, which all DNA atoms were kept frozen with a positional restraints force of 100 kcal mol^{-1} $Å^{-2}$. For the equilibration, 60 ps heating up from 0 to 300 K (another simulation condition from 0 to 315 K) was performed with harmonic restraints of 5 kcal mol^{-1} $Å^{-2}$. Then, two steps of the restrained MD simulation at constant-pressure and constant-temperature conditions were carried out for relaxing the modeled systems with the restrain factors of 5.0, 2.5 kcal mol^{-1} $Å^{-2}$ for 200 ps in each restrain cycle. For the first 60 ps, After that, the harmonic restrain of 1.0 were kept only for DNA end chains and the simulation were continued to complete the total time of 1 ns. The temperature-bath coupling was achieved by the Berendsen algorithm. Long-range interactions were taken into account, via the particle mesh Ewald method (PME). The time step is 2 fs using SHAKE, and snapshots were taken every 0.2 ps. All the PME and SHAKE parameters were set to default. For data analysis, we used program ptraj to obtain the average structures over the final nanosecond and the root-mean-square deviation (RMSD) over the trajectories of the 500-1000 ps simulations. The selected structures were minimized and Normal mode analysis and the vibrational spectra were calculated using Discover combined with use of AMBER forcefield in Materials Studio. The Hessian matrix, a matrix of the second derivatives of the energy, is used to calculate the normal modes of vibration.

RESULTS AND DISCUSSION

From our MD investigation, Figure 2 shows the RMSD of all the atoms in the DNA during the time from 450-1000 ps indicating the equilibrium of a system had been reached after 500 ns. The average RMSDs for the simulation were: 1.67 Å for A2; 1.18 Å for B2 and B3; 1.26 Å for B4; 1.18 Å for B5. A DNA seems to change conformation more than B-DNA in water. However, the RMS values are very similar and did not change much from the starting conformation. The crucial parameters in identified the two forms of DNA were identified by the shortest O (sugar) –O (sugar) distance across the minor groove which summarized in Table 1.

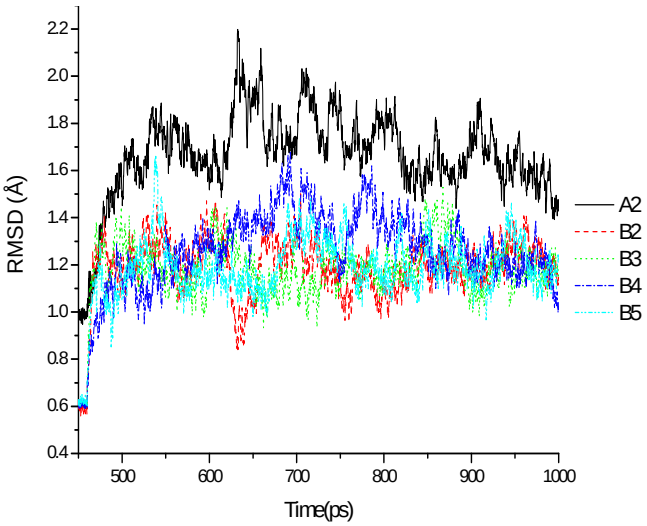

Fig. 2: The RMSDs in comparison to the starting structures

Since our study was done in the extreme case of high salt concentration. Therefore, the change from B-DNA to A-DNA would be transformed in the fast dynamics process during the simulation time which is obviously seen in our calculation. From Table 1, the change in the minor-groove width was observed in all B model, however, we can not conclude clearly from such parameter whether which form is more dominant in the end of simulation.

Table 1 The minor-groove width (Å) of the final MD simulation

	A1	A2	B1	B2	B3	B4	B5
Minor-groove Width (Å)	13.64	15.14	6.48	8.49	8.29	8.43	8.46

In contrast, the transformation of B-DNA to A-DNA in high salt concentration can be observed quite clear from the spectra in the far infrared region. The calculated infrared spectra in Figure 3 show the significantly different of the peak in 0-60 cm^{-1} region between the two forms of DNA. The peaks from the solvent are attributed to bending and torsional motions associated with the local structure of liquid water and are located in the 55-70 cm^{-1} spectral region. In comparison with the midinfrared measurements, the DNA samples were measured by synchrotron Fourier transform infrared (FTIR) spectromicroscopy at the Advanced Light Source at Lawrence Berkeley National laboratory at beamline 1.4. [16-17]

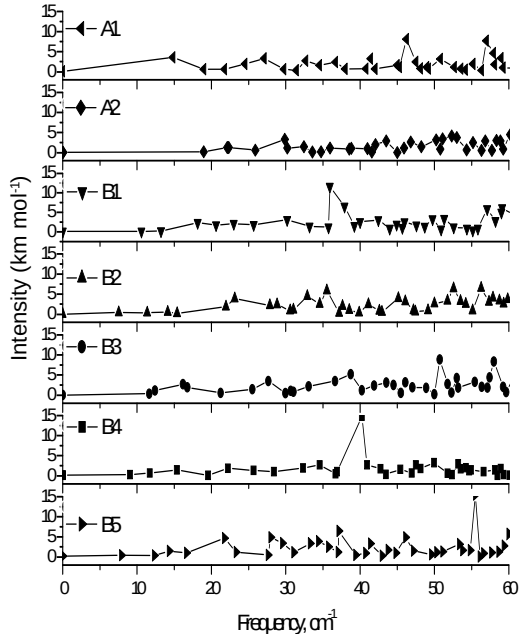

Fig.3 Calculated absorption spectra of poly(A)-poly(T).

Most of the measured resonance peaks are found and correlated well with the modeled spectrum. The list of normal modes of A-DNA and B-DNA from the midinfrared experiment were reported in Table 2. The DNA in aqueous (A2 and B) exhibits the diffuse peak than the minimized DNA (A1 and B1), which show more strong peak, in gas phase due to the diffusion properties and interaction of solvents in and around DNA. The high temperature accelerated the transformation to A-form in high salt concentration as indicated in B5 model. Unclear result on the calculated spectra of high salt concentration at 300 K which is more similar to B-form in gas phase need to be further discussed.

Table 2 Normal modes in cm^{-1} from midinfrared experiment.

A-DNA	B-DNA
13.71	8.82
25.74	20.86
37.76	32.89
49.79	44.93
61.82	56.97

CONCLUSION

Fast structural transformation of poly(A)-poly(T) from B-form to A-form is observed by high salt concentration and temperature during molecular dynamics simulation. The signature of the peak in far infrared region could be a better indicator for such transformation than the conformational parameter such as the width of minor groove. Our absorption calculation agrees reasonably well with the measured absorption spectra.

ACKNOWLEDGEMENTS

We would like to acknowledge Computational Simulation and Modeling (CSML), Department of Chemistry, Chiang Mai University, Chiang Mai, Thailand, NANOTEC Thailand, and The Center for Innovation in Chemistry: Postgraduate and Research Program in Chemistry (PERCH-CIC) for the contribution and for providing the grant to support this project.

REFERENCES

1. Kubinec M.G., Wemmer, D.E., 1992. J. Am. Chem. Soc. 114:8739–8740.
2. Rau, D.C., Parsegian, A., 1992. Biophys. J. 61:246–259.
3. Urabe, H., Kato, M., Tominaga, Y., 1990. J. Chem. Phys. 92:768–774.
4. Forester, T.R., McDonald, I.R., 1991. Mol. Phys. 72:643–660.
5. Feig, M., Pettitt, B. M., 1999. Biophys. J. 77:1769–1781.
6. Nishimura, Y., Torigoe, C., Tsuboi, M., 1986. Nucleic. Acids. Res.14:2737–2748.
7. Wang, Y., Thomas, G.A., Peticolas, W.L., 1989. J. Biomol. Struct. Dyn. 6:1177–1187.
8. Misra, V.K., Sharp, K.A., Friedman, R.A., Honig, B.J., 1994. J. Mol Biol 238:245–263.
9. Woolard, D. L., Loerop, W. R., Shur, M. S., 2003.Terahertz SensingTechnology, Volume 1: Electronic Devices and Advanced SystemsTechnology; Volume 2: Emerging Scientific Applications & Novel Device Concepts, Singapore: World Sci.
10. Mittleman, D., 2003. Sensing with Terahertz Radiation, ser.Opt. Sci., Berlin, Germany: Springer-Verlag.
11. Siegel, P. H. 2004.Terahertz Technology in Biology and Medicine," IEEE Trans. Microwave Theory Tech. 52:2438-2447.
12. Woolard, D. L., Brown, E. R., Samuels, A. C., Globus, T., Gelmont, B., Wolski, M., 2003. IEEE MTT-S Int. Microwave Symp. Dig., Philadelphia, PA, June 8-13, pp. 763-766.
13. Brown, E.R., Bjarnason, J.E., Chan, T.L.J., Lee, A.W.M., Celis, M.A., 2004. Appl. Phys Letters, 84:3438-3440.
14. Material Studio 4.3©2008 Accelrys Software Inc.
15. Case, D.A., Darden, T.A., Cheatham, III,T.E.,Simmerling, C.L., Wang, J. , Duke, R.E., Luo, R., Merz, K.M., Pearlman, D.A., Crowley, M., Walker, R.C., Zhang, W., Wang, B., Hayik, S., Roitberg, A., Seabra, G., Wong, K.F., Paesani, F., Wu, X., Brozell, S., Tsui, V., Gohlke, H., Yang, L., Tan, C., Mongan, J., Hornak, V., Cui, G., Beroza, P., Mathews, D.H., Schafmeister, C., Ross, W.S., Kollman, P.A., 2006, AMBER 9, University of California, San Francisco.
16. Martin, M. C., McKinney, W. R., 1998. Proc. Mater. Res. Soc. 524, 11.
17. Holman, H-Y. N., Martin, M. C., McKinney, W. R., 2003. Spectroscopy-An International Journal 17, 139.

QM& MD Methods for Simulations of Two Liposome Phospholipid Layers Structure

Mehrnoosh Khaleghian[1] , Sima Afsharnezhad[2], Majid Monajjemi[3]
Mehr_khaleghian@yahoo.com
[1] Department of Physical Chemistry, Young Researchers Club, Science & Research Branch ,Islamic Azad University, Tehran. IRAN
[2]Department of Biochemistry, Mashhad Islamic Azad University Branch, Mashhad. IRAN.
[3]Department of Physical Chemistry, Science & Research Branch ,Islamic Azad University, Tehran. IRAN

Abstract: Since phospholipids constitute more than 70% of liposome lipids, so in the liposome two lipid layers of phospholipid are used. For this purpose, first one phosphalipid molecule should be simulated. In this study, we use DPPC (1,2 dipalmitoyl- sn- glycerol- 3- phosphatidyl choline) phospholipid. DPPC is the most current phospholipid that constitutes liposome. To abtain optimal molecule structure, ab initio calculations were performed on the basis of levels (quantum mechanic calculations) on a single DPPC molecule. In this research, in order to selcet the most appropriate base collection, for optimizing the relative molecule energy the calculations were accomplished in the gas phase and the geometric structure of DPPC molecule was minimized with three basis set of 6-31G, 3-21-G, and STO-3G. In order to final confirmation of primary simulated structure, calculative data of simulated model should be compared with empirical data considering that NMR method is the only way of obtaining information about DPPC molecule structure.After getting the primary optimized structure, H_2O molecules around the single- molecule should be simulated. For this purpose, ab initio calculation was used, and by using this method, situation of 16 H_2O molecules around the molecule top was considered so, that corresponds with practical results of previous mentioned studies. Then the distance of H_2O molecules according to DPPC should be optimized.

For this reason, forth distance of 1, 2, 3 and 4 angstroms for each of 16 H_2O molecule with DPPC phospholipid were selected and by using lennard - jones potential model the distance two- layer liposome by using the molecular dynamic method. After DPPC and water around optimizations, the moderation stages of dynamic molecules were carried out by two dynamic methods of NRT (instant volume and temperature) and NPAT (instant potential, area, and temperature) for two DPPC layers in 323^{o}k. Finally, system in 2ns period by using molecular dynamic method was moderated.

Key words: liposome, DPPC, Quantum Mechanic, Molecular Dynamic Simulation

1. Introduction

Today, liposomes are used as a matrix for proteins like enzymes fixation [1]. Since one of the most successful immoblizatin methods is to enclose them in the liposome [2], hence, dynamic molecullar simulation of liposome proteins helps in understanding more about their function and interaction with their surrounding environment [3].

Since phospholipids constitute more than 70% of liposome lipids, so in the liposome two lipid layers of phospholipid are used. The shape and amphiphilic nature of the phospholipid molecules cause them to form bilayers spontaneously in aqueous environments. Thus, lipid molecules spontaneously aggregate to bury their hydrophobic hydrocarbon tails in the interior and expose their hydrophilic heads to water [4]. For modeling of liposme, a part of it's lipid bilayer is simulated then protein add in it. Two basic methods are used to add protein to the liposome system. First, protein radius is estimated, then lipid structures add to a protein and two lipid layers are formed around protein. Finally, through intellectual optimizing stage worst connections are eliminated and an appropriate structure including protein- liposome is obtained (CHARMM) program uses this method [5]. The most common biological phospholipids one encounters in studies are glycerol-backbone lipids, like DPPC is predominantly found in animal cell membrane [6]. On DPPC molecular level it has been of interest to explore to what extent molecular conformations, lateral interactions, and dielectric constant and how these features affect the properties and topology of the membrane surface.

Corresponding Author: Mehrnoosh Khaleghian, Department of Physical Chemistry, Young Researchers Club, Science & Research Branch ,Islamic Azad University, Tehran. IRAN

Many techniques have been used to study specific bilayer properties such as ESR spectroscopy, Xray differaction, IR/Raman spectroscopy to study tail dihedral gauche-defects and differential scanning calorimetry (DSC) to study phase transition [7]. But in some of phospholipid structures, it is limited to measure the transition temperature and also the effect of solvents practically. Therefore, studding on this model for consideration of phospholipids function to expose to different solvents and specific selective of solvents across of transmembrane is very important.
In this research, in order to modeling of lipid bilayer, the first, the geometric structure of a DPPC molecule was minimized Then, in order to final confirmation of primary simulated structure, calculative data of simulated model compared with empirical data considering that NMR method is the only way of obtaining information about DPPC molecule structure. After getting the primary optimized structure, H_2O molecules around the single- molecule should be simulated and optimized.

Finally, the moderation stages of dynamic molecules were carried out by two dynamic methods of NRT (instant volume and temperature) and NPAT (instant potential, area, and temperature) for two DPPC layers in 323^{o}k. Finally, system in 2ns period by using molecular dynamic method was moderated.

2. Computational method and Theory

2.1 QM calculations: the GAIO method and Solvent Model

All of the geometries compound were full optimized at the RHF/6-31G level of the theory. This procedure was followed both in the gas-phase and solvent phases and also using the simple Onsager cavity salvation model (SCRF). The solvent effect was calculated using SCRF model. According to this method, the total energy of solute and solvent, which depends on the dielectricity constant ε, is denoted as Es [8]. Only the electrostatic effects of salvation are included in the Onsager model, and other forces such as cavity work, dispersion, or exchange repulsion effects are neglected [9] this is a reasonable approximation when zwitterions or strongly polar molecules are studies in polar solvents where the electrostatic effects of salvation are expected to predominant. For computation of the corresponding energies and NMR shielding were evaluated using the gauge-included atomic orbital (GIAO) method.
Nuclear magnetic resonance (NMR) spectroscopy has become one of the more powerful methods for probing molecular structure in solution [10].The isotropic part <σiso> of σ is measured by taking the average of σ with respect to the orientation to the magnetic field,

i.e. $< \sigma iso >= \frac{\sigma_{11} + \sigma_{22} + \sigma_{33}}{3}$

Where σ_{xx}, σ_{yy} and σ_{zz} are principal axis values of σ. The obtained result of calculated by using HF theory.

The anisotropy is: $\Delta\sigma = |\sigma_{33} - < \sigma iso >|$

And the asymmetry is: $\eta = \frac{\sigma_{22} - \sigma_{33}}{\Delta\sigma}$

2.2. NMR sample preparation and experiment

DPPC was obtained from Avanti Polar Lipids. Pure lipid sample was prepared by mixing the lipid with de-ionized water (PH= 7) in a conical vial with a vortex mixer. This was followed by a minimum of 5 freeze-thaw cycles in dry ice and a warm water bath set to 300 K (low the liquid crystalline phase transition for DPPC).

Thus, the samples in this study are large MLV's greater than ~ 1 μm in diameter. Samples containing lipid constituents were first combined and dissolved in chloroform followed by vacuum drying overnight to remove the solvent. The samples were than hydrated in chloroform, Benzene, Carbon Tetrachloride and methanol solvents with the above procedure. All lipid sample were 33 wt% DPPC. Therefore a solution of 50 mg DPPC was prepared. ^{13}C-NMR spectra were recorded at 20 °C on a DRX 500 MHz spectrometer (Burker Analytische Messtechnik, Karlsruhe, FRG) and a B-VT-1000 heating unit. Natural abundance solution ^{13}C NMR spectra yielded cholin and glycerol resonances that are accessible to conformational analysis. Reduced chemical shift anisotropies have been estimated for the cholin C_α, C_β, and C_γ carbons and for glycerol C1, C2 and C3 carbons (Figure 1)

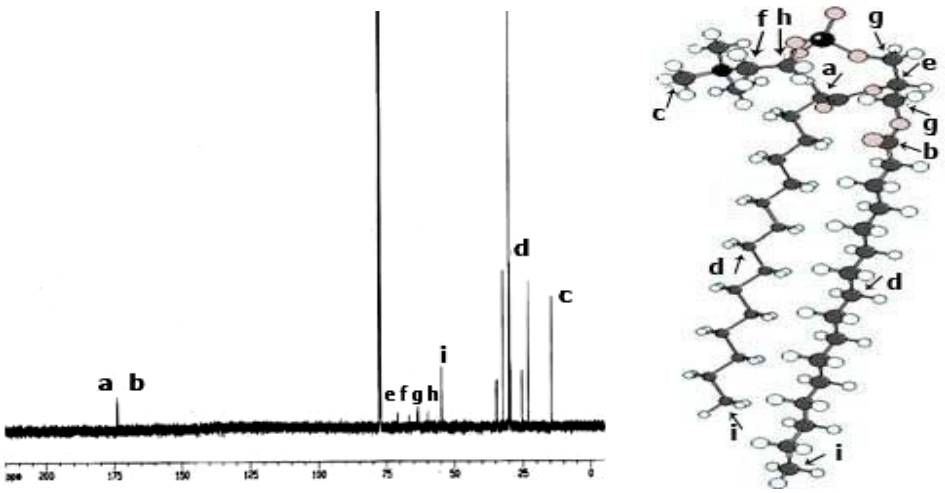

Figure 1, a plot of the peak position of natural abundance 13C NMR spectra yielded choline and glycerol resonance in Chloroform that is accessible to conformational analysis. Chemical shifts have been estimated for the choline C_α(h), C_β(f), and C_γ(c) carbons and for glycerol C1(g), C2(e), and C3(g) carbons and Sn2-CO (a) and Sn1-CO (b).

2.3 MD Simulation of phospholipid bilayers

After the building of the structure of one DPPC with a molecular editor, a topology for the lipid is generated by CHARMM, a good method is to start with the topology of DPPC lipid. Then actual bilayer is created the. DPPC randomly rotated around its long axis and randomly translated over 0.4 nm laterally, the monolayer to obtain the second leaflet of a bilayer is rotated in vacuum with pressure coupling to high lateral pressures 200 bar. This will compress the bilayer. After that, the periodic boundary conditions are used that multiply it to the desired system size. All system started as multiples of 4_4, with most systems having 64 lipids in each leaflet. Dynamic methods of NRT (instant volume and temperature)
and NPAT (instant potential, area, and temperature) for two DPPC layers in 323^{o}K are used [11]. Finally energy is minimized the resulting system.

3. Result and Disscussion

For the simulation of phospholipid bilayers, first one phosphalipid molecule should be simulated. In this study, we use DPPC (1,2 dipalmitoyl- sn-glycerol- 3- phosphatidyl choline) phospholidid. it is named a test molecule because it has both many practical data, and a lot of simuluation have been performed on it. Accorodingly, DPPC structure was described by using chemdraw software. To obtain optimal molecule
structure, ab initio calculations were performed on the basis of levels (quantal mechanic
calculations) on a single DPPC molecule. In this research, quantom mechanic calculations were performed both in gas phase and in H_2O solvent. The situation of H_2O molecules around the molecule top was considered so, that corresponds with practical results of previous mentioned studies. Then the distance of H_2O molecules according to DPPC should be optimized. For this reason, 4 distance of 1, 2, 3 and 4 angestrom for each of 16 H_2O molecule with DPPC phospholipid were selected and by
using lenard jones potential method the distance two- layer liposome by using the dynamic molecullar method. All the calculations of quantom mechanic were accomplished by using Goussian 2003 [12] and Molecular dynamic simulation was performed by CHARMm program.

3.1 Results of conformation energies for optimizing DPPC geometric structure in different basis sets in gas phase.

Table 1, shows the conformation energies resulting from three basis sets, STO-3G, 3-21-G, and 6-31G.

Table 1, the conformation energies in diferent basis sets.

Basis set	E(kcal/mol)
STO-3G	-1583811.262
3-21G	-1594584.634
6-31G	-1602682.003
6-31G*	-1603386.341

3.2 Adding H_2O in different distances between H_2O molecules aroud DPPC molecule.

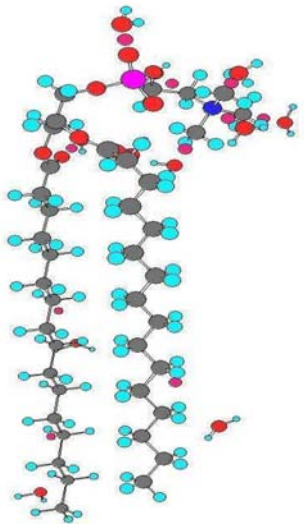

Figure 2. DPPC molecule with 16 water molecules

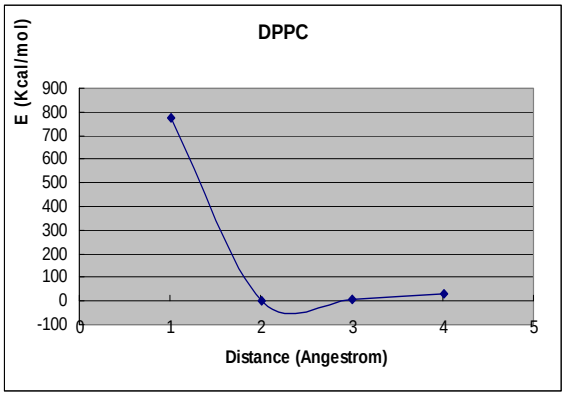

Figure 3, the changes of potential energy between H_2O molecules with DPPC according to various distances of H_2O moleculs with DPPC

Results of figure 3 shows that minimum enetgy is related to 2.02 distance of H_2O molecules with DPPC molecule which is the most stable form, therefore, distance of H_2O molecules with DPPC was selected 2.01.

Finally, after considering all the aspects such as the number and distance of H_2O molecules around phospholipid, part of simulated membrane.

3.3. Experimental Results and Comparison with GIAO Calculations

We reproduce in Table 2, a comparison of our theoretical data and the experimental data of DPPC molecule in different solution. All chemical shifts were referenced to Tetramethylsilane. For comparing the results, chemical shift value (δ) has been calculated was considered with the obtained results from GIAO calculations. The ab initio quantum chemical results are fragmentary in that the large molecule like DPPC was typically not studied. However, it is apparent that the our experimental results are similar to the GIAO calculations (Table 2).

Table 2. Comparison between calculated and experimental ^{13}C isotropic shift values for DPPC in Chloroform, Methanol and Benzene solution.

	Isotropic value in ppm					
	CDCL3		CD3OD		C6O6	
Atom[a]	calculated[b]	experiment	calculated[b]	experiment	calculated[b]	experiment
i	54.7	48.7	50.3	48.8	48.8	48.7
h	59.7	51.6	50.5	52.0	48.9	51.3
g1	63.4	61.1	50.6	61.2	49.1	60.9
g2	63.7	61.9	50.8	61.9	49.3	62.0
f	66.7	63.4	66.5	52.0	69.1	63.1
e	70.9	82.5	51.0	82.6	49.4	82.6
a	173.9	240.2	176.6	239.7	173.5	231.6
b	173.6	231.6	176.2	231.7	173.7	240.7

[a] The numbering corresponds to the atom numbers given in Figure 2.
[b] Value obtained for the minimum energy conformation at 6-31G level and standard; TMS: Isotropic carbon shielding tensor=208.2102,

3.4. Simulation of phospholipid bilayers

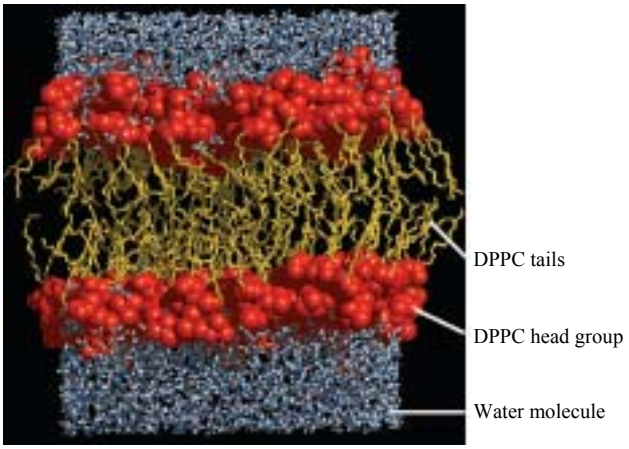

Figure4: a model of DPPC bilayer

References:

1- Armen, R. S., O. D. Uitto, and S. E. Feller. 1998. Phospholipid component volumes: determination and application to bilayer structure calculations. *Biophys. J.* 75:734 -744
2- Zaborsky, O.R. 1973 Immobilized enzymes, CRC Press, Cleveland.
3- Marrink, S. J., M. Berkowitz, and H. J. C. Berendsen. 1993. Molecular dynamics simulation of a membrane water interface - the ordering of water and its relation to the hydration force. Langmuir 9:3122–3131
4- Gennis, R. B. 1989. Biomembranes Molecular Structure and Function. Springer-Verlag, New York.
5- Brooks, B. R., R. E. Bruccoleri, B. D. Olafson, D. J. States, S. Swaminathan, and M. Karplus. 1983. CHARMM: A program for macromolecular energy minimization and dynamics calculations. *J. Comput. Chem.* 4:187-217.
6- Lawerence M. Philip W. 1985. A model of orientational ordering in phosphatidylcholin bilayers based on conformational analysis of the glycerol backbone region. Biophys J., 756-773.

7- Wei-Chin Hung and Fang-Yu Chen, 2003. The hydrocarbic-hydrophilic interface of phospholipids membranes studies by lamellar X-Ray diffraction. *Chines Jouranl of Physic* 41:85-91.
8- Truong, Truong and Stefanovich. .1997. Free energy profile of reactions in solution. J. Chem. Phys., 107, No. 6, 8.
9- Bryan. M., Kyungsun. K. 1996. New model for calculation of salvation free energies. J. Phys. Chem., 100, 11775-11788.
10- Salsbury, N. J., A. Dark, and D.Chapman. 1972. Deuteron magnetic resonance studies of water associated with phospholipids. Chem. Phys. Lipids. 8:142-151.
11- Feller, S. E., R. M. Venable, and R. W. Pastor. 1997. Computer simulation of a DPPC phopholipid bilayer: structural changes as a function of molecular surface area. *Langmuir.* 13:6555- 6561.
12- M.J. Frisch, G.W.Trucks, H.B. Schlegel , et al, 2003. Gaussian, Inc., Pittsburgh PA

Theoretical Investigation of Monte Carlo Simulation on DHA-Containing Phospholipids in Nerve Cell's Membrane

N .Khodayari[1], B .Honarparvar[2], Monajjemi.M[2,*]
[1]Department of Biology, Science and Research Branch, Islamic Azad University, Tehran, Iran
[2]Department of Chemistry, Science and Research Branch, Islamic Azad University,
P.O. Box: 14155-775 Tehran, Iran

Abstract: Phospholipids involved in Docosa - hexaenoic acid (DHA, 22:6n-3) are the ubiquitous components of the central nervous system. In such metabolically challenged cells including nerve cells specific enzymes transfer DHA as new tails onto phospholipids molecules. Enrichment of membranes with DHA-containing phospholipids enables their proteins to "flip" or "spin" faster in the membrane environment. In this study, we have simulated a novel DHA-containing phosphatidylcholine (PC) found in a marine single cell eukaryote, "Schizochytrium sp F26-b". We have used Monte carol as well as molecular dynamics as simulation methods. The agreement between our obtained simulation data and experimental results seems excellent which validates subsequent simulation outcome for docosahexaenoic acid.

Keywords: Docosahexaenoic acid (DHA); Nervous System; Schizochytrium sp; AM1; Monte Carlo Simulation

Introduction

Biomembrane is the most important part of each cell which surrounds the cell and each organelle. The cell membrane contains lipids, proteins, and carbohydrates. Phospholipids are major components of the cell membrane. They are similar to fats, and have only two fatty acids and this is the difference between them [1, 3]. The third hydroxyl group of glycerol is joined to a phosphate group, which holds negative charge. Additional small molecules which usually charged or polar linked to the phosphate group to make different forms of phospholipids [4]. Cells that are the most metabolically active require more fluid membrane systems, and fluidity requires that more membrane phospholipids carry long-chain unsaturated fatty acids[1, 5-7]. Among these, the polyunsaturated lipids probably increase and regulate fluidity of the membranes[1]. Docosahexaenoic acid (DHA) is the major unsaturated fatty acid and one of the most abundant polyunsaturated fatty acids (PUFAs) in membrane phospholipids of the central nervous system and retina which mentioned that they need more flexibility [7-11]. DHA is paired in glycerophospholipids often with palmitic acid (16:0) and stearic acid (18:0) and in some cases with another long-chain polyunsaturated fatty acid such as 22:6 in position sn-1 and accumulates in phosphatidylethanolamines [12]. It has been postulated that optimal neurological development, information processing, the capacity of nerve cells to conduct electrical signals [10] and cognitive functions [11, 13, 14]. Depend on an adequate supply of this fatty acid. It should be mentioned that in humans little DHA is produced de novo and most of that is supplied by dietary sources [8]. Nowadays, the main industrial source of DHA and polyunsaturated fatty acids is marine fish oils. Among the benefits of DHA, the supply of fish oils may be unreliable because of seasonal variation, variability of various fisheries, marine pollution, and high processing costs [8, 15]. Microorganisms are also used to provide DHA and it seems that some microorganisms are considered as a new source of DHA [16]. Schizochytrium sp is an algae-like microorganism used for industrial production of docosahexaenoic acid (DHA) -rich oil and dried microorganism for use as a source of this fatty acid in foods, and nutritional supplements [17]. It has been found out that in Schizochytrium sp. Strain F26-b the major phospholipid is a novel PC which contains pentadecanoicacid (C15:0) at sn-1 and docosahexaenoic acid at sn-2, i.e., the systematic name of this new ph ospholipid is 1-pentadecanoyl-2-docosahexaenoyl-sn–glycerol-3-phosphocholin (see Fig.1) and this opened a new insight into the methods for producing DHA.

Corresponding Author: N .Khodayari, Department of Biology, Science and Research Branch, Islamic Azad University, Tehran, Iran

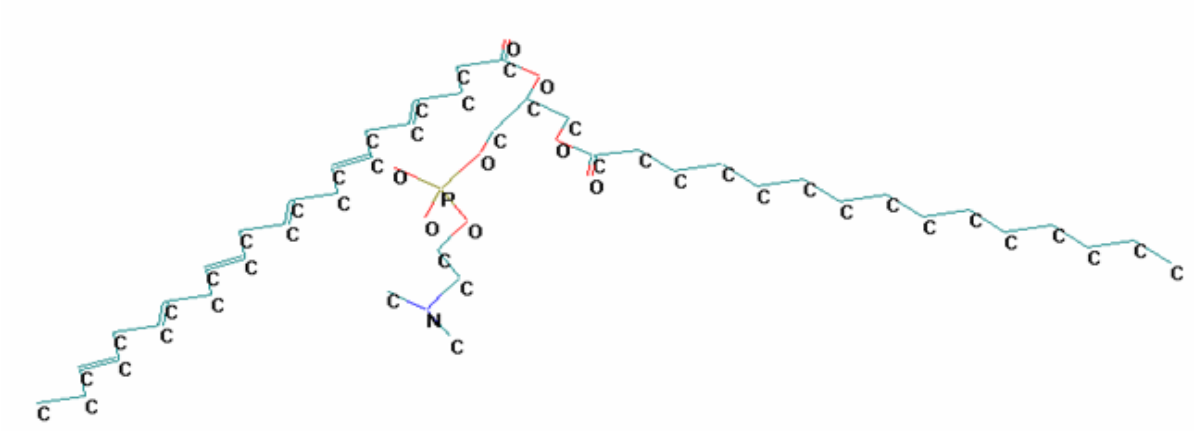

Figure1. The optimized structure of 1-pentadecanoyl-2-docosahexaenoyl-sn- glycerol-3-phosphocholin.

Previously, Lange in and BD simulations were used to simulate a DPPC bilayer in the liquid- crystal [19, 20] and gel [21] states and also the effect of environmental exposure to some chemical solvents on it [22, 23] and unsaturated molecules in a bilayer membrane [24]. Also Brownian dynamics has been used to simulate both oleic acid and DHA molecules.

Nowadays, production of DHA-containing phospholipids has drawn significant attention and although there is some problem to use fish oils as a source of DHA, it is used for their production. Because of some toxic compounds such as dioxins and heavy metals including mercury compounds which could be concentrated in fish oils, the microbial production of DHA is expected to be safer than fish oils [25].

If one of the candidate sources for DHA-containing phospholipids are microorganisms such as Schizochytrium sp. Strain F26-b , we have to know all information about this unsaturated molecule and it's exact both equilibrium and dynamic properties in atomic level. Our main goal of this study is to obtain mentioned details to compare them with the experimental results.

MATERIALS AND METHODS

For membrane's molecules, the experimental studies are so difficult and NMR studies of unsaturated fatty acids in membranes provide equilibrium and dynamic properties but to get atomic level data of those properties for such molecules, we have to use computer simulation. Surely molecular dynamics (MD) is the most common used technique to simulate membrane systems [18]. However, one may gain more detailed description of a system in short time range simulation, generally in the order of picoseconds [1].

The first step in our study was to model the 1-pentadecanoyl-2-docosahexaenoyl-sn- glycerol-3-phosphocholin molecule with HYPER 6 software. After modeling the bacteria's structure we have set it in different water boxes for optimization. For this purpose we chose 10 boxes with different number of water molecule as listed in Table1.

To investigate the temperature effect on the structural stability the simulation temperature have been changed from 300k up to 330k during the optimization and for each state , potential energy and optimized molecule have been obtained using molecular mechanic, Monte Carlo method and reported in Table1 and the related graph has been displayed in Figure2.

Table1. The energy values (kcal/mol) of 1-pentadecanoyl-2-docosahexaenoyl-sn-glycerol-3-Phosphocholin located in different water boxes at different temperatures using Monte Carlo simulation.

Number of Water molecules	300k	305k	310k	315k	320k	325k	330k
548 water	12345.5	12350.2	12257	12259.6	12263.5	12243	12245
561 water	12649.7	12742.5	12507.6	12517	12519.5	12520.6	12533.7
566 water	11077.4	11082.5	11067.8	11067.6	11073.3	11167.1	8609.06
578 water	8093.21	8099.56	8108.94	7842.05	7847.24	7848.27	7849.21
613 water	17254.9	15643.7	19179.4	15576.6	26520.5	26523.9	26527.1
629 water	20411.9	19499.5	20419.9	15199.3	20329.8	19419.2	19424.5
692 water	18933.9	21918.6	21711.9	21733.5	21837.6	21889.1	21895.2
707 water	18595.6	18600.4	18631.3	18628.9	18636.3	18637.9	17986.9
777 water	13069.9	13067	12825.1	12822.8	12825.7	12832.9	12834.9
884 water	19268.9	19269.6	19301.1	19301.2	19302.1	19305.04	19292.8

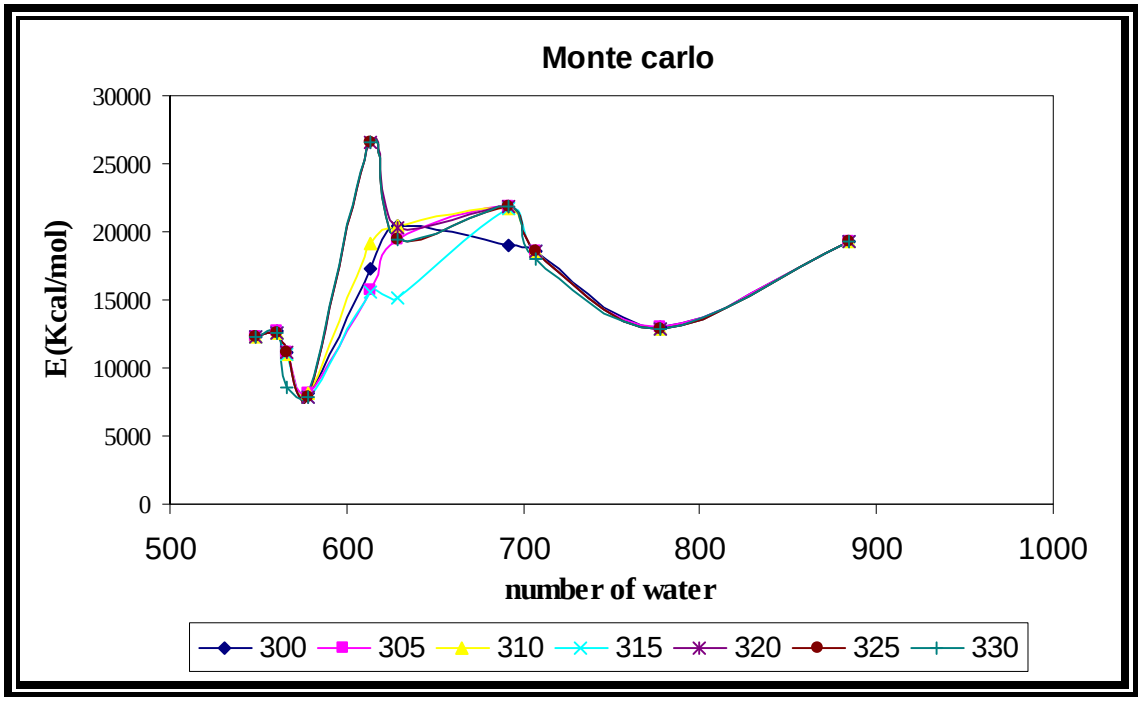

Figure2. The graph of energy values (kcal/mol) of 1-pentadecanoyl-2-docosahexaenoyl-sn-glycerol-3-Phosphocholin versus different temperatures using molecular mechanic, Monte Carlo method.

Second, as a comparative study we have repeated our calculation at AM-1 level of theory using, for this state we Gaussian 98 software [26]. First we have molecules with all water molecules. But this time we chose only 3 biologic temperatures which were 300k (laboratory temperature), 310k (body temperature) removed all water molecules of water boxes and then obtained optimized molecules. Then we continued the computation with UFF method with optimized and 313k (fever temperature). So we got energies which were different from the previous step and have shown in Table3.

Table2. The energy values (kcal/mol) of optimized 1-pentadecanoyl-2-docosahexaenoyl-sn-glycerol-3-Phosphocholin molecules without water obtained at AM1 level of theory at different temperatures.

Number of Water molecules	300k	305k	310k	315k	320k	325k	330k
548 water	6.368761	6.368761	6.362833	6.362833	6.369238	6.369243	6.369243
561 water	6.368762	6.368763	6.362841	6.369246	6.369246	6.369246	6.369244
566 water	6.368759	6.368758	6.373617	6.373617	6.373619	6.373615	0.657563
578 water	5.424561	6.387942	3.99012	5.707408	5.707408	5.619212	5.707392
613 water	6.389847	6.389848	0.656185	6.352666	6.352669	6.352669	6.352669
629 water	6.383705	6.3837	6.380628	0.659395	6.35729	6.357292	6.357295
692 water	0.656186	6.371922	6.368845	6.368845	6.36885	6.368845	6.375459
707 water	6.244059	6.244057	6.240996	6.240981	6.248187	6.248187	5.472913
777 water	6.396743	6.396751	6.386004	5.710963	5.710965	5.710971	5.710971
884 water	5.736647	5.73666	5.733649	5.7109	5.710964	5.710971	5.710974

Table3. The energy values (kcal/mol) of optimized 1-pentadecanoyl-2-docosahexaenoyl -sn-glycerol-3-Phosphocholin molecules including different number of water molecules using UFF method at different temperatures

Number of Water molecules	300k	310k	313k
548 water	234.1378	229.1155	229.1397
561 water	235.1184	235.1232	235.1076
566 water	236.1091	236.13871	236.3579
578 water	116.0159	167.11903	215.3754
613 water	237.7326	219.2787	237.8413
629 water	239.1759	239.3568	239.4248
692 water	222.4502	239.8061	239.9235
707 water	241.0956	241.2791	241.0459
777 water	248.5212	250.2783	248.6568
884 water	254.6160	254.7821	254.9270

RESULTS AND DISCUSSION

The energy values of 1-pentadecanoy l-2-docosahexaenoyl-sn-glycerol-3-phosphocholin molecules in both water boxes and without water at different temperatures at the UFF as well as AM1 approximations available in Gaussian 98 program have been listed in Table 1, Table 2, and Table 3. So, the potential energy surface for the interaction of 1-pentadecanoyl-2-docosahexaenoyl-sn-glycerol-3-phosphocholin with numerous water molecules has been explored using. Moreover, to find out more about the trend of energy variation in terms of different number of water molecules and different temperatures, several graphs of energy values versus various temperatures in the range of 300k up to 330k have been displayed in Figure (1) and analyzed.

Based on our obtained results, we can clearly found out that by increasing the number of water molecules the energy values tends to be increased at all employed temperatures. Of course, it is notable that in the case of 1-pentadecanoyl-2-docosahexaenoyl-sn-glycerol-3-phosphocholin molecules including 548 water molecules shows deviation from the mentioned trend. Therefore, we may realize that properties of water have a profound influence on the physical and chemical processes due to hydrogen bonding interactions in biological systems.When the molecule optimized in a box containing 548 water molecules, a dramatically decreasing trend can be seen in the energy values (see Figure3). The same fact has been repeated in the case of molecule optimized in 561 water molecules and for this case the significant variation obtained in the range of 310k-315k.

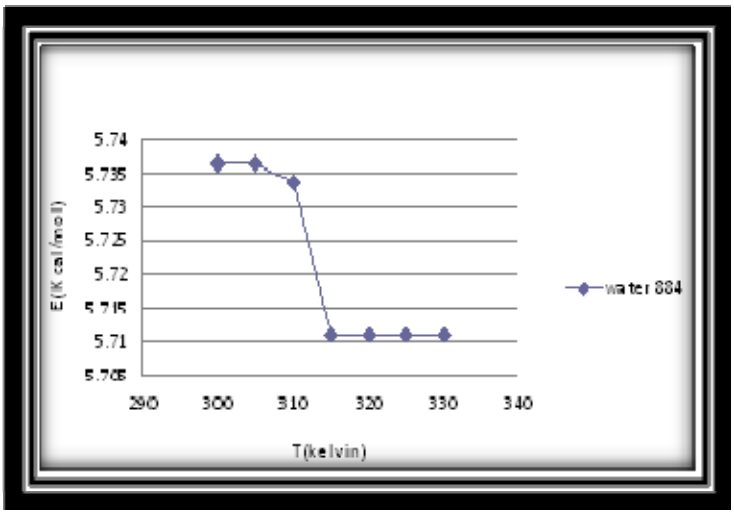

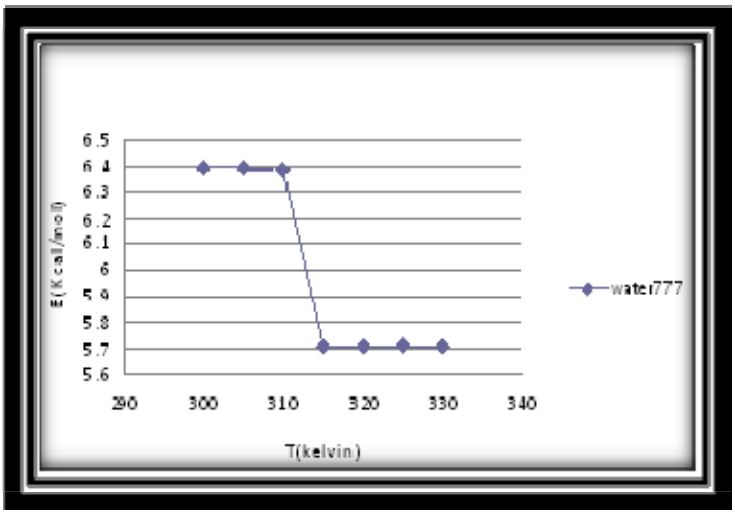

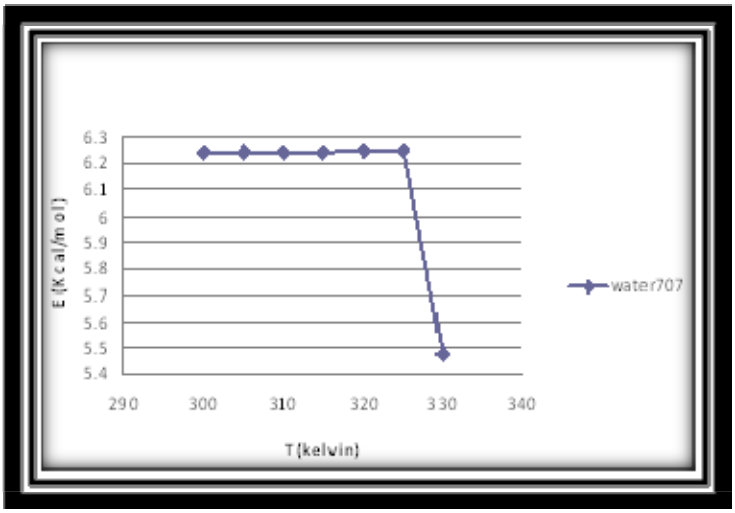
6.3
6.2
6.1
6
5.9
5.8
5.7
5.6
5.5
5.4
E (Kcal/mol)
290
300
310
320
330
340
T(kelvin)
water707

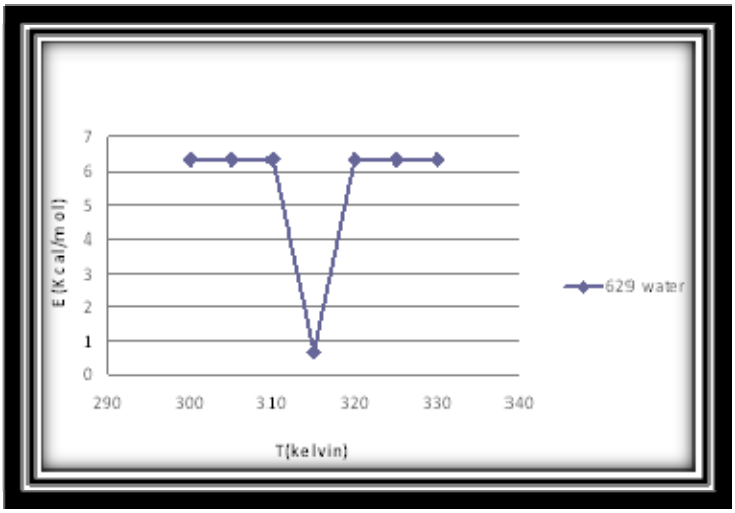
7
6
5
4
3
2
1
0
E (Kcal/mol)
290
300
310
320
330
340
T(kelvin)
629 water

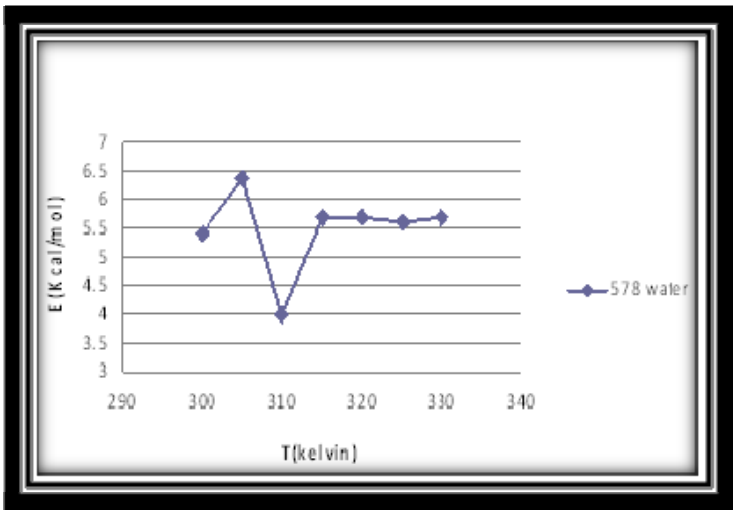
7
6.5
6
5.5
5
4.5
4
3.5
3
E (Kcal/mol)
290
300
310
320
330
340
T(kelvin)
578 water

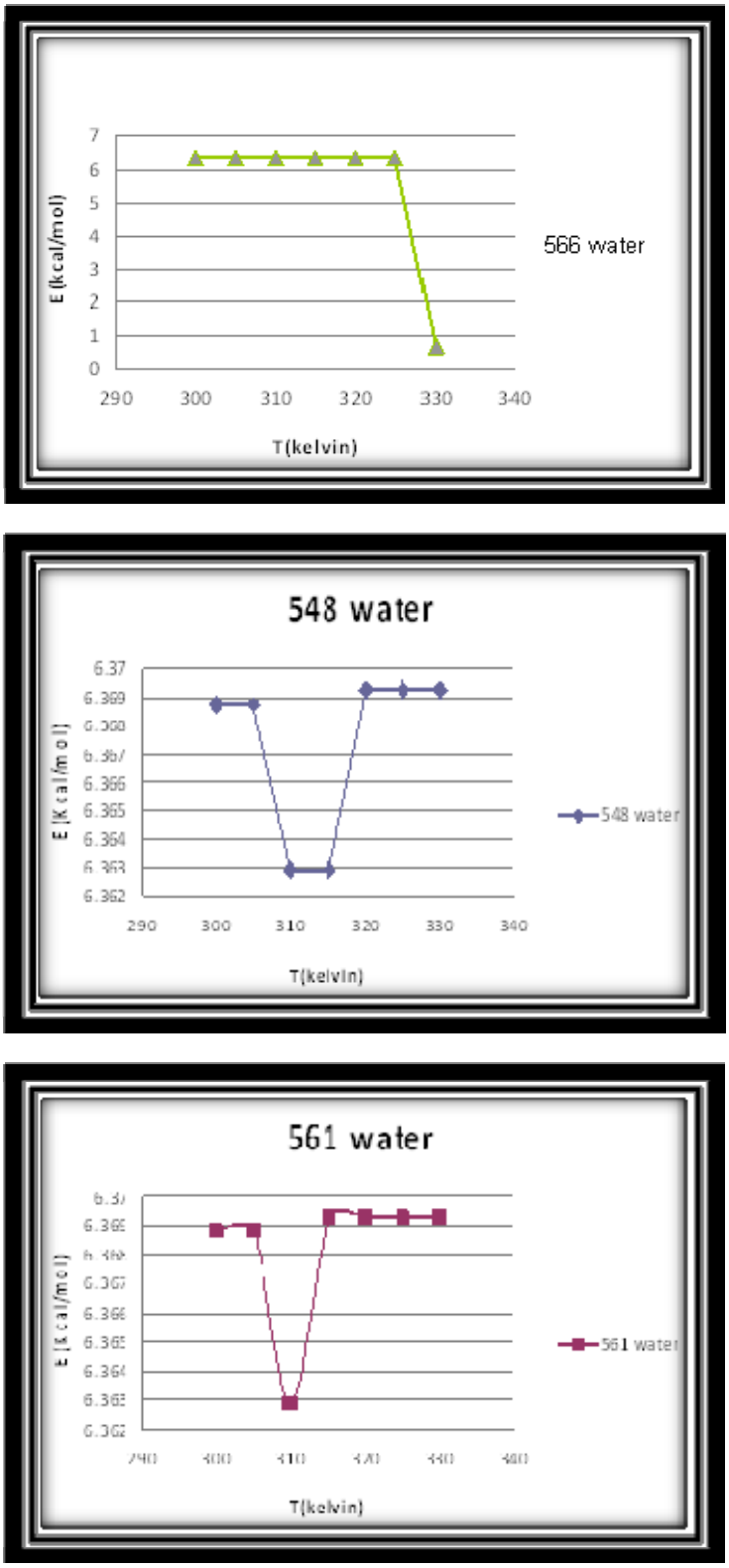

Figure3. The graphs of energy values (kcal/mol) of 1-pentadecanoyl-2-docosahexaenoyl-sn-glycerol-3-Phosphocholin versus different temperatures using AM1method.

Also, a similar tendency of variations has been observed for molecules which optimized in 578, 613and 629 water molecules as can be easily seen in the plotted energy graphs (see Figure 3). A different trend has been observed in the case of optimized molecules in the boxes containing 566 and 707 water molecules which exhibited a decreasing slope of energy at 325k. Conversely, for 1-pentadecanoyl-2-docosahexaenoyl-sn-glycerol-3-phosphocholin Optimized in a box containing 692 water molecules a different observation is notable. The obtained energy at 300k is very low, but suddenly the energy values reaches to the highest values. The two former cases are corresponded to molecules which optimized with 777 and 884 water molecules.

According to obtained energy of optimized 1-pentadecanoyl-2-docosahexaenoyl-sn-glycerol-3-phosphocholin listed in all three theoretical methods including AM1, UFF and Monte Carlo simulation, the lowest energy value and then the highest structural stability has been yielded with water boxes containing 578 water molecules. For further information about the structural stability in view of the most proper temperature, we may conclude that the most stability has been found at 310k so called body temperature, however supposing the highest temperature i.e. 313k (fig.4). Strikingly, in the case of optimized 1-pentadecanoyl-2-docosahexaenoyl-sn-glycerol-3-phosphocholin using Monte Carlo simulation, the lowest energy values have been found in each seven employed temperatures.

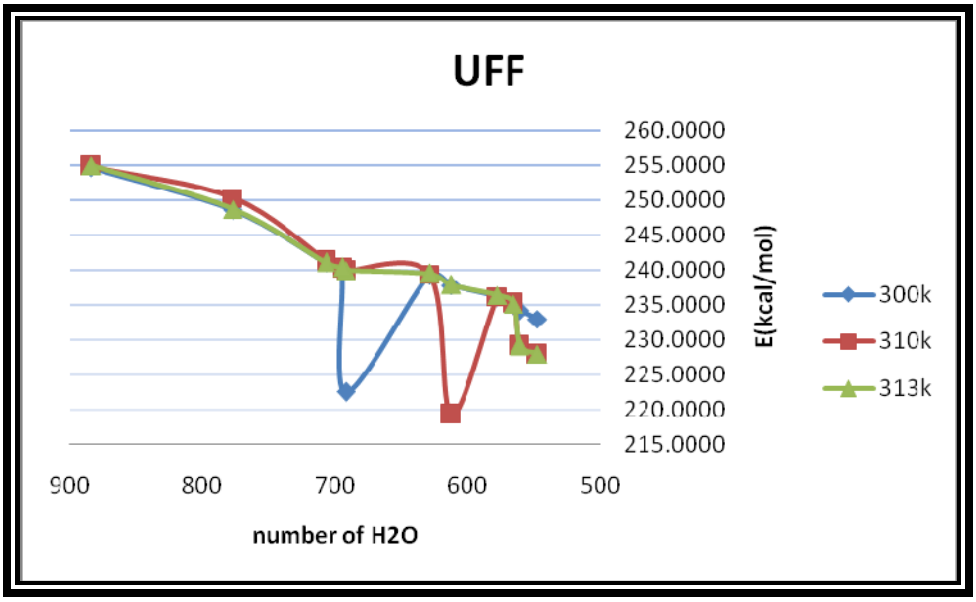

Figure4. The graph of energy values (kcal/mol) of 1-pentadecanoyl-2-docosahexaenoyl-sn-glycerol-3-Phosphocholin versus different temperatures using UFF method.

CONCLUSION

Computer technology has an important role in structuring biological systems. The explosive growth of high performance computing techniques in recent years with regard to the development of good and accurate models of biological systems has contributed significantly to new approaches to fundamental problems of modeling transient behavior of biological system.

A novel DHA-containing phosphocholin have found in Schizochytrium sp. Strain F26-b which is expected to consider as a new commercial source for DHA and DHA-containing phospholipids. This new molecule has been chosen for Monte Carlo and semi-emperical computational methods.

Besides the fact that changes in the properties of water can affect cell integrity, water is also essential for most biochemical reactions. This tendency of water molecules to attract each other strongly through hydrogen bonds is responsible for the unusual properties of water.

It has been found out that through increasing the number of water molecules the energy values increase. More interestingly, for 1-pentadecanoyl-2-docosahexaenoyl-sn-glycerol-3-phosphocholin molecules with 548 water molecules shows deviation from the mentioned trend.

A dramatically decreasing trend can be seen in the energy values have been observed when the molecule optimized in a box containing 548 water molecules. The same fact has been occurred in the case of molecule optimized in 561 water molecules and for this case the significant variation obtained in the range of 310k-315k.

The theoretical results obtained clarify the interpretation of potential energy surface studies. Future research in these areas should boost our understanding of how physicochemical effects caused by inserting a number of water molecules.

REFERENCES

1. Miguel X. F, Miguel A.R.B. Castanho, De la Torre Jose Garsia, 2002, Brownian dynamics simulation of the unsaturated lipidic molecules oleic and docosahexaenoic acid confined in a cellular membrane. *Biochemical et Biophysyca Acta.* 1565**,** 29-35.
2. Shaikh.S.R., Edidin.M, 2006, Poly-unsaturated fatty acids, membrane organization, T cells, and antigen presentation. *Am J Clin Nutr*. 84, 1277– 89.
3. Heller .H, Schaefer .M, Schulten .K, 1993, Molecular Dynamic Simulation of a Bilayer of 200 Lipids in The Gel and in the Liquid Crystal Phase. *J. Phys. Chem.* 97, 8343-60.
4. Cooper. G. M. and Hausman.R.E. The Cell: A Molecular Approach, Fourth Edition
5. Kidd. M, 2005, Glycero Phospho Choline (GPC), Mind-Body Nutrient for Active Living and Healthy AgingScience&Ingredients, Mind-Body Parris, 1-21.
6. Alberts B, et al, 2002, Molecular Biology of the Cell, New York press, Fourth Edition.
7. Salem, N.,1989, Omega-3 fatty Acids:Molecular and Biochemical Aspect, in current Tropic in Nutrition and Disease..22, 109-228.
8. Abe.E, et al, 2006, A Novel phosphatidylcholine which contains penta-decanoic Acid at sn-1 and docosahexaenoic Acid at sn-2 in schizochytrium sp. F26-b. *J.Biochem*, 140,247-253.
9. Alessandri .J. M., et al, 2003, Incorporation of docosahexaenoic acid into nerve membrane phospholipids: bridging the gap between animals and cultured cells. *Am J. Clin Nutr***,** 78, 702-10.
10. Crawford M.A, Costeloe, K., Phylactos, A., Skirvin, L, Stacey.F, 1997, Are deficits of arashidonic and docosahexanieic acids responcible for the neural and vascular complications of premature babies?, *Am. J. Clin. Nutr.*66, 1032-1041.
12. Tibor Farkas et al (2000) Docosahexaenoic acid-containing phospholipids' molecular species in brains of vertebrates. Vol. 97**,** No.12 ,6362–6366.
13. Burdge. G.C, 1998, Docosahexaenoic acid-containing phospholipid molecular species in brains of vertebrates. *biochem.soc.trans*.26, 247-252.
14. Werkman, S. H, Carlson. S. E, 1996, A randomized trial of visual attention of preterm infants fed docosahexaenoic acid until two months. *Lipids* 31**,** 91–97.
15. Yehuda.S, Rabinovitz. S, Mostofsky. D. I, 1998, Modulation of Learning and Neural Membrane Compositions in the Rat by Essential Fatty Acid Preparation. *Neurochem. Res.* 23**,** 627–634.
16. Ashford A, Barclay W.R, Weaver C. A, Giddings T.H, Zeller. S, 2000, Electron Microscopy may Reveal Structure of Docosahexaenoic Acid-rich oil within Schizochytrium sp, *Lipids*, 35(12) 1377-86.
17. Lewis,T., Nichols, P, Mcmeekin,T,2000, Production of Polyunsaturated fatty acids by Australian Thraustochytrids*:Aquaculture Applications*, 1-21.
18. Li, Z.Y. and Ward, O. P., 1994, Production of docosahexanieic acids by Thraustochytrium roseum. *J. Ind. Microbiol.* 13, 238-241.
19. D.P. Tieleman, S.J. Marrink, H.J.C. Berendsen,1997, *biochim. Biophys. Acta* 1331 235-270.
20. Pastor. R, Venable.W, Karplus. M, 1988, *J.Chem.Phys.* 89 1112-1127.

21. Monajjemi,M., Afsharnezhad, S., et al. (2008) Theoretical Study of Solvent Effects and NMRShielding Tensors of DLPC. *Indo. J. Chem.*, 8, 58-64.
22. Monajjemi.M, Afsharnezhad. S, et al., 2007, NMR shielding and a Thermodynamic study of the effect of environmental exposure to petrochemical solvent on DPPC, an important component of lung surfactant. *Russian Journal of Physical Chemistry A.*Vol**.**81, No.12, 1956-1963.
23. Monajjemi,M., Afsharnezhad,S, et al.,2006, The effect of environmental exposure to some chemical solvents on DPPC as important component of lung surfactant:an ab initio study. *Journal of Physical and Theoretical Chemistry.Islamic Azad University of Iran.*Vol, 3**.**159-166.
24. Ramsey.R.B, Scott. T, Banik. N.L., 1997, Fatty acid composition of myelin isolated from the brain of a patient with cellular deficiency of co-enzyme forms of vitamin B12. *J. Neurol. Sci.* 34, 221-232.
25.Teague.W, Fuller.N,Rand.R.P ,2002, Polyunsaturated lipids in membrane fusion events.*Cell.Mol.Biol.Lett*, Vol **7.** 262-264.
26. M.J. Frisch, G.W.Trucks, H.B. Schlegel, G.E. Scuseria, M.A. Robb, J.R Cheeseman, V.G . Zakrzewski,J.A. Montgomery, Jr., R.E. Stratmann, J.C. Burant,`S. Dapprich, J.M. Millam, A.D. Daniels, K.N. Kudin, M.C. Strain, O. Farkas, J. Tomasi, V. Barone, M. Cossi , R. Cammi, B. Mennucci, C. Pomelli, C. Adamo, S. Clifford, J. Ochterski, G. A. Petersson, P.Y. Ayala, Q. Cui, K. Morokuma, D.K. Malick, A. D. Rabuck, K. Raghavachari, J. B. Raghavachari, J. Cioslowski, J. V. Ortiz, A.G . Baboul, B.B. Stefanov, G. Liu, A. Liashenko, P. Piskorz, I. Komaromi, R. Gomperts, R.L. Martin, D. J. Fox, T. Keith, M. A. Al-Laham, C. Y. Peng, A. Nanayakkara, C. Gonzalez, M. Challacombe, P. M. W. Gill, B. Johnson, W. Chen, M. W. Wong, J. L. Andres, C. Gonzalez, M. Head-Gordon, E. S. Replogle, J. A. Pople. Gaussian, Inc., Pittsburgh PA, 199818) M.Kato, K. Nihikawa, M. Untani, M. Mlyazaki , M.Takcmura , J Bmehem (1990) Gaussian 98 Revision A.7,107, 242-247.

Corporate Cash Holdings: Evidence from Thailand

Suchada Manunphongpan,
Faculty of commerce and accountancy, Chulalongkorn University

Abstract: The objective of this paper is to investigate the empirical determinants of corporate cash holdings for a sample of Thai firms over the period 1988-2007 and to find out whether Thai firms try to adjust their cash holdings towards the target cash level. In this paper, we find evidence supportive of the trade-off theory of cash holdings. The results reveal that firms' growth opportunity, debt maturity structure, dividend's payment, liquidity assets substitute, and leverage are important in determining cash holdings. Our results show that firms' growth opportunity, debt maturity structure, dividend's payment are positively related to cash holdings while liquidity assets substitute and leverage are negatively related to cash holdings. Furthermore, in dynamic panel estimation indicates that Thai firms do not adjust their cash holdings to the target cash ratio. We suspect that the most reasonable explanations for these results are based on the adjustment costs are so large which preventing firms from making adjustments in their cash holdings to reach the target cash ratio and/or there is no the existence of the target cash holding in long-run for Thai firms.

Keywords: Cash holdings, Dynamic adjustment, Panel data, Trade-off theory.

INTRODUCTION

The decision of firms in order to hold cash has recently been focus of attention in finance literature. Many international studies demonstrate that firms maintain important cash holdings for example, Opler et al. (1999) find that U.S. firms hold on average 17% of their total assets in cash and cash equivalents and Ferreira and Vilela (2004) observe an average cash ratio of 15% in EMU countries. According to existing studies on corporate cash holdings (e.g.,Opler et al.,1999; Ozkan and Ozkan,2004; Guney et al.,2003), they argue that the main benefit of holding cash is to reduce costs associated with dependence on external financing. In this view, cash holding decision may be affected by the existence of market imperfections such as information asymmetry, agency conflicts that make firms difficult and expensive to obtain funds. However, there are also potential adverse effects of cash holdings. Central of this argument is the agency conflicts between shareholders and managers can be most severe when firms have large free cash flows (Jensen, 1986). Managers can pursue their own private objectives that need not coincide with those of shareholders. Therefore, cash holdings obviously play an important role in financial management of corporations.

Due to the arguments of the costs and benefits of holding cash , one of the main questions that the previous studies try to answer is whether firms have target cash ratio. There are two main theoretical models that can help to explain the cash holding decision : the trade-off model (Myers, 1977) and the pecking order model (Myers and Mailuf, 1984). By utilizing the trade-off model on the case of detention of cash, we are able to conclude that firms identify their optimal level of cash holdings by weighting the marginal costs and marginal benefits of holding cash. In contrast, extending the pecking order theory in an attempt to explain the determinants of cash, leads to a contradictory conclusion of no optimal cash level. Cash is used as a buffer between retained earnings and investment needs.

Wichada (1998) reports that Thai listed firms have mean cash ratio ranging between 6% to 12% and standard deviation around 12% over the period of 1993 to 1998. From this data, it means that there are different in cash holdings among Thai firms. Therefore, in this paper we study cash holdings behavior of Thai firms and our question is that whether Thai firms have optimal levels of cash holdings. To answer this question, we test what are factors determining levels of cash holdings. For this test, we based on trade-off and pecking order theories that help to explain which firm characteristics influence cash holding decisions in order to investigate the determinants of Thai corporate cash holdings.

Another objective in this paper lies in the dynamic analysis of corporate cash holding decision. Because of previous Thai studies focus only on the static analysis of cash holdings in order to examine the determinants of Thai corporate cash holdings (Wichada ,1998 ; Chayanin ,2001), in this paper we adopt a more realistic recognizing that when cash holdings change due to firm characteristics change or random shocks occur. Market imperfections such as adjustment costs may prevent firms from adapting the current cash ratio immediately adjust to new desired cash level. Therefore, the objective for dynamic analysis of corporate cash holding is to investigate whether firms have long-run target cash ratio and if so how quickly that firms adjust toward the optimum. The important is that the interpretation from speed of adjustment towards

Corresponding Author : Suchada Manunphongpan, Master of Science degree in finance, Faculty of commerce and accountancy, Chulalongkorn University

the target cash ratio can evaluate the credibility of competing capital structure theories. In this view, a fast speed of adjustment is interpreted as support for the trade-off theory while a slow adjustment is consistent with pecking order theory.

However, most of empirical studies on the speed of adjustment towards the target cash ratio are based on the implicit assumption that firms follow a uniform adjustment rule and the speed of adjustment is linear and symmetric (e.g., Opler et al.,1999 ; Ozkan and Ozkan ,2004 ; Bruinshoofd and Kool, 2004). This means that all firms within a country have the same speed of adjustment at average value. According to Flannery and Hankins (2007), a theory of capital structure adjustment speed postulate that the speed of adjustment is not equal across all firms and the speed of adjustment depend on the costs of deviating from the target and the costs of adjusting toward the optimum. Therefore, in this paper we apply this theory to examine the determinants of speed adjustment towards the target cash ratio. To our knowledge, no research study on the determinants of speed adjustment towards the target cash ratio, this paper is the first to investigate that what are factors determining the speed of adjustment towards the target cash ratio.

DATA AND METHODOLOGY

Data

For our empirical analysis of corporate cash holdings, we use a sample of publicly traded Thai firms over the period 1993-2007. Our initial sample is the set of all firms for which data are available on the Datastream database. These data include survivors and non-survivors that appeared on Datastream at any time during the sample period. We exclude firms which operate in the financial sector since their cash policy differs from that of industrial firms. These criteria have provided us with a total of 426 firms, which represents 6,840 firm-year observations.

Methodology

This paper investigates the determinants of corporate cash holdings, estimates the speed of adjustment towards the target cash ratio and examines the determinants of speed of adjustment towards the target cash ratio of Thai firms. To answer all of these questions, we will examine corporate cash holdings in two sections which are static and dynamic panel data estimation.

Static Panel data estimation

The objective in this section is to investigate whether firms have target cash ratio. To answer this question, we test that what are factors determining levels of cash holdings. Because of previous studies find that proxies for agency and asymmetric information problems are important determines cash holdings (e.g., John, 1993; Kim et al.,1998; Harford,1999 ;Opler et al.,1999), therefore the explanatory variables that we use for this test reflect these problems and based on trade-off and pecking order theories explanation in order to describe the relationship between these variables and cash holding decision.

To test that what are factors determining levels of cash holding, we will estimate the following equation.

$$CASH_{i,t} = \beta_0 + \beta_1 MB_{i,t} + \beta_2 SIZ_{i,t} + \beta_3 CF_{i,t} + \beta_4 LIQ_{i,t} + \beta_5 DIV_{i,t} + \beta_6 LEV_{i,t} + \beta_7 DBT_{i,t} + \alpha_i + \varepsilon_{i,t} \quad (1)$$

where, $CASH$ is the dependent variable

$CASH_{i,t}$ = Cash + Cash equivalents/ Total assets – (Cash + Cash equivalents).

$MB_{i,t}$ = (Book value of total assets – Book value of equity + Market value of equity) / Book value of assets.

$SIZ_{i,t}$ = Natural logarithm of total assets.

$CF_{i,t}$ = Operating cash flow/ Total assets.

$LIQ_{i,t}$ = Net working capital – (Cash + Cash equivalents) / Total assets.

$DIV_{i,t}$ = Dividend Yield

$LEV_{i,t}$ = Total debt (Long-term debt + Short-term debt) / Total assets.

$DBT_{i,t}$ = Long-term debt / Total debt.

From equation (1), i and t represent firms and time respectively. α_i represents time-constant firm-specific effects. It is assumed that firm-specific effects α_i (firm-heterogeneity term) are unobservable but have a significant impact on cash holdings. They change across firms but fixed for a given firm through time.

In this paper, we use three different regression methodologies to examine the determinants of corporate cash holdings which are the Fama-Macbeth methodology, pool regression and fixed-effect regression. The reason that we use fixed-effect method in this study is to control for unobserved heterogeneity (α_i). This method is wildly uses in various empirical studies on corporate cash holdings (e.g.,Ozkan and Ozkan, 2004; Guney et al., 2003; Drobetz and Gruninger, 2006). We use Fixed-effects method because there are relevant unobservable characteristics in the underlying model, estimated coefficients in cross-sectional regression will be biased due to the correlation generated between the regressors and error term. The extent to which these unobserved effects remain relatively stable over time, we could control for them by using a fixed-effects estimator to obtain consistent coefficient estimates (Wooldridge, 2002).

Dynamic Panel data estimation

Estimate the speed of adjustment towards the target cash ratio.

In this section, the purpose is to examine whether firms have long-run target cash ratio and if so how quickly that firms adjust toward the target. The static cash holding model implicitly assumes that firms can instantaneously adjust towards the target cash level in response to changes in firm-specific characteristics or random shocks. In this paper, we adopt a more realistic recognizing that there may be delays in the adjustment process because of positive costs of adjustment causing the current cash ratio not to be immediately adjusted to the desire cash level. Following Ozkan and Ozkan (2004) and applying the partial adjustment toward target capital structures from Flannery and Rangan (2006), we estimate dynamic panel model. The process of firms in order to partially adjust to the target cash ratio can be represented by partial adjustment model :

$$CASH_{i,t} - CASH_{i,t-1} = \lambda\left(CASH^{*}_{i,t} - CASH_{i,t-1}\right) + \delta_{i,t} \quad (2)$$

where, $CASH_{i,t}$ is the actual cash ratio and $(CASH^{*}_{i,t} - CASH_{i,t-1})$ can be interpreted as the target change whereas only a fraction λ of it is achieved. The value of adjustment coefficient λ, capturing the ability of firms to adjust to their target cash levels. λ lies between 0 and 1. If λ=1, firms will adjust their cash levels to optimal level immediately, i.e., $CASH_{i,t} = CASH^{*}_{i,t}$. On the other hand, if λ=0, this indicates that adjustment costs are so large that firms cannot change their existing cash structure, i.e., $CASH_{i,t} = CASH_{i,t-1}$.

However the target cash ratio $CASH^{*}_{i,t}$ cannot be observed directly, the proxy is used. The target cash ratio can be determined as follow :

$$CASH^{*}_{i,t} = \sum_{k} \beta_k x_{k,i,t} \quad (3)$$

where, $CASH^{*}_{i,t}$ is a function of explanatory variables, X, which describe in equation (1).

We use equation (3) as a proxy for target cash ratio in equation (2), then combining equation (2) and (3), the result is obtained as follow:

$$CASH_{i,t} - CASH_{i,t-1} = \lambda(\sum_{k} \beta_k x_{k,i,t} + \alpha_i - CASH_{i,t-1}) + \delta_{i,t}$$

Then rearrange the above equation, we get

$$CASH_{i,t} = (1-\lambda)CASH_{i,t-1} + \lambda\sum_{k} \beta_k x_{k,i,t} + \delta_{i,t}$$

which can be simplified to :

$$CASH_{i,t} = \gamma_0 CASH_{i,t-1} + \sum_{k} \gamma_k x_{k,i,t} + \delta_{i,t} \quad (4)$$

where, $\gamma_0 = 1-\lambda$, $\gamma_k = \lambda\beta_{k..}$ The most important is the estimated value of $\lambda = 1-\gamma_0$ measures the speed of adjustment towards the target cash ratio. Estimation equation.

$$CASH_{i,t} = \gamma_0 CASH_{i,t-1} + \gamma_1 MB_{i,t} + \gamma_2 SIZ_{i,t} + \gamma_3 CF_{i,t} + \gamma_4 LIQ_{i,t} + \gamma_5 DIV_{i,t} + \gamma_6 LEV_{i,t} + \gamma_7 DBT_{i,t} + \alpha_i + \varepsilon_{i,t} \quad (5)$$

However in dynamic panel model a problem arises from the lagged dependent variables $CASH_{i,t-1}$ as mentioned in many studies (Ozkan and Ozkan, 2004; Guney et al., 2003; Drobetz and Gruninger, 2006; Garcia-Teruel and Martinez-Solano,2004). In this view, OLS regression does not consistently estimate coefficients in equation (5) because there is an autocorrelation between the disturbances. The OLS estimators are no longer minimum variance. To solve this problem, we use the two-stage least square (2SLS) regression and the unbiased estimation of equation (4) and (5) can provided by the two-stage least square regression if an instrument variable can be found that there is highly correlated with $CASH_{i,t-1}$ but not for the error term (Gujarati, 2003). In this paper, we use $CASH_{i,t-2}$ as an instrument variable.

Using the two-stage least square (2SLS), $CASH_{i,t-1}$ is regressed first on the instrument variable $CASH_{i,t-2}$ and the explanatory variables $x_{k,i,t}$.

$$CASH_{i,t-1} = \rho CASH_{i,t-2} + \sum_{k} \prod_k x_{ki,t-1} + \varepsilon_{i,t-1} \quad (6)$$

The fitted value of $CASH_{i,t-1}$ is obtained from equation (6).

$$\hat{CASH}_{i,t-1} = \hat{\rho} CASH_{i,t-2} + \sum_{k} \hat{\prod}_k x_{k,i,t-1} \quad (7)$$

where, $\hat{CASH}_{i,t-1}$ is the fitted value of $CASH_{i,t-1}$.

Therefore the equation (4) can be written as

$$CASH_{i,t} = \gamma_0 \hat{CASH}_{i,t-1} + \sum_{k} \gamma_k x_{k,i,t} + \delta_{i,t} \quad (8)$$

The speed of adjustment towards the target cash ratio can be examined by running the regression on equation (8).

Examine determinants of speed of adjustment towards the target cash ratio.

In this section, we recognize that the speed of adjustment towards the target cash ratio depends on the costs of deviating from the target and the costs of adjusting toward that optimum. This means that firms within a country may have difference speed of adjustment towards the target cash ratio due to the variation in adjustment costs and adjustment benefits. Therefore, in this study we will investigate that what are factors determining the speed of adjustment towards the target cash ratio.

Based on theory of capital structure adjustment speed of Flannery and Hankins (2007), we recognizing that the adjustment costs depend on firm's external financing costs and the benefits of achieving the target vary with the costs of financial distress. The main idea

is that firms that face lower external financing costs, can raise funds easily and have flexibility to adjust their cash holdings. Therefore, firms with lower external financing costs will have faster speed adjustment towards the target cash ratio than firms with higher external financing costs. Furthermore, the faster speed of adjustment towards the target cash ratio is predicted for firms with higher probability of financial distress.

To investigate the determinants of speed of adjustment towards the target cash ratio, we use firm size and debt capacity as the proxies for external financing costs and to capture the costs of financial distress, we examine relative leverage, relative cash and fixed assets.

Large firms imply faster speed of adjustment because they have low asymmetric information and face low cost of financing. Debt capacity measures firm's ability to access the external capital. High debt capacity, imply that firms easy to access capital markets and have faster speed of adjustment. Overleveraged firms and firms with cash below target level are expected to have faster speed of adjustment because they are more likely to distress. On the other hand, firms with more collateral reflect low costs of financial distress. Therefore, firms with more fixed assets have slower speed of adjustment than firms with low fixed assets. In this paper, firms are categorized as high or low in terms of firm size, debt capacity and fixed assets based on whether they are in the top (Q_4) or bottom (Q_1) quartile. Leverage and cash ratio are classified into two groups which are over or under the target level.

To investigate the determinants of speed of adjustment towards the target cash ratio, we hypothesis that differences in adjustment costs and benefits generate cross-sectional and variation in cash rebalancing. In this paper, we identify Z to represents the adjustment speed factors (firm size, debt capacity, relative leverage, relative cash and fixed assets) and the baseline model presented in equation (2) can be modified to allow the adjustment speed to vary with Z. The adjustment speed coefficient, λ, is replaced with a multi-factor coefficient which contain of a base adjustment speed estimate, λ_0, and the adjustment speed factor estimate, λ_1.

$$\lambda_{NEW} = \lambda_0 + \lambda_1 Z \qquad (9)$$

The modified partial adjustment model is:

$$CASH_{i,t} - CASH_{i,t-1} = (\lambda_0 + \lambda_1 Z)(CASH^*_{i,t} - CASH_{i,t-1}) + \delta_{i,t} \qquad (10)$$

We estimate equation (10) with a two-stage process. The first stage predicts the target cash ratio *CASH** and the second stage tests whether the adjustment speed factors are significant cash determinants.

A two-stage methodology is common uses in capital structure literature and authors frequently estimate the target based on the leverage factors, X, (Hovakimian, Opler and Titman, 2001; Fama and French,2002). This omits two important facts. First, it ignores the unobserved firm effects that may influence target ratio. Furthermore, it assumes that firms are in equilibrium. This assumption does not require for the partial adjustment model. Although in this paper we study the corporate cash holdings, we also concern about these two facts. Because of the previous studies on corporate cash holdings estimate the target ,*CASH**, based on firm characteristic factors, X (e.g., Ozkan and Ozkan, 2004; Guney et al., 2003). Therefore, we estimate the target cash ratio based on the partial adjustment framework.

Following Flannery and Hankins (2007), we can indicate that estimation in equation (4) does not require β or λ to be specified. The two-stage approach requires *CASH** to be calculated for each firm-year.

First, rearranging equation (4) shows that the target cash ratio can be estimated.

$$\sum_K \beta_k x_{k,i,t} + \alpha_i = \frac{1}{\lambda}\{CASH_{i,t} - (1-\lambda)CASH_{i,t-1}\} + \delta_{i,t} \qquad (11)$$

From equation (11), the predicted target cash ratio can be calculated based on the fitted values for the dependent variable, $\hat{CASH}_{i,t}$, the lagged dependent variable,$CASH_{i,t-1}$, and the estimated adjustment speed, $\hat{\lambda}$.

$$\hat{CASH}^*_{i,t} = \left(\sum \hat{\beta}_k \hat{x}_{k,i,t} + \alpha_i\right) = \frac{1}{\hat{\lambda}}\{\hat{CASH}_{i,t} - (1-\hat{\lambda})CASH_{i,t-1}\} \qquad (12)$$

In this paper, we estimate equation (4) using fixed-effect method and find the fitted values for $\hat{CASH}_{i,t}$ and $\hat{\lambda}$. These values are substituted in to equation (12) and the predicted target cash ratio is calculated.

Then the target is used in the second stage to estimate the impact of the adjustment speed factors. Due to the target determined from the first stage, we will know the difference between the target and the current cash ratio.

$$Deviation_{i,t-1} = \hat{CASH}^*_{i,t} - CASH_{i,t-1} \qquad (13)$$

And we also know the actual change in cash.

$$Change_{i,t} = CASH_{i,t} - CASH_{i,t-1} \qquad (14)$$

Substituting equation (13) and (14) into equation (10), we will get that only the adjustment speed coefficients λ_0 and λ_1 are estimated.

$$Change_{i,t} = (\lambda_0 + \lambda_1 Z)(Deviation_{i,t-1}) + \delta_{i,t} \qquad (15)$$

From equation (15), we can estimate the impact of the adjustment speed factors, Z by OLS regression.

RESULTS

Panel regression tests

We study the determinants of cash holdings using a regression of cash holdings, where CASH is the dependent variable. In this paper, we use three different regression methodologies. First, we use the Fama-Macbeth methodology: we run cross-sectional regression each year and use the time series of regression coefficients to make our inferences. Second, we run pool regression. Finally, we run a fixed-effect regression in order to control the unobserved firm heterogeneity problem. In this study, we examine the determinants of cash holdings in three samples period. The regression results are presented in table 1. Panel A,B and C show the results in whole period, before crisis and after crisis, respectively.

Table 1 Panel regression results

The dependent variable in all regressions is CASH, which is calculated as cash and cash equivalents divided by net assets. Panel A shows results in period 1993 to 2007. Panel B and C show results in the period of before crisis (1993-1996) and after crisis (1998-2007), respectively. MB is measured as the book value of total assets minus the book value of equity plus the market value of equity to book value of assets. SIZ is defined as the natural logarithm of total assets. CF is the ratio of operating cash flow to total assets. LIQ is the ratio of current assets minus current liabilities and total cash to total assets. LEV is the ratio of total debt to total assets. DBT is the ratio of long-term debt to total debt. DIVYIELD is the ratio of dividend to the stock price. The Fama-Macbeth model gives the average of the time series of coefficients from annual cross-sectional regressions. The cross-sectional regression uses the means of all variables for each firm. Only firms for which a full panel of data is available are used in the cross-sectional specification**.** ***, ** and * indicate significance at the 1 percent, 5 percent , and 10 percent level, respectively.

Dependent Variable : CASH

Panel A : Period 1993 to 2007 (Whole period)

Independent variable	Fama-Macbeth model	Pool regression	Fixed-effects regression
Intercept	0.0526	0.1025	0.0178
	(0.79)	(2.63)	(0.15)
MB	0.0609***	0.0427***	0.0243***
	(3.94)	(10.6)	(6.03)
SIZ	0.0032	0.0023	0.0078
	(0.81)	(0.86)	(1.02)
CF	0.0608	0.0034	0.0005
	(0.95)	(0.89)	(0.15)
LIQ	-0.1355***	-0.1579***	-0.2662***
	(-5.94)	(-9.44)	(-10.62)
LEV	-0.2866***	-0.2948***	-0.2674***
	(-9.75)	(-16.53)	(-11.1)
DBT	0.0644**	0.0329***	0.0967***
	(2.56)	(2.82)	(6.84)
DIVYIELD	0.0029**	0.0025***	0.0003
	(1.78)	(3.44)	(0.46)
N	15	3087	3087
Adjusted R-square	0.198	0.13	0.488

Panel B : Period 1993 to 1996 (Before crisis)

Independent variable	Fama-Macbeth model	Pool regression	Fixed-effects regression
Intercept	-0.1802	-0.3098	-1.8717
	(-0.97)	(-2.39)	(-2.66)
MB	0.0313**	0.0494***	0.0389***
	(3.82)	(6.16)	(3.38)
SIZ	0.0140	0.0193**	0.1294***
	(1.13)	(2.16)	(2.71)
CF	0.2032	0.3955***	0.5678***
	(0.86)	(4.64)	(7.53)
LIQ	-0.1506*	-0.1027*	-0.1537
	(-2.18)	(-1.81)	(-1.26)
LEV	-0.2012**	-0.0719	-0.233*
	(-3.10)	(-1.1)	(-1.8)
DBT	0.1474*	0.0662*	0.0859
	(1.80)	(1.79)	(1.29)
DIVYIELD	0.0081**	0.0091***	0.0029
	(3.50)	(3.26)	(0.88)
N	4	493	493
Adjusted R-square	0.181	0.196	0.634

Panel C : Period 1998 to 2007 (After crisis)

Independent variable	Fama-Macbeth model	Pool regression	Fixed-effects regression
Intercept	0.1527	0.1667	0.0366
	(3.33)	(3.91)	(0.28)
MB	0.0738***	0.0365***	0.0082
	(3.33)	(6.71)	(1.55)
SIZ	-0.0015	-0.0005	0.0096
	(-0.55)	(-0.16)	(1.11)
CF	0.0103	0.0022	-0.0007
	(0.37)	(0.6)	(-0.23)
LIQ	-0.1382***	-0.1629***	-0.2006***
	(-6.29)	(-8.9)	(-7.13)
LEV	-0.3290***	-0.3145***	-0.2705***
	(-11.27)	(-15.73)	(-9.8)
DBT	0.0266**	0.0177	0.0379**
	(2.66)	(1.4)	(2.45)
DIVYIELD	0.0011	0.002**	-0.001
	(0.55)	(2.47)	(-1.35)
N	10	2403	2403
Adjusted R-square	0.206	0.134	0.573

For whole period, the results from all three methodologies report that cash holdings increase significantly with market-to-book ratio and debt maturity structure and cash holdings decrease significantly with liquid assets substitutes and leverage. In addition, we also find that cash holdings increase significantly with dividend's payment in the Fama-Macbeth and Pool regression. However, the coefficients obtained for firm size and cash flow are not significant across all methodologies.

The market-to-book ratio coefficient is positive and significant at the 1% level, consistent with the view that firms with higher levels of growth opportunities prefer to hold more cash to avoid situations in which they give up profitable investment opportunities because they are short of cash. This result coincides with that found in previous studies (Kim et al.,(1998), Opler et al.,(1999), Ozkan and Ozkan(2004), Ferreira and Vilela (2004)).

The effect of liquidity asset substitutes on cash holdings is negative and significant at the 1% level. This result can possibly indicate that firms can use their non-cash liquid assets as substitute to cash holdings.

There is strong support for the negative relationship between leverage and cash holdings, as previously shown by Opler et al.,(1999), Ozkan and Ozkan(2004), Ferreira and Vilela (2004). The coefficient of leverage is significant at 1% level. The negative coefficient supports the pecking order theory, where cash holdings fall when investments exceed retained earnings.

We also provide strong evidence that the coefficient of dividend's payment is positive and significant. This finding is similar to the result that found in Ozkan and Ozkan (2004), Drobetz and Gruninger (2006) and the result is consistent with the view that dividend payers are particularly reluctant to omit dividends. Therefore, firms will hold large amounts of cash.

One interesting result is on the effects of firm size on cash holdings, the result indicates that the coefficient of firm size is positive but insignificant. This finding contradicts to the previous empirical studies (Opler et al.,(1999), Drobetz and Gruninger (2006)) and does not support the view that larger firms hold lower cash because they have better excess to external financing and less likely to experience to financial distress.

When we estimate our regression for the two sub samples period, we find that the results from the regressions lead to the same conclusions as the whole period, except for firm size and cash flow. During before crisis and after crisis, we still find strong evidence that the coefficients of market-to-book ratio, debt maturity structure and dividend's payment are positive and significant and the coefficients of liquidity asset substitutes and leverage are negative and significant. However, only the results from during before crisis reveal that firm size and cash flow coefficients are significant and positive related to cash holdings.

Dynamic panel data estimation

Estimate the speed of adjustment towards the target cash ratio.

In table 2, we report the results obtained for the estimation of the dynamic panel model. In this paper, we examine dynamic panel model in three samples period. Column (1) shows the result for the whole period (1993-2007) and Column (2),(3) show the results during before crisis and after crisis, respectively. All the estimations have been carried out using the two-stage least squares estimator.

Table 2 Dynamic panel data estimation results – Two-stage least squares estimations

This table presents the results from two-stage least squares estimations. Column (1) shows the results over the period from 1993 to 2007. Column (2) and (3) show the results in the period of before crisis (1993-1996) and after the crisis (1998-2007), respectively. CASH is calculated as cash and cash equivalents divided by net assets. MB is measured as the book value of total assets minus the book value of equity plus the market value of equity to book value of assets. SIZ is defined as the natural logarithm of total assets. CF is the ratio of operating cash flow to total assets. LIQ is the ratio of current assets minus current liabilities and total cash to total assets. LEV is the ratio of total debt to total assets. DBT is the ratio of long-term debt to total debt. DIVYIELD is the ratio of dividend to the stock price. ***, ** and * indicate significance at the 1 percent, 5 percent , and 10 percent level, respectively.

Dependent Variable : CASH			
Independent Variable	**(1) Whole period**	**(2) Before crisis**	**(3) After crisis**
CASH(t-1)	1.0667***	0.9529***	1.1033***
	(46.13)	(17.21)	(40.69)
MB	-0.0214***	-0.0458***	-0.0118**
	(-5.03)	(-4.19)	(-2.32)
SIZ	0.001	0.0059	0.0002
	(0.49)	(0.84)	(0.09)
CF	-0.0019	-0.083	-0.0019
	(-0.72)	(-0.98)	(-0.73)
LIQ	0.0065	-0.0346	0.0138
	(0.51)	(-0.73)	(1)
LEV	0.0139	0.0398	0.0128
	(0.94)	(0.71)	(0.76)
DBT	0.0013	0.0761***	-0.0094
	(0.15)	(2.6)	(-1.03)
DIVYIELD	-0.0002	0.0034	-0.0006
	(-0.4)	(1.59)	(-1.06)
C	-0.0009	-0.0795	0.0025
	(-0.03)	(-0.78)	(0.08)
N	2793	325	2292
Adjusted R-squared	0.515	0.536	0.518

For the whole period, the coefficient of the lagged dependent variable CASH(t-1) is negative and significant at the 1% level. The estimated speed of adjustment coefficient for Thai firms, $\lambda = 1-\gamma_0$, is -0.0667 which does not support the dynamic behavior of cash holding decisions. This result implies that adjustment costs are so large, preventing firms from making adjustments in their cash holdings to reach the target cash ratio. This finding is inconsistent with the previous empirical studies from Guney et al. (2003), Ozkan and Ozkan (2004), Garcia-Teruel and Martinez-Solano (2004), Drobetz and Gruninger (2006), which confirm the dynamic nature of cash holdings and firms adjust their cash holdings to the target cash ratio.

However, we find that the result during before crisis contradicts to the whole period. The coefficient of lagged dependent variable CASH(t-1) during before crisis is positive and significant at the 1% level. The estimated speed of adjustment coefficient, $\lambda = 1-\gamma_0$, is 0.0471 which confirms that Thai firms adjust their cash holdings to the target cash ratio at low speed of adjustment. This can be taken as the support to the view that firms trade-off between costs of adjustment towards target cash holdings and costs of being off target.

The result during after crisis is consistent with the result for the whole period. The coefficient of the lagged dependent variable CASH(t-1) is negative and significant at the 1% level. The estimated speed of adjustment coefficient, $\lambda = 1-\gamma_0$, is -0.1033 which does not support the dynamic behavior of cash holding decisions.

In summary, our results indicate that Thai firms do not adjust their cash holdings to the target cash ratio. We suspect that the most reasonable explanations are based on the adjustment costs are so large which preventing firms from making adjustments in their cash holdings to reach the target cash ratio and/or there is no the existence of the target cash holding in long-run for Thai firms.

Examine determinants of adjustment speed to target cash ratio

Table 3-7 present the results of the determinants of speed adjustment to the target cash ratio. The main factors that we study the impact to speed of adjustment are firm size, debt capacity, relative leverage, relative cash, and fixed assets. Firms are categorized as high or low in terms of firm size, debt capacity, and fixed assets based on whether they are in the top (Q_4) or bottom (Q_1) quartile. Leverage and cash ratio are classified into two groups which are over or under the target level. In all tables, we investigate the determinants of speed to target cash level in three samples period. Column (1) shows the result for the whole period (1993-2007) and Column (2),(3) show the results during before crisis and after crisis, respectively. All the estimations have been carried out using the two-stage least squares estimator. In this paper, the results from table 3-7 show that the speed of adjustment coefficient CASH(t-1) significant at the 1% level.

Table 3 The result of determinant speed of adjustment – Firm size

This table examines firms in the top and bottom quartile for size. The speed of adjustment is estimated with a two-stage least squares methodology. Column (1) shows the results over the period from 1993 to 2007. Column (2) and (3) show the results in the period of before crisis (1993-1996) and after the crisis (1998-2007), respectively. CASH is calculated as cash and cash equivalents divided by net assets. MB is measured as the book value of total assets minus the book value of equity plus the market value of equity to book value of assets. SIZ is defined as the natural logarithm of total assets. CF is the ratio of operating cash flow to total assets. LIQ is the ratio of current assets minus current liabilities and total cash to total assets. LEV is the ratio of total debt to total assets. DBT is the ratio of long-term debt to total debt. DIVYIELD is the ratio of dividend to the stock price. ***, ** and * indicate significance at the 1 percent, 5 percent , and 10 percent level, respectively.

Dependent Variable : CASH						
	(1) Whole period		(2) Before crisis		(3) After crisis	
Independe	Small	Large	Small	Large	Small	Large
CASH(t-1)	1.0549***	1.1751***	0.5053***	0.9013***	1.2248***	1.3348***
	(24.97)	(25.17)	(4.75)	(6.63)	(26.69)	(25.74)
MB	-0.0639***	-0.0011	-0.0563***	0.0185	-0.0234**	-0.0116
	(-7.3)	(-0.15)	(-2.66)	(0.8)	(-2.22)	(-1.56)
SIZ	-0.0048	-0.0116**	0.0043	-0.0365	-0.0083	-0.0099**
	(-0.45)	(-2.46)	(0.16)	(-1.45)	(-0.72)	(-2.27)
CF	-0.002	0.0846*	-0.0832	-0.6086***	-0.0032	0.2227***
	(-0.45)	(1.83)	(-0.66)	(-3.69)	(-0.75)	(4.82)
LIQ	-0.0338	0.0155	-0.0924	-0.3003**	-0.009	0.0645***
	(-1.28)	(0.67)	(-1.49)	(-2.54)	(-0.32)	(2.89)
LEV	-0.0148	0.13***	-0.1461*	0.0176	0.0177	0.1934***
	(-0.47)	(5.15)	(-1.7)	(0.14)	(0.52)	(7.41)
DBT	-0.0238	-0.0009	0.0532	0.0511	-0.0381**	-0.0108
	(-1.49)	(-0.05)	(1.26)	(0.68)	(-2.25)	(-0.72)
DIVYIELD	-0.0007	0.0005	0.0025	0.01	-0.0008	-0.0002
	(-0.73)	(0.43)	(0.91)	(1.12)	(-0.78)	(-0.18)
C	0.136	0.1217	0.0588	0.5501	0.1206	0.0652
	(0.96)	(1.56)	(0.17)	(1.34)	(0.79)	(0.9)
N	698	698	81	81	573	572
Adjusted R	0.574	0.611	0.39	0.484	0.647	0.671

Table 4 The result of determinant speed of adjustment – Debt capacity

This table examines firms in the top and bottom quartile for debt capacity. The speed of adjustment is estimated with a two-stage least squares methodology. Column (1) shows the results over the period from 1993 to 2007. Column (2) and (3) show the results in the period of before crisis (1993-1996) and after the crisis (1998-2007), respectively. CASH is calculated as cash and cash equivalents divided by net assets. MB is measured as the book value of total assets minus the book value of equity plus the market value of equity to book value of assets. SIZ is defined as the natural logarithm of total assets. CF is the ratio of operating cash flow to total assets. LIQ is the ratio of current assets minus current liabilities and total cash to total assets. LEV is the ratio of total debt to total assets. DBT is the ratio of long-term debt to total debt. DIVYIELD is the ratio of dividend to the stock price. ***, ** and * indicate significance at the 1 percent, 5 percent , and 10 percent level, respectively.

Dependent Variable : CASH						
	(1) Whole period		(2) Before crisis		(3) After crisis	
Independe	Low Debt	High Debt	Low Debt	High Debt	Low Debt	High Debt
CASH(t-1)	0.9431***	1.2297***	0.4125***	1.405***	1.0155***	1.1915***
	(20.49)	(22.08)	(6.13)	(12.09)	(20.03)	(15.95)
MB	-0.0288***	-0.0004	-0.0175	0.044	-0.0088	-0.0067
	(-3.49)	(-0.03)	(-1.63)	(1.24)	(-0.93)	(-0.39)
SIZ	-0.0009	0.0021	0.0073	0.0192	-0.0095*	0.0029
	(-0.17)	(0.44)	(1.02)	(0.94)	(-1.66)	(0.55)
CF	-0.0025	0.0916*	0.0615	0.1653	-0.004	0.0993*
	(-0.45)	(1.84)	(0.58)	(1.01)	(-0.73)	(1.75)
LIQ	-0.172***	-0.0586*	-0.0643	-0.1405	-0.1871***	-0.033
	(-4.57)	(-1.69)	(-1.12)	(-1.2)	(-4.59)	(-0.88)
LEV	-0.9565***	-0.0615	-0.3127***	-0.0705	-1.1134***	-0.0275
	(-8.42)	(-1.08)	(-3.54)	(-0.32)	(-7.73)	(-0.44)
DBT	-0.0038	0.0695***	0.1109***	0.1381*	-0.0314	0.0477*
	(-0.18)	(2.65)	(3.8)	(1.73)	(-1.39)	(1.68)
DIVYIELD	-0.0031**	0	-0.0005	0.0052	-0.0042***	-0.0006
	(-2.36)	(0)	(-0.21)	(1.25)	(-2.93)	(-0.43)
C	0.1503**	-0.0115	-0.0311	-0.3647	0.2615***	-0.028
	(2.01)	(-0.16)	(-0.29)	(-1.23)	(3.14)	(-0.35)
N	698	698	81	81	573	573
Adjusted R	0.554	0.5	0.602	0.798	0.598	0.37

Table 5 The result of determinant speed of adjustment – Relative leverage

This table examines firms that are over or underleveraged. The speed of adjustment is estimated with a two-stage least squares methodology. Column (1) shows the results over the period from 1993 to 2007. Column (2) and (3) show the results in the period of before crisis (1993-1996) and after the crisis (1998-2007), respectively. CASH is calculated as cash and cash equivalents divided by net assets. MB is measured as the book value of total assets minus the book value of equity plus the market value of equity to book value of assets. SIZ is defined as the natural logarithm of total assets. CF is the ratio of operating cash flow to total assets. LIQ is the ratio of current assets minus current liabilities and total cash to total assets. LEV is the ratio of total debt to total assets. DBT is the ratio of long-term debt to total debt. DIVYIELD is the ratio of dividend to the stock price. ***, ** and * indicate significance at the 1 percent, 5 percent , and 10 percent level, respectively.

Dependent Variable : CASH						
	(1) Whole period		(2) Before crisis		(3) After crisis	
Independe	Under Lev	Over Lev	Under Lev	Over Lev	Under Lev	Over Lev
CASH(t-1)	0.948***	1.1645***	0.8153***	1.1405***	0.9726***	1.2247***
	(24.66)	(45.64)	(8.05)	(17.2)	(22.6)	(41.71)
MB	-0.0241***	-0.0107**	-0.0523***	0.0166	-0.0068	-0.0158***
	(-3.72)	(-2.03)	(-2.93)	(1.07)	(-0.91)	(-2.64)
SIZ	0.0003	0.0009	0.0128	0.0004	-0.0016	0.0016
	(0.09)	(0.36)	(1.01)	(0.05)	(-0.5)	(0.64)
CF	-0.0019	0.0625**	0.0981	-0.3102***	-0.0021	0.1243***
	(-0.65)	(2.35)	(0.58)	(-3.19)	(-0.7)	(4.34)
LIQ	-0.0291	0.0463***	0.022	-0.0713	-0.023	0.0683***
	(-1.41)	(3.21)	(0.25)	(-1.31)	(-1.07)	(4.39)
LEV	-0.0757***	0.0985***	0.1754	-0.0299	-0.0849***	0.1305***
	(-2.75)	(5.4)	(1.53)	(-0.49)	(-2.79)	(6.35)
DBT	-0.0096	0.0113	0.0323	0.0777**	-0.0167	-0.0031
	(-0.72)	(1.14)	(0.6)	(2.35)	(-1.19)	(-0.29)
DIVYIELD	-0.001	0.0004	-0.0036	0.0081***	-0.0009	-0.0003
	(-1.09)	(0.75)	(-0.99)	(3.2)	(-0.98)	(-0.41)
C	0.0562	-0.0643*	-0.1863	-0.0751	0.068	-0.0846**
	(1.27)	(-1.94)	(-1)	(-0.64)	(1.48)	(-2.35)
N	1482	1309	109	214	1338	954
Adjusted R	0.409	0.669	0.442	0.645	0.411	0.707

Table 6 The result of determinant speed of adjustment – Relative cash

This table examines firms that cash are above or below the target. The speed of adjustment is estimated with a two-stage least squares methodology. Column (1) shows the results over the period from 1993 to 2007. Column (2) and (3) show the results in the period of before crisis (1993-1996) and after the crisis (1998-2007), respectively. CASH is calculated as cash and cash equivalents divided by net assets. MB is measured as the book value of total assets minus the book value of equity plus the market value of equity to book value of assets. SIZ is defined as the natural logarithm of total assets. CF is the ratio of operating cash flow to total assets. LIQ is the ratio of current assets minus current liabilities and total cash to total assets. LEV is the ratio of total debt to total assets. DBT is the ratio of long-term debt to total debt. DIVYIELD is the ratio of dividend to the stock price. ***, ** and * indicate significance at the 1 percent, 5 percent , and 10 percent level, respectively.

Dependent Variable : CASH						
	(1) Whole period		(2) Before crisis		(3) After crisis	
Independe	Cash below	Cash above	Cash below	Cash above	Cash below	Cash above
CASH(t-1)	0.324***	0.7864***	0.218***	0.9505***	0.3718***	0.7551***
	(19.92)	(18.45)	(7.01)	(8.74)	(18.77)	(15.51)
MB	0.0001	0.0009	0.0085***	-0.0905***	-0.0012	0.0316***
	(0.04)	(0.09)	(2.64)	(-3.57)	(-0.7)	(2.66)
SIZ	0.0026***	-0.0045	0.0023	-0.0092	0.0025***	-0.0052
	(4.32)	(-0.92)	(1.24)	(-0.42)	(3.73)	(-0.99)
CF	0.0002	-0.0057	-0.0691***	0.1997	0.0002	-0.005
	(0.31)	(-0.87)	(-2.93)	(0.85)	(0.28)	(-0.77)
LIQ	-0.0106**	-0.1748***	-0.0411***	-0.284**	-0.0064	-0.1534***
	(-2.42)	(-5.97)	(-3.11)	(-2.15)	(-1.3)	(-4.93)
LEV	-0.0532***	-0.2438***	-0.0781***	0.0705	-0.046***	-0.2729***
	(-8.82)	(-7.81)	(-4.93)	(0.48)	(-6.41)	(-7.76)
DBT	0.0149***	0.0275	0.029***	0.1169	0.0136***	0.0124
	(5.7)	(1.34)	(3.47)	(1.64)	(4.84)	(0.56)
DIVYIELD	0.0005***	-0.0025	0.0007	-0.0044	0.0007***	-0.0047***
	(3.52)	(-1.63)	(1.18)	(-0.81)	(3.72)	(-2.59)
C	-0.0139	0.2684***	-0.0089	0.289	-0.0165*	0.2685***
	(-1.59)	(3.84)	(-0.34)	(0.89)	(-1.71)	(3.61)
N	1851	942	227	98	1511	781
Adjusted R	0.417	0.53	0.405	0.527	0.428	0.543

Table 7 The result of determinant speed of adjustment – Fixed assets

This table examines firms in the top and bottom quartile for fixed assets. The speed of adjustment is estimated with a two-stage least squares methodology. Column (1) shows the results over the period from 1993 to 2007. Column (2) and (3) show the results in the period of before crisis (1993-1996) and after the crisis (1998-2007), respectively. CASH is calculated as cash and cash equivalents divided by net assets. MB is measured as the book value of total assets minus the book value of equity plus the market value of equity to book value of assets. SIZ is defined as the natural logarithm of total assets. CF is the ratio of operating cash flow to total assets. LIQ is the ratio of current assets minus current liabilities and total cash to total assets. LEV is the ratio of total debt to total assets. DBT is the ratio of long-term debt to total debt. DIVYIELD is the ratio of dividend to the stock price. ***, ** and * indicate significance at the 1 percent, 5 percent , and 10 percent level, respectively.

Dependent Variable : CASH						
	(1) Whole period		(2) Before crisis		(3) After crisis	
Independe	Low	High	Low	High	Low	High
CASH(t-1)	1.0814***	0.7678***	1.26***	1.0337***	1.0456***	0.7011***
	(22.89)	(13.94)	(13.55)	(7.69)	(18.03)	(10.91)
MB	-0.0129	-0.0133	-0.0205	0.0016	-0.0076	-0.0115
	(-1.13)	(-1.61)	(-0.86)	(0.05)	(-0.55)	(-1.22)
SIZ	0.0009	0.0062*	-0.0019	0.0083	0.0027	0.0062*
	(0.13)	(1.95)	(-0.11)	(0.49)	(0.35)	(1.96)
CF	0.2309***	-0.0006	0.0812	-0.5521***	0.2332***	0.0914*
	(4.31)	(-0.01)	(0.51)	(-3.62)	(3.8)	(1.89)
LIQ	-0.1636***	-0.0446	-0.0634	-0.1707*	-0.1689***	-0.0543*
	(-4.59)	(-1.57)	(-0.68)	(-1.67)	(-4.12)	(-1.7)
LEV	-0.0423	-0.0347	0.1701	-0.1435	-0.0771	-0.0543*
	(-1.01)	(-1.2)	(1.56)	(-1.28)	(-1.54)	(-1.68)
DBT	0.0726***	0.0131	0.1078*	0.0288	0.0668**	0.0184
	(2.74)	(0.83)	(1.86)	(0.46)	(2.12)	(1.05)
DIVYIELD	-0.0016	0.0002	0.0038	0.0063	-0.0026*	-0.0017
	(-1.24)	(0.15)	(1.1)	(1.45)	(-1.7)	(-1.27)
C	0.0494	-0.0829*	-0.0632	-0.1165	0.0393	-0.0813*
	(0.54)	(-1.78)	(-0.28)	(-0.46)	(0.37)	(-1.74)
N	698	698	81	81	573	573
Adjusted R	0.606	0.282	0.818	0.469	0.556	0.27

Table 3 and 4 present the impact of external financing costs to adjustment process. Higher external financing costs are expected to slow the rate of adjustment. Because of external financing costs fluctuate with asymmetric information and firm's ability to access the capital markets. In this paper, we use firm size as the proxy for information asymmetry and debt capacity to evaluate access to the capital markets.

Table 3 shows the impact of firm size. For the whole period, the results indicate that small and large firms do not adjust their cash holdings to the target cash ratio. The speed adjustment coefficients for both firms are negative at the rate of
-0.0549 and -0.1751, respectively. These results show that there are not different in speed of adjustment due to firm size and do not support the hypothesis that larger firms have lower information asymmetry which would imply a lower cost of financing and have faster speed of adjustment towards the target cash ratio.

On the other hand, when we consider the impact of firm size into two sub periods, we find that small and large firms adjust their cash holdings to the target cash ratio during before crisis. The result shows that small firms have faster speed of adjustment than large firms (0.4947 compare to 0.0987). This finding is opposite to the prediction of the relationship between firm size and speed of adjustment to target cash ratio. However, the result during after crisis is similar to the result for the whole period. For during after crisis, we still find that both of small and large firms do not adjust their cash to the target level.

Table 4 shows the impact of debt capacity. For the whole period, the result shows that firms with low debt capacity adjust their cash holdings to the target cash level at low speed of adjustment (0.0569) while firms with high debt capacity do not adjust their cash to the target cash ratio(the speed of adjustment coefficient is negative at the rate of -0.2297). Moreover, we find that the result during before crisis is similar to the result for the whole period. However, for during after crisis the result indicates that both of firms with low debt capacity and firms with high debt capacity do not adjust their cash holdings to the target cash level. All these findings are not consistent with the conclusion of Leary and Roberts (2005) that firms with low debt capacity have limited potential for distress and less need for rapid adjustment.

Table 5-7 present the impacts of financial distress costs to adjustment process. The main idea is that faster adjustment is predicted for firms with a higher probability of distress. To capture costs of distress, we use relative leverage, relative cash and fixed assets as proxies.

Table 5 shows the impact of relative leverage. For the whole period, the result shows that underleveraged firms adjust their cash holdings to the target cash level at low speed of adjustment (0.052) while overleveraged firms do not adjust their cash to the target cash level (the speed of adjustment coefficient is negative at the rate of
-0.1645). In addition, the conclusions of the results for during before crisis and after crisis are the same as the result for the whole period. All these results opposite to the conclusion that overleveraged firms have higher speed of adjustment than underleveraged firms because of the costs of financial distress for overleveraged firms are higher.

Table 6 shows the impact of relative cash. For the whole period, the result shows that firms with cash below target have faster speed of adjustment than firms with cash above target (0.676 compare to 0.2136). And we also find that the conclusions of the results during before crisis and after crisis are the same as the result for the whole period. These results are consistent with the view that firms with cash below target are expected to have faster speed of adjustment than firms with cash above target because they are more likely to distress.

Table 7 shows the impact of fixed assets. For the whole period, the result shows that firms with high fixed assets adjust their cash holdings to the target cash level at the rate of 0.2322 while firms with low fixed assets do not adjust their cash to the target cash ratio(the speed of adjustment coefficient is negative at the rate of
-0.0814). Furthermore, we find the same results as the whole period in during after crisis. However, the result during before crisis reports that firms with low fixed assets and firms with high fixed assets do not adjust their cash holdings to the target cash ratio. Therefore, we can conclude that all these results contrast to the conclusion that firms with higher fixed assets have slower speed of adjustment than firms with lower fixed assets.

CONCLUSIONS

We examine firms' cash holding decisions by using Thai non-financial firms during the period 1993-2007. First, we investigate the determinants of corporate cash holdings. We observe significant influences from firm-specific variables on cash holdings. Our results indicate that cash holding is positively related to the firms' growth opportunity and negatively related to leverage and liquidity assets substitute. These findings are similar to the previous findings in Opler et al.,(1999), Ferreira and Vilela (2002), Ozkan and Ozkan (2004) and support the trade-off model which postulates that firms identify their optimal level of cash holdings by weighting the marginal benefits and marginal costs of holding cash.

The strong positive relationship between firms' growth opportunity and cash holdings indicates that firms will avoid foregoing valuable investment opportunities due to cash shortages. And according to the transaction cost motive, the observation that firms with higher leverage tend to hold less cash is consistent with the view that opportunities costs of holdings cash increase with leverage. However, the negative relationship between leverage and cash holdings also support the pecking order theory, where cash holdings fall when investments exceed retained earnings.

In addition, we also find the positive relationship between dividend's payment and cash holdings. This result supports for the hypothesis that dividend paying firms hold more cash because they reluctant to cut or omit dividend payments. However, our result indicates that debt maturity structure is positively related to cash holdings which contrast to the result from previous study (Garcia-Teruel and Martinez-Solano, 2004). This finding is not support the view that firms with more short-term debt, which are likely to have greater information asymmetry, hold more cash. In this paper, we cannot observe a significant relationship between firm size and cash holdings.

Second, we analyze speed of adjustment towards the target cash ratio of Thai firms by two-stage least square estimator. The results show that the estimated adjustment coefficients from dynamic panel models are negative, indicating that Thai firms do not adjust their cash holdings to the target cash ratio. We suspect that the most reasonable explanations are based on the adjustment costs are so large which preventing firms from making adjustments in their cash holdings to reach the target cash ratio and/or there is no the existence of the target cash holding in long-run for Thai firms.

Finally, we focus on the determinants of speed of adjustment towards the target cash ratio. In this paper, we examine the impact of firm's external financing costs and financial distress costs to the speed of adjustment. Most of our findings demonstrate that we cannot observe adjustment behavior to target cash ratio for Thai firms. However, we find some adjustment towards target cash level and support the reasons of theory of adjustment speed. The results show that firms with cash below target have faster speed of adjustment towards target cash ratio than firms with cash above target in all three samples period.

On the other hand, we also find the results that are not consistent with the reasons of theory of adjustment speed. Our findings indicate that underleveraged firms have faster speed of adjustment towards target cash ratio than overleveraged firms in all three samples period and firms with high fixed assets adjust their cash holdings faster than firms with low fixed assets in the whole period and during after crisis.

REFERENCES

1. Baskin, J. (1987): "Corporate Liquidity in Games of Monopoly Power", *Review of Economics and Statistics*, vol. 69, pp. 312-319.
2. Brennan, M., Hughes, P. (1991): "Stock prices and the supply of information", *Journal of Finance,* vol. 46, pp. 1665-1691.
3. Bruinshoofd, A.W., Kool, C.J.M. (2004): "Dutch corporate liquidity management:New evidence on aggregation", *Journal of Applied Economics,* vol. 7, pp. 195-320.
4. Chayanin Chavanabutvilai, 2001, "An empirical study on the determinants of cash holdings of Thai firms". A special project submitted in partial fulfillment of the requirements for the degree of Master of Science in Finance, Faculty of Commerce and Accountancy, Chulalongkorn University.
5. Collins, D., Rozeff, M., Dhaliwal, D. (1981): "The economic determinants of the market reaction to proposed mandatory accounting changes in the oil and gas industry", *Journal of Accounting and Economics,* vol. 3, pp. 37-71.
6. Couderc, N. (2005):"Corporate cash holdings: financial determinants and consequences", Working Paper.
7. Dittmar, A., J. Mahrt-Smith and H. Servaes (2002): "International CorporateGovernance and Corporate Cash Holdings", *Journal of Financial and Quantitative Analysis,* vol. 38, pp. 111-133.
8. Drobetz,W. and M.C. Gruninger (2006) :"Corporate Cash Holdings : Evidence from Switzerland", Working paper.
9. Fama, E. F. and K. R. French (2002): "Testing Trade-Off and Pecking Order Theories of Capital Structure", *Review of Financial Studies,* vol. 15, pp.1-33.
10. Faulkender, M. (2004): "Cash holdings among small businesses", Working Paper.

11. Fazzari, S.M., Petersen, B. (1993): "Working capital and fixed investment: New evidence on financing constraints", *Rand Journal of Economics,* vol. 24, pp. 328-342.
12. Ferreira, M. A. and A. Vilela (2004): "Why do Firms Holds Cash? Evidence from EMU Countries", *European Finance Management*, vol. 10, pp. 295-319.
13. Flannery, M. J. (1986): "Asymmetric Information and Risky Debt Maturity Choice", *Journal of Finance*, vol. 41, pp. 19-37.
14. Flannery, M. J. and K. P. Rangan. (2006): "Partial Adjustment toward Target Capital", *Journal of Financial Economics,* vol . 41, pp. 41-73.
15. Flannery, M.J. and K. W. Hankins (2007): "A Theory of Capital Structure Adjustment Speed", Working paper.
16. Garcia-Teruel, P.J., Martinez-Solano, P. (2004): "On the determinants of SMES cash holding: Evidence form Spain", Working Paper.
17. Gujarati, D.N. (2003): Basic Econometrics.
18. Guney, Y., A. Ozkan and N. Ozkan (2003): "Additional International Evidence on Corporate Cash Holding", Working paper, SSRN Electronic Library.
19. Harford, J. (1999): "Corporate cash reserves and acquisitions", *The Journal of Finance*, vol. 64, pp.1969-1997.
20. Harris, M., Raviv, A., (1990): "The theory of the capital structure", *Journal of Finance,* vol. 46, pp. 297-355.
21. Hovakimian, Armen, T. Opler, and S.Titman (2001): "The Debt-Equity Choice",*Journal of Financial and Quantitative Analysis*, vol. 36, pp.1-24.
22. Jensen, M. C. (1986): "Agency Costs of Free Cash Flow, Corporate Finance and Takeovers", *American Economic Review,* vol. 76, pp. 323-339.
23. John, T. C. (1993): "Accounting Measures of Corporate Liquidity, Leverage and Costs of Financial Distress", *Financial Management*, vol. 22, pp. 91-100.
24. Kale, J. R. and T. H. Noe (1990): "Risk Debt Maturity Choice in a Sequencial Game Equilibrium", *Journal of Financial Research*, vol. 13, pp. 155-165.
25. Kim, C. S., D. Mauer and A. E. Sherman (1998): "The Determinants of Corporate Liquidity: Theory and Evidence", *Journal of Financial and Quantitative Analisys*, vol. 33, pp. 335-359.
26. Kytonen, E. (2005): "Corporate liquidity holdings: An empirical investigation of Finnish firms", Working Paper.
27. Miller, M. H. and D. Orr (1966): "A Model of the Demand for Money by Firms",*Quarterly Journal of Economics*, vol. 80, pp. 413-435.
28. Myers, S. (1977): "Determinants of corporate borrowing", *Journal of Financial Economics,* vol. 5, pp. 147-175.
29. Myers, S.C.(1984): "The capital structure puzzle", *Journal of Finance,* vol. 39, pp. 575-92.
30. Myers, S. C. and N. S. Majluf (1984): "Corporate Financing and Investment Decisions when Firms Have Information that Investors Do Not Have", *Journal of Financial Economics*, vol. 20, pp. 293-315.
31. Opler, T., L. Pinkowitz, R. Stulz and R. Williamson(1999):"The Determinants and Implications of Corporate Cash Holdings", *Journal of Financial Economics*, vol. 52, pp. 3-46.
32. Ozkan,A. (1996): "Corporate bankruptcies, liquidation costs and the role of banks", *The Manchester School,* vol. 64, pp.104-119.
33. Ozkan, A. and N. Ozkan (2004): "Corporate Cash Holdings: an Empirical Investigation of UK Companies", *Journal of Banking and Finance*, vol. 28, pp. 2103-2134.
34. Shleifer, A., Vishny, R.W. (1992): "Liquidation values and debt capacity: A market equilibrium approach", *Journal of Finance*, vol. 47, pp.1343-1366.
35. Titman, S. and R. Wessels (1988): "The Determinants of Capital Structure Choice", *Journal of Finance,* vol. 43, pp. 1-19.
36. Wichada Leawnanonchai, 1998, "The determinants of corporate liquidity : Evidence from Panel Data of Thai Industrial Firms". A special project submitted in partial fulfillment of the requirements for the degree of Master of Science in Finance, Faculty of Commerce and Accountancy, Chulalongkorn University.
37. Wiliamson, O. (1988): "Corporate finance and corporate governance", *Journal of Finance*, vol. 43, pp. 567- 591.
38. Whited, T. (1992): "Debt, liquidity constraints, and corporate investment: Evidence from panel Data", *Journal of Finance,* vol. 47, pp.1425-60.
39. Wooldridge, J.M. (2002): Econometric analysis of cross section and panel data. MIT Press.

The Investigation of Target Leverage Role When Firms Make Financial Decision: Empirical Evidence In Australia Singapore And Thailand

Eakkachai Tangsageamvisai
Department of Banking and Finance, Faculty of Commerce and Accountancy
Chulalongkorn University
Bangkok, Thailand

Abstract: Target capital structure explains that firms will trade off between the benefit of using debt and the cost of debt to reach their target capital structure. At this level, firms will maximize their value. Base on this theory, firms will adjust their capital structure to move toward target that means firms consider target as important factor when they make external finance. In contrast to previous target capital structure work, this paper will classify the role of target capital structure into 2 different levels. Given investment plan, firms will try to make external finance (debt or equity) that minimize deviation from target. Another is firms will adjust their capital structure over time when they deviate further from target. Binary logit regression method will be applied to the test. Binary logit regression can take into account other control variables. The results show that when firms make external finance, firms will have their target level in mind and try to finance in the way that minimize their deviation from target. Firms also try to adjust their capital structure overtime when they deviate from target leverage ratio. This evidence shows that capital structure is relevant when firms do financial transaction.

Keywords: Trade-off, Target Leverage Ratio

INTRODUCTION

The trade-off theory is one of main theories that explain the relevance of capital structure. According to this theory, firms choose their capital structure that balance marginal benefits and marginal costs of debt and try to maintain to the target structure. This target will maximize the value of the firm and so, according to this theory, a firm will consider its target as one important factor when making a financial decision.

The study of debt-equity choice which is the one implication of trade-off theory examines how firm characteristics affect the choice between debt and equity when firms want external fund. This study hypothesizes that firms tend to move toward target leverage ratio when they either raise capital or retire existing capital.

Hovakimian [1] proposes that earlier studies of debt-equity [2,3,4,5] choice have overlooked some aspects of firms' behavior which are also consistent with the tradeoff theory. Firms might consider the target as an important determinant in their financial decision at different situations. The first involves a situation in which firms considering for external fund tend to select the transaction that can minimize the absolute deviation from target. This is called debt-equity hypothesis. Second, firms when deviate from target tend to make a transaction which moves their leverage ratio toward the target leverage ratio. This is called target adjustment hypothesis. The first situation assume that firms do have financial need so they have to decide either to raise fund with equity or debt by considering which type of transaction can minimize the absolute deviation. Contrast with the first situation, second situation involves the firms that decide to make transaction and decide not make any transaction. To investigate, firms make transaction because of adjusting toward target leverage ratio. For example, overleveraged firms, by the target adjustment hypothesis, tend to issue equity or reduce debt rather than making no transaction because firms want to adjust their leverage ratio toward the target leverage ratio.

This paper will examine whether target capital structure determines corporate financial decisions by differentiating between two aspects of the role of target leverage. The countries in the study are Australia, Singapore and Thailand. These countries are in the Asia Pacific region where study on the role of target capital structure is less documented. Previous debt-equity choice studies are concentrated in US, UK and Europe

Corresponding Author: Eakkcahi Tangsageamvisai, Department of Banking and Finance, Faculty of Commerce and Accountancy, Chulalongkorn University, Bangkok, Thailand Tel: +662-6936838, E-mail: eakkachai12@gmail.com

[1,2,6]. The different environments in each country, such as the legal and institutional settings, will also provide a good opportunity to examine the role of target leverage in this region. For example, Australia and Singapore are developed capital market while Thailand is emerging market. La Porta, Lopez-de-Silanes, Shleifer, and Vishy [7] find that a better protection of outside investor increases external financing. These countries in investigation have the different level of protection of outside investors. Australia and Singapore have the same level of shareholders right protection at 4 which is greater than Thai shareholders that score only 2 (high score means high level of protection). This implies that Australia and Singapore can easier access to stock market than Thailand. In term of debt financing, the legal protection for creditor rights in Australia, Singapore and Thailand are 1, 4 and 3 respectively. Comparing between shareholders and creditors protection right imply that when external fund needed, Australia firms tend to issue more equity. Singapore can use either debt or equity. Thai firms will depend more on debt. These differences could affect the firms' decision when decide for external fund.

This paper also classifies firms into two different types, namely those overleveraged and those underleveraged. Classifying these two kinds of firms in the study can identify the role of target leverage more clearly because over- and under- leveraged firms are in different positions so they have different incentives. Pooling these two types of firm together might give a biased result; for example, if overleveraged firms concern more on target leverage ratio than underleveraged firms because they have higher costs of deviation from the target [6].

METHODS AND DATA

The sample contains firms in stock exchange of Australia, stock exchange of Singapore and stock exchange of Thailand. Firms in financial sector are excluded from the sample because they are highly regulated and their capital structures are significantly different from other sectors. The period of this study is during 1996-2006.

There are 4 main transactions in this study, namely Equity issue, Debt issues, Equity repurchase and Debt reduction. All transactions will be net transactions, net equity issue (net equity repurchase) = proceeds from sale of common stock and preferred stock – amount of common and preferred stock repurchased. Net debt issue (net debt reduction) = proceeds from issuing short or long term borrowing – amount of repayment of amount borrowed

Following Hovakimian, Opler and Titman [5], this paper will focus on firms having financing transactions defined as being greater 5% of the pre-issue book value of total assets. Firms that being less than 5% for both debt and equity transactions define as No transaction firms. For example, in a given financial year if net equity issue of firm A is positive and is greater than 5% of the pre-issue book value of total assets. A is classified as equity issue transaction. However, if net equity issue of firm A is negative and is greater than 5% of pre-issue book value of total assets. A is classified as equity repurchase transaction.

Net equity issue, net equity repurchase, net debt issue and net debt reduction are tracked from the cash flow from financing as reported on Reuter. The reason that uses cash flow statement because debt that comes from operating activity should be excluded. Other accounting variables are collected from DataStream database.

To examine to role of target leverage ratio, two stages procedure are required by the following equations.

$$Lev_{i,t} = \alpha_0 + \beta_1 PROF_{i,t-1} + \beta_2 TANG_{i,t-1} + \beta_3 SIZE_{i,t-1} + \beta_4 NDTS_{i,t-1} + \beta_5 MTB_{i,t-1} + \beta_6 SE_{i,t-1} + \beta_7 RD_{i,t-1} + \beta_8 DUM\_RD_{i,t-1} + v_i + \lambda_t + \varepsilon_{i,t} \quad (1)$$

First, target leverage ratio is estimated. This paper will proxy the target by regress the debt ratio against the set of the variables that are used in past studies of debt determinants Lev is the book value of debt ratio. The reason the book value of debt ratio is used because managers consider the accounting number as their information before making any financial decisions. The natural logarithm of sale used as a proxy for firms size (SIZE) which is a common measure for size[8]. Larger firms tend to be more diversified and have more access to capital market so they can use more debt. The ratio of net property plant and equipment to total asset (TANG) is used to proxy for tangible asset [8]. Tangible asset can be used as collateral for debt financing can thus be associated with high debt capacity. ROA proxies for internal finance capacity [5]. ROA is defined as the ratio of earnings before interest, taxes, depreciation and amortization (EBITDA) to total assets. The market to book ratio (MTB) is a common measure for growth opportunities [8]. Firms with high growth opportunities tend to use less debt because an increase in market to book decrease weight of assets in place against growth opportunities and therefore reduces the relative value in case of liquidation. The ratio of depreciation and amortization to total asset (NDTS) as

an explanatory variable to proxy for non-debt tax shields [6]. High depreciation means less benefit of tax shield from using debt. Selling expense to sales (SE) is used to proxy for firms' uniqueness [5]. High uniqueness means that firms have lack of liquidity when they are force to liquidation so low leverage is expected. Another proxy for uniqueness which is used in this study is the ratio of research and development expense to sales (RD). A dummy variable for research and development is used because there are a number of missing observations. This dummy variable is assign as zero when research and development expense is not reported otherwise set to 1.

To estimate the target, the panel data will be used as it includes time effect (λ_t) as well as acts as a control for the heterogeneity of the firms through firm-specific effect (v_i).

To test debt-equity choice hypothesis and target adjustment hypothesis, binary logit estimation is applied by following equation.

$$Y_{i,t} = \alpha + \beta_1(LEV_{i,t-1}\text{-}TARGET_{i,t}) + \beta_2 DTLD_{i,t-1} + \beta_3 ROA_{i,t-1} + \beta_4 CASH_{i,t-1} + \beta_5 MTB_{i,t-1} + \beta_6 RET_{i,t-1} + \varepsilon_{i,t} \quad (2)$$

The binary logit regression which is suitable for debt-equity choice study is used for the examinations. The set of explanatory variables in includes deviation from target (LEV-TARGET). Positive is overleveraged firm and negative is underleveraged firm. This variable will capture whether firms deviate from target adjusting toward target. DTLD [5] is defined as the projected difference between the absolute deviation from target if a firm issues debt, $|LEV_d\text{-TARGET}|$ and the absolute deviation from target if a firm issues the same amount of equity, $|LEV_e\text{-TARGET}|$. A positive value of this variable indicates that firms would end up closer to the target if they issue equity rather than debt. The following example clarifies the motivation for this variable. Consider a firm with leverage ratio of 0.2 and target leverage of 0.21 that needs new financing in the amount of 0.1 of total assets. Currently this firm is underleveraged, one might think that is should issue debt to move toward target. However, issuing equity for this firm makes its leverage ratio became 0.182. If firm chose to issue debt instead, its leverage ratio becomes 0.273. Thus, despite the fact that the firm is underleveraged, it stays closer to target if is issues equity rather than debt. ROA show firms' operating performances [1].This variable is defined as EBITDA to total assets. This variable relates to the availability of internal funds. Firms that have more internal funds tend to use such funds first. Cash or cash equivalent to total asset (CASH) is a control variable [9]. Market to book (MTB) will capture the effect of the market conditions [1]. This variable is also a proxy for growth opportunity (control for market timing). Stock return is also a measure of market performance and can also be interpreted as a proxy for the market timing effect. This variable has a negative relation with debt ratio which provides evidence that firms are more willing to issue equity when firms experience relatively high market valuation. (control for market timing).

RESULTS AND DISCUSSION

The two hypothesis of the role of target leverage ratio are tested as follow.

Table1: Debt-Equity Choice Hypothesis Test

Variable	Thailand Coefficient	Singapore Coefficient	Australia Coefficient
LEV-TARGET	-3.78**	-4.34**	-0.25
DTLD	-574***	-434**	-7.60***
ROA	3.81***	0.59	1.78***
RET	-0.07	1.03***	0.23
MTB	-0.09	- 0.67***	0.18**
CASH	-1.84	- 1.63	- 3.93***
Intercept	1.22***	2.37***	0.21
MacFadden R-squared	0.18	0.21	0.24
Obs Dep=0	121	96	331
Obs Dep=1	501	269	251

1 represent debt issue and zero represent equity issue transaction

*** indicates significance at the 1% level.

** indicates significance at the 5% level

* indicates significance at the 10% level.

Overall, the result the strong evidence of target leverage role in Singapore and Thailand. Both (LEV_B-TARGET) and DTLD are significant and have expected sign which consistent with the debt-equity choice hypothesis. Firms try to get as close as possible to the target when they have to decide for external fund. Australia show weaker evidence of target leverage role that Australia firms do consider which type of transaction can minimize absolute deviation from target.

Table 2: Difference between over and under leveraged firms

Variables	Thailand Coefficient	Singapore Coefficient	Australia Coefficient
LEV-TARGET	-1.59	-6.24	0.71
DTLD	-6.63**	-2.73	-7.15***
ROA	4.98***	3.21*	2.49***
RET	-0.17	0.61	0.09
MTB	-0.001	-0.62***	0.21*
CASH	-2.51	-3.36**	-4.91***
Intercept	1.09**	2.22***	0.33
Dum	0.66	0.80	0.09
Dum*LEV-TARGET	-4.05	3.32	-2.37
Dum*DTLD	-0.75	-3.8	-1.61
Dum*ROA	-2.91	-4.66**	-2.1**
Dum*RET	0.11	1.07*	0.43
Dum*MTB	-0.12	-0.71	-0.09
Dum*CASH	2.91	5.32*	3.09
Log Likelihood	-249.18	-162.39	-297.59
Obs Dep=0	121	96	331
Obs Dep=1	501	269	251

1 represent debt issue transaction and zero represent equity issue transaction. Dum is dummy variable where set to 1 if firms are overleveraged (LEV-TARGET) greater than zero or set to 0 if firms are underleveraged (LEV-TARGET) less than zero.
*** indicates significance at the 1% level.
** indicates significance at the 5% level
* indicates significance at the 10% level.

One of question in this study is that do overleveraged firms give more concern on target leverage. This study uses dummy variable where assign 1 for overleveraged firm and 0 for underleveraged firms. The results in Table 2 show that the role of target leverage is indifference between over and under leveraged firms in all country samples. Dum*(LEV - TARGET) and Dum*DTLD are not significant in all samples. These result rejected the hypothesis that overleveraged firms will give more important on target leveraged than underleveraged because they have more possibility of bankruptcy. The results imply that firms do consider tax benefit and cost of bankruptcy at the same important level.

Table 3: Target Adjustment Hypothesis Test
Debt Issue Transaction

Variable	Thailand Coefficient	Singapore Coefficient	Australia Coefficient
LEV-TARGET	-3.32***	-5.45***	-4.16***
ROA	0.09	1.36	-0.24
RET	0.23*	0.37**	0.46**
MTB	0.27**	0.001	0.20**
CASH	-6.67***	-4.66***	-4.13***
Intercept	0.41**	-0.28*	-0.14
Log Likelihood	-491.17	-476.66	-338.12
Obs Dep=0	290	552	276
Obs Dep=1	501	260	251

1 represent debt issue and zero represent no transaction.
*** indicates significance at the 1% level.
** indicates significance at the 5% level
* indicates significance at the 10% level.

The results from Table 3 of debt issue transaction support the target adjustment hypothesis that underleveraged firms tend to issue debt to move toward target leverage ratio. The significant of LEV-TARGET which negative sign confirm the hypothesis that firms when deviate from target do adjust their leverage ratio overtime.

Table 4: Target Adjustment Hypothesis
Equity Issue Transaction

Variable	Thailand Coefficient	Singapore Coefficient	Australia Coefficient
LEV-TARGET	5.09***	4.98***	3.35***
ROA	-1.71	-2.15**	-1.88
RET	0.23	-0.64**	0.08
MTB	0.44***	0.45***	0.15**
CASH	-4.44**	-1.1	-0.16
Intercept	-1.05***	-2.22***	-0.06
Log Likelihood	-221.39	-241.32	-381.76
Obs Dep=0	290	552	276
Obs Dep=1	121	96	331

1 represent equity issue and zero represent no transaction.
*** indicates significance at the 1% level.
** indicates significance at the 5% level
* indicates significance at the 10% level.

The results from Table 4 of equity issue transaction also support the hypothesis. This time, overleveraged firms tend to issue equity to offset the deviation from target leverage ratio and move toward target. LEV-TARGET which positive sign confirm the hypothesis.

Table 5: Target Adjustment Hypothesis
Debt Reduction Transaction

Variable	Thailand Coefficient	Singapore Coefficient	Australia Coefficient
LEV-TARGET	7.37***	7.14***	9.66***
ROA	1.15	-0.59	-0.84***
RET	-0.05	-0.33*	-0.13
MTB	-0.11	0.08	0.06
CASH	-5.13***	-3.15***	-3.14***
Intercept	0.87***	0.52***	-0.05
Log Likelihood	-500.62	-441.71	-304.87
Obs Dep=0	290	552	276
Obs Dep=1	637	245	254

1 represent debt reduction and zero represent no transaction.
*** indicates significance at the 1% level.
** indicates significance at the 5% level
* indicates significance at the 10% level.

Table 5 reports the evidences of debt reduction transaction. Firms when deviate above the target leverage ratio tend to reduce debt and move toward the target.

Overall, the target adjustment hypothesis is strongly supported in Thailand, Singapore and Australia. Though, firms cannot maintain at target leverage all the time, firms do have behavior to adjust their leverage ratio toward target.

CONCLUSION

The role of target leverage play important role when firms decide to make external transaction. Firms consider target as important factor when they decide either debt or equity to issue for raising fund. Though, firms cannot maintain at that target, firms try to stay as close as possible to that target. Second, firms do not adjust their leverage ratio all the time due to high adjustment and transaction cost. However, firms when deviate from target tend to do the type of transaction which can move their leverage ratio toward target leverage ratio.

ACKNOWLEDGMENTS

I would like to give my pleasure to those who have contributed to this paper. Firstly, I would like to thank to Ruttachai Seelajaroen Th.D., my adviser for encouragement and guidance through the achievement of this paper.

In addition, I am thankful to all of my friends in MSF program for helpful advice. I would like to give my gratitude to my mother and my family for their encouragement and inspiration given to me throughout my study.

REFERENCES

1. Hovakimian, A., 2004. The role of target leverage in security issue and repurchase. Journal of Business, 77, 1041-1071
2. Marsh, P., 1982. The choice between equity and debt: An empirical study. Journal of Finance, 37, 121-144
3. Jalivand, A., and R.S. Harris, 1984. Corporate behavior in adjusting to capital structure and dividend targets: An econometric study. Journal of Finance, 39, 127-145.
4. Mackie-Mason, J.K., 1990. Do firms care who provides their financing? In: Asymmetric Information, Corporate Finance and Investment, ed. R.G. Hubbard. Chicago and London: University of Chicago Press.
5. Hovakimian, A., T. Opler and S. Titman, 2001. The debt-equity choice. Journal of Finance and Qualitative Analysis, 36,1-25.
6. Bender, A., P. Gaud and M. Hoesli, 2007. Debt-equity choice in Europe. International Review of Financial Analysis, 16, 201-222.
7. La Porta, R., F. Lopez-de-Silanes and R. Vishny, 1997. Legal determinants of external finance. Journal of Finance, 52, 1131-1150.
8. Rajan, R. and L. Zingales, 1995. What do we know about capital structure? Some evidence from international data. Journal of Finance, 50, 1421-1460.
9. Lie, E., 2002. Do firms undertake self-tender offers to optimize capital structure? Journal of Business, 75, 609-39.

Development of Successful Indicators Derived from Standards of the Distance Education via Satellite Management in Basic Education

Ameacha Pongpanpanu
Doctoral Student, Educational Technology,
Kasetsart University, THAILAND
kheanjan@hotmail.com

Abstract: This research was aimed at developing the successful indicators derived from the standards of the distance education via satellite in basic education. The following indicators, which consisted of input factors, procedures, and results of distance education, were purposely marked for the development of successful indicators derived from standards. In the first phase, the cross sections were the experts from the Distance Learning via Satellite Foundation, Office of the Elementary Education Commission, Bureau of Technology for Teaching and Learning, and the school administrators affiliated to the distance education via satellite management in basic education amounted to 20 persons. In the second phase, the cross sections were 300 administrators and teachers from schools subordinate to the remote education. The conclusion was to be noted that the indicators derived from standards of the distance education via satellite in basic education composed of 41 indicators and performance criteria.

Introduction

From the first move of the distance education via satellite in basic education to present time, the following distance education management was appointed but there were lack of purpose and apparent successful indicators. The indicators implied the status and reflected the appearance of overall operation. Indicators could display the alterations or consequences which were effective in practice and most gainful to the distance education via satellite management. Sixteen standards of distance education via satellite could be categorized as follows;

1st Standard: Properly arranging room for input and output satellite control board to be convenient for activities, to encourage learning, and develop learner's skill.

2nd Standard: Properly Arranging classrooms for distance education via satellite to be convenient for activities, to encourage learning, and develop learner's skill.

3rd Standard: Schools must be administered systematically and effectively in education terms.

4th Standard: Schools must organize plans for distance education via satellite.

5th Standard: Schools must be corporate to all sides to generate distance education via satellite.

6th Standard: To plan the schooling correspondent with teachers' distance education via satellite handbooks in agreement with the schools and locals.

7th Standard: Arranging or improving schooling activities to practically develop thinking process and evaluation for schooling development to be correspondent with learner's quality of life, family and community.

8th Standard: Available for various instructional media for learners.

9th Standard: Arranging or improving schooling via satellite to indoctrinate students with pursuit of knowledge by themselves.

10th Standard: Arranging or improving schoolings for learners to improve skills and potentially reach the fullest aptitude by increasing the strength and fix the weakness of learners individually and in groups.

11th Standard: Arranging schooling due to matters of learning by utilizing distance education via satellite as acquisition of knowledge.

12th Standard: Arranging schooling by implanting morality and ethic which matter to learner's way of life.

13th Standard: Consecutively evaluating learner's quality in every side by equipment and optimal procedures.

14th Standard: Schools must be utilizing distance education via satellite media as equipment to support and develop personnel effectively at a stretch.

15th Standard: Schools must be systematically evaluated in each progress.

16th Standard: Students had abilities to acquire knowledge and were driven to seek for knowledge.

Researcher had considerably realized that the studies of summarizing the following indicators collateral to reach the goal of development was essential and necessary to develop indicators of distance education via satellite to be useful in utilizing

Corresponding Author : Ameacha Pongpanpanu,Doctoral Student, Educational Technology, Kasetsart University, THAILAND, kheanjan@hotmail.com

equipment for the follow up, controlling, sustaining, and operating plans in order to hit the right target. At the same time, the studies indicated the effective evaluation and proper administration led to alteration which benefited national education development in the future.

Materials and Methods

The first phase was proceeded as follows;

1. Researcher gathered all documents in order to be basic information.
2. Researcher analyzed contents from gathering information and create set of ideas about standard element of distance education via satellite.
3. Studied from experts by utilizing Delphi Technique as follows;

Researched opinions of 20 experts by assigning cross sections to consider and give opinions about the element and successful indicators derived from standards of distance education via satellite in basic education. Research instruments were open ended in round 1.

Gathered open-questionnaire opinion and created 5 scale-rating questionnaires and appointed 20 cross sections considering the importance of following indicators. Research instruments were ended in round 2.

Handed in the same questionnaires as in the 2nd round end and returned to cross sections to reconsider answers counted in third round by showing value of median, Interquartile range, and answers of cross sections of 2nd round. Each cross section might alter the answers or insist on former answer as well. The answer could merely be made outside the Interquartile range.

Added in information of indicators which were shown in the correspondent answers of cross sections as the successful indicators from the standards of distance education via satellite in basic education.

4. Researcher aggregated all the studies for dissertation advisory committees to consider and specify elements and indicators of distance education via satellite.

The second phase was proceeded as follows;

Researcher sought for consensus from experts whose opinions were concordant towards each other and no less than 80 percentages. The cross sections were 300 administrators and teachers from educational institutions subordinate to distance education via satellite.

1. Aggregated results from the first phase and sought for consensus of experts.
2. Gathered information about indicators in first round which were shown in the correspondent answers of cross sections as the successful indicators from the standards of distance education via satellite in basic education.
3. Gathered and summarized the studies.

Results

The research indicated that indicators which derived from standards of distance education via satellite in basic education had received 80 percentages of consensuses as follows;

In 1st Standard, properly arranging room for input and output satellite control board to be convenient for activities, to encourage learning, and develop learner's skill. The consensuses of cross sections were correspondent 95 percentages. Indicators were input and output satellite control room, additional apparatus, and sizes which were convenient to create sufficient and proper activities. Performance criteria was input and output satellite control room sufficient to numbers of classes, air-conditioners, recorders, contacting phone lists of affiliated schools and proper size of rooms.

Consensus of cross sections consisted of 90 correspondent percentages. Indicators were service system, usability, and maintenance of media and technology. Performance criteria were utilizing and maintaining media and technology for systematic administration as well as the convenience from the service.

Consensus of cross sections consisted of 85 correspondent percentages. Indicators were technicians in control rooms. The performance criteria were to have1 technician in each control room.

Consensus of cross sections consisted of 80 correspondent percentages. Indicators were to create nice surroundings in the input and output satellite control room. Performance criteria were nice surroundings in the input and output satellite control room, clean, safe, and containing regulations for controlling equipment, input and output satellite control board, schooling schedules of parent schools and destination schools and categorized input and output satellite control equipment.

In 2nd standard, properly arranging classrooms for distance education via satellite to be convenient for activities, to encourage learning, and develop learner's skill. Consensus of cross sections consisted of 95 correspondent percentages. Indicators were broadcasting schedules in each class. Performance criteria were to have every channel broadcasting schedules in every class.

Consensus of cross sections consisted of 90 correspondent percentages. Indicators were distance education via satellite classrooms and additional apparatus which were convenient to create sufficient and proper activities. Performance criteria were at least 2 televisions or projectors in each classroom, phones to contact with parent schools, black boards or white boards, stereos, lighting systems, ventilated air, and proper size of rooms.

Consensus of cross sections consisted of 80 correspondent percentages. Indicators were phones or faxes in each class. Performance criteria were at least 1 phone or fax in each class.

In 3rd Standard, schools must be administered systematically and effectively in education terms. Consensus of cross sections which consisted of 90 percentages correspondent indicators and evaluation of performance criteria were at least 3 responsible working groups consisted of administrator, academic section, and technician. The follow-up, further progress, evaluation, and analysis must be consecutively and entirely advanced.

Consensus of cross sections consisted of 85 correspondent percentages. Indicators were support allowance. Performance criteria were yearly support allowance.

Consensus of cross sections consisted of 80 correspondent percentages. Indicators were schools must organize the plan about the distance education via satellite. Performance criteria were to specify the proper classes for distance education via satellite, manage to have all kinds of facilities, and build up understandings among teachers and learners.

In 4th Standard, schools must organize plans for distance education via satellite. Consensus of cross sections consisted of 90 correspondent percentages. Indicators were schools must organize plans for distance education via satellite. Performance criteria were organizing plans for distance education via satellite correspondent to the target education policy, the potentiality of the academy and the needs of locals. Further, schools must build clear strategies of development which could potentially be fulfilled. Schools must rearrange working procedures reasonably and create good comprehension among teachers and learners as well as to follow the regulations of handbooks and design development of schooling process.

Consensus of cross sections consisted of 85 correspondent percentages. Indicators were reporting the advancement to all parents in communities and other relevant educational institutions. Performance criteria were spreading overall operation in various and interesting forms.

In 5th Standard, schools must be corporate to all sides to generate distance education via satellite. Consensus of cross sections consisted of 90 correspondent percentages. Indicators were direct coordinators of the remote education via satellite. Performance criteria were at least 1 direct coordinator of the remote education via satellite.

Consensus of cross sections consisted of 85 correspondent percentages. Indicators were to create local school networks of which utilized distance education via satellite systems. Performance criteria were to create local school networks of which utilized distance education via satellite systems and other relevant schools, such as, Rachaprachanusongkror School and Suksasongkror School.

Consensus of cross sections consisted of 80 correspondent percentages. Indicators were prescribing visions and targets about educational management. Performance criteria were schools, parents, and relevant institutes must prescribe visions and targets onto apparent distance educational management together.

In 6th Standard, to plan the schooling correspondent with teachers 'distance education via satellite handbooks in agreement with the schools and locals. Consensus of cross sections consisted of 95 correspondent percentages. Indicators were teachers who comprehended in psychology theory and growth of learners which could be individually used in student's development.

Consensus of cross sections consisted of 85 correspondent percentages. Indicators were teachers who must organize the schooling conformed to distance education handbooks. Performance criteria were to rectify schooling methods conformed to distance education handbooks in every academic year.

Consensus of cross sections consisted of 80 correspondent percentages. Indicators were teachers who were well-trained in organizing schoolings. Performance criteria were teachers who were trained in organizing schoolings at least once per year.

In 7th Standard, arranging or improving schooling activities to practically develop thinking process and evaluation for schooling development to be correspondent with learner's quality of life, family and community. Consensus of cross sections consisted of 90 correspondent percentages. Indicators were to arrange schoolings which allowed students to analyze and take action by working in groups and various sources of knowledge. Performance criteria were to arrange schoolings which allowed students to analyze and take action and supporting work-in-group methods and various sources of knowledge which covered the whole institutes.

Consensus of cross sections consisted of 85 correspondent percentages. Indicators were teaching conferences or seminars. Performance criteria were at least once per year conference or seminar to sum up trouble condition of the process and rectify seminar's results every academic year.

In 8th Standard, schools must be available for various instructional media for learners. Consensus of cross sections consisted of 90 correspondent percentages. Indicators were schools must have proper instructional media which supported to acquisition of knowledge. Performance criteria were suitable natural, indigenous, and technology media which were supportive to acquisition of knowledge, able to interchange or be connected with source of knowledge.

Consensus of cross sections consisted of 85 correspondent percentages. Indicators were evaluation

of media usage. Performance criteria were to evaluate media at least once per year in various methods.

Consensus of cross sections consisted of 80 correspondent percentages. Indicators were service and maintenance system of media and technology. Performance criteria were to plan usage and maintenance of media and technology to reach systematic management. Every relevant authority must be satisfied in the service.

In 9th Standard, arranging or improving schooling via satellite to indoctrinate students with pursuit of knowledge by themselves. Consensus of cross sections consisted of 85 correspondent percentages. Indicators were to arrange or improve schooling via satellite to indoctrinate students with pursuit of knowledge by themselves. Performance criteria were schools must record schooling activity lists from parent schools, construct electronic libraries to store media which contained uncomplicated knowledge retrieving center, and organize activities mainly for learners. Teachers must be assured that every student had watched televisions or projectors and acted on learning procedures, audition learners, and provide facilities to students so that they could enjoy their learning.

Consensus of cross sections consisted of 80 correspondent percentages. Indicators were schools must be composed of televisions as a media of distance education via satellite in various places. Performance criteria were schools must be composed of at least 1 television as a media of distance education via satellite in various places, such as, conference room or multi-functional building.

In 10th Standard, arranging or improving schoolings for learners to improve skills and potentially reach the fullest aptitude by increasing the strength and fix the weakness of learners individually and in groups. Consensus of cross sections consisted of 90 correspondent percentages. Indicators were to arrange systems and activities to aid students individually. Performance criteria were to familiarize each student and organize systematically and consecutively supportive activities.

Consensus of cross sections consisted of 85 correspondent percentages. Indicators were designing educational system according to institute's ability. Performance criteria were to design educational system according to institute's ability at least 1 grade.

In 11th Standard, schools must arrange schooling due to matters of learning by utilizing distance education via satellite as acquisition of knowledge. Consensus of cross sections consisted of 85 correspondent percentages. Indicators were schoolings according to acquisition of knowledge. Performance criteria were schools must arrange schooling due to matters of learning by utilizing distance education via satellite as acquisition of knowledge in every grade.

Consensus of cross sections consisted of 80 correspondent percentages. Indicators were to convert schools into local learning centers. Performance criteria were to establish at least 1 system of local learning center.

In 12th Standard, schools must arrange schooling by implanting morality and ethic which matter to learner's way of life. Consensus of cross sections consisted of 90 correspondent percentages. Indicators were to organize activities in supporting desirable attribute of learners. Performance criteria were setting policy to support ethic, morality, and desirable value of institute which were connected to visions. At the same time, schools must organize interesting activities which had clear evaluation purpose and allowed learners to participate willingly. In addition, the group activity process must be achieved.

Consensus of cross sections consisted of 85 correspondent percentages. Indicators were learners must have disciplines due to local virtuous culture. Performance criteria were 80 percentages of students must be punctual, responsible for given assignment, interested in schooling activities, polite, and paying homage to local custom.

Consensus of cross sections consisted of 80 correspondent percentages. Indicators were to organize practical activities in various opportunities. Performance criteria were every learner must be practiced for practical activities in various opportunities.

In13th Standard, consecutively evaluating learner's quality in every side by equipment and optimal procedures. Consensus of cross sections consisted of 90 correspondent percentages. Indicators were premium and various kinds of evaluation equipment. Performance criteria were every relevant authority must have evaluation equipment correspondent to anticipating consequence by utilizing assorted evaluation methods, emphasizing analysis and synthesis questions, evaluating, and measuring learner's behavior in suitable proportion at least once a year.

Consensus of cross sections consisted of 85 correspondent percentages. Indicators were to arrange school-record decision for upgrading learner's ability. Performance criteria were to identify the source of school-record decision yearly or in every semester. Every acquisition of knowledge section must be leveled up to challenge learner's ability as well as the upgrading courses for advanced ability test of learners.

Consensus of cross sections consisted of 80 correspondent percentages. Indicators were to utilize school-records as a method in developing student's potentiality, schooling, and institute. Performance criteria were to report advancement of learners individually and in every degree. Likewise, the enhancement must be based on learner's school-record before viewing overall school-record.

In 14th Standard, schools must be utilizing distance education via satellite media as equipment to support and develop personnel effectively at a stretch. Consensus of cross sections consisted of 85 correspondent percentages. Indicators were teachers who utilized distance education via satellite media as equipment to support and develop themselves. Performance criteria were teachers who utilized distance education via satellite media as equipment to support and develop themselves effectively at a stretch.

Consensus of cross sections consisted of 80 correspondent percentages. Indicators were teachers who were from remote education system. Performance criteria were to set up principal policy of schools which consisted of teacher's schooling arrangement by distance education via satellite.

In 15th Standard, schools must be systematically evaluated in each progress. Consensus of cross sections consisted of 90 correspondent percentages. Indicators were the follow-up and systematic evaluation. Performance criteria were to proceed systematically plans in every activity.

Consensus of cross sections consisted of 85 correspondent percentages. Indicators were the follow-up plan, inspecting, evaluating, developing, evaluation system according to regulations of testing and evaluating which consisted of responsible and ready-to-act authority.

In 16th Standard, students had abilities to acquire knowledge and were driven to seek for knowledge. Consensus of cross sections consisted of 85 correspondent percentages. Indicators were students who could creatively apply knowledge and technology to their real lives. Performance criteria were more than 80 percentages of students who could utilize knowledge and experience together with new information from researching of distance education via satellite media and applying to develop them, others, and would remain incessantly.

Consensus of cross sections consisted of 80 correspondent percentages. Indicators were students who sought for knowledge from different sources. Performance criteria were 80 percentages of students, who sought for knowledge, longed for self-development, knew their strength and weakness, and developed themselves creatively and concretely.

Discussion

Quality development of distance education via satellite had given precedence to instructional technology media. Office of the Elementary Education Commission had set a policy for institutional media usage as follows; providing technology to educational institutes, supporting the usage of effective technology, developing personnel in comprehension of technology utilization, arranging technology system for management terms, cooperating with state and private agency on technology matters, and following up the quality of effective technology usage in educational institution which were correspondent to effective technology utilization of schools in the United States of America.

Results of synthesis research from 176 issues in total revealed that since 1995 to 1996 proper technology utilization for acquisition of knowledge positively affected to the achievement of student's learning from primary school level to higher education. In addition, technology usage positively culminated to learner's attitude and learners were the major key terms in the following schooling.

At the same time, Office of the National Education Commission had proposed a principle of desirable attribute, quality, and standard which were a must in educational institute including the follow-up, inspection, evaluation, and quality assurance of education.

1st Standard: Desirable attribute of Thais in both citizen and humankind terms. (Thais are intelligent, good-hearted, and happy)

Indicators: Physical and mental elements as follows;

- Thais had good physical and mental health as well as physical, mental, and intellectual development in complete form ageing period development.

Indicators: Knowledge, sufficient and necessary skills applying in real life, and social development as follows;

- Thais reached the fullest of learning potentiality.
- Thais were employed, applied knowledge to their careers, and made benefits to society.

Indicators: Acquisition of knowledge skill and adaptation as follows;

- Thais were able to learn by themselves, sought for knowledge, were cognizant to the world, and had abilities in applying knowledge and media to develop themselves and society.
- Thais were well-adjusted, friendly, and able to participate with others.

Indicators: Social skills as follows;

- Thais understood and paid respect to nature, surroundings, and society. They had abilities and skills which were essential to live a happy life.
- Thais had responsibilities, understandings, acceptances, and realized in value of different culture. They had abilities to solve problems as members of Thai and world society in peaceful means.

Indicators: Moral, public mind, and consciousness of Thai citizens and humankinds as follows;

- Thais had good conduct in action, verbal good conduct, and mental good conduct.
- Thais had moral and social responsibilities. They had consciousness in prestige of Thailand. They loved and lived up to democracy and volunteered to help communities and social as Thai and world citizens.

Acknowledgements

The author wish to thank, the following graduate research was funded by the Gruduate School of Kasetsart University.

References

1. Department of Non-Formal Education. 2541. Summary of evaluation and inspection of distance education via satellite project. Academic journal. Department of Vocational Education. 2542. The national education act 1999 BC. Bangkok: Prikwan Graffic Company Limited.
2. Distance Learning Via Satellite, Foundation. 2006. Distance education via satellite administration for educational institute. Bangkok: Amarin Printing and Publishing Company Limited. Khwankaew Watcharothai. 2003. Distance education via satellite: Forever learning with technology. Bangkok: Amarin Printing and Publishing Company Limited.
3. Boonreang Kajornsin. 2000. Educational research means. Bangkok: P.N. Publishing Limited Partnership.
4. Distance Learning Via Satellite, Foundation. 2006. Distance education via satellite administration. Bangkok: Amarin Printing and Publishing Company Limited.
5. Office of the National Education Commission. 1999. The national education act 1999 BC. Bangkok: Prikwan Graffic Company Limited. Secretariat of the Teacher Council of Thailand Ministry of Education. 2004. Concise of Teachers and Educational Personnel Council Act, 2003. Bangkok: Press of The Teachers' Council of Thailand.

Simulation of Landform Evolution by Seepage Erosion

Adichai Pornprommin[1,2] and Norihiro Izumi[2]
[1]Department of Water Resources Engineering, Kasetsart University
50 Phaholyothin Rd., Jatujak, Bangkok 10900, Thailand
[2]Department of Civil Engineering, Hokkaido University
Nishi 8, Kita 13, Kita-ku, Sapporo, Hokkaido 060-8628, Japan

Abstract: Gully erosion is one of the fruitful studies in geomorphology. It causes severe soil erosion and induces landform evolution. Overland flow and seepage have been hypothesized as the dominant factors of gully erosion. In this study, the numerical model is performed using the finite difference method with the center scheme. The Dupuit-Forchheimer equation is employed to calculate groundwater flow, and only seepage flow is considered for the propagation of gully front. As the first step, the retreat speed of the front is assumed to be an exponential function of groundwater unit discharge. In order to increase the accuracy of the computation of groundwater flow at the front, the 8 direction vectors (N, NE, E, SE, S, SW, W and NW) are introduced to detect the front location. If we impose a random function to the hydraulic conductivity, gullies are easily initiated and migrate upstream very fast. However, if the threshold groundwater discharge for seepage erosion is introduced, gullies migrate slower and their widths are narrower. Channel bifurcation is found in every case. However, the results depend on the model grid scale and the random function. We introduce the concept that the retreat speed also depends on the front curvature and this will be done in the future.

Key words: Seepage erosion, front propagation, finite difference method

INTRODUCTION

A gully is an incised, steep-sided channel, with an eroding headcut and slumping sidewalls[1,2]. By widening, deepening and head cutting, gullies cause severe soil erosion. Gully erosion affects agricultural productivity, restricts land use and can threaten roads, fences and buildings. Soil eroded from the gullied area induces a high rate of sediment runoff and causes rapid siltation and bed aggradation downstream. Furthermore, suspended sediments from the erosion, which may have attached nutrients and pesticides, can adversely affect water quality. They may clog groundwater aquifers, pollute water courses and affect aquatic life. Small rills or channels that appear at the initial stage of channelization can develop into large gullies by the concentration of flow, and it can be difficult and costly to control the erosion[3].

Erosions by overland flow and seepage have been hypothesized as the dominant factors in the initiation and evolution of gullies and channels in both sediment and rock. Many studies on channelization due to erosion by overland flow have been carried out, whereas fewer studies have focused on channelization due to seepage erosion[4,5,6]. Many landforms exhibit distinct boundaries between dissimilar terrain and can be well characterized by planimetric outlines[7]. In this study, the simulation of landform evolution (the development of gullies or channels) by seepage erosion was developed. The model is composed of the groundwater flow model and the seepage front propagation model. Thus, the characteristics of gully formation can be investigated by the evolution of the planimetric outline of the seepage front.

GROUNDWATER MODEL

Let us consider groundwater flow in an unconfined aquifer with a free water surface above an inclined impermeable layer as shown in Figure 1. If the gradients of the piezometric surface are assumed to be sufficiently small, the pressure distribution can be approximated to be hydrostatic, and the movement of groundwater flow can be described by the following Dupuit-Forchheimer equation:

$$\frac{1}{\phi}\frac{\partial h}{\partial t}-\frac{\partial}{\partial x}\left[Kh\left(\frac{\partial h}{\partial x}-S\right)\right]-\frac{\partial}{\partial y}\left(Kh\frac{\partial h}{\partial y}\right)=R \qquad (1)$$

where t is time, x and y are the streamwise and lateral directions respectively, h is water depth, K is the hydraulic conductivity, ϕ is porosity, S is the slope of the impermeable layer, and R is the recharge (positive) or withdrawal (negative) rate (volume of water per unit time per unit surface area).

In Figure 1, groundwater with a constant water depth at the upstream end flows through the media and emerges at the downstream end, whereas the left and

Corresponding Author: Adichai Pornprommin, Department of Water Resources Engineering, Faculty of Engineering, Kasetsart University, 50 Phaholyothin Rd., Jatujak, Bangkok 10900, Thailand

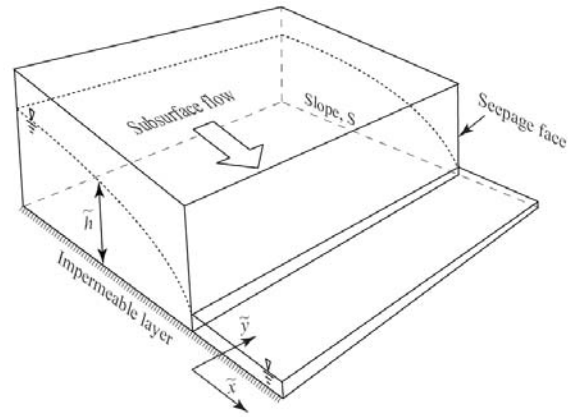

Fig. 1: Seepage face and groundwater flow.

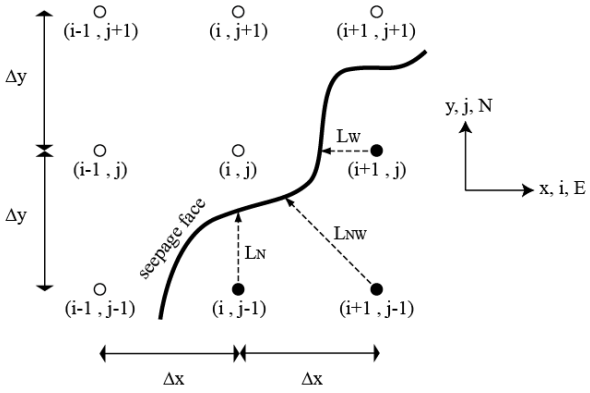

Fig. 2: Grid layout for the numerical simulation.

right banks are assumed to be walls. Thus, at the downstream end where the seepage front is located, seepage erosion can occur and induce the development of gullies. If the groundwater depth is zero, the groundwater velocity, however, becomes infinity in the Dupuit approximation in which it will violate our model. As a result, a constant non-zero value of water depth is necessary to be assumed at the seepage front in our model.

With the use of the finite difference method, we discretized (1), and, in order to increase the accuracy of the calculation near the seepage front, each node possesses 8 vectors pointing to the 8 directions (N, NE, E, SE, S, SW, W and NW) as shown in Figure 2. If the seepage front is detected to be between the computing node (i, j) and the surrounding nodes (i±1, j±1), the vectors are used to express the location of the front. We employed the fully implicit discretization with the central scheme as described by Patankar[8]. As a result, the discretization equation of the groundwater flow equation (1) is

$$a_P h_P = a_E h_E + a_W h_W + a_N h_N + a_S h_S + a_P^0 h_P^0 + b_P \qquad (2)$$

where the subscripts P, E, W, N, S are the computing point, the points in the East, West, North and South of the computing point respectively, the superscript 0 denotes the present time, and a_P, a_E, a_W, a_N, a_S, a_P^0, b_P are the coefficients, such that

$$a_P = a_P^0 + a_E + a_W + a_N + a_S \qquad (3a)$$

$$a_P^0 = \frac{1}{\phi_P \Delta t} \qquad (3b)$$

$$(a_E, a_W) = \left(\frac{T_E}{\Delta x_P \Delta x_E}, \frac{T_W}{\Delta x_P \Delta x_W} \right) \qquad (3c,d)$$

$$(a_N, a_S) = \left(\frac{T_N}{\Delta y_P \Delta y_N}, \frac{T_S}{\Delta y_P \Delta y_S} \right) \qquad (3e,f)$$

$$b_P = R_P - \frac{T_E S}{\Delta x_P \Delta x_E} + \frac{T_W S}{\Delta x_P \Delta x_W} \qquad (3g)$$

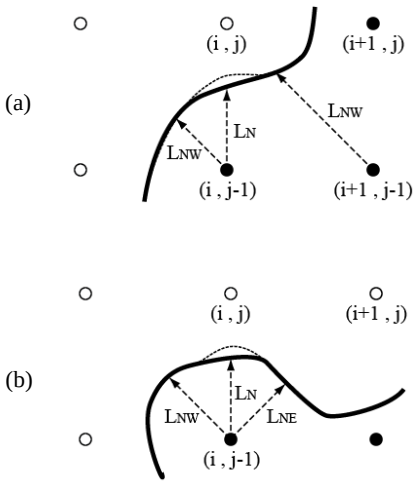

Fig. 3: Concept to compute the front curvature.

where T denotes the multiplication between the hydraulic conductivity K and the water depth h.

FRONT PROPAGATION MODEL

As the first step of our study, we assume that the retreat speed of the front (seepage face) can be expressed by an exponential function of a unit discharge as follows:

$$\frac{\partial L_n}{\partial t} = \alpha (q_n - q_{th})^{\gamma} \qquad (4)$$

where the subscript n denotes the vector direction (N, NE, E, SE, S, SW, W or NW), L is the length of the vector n, q_n and q_{th} are a unit discharge in the n direction and the threshold unit discharge for seepage erosion respectively, and α and γ are the coefficients. If a vector of any 8 directions reaches an adjacent point, that point will be considered as a point at the downstream of the seepage front in the next time step.

According to *Howard*[7], the retreat speed of the front due to backwasting can be enhanced by the front convexity. In this study, we show the possibility to extend our model to compute the convexity of the seepage front in Figure 3. In order to compute the curvature, three points on the seepage front are needed. Figure 3 shows two cases to find three points on the front to compute the front curvature at the north direction of the point (i, j-1). In the case of Figure 3a, the 1st and the 2nd points are provided by the vectors L_{NW} and L_N of the point (i, j-1), respectively. However, the 3rd point has to use the vector NW of the point (i+1, j-1) because the point (i+1, j) is found to be at the downstream of the seepage front in Figure 3a. If the point (i+1, j) is at the upstream of the seepage front as shown in Figure 3b, the 3rd point will be provided by the vector NE of the point (i, j-1). With this concept, the model can calculate the curvature of the planimetric outline of the seepage front and consider the front curvature as a factor in the front propagation.

RESULTS AND DISCUSSION

In this study, we simulated 3 cases in order to investigate the characteristics of gully formation as shown in Table 1. The simulation no. 1 and no. 2 are given the same conditions except that we imposed a random function to the normal hydraulic conductivity in the simulation no. 2 as follows:

$$K_a = K_n \exp(CM) \tag{5}$$

where K_a and K_n are the actual and the normal hydraulic conductivity, C is a scaling factor and M is a random normal deviate (zero mean and unity standard deviation).

The simulation no. 2 and no. 3 are given the same conditions except that we add the threshold discharge for seepage erosion (q_{th}) of 0.0024 m^2/s in the simulation no. 3. Thus, the effect of the threshold discharge can be studied by comparing the results of the simulation no. 2 and no. 3.

Figure 4 shows the comparison of the streamwise water depth between the simulation no.1 and the theory at the beginning period where the erosion still does not occur. In theory, the relation between the streamwise distance x and the water depth h is

$$\frac{h_0^2 - h^2}{h_0^2 - h_L^2} = \frac{x}{L} \tag{6}$$

where h_0 and h_L are the water depth at the upstream end and the downstream end, respectively. Thus, water depth decreases in the streamwise direction in the parabolic form. It is found that the model can simulate the groundwater depth accurately.

Figure 5 shows the results of gully formation in the simulation no. 1 at 5 different times (0 s, 100000 s, 200000 s, 300000 s and 400000 s). Since all variables are laterally uniform, the propagation of seepage front becomes laterally uniform. However, when t = 300000 s, the disturbance of seepage front can be seen at the left and right banks, and then the front become more irregular as time progresses to 400000 s. It implies that if the disturbance is imposed, it will grow in time and finally become gullies.

Table 1: Conditions for the simulation.

Simulation no.	1	2	3
Porosity, ϕ	0.3		
Bed slope, S	0		
Recharge rate, R	0		
Hydraulic conductivity, K	0.3 m/s (constant)	0.3 m/s (random)	
Length x Width	50 m x 50 m		
Upsteam water depth, h_{max}	1 m		
Downstream water depth, h_{min}	0.01 m		
Threshold discharge, q_{th}	0		0.0024 m^2/s
α	0.01		
γ	1		
Δt, Δx, Δy	0.1 s, 1 m, 1 m		

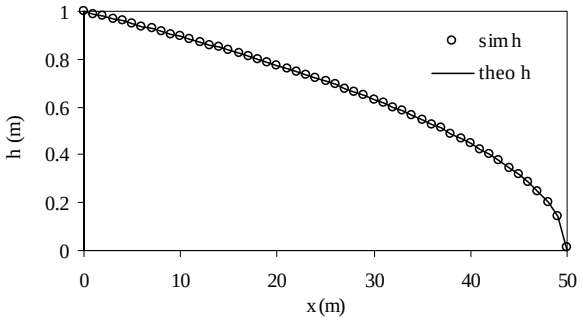

Fig. 4: Comparison of water depth along the streamwise direction between the simulation no. 1 and the theory.

In the simulation no. 2, the random function in (5) is imposed on the hydraulic conductivity K, and the time evolution of gully formation is shown in Figure 6. While the results from the simulation no. 1 in Figure 5 show the laterally uniform retreat of seepage front, the result from the simulation no. 2 in Figure 6 show that gullies can be developed from the beginning. As the heads of gullies can gather more water than other portions, their retreat speeds (headcutting) are faster. Many channel bifurcations are seen in 3 large gullies. The largest gully is located at the center, which may be due to that at the center more flow can be concentrated. Water piracy is also found, in which larger gullies receive more water, grow faster and cause adjacent, smaller gullies stop their development because of receiving less groundwater. At t = 400000 s, the largest gully at the center in Figure 6 almost reaches the

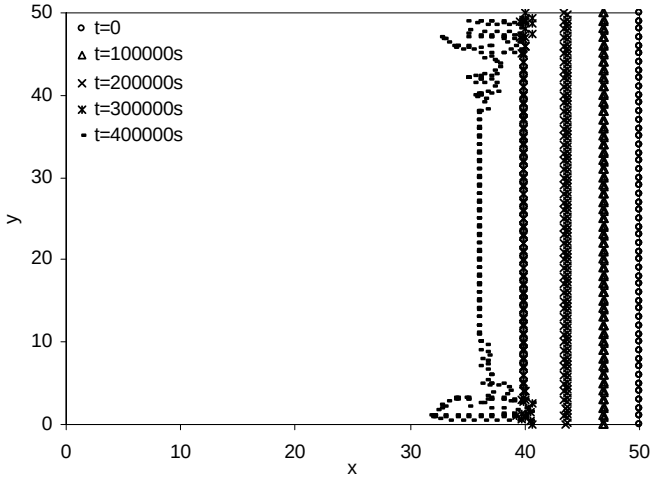

Fig. 5: Gully formation of the simulation no. 1.

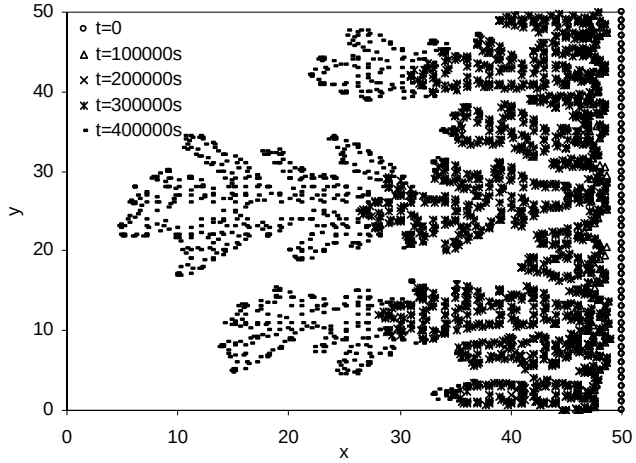

Fig. 6: Gully formation of the simulation no. 2.

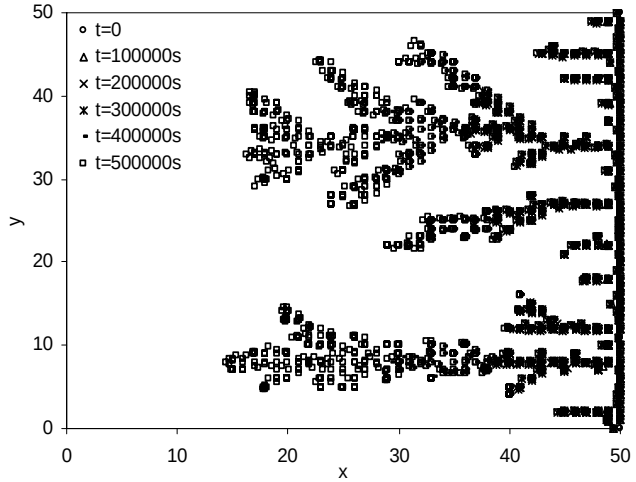

Fig. 7: Gully formation of the simulation no. 3.

upstream end, whereas, the seepage front in Figure 5 can just migrate to somewhere around one third of the total length. Thus, it implies that the imposed random function in the hydraulic conductivity induces the initiation and development of gullies.

Figure 7 shows the evolution of gully formation for the simulation no. 3. In this simulation, the threshold discharge for seepage erosion q_{th} is set to be 0.0024 m^2/s, which is about 80% of the normal unit discharge at the beginning. The hydraulic conductivity is as same as that in the simulation no. 2. The remarkably difference of gully formation between the simulation no. 2 in Figure 6 and the simulation no. 3 in Figure 7 can be seen. The width of gullies in Figure 6 is much larger than that in Figure 7. The threshold discharge also causes the gully development to be retarded. However, since the heads of gullies can receive more groundwater than other portions, this is the reason that the heads can be eroded further upstream, whereas other portions stop their development. Thus, gullies in this case possess narrow widths.

According to *Howard*[4],[7], although the channel spacing can be initiated by imposing a random function in the hydraulic conductivity, the characteristics of gully formation is found to depend on the inputs of the model grid scale and the characteristics of the imposed random function. Thus, the results cannot provide the self-organized characteristics of gully formation. Due to this shortcoming, we hypothesize that using water discharge alone to compute seepage erosion may be not sufficient. It is possible that if the effect of front curvature is included, the self-organized gully formation can be developed. Figure 8 shows our concept of the retreat speed affected by the groundwater discharge and the front curvature. In Figure 8a, if the disturbance with small wavenumber *k* is imposed on the seepage front, the effect of the front curvature is not strong and, thus, the heads of gullies migrate faster than other portions. However, in Figure 8b, if the disturbance with large wavenumber *k* is imposed on the seepage front, the effect of the front curvature become stronger and the retreat speeds of heads of gullies can be retarded due to the concave shape of the front and, thus, the heads may migrate slower than other portions. As a result, the seepage front becomes laterally uniform and is stable from the inception of gullies if a small disturbance possesses sufficiently small wavenumber *k*. This concept will be done in the future study.

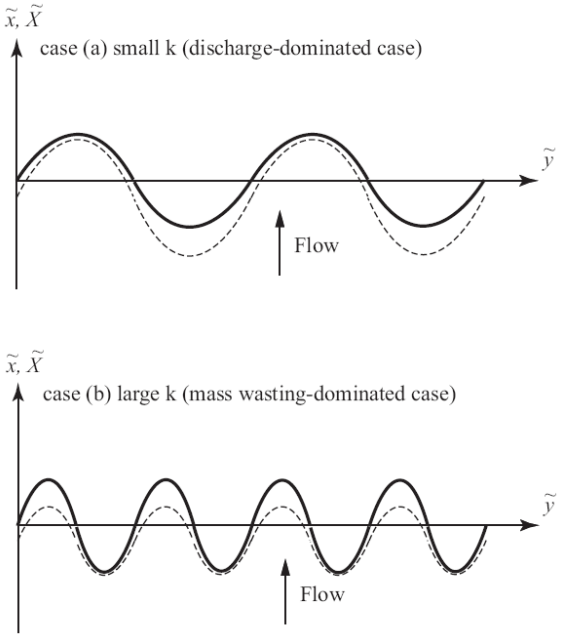

Fig. 8: Concept of the retreat speed affected by the groundwater discharge and the front curvature.

CONCLUSION

The numerical simulation of landform evolution by seepage front propagation was performed. The front propagation is assumed to be an exponential function of groundwater unit discharge. We found that, with the use of a random function imposing to the hydraulic conductivity, gullies can be initiated. However, they are found to depend on the model grid scale and the imposed random function. The development of gullies becomes slower and the width of gullies is narrower if the threshold discharge for seepage erosion is introduced. The concept to compute the front curvature is introduced and we hypothesize that it can improve the results especially when the self-organized channel spacing is needed to be investigated.

ACKNOWLEDGEMENT

This work was supported by the Japan Society for the Promotion of Science Postdoctoral Fellowship Program (grant-in-aid P 07116). We thank Prof. Dr. Yasuyuki Shimizu for valuable suggestions.

REFERENCES

1. Bradford, J. M. and R. F. Piest, 1980. Erosional development of valley-bottom gullies in the upper midwestern United States, in Thresholds in Geomorphology, edited by D. R. Coates and J. D. Vitek, Allen and Unwin, St. Leonards, NSW, Australia: 75-101.
2. Schumm, S. A., M. D. Harvey and C. C. Watson, 1984. Incised Channels: Morphology, Dynamics and Control, Water Resour. Publ., 200 pp.
3. Carey, B., 2006. Gully erosion, in Fact Sheets: Land Series, the Department of Natural Resources and Water, the Queensland Government, Australia.
4. Howard, A. D., 1988. Groundwater Sapping Experiments and Modeling, in Sapping Features of the Colorado Plateau: A Comparative Planetary Geology Field Guide, edited by A. D. Howard, R. C. Kochel, and H. Holt, NASA Spec. Publ., SP-491: 71-83.
5. Kochel, R. C. and J. F. Piper, 1986. Morphology of large valleys on Hawaii: Evidence for groundwater sapping and comparisons with Martian valleys, J. Geophys. Res., Proc. Lunar Planet Sci. Conf. 17th Part 1, Vol. 91, suppl.: E175-E192.
6. Gomez, B. and V. T. Mullen, 1992. An experimental study of sapped drainage network development, Earth Surf. Processes Landforms, Vol. 17: 465-476.
7. Howard, A. D., 1995. Simulation modeling and statistical classification of escarpment planforms, Geomorphology, 12: 187-214.
8. Patankar, S. V., 1980. Numerical heat transfer and fluid flow, Series in computational methods in mechanics and thermal sciences, Hemisphere publishing corporation, pp. 197.

A Neural Network Model for Prediction Puddling Index

[1]Bandit Suksawat
[1]Department of Teacher Training in Mechanical Engineering
Faculty of Technical Education
King Mongkut's University of Technology North Bangkok (KMUTNB), Bangkok, Thailand

Abstract: Rice is one of the most important cereal and economic crops in Thailand. Paddy is usually grown under wet land conditions. Transplanting of paddy needs a well prepared soft soil bed, which can be obtained through puddling. The quality of puddling is determined by the value of the puddling index (*PI*), ratio of initial to final volume of settled sediments. For determining the *PI* value, soil water suspension samples are taken from the puddled soft top soil. However, the soft soil samples sedimentation is a time consuming process which requires 48 h to obtain the settled sediments. Therefore, this project aims to develop and apply an artificial neural network for prediction of *PI* value. The back propagation model of the feed-forward multi-layer neural network is selected for development of a prediction program made by visual basic programming. The developed program is performed to predict tilled soil with rotary tiller for puddling soil preparation. The input parameters of four hidden layers neural network consist of cone index, depth of tillage, soil hardness, rotary speed, traveling slip and tractor speed. Thirty samples from rotary tillage paddy soil, composed of sand (44.029%), silt (34.788%), and clay (21.183%) are used for neural network training with optimum parameters consisting of training rate and momentum equals 5 and 0.4, respectively. These data are also used in the prediction of *PI* value. The results revealed that the proposed neural network model performs high precision of prediction more than 94.02 % confidence with mean square error of 0.01.

Keywords: Neural Network, Prediction Modeling, Puddling Index

INTRODUCTION

Rice in Thailand is mostly grown under lowland conditions with 1–3 crops a year depending on the availability of irrigation water and the use of modern, short season varieties. Transplanting of rice seedling in puddled soil is one of the most widely used cultivation practices.

The most common method of land preparation for wetland rice in Thailand and Southeast Asia is puddling. This method primarily helps water saving, by decreasing percolation and preventing leaching losses of plant nutrients. Puddling generally refers to breaking down soil aggregates at near saturation into ultimate soil particles. The degree of puddling also depends on tillage implement and intensity of puddling[1].

Puddling or working soil above saturation moisture during rice cultivation, eliminates most macropores, which transmit water. The remaining macropores are partially filled by dispersed fine particles, resulting in drastic reduction in percolation losses of water. Apart from reducing percolation losses, puddling makes the soil soft for transplanting and controls weeds. The extent of reduction in water losses depends on puddling intensity and puddling depth among other factors[2].

Nowadays, most of farmers in Thailand use mechanized rice cultivation method especially rotary tillage to prepare puddled soil for rice growing. In the past decade, many researchers considered quality of puddle soil by puddling index value assessment[2], [3], [4]. However, the soft soil samples sedimentation is a time consuming process which requires 48 h to obtain the settled sediments. Therefore, the prediction of pudding index is required to reduce time consumption.

The artificial neural network (ANN) has become an alternative approach to model in engineering field. ANN has a flexible mathematical structure which is capable of identifying complex nonlinear relationships between the sets of input and output data. Therefore, the researcher aims to apply a new approach ANN from engineering field for solving the agricultural

Corresponding Author: Bandit Suksawat, King Mongkut's University of Technology North Bangkok, Pibulsongkram Road, Bangsue, Bangkok, 10800, Thailand, E-mail: mail2bandit@gmail.com

problems. In this paper, multi-layer perceptron of back-propagation ANN is proposed as a tool to predict puddling soil index which puddled soil was tilled by rotary tiller for puddling soil preparation in paddy soil, composed of sand (44.029%), silt (34.788%), and clay (21.183%).

PUDDLING SOIL PREPARATION

Puddling Soil Preparation with Rotary Tillage

The puddling soil preparation in paddy field consists of conventional tillage and rotary tillage method. The conventional puddling soil preparation for rice growing in Thailand consists of primary-tillage, secondary-tillage and thirdly-tillage. The primary-tillage uses plough for cutting soil and dead leaves or plants with 20 cm of depth. The secondary-tillage crushes the cold soil from primary-tillage into small size by using puddler. Usually, the secondary-tillage performs two times or more than which depend on soil hardness, soil size and quantity plants in paddy field. The thirdly-tillage uses tine to plane level of top soil surface.

On the other hand, the farmers use the C-type blade rotary tiller which attached to the tractor for puddling soil preparation. Because, this method can integrates the primary-tillage and secondary-tillage into one process. Therefore, the energy consumption and tilling time are reduced. Furthermore, the high efficiency rotary tiller can performs a good quality of puddle soil by eliminate the thirdly-tillage.

Measurement of Puddled Soil

For measuring the degree of puddling, the viscosity of puddle soil has been used as an index[5]. Some other indices used are aggregate size distribution, decrease in percolation rate and specific weight of puddled soil. It must be noted that no single index can be used to describe quality of a puddled bed because of various limiting soil characteristics. In this paper, the quality of puddling is assessed by sediments settlement method[6]. Just after final puddling operation, puddled soil sample is collected to determine the puddling index. The volume of soil sample is noted after allowing it to settle for 48 h. Puddling index was then calculated by using the following formula:

$$PI(\%) = \frac{V_s}{V_t} \times 100 \qquad (1)$$

where, PI is puddling index, V_s is volume of soil after settlement (cm^3) and V_t is total volume of soil before settlement (cm^3).

ARTIFICIAL NEURAL NETWORKS

ANN is used because it could accommodate non-linear mapping with limited discontinuous points between input and output data without any hypothesis. Two types of networks, the feed-forward multi-layer perceptron (MLP) network and the counter propagation network (CPN) network, are usually used for prediction modeling problems. MLP is selected for application in this paper. MLP is consisted of a number of computational elements described as neurons. The neurons are organized in three layers consisting of input layer that receive information from the outside world, hidden layer of computation neurons and output layer of computation neurons[7].

The input layer and output layer was connected by a hidden layer. The number of nodes of the hidden layer determines the complexity of the model. Two neighboring layers are connected with links and each node in one layer is linked with all nodes of the next layer. All links between input layers and hidden layers composes the input weight matrix and all links between hidden layers and output layers composed the output weight matrix. Weight (w) which controls the propagation value (x) and the output value (O) from each node is modified using the value from the preceding layer according to Eq. (2).

$$O = f(-T + \Sigma w_n x_n) \qquad (2)$$

Where, T is a specific threshold (bias) value for each node. f is a non-linear sigmoid function, which increased monotonically.

The activity at a neuron is computed as the weighted sum of the outputs of the neurons of the previous layer. The output of the neuron is computed from a nonlinear activation function. The most commonly used in this type of network is the sigmoid function. This activation function is continuously differentiable, symmetric and bounded between 0 and 1. The mathematical expression of the sigmoid function is given by Eq. (3).

$$f(n) = \frac{1}{1 + e^{-n}} \qquad (3)$$

All input to a neuron in a particular layer is from the proceeding layer and these unidirectional strengths are known as weights. A gradient descent

procedure known as generalized error-back propagation or back-propagation is usually employed for training the MLP network. Thus MLP network is known as a back-propagation network (BPN).

BPNs are trained with a back-propagation technique which adjusted the weight and bias values along a negative gradient descent directed in an attempt to minimize the mean squared error (MSE) between the input and output vectors of the training set. The model is trained by adjusting model structure and coefficients according to different rules or algorithms. One presentation of the training data with the associated weight and bias adjustment is called an epoch. The MSE between the network outputs (predicted values) and the targeted values (measured values) is calculated through each epoch. Training is stopped when the MSE could not be reduced further[8].

In this study, a model of back-propagation ANN was developed to predict puddling soil index based on the schematic diagram in Fig. 1.

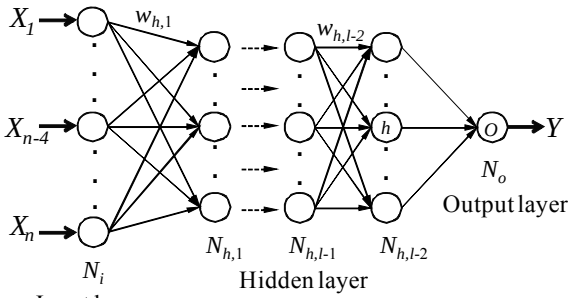

Fig. 1: A multi-layer net work with *l* layers of units

METHODOLOGY

Neural Network Prediction Program Development

The prediction program is made by visual basic programming as shown a program window in Fig.2. The main input of program consist of training iteration, hidden layer, number of sample, input node, output node, training rate, momentum and mean square error. These inputs are design for simple adjustment by the user. The program operation is divided into pre-process and post-process. The pre-process is designed for data training operation which excel filed is imported in the process. The output from this process is training results and optimum weights (*w*) of ANN model. These weights are also used in the post-process. The post-process is the prediction process which the data for prediction are also imported in the excel format. The number of prediction sample can change by the user. The computational process is following the above mentioned and a model of back-propagation ANN as shown in the Fig.1. The prediction results save automatically on the sheet No. 2 of prediction data file with excel format.

Input Parameters for Neural Network

The input parameters of neural network consist of cone index, depth of tillage, soil hardness, rotary speed, traveling slip and tractor speed.

Soil cone index is an empirical measure of soil strength and is widely used for assessment of the compacting and loosening effects of agricultural.

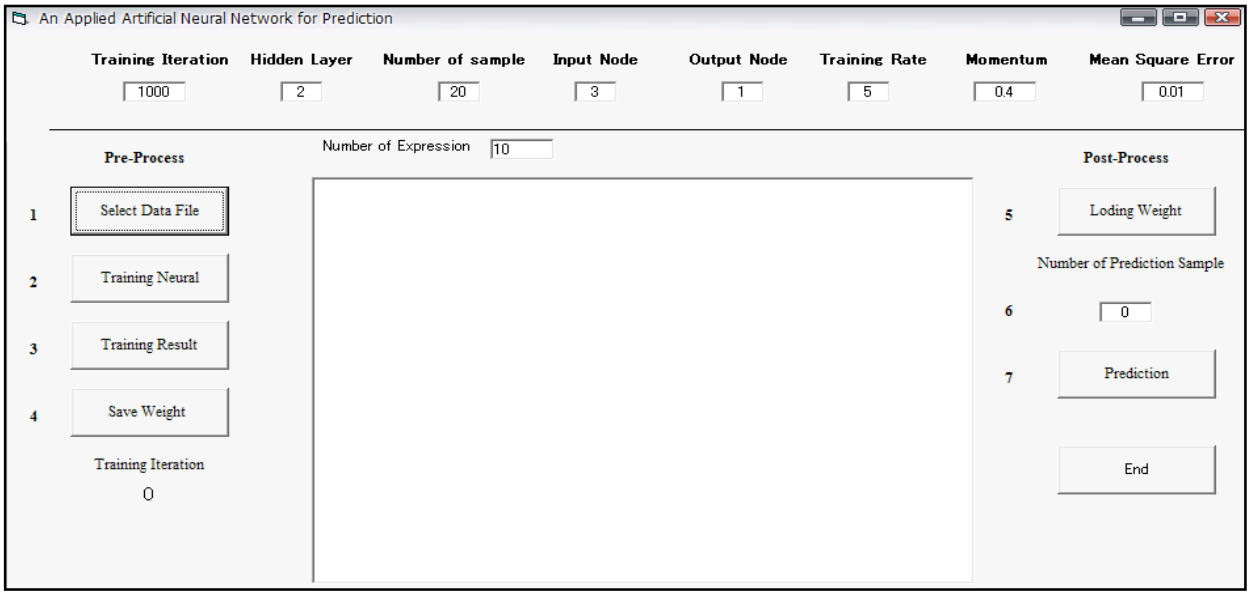

Fig. 2: A program window of neural network for prediction of puddling soil index

Table 1: Data set for neural network training and training results

Input Parameters									Target	Training Results	
Soil Cone Index (kPa)				Depth of Tillage	Soil Hardness	Rotary Speed	Traveling Slip	Tractor Speed	Pudding Index	Pudding Index	Error
5 cm	10 cm	15 cm	20 cm	(cm)	(cm)	(rpm)	(%)	(m/s)	(none unit)	(none unit)	(%)
125.22	325.58	548.80	788.36	12.00	8.33	300.00	1.38	0.75	69.53	69.96	0.62
125.22	325.58	548.80	788.36	13.00	9.84	300.00	1.38	0.75	67.91	67.94	0.05
125.22	325.58	548.80	788.36	11.33	8.96	300.00	1.38	0.75	69.47	69.26	0.30
142.79	350.98	734.66	808.78	11.00	10.60	407.00	1.99	0.81	77.17	77.67	0.65
130.80	281.22	523.20	727.03	11.99	9.46	315.00	1.25	0.74	70.68	70.92	0.35
130.80	281.22	523.20	727.03	12.32	10.60	315.00	1.25	0.74	70.49	70.68	0.26
130.80	281.22	523.20	727.03	11.99	8.39	315.00	1.25	0.74	71.32	71.74	0.59
135.16	327.00	656.18	800.06	12.68	9.02	309.00	1.96	0.76	69.53	68.07	2.10
142.79	350.98	734.66	808.78	11.33	10.28	407.00	1.99	0.81	82.73	81.48	1.51
135.16	327.00	656.18	800.06	11.33	8.39	309.00	1.96	0.76	68.50	68.29	0.31
135.16	327.00	656.18	800.06	13.01	8.46	309.00	1.96	0.76	68.07	68.16	0.13
126.44	304.11	577.70	765.18	12.68	10.41	355.00	2.09	0.82	75.76	76.36	0.79
126.44	304.11	577.70	765.18	13.34	7.70	355.00	2.09	0.82	77.69	78.24	0.71
142.79	350.98	734.66	808.78	11.66	10.03	407.00	1.99	0.81	75.00	75.94	1.25
126.44	304.11	577.70	765.18	12.32	8.08	355.00	2.09	0.82	73.85	74.76	1.23
146.06	327.00	608.22	780.44	12.68	9.72	358.00	1.95	0.78	72.50	73.04	0.75
146.06	327.00	608.22	780.44	12.32	9.46	358.00	1.95	0.78	74.80	75.32	0.70
146.06	327.00	608.22	780.44	12.32	10.41	358.00	1.95	0.78	71.43	72.28	1.19
144.97	322.64	675.80	793.52	12.32	9.78	348.00	1.80	0.77	78.13	79.69	1.99
144.97	322.64	675.80	793.52	12.68	8.96	348.00	1.80	0.77	79.34	80.42	1.36
144.97	322.64	675.80	793.52	12.68	8.46	348.00	1.80	0.77	81.08	81.18	0.13
144.97	322.64	675.80	793.52	11.66	8.58	348.00	1.80	0.77	74.80	76.21	1.89
111.18	253.97	477.42	719.40	13.01	12.99	390.00	2.13	0.84	77.27	77.97	0.91
111.18	253.97	477.42	719.40	14.00	14.00	390.00	2.13	0.84	77.87	78.35	0.62
111.18	253.97	477.42	719.40	11.99	11.98	390.00	2.13	0.84	76.98	77.32	0.45
144.97	313.92	647.46	758.64	11.33	10.98	410.00	1.98	0.77	75.86	76.75	1.18
144.97	313.92	647.46	758.64	12.68	10.16	410.00	1.98	0.77	77.87	78.17	0.38
144.97	313.92	647.46	758.64	12.32	10.54	410.00	1.98	0.77	75.63	76.12	0.65
144.97	313.92	647.46	758.64	11.66	10.47	410.00	1.98	0.77	78.57	79.02	0.57
142.79	350.98	734.66	808.78	11.99	10.98	407.00	1.99	0.81	75.81	76.16	0.47

For the experiment, the soil cone index before tillage of flood paddy field at 5, 10, 15 and 20 cm of depth is measured by using the standard cone penetrometer of 3.14 cm^2 base area.

Soil hardness is measured by using falling cone penetrometer, specification characteristic is 3.6 cm in diameter, 4.4 cm of height, and 115 g of weight. Soil hardness is measured after soil is tilled by rotary tiller.

Depth of tillage and rotary speed are measured by level indicator and tachometer, respectively. The rotary speed in the experiment is fixed at 300, 350 and 400 rpm. Tractor traveling slip and tractor speed are measured by timer and tape-measuring device.

The training and testing data set collected from the rotary tillage for pudding soil preparation field experiments are used. Thirty data from the experiments as shown in Table 1 are used for training the neural network and nine data from the experiments are used for prediction and evaluation of prediction accuracy.

SIMULATION RESULTS

Data Training Results

The simulation was performed by determining MSE constrain at 0.01. The simulation results revealed that the optimum training rate, momentum and number of hidden layers of neural network model were 5, 0.4 and 4, respectively. The data training results are shown in Table 1. The average absolute error of learning the target value was 0.8 %. However, the maximum and minimum absolute errors were 2.10% and 0.05%, respectively. Almost of results have absolute error less than 1% with average errors about 0.49%, whereas, 9 data have absolute error more than 1% with an average

error about 1.48%. From data training results, it can be concluded that the neural network model performs the accuracy 99.5% – 97.9% of data learning.

Table 2: Prediction input parameters and results

Input Parameters									Real Value	Prediction Results	
Soil Cone Index (kPa)				Tilling Depth	Soil Hardness	Rotary Speed	Traveling Slip	Tractor Speed	Pudding Index	Pudding Index	Error
5 cm	10 cm	15 cm	20 cm	(cm)	(cm)	(rpm)	(%)	(m/s)	(none unit)	(none unit)	(%)
125.22	325.58	548.80	788.36	13.00	8.80	300.00	1.38	0.75	72.00	67.95	4.05
130.80	281.22	523.20	727.03	13.00	8.50	315.00	1.25	0.74	70.54	76.52	5.98
135.16	327.00	656.18	800.06	13.00	8.63	309.00	1.96	0.76	70.45	68.04	2.41
126.44	304.11	577.70	765.18	12.00	8.73	355.00	2.09	0.82	77.27	73.55	3.72
146.06	327.00	608.22	780.44	12.33	9.87	358.00	1.95	0.78	72.59	74.03	1.44
144.97	322.64	675.80	793.52	11.67	9.90	348.00	1.80	0.77	68.66	68.67	0.01
111.18	253.97	477.42	719.40	12.67	12.67	390.00	2.13	0.84	77.05	77.77	0.72
144.97	313.92	647.46	758.64	11.67	10.83	410.00	1.98	0.77	78.33	76.33	2.00
142.79	350.98	734.66	808.78	11.83	10.53	407.00	1.99	0.81	80.34	75.34	5.00

Prediction Results

In an attempt to access predictive capability, the trained ANN model was used to estimate puddling soil index value as shown in Table 2. The results showed that an average absolute error was 2.82%. The maximum and minimum absolute errors were 5.98% and 0.01%, respectively. As the results, the simulation performed that ANN performs accuracy of 99.9% – 94.02% for prediction. The results indicated that accuracy of range of prediction value from trained model of ANN was consistently wider than the learning results. Based on these results the simulation could speculate that the ANN model, trained with data from the paddy field tillage experiment had good predictive capability when range of input data was similar or not significantly change. However, predictive accuracy could be reduced when the range of input data was drastically different from the input data used to train the model.

CONCLUSION

A back-propagation ANN model was developed and trained to estimate the puddling soil index by using the rotary tiller for puddling soil preparation in the paddy field. The training and prediction results indicated that the developed ANN model performs high-accuracy more than 94.02 % for learning and prediction with constrain mean square error for ANN model at 0.01. However, this ANN model can use only for paddy soil, consisting of 44.029% of sand, 34.788% of silt, and 21.183% of clay. The results also confirmed that an engineering approach ANN model can apply to solve agricultural problems. For further work, different percentages of sand silt and clay will be determined as input parameters for ANN model. The practical using the prediction model can manipulate for decision to increase or decrease number of tillage and operation for saving energy consumption in the paddy soil preparation by rotary tiller.

REFERENCES

1. So, H.B. and A.J. Ringrose-Voase, 2000. Management of clay soils for rainfed lowland rice-based cropping systems: an overview, Soil&Tillage Research 56: 3 – 14.
2. Kukal, S.S. and G.C. Aggarwal, 2003. Puddling depth and intensity effects in rice-wheat system on a sandy loam soil I. Development of subsurface compaction, Soil&Tillage Research 72:1–8.
3. Shivastava, A.K. and R.K. Datta, 2001. Performance evaluation of an animal drawn puddling implements under controlled soil-bin conditions,Journal of Terramechanics 38: 121–131.
4. Kukal, S.S. and A.S. Sidhu, 2004. Percolation losses of water in relation to pre-puddling tillage and puddling intensity in a puddle sandy loam rice (*Orayza sativa* L.) field, Soil&Tillage Research 78:1–8.
5. Salokhe, V.M. and N. Ramalingam, 2001. Effects of direction of rotation of a rotary tiller on properties of Bangkok clay soil, Soil&Tillage Research 63: 65–74.
6. Sinha, M.P., 1964. A study of the measurement of Puddling and Comparative Performance of Different Implements for Puddling in Rice Cultivation, Food and Agriculture Organization of The United Nation, International Rice Commission, Manila,Philippines, pp: 1– 5.
7. Zhao, Z., T.L. Chow, H.W. Rees, Q. Yang Z. Xing and F. Meng, 2008. Prediction soil ttexture distributions using an artificial neural network

model, Computers ans Electronics in Agriculture: pp.1–13. (Article In Press)
8. Galushkin, A.I., 2007. Neural Network Theory, Springer, New York.

Crop Monitoring Using Remote Sensing Data

Aye Mya Thein[a] Myint Myint Khaing[b] and R.P Singh[c]
[a] Remote Sensing Deparatment, Mandalay Technological University, Myanmar
[b]Head of Remote Sensing Department, Mandalay Technological University, Myanmar
[c]Agricultural Forestry & Environment Division, Indian Space Application Center, ISRO, Ahmedabad, India.

Abstract: This study focuses on the investigations related to crop classification using relatively high spatial resolution (56m) IRS-AWiFS data and crop growth profile assessment using high temporal resolution (10day) SPOT-Vegetation data. Crop growth was monitored over central India as well as Myanmar region using SPOT-Vegetation NDVI product. It was observed that multi spectral information is most important in classification of crops. The overall accuracy increased from 50% to 89% when compared with one (Green) band classification and four bands (Green, Red, NIR and SWIR) classification. The validation of NDVI product over a transact showed high correlations (0.8) between AWiFS and SPOT-Vegetation data. A distinct temporal crop growth profile was observed over the two representative sites. Two-peak pattern associated with soyabean and wheat crops was observed over central India and one peak of rice was observed in Myanmar region.

Key Words: NDVI, Crop Classification, fAPAR.

1. Introduction

The monitoring of the crop involves crop identification and estimation of biophysical parameters. Remote Sensing techniques are used for discrimination of crops as well as for the determination of their biophysical parameter such as Leaf Area Index (LAI) fraction of absorbed photosynthetic active radiation (fAPAR) and Net Primary Productivity (NPP) etc..

2. Objectives

- Study on effect of different spectral bands on crop classification using IRS_AWiFS Data over central India.
- Estimation of surface radiance, reflectance and NDVI using IRS-P6-AWiFS data and comparison with SPOT-Vegetation NDVI product.
- Assessment of crop growth profile over representative sites in central India and Myanmar.
- Study on inter annual variability in fAPAR over representative sites in Central India and Myanmar.

3. Crop Classification

Analysis of crop classification was focused on studying the spectral signature in terms of DN, radiance and apparent reflectance and quantification of role of difference spectral band on classification accuracy and crop separability. It can be seen that vegetation in red band looks darker with respect to NIR band. The water shows low values in all the bands while sand shows high values in all the bands.

The class wise DN values, radiance values, apparent reflectance values and NDVI are respectively. Higher mean reflectance was observed as 23% in NIR band as compared to lowest mean reflectance of 7% in Red band in vegetation dominated image of central India Forest showed 9%, 5%, 20% & 16.5% reflectance in Green, Red, NIR and SWIR bands respectively. Crop shows 11%, 29%, 25% and 19% reflectance in Green, Red, NIR & SWIR bands respectively. The NDVI values of forest, crop, fallow land, water and sand varied as 0.68, 0.53, 0.283, -0.03 and 0.105 respectively. The shows NIR & Red band scatter gram in terms of distribution of DN values of difference land cover classes.

Based on the training signatures of difference bands, the IRS-AWiFS data was classified into forest, crop, wasteland & fallow land, water and sand classes using different spectral band combinations. The classified image output when classified with green band, green & red band and green, red & NIR band

Corresponding Author: Aye Mya Thein, Assistant Lecturer, Remote Sensing Department, Mandalay Technological Universtiy. Myanmar. Tel .0952-88704.Fax: 0952-88702, E-mail: ayemyathein@gmail.com

combinations. The figure 1 shows the false color composite of IRS-AWiFS and four bands (Green, Red, NIR and SWIR) classified image. It can be inferred from the field survey data as well as overall accuracy that classification accuracy increased gradually when more number of bands was used in classification (figure 2). Single band (Green) classification gave 50% overall accuracy which gradually increased to 73%, 88% and 89% when two bands (Green, Red), three bands (Green, Red, NIR) and four bands (Green, Red, NIR & SWIR) respectively were used in classification.

Similar results were observed when crop separability in terms of transformed divergence distance was analyzed. The transformed divergence increased from 1.29 to 1.68 subsequently to 1.92 and finally 1.96 when analyzed with one band (Green) to two bands (Green & Red) thereafter three bands (Green, Red, NIR) and finally four bands (Green, Red, NIR & SWIR) & False Color Composite (IRS P6-AWiFS) Figure 3.

3.1 Spectral Band Combination

Green Band Red Band

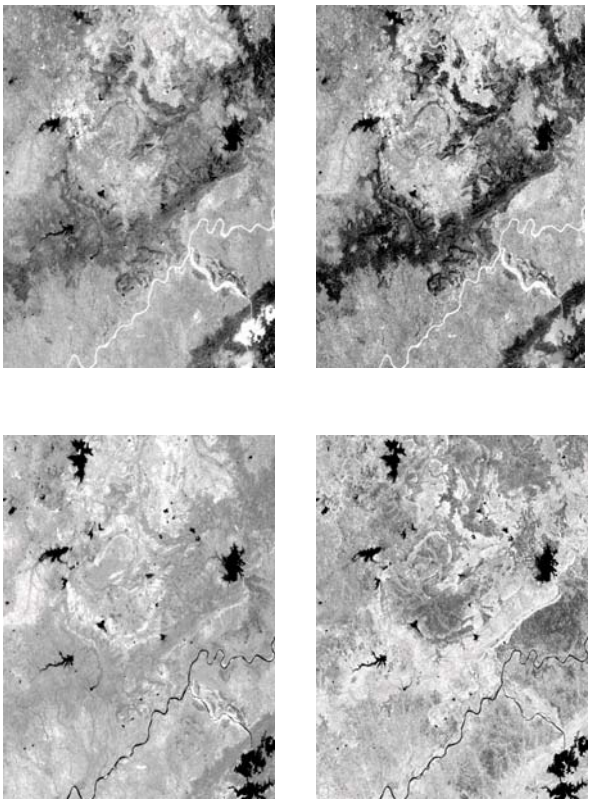

NIR Band SWIR Band

Figure 1. Four band data & IRS-P6-AWiFS

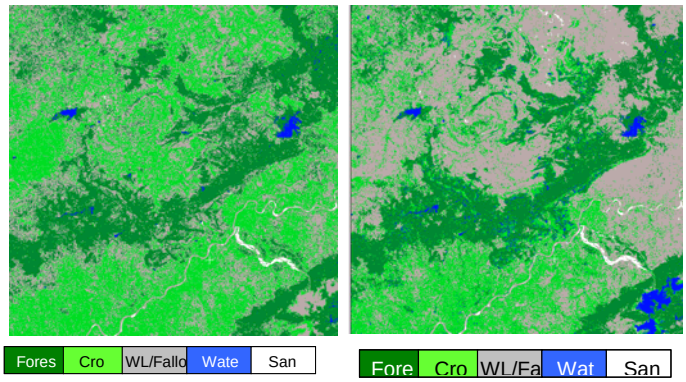

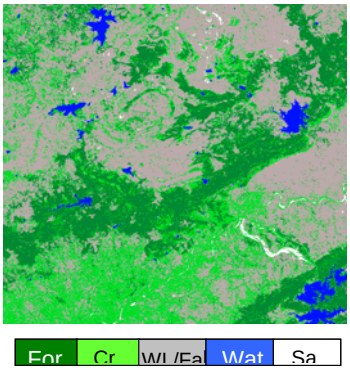

Figure-2. Classified images of different band combinations

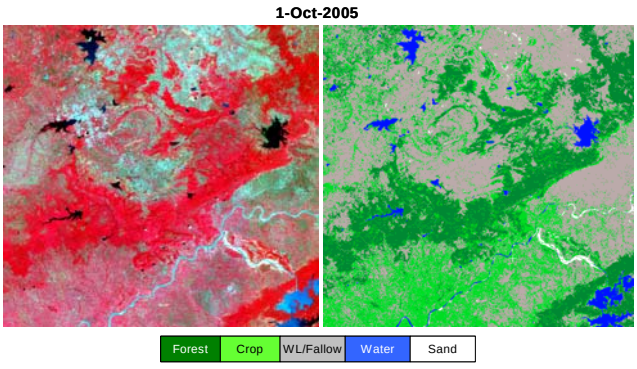

Figure 3. Comparison of IRS-AWiFS image and classification image

4. Methodology

Study was carried out with data at different spatial resolution ranging from 56 m to 16km using procedures according to figure 4. The study was based

on single day analysis of AWiFS data to one-year analysis of SPOT-NDVI data to decadal (1982-1999) analysis of NOAA-AVHRR derived fAPAR product. Analysis was focused broadly an three themes (a) classification and accuracy assessment using AWiFS data (b) estimation of NDVI from AWiFS data and its comparison with of SPOT –Vegetation NDVI data and (c) NOAA-AVHRR – fAPAR data analysis over representative sites in central India and Myanmar. The major image analysis steps for crop classification consisted of data acquisition as the proper bio window (peak vegetation stage), extraction of study area, training site signature generation based on available field survey data. The maximum likelihood approach was followed for classification.

Analysis also involved development of an affine transformation equation between IRS-P6-AWiFS data and SPOT-NDVI data using common ground control points (GCP) for NDVI comparison. SPOT-NDVI product was resampled to AWiFS data using nearest neighbors approach for comparison of NDVI product generated from two sensors. Based on the field survey information, sites of various crops and other land cover classes were identified and marked as training sites on the image. Training signatures were used for classification as well as separability analysis. Transformed divergence measure was used to quantity the effect of difference band combination on crop separability. Classification accuracy assessment was carried out using overall accuracy estimated using training site based confusion matrix.

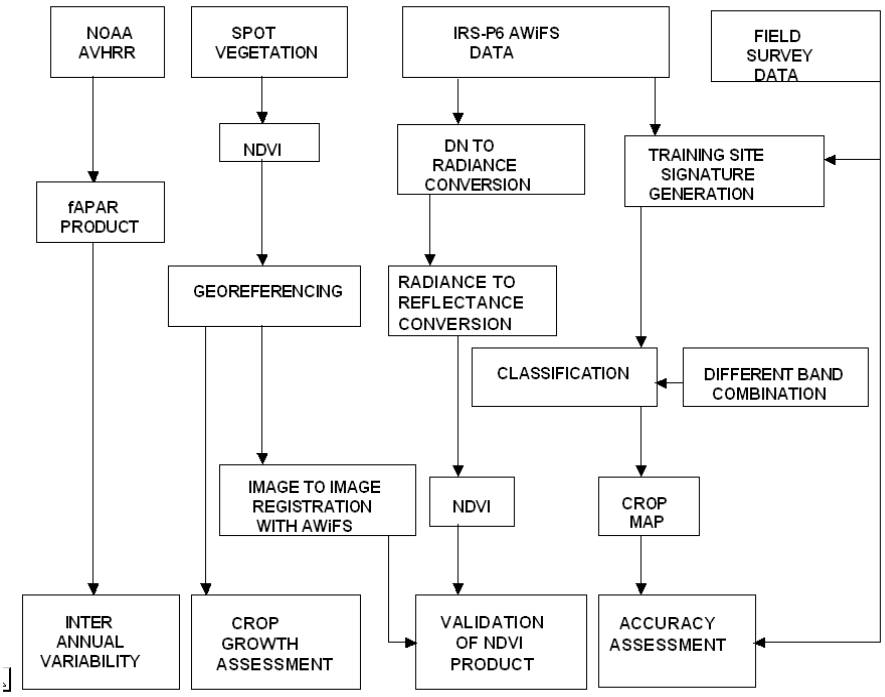

Figure.4 The steps followed in the crop assessmenusing remote sensing Data

5. Vegetation Growth observed using SPOT-VEGETATION data during (May 2005 To March 2006 see fig. 5)

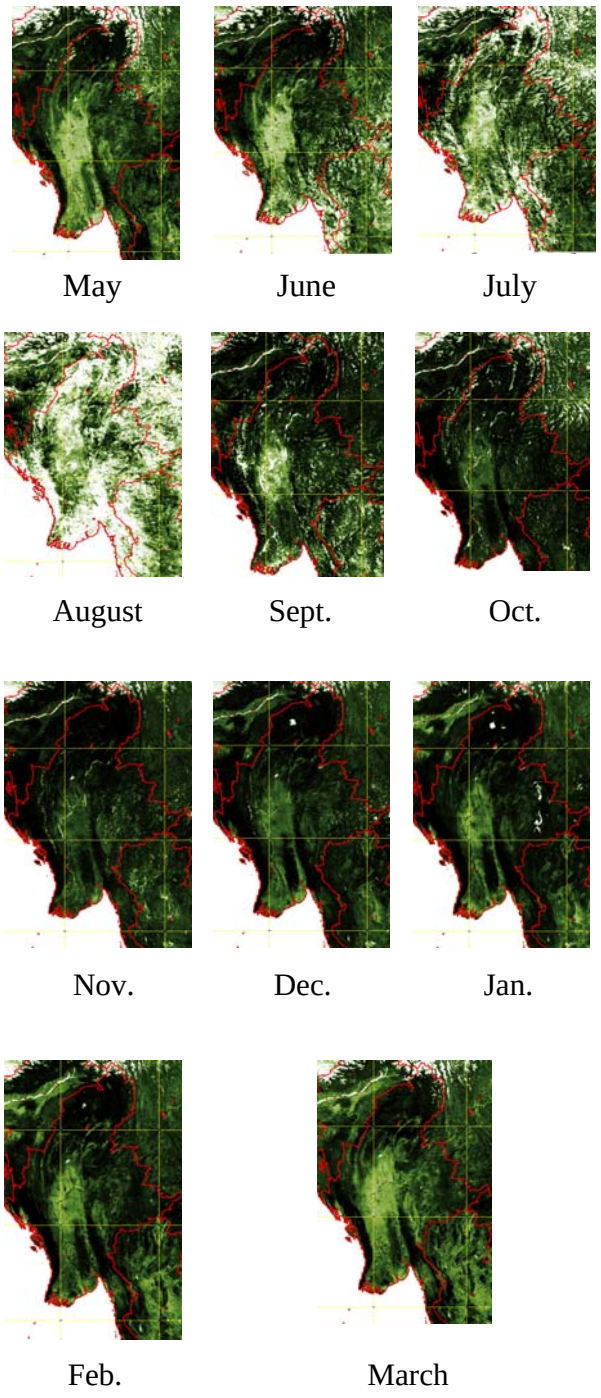

Figure.5 Distinct crop growth characteristic was observed during May 2005 – March 2006

6. Seasonal Growth Profile

Quantification of spatial and temporal NDVI variability is another important component of crop monitoring. Overall high NDVI in forest and crop regions and low NDVI in sand, fallow and wastelands can be seen in both sensor data with different spatial details. The quantification of the estimated NDVI from AWiFS and SPOT-Vegetation data over a horizontal transect is shown in figure 8.

The correlation coefficient of 0.8 was observed between the two NDVI estimates. The IRS-P6 AWiFS NDVI showed more variability due to high spatial resolution as compared to SPOT-NDVI data. Over all SPOT- NDVI product showed an over estimation as compared to IRS-P6 AWiFS data. The characteristic response to crop growth over Myanmar and Central India (figures 6 and 7). The NDVI from Myanmar region starts with bare soil NDVI of 0.2 in May and reaches up to 0.6 during October and drops back to 0.2 in March. The NDVI profile over Hoshangabad site, central India starts with bare soil NDVI of 0.2 and reaches first peak up to 0.8 in September and falls back to lower value in November with another peak (0.8) and fall (0.2) in January and March respectively.

It can be inferred from Myanmar is associated with one crop (rice) system while central India has two crop rotation of soyabeam and wheat during monsoon and winter season. The growth profiles are associated with weather conditions as well as agricultural practices. The representative station wise NDVI profiles along with the climatic rain

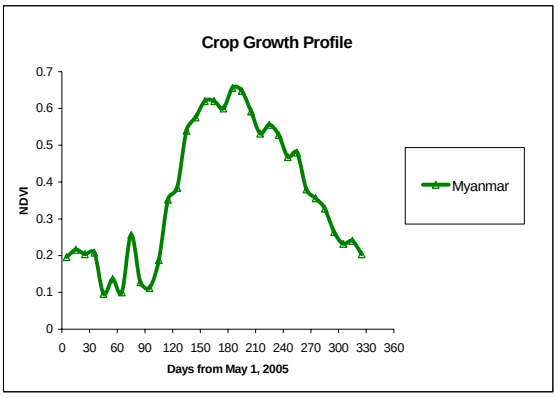

Figure 6. The Crop Growth Profile of Myanmar region

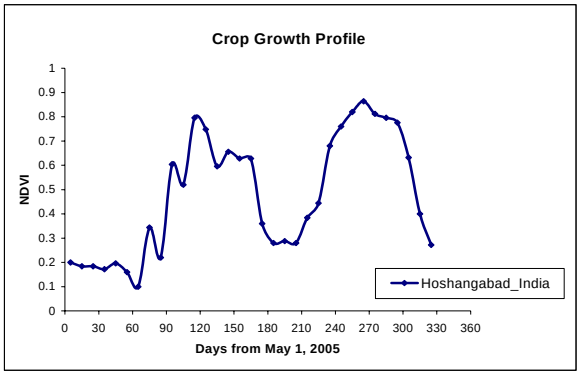

Figure 7. The Crop Growth Profile of Hoshangabad region

Inter Annual Variability

Inter annual variations in crop phenology (Singh *et al.* 2006) is needed to understand the cause and effect relationship of weather and other human induced changes. Monthly fAPAR values were analyzed at two representative locations in Hoshangabad, central India and Myanmar regions between 1982 to 1999.

Inter annual analysis of fAPAR data showed both seasonal variations and as well as temporal trend in Hoshangabad site, India. In contrast to Hoshangabad site in India, Myanmar site showed only seasonal variations but did not show any increasing trend in vegetation activity. Increasing trend of 7.4 percent in fAPAR over a decade in central India indicates the positive feed back of improvement in agricultural technology and favorable weather conditions.

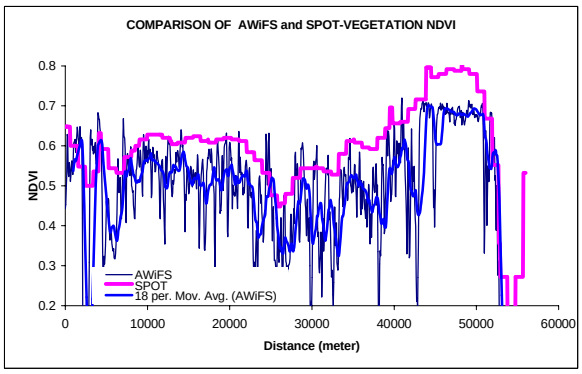

Figure 8. Comparison of AWiFS and SPOT-Vegetation NDVI

7. Results and Discussion

Analysis was carried out to address mainly three issues involved in crop monitoring (a) crop classification (b) seasonal growth profile and (c) inter annual variability. It was observed that multi spectral information is needed to accurately classify different land cover classes. Overall classification accuracy increased from 50% to 89% when single band (Green) and four band (Green, Red, NIR, SWIR) data was used in classification. A distinct crop growth profile was observed over agricultural sites in central India (soyabean and wheat rotation) and Myanmar region (Rice).Inter annual analysis of fAPAR data showed temporal trend in Hoshangabad site, India but no such trend was found in Myanmar site. Increasing trend of 7.4 percent in fAPAR over a decade in central India indicates the positive feed back of improvement in agricultural technology.

8. Summary & Conclusions

Study was carried out to address some of the important components of crop monitoring such as crop classification, crop growth characteristic and inter annual variations in crop biophysical property. Multi source data including IRS-AWiFS, SPOT-Vegetation and NOAA-AVHRR at varying spatial and temporal resolution were used in analysis at two representative agricultural sites in central India and Myanmar region. It was observed that multi spectral bands play a major role in classification. A systematic analysis showed that overall accuracy increased 50% to 89% when one band (Green) and four bands (Green, Red, NIR, SWIR) respectively were used in classification. Comparative analysis between AWiFS and SPOT-Vegetation derived NDVI showed good correlation (0.8) over a horizontal transect in central Indian site.

Distinct crop growth characteristic was observed during May 2005- March 2006 season over two representative agricultural sites in India and Myanmar. The Hoshangabad site of central India showed two peak crop growth profile associated with soyabeam and wheat crop while Myanmar region showed only one peak pattern associated with rice cultivation. Analysis of monthly fAPAR data set derived for NOAA-AVHRR data using an RT model of Myneni *et. al.* (1997) covering period Jan. 1982 to Dec. 1999 showed decadal increase in fAPAR about 7.4% over Hoshangabad site in central India.

Results obtained from the present study indicate the potential use of remote sensing based inputs in assessment and monitoring of crop at regional and global level. The present study is limited by using mainly the optical data and product derived from the same but an integrated technique of crop monitoring such as FASAL (Parihar & Oza, 2006) would also require the data from other electromagnetic spectrum such as thermal and microwave region. Data available in thermal and microwave spectral regions would be used in future for assessment of the surface temperature, soil moisture and evapo-transpiration.

Acknowledgements

This work was supported by CSSTEAP Pilot Project for post graduate diploma project work. The author wish to thanks Director from CSSTEAP (UN Affiliated), Dr. George Joseph, Course Director, Associated Professor Dr.Myint Myint Khaing ,Head of Remote Sensing Department ,SATMET course Dr.B.M. Rao and Dr R.P. Singh, Agricultural Forestry & Environment Group Space Applications Center, ISRO and all respectable teachers from ISRO Campus.

9. References

1 Asrar, G., Fuchs, M., Kanemasu, E.T., and Hatfield, J.L., 1984, Estimating absorbed photosynthetic radiation and leaf area index from spectral reflectances in wheat. *Agronomy Journal*, 76, 300-306.

2. Badhwar, G. D., 1980, Crop emergence date determination from spectral data. *Photogrammetric Engineering and Remote Sensing*, 46, 369-377.

3. Bannari, A., Morin, D., and Bonn, F., 1995, A review of vegetation indices. *Remote Sensing Reviews*, 13, 95-120.

4. Baret, F., and Guyot, G., 1991, Potentials and limits of vegetation indices for LAI and APAR assessment. *Remote Sensing of Environment*, 35, 160-173.

5. Dadhwal, V. K., Parihar, J. S., Medhavy, T. T., Ruhal, D. S., Jarwal, S. D. and Khera, A. P.,1996, Comparative performance of thematic mapper middle-infrared bands in crop discrimination. *International Journal of Remote Sensing*, 17, 1727-1734.

6. MacDonald, R.B., 1984, A summary of the history of the development of automated remote sensing for agricultural applications. *IEEE Transaction Geoscience & Remote Sensing*, 22, 473-481.

7. Myneni, R.B, Nemani, R.R., Running S.W, 1997, Estimation of global leaf area index and observed par using radiative transfer model. IEEE Transations on Geoscience and Remote Sensing, 35, 1380-1393.

8. Navalgund, R.R., Parihar, J.S., Ajai and Nageshwar Rao, P.P., 1991, Crop inventory using remotely sensed data. *Current Science*, 61, 162 – 171.

Spatial Pattern Analysis of Land Degradation Using Satellite Remote Sensing Data and GIS in Mandalay Watershed, Central Myanmar

Kyaw Zaya Htun[1], Myint Myint Khaing[2], Swe Swe Aye[3]and Lal Samarakoon[4]
[1] Remote Sensing Department, Mandalay Technological University, Myanmar
[2] Associate Professor, Remote Sensing Department, Mandalay Technological University
[3] Pro-Rector, Yangon Technological University, Myanmar
[4] Director, Geoinformatics Center, Asian Institute of Technology, Thailand
kyawzaya.htun@gmail.com

Abstract: Land degradation in term of soil erosion is the single most important environmental concern in the developing countries. Eroded sediment also acts as both a physical and chemical pollutant. It has been become an ecological, social and economic problem. This study explored the influence of major socioeconomic factors on erosion processes and conservation measures in a Dry Zone farming context for producing Erosion Risk Map of the study area. We also put forward a way of studying soil Erosion and relations of soil erosion factors by integrated GIS and RS. Knowing extent and severity of the land is important as a decision support system to policy makers, resource managers as well as local communities and farmers. Firstly, satellite images (ETM) and the ground real conditions have been rectified. Secondly, according to the ecological environmental factors, the spatial database and Digital Elevation Model of the study area have been built. Finally, referring to Universal Soil Loss Equation, the quantization and distribution of the soil erosion, risks and changes have been obtained. The result of this assessment showed spatial distribution of different land degradation severity across the area in watershed basis. Soil erosion susceptibility was estimated through Universal Soil Loss Equation USLE. To examine land potential, land capability classification was carried out using Storie Index Rating SIR. Population density was included in the model since human pressures on the land was considered as a major contribution factor for land degradation. Soil erosion, land capability and population density parameters were modeled in GIS platform. Though modeling of land degradation assessment is specific and involving much basic information such as suitability of crops, soil fertility, social and environment benefits etc., this study was only intend to develop a model based on spatial information and demographic data.

INTRODUCTION

Mandalay watershed is located in the heart of Dry Zone, in Mandalay District, Central Myanmar a distinct semi-arid region within the country, lying between N 21 17 57 to N 22 34 16 and E 95 10 24 to 96 18 59 with approximate 9936 km 2 watershed area.

This watershed is situated on Mandalay-Kyaukse plain which is between the Irrawaddy River in the west and Shan Highland in the east. In general, the topography of this watershed is high in the eastern parts from which the ground surface gradually slopes towards the western and southern parts of the city.

In Dry Zone Area of Central Region of Myanmar, soil erosion is high in river bank, particularly in the form of water erosion during the rainy season. Rills, gullies and rivers full of sediments show that a considerable amount of soil is carried away, mainly during the destructive intense storms which characterize Myanmar dry zone rainfall patterns. In the Myanmar Dry Zone, although annual rainfall ranges between 500 mm and 1000 mm, heavy individual storms and destructive showers occurring within a very short period causing flood and severe erosion. In addition, due to deforestation, soil degradation is now taking place particularly in the central dry zone of the country (NCEA, 1997).

Loss of vegetation cover, and unfavorable agricultural practices such as slash and burn cultivation and shifting cultivation are found in the dry zone area of central Myanmar. Shifting cultivation still continues because the punishment is small and the farmer can legally obtain their agricultural products in exchange with little fine. Measures to prevent slash and burn cultivation, shifting cultivation and illegal logging. The problem is that the local authority does not respect the plan as plan is not consistent with the local development
plan. Land degradation occurs representing 7.8 % of the cultivable land area. Annual deforestation rate during 1980s is estimated to be 2.3 %.

Corresponding Author: Kyaw Zaya Htun, Remote Sensing Department, Mandalay Technological University, Myanmar

Assessment of erosion occurring at this watershed is a very difficult task when it is done following ground based conventional methods. It is time consuming and almost impractical when it is required to be done repetitively. Synoptic view offered by the remote sensing satellites has made the task comparatively easy.

The assessment of soil erosion and land degradation is a wide range of field that needs long-term and multidisciplinary studies. The results of this study are expected to help analyze land-use problems, and plan and develop activities for soil-erosion control in the Dry Zone area of Central Myanmar.

METHODOLOGY

Land capability and soil erosion susceptibility could be determined using biophysical aspect of land use which could be understanding potential of the land. Theoretically, integration of population as possible human activities, disturbances on the land can be identifiable. The concept of geospatialized land degradation assessment was used in this research.

The most widely used method for predicting soil loss from overland areas is the Universal Soil Loss Equation (USLE) (Mitchel, J. K et al. 1980). This was used to determine soil erosion susceptibility. The general form of the USLE, as expressed in metric units, is as follows (Goldman et al. 1986):

E= R*K*L*S*C*P

where,
E = erosion (ton/ha/yr)
R = rain fall erositivity factor
K = soil erodibility factor
L = slope length factor
S = slope steepness factor
C = crop management factor
P = erosion control practice factor

Land capability classification was carried out using Storie Index Rating (SIR) to examine land potential. As an element of land degradation, population density was classified and included in the model. Soil erosion, land capability and population density parameters were overlaid and modeled in GIS platform.

Rainfall Erosivity (R)

Wischmeier and Smith (1958) stated soil loss is directly proportional to rainfall factor. The rainfall factor, R, accounts for the potential of falling rain drops and flowing water in a particular area to produce erosion. Two components of the factor are the total energy (E) and the maximum 30-min intensity of storms I30 (Wischmeier and Smith, 1978). The R-factor is the sum of the product of these two components for all major storms in the area during an average year. Even though EI30 is the most reliable source for computing R, other equations might be used where E and I30 were not available. R = 38.5 + 0.35*P (P = mean annual precipitation) gives acceptable erosivity index for tropical and subtropical ecological zones (Eiumnoh, A., 2000). In the study area, there was only one rainfall station in the study area and R-value was interpolated through average annual rainfall data (1973 to 2006) from surrounding stations instead. Resultant R- value ranged from 99 to 356 (Figure 3).

Soil Erodibility Index (K)

K factor calculated from soil organic matter content, texture, structure, and the permeability of the soil to water. Soil erodibility index (K) is influenced by soil structure, organic matter content, soil texture and soil permeability, it should be based on measured value wherever possible (Morgan, 1995). The K value can be calculated with the use of nomograph, derived by Wischemier and Smith (1978), when all the values of K influencing factors are available.From the analysis report, all the soil types in the study area showed strong sand component, up to 70%. Sands being non-coherent and structureless are easily erodible, high specific gravity, low total porosity, low available water range, and high infiltration and course textured soil (FAO, 1975). K- values ranged from 0.22 to 0.62 in the study area(Figure 3).

Topographic Factor (LS)

The factors of slope length (L) and slope steepness (S) are combined in a single topographic index termed LS factor. Wischmeier and Smith defined the slope length as the distance from the point of origin of overland flow to the point where either the slope gradient decreases enough that deposition begins or the runoff water enters a well-defined channel that may be part of a drainage network or a constructed channel. Slope and aspect maps were generated from digital elevation model (DEM) formed from contour map of 50 feet (15.24 m) interval. The following equations were applied to produce LS(Figure 3).

$L = (l / 22)m$
$m = \sin 2\theta + 0.269 (\sin\theta) 0.8 + 0.05$
$s < 9\% , S = 10.8 \sin \theta + 0.03$
$s > 9\% , S = 16.8 \sin \theta - 0.50$

where,
L = slope length factor
l = slope in m
m = dimensionless exponent

θ= field slope steepness in degrees = $\tan^{-1}$ (s / 100)
s = field slope in percent
S = slope steepness

Crop Management factor (C)

Crop management factor (C) was represented by the ratio of soil loss under given crop to that from bare soil. In order to determine C factor, Mandalay watershed was classified into 6 land uses generated from Landsat TM images (2005), applying maximum likelihood of supervise classification. C- values were assigned 0.06 for natural woodland (heavy vegetative cover), 0.014 for scrub and grass lands, 0.01 for built-up area, 1 for bare land (low vegetative cover) and 0.377 for agriculture land as recommended by Morgan, 1995(Figure 3).

Erosion Control Practice Factor (P)

This factor accounts for control practices that reduce the erosion potential of the runoff by their influence on drainage patterns, runoff concentration and runoff velocity. Therefore, erosion control practice factor is based on the soil conservation practices operated in a particular area. In this study, P value was defined according to tillage system, 1.0 for fall plow, 0.9 for spring plow, 0.60 for mulch tillage, 0.25 for zone tillage and no tillage(Figure 3).

Soil Erosion Potential

Estimation of soil erosion by water in the study area was modeled using the USLE. USLE estimates the average annual soil loss (A) by using a functional relation of several factors expressed as E=RKLSC. Modeling in the present study used a raster based approach where a square cell of 50 meters was chosen. It was taken that this resolution would be suitable for a reasonable accuracy considering that the original data were mostly from 1:50,000 maps. Grids of rainfall, soil land use and elevation data created using ArcGIS software were used for the computation for the USLE.

Land Capability Classification

Land capability classification shows the suitability of soils for most kinds of field crops. Land capability classification was executed to determine land potential as well as relationship between soil erosion and land capability classes. Storie Index Rating (SIR) developed by Storie, R.E. (1933 and 1978) was chosen for its simplicity. The SIR system is an index for numerical rating of soils and expresses numerically the relative degree of suitability, or value of a soil for general land use and agriculture. The rating is based on soil and topographic characteristics only and obtained by evaluating specific soil factors. Four general factors are considered in the Storie index rating (SIR) as follows;

SIR = a * b * c * x * 100

where

a = rating on characteristics of physical profile (color, depth)
b = rating on basis of surface texture
c = rating on basis of slope
x = rating on conditions other than those factor a,
b, c and x such as nutrient, salinity, acidity.

Population Density

Accelerated erosion and excessive runoff are connected with development activities and human disturbances: clearance of fragile zones, denudation and compaction of soil through overgrazing, exhaustion of soil through intensive cropping. Erosion increases as a function of population density in a given agrarian system, if the population passes a certain threshold, land starts to run short, and soil restoration mechanisms seize up (Pieri, 1989). In Sudano-Sahelian zones, when the population exceeds 20-40 inhabitants/km², the fallow period is shortened to the point of ineffectiveness, and one speaks of a densely populated degraded area when the population reaches 100 inhab/km² (FAO, 1996).

Dry zone, central Myanmar, being semi-arid region, assuming similar trend as in Sahel, population density was classified in to 3 classes, < 50 inhab/km2 as sparse, 50- 100 inhab/km2 as moderate and >100 inhab/ km2 as dense population. Finally, Land degradation extent was determined using spatial overlay function with weighing system in GIS.

RESULTS AND DISCUSSION

From USLE analysis, while moderate erosion rates were found at virgin lands which account for 10% of the total land area, more than 79% of total area covered by agriculture land with gentle slopes has low soil loss, 1-10 tons/ha/year. High soil loss can be seen in the middle part of upper watershed region, in the acrisol soil type. If annual soil loss of more than 10 ton/ha/yr is considered as critical value in South East Asia, almost one third is under critical condition in Mandalay watershed. It is rather large area compare with the watershed as a whole.

According to index rating for a soil, a rating of 100 per cent expresses the most favorable or ideal condition (class 1), and lower percentage ratings are given for conditions that are less favorable to crop production (class 10). Almost 80 % of the watershed occupied in class 1 and class 2 accounts for 27 % and the rest for 3%.

Population Density map was prepared and classified into 3 groups. Dense populations were found in central portion and south-east part of watershed where vast arable land with good accessibility. Population density, more than 100/km2, is found in regions located near to the highway and Irrawaddy River. The lowest population can be seen in steep slope occupying forest and limited cultivation land while moderate density is in large cultivation land and gentle slope.

Soil loss from all heavy vegetative area was the lowest i.e., 0-10 ton/ha/yr, among all land use classes. Soil loss and land capability were largely influenced by soil properties. The very severe erosion was occurred at high land capability class in this case because vegetation cover is a very little in this region.

There was a slight significant contribution in soil erosion by class (>100 inhab/km2) than the other two.

It was found that the estimated soil loss in 2005 by USLE was directly related to land degradation severity assessment. Soil erosion rate of 10-50 ton/ha/yr was account for the most severe land degradation since almost all of combined very severe and severe classes (15.02 % out of 17.69%) was fall into 10-50 ton/ha/yr annual soil loss class.

ACKNOWLEDGMENTS

My sincere thank and gratefulness to the Ministry of Science and Technology and our minister for giving me a chance to make this research. I am thankful to all staffs from Remote Sensing Department for their assistance and suggestion during my study. I could not forget to express my deepest gratitude and appreciation to my supervisor, Dr. Swe Swe Aye (Pro-Rector, Yangon Technological University), and my co-supervisor, Dr. Myint Myint Khaing(Associate Professor, Remote Sensing Dept., Mandalay Technological University), for their constant inspiration, invaluable guidance and support in my research from the early stage of forming proposal to the completion stage.

REFERENCES

[1] Environmental Monitoring. Stuttgart, German, E. Schweizerbart'sche Verlagsbuchhandlung, 1999.

[2] Friend A. J., "Achieving Soil Sustainability",Journal of Soil and Water Conservation, Vol.47,Number 2, 156-157, 1992.

[3] Jenson, J.R., Introductory Digital ImageProcessing, Prentice Hall, New Jersey, 1986.

[4] Lambin, E.F., Turner, B.L. II, Geist, H.J., Agbola,S.B., Angelsen, A. et al., "The causes of land-use and land-cover change: Moving beyond the myths", Global Environmental Change: Human and Policy Dimensions 11(4):5-13, 2001.

[5] Morgan, R.P.C., Soil Erosion and Conservation (Second Edition), Longman Group, UK Limited, 1995.

[6] Robert A. Schowengerdt, Techniques for Image Processing and Classification in Remote Sensing (Second Edition), Academic Press, INC, Londom Limited, 1983.

[7] Symeonaki,.E., Drake, N., "Monitoring Desertification and Land Degradation over Sub-Saharan Africa", Internationa Journal of Remote Sensing, 25(3),573-592, 2003.

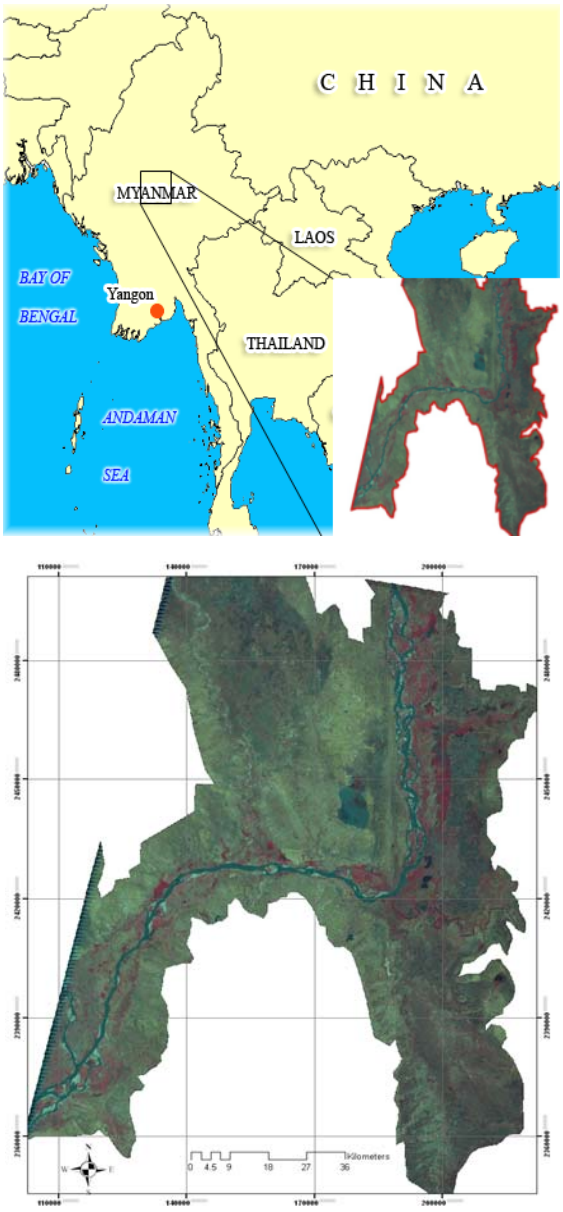

Figure1. Location of Study Area and False Color Composite of Study Area

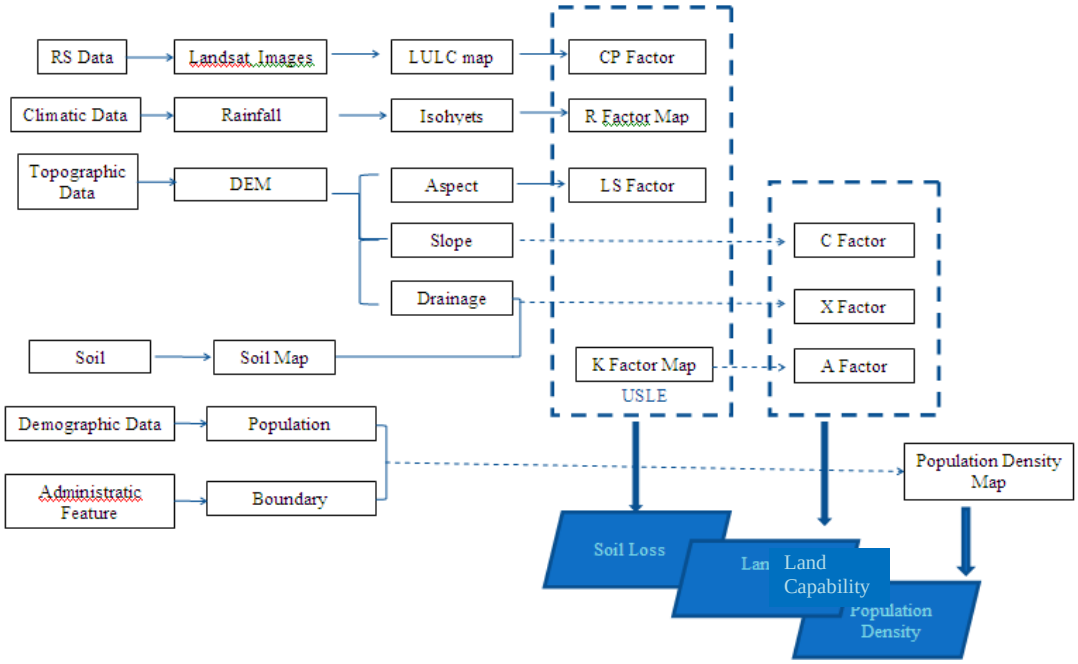

Figure2. Land degradation assessment methodology

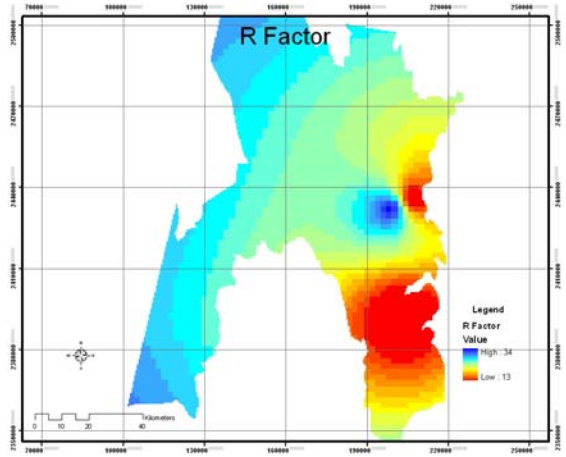
R Factor
Legend
R Factor
Value
High : 34
Low : 13

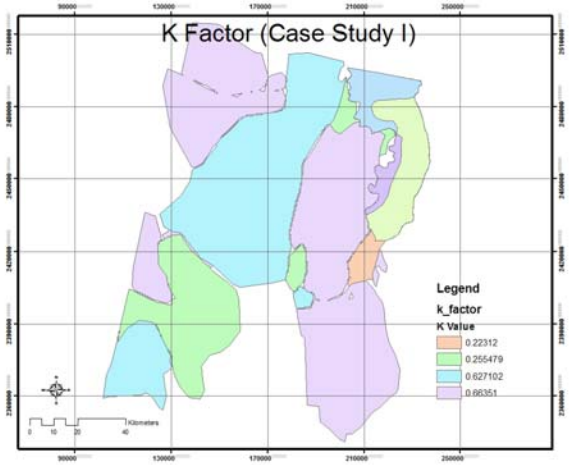
K Factor (Case Study I)
Legend
k_factor
K Value
0.22312
0.255479
0.627102
0.86351

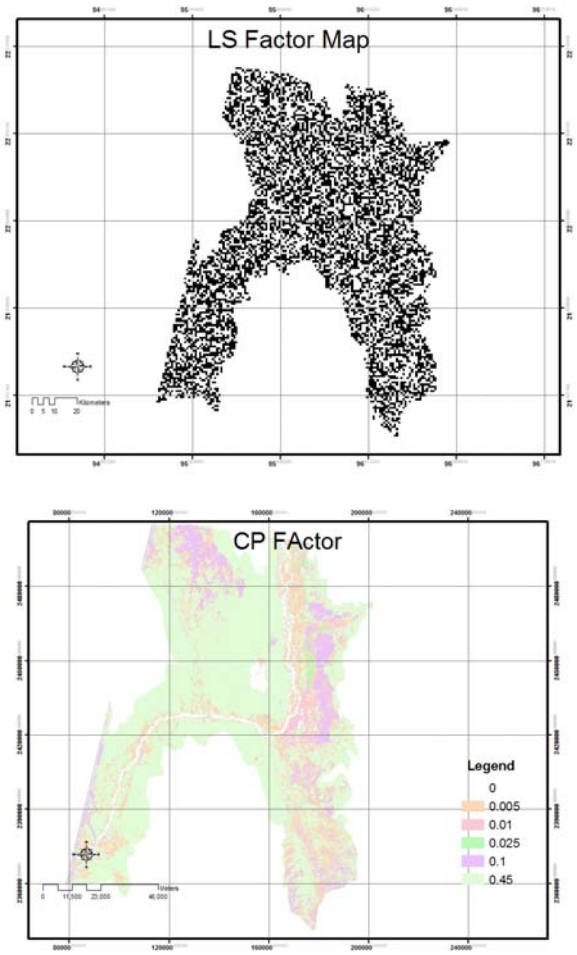

Figure3. Maps of Soil Erosion Parameters

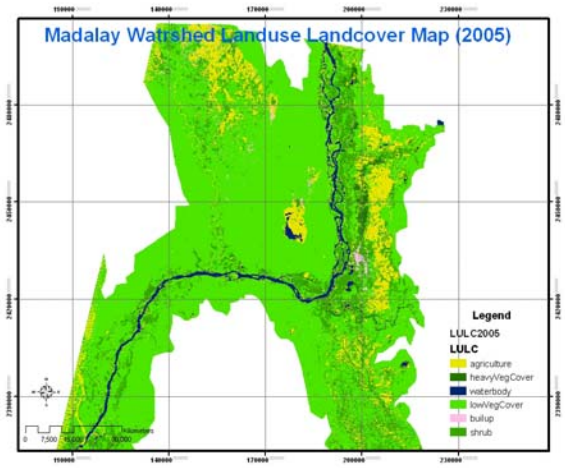
Madalay Watrshed Landuse Landcover Map (2005)
Legend
LULC2005
LULC
agriculture
heavyVegCover
waterbody
lowVegCover
builup
shrub

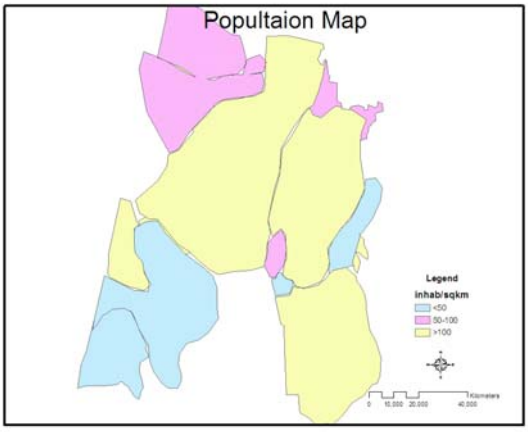
Populaion Map
Legend
inhab/sqkm
<50
50-100
>100

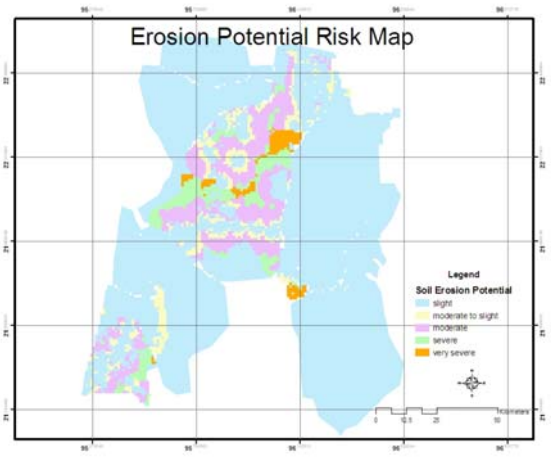
Erosion Potential Risk Map
Legend
Soil Erosion Potential
slight
moderate to slight
moderate
severe
very severe

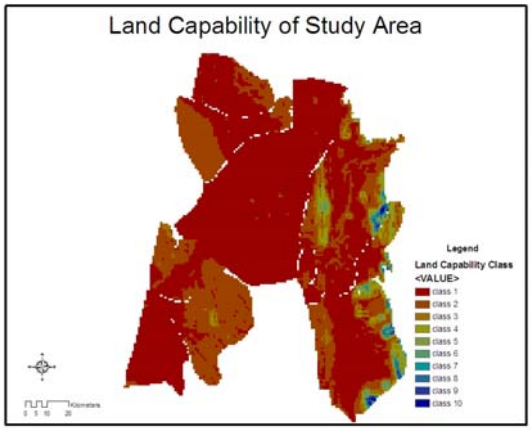

Figure4. Resultant maps of land degradation assessment

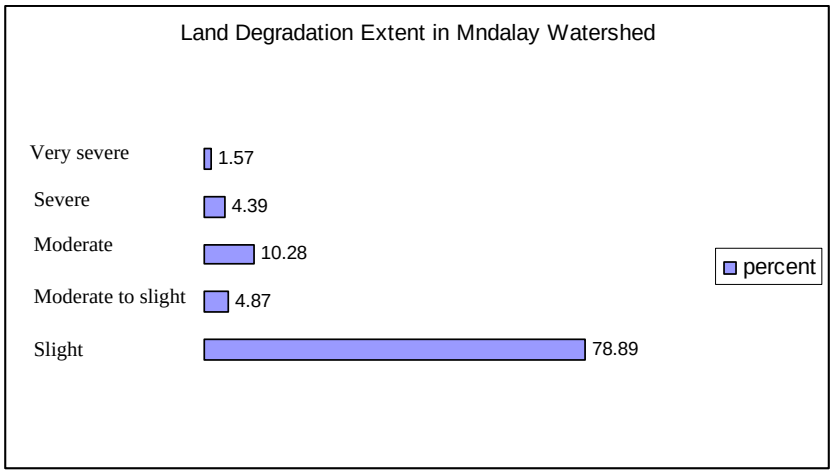

Figure5. Land degradation extent in Mandalay Watershed

A Process-based Model for Methane Emission from Flooded Rice Production

Kruamas Smakgahn
Faculty of Liberal Arts and Science, Kasetsart University Kamphaeng Saen Campus,
Kamphaeng Saen district, Nakornpathom province 73140 THAILAND

Abstract: In this study, the revised DeNitrification DeComposition (DNDC) model was validated against field observations for methane emission from irrigated rice fields in Thailand. The model was used for sensitivity test of important cultivation factors and soil properties in order to discuss feasible mitigation options. The revised DNDC model agreed well with observation. Possible option to reduce methane emission by controlling cultivation practices were suggested from simulated results. Organic carbon available in rice soil, particularly fresh residues from rice biomass, was considered as an important factor that affected simulated methane emissions. In addition, the content of electron acceptors in soil, especially reducible iron, is a major factor controlling methane emissions. Less available reducible iron in soil enhances methane emission. Management of rice cultivation including rice straw application is helpful for methane mitigation. In order to control the methane emission together with maintaining rice yield, the optimal rice cultivation practice needs to be considered and encouraged.

Keywords: greenhouse gas, methane, revised DNDC model, rice

INTRODUCTION

Methane (CH_4) is the second most important greenhouse gas after CO_2, which is 23 times more radioactively active than CO_2. The average global concentration of CH_4 in the atmosphere was 1,745 parts per billion by volume (ppbv) in 1998 (IPCC, 2001). It is estimated that 60 to 80 percent of current CH_4 emissions are the result of anthropogenic activities. Carbon isotope measurements indicate that roughly 20 percent of CH_4 methane emissions are from fossil fuel consumption, and an equal percentage is produced by natural wetlands, which will likely increase with rising temperatures and rising microbial action (IPCC, 1996). The concentration of CH_4 in the atmosphere has more than doubled over the last 200 years, and in particular, has increased by about 50% in the last 40 years. Rice paddy soils emitted approximately 15-20% of total methane emitted to the atmosphere. Anaerobic conditions do occur in wetland rice fields that are flooded for at least part of the rice-growing season. In irrigated rice fields the floodwater is controlled and usually maintained throughout the growing season. These conditions are favorable for both rice production and CH_4 production (Denier van der Gon, 1996). Methane production is a microbiological process by strict anaerobic bacteria (methanogens), which use compounds from the decay of organic matter as their food source and produce methane as a by-product.

The linkage among microbial processes and the related influence factors are relatively unexplored for Thai rice fields. Measurement of CH_4 emission from variation of location and variation of cultural practice are difficult. Moreover, estimated CH_4 fluxes from rice fields have a large range and depend on variability in soil flooding and sampling methodologies. As such, the model implementations are useful in order to predict the CH_4 pool and correlation among influencing factors on CH_4 emission.

In this study, the revised DNDC model was validated against field observations of CH_4 emission from irrigated rice fields in Thailand. The model was used for sensitivity test of important cultivation factors and soil properties in order to discuss feasible mitigation options.

MATERIALS AND METHODS

The revised DNDC model description

The DNDC model (Li, 1994) is a process oriented computer simulation model of soil carbon and nitrogen biogeochemistry. The DNDC model contains information on the fundamental biochemical and geochemical processes. This model was constructed to

Corresponding Author: Kruamas Smakgahn, Faculty of Liberal Arts and Science, Kasetsart University Kamphaeng Saen Campus, Kamphaeng Saen district, Nakornpathome province 73140 THAIALAND Phone: (+66 34) 281105-7 ext. 6781, Fax: (+66 34) 281057, E-mail: kruamas.s@ku.ac.th

include two components. The first component, consisting of the soil climate, crop growth and decomposition sub-models, predicts soil temperature, moisture, pH, Eh and substrate concentration profiles driven by ecological drivers (e.g., climate, soil, vegetation and anthropogenic activity). The second component, consisting of the nitrification, denitrification and fermentation sub-models, predicts NO, N_2O, N_2, CH_4 and NH_3 fluxes based on the modeled soil environmental factors. The revised DNDC model, (Fumoto et al., 2008) was modified from the DNDC model (Li, 1994) by focused on crop growth sub-model of Japanese rice production system. The crop growth sub-model was revised by incorporated an established model of crop carbon metabolism to explicitly describe photosynthesis, respiration and carbon (C) allocation with additional effects of N availability and atmospheric carbon dioxide (CO_2) concentration on photosynthesis. The crop carbon balance included carbon flux from root activity or root respiration to soil turnover and root exudation. Hence, CH_4 production is directly associated with the plant C metabolism. The CH_4 conductance to atmosphere was a function of the number of tiller and O_2 release from rice root is described CH_4 oxidation. The main idea of revision was to quantify production and consumption of electron donors (H_2 and DOC) as the substrates for CH_4 production and other reductive reactions. While only dissolve organic carbon (DOC) was play importance role as substrates for CH_4 production of current DNDC model. The revised DNDC model calculates production of electron donors due to anaerobic decomposition and root exudation, and the rates of reductive reactions are calculates by kinetic equations dependent on availabilities of electron donors and acceptors. Methane emission rate is function of conductance and density of rice tillers (Fumoto et al., 2008).

Sources: [a] Katoh et al. (1999a), ,[b] Katoh et al. (1999c), [c] Katoh et al. (1999b), [d] Yagi et al. (1994), [e] Total carbon, [f] Easily reducible Mn.

Field observation data for model simulations

There are five locations of study sites in this study, of which two sites are located in the central plains of Thailand, one site is in the Northeast, and two sites are in the North. The central plains sites were at Bangkhen (Bkn) and Suphanburi (Spr). Phrae and San Pa Thong (Spt) were used for representative Northern rice fields. Khon Kaen (Kkn) is located in the Northeast. The soil properties for the study sites are shown in Tables 1 and 2.

RESULTS AND DISCUSSION

Methane emissions predicted by the revised DNDC model from 5 fields in Thailand present on Figure 1. Large discrepancy of emission (> 70 % deviated from observation) predicted by revised DNDC model occurred in Bkn and Kkn sites, which was 80% and 60% over observation, respectively. Successfully simulation results in this study was found at Spr, and Phrae site, which shown only 3% and 17% under field observation, respectively. In addition, validated result at Spt site showed 17% over field observation. Large discrepancy between model and observed data under heavy clay at Bkn site was unexplainable by observed data. However, heavy clay texture may lead to low soil redox potential (Eh) during growing period and

maintain anaerobic condition suitable for methane production predicted by the revised DNDC model.

Site	Soil texture	Carbon[e] (%)	Total N (%)	Free Fe (mmol/ kg)	Mn_{ER}[f] (mmol/ kg)	SO_4^{2-} (mmol/ kg)
Bangkhen (Bkn)[a]	Heavy clay	0.188	0.2	100	0.9	7
Khon Kaen (Kkn)[b]	Sandy loam	0.049	0.002	12	0.2	–
Phrae[c]	Silty clay loam	0.089	0.009	57	3.3	0.7
San Pa Thong (Spt)[c]	Light clay	0.103	0.011	188	5.3	0.5
Suphanburi (Spr)[d]	Clay	1.30	0.010	183	0.5	0.6

Table 1: Soil properties at study sites

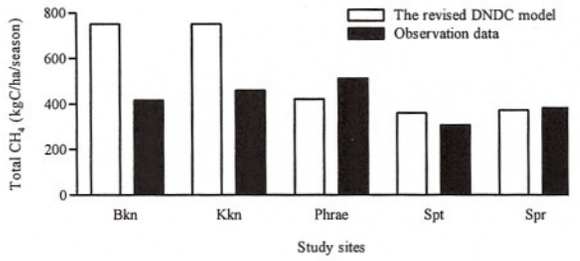

Fig. 1: Total seasonal methane emission from field observation and model validation at Bangkhen, Khon Kaen, Phrae, San Pha Thong, and Suphanburi sites

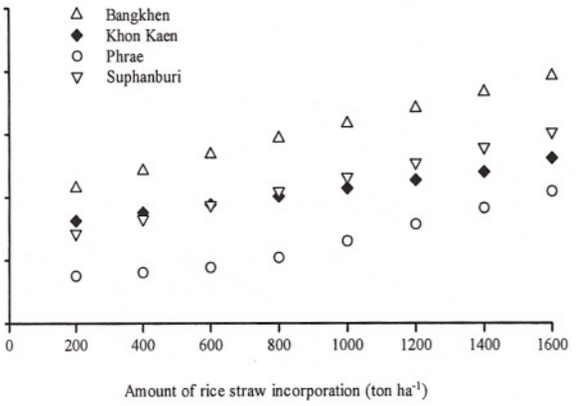

Fig. 2 Influence of rice straw incorporation on methane emission simulated by the revised DNDC model at Bangkhen, Khon Kaen, Phrae and Suphanburi sites

Straw incorporated into field strongly enhances CH_4 emission from field observation. The revised DNDC model agreed with observed data for all cases. The results agreed well with previous researches that CH_4 production increased in proportion to the rice straw application rate (Kimura *et al.* 1992; Wang *et al.* 1992; Lindua *et al.* 1993; Nagroho *et al.* 1994a, Jermsawatdipong *et al.* 1994; and Kongchum *et al.* 2006) and CH_4 emissions rate increased linearly with the amount of rice straw supplementation (Yang and Chang 1998) as shown on Figure 2. Sensitivity of the model to rice straw application was tested by varying the application rate over the range of 200-1600 kg C/ha at the sites of Bkn, Kkn, Phrae, and Spr site (Fig. 2). Simulated seasonal CH_4 emissions monotonously increased with straw application rate, and increase in straw application rate from 200 to 1200 kg C/ha enhanced CH_4 emission by approximately 166 – 202 kg C/ha from major rice at Phrae, Spr and Kkn site, respectively. These results imply that about 40% of the rice straw applied was decomposed during the next rice season at these sites. From these results, it is also clear that revised DNDC model is so sensitive to rice straw application rate that this parameter has to be quantified appropriately for reliable prediction of CH_4 emission.

The observed CH_4 emissions were negatively correlated with the free Fe concentration (Fig. 4), indicating that soil Fe^{3+} is a major inhibitory factor for CH_4 emissions. As the level of reducible soil Fe^{3+} increased, the simulated seasonal CH_4 emissions decreased monotonically. The simulation in this study agree with the results of soil incubation tests, in which CH_4 production was almost completely suppressed during Fe^{+3} reduction (Van Bodegom and Stams, 1999), and in field trials, in which CH_4 production was inhibited by the addition of Fe^{3+} (Chidthaisong and Conrad, 2000).

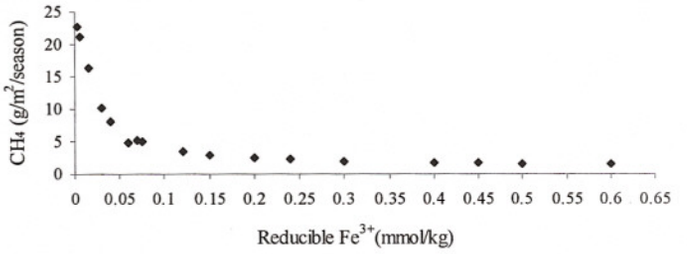

Fig. 3 Influence of reducible Fe on seasonal methane emission

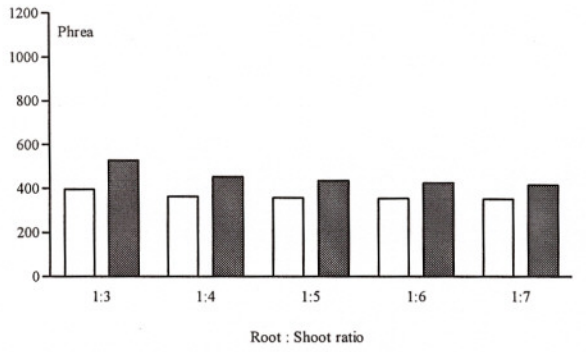

Fig. 4 Influence of root:shoot ratio on seasonal methane emission

Regarding the effects of rice root on CH_4 emission, it has been previously reported that (1) increase in biomass usually results in increase in CH_4 emission (Bronson *et al.* 1997, Singh *et al.* 1997, Denier Van Der Gon 2002, Yagi and Minami, 1994, Mitra *et al,* 1999), and (2) rice plant provides labile C through root exudates and contributes to CH_4 production (Cheng 1999, Li *et al.* 2004; Aulakh *et al.* 2001b, Mitra *et al.* 2005). Sensitivity of the model to root biomass was tested by running the model at the sites of Phrae, varying the root: shoot ratio between 1:7 and 1:3 (Fig. 4). Clearly, larger root biomass (higher root: shoot ratio) enhanced simulated CH_4 emission: when root: shoot ratio was raised from 1:5 to 1:3, simulated seasonal CH_4 emission was increased by 100-200 kg C/ha.

CONCLUSION

The revised DNDC model shows potential to estimate the variations in CH_4 emissions due to factors such as concentrations of soil Fe^{3+}. The predicted emissions still contain considerable uncertainties that result from a number of influential factors, such as the estimated concentration of reducible soil Fe^{3+}, quantification of the rate of straw incorporation, and calculation of rice root biomass. The results also showed the potential of the revised DNDC model to evaluate possible mitigation options for CH_4 emissions from rice fields, such as reducing the amount of rice straw incorporated into the soil and selecting rice varieties with low production of root exudates. By reducing the uncertainties in the model input factors, the revised DNDC model will become an increasingly useful tool to evaluate and design practical mitigation options for rice fields in Thailand.

ACKNOWLEDGEMENTS

The author would like to thanks Prof. C.S. Li for his guidance. Thank you Dr. Tamon Fumoto and Dr. Kazuyuki Yagi for the revised DNDC model, valuable suggestion and comment on model simulation. Also thank Prof. Shu Fukai for providing valuable data on Thai rice plants. The author thanks Dr. Naruo Matsumoto, Dr. Niwat Nabheerong, and Mr. Chitnucha Buddhaboon for their suggestions on the values of certain parameters used in this simulation.

REFERENCES

1. Intergovernmental Panel on Climate Change, 2001, Climate Change 2001: The Scientific Basis, Cambridge University Press, New York.
2. Intergovernmental Panel on Climate Change, 1996, IPCC guidelines for national greenhouse inventories, IPCC greenhouse gas inventory reference manual. Vol. 3.
3. Denier van der Gon, H. A. C., 1996, Methane Emission from Wetland Rice Fields, Doctoral Thesis, Wageningen Agriculture University, Wageningen, 182 p.
4. Li, C. S., Frolking, S., and Harriss, R. 1994, Modeling carbon biogeochemistry in agricultural soils, Global Biogeochemical Cycles., 8 (3), 237-254.
5. Fumoto, T., Kobayashi, K., Li, C. S., Yagi. K., and Hasegawa, T., 2008, Revising a process-based biogeochemistry model (DNDC) to simulate methane emission from rice paddy fields under various residue managements and fertilizer regimes. Global Change Biology. 4, pp. 382-402.
6. Katoh, K., Chairoj, P., Yagi, K., Tsuruta, H., Minami, K., and Cholitkul, W., 1999a, Diel and seasonal variations of methane flux from Bang Khen paddy field in Thailand. JIRCAS Journal., 7, pp. 65-75.
7. Katoh, K., Chairoj, P., Yagi, K., Tsuruta, H., Minami, K., and Cholitkul, W., 1999b, Methane emission from paddy fields in Northern Thailand. JIRCAS Journal., 7, pp. 77-85.
8. Katoh, K., Chairoj, P., Yagi, K., Tsuruta, H., Minami, K., and Cholitkul, W., 1999c, Methane emission from paddy fields in Northeast Thailand. JIRCASJournal., 7, pp. 87-96.

9. Yagi, K., and Minami, M., 1994, Effect of organic matter application on methane emission from some Japanese paddy fields. Soil Science Plant Nutrition., 40, pp. 29-37.
10. Kimura, M., Miura, Y., Watanabe, A., Murase, J., and Kuwatsuka, S., 1992, Methane production and its fate in paddy fields. I. Effects of rice straw application and percolation rate on the leaching of methane and other soil components into the subsoil. Soil Sci. Plant Nutr., **38,** 665-672
11. Wang, Z. P., Delaune, R. D., Lindau, C. W., and Patrick, W. H. Jr., 1992, Methane Production from anaerobic soil amended with rice straw and nitrogen fertilizers. Fertilizer Research., 33, 115-121.
12. Lindau, C. W., Bollich, P. K., DeLaune, R. D., Mosier, A. R., and Bronson, K. F., 1993, Methane mitigation in flooded Louisiana rice fields. Biology Fertilizer Soils., 15: 174-178.
13. Nagroho, S. G., Lumbanraja, J., Suprpto, H., Sunyoti, W. S., Ardjasa, H., and Kimura, M., 1994, Methane emission from an Indonesian paddy field subjected to several fertilizer Treatments. Soil Science and Plant Nutrition., 40 (2), 275-281.
14. Jermsawatdipong, P., Murase, J., Prabuddham, P., Hasathon, Y., Khomthong, N., and Kimura, M., 1994, Methane emission from plots with differences in fertilizer application in Thai paddy fields. Soil Science Plant Nutrition., 191, 233-240.
15. Kongchum, M., Bollich, P. K., Hudnall, W. H., DeLaune, R. D., and Lindau, C. W., 2006, Decreasing methane emission of rice by better crop management. Agron. Sustain. Dev., 26, 45-54.
16. Yang, S. S., and Change, H. L., 1998, Effect of environmental condition on methane production and emission from paddy soil. Agriculture, Ecosystems and Environment., 69, 69-80.
17. Van Bodegom, P. M., and Stams, A. J. M, 1999, Effects of alternative electron acceptors and temperature on methanogenesis in rice paddy soils. Chemosphere., 39, 167-198
18. Chidthaisong, A., and Conrad, R., 2000, Turnover of glucose and acetate coupled to reduction of nitrate ferric iron and sulfate and to methanogenesis in anoxic rice field soil. FEMS Microbiology Ecology., 31, 73-86.
19. Bronson, K. F., Neue, H. U., Singh, U., and Abao, E. B., 1997, Automated chamber measurements of methane and nitrous oxide flux in a flooded rice soil: I. Residue, nitrogen, and water management. Soil Society American Journal., 6 (3), 981-987.
20. Singh, S., Kumar, S., Jain, M. C., 1997, Methane emission from two Indian soils planted with different rice cultivars. Biol. Fertil. Soil., 25, 285-289.
21. Denier van der Gon, H. A. C., Kropff, M. J., van Breemen, N., Wassmann, R., Lantin, R. S., Aduan, E., Corton, T. M., and van Laar, H. H., 2002, Optimizing grain yields reduces CH_4 emissions from rice paddy fields, Proceeding of the nation academy sciences of the United States of America. , 99, 12021-12024.
22. Mitra, S., Jain, M. C., Kumar, S., Bandyopadhyay, S. K., and Kalra, N., 1999, Effect of rice cultivars on methane emission. Ecosystems and Environment., 73, 177-183.
23. Cheng, W., 1999, Rhizosphere feedbacks in elevated CO_2. Tree Physicology., 19, 313-320.
24. Li, C. S., Mosier, A., Wassmann, R., Cai, Z., Zheng, X., Huang, Y., Tsuruta, H., Boonjawat, J., and Lantin, R., 2004, Modeling greenhouse gas emissions from rice-based production system: Sensitivity and upscaling. Global Biogeochemical Cycles., 18, GB1043, doi:1029/2003GB002045, 1-19.
25. Aulakh, M. S., Wassmann, R., Bueno, C., and Rennenberg, H., 2001, Impact of root exudates of different cultivars and plant development stage of rice (*Oryza sativa L.*) on methane production in a paddy soil. Plant soil., 230, 77-86.
26. Mitra, S., Aulakh, M. S., Wassmann, R., and Olk, D. C., 2005, Triggering of methane production in rice soils by root exudates: Effects of soil properties and crop management. Soil SCL. SOC. AM. J., 69, 563-570.

Application of Geostatistical Analysis in Snow Depth and Density in Orazan Watershed

Mahdi Vafakhah[1] Mohsen Mohseni Saravi[2] Mohamad Mahdavi[3] Seyyed Kazem Alavipanah[4]
[1] Ph.D.Student, Natural Resources Department, Tehran University, Email:Vafakhah@modares.ac.ir.
[2] Associate Professor and Professor, respectively, Natural Resources Department, Tehran University.
[3] Professor, Natural Resources Department, Tehran University.
[4] Associate Professor, Geographical Department, Tehran University.

Abstract: Geostatistical analysis was applied for snow depth and density estimation. This research was conducted in Orazan sub-basin located in Taleghan watershed which comprises 2706 km^2 in area. Field sampling was performed based on random-systematic method with random start in different heights and the distance between samples was equally 100 m. Depth and density of snow was measured in every point. The experimental variogram was plotted by using 98 field sampling points.The experimental variogram of snow depth revealed more than 80% sill, implying strong spatial auto-correlation between samples but the experimental variogram of snow density revealed more than 80% nugget effect, implying weak spatial auto-correlation between samples. Estimation of snow depth and density was performed by using ordinary kriging and spherical model. Cross validation results indicated that kriging could make a precise estimation of snow depth and density due to low variability of snow depth and density and the strong spatial structure of snow depth.

Keywords: Geostatistical analysis, snow depth, snow density, variogram, Talaghan.

Introduction

The snow depth and density measurements provide a basis for snow conditions avalanche forecasting, hydrological snowmelt runoff, long-term changes in snow depth and density (Erxleben *et al.*, 2002). Collection of snow basic data is a hard and expensive task in the Iran because of both vast mountainous areas and snowy and financial difficulty and time limitation (Sharifi *et al.*, 2008). One way to approach this problem is to asses the performance of spatial interpolation techniques in estimating snow depth and density. One of the spatial interpolation techniques is Kriging procedure on base of geostatistic analysis that has been established based on spatial change approach. The first application of geostatistics happened in mine exploitation and extended to other branches of earth science. These models can be used to simulate hydrological processes at a daily or monthly time steps and the interpolation of cilmatological variables such as rainfall, temperature, evapotranspiration and snow. There has been a range of studies which compared different algorithms for deriving estimates of precipitation from point data (for example, Bastin et al.(1984), Tabios and Salas (1985), Hevesi et al.(1992a,b), Hutchinson (1995 and 1998a,b), Hay et al.(1998), Prudhomme and Reed (1999), Goovaerts (2000),Gomez-Hernandes et al. (2001), Deraisme et al. (2001), and Hofierka et al. (2002)). Application of geostatistic techniques in hydrological sciences is a useful approach to avoid such errors and increase of calculation accuracy as well. In classic statistics samples taken from a population lack the spatial properties. Therefore the calculated values of a parameter in a homogenate sample do not include any information of the same parameter in another sample with a defined distance. Geostatistics consider the value as well as location of the sample. Then it is possible to analyze value and location of the samples together. To achieve this purpose it is necessary to relate spatial properties (distance, direction) of different samples using mathematical formula called spatial structure.

Marchand and Killingtveit (2001) analyses the relation between spatial snow distribution and terrain characteristics including height, aspect, slope and land form for near 36 km^2 study site. The linear regression and nonlinear regression models could explain 15.6% and 20.1% of the observed variability in spatial snow depth distribution. Erxleben *et al.* (2002) evaluate to estimate snow water equivalent for three 1 km^2 study sites in the Colorado Rocky Mountains. Each study site is representative of different topographic and vegetative characteristics. The tree-based models provided the most accurate estimates for all study sites, explaining 18-30% of the observed variability in snow depth. Kriging of the regression tree residuals did not substantially improve the models. Molotch *et al.* (2005) estimate the spatial distribution of snow water equivalent in an alpine basin of 19.1 km^2 in area using binary regression tree models. The binary regression tree models provided 37% of the observed variability for April with mean snow depth of 255 cm. Erickson *et al.* (2005) use the persistence of topographic controls on the spatial distribution of snow depth using binary

Corresponding Author: Mahdi Vafakhah, Ph.D.Student, Natural Resources Department, Tehran University, Email:Vafakhah@modares.ac.ir.

regression tree model in Rugged Mountain, Colorado. The binary regression tree and nonlinear regression integration had better than the binary regression tree. Sharifi *et al.* (2007) assess the spatial distribution of snow depth using Kriging and linear regression in Samsami watershed, Iran. The linear regression and Kriging provide 67% and 62% of the observed variability of snow depth using height, aspect and wind index factors, respectively. The aim of this study evaluates the performance of Kriging for snow depth and density predict in Orazan watershed.

Materials and Methods

Study Area

Orazan is one of the sub-basins of Taleghan watershed in north-central part of Iran between 36˚06´ 25˝ to 36˚10´ 45˝ N latitude and 50˚52´ 05˝ to 50˚54´ 25˝ E longitude and is chosen as study area. This part of Taleghan watershed is mainly a mountainous area and it maximum, minimum and mean height is 3280, 1870 and 2506 meters, respectively. It covers an area of 2706 ha with annual average precipitation of 690 mm and temperature of 3.06$^{\circ C}$. The majority of precipitation has a Mediterranean regime. Usually, most of the precipitation in Orazan sub-basin occurs in February, March, and April with high intensity and in short periods. The region climate is semi-humid cold and upper heights by using De Martonne Modified and Emberger methods, respectively (Irrigation and Reclamation Department, 1993) (Fig. 1).

Figure 1 Study area (Orazan sub-basin) on the Iran map (■)

Methods

Field Methods

Ground observations of snow depth and density were collected during 5–7 February 2008 in 98 locations. Depth and density measurements were made on a relatively evenly spaced grid pattern across the Orazan sub-basin, with measurement locations separated by approximately 100m. Snow depth measurements were made using aluminium probes graduated in 5cm increments. Snow density measurements were derived from snow pits in which samples were taken at 10 cm vertical intravels over the entire snow pit depth using a 1000 cc stain less steel cutter. At each sampling location three depth and density measurements were collected 5 m apart along transects oriented in the direction of travel with the centre measurement recorded using global positioning systems. The three measurements were averaged to obtain snow depth and density values at the sampling location.

Geostatitical Analysis

Geostatistical prediction includes two stages which is first identification and modeling of spatial structure. At this stage continuity, homogeneity and spatial structure of a given variable is studied using variogram. Second stage is geostatistical estimation using Kriging technique which depends on the properties of the fitted variogram which affects all stages of the process.

Variogram analysis

Variogram method is a suitable technique for estimating spatial variability of a variable. Calculation of variogram graph is one of essential stages in geostatistics which is defined as follow:

$$\gamma(h) = \frac{2}{2n(h)} \sum_{i=1}^{n(h)} [Z(xi) - Z(xi+h)]^2$$

(1)

where:

γ(h): value of variogram for pair points with distance h

n(h): number of pair points with distance h

Z(xi): observed value of vaiable xi

Z(xi+h): observed value of the variable with distance h from xi.

For variogram plotting it is necessary to compute γ (h) for different values of h and then to plot the values for different distances of h. In other words variogram is the variance of different points with distance h. The obtained variograph of measured samples is called experimental variogram which is a vector value that is a dependent of distance and direction.

The variogram properties include threshold (sill=C_0). The threshold is the maximum value of variogram which is spatial variance of the variable. The lowest value of variogram includes partial effect which shows variance of errors of measurements. The effective distance demonstrates the distance. That variogram has the highest value. Instead of variance, covariance shows the similarity of variables. Since arithmetic summation of similarity and dissimilarity is constant then it is possible to replace it with the average difference of points of distance h. The relation between variogram and co-variogram is defined as:

$$\sigma^2 = \gamma(h) + c(h) \quad (2)$$

Where:

σ^2 = Threshold

$\gamma(h)$ = Variogram value

$c(h)$ = Co-variance value

Kriging

Kriging is a prediction that considers values of a variable in unsampled points as a linear composition of the values of surrounding points. Considering the values of variable Z in n measured points as follow:

Z= (z(x,), Z (x2)….Z (xn))

(3) Estimation of Z in point X_0 using kriging estimation is defined as:

$$Z^*(x_0) = \sum_{i=1}^{n} \lambda_i z(x_i)$$

(4) The most important part of Kriging is statistical weights assigned to λ_i .To avoid bias of estimation, the weight should be determined in a way that summation is equal to one $(\sum_{i=1}^{n} \lambda_i = 1)$ and the variance of estimates should be minimized as:

$$\text{var}[Z^*(x_0)] = E[(Z^*(x_0) - Z(x_0))^2] = \text{Min} \quad (5)$$

Accuracy Assessment

The Geostatistical analyst provided an indication of which model produces minimal prediction error though cross-validation. Cross-validation uses all of the data to estimate trend and autocorrelation models, and then removes each data location, one at a time, and predicts the associated data value(Johnston *et al.*, 2001). The prediction is based on four measures of accuracy: the mean bias error (MBA), the mean absolute error(MAE), and the mean squared standardized deviation ratio(MSDR):

$$MAE = \frac{1}{n}\sum_{i=1}^{n}\left|Z^{*}{}_{(x_i)} - Z_{(x_i)}\right| \quad (6)$$

$$MBE = \frac{1}{n}\sum_{i=1}^{n}\left(Z^{*}{}_{(x_i)} - Z_{(x_i)}\right) \quad (7)$$

$$MSDR = \frac{1}{n}\sum_{i=1}^{n}\left(\frac{Z^{*}{}_{(x_i)} - Z_{(x_i)}}{\sigma(x)}\right)^2 \quad (8)$$

Where: n is the number of observations, $Z^{*}{}_{(x_i)}$ the predict value, $Z_{(x_i)}$ the observed value, i the counter for the individual observed and predicted values and $\sigma(x)$ the root mean squared error (RMSE):

$$RMSE = \sqrt{\frac{1}{n}\sum_{i=1}^{n}\left(Z^{*}_{(x_i)} - Z_{(x_i)}\right)^2} \quad (9)$$

Since the MBE reveals the tendency for systematic overestimation or underestimation, it should be zero in the ideal case. Caution must be exercised in the interpretation of bias because it is possible for large, compensating sub-regional biases to produce a mean zero estimate. Small MAE values indicate a method with few errors, overall. The MAE measure, however, does not reveal the magnitude of error that might occur at any point. For this reason, we chose to calculate the RMSE measure, which is a measure of the root of the sum of the squared residuals. MSDR shows ratio between experimental and theoretical variance. It should be one in the ideal case.

Results

The normality test was examined for the data using Colmogorov-Smirnov test. Snow depth data was not normal neither was snow density because logarithm of the snow depth data was used to avoid skewness. Table 1 presents a summary of statistical characteristics of data.

Table 1. Statistical characteristics of field survey data(after transformation)

Parameter	Mean	Variance	Minimum	Maximum	Range
Snow Depth(cm)	24.19	13.27	11	73	62
Snow Density(gr/cm^3)	0.803	0.147	0.51	1.05	0.54

Since the first step for geostatistical application for a set of data is variogram analysis then the results of variogram analysis in the study area were calculated (Table 2).

Table 2. The properties of suitable variogram model of variables

Variable	Model	Nugget	Sill	Range Parameter	Effective Range
Snow depth	Spherical	0.0010	0.05	186	186
Snow density	Spherical	0.0103	0.0485	7368	7368
Variable	$\frac{C}{Co+C}$	r^2	RSS	Lag (m)	
Snow depth	0.998	0.022	0.0529	100	
Snow density	0.788	0.13	0.014	100	

Theoretical variograms were estimated from the snow depth and density data (Fig. 2 and 3).

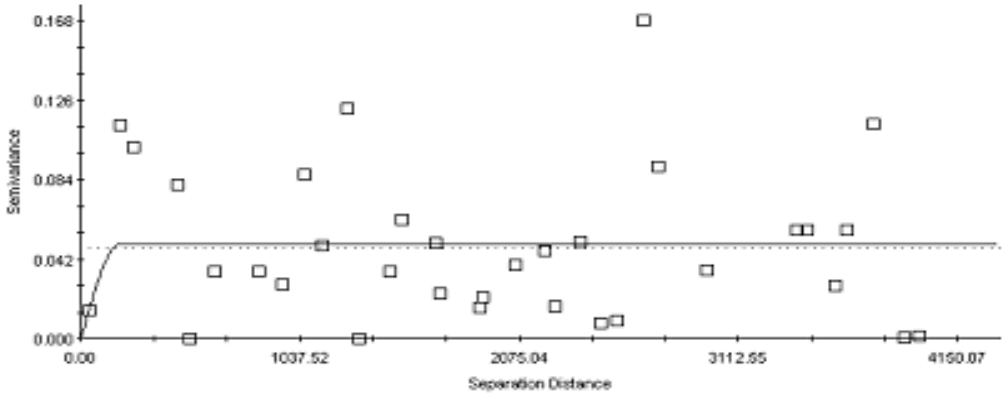

Fig 2.Theoretical variogram of snow depth

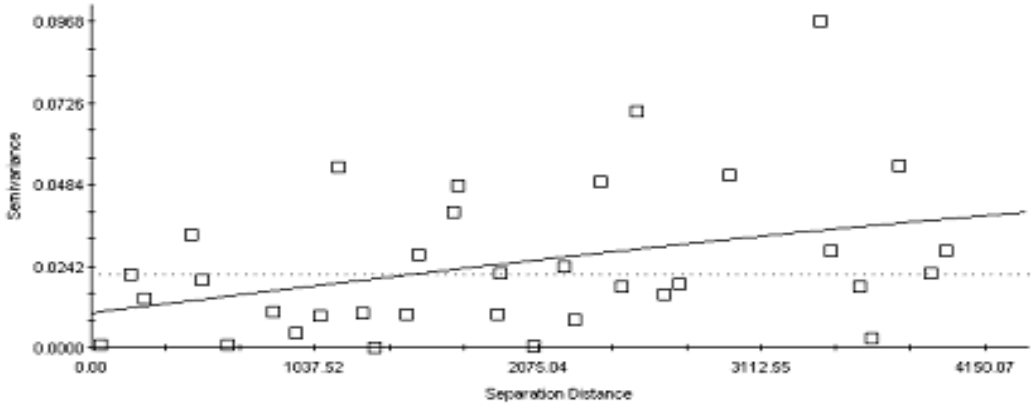

Fig 3.Theoretical variogram of snow density

The calculation of variogram in different directions shows that there are not any geometric or zonal anisotropy. In this reason, the variogram is multi-directions. Based on Table 2 and Figures 3 and 4 about snow depth, nugget (0.0010) is very low in comparison with sill (0.05), this means that the space structure of data is very strong. Also, a high part from total variance amount (207.67) is explained by variogram and its low part (20%) is defined by random and nonstructural part but due to low nugget effect amount, there is the strong space structure among data to a low distance (186 m). About snow density, the nugget of variogram(0.0103) in comparison with the sill(0.0485) is very high. This means that the space structure of data is very weak. Despite high nugget effect (7368 m), due to a high sill amount, a low part from total variance(0.023) is explained by variogram and its high part(79%) is defined by random and nonstructural part.The ordinary kriging was done using ESRI's Arc/GIS (Fig. 4 and 5).

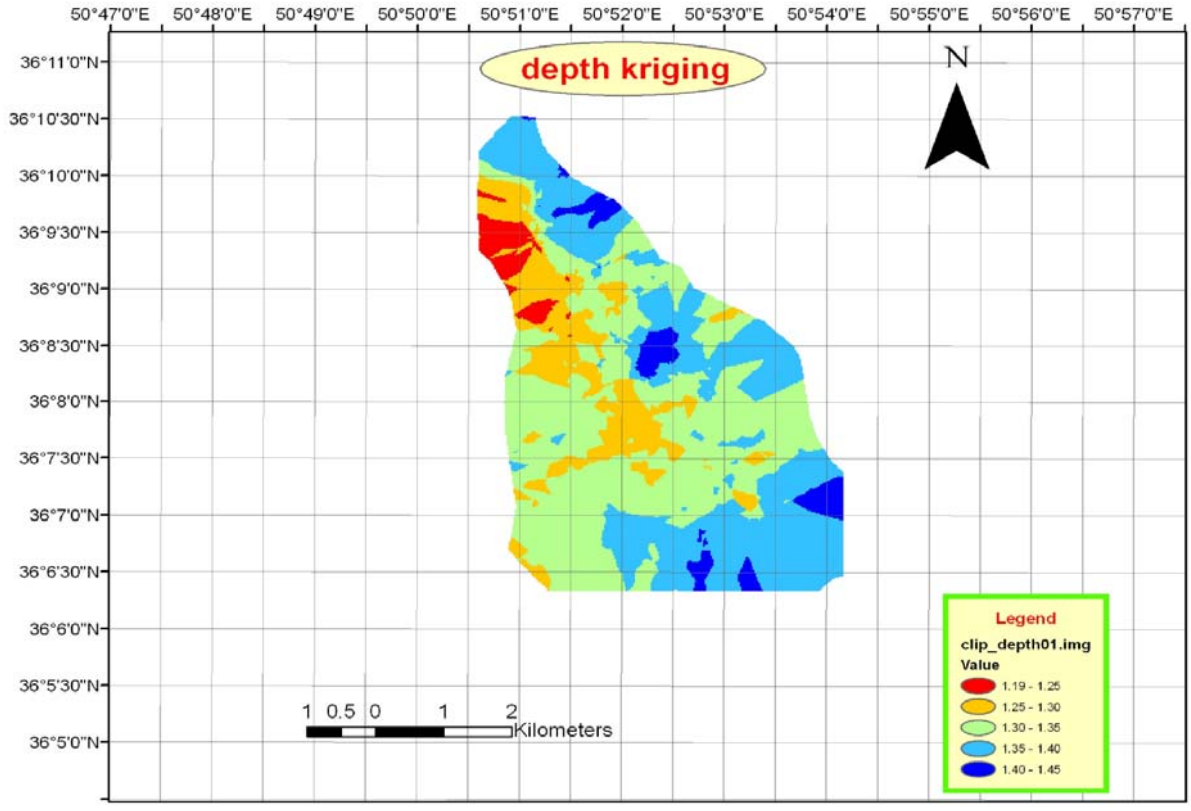

Fig.4. Kriging map of snow depth

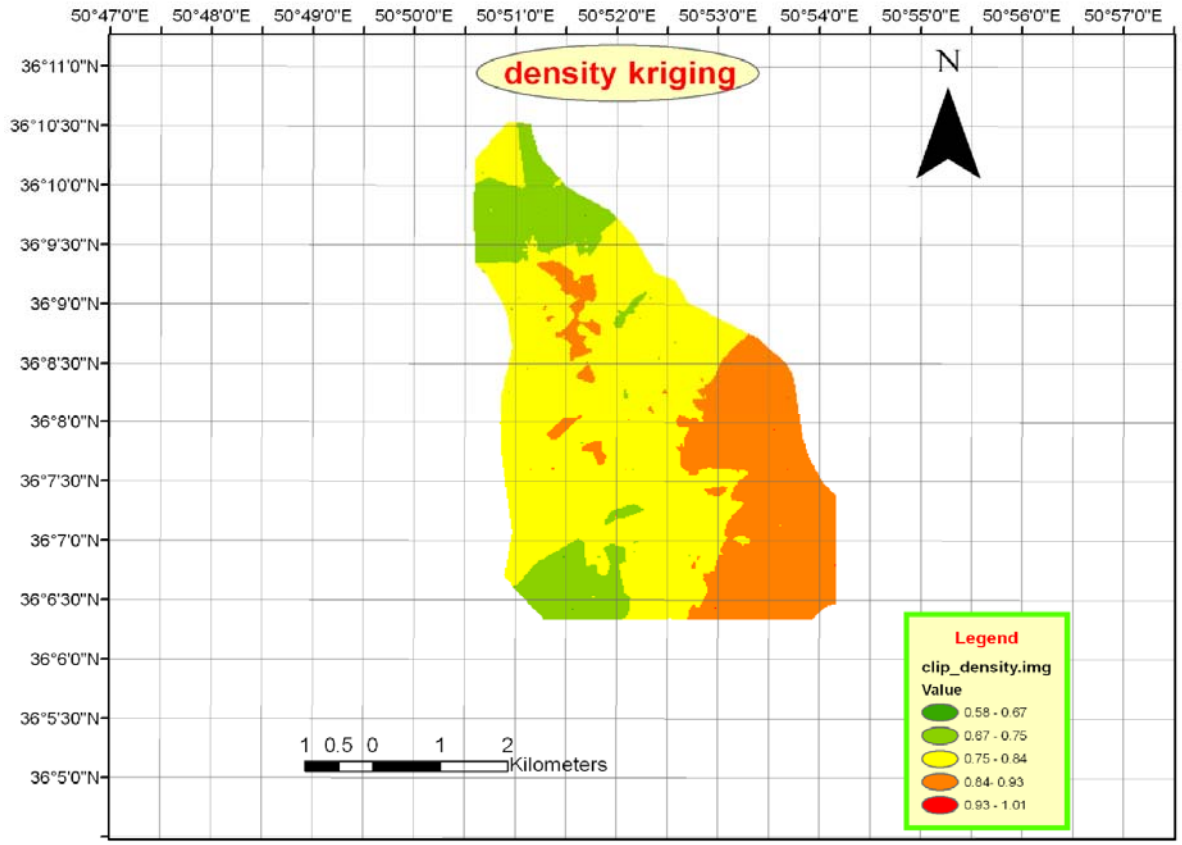

Fig.5. Kriging map of snow density

Table 3.Error statistics

Parameter	MAE	MBE	MSDR	RMSE
Snow depth	0.143	-0.01831	1	0.22
Snow density	0.1005	-0.0015	1	0.12

Based on table 3, MAE and MBE are near zero, it indicates that Kriging can estimate snow depth and density accurately. Also, MSDR is one; it indicates that there are not differences between Kriging variance and variance estimation from theoretical variogram.

Conclusion and discussion

All of information estimated by Kriging interpolation in geostatistical analysis depends on overall structure of theoretical variogram and particularly nugget effect amount in variogram. The higher the nugget effect, the lower the potential of prediction by variogram model. In variogram related to snow depth, the nugget effect is low due to strong space structure among snow depth amount in different distances. Also, effect range has a low amount that it is indictor on a strong space structure in shortage distance and because of this geostatistical analysis has been made based on spatial continuous changes of environmental parameters. This characteristic shows homogeneity in snow depth collection data (The low amount of nugget effect shows this subject). The low of nugget effect in the estimating variogram, can be due to low changes of snow depth in shortage distance. In variogram related to snow density, nugget effect is high due to weak space structure among snow density amount in different distances. This characteristic shows that there are no homogeneity among snow density data in different distances (The high amount of nugget effect shows this subject). The results of cross validation showed that Kriging has high capability in snow depth and density estimation in region because of low amount of effect nugget in snow depth variogram and high amount of effective range in snow density variogram.
The topographic factors include height, aspect, angle of slope and land form and velocity and direction of wind and also vehicle roads are effective factors on random distribution of snow depth and density in study region. Low amount of effective range related to snow depth and high amount of nugget effect related to snow density show the severe variability of these parameters in high distance. This variability of data is hidden in each kind of anisotropy. It seems that the field samples collection method based on a region homogeneity and classification of suitable data using satellite images and photoarial is caused isotropy among data both spatial data variability decrease and suitable of geostatistical analysis increase. Totally, geostatistical analysis in both local scales and limit to effective range data as well as when region is homogenous, will has the better results than ordinary statistic(e.g. multiple regression). Also, the selection of suitable of data effect on application of this method.

References

1. Bastin, G., Lorent, B., Duque, C. and Gevers, M., 1984. Optimal estimation of the average rainfall and optimal selection of raingauge locations. Water Resources Research, 20, 463–470.
2. Deraisme, J., Humbert, J., Drogue, G. and Freslon, N., 2001. Geostatistical interpolation of rainfall in mountainous areas,in: Monestiez, P., Allard, D..
3. Erxleben, J., Elder, K. , Davis, R., 2002, Comparison of spatial interpolation methods for estimating snow distribution in Colorado Rocky Mountains, Hydrological Processes, 16:3627-3649.
4. Erickson, T.A., Williams, M.W. and Winstral, A., 2005, Persistence of topographic controls on the spatial distribution of snow in Rugged mountain, Colorado, United States, Water Resources Research, 41:1-17.
5. Froidevaux, R. (Eds.), GeoENVIII: Geostatistics for Environmental Applications.Kluwer Academic Publishers, Dordrecht, pp. 57–66.
6. Go`mez-Herna`ndez, J., Cassiraga, E., Guardiola-Albert, C. and A´ lvarez Rodri´guez, J., 2001. Incorporating information from a digital elevation model for improving the areal estimation of rainfall,in: Monestiez, P., Allard, D., Froidevaux, R. (Eds.), GeoENV III: Geostatistics for Environmental Applications. Kluwer Academic Publishers, Dordrecht, pp. 67–78.
7. Goovaerts, P., 1997, Geostatistics for Natural Resources Evaluation, Oxford University Press, New-York, 483p.
8. Goovaerts, P., 2000. Geostatistical approaches for incorporating elevation into the spatial interpolation of rainfall. Journal of Hydrology, 228:113–129.
9. Hay, L., Viger, R. and McCabe, G., 1998. Precipitation interpolation in mountainous regions using multiple linear regression, in: Kovar, K., Tappeiner, U., Peters, N.E., Craig, R.G. (Eds.), Hydrology, Water Resources and Ecology in Headwaters. Proceedings of the Headwater 1998 Conference, Mean/Merano, Italy, April IAHS Publication, 248pp.
10. Hevesi, J.A., Istok, J.D. and Flint, A.L., 1992a. Precipitation estimation in mountainous terrain using multivariate geostatistics. Part I: structural analysis. Journal of Applied Meteorology, 31, 661–676.
11. Hevesi, J.A., Flint, A.L. and Istok, J.D., 1992b. Precipitation estimation in mountainous terrain using multivariate geostatistics. Part II: isohyetal maps. Journal of Applied Meteorology, 31, 677–688.
12. Hofierka, J., Parajka, J., Mitasova, M., Mitas, L., 2002. Multivariate interpolation of precipitation using regularized spline with tension. Transactions in GIS, 6, 135–150.

13. Hutchinson, M.F., 1998a. Interpolation of rainfall data with thin plate smoothing splines—Part I: two dimensional smoothing of data with short range correlation. Journal of Geographic Information and Decision Analysis, 2, 139–151. http://www.geodec.org/gida_4.htm.
14. Hutchinson, M.F., 1998b. Interpolation of rainfall data with thin plate smoothing splines—Part II: analysis of topographic dependence. Journal of Geographic Information and Decision Analysis, 2, 152–167 http://www.geodec.org/gida_4.htm.
15. Irrigation and Reclamation Department (Agriculture Faculty at Tehran University), 1994, Watershed Management Studies in Taleghan Watershed(In Persian), Regional Water Organization (Branch of Tehran Province).
16. Marchand, W. D. and Killingtveit, A., 2001, Analyses of the Relation between Spatial Snow Distribution and Terrain Characteristics, 58th Eastern Snow Conference Ottawa, Ontario, Canada.
17. Molotch, N.P., Colee, M.T., Bales, R.C. and Dozier, J., 2005, Estimating the spatial distribution of snow water equivalent in an alpine basin using binary regression tree models: the impact of digital elevation data independent variable selection, Hydrological Processes, 19:1459-1479.
18. Najafi, M., Shikhvand, J. and Pourhamat, J., 2004, Snowmelt runoff estimation in snow affect watersheds using SRM (Case study: Mahabad dam watershed)(In Persian), Iranian Journal of Gorgan Natural Resources and Agricultural Sciences, 11(3): 111-122.
19. Prudhomme, C. and Reed, D.W., 1999. Mapping extreme rainfall in a mountainous region using geostatistical techniques: a case study in Scotland. International Journal of Climatology, 19, 1337–1356.
20. Sharifi, M.R., Akhondali, E.M., Pourhamat, J., and Mohamadi, J., 2008, Assessment of two linear regression and ordinary Kriging methods for spatial distribution of snow depth in Samsami watershed (In Persian), Iranian Journal of Watershed Management Sciences, 1(1): 24-38.
21. Tabios, G.Q. and Salas, J.D., 1985. A comparative analysis of techniques for spatial interpolation of precipitation. Water Resources Bulletin, 21, 365–380.

Dynamic Mathematical Model for Site Specific N Fertilizer Recommendation

Kumut Sangkhasila, Sirisuda Butpetch, and Raweewan Chotiphan
Depaerment of Soil Science, Kasetsart University, Kamphaeng Saen Campus
Nakhon Pathom, 73140, Thailand

Abstract: Dynamic mathematical model has been developed and presented in this manuscript. The model aimed at finding N fertilizer recommendation rates for site specific crop production. The model was developed by considering processes involved in the N availability in soil. Based on processes, the model was expected to be applied in the different climatic conditions, soil properties, and plant types. Processes included the mineralization of organic materials, adsorption of N, leaching and denitrification of N loss. Available N in the soil profile was treated to be a major role of this model. The N availability, as model results, was the solution after the interactions of selected processes. The rate of organic material mineralization was treated to be the function of the amount of daily rainfall and the soil texture of the cropping location. The N adsorption was treated to be a function of total amount of organic material of the soil profile. The N loss via leaching and denitrification was treated to be a function of the daily amount of rainfall. The model used the S-shape curve to depict the shape of N uptake by plants along their growth period. The amount of available N would be partition mathematically into N adsorption, N loss, and N uptake by plants. The product of mineralization of SOM was treated to be amount of N which would be added to the soil N availability. The N uptake by plants was treated to be specific proportion of total N availability. The model required some soil tests, i.e. contents of SOM and total soil N as input for initial condition. Daily amount of rainfall and amount of N fertilizer rate were treated to be a boundary condition of the model. The daily amount of N uptake by plants must be prescribed and fed to the model. Two data sets of fertilizer trial on the growth and yield for cassava were used to calibrate and verify the applicability of the model. Simulation results agreed well with those two data sets. The model was sensitive to values of model constants. This model might be another choice to be selected for determining the optimal rate of N fertilization to produce any field crops economically and environmental friendly.

Key words: N recommendation, field crops, Dynamic model

INTRODUCTION

Element N is an essential plant nutrition. Continuous cropping at the same piece of land made decreasing soil N continually. To maintain the N fertility for crop production, farmers applies N fertilizer in terms of either inorganic N or organic N, or both of them. The application of N fertilizer might not be efficient due to N loss via leaching and volatilization[2]. To increase the efficiency of N fertilizer use, the optimal N application rate must be recommended to enhance the growth of plants to be produced, and be sound economically and environmental friendly[6]. Three important factors must be considered for N recommendation, namely climatic conditions, soil properties, and crop types[2]. Climatic conditions of the cropping areas provide soil water availability through rainfall, temperature for activities of microorganisms and plant enzyme activities. Soil properties provide condition for amount of available N for plant to uptake. Plant types specify their N requirements. The site specific recommendation rate is very difficult to be made since the highly interaction among those 3 factors. Conventional N recommendation for crop production comes from the N fertilizer trial experiments. Experimental results assumingly can be applied satisfactorily to other locations[2]. Many N recommendation models have been established in order to refine recommendation rate to suit the site specific problem[1,6]. In this manuscript, we presented another choice of such a model which was the mathematical model describing the dynamic nature of available N in soils for the whole course of cropping production period. Solution of the proposed model included the N fertilizer application rate that fits to the 3 factors of consideration.

MODEL DEVELOPMENT

The principle of Nitrogen Fertilizer Recommendation (N-Rec) model was developed by applying processes involved in N availability, namely losses and gains, and transformations of N forms within the soil profile. Model was written in the form:

$$\frac{\partial}{\partial t}N = f_{SOM}\frac{\partial}{\partial t}SOM + f_{FOM}\frac{\partial}{\partial t}FOM + f_{LOM}\frac{\partial}{\partial t}LOM + f_{FN}\frac{\partial}{\partial t}F_N + N_{Trap} + N_{Loss} + N_{uptake} \quad (1)$$

Corresponding Author : Kumut Sangkhasila, Depaerment of Soil Science, Kasetsart University, Kamphaeng Saen Campus Nakhon Pathom, 73140, Thailand

where $\frac{\partial}{\partial t}N$ was the rate of change of available N-mass within the soil profile. Terms $f_{SOM}\frac{\partial}{\partial t}SOM$, $f_{FOM}\frac{\partial}{\partial t}FOM$, and $f_{LOM}\frac{\partial}{\partial t}LOM$ were rates soil organic matter (SOM), organic fertilizer (FOM), and litter (LOM) mineralization. The prefixes f of these terms were N mass fraction of the corresponding materials. Units of SOM, FOM, and LOM were kg per unit area, i.e. kg ha^{-1}. $f_{FN}\frac{\partial}{\partial t}F_N$ was the rate of N-chemical fertilizer dissolution after its application. f_{FN} was N mass fraction of the fertilizer, and F_N was the amount of N-fertilizer application with the unit of kg ha^{-1}. N_{Trap} was the rate of N-mass which would be adsorbed by soil colloids and organic materials in the soil profile. N_{Loss} was the rate of N-mass removal from the soil profile via the leaching and denitrification processes. N_{uptake} was the rate of N-mass uptake by plants. All terms in (1) held the units of kg-N per unit area and per unit time, i.e. kg-N ha^{-1} day^{-1}.

Mineralization rate of SOM used in this model was in the form of modified first order kinetic, namely

$$\frac{\partial}{\partial t}SOM = k_1 SOM \qquad (2)$$

where k_1 was the kinetic rate constant which was treated to be a function of daily amount of rainfall ($Rain$, mm day^{-1}). This treatment aimed at mimicking the mineralization rate which was also soil moisture dependency (Ref…….). The k_1 was in the form

$$k_1 = \left(\frac{Sand^{V_{mSOM}} \cdot Rain}{K_{mSOM} + Rain}\right) + k_{2SOM} \ . \qquad (3)$$

where V_{mSOM}, K_{mSOM}, and k_{2SOM} were constants. Sand was a sand fraction of soil texture. Terms k_{2SOM}, and $Sand^{V_{mSOM}}$ held units of day^{-1} while K_{mSOM} held a unit of mm day^{-1}. Terms $\frac{\partial}{\partial t}FOM$ and $\frac{\partial}{\partial t}F_N$ were defined in the same manner as $\frac{\partial}{\partial t}SOM$. However, their constants were different.

The mineralization rate of litter, $\frac{\partial}{\partial t}LOM$, was introduced since during the plant growth period, some leaves might be dropped and became another source of organic material of the system (ref, …). The model proposed this kind of mineralization as

$$\frac{\partial}{\partial t}LOM = k_1 LOM + \frac{\partial}{\partial t}L_{gen} \ . \qquad (4)$$

A term k_1 was defined in the same manner of the mineralization of SOM. A term L_{gen} was the litter mass generated and accumulated along the whole period of plant growth. This term held a unit of kg litter ha^{-1}. S-curve was used to described this behavior, namely

$$L_{gen} = \left(\alpha_L - \frac{1}{\beta_L + \gamma_L \exp \delta_L (1-t)}\right)\kappa_L \qquad (5)$$

where α_L, β_L, γ_L, and δ_L were shape factors. A term t was normalized plant age to the time at harvest. κ_U was amount of litter (in kg ha^{-1}) at harvesting.

Since surface charges of organic material greatly affected the adsorption of both $NO_3^- - N$ and $NH_4^+ - N$ forms in soil, the model treated the rate of N adsorption due to these material left over in the soil as

$$N_{Trap} = \left(\frac{V_{trap} \cdot OM}{K_{mtrap} + OM}\right) \cdot N \qquad (6)$$

where V_{trap} and K_{mtrap} were constants. Please be noted that OM (kg ha^{-1}) in (6) were the left over contents of organic materials after the mineralization of SOM, FOM, and LOM. V_{trap} held a unit of day^{-1}, while K_{mtrap} held a unit of kg ha^{-1}.

The loss of nitrogen occurred from the 2 processes, namely denitrification and leaching. Both processes were soil moisture dependent (Ref…..). The model treated the amount of these losses depending on the amount of daily rainfall. The equation, thus, was in the form

$$N_{Loss} = \left(\frac{V_{Loss} \cdot Rain}{K_{mLoss} + Rain}\right) \cdot N \ . \qquad (7)$$

Terms V_{loss} and K_{mloss} were constants, while $Rain$ was the daily amount of rainfall, mm day^{-1}. N was available N mass left in the soil. V_{loss} held a unit of day^{-1}, and K_{mloss} held a unit of mm day^{-1}.

In this model the rate of N-uptake was defined by the changes of N accumulation in plants over time along their growth period. The N accumulation had the form

$$N_{acc} = \left(\alpha_U - \frac{1}{\beta_U + \gamma_U \exp \delta_U (1-t)}\right)\kappa_U \qquad (8)$$

where α_U, β_U, γ_U, and δ_U were S-shape factors. A term t was defined in the same manner as in (5). κ_U was the total amount of N uptake (in kg-N ha^{-1}) by plants for a specific yield. The term N_{uptake} could be obtained by

$$N_{uptake} = \frac{d}{dt}N_{acc} \ . \qquad (9)$$

MODEL INPUT

N-Rec model required contents of OM, total N, and organic fertilizer as its initial condition. The model also required amount of daily rainfall, the amounts of N fertilizer application, and N uptake by plants along the course of growth period as its boundary condition. Output of the model is the suitable amount of N-fertilizer that should be applied, and it is the main objective of this model.

N-Rec model required several constants, as implicitly shown in equations (1) through (9), to solve for its solution numerically. Implicitly finite difference with 1day time step size was used[3].

MODEL CALIBRATION AND VERIFICATION

Two sets of experiment had been set for model calibration and verification. These two sets were conducted in the same manner. Cassava (*Manihot esculenta*, Crantz; Huai Bong variety) were grown under rainfed conditions. Cassava for the 1st set were grown in Kamphaeng Saen (Ks) soil series (fine-silty, mixed, sub-active, isohyperthermic Typic Haplustalfs) located in Kamphaeng Saen Campus of Kasetsart University (N 14.035, E99.958), called Ks site, while those of the 2nd set were grown in Fang Daeng (Fd) soil series (fine-loamy, kaolinitic, isohyperthermic Rhodic Kandiudults) located in Prachuab Kririkhan Province (N11.833, E99.833), called Fd site. Ks and Fd soils have respectively the sandy loam (with 71% sand, 17% silt, 12% clay) and the loamy sand (with 84% sand, 11% silt, 5% clay) textures. There were several N-fertilizer treatments in these experimental sties. Amount of N-fertilizer of each experimental treatment was equally divided and applied at 2 and 4 months after cassava planting. Total rates of N treatments of the Ks site included 0, 63, 100, 250, and 375 kg-N ha^{-1}, while those of the Fd site included 0, 100, 150, 300, and 450 kg-N ha^{-1}. Urea and NH_4SO_4 were used as sources of N-fertilizer. Each experimental unit received the same cultural practices, except its amounts of daily rainfalls and of N-fertilizer treatments which were varied, respectively, by sites of experiment. Cassava was grown with spacing of 1.0x1.0 m^2. Each experimental unit covered an area of 30.0 m^2 (3 rows with a length of 10.0 m plot). Herbicide was applied at recommendation rate at planting. Hand-weeding was performed to all experimental units at 2 month after planting. Organic fertilizer was not applied for both experiments. Both experiments commenced in Nov 2006 and lasted in Nov 2007. The amounts of annual rainfall were 1191 and 1721 mm yr^{-1} for Ks and Fd sites, respectively.

Soil test values such as contents of OM and total N were collected at planting and at harvesting, Cassava yields (root biomass) obtained from each experimental units were collected at harvest. %N of leaf, stem, and root biomass were also collected along the growing period and at harvest. Biomass along with their %N was used for calculating the N_{uptake} term of equations (1), (8) and (9). Contents of soil OM and total N and organic fertilizer rate were treated as initial condition, while those of soil OM, and total soil N at harvest were used for reliable checking of N-Rec model.

Table 1. Data set of the Ks site used for finding model constants.

	N-rate, kg-N ha^{-1}				
	0	**63**	**100**	**250**	**375**
OM^1	0.65	0.79	0.79	0.58	0.46
N^1	0.046	0.051	0.054	0.057	0.060
OM^2	0.51	0.61	0.63	0.58	0.48
N^2	0.042	0.045	0.046	0.046	0.046
Yield	49.9	65.4	76.8	84.1	78.6
Shoot	22.3	24.4	42.6	55.3	61.3
N in root	0.143	0.151	0.168	0.188	0.224
N in shoot	1.242	1.151	1.137	1.209	1.202
N uptake	78.11	84.87	136.58	182.69	202.89
$N\text{-loss}^*$	14.66	15.65	16.09	16.18	16.46
$N\text{-avai}^*$	124.74	200.93	294.34	485.63	625.35
$N\text{-ad}^*$	0.31	0.37	0.40	0.38	0.36

N-rate: N-fertilizer rates in kg-N ha^{-1}; OM^1: OM contents at initial (%); N^1: total N contents at initial (%); OM^2: OM contents at harvest (%); N^2: total N contents at harvest (%); Yield: cassava root yields in ton ha^{-1} at harvest; N in root: total N in roots (%) at harvest; N in shoot: total N in leaves and stem (%) at harvest; N uptake: total N content uptaken by cassava (kg-N ha^{-1}) at harvest; superscript * indicated that these items were the model solution; $N\text{-loss}^*$: amount of N loss due to leaching and denitrification (kg-N ha^{-1}); $N\text{-avai}^*$: amount of available N in the soil profile (kg-N ha^{-1}); and $N\text{-ad}^*$: amount of adsorped N by clay and organic materials in the soil profile (kg-N ha^{-1}).

The calibration and verification were made for evaluating values of model constants. They were just the initial-boundary value problem. Obtaining values of model constants by trial and error method was chosen here[3].

DESCRIPTION OF COLLECTED DATA

The two data sets showed that the higher rates of N fertilizer application, the higher rates of N uptake by cassava (Tables 1 and 2). However, the N uptake rates were not linearly responses. The accumulations of N in cassava shoots at harvest were 6-10 folds higher than those of in the roots. N-application with rates lesser than 250 kg-N ha^{-1} help increase in root yields for both data sets. However, the two experiments gave yield reductions when N-fertilizer rates were more than 250 kg-N ha^{-1}. However, both data sets showed that total biomass production increased as a result of increase in fertilizer application. These results might be caused by excess N fertilization[5]. The two experimental sites gave a little difference in N uptake. The Fd site with its higher annual rainfall and % sand of soil texture seemed to have at least 1.5 folds higher in N accumulation in both shoot and root tissues, when comparing with results obtained from the Ks site. This result suggested that N in the Fd site was more available than that of in the Ks site. The more N available in soil profile, the more N uptake by plants[7].

Table 2. Data set of the Fd site used for finding model constants.

	N-rate, kg-N ha^{-1}				
	0	**100**	**150**	**300**	**450**
OM[1]	0.44	0.54	0.44	0.34	0.51
N[1]	0.036	0.040	0.042	0.037	0.047
OM[2]	0.30	0.28	0.31	0.25	0.35
N[2]	0.030	0.029	0.029	0.021	0.027
Yield	46.0	61.1	67.6	71.3	68.1
Shoot	28.0	43.6	63.8	66.6	68.8
N in root	0.325	0.397	0.443	0.469	0.569
N in shoot	1.686	1.676	1.575	1.638	1.773
N uptake	141.75	222.73	295.96	324.25	367.79
N-loss[*]	15.58	15.77	16.12	12.40	15.26
N-avai[*]	213.45	406.28	519.53	685.02	898.70
N-ad[*]	0.22	0.28	0.27	0.21	0.34

Column 1: The same abbreviation as used in Table 1.

VALUES OF MODEL CONSTANTS

After the calibration and verification processes, values of constants needed for the model were classified into to sets, i.e. common and site specific sets (Tables 3, 4 and 5). To obtain the solution of the model, both of data sets were needed. The common data set mostly included parameters for organic matter mineralization, adsorption, leaching, and litter generation processes, while the specific set included kinetic constant of soil organic matter mineralization, amount of N-uptake by cassava at the different level of biomass production, and amount of litter generation at the different rates of N-fertilizer application. Uses of these values of constants made results of the model were less than 2% deviation from those of the collected data.

Table 3. Values of constants for a common set.

Constant	Value	Constant	Value
V_{mSOM}	10.1169	V_{trap}	0.000444
K_{mSOM}	850.0	K_{mtrap}	30000.0
f_{SOM}	0.0055	k_{2trap}	2.99
V_{mFOM}	10.1169	V_{loss}	0.00512
K_{mFOM}	850.0	K_{mloss}	750.0
f_{FOM}	0.0055	α_U	0.99999
V_{mLOM}	20.1169	β_U	1.0
K_{mLOM}	850.0	γ_U	125.0
f_{LOM}	0.012243	δ_U	-7.50
V_{mFN}	0.0325	α_L	1.025
K_{mFN}	300.0	β_L	0.976
k_{2FN}	0.0465	γ_L	160.0
f_{FN}	1.0	δ_L	-15

Units of these constants were given in the content.

The site specific data sets explicitly showed that SOM of the Fd site was more rapidly mineralized than that of in the Ks site. The higher %sand of the soil texture might be the cause of this result (ref,…..). The N uptake rates were high with the higher rates of N fertilizer application. Please be note that these constants of the Fd site were about 3 folds higher than those of the Ks site. This might be caused by the higher %sand and higher annual rainfall which raised the soil N availability (ref,…). Values of amount of litter generation for the two sites were not too much different.

Table 4. Values of constants of the site specific set for the Ks site.

	N-rate, kg-N ha^{-1}				
Constant	**0**	**63**	**100**	**250**	**375**
k_{2SOM}	0.000293	0.000293	0.000293	0.000293	0.000293
κ_U	0.04411	0.04381	0.06807	0.08720	0.09353
κ_L	8750	10250	14000	15400	15400

Units of these constants were given in the content.

Table 5. Values of constants of the site specific set for the Fd site.

	N-rate, kg-N ha^{-1}				
Constant	**0**	**100**	**150**	**300**	**450**
k_{2SOM}	0.000612	0.000612	0.000612	0.000612	0.000612
κ_U	0.10450	0.15802	0.20280	0.27751	0.25310
κ_L	8752	9966	10590	11649	11649

Units of these constants were given in the content.

SENSITIVITY ANALYSIS

The selected responses were sensitive to changes of value of selected constants (Table 6). The amounts of N loss and N adsorption were sensitively to V_{loss} and V_{trap} values, while the amounts of soil N availability and N uptake were greatly sensitive to any changes in constant values. This result suggested that processes used to develop the model satisfactorily explain the interaction of N availability in soil. The amount of higher N adsorption leaded to the condition of lesser N availability, thus, the lesser N was uptaken by plants (ref…). The amount of higher SOM mineralization (higher value of k_{2SOM}) raised the N availability in the soil profile. This condition leaded to the higher rates of N uptake by plants, N loss, and N adsorption[7].

Table 6. Averaged sensitivity of selected model solutions in response to selected model constants, $\partial Y / \partial X$'s.

	X			
Y	V_{loss}	k_{2FN}	V_{trap}	k_{2SOM}
N-uptake	-29.36 (10.72)	23.73 (30.67)	-118.24 (40.35)	1286.35 (299.36)
N-loss	3075.31 (129.57)	1.18 (1.08)	-14.64 (1.19)	279.52 (58.49)
N-avai	-3046.23 (120.56)	33.77 (33.05)	-693.02 (60.18)	51076.45 (10689.40)
N-ad	-0.21 (0.06)	0.00 (0.00)	825.68 (77.41)	27.65 (2.52)

Numbers in parentheses were standard deviation of sensitivity.

MODEL APPLICATION

The model created outputs which were in a good agreement with two sets of collected data. The outputs were strongly constant value dependent, especially

values of k_{2SOM} and κ_U. These 2 constants were site specifically dependent. Knowledge of these 2 constants needed to be used with the model. To generate general relation formula for these quantities required more fertilizer trial experiments. The optimal N-fertilizer application rate will be obtained by providing values of these 2 constants. The value of κ_U were total N requirement which will be uptake by any field crop plants with the optimal yield expectation. The value of k_{2SOM} is site specific which strongly depends on types of climate, soil properties, and soil organic matter. Reviewing of published papers related to field crop fertilizer trial and regression analysis would give the knowledge k_{2SOM} and κ_U of values. The optimal yield expectation would be determined either by economic or environmental aspects.

CONCLUSION

The N-Rec model had been developed in terms of a system of equations. Equations included the balance of N mass for 1) rate of change of N availability in soil, 2) rate of SOM mineralization, 3) rate of FOM mineralization, 4) rate of LOM generation and mineralization, and 5) rate of N-fertilizer dissolution. The model required amounts of SOM, FOM, LOM, and soil N availability priori of planting. These quantities would be treated as its initial condition. The daily rainfall, amount of N fertilizer application, and rate of N uptake by plants were treated as its boundary condition. The solution of the model was amount of available N in the soil dynamically changes over the course of plant growth. Changes in amounts of N adsorbed by organic materials, N lost by leaching and denitrification were also the model solution. Two sets of cassava fertilizer trial experiments were used to calibrate and verify the model. Values of model constants used made model outputs be in good agreement with experimental data. Change in soil available N over the course of simulation was sensitive to values of model constants, especially the constants which were represented the mineralization rate of SOM, N adsorption, and N loss by leaching and denitrification, and amount of N uptake by plants. The model outputs might be used to judge an optimal N fertilizer application rate under a specific plant type and a specific climatic condition.

ACKNOWLEDGEMENTS

We would like to acknowledge Kasetsart University Research and Development Institute (KURDI) for providing the grant to support this project.

REFERENCES

1. Bonneau, M. and C. Nys. 1993. A nitrogen cycle model for calculating the reduction of N-input necessary to reduce soil acidification and nitrate leaching and the consequences of this for wood production. Water, Air, and Soil Pollution. 69:1-20.
2. Glendinning, J. S. 1999. Australian Soil Fertility Manual. CSIRO Publishing, Collingwood, Australia.
3. Hall, C. A. and T. A. Porsching. 1990. Numerical Analysis of Partial Differential Equations. 1990. Prentice-Hall, New Jersey, USA.
4. Hirobe, M., K. Koba., and N. Tokuchi. 2003. Dynamics of the internal soil nitrogen cycles under moder and mull forest floor types on a slope in a *Cryptomeria japonica* D. Don plantation. Ecological Research. 18:53-64.
5. Lemus, R., E. C. Brummer, C. L. Burras, K. J. Moore, M. F. Baker, and N. E. Mostad. 2008. Effects of nitrogen fertilization on biomass yield and quality in large fields of established switchgrass in southern Iowa, USA. Biomass and Energy. 32:1187-1194.
6. Nesme, T., F. Lescourret, S. Bellon, and R. Habib. 2008. A modelling approach to explore nitrogen fertilization practices of growers and their consequences in apple orchards. Agricultural Systems (in press).
7. Smolen, S. and W. Sady. 2009. The effect of various nitrogen fertilization and foliar nutrition regimes on the concentrations of nitrates, ammonium ions, dry matter and N-total in carrot (*Daucus carota* L.) roots. Scientia Horticulturae. 119:219-231

Spatial Cd stock and flow analysis on Australian regional agricultural land

[1]Napat Jakrawatana, [1]Stephen Moore, [2]Samsung Lim and [3]Iain MacGill
[1]School of Civil and Environmental Engineering
[2]School of Surveying & Spatial Information Systems
[3]Centre for Energy and Environmental Markets and School of Electrical Engineering and Telecommunications
University of New South Wales, Sydney, Australia 2052.

Abstract: Cadmium (Cd) is the highly toxic bioaccumulative substance, which can cause serious health impact to humans. Cd accumulation in agriculture soil and contamination of the food chain is a challenging problem for agricultural systems. Cd inputs to land comes from various sources including; phosphate fertilizer, atmospheric deposition, gypsum, lime and manure. Cd outputs from agriculture are harvested crop, leaching and runoff. Different areas or different crop growing have different Cd input, output and stock accumulation on land. This paper demonstrates a new method to estimate input, output and stock accumulation of Cd on soil spatially, using integrated Substance Flux Analysis (SFA) method and Geographic Information System (GIS). This method is demonstrated in the application on an intensive agricultural area in Australia, the Murrumbidgee Irrigation Area (MIA). The results can be used to evaluate the trend of Cd exceeding an acceptable limit, and development of an effective policy and limit to control Cd input to soil.

Key words: Cadmium, Material Flux Analysis, Agriculture

INTRODUCTION

Accumulation of cadmium (Cd) on agricultural land and contamination of the food chain is a challenging problem for agricultural systems in Australia. Although Australian soils have inherently low Cd levels, the Cd concentration in food is similar to other countries. This may be because chemical processes and soil conditions in Australia are prone to causing high Cd uptake in plants[1]. Australia has the current maximum level of Cadmium allowed in phosphate fertilizer of 300 mg/kg of P and a recommended maximum soil concentration of 1.0 mg Cd/kg soil[2]. Even though Cd contamination in Australia doesn't yet exceed Australian food standard limits[3,4], however the increasing accumulation of Cd stock is deteriorating the quality of soil and can lead to contamination of food that will exceed the limit in the future. Therefore, Cd inputs to soil need to be monitored, controlled and reduced.

Material Flux Analysis (MFA) method has been used to trace and monitor toxic substances through anthropogenic and environmental process since 1985[5]. However, conventional MFA quantifies the flow of inputs and outputs through the processes in the region and the total stock accumulation in the region as a whole, without connecting these flows to spatial land use within the region. Stock accumulation of Cd on land will be different relating to different land uses which have different inputs of Cd from different fertilizer types and application rates and also different outputs from various harvested crops. Therefore, a model that can account for this spatial effect will be very useful for management of Cd on land.

This paper describes a method to estimate spatial accumulation of Cd on agricultural land, so that trends can be followed, enabling the time remaining before acceptable limits are exceeded to be estimated on a spatial basis. Then a more detail policy can be developed to limit and control Cd input to soil within the region. The method is the integrated Material Flux Analysis (MFA) and Geographic Information System (GIS) model and is demonstrated in the application to the Murrumbidgee Irrigation Area (MIA), one of Australia's major producers of rice, cereal, citrus and winegrape, using available land use data in the period 1992-2002.

Corresponding Author: Napat Jakrawatana, School of Civil and Environmental Engineering University of New South Wales, Sydney, Australia 2052.

MATERIALS AND METHODS

2.1 Material Flux Analysis (MFA)

Material Flux Analysis is an environmental accounting tool that traces and provides an account of valuable resources or toxic substances flowing through a process or region[5,6]. MFA comprises the following iterative steps:

- Problem definition.
- Selection of substances.
- Determination of system boundary.
- Determination of related processes and goods.
- Determination of mass flows of goods.
- Determination of substances concentration in these goods.
- Calculation of substances flow from goods flows and substances concentration in these goods.
- Illustration, interpretation and policy development.

Problem definition and substances selection

The Australian agricultural sector faces a number of environmental sustainability issues. One important challenge is Cd accumulation in agricultural soil and contamination of the food chain. Cd is a bioaccumulative toxic heavy metal contaminant of phosphate fertilizer, and continuing application of fertilizer and soil conditioner on agricultural soils may contribute to excessive levels of Cd in the soil. Therefore, Cd is selected for this study.

System boundary

The system boundary of this project is the geographical boundary of the Murrumbidgee Irrigation Area (MIA), shown in Figure 1, the intensive agriculture area in the southwest of the Australian state of New South Wales (NSW) and about 600 km from Sydney. The area of is one of the largest agricultural areas in Australia. The area is a major producer of rice, cereal, oilseed, citrus, winegrape and other fruit and vegetables. The MIA produces almost 20% of total Australian winegrape production, 35% of total Australian citrus production and almost 20 % of total Australian rice production. A number of food processing facilities are located in the region including wineries, rice mills, juice making, and fruit and vegetable processing. The MIA also has two intensive cattle feedlots and a beef processor, which carry a total of 140,000 head of cattle, and one of Australia's largest chicken producer and processors, processing approximately 28 million chickens a year[7].

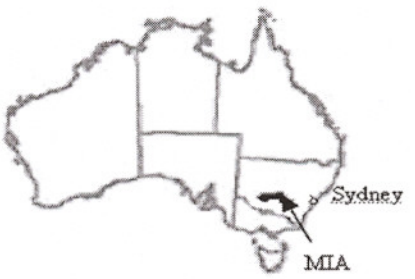

Figure 1 Map showing location of MIA in Australia (not to scale)

Related process and goods.

The diagram in Figure 2 shows sources of Cd inputs to and outputs from crop production soil in the MIA. There are five inputs of Cd to crop production soil in the MIA, including: fertilizer, manure, atmospheric deposition, gypsum and lime.

There are three outputs of Cd from crop production soil in the MIA, including: harvested crops, harvested residue for feed and burnt residues.

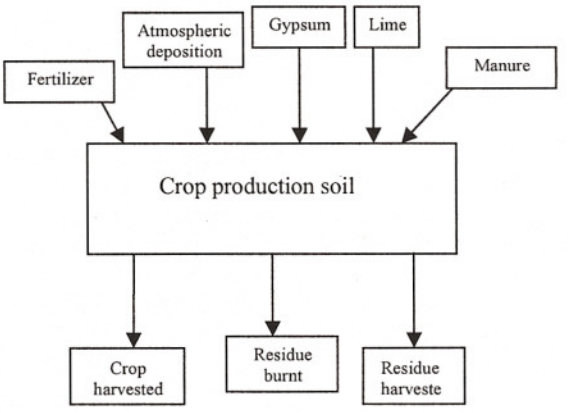

Figure 2 Sources of Cd inputs to and outputs from the crop production soil in MIA

2.2 Geographic Information System (GIS)

GIS is defined as an information system that is used to input, store, retrieve, manipulate, analyse and output geographically referenced data or geospatial data, in order to support decision making for planning and management of land use, natural resources, environment, transportation, urban facilities, and other administrative records[8]. The GIS software used in this study is ArcGIS 9 developed by Environmental System Research Institute ESRI (www.esri.com).

2.3 Integrated MFA and GIS

Figure 3 shows the concept of the integration. Firstly, GIS land use data is obtained, then input and and output data is added to the GIS files by adding into the attribute table in the GIS files. These inputs and outputs are related to type of crops and land use. Secondly, calculate the net Cd balance from each year by deducting inputs from outputs for each parcel of land. Thirdly, the net balance of each year is combined together to find the total accumulation from the base year to the final year. Finally, transform the net balance accumulation to soil Cd concentration and combine them with the previous soil Cd concentration (before the base year) to obtain the estimated Cd concentration in the final year.

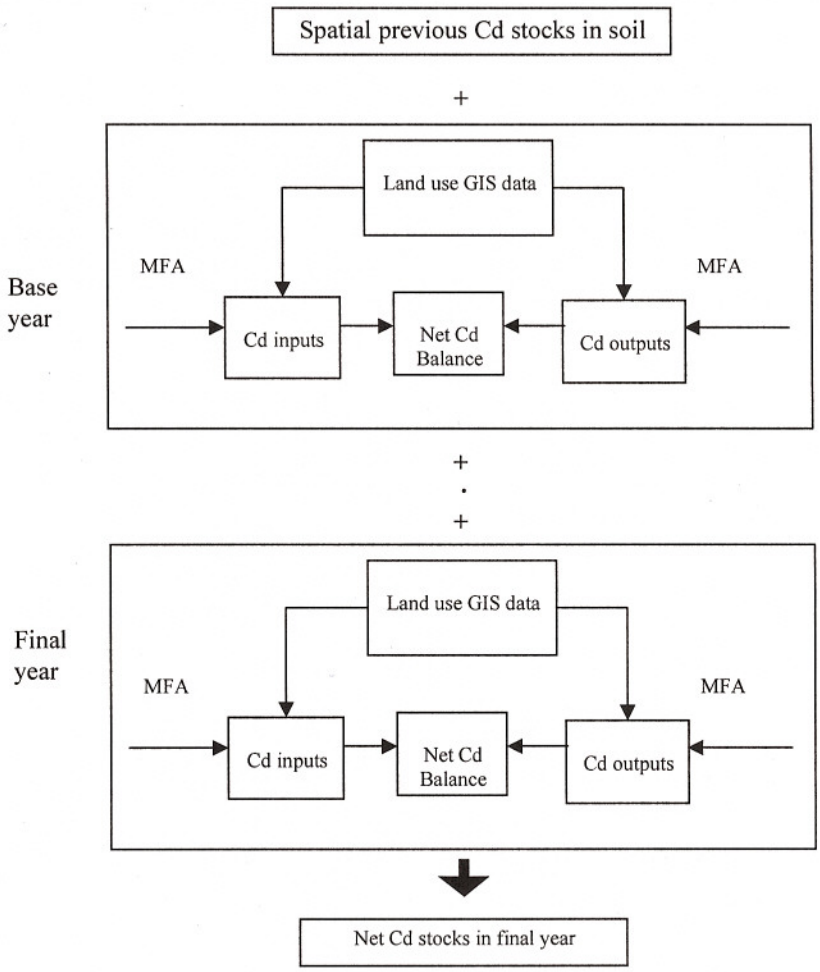

Figure 3 Method to integrate MFA and GIS The method to integrated MFA and GIS is described in the following sections:

2.3.1 Prepare land use GIS data

GIS land use data for the MIA from 1992-2002 are obtained from the Australian collaboration land use mapping program (www.brs.gov.au/landuse). The GIS data for the boundary of MIA is obtained from Murrumbidgee Irrigation limited.

2.3.2 Formulate Cd inputs in attribute data table

Sources of Cd inputs to crop production soil in MIA comprise: Fertilizer, Manure, Atmospheric deposition, Gypsum and Lime.

Input from fertilizer (F_{input})

The Cd input from fertilizer is estimated by following formula:

$$F_{input} = F_{rate} \times Cd_{ratio} \qquad (1)$$

F_{input} = Cd input from fertilizer (g Cd/ha)

F_{rate} = Fertilizer application rate (kgP/ha)

Cd_{ratio} = Cd per P ratio (g Cd/kg P)

To include this input, add the fields of F_{input}, F_{rate}, and Cd_{ratio} into the attribute table of land use data of each year. Add the data for fertilizer application rate and Cd/P ratio in the attribute table. These fertilizer application rates and type of fertilizers are related to the type of crops and this data assumption is adopted from the recommended fertilizer application rate for crops production in NSW and from the literature[9,10,11,12,13,14,15,16]. Cd/P ratio is adopted from[17]. To add these data in relation to crop type automatically to the attribute data, SQL and Visual Basic language are used to allocate this data. Then, F_{input} is calculated using formula (1) and SQL in the field calculator.

Input from Atmospheric deposition (A_{input})

Due to the MIA being distant from heavy industry and a power plant, Cd from atmospheric deposition is assumed to be very low[4]. This input is conservatively estimated to be equal to the output of Cd to air from burning of rice straw. The total Cd emission to air from burning of rice straw in MIA is estimated to be 19 kg/y. Dividing this input by the total area of MIA of 362,400 ha, the input flux from atmospheric deposition is estimated to be 0.05 g/ha. To formulate this input, the field of A_{input} = 0.05 g/ha is added into the attribute table.

Input from Gypsum (G_{input})

Data from Australian Bureau of Statistics (ABS) shows that total Cd in Gypsum applied to soil in MIA is 8.3 kg/y[18]. Divided by the area that it has been applied, the input from gypsum to this area is 0.06 g/ha. To formulate this input, the field of G_{input} = 0.06 g/ha is added into attribute table.

Input from Lime (L_{input})

Data from Australian Bureau of Statistics (ABS) shows that total Cd in Lime applied to soil in MIA is 8.3 kg/y[18]. Divided by the area that it has been applied, the input flux from lime to this area is 0.06 g/ha. To formulate this input, the field of L_{input} = 0.06 g/ha is added into attribute table.

Input from Manure (M_{input})

Here, the main manure used as Phosphorus source in the region is chicken litter (chicken manure plus bedding material). This manure is mainly applied to vegetables, fruits and winegrape. Application rate and Cd/P ratio of the manure are assumed from the recommended application rate from the literature[9,10,11,15] and Cd/P ratio from [17]. Input from manure is given by the following formula:

$$M_{input} = M_{rate} \times Cd_{ratio} \qquad (2)$$

M_{input} = Cd input from manure (g Cd/ha)

M_{rate} = Manure application rate (kgP/ha)

Cd_{ratio} = Cd per P ratio (g Cd/kg P)

Total Cd input (g/ha) ($Total_{input}$)

Total Cd input can be obtained by summing all the inputs using field calculator.

$$Total_{input} = F_{input} + A_{input} + G_{input} + L_{input} + M_{input} \qquad (3)$$

2.3.3 Formulate Cd outputs in attribute data table

Sources of Cd outputs from crop production soil in MIA comprise: harvested crop, harvested cereal straw for feedstuff, burning of rice straw.

Output from harvested crop ($Crop_{output}$)

Output from harvested crop can be estimated by the following formula:

$$Crop_{output} = Crop_{yield} \times Crop_{Cd} \quad (4)$$

$Crop_{output}$ = Cd output from crop harvested (g Cd/ha)

$Crop_{yield}$ = Crop yield (tonnes/ha)

$Crop_{Cd}$ = Cd concentration in crop (mg Cd/kg crop)

To calculate this output, first, add fields of $Crop_{output}$, $Crop_{yield}$ and $Crop_{Cd}$ into the attribute table of land use data for each year. Add the data for crop yield obtained from Australian Bureau of Statistics[18,19,20,21] and crop Cd concentration obtained from the literature[22,23,24], in the attribute table. To add these data related to crop type automatically to the attribute data, SQL and Visual Basic language are used to allocate this data. Then, $Crop_{output}$ is calculated using formula (4) and SQL in the field calculator.

A simple assumption is adopted from the model from [4], where according to the current Cd concentration in fertilizer; Cd concentration in crops will increase almost linearly by either about 1 % or 5% each year, for two groups of crops. The first group is crops that have been applied with low Cd fertilizer including: rice, cereal legume, potatoes and vegetable. Cd concentrations in these crops are increasing by 1 % every year. The second group is crops that have been applied with high Cd fertilizer including: oilseed, sown pastures, citrus, grape, stone fruit, apples, pears. Cd concentration of crops in this group is increasing by 5 % every year.

Output from harvested cereal straw for feedstuff ($Feed_{output}$)

From the site visit and interviews, the following assumptions are made:

- 60% of total cereal straw is harvested for feedstuff
- Cd concentration in cereal straw is increasing linearly 1 % every year

Output from harvested cereal straw for feedstuff is obtained by following formula:

$$Feed_{output} = Straw_{yield} \times Straw_{Cd} \times 0.6 \quad (5)$$

$Feed_{output}$ = Cd output from cereal straw harvested for animal feed (g/ha)

$Straw_{yield}$ = Straw yield (tonnes/ha)

$Straw_{Cd}$ = Cd concentration in straw (mg/kg)

To calculate this output, add fields of $Feed_{output}$, $Straw_{yield}$ and $Straw_{Cd}$ into the attribute table of land use data for each year. Add the data for straw yield, which assumed to be 1.5 times cereal yield, and straw Cd concentration estimated from [22], into the attribute table. To add these data related to crop type automatically to the attribute data. SQL and Visual Basic language are used to allocate this data. Then, $Feed_{output}$ is calculated using formula (5) and SQL in the field calculator.

Output from burning rice straw ($Burnt_{output}$)

From the site visit and interviews, the following assumptions are made:

- rice straw: 90% is burnt in the field and 10% is used for animal bedding
- When rice straw is burnt, 35% of Cd is emitted to the air, the remainder to the bottom ash on the soil.
- Cd concentration in cereal straw is increasing linearly 1 % every year

Output from burning rice straw is obtained by following formula:

$$Burnt_{output} = Straw_{yield} \times Straw_{Cd} \times 0.9 \times 0.35 \quad (6)$$

$Burnt_{output}$ = Cd output in rice straw burnt (g/ha)

$Straw_{yield}$ = Straw yield (tonnes/ha)

$Straw_{Cd}$ = Cd concentration in straw (mg/kg)

To calculate this output, add fields of $Burnt_{output}$, $Straw_{yield}$ and $Straw_{Cd}$ into the attribute table for land use data of each year. Add the data for straw yield which is assumed to be 1.5 times rice yield and straw Cd concentration estimated from [22], into the attribute table. To add these data related to crop type automatically to the attribute data, SQL and Visual Basic language are used to allocate these data. Then, $Burnt_{output}$ is calculated using formula (6) and SQL in the field calculator.

Total Cd output (g/ha) ($Total_{output}$)

Total Cd output is calculated by summing all the outputs using the field calculator:

$$Total_{output} = Crop_{output} + Feed_{output} + Burnt_{output} \quad (7)$$

2.3.4 Calculate Net Cd balance for each year.
Cd Balance can be calculated from the following formula:

$$Net_{Cd/ha} = Total_{input} - Total_{output} \quad (8)$$

$Net_{Cd/ha}$ = Net Cd balance (g Cd/ha)

2.3.5 Reclassify the data under the field $Net_{Cd/ha}$ and generate the new file of $Net_{Cd/ha}$ for each year from 1992-2002.

This is conducted by using ArcToolbox - Spatial Analysis tool, using the Reclass- Reclassify function.

2.3.6 Combine Net Cd balance for each year together to obtain total net Cd accumulation from 1992-2002 ($Accum\_Net_{Cd/ha}$).

This is conducted by using ArcToolbox - Spatial analysis tool , using the Math - Plus function.

2.3.7 Transform accumulation net Cd balance ($Accum\_Net_{Cd/ha}$) (g/ha) to accumulated soil Cd concentration ($Accum\_soilCd_{Conc}$) (mg Cd /kg soil).

$$Accum\_soilCd_{Conc} = \frac{Accum\_Net_{Cd/ha}}{10\rho d_p} \quad (9)$$

Accumulated Cd concentration in soil (1992-2002) is given by the following formula:

$Accum\_soilCd_{Conc}$ = Accumulated soil Cd concentration (mg Cd /kg soil)

$Accum\_Net_{Cd/ha}$ = Total net Cd accumulation from 1992-2002 (g/ha)

ρ = soil bulk density (1300 kg/m^3)

d_p = depth of plough layer (0.1 m)

2.3.8 Calculate total stock Cd concentration in soil in the final year (2002).
This can be obtained by the following formular:

$$SoilCd_{Conc} = \mathrm{Pr}esoilCd_{conc} + Accum\_soilCd_{conc} \quad (10)$$

$SoilCd_{Conc}$ = Soil Cd concentration in 2002

$Accum\_soilCd_{Conc}$ =Accumulated Cd concentration in soil (1992-2002)

$\mathrm{Pr}esoilCd_{Conc}$ = Previous stock Cd concentration in soil (before 1992)

Average Cd concentration in MIA before 1992 of 0.1 mgCd/ kg soil is assumed (Mclaughlin et al., 2006).

RESULTS AND DISCUSSION

GIS land use map in 1992 in Figure 4 shows that major land use in 1992 is sown pasture and rice paddy, with cereal growing scattered around those areas. Grape vine and citrus plantation area are concentrated in the middle-east part of the MIA. After 1992 sown pasture land is reducing gradually, with increasing rice and cereal growing. Grape vine and citrus growing areas also have small increases.

Spatial Cd flux inputs to MIA in 1992 are shown in Figure 5. Cd input is high in crops that are applied with phosphate fertilizer that contain high Cd, including: oilseed (8-10 g Cd/ha), sown pastures (6-8 g Cd/ha), citrus (6-8 g Cd/ha), grape (6-8 g Cd/ha), stone fruit (6-8 g Cd/ha), apples (6-8 g Cd/ha), pears (6-8 g Cd/ha). Other crops, including: rice and cereal, were

applied with low Cd phosphate fertilizer, resulting in lower Cd input (2-4 g Cd/ha).

Spatial Cd flux outputs from MIA in 1992 are shown in Figure 6. Some crops especially citrus and grape take up very low Cd, therefore, the Cd outputs in those harvested crop area are low (0-0.3 g Cd/ha). Sown pastures area has the medium output of 0.3-0.6 g Cd/ha. Other crops, including: cereals (1.2-1.5 g Cd/ha), oilseed (1.2-1.5 g Cd/ha) and rice (0.6-0.9 g Cd/ha) and have high Cd outputs because their residues such as straw contain high Cd concentrations. Therefore, when these residues are harvested for feed or burnt, there is a high overall output.

The spatial net Cd balance, derived from subtracting Cd output from Cd input, is shown in Figure 7. The results from the model show Cd the balance that remains in the soil in 1992 is high in the crop areas of oilseed (8-10 g Cd/ha), sown pastures (6-8 g Cd/ha), citrus (6-8 g Cd/ha), grape (6-8 g Cd/ha), stone fruit (6-8 g Cd/ha), apples (6-8 g Cd/ha), pears (6-8 g Cd/ha). This indicates that Cd soil accumulation is mainly concentrated in crop land with high Cd input from phosphate fertilizer, especially where the crop has low output of Cd ,such as citrus and grape, because there is no residue output.

The 10 years accumulated Net Cd balance from combining net Cd balances for 1992-2000 is shown in Figure 8.The results show that the land area that have high Cd accumulation include: oilseed (66.8 - 83.4 g Cd/ha), sown pastures (50.2 – 83.3 g Cd/ha), citrus (66.8 - 83.4 g Cd/ha), grape (66.8 - 83.4 g Cd/ha), stone fruit (66.8 - 83.4 g Cd/ha), apples (66.8 - 83.4 g Cd/ha), pears (66.8 - 83.4 g Cd/ha). Other crops, including: rice and cereal, were applied with low Cd phosphate fertilizer, resulting in lower Cd input (17.1 – 50.2 g Cd/ha). Even though there have been some changes in land use over 10 years, the spatial-temporal track of Cd input to the region indicates stock accumulation of Cd has increased by nine times the annual net Cd balance in this period.

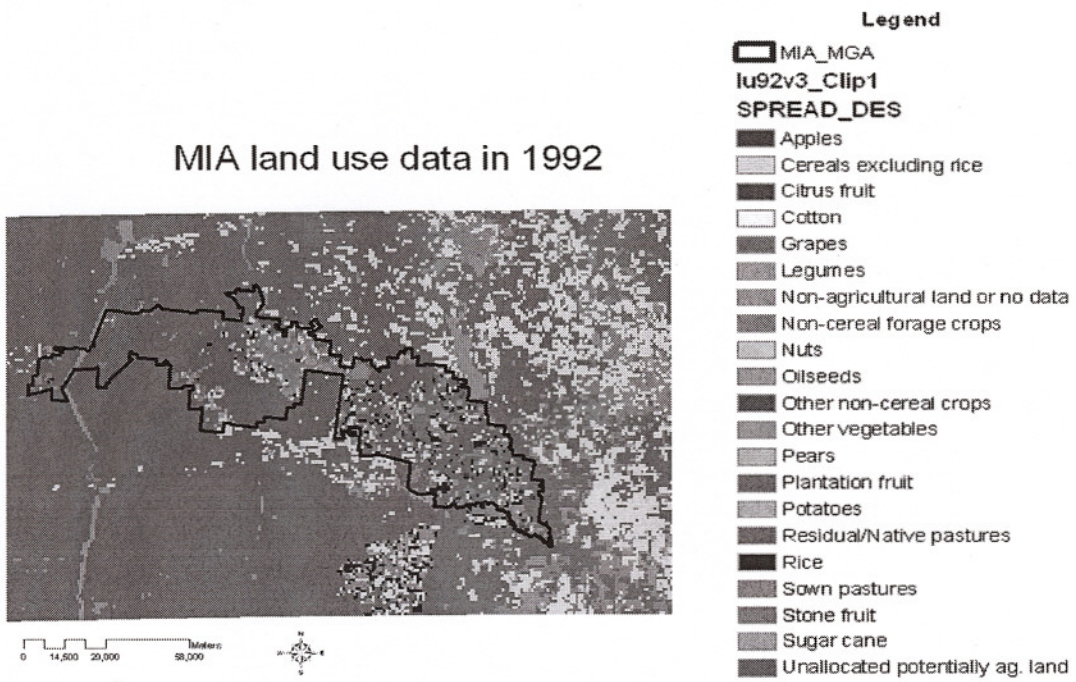

Figure 4 MIA land use data in 1992 (the boundary of MIA is the black line)

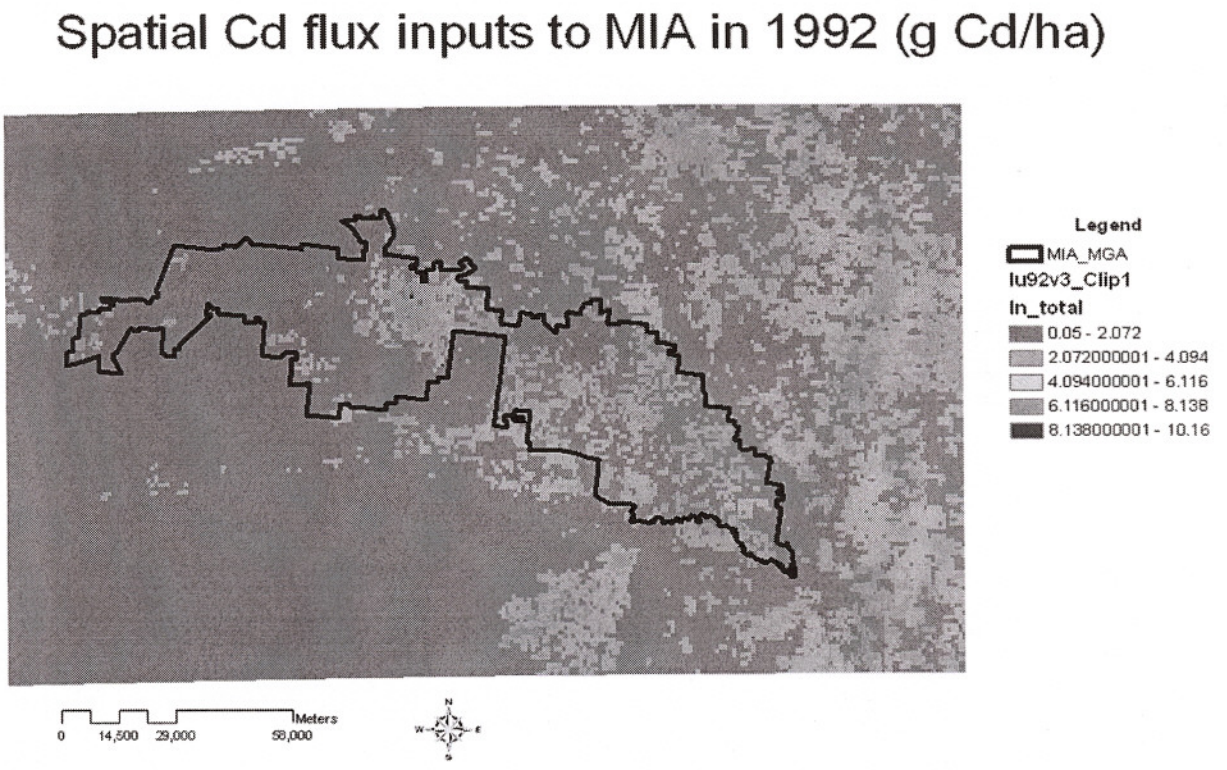

Figure 5 Spatial Cd flux inputs to MIA in 1992 (g Cd/ha)

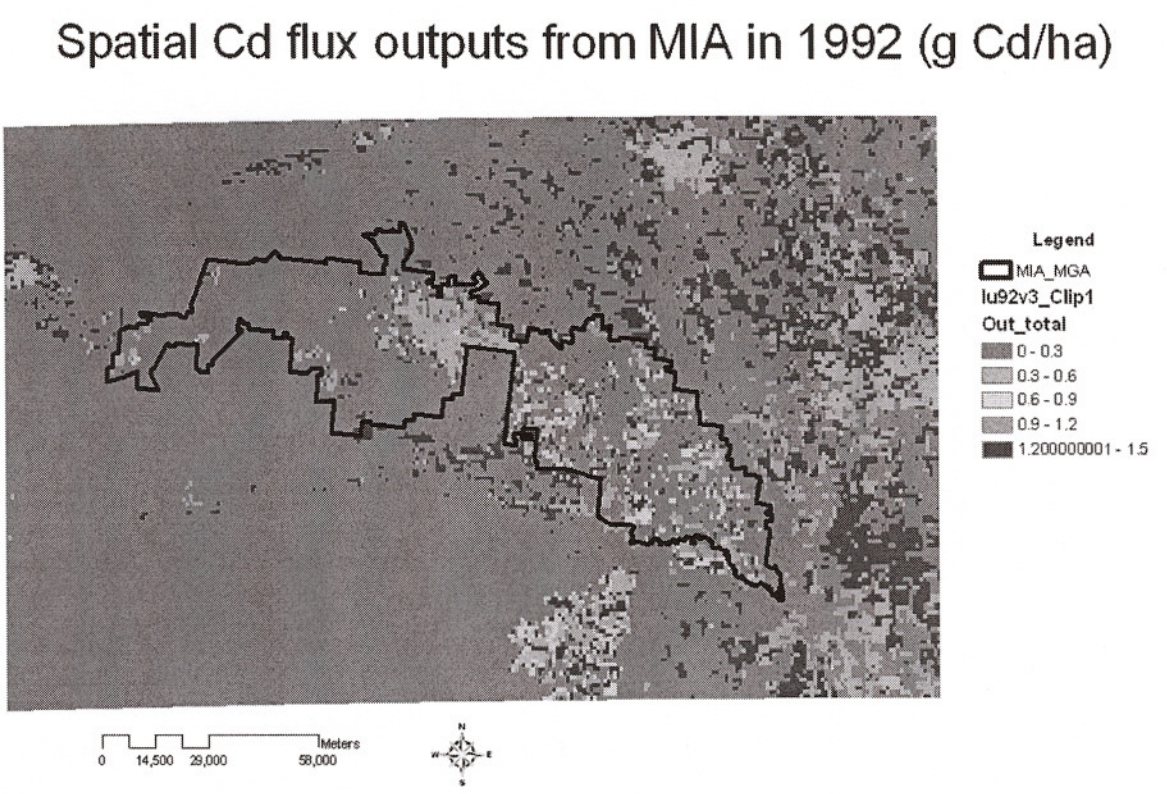

Figure 6 Spatial Cd flux outputs from MIA in 1992 (g Cd/ha)

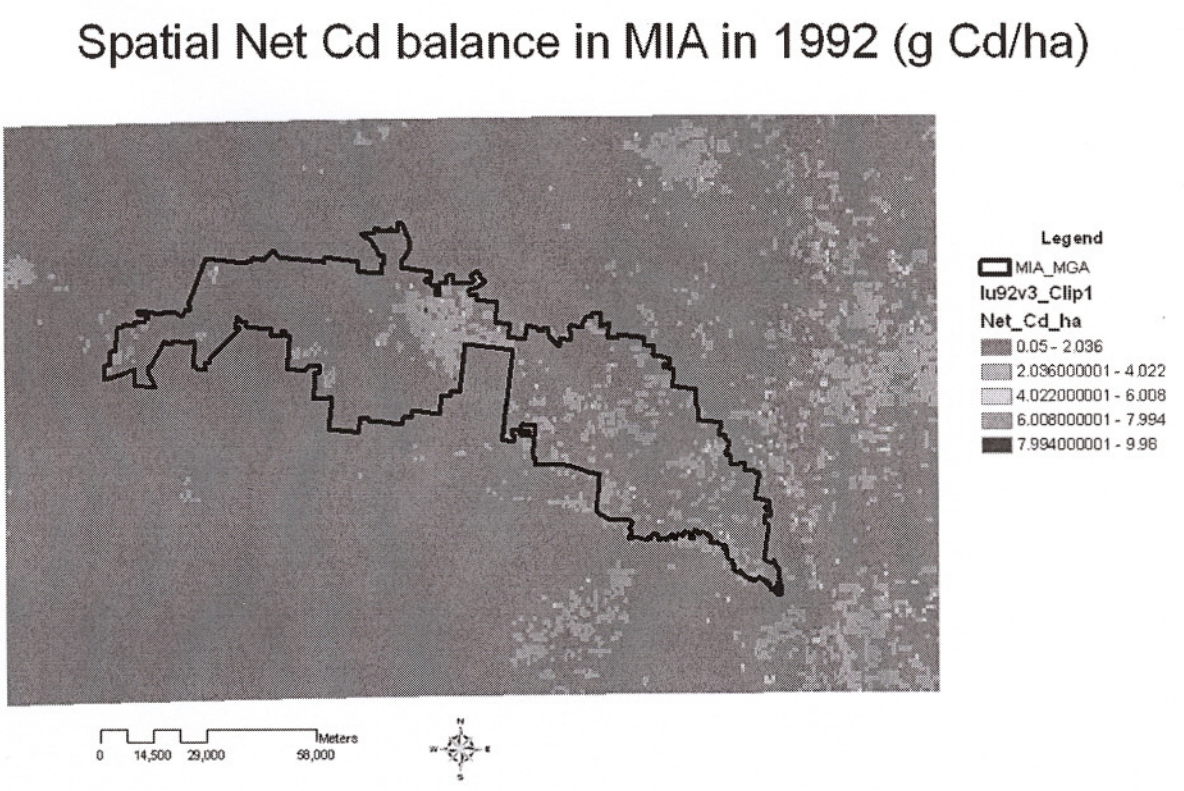

Figure 7 Spatial net Cd balance in MIA in 1992 (g Cd/ha)

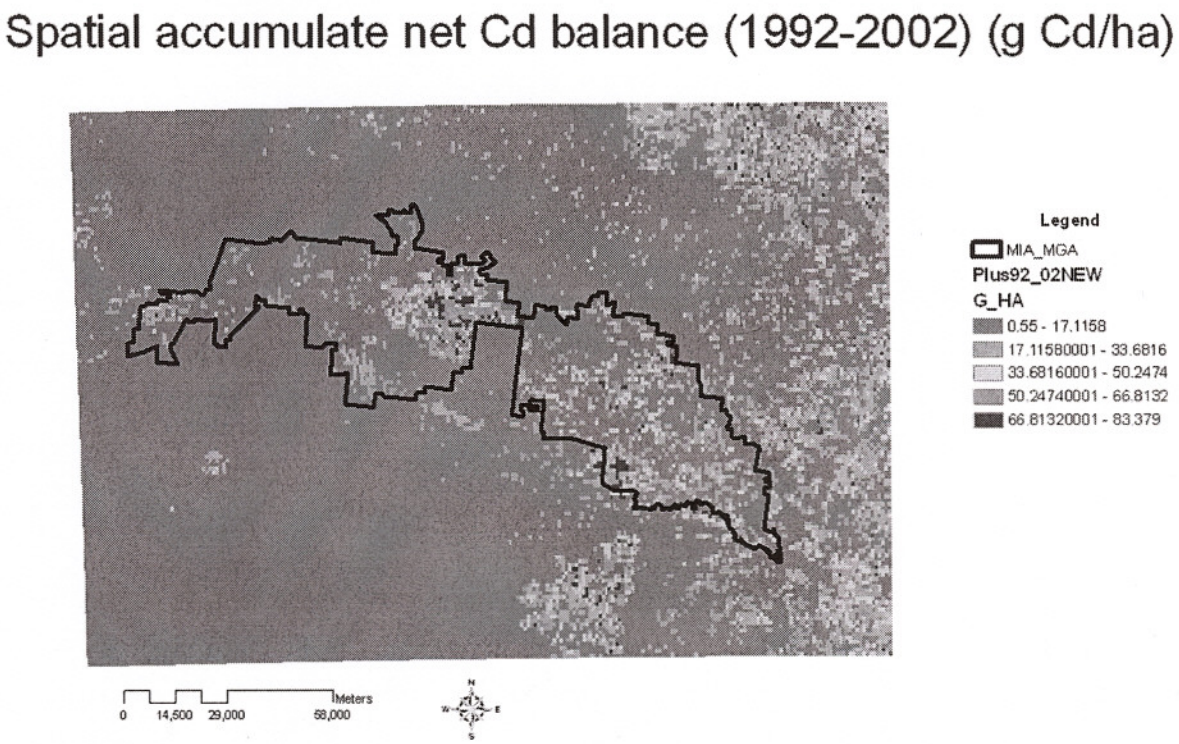

Figure 8 spatial accumulated net Cd balance in MIA (1992-2002) (g/ha)

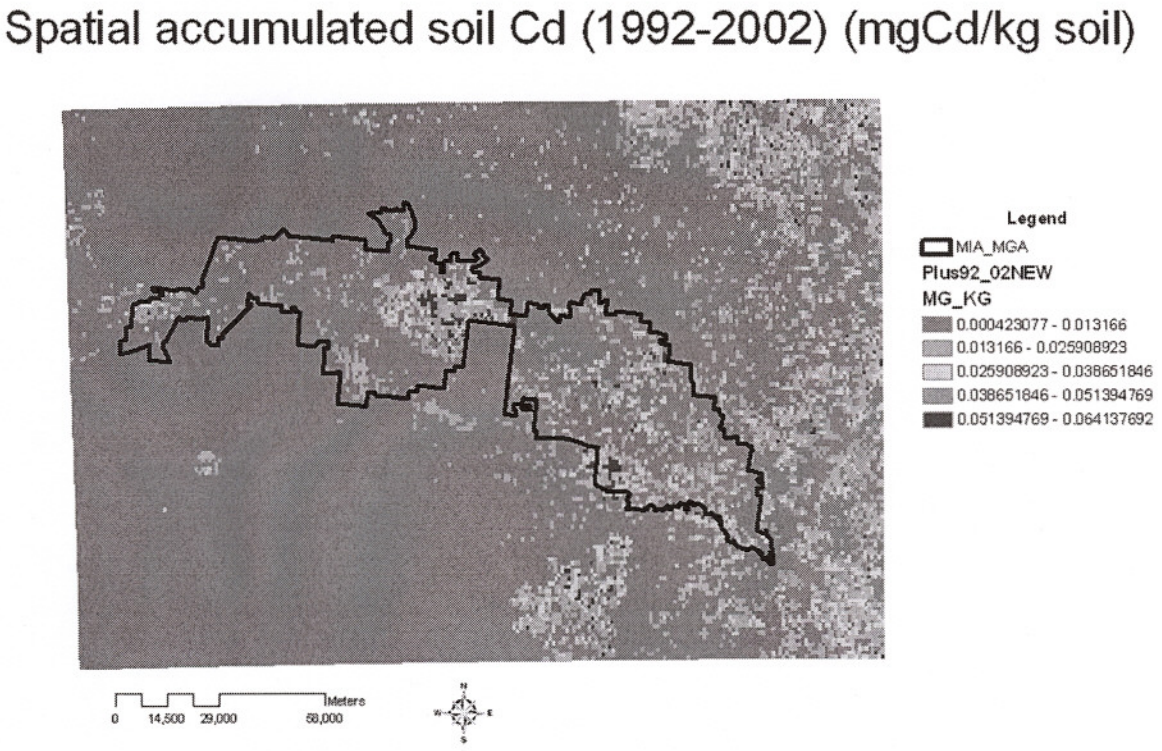

Figure 9 Spatial accumulated soil Cd concentration in MIA (1992-2002) (mgCd/kg soil)

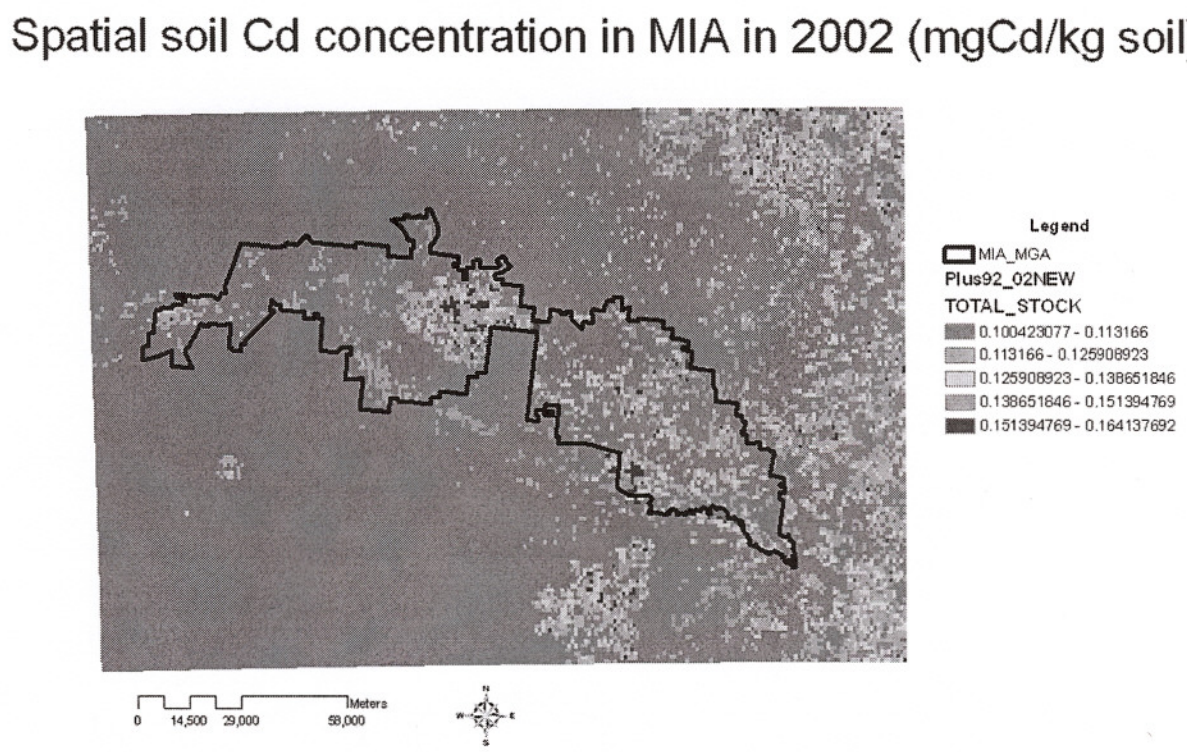

Figure 10 Spatial soil Cd concentration in MIA in 2002 (mgCd/kg soil)

The increase in soil Cd concentration from 1992 – 2002 (mgCd/kg soil), which is calculated using formula (9), is shown in Figure 9 , The results show that the land areas that have high increase in Cd accumulation in soil include: oilseed (0.051 – 0.064 mg Cd/kg soil), sown pastures (0.038 - 0.064 mg Cd/kg soil), citrus (0.051 – 0.064 mg Cd/kg soil), grape (0.051 – 0.064 mg Cd/kg soil), stone fruit (0.051 – 0.064 mg Cd/kg soil), apples (0.051 – 0.064 mg Cd/kg soil), pears (0.051 – 0.064 mg Cd/kg soil). Other crops, including: rice and cereal, were applied with low Cd phosphate fertilizer, resulting in lower soil Cd concentration (0.013 – 0.039 mg Cd/kg soil).

Estimated soil Cd concentration in 2002, calculated from formula (10), assuming the average soil Cd concentration in MIA is 0.1 mg Cd/kg soil in 1992, is shown in Figure 10. In 2002, Cd concentration in soil is high in crop lands that have been applied with high Cd fertilizer, including: oilseed (0.151 – 0.164 mg Cd/kg soil), sown pastures (0.138 - 0.164 mg Cd/kg soil), citrus (0.151 – 0.164 mg Cd/kg soil), grape (0.151 – 0.164 mg Cd/kg soil), stone fruit (0.151 – 0.164 mg Cd/kg soil), apples (0.151 – 0.164 mg Cd/kg soil), pears (0.151 – 0.164 mg Cd/kg soil). These crops especially citrus and grape take up very low Cd, so the output in terms of harvested crops contain low Cd, therefore a large part of Cd still remains in the soil. In these area soil Cd concentration in 2002 is almost 1.5 times the soil Cd concentration before 1992 (i.e., soil Cd concentration increase 0.5-0.6 times in 10 years). This means the soil Cd concentration can exceed the recommended limits of 1 mg Cd/ kg soil in 200 years. However, Cd contamination in crops can exceed the food standard in 100 years before exceeding soil concentration limit. Therefore, the recommended soil concentration limit needs to be re-considered, to be compatible with the risk of Cd contamination in

particular crops, relating to their uptake characteristics. The agriculture use zoning of these high soil Cd areas needs to be reconsidered. These areas should not be used to grow high Cd uptake crops such as, potatoes cereals, rice and vegetables in the future. Cd input to the areas where these crops are to be grown needs to be reduced.

In the areas which are applied with low Cd phosphate fertilizer, including rice and cereal, result in lower soil Cd concentration (0.113 – 0.139 mg/kg). The soil Cd concentration in these areas in 2002 is about 1.01-1.3 times the soil Cd concentration before 1992. The upper rate still can cause the risk of exceeding Cd in the food standard[3], even though this is in the medium term of 200 years.

The model in this paper made a number of assumptions such as, type of fertilizer and fertilizer and manure application rate, which are normalized across the region. Due to limit of contacts, time and resources in this study, such data from every farm could not be acquired. The model will be more precise if all the data can be obtained routinely from every farm, and used in the model in an annual update.

A government agency should undertake such data collection from each farm; so that a detail routinely updated spatial material flux analysis of Cd on land can be developed to provide ongoing monitoring of the study of the status of Cd contamination and action that needs to be taken to avoid future adverse impacts on the agricultural use of the land. In Australia this could be undertaken by including farms in the National pollutant inventory (NPI), where Cd emission to land are already covered for other industries (www.npi.gov.au).

CONCLUSION

This paper describes a new methodology for integrating Material Flux Analysis (MFA) and Geographic Information System (GIS) to estimate spatial inputs, outputs and accumulation of stock of Cd in agriculture areas and demonstrates this with application to the Murrumbidgee Irrigation Area (MIA) in Australia between 1992-2002.

The methodology begins with adding inputs and outputs fields and data, into a GIS land use data attribute table. These inputs and outputs are formulated by allocating different data associated with types of crops growing and land use. Secondly, calculation of the net Cd balance from each year is undertaken by deducting outputs from inputs for each parcel of land. Thirdly, the net balance of each year is combined together to find the total accumulation from the base year to the final year. Finally, the net balance accumulation to Cd soil concentration is calculated and combined with the previous soil Cd concentration in the base year to obtain the estimated Cd concentration in the final year.

In the case study in this paper, the result presents the spatial estimated Cd accumulation and concentration in the MIA in 2002. The areas that have high Cd concentration are revealed. In these areas, Cd concentration in soil is as high as 1.5-1.6 times of the soil Cd concentration before 1992; namely crop land that has been applied with high Cd fertilizer, such as oilseed, sown pastures, citrus, grape, stone fruit, apples, pears. The areas which have been applied with low Cd fertilizer, such as cereals and rice and vegetables, have lower soil Cd concentration. The Cd accumulation to soil and crops need to be reduced by: reducing Cd concentration in fertilizer, designate of Cd vulnerable and risk zones and control crops that will be planted in such a zone, reduce the use of phosphate fertilizer, decrease Cd availability to crop and remove Cd from soil.

The integration of MFA for Cd with GIS over a time period greater than the conventional one year enables the spatial accumulation of Cd to be tracked in more detail than could be undertaken by relatively unreliable random sampling and analysis of soils. It also allows a more detailed spatial-temporal plot of Cd accumulation in the region to be projected. Where adverse impacts can be anticipated, the model facilitates the design of alternative agricultural management practices to be developed to avoid these impacts. The method can also be applied to a range of substances from associated economic processes in all regions, enhancing the application of MFA to the development of preventive strategies to protect the quality of receiving environments for future generations.

ACKNOWLEDGEMENTS

This research is supported by a Research Grant from the Faculty of Engineering at the University of New South Wales. The authors would also like to acknowledge the willing supply of data and background knowledge from the MIA agricultural industries and local government interviewed during this study. We would also like to thank the referees for their comments.

REFERENCES

1. Mclaughlin, M., 2000. Australian agriculture acts to reduce Cadmium Levels, CSIRO Land and Water, Australia.
2. Warne, M, S., Brent, P., Drew, N., Klim, E., Mclaughlin, M., Milham, P., Rayment, G., Shelly, B., Sparrow, L., 2006. Aims of the NCMC, Raising Public Awareness and Co-ordinating Cadmium Activities in Australia.. Effective management of Cadmium: A case study. National Cadmium management committee, Australia
3. ANZFA. (1997). Food standards code, amendment 35, Australia and New Zealand Food Authority, Canberra.
4. Mclaughlin, M., Warne, M, S., Brent, P., Drew, N., Klim, E., Milham, P., Rayment, G., Shelly, B., Sparrow, L., 2006. Australia's National Cadmium Database and National Cadmium Budget. National Cadmium Management Committee, CSIRO, Canberra, Australia
5. Brunner, P. H. and Rechberger, H., 2004. Practical Handbook of Material Flow analysis. Lewis Publishers, Vienna.
6. Daniels, P. L. and Moore, S. J., 2002. Approaches for quantifying the metabolism of physical economies: part 1 methodological overview, Journal of Industrial Ecology, **5:** 69-93.
7. Murrumbidgee Irrigation Ltd., 2006. Regional Production in Murrumbidgee Irrigation Area. [online],Available: http://www.mirrigation.com.au/AboutUs/Water_for_Life.htm#Production
8. Bernhardsen, T., 2002. Geographic Information Systems: An Introduction, Wiley, New York. Wiley. New York.
9. Singh, S., 2006. Grapevine nutrition literatures review, Cooperative Research Centre for Virticulture, SA, Australia.
10. Chvyl, L. and Maier, N., 2005. Grapevine nutrition 2: Phosphorus fertilization, Cooperative Research Centre for Virticulture, SA, Australia
11. Bright, J., 2005. Apple and pear nutrition. Primefacts 85, NSW department of primary industries, State of New South Wales, Australia.
12. Farrel, T., Serafin, L., Kneipp, J., 2007. Summer crop production guide. NSW department of primary industries, State of New South Wales, Australia.
13. Jenkins, A., 2004. Managing soil amendments and fertilisers for a cleaner environment. AGFACTS, NSW department of primary industries, State of New South Wales, Australia.
14. Edwards, J., Roberts, K., 2006. Soil-phosphorus after drought, NSW department of primary industries, State of New South Wales, Australia.
15. NSW Department of primary industries, 2005. Best practice guidelines for growing vegetables, NSW department of primary industries, State of New South Wales, Australia.
16. NSW Department of primary industries, 2007. Ricecheck recommendations, NSW department of primary industries, State of New South Wales, Australia.
17. Kwonpongsagoon, S. (2007). Integration of substance flow analysis, transport and fate of materials in the environment, and environmental risk assessment for provision of information for environmental management: cadmium as a case study in Australia, PhD thesis, The University of New South Wales, Sydney, Australia.
18. Australian Bureau of Statistics (ABS), 2002. The Agricultural Census 2000-2001, Commonwealth of Australia, Canberra.
19. Australian Bureau of Statistics (ABS), 1994. Agricultural statistics-selected small area data, New South Wales 1992-1993, Commonwealth of Australia, Canberra.
20. Australian Bureau of Statistics (ABS), 1997. Agricultural statistics, New South Wales 1995-1996, Commonwealth of Australia, Canberra.
21. Australian Bureau of Statistics (ABS), 1998. Agricultural statistics, New South Wales 1996-1997, Commonwealth of Australia, Canberra.
22. McLaughlin, M. J., Tiller, K.G., Naidu, R., and Stevens, D.P., 1996. Review: the behaviour and environmental impact of contaminants in fertilizers, Australian Journal of Soil Research **34**: 1-54.
23. Jinadasa, K. B. P. N., Milham, P.J., Hawkins, C.A., Cornish, P.S., Williams, P.A., Kaldor, C.J., and Conroy, J.P., 1997. Heavy metals in the environment: survey of cadmium levels in vegetables and soils of Sydney, Australia, Journal of Environmental Quality Vol. 26, pp 924-933.
24. Bureau of Resource Sciences, 1997. Report on the National Residue Survey: 1993-1994, 1995, 1996 Results, Bureau of Resource Sciences, Commonwealth of Australia, Canberra

Autonomous Security Hexapod Agent for Crop Production

[1]Md. Masum Billah, [1]Soheli Farhana and [2]Md. Motasim Billah
[1]Faculty of Engineering, International Islamic University Malaysia (IIUM), Jalan Gombak, 53100 Kulala Lumpur, Malaysia.
[2]Department of Physics, Jahangirnagar University, Dhaka, Bangladesh

Abstract: This paper presents a secured engineering solution to the crop production hazards involved in spraying chemicals to the insects in the crop production field or sends information to the central security unit to alert them whenever the enemy is out of control. This is achieved by the design and construction of an autonomous hexapod agent robot for use in production security and enemy prevention applications in crop production field where people can not go to prevent anti crop production animal. The effectiveness of this platform is shown by the platforms ability to successfully navigate itself everywhere of a crop field, while the spraying system efficiently covers the insects in the set dosages, whenever it fail to cover then it will inform control room automatically from its self learning intelligence. Finally the design and simulation of a hexapod agent for crop production field is developed here.

Keywords: Autonomous, hexapod, crop field.

INTRODUCTION

The function of a crop field is to create the optimal growing conditions for the full life of the plants[1]. Achievement of the desired conditions often requires the use of spraying, high temperatures and increased carbon dioxide and humidity levels[2]. Prolonged exposure of crop workers to these conditions leads to an uncomfortable and hazardous work environment[3][4]. Often, there are substantial risks involved in crop field work due to the hazardous environment. Specific examples of these include: Repetitive strain injury, toxic chemical exposure, ex-termed heat exposure, extreme humidity (heatstroke)[3], and working at heights to protect insects. Automating tasks within the crop field will enable the avoidance of unwanted or hazardous human exposure whilst potentially leading to an increase in overall efficiency and productivity. The main application of robots in the production sector has been concerned with the substitution of manual human labor by robots or mechanized systems to make the work more time efficient, accurate, uniform and less costly[5]-[10]. One may argue the social implications of such developments, for example, the effects on employment through loss of blue collar jobs to the more efficient robotic counterpart; there are also ethical considerations that may be argued. Whilst there may well be some validity to the argument in some cases, this current project s unique in the number of stakeholders that are affected in a positive sense. The farmers' benefits are found in more efficient maintenance of the crops and either less work for themselves or a decreased need for the employment of others (arguably, an expensive process). Increased demand on growers has begun to be met with increased specific automation in many fields, as producers believe that automation is a viable and sometimes necessary[7] method to ensure maximum profits with minimum costs[6]. Indeed Hopkins[6] argues that automation enables the expansion of a crop field without having to invest more financial resources on labor. Merchants may benefit from increased sales due to a lower cost product; the consumers will benefit, likewise, a lower cost product of comparable quality. The stakeholders that benefit most, at least from an ethical or social perspective, however, are the crop field workers. This paper presents the design and construction of an autonomous hexapod agent robot that seeks to give the security to the crop field. This robot is designed as a base for developing systems to enable the automation of crop production security processes such as the spraying to the insects, send alert

Corresponding Author: Md. Masum Billah, Department of Mechatronics Engineering, Faculty of Engineering, International Islamic University Malaysia (IIUM), Jalan Gombak, 53100 Kuala Lumpur, Malaysia, E-mail: liton_aub@yahoo.com.

information to the security center for the uncontrolled animal. The system is designed to be as modular as possible, enabling the development and modification of any of the individual tasks.

LITERATURE REVIEW

This is proposed current technique for spraying insect killer. To controlling the anti crop insect, carbon dioxide enrichment, temperature, humidity, root moisture, fertilizer feed, pest and fungus control allow the crop field to produce fruits, vegetables all year round. For example, carbon dioxide levels in a controlled crop field are approximately five times the normal atmospheric levels[11]. The optimal height of crop field during the normal production time can be quite high, making it very difficult and impossible for worker to prevent anti crop production kit. This can subject the worker to risks to help the crop to grow up. The inhalation of spraying insect killer used within a crop field can, in some cases, be fatal or cause permanent damage to the lung tissue. Even relatively small amounts of exposure to many chemicals over long periods of time can be damaging to the worker. Due the hazards of such exposure, protective clothing and equipment must be used. However, research has showed that protective clothing does reduce the possible amount of exposure but does not stop it[3].Many insect killer spray have been found to be able to penetrate clothing and even rubber gloves within half an hour and a manual spraying task can take several hours depending on the size of the crop field. Fig. 1 shows a typical crop of the crop field. Contemporarily, a human worker would walk inside field with an insect killer spraying gun, in an attempt to cover the foliage of the plants with an even coat of spray. An experienced worker will attempt to coat the surface of the plants with the appropriate calculated dosage to the insect. This manual application of spraying is, as mentioned above, a time consuming, tedious and dangerous task, requiring the worker to wear protective clothing and breathing apparatus for all times. Hence, this manual application technique is largely open for error. It is often difficult to know exactly the insect places of each plant to spray, mostly to detect on ground close with the root of the plant. In this harsh environment, it is possible that the worker may also apply an inappropriate amount of spray to the unexpected area through either fatigue or haste, resulting in the inefficient application of spraying. The alternative method to manual spraying is Fog spraying to kill the insect. This involves using a fogging sprayer to spray the whole crop field with a fine mist that covers every surface[12]. This is useful where the crop field is infested with small flying medicine and the entire field requires spraying. This method is not always desirable and cannot cure all enemy. An autonomous hexapod insect killer spraying device would be invaluable in the avoidance of human exposure to hazardous chemicals and to ensure the optimal calculated amount of spray is applied to all insect evenly, minimizing waste due to increased accuracy and precision[13]. A further advantage of using an autonomous hexapod agent is that various concentrations of enemy can be applied at levels where there would normally be an increased the risk of toxin exposure to the human applicator. And it can also be easily navigate all the places to detect the enemy by an active vision system[16]-[19].

Fig. 1: Typical crop field

For the future implementation of a crop field robot to be commercially viable, such a product would have to be at a low cost, or have the potential to make sure perfect security, or most, of the current manual tasks within a crop field. Some of these potential applications include monitoring plant health, destroy insects, inform against uncontrolled enemy, plant growth rates, removing unwanted leaves and picking the produce. In principle, a system able to satisfy these requirements seems viable, as the requirements may be met via a common basic pathway. Whilst it is recognized that there is generally more than one solution to an engineering problem, an example of a system able to achieve this would be that consisting of a mobile platform with a robot on an elevating plat- form, which would then satisfy the pruning, picking and monitoring of produce, essentially adding to the robot this paper has outlined. As mentioned, the considerable economic

and social costs related to the manual process of security application within crop field (specifically labor costs and the human health risks respectively) is far outweighed by the economic and social benefits of an autonomous robot such as that discussed by this paper. The benefits include the decreased labor costs, reduced spraying medicine wastage costs and the obvious reduction in human health hazards[14][10]. The commercial aspirations of this project require the total cost to be kept to a minimum. Such cost effective automation should therefore be relatively attractive to growers. In addition to the cost considerations, all parts and materials have been purchased from local distributors. Whilst this has been done to simplify the future manufacturing of the commercial product, finally, to enable the ease of reproduction, modification and replacement, almost all components are assembled from off the shelf parts.

DESIGN OF THE AGENT

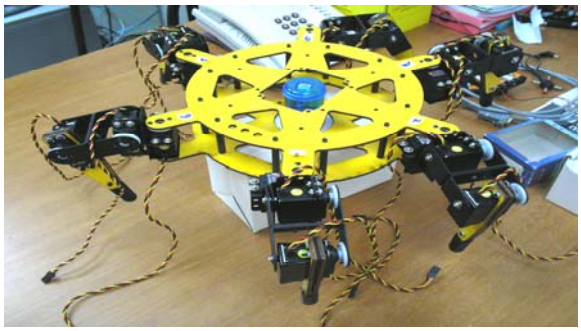

Fig. 2: Frame of Hexapod agent

The basic frame of the hexapod agent is shown in Fig. 2. The full configuration is shown in Fig. 3, is a standard installation for crop field and can reach every complex environment. To attack against the enemy it will rotate in any direction, heavy legs with powerful motors are chosen over other types as they can withstand heavy loads and high temperatures with no deviation to travel height. Fig. 4 shows the central control alarm unit, where robot can send signal to alert by turn on the alarm.

Fig. 3: Organization of all components

For its legs, it can navigate all the area of the crop field and try to detect the insects by its proposed camera with active vision system technique, then it will able to make decision to automatically spray against to the insects by its proposed sprayer configuration, if the agent assume that the insect/enemy is uncontrolled then it transfer signal to the alarm unit by its wireless system. The proposed induction sensor will be connected directly to the microcontroller; allowing the robot to sense that it is indeed on the correct area. The arranged legs assembly keeps the robot on the tracks allowing the robot to drive along without the need for any expensive and complicated navigation ability. For ease of design and reproduction, as few parts as possible require special machining or manufacturing in an attempt to minimize the cost of manufacturing this and repeat robots. This choice to use as many off the shelf products as possible carried with it significant challenges, but is mostly regarded as an important reality check in the design process enabling the optimization of a simple and flexible design to be realized. The robot is designed for simplicity and value for money, while it will be able to effectively spray insects in the crop field. The robot is capable of walking to the end and back along in the field, requiring then to be automatically moved to another part. From the micro-controller placement to aligning individual nut and bolts, each component is modeled into place to ensure the most space efficient design, minimizing the physical dimensions of the robot, while keeping all simplicity and functionality.

Fig. 4: Central Control unit Alarm System

SAFETY CONSIDERATION

As this system is possibly working without supervision, safety aspects must be considered to ensure the safety of the robot, the people that may be within the crop field. Easily accessible Emergency Stop buttons, anti-bump start button, separate enable switches for pump (proposed) and servo motor, Key activated power switch, fast blow fuses and bump sensors are the main safety components built into the design of this robot and it also be detecting obstacle. If an emergency stop button is triggered by either button or microcontroller, the robot will stop and user intervention is required to restart to robot. Onboard RF connectivity allows for the future realization of wireless control of the robot. This allows for remote monitoring and control of robot functions. The bump sensors are located at the down of the six leg of the robot to stop the robot from bumping into any objects that may be in the path of travel. If triggered, the microcontroller will promptly stop the robot within its buffer zone. Unlike the Emergency stop buttons, the robot will continue its path of travel when the obstruction that triggered the sensor is cleared and it is safe to move.

CONTROL SYSTEM

Fig. 5 shows the control environment currently implemented. The user interfaces have control over the running of the microcontroller and are fed back information about the status of the robot. The microcontroller reads the information and controls the movements of the robot and actions of the proposed spraying system. The drive system consists of servo motors capable of a maximum speed is 10”/sec. The motor is driven by a high powered PWM (Pulse Width Modulation) controller board, signal from the microcontroller.

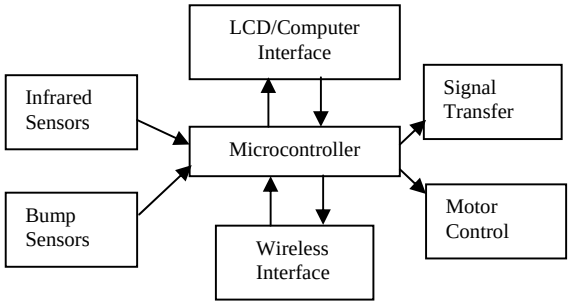

Fig. 5: Control environment of the developed system

The servo motor controller has its own soft start and stop facilities allowing smooth stopping and starting with no processing time required for the microcontroller. The 0-5v analogue signal input also allows the microcontroller to control the speed, acceleration and declaration. The induction proximity sensors accurately detect the presence of the metal rails beneath the robot. This allows for safe, hassle free operation of the robot within the crop field requiring no changes to the existing crop field configuration. The SICK infra-red sensors accurately sense the placement of the reflective sensors as they pass beneath the robot. The reflective sensors are a simple and efficient method of marking a selected insect. The sensors can be replaced with a more advanced method if detecting a selected insect as the technology advances, allowing the potential for the robot to almost fully automated. The LCD/Computer module shows the user relevant information on the robots status and allows the user to control the robot directly with ease. The wireless interface able to pass signal from the microcontroller to the alarm control centre which is potential for the robot to be monitored, controlled and detect enemy from a remote location. Keeping the user at a safe distance to prevent the enemy.

CONTROL ALGORITHM

The on-board microcontroller controls all of the inputs and outputs of the system. The software running on the processor is Dynamic PIC C language. Extra libraries and functions have been added to the original PIC C language that is specific to the PIC-microcontroller. Of particular notice are the multi-tasking functions. Both the Preemptive multitasking and Cooperative multitasking is available. Pre-emptive, being the ability to time slice the program code so that many processors can be sharing the processor times to make it seem like the processes are running at the same time. In the Co operative multitasking environment, each process voluntarily passes control to the other processes. Usually done while waiting for something to happen. For example, a button press, or a delay to finish. The processor uses this usually wasted 'waiting time' to execute other processes. Figure 6 shows the current basic program flow chart. The Platform Control program is used to control the mobility of the base platform. It carefully monitors the autonomous intelligence of the robot and monitors sensor inputs. Our algorithm Hypotheses: In a homogeneous population of agents is considered for this hexapod agent, i.e. the robot has the same capabilities of sensing, acting, communicating and processing. Moreover, the considered task is safe and robust reactive navigation in a clustered environment for exploration purposes. The robot is programmed a priori neither for obstacle avoidance nor for enlarging the explored area, and nor for executing more complex actions like, Finding a task, Analyze the task, then take the decision. On the contrary, the agent has to find by itself an efficient policy for performing the complex task. The online self-learning procedure is based upon the principles of genetic algorithms that allow a faster convergence rate than the classical learning algorithms, as it is shown in what follows.

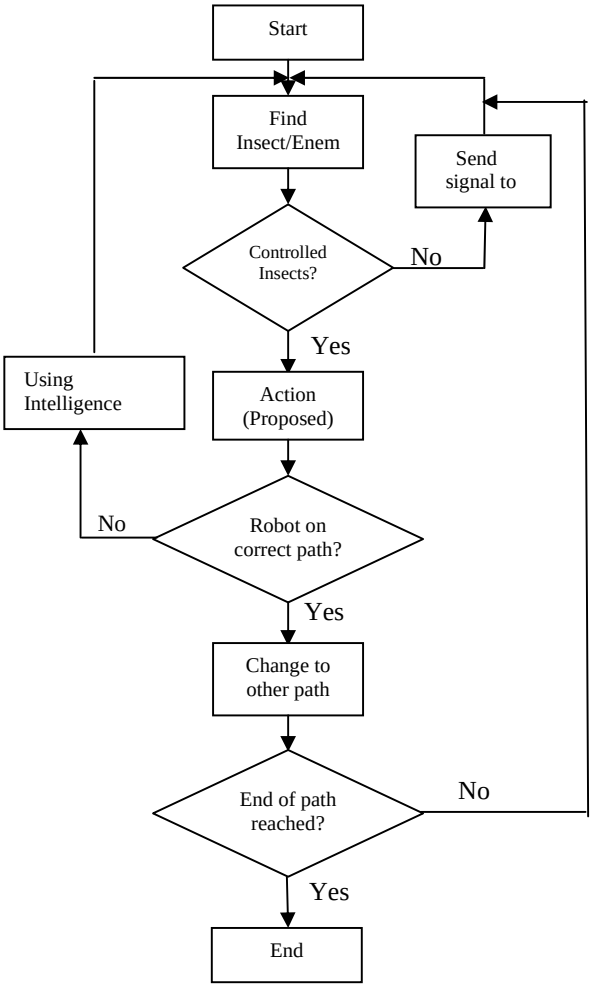

Fig. 6: Control program Flow Chart

The algorithm's operation is then illustrated by considering the exploration problem, which is simple to evaluate and to implement on real robots. The inputs of the sensor motor system are composed of five states listed in Table 1. These states can easily be recognized by the proximity sensors of the robot. On the other hand of the control system is the elementary behaviors of the robots are given in Table 2. It actuates immediately and properly the leg motors. By getting knowledge from these two tables, robot will perform correct activities mention in Table 3. An individual of the population considered for the evolutionary learning is the list of connections between inputs and outputs. It encodes thus the "synapses" of the robot's sensor motor control system. Such states and elementary actions have been choosing to guarantee that the behavior is learnable during the battery life. The manipulations of optimal state are showing in Fig. 7.

Table 1: Different states of an agent's sensory system

State 1	No obstacle
State 2	Left obstacle
State 3	Right obstacle
State 4	Front obstacle
State 5	Robot is jammed

Table 2: Set of elementary reactions

Behavior 1	Go forward
Behavior 2	Turn right
Behavior 3	Turn left
Behavior 4	Go backward

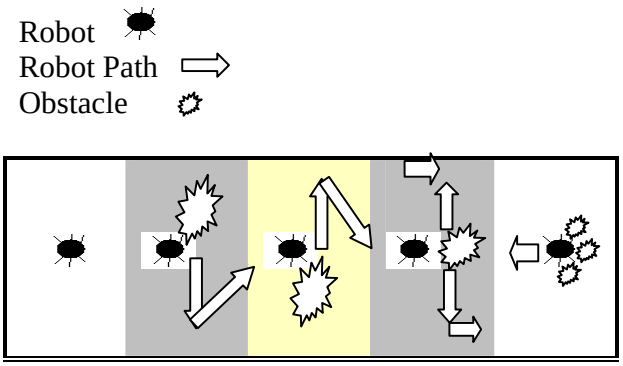

Fig. 7: Optimal State

Table 3: Optimal decision by robot

1: No obstacle	1: Go forward
2: Left obstacle	2: Turn right
3: Right obstacle	3: Turn left
4: Front obstacle	2 or 3 Turn left or right
5: Robot is jammed	4: Go backward

TESTING

The robot was tested in the crop field at The International Islamic University Malaysia, where pumpkin plants are grown. Figure 8 shows the on-site experiment with the developed robot where the robot will take action against the enemy. Robot takes action (proposed) by using intelligence only. The testing consisted of single runs down to the end of a row of the crop field and back to the work area while taking action to the enemy. Along the run, the enemies were marked out by the robot. While in operation, emergency stop buttons and bump sensors were tested for their effectiveness in a real situation.

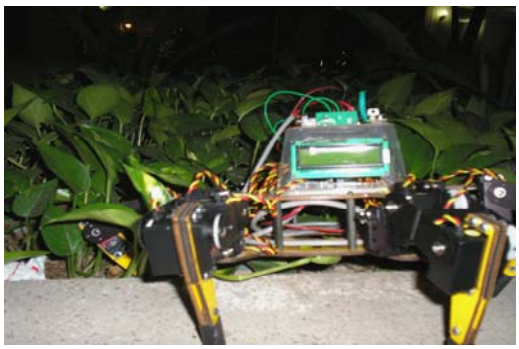

Fig. 8: Control program structure

The platform was able to successfully and smoothly drive up and back along a row in the crop field and return to the work area at the end of the row. The intelligence worked sufficiently to turn the robot around and stop the robot when it returned to the start. The identification of the reflectors was excellent until taking action from one of the Infra-Red sensors. It also send signal to the alarm unit for the uncontrolled insects.

CONCLUSION

The experiments show that the robot was able to successfully fulfill the physical specifications outlined by International Islamic University, so as to be able to function within their crop production field. The robot also met the economic and time constraints that it was subject to. The robot was able to move up and back along the pathway in the crop field. The Sensors detected the path way and operated satisfactorily against the insects. The coverage of the insects for taking action will be decided by the robot owns self. Even though the agent is unable to do any action against insect it will pass signal to help it to prevent enemies. At the far end of the crop field the sensors successfully detected the end of the path way, enabling the platform to change direction, coming back along the path way and returning to the start. The legs assembly was successful in delivering a smooth transition to every conditional path way. The bump sensors were tested for situations where people and obstacles such as branches were in the path of motion. The bumpers were successfully activated and the robot was able to be stopped within a safe distance so that no damage or injury was or could be caused. The design and successful construction of the robot using of the shelf components to under take the task of autonomously spraying insect killer within a crop field shows that it is possible and can be done via a simple and cost effective manner. Being a prototype, the robot has some components (namely servo motor and microcontroller) that are over designed for the simple task of action and taking self decision, resulting in the robot having surplus capacity. The use of this more sophisticated microcontroller enables greater cost efficiency when reproducing a commercial product, as a dedicated microcontroller with less capability and a correctly designed motor for the internal weight and performance requirements would be correspondingly cheaper. Conversely, as a result of this over design there is a lot of further work that can be done to improve this robot without increasing the price by the additional cost of a more sophisticated microcontroller. The over design can be justified because it can cope with multitasking additional attachments.

REFERENCES

1. Badgery-Parker, J. (1999), Agnote DPI/249, Edition1, pp. 1-2.
2. Van Henten, E.J., Hemming J., Van Tuijl, B.A.J., Kornet, J.G., Meuleman, J., Bontsema J., & Van Os,E.A. (2002), An Autonomous Robot For harvesting Cucumbers in Greenhouses", Autonomous Robots, Vol 13, pp. 241-258.
3. Riley B., Siemsen-Newman L., (2003) Health Haz-ards Posed to Pesticide Applicators", Northwest Coalition for Alternatives to Pesticides, pp. 17-24. [4] Tosaki K., Miyahara S., Ichikawa T, Taniai S., Mizukura Y, Moriki H., and Miyashita S. (1998), Development of Microcomputer-Controlled Un- manned Air Blast Sprayer" JARQ Japan Agricul- tural Research Quarterly, Vol 32, No. 3, pp. 83-90.
4. Sezen, B. (2003), Modelling Automated Guided Ve-hicle Systems in material Handling", Dogus Univer-sitesi Dergisi, Vol 4, No. 3, pp. 207-216.
5. Hopkins, M. (2000), Automating in the 21st Cen- tury Career and Technical Education", Greenhouse Grower, pp. 4-12.
6. Giacomelli G.A., and Ting K.C. (1995) Transportation and Robotics for Greenhouse Crop Production Systems", Acta Hort (ISHS), Vol 399, pp. 49-60.
7. Van Henten, E.J., Hemming J., Van Tuijl, B.A.J., Kornet, J.G., Meuleman, J., Bontsema J. (2003), Collision-free Motion Planning for a Cucumber Picking Robot", Biosystems Engineering, Vol 86, No. 2 pp. 135-144.
8. Pilarski, T., Happold, M., Pangels, H., Ollis, M., Fitzpatrick, K., Stentz A. (2002), The Dementer System for Automated Harvesting", Autonomous Robots, Vol 13, pp. 9-20.
9. Gan-Mor S., Ronen B., Kazaz I., Josef S., Bilanki Y. (1997), Guidance for Automatic Vehicle for Greenhouse Transportation", ACTA Horticulture, Vol 443, pp. 99-104.
10. Kellerman, D. (2002) Pickling Cucumbers", Com-mercial Vegetable - Production Guide, Agriculture Magazin, pp. 22-25.
11. Austerweil M., Grinstein A., (1997), Automatic Pesticide Application in Greenhouses", Phytopara- sitica, Vol 25, pp. 37-42.
12. Hetzroni A., Meron M., (2003) Mapping Tree Canopy for Precision Spraying", Technical Report, Department of Agriculture, Illinois, pp. 75-83.
13. Haire, B. (2003), UGA Scientists Develop 'row-bot' - Farming Robots not Science ¯ction but technical fact", Technical Report, Georgia Faces, University of Georgia.
14. Michelini R. C., Razzoli R. P, Acaccia G. M, Mol¯no R. M., (1998), "Mobile Robots in greenhouse Culti- vation: Inspection and Treatment of plants" ACTA Horticulture, Vol 453, pp52-60.
15. Franklin, D., Kahn, R.E., Swain, M.J. and Firby, R.J. 1996. Happy atrons Make Better Tippers: Creating a Robot Waiter Using Perseus and the Animate Agent Architecture. International Conference on Face and Gesture Recognition.
16. Huber, E. 1994. Object Tracking with Stereo Vision. AMA/NASA Conference on Intelligent Robots in Factory, Service and Space (CIRFFSS '94).

17. Olson, T.J. and Coombs, D.J. 1991. Real-Time Vergence Control for Binocular Robots. International Journal of Computer vision 7(1): 67-89.
18. Uhlin, T., Nordlund, P., Maki, A., and Eklundh, J.O. 1995. Toward and Active Visual Observer. ZCCV: 679-686.
19. H-S Lin, J. Xiao and Z. Michalewicz (1994) "Evolutionary Navigator for a mobile robot", ICRA'94, San Diego volume 3, pp.2199-2204.

Comparison of Thermal Time Calculated using Different Time Steps for Use in Crop Simulation Models

[1]Afshin Soltani, [2]Manouchehr Gholipoor and [1]Benyamin Torabi

[1]Department of Agronomy, Gorgan University of Agricultural Sciences and Natural Resources, Gorgan 49138-15739, Iran, [2] Department of Agronomy and Plant Breeding, Shahrood University of Technology, P.O. Box 36155-316, Shahrood, Iran

Abstract: Crop phenology prediction using thermal time (TT) concept has important applications in crop management and in crop simulation modeling. TT is calculated based on different time steps, varying from hourly to daily. In this study, a sensitivity analysis was performed over a wide range of daily temperatures and at temperature amplitudes (= $T_{max} - T_{min}$) of 0, 6, 12 and 18 ^oC to compare TT calculated using hourly, 3-hourly and daily time steps. Further, these time steps were compared in a simulation model of phonological development in chickpea (*Cicer arietinum* L.). The sensitivity test showed that absolute value of cumulative TT are different for daily and hourly time steps, but not between time steps of 1 and 3 hours. The difference was greater around cardinal temperatures and increased with increase in temperature amplitudes. Using hourly time step, higher absolute values of TT were obtained around the base and ceiling temperatures and the lower values around optimal temperature. However, when implemented in a simulation model of chickpea phenology, there was no difference between all the time steps. Therefore, it was concluded that there is no preferred time step, at least in chickpea, in calculation of TT and either hourly or daily time steps are adequate.

Key words: Thermal time; Time step; Phenology; Model; Simulation

INTRODUCTION

Thermal time (TT) concept has been widely used to quantify phenological development. TT is calculated based on cardinal temperatures and then is corrected for photoperiod if the crops or developmental stages are sensitive to photoperiod. Different time steps have been used by different researchers in calculating temperature and hence TT (Cesaraccio et al., 2001; Dwyer et al., 1999). Daily (DTT), 3-hourly (3HTT) and hourly (HTT) time steps are common in this regard.

There is no report assessing the difference between these time steps. In one study, Purcell (2003) only compared absolute values of TT derived from daily and hourly temperatures. Therefore, this study was aimed to determine: (1) under what conditions the absolute values of DTT, 3HTT and HTT are different, and (2) what time step is more suitable to be used in chickpea phenology modeling.

METHODS

A sensitivity analysis was conducted based on 3 temperature functions that describe response of development rate to temperature. These were (Fig. 1; Soltani et al., 2006ab):

Segmented function:

$f(T) = (T - T_b) / (T_o - T_b)$ *if* $T_b < T \le T_o$
$f(T) = (T_c - T) / (T_c - T_o)$ *if* $T_o < T < T_c$
$f(T) = 0$ *if* $T \le T_b$ *or* $T \ge T_c$

Beta function:

$$f(T)= \left\{\left[\left(\frac{T-T_b}{T_o-T_b}\right)\left(\frac{T_c-T}{T_c-T_o}\right)\right]^{(T_c-T_o)/(T_o-T_b)}\right\}^{\alpha}$$

if $T > T_b$ *and* $T < T_c$

$f(T)= 0$ *if* $T \le T_b$ *or* $T \ge T_c$

Dent–like function:

$f(T) = (T - T_b) / (T_{o1} - T_b)$ *if* $T_b < T < T_{o1}$
$f(T) = (T_c - T) / (T_c - T_{o2})$ *if* $T_{o2} < T < T_c$
$f(T) = 1$ *if* $T_{o1} < T < T_{o2}$
$f(T) = 0$ *if* $T \le T_b$ *or* $T \ge T_c$

where $f(T)$ is the temperature function that ranges between 0 and 1, T is the daily, 3-hourly or hourly temperature, T_b the base temperature, T_o the optimum temperature, T_{o1} the lower optimum temperature (for dent-like function), T_{o2} the upper optimum temperature (for dent-like function), T_c the ceiling temperature and α is the shape parameter for the beta function which determines the curvature of the function.

Corresponding Author: Afshin Soltani, Department of Agronomy, Gorgan University of Agricultural Sciences and Natural Resources, Gorgan 49138-15739, Iran

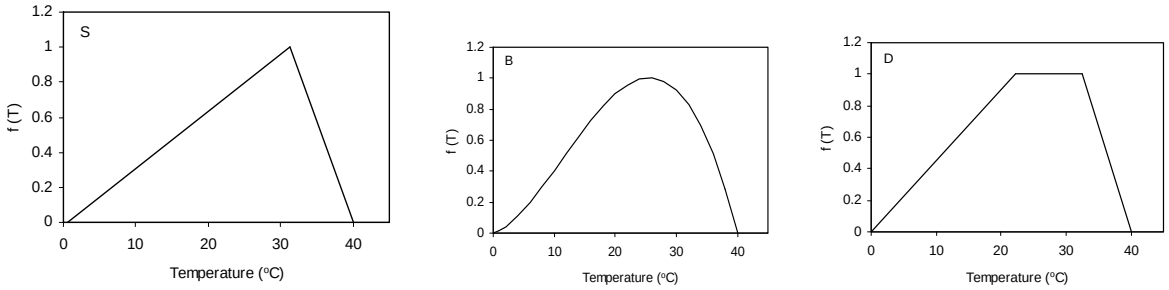

Fig. 1. Temperature response functions used to calculate thermal time. Functions are segmented (S), beta (B) and dent-like (D).

Various series of daily values of minimum (T_{min}) and maximum (T_{max}) temperatures were generated to have different means (from 0 to 40 °C) and amplitudes (= $T_{max} - T_{min}$) (0, 6, 12 and 18 °C). The values of 3-hourly and hourly temperature data were then calculated according to Jones and Kiniry (1986) and Yin et al. (1997), respectively. For each series, daily values of TT were calculated as:

$DTT_i = (T_{o1} - T_b).\ f(T_i)$ for DTT
$DTT_i = [\Sigma (T_{o1} - T_b).\ f(T_j)] / 8$ for 3HTT
$DTT_i = [\Sigma (T_{o1} - T_b).\ f(T_j)] / 24$ for HTT

where DTT_i is accumulated thermal time in day i, T_i is mean daily temperature in day i, T_j is temperature at every 3 (3HTT) or 1 (HTT) hour during the day i, $f(T_i)$ is $f(T)$ calculated using daily temperature and $f(T_j)$ is $f(T)$ calculated based on 3-hourly or hourly temperature. For segmented and beta functions T_{o1} is equal to T_o.

The values of 1 for T_b, 31 for T_o and 39 °C for T_c were used in segmented function. For beta function values of 0 for T_b, 26 for T_o, 39 °C for T_c and 1.8 for α were considered. For dent-like functions these were 0 for T_b, 22 for T_{o1}, 33 for T_{o2} and 39 °C for T_c. All the estimates are from Soltani et al. (2006ab).

In the second section of this study, we calculated DTT, 3HTT and HTT for sowing-emergence, emergence-flowering and flowering-maturity intervals, observed in the field under different sowing dates (7-9 sowings) and for four chickpea cultivars as reported by Soltani et al. (2006ab). And then the calculated values of TT were used to predict chickpea phenological development using independent data sets (Soltani et al, 2006ab).

RESULTS AND DISCUSION

The calculated TT versus mean temperature at various temperature amplitudes are indicated in Fig. 2 for segmented function, Fig. 3 for Beta function and Fig. 4 for dent-like function. The greater temperature amplitude, the greater was the difference between time steps with respect to absolute value of TT. At constant temperature (temperature amplitude of 0 °C) there is no difference between time steps. Around the cardinal temperatures, the difference between time steps were greater compared to other mean temperatures. It was found that there is no difference between hourly and 3-hourly time steps with respect to absolute value of TT. The value of TT was higher with hourly and 3-hourly time steps around the base and ceiling temperatures, but at optimum temperature the inverse was true.

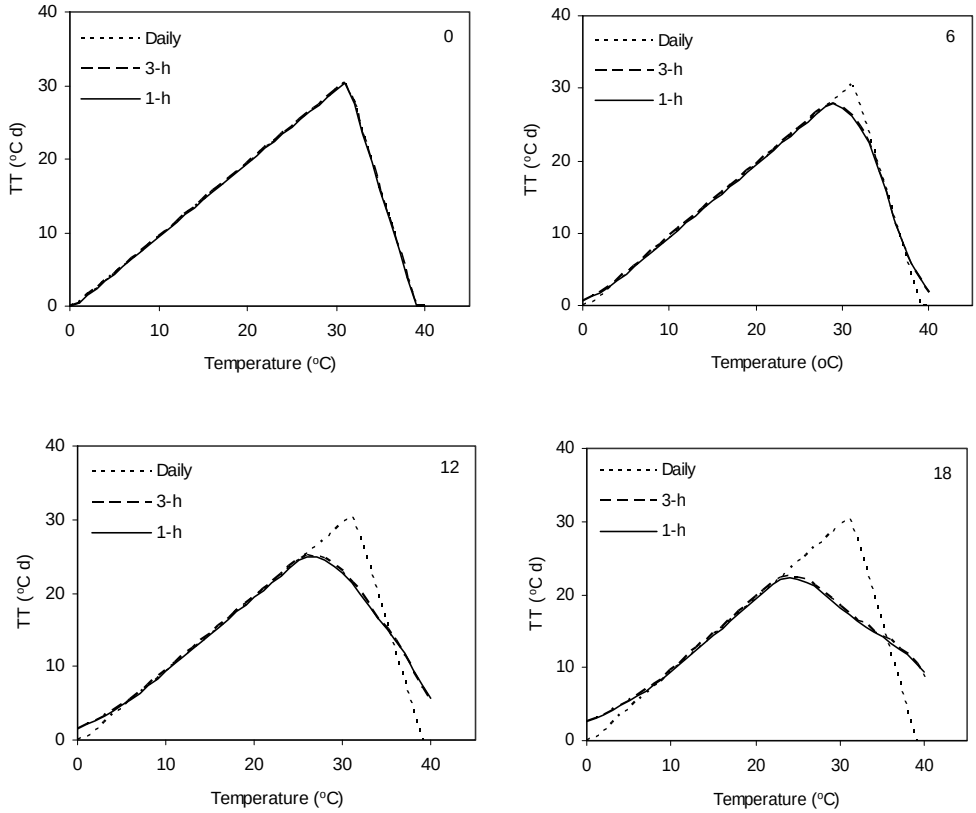

Fig. 2. Calculated thermal time based on segmented function versus mean temperature at temperature amplitudes (= Tmax – Tmin) of 0, 6, 12 and 18°C. Time steps used are 1, 3 and 24 h (daily).

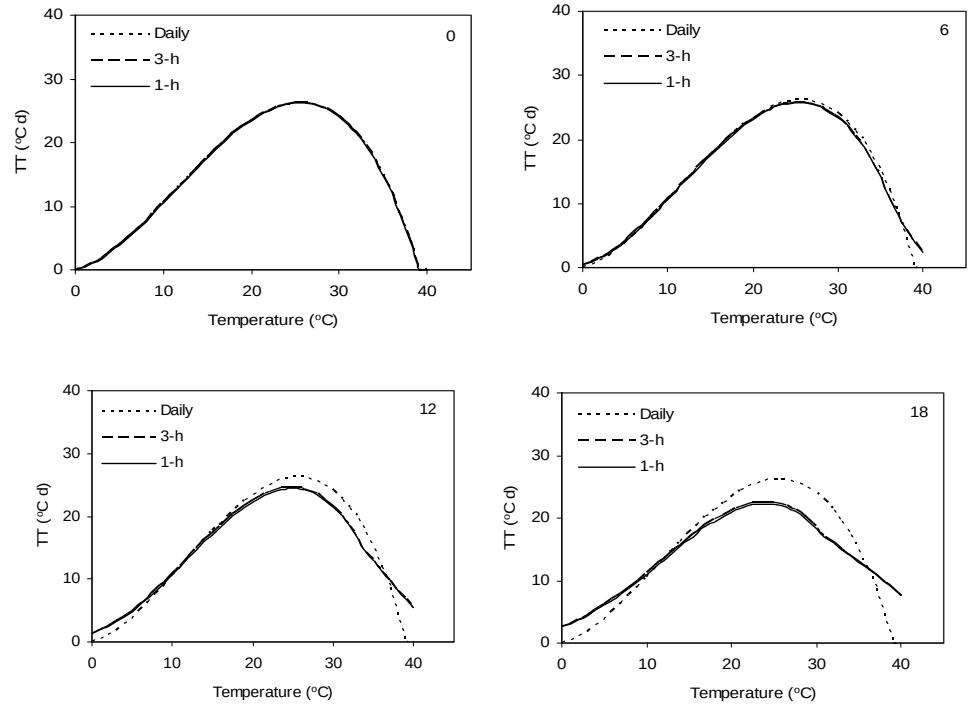

Fig. 3. Calculated thermal time based on beta function

versus mean temperature at temperature amplitudes (= Tmax – Tmin) of 0, 6, 12 and 18 ^{o}C. Time steps used are 1, 3 and 24 h (daily).

Purcell (2003) compared TT derived from daily and hourly temperatures. He compared the daily and hourly calculations of TT for two sets of cardinal temperatures for representative warm-season crops. His simulations across 43 years of weather data (Fayetteville, AR, USA) comparing the time required to cumulate 200 ^{o}Cd showed that nearly identical number of days was required for both DTT and HTT to reach to 200 ^{o}Cd. So, he concluded that for warm-season crops, there is no advantage in hourly calculations of TT over daily values. In fact, he compared absolute values of DTT and HTT and concluded that they are similar. However, as indicated in this study, DTT, 3HTT and HTT may be different with respect to absolute value and this does not show which one is better or more precise. The greater difference between daily maximum and minimum temperatures, the greater will be the difference between DTT, 3HTT and HTT. At Fayetteville, the difference between maximum and minimum temperature is 10 ^{o}C.

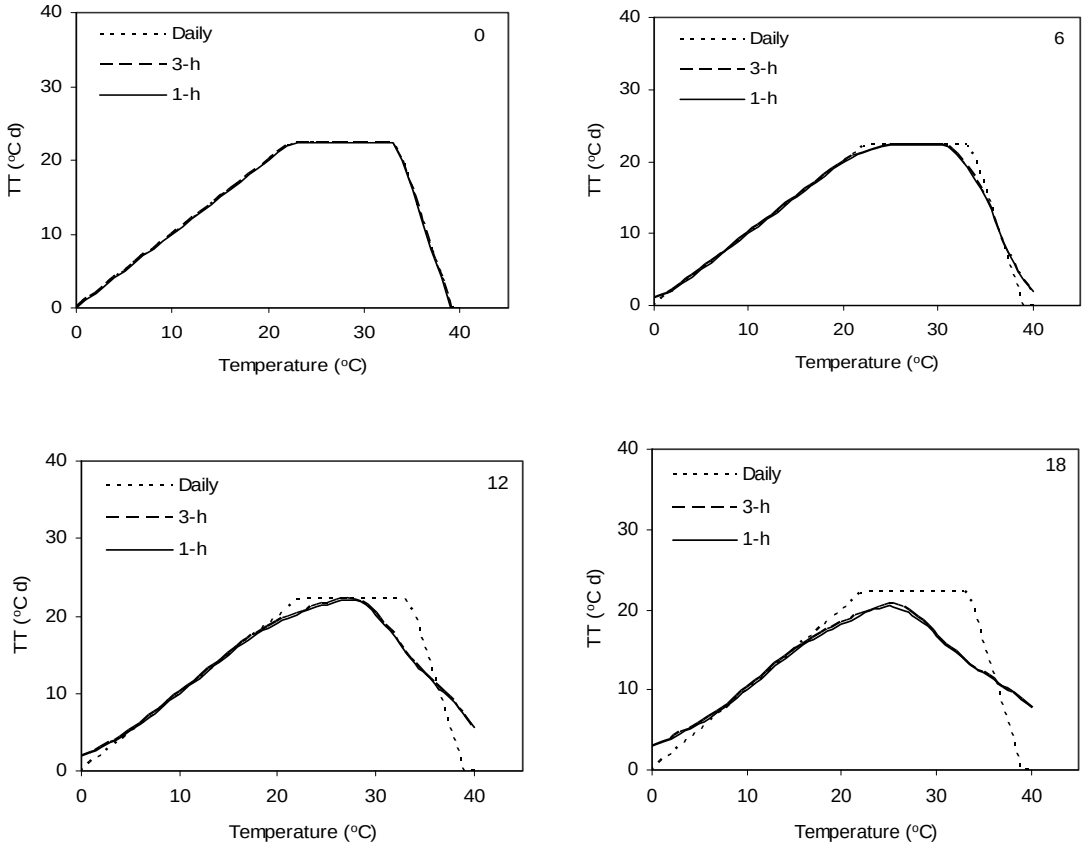

Fig. 4. Calculated thermal time based on dent-like function versus mean temperature at temperature amplitudes (= Tmax – Tmin) of 0, 6, 12 and 18 ^{o}C. Time steps used are 1, 3 and 24 h (daily).

Fig. 5 compares simulated versus measured days to flowering (R1) and to maturity (R7) in chickpea. In these simulations, desired values of TT based on daily, 3-hourly and hourly time steps were implemented in the simulation model. Actually, there is no clear difference between time steps. Therefore, it can be concluded that there is no preferred time step, at least in chickpea, in calculation of TT and either hourly or daily time steps are adequate.

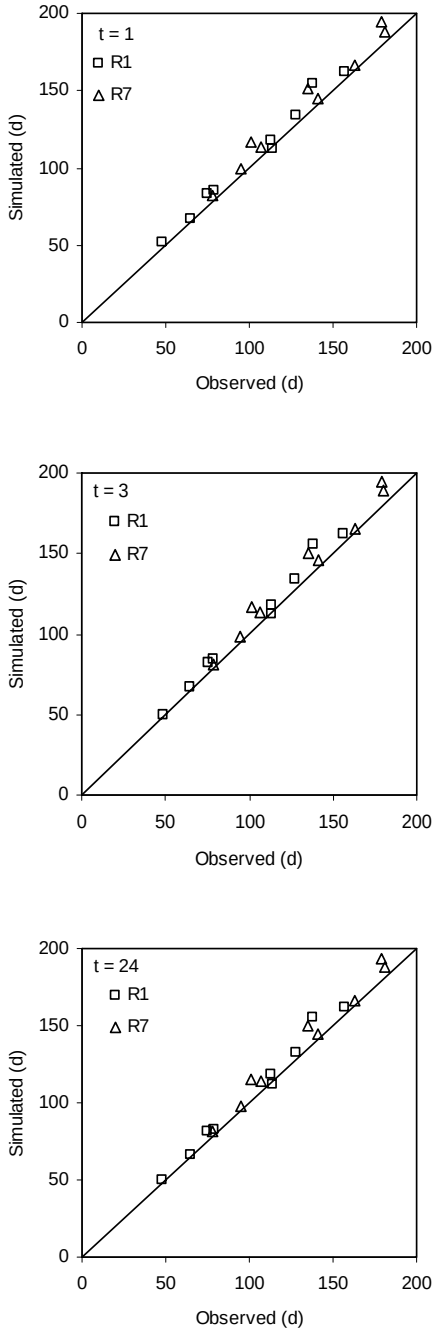

Fig. 5. Predicted versus observed days to flowering (R1; squares) and maturity (R7; triangles) on independent data set using time steps (t) of 1, 3 and 24 h.

REFERENCES

Cesaraccio, C, D. Spano, P. Duce and R.L. Snyder, 2001. An improved model for degree-days from temperature data. Int J Biometeorol 45(4): 161-169.

Dwyer, L.M., W. Douglas, L. Stewart, B.L. Carrigan, P. Neave and D. Balchin, 1999. A general thermal index for maize. Agron J. 91: 940–946.

Jones, C.A., and J.R. Kiniry, 1986. CERES-Maize: A Simulation Model of Maize Growth and Development. Texas A&M University Press, College Station, Texas.

Purcell, L.C. 2003, Comparison of thermal units derived from daily and hourly temperatures. Crop Sci 43: 1874-1879.

Soltani, A., G.L. Hammer, B. Torabi, M.J. Robertson and E. Zeinali, 2006a. Modeling chickpea growth and Development: phenological development. Field Crops Res. 99: 1-13.

Soltani, A., M.J. Robertson, B. Torabi, M. Yousefi-Daz and R. Sarparast, 2006b. Modeling seedling emergence in chickpea as influenced by temperature and sowing depth. Agric. For. Meteorol. 138: 156-167.

Yin, X., M.J. Kropff, P.K. Aggarwal, S. Peng, T. Horie, 1997. Optimal preflowering phenology of irrigated rice for high yield potential in three Asian environments: A simulation study. Field Crop Res. 51: 19-27.

Material Flow Analysis of Nitrogen and Phosphorus for Rice Paddy in Bang Pakong Basin of Thailand

Wallapa Kupkanchanakul and Suphaphat Kwonpongsagoon
Department of Sanitary Engineering, Faculty of Public Health,
Mahidol University, Bangkok, Thailand

Abstract: This paper is to investigate nitrogen (N) and phosphorus (P) flows through rice paddy in Bang Pakong basin (including Nakhonnayok, Chachoengsao, and partly of Chonburi province) by using Material Flow Analysis (MFA) based on the mass balance approach. Reliable data sources have been gathered and used to support this study. The models of N and P representing flows and stocks through rice paddy in the basin are presented here. The results show that the N and P flows can be found in air, water and goods, such as fertilizers, irrigated water, rain, rice yields, and drainage/runoff. The key inflows of N and P as in fertilizers are initially estimated at 28,000 tones/year and 9,000 tones/year respectively. The key outflows of N as in emissions (volatilization and burning) and drainage/runoff are 22,000 tones/year and 10,000 tones/year respectively, while the key outflow of P in drainage/runoff is about 1,200 tones/year. This study indicates that rice paddy, one of the main agricultural activities of the basin, can significantly contribute to the high N and P loads, subsequently cause the water pollution problems to streams and the Bang Pakong River of the basin.

Keywords: Material Flow Analysis, Nitrogen, Phosphorus, Bang Pakong basin

INTRODUCTION

World demand of rice production for trade and consumption has increased. Thailand is one of important rice-growing countries, approximately 10 million ha of the total area[1]. Applying nutrients, especially nitrogen (N) and phosphorus (P) fertilizers, is an essential part of rice growing. It can increase the rice yield markedly, however, the overuse of these nutrients has become an environmental pressure in water bodies including eutrophication, oxygen depletion and decline in wildlife habitat. Such problems have already occurred in waterways in Thailand, like Thachin, and Bang Pakong River[2,3,4]. Excess nitrogen and phosphorus are transported and transformed to the waterways, leading to the water quality problems by leaching and runoff processes, mostly as nitrate (NO_3) and particulate P form[5,6]. In order to determine how to best prevent such problems, all inputs that contribute to the total nitrogen and phosphorus loading must be identified.

Material Flow Analysis (MFA), a tool of environmental management analysis, has been developed to investigate the efficiency of material (e.g. paper, plastic), substance (Pb, Cd, Zn, N, P), and energy use[7,8]. The approach is often used in country, regional, and basin scale to understand a holistic structure of related pollutant sources and pathways. It has been applied in many studies for pollution management, for example, to track the flows and stocks of phosphorus in Sydney[9], to evaluate measure to reduce the cadmium flows in Australia[10,11], and to develop a systematic methodology for mass integration in drainage systems and watersheds for ammonium management case[12,13]. In Thailand MFA has been recently applied to study domestic solid waste and wastewater management[14], to analyze heavy metal in canals of Ratchaburi and Samut Songkhram province[15]. Another significant application for assessing river water pollution and mitigation potentials for N and P in Thailand, Schaffner[16], Hans-Peter Bader and Ruth Scheidegger from Swiss Federal Institute of Aquatic Science and Technology firstly developed the model of N and P flows for the Thachin River basin.

This study has been applied from the Monika Schaffner's thesis[16], and focused on the nutrients nitrogen (N) and phosphorus (P) only in rice paddy in Bang Pakong basin, Thailand. The study area is located in eastern Thailand covering Nakhonnayok, Chachoengsao and partly Chonburi province, with the area of 1,030,000 ha. The land use in the basin consists of agriculture, aquaculture, livestock, community, and industry. Rice paddy is one of significant agricultural areas, about 320,000 ha and 3,700 kg/ha of the annual yield[1]. The quantity of fertilizer is applied about 280 kg/ha.

Corresponding Author: Wallapa Kupkanchanakul, Department of Sanitary Engineering, Faculty of Public Health, Mahidol University, Bangkok, Thailand, Tel/Fax: +66 2354 8540,
E-mail: pum_wallapa@hotmail.com

This paper aims at investigating nutrients nitrogen (N) and phosphorus (P) flows through rice paddy in Bang Pakong basin by using Material Flow Analysis (MFA) based on the mass balance approach.

METHOD AND DATA ACQUISITION

The method applied is Material Flow Analysis (MFA) as described above in the introduction section. It is based on the mass balance concept which is described as the conservation of mass to the analysis of physical flows, and is applied to a specific area over a time interval. The concept is used to calculate the N and P flow in this study. Each flow is expressed as a unit of tones/year. The studied procedure consists of two main parts, namely system analysis and data collection[10]. After selecting a concerned substance, reference year, and the studied area, in the first part system analysis is to identify goods and processes related to the N and P in the rice paddy. The collection of data is then the next important step of this study, particularly statistical data and the N and P content. The reliable data is required and gathered from several sources as follows:

- Department of Agricultural Extension (DOAE)
- Thesis and journal articles
- Government reports
- Interview with experts and farmers

All statistical data is based on the year of 2005.

DESCRIPTION OF BANG PAKONG BASIN

In Figure 1, Bang Pakong basin as described in the introduction comprises three provinces, namely Nakhonnayok, Chachoengsao, and Chonburi. The topography of the basin is highland in the upper part, but flat to slightly sloping in the middle and the lower part. The basin can be classified into five sub-basins as follows: Bang Pakong (main river), Bang Pakong plain, Nakhonnayok, Klong Tha Lad, and Klong Luang. The main river of the basin is the Bang Pakong River that is originated from the combination of Prachinburi River and Nakhonnayok River, running about 122 kilometers into the Gulf of Thailand. Mean annual rainfall is about 1,400 mm/year. The main crop is rice, accounting for 30% (320,000 ha) of the total basin area. Table 1 shows the total area, planting area, yield, and fertilizers applied in each province. There are two cultivation systems of rice, namely irrigated and rainfed paddy field. In the tropical zone, like Thailand where rainfall is high, the irrigated crop is dominant, has higher productivity than the rainfed crop. Both systems require a lot of water from rain, river and canals, and nutrients from applying fertilizers.

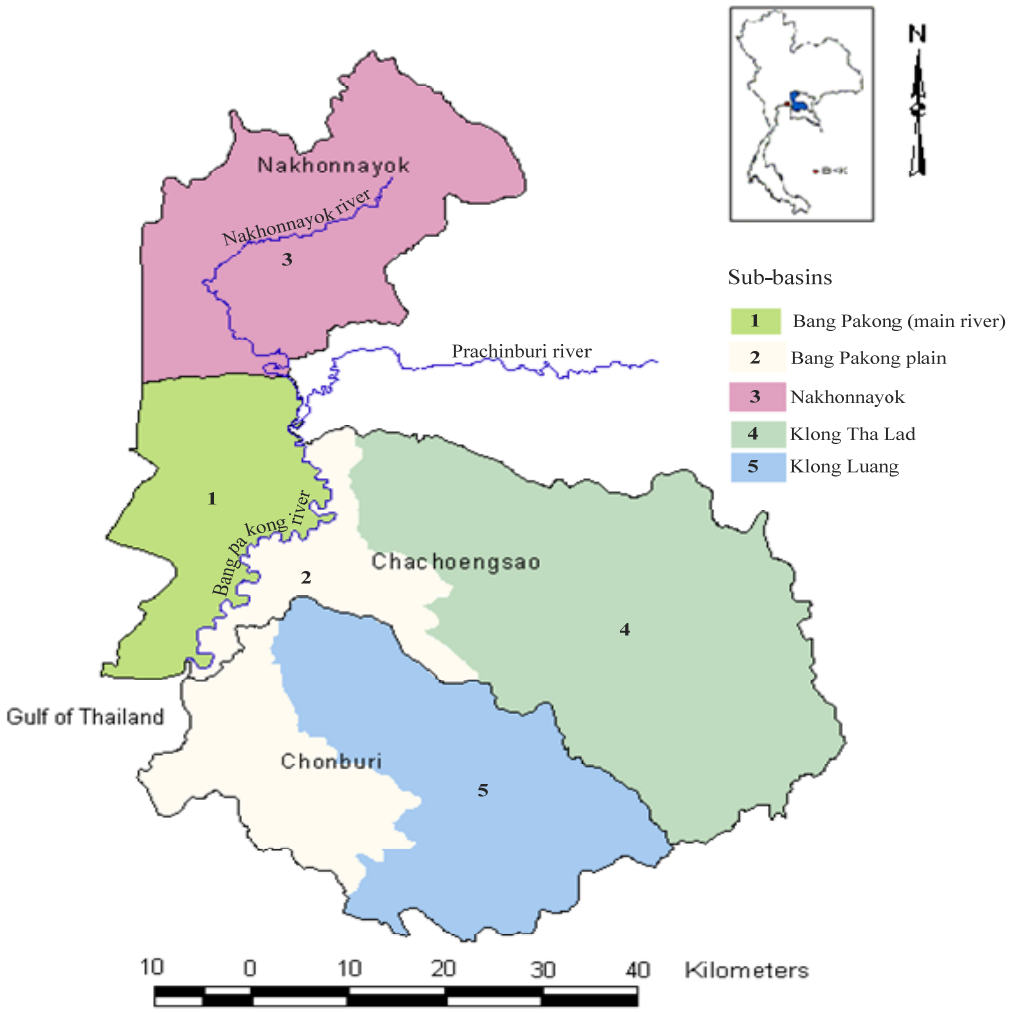

Fig. 1: A schematic of the Bang Pakong basin

Table 1: Rice paddy in Bang Pakong basin[1]

Province	Total area (ha)	Planting area (ha)	Rice yield (kg/ha)	Applied fertilizers (kg/ha)
NY	212,220	100,692	3,259	253
CCS	535,100	202,446	4,075	309
CB	282,851	17,147	1,732	142
Total BPK	1,030,151	320,285	3,693	282

Note : NY = Nakhonnayok province
CCS = Chachoengsao province
CB = Chonburi province
BPK = Bang Pakong basin

RESULTS

The models of mass, N and P representing flows and stocks through rice paddy in the basin are presented in Fig. 2A for mass flow, Fig. 2B for N flow, and Fig.2C for P flow. It consists of fourinputs: (1) fertilizer, (2) irrigation, (3) fixation (see Fig. 2B), and (4) rain/deposition; and four outputs: (1) evapotranspiration (EVTP) (see Fig.2A), (2) emission (see Fig. 2B), (3) yield, and (4) drainage/runoff.

The results show that the N and P flows can be found in air, water and goods, such as fertilizers, irrigated water from the river and canals, rain, rice yields, and drainage/runoff. The key inflows of N and P as in fertilizers are initially estimated at 28,000 tones/year and 9,000 tones/year respectively. It can be seen that although high level of mass inflows are rain/deposition and irrigation (Fig. 2A), the high N and P inflow come from fertilizer (Fig. 2B and 2C). This is due to the presence of high concentration of N and P in fertilizers (urea and mono-ammonium phosphate) applied in the paddy field. The content of N in urea ($CO(NH_2)_2$) and mono-ammonium phosphate ($NH_4H_2PO_4$) is about 46 and 16 g/ 100 g of fertilizer respectively, and about 20 g P/ 100 g of fertilizer found in mono-ammonium phosphate[17].

In concerning about the environmental problems, especially water quality in the river and canals, the key outflows of N in emissions (volatilization and burning) and drainage/runoff are 22,000 tones/year and 10,000 tones/year respectively, while the key outflow of P in drainage/runoff is about 1,200 tones/year.

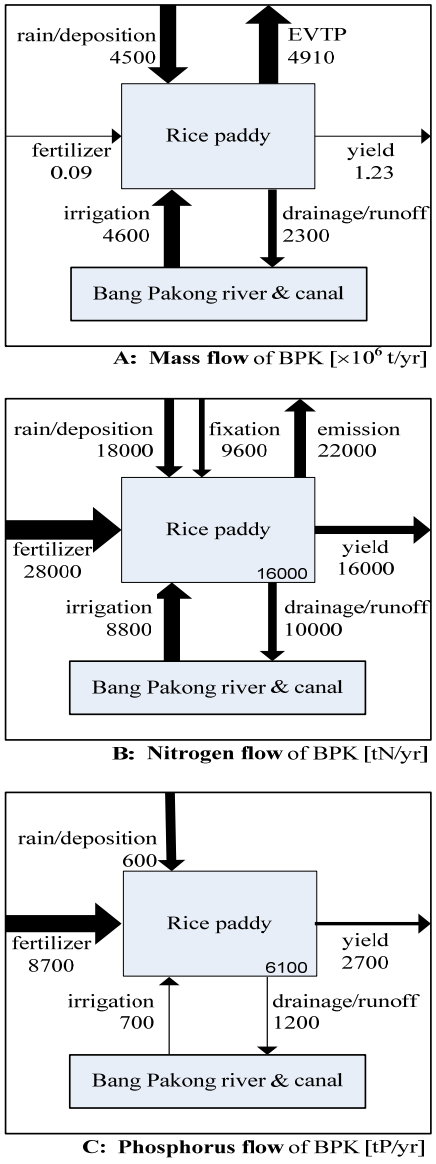

Fig. 2: Mass, nitrogen, and phosphorus flow for rice paddy in Bang Pakong basin.

CONCLUSION

To conclude, this study indicates that rice paddy, one of the main agricultural activities of the basin, can significantly contribute to the high nitrogen and phosphorus loads, subsequently cause the water pollution problems to streams and the Bang Pakong River of the basin. There are not only rice-growing activities in the basin, but also livestock, aquaculture, community, and industry located in the basin. Therefore, the Material Flow Analysis (MFA) of nitrogen and phosphorus for all these activities has to be conducted. Both point and non-point sources will then be taken into account. Ultimately, measures and options to reduce the nitrogen and phosphorus pollution in the river and canals can be discussed and managed properly.

ACKNOWLEDGEMENTS

Authors would like to thank Assoc. Prof. Dr.Prayoon Fongsatitkul at Department of Sanitary Engineering, Mahidol University for his advice and comments. We are deeply grateful to Dr.Monika Schaffner, Dr.Hans-Peter Bader and Ruth Scheidegger at the Swiss Federal Institute of Aquatic Science and Technology for supporting the model and useful data throughout the study.

REFERENCES

1. DOAE, 2007. Production statistic in year 2005. Department of Agricultural Extension. http://production.doae.go.th/ Last Updated: n/a. Access: 30 January 2007.
2. Pollution Control Department, 2005. State of Thailand's Pollution in Year 2005. Ministry of Natural Resources and Environmental, Bangkok.
3. Pollution Control Department, 2007. Water quality monitoring data for Nakhonnayok, Prachinburi, and Bangpakong River. http://iwis.pcd.go.th/IWIS/index.php Last Updated: n/a. Access: 8 May 2007.
4. Simachaya, W., 2003. A decade of water quality monitoring in Thailand's four major rivers: the results and the implication for management, the 6th International Conference on the Environmental Management of Enclosed Coastal Seas, November 18-21, Bangkok, Thailand.
5. Cao, Z.H. and Zhang, H.C., 2004. Phosphorus losses to water from lowland rice field under rice-wheat double cropping system in the Tai Lake region. Environmental Geochemistry and Health, 26: 229-236.
6. Kuroda, H., Kato, T., and Nakasone, H., 2005. The nitrate nitrogen pollution and the nitrogen removal by paddy field in agricultural area. Journal of Water and Environment Technology, 3(2): 165-168.
7. Baccini, P. and Bader, H.P., 1996. Regionaler Stoffhaushalt: Erfassung, Bewertung und Steuerung. Spektrum Akademischer Verlag, Heidelberg.
8. Baccini, P., and Brunner, P.H., 1991. Metabolism of the anthroposphere. Springer, Berlin.
9. Tangsubkul, N., Moore, S., and Waite, T.D., 2005. Incorporating Phosphorus Management Considerations into Wastewater Management Practice. Environment Science and Policy, 8: 1-15.
10. Kwonpongsagoon, S., Waite, D., Moore, S., and Brunner, P., 2007a. A substance flow analysis in the southern hemisphere: cadmium in the Australian economy. Clean Technologies and Environmental Policy, 9(3): 175-187.
11. Kwonpongsagoon, S., Bader, H.P., and Scheidegger, R., 2007b. Modelling cadmium flows in Australia on the basis of a substance flow analysis. Clean Technologies and Environmental Policy, 9: 313-323.
12. El-Baz, A.A., Ewida, M.K.T., Shouman, M.A., and El-Halwagi, M.M., 2005a. Material Flow Analysis and integration of watersheds and drainage systems: I. simulation and application to ammonium management in Barh El-Baqau drainage system. Clean Technologies and Environmental Policy, 7: 51-61.
13. El-Baz, A.A., Ewida, M.K.T., Shouman, M.A., and El-Halwagi, M.M., 2005b. Material Flow Analysis and integration of watersheds and drainage systems: II. integration and solution strategies with application to ammonium management in Barh El-Baqau drainage system. Clean Technologies and Environmental Policy, 7: 78-87.
14. Sinsupan, T., 2004. Material Flux Analysis (MFA) for Planning of Domestic Wastes and Wastewater Management: Case Study in Pak Kret Municipality, Nonthaburi, Thailand. Master Thesis, Asian Institute of Technology, Bangkok.
15. Krisuwansan, N., 2008. Mass Flow Analysis of some heavy metals in the canal system of Ratchaburi and Samut Songkhram provinces. Master Thesis, Mahidol University, Nakhonpathom.

16. Schaffner, M., 2007. Applying a Material Flow Analysis Model to assess river water pollution and mitigation potentials: a case-study in the Thachin River Basin, Central Thailand. Doctoral Thesis, Swiss Federal Institute of Aquatic Science and Technology, Zürich.
17. Bureau of Rice Research and Development, 2006. Potential zoning of rice production in Nakhonnayok province (in Thai). Pathumthani

The Rainmaking Decision Model over River Basins of Thailand

[1]Veerasak Udomchoke, [2]Prasert Aungsuratana, [1]Nitaya Lauhachninda, [1]Unnop Homchan, [1]Pongsakorn Jiwapornkupt and [1]Krongjit Kesjinda
[1]Environmental Geotechnology and Natural Disasters Research Unit, Department of Earth Science, Faculty of Science, Kasetsart University (KU), 5 Phahol Yothin Rd, Chatuchak, Bangkok, 10900
[2]Bureau of Royal Rainmaking and Agricultural Aviation, Office of the Permanent Secretary for Ministry of Agriculture and Cooperatives.

Abstract: The rainmaking decision model over all river basins of Thailand were considered on the basis of urgent need and appropriate rainmaking conditions. An urgent need condition was defined in 3 criteria: firstly, the urgent need of planting-system were weighted as 3, 2 and 1 for areas of high, moderate and low water-demand respectively. Secondly, climatic situations for probability to operate rainmaking or amount of monthly rainy days which were also weighted as 3, 2 and 1 for high (> 10 rainy days), moderate (6-10 rainy days) and low (1-5 rainy days) respectively. Finally, weather situation criteria which were analyzed on the basis of a Multivariate ENSO Index (MEI) and were classified into 3 levels: the COLD ENSO (La-Nina), MEDIUM ENSO (Normal) and WARM ENSO (El Nino) of little need of rainmaking, moderate need of rainmaking and urgent need of rainmaking, which weighted as 1, 2 and 3 respectively. Therefore, if the rank of total marks were 3-4, 5-6 and 7-9 it means low, medium and high need for rainmaking respectively. An appropriate rainmaking conditions were analyzed on the basis of 3 criteria: synoptic conditions, climatic model from radiosonde data and daily cloud-radar prediction model. Firstly, the situation on weather synoptic conditions were ranked into 3 levels by the Synoptic Index (SYNI): 2–4, 5–7 and 8–10 for low appropriated condition for rainmaking, medium appropriated condition and high appropriated condition and such conditions were weighted as 1, 2 and 3 respectively. Secondly, the rainfall amount estimated from radiosonde data for upper climatic simulation model were divided into 3 levels: low, medium and high appropriate conditions for rainfall amount lower than 10 mm (or cover the area less than 10%), 10-30 mm (or cover 10-50% of the area) and higher than 30 mm (or cover more than 50% of the area). Those levels also weighed as 1, 2 and 3 respectively. Thirdly, daily cloud-radar prediction models were classified as 1, 2 and 3 for the all day clear sky referred to low and means a low appropriation to inappropriate condition for rainmaking, the presence of cumulus cloud in late morning referred to moderate rainmaking condition and was weight as 2 and the cumulus morning cloud coupled with Cumulonimbus cloud (CB) was weight as 3 respectively. Base on these 3 main criteria in rainmaking decision of the total weight points of 3-4 was low and inappropriate condition to make rain while 5-6 and 7-9 mean moderate and high appropriations respectively. As the final conclusion, both urgent need and appropriate conditions were taken into account for decision making as follow 1) low need in case of low appropriated condition, don't operate rainmaking; medium appropriated condition, don't operate rainmaking and high appropriated condition, don't operate rainmaking 2) moderate need in case of low appropriated condition, don't operate rainmaking; medium appropriated condition, operate rainmaking and high appropriated condition, operate rainmaking 3) urgent need in case of low appropriated condition, operate rainmaking; medium appropriated condition, operate rainmaking and high appropriated condition, operate rainmaking.

Keywords: Decision Model, Royal Rainmaking, Thailand River Basins

Corresponding Author: Veerasak Udomchoke, Environmental Geotechnology and Natural Disasters Research Unit, Department of Earth Science, Faculty of Science, Kasetsart University (KU), 5 Phahol Yothin Rd, Chatuchak, Bangkok, 10900, Thailand, Tel: +66 02-562-5555, Fax: +66 05-579-3711, E-mail: fscivsu@yahoo.com

INTRODUCTION

Thailand is located in an appropriate area surrounding with countries those are subjected to prior confront with tropical storms. The influent of monsoons in southwest and northeast direction governs this land rather wet in the rainy season and cool and dry in winter season. Almost half of a year, during winter (120 days) and summer (61 days) seasons, there are only eight to ten rainy days which implies drought condition or semi arid condition even though the range of mean annual rainfall in this area is greater than 1,000 millimeter.

Farmers always request the rainmaking operation during the end of farming to the early of planting period in order to moist the land and fresh the plants. Rainmaking operation is a scientific method that can activate cloud formation in order to increase rainfall amount. Moreover, such method can specify the rain to fall on the target area. However, due to many climatic uncertainties and different requirements of farmer, each rainmaking operation should be done on the basis of careful decision case by case because each decision will relate with not only a successful opportunity but a budget also (Battan, 1962; Dennis, 1980 and Roger, 1985). Recent rainmaking decision criteria still need more precised know how and detail research for reaching complete criteria (Udomchoke et.al., 2007). Rainmaking decision model is a very important task to support the committees who have to make a decision to operate rainmaking.

OBJECTIVES

The main targets of this research work are the criteria for rainmaking those depend on demand of crops and weather situation both upper atmospheric conditions and synoptic conditions, then established decision model to Geographic Information System (GIS).

MATERIALS AND METHODS

Two conceptual ideas those applied to this study were the water demanded levels and the appropriate climatic situation for rainmaking as follow.

1. Analysis on water demand period in agricultural area.

1.1 Data acquisition by questionnaire and agricultural survey map from Agricultural Extension Departments.

1.2 Define a water demanded map based on data from questionnaire into GIS.

1.3 Define a water demanded index of major crops such as paddy field, field crop, vegetable and orchard on each district.

1.4 Integrate both two demanded maps with an agricultural zone map and suitable land-use map in order to produce a suitable water demanded map of Thailand River Basins.

2. Analysis on appropriated climatic condition for rainmaking

Meteorological data collection

2.1 The meteorological forecasting data during 2003-2007 were acquired from Department of Meteorology.

2.2 The upper climatic condition which have been recorded by the Royal Rainmaking Station, at Phimai, Nakhon Ratchasima Province and at Omkoi Station, Chiang Mai Province and recorded by the Meteorological Department of Thailand were used in this analysis. Such observational data such as temperature, humidity, stratosphere height, stability index of some typical air mass and direction as well as velocity of air mass were used in identification of synoptic index. The Synoptic Index will be compared with seasonal rainfall in Thailand in order to formulate a model of the relationship between rain and upper climatic parameters.

2.3 Radar data were collected from 4 radar stations as followings.

1) Bureau of Royal Rainmaking and Agricultural Aviation supported data from three radars at Phimai District, Nakhon Ratchsima Province, at Omkoi District, Chiang Mai Province and at Hua Hin District, Prachuap Khiri Khan Province which emit S-Band (2.8 GHz) with wavelength of 10.7 cm, power 850 kilowatts, resolution of 1x1 kilometers and 160 kilometers detectable radius.

2) The Meteorological Department supported data from Radar at Mueang District, Phitsanulok Province and at Don Mueang Airport, Bangkok which emits S-Band (2.8 GHz) with wavelength of 10.7 cm, power 850 kilowatts, resolution of 1x1 kilometers and 160 kilometers detectable radius.

3) Collect data from radar those related with each typical synoptic weather situation in order to understand growth and decay behavior, coverage area, movement, reflection energy and rain volume estimation of the selected cloud.

4) Descriptive statistical analysis were applied to analyze the cloud radar data related with the each weather situation in term of duration, maximum,

minimum, mean, standard deviation, F-test and T-test that revealed cloud physics characteristics of each typical cloud from each weather situation.

2.4 Rainfall data from automatic raingage were consequently classified based on synoptic situation i.e. southwest monsoon related or tropical storm related rains and were analyzed same as the radar data then it will represent an estimated daily rainfall of each synoptic situation. Such method yields a simulated model of pattern and distribution of rainfall of each synoptic situation in Thailand.

2.5 Integration of simplified model

The rank of appropriated rainmaking index will be defined as high, moderate and low in term of ranking number. In addition, a weight of each physical parameter will be defined and multiplied in order to obtain the simplified models as follows:

1) The Weather Situation Model which simulate a rain formation in each weather situation.

2) The Cloud Physic Model which was simulated from radar data and the upper-air observation.

3) The Climatic Model which displays the seasonal and spatial variations of the weather situation model and the cloud physic model couple with a rain formation model in each physiography of the upper Thailand river basins.

4) The Physical Rain-required Model which represents the monthly need on water of main crops in each district.

3. Decision Supported Model on the appropriated rainmaking operation

This model was formulated by the integration of all simplified models and also be described as degree of rain requirement and weighting factors, then compited in to model in GIS form.

4. Modeling Verification

The model was verified by the recent data and, consequently, the model's efficiency was also concluded. Finally, some suggestion should be recommended in order to adjust the model for higher efficiency.

RESULTS AND DISCUSSION

Rainmaking criteria

Rainmaking criteria which were used in rainmaking processes over all river basins of Thailand comprised of rain requirement criteria, cropping system criteria, climatic condition criteria, weather situation criteria and cloud physic criteria as follow:

1. Model criteria from cropping system

1.1 Cropping system in climatic zone

On the basis of topography and climatic conditions such as mountain range, alluvial plain, terrace, rainfall amount, temperature and humidity climatic zone in Thailand were establish in 1973. The climate of over all river basins of Thailand can be classified into 12 sub-regions with in 4 regions by the criteria of topography and amount of rain in each monsoon season as follow.

1) Equatorial climate (8-11 humid months) dividing into 2 sub-regions ,i.e., region with high rainfall during long southwest monsoon season (A1) and region with high rainfall during long northeast monsoon season (A2)

2) Tropical monsoon climate with long rainy season (6.5-8 humid months) including 5 regions ,i.e., region with high rainfall (B1) region with moderate rainfall (B2) region with low rainfall (B3) region with moderate to high rainfall and cool dry season (B4) and mountainous region with cool dry season in valleys (B5)

3) Tropical monsoon climate with rainy and dry season (5.5-6.5 humid months) dividing into 3 sub-region ,i.e.,region with moderate to high rainfall (C1) region with low rainfall (C2) and region with low rainfall and cool dry season (C3)

4) Tropical Monsoon climate with long dry season (4.5-5.5 humid months) including 2 sub-regions, i.e., region with low rainfall (D1) and region with very low rainfall (D2)

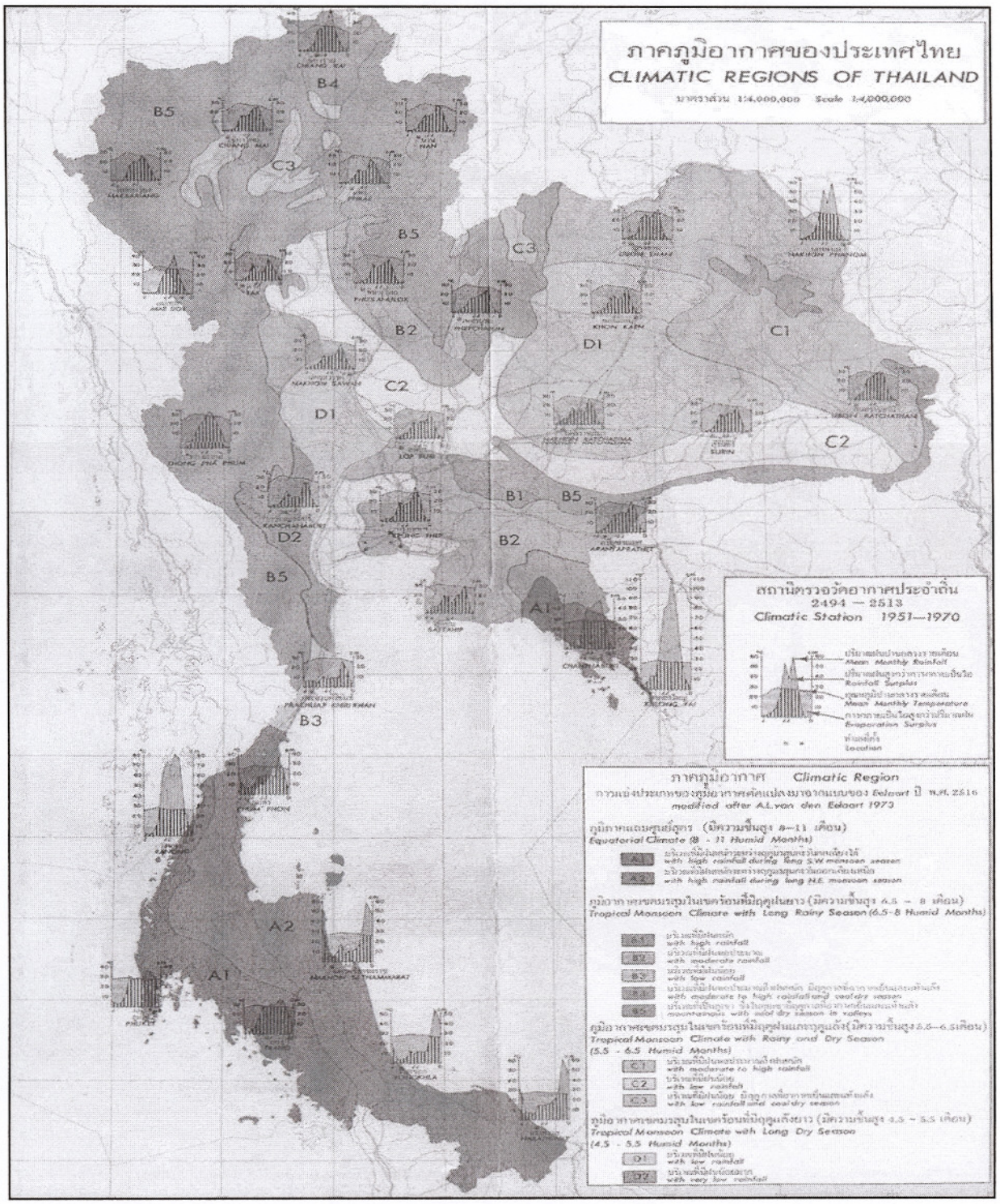

Figure 1. Climatic regions of Thailand
from: Meteorological Department of Thailand (1976)

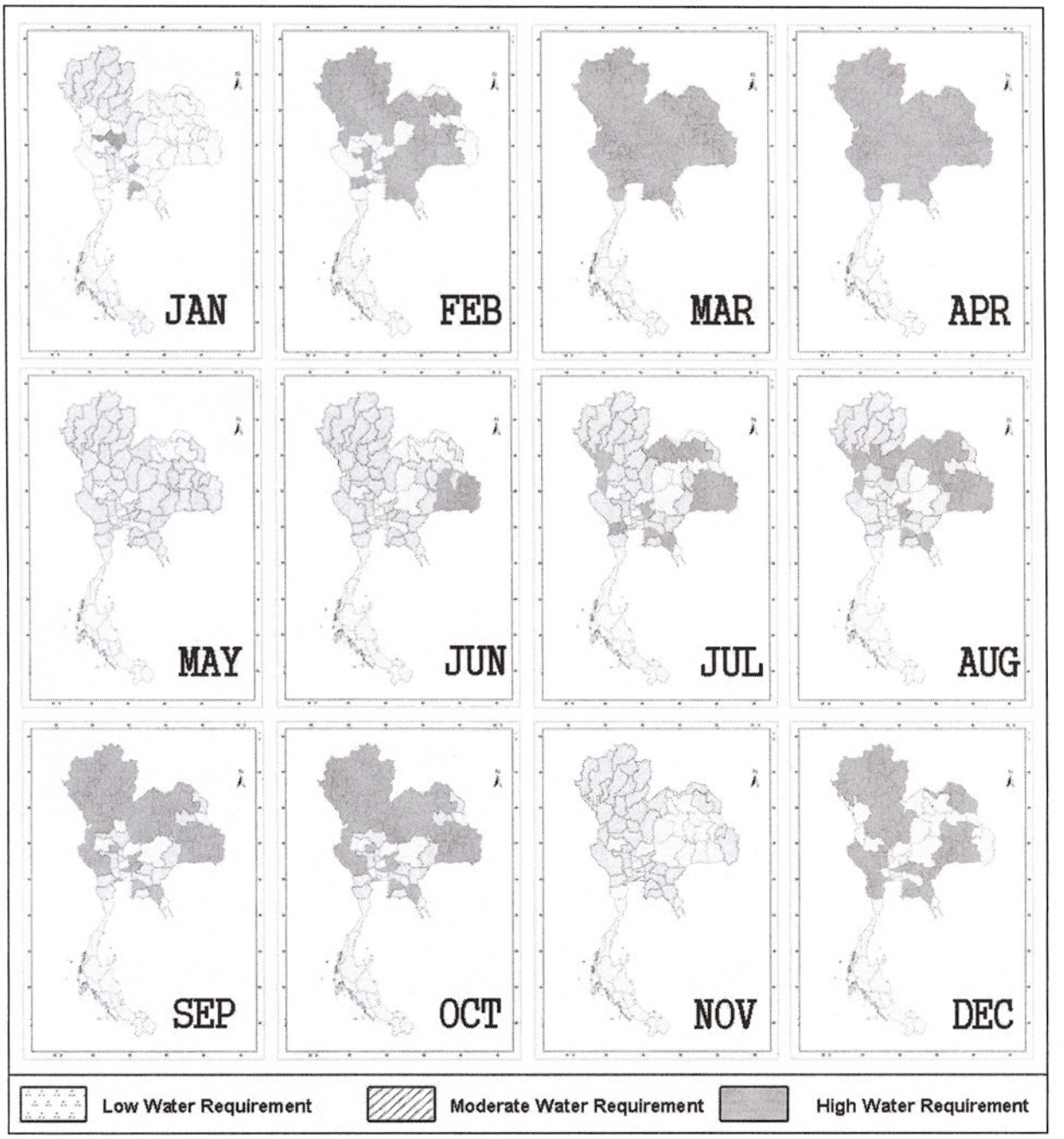

Figure 2. Water requirement for each month and each Province of Thailand

1.2 Agricultural water demanded map

The cropping system map of each climatic region was carried out on the basis of combination between cropping system data and data which collected through the questionnaire. Then the maps will be separately presented as monthly map based on planting time of 5 major cropping system such as rice, corn, cassava, vegetable and fruit, and forest. Such map will be resented a time-based water requirement of each zone as shown in Figure 2. The water demand was defined into 3 ranks depended on urgent need of cropping system as 3, 2 and 1 for high, moderate and low water demand (FAO, 1982).

2. Criteria on the basis of climatology

Daily weather forecasting data and upper level climatic data since 1993 to present year were accompanied to analyze statistically. Synoptic weather condition which result rainfall in tropical zone should be affected by 3 main factors. (i) Relationship between energy storage in continent and ocean. (ii) Seasonal air-mass movement which affected by the solar and terrestrial energy transfer. (iii) Geography and topography of the site.

In case of Thailand River basin, the major synoptic weather condition (Udomchoke and Augsurattana, 2002) which result rainfall are:

2.1 The active high pressure or cold surges accompanied with heat low cell (AH&HL), usually occur during the winter season.

2.2 Confluence (CON) of the low level flow (streamlines) between warm and moist airmass from the South China sea joining with warm and very moist airmass from the Andaman sea.

2.3 Westerly Trough (WT) from north hemisphere westerlies winds bring temperate airmass mixing with the tropical airmass.

2.4 The influential movement of tropical storm and low depression (LOW & DEP) from the Andaman sea and the South China sea.

2.5 The influential of active intertropical convergence zone (AITCZ).

2.6 The influential of southwest monsoon (SWS).

2.7 The active southwest monsoon winds and the influential of moderate and weak intertropical convergence zone (ASW & WITCZ).

2.8 The easterly winds from Pacific Subtropical High and South China sea (EWIND).

2.9 The southerly wind from Gulf of Thailand to the heat low cell inland over Indo-China Peninsular (SWIND).

These nine synoptic weather situations take place in different period of time therefore they influent on five monsoon seasons (Silvermann et.al., 1986) of this region as show in Table 1.

Table 1. Major synoptic weather conditions those influent in different period of time of five seasons.

Seasons	Period of time	Synoptic weather condition
Northeast Monsoon	November to February	AH & HL, CON and WT
Summer Intermonsoonal	March to April	AH & HL and WT
Onset southwest Monsoon	May to June	LOW & DEP and AITCZ.
Southwest Monsoon	July to September	AITCZ, ASW and LOW & DEP
Winter Intermonsoonal	October	LOW & DEPand AITCZ

Monthly probable ranks for rainmaking operation over all river basins was calculated from daily weather data which collected since 1981 to 2007. Consequently, monthly probability of each synoptic weather condition will be generated. As a result, the lowest probability of rainmaking takes place in November, December, January, February and March. The moderate probability takes place during April to May and, finally, the most probability takes place during June to October. Appropriated criteria for monthly-rainmaking consideration in Thailand are classified, on the basis of number of rainy day and monthly probability, into 3 ranks as follow.

(i) Low monthly probability exists on 1-5 rainy days and was weighted as 1.

(ii) Moderate monthly probability exists on 6-10 rainy days and was weighted as 2.

(iii) High monthly probability exists on more than 10 rainy days and was weighted as 3.

Based on these above criteria, a weight of monthly probability of each region is defined as in Table 2.

Table 2. Decision criteria of rainmaking based on number of rainy days and monthly probability of each month.

Month	Regions River Basins in Thailand				
	North	Northeast	Central	East	South
January	1	1	1	1	3
February	1	1	1	1	2
March	2	1	2	1	1
April	2	2	1	1	1
May	3	3	3	2	2
June	3	3	3	3	3
July	3	3	3	3	3
August	3	3	3	3	3
September	3	3	3	3	3
October	3	2	3	2	3
November	1	1	1	1	3
December	1	1	1	1	3

3. Criteria on the basis of Synoptic Weather Situation

Amount of rainfall over the study area was estimated based on the relationships between daily synoptic weather situation and daily rainfall amount. as following. The low pressure and tropical storm revealed highest rainfall amount approximately 63.9 mm, over 97% of area of the Upper Northern Thailand. Active intertropical convergence zone (AITCZ) result a moderate rainfall amount over 75% of the study area. High pressure airmass can conduct moderate rainfall amount as well as covering area similar to the result of convergence wind between southwest and northeast monsoons (CON). The last group of monsoon which result immeasurable rainfall amount composed of the southerly wind from Gulf of Thailand to the heat low cell inland over Indo-China Peninsular (SWIND) and the easterly winds from Pacific Subtropical High and South China sea (EWIND). This group usually cover approximately 5% of whole area only.

Different synoptic weather situation result the different pattern of rainfall, amount and distribution especially on daily rainfall. Therefore, rainfall amount can be weighted through assessment of synoptic weather situation (Table 3). By such weight, rainfall amounts are divided into 5 ranges. In addition, covering area also divided into 5 ranges based on number of station which rainfall take place. The quantitative result from Table 3 will assessed in order to formulate the Synoptic Situation Index, SYNI. The analyzed results reveal that the highest, moderate and lowest SYNI values result from DEP & LOW, AITCZ and WIND climatic situations, respectively.

Based on rainfall data during 1993 to 2007, monthly SYNI were analyzed through method of Arkin (1974). The suitable number of sample at reliability of 0.05 is 46 samples or 46 months. Analysis was done by regression equation. In this analysis, SYNI value is defined as free variable while monthly rainfall amount (Pm) is defined as fixed variable. The analysis yield following relationships. (Table 4.)

Table 4. Relationship between monthly rainfall amount and synoptic index for each region of Thailand.

Region	R-square	Rain-Synoptic Model
UP-N	0.9089	Pm = 1.155SYNI +7.635
LO-N	0.9633	Pm = 1.160SYNI +1.686
UP-NE	0.8870	Pm = 1.799SYNI + 8.892
LO-NE	0.9596	Pm = 1.3198SYNI + 1.189
Central	0.9549	Pm = 1.759SYNI + 3.836
East	0.9612	Pm = 1.4461SYNI + 0.972
SSE	0.8646	Pm = 1.8221SYNI + 45.46
SSW	0.9716	Pm = 1.0441SYNI + 1.0451

It might be concluded that the SYNI can describe or estimate monthly rainfall amount with high reliability. Furthermore, based on SYNI, appropriation on rainmaking can be divided into 3 levels and their weights are listed in Table 5.

Table 5. Appropriated criteria for rainmaking classification on the basis of SYNI

SYNI	Appropriated Rainmaking Criteria	Weight
2-4	Low	1
5-7	Moderate	2
8-10	High	3

Table 3. Synoptic Weather Situation Index (SYNI) assessment based on analysis of rainfall amount and covering area.

Synoptic Weather Situation	Upper North		Lower North		Upper Northeast		Lower Northeast		Central		East		Southern East Coast		Southern West Coast	
	Plus	SYNI	Plus	SYNI	Plus	SYNI	Plus	SYNI	Plus	SYNI	Plus	SYNI	Plus	SYNI	Plus	SYNI
1) AH&HL	1*4	4	1*4	4	1*4	4	1*4	4	2*4	8	1*4	4	4*5	20	1*4	4
2) - LOW&DEP1	2*5	10	2*5	10	2*5	10	1*5	5	2*4	8	2*4	8	2*5	10	2*4	8
- LOW&DEP2	3*5	15	3*5	15	2*5	10	2*5	10	1*5	5	1*5	5	3*5	15	2*4	8
3) AITCZ	2*5	10	2*5	10	2*4	8	2*5	10	2*5	10	2*5	10	2*4	8	3*5	15
4) SWIND	1*2	2	1*2	2	1*2	2	1*3	3	1*2	2	1*2	2	1*4	4	1*4	4
5) ASW	1*4	4	1*5	5	1*4	4	1*3	3	1*3	3	1*3	3	1*4	4	3*5	15
6) EWIND	1*1	1	1*1	1	1*1	1	1*1	1	1*1	1	1*1	1	1*4	4	1*3	3
7) CON	1*4	4	1*4	4	1*4	4	1*4	4	1*4	4	1*4	4	1*4	4	2*4	8
8) WT	1*4	4	1*4	4	1*4	4	1*3	3	1*4	4	1*2	2	1*4	4	1*3	3

Remark : (1) multiplied number such as 1*4 means synoptic rainfall of rank 1 multiply with percent of covering area of rank 4. These number are selected from the following list.

Rank on median of synoptic rainfall (mm)	Rank on percentage of station which rainfall take place
< 10 mm = 1	< 10% = 1
10-20 mm = 2	10% - 30% = 2
20-30 mm = 3	31% - 50% = 3
30-40 mm = 4	51% - 80% = 4
> 40 mm = 5	> 80% = 5

4. Criteria on the basis of Cloud Physic

4.1) Cloud Radar data

The data from doppler radar have been collected from 4 stations, at Omkoi, Phimai, Sattahip and Hua Hin Radar Station of Bureau of Royal Rainmaking and Agricultural Aviation, and at Phitsanulok Radar Station of Department of Meteorology.

According to radar data, heavy rain take place in the day which either all day cumulus cloud or cumulonimbus cloud occur in the morning. Any day that cumulus cloud occur lately in the morning, rainfall amount will be moderate. Any day that without any cloud will without or lack of rain also. Therefore, radar data of every 6 minutes is can used in order to adjust a rainmaking plan.

Some cloud physic data reveal that, during late of 2007, raining took place until October. Cloud which found over northern, northeastern and central of Thailand show duration, covered area, and rain volume rate much more than eastern Thailand (Table 6).

Table 6. Appropriated criteria for rainmaking on the basis of cloud radar data

station	Zmax (dBz)	time (min)	Area (km)	Rain Volume Rate (mm/hr)
Donmuang	33-46	30-240	72-1770	0.52-3.51
Phimai	37	102-234	126-2364	3.10-4.75
Rayong	32	21-166	32-302	7.14
Omkoi	27-34	175-307	2377-30759	1.28-4.02
Phitsanulok	33-42	60-480	60-2635	0.63-5.01

As a result, appropriations for rainmaking are divided into 3 levels based radar data that have been observed every 6 minutes and then their weights are as shown in Table 7.

Table 7. Appropriated criteria for rainmaking on the basis of radar data.

Cloud occurrence	Rainfall amount	Weighting rank
Without cloud	Low rainfall	1
Cumulus cloud occur in late morning	Moderate rainfall	2
Cumulus cloud occur in morning with Cumulonimbus	High rainfall	3

4.2) Upper-air observation data

This data comprised of atmospheric water content (cm), convective condensation level (CCL), relative humidity (RH), wind speed (kts), Sholwalter Index (SI), the lifted index (LI), K, Cape 1 and Cape 2.

Such data have been collected during both in rainy season (during 16th May to 15th October) and out of rainy season (after 16thOctober to 15thMay) from 1999 to 2007. The samples which collected by method of Arkin (1974) are composed of 72 samples of rainy season and 68 samples of other season with the reliability of 0.02. Data of upper climatic observation from 4 stations were input in the multiple linear regression analysis on step wise technique in order to forecast the rainfall amount. Relationship between mean rainfall amount (P) and percentage area of mean rainfall (P(%)) with upper atmospheric parameters of each region in Thailand are tabulated in Table 8 as follow

Table 8. The upper atmospheric influential parameters on mean rainfall amount and percentage area of mean rainfall for each region of Thailand.

Rainy season

VALUE	Depend on
P(UP-N)	RHAb, LI, CAPE1
P(%UP-N	RHAb, CAPE1
P(LO-N)	Ws, RHAb
P(%LO-N)	RHccl, CAPE1
P(UP-NE)	KI
P(%UP-NE)	RHAb
P(LO-NE)	Pw
P(%LO-NE)	RHAb, XLi
P(CEN)	RHAb
P(%CEN)	RHAb
P(EAST)	RHAb
P(%EAST)	RHAb, CAPE1
P(SSE)	RHAb
P(%SSE)	RHAb
P(SSW)	RHAb
P(%SSW)	RHAb

Other season

Value	Depend on
P(UP-N)	Ws, RHAb
P(%UP-N)	Ws, RHAb
P(LO-N)	RHAb
P(%LO-N)	RHAb
P(UP-NE)	Pw, RHlo, KI
P(%UP-NE)	Pw, LI, SI
P(LO-NE)	Pw
P(%LO-NE)=	RHAb
P(CEN)	LI, CCL
P(%CEN)	Ws, CCL
P(EAST)	LI, RHAb, CAPE1
P(%EAST	RHAb, Cape1
P(SSE)	RHAb
P(%SSE)	RHAb
P(SSW)	RHAb
P(%SSW)	RHAb, CAPE1

Note: P=Mean rainfall amount (mm),
P(%) = percentage area of mean rainfall (%)

Regional meaning
UP-N = Upper Northern Thailand

LO-N = The Lower Northern Thailand
UP-NE = The Upper Northeastern Thailand
LO-NE = The Lower Northeastern Thailand
CEN = The Central Thailand
EAST = The Eastern Thailand
SSE = The Southeastern Coastal Thailand
SSW = Southwestern Coastal Thailand

Upper atmospheric parameters
Pw = precipitation water content, Pw
CCL = Convective condensation level
RHccl = Relative humidity at CCL
RHlo = Relative humidity at 0–10,000 feet
RHAb = Relative humidity at 10,000–18,000 feet
WS = Wind speed
SI = Stable index, SI
LI = Stable index, LI
KI = Stable index, KI
Capel = Uplift energy of air mass 1
Cape2 = Uplift energy of air mass 2

While value of upper atmospheric parameters are replaced into equations as independent variable the mean rainfall amount (P) and covered area P(%) will be obtained. Consequently, appropriation for rainmaking and weight of estimated rainfall amount are defined as in Table 9.

Table 9. Appropriation and weight of each estimated rainfall amount

Estimated rainfall amount	Appropriation	Weighting rank
P<10, P(%)<10	Low	1
P=10-30, P(%)=10-50	Moderate	2
P>30, P(%)>50	High	3

5. Climatic situational forecasting

Aungsuratana (2003) have analyzed rainfall amount from synoptic situation of different region which characterized by specific physiography. He found that weather in different time affect on rainfall amount significantly i.e. lack of rain took place in early the Southwest monsoon season (OSM) during May to June of 1992 while heavy rain took place in the both same season and same place of 1994. In addition, he also concluded, from analysis on frequency of each climatic situation, that the beginning of southwest monsoon of each year start at different time. Moreover, El-Nino and La-Nina phenomenon also affect on variation in beginning time of season as follow.

5.1) Effect of regional climatic situation on beginning of southwest monsoon season

According to Chi-square Tests on effect of regional climatic situations on beginning of southwest monsoon which were done based on rainfall amount data which collected since 1981 to 2007, early onset, normal onset and late onset affect on the monthly rainfall ratio as <0.75, 0.75-1.0 and > 1.0, respectively (Table 10).

Table 10. Relationship between beginning of rainy season and rainfall ratio in March of each region

Parameters	Chi-square	Correlation coefficient
UP-N	11.017*	0.6
LO-N	10.84*	0.59
UP-NE	10.349*	0.58
LO-NE	6.9	0.5
CEN	10.937*	0.6
EAST	15.44**	0.66

Remark: 1) N=20, critical value, df=4, (α = 0.5) = 9.348

As a result, it can be concluded that during the beginning of the southwest monsoon result a high rainfall amount in April while late beginning of the monsoon result a low rainfall amount.

5.2) Effect of southern pressure oscillation on Thai weather.

The southern pressure oscillation closely relates with El-Nino and Southern Oscillation (ENSO). Walter (1998) suggested that index have to be defined by variable in order to classify Multivariate ENSO Index (MEI). Those variables including sea-level pressure (P); East-West Circulation (U); North-South Circulation (V); sea surface temperature (SST), surface air temperature (A); and cloudiness fraction of the sky (C).

Analytical result of El-Nino and La-Nina during analysis, El-Nino during 1991-1993 and 1995-1997 and La-Nina 1988-1989, revealed that ENSO affect on rainfall amount in this region significantly. It result low rainfall amount lesser than normally and its arrival late was 2 months.

La-Nina result high rainfall amount of southwest monsoon season, negative MEI and maximum slope of MEI decreasing rainfall amount ad

also came late approximately 1 week. Such phenomenon means rainfall tool placed since southwest monsoon season to northeast monsoon season.

Based on MEI, ENSO will be classified into 3 levels which according to requirement for rainmaking and weight as Table 11.

Table 11. Rainmaking requirement for each MEI

MEI	Requirement for rainmaking	Weighting Rank
COLD ENSO (La-Nina)	Low	1
MED	Moderate	2
WARM ENSO	High	3

6. Decision model for rainmaking over Thailand river basins.

Rainmaking will be operated based on the following items.

6.1) Critical need for rainmaking

This item is concerned based on 3 criteria: cropping system, climatology, and weather situation. Their weight and details are concluded in Table 12.

Table 12. Critical need for rainmaking over the Upper Northern Thailand River basin

Criteria	Weighting Rank	Remark
Cropping system	1	Low requirement
	2	Moderate requirement
	3	High requirement
Monthly synoptic index, SYNI	1	Low probability
	2	Moderate probability
	3	High probability
Multivariate ENSO Index, MEI	1	COLD ENSO
	2	MED
	3	WARM ENSO

Remark: If total weighting Rank = 3-4 means low need for rainmaking
If total weighting Rank = 5-6 means need for rainmaking
If total weighting Rank = 7-9 means critical need

6.2) Appropriation for rainmaking

This item is recognized based on 3 criteria: daily climatic type, upper-air model, and radar model. Their weights are as Table 13.

Table 13. Appropriation for rainmaking in study area.

Appropriated criteria	Weight	Remark
Daily climatic type	1	Low requirement
	2	Moderate requirement
	3	High requirement
Upper-atmosphere model	1	Low rainfall amount
	2	Moderate rainfall amount
	3	High rainfall amount
Radar model	1	Cloud absent
	2	Cloud occur at noon
	3	Cloud occur from morning couple with Cumulonimbus

Remark: If total weight = 3-4 means low appropriation for rainmaking
If total weight = 5-6 means moderate appropriation for rainmaking
If total weight = 3-4 means high appropriation for rainmaking

Consequently, decision criteria for rainmaking are defined as Table 14.

Table 14. Decision criteria definition from rainmaking in the study area.

Need for rainmaking	Appropriated criteria	Decision criteria
Low need	Low appropriation	No Operation
	Moderate appropriation	No Operation
	High appropriation	No Operation
Moderate need	Low appropriation	No Operation
	Moderate appropriation	Operation
	High appropriation	Operation
Urgent need	Low appropriation	Operation
	Moderate appropriation	Operation
	High appropriation	Operation

For easy application of this model, the GIS software named Mapserver is employed to this model. The decision criteria are installed in the Mapserver program in order to make a suitable using.

CONCLUSION

Analysis of decision criteria in order to make an artificial rain over all river basins of Thailand which based on need or requirement and appropriation composed of the following details.

Critical need for rainmaking

This criteria is recognized on the basis of cropping system, climatology, and weather situation. Its weights are concluded as follow.

1) Cropping system criteria, the weight of 3, 2 and 1 are defined for the highest, moderate and lowest requirement for water in agricultural activities, respectively.

2) Climatology criteria. Probabilities of rainfall making or rainfall amount are divided into 3 levels: low, moderate and high. Probability for monthly rainmaking is assessed from climatic situation. The weight of 3,2 and 1 are defined for highest probability for monthly rainmaking (rainy day > 10 days), moderate probability for monthly rainmaking (rainy day = 6 - 10 days), and lowest probability for monthly rainmaking (rainy day = 1 – 5 days), respectively.

3) Climatic situation criteria is recognized based on MEI and need for rainmaking then climatic forecasting is divided into 3 levels: 1, 2 and 3 for COLD ENSO (La-Nina), MED and WARM ENSO, respectively. Such weights mean low need, moderate need and critical need, respectively.

Appropriation for rainmaking

The appropriation is concerned on the basis of 3 criteria: type of daily climatic situation, upper-air model and radar model. Weight of each appropriation for rainmaking is concluded as follow.

1) Type of daily climatic situation can be used for categorization of appropriation for rainmaking which composed of 3 levels: low appropriation (SYNI = 2-4), moderate appropriation (SYNI = 5-7), and high appropriation (SYNI = 8-10). These levels are weighted as 1, 2, and 3, respectively.

2) The upper-air model will be used to estimate rainfall amount. Consequently, appropriation for rainmaking is divided into 3 levels: rainfall amount is lesser than 10 or % of area is lesser than 10%, rainfall amount is 10-30 or % of area is 10-50%, and rainfall amount is higher than10 or % of area is higher than 10% with the weight of 1, 2, and 3 respectively.

3) Radar model also can be used to divide an appropriation for rainmaking into 3 levels based on cloudiness in the sky: cloud absent through whole day means low appropriation, cloud occur on afternoon mean moderate appropriation, and cloud occur since morning couple with cumulonimbus means high appropriation. Such appropriations are weighted with 1, 2, and 3, respectively.

4) According to need and appropriation for rainmaking, decision criteria for rainmaking can be concluded as no operation and operation.

ACKNOWLEDGEMENT

The authors wish to gratefully thanks The Bureau of Royal Rainmaking and Agricultural Aviation and the Department of Earth Science, Kasetsart University for granting and supporting to carried out the research task till successful.

REFERENCES

1. Arkin, H. 1974. Handbook of Sampling for Auditing and Accounting. 2nd rd. Mc Grow-Hill, USA.

2. Aungsuratana, P. 2003. The Incluencing Parameters on Hydrological Characteristics of Atmospheric Water Resources Over Main River Basins of Thailand. Dissertation of Graduate school, Kasetsart University.

3. Bureau of Royal Rainmaking and Agricultural Aviation. Office of the Permanent Secretary for Ministry of Agricultural and Cooperatives. 2007. The Upper Atmospheric Data and Radar Data.

4. Meteorological Department (1976) Map of Regional Climatic Conditions of Thailand.

5. Meteorological Department. 2008. Climatic Data of Thailand and Radar Data of Phitsanulok Airport.

6. Silverman, B.A., S.A. Changnon., Flueck J.A. and Lintner S.F.. 1986. Weather Modification Assessment: Kingdom of Thailand. Bureau of Reclamation, United Stated Department of Interior, Denver, Colorado, USA.

7. Udomchoke, V., and P. Angsurattana. 2002. The Role of Agro-environmental Education and Water Resources on Related Disasters in Thailand. in the

Preceeding of the Annual Tsukuba Asian Seminar on Agricultural Education (TASAE) for Asia and the Pacific Programme of Education Innovation for Development (APEID) Tsukuba, Japan.

8. Udomchoke, V., Lauhachinda, N., Homchan, U., Jiwapornkupt, P. and Kesjinda, K. 2007. The Criteria for Rainmaking of watershed in the Upper Thailand. In the Proceeding on the Seminar of the Bureau of Rainmaking and Agriculture Aviation.

SCS-CN model : tool of head watershed management in Thailand.

P.Witthawatchutikul and P.Thitirojanawat
Watershed Reasearch Section,
Department of National Park, Wild Life and Plant Conservation, Thailand.

.

Abstract: Up till now, the continuous deforestation of Thailand in the past has introduced soil erosion, flash flood and drought to the people. They are more severity by the incident rainfall due to climate change. Watershed Research Section, Department of National Park, Wild Life and Plant Conservation has tried to safe the people from flooding and introduce them to have better living in the future. The API flood warning model has been developed to safe the people from flooding. The Biodiversity value model and Land use simulation model has been developed to change the attitude of people and help the government to protect the existing forest. Lastly, the Sustainable watershed model has been developed to monitor the sustenance of watershed after allocating the various land uses over any area of head watershed by head watershed community and lower reach community. Because of lacking the data in Thailand, SCS-CN method was selected to be a tool for developing these models

Keywords: SCS-CN Model, Head Watershed, in Thailand

INTRODUCTION

Although the cabinet defined the head watershed area of Thailand which is about 24.18 percent of total area as forest protection area, the forest area has been continuously destroyed. According to statistic estimation, the forest area in 2008 is about 23.08 percent of country area (Witthawatchutikul, 2008). The forest encroachment on head watershed area induces soil erosion and increases in peak flood discharge.

There is now firm evidence that climate change is likely to affect rainfall, altering the incidence and severity of landslide, flood and drought. Such changes may have significant impacts on agriculture, water resources, infrastructure and the environment both on head watershed and lower reach. (Harrold and Jones, 2003)

In order to save the people from these disasters including induce the better of life quality in the future, Watershed Research Section, Department of National Park, Wild Life and Plant Conservation has tried to study and develop the tools for suitable operations. Finally, SCS-CN method was applied to be the models for solving these problems. This paper would like to propose the new strategies of head watershed management and apply the SCS-CN method to be the models for management.

CONCEPT OF WATERSHED MANAGEMENT

Before 1975, the operation of watershed management in Thailand was the forest plantation instead of shifting cultivation. During 1975-2000, the operation emphasized the participation of local people to protect the existing forest and developed the deteriorated lands.

After that time, however, the climate change increased in flood and landslide in rainy season due to heavy rain over head watershed area. Thai government tried to solve these problems by changing the target of watershed management to be safe the people from landslide and flash flood including introduce the better of life quality in the future with sustainable land use.

Watershed research section, Watershed management division, Department of National park, wild life and plant conservation has tried to develop the tool for defining the system approach of head watershed management operations and evaluation the successful of these operations.

Corresponding Author: P.Witthawatchutikul, Watershed Reasearch Section, Department of National Park, Wild Life and Plant Conservation, Thailand. Tel: +66 02-562-5555 Email: dmuay@yahoo.com

According to safe the people from landslide and flooding, the API flood warning model must be developed. In order to change the attitude of people and help the government to protect the existing forest, and determine the sustained land use, the Biodiversity value model of watershed ecosystem and Land use simulation model must be developed. And the Sustainable watershed model must be developed for testing the sustenance of watershed after the allocation of the land use patterns over any area of head watershed by head watershed community and lower reach community, as well. Finally, the working plan is presented as flow chart as shown in Figure 1.

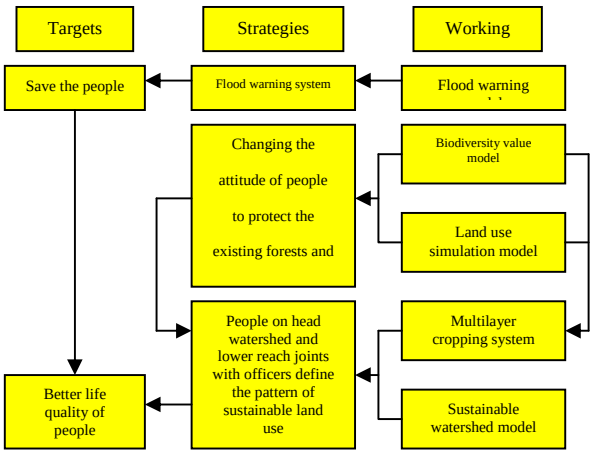

Figure 1. Strategies and working plan of watershed management.

SCS-CN METHOD

Mishra and Singh (2003) indicated that the SCS-CN method is simple, easy to understand and apply, stable, and useful for ungauged watersheds. The primary reason for its wide applicability and acceptability lies in fact that it accounts for most runoff producing characteristics : soil type, land use/treatment , surface condition , and antecedent moisture condition.

The SCS-CN method is based on the water balance equation and two fundamental hypotheses. The first hypothesis equates the ratio of the actual amount of direst runoff (Q) to the total rainfall (P) (or maximum potential surface runoff) to the ratio of the amount of actual infiltration (F) to amount of the potential maximum retention (S). The second hypothesis relates the initial abstraction (Ia) to the potential maximum retention. Thus the SCS-CN method consists of

(a) water balance equation:

$$P = Ia + F + Q \qquad \ldots(1)$$

(b) proportional equality hypothesis :

$$\frac{Q}{(P - Ia)} = \frac{F}{S} \qquad \ldots(2)$$

and (c) $Ia - S$ hypothesis :

$$Ia = \lambda S \qquad \ldots(3)$$

The fundamental hypothesis (equation (2)) is primarily a proportionality concept, as shown in Figure 2. Apparently, as $Q \to (P - Ia), F \to S$. This proportionality enables partitioning (or dividing) $(P - Ia)$ into two surface water (Q) and subsurface water (F) for a given watershed characteristics or S.

Parameter S of SCS-CN method depends on the soil type, land use, hydrologic condition and antecedent moisture content (AMC). The initial abstraction (Ia) accounts for short term losses, such as interception, surface storage and infiltration. Parameter λ is frequently viewed as a regional parameter dependent on geologic and climatic factor. The existing SCS-CN method assumes λ to be equal to 0.2 for practical application.

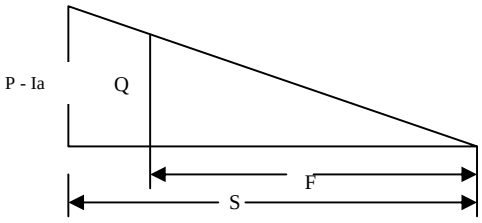

Figure 2. Proportionality concept.

According to the SCS-CN method, the extent of runoff contribution of a storage element depends on its capacity or, alternatively, the magnitude of S and, therefore, the whole watershed should be contribute to runoff, if S is taken to be the definite quantity. S is that constant and is the maximum difference of (P-Q) the

can occur for the given storm and watershed conditions. S is limited by either the rate of infiltration at the soil surface or the amount of water storage available in the soil profile, whichever gives the smaller S value. Since infiltration rates at the soil surface are strongly affected by the rainfall impact, they are strongly affected by the rainfall intensity.

Since parameter S can vary in the range of $0 \leq S \leq \infty$, it is mapped into a dimensionless curve number (CN) varying in a range $0 \leq CN \leq 100$. Using more than 3,000 soil typed divided into four hydrologic soil groups the SCS developed runoff curve number (CN) to estimate S in equation (4).

$$S = \frac{25{,}400}{CN} - 254 \qquad \ldots(4)$$

Wanielista et al. (1997)

API FLOOD WARNING MODEL

Concept of model

The factors affecting flood compose of rainfall and watershed runoff producing characteristics such as topography, soil infiltration and vegetative cover. Therefore, the flood warning system was developed by using the peak flow model of Cook's method, SCS-CN method and the equation of antecedent precipitation index or API (Schawab et al.,1971; Mishra and Singh, 2003 and Linsley et al, 1982).

Model operation

There are four steps in the process of model. Firstly, the score of topography, soil infiltration and vegetative cover are input. Total score is changed to be initial API with the last annual rainfall. Secondly, the recession factor of daily API, (k) was determined by the data of daily water level of the stream due to single heavy rain. Thirdly, the initial API is taken to determine daily API, ($API_{(t)}$) by k and daily rainfall as shown in equation (5)and Figure 3.

4. Daily API

Date	Rainfall(mm)	API	k	critical level	Accepted rainfall (mm)
1 April 20..	0	53	0.41689	Risky	32.9048
2 April 20..	0	22.0952	0.75263	Normal	38.3704
3 April 20..	5.6	22.2296	0.74956	Normal	38.3376
4 April 20..	0	16.6624	0.91062	Normal	39.8269
5 April 20..	0	15.1731	0.97005	Normal	40.2814
6 April 20..	0	14.7186	0.99017	Normal	40.4261
7 April 20..	0	14.5739	0.9968	Normal	40.4728
8 April 20..	0	14.5272	0.99896	Normal	40.4879
9 April 20..	0	14.5121	0.99966	Normal	40.4928

Figure 3. Output of flood warning model.

$$API_{(t)} = [API_{(t-1)} * k_{(t-1)}] + R_{(t)} \qquad \ldots(5)$$

where $API_{(t)}$ is the antecedent precipitation index (API) of that day (dimensionless),
$API_{(t-1)}$ is the antecedent precipitation index (API) of the day before (dimensionless),
$k_{(t-1)}$ is the recession factor at the $API_{(t-1)}$ value (dimensionless),
$R_{(t)}$ is the rainfall occur on the considered day (mm).

Lastly, the API value must be taken to determine the critical level of flood warning by observing the sediment in the stream water and runoff characteristics.

BIODIVERSITY VALUE MODEL

Concept of model

Biodiversity value of forested watershed ecosystem is defined as the economic value of impacts due to deforestation. These impacts are separated into structural impacts like as soil, water and nutrient losses by soil erosion and functional impacts such as increasing in runoff and air temperature.

There are three steps for model development. Firstly, biodiversity model was developed. At this step, SCS-CN method was applied to define the score and level of biodiversity. The crown cover percentage and canopy strata were defined as the structural variables. As well as the basal area percentage and soil depth were

defined as functional variables. Finally, the mathematical model for estimation the biodiversity score from these variables were determined.

Secondly, five forested watershed ecosystems were selected to study the impacts of deforestation at Doi Chiang Dao, Chiang Mai province. Climatic stations, erosion plots and weirs were installed to compare soil erosion, air temperature and runoff characteristics between forested watershed and denuded watershed. According to the study on impact of runoff characteristics, SCS-CN method was applied to develop runoff simulation model.

Thirdly, the cost replacement method was taken as a tool to estimate the value of impacts in terms of monetary unit.

Model operation

There are three steps of the model operation. Firstly, the crown cover percentage, canopy strata, basal area percentage and soil depth are input. The model will calculate the biodiversity score by equation as fallow,

$$BDV = 0.45*(10.46 + (0.11*CC*CS))^{0.62} * (25.16 + (45.26*BA*SD)^{0.59} \quad \ldots(6)$$

where BDV is biodiversity score (dimensionless),
CC is crown cover percentage (%),
CS is canopy strata,
BA is percent of basal area per unit area (%),
SD is soil depth (m).

Secondly, the biodiversity score is taken to calculate the impacts of deforestation such as soil, water and nutrient losses due to soil erosion, the changing in runoff characteristics and temperature increasing. Finally, the cost replacement method is used to be as tool for estimation the values of head watershed ecosystem as shown in Figure 4. as follow;

Impacts	No. of impact	Cost per unit	Cost (bath/rai/yr)
Soil loss (kg/rai/yr)	598.97	1800	1800.00
Nitrogen loss (kg/rai/yr)	835.45	0.035	29240.87
Phosphorus (gm/rai/yr)	397.13	0.093	36.93
Potassium (gm/rai/yr)	1.52	0.88	1.34
Water loss (mm/yr)	261.20	1800	39180.50
Temperature increase (celsius)	2.22	2.5	55547.46
Total value (bath/rai/yr)			125807.09

Figure 4. Output of Biodiversity value of head watershed ecosystem.

(CN) is changed to be initial API (initial CN) with the last annual rainfall. The infiltration data of forest area and considered agriculture land must be also input. These **LAND USE SIMULATION MODEL**

Concept of the model

Functional impact in term of variation of runoff characteristics due to the changing the forest area to be an agriculture land was taken to be a concept of this model. Therefore, SCS-CN method was applied for model development (Mishra and Singh (2003).

Model operation

As well as the API flood warning model, the score of topography, soil infiltration and vegetative cover are input. Total score data shall determine monthly API (monthly CN) of these area. Daily API of these two area are calculated by effective monthly API and daily effective rainfall as in equation (7). Then, daily runoff of forest area and agriculture land are estimated by the equation (8);

$$API_{(t)} = (a_{(m)} * API_{(m)}) + (b_{(m)} * R_{(t)}) \quad \ldots(7)$$

where $API_{(t)}$ is API of considered day (dimensionless),
$API_{(m)}$ is API of considered month (dimensionless),
$a_{(m)}$ is the correction factor of API for considered month,
$R_{(t)}$) is daily rainfall of considered day (mm),
$b_{(m)}$ is the correction factor of effective rainfall of considered month.

$$Q_{(t)} = (0.12 * R_{(t)}) + (0.06 * API_{(t)}) - 0.93 \quad \ldots(8)$$

Where $Q_{(t)}$ is daily runoff of considered day (mm).

Finally, daily runoff of these area are compared with graph as shown in Figure 5. as follow;

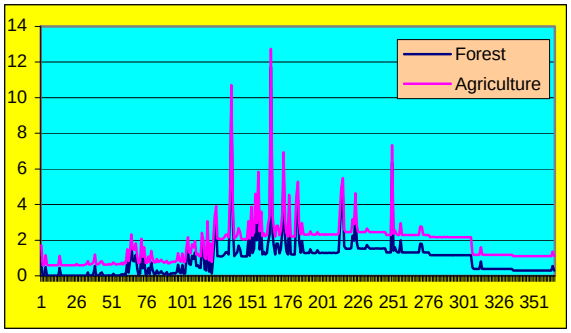

Figure 5. Output of land use simulation model.

SUSTAINABLE WATERSHED MODEL

Concept of model

The Critical Watershed Model of Witthawatchutikul (1997), Biodiversity model and SCS-CN method were applied for this model. The annual low flow per unit area and sediment yield per unit area were selected to be indicators of the model. These estimated data must be compared with the representative data of the region of Thailand in order to determine the level of sustainable watershed.

Model operation

There are four steps of model operation. Firstly, the biodiversity score of the existing forest is determined. Secondly, the score of forest area over head watershed and the score of main type of agriculture land are included to define the score of vegetative cover. Thirdly, the score of topography, and the score of soil infiltration including annual rainfall data are added to estimate the low flow per unit area and sediment yield per unit area by the equations as follow;

$$Ql/A = (8.51*10*Ra)-(0.00013*CNto)+(0.00136*CNso)\ (0.01058*CNve)-0.02924 \quad \ldots(9)$$

$$Sd/A = 27.68 + (0.018*Ra)+(0.71*CNto)-(0.53*CNso)-(5.32*CNve) \quad \ldots(10)$$

where Ql/A is low flow per unit area (MCM/sq km),

Sd/A is sediment yield per unit area (ton/sq km),

Ra is annual rainfall (mm),

CNto is score of topographic factor (dimensionless),

CNso is score of soil infiltration factor (dimensionless),

CNve is score of vegetative cover (dimensionless).

These estimated data are taken to compare with the representative data of the region for defining the level of sustenance. Lastly, the least sustenance of two indicators is compared to select the level of sustainable watershed as shown in Figure 6.

Ql/A	
Low flow amount per unit area (MCM/sq km)	0.03831
Sustained score of low flow per unit area	4
Sustained level of low flow per unit area	sustenance
Sd/A	
Sediment yield per unit area (tons/sq km)	60.395
Sustained score of sediment yield per unit area	3
Sustained level of sediment yield per unit area	warning
Head watershed area	
Sustained score of head watershed	**3**
Sustained level of head watershed	**warning**

Figure 6. Output of sustained watershed model.

CONCLUSION

In order to safe the people from flooding, the API flood warning model has been developed. At the same time, the Biodiversity value model and Land use simulation model has been developed to be the tool for changing the attitude of people and help the government to protect the existing forest and allocate the various land uses over any area of head watershed. Lastly, the sustenance of watershed will be tested by the Sustainable watershed model. According to succeed these proposes, however, the local people including the people at lower reach must be participant the model operations.

REFERENCES

1. Harrold, T.I. and R.N.Jones. 2003. Generation of local-scale rainfall scenarios using changes in GCM rainfall : a refinement of the perturbation method. Pp.11-16 *In* Proceedings MODSIM 2003. Modelling and Simulation Society of Australia and New Zealand Inc.

2. Linsley, R.K., M.A.Kohler and J.L.H. Paulhus. 1982. Hydrology foe Engineers. (Third edition). McGraw-Hill Book Company. Singapore. 508 P.

3. Mishra, S.K. and V.P. Singh. 2003. Soil Conservation Service Curve Number (SCS-CN) Methodology. Kluwer Academic Publishers. Dordrecht. 513 P.

4. Schwab, G.O., K.K. Barner, R.K. Frevert and T.W. Edminter. 1971. Rainfall and runoff, pp.63-81. *In* Elementary Soil and Water Engineering. John Wiley & Sons.Inc., New York.

5. Wanielista, M., R. Kersten and R. Eaglin. 1997. Hydrology: Water quantity and quality control. John Wiley & Sons, Inc. 567 P.

6. Witthawatchutikul,P. 1997. Modelling for Evaluation of Critical Condition of Watershed in Thailand. Ph.D.Thesis. Kasetsart University. Bangkok, Thailand.

Application of Remote Sensing and GIS in Land Use Land Cover Change and Soil Erosion

Kyaw Zaya Htun[1], Swe Swe Aye[2], Lal Samarakoon[3]
[1] Remote Sensing Department, Mandalay Technological University, Myanmar
[2] Pro-Rector, Yangon Technological University, Myanmar
[3] Director, Geoinformatics Center, Asian Institute of Technology, Thailand
kyawzaya.htun@gmail.com

Abstract: Geographic Information Systems are becoming a popular tool when seeking solutions to issues of these kinds, which are spread over large spatial extents and require a study of many alternatives. Most common method for soil erosion assessment is the use of Universal Soil Loss Equation (USLE). Many have proposed modifications to the USLE but all are woven around the same concept where rainfall erosivity, soil erodibility, slope length, slope class, land cover and land management factors are taken as directly proportional to the rate of annual erosion (Brooks et al 1991, Renard et al 1997,Morgan 1986). Present study describes the methodology adopted to compute these factors and a comparison of results with the polygon based study done by Ijesekera & Chandrasena (2001).The relationship between land use land cover changes and soil erosion is investigated using digital image processing integrated with Remote Sensing (RS) and Geographic Information System (GIS) in Tonle Sap Watershed, Cambodia. The Universal Soil Loss Equation (USLE –Wischmeier and Smith, 1978) was applied to build a model to estimate the annual soil loss from the watershed in 1976 and 2002. The analysis process on land use land cover change is based on geo-processing of GIS utilizing the raster and vector analysis. The analysis result of land use land cover change between 1976 and 2002 show that the agriculture land was expanded and the forest area was decreased in the study area. A grid based and polygon based GIS were used to comparatively calculated soil loss map. The result shows that grid based method also enables the meaningful use of pixel based remotely sensed land cover information for modeling soil erosion. The result also shows that increased soil erosion in the agriculture land and suggests that mitigation measure should be taken for prevention of further degradation. High resolution satellite images are very effective tool for not only monitoring the land use land cover change but also estimating soil erosion in the watershed. Similarly, GIS is also an effective tool in analyzing by overlaying various vector maps related to factors affecting in soil erosion. C++ programs were also developed for digital image processing such as solving LS factor and converting raw Digital Number (DN) value to reflectance valves. The main data used in this study are Landsat ETM satellite images.

Corresponding Author : Kyaw Zaya Htun, Remote Sensing Department, Mandalay Technological University, Myanmar

1. Introduction

Soil erosion is a very complex process monitored or determined by mutual interaction of numerous factors. To assess the spatial extent and severity of environmental risk of this process, extensive data sets related land cover and soil are necessary. The hardware and software facilities, as well as the new methodological approaches, integrated into digital image processing with Remote Sensing & Geographical Information Systems (RS_GIS) allow to model soil erosion at different land cover and analyze the change detection.

2. Study Area and Data

Tonle Sap Watershed is located in the northwest part of Cambodia between longitudes 102° 15' to 105° 50' E and latitudes 11° 40' to 14° 28' N covering an area of about 80 000 km^2, including Tonle Sap Lake. The Watershed consists of six provinces and it covers about 44% of the total land area of Cambodia. Population is about 5.14 million (Population Census of Cambodia. 2002) which represents nearly 43% of the total population of Cambodia (11.50 million persons). Tonle Sap Watershed is an important region for socio-economic development of Cambodia. (Dr Geoff Wright, Dr David Moffatt, Dr Jonathan Wager,2004). It consists chiefly of plains with elevations generally of less than 100 meters. Mountainous area is in north and south of study area and rise to more than 1 500 meters. 53% of the total land resources of the Watershed is covered by forest. The land use for agriculture is 2,368,059 ha or 30.92% and urban area is 12,256 ha or 0.15% of the total land use in Tonle Sap Watershed (Keskinen, 2003) (Figure 2 and 3).

3. Methodology

Detail discussion of the methodology of each digital image processing phase and its stepwise procedures has been described in separated flow diagrams for change detection and soil erosion. Each

step includes Remote Sensing (RS) section and GIS section (Figure 1 and 11).

3.1. Remote Sensing Data Classification

Raw digital number (DN) was converted to reflectance for each band of Landsat ETM satellite images of the year 1976 and 2002 using C++ program which was developed based on the formula describing in Landsat ETM Science Data Users Handbook (Irish, 2000) before image processing step because acquisition date of two satellite images changing sun illumination geometry strongly affects DN.

Firstly, DN value was converted into radiance using the following equation 1.

$$L_\lambda = (L_{\max,\lambda} - L_{\min,\lambda}) / 255 * DN + L_{\min,\lambda} \quad (1)$$

And then conversion of radiance into reflectance was carried out by using the equation 2, 3 and 4.

$$\rho_\lambda = \frac{\pi . L_\lambda . d^2}{E_\lambda . \cos\theta} \quad (2)$$

$$d = 1.00011 + 0.034221 \cos x + 0.00128 \sin x + 0.000719 \cos 2x + 0.000077 \sin 2x \quad (3)$$

$$x = 2\pi (DOY) / 365 \quad (4)$$

where, ρ_λ = unitless planetary reflectance

L_λ = spectral radiance at the sensor's aperture

d = earth- sun distance in astronomical units

E_λ = mean solar exoatmospheric irradiances

θ = solar zenith angle in degrees

The unsupervised classification image produced 40 classes through the satellite data and then using Maximum likelihood to reclassify them to seven classes according to the existing land use map of 2001 and ground control points (ground truth data) which were collected during the field survey. There was some confusion in satellite images during classification step. The wet season image and NDVI images of each year also was used as reference images during the classification step because deciduous forest, harvested paddy field, urban area and bare land were confused with the other classes or each other. Both classified images accuracies were an acceptable accuracy of 85% (Figure 4). Image Segmentation separated classified image into each layer and then each was converted into vector format.

3.2. Change Detection

Geo-processing tool and logical function was applied two satellite images to detect and quantify the land use changed in ArcGIS 9.0 software. The basic tools used in landuse/ landcover change are shown in Table 1. Detail methodology is shown in Figure 3. The result is shown in Figure 5 and the statistical data is shown in Table 2. The most significant changed was occurred in agricultural land and forest area.

3.3. DEM Generation

Digital Elevation Model (DEM) provides a digital representation of a portion of the earth's surface terrain over a two dimensional surface. We can derive much useful topographic information such as slope, aspect, stream networks and watershed boundaries. Digital elevation models may be prepared in a number

of ways, but they are frequently obtained by remote sensing rather than direct survey. At present study, older methods of generating DEM is used and it involves interpolating digital contour map having 10 m interval that may have been produced by direct survey of the land surface. DEM was interpolated from elevation contours and was employed to generate the slope and LS-factor. It is a time saving and cost effective procedure to calculate the LS factor.(Panda et al.,2000) (Figure 6).

3.4. Potential of Soil Erosion Estimation

This study of estimation of soil erosion potential by water between the year 1976 and 2002 using Universal Soil Loss Equation (USLE) based on raster calculation. Preparation of USLE parameters are described in following section.

3.4.1. Rainfall Erosivity (R) Factor

According to R factor vector image (Figure 7), there is no too much different amount of rainfall among provinces in study area. The rainfall data of fourteen rainfall stations of Tonle Sap Watershed including neighboring stations were used. The annual rainfall data was calculated based on the equation used by El-swaify et al, 1985; Harper, 1987; Funnpheng et al 1993 for computation of R factor. This equation is as follow:

$$R=38.5 + 0.35\ r \qquad (5)$$

where,
R = rainfall erosivity index
r = total rainfall amount in millimetre
Total rainfalls of fourteen stations of the watershed were interpolated based on location.

3.4.2. Soil Erodibility (K) Factor

As the soil information is not available in soil map (1998, 1:100,000 scale) of the Tonle Sap Watershed, FAO Soil Map of the World book was used to match local soil name and global soil name of FAO. Assigning the soil information (organic matter, silt percent, very fine sand percent, clay percent, permeability and soil texture) was done in soil database using following equation (Figure 8).

$$K=[\,2.1 * 10\text{-}4\,(12 - OM)\,M1.14 + 3.25\,(s-2) + 2.5\,(P-3)\,]\,/\,100 \qquad (6)$$

where,
K = soil erodibility
OM = % of organic matter (%OM= 1.724 * %OC)
OC = Organic Compound
M = particle size parameter [(%silt + % very fine sand) *100 - %clay]
s = classes for structure
(1= very fine granular, 2= fine granular, 3= medium or coarse granular, 4 = blocky, platy or massive)
p = permeability class
(1= rapid, 2 = moderate to rapid, 3= moderate, 4= slow to moderate, 5= slow, 6 = very slow)

3.4.3. Topographic (LS) Factor

In modeling erosion in GIS, it is common calculating the LS combination using a formula:

$$LS = (\text{Flow Accumulation} * \text{Cell Size}/22.13)^{0.4} * (\sin \text{slope}/0.0896)^{1.3} \qquad (7)$$

Where Flow Accumulation is the number of cells contributing to flow into a given cell and Cell Size is the size of the cells being used in the grid based representation of the landscape. This formula is based on the suggestion by Moore and Burch (1986a, b) that there was a physical basis to the USLE L and S factor combination. A C++ program based on above equation was also developed to calculate LS factor. This program involved four steps: removing sink, calculation of slope, slope direction (aspect) and then GRID accumulation (flow accumulation), which were calculated on centre pixel of 3*3 window (Figure 9).

3.4.4. Crop Management and Practice (C and P) Factor

The value of C factor was derived by the expert assessment of the values published by Wischmeier, Smith (1975), Morgan (1996) and Pasak et. al. C value was assigned according to land use classes of land use map 1976 and 2002. The agriculture land was covered with annual crop such as paddy, wheat, barley, maize, etc., and the C value is assigned as 0.377 to the whole agriculture land. Moreover, people have to collect wood for fuel supply. So, the woodlands were consequently opened in some part of the watershed and so equally assigned to 0.006 which is recommended by Wischmier and Smith (1978). P value is assigned 0.5 equally to all the agriculture land because of the practices of all agriculture are traditionally ploughed with contour and assigned 1 to built-up area, bare land, scrub, grass and forest which has no conservation practices (Figure 10).

3.5. Intervention Analysis Using GIS

Estimation of soil erosion by water in the study area was modelled using the USLE. USLE estimates the average annual soil loss (A) by using a functional relation of several factors expressed as A=RKLSCP where R is the rainfall erosivity, K is the

soil erodibility, L & S are slope length and slope angle factors, C is the crop management factor and P is the eros ion control practice factor. Modeling in the present study used a raster based approach where a square cell of 50 meters was chosen. It was taken that this resolution would be suitable for a reasonable accuracy considering that the original data were mos tly from 1:50,000 maps. Grids of rainfall, soil land use and elevation data created using ArcGIS software were used for the computation for the USLE (Figure 11).

4. Comparison

Comparison of computed spatial distribution of erosion levels on polygon and grid based calculation method is checked for the year 2002 in Figure 12. Modeling results showed that about 3.3% of watershed could be ranked in the severe erosion level category. Investigation of the individual cell values showed that 3.3% of the area had resulted in annual soil loss values greater than 126. Both methods resulted in similar values through model calculations. Calibration of USLE values in the polygon -based method had 26 and 45 tons/ha/year as threshold values between insignificant, moderate and severe erosion classes. Though the values from both methods do not drastically differ from one another, it is prudent to be cautious of the averaging effect over spatial extents when model computations are used for planning purposes. Investigation of computations at each cell showed that in most cases such flat area represented insignificant soil erosion zones as expected in nature. This deficiency was noted in both methodologies. Percentage of extents classified at moderate level of erosion in polygon based computation shows a reduction in the raster -based approach. Comparison shows that there had been a tendency for values of polygon approach to move from the moderate category to the insignificant category when raster approach is used. This suggests that polygon -based approach may lead to an over estimation of extents that require precautionary measures. However it is noted that a careful selection of manageable polygon sizes may look after this concern. Comparison shows that both methods estimated similar annual erosion levels for approximately 70% of the watershed with a well matched spatial distribution. Estimations were quite close in the severe category indicating the greater emphasis on this category when using a weighted function for optimization (Figure 13).

5. Results and Discussion

Erosion was mostly occurred in agriculture land within 7 km along National 6 road in the year 1976 and 2002(Figure 12 and 13). It was found that soil loss had increased from 105,385 ton/ha/yr in the year 1976 to 161,035 ton/ha/yr in the year 2002 along this road. It was also clearly found that total soil erosion potential had increased more than double in Kampong Thom Province, Preah Vihear Province and Poussat Province. In former two Provinces, the percent of change from forest to agriculture was 45 % (951.15 sq km) and 13% (290.60 sq km) of total change area of forest to agriculture (2,104.67 sq km) in Tonle Sap Watershed. The reason is that the agriculture land was expanded in these sites after 26 years because of population pressure. This expansion was mostly happened in forest area around Tonle Sap Lake. In Preah Vihear Province, agriculture land was also expanded, which was occurred by clearing forest in high land area.

It can be conclude that population pressure affected the soil erosion. The population data of some provinces are shown in table3. The populations have increased almost double in some provinces over the past 26 years. In 2010, this may be increased at least 15% more in each province according to the growth rate formula (Table 3). As a result, agriculture land expanding will increase in lowland as well as upland area. In the uplands, farming is generally practiced along slopes without any soil conservation measures where the erosion potential is high. Three months after clearing, one to 1.5 cm of the topsoil is typically lost (Yang Saing Koma 1997). The exploitation of forests has also led to reduced availability of resources to local communities; increased run off and siltation from commercial logging; reduced soil fertility (Shams and Ahmed 1996; CEDAC 1997).

The average depth of the lake has decreased from 4.5 m in January 1979 to 3.5 m in January 1994 (Global Witness 1997). According to filed data, the depth of the lake has decreased to 1m in January 2004 and frequency of flood was also increased. The flood area has expanded by 43.92 km2 during this period. Changed flood patterns leading to food shortages in some parts of the country. Mottet (1997) claimed that if the present pace of deforestation remained unabated, the Tonle Sap Watershed would very soon stop producing rice and fish.

In this study, limitation of data about soil erosion cause difficult to validate. So estimated erosion rate of some classes were compared with some sites of soil loss rate which are published to evaluate the soil yield. The reference information about soil erosion rate is shown in Table 4.

6. Recommendation

The results of this study have confirmed that digital image processing with RS-GIS data integration and analysis is an efficient approach for obtaining

information on spatial variability of soil erosion at regional scale. The contemporary hardware and software systems enable to process the data sets representing large territories in scale useful for regional studies but also for global. The methodology used in this study is rather simple and straightforward and alternative solutions based on similar models integrated with simulation can be also applied. In this study, land use land cover change categories only considered seven major types of land. The categories should be considered more detail as further analysis based on the classification criterion of the world. Upland planting should be established in high land area to control erosion. Long term shrub fallow should be cultivated along farm boundaries, scattered over the plot or in house compound because they contribute to control of soil erosion.

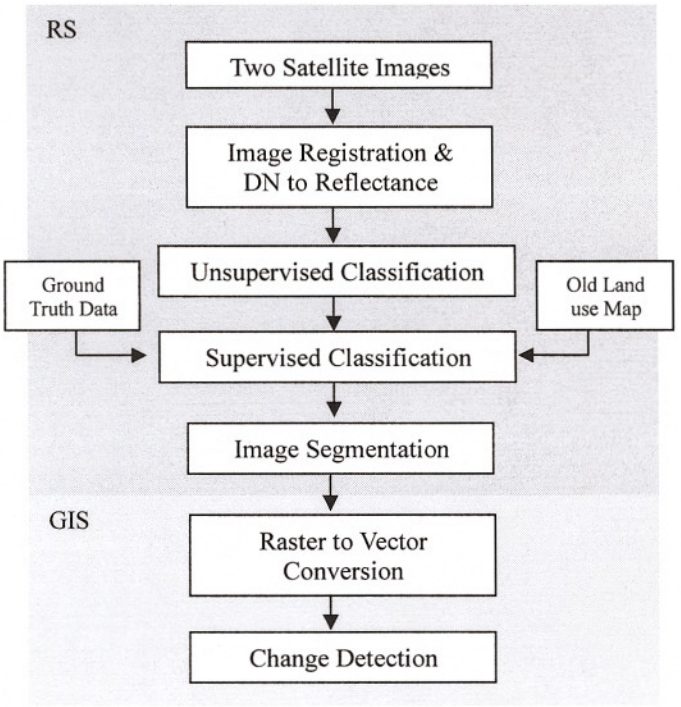

Figure. 1. Flow Chart of Change Detection

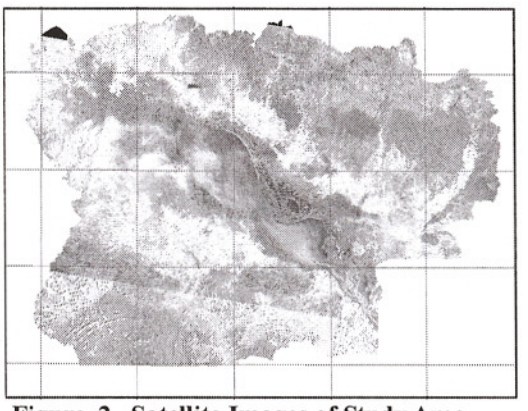

Figure. 2. Satellite Images of Study Area (Landsat_MSS _1976)

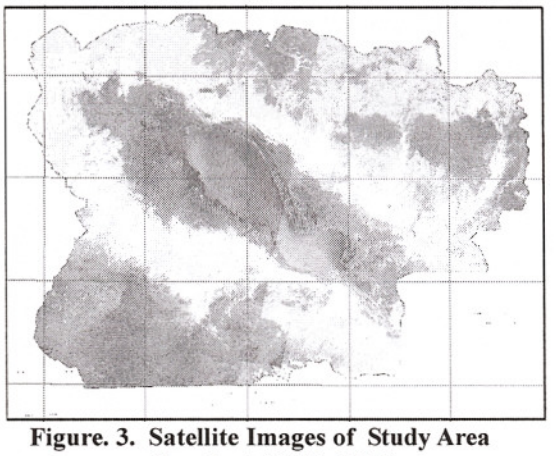

Figure. 3. Satellite Images of Study Area (Landsat_ETM_2002)

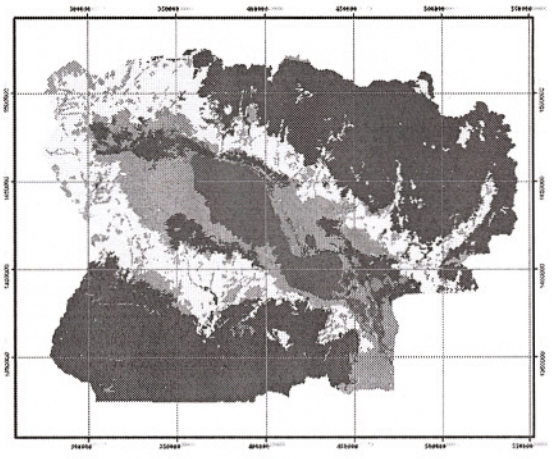

(a)

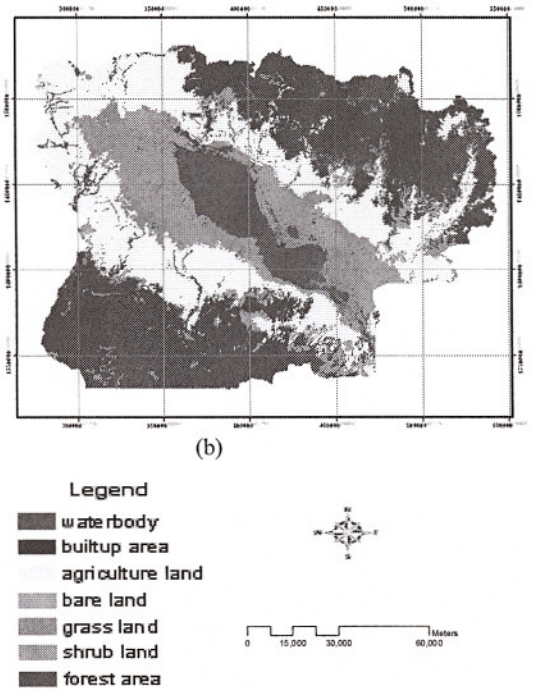

Figure. 4. Vector Images of Land Cover of Study Area : (a) 1976 and (b) 2002

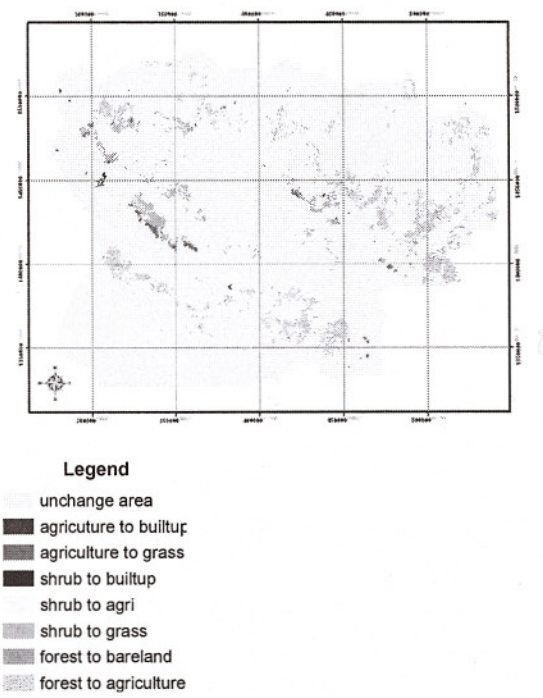

Figure. 5. Change Detection Analyses between 1976 and 2002

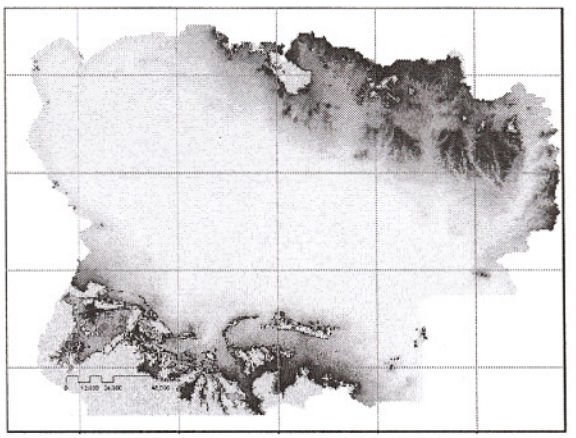

Figure. 6. DEM Raster Image

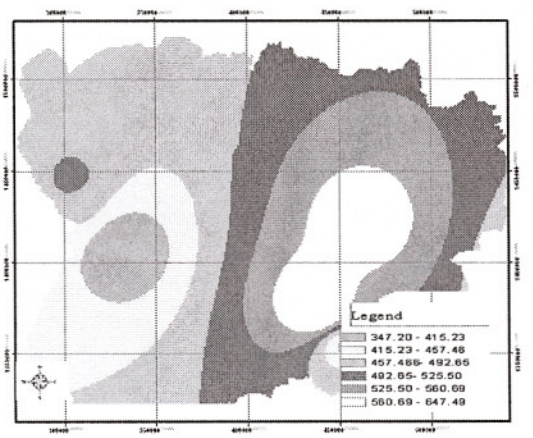

(a)

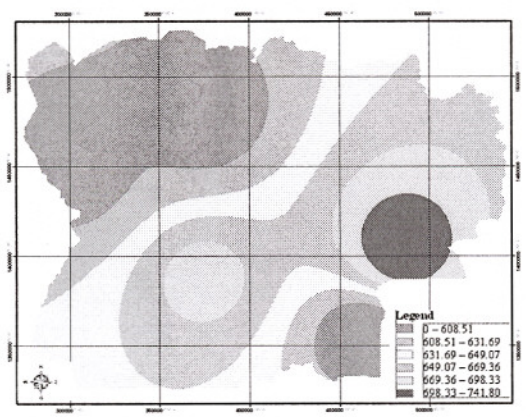

(b)

Figure. 7. Vector Image of R Factor: (a) 1976 and (b) 2002

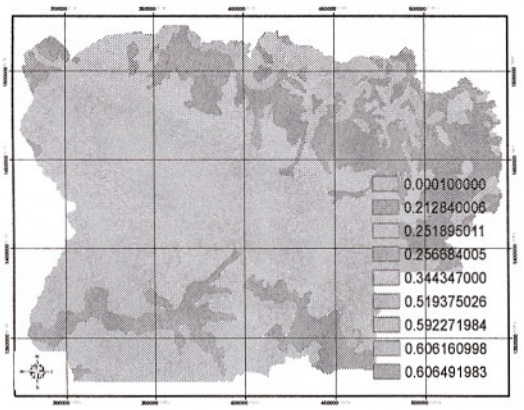

Figure. 8. Vector Image of K Factor

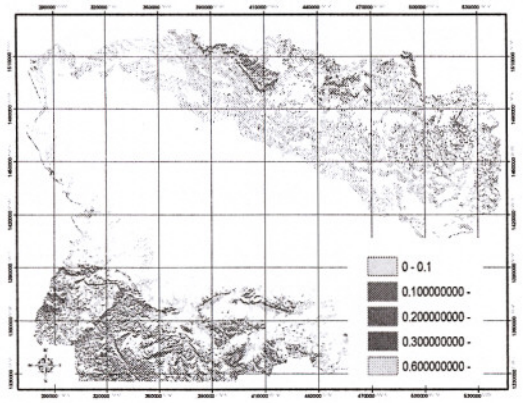

Figure. 9. Vector Image of LS Factor

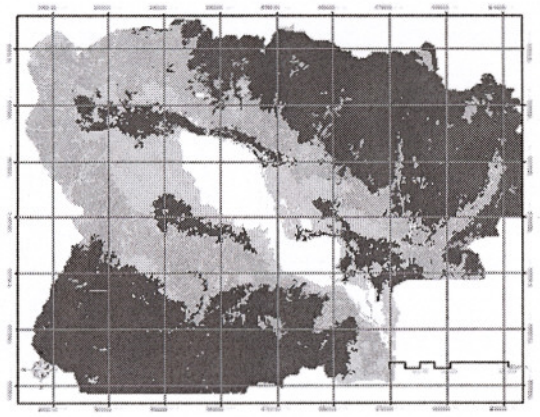

(a)

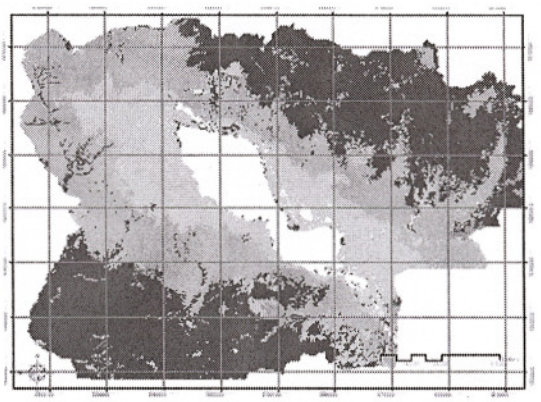

(b)

Figure. 10. Vector Image of CP Factor: (a) 1973 and (b) 2002

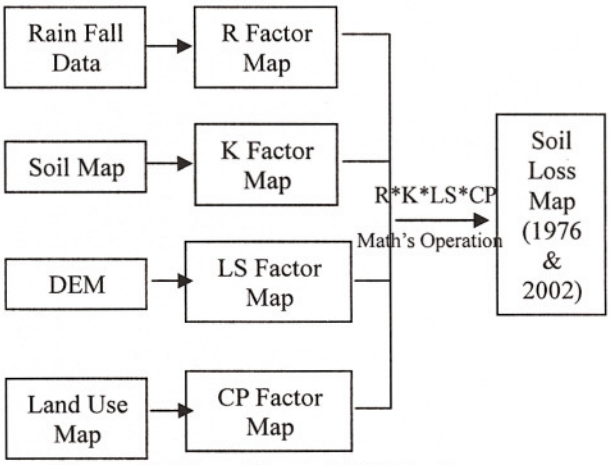

Figure. 11. Flow Chart of Soil Erosion

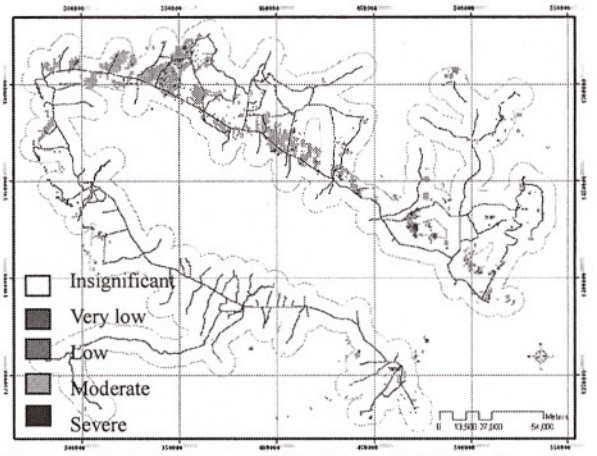

Figure. 12. Soil Loss on Grid Based Calculation: (1973)

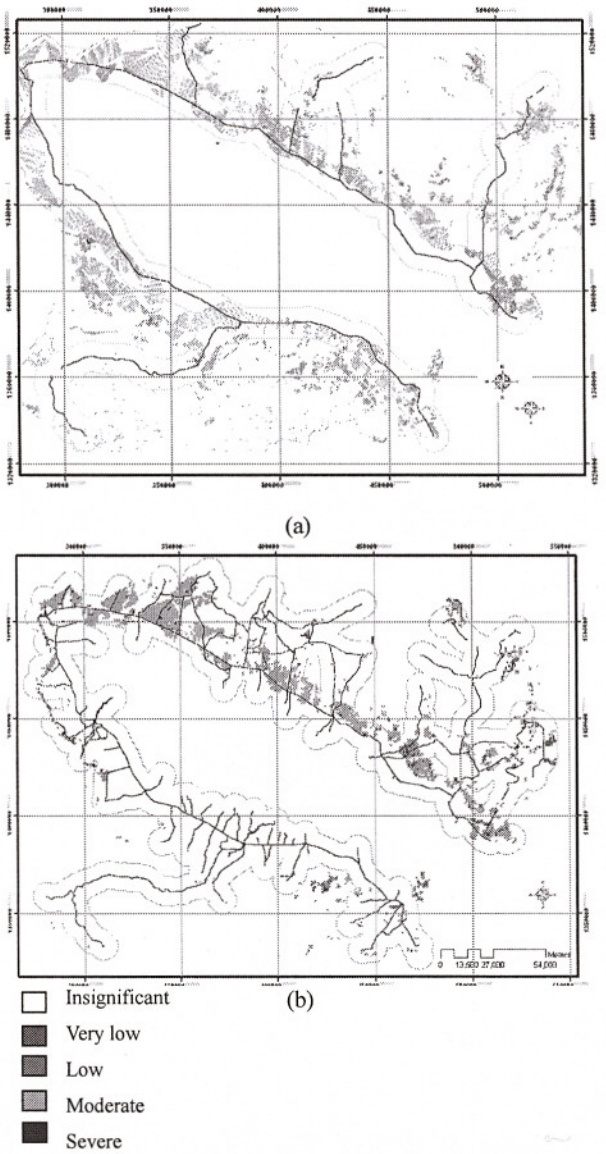

Figure. 13. Soil Loss on (a) Polygon Based Calculation (2002) (b) Grid Based Calculation (2002)

Table 1. GIS function in land use/ land cover analysis

Geo-processing	GIS function	Result in land use/ land cover change
	Intersection	Unchanged area between 1976 and 2002
	Intersection and Erase	Area lost between 1976 and 2002
	Union	Not immediate interest
	Union, Intersection and Erase	Area gained at 2002

Table 2. Land Cover Change between 1976 & 2002

No.	Land Use	Land Use in 1976 (sq km)	Land Use Percent in 1976	Land Use in 2002 (sq km)	Land Use Percent in 2002	Change Percent
1	water body	3,171.73	7.89	3,216.97	7.89	0.00
2	built-up area	11.10	0.03	37.41	0.09	0.06
3	agriculture land	8,421.76	20.95	12,633.11	31.42	10.47
4	bare land	51.78	0.13	97.20	0.24	0.11
5	grass land	515.53	1.28	1,465.17	3.64	2.36
6	shrub land	6,771.20	16.84	6,556.98	16.31	-0.53
7	forest cover	21,261.67	52.88	16,241.86	40.40	-12.49
	Total	40,204.77	100.00	40,248.69	100.00	

Table 3. Population Data

SrNo.	Province	Estimated Population (1976)	Actual Population (2002)
1	Siem Reab	221,035	696,164
2	Kampong Thum	271,907	569,060
3	Kampong Cham	170,907	371,357
4	Kampong Chnang	181,272	417,693
5	Pousat	110,120	360,445
6	Bat Dambang	314,906	793,129
7	Bantaey Mean Chey	318,463	577,772
8	Kaoh Kong	-	131,912
9	Prean Vinear	60,595	119,261

Table 4. Soil Erosion in Some Sites

unit (ton/ha/yr)

Land Use Type	Mayaguez, US	Japan: Asio region (30°)	Siwalik: Far West Nepal Sandstone foothill	Tonle Sap Watershed(2002)
Grass land	-	20.27 (1mm/yr)	-	6.59
Agriculture Land	39.7	-	-	27.56
Forest	-	2.027 (0.1 mm/yr)	20.00	1.098
Bare land	339.7	-	-	139.86
reference	Smith and Abruna,1995	Honda,1993	Laban,1978	model result

Degraded forest, sandstone foot hill, Siwalik, Far West Nepal

References

[1] Bähr, H. P. & T. Vögtle (ed), GIS for Environmental Monitoring. Stuttgart, German, E.Schweizerbart'sche Verlagsbuchhandlung, 1999.

[2] Friend A. J., "Achieving Soil Sustainability", Journal of Soil and Water Conservation, Vol.47, Number 2, 156-157, 1992.

[3] Jenson, J.R., Introductory Digital Image Processing, Prentice Hall, New Jersey, 1986.

[4] Lambin, E.F., Turner, B.L. II, Geist, H.J., Agbola, S.B., Angelsen, A. et al., "The causes of land-use and land-cover change: Moving beyond the myths",

Global Environmental Change: Human and Policy Dimensions 11(4):5-13, 2001.

[5] Morgan, R.P.C., Soil Erosion and Conservation (Second Edition), Longman Group, UK Limited, 1995.

[6] Robert A. Schowengerdt, Techniques for Image Processing and Classification in Remote Sensing (Second Edition), Academic Press, INC, Londom Limited, 1983.

[7] Symeonaki,.E., Drake, N., "Monitoring Desertification and Land Degradation over Sub-Saharan Africa", International Journal of Remote Sensing, 25(3),573-592, 2003.

Participatory Agent-Based Modeling and Simulation of Rice Farming in the Rainfed Lowlands of Northeast Thailand

W. Naivinit[1], C. Le Page[2], M. Thongnoi[3], and G. Trébuil[2]
[1] Ph.D. student, Chulalongkorn University, Thailand and Paris X University, France;
[2] Cirad, UPR Green, Montpellier, F34000 France and
CU – Cirad ComMod Project, Chulalongkorn University, Bangkok, Thailand;
[3] M.Sc. student, Faculty of Agriculture, Ubon Rajathanee University, Thailand

Abstract: Rainfed lowland rice production in lower northeast Thailand is a complex and adaptive farming activity. Complexity arises from interconnections between multiple and intertwined processes, particularly agronomic practices and labor migration. Having faced a heterogeneous and very variable environment for centuries, local rice farmers are very adaptive and used to adjust their behavior in unpredictable farming conditions. Based on the principles of the Companion Modelling (ComMod) approach, indigenous and academic knowledge was integrated in an Agent-Based Model (ABM) to build a shared representation of this complex and adaptive system. The ABM was co-designed over a 3 years long process with a group of different types of rice growers from Ban Mak Mai village in southern Ubon Ratchathani province. This participatory modeling process also aimed at stimulating participants' thinking and co-learning through the collective exploration of simulated scenarios with varying levels of water and labor availability, with the ultimate goal of further strengthening their adaptive management ability.
The ABM consists of three interacting modules in a virtual rainfed lowland rice environment: Water (hydro-climatic processes), Rice, and Household. "Household" is a rule-based agent making daily decisions based on its available means of production depending on the stage of the rice crop, and water and labor availability. Key decisions made are related to: i) rice nursery establishment, ii) rice transplanting, iii) rice harvesting, and iv) migration of household members. The spatially-explicit model interface represents an archetypical toposequence made of upper to lower paddies in a mini-catchment farmed by 4 different households and includes also water bodies and human settlements. According to participating farmers, after many iterations between the lab. and the field, this ABM adequately represents their rice farming and labor migration management practices. Using the model to raise farmers' awareness of the system emergent properties as a consequence of interactions between rice farming and labor migration is also discussed.

Keywords: Agent-based modeling and simulation, Companion Modelling, rainfed rice farming, labor migration, northeast Thailand.

INTRODUCTION

85% of the 5.2 million ha of rice areas in Northeast Thailand are farmed under rainfed conditions with a single crop per year and low productivity of paddy rice averaging 1.8 t ha^{-1}. This is mainly the result of low water-holding and infertile coarse-textured soils and erratic rainfall distribution[15, 29]. Notwithstanding, 25% of the households living in this most populated region of the kingdom are still engaged in rice production[25]. But cash incomes generated from rice production are inadequate to meet their basic needs, leading to a relatively high rate of poverty in this region. Therefore, to improve their livelihoods, these resource-poor rice farmers have been involved in labor migration for a long time to access off-farm jobs in urban areas, causing labor scarcity at household and community level. More than a third of all interregional migrations still originates from this region[28]. Successive state policies have been implemented to upgrade farmers' livelihoods by mitigating agro-ecological constraints, but met with limited success. Today, in particular, a new water improvement scheme proposes to invest 15 billion US dollar in the construction of a future ambitious "hydro-shield tunnel" to divert water from the Mekong River to supply 19 provinces in the Northeastern region. As in the past, the success of water improvement schemes could be

Corresponding Author : Warong Naivinit, Faculty of Agriculture, Ubon Rajathanee University, Ubon Ratchathani 34190, Thailand, Tel: 081-855-1205, E-mail: wnaivinit@yahoo.com

limited if they are not based on an in-depth understanding of the interactions between water use, farmers' rice production practices, and labor migration.

Rainfed lowland rice (RLR) farming in lower northeast Thailand is a very complex and adaptive system (CAS). Complexity arises from the interconnections between multiple and intertwined processes, particularly rice production practices and labor migration. Having faced a heterogeneous and very variable environment for centuries, local rice farmers are very adaptive and used to adjust their behavior in unpredictable farming conditions. Agent-Based Modeling and simulation is more and more widely used to represent, track, and analyze the dynamics of such CAS. Agent-Based Models (ABM) explicitly represent human decision-making processes[14] by means of agents set as autonomous computer entities interacting directly among themselves and with their common environment, in order to achieve their goals [12, 30]. An agent has some specified knowledge about the system in which it is situated and operates (but it is not omniscient). By nature, an ABM provides a representation of a real system that is less abstract than a mathematical model. Therefore, it is a promising tool to promote discussion and further exploration among researchers and model developers, but also subject matter specialists, policy-makers as well as local stakeholders [24]. The Companion Modelling (ComMod) approach has been designed for such a purpose: it is an iterative, continuous, evolving approach to facilitate dialogue, shared learning and collective decision-making through interdisciplinary and research in action processes to strengthen the adaptive management capacity of stakeholders facing a common resource management problem [5].

Past studies have examined labor migration as a result of economic drivers, such as push and pull factors in the neoclassical economic theory [7, 8, 19, 26], often at macro level. Some studies [10, 13] focused on the migration decision-making process as a result of the interaction between individual or micro-factors (often referring to demographic and social characteristics) or macro factors ranging from household to community levels (often referred to economic-related factors). But few studies have examined the relationship between renewable natural resource use and labor migration [27, 28]. And fewer of them used ABMS to assess changes in technologies and land use in relation to labor migration [17, 18]. Recent studies of RLR systems and RLR crop modeling carried out in this region took rainfall variability and the risk of drought into account. But none of them integrated the key interaction between rainfall distribution and farmers' decisions regarding RLR crop management [3, 4].

Therefore, the purpose of this research is to build a shared representation of the interactions between RLR farming, water availability, and labor migration by integrating indigenous and academic knowledge through a process of collaborative construction of an ABM with local RLR growers. We also aim at stimulating the participants' thinking and co-learning through the collective exploration of simulated scenarios displaying varying water and labor availability, with the ultimate goal of further strengthening their adaptive management ability throughout this very interactive participatory modeling and simulation process.

First, the structure of the ABM and the main processes represented in it are described. Then, the simulated scenarios identified by the participating local farmers are introduced and the salient points of the simulation results discussed with the researchers are presented. Finally, the effects of such collaborative modeling activity on farmers' awareness of the system emergent properties resulting from the simulated interactions between RLR farming and labor migration are discussed.

THE BanMakMai AGENT-BASED MODEL

The development of the ABM involved a heterogeneous group of RLR farmers from the Ban Mak Mai village since the beginning of the design process, hence its name: the BMM agent-based model.

A model designed with farmers

In agreement with the ComMod approach, our objective in designing and using an ABM with farmers was to support a co-learning process on the complex situation to be examined to improve farmers' and scientists' knowledge on its functioning by elucidating, and sharing diverse perceptions. Thus, the RLR growers' involvement to explain their decision-making processes regarding farm management was needed to allow such exchanges and the integration of indigenous and academic knowledge.

The study area is located in the Lam Dome Yai watershed, south of Ubon Ratchathani province. It is covering 1,680 km^2 in Det Udom and the northern part of Na Chaluay districts where 80% of the land is planted to RLR[21]. Within that area, the Ban Mak Mai village was selected, as it typically represents the regional RLR-based farming system.

Within this village, 11 farming households ranging from small farms (average size of 3.2 ha), to larger holdings (average size of 7.2 ha), were recruited

to take into account the diversity of farming conditions among households having different amounts of productive assets, socio-economic strategies regarding RLR production and labor employment. Husband and wife of each selected household were invited to participate in each of the successive modeling field workshops held in this village.

A 3 years long iterative collaborative modeling process

In this experiment, 6 successive participatory workshops were held in the village to co-design the ABM with the different types of rice growers. In the early stages of the process, participants were requested to make decisions under circumstances very similar to their actual ones (farm size, pond size, location of farm, family labor and members, etc.) and the participants played their own roles in role-playing games (RPGs) [22]. During the first 3 workshops, this particular type of participatory simulations was used to facilitate interactive knowledge sharing between participating farmers and researchers, and to acquire new information emerging from players' interactions when facing different situations regarding water availability. On the way from the RPG to the ABM, a couple of additional participatory workshops using prototype versions of the ABM derived from the previous RPGs were organized to agree on the formalization of the main decision-making processes regulating the relationships between water dynamics and farm management including labor migration (Figure 1).

Model description

The BMM model is a spatially-explicit agent-based model made of three interacting modules i.e. a water module (to account for hydro-climatic processes), a RLR module, and a household module (Figure 2). The BMM model is run with a daily time step. The initial date is set on 1st of April, at the end of the dry season. In every step, each simulated household has to make rice production and/or labor management decisions. The BMM model is designed to allow up to 10 years long simulations.

Spatial settings

The BMM model spatial configuration is based on field, farm, and community levels representing three land use types: upper to lower paddy fields, water bodies such as farm ponds and stream, and human settlements such as houses, village, and city (Figure 3). The smallest spatial unit, or cell, is equal to 0.04 ha (1 *ngan*, a Thai area unit). Elevation ranges from 97 to 133 meters to represent a regular slope from lower (close to the stream) to upper paddies (close to roads). The properties of the sandy Korat soil series found in this area are applied to each cell [2]. A paddy field is an aggregation of cells, and a farm is an aggregation of paddy fields. To represent the heterogeneity of farm size and water availability, two small farms (3.3 ha) and two large farms (6.5 ha) with

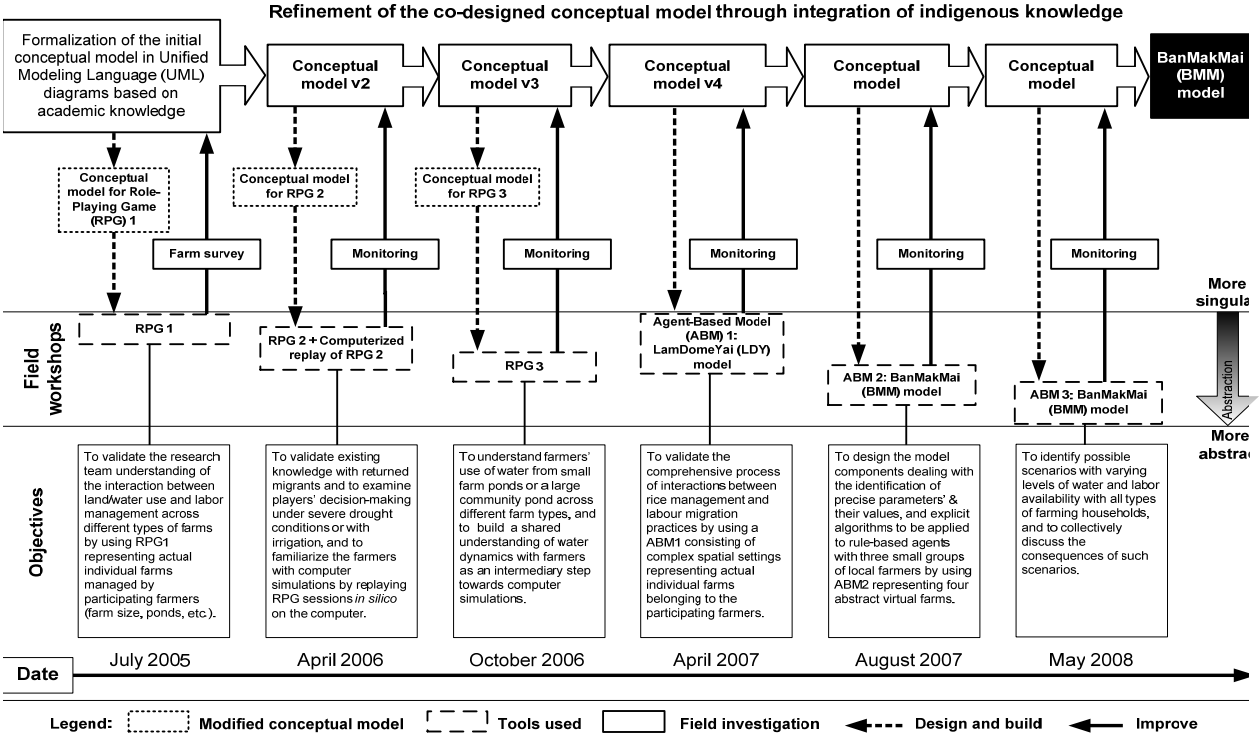

Figure 1. ComMod process conducted with 22 rice farmers in Ban Mak Mai village, Det Udom district, Ubon Ratchathani province showing objectives and tools used of 6 participatory workshops.

different farm pond size were implemented.

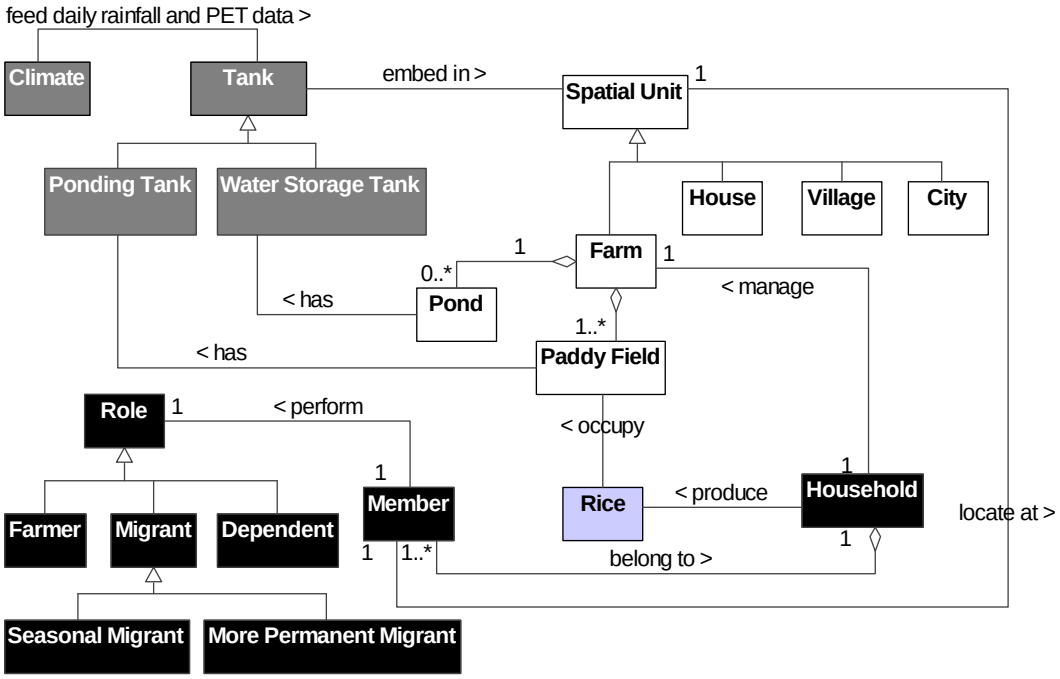

Figure 2. The BMM conceptual model in a UML class diagram representing key entities and their relationships.

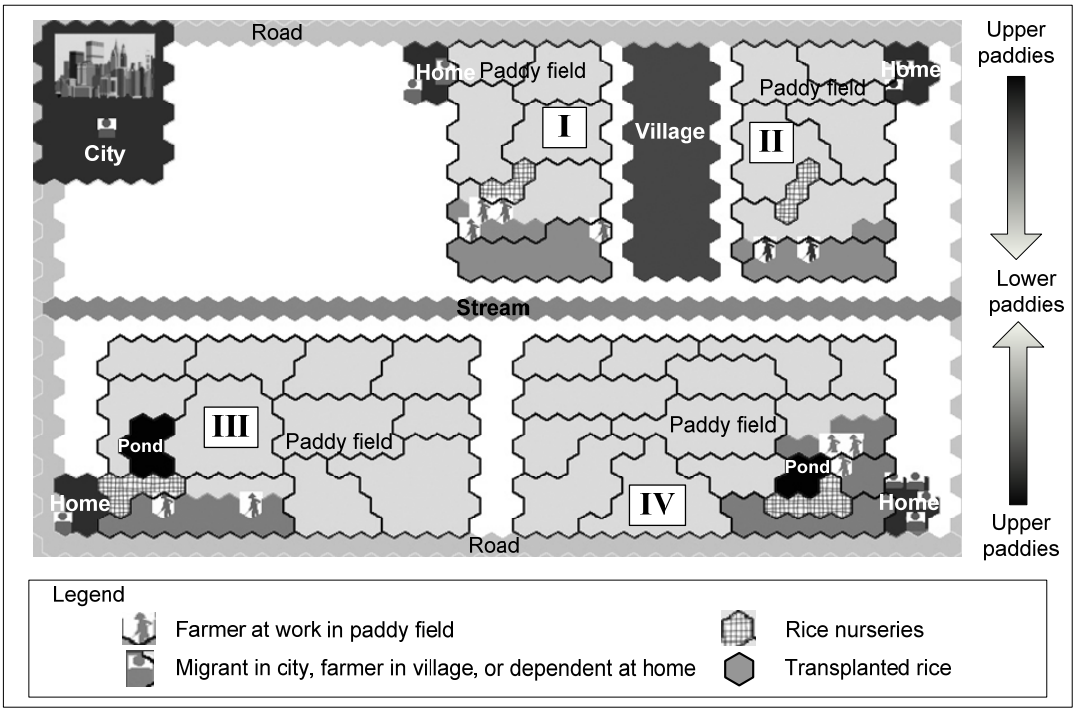

Figure 3. Spatial configuration of the BMM model representing two small farms (I and II) and two large farms (III and IV) during rice transplanting.

Water module

Water is entering the system via the input of daily rainfall data. A predefined set of daily precipitations over 10 years (duration of a simulation run) obtained from the Ubon Ratchathani regional meteorological center is used in the simulation runs. Two types of hydrological tanks are defined: a ponding tank for each paddy field, while a single water storage tank is associated to each farm pond. In addition to the direct input of rainfall in each tank, overflowing tanks are filling lower neighboring paddies through runoff. Finally, a constant (10 mm) quantity of water is deducted each day from each ponding tank to account for the overall functioning of the soil-plant system.

Rice module

This module provides information to Households about the RLR growth stage at any given time. Two, early and late maturing, photo-sensitive rice varieties are used in the BMM model as these two types of cultivars are combined on the local farms. They have different parameters affecting the decision to harvest: the early maturing rice variety is ready for harvest on November 10, while the late maturing one is ripe on November 21. Information from this module prompts Households to act accordingly. However, climatic conditions (dry spells early in the season, or rainy days during harvest affecting paddy quality) also determine whether such actions are possible or not.

Household module

This module integrates three aggregated social levels: individual, household, and village. Each individual household member is holding one out of three possible roles i.e. Farmer, Migrant, or Dependent depending on his/her activity at a given time (Figure 2). The location of an individual member on the spatial grid indicates his/her role (Figure 3): Migrants are in the city; Farming members are located in paddy fields (when growing RLR) or in the village (when waiting for employment on other farms). The four households represented were created with different size, assets and number of workers. Smallholdings I and II have six members with household I having three laborers and three dependents while household II has four laborers and two dependents. Larger farming units III and IV have two laborers and one dependent, and three laborers and four dependents respectively (Figure 3).

Sequence of farming activities throughout a crop year

The Household agent controls the activation of a sequence of farming activities, updated on a daily basis, as the result of the interactions between the availability of water and the successive RLR growth stages. The key successive farming activities are as follows: establishment of RLR nurseries and production of seedlings, transplanting, and harvesting. After RLR harvest, each household computes the results of the rice season and decisions about labor migration are individually considered by each member.

Nursery establishment and production of seedlings

Following the 2nd week of May and the Royal Plowing Ceremony in Bangkok, Households consider the possibility to establish rice nurseries. Without a pond or without sufficient water volume in the pond (less than 10% of pond capacity), the decision to establish a nursery relies only on rainfall (see corresponding threshold in table 1). Once the nursery is established, a water stress occurs if there are 12 successive days without rainfall higher than 10 mm/day. Under such circumstances, if the household has a pond with enough water, it is pumped to alleviate the water stress, otherwise the nursery is partly (1/3) destroyed and the household has to re-establish another one to produce this quantity of seedlings. At the age of 30 days, RLR seedlings are ready for transplanting.

Transplanting

All Households wait for a daily rainfall higher than 20 mm to start transplanting and all seasonal migrants return home at that time. Early-maturing rice is first transplanted in the upper paddies, then late-maturing rice starting from the lowest paddies. When a Household sees that it cannot complete transplanting with family labor by September 15 (after that date the duration of the RLR vegetative phase would be too short to achieve satisfactory yields), additional labor is hired. Farm ponds are not used for this activity implemented during a usually very wet period.

Harvesting

RLR varieties are photo-sensitive and are ripe one month after flowering. Therefore, all households start to harvest rice at the same time. Once harvesting has started, if the daily rainfall is over 30 mm (wet day threshold), this activity will be paused and resumed one day later. The labor availability is critical for the production of quality late-maturing rice variety for sale, as a fast harvest yields a higher paddy quality sold at a higher farm gate price (Table 1). Therefore, hiring labor is considered necessary for all farms to accelerate harvesting, so that it can be completed before December 1. When harvesting is under way, all farms have the same objective of getting high quality paddy but if it not possible (as December 1 already passed),

then to get fair quality paddy. If it is not possible (after December 10), there is no more reason to rush to finish harvesting RLR and therefore no labor is hired.

Relations between RLR production and decisions on labor migration

Once RLR production activities are completed, late-maturing rice sales, local off-farm incomes (wages received when transplanting and harvesting on other farms) and labor costs (wages paid to hired labor) are calculated for each household. Afterwards, the demographic characteristics of their members, which are important to determine potential migrants and migration patterns, are updated. Two kinds of migration are taken into account. Seasonal migrants always return home to help in RLR production at transplanting and harvest, while more-permanent migrants are removed from the list of family farm laborers. The criteria to become a potential migrant, and selection of migration patterns are based on the Value-Expectancy model (De Jong 1997) [10].

First, a member evaluates its migration intention (none, low, or high) based on its personal characteristics (age, gender, marital status, migration experience). The member also considers its Household's socioeconomic conditions (presence of dependents, financial situation after rice sales and wage earned as hired labor, subtracted by farm input and labor cost). After combining these two dimensions, the member finally makes his/her decision whether to migrate to the city in the dry season (seasonal migrant), to work in urban areas without returning home to help on the farm (more-permanent migrant), or stay at home.

COLLECTIVE DEFINITION AND EXPLORATION OF SIMULATED SCENARIOS

The spatial settings and characteristics of the four households and their members presented in the previous section were used to define a baseline scenario. We used it to calibrate the model and as a reference for comparisons with other scenarios. Two of them emerged from the discussions with participating farmers held in May 2008. The first one includes the availability of cheap foreign laborers from the Lao PDR and Cambodia during transplanting and harvest. The second proposed scenario assumed that enough water is accessible to all farms (for instance through an irrigation canal).

Cheap foreign labor scenario

The simulation of this scenario, based on the availability of 30 hired laborers from neighboring countries ready to work at low wages, showed a high income differentials across farm types compared to the baseline scenario. Incomes from rice sales of

Table 1.Default values, units and sources of key parameters for each module of the BMM model.

Module	*Parameter*	*Default value*	*Unit*	*Source & main tool used*
Water	Water quantity needed to supply a 0.04 ha RLR nursery	40	m^3	Field workshop based on RPG3
	Minimum depth of water level needed in farm ponds	10	%	Field workshop based on RPG1
	Daily volume of water (related to soil-plant system) deducted from a ponding tank	10	mm	ABM calibration
	Daily rainfall threshold to initiate RLR nursery establishment	30	mm	Field workshop based on RPG3
	Daily rainfall threshold to start transplanting	20	mm	
	Daily rainfall threshold to stop harvest for one day	10	mm	
Rice	Minimum daily rainfall of a wet day at nursery stage	10	mm	Field workshop based on ABM2
	Duration of dry spell for water stress to occur in RLR nurseries	12	day	Field workshop based on ABM1
	Maximum RLR paddy yield	2,250	kg/ha	Field workshop based on RPG1
	Minimum RLR paddy yield	938	kg/ha	
	Age of RLR seedlings ready for transplanting	30	day	
	Duration of transplanting after rice seedlings reach 30 days	21	day	Field workshop based on ABM2
	Last week to establish RLR nurseries	3rd week of July	week	Field workshop based on RPG1
	Last week for RLR transplanting	2nd week of September	week	
	Starting date of early maturing rice harvest	10th November	day	Bureau of Rice Research and Development, 1999
	Starting date of late maturing rice harvest	21st November	day	
	Maximum harvesting date to get high quality paddy	1st December	day	Field workshop based on ABM2
	Maximum harvesting date to get fair quality paddy	10th December	day	
	Farmgate price of high quality paddy	18	baht/kg	Thai Rice Mills Association, 2008
	Farmgate price of fair quality paddy	12	baht/kg	
	Farmgate price of low quality paddy	9	baht/kg	
Household	Beginning of RLR nursery establishment	2nd week of May	week	Field workshop based on RPG1
	Maximum age of migrant villagers	45	years	Field workshop based on ABM2
	Average annual net income per household	20,000	baht	NSO, 2007
	Average farm input cost excluding labour cost	3,750	baht/ha	OAE, 2005
	Volume of paddy for self-consumption	350	kg/person/year	Authors' farm survey in 2004
	Rate of daily wage at RLR transplanting	120	baht/person	Field workshop based on ABM2 in 2008
	Rate of daily wage at RLR harvest	150	baht/person	

smallholdings I and II were not significantly different, but they lost off-farm income usually received from household III and IV. In contrast, without any labor constraint, the large farming households III and IV earned higher incomes from selling high quality paddy thanks to faster harvests despite high labor costs.

However, the participating farmers argued that, actually, small farms may not lose their off-farm income as much as showed by the simulated results because these immigrant workers are less likely to be hired because they are not considered as meticulous rice farmers. Furthermore, local farmers seem to prefer to hire laborers within their kinship networks.

No water constraint scenario

The simulated results showed that the synchronization of rice farming activities (here all farms are able to start producing rice at the same time) was unlikely to change the situations of larger farm III and IV compared to the baseline scenario. Farm III and IV could not hire extra workers at the beginning of transplanting like they did in the baseline scenario. However, transplanting can be prolonged without critical damage to rice productivity. Therefore, farmer III and IV could complete transplanting by hiring extra workers from household I and II once these households finished this activity on their small holdings. In this scenario, a small virtual farm II could not complete transplanting of its entire farm when the heavy rains came late, and by then some rice seedlings were too old to be used. Compared to the baseline scenario, it shows little difference in terms of local off-farm income gained by small farms and labor cost paid by large farms.

However all participants said that the impossibility to transplant paddy fields was unlikely to happen in reality because rice farmers take adaptive measures like establishing more nurseries or buying rice seedlings from their neighbors. Nevertheless, this simulated outcome helped the participants to reflect on such a risk-taking decision in relation to water dynamics that may cause them to spend more cash on additional rice seedlings.

DISCUSSION

KIDS or KISS? Or both!

As expressed by the familiar motto "Keep It Simple and Stupid" (KISS), simpler models are widely considered as more useful than complex ones [9]. In the field of social simulation, in contrast to the KISS motto that praises ambitious abstract, high-level modeling, Edmonds and Moss (2004) [11] have proposed a new slogan -"Keep It Descriptive, Stupid" (KIDS)- to claim that the systematic reference to the law of parsimony should not prevent for more low-level, descriptive modeling. This provocative slogan seems to call for a radical positioning of modelers among those who would rather place a colon or a comma between "keep it descriptive" and "stupid".

However, we believe that both KISS and KIDS principles are worthwhile, especially when the aim of the modeling process is to foster co-learning among scientists and stakeholders. Before starting to directly interact with the local farmers, researchers engaged in the modeling process to synthesize the existing scientific knowledge. At this stage, any relevant information was integrated into the prototype model, according to the KIDS principle. For instance, an existing hydrological module that was previously developed to precisely simulate the availability of water in paddy fields and ponds in this Lam Dome Yai watershed[16] was integrated into the first version of the BMM model. During the collaborative modeling process, we realized that farmers were making decisions about rice-growing activities in relation to water availability by directly referring to daily rainfall conditions. Furthermore, we had difficulty to make transparent to participating farmers complicated hydrological processes such as infiltration, percolation, and diffusion. For these reasons, the sophisticated hydrological module was replaced by a simple parameter set to a constant value (10 mm) to account for daily water outflow from a paddy field in this RLR ecosystem.

Validation: a shared representation of the interactions between land & water use and labor migration

Validation relates to the extent to which the model adequately represents the system being modeled [6]. The canonic view of validation mainly considers the difference between simulated and observed data. The goodness of fit makes the model "right". However, the correlation between observed and simulated data might be induced by irrelevant mechanisms introduced in the model [1].In any case, the validity of a model should not be thought of as binary event (i.e. a model cannot simply be classified as valid or invalid). The adequacy of the representation provided by the BMM model refers to its acceptance by the local farmers who participated to its collaborative design as a fair and useful representation of the interactions between land & water use and labor migration in their village. According to the ComMod principles, this representation was built through the confrontation of the views of different types of stakeholders and the

views of the researchers in order to clearly express scenarios built to explore the opportunities and dangers of an uncertain future [20].

The BMM model has been recognized by the participating farmers to be sufficiently accurate to represent their current situation. As a result, they eventually proved to be comfortable and confident enough with it to present and comment the BMM model in front of master students and lecturers-researchers -who did not participate to the modeling process - at the Faculty of Agriculture, Ubon Rajathanee University, on October 18, 2008. The discussion that followed the demonstration showed that most of the students have different views and understandings and even concepts about RLR farming in northeast Thailand. This confirmed the fact that any model might be an accurate representation of some stakeholders' views, but at the same time, an inaccurate (though precise) one for other differing stakeholders' views [20]. Such collaborative modeling practice is valuable because of its efficiency in communicating and therefore sharing such diversity of viewpoints.

From singular representations of actual households to the abstract concept of a BMM household

The first ABM was introduced to the participating farmers in a workshop organized in April 2007. This ABM was initialized from the exact circumstances of the 11 households who participated in the process. During this workshop, we had difficulty to stimulate collective discussions to refine the model, and to get a collective agreement on the validation of this model. This was because all the participants attempted to correct the individual dissemblance that they found in the model compared to their actual situation.

To enhance such a collective discussion, we simplified the model to represent only 4 farms, with characteristics based on a previous farm survey and typology [23], as shown in the latest version of the BMM model described above. We organized 4 sub-workshops, with small groups of farmers belonging to the same farm type, to fine-tune this simplified model. Although this latest version is more abstract than the first one, it was accepted by all the participating farmers to sufficiently represent their system in the last workshop held in May 2008.

CONCLUSION

The BMM model is undoubtedly a site-specific model, far from a generic tool. The process of designing it was a long and costly one with only a local impact so far. This inescapably raises the question of the cost-benefit of the whole approach. In term of out-scaling, the current model can be considered as a communication tool to be reused in villages similar to BMM to stimulate knowledge sharing, leading to the enrichment of the underlying conceptual model. We believe that the computer model could be introduced straightforwardly to other farmers without being perceived as a "black box" if the presentation is made by the BMM farmers themselves: there is no reason why the communication of the model among farmers would be more problematic than the communication of the model from farmers to scientists.

Finally, from this experiment, we found that it is possible to use collaborative modeling with marginal rice farmers. We both researchers and participating farmers gained benefits through knowledge sharing by co-constructing the model.

ACKNOWLEDGEMENTS

The paper presents findings from PN 25 "Companion modelling for resilient water management", a project of the CGIAR Challenge Program on Water and Food, and Echel-Eau Project. The authors also thank the bilateral MAE-CHE Franco-Thai cooperation program in higher education and research for its financial support.

REFERENCES

1. Amblard, F., Bommel, P., and Rouchier, J., 2007. Assessment and validation of multi-agent models. In: Phan, D., and Amblard, F., Eds., Multi-Agent Modelling and Simulation in the Social and Human Sciences. Bardwell Press. Pp: 93–114.
2. Aumsamut, S., and Boonsomphonphan, B., 1999. Established soil series in the Northeast Thailand reclassified according to Soil Taxonomy 1998. Land Development Department, Ministry of Agriculture and Co-operatives, Bangkok. 154 p.
3. Boling, A. A., Tuong, T. P., Suganda, H., Konboon, Y., Harnpichitvitaya, D., Bouman, B. A. M., and Franco, D. T., 2008. The effect of toposequence position on soil properties, hydrology, and yield of rainfed lowland rice in Southeast Asia. Field Crops Research 106**,** 22-33.
4. Boonjung, H., 2000. Climatic variability and rice production in rainfed rice area in Northeast Thailand: risk analysis and management applications. Proceedings of the International Forum on Climate Prediction, Agriculture and Development, Palisades, New York, USA, 2000. Pp: 202-205.

5. Bousquet, F., and Trébuil, G., 2005. Introduction to companion modeling and multi-agent systems for integrated natural resource management in Asia. In: Bousquet, F., Trébuil, G., and Hardy, B., Eds., Companion Modeling and Multi-Agent Systems for Integrated Natural Resource Management in Asia. IRRI, Los Baños, the Philippines. Pp: 1-20.
6. Casti, J. L., 1997. Would-be worlds: how simulation is changing the frontiers of science. Jonh Wiley and Sons, Inc., New York. 242 p.
7. Chamratrithirong, A., Archavanitkul, K., Richter, K., Guest, P., Thangthai, V., Boonchalaksi, W., Piriyathamwong, N., and Vong-Ek, P., 1995. National migration survey of Thailand. Institute for Population and Social Research, Nakonpathom. 87 p.
8. Chantavanich, S., and Risser, G., 2000. Intra-regional migration in Southeast and East Asia: theoretical overview, trends of migratory flows, and implications for Thailand and Thai migrant workers. In: Chantavanich, S., Germershausen, A., and Beesey, A., Eds., Thai migrant workers in East and Southeast Asia 1996-1997. Asian Research Center for Migration (ARCM), Bangkok. Pp: 10 - 27.
9. Chwif, L., Barretto, M. R. P., and Paul, R. J., 2000. On simulation model complexity. Proceedings of the 2000 Winter Simulation Conference, IEEE, Piscateway, NJ, 2000. Pp: 449–455.
10. De Jong, G. F., 1997. Temporary and more permanent rural-urban migration in Thailand. Proceedings of Population Association of America Annual Meeting, Washington, D.C., 1997. Pp: 23-32.
11. Edmonds, B., and Moss, S., 2004. From KISS to KIDS: An 'anti-simplistic' modelling approach, MAMABS.
12. Ferber, J., 1999. Multi-agent systems: an introduction to distributed artificial intelligence. Addison-Wesley Longman, New York. 499 p.
13. Fuller, T. D., Lightfoot, P., and Kamnuansila, P., 1985. Rural-urban mobility in Thailand: a decision-making approach Demography 22**,** 565-579.
14. Gilbert, N., 2008. Agent-Based Models. In: Liao, T. F., Ed., Book Agent-Based Models. Sage Publications. 98 p.
15. Jintrawet, A., 1995. A decision support system for rapid assessment of lowland rice-based cropping alternatives in Thailand. Agricultural Systems 47**,** 245-258.
16. Lacombe, G., and Naivinit, W., 2005. Modeling a biophysical environment to better understand the decision-making rules for water the use in the rainfed lowland rice ecosystem. In: Trébuil, G., Bousquet, F., and Hardy, B., Eds., Companion Modeling and Multi-agent system for Integrated Natural Resource Management in Asia. IRRI, Los Banos, Philippines. Pp: 191-210.
17. Laine, T., and Busemeyer, J., 2004. Comparing agent-based learning models of land-use decision making. Indiana University, Bloomington, IN. 6 p.
18. Loibl, W., Giffinger, R., and Toetzer, T., 2002. Growth and densification processes in suburban landscapes - a spatial agent - simulation. 5th AGILE Conference on Geographic Information Science, Palma (Balearic Island, Spain). 11 p.
19. Matsumura, M., Isarabhakdi, P., and Pleumcharoen, S., 2003. Rural industrialization and return migration: a case study of female factory workers in Northeast Thailand. Journal of Population and Social Studies 10**,** 105-130.
20. Moss, S., 2008. Alternative aproaches to the empirical validation of agent-based models. Journal of Artificial Societies and Social Simulation (JASSS) 11**,** 5.
21. Naivinit, W., 2005. Companion modelling to understand interactions between land&water use and labour migration in lower northeast Thailand: context, methodology, and preliminary findings. Proceedings of the International Conference on Simulation and Modeling (SIMMOD) 2005, Nakornpathom, Thailand, 2005. Pp: 444-452.
22. Naivinit, W., Le Page, C., Thongnoi, M., Trébuil, G., and Sribombat, N., 2007. Use participatory modelling to validate and build Multi-Agent System model regarding rainfed lowland rice and labour management in lower northeast Thailand. Proceedings on CD-ROM of 2nd International Conference on Asian Simulation and Modeling (ASIMMOD) 2007, Sheraton Hotel, Chiang Mai, Thailand, 2007. Pp: 306-312.
23. Naivinit, W., Trébuil, G., Thongnoi, M., and Le Page, C., 2008. Collaborative Multi-Agent Modelling to improve Farmers' Adaptive Capacity to Manage Water and Migrations Dynamics in Northeast Thailand, Proceedings on CD-ROM of 13th IWRA World Water Congress 2008, Montpellier, France. 15 p.
24. O' Sullivan, D., 2008. Geographical information science: agent-based model. Progress in Human Geography 32**,** 541-550.
25. OAE, 2005. Agricultural statistics of Thailand, crop year 2004/2005. Office of Agricultural Economics (OAE), Ministry of Agriculture and Co-operatives, Bangkok. 151 p.

26. Paris, T., 2003. Labor out-migration, rice farming and gender roles: synthesis of important findings in major rice production environments in Southeast and South Asia. International Rice Research Institute. 21 p.
27. Rattanawarang, W., and Punpuing, S., 2003. Migration and land size change: a case study in Nang Rong, Buriram, Thailand. Journal of Population and Social Studies 11**,** 95-119.
28. Santiphop, T., 2000. The relevant population dynamics to land degradation in the northeast region. Journal of Population and Social Studies 8**,** 67-89.
29. Somrith, B., 1997. Cultivar improvement for rainfed lowland rice in Thailand. Proceedings of Breeding strategies for rainfed lowland rice in drought-prone environments, ACIAR Proceedings 77, Ubon Ratchathani, Thailand, 1997. Pp: 36-42.
30. Valbuena, D., Verburg, H. P., and Bregt, K. A., 2008. A method to define a typology for agent-based analysis in regional land-use research. Agriculture, Ecosystems and Environment 128**,** 27-36.

Sand Dune Simulation of Nonuniform Sediment

Wandee THAISIAM and Yasuyuki SHIMIZU
Graduate School of Engineering, Hokkaido University
North 13, West 8, Kita-ku, Sapporo 060-8628, Japan

Abstract: In general, bed material in the natural rivers is composed with a variety of sediment sizes. Thus, their morphodynamics are affected by nonuniform sediment transport conditions. In this study, we propose a numerical model for the sand dune migration simulations and grain sorting simulations inside the sand dunes. In our numerical codes, the sediment transport model explicitly takes the turbulence flow model into account during the morphodynamic computation. The sediment transport model is composed of a nonuniform sediment transport model and a bed layer model. The concept of size fraction transport is employed for nonuniform sediment transport calculation. Moreover, non-equilibrium bed load sediment transport of each size fraction is treated using Eulerian stochastic formula for the sediment exchange process. The bed layer model is used for grain sorting simulation inside the bed forms. The results of the simulations are compared with the experimental results of nonuniform sediment. The comparison shows a good agreement in the grain sorting evolution inside the sand dunes. The computed results show that the pattern of grain sorting inside the bed forms is down coarsening from the crest of sand dune through the trough of sand dune. However, the discrepancy of the waveheight between the simulations and the experiments are within ± 25%.

Key words: Non-unifom sediment transport, numerical simulation, grain sorting

INTRODUCTION

Bed material in natural rivers is generally a non-uniform material. Thus, their morphodynamics are affected by the non-uniform sediment transport conditions. Over the past few decades, the sediment transport model has been introduced into the field of river engineering. A variety approaches have been developed in order to clarify the morphologic features in alluvial channels. Most of the presented models, the bed material was specified by single grain size (uniform sediment). However, many research found that considering only one grain size cannot explain some important mechanisms of river morphology sufficiently such as the geometry of bed forms and their evolutions.

In the fields of river morphologic study, non-uniform sediment transport models are important tool to analyze and predict the flow features and morphologic process in the natural river. Various researches of non-uniform sediment transport model were conducted to study the mechanisms of sand dune migration process. The features and mechanisms of sand dunes were also approached by laboratory studies[1,2,3]. For instance, Miwa and Daido[1] performed the experiment of dunes and compared the migration process and sand dune geometries between uniform and non-uniform sediment cases. They also investigated grain sorting at various locations of sand dunes in the experiments of non-uniform sediment. Their experimental results showed that grain sorting on the upstream part of sand dune crests causes the sediment coarsening on the lee side and, finally, affects wave height. As a result, with the same mean diameter and hydraulic conditions, wave height of the non-uniform sediment case was found to be smaller than that of the uniform sediment case, but the migration speed of the non-uniform sediment case is faster. Blom et al.[3] indicated that three mechanisms contribute the formation of a coarse layer underneath migrating dune: (1) the avalanching process at the lee face (2) partial transport in which a relatively large amount of coarse material does not participate in the transport process and (3) the winnowing of fines from the trough surface and subsurface. All mentioned studies show that the non-uniform sediment has a complicated process and also affects sand dune morphology significantly.

The morphodynamic numerical models have been extensively developed in this decade for simulating hydrodynamic and morphodynamic under the uniform bed material condition. For example, Shimizu et al.[4] performed a three-dimensional direct numerical simulation. The model provided a complete approach for flow computation and turbulence over the bed forms. Although the model carried out a good agreement in turbulence flow simulation, the sediment transport model for morphodynamic simulation was impractical. Thus, Giri and Shimizu[5] proposed a vertical two-dimensional morphodynamic model with non-hydrostatic and free surface flow for the uniform bed material. The proposed model was simplified from a three-dimensional direct numerical simulation[4]. In the study, an enhance k-ε turbulence closure with non-

Corresponding Author: Wandee THAISIAM, Graduate School of Engineering, Hokkaido University, North 13, West 8 Kita-ku, Sapporo 060-8628, Japan

linear term was incorporated to the hydrodynamic model, including the morphologic condition. They found that the hydrodynamic model with a nonlinear k-ε turbulence closure adequately reproduced flow and vorticity field in the separation region. The model succeeded simulating some features of the bed form evolution, such as amalgamation and asymmetric geometry. The simulation results complied well with the experimental results.

Recently, numerical models of the non-uniform bed materials have been introduced in various applications of river engineering[6,7,8]. Ashida et al. [7] performed a two-layer flow model simulating the bed deformation and the non-uniform sediment phenomena in meandering channels with flood plain flows. In their model, a boundary-fitted orthogonal coordinate system was employed in order to avoid the complexities and the substantial computing time and storage, and also increase the accuracy of the computed solutions. The model was constructed to deal with mixed sediment for evaluating the influences of sediment sorting on bed deformation. The model had the ability of simulating the bed deformation and sediment sorting phenomenon in meandering channels with flood plain flow. Consequently, a reliable and more complete numerical model for microscale bed form simulation of non-uniform sediment is still important for advancing our understanding of morphologic features and grain sorting inside the bed forms.

This study is the extension work from the vertical two-dimensional flow model[5] with the goal to develop a morphodynamic numerical model for the non-uniform bed materials. The model performance is significantly improved using the bed layer model[7] for grain sorting simulation. The total bed material transport is summarized from each sediment size fraction. The sediment exchange process of each size fraction, namely pickup and deposition, is calculated by using an Eulerian stochastic formulation which proposed by Nakagawa and Tsujimoto[9]. In this study, the model is proposed for low flow regime focusing the sand dune simulation.

SEDIMENT TRANSPORT MODEL

The non-uniform sediment transport model is employed for sediment transport calculation which includes sediment pickup rate, sediment deposition rates, and bed deformation. The bed layer model is applied for grain sorting simulation. The total bed material transport can be modeled by two different approaches, either dividing the model into bed load and suspended load transport, or considering only the bed load transport. Presently, our sediment transport computation considers only the bed load transport.

(1) Non-uniform Sediment Transport Model

The sediment transport of non-uniform bed materials normally depends on a potential size fraction transport and is influenced by complicated flow features. The concept of size fraction transport is to divide bed material into size fractions which consider each size fraction as a uniform material. The sediment transport rate is determined by the summation of the potential transport rate of each size fraction which is in turn related to its concentration existing in the bed material. The bed material transport rate can be calculated by multiplying the potential transport rate corresponding to a given size fraction with the percentage of material which can be read as follows:

$$q_b = \sum_{k=1}^{nk} q_{bk} = \sum_{k=1}^{nk} P_k . q_k \qquad (1)$$

where q_b is the bed load transport rate per unit width, q_{bk} is the bed load transport of sediment size fraction k per unit width, P_k is the concentration of sediment fraction size k, q_k is the potential transport rate for a given size fraction k, subscripts k and nk are the number and the total number of size fraction, respectively.

An Eulerian stochastic formulation of sediment transport, proposed by Nakagawa and Tsujimoto[9], is used in our model for the bed load transport calculation in which can be expressed in term of the dimensionless pickup rate of sediment size fraction k as:

$$p_{sk} = \frac{0.03\tau_k^* \left(1 - 0.7\tau_{ck}^* / \tau_k^*\right)^3}{\sqrt{d_k / (\rho_s / \rho - 1)g}} \qquad (2)$$

where p_{sk} is the pickup rate of sediment size fraction k, ρ and ρ_s are fluid and sediment density respectively, τ_k* is dimensionless local bed shear stress of sediment fraction size k, and τ_{ck}* is dimensionless critical bed shear stress of sediment fraction size k.
The sediment deposition rate is expressed as:

$$p_{dk} = \int p_{sk} f_s(s) \qquad (3)$$

where p_{dk} is the deposition rate of sediment fraction size k and $f_s(s)$ is the distribution function of step length.

The exponential distribution function of step length by Nakagawa and Tsujimoto[9] is written as:

$$f_s(s) = \frac{1}{\Lambda} \exp\left(-\frac{s}{\Lambda}\right) \qquad (4)$$

where Λ is the mean step length and s is the distance of sediment motion from the pickup point. On the basis of

probability theory, Einstein[10] proposed $\Lambda = \alpha d$, in which α is an empirical constant proposed to be 100.

Then, the bed deformation is computed by using the sediment continuity equation which is

$$\frac{\partial z_b}{\partial t} + \frac{1}{1-\lambda} \cdot \frac{\partial}{\partial x}\left(\sum_{k=1}^{nk} q_{bk} \right) = 0 \qquad (5)$$

where z_b is the bed elevation and λ is porosity of bed material.

(2) The Bed Layer Model

The bed layer model proposed by Ashida et al. [7] is employed for the grain sorting simulation of non-uniform sediment in our numerical model. In the bed layer model, bed material is divided into sublayers as shown in Figure 1.

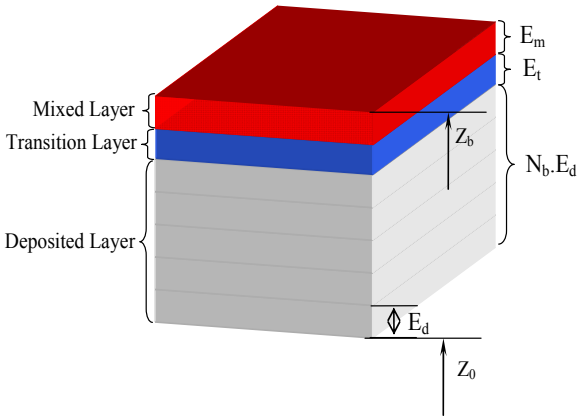

Fig.1 The bed layer model

The mixed layer represents the exchange layer or top layer containing the bed materials which is active to the transport process. The mixed layer thickness is assumed to be constant and equivalent to the size d_{90} of initial bed material distribution. The transition layer acts as a buffer layer between the mixed layer and the deposited layer. The thickness of transition layer is a function of time and streamwise direction and is restricted between $0 < E_t \leq E_d$. The deposited layer is divided into N_b layers in which thickness of sublayers is equal to E_d. Therefore, thickness of the deposition layer is equal to the multiplication of N_b and Ed.

The initial non-uniform bed material in Figure 1, the bed elevation is calculated by

$$z_b = E_m + E_t + N_b.E_d + z_0 \qquad (6)$$

where z_b is the bed elevation, E_m is thickness of mixed layer, E_t is thickness of transition layer, N_b is total number of sub-layers in the deposited layer, E_d is thickness of multiple layers, and z_0 is the datum elevation.

In our calculation codes, the non-uniform sediment transport model is employed to calculate sediment pickup rate, sediment deposition rate and bed deformation in each calculated cell. Then, the concentration of sediment size fractions can be calculated from the bed layer model.

HYDRODYNAMIC MODEL

Giri and Shimizu[5] proposed a vertical two-dimensional flow model for simulating morphodynamic process for free surface flows over bed forms under uniform sediment conditions. The model was coupled with a hydrodynamic and a mophodynamic models which are two-dimensional in streamwise and vertical directions. The flow model can perform accurately simulations both of mean flow and turbulence structures influenced by bed forms under free surface flow. In present study, the hydrodynamic model proposed by Giri and Shimizu[5] is employed for the hydrodynamic simulation. The brief description of the model can be shown as following:

The governing equations for unsteady vertical two-dimensional flow can be written in Cartesian coordinate system as follows:

Continuity equation

$$\frac{\partial u}{\partial t} + \frac{\partial v}{\partial t} = 0 \qquad (7)$$

where x and y are coordinates in horizontal and vertical direction respectively; u and v are components of velocity in horizontal and vertical direction, respectively.

Momentum equations

$$\frac{\partial u}{\partial t} + u\frac{\partial u}{\partial x} + v\frac{\partial u}{\partial y} = -\frac{1}{\rho}\frac{\partial p}{\partial x} + \frac{\partial}{\partial x}\left(-\overline{u'u'}\right) + \frac{\partial}{\partial y}\left(-\overline{u'v'}\right) \qquad (8)$$

$$\frac{\partial v}{\partial t} + u\frac{\partial v}{\partial x} + v\frac{\partial v}{\partial y} = -\frac{1}{\rho}\frac{\partial p}{\partial y} + \frac{\partial}{\partial x}\left(-\overline{u'v'}\right) + \frac{\partial}{\partial y}\left(-\overline{v'v'}\right) - g \qquad (9)$$

where $\overline{u'u'}$, $\overline{u'v'}$ and $\overline{v'v'}$ are Reynolds stress tensors, ρ is fluid density, g is gravitational acceleration and p is pressure.

Table 1 Experimental cases and conditions
(H-1 and H-2 denote the study by Hagiwara, M-1 and M-2 denote the study by Miwa and Daido[1])

Run no.	q_w (cm^2/s)	Sediment mean diameter (cm)	Standard deviation	I_e ($x10^{-3}$)	u_* (cm/s)	L (cm)	Δ (cm)
H-1	300	0.040	2.74	3.00	4.21	23.20	1.20
H-2	800	0.065	2.12	4.00	6.66	78.13	1.25
M-1	350	0.070	1.70	350	3.31	30.70	0.67
M-2	400	0.070	1.70	400	3.69	54.00	1.16

The governing equations for unsteady two-dimension flow in the Cartesian coordinate system (x,y,t) is transformed to the moving boundary fitted coordinate system (ξ, η, τ) [11]. The transformed equations are solved by splitting into non-advection and pure advection terms. The non-advection terms are solved by using central difference method. The pure advection term is calculated by using a high-order Godunov scheme known as the cubic interpolated pseudoparticle (CIP) technique. The pressure term is resolved using SOR method considering dynamic pressure.

In the turbulence model, a 2nd order non-linear k-ε turbulence closure is employed to reproduce turbulence characteristics in shear flow with separation zone. Kimura and Hosoda[12] carried out a detailed analysis and comparison of the 2nd order non-linear k-ε model with other turbulence closures. They found that the 2nd order non-linear k-ε model is more efficient than RSM or LES model in terms of CPU time. Giri and Shimizu[5] found that the 2nd order non-linear k-ε turbulence closure is adequate to reproduce flow and vorticity field in the separation region in the case of fixed dunes, while linear k-ε model was found to be over dissipative. On the other hand, the zero-equation turbulence model showed poor results for both flow and morphodynamic simulation. Comparing among all approaches, the 2nd order non-linear k-ε turbulence closure is satisfactorily predicts mean flow and turbulence properties over the bed forms.

The time-dependent water surface change computation is used for realistic reproduction of free surface flow over migrating bed forms. Along with the flux continuity, the kinematic condition was imposed along the free surface to compute the temporal changes in water surface elevation.

The boundary condition at the bed is no slip and a logarithmic expression for near-bed region is adopted.

$$\frac{u_p}{u_*} = \frac{1}{\kappa} \ln \frac{y_p}{y_0} \qquad (10)$$

where up is velocity at near-bed grid point, u_* is local bed shear velocity, κ is Karman constant, $y_0 = k_s/30$, $k_s = 2.5d$, in which k_s is roughness height and d is bed particle diameter. In our calculated codes, d is equivalent to mean diameter (d_{50}) of bed material. The periodic boundary conditions are employed in the computational domain, in which output at the downstream end is set to be input at the upstream end.

EXPERIMENT

Laboratory investigations of sand dune migration process were conducted in the hydraulic research laboratory at Hokkaido University. Experiments were carried out in a straight rectangular open channel, 10.0 m long, 0.2 m wide, and 0.3 m deep. The middle part of the flume (7.5 m) was covered with a 5 cm thick non-uniform sediment layer. The bed material was mixed from three types of uniform sediment. Samples 1 and 2 were graded sediments with the mean diameter of 0.040 and 0.065 cm and the geometric standard deviations (σ) are 2.74 and 2.12, respectively. Sample 1 and 2 were used in the experiment H-1 and H-2 respectively. The specific gravity of both sediment samples is 2.65. Sand dune geometries were measured after the bed forms reached to equilibrium stage over the course of the evolution process by referring to the experimental pictures. Dune length and dune height were measured by the trough to trough method. In addition, two experiments, M-1 and M-2, performed by Miwa and Daido[1] were also used to verify our numerical model. Hydraulic conditions of all experiments are given in Table 1 in which parameters were measured after the bed forms reached to an equilibrium stage. In the table, q_w is water discharge per unit width, I_e is the energy slope, u_* is the mean shear velocity, L and Δ are wave length and wave height of sand dunes, respectively.

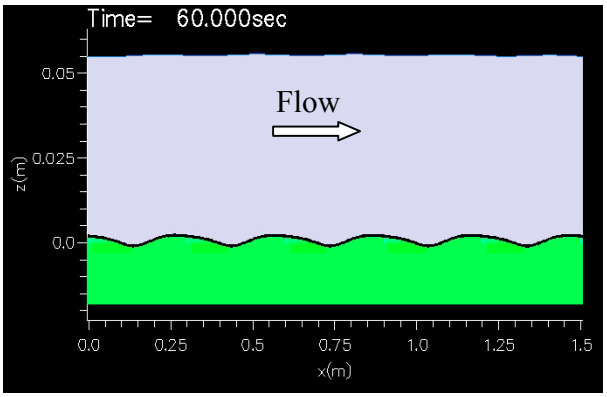

(a) sand dune evolution after 60 seconds

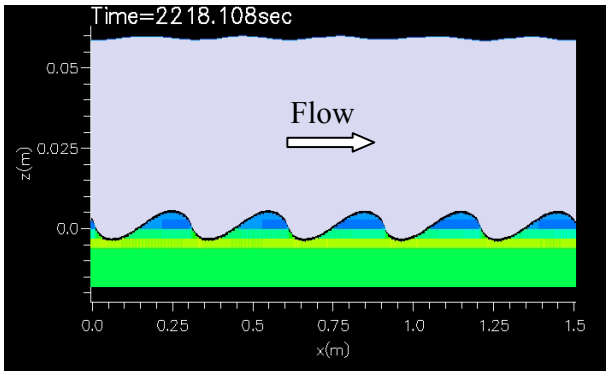

(b) sand dune migration with grain sorting inside sand dunes after the bed forms reached to equilibrium stage.

MODEL VERIFICATION

In present study, only the numerical model for the non-uniform sediment is needed to be verified. The non-uniform sediment transport model has been verified with several experimental cases. The experimental results are used to evaluate the model prediction ability on grain sorting evolution inside the sand dunes and sand dune geometric simulations. Quantitative comparisons are made after the analogous time increment. The comparisons are made in various features of grain sorting process inside the sand dunes, for instant, grain sorting inside the sand dunes in various locations, wave height of sand dune.

We noted that the simulations of experiment H-1 and H-2 denote Run H-1 and Run H-2, respectively while the simulations of experiment M-1 and M-2 denote Run M-1 and Run M-2, respectively. Some pictures from simulation Run M-1 are shown in Figure 2. In our calculations, the simulation was performed for an almost flat bedded initial condition with a very small random field perturbation as shown in Figure 2(a). Figure 2(b) shows the equilibrium bed forms which reached to steady stage within 1800 seconds.

Conditions of all experimental cases are used in numerical calculations of bed form growth and geometry. The computed results of wave height of sand dunes were compared with the observed data after analogous time increment. The comparison results of wave height are depicted in Figure 3. The comparison results in wave height of sand dunes provided by the present model shows good agreement with the discrepancy within ±25% for most observed cases. The wave height appears to be underestimated for Run H-1 and Run H-2 and overestimated in Run M-2 by the present model.

In present study, the mechanisms of grain sorting inside the sand waves are also investigated through the numerical simulations. From the calculated results, we plot the grain size distribution of sediment in the crest down to the trough of sand dunes for all experimental cases. The grain size distributions of four simulations show that pattern of grain sorting is down coarsening from the crest down to the through of sand dunes. The simulation result of experiment M-1 is depicted in Figure 4 which shows the finest grain size distribution on the crest and becomes coarser in the downward direction. As the results, the coarser grains are deposited in the trough of sand dunes. The calculated results found to be the same trend as the experiment results.

CONCLUSION

The proposed numerical model for non-uniform sediment satisfactorily predicts grain sorting at various locations of sand dunes and wave heights of sand dunes. The simulation results found to be good agreement in the wave height of sand dunes between the experiment and the simulation with the discrepancy within ±25%. The grain sorting simulations inside the sand dunes also show the same results as the experiment.

REFERENCES

1. Miwa, H. and A. Daido, 1992. Sand wave development with sediment sorting. J. Hydrosc. Hydr. Eng., Vol.10 (2), pp.39-50.
2. Kleinhans, M. G., 2004. Sorting in grain flows at the lee side of dunes, Earth Sci. Rev., 65, pp. 75–102.
3. Blom, A., J. S. Ribberink and H. J. de Vriend, 2003. Vertical sorting in bed forms: Flume experiments with a natural and a trimodal sediment mixture, Water Resour. Res., 39(2), 1025, doi:10.1029/2001 WR001088.
4. Shimizu, Y., M. W. Schmeeckle, and J. M. Nelson, 2001. Direct numerical simulation of turbulence over two-dimensional dunes using CIP methods, J. Hydrosci. Hydraul. Eng., 19(2), 85– 92.

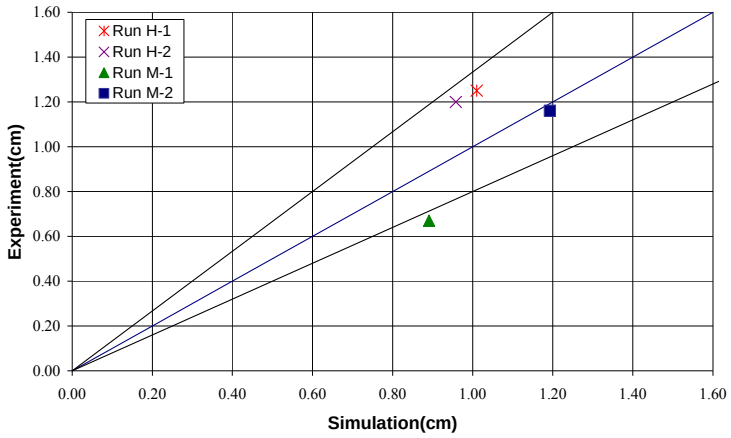

Figure 3 The comparison between the experimental results and simulated results of the wave height of sand dunes.

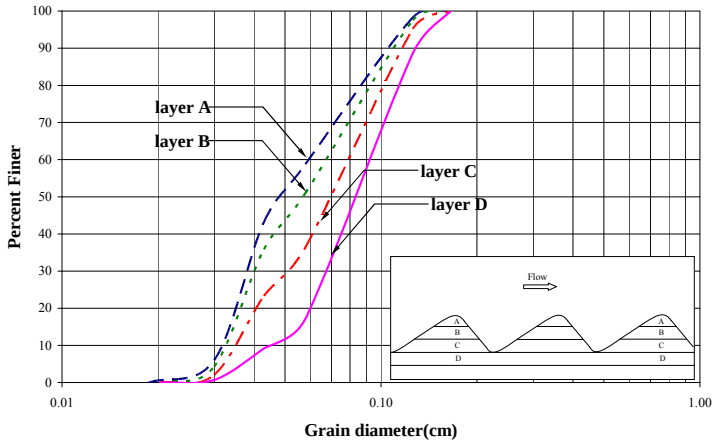

Figure 4 Grain size distributions at various locations inside sand dunes (Run M-1) where the locations of measured mixture are shown as a small figure.

5. Giri, S., and Y. Shimizu, 2006. Numerical computation of sand dune migration with free surface flow, Water Resour. Res., 42, W10422, doi:10.1029/2005WR004588.
6. Takebayashi, H. and S. Egashira, 2007. Spatiotemporal change characteristics of alternate bar geometry on bed with non-uniform sediment, Ann. J. Hydrau. Engrg, JSCE, Vol.51, pp. 1033–1038.
7. Ashida, K., S. Egashira and B. Lui, 1992. Numerical calculation of flow and bed evolution in compound channels by a two-layer flow model, Ann. Disas. Prev. Res. Inst., Kyoto University, No. 35 B-2, pp. 41-62.
8. Wu, W.: Depth-averaged two-dimensional numerical modeling of unsteady flow and nonuniform sediment transport in open channels, J. Hydraul. Eng., Vol. 130(10), pp. 1013–1024, 2004.
9. Nakagawa, H., and T. Tsujimoto, 1980. Sand bed instability due to bedload motion, J. Hydraul. Div. Am. Soc. Civ. Eng., 106(12), pp. 2029–2051.
10. Einstein, H. A., 1942. Formulas for the transport of bed load, Trans. Am. Soc. Civ. Eng., 107, pp. 561-597.
11. Itakura, T., Y. Yamaguchi, Y. Shimizu, T. Kishi and M. Kuroki, 1986. Observation of bed topography during the 1981-flood in the Ishikari River, J. Hydrosci. Hydraul. Eng., 4(2), pp. 11 – 19.
12. Kimura, I., and T. Hosoda, 2003. A nonlinear k-e model with realizability for prediction of flows around bluff bodies, Int. J. Numer. Methods Fluids, 42, 813–837.

Simulation of Turbulent Cavitating Flows around a Hydrofoil

[1]Thaithacha Sudsuansee, [1]Udomkiat Nonthakaew and [2]Yodchai tiaple
[1]Department of Mechanical Engineering
King Mongkuth University of Technology North Bangkok
1518 Pibulsongkram Road, Bangsue, Bangkok Thailand 10800
[2]Naval architecture and Marine Engineering
International Maritime College, Kasetsart University, Si Racha Campus
199 Moo 6, Sukhumvit Road,Sriracha, Chonburi Thailand 20230

Abstract: Cavitating flows are complex because of they are highly turbulent and unsteady flows involving two species (liquid/vapor) with a large density difference.The effect of cavitating flows is also decrease an overall efficiency of turbomachinery. These features pose an importance and a challenge to numerical modeling works. This paper presents CFD simulations of the cavitating flow around the symmetrical 2D hydrofoil. The numerical model used an implicit finite volume scheme (based on the SIMPLE algorithm) to solve Reynolds-averaged Navier-Stokes equations, associated with a mixture model approach of the cavitating flow. the liquid/vapour mixture is treated as a homogeneous fluid. Results presented in the paper focus on cavitation inception, the cavitation length and the general behaviour of the sheet cavitation, lift coeficient around the foil. A numerical estimation of the void fraction evolution inside the cavity is also presented.

Key words: turbulent , cavitating flows , finite volume

INTRODUCTION

In the design and use of hydraulic turbomachines cavitation and the effects related to cavitation are playing an important role. Of special interest are the mechanisms of cavitation yielding to noise generation, loss of efficiency and erosive damage of the exposed surfaces. To avoid or to reduce the effects of cavitation by design and operation, there is a persistent need of improving the detailed understanding of the physical phenomena and their modelization for numerical calculations.

Numerical modeling of cavitation has, until recently, only been possible using cutting edge inhouse CFD codes. Special challenges occur since cavitating flows are highly dynamic in nature. Also,such flows are Characterized by large gradients in the density feild, which is known to cause numerical instabilities. With the release of the CFD solver Fluent6, a cavitation model is available with a general-purpose Commercial software package. Fluent6 is a finite volume based solver that fully supports unstructured Multiblock meshes. The cavitation model shipped with Fluent6 is essentially based on the paper by Kubota Et al. (1992). This paper is meant as a reference for validation of the cavitation model in Fluent6. The Software will, in later studies,be used to enhance the understanding of the cavitation phenomenon.

CAVITATION MODEL

The cavitation model employed in the present study is based on the so-called “full cavitation model” by Singhal et al. The flow solution procedure is the SIMPLE routine presented by Patankar & Spalding (1972). This solution method is designed for incompressible flows, thus being implicit. The full Navier Stokes equations are solved. The cavitation model itself is highly physical utilizing the Rayleigh-Plesset equation to calculate bubble growth and collapse, while a vapor transport equation is implemented to track the resulting vapor mass fraction field. The transport equation is based on equation 1, and will when solved along with the flow equations, give the vapor mass fraction at any solution point in the computational domain.

$$\frac{\partial}{\partial t}(\rho f)+\nabla\left(\rho \vec{v}_v f\right)=\nabla(\gamma\nabla f)+R_e-R_c \qquad \textbf{(1)}$$

Here ρ is the mixture density and $\vec{v}_v$ is the velocity vector of vapor phase, γ is the effective exchange coefficient, R_e and R_c are the vapor generation and condensation rate terms (or phase change rates). The rate expression are derived from the Rayleigh-Plesset equations, and limiting bubble size considerations (interface surface area per unit volume of vapor). These

Corresponding Author: Thaithacha Sudsuansee, Department of Mechanical Engineering, King Mongkuth University of Technology North Bangkok, 1518 Pibulsongkram Road, Bangsue, 10800 Bangkok, Thailand Tel: +669-1248701, E-mail: ttc_sss@hotmail.com

rates are functions of instantaneous, local static pressure and are given by

When $p < p_{sat}$

$$R_e = C_e \frac{V_{ch}}{\gamma} \rho_l \rho_v \sqrt{\frac{2(P_{sat} - P)}{3\rho_l}} (1 - f) \quad (2)$$

when $p > p_{sat}$

$$R_c = C_c \frac{V_{ch}}{\gamma} \rho_l \rho_v \sqrt{\frac{2(P - P_{sat})}{3\rho_l}} f \quad (3)$$

where the suffixes l and v denote the liquid and vapor phases, V_{ch} is a characteristic velocity, which is approximated by the local turbulence intensity, (i.e. $V_{ch} = \sqrt{k}$), σ is the surface tension coefficient of the liquid, P_{sat} is the liquid saturation vapor pressure at the given temperature, and C_e and C_c are empirical constants. The default values are C_e = 0.02 and C_c = 0.01

The cavitation model suffers from several simplifications, where the most critical is probably that both phases has to be treated as incompressible. Similar calculations by Song et al. (1997) indicates that the compressibility of the vapor phase is important.

Computational Setup

The 2D geometry was made to resemble the test section of the high speed water tunnel at the Saint Anthony Falls laboratory in Minneapolis, MN (SAFL)[1]. The chord length of the NACA 0015 foil is 100 mm and the domain stretches 2.5 chord lengths upstream and 5 chord lengths downstream measured from the trailing edge. Simulations for 8 and 6 degrees angle of attack are presented. In the direction from the upper and lower foil surface, the computational domain stretches one chord length in both directions. The lengths are chosen from the test section in the water tunnel and the purpose of the calculations is to reproduce experiments. Test calculations show that the blockage effect is negligible for the SAFL tunnel set-up.

Figure 1(a) shows a closeup of the 2D grid at 8 degrees angle of attack. The grid is a C-grid type with a total of about 30000 cells. The smallest cell size in the direction from the wall is 0.01 mm, which corresponds to approximately $1/100 \cdot \mathrm{Re}^{-1/2}$. This results in the first grid point being at $y^+ < 5$ on both surfaces.

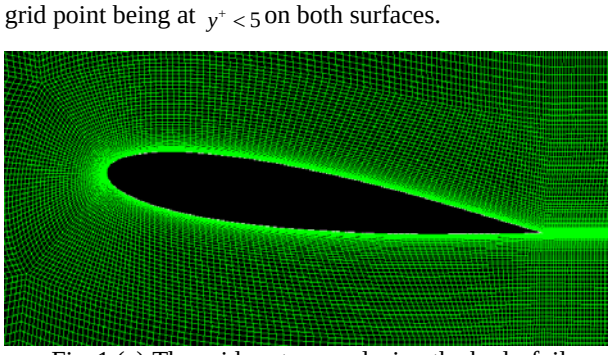

Fig. 1 (a):The grid system enclosing the hydrofoil

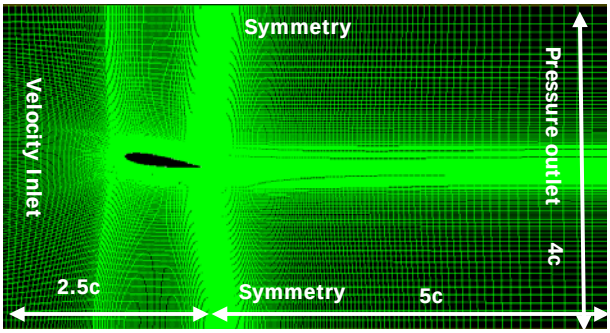

Fig. 1 (b): Computational flow configuration

Boundary Conditions

Figure 1(b) shows the total 2D computational domain with lengths and boundary conditions showing. The inlet bondary condition is specified velocity, using a constant velocity profile. Upper and lower boundaries are slip walls, i.e a symmetry condition. The outlet used is a constant pressure boundary condition. The foil itself is no-slip wall. The inlet is set to 10 m/s which corresponds to a Reynolds number equal to 1.2×10^6 based on chord length. This is in the same range as the experimental data. The computational domain stretches 2.5 chord lengths upstream and 5 chord lengths downstream.

Numerical method

The solving strategy used is the unsteady SIMPLE algorithm, Patankar & Spalding (1972). The convective flow terms are discretisized using second order upwind schemes. This is also used for the Mixture of Fluid equation and the Rayleigh-Plesset equation. The pressure is discretisized using a second order central scheme. The implicit time formulation used is also of second order accuracy. Internally, all numbers are stored and calculated with double precision. The time step used was 0.0005s. This gives 20-30 time steps per cycle. The cavitation model itself was configured with a noncondensable gas mass fraction is 1.5×10^5. It is believed that increasing a noncondensable gass mass fraction in the numerical model will increase the dynamics of the system, thus adding instability, however this was not a problem in the study. The water vapor pressure P_v ,was set to 3540 Pa. The cavitation number was adjusted by changing the reference pressure, P_{ref}, in the solver. The same effect can also be achieved by having a constant reference pressure and adjusting the vapor pressure.

Turbulence model

Once the Reynolds averaging approach for turbulence modeling is applied.The $k-\omega$ turbulence model, which is based on the Boussinesq hypothesis and incorporates transport equations for turbulent kinetic energy, k,and specific dissipation rate, ω, was used for the mixture. The specific dissipation rate can be thought of as the ratio of the turbulent kinetic energy dissipation rate to k. The turbulent viscosity μ_t is computed by combining k and ω as $\mu_t = \rho_m (k/\omega)$. The wall boundary conditions for the $k-\omega$ model are treated in such a way that when the wall-adjacent cells are located in the log-law region, the wall function approach, based on the law of the wall, is applied. When the wall-adjacent cells are closer to the solid surface and inside the sublayer region, and alternative approach that ensures the no-slip condition on the solid surface is applied. For cells in the buffer region, the above two are blended. The $k-\omega$ model is one of the most widely used turbulence models for external aero and hydrodynamics as well as for the complex flow field on both the sublayer level and wall function grids.

Simulation Results

An important parameter in cavitating flows is the cavity length. Experimentally, this is determined by analysis of high speed movies. The cavity length will generally vary a lot during a cycle, thus an maximum value is plotted. The same technique is used in the numerical approach, where a combination of velocity vector plots, and contours of constant vapor fraction plots are analyzed. An example of an instantaneous contour plot and velocity vector plot at the same instant in time is shown in figure 2. Here we can see that the cavity length is not easily identified from the contour plot alone, while the velocity vector plot clearly shows the reentrant jet and the closure of the attached cavity. The cavity length for a flat plate at an angle of attack, α, was shown to scale with the composite parameter, $\sigma/2\alpha$ by Acosta (1955). Arndt (1981) suggested the use of this parameter for thin hydrofoils. The cavity length, l, is normalized with respect to chord length, c, and plotted versus the parameter $\sigma/2\alpha$. In Figure 3, the numerical results are plotted with the corresponding experimental results. As we can see, the code can predict the cavity length with high accuracy. The reentrant jet will transport liquid phase into the cavitation regime at the end of the cavity. Visually, this will result in a closure of the cavity in a phase contour plot. It is also worth mentioning that the cavity length alone does not describe the flow. This can be seen clearly from the contour of constant void fraction plots shown in Figure 4. Both pictures are from $\sigma/2\alpha = 4$ but different angles of attack. The cavity length is the same, but the flow is very different. At 8 degrees angle of attack, the flow is much more violent with structures shedding of the suction side while the 6 degrees case is practically stable.

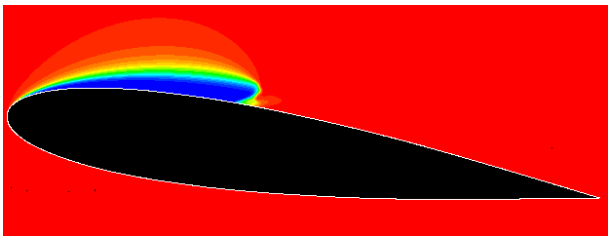

Fig 2 (a):The volume fraction contour for $\sigma/2\alpha = 6$ at 8 degree angle of attack.

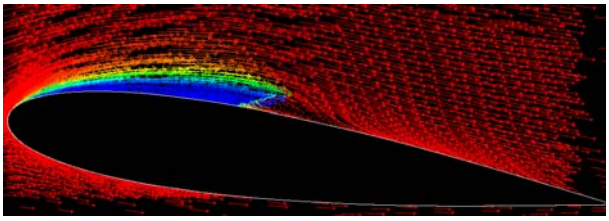

Fig 2 (b):The corresponding velocity vector at the same time.

Kjeldsen et al. (2000) shows that the flow over this hydrofoil passes through several cavitation regimes ranging from inception to supercavitating. The same sequence of cavitation regimes are found in the numerical model as reported from the experiments. It must be emphasized that the difference between patch and bubble cavitation as reported by Fluent, is determined based on whether the patch sheds itself (bubble cavitation) or is sustained for a certain period of time. The determination of the cavitation regimes was done by visual inspection of contour plots of the numerical solution.

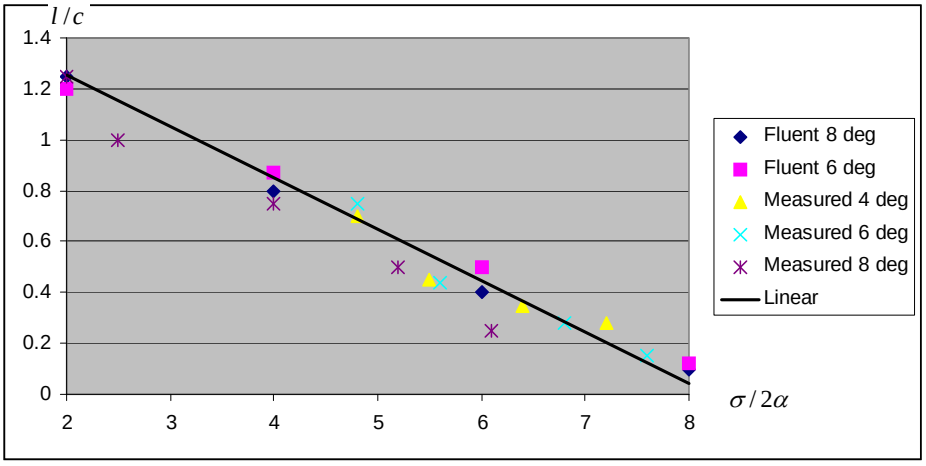

Fig 3:Cavity length as a function of $\sigma / 2\alpha$

In engineering applications, prediction of lift breakdown is important. This was also calculated and compared to experimental results. The lift is oscillating with different amplitudes at different cavitation numbers. The lift fluctuates with largest amplitudes when the cavity length is about 0.75 chord lengths, corresponding to $\sigma / 2\alpha$ of about 4. Experimental results are not available for 8 or 6 degrees angle of attack, and the lift does not seem to scale with the parameter $\sigma / 2\alpha$. The general shape of the lift breakdown curve can still be compared. The results are plotted in Figure 5. The cavitation model does not seem to capture the distinct breakdown that is measured. It is believed that this is caused by the lack of compressibility in the vapor phase, i.e. the flow that is closest to the suction side in the foil.

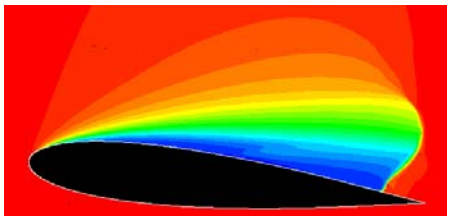

Fig 4 (a): A volume fraction contour for $\sigma / 2\alpha = 4$ at 6 degree angle of attack.

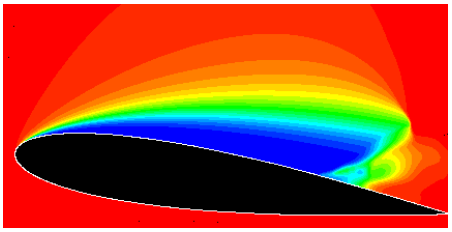

Fig 4 (b): A volume fraction contour for $\sigma / 2\alpha = 4$ at 8 degree angle of attack.

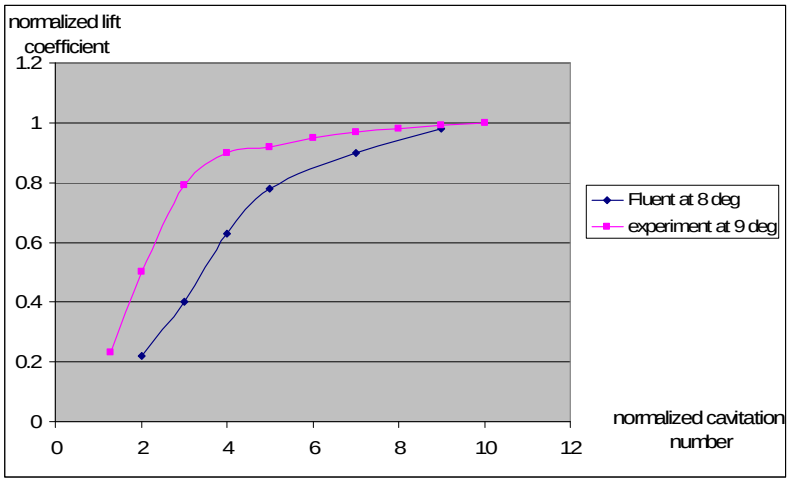

Fig 5: Normalized lift coefficient as a function ofnormalized cavitation number $\sigma / 2\alpha$

Conclusions

In general, the results are very promising. Several aspects of cavitation can be accurately captured with the current cavitation model. Visually, the flow is very well predicted. Especially, the cavity length can be calculated with a high degree of accuracy. This is an important feature in engineering aspects, since cavity collapse close to surfaces will cause damage. Also, with this code, it is easy to quantitatively adjust the overall cavitation number in the computational domain accurately. This is demonstrated by the good agreement between cavitation regimes and cavity length from experimental data and the numerical data respectively. The different cavitation regimes were found to match the reported experimental data.

Lift characteristics is fairly well calculated. The lift seems to drop in a more gradual manner. The calculations are still within reasonable accuracy.

REFERENCES

1. Song, C.C.S., He, J., Zhou, F.&Wang, G. 1997 Numerical simulation of cavitating and non-cavitating flows over a hydrofoil. Tech.Rep. 402. University of Minnesota, St. Anthony Falls Laboratory. Tylor H.F.W., 1997. Cement Chemistry, Thomas Telford Publishing, London, pp: 12 – 28.
2. Patankar, S.V. & Spalding, D.B. 1972 A calcuation procedure for heat, mass and momentum transfer in three-dimensional parabolic flows. International Journal of Heat and Mass Transfer 15,1787+.
3. Kubota, A., Kato, H.&Yamaguchi, H. 1992 A new modeling of cavitating flows: a numerical study of unsteady, cavitation on a hydrofoil section. Journal of Fluid Mechanics 240, 5969.
4. Acosta, A.J. 1955 A note on partial cavitation of flat plae hydrofoils. Tech. Rep. E-19.9. California Institute of Technology.
5. Singhal, A.K. 2002 Mathematical Basis and Validation of the Full Cavitation Model. Journal of Fluids Engineering, Vol.124 pp:617 - 624.

Frequency of Coherent Vortices in Rigid Submerged Vegetation

[1]Sandeep Patil, [2]Enda Murphy [3]Vijay P. Singh and [4]A. K. Rastogi
[1]School of Engineering and IT, Charles Darwin University, NT, Australia. 0909.
[2]Scott Wilson Ltd., Alencon Link, Basingstoke RG21 7PP, UK.
[3]Caroline and William N. Lehrer Distinguished Chair in Water Engineering
Department of Biological and Agricultural Engineering, Texas A and M University
Scoates Hall, 2117 TAMU, College Station, Texas 77843-2117, U.S.A.
[4]Department of Civil Engineering, Indian Institute of Technology, Bombay. 400076. India

Abstract: Flow through submerged vegetation exhibits periodic oscillations at the interface called Kelvin-Helmholtz vortices. In this paper, we adopt a two-layer model of the system, consisting of overflow and vegetation regions, which are linked by a strong shear transition. A dispersion relation for the vortices is derived as a function of vegetation parameters. The relation provides a means to calculate vortex frequency in terms of measurable flow characteristics. Results show that the vortex frequency for rigid plants is a function of flow hydraulics and plant material density, whereas in case of flexible stems, it is a function of stem geometry of bending stems (Patil et al., 2006).

Keywords: Kelvin-Helmholtz vortices, rigid vegetation

INTRODUCTION

In flow through submerged vegetation, the magnitudes of velocity in the overflow region (U_o) and that in the vegetation region (U_v) (Carollo et al., 2002) are distinctly different, owing to obstruction of the flow in the latter region by plant stems. These velocities are joined by a depth-wise transition of strong shear with a point of inflection at the interface (Raupach et al., 1996). The existence of a point of inflection provides Rayleigh's necessary condition for instability that induces vorticity with a local maximum at the interface. As a result, flow at the interface rolls into coherent vortex structures called Kelvin-Helmholtz (KH) vortices (Grizzle et al., 1996) (Fig.1).

In laboratory measurements, Ghisalberti and Nepf (2002) observed periodic fluctuations at the interface of the vegetation canopy and the overflow and attributed them to the presence of KH vortices. The center of these vortices remains close to, but slightly above, the top of the vegetation (Ghisalberti and Nepf, 2006) and exhibit motions that are stronger while moving into the canopy (sweeps) and weaker while coming out into the overflow (ejections). Poggi et al.

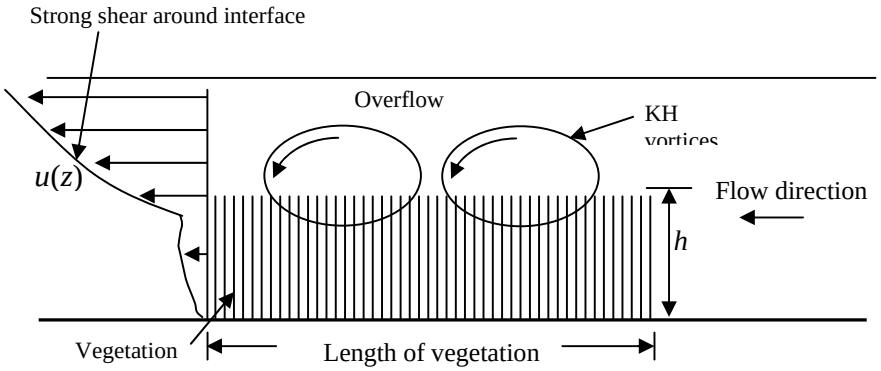

Fig 1: Schematic diagram of KH vortices in rigid submerged vegetation

Corresponding Author : Sandeep Patil, School of Engineering and IT, Charles Darwin University, NT 0909, Australia,
Tel: +618-89467367, Fax: +618-89466680, E-mail: sandeep.patil@cdu.edu.au, coastlab1@yahoo.com

(2004) investigated the effect of vegetation density on KH vortices and stated that the vortices appear only for a certain magnitude of stem density. These oscillations, being coherent and periodic, have potential to significantly influence the exchange of flow and turbulence between the free and obstructed regions (Nepf and Vivoni, 2000). In this paper, we assume that the two regions behave as co-flowing layers of fluid of different density, ρ_o being the density of the overflow and ρ_v being the effective density of the vegetation region, which is influenced by the presence of stems. For simplicity a relative motion between U_o and U_v is considered, meaning that the net velocity of overflowing water becomes $(U_o - U_v)$, whereas the vegetation flow has zero velocity. Applying the linear instability theory to this flow field, a dispersion equation relating the frequency of KH vortices to hydraulic and vegetative parameters is derived and is verified using experimental data.

DISPERSION RELATION FOR KH VORTICES

The vegetation density for the vegetation region can be calculated on the basis of the volumetric contributions of the stems and the surrounding water. The volume of a stem is $(\pi d^2 h/4)$. If the number of stems per unit volume is $1/h\Delta S^2$, then the volume occupied by plants in the vegetation region is $= \pi d^2/(4\Delta S^2)$. The remaining volume is occupied by water which can be expressed as $= 1 - [\pi d^2/(4\Delta S^2)]$. The vegetation density can be written as

$$\rho_v = \rho_m \left(\frac{\pi d^2}{4\Delta S^2} \right) + \rho_o \left(1 - \frac{\pi d^2}{4\Delta S^2} \right)$$

$$\rho_v = \rho_o + (\rho_m - \rho_o) \left(\frac{\pi d^2}{4\Delta S^2} \right) \quad (1)$$

where $\rho_m = 700$ kg/m^3 is on average, the material density of wood and $\rho_o = 1000$ kg/m^3 is the water density. Assuming irrotational flow and the two regions to be immiscible, a linearized inviscid analysis is applied. Due to instability, there are disturbances in the overflow as well as in the vegetation region which can be expressed as

$$u_1 = (U_o - U_v) + u_o' \qquad u_2 = u_v' \quad (2)$$

where u_o' and u_v' are, respectively, the small vector disturbances in the overflow and vegetation. Substituting Eq. 2 into the conservation of mass equation

$$\nabla u_o' = 0 \qquad \nabla u_v' = 0 \quad (3)$$

and into the conservation of momentum equation

$$\frac{\partial u_o'}{\partial t} + (U_o - U_v)\frac{\partial u_o'}{\partial x} = \frac{\nabla p_o}{\rho_o} \quad (4)$$

$$\frac{\partial u_v'}{\partial t} = \frac{\nabla p_v}{\rho_o + (\rho_m - \rho_o)\left(\frac{\pi d^2}{4\Delta S^2} \right)} \quad (5)$$

where p_v and p_o are the dynamic pressures due to disturbance. The kinematic boundary condition at the interface can be defined as $F = z_i - \tau(x,t) = 0$ where z_i is the height of interface from the channel bottom and τ is the surface of the monami wave. For only vertical movement of disturbance, it becomes

$$\frac{\partial F}{\partial t} + U \nabla F = 0 \quad (6)$$

where U is the velocity which for the upper layer is $(U_o - U_v)$ and zero for the lower layer. Linearizing the equations, one obtains

$$\frac{\partial \tau}{\partial t} + (U_o - U_v)\frac{\partial \tau}{\partial x} = w_o \quad (7)$$

$$\frac{\partial \tau}{\partial t} = w_v \quad (8)$$

Further, the dynamic free surface boundary condition provides equal pressure at interface, i.e.,

$$p_o - \rho_o g \tau = p_v - \left[\rho_o + (\rho_m - \rho_o) \left(\frac{\pi d^2}{4\Delta S^2} \right) \right] g \tau$$

at $z = 0$ (9)

As a first order approximation, the disturbances are assumed to be of sinusoidal form, $(p_o, w_o, p_v, w_v, \tau) = (P_o, W_o, P_v, W_v, Z)\, e^{i(kx - \omega t)}$,

where *k* is the wave number, and $\omega = \omega_r + j\omega_j$ is the wave frequency in which ω_r is sinusoidal and ω_j is monotonic, and *j* is the complex notation similar to *i*. The right side bracketed quantities are the amplitudes of the left side bracketed quantities. For developing vortices, which grow from the leading edge of the canopy to the fully developed steady state, $\omega_j \rangle 0$, whereas for fully developed coherent vortices, $\omega_j = 0$. Substituting the disturbances in Eqs. 4 and 5, one can write:

$$-i\omega W_o + ik\left(U_o - U_v\right) W_o = \frac{P_o}{\rho_o}(ik) \quad (10)$$

and

$$-i\omega W_v = \frac{P_v}{\left[\rho_o + \left(\rho_m - \rho_o\right)\left(\frac{\pi d^2}{4\Delta S^2}\right)\right]}(ik) \quad (11)$$

Similarly for Eqs. 7, 8 and 9,

$$Z\left[-i\omega + ik\left(U_o - U_v\right)\right] - W_o = 0 \quad (12)$$

$$-i\omega Z - W_v = 0 \quad (13)$$

$$P_o - P_v + Zg\left[\left(\left[\rho_o + \left(\rho_m - \rho_o\right)\left(\frac{\pi d^2}{4\Delta S^2}\right)\right]\right) - \rho_o\right] = 0 \quad (14)$$

Eqs. 10, 11, 12, 13 and 14 can be expressed in matrix form as:

$$\begin{bmatrix} i\left[k\left(U_o - U_v\right) - \omega\right] & -1 & 0 & 0 & 0 \\ -i\omega & 0 & -1 & 0 & 0 \\ g\left[\left(\rho_o + \left(\rho_m - \rho_o\right)\left(\frac{\pi d^2}{4\Delta S^2}\right)\right) - \rho_o\right] & 0 & 0 & 1 & -1 \\ 0 & 0 & -i\omega & 0 & \frac{k}{\left(\rho_o + \left(\rho_m - \rho_o\right)\left(\frac{\pi d^2}{4\Delta S^2}\right)\right)} \\ 0 & i\left[k\left(U_o - U_v\right) - \omega\right] & 0 & \frac{-k}{\rho_o} & 0 \end{bmatrix} \begin{bmatrix} Z \\ W_o \\ W_v \\ P_o \\ P_v \end{bmatrix} = \begin{bmatrix} 0 \\ 0 \\ 0 \\ 0 \\ 0 \end{bmatrix} \quad (15)$$

For a non-trivial solution of Eq. 15, the determinant of the matrix is equated to zero. This provides

$$\omega = \frac{k\left(U_o - U_v\right)\rho_o \pm i\sqrt{\left[k^2\left(U_o - U_v\right)^2 \rho_o\left(\rho_o + \left(\rho_m - \rho_o\right)\left(\frac{\pi d^2}{4\Delta S^2}\right)\right)\right] + \left[k\,g\left(\left(\rho_o + \left(\rho_m - \rho_o\right)\left(\frac{\pi d^2}{4\Delta S^2}\right)\right) - \rho_o\right)^2\right]}}{2\rho_o + \left(\rho_p - \rho_o\right)\left(\frac{\pi d^2}{4\Delta S^2}\right)} \quad (16)$$

Eq. 16 is the dispersion equation for the interfacial periodicity. For neutral stability in which vortices are neither growing nor dampening, the entire square root term in Eq. 16 will be zero. Thus, the monami frequency for coherent vortices becomes

$$\omega = \frac{k\left(U_o - U_v\right)\rho_o}{2\rho_o + \left(\rho_p - \rho_o\right)\left(\frac{\pi d^2}{4\Delta S^2}\right)} \quad (17)$$

Eq. 17 provides a dispersion equation for the oscillatory motion at the interface of rigid canopy with which the frequency of vortices can be calculated.

EXPERIMENTAL VALIDATION

The experimental data of Ghisalberti and Nepf (2006) was used to validate the model. Wooden stems (density ~ 700kg/m^3) with varying frontal area per unit volume, $a = d/\Delta S^2$ (ΔS = stem spacing), ranging from 0.025 to 0.08 were used to represent the vegetation canopy. Measured velocities in the overflow and vegetation regions were used to calculate the observed frequency vortices, $f = 0.032\overline{U}/\theta$ (Ho and Huerre, 1984) where $\overline{U} = \left(U_o + U_v\right)/2$. The momentum thickness, $\theta \sim 6t_{ml}$, was used, where t_{ml} is the measured value of the mixing length and six is the constant factor. In the flexible vegetation, this factor is ~7 (Ghisalberti and Nepf, 2002) which for the rigid vegetation will be reduced as the momentum penetration is easier in flexible vegetation. Thus, a value of six was selected for the factor. The sensitivity of the factor was checked and found to be not affecting the computed match between observed and predicted frequencies. As the phase speed of vortices (*C*) is higher than the interfacial flow velocity (Ikeda and Kanazawa, 1993), the measured interfacial velocity was increased by 10% to get the phase speed and the corresponding wave number *k* was calculated using the measured frequency and phase speed.

The predicted frequencies from Eq. 17 were compared with the observed frequencies, as shown in

Fig. 2. The trend of observed frequencies was simulated satisfactorily. The discrepancies in the predicted values may be due to the non-linear characteristics of the vortices observed in the experiments, including strong sweeps and weak ejections, which could not be captured by the linear theory. The theory assumes the overflow and vegetation regions to be immiscible, which is an approximation. Other sources of non-linearity in real KH vortices include interactions between neighbouring vortices (Ikeda and kanazawa, 1996) and three-dimensional effects (Finnigan, 2000).

CONCLUSION

A theoretical framework for predicting the frequency of Kelvin Helmholtz vortices in flows through submerged vegetation is proposed. A two layer model is presented, where the two distinct regions of the flow, the overflow and the vegetated region, are analogous to layers of fluid of different density. Linear instability theory is used to develop a dispersion relationship for the vortices. As expected, the frequency of the vortices is found to be a function of the wave number, the net velocity difference between the overflow and vegetation regions, and the plant stem density.

The model is validated using the results of laboratory flume experiments (Ghisalberti and Nepf, 2006). The predictions are accurate to about 20%, which is within the range of uncertainty expected for the linear instability theory adopted.

This research gives some insight into the physical characteristics of turbulent flows through submerged vegetation. In particular, the paper provides a better understanding of the behaviour of fluid at the interface between the vegetation and overflow regions, which is important in predicting residence times, mass transport and the distribution of organisms.

REFERENCES

1. Carollo, F. G., Ferro, V. and Termini, D. 2002. Flow velocity measurements in vegetated channels. *J. Hydraulic. Eng.*, 128(7), 664–673.
2. Ghisalberti, M., and H. M. Nepf, 2002, Mixing layers and coherent structures in vegetated aquatic flows. J. Geophysical Research, 107 C2, 1-11.
3. Ghisalberti, M., and H. M. Nepf, 2006, The Structure of the Shear Layer in Flows over Rigid and Flexible Canopies. Environmental fluid mechanics, 6(3), 277-301.
4. Grizzle, R. E., F. T. Short, C. R. Newell, H. Hoven, and L. Kindblom, 1996, *Hydrodynamically induced synchronous waving of seagrasses: 'monami' and its possible effects on larval mussel settlement.* J. Experimental Marine Biology and Ecology, 206, 165-177.
5. Ho, C. H. and Huerre, P. 1984. Perturbed free shear layers. Annual Review of Fluid Mechanics, 16: 365-422.

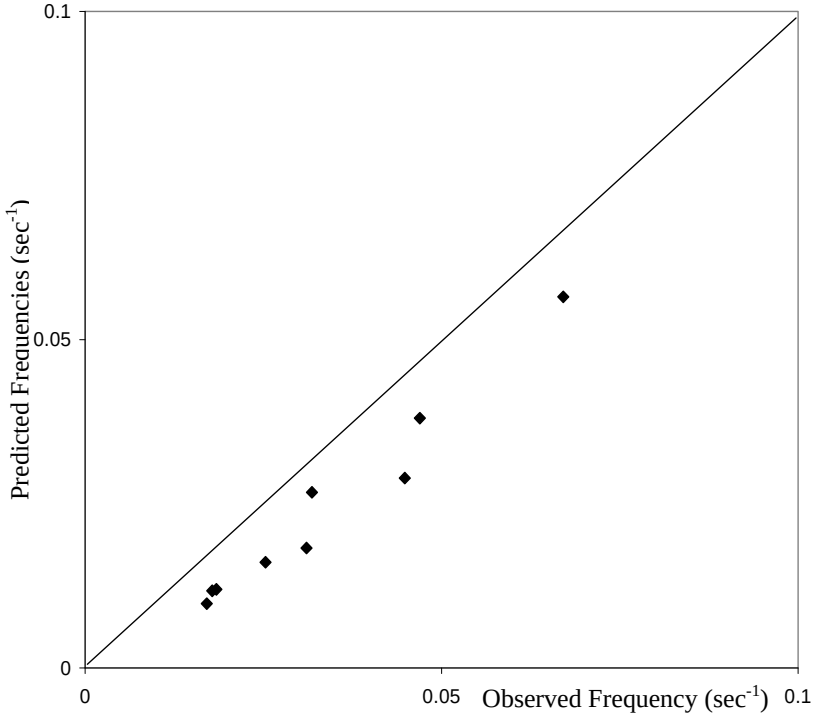

Fig 2: Predicted frequencies v/s observed frequencies of vertical vortices

6. Ikeda, S. and Kanazawa, M., (1993). On the velocity distribution in and above flexible plant canopy. In: Proceedings of the 48th Annual Meeting of JSCE, JSCE, No. 2, pp. 718–719.
7. Ikeda, S. and Kanazawa, M. (1996). Three-dimensional organized vortices above flexible water plants, *J. Hydraulic Eng*, 122 (11), 634-640.
8. Nepf, H. M., and Vivoni, E. (2000), Flow structure in depth-limited vegetated flow. J. Geophysical Research, 105(C12), 547-557.
9. Poggi, D., A. Porporato, L. Ridolfi, J. D. Albertson, and G. G. Katul, (2004), The effect of vegetation density on canopy sub-layer turbulence. Boundary Layer Meteorology, 111, 565–587.
10. Patil S., V. P. Singh, and A. K. Rastogi, 2006, Monami wave in submerged vegetation, 6th international symposium on stratified fluid. (Perth, Western Australia , Australia), pp. 348-353.
11. Raupach, M. R., J. J. Finnigan, and Y. Brunet, 1996, Coherent eddies and turbulence in vegetation canopies: The mixing layer analogy. Boundary Layer Meteorology, 78, 351-382.
12. Finnigan, J. J., 2000, Turbulence in waving plant canopies. Annu. Rev. Fluid Mech., 32, 519-571.

FEA Study on Parameters Affecting Springback of Forming of Advance High Strength Steel sheets (AHSS)

Watcharapong Sirigool[1],Nattawoot Depaiwa[1], Suwat Jirathearanat[2], Adachi Tadaharu[3]
Department of Mechanical Engineering, Faculty of Engineering,
King Mongkut's Institute of Technology Ladkrabang[1]
Near Net Shape Metal Manufacturing Research Group, National Metal and Materials Technology Center[2]
Department of Mechanical Sciences and Engineering, Tokyo Institute of Technology[3]

Abstract: Recently, advanced high strength steels (AHSS) are becoming widely used in many applications in place of mild steels, especially in automotive part manufacturing, due to its low weight, high strength and fairly good formability. However, the unavoidable obstacle of AHSS sheet metal forming is springback, which is a result of elastic recovery and residual stress. The aim of this study is to determine proper process parameters enabling reduction of springback defects in AHSS forming process. In this paper, a U-shape and a Butt-shape forming were used to examine springback behaviors, which are springback angle, sidewall curl, and twist, through finite element analyses. Simulation numerical parameters affecting springback prediction, which are element size, number of integration poinnts through thickness, adaptive meshing, and mass scaling increase were investigated to identify suitable simulation numerical settings for accurate springback prediction. Then, the simulation model was applied to study effects of blank holder force on springback behaviors and formability of the U-shape and Butt shape forming in an attempt to find proper blank holder force profiles for springback reduction emphasized die design guidelines.

Key words: Springback, AHSS, Stamping die designs

1. Introduction

Recently, advanced high strength steels (AHSS) such as dual-phase steels are becoming widely used in many applications in place of mild steels, especially in automotive parts manufacturing, owning to its light weight, high strength and good formability. However, the unavoidable obstacle of AHSS sheet metal forming is springback, which is referred to as the geometry changes of a part after tool removal. In metal forming process, springbacks are mainly caused by residual stress distributions after elastic recovery both in plane and through thickness of product. The severity of that residual stress depends on sheet metal mechanical properties (E, YS and n-value), material thickness, die geometry (die & punch radii, tool clearance), as well as forming process parameters (blank holder force and part-die lubricity) used during forming. With severe spring back defects, AHSS part assembly are difficult if not possible at all due to each individual part geometric deviations. Consequently, inevitably die geometry and process parameters need to be adjusted in the expense of time and money. This paper focuses on shape fixation techniques based on proper application of blank holder force profiles determined through well-adjusted FE simulations.

Many studies have been carried out in various aspects of springback in sheet metal forming. Specifically, as for numerical simulation related issues, Xu [1], Li and Wagner [2], Maker [3], Shi et al. [4], Lee and Yang [5] Yao and Lui [10] found that FEM simulations of springback are much more sensitive to numerical tolerances than forming simulations. The numerical parameters include the number of integration point [1-5] [10], size of element [1-5] [10], adaptive angle in tolerance and minimum time step [10]. According to the literature review, the numerical parameters such as the size of element, number of integration through thickness and adaptive meshing tolerance degree can affect the accuracy of FEA simulation. In this paper, finite element analyses were conducted to study effects of simulation numerical parameters on calculation of springbacks and, thus, to define their suitable values for accurate springback simulation. The simulation model was then utilized to determine proper process parameters, i.e. blank holder force profiles, for reducing springback defects in AHSS, SPHC590, forming process.

2. Methodology

In this study, simplified part geometries, which are U-shape and Butt-shape were used for forming and springback simulations. The geometry of U-shape resembling to rail components and pillar-like Butt-shape were chosen to examine part springback angle,

Corresponding Author: Watcharapong Sirigool , Department of Mechanical Engineering, Faculty of Engineering, King Mongkut's Institute of Technology Ladkrabang, Thailand

curvature of sidewall curl, and twisting. The punch and die radii of the U-shape and Butt shape are 12 mm. which is 10 times of its thickness. Fig. 1 shows the geometry of U-shape and Butt-shape.

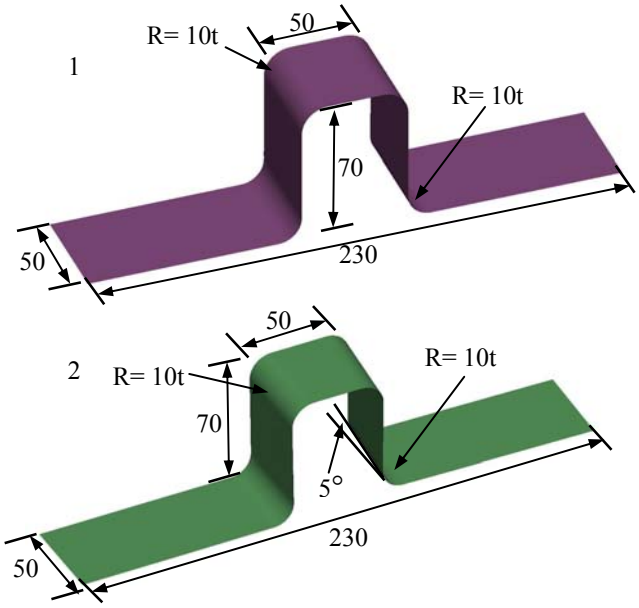

Fig. 1: top) U-shape bottom) Butt-shape

Fig. 2 shows three types of springback, which are springback of wall opening angle (θ_1), curvature of sidewall curl (ρ) and twist angle(θ_2).

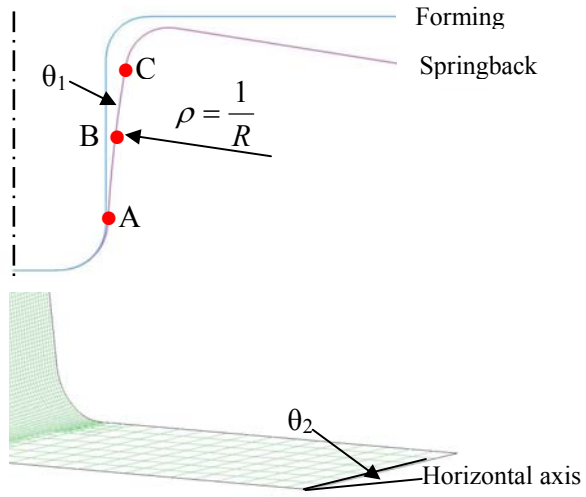

Fig. 2: Mesurement for U-shape and Butt-shape

θ_1 is an angle that a straight line passing through point A, C makes to the referenced vertical axis. ρ is a curvature of the sidewall curl constructed by point A, B and C. θ_2 is a twisting angle that the part flange line makes to the referenced horizontal axis.

3. Simulation

3.1 Numerical Parameter Investigation

Dynamic explicit and static implicit finite element analyses of the part forming and the formed part springback were performed by Dynaform 5.5 code [7]. First, the forming simulation was done using dynamic explicit analysis. Then, the data obtained form the forming simulation such as blank property, stress , plastic strain distributions and, deformed geometry, were saved to apply in the springback simulation using static implicit analysis. In forming and springback simulations, the blank was modeled with fully integrated shell element type having nine integration points along the thickness direction [7]. The material model was applied following the research work of Barlat–Lian [6], with isotropic hardening and m= 6. The dimension of initial blank is 350x50x1.2 mm. The material used in this study was SPHC 590 high strength steel sheets. The sheet metal mechanical behavior was characterized by tensile tests as shown in table1 below. Coulomb friction coefficient of 0.125 was assumed. A constant blank holder force profile of 10 tons was used to form the part in all the simulation cases.

Table1 Mechanical properties

Material	t,mm	E,GPa	YS,MPa	K,GPa	n
SPHC590	1.2	198.821	336.297	937.942	0.195

R_0=1.372, R_{45}=1.167, R_{90}=1.543

An array of U-shape forming and springback simulations was conducted to investigate numerical parameters affecting accuracy of springback prediction. The procedure of numerical parameter investigation followed was to study one parameter at a time, shown in Fig. 3, in such an order that interactions between these parameters are made minimum. First, the effect of element size is investigated, and then a proper element size was chosen to analyze effect of adaptive remeshing. The proper element size and adaptive remeshing are chosen to further analyze effect of number of integration point. Then, effect of mass scaling (time-step size) was studied with a proper set of previously determined parameters. Finally, the proper set of all numerical parameters was determined to conduct simulation analyses determination of proper blank holder force profiles with confidence.

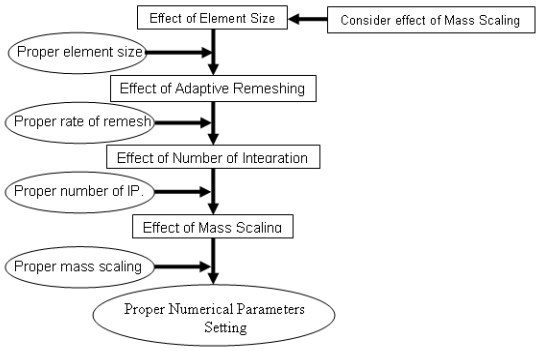

Fig. 3: Flowchart of numerical parameters simulation

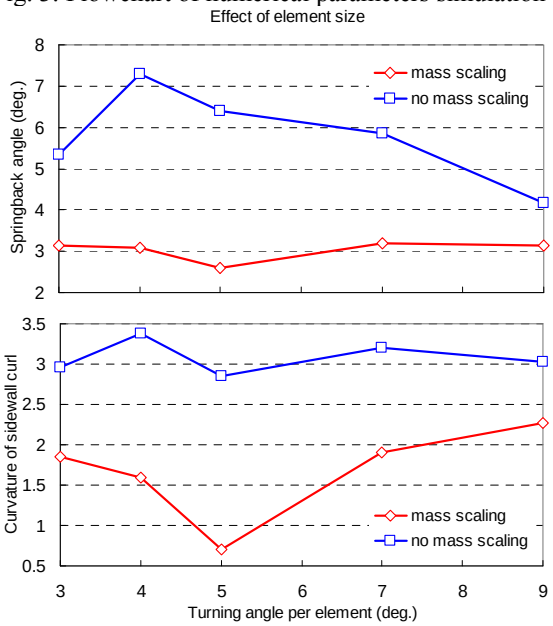

Fig. 4 Effect of element size

Fig. 4 shows effects of element size and use of mass scaling on calculation of springback opening angle and curvature of sidewall curl. The effect of mass scaling was consistent; simulations without mass scaling predicted more springbacks than with mass scaling for all the element sizes considered. Generally, a no mass scaling model should give more accurate results, because it has no additional inertial force incurred by the added mass. The element size per turning degrees of tool radii is known to greatly affect accuracy of springback prediction as it can better represent part geometry when it becomes smaller but at the expense of increased computation time, Fig. 4. From the figure, springbacks seem to increase as the element size becomes smaller except at element size of 3 degrees. With the absence of experimental data, the size of element per 4 degree seems to be a proper choice considering it giving maximum springbacks at reasonable computational time (about one third of the simulation with element size of 3 degrees).

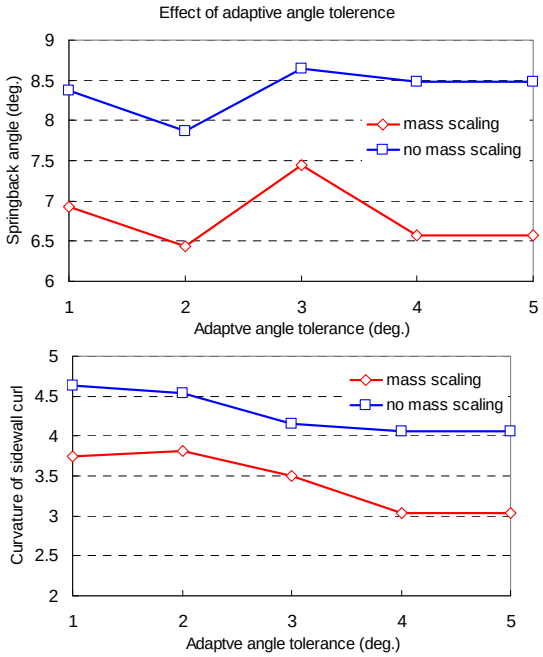

Fig. 5: Effect of adaptive angle tolerance

Fig. 5 shows effect of adaptive angle tolerance, by which the part mesh is refined when the angle between any adjacent elemental normal vectors exceed. In the case without mass scaling simulation, the springbacks were again larger than the case with mass scaling for all the adaptive angle tolerance. The springback predictions are stagnant at first but later become larger as the adaptive angle tolerance is much smaller; elements become smaller at a faster rate. The small adaptive angle tolerance of 1 degree is much more sensitive to part geometry based mesh refinement than 5 degree tolerance. Therefore, 1 degree tolerance is chosen as a proper adaptive angle tolerance.

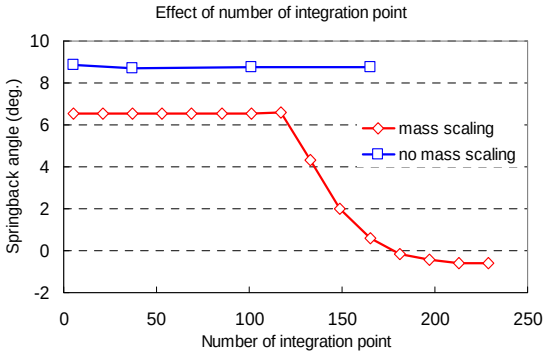

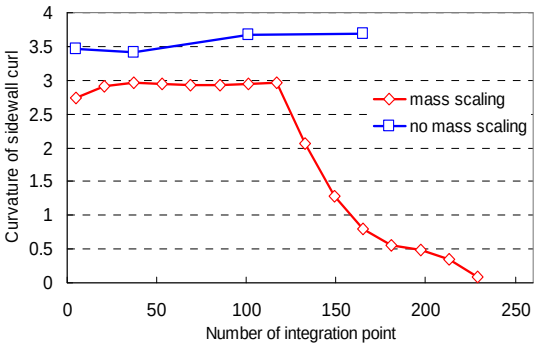

Fig. 6: Effect of number of integration point

Effect of number of integration point through thickness is shown in Fig. 6. With no mass scaling applied, springback angle prediction seemed somewhat constant while the curvature of sidewall curl increased slightly as the number of integration points increased. Interestingly, it can be found from the figure that the proper number of integration point is low for springback angle calculation compared to that of curvature of sidewall curl calculation. Considering computational time spent, in this case, the number of integration point of 9 was chosen to be proper. The simulations employing mass scaling clearly underpredicted the springbacks, especially when the number of integration point was larger than 125.

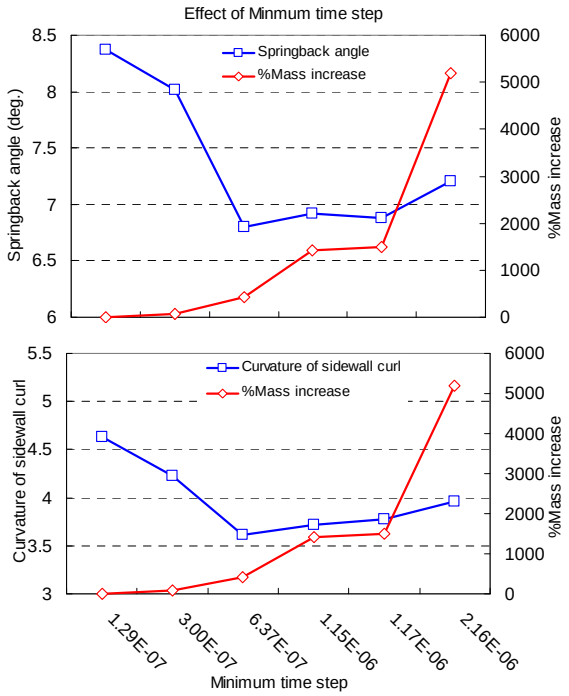

Fig. 7: Effect of minimum time step

Based on the simulation results up to this point, it is evident that simulations with mass scaling technique give erroneous springback prediction. However, it is usually more time-efficient to allow a careful application of mass scaling when adaptive mesh refinement is used to avoid too small of minimum time step leading up to extremely long computational time. Fig. 7 shows relationship of mass scaling increase and minimum time step, and their effect on springback prediction. The necessary minimum time step decreases as the mass scaling decreases requiring more computational time. Springback is predicted larger as minimum time step decreases. In this case, the minimum time step is 1.29E-07 sec when no-mass scaling is used. However, if only a small amount of mass scaling is applied (i.e. 70% mass increase) the necessary minimum time step is increased to 3.0E-07 sec resulting in 50% computational time reduction but with similar springback prediction. Thus, minimum mass increase (i.e. less than 100%) or equivalent to necessary minimum time step of 3.0E-07 sec seems to be a proper numerical setting for the proceeding process simulations.

3.2 Process Parameter Investigation

Effect of various Blank Holder Force (BHF) profiles on springback behavior and formability of the U-shape and Butt shape forming is investigated in an attempt to find proper BHF profiles for part springback reduction. Fig. 8 shows various profiles of BHF used in this study for both part geometries. Many researchers [8] [9] have suggested that proper part stretching during forming can reduce part springback. The underlying idea of these various BHF profiles is to determine when and how much to stretch the part through BHF action as to reduce part springbacks. All the numerical parameter settings determined previously were used here.

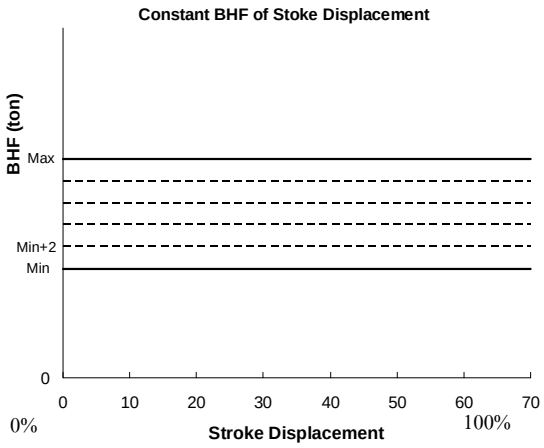

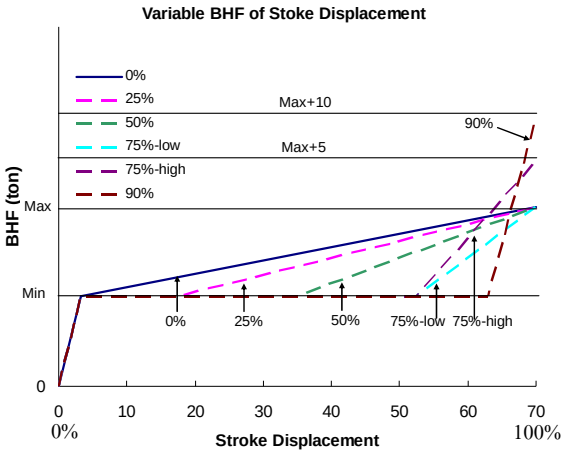

Fig. 8: Constant blank holder force profiles (top) and variable blank holder force profiles (bottom)

All the trial BHF profiles can be grouped in two; 1) BHF is kept constant throughout the forming stroke – "constant BHF profiles", and 2) BHF is kept constant up to certain forming strokes then increased linearly up to the end stroke – "variable BHF profiles". For each part geometry all constant BHF profiles are bounded by the lowest BHF, which is 10 tons as it is the lowest BHF available in our hydraulic press, and the highest BHF, by which the part can be form without necking. It was found that the highest BHF is 20 tons for U-shape and 22 tons for Butt shape. Most of the trial variable BHF profiles run between these lowest and highest values of BHF applied in the cases of constant BHF. However, two variable profiles exceeding the highest BHF value were applied without any part fracture.

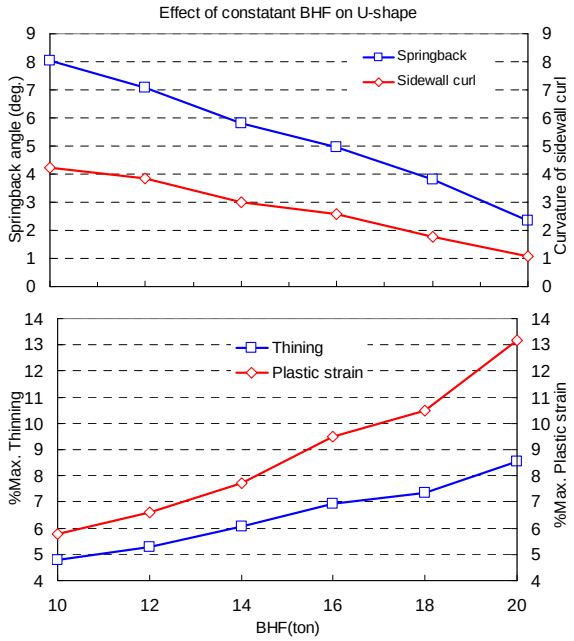

Fig. 9: Effect of constant BHF on U-shape

Fig. 9 shows effect of constant BHF profiles and corresponding part formability. The tendency of springback behavior was reducing. When blankholder forces increase springback and curvature of sidewall curl, the blank holder force was limited to 20 ton because higher values led to broken parts. The spring-back angles θ_1 and curvature of sidewall curl vary more substantially for smaller values of blankholder force. An increase of blank holder force from 10 ton to 20 ton, the %max thinning and %max plastic strain were increment.

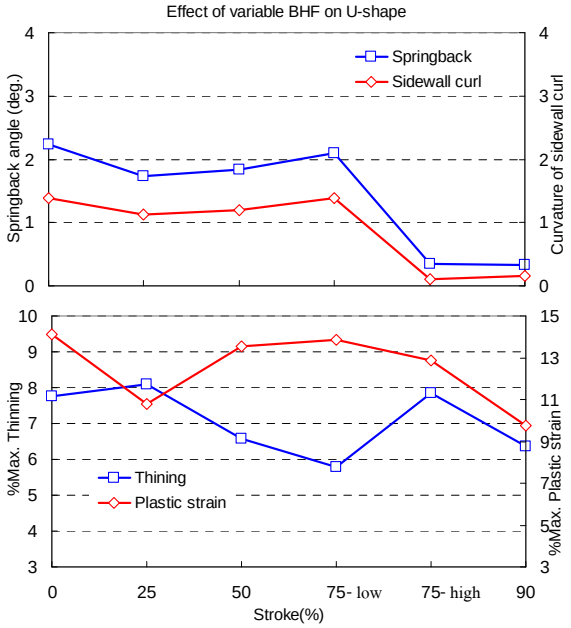

Fig. 10: Effect of variable BHF on U-shape

Fig. 11: Effect of variable BHF profiles and correspondimg part formability. The tendency of springback behavior was reducing then the springback behavior was increment at 50% stroke. The variable blankholder forces were the most reductional springback behavior especially in cases 75%-high and 90%. The value of %maximum thinning was reducing, when the stroke% was increment until 75%-low. In case 75%-high, the thinning was increment then the 90% was reduce thinning. The % maximum plastic strain was reducing. When blankholder forces increase %maximum plastic strain.

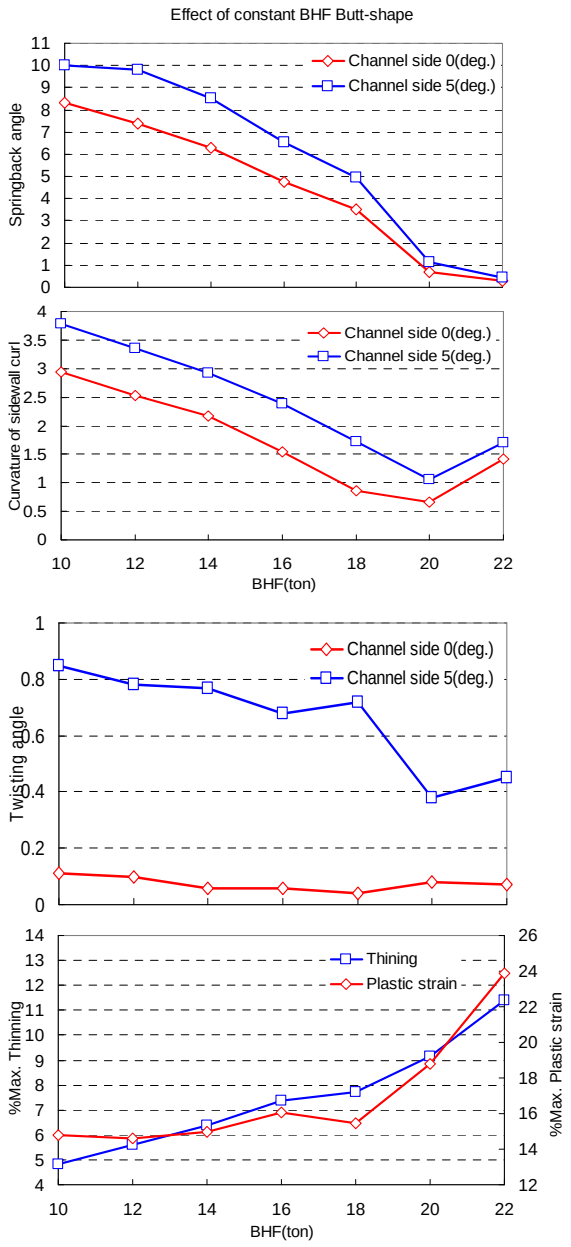

Fig. 12: Effect of constant BHF on Butt-shape

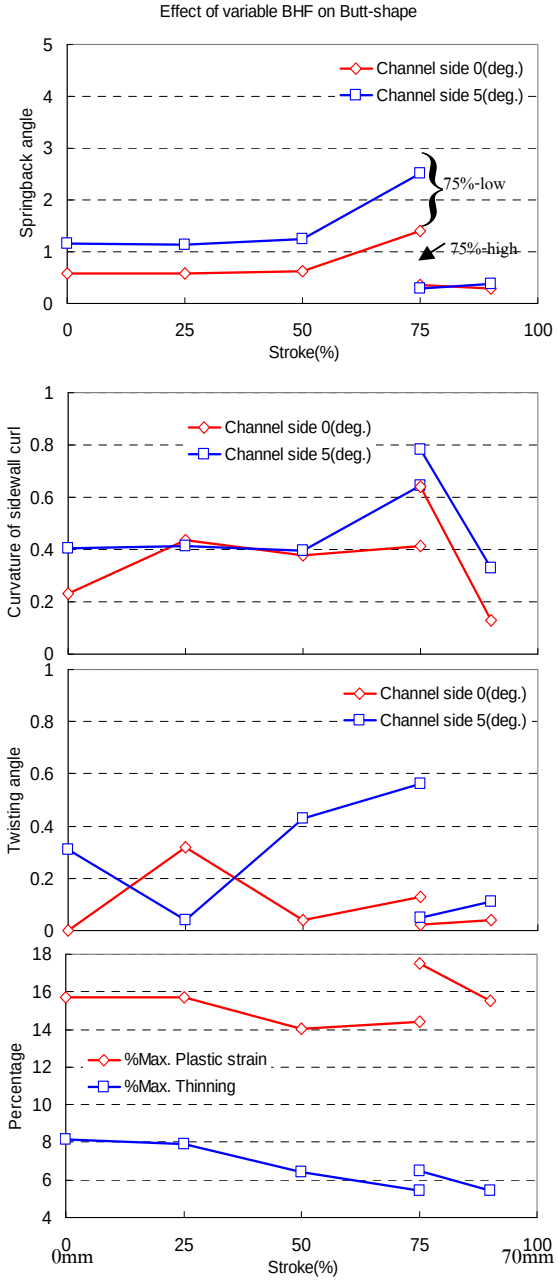

Fig. 13: Effect of variable BHF on Butt-shape

Fig. 11 shows effect of constant BHF profiles and corresponding part formability. The tendency of springback behavior was reducing. When blankholder forces increase springback and curvature of sidewall curl, the blank holder force was limited to 22 ton because higher values led to broken parts. The spring-back angles θ_1 and curvature of sidewall curl vary more substantially for smaller values of blankholder force. An increase of blank holder force from 10 ton to 22 ton The twists of flange θ_2 on channel side 5° can be reducing twist angle depend on blankholder force. The thinning and plastic strains were increment percentage when the BHF increase force.

Fig. 12 shows effect of variable BHF. The springback angle was similar until case 75%-low, which are both of channel side angle increase. In cases 75%-high and 90% stroke, the springback angles were decrease both of channel side. The curvature of channel side 0° was smaller at 0% of stroke and then increase to constant about 0.4, but the channel side 5° was constant 0.4 and then raise up of curvature at 75%-low. In case

75%-high, the curvature of sidewall curl has high curvature and 90% the curvature of sidewall curl was lower than case 75%-high. The twist angle of flange could reduce twisting at 75%-high. The thinning and plastic were reducing at 0% to 75%-low of stroke. However, the thinning and plastic strain at 75%-high was higher than 75%-low but springback angle smaller than 75%-low. The effect of variable blank holder force can be reduce springback behavior, %maximum thinning and %maximum plastic strain better than constant blankholder force.

4. Conclusion

The numerical parameters are affecting springback simulation accuracy. In this paper investigate numerical parameters influence springback prediction.

- The proper mass scaling and element size are very crucial.

- The number of integration point was important parameter, which is more the number of integration points. The springback behavior simulation was accurate simulation

- The minimum time step should be avoid small minimum time step, the minimum time step shall not exceed 3.0E-07.

- Proper levels of constant blankholder force can reduce springback behavior in U & butt shape, but the variable blank holder force can reduce not only springback behavior more than constant blank holder force but also %maximum thinning and %maximum plastic strain, which can be improve capability of parts

References

[1] W.L. Xu, Sensitive factors in springback simulation for sheet metal forming, J Mater Process Technol 151 (2004) 217–222

[2] Li, K. and Wagoner, R. H., "Simulation of Springback", Simulation of Material Processing: Theory, Methods and Applications, Huetink and Baaijens (eds),1998, 21-31.

[3] Maker, B. N., "implicit Springback Calculation using LS-DYNA", Livermore Software Technology Corporation, 1998.

[4] Shi, M. F., Prince, D. G., and Song, W., "A Sensitivity Study of Simulation Parameters in Sheet Metal Forming and Springback Simulation using LSDYNA". Proc. 5th Intl. LS-Dyna User Conf. Southfield, USA,1998.

[5] S.W. Lee, D.Y. Yang, An assessment of Numerical parameters influencing springback in explicit finite element analysis of sheet metal forming process, J. Mater. Process Technol 80–81 (1998) 60–67.

[6] F. Barlat and J. Lian, Plastic behaviour and stretchability of sheet metals. Part I. A yield function for orthotropic sheets under plane stress conditions, Int. J. Plast. 5 (1989) 51–66.

[7] LS-DYNA Dynaform5.6 User's Manual,Livermore Software Technology Corporation, Livermore, 2003.

[8] Gang Lui, Variable blankholder force in U-shape part forming for eliminate springback error, J Mater Process Technol 120 (2002)259-264

[9] B. CHIRITA, Experimental study of the influence of blankholder force on spring-back of sheet metal, Archieves of Civil and Mechnical Engneering, vol. 3, 2003

[10] H. Yao and S.-D. Liu, Techniques to Improve Springback Prediction Accuracy Using Dynamic Explicit FEA Codes, Society of Automotive Engineers, 2002, 01-0159

Applications of Ray Tracing Method in Illumination Design

Piyapong Premvaranon, Apichart Teralapsuwan, and Foifon Srisawat
Automotive Laboratory, National Metal and Materials Technology Center (MTEC)
114 Thailand Science Park, Paholyothin Rd, Klong 1, Klong Luang,
Pathumthani 12120, Thailand

Abstract: This paper proposed applications of the Computer Aided Lighting (CAL) technology, so called "Ray Tracing Method", which is widely used in various industries such as automotive lamp, building lighting, medical optics, display instrument, or aerospace. In this project, the ray tracing method was demonstrated and employed to calculate the illuminance, intensity, and beam patterns of recessed luminaires and tractor's headlamp in order to assess their beam quality. Besides, the ray tracing method was applied to improve the beam quality of the lamps and explore the effects of geometry changes to the beam pattern of the lamp for specific lighting application. With ray tracing method, the beam quality of the lighting system can be effectively assessed in the early design stage prior to the generally costly prototype fabrication, which results in the fabrication cost reduction and the shorter trials and errors period. Furthermore, the conceptual methodology gained from this project can be applied on other complex lighting systems, especially automotive headlamp, for soothing the beam shift problem, which is taken seriously into account as a key criterion in automotive lamp design.

Keywords: Ray tracing, luminaire design, headlamp design

INTRODUCTION

For lighting engineers, the science of light has been used to design various practical systems that control light and other forms of radiation of electromagnetic wave. The systems that engineers deal with include medical optics and laser, display instruments, luminaires, automotive headlamp, and many others. Recently, the Computer Aided Lighting (CAL) technology, such as ray tracing method, has become a very useful tool and widely used in the field of lighting design[1]. The ray tracing method has been developed for lighting design and calculation in order to simplify and speed up the design process to enable engineers to examine more aspects of system performance and to explore a larger number of solutions.

In the past, the illumination of luminaire and headlamp is very difficult to calculate due to a number of reflective surfaces inside. To controlling the light distribution, the reflector design mainly depends on the measured data and experience of engineers. For instance, the efficiency and the basic parameters related to light distribution are stipulated, or the reflector geometry is assumed to be fixed, or the illuminance can be found approximately by the integral equations[2][3]. Consequently, the results obtain from those methods can neither express the intensity distribution directly, nor reflect the effect of the reflector geometry obviously.

Nowadays, by using the ray tracing method, the interaction of light with optical and mechanical structure is able to simulate efficiently in a single, global, three-dimensional coordinate with any complex geometry. Light rays obey the geometrical optics[4] and can be split into reflected, refracted, and scattered components as they propagate through the system. Each ray proceeds independently, following the realizable path determined by relatively simple formulae, and sequentially or non-sequentially encountering the objects in the system.

In this paper, the ray tracing method was employed to calculate the ray path, illuminance, intensity, and beam pattern of two study cases, a recessed luminaire and a tractor's headlamp, in order to assess the beam quality of the initial models. Then, the simulation results were used as a guideline for redesigning the shape of reflector to improve their function and beam quality. Furthermore, the data gained from ray tracing method in tractor's headlamp analysis could be adapted to use with finite element method to predict the failure due to the excessive heat within the headlamp, which is

Corresponding Author: Piyapong Premvaranon, Automotive Laboratory, National Metal and Materials Technology Center, 114 Thailand Science Park, Paholyothin Rd, Klong 1, Klong Luang, Pathumthanee 12120, Thailand, Tel: +662-5646500 ext 4355, Fax: +662-5646370, E-mail: piyapp@mtec.or.th

taken seriously into account as a key criterion in automotive lamp design.

MONTE CARLO RAY TRACING METHOD

In ray tracing method, light is considered as an electromagnetic wave traveling through space. A light ray is defined as a line normal to the direction of wave propagation. A light ray or ray obeys the laws of geometrical optics and can be transmitted, reflected, and refracted through an optical-mechanical system following the Snell's law as described below

$$n_1 \sin\theta_1 = n_2 \sin\theta_2 \quad (1)$$

where n_1 and n_2 are the refractive indices of medium 1 and 2, respectively, θ_1 is the incident angle of light ray with respect to the normal, and θ_2 is the refracted angle.

For Monte Carlo ray tracing, the luminous flux of light source can be expressed with photon bundles P. The emission and direction of the luminous flux can be directly measured or determined randomly based on the emission characteristics of light source. The emitted photon bundles (rays) from the light source travel through the system following the ray paths determined by the law of geometrical optics. When each photon bundle encountering the surface, its reflection, refraction or absorption is determined with a random number. After each ray passes all of surfaces in the system, the illuminance E of each surface is calculated from the number of photon bundles

$$E = \frac{P}{P_O} \times \frac{F}{A} \quad (2)$$

where P_O is the total number of photon bundles emitted from the light source, P is the number of photon bundles intercepted by the surface, F is the total luminous flux of light source, A is the area of the surface.

The principle of inverse square law is used in the simulation. The luminous intensity is related to illuminance, shown as the following,

$$I = E \times D^2 = \left(\frac{P}{P_0} \times \frac{F}{A} \right) \times D^2 \quad (3)$$

where D is the distance between light source and the detector surface.

SIMULATION PROCEDURE

The simulation procedure for predicting the beam quality of lighting systems by using ray tracing analysis is shown in Fig. 1. Generally, at the beginning of the simulation process, the problem statement must be defined. In this step, the goal of design must be specified. This includes the dimension, weight, power consumption, heat generation, testing standard, and etc. Next, the materials and their optical properties such as the reflectance, transmittance or scattering characteristic must be defined. Then, the 3D CAD model of the initial geometry was built. Commonly, the initial geometry is obtained by the design of an engineer, the past designs of manufacturer, or from the technical patents. After that, the working or testing environment was set up for analysis. Then, the beam pattern, illuminance, and intensity distribution of the initial model were calculated with ray tracing method to evaluate their beam quality. Finally, the reflector shape is redesigned until the lighting system has a function and beam quality as the design specification.

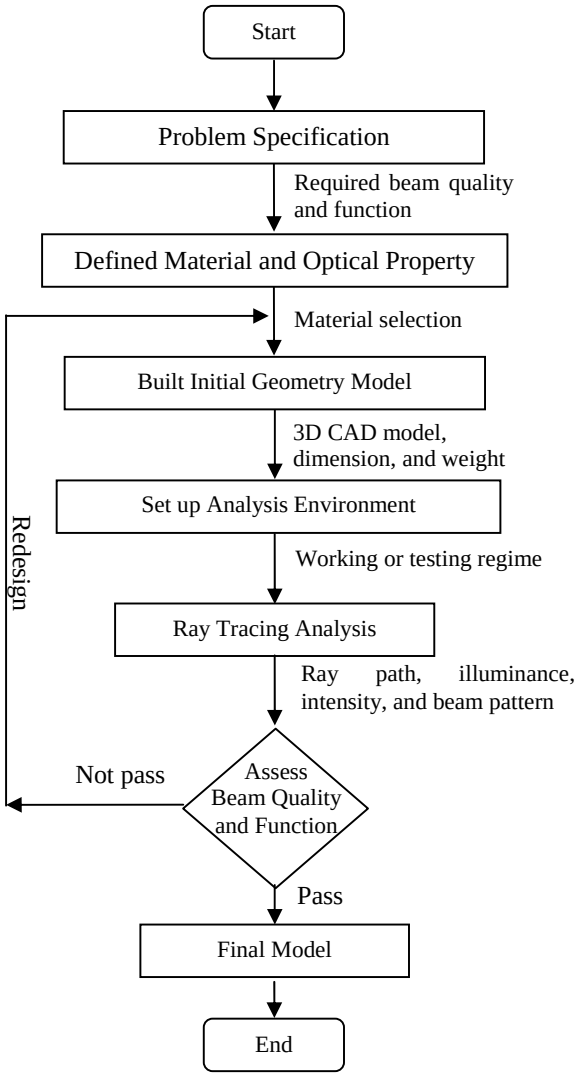

Fig. 1: Simulation Procedure

In this paper, a recessed luminaire and a tractor's headlamp are used as study cases. For both lighting systems, the beam pattern and illuminance of final design were predicted by ray tracing analysis and compared with those of initial geometries to assess their beam quality instead of those time-consuming trials and errors and the costly physical testing.

SIMULATION AND RESULTS

Study Case 1 : Recessed Luminaire

A twin 36W fluorescent recessed lamp (SL-T236L) with 2x11 cells louver and two reflectors are taken as the luminaire model. Fig. 2 shows a 3D CAD model and the overall dimensions of the recessed luminaire. The aluminum reflectors and louver blades have 95 and 5 percent reflectance, consecutively. The 36W florescent lamp gives the luminous flux at 2250 lumens with day light spectrum.

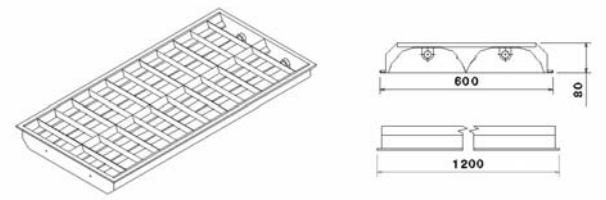

Fig. 2: 3D CAD model and dimension of the recessed luminaire

For ray tracing analysis, the CAD model was imported and material's optical properties including the surface characteristics of each component were applied. The simulation environment is set up following the testing standard. According to the testing standard, the recessed luminaire is installed at 2.7 meter height above the 10x10 m^2 detector on the floor ground as shown in Fig. 3 and Fig. 4 shows the cross section of initial luminaire's geometry.

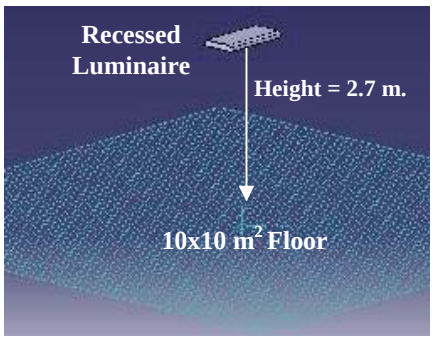

Fig. 3: Simulation set up following standard testing

After launching the ray tracing analysis, the position and direction of a photon bundle is firstly calculated, this photon bundle is traced from the light source to the reflector surface until it leaves the luminaire and strikes on the detector. The ray paths of each luminous flux from the florescent lamp are shown in Fig. 5.

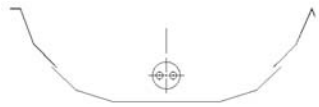

Fig. 4: The cross section of initial geometry

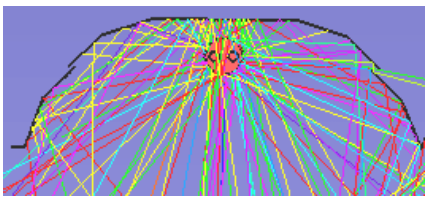

Fig. 5: The calculated ray paths of the light source and reflector

At the detector, the intersection of rays and detector surface are found and accounted for beam pattern, illuminance and intensity following the previous formulae. The beam pattern and intensity distribution of the initial geometry were reckoned out as shown in Fig. 6. From the simulation results, the maximum illuminance of the initial luminaire is 205.64 lux at the center of the beam pattern and its intensity is not quite a bat wing distribution due to a down light characteristics.

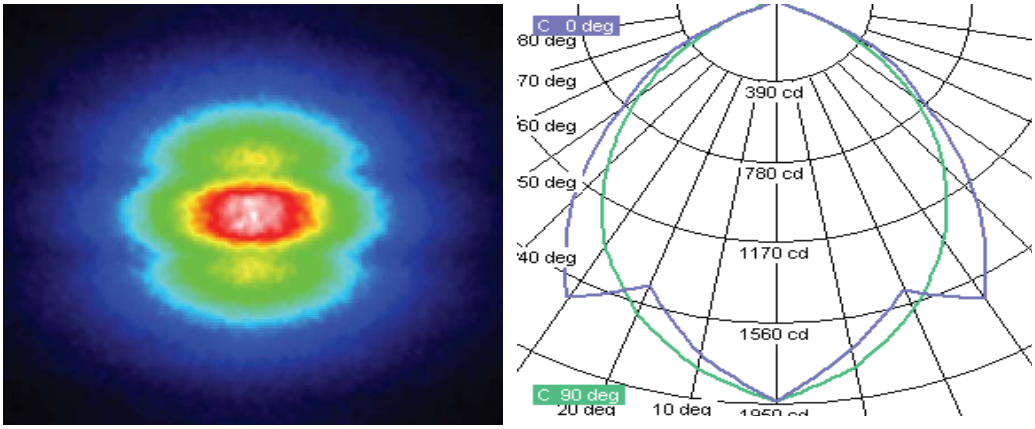

Fig. 6: The illuminance and intensity distribution of initial model

	Initial Model	Redesign Model
Beam Pattern	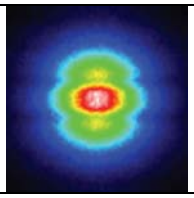	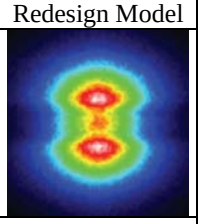
Max. Illuminance	205.64 lux	160.41 lux
Intensity Distribution	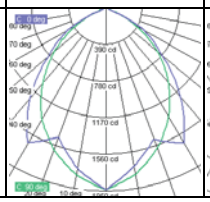	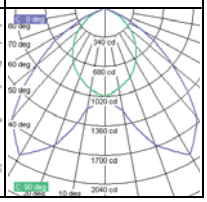

According to the requirement of manufacturer, the luminaire's reflector was redesigned to obtain a bat wing intensity distribution in order to increase the illumination area. The previous ray path simulation suggested that the upper part of the reflector controls light incidented on the inner part of the beam pattern, while, the lower reflector controls the outter shape of the beam pattern. With those ray path data, the angle and length of the reflector surfaces can be altered to get the required beam pattern and intensity distribution. Fig. 7 shows the cross section of redesigned reflector compared to its initial geometry.

Fig. 7: The cross section of redesigned reflector compared to the initial geometry.

Table 1: Comparison of the simulation results between the initial model and redesigned model

From table 1, the illuminance and intensity distribution of recessed luminaire were changed. The redesigned model gives the bat wing distribution as required. However, the maximum illuminance reduces due to the wider distribution of light on the floor. Then, the redesigned model is used for prototyping and testing following the IESNA standard. In accord with the testing result, the maximum illuminance from testing is 178 lux, which is 2.2 % error comparing to the simulation value. In conclusion, the function of the recessed luminaire was improved with the acceptable illuminance values for the manufacturer.

Study Case 2 : Tractor's Headlamp

In this study case, the ray tracing and finite element method was applied to study the melting cause of headlamp's plastic covered lens as shown in

the Fig. 8 below. The ray tracing method was employed to gain the ray path and illuminance data, then the finite element analysis was used to predict the failure of covered lens due to the thermal effect.

Fig. 8: The melting of plastic covered lens

Firstly, the original model of tractor's headlamp is imported and the optical properties, such as reflectance and transmittance, were applied. The headlamp system consists of 2.5 mm.-thick thermoplastic reflector part, the polycarbonate lens with 2 mm. in thickness, and the H4 Bulb 75/70 watts at an operating voltage 24 Volts. The 3D CAD model of the original headlamp system is shown in Fig. 9.

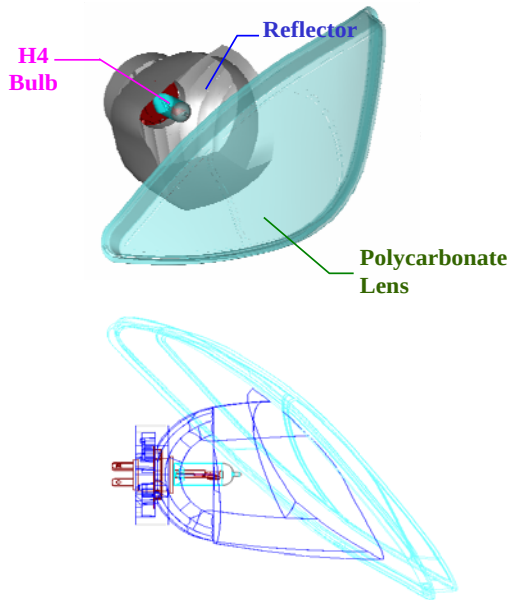

Fig. 9: CAD Model for forward lighting analysis

In ray tracing analysis, thermoplastic reflector's surface is assumed to be an aluminized surface that reflects light at 96 percent. The polycarbonate lens has index of refractive at 1.591 and transmits light at 85 percent for 2 mm. in thickness. A 4x6 m^2 screen is located at the distance 5 meters from the lamp to receive rays and simulate the beam pattern. The surface of reflector and lens are assumed to be a well-polished surface to neglect the effect of scattering. After tracing rays, the ray paths within the headlamp and its beam pattern were figured out as shown in Fig. 10.

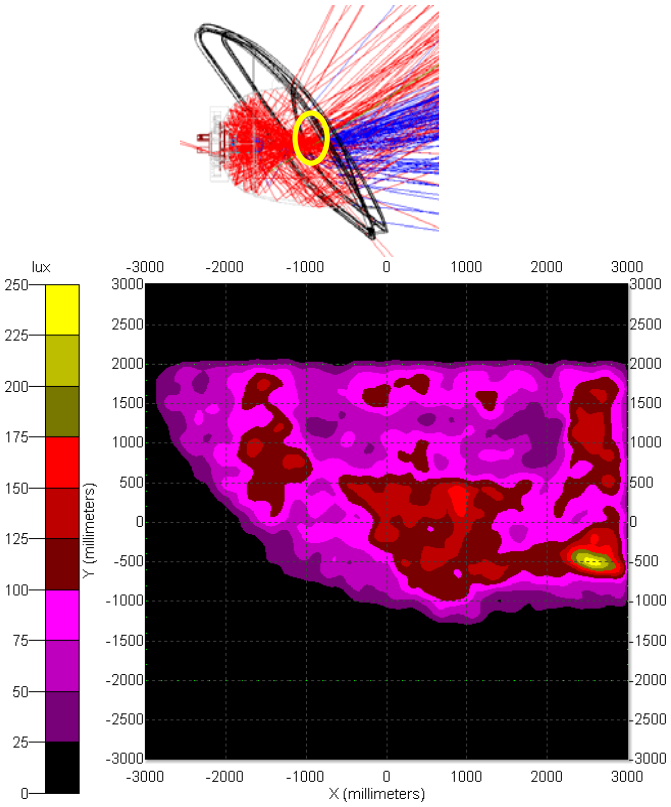

Fig. 10: The predicted ray paths and illuminance of the headlamp

Fig. 10 shows that most of the reflected rays focus on the surface of covered lens, while the discontinuity of beam pattern implies that the illumination of this original lamp model is quite unpleasant. With high and low beam filaments, the illumination on the working area is approximately 75-175 lux, which is not enough for working. According to ray tracing analysis, the maximum illuminance value locates at the focus area of rays on the covered lens as shown by Fig. 11. Next, this illuminance distribution (in Watt/m^2) on the inner surface of the covered lens was exported to map on 3D finite element model as thermal load for heat transfer analysis. The exported data composed of the flux value (in Watt) of each incident ray, XYZ

coordinate of each ray in global coordinate and the vector of ray direction.

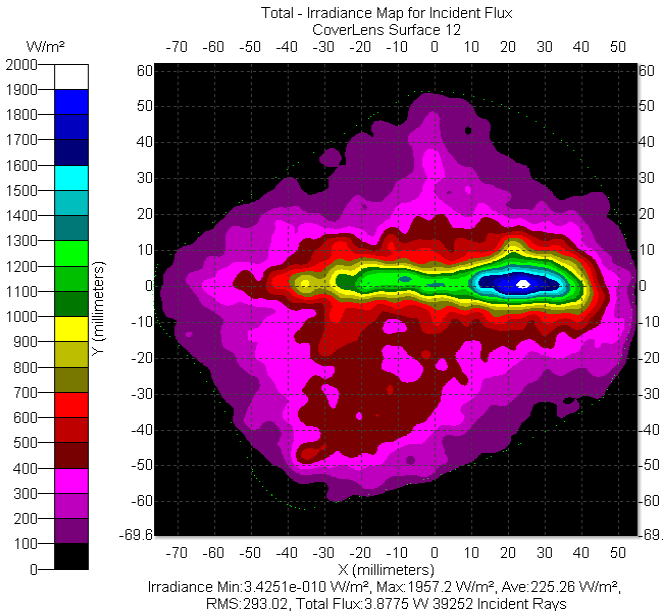

Fig. 11: The illuminance distribution on the inner surface of the covered lens

For thermal analysis, the covered lens of the original headlamp model was modeled as solids that transport energy by conduction. At the inner surface of the covered lens, temperature of the enclosed air is 40 degree Celsius and at the outer surface of the lens, heat is naturally convected to the ambient air. By using interpolation function, the illuminance distribution gained from ray tracing analysis was applied as a heat flux boundary condition in the finite element model. The finite element model and the boundary conditions as described above were applied for the heat transfer analysis. At the ambient temperature, the heat transfer coefficient of air is 10 W °C/m^2. In Fig. 12, the melting area is shown by setting the display temperature from 111 to 144 degree Celsius which is the melting temperature of polycarbonate plastic and then comparing with the melting covered lens sample from the field test. As shown in Fig. 12, the simulation result and the sample from field test are in good agreement.

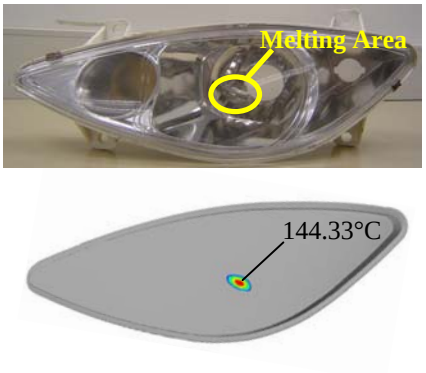

Fig. 12:Comparison of simulation result and thefield test sample

According to analysis results above, the melting problem of covered lens is caused by the focus of reflected light. Therefore, the shape of reflector can be redesigned so that the reflected rays are distributed and do not focus at the covered lens as shown in Fig. 13.

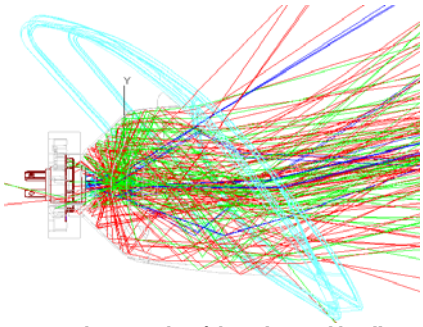

Fig. 13: The ray paths of the redesigned headlamp

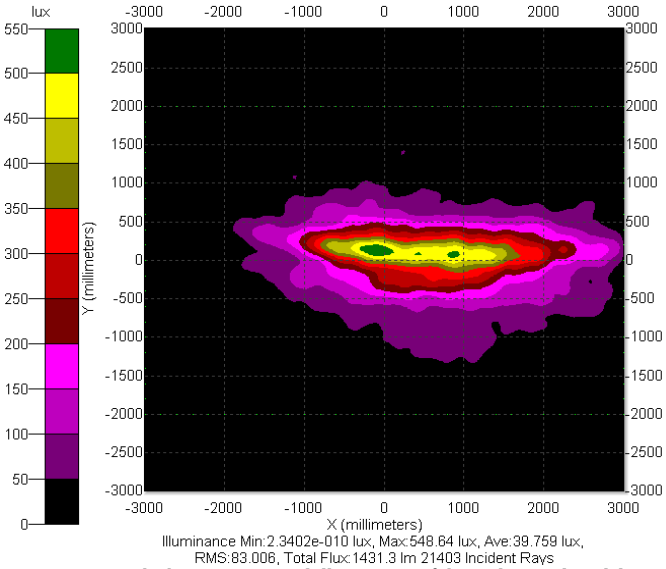

Fig. 14:The beam pattern and illuminance of the redesigned model

By using the proper parabolic based surface, the redesigned reflector can distribute the reflected rays better than the original model as shown in Fig. 14. The illuminance contour of redesigned model is continuous and beam pattern better illuminates on the working area with the increasing illuminance comparing to its original model.

In the aspect of thermal analysis, the temperature distribution of redesigned model is quite pleasant. The finite element simulation result suggests that the covered lens can resist the excessive heat from the filaments, when switching on high beam and low beam filaments at the same time. The Fig. 15 illustrated that the maximum temperature on the covered lens was reduced from 144.33 degree Celsius to 92.71 degree Celsius which lower than the melting temperature of the polycarbonate.

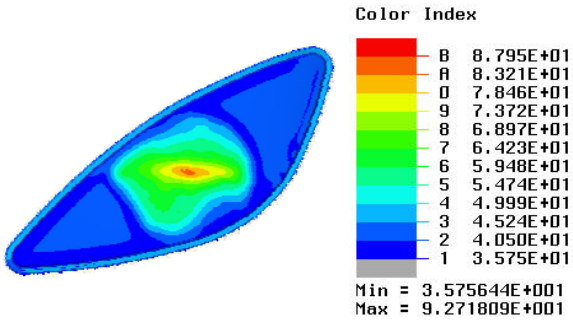

Fig. 15: Temperature distribution on the covered lens of redesigned model

Consequently, the beam quality of this lamp was improved and the melting problem of plastic lens due to the excessive heat from the filament bulb was solved.

CONCLUSION

In this paper, the ray tracing method is demonstrated and employed to evaluate the beam quality of the lighting systems such as luminaire and headlamp. Engineers can determined the illuminance and beam pattern of those lighting systems in the early design stage. The information gained from the ray tracing method can give useful information on an optical redesign. Besides, with the integration of ray tracing and finite element methods, the optical and thermal performance of a lighting system can be predicted in the design step without involving the costly fabrication and testing of multiple prototypes.

ACKNOWLEDGEMENTS

We would like to acknowledge Silver Light Enterprise and Sakpatthana Karn Kaset Company for their great cooperation and allowing us to use their product as study cases and thanks to the National Metal and Materials Technology Center (MTEC) for software and high performance computers used in this project.

REFERENCES

[1] V. Prasanna Kumar, R. Lakkumanan, and K. Prakasan, 2005. Computer aided optical design of reflectors in automotive headlights, IMechE, 220: 415-424.

[2] Y. Tabuchi, M. Hirata, M. Nakau, M. Nishimura and H. Satone, 1985. Lighting Calculation Procedure in the Room with the Louvered Ceiling and its Experimental Evaluation, J. Illm. Engng. Inst. Jpn., Vol 69, No.2: 25-37.

[3] M. Nishimura, M. Wada, S. Aiba and H. Satone, 1997. Theoretical Analysis of Lighting Calculation of Chromatic Color Louver, J. Illum. Engng. Inst. Jpn., Vol.81, No.2: 10-18.

[4] Hecht, E. Optics, 2003, Pearson Education, Inc.

[5] Murdoch, J.B., 1985. Illumination Engineering – From Edison's Lamp to the Laser, First Ed., Macmillan Publishing Company, New York, USA : 27-35.

[6] J. Hyaung Park, and J. Youb Sah, 2001. Design of Reflector Optics with Smooth Surface for Automotive Lamps, SAE, No. 2001-01-0457

A Study for Improvement of Production Efficiency in Hot Forging Processes Using the Finite Volume Method

Surasak Suranuntchai, Prarop Kritboonyarit,
Excellence Center in Sheet and Bulk Metal Forming Technology, Faculty of Engineering
King Mongkut's University of Technology Thonburi (KMUTT)
126 Prachauthit Rd., Bangmod, Thungkru, Bangkok 10140
Tel. 0-2470-9211 Fax: 0-2872-9080
*Email: surasak.sur@kmutt.ac.th

Abstract: When bulk materials are deformed by forging processes, they will flow in perpendicular to the motion of tools direction and their shapes are also followed by the geometry of designed dies. The limitation of forging processes depends on the tools life and the quality of finished products such as dies fracture, surface tearing and dimensional accuracy on workpieces. In the current research work, some critical problems found in industry where fabricates agriculture engine parts by hot closed-dies forging process have been studied. The main objective of this project focuses on the productivity improvement of such the product. Under the manufacturing circumstance of 1250 units by average observed, wrinkles were occurred on the workpiece surface near the shoulder area of deformed part as well as cracks were taken place on and insight forging dies. The closed-dies forging were made of SKD61 steel, which was hardened to the constant level of hardness about 56 HRC. The material for workpiece was S45C. The forging temperature was in the range of 1100◦C to 1250◦C and graphite was used as a lubricant. In order to search the causes of such defects formation above in the products during deformation, this investigation emphasized on two process parameters: the radius values in the region of corner and fillet of closed-dies forging. The reason for this is that both parameters affect the material flow inside the dies. From the numerical simulation results of forging processes obtained by employing the finite element (FE) commercial package called: MSC. SuperForge, it could be found that the material flow was improved when increasing the values of radius corner and fillet of forging dies. It has also been seen that a maximum density of material flow was happened in the position near the edge radius corner of closed-dies. With real experimental tests, in addition, it was shown that wrinkles occurred in the region around the shoulder of forged products tended to decrease with the increment of two process parameters mentioned, as well. After modification of dies shape by increasing the values of radius corner and fillet about 12.5 percents, the good numerical predictions have been achieved. However, when adding the blocker into such forging process, the results from simulation obtained showed that the deformation forces of finished dies tend to decrease. Thus, forging dies can make the number of products more than 5,000 units

Keywords: Production Efficiency Improvement, Hot Forging Processes, Finite Volume Method, MSC. SuperForge

INTRODUCTION

The production processes in the industries have very high competition in the present market. The objective is to meet all of customer satisfactions. Hot forging process is one of the processes that have great competition; therefore, technical design should be studied in details to reduce the cost. Mostly, the factory practices in solving manufacturing problems by trial and error, which consumes much of the cost and times.

Consequently, the analysis for the flow of metal during the deformation had been applied by using computer program which described by mathematical equation. The process parameters are designed and simulate in hot forging process in order to find out the suitable process conditions. Thus, reduced costs, save production times, and less wasted materials can be achieved which further increased process efficientcy and product qualities.

Corresponding Author: Surasak Suranuntchai, Excellence Center in Sheet and Bulk Metal Forming Technology, Faculty of Engineering King Mongkut's University of Technology Thonburi (KMUTT) 126 Prachauthit Rd., Bangmod, Thungkru, Bangkok 10140, Thailand

FORGING THEORY AND METHODS

Forging is the process by which metal is heated and is shaped by plastic deformation by suitably applying compressive force. Forging refines the grain structure and improves physical properties of the metal. With proper design, the grain flow can be oriented in the direction of principal stresses encountered in actual use[1]. Grain flow is the direction of the pattern that the crystals take during plastic deformation. Physical roperties such as strength, ductility and toughness are much better in a forging than in the base metal, which has, crystals randomly oriented[2]. Most machines in forging are power hammer, eccentric press, or hydraulic press. There are three different kind of forging which included:

1. Upsetting consist of blows that transfer the compressive energy to the outside of the product. Upseting increases cross-section by compressing the length of workpieces[3].
2. Spreading is a slow squeezing action of a press, to transfer a great amount of compressive force to the workpiece. The finished product is a rough approximation of the die[3].
3. Rising is impressions die forging and good precision are further refinements of the die surface. The finished part more closely resembles the die impression[3].

Comparision to Other Processes

Advantages

1. Good mechanical properties
2. Reduced voids between grain boundaries
3. High productivities
4. Grain refined
5. Less wasted material
6. Moderate surface finish and dimension accuracy
7. Most material can be forged

Disadvantages

1. Hot forging cause oxidation on part surface
2. High cost for tools and maintenance
3. Can not do complicated shape
4. Cost is higher than casting

Forging Die Design

In the design of forging die, several parameters should be considered for ease of to metal flow, precision parts, and good surface, which descibed as follow[4]:

• Draft angle on die all should be inclined which make possible removal of parts as shown in Fig. 1. Recommended draft angles are described in the following table.

Material Draft Angle	(°)
Aluminum	0 - 2
Copper Alloys	0 - 3
Steel	5 - 7
Stainless Steel	5 – 8

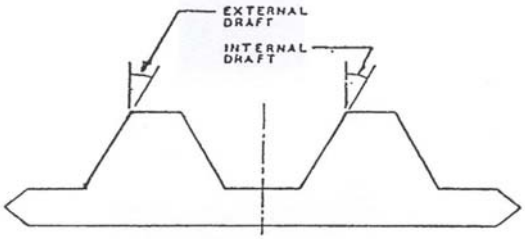

Fig. 1: Draft angle in forging die design

• Generous fillets and radius should be provided to aid in material flow during the forging process as shown in Fig. 2.

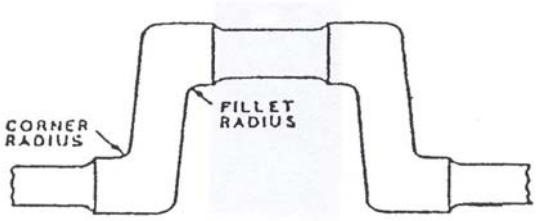

Fig. 2: Radius of corner and fillet design in forging parts.

Sharp corners are stress-risers in the forgings, as well as make the dies weak in service. Recommended minimum radiuses are described in the following table.

Height of Protrusion mm (in)	**Min. Corner Radius** mm (in)	**Min. Fillet Radius** mm (in)
12.5 (0.5)	1.5 (0.06)	5 (0.2)
25 (1.0)	3 (0.12)	6.25 (0.25)
50 (2.0)	5 (0.2)	10 (0.4)
100 (4.0)	6.25 (0.25)	10 (0.4)
400 (16)	22 (0.875)	50 (2.0)

• Parting surface should be along a single plane if possible, else following the contour of the part. The parting surface should be through the center of the part, not near the upper or lower edges. If the parting line cannot be on a single plane, then it is good practice to use symmetry of the design to minimize the side thrust forces.
• As in most forming processes, use of undercuts should be avoided, as these will make the removal of the part difficult, if not impossible.
• Ribs should not be high or narrow; this makes it difficult for the material to flow.
• A proper lubricant is necessary useful in preventing sticking of the workpiece to the die, and also acts as a thermal insulator to help reduce die wear.
• Finish allowance for precise forge part in further finishing surface should be 0.3~0.8 mm. which depend on different type of materials and size.

Tolerances:

• Dimension tolerances are usually positive and are approximately 0.3 % of the dimension, rounded off to the next higher 0.5 mm
• Die wear tolerances are lateral tolerances parallel to the parting plane and are roughly +0.2 % for Copper alloys to +0.5 % for Aluminum and Steel.
• Die closure tolerances are in the direction of opening and closing, and range from 1 mm for small forgings, die projection area < 150 cm ^{2}, to 6.25 mm for large forgings, die projection area > 6500 cm ^{2}.
• Die match tolerances are to allow for shift in the upper die with respect to the lower die. This is weight based and is shown in the the following table.
• Flash tolerance is the amount of acceptable flash after the trimming operation. This is weight based on type of materials and part weight.

Initial Billet Mass Calculation

$$m_A = m_E + m_G + m_Z \qquad (1)$$

which m_A = initial billet mass (kg.)
m_E = final part mass (kg.)
m_G = flash mass (kg.)
m_Z = burned scrap mass (kg.)

Forming Strain Rate

$$\dot{\varepsilon} = \frac{v}{h_0} \qquad (2)$$

which $\dot{\varepsilon}$ = strain rate (s^{-1})
v = blow velocity (mm/s)
h_o = initial height (mm.)

Forming Stress

$$k_f = k_{f1} \times \dot{\varepsilon}^{m} \qquad (3)$$

which k_f = initial stress / yielding for billet (N/mm^2) (temperature dependence)
k_{f1} = final forming stress (N/mm^2)
$\dot{\varepsilon}$ = strain rate (s^{-1})
m = power coeficient

Finite Volume Method, FVM

FVM handles basic regtangular element overall geometry as shown in Fig 3. These othogonal component grids satisfy normal and tangential fields at interfaces for various differential equations that describes discretized problems. Incontrary, finite element method FEM can represents better element nearly fit to geometry boundaries, which comsumes much of computational times[5].

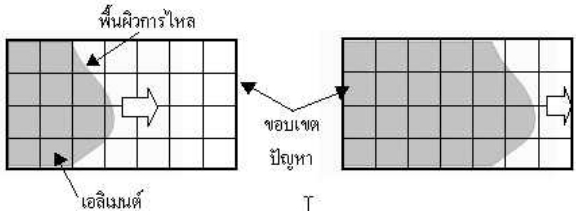

Fig. 3: Element structure in finite volume method.

RESULTS AND DISCUSSION

The forging parts were used in the agricultural machines for "Rotor Boss" as shown in Fig 4. The parts are made from steel S45C by hot forging process. Customers will order monthly for 4,500 pieces, which cost 47 baht per piece. The initial billet has diameter of 42 mm. and length 57.7 mm. which weights 0.627 kilograms. From the production reports, the factory found most of defect parts show in Fig 4. on November 2006 were approximately 10 percent as follow:

1. Wrinkle Overlap 267 pieces
2. Crack at corner 86 pieces
3. Out of Dimension 59 pieces
4. Unfilled part 38 pieces

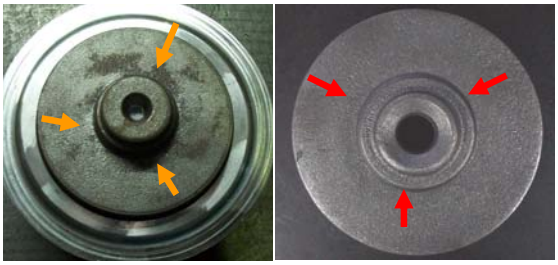

Fig. 4: "Rotor Boss" produced by hot forging. Wrinkle mostly occurred at part fillet.

From this experiment, the corner radius was designed at 1.75 mm., which had acceptable machining tolerance, and the fillet radius was designed at 2.25 mm. shown in Fig 5. By increasing the radius, metal flow during die impression increased linearly as shown in Fig 6. Thus the formability also increased as the radius increased[6] which favor metal force to squeeze excess materials to flash out through side gutter and reduced die impression pressure[7].

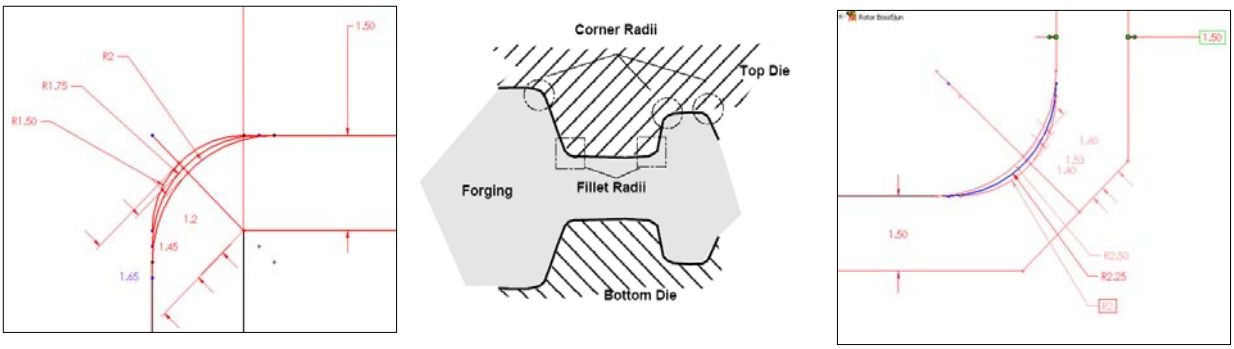

Fig. 5: Corner and fillet radius implemented on die.

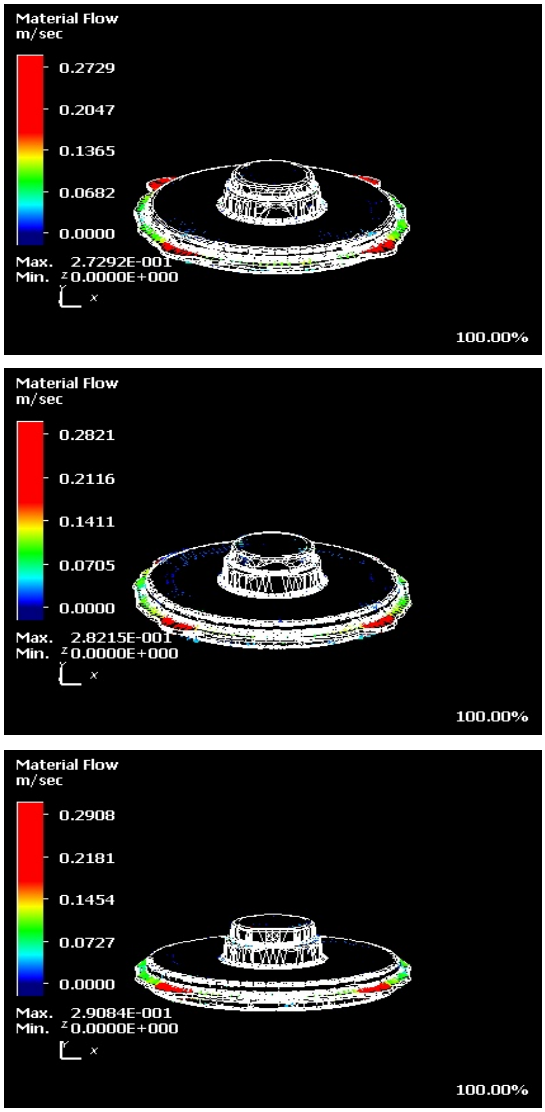

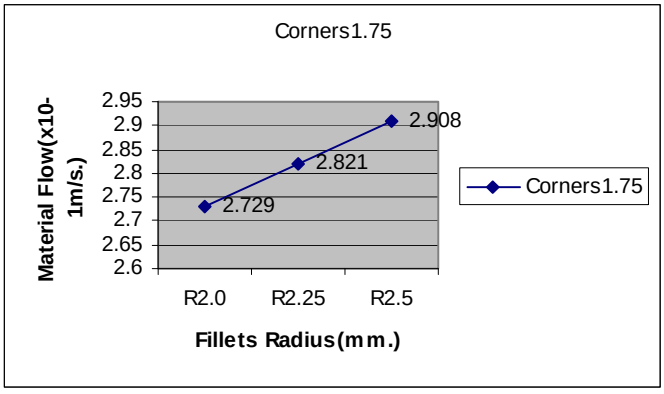

Fig. 6: Results for material flow using finite program MSC.SuperForge.

Cost Break Down Details	Old Design Cost (Baht)
Customer Order 4,500 pieces Defected parts 11% Produced = 4,995 pieces/order	
Materials: S45C Dia. 42. x 6,000 mm = 1,887 baht 6,000 ÷ 57.7 = 98 pieces 1,887 ÷ 98 = 19.255 baht/piece 4,995 x 19.255 =	96,178.73
Die Cost = 53,500 baht Die Life = 5,000 pieces 53,500 ÷ 5,000 = 10.70 baht/piece 4,995 x 10.70 =	53,447.50
Labor Cost: Man Hour 8 hours/day = 280 baht 1 piece produced for 8 seconds 4,995 x 8 ÷ 60 ÷ 60 = 11.10 hours 280 ÷ 8 x 11.10 =	388.50
Electricity: Electric cost 2.8 baht/Kwatt/hours Warm up 40 Hp machine 0.5 hour Included vat 7%: 2.8 x0.746 x40 x 1.07 x (11.1+0.5)=	1,037.05
Machine depreciated cost:	3,000.00
Total Cost Cost + 10% Accessories	169,456.96
Cost per pieces: 169,456.41 ÷ 4,500 =	. 37.66
Sale per order: 4,500 x 47 =	211,500.00
Benefits: 211,500 - 169,456.96 =	42,043.04
Break Even Point: 169,456.96 ÷ (47 – 37.66) = 18,143 pieces	

Cost Break Down Details	New Design Cost (Baht)
Customer Order 4,500 pieces Defected parts 6% Produced = 4,770 pieces/order	
Materials: S45C Dia. 42. x 6,000 mm = 1,887 baht 6,000 ÷ 57.7 = 98 pieces 1,887 ÷ 98 = 19.255 baht/piece 4,770 x 19.255 =	91,846.35
Die Cost = 53,500 baht Die Life = 6,300 pieces 53,500 ÷ 6,300 = 8.492 baht/piece 4,770 x 8.492 =	40,506.84
Labor Cost: Man Hour 8 hours/day = 280 baht 1 piece produced for 8 seconds 4,770 x 8 ÷ 60 ÷ 60 = 10.60 hours 280 ÷ 8 x 10.60 =	371.00
Electricity: Electric cost 2.8 baht/Kwatt/hours Warm up 40 Hp machine 0.5 hour Included vat 7%: 2.8 x0.746 x40 x 1.07 x (10.6+0.5)=	992.35
Machine depreciated cost:	3,000.00
Total Cost Cost + 10% Accessories	150,388.19
Cost per pieces: 150,388.19 ÷ 4,500 =	. 33.42
Sale per order: 4,500 x 47 =	211,500.00
Benefits: 211,500 - 150,388.19 =	61,111.81
Break Even Point: 150,388.19 ÷ (47 – 33.42) = 11,074 pieces	

CONCLUSION

From the experiment, hot forging had been analysis by using commercial software FVM program MSC.SuperForge. The modeling simulations were effectively describe the variation of design parameter that affected to forming process[8]. By varying fillet radius from 2 mm. to 2.25 mm. and corner radius from 1.5 mm. to 1.75 mm., the metal flow during the deformation from 2.554 m/s to 2.821 m/s, which increase by 10.45 percent. With redesign die, the wrinkle and others defects on parts greatly decreased from 11 percent to 6 percent. Lower stress on die can be appreciated by longer die life from 5,000 pieces to 6,300 pieces, which productivity increase 26 percent.

In the production of Rotor Boss, total costs were 169,456.96 baht, the part cost 37.66 baht, and the break even point was at 18,143 pieces for old die design. For the redesign die, total cost was 150,388.19 baht, the part cost 33.42 baht, and the break even point was at 11,074 pieces. Thus the company could earn higher profits of 19,068.77 baht. Aided by FVM in the analysis of particular hot forging problem[9][10], common benefit can be achieved by increase the overall productivity, process efficiency, and decrease trial and error time. The mechanical properties of part increase strength, more refine grain structure, and good surface fisished[11][12]. Thus the company was able to develop more technical skill designing more complicated parts in order to compete in the further market.

REFERENCES

1. American Society for Testing and Material, 1978, Standard Test Methods for Compression Testing of Metallic Materials Book of ASTM Standards, Vol. 3.01, Easton, p.266.
2. Dieter, G.E., 1988, Mechanical Metallurgy SI Metric ed., McGraw-Hill, Singapore, p.546.
3. Edward, M., 1991, Metalworking Science and Engineering, McGraw-Hill, New York, pp. 198-205.
4. Lange, K., 1985, Hand Book of Metal Forming, McGraw-Hill, New York, pp. (10.1)-(11.1).
5. Bhavin, V., Ibrahim., A.Z., and Jay., S., 2001, "Evaluations of MSC.SuperForge for 3D Simulation of Streamlined and Shear Extrusion Dies", Journal of Mechanical Engineering Ohio University ,Ohio, September, 2001.
6. Slagter, W.J., Florie, C.J.L., and Venis, A.C.J., 1999, "Forging Simulation Tool Based on Breakthrough Technology", MSC. Softeware Corporation, Netherlands.
7. J. Slagter, Hans, C.A., 2001, "Quality of Simulation Packages for Flashless Hot Forging Operations", Journal of Simulation of Material Processing, Hannover, September 2001.
8. Harshil, P., Bhavin, M., and Jay, G., 2001, "Forging Process Analysis and Preform Design", Journal of Ohio University, Mechanical Engineering Department, Faculty of Engineering Ohio University, Ohio.
9. C. Florie, A. Venis., 2000, "Advances in 3-D Forging Process Modelling", Journal of MSC. Software Corporation , Netherlands.
10. Arjaan, J. Buijk., 2000, "Application of the Finite Volume Method to Upset Forging of Cylinder", Journal of Forging Fair 2000, Ohio, April 2000.
11. Japanese Standards Association, 2001, "Ferrous Material & Metallurgy I", JIS Handbook, p. 303, 1140, 1516.
12. Olivier, B., Bernhart, G., 1999, "Methodology for service life increase of hot forging tools", Journal of Materials Processing Technology, Vol.87 101, France, pp. 237-246.

Effect of Co and Counter Flow to Transport Phenomena for Proton Exchange Membrane Fuel Cell by Numerical Simulation

Keerasut Suttanarak[1] Nirut Naksuk[2] and Jarruwat Charoensuk[1]
Department of Mechanical Engineering, Faculty of Engineering, King Mongkut's Institute of Technology Ladkrabang[1], National Metal and Materials Technology Center[2]

Abstract: The objective of this research is to study the effect of co-flow and counter-flow patterns in transport phenomena by taken into account temperature distribution along flow channels and mass fraction of hydrogen, oxygen and water from electrochemical reaction. The results are shown at two conditions i.e., 0.75 volt and 0.4 volt by taking into account the effect of electro-osmotic drag and back diffusion between anode and cathode. We found that at low current density co-flow gives slightly higher cell voltage than the counter-flow pattern due to better reaction, which reduces activation losses. On the other hand, at high current density, the counter-flow pattern gives higher voltage than the co-flow pattern apparently due to decrease in the concentration loss.

Key words: PEMFC, Electrochemical reaction, co flow, counter flow

INTRODUCTION

Proton Exchange Membrane Fuel Cell (PEMFC), with its zero emission and numerous future commercial prospects, is a promising future energy technology. To develop an efficient fuel cell system, it is necessary to understand its underline mechanisms such as non-uniform concentration, current density distributions, high ionic resistance due to dry membrane, or high diffusive resistance due to the flooding on the cathode. These phenomena can cause performance loss. Water management is a key challenging problem in PEMFC design and operation. Effective water management is a criticalrequirement to operate PEMFC at high current density. Membrane in PEMFC needs to be fully hydrated to conduct ionic current thus low resistive loss. However, excessive water can result in flooding in the catalyst layer or the diffusion layer. In the worst case, water in form of liquid will block the reactant flow channels. Numerical simulation is used to predict transport phenomena such as velocity, pressure and temperature distribution as well as investigate hydrogen, oxygen and water concentration along the channels, which contribute to different of flow distribution. Our investigation covers co-flow and counter-flow configuration at low and high current density.

Electrochemical Reaction in Fuel Cell

Fuel cell uses reactant gases in electrochemical process to generate electricity. The reaction could be explained as a hydrogen molecule flows into the channel and was broken into protons and electrons at the catalyst layer (on the surface of the catalyst) as shown in Eq. (1). The protons are carried through the membrane while electrons as negative current go through external load and ends up at the cathode side. At the cathode side, oxidation reaction takes place as an oxygen molecule combines with electrons and protons (hydrogen ion) and forming water molecules in vapor form as shown in Eq. (2). This process is called reduction. Thus, the products from the reaction are water and electrons. This process is shown in Fig.1

$$H_2 \rightarrow 2H^+ + 2e^- \quad (1)$$

$$O_2 + 4e^- + 4H^+ \rightarrow 2H_2O \quad (2)$$

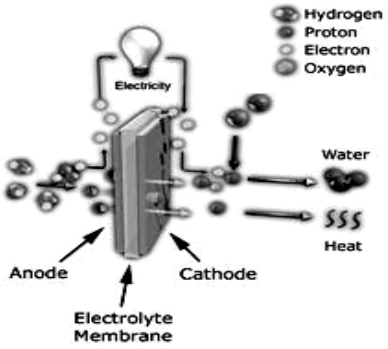

Fig. 1 Diagram of Fuel Cell operation [4]

Fuel Cell Efficiency

Electrical energy is obtained from a fuel cell only when reasonable current is drawn. Actual cell potential is decreased from its equilibrium potential because of irreversible losses as shown in figure 2. Several sources contribute to the irreversible losses. The losses, which are often called polarization, over potential, or over voltage, originate primarily from three sources including activation polarization, ohmic polarization and concentration polarization, respectively. These losses result in cell voltage less than its ideal potential.

Corresponding Author: Keerasut Suttanarak , Department of Mechanical Engineering, Faculty of Engineering, King Mongkut's Institute of Technology Ladkrabang, Thailand

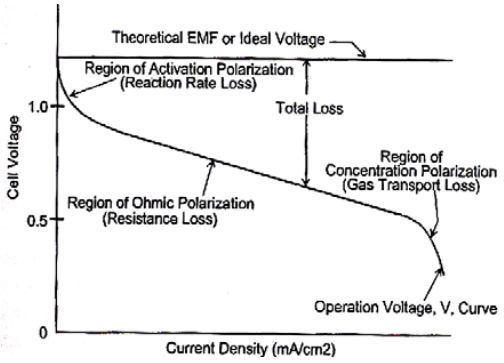

Fig 2 Fuel Cell Polarization Curve [4]

The activation polarization loss is dominant at low current density. At this region, electronic barriers have to be overcome prior to the flow of current or ion. Activation losses show some increase as current increases. Ohmic polarization loss varies linearly with the current, increasing over the whole range of current because cell resistance remains essentially constant through out the current density region. Gas transport losses occur over the entire range of current density, but these losses become prominent at high limiting currents where it becomes difficult to provide enough reactant flow to the cell reaction sites.

Mathematical modeling and computational Domain

The simulation based on conservation equation of mass, momentum, energy, current and species implementing on CFD software. The key elements of modeling are transport phenomena in porous media, heterogeneous reaction in porous electrodes and coupling between mass transport, electrochemical and current potential fields.

The Computational Domain includes anode and cathode flow channels, anode and cathode current collectors, anode and cathode Gas Diffusion Layers, anode and cathode Catalyst Layers and Membrane as shown in fig 3 and fig 6. In case of co flow, fuel and the reactant flow in same direction as shown in fig 4. Conversely, fuel and the reactant flow in the opposite direction in the flow channels as shown in fig 5.

In this section, we will present all governing equations involve in the process. First, the mass conservation equation can be written as Mass conservation

$$\nabla.(\varepsilon\rho u) = s_m$$

Where ε is porosity, ρ is mixture density and u is velocity vector.

s_m denote source terms corresponding to the consumption of hydrogen and oxygen in the anode and cathode, and the production of water in the cathode.

$$s_m = s_{H_2} + s_{aw} \quad : Anode\ side$$

$$s_m = s_{O_2} + s_{cw} \quad : Cathode\ side$$

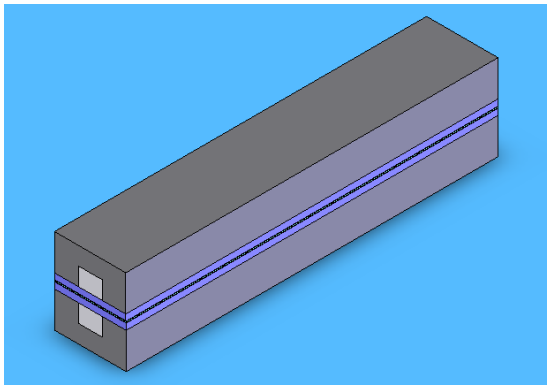

Fig 3 Computational Domain

Fig 4 Schematic of Co-flow

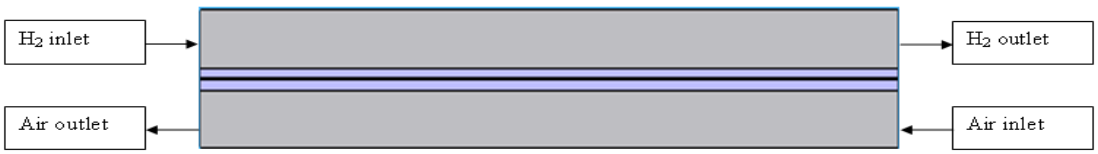

Fig 5 Schematic of Counter-flow

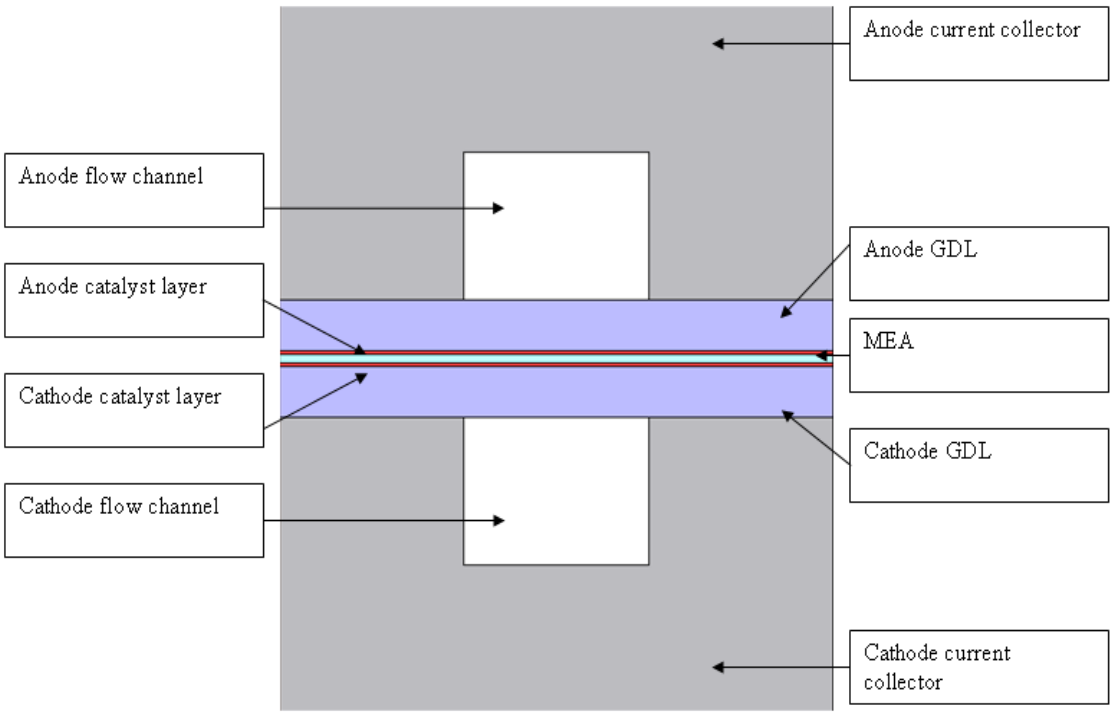

Fig 6 Cross-section Schematic of PEM Fuel Cell

Where subscript 'a' and 'c' refer to the anode and cathode respectively.

Momentum conservation

$$\nabla(\varepsilon\rho uu) = -\varepsilon\nabla p + \nabla(\varepsilon\mu\nabla u) + s_u$$

where p is pressure, μ is dynamic viscosity

s_u denote source term based on Darcy's law

$$s_{ux} = -\frac{\mu u}{\beta_x},\ s_{uy} = -\frac{\mu u}{\beta_y}\ and\ s_{uz} = -\frac{\mu u}{\beta_z}$$

where β is the permeability.

And the energy conservation relation can be written as

$$\frac{\partial}{\partial t}(\varepsilon\rho h) + \nabla.(\varepsilon\rho uh) = \nabla.q + \varepsilon\frac{dp}{dt} - j_T\eta + \frac{i.i}{\sigma} + S_h$$

Where h is mixture static enthalpy, i is current density, J_T is the transfer current, η is electrode over potential, σ is electrical conductivity, S_h is latent heat of phase change and q is heat flux due to thermal conductivity. The species diffusion equation above can be written as

$$q = k\nabla T + \sum J_i h_i$$

where k is the thermal conductivity, T is the mixture temperature and J_i is species diffusion flux. The species conservation equation can be written as

$$\nabla(\varepsilon\mu C_k) = \nabla(D_k^{eff}\nabla C_k) + s_k$$

Where C_k is Molar concentration of chemical species

D_k^{eff} is the effective diffusion coefficient and s_k denote source term

$$s_k = -\frac{I(x,y)}{2F}M_{H_2}A_{CV} \qquad :s_{H_2}$$

$$-\frac{\alpha(x,y)}{F}I(x,y)M_{H2O}A_{CV} \qquad :s_{aw}$$

$$-\frac{I(x,y)}{4F}M_{O_2}A_{CV} \qquad :s_{O_2}$$

$$-\frac{1+2\alpha(x,y)}{2F}I(x,y)M_{H2O}A_{CV} \qquad :s_{cw}$$

where M_{H2}, M_{H2O} and M_{O2} are the molecular weight of hydrogen, water and oxygen respectively and $I(x,y)$ is the local current density, F is Faradays constant, $\alpha(x,y)$ is the local net water transfer coefficient per proton and A_{CV} is the specific surface area of control volume element in the domain.

Water management is a critical issue for the performance of a proton electrolyte membrane fuel cell.

The transport phenomena of water can be described as follows.

First, the water molecules are transported through the polymer electrolyte membrane by the hydrogen protons and this process is called electro-osmotic drag. In addition to the molecular diffusion and electro-osmotic drag, water is generated in the cathode catalyst layer due to electrochemical reaction.

1) Electro-osmotic water flux going through the membrane can be calculated from the proton flux going through the membrane, given by the specified current density and Faraday law as

$$j_{H2O} = 2\,x\,n_d\,\frac{I(x,y)}{2F}$$

n_d is Electro-osmotic drag coefficient which depend on water activity as follow

$$n_d = 0.029\lambda^2 + 0.05\lambda - 3.4x10^{-19}$$

where λ represents water content of the membrane described as

$$\lambda = 0.043 + 17.81a_k - 39.85a_k^2 + 36a_k^3 \;; 0 < a_k < 1$$

$$\lambda = 14 + 1.4(a_k - 1) \;; 1 < a_k < 3$$

where a_k is water activity

$$a_k = \frac{x_{wk}\,p(x,y)}{p_{wk}^{sat}} \quad ;\ k \text{ is Anode or Cathode}$$

Where x_{wk} *and* p^{sat} are water mole fraction and saturation pressure at each electrode respectively therefore

$$\log_{10} p^{sat} = -2.1794 + 0.02953T - 9.1837x10^{-5}T^2 + 1.4454x10^{-7}T^3$$

2) For the back diffusion flux, the water formation at the cathode results in a gradient in the water content between the cathode side and anode side of the membrane. For PEMFC, this gradient causes a water flux back to anode side which is superimposed to the electro-osmotic flux. This back diffusion is expressed as following water flux as

$$J_{H2O} = -\frac{\rho}{M}\,xD_w\,x\frac{d\lambda}{dz}$$

where ρ is the dry density of electrolyte, M is electrolyte equivalent weight, z is the direction through the membrane thickness and D_W is water diffusion coefficient therefore

$$D_w = D_\lambda \exp(2416x(\frac{1}{303} - \frac{1}{T_{cell}}))$$

where

$$D_\lambda = 10^{-10} \;; \lambda < 2$$

$$D_\lambda = 10^{-10}(1 + 2(\lambda - 2)) \;; 2 \le \lambda \le 3$$

$$D_\lambda = 10^{-10}(3 - 1.67(\lambda - 3)) \;; 3 < \lambda < 4.5$$

$$D_\lambda = 1.25x10^{-10} \;; \lambda \ge 4.5\,.$$

The model assumptions we adopted in this paper are

1) Steady state
2) Laminar flow
3) Isothermal
4) Incompressible fluid
5)Butler-volmer equation is used describe electrochemical reaction.
6) Reactant species include H_2, O_2, N_2 and H_2O (vapor) were considered.
7) The volume of liquid H_2O was assumed to be negligible in the domain.
8) The gravity effect was negligible.

Table 1 Model parameters

Parameters	value
Channel width (mm)	0.8
Channel high (mm)	0.6
Channel length (mm)	125
Rip width (mm)	0.8
GDL thickness (mm)	0.21
Catalyst thickness (mm)	0.012
Membrane thickness (mm)	0.036
Operating pressure (Mpa)	0.1
Operating temperature (K)	353

Results and discussion

Based on the computational result of the temperature distribution along the channels at the cell potential of 0.75 volt in both co-flow and count-flow cases, we found that the temperature in anode flow channel is higher than cathode flow channel. The higher temperature could be the result of higher specific heat and velocity of hydrogen.

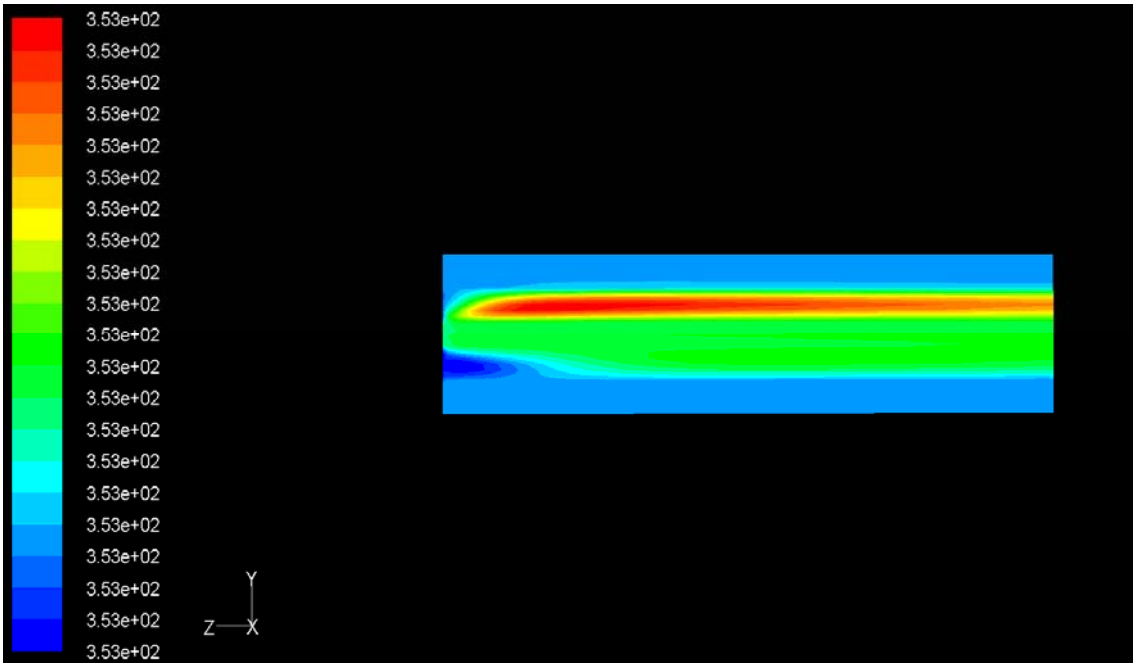

(a)

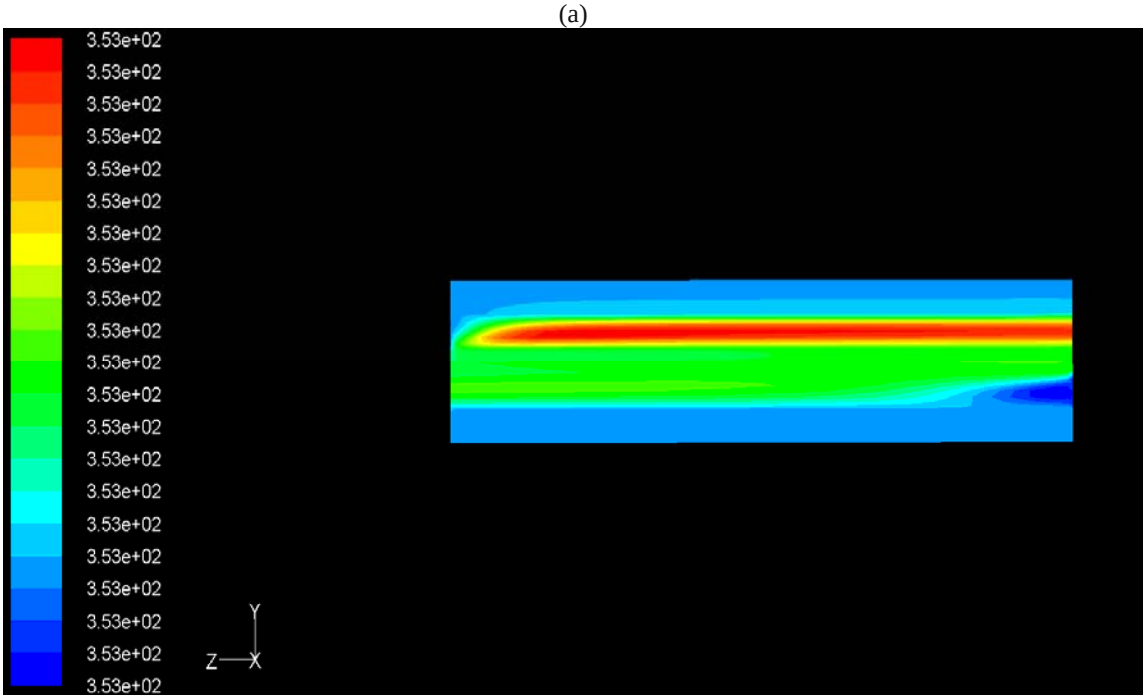

(b)

Fig 7 Temperature distribution at 0.75 volt
(a)Temperature distribution of Co-flow
(b)Temperature distribution of Counter-flow

Electrochemical reaction occurred at the cathode side in shown in fig 7. The temperature distribution of hydrogen in the co-flow pattern was higher initially then it decreased gradually. In contrast, the temperature in the counter flow configuration does not decrease along the length of the channel as illustrated in fig 7a and 7b. The mass fraction of hydrogen and oxygen gas was slightly decreased along the channel. We also noticed that the hydrogen gas in co-flow configuration was diffused with higher amount than in the counter flow pattern, while the water mass fraction at anode was increased due to the water diffuse though the membrane from cathode side. Water mass fraction at cathode side was decreased along the flow channel as shown in fig 8.

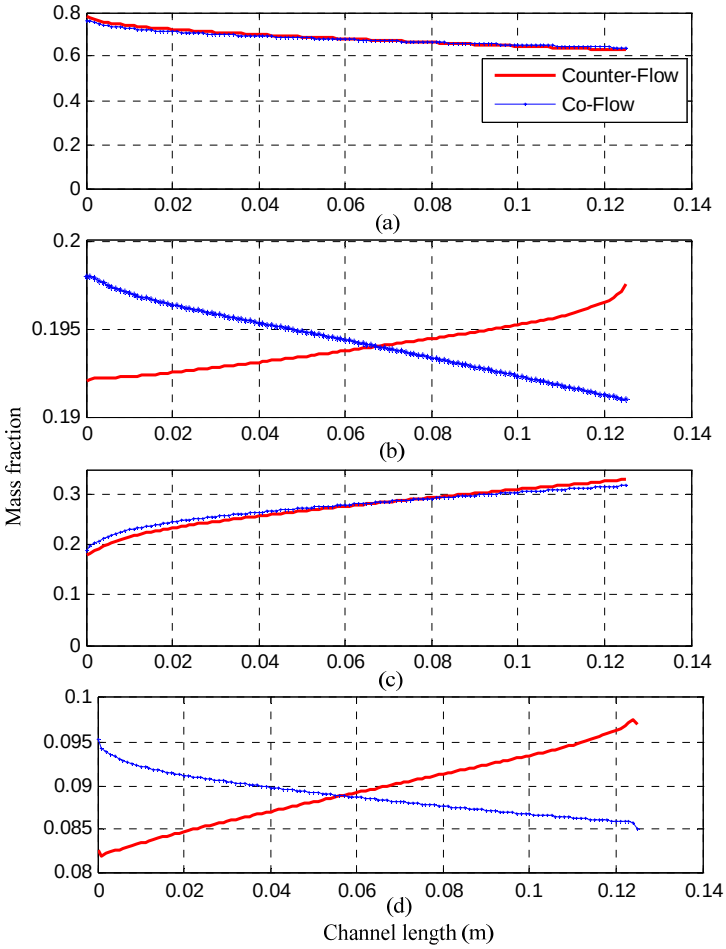

Fig 8 Mass fraction along channel of co and counter flow at 0.75 volt
(a) Hydrogen mass fraction along channel
(b) Oxygen mass fraction along channel
(c) Water mass fraction at anode catalyst layer
(d) Water mass fraction at cathode catalyst layer

Temperature distribution along the channels, mass fraction of hydrogen and oxygen, and water mass fraction of both flow configurations at the cell potential 0.4 volt are shown in fig 9 to 10. At cell potential equal to 0.4 volt, we found that the counter-flow pattern yield more even temperature distribution in the high temperature area comparing with the co-flow pattern.

We also found that high temperature occurred around membrane, catalyst layer and GDL especially in cathode side (the highest). As we known that the water product takes place at this area, thus this heat is reasonably the result of formation and latent heat of water.

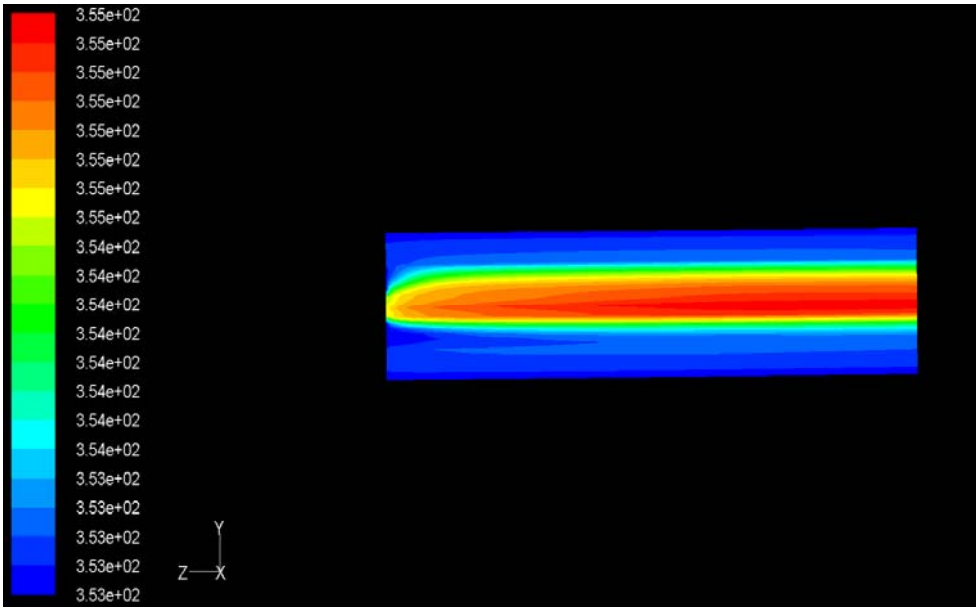

(a)

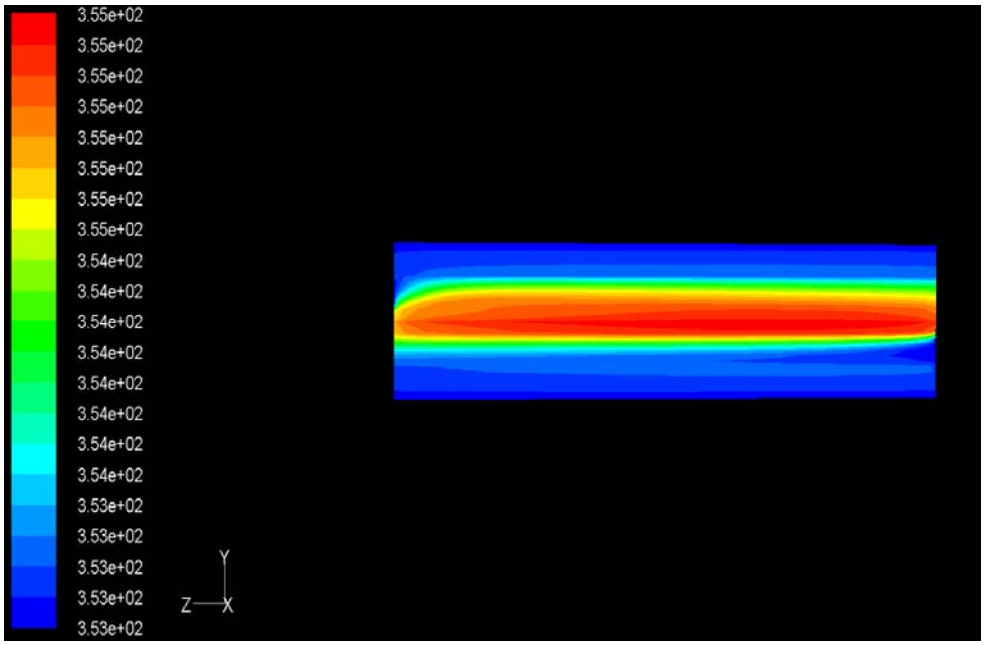

(b)

Fig 9 Temperature distribution at 0.4 volt
(a) Temperature distribution of co-flow
(b) Temperature distribution of counter-flow

We also found that the hydrogen mass fraction was decreased gradually along the channel in anode side especially in case of counter flow. In this case, hydrogen as well as oxygen was consumed more than co flow. This is due to the higher electrochemical reaction. The water mass fraction in the anode side was increased gradually along the channel due to the effect of water back diffusion from the cathode side. Meanwhile the higher water mass fraction was occurred at the cathode side due to the effect of electro-osmotic drag and the water formation from electrochemical reaction. When we compare water mass fraction of co and counter flow,

we found that the water mass fraction at the cathode catalyst of the counter flow was higher than the co flow, which implied that it achieved better reaction.

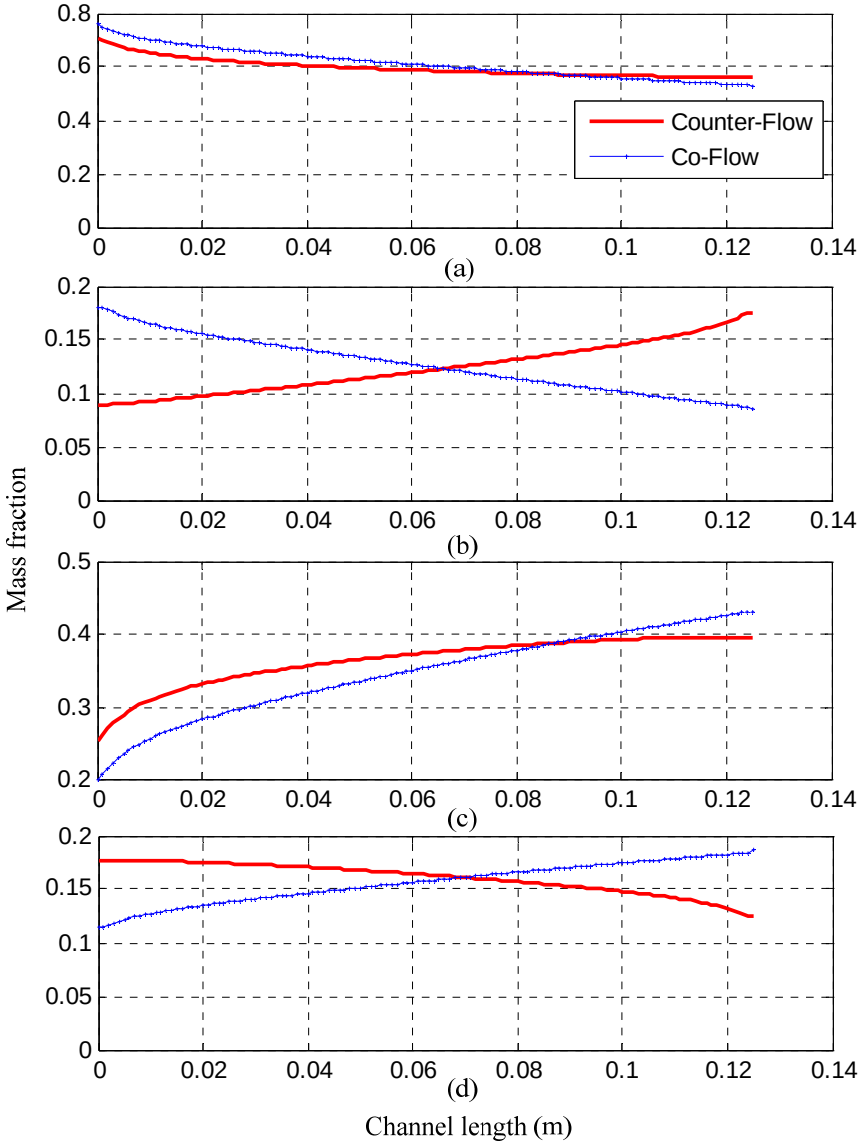

Fig10 Mass fraction along channel of co and counter flow at 0.4 volt
(a) Hydrogen mass fraction along channel
(b) Oxygen mass fraction along channel
(c) Water mass fraction at anode catalyst layer
(d) Water mass fraction at cathode catalyst layer

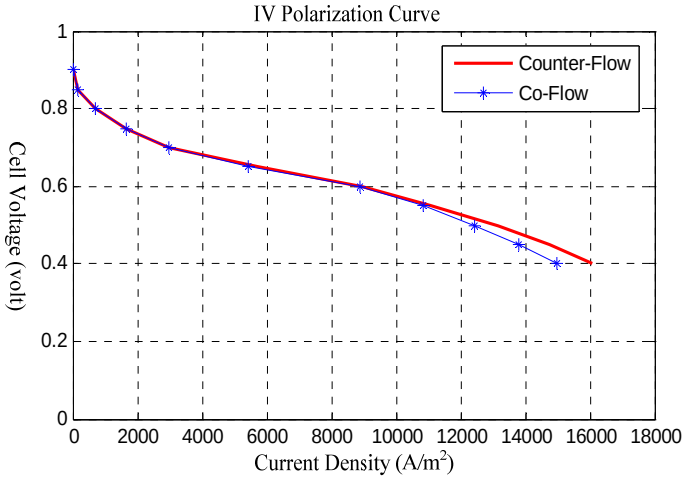

Figure 11 IV Polarization Curve

In Fig 11 is shown the comparison between IV Polarization Curve of Co-flow and Counter-flow patterns in low current operating condition. The result shows that the co-flow pattern gives slightly higher cell voltage than the counter-flow pattern. The reason may due to better reaction resulting in the reduction of the activation losses. On the other hand, at high current density, we found that the counter-flow pattern gives better cell performance than the co-flow pattern. This could be due to the counter-flow pattern can reduce concentration losses at high current density.

Conclusion

In this paper, numerical simulations are used as a tool to investigate the transport phenomena of Proton Exchange Membrane Fuel Cell. The study includes the temperature distribution of hydrogen, oxygen and water concentration along the flow channels. Particularly, co-flow and counter-flow patterns were studied at the operating potential of 0.75 and 0.4 volt. The results show that at low current, co-flow pattern gives slightly higher cell voltage than counter flow due to better reaction. We also found that at high current density the counter-flow pattern has higher cell voltage than co-flow pattern obviously due to the reduction of concentration losses.

Acknowledgement

The author would like to thank Electrochemical Materials and Systems Laboratory, National Metal and Materials Technology Center for the software package used in this research.

References

1. Barbir, F.**, "**PEM fuel cell theory and practice,**"** California Elsevier Academic Press, 2005.
2. Larminie, J., and Dick, A., **"**Fuel cell system explained**,"** Chichester John Wiley & Son, 2000.
3. Kumar, A., and Reddy, G.**, "**Effect of channel dimensions and shape in the flow-field distributor on the performance of polymer electrolyte membrane fuel cells,**"** Journal of Power Sources, vol. 113, pp 11–18, 2003.
4. N. Jaruwasupant and Y. Khunatorn "Three-dimensional model and experiment of new flow field for proton exchange membrane fuel cell using CFDRC**"** International Conference on Green and Sustainable Innovation, November 29th – December 1st 2006 Chiang Mai, Thailand. 7. Barabesi, L. and C. Pisani, 2002. Ranked set sampling for replicated sampling designs. Biometrics, 58: 586-592.

5 ZHUGE,W.,ZHANG, Y., MING, P., LAO, X., CHEN X., "Numerical simulation of three-dimensional gas/liquid two-phase flow in a proton exchange membrane fuel cell**"** Energy Power Eng. China, pp 305-310, 2007.

6. Pil Hyong,L., Sang Seok ,H.,Sang Soon, "Three-Dimensional Transport Modeling for Proton Exchange Membrane(PEM) Fuel Cell with Micro Parallel Flow Field", 2008.

Monochromator Selection, Crystal Design & Replacement of X-ray Tubes

[1]Md. Motasim Billah, [2]Md. Masum Billah and [2]Soheli Farhana
[1]Department of Physics, Jahangirnagar University, Dhaka, Bangladesh
[2]Faculty of Engineering, International Islamic University Malaysia (IIUM), Jalan Gombak, 53100 Kulala Lumpur, Malaysia.

Abstract: The investigation of Al, Ca, Cr, Co, Au, Ir, Fe, Pb, Ni, Pd, Pt, Si, Ag, Ta and W have been done to calculate the atomic scattering factors, structure factors, refraction effects, energy resolution to identify the good monochromatic behavior of thirteen elements. We have also considered the effect of temperature on the atomic scattering factor of every element by using the formula $f = f_0 e^{-M.}$ The results have been utilized to design a suitable monolithic monochromator which would provide a fixed wavelength device. Silicon is found to be the best selection out of all the thirteen elements. All X-ray tube wavelengths can be replaced by silicon monolithic monochromator in synchrotron X-ray beam line. We have designed the mono chromator corresponding to the X-ray tube wavelengths of λ = 0.711Å (Mo Kα), 0.632Å (Mo Kβ), 1.542Å (Cu Kα), 1.392Å (Cu Kβ), 1.790Å (Co Kα), 1.621Å (Co Kβ), 2.291Å (Cr Kα) and 2.085Å (Cr Kβ) by simply choosing the (h_1,k_1,l_1) and (h_2,k_2,l_2) indices of Silicon.
Keywords: scatter, refraction effects, monolithic monochromator

INTRODUCTION

The high power associated with the X-ray beams generated by the third generation synchrotron radiation facilities has created new challenges in the design of the beam line components that intercept the X-ray beams. The challenge is especially critical in the design of the monochromators, which must provide acceptable performance under the thermal load of the X-ray beams. Research activities in the development of monochromators for more stable and less complicated beam lines has led to examination of many aspects of the monochromators design[1]. In synchrotron radiation, it is of high importance to have the fixed wavelength for lattice parameter determination and many solid state experiments. We can get the any desired wavelength by tuning the Bragg angle of Si (111) in general. X-Ray tubes has a wavelength of λ = 0.711Å (Mo $K\alpha$), 0.632Å (Mo $K\beta$), 1.542Å (Cu $K\alpha$), 1.392Å (Cu $K\beta$), 1.790Å (Co $K\alpha$), 1.621Å (Co $K\beta$), 2.291Å (Cr $K\alpha$) and 2.085Å (Cr $K\beta$). We intended to obtain those wavelengths from synchrotron radiation X-ray beam line. From this point of view we have considered 13 elements to characterize them in terms of their structure factors, effect of temperature factors on atomic scattering factors[2] by using the equation $f = f_0 e^{-M}$, refraction effects, and energy resolution. We have calculated all these factors and effects. Finally we found silicon is the best choice for the monochromator. In addition, monolithic structure gives the stability of the wavelength. Finally we have designed the monolithic monochromator corresponding to the X-ray tube wavelengths, perhaps for the first time.

We select a monochromator from its four characteristics, which are discussed below:

- **Effect of Temperature Factor on the atomic Scattering Factor**

The thermal vibrational amplitude of the atom will have an affect on X-ray scattering[3]. We need any quantitive information about the temperature factor e^{-2M}, but it is convenient to describe the calculation. Formally, we allow for the effect by defining f as the atomic scattering factor of an atom undergoing thermal vibration, f_0 as the same quantity for an atom at rest, and relating the two by, $f = f_0 e^{-M}$.

- **Resolution Provided by the Monolithic Monochromator (MM)**

The full width at half maximum (FWHM) of the reflection range of MM is also determined by the dynamical theory of diffraction & is given by[4]:

Corresponding Author: Md. Motasim Billah, Department of Physics, Jahangirnagar University, Savar, Dhaka, Bangladesh, E-mail: lipu_ju@yahoo.com / liton_aub@yahoo.com

$$\Delta\theta = 2C\frac{\chi_g\left(\gamma_g/\gamma_o\right)^{1/2}}{\sin 2\theta_B} \quad (1)$$

$$\chi_g = -\frac{\chi_e\lambda^2 F_h}{\pi V_c}$$

Where χ_e is the classical electron radius, F_h is the atomic structure factor, V_c is the volume of the unit cell, λ is the wavelength, C is the polarization factor & c=1 for σ polarization & C = cos $2\theta_B$ for π polarization vector. We note that (γ_g/γ_o) = 1 for symmetric reflection. The energy resolution is given by $\Delta\lambda/\lambda$ or $\Delta E/E = \cot\theta\,\Delta\theta$

Then from equation (1),

$$\Delta\theta = \frac{2c\left(\gamma_e\right)\lambda^2 F_h}{\pi V_c \sin 2\theta_B} = \frac{2\lambda^2 F_h}{\pi V_c \sin 2\theta_B}$$

- **Refractive Index**

For the correction of wavelength measurement, refractive index plays an important role. The refractive index is defined as the ratio of the phase velocities in vacuum & in the medium c/v_q because v_q is complex, we get complex refractive index μ_c. The partial refractive index for q-type electron[4]:

$$\mu_{c,q} = \mu_q - i\mu_{i,q} = 1 - \delta_q - i\beta_q$$

$\mu_q = 1-\delta_q$ is the real part of $\mu_{c,q}$. The unit determent δ_q gives the departure of μ_q from 1 for x-ray frequencies.

$$\delta_q = \frac{2\pi n_q e^2 m\left(w^2 - w_q{}^2\right)}{\left[m^2\left(w^2 - w_q{}^2\right) + 4e^4 w^6/9c^6\right]}$$

$$\Rightarrow \delta_q \approx \frac{2\pi n_q e^2}{m\left(w^2 - w_q{}^2\right)}$$

For the X-ray frequencies ($w >> w_q$)

$$\delta = \sum\delta_q = \frac{2\pi e^2\sum n_q}{\left[m^2\left(w^2 - w_q{}^2\right)\right]}$$

$$\Rightarrow \delta = 2\pi e^2\sum n_q/m(w^2)$$

$$\Rightarrow \delta = e^2 n\lambda^2/(2\pi mc^2)$$

For X-rays being dispersed by crystals, the unit determinant δ is a small positive quantity & $\mu = 1-\delta \le 1\,(for\ x-rays)$, [in the glass prism $\mu \ge 1$]. It follows that for x-rays the medium of a crystal is less dense than a vacuum. If $N_A = 6.0225\text{x}10^{23}$ is Avogadro's number, A = Atomic weight, Z = Atomic number, ρ = density, then the above equation gives with

$$n = ZN_A\rho/A \;\&$$

$$\delta/\lambda^2 = e^2 ZN_A\rho/\left(2\pi mAc^2\right)$$

$$\delta/\lambda^2 = 2.7\times10^{10} Z\rho/A = cons\tan t\left(\lambda \le \lambda_k\right)$$

- **Structure Factor Variation in Lower & Higher Indices**

The resultant wave scattered by all the atoms of the unit cell is called the structure factor, because it describes how the atom arrangement, given by *uvw* for each atom, affects the scattered beam. The scattered factor, designated by the symbol *F*, is obtained by simply adding together all the waves scattered by the individual atoms. If a unit cell contains atoms 1, 2, 3… N, with fractional coordinate's $u_1\ v_1\ w_1$, $u_2\ v_2\ w_2$, $u_3\ v_3\ w_3$, … and atomic scattering factors f_1, f_2, f_3, …., then the structure factor for the *hkl* reflection is given by

$$F = f_1 e^{2\pi i(hu_1+kv_1+lw_1)} + f_2 e^{2\pi i(hu_2+kv_2+lw_2)} + f_3 e^{2\pi i(hu_3+kv_3+lw_3)} + \ldots$$

This equation may be written more compactly as

$$F_{hkl} = \sum f_n e^{2\pi i(hu_n+kv_n+lw_n)}$$

where the summation extends over all the N atoms of the unit cell. We have calculated the structure factor for the thirteen elements (Al-W). From Table-4, we find the lowest value of the structure factor for $Si_{(111)}$ = 40.7,

thus provides the good energy resolution from other elements.

MONOCHROMATOR SELECTION CALCULATION

(1) Atomic scattering factor with and without the effect of temperature factor

Table 1, represents the difference 'Δf' of atomic scattering factor with and without the effect of temperature factor, at the end point of the curves. Silicon is found to have the lowest Δf as shown in Fig-1.

Table 2,3 & 4 represents the calculation for energy resolution, refractive index correction and structure factors for the elements Al, Ca, Cr, Co, Au, Ir, Fe, Pb, Ni, Pd, Pt, Si, Ag.

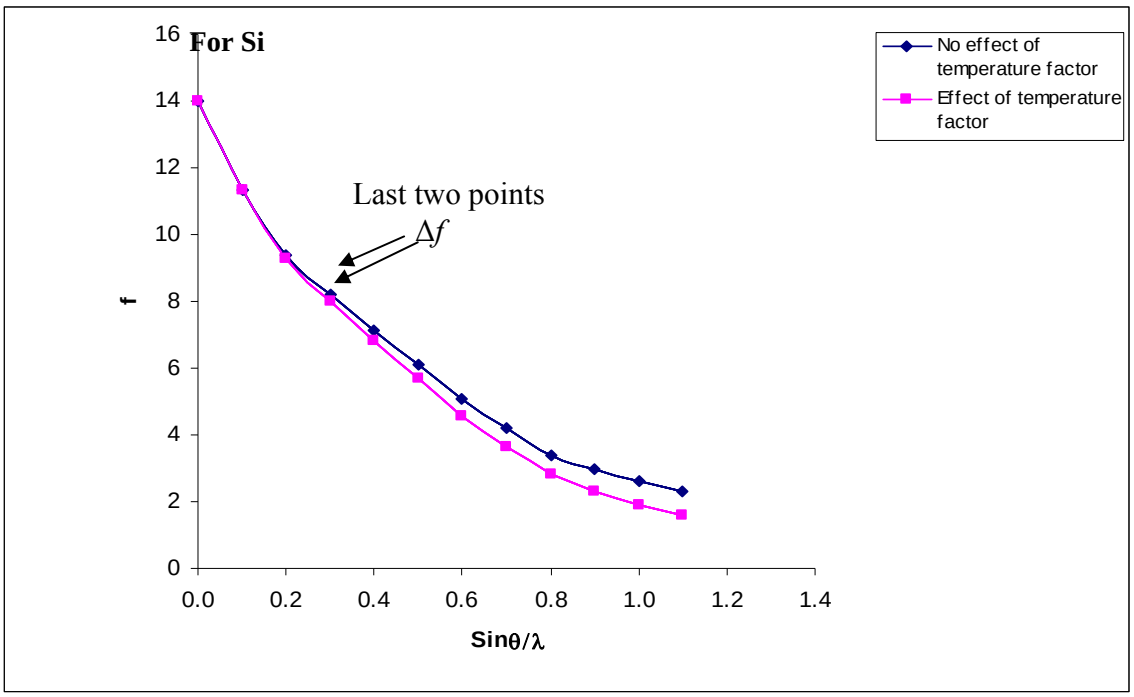

Fig. 1: Silicon graph

Table 1: Difference of atomic scattering factor with and without the effect of temperature factor line(Δf)

Name of the elements	(Δf)Difference between last two points
Cu	3.27
Al	1.3
Ca	3.28
Ir	6.24
Fe	2.04
Ni	2.44
Co	2.22
Pb	23.50
Si	0.71
Au	13.23
Pd	5.33
Pt	8.89
Ag	7.72

(2) Energy Resolution:

Table 2: calculation for energy resolution

Element	$\Delta\theta$ for lower indices	$\Delta\theta$ for higher indices
Cu	4.12 (111)	2.48 (420)
Al	3.23 (111)	1.27 (422)
Ca	1.18 (111)	0.43 (444)
Ir	10.10 (111)	11.21 (422)
Fe	3.21 (111)	2.08 (420)
Ni	3.80 (111)	3.76 (420)
Co	3.59 (111)	2.93 (420)
Pb	6.74 (111)	2.92 (620)
Si	0.80 (111)	0.48 (444)
Au	9.26 (111)	9.23 (333)
Pd	5.58 (111)	4.37 (422)
Pt	9.77 (111)	7.40 (422)
Ag	5.19 (111)	5.44 (333)

(3) Refractive Index Correction:

Table 3: calculation for refractive index correction

Element	Refractive Index 'δ'
Cu	2.61×10^{-5}
Al	8.35×10^{-6}
Ca	4.90×10^{-6}
Ir	5.80×10^{-5}
Fe	2.35×10^{-5}
Ni	2.6×10^{-5}
Co	2.58×10^{-5}
Pb	2.9×10^{-5}
Si	7.44×10^{-6}
Au	4.96×10^{-5}
Pd	3.3×10^{-5}
Pt	5.5×10^{-5}
Ag	2.9×10^{-5}

(4) Structure Factor Variation for Lower and Higher Indices

Table 4: calculation for Structure Factor

Element	F for lower indices	F for higher indices
Cu	88.3 (111)	44.3(420)
Al	88.4 (111)	16.7 (422)
Ca	632 (111)	28.4 (444)
Ir	246.2 (111)	150.2 (422)
Fe	70.3 (111)	40.2 (420)
Ni	77.2 (111)	42.55 (420)
Co	73.7 (111)	41.1 (420)
Pb	280.8 (111)	168.0 (620)
Si	40.7 (111)	18.9 (444)
Au	256.8 (111)	153.4 (333)
Pd	139.7 (111)	80.4 (422)
Pt	249.7 (111)	153.9 (422)
Ag	145.4 (111)	81.5 (333)

CRYSTAL DESIGN

The starting point of our Monolithic Monochromator design is the Bragg's law. In order to obtain suitable wavelength from Monolithic Monochromator, we solve the following equations:

$$\lambda_1 = 2d_1 \sin\theta_1 \left(1 - \frac{\delta}{\sin^2\theta_1}\right)$$

$$\lambda_2 = 2d_2 \sin\theta_2 \left(1 - \frac{\delta}{\sin^2\theta_2}\right)$$

$$\theta_1 + \theta_2 + \beta_0 = \pi$$

$$\lambda_1 = \lambda_2$$

Solving the four equations yields after simplifications, we get

$$\lambda = \frac{2d_1 \sin\beta_0}{\left[\left(\sqrt{\frac{d_1}{d_2}} - \cos\beta_0\right)^2 + \sin^2\beta_0\right]^{1/2}}$$

where δ represents the refraction related correction and β_0 is the interplanar angle between the two planes, d_1 and d_2 are the two lattice planes of monochromator and θ_1 and θ_2 are corresponding two Bragg angles in vacuum. Monolithic monochromator crystal design MMCD computer program[4] can generate different wavelengths using (h_1, k_1, l_1) & (h_2, k_2, l_2). We can generate this planes using Bragg equation $2d \sin\theta = n\lambda$. Several monolithic monochromators of wavelengths λ = 0.711Å (Mo $K\alpha$), 0.632Å (Mo $K\beta$), 1.542Å (Cu $K\alpha$), 1.392Å (Cu $K\beta$), 1.790Å (Co $K\alpha$), 1.621Å (Co $K\beta$), 2.291Å (Cr $K\alpha$), 2.085Å (Cr $K\beta$) are designed by the Si of suitable lattice planes. In silicon we can find the lattice parameter a = 5.431061 Å. Now one can design the monochromatic crystal using the parameters given in Table-1. As an example, designing of 0.711Å (Corresponds to Mo $K\alpha$) monochromator is given below:

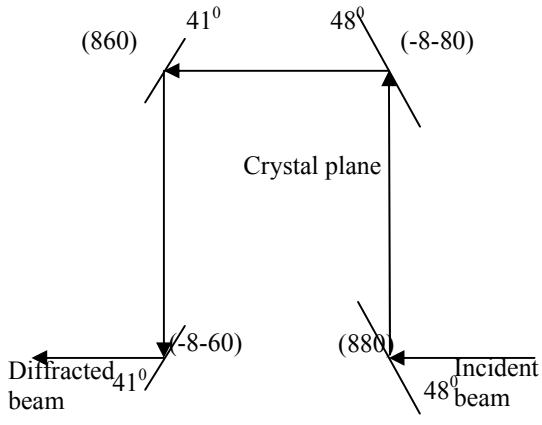

Fig. 2: Design of Si monolithic monochromator for λ = 0.711Å

RESULTS AND DISCUSSION

From all the studies, we select the silicon is the averaging best monochromator for its various characteristic properties as it has low temperature effect, it has a low $\Delta\theta$, it has a lower value of refractive index and structure factor. We have designed the monolithic monochromator by using the Silicon element. For the replacement of X-ray tubes, various design parameters and lattice planes (h_1 k_1 l_1, h_2 k_2 l_2), are given below (Table 5):

Table 5: Design parameters and lattice planes

$\lambda = \lambda_1 = \lambda_2$	θ_1	θ_2	β_0	$h_1k_1l_1$	$h_2k_2l_2$
0.711Å (Mo $K\alpha$)	48^0	41^0	91^0	8 8 0	8 6 0
0.632Å (Mo $K\beta$)	51^0	38^0	91^0	9 7 7	7 7 3
1.542Å (Cu $K\alpha$)	65^0	24^0	91^0	6 2 0	2 2 0
1.392Å (Cu $K\beta$)	64^0	25^0	91^0	7 0 0	3 1 1
1.790Å (Co $K\alpha$)	60^0	29^0	91^0	5 1 1	3 0 0
1.621Å (Co $K\beta$)	58^0	31^0	91^0	4 4 0	2 2 2
2.291Å (Cr $K\alpha$)	65^0	24^0	91^0	3 3 1	1 1 1
2.085Å (Cr $K\beta$)	53^0	36^0	91^0	3 3 0	3 1 0

CONCLUSION

X-ray tubes are very expensive. In X-ray tube we get the wavelengths of 0.711Å (Mo $K\alpha$), 0.632Å (Mo $K\beta$), 1.542Å (Cu $K\alpha$), 1.392Å (Cu $K\beta$), 1.790Å (Co $K\alpha$), 1.621Å (Co $K\beta$), 2.291Å (Cr $K\alpha$) and 2.085Å (Cr $K\beta$) respectively. Now, we replace all the tubes by simple silicon. If we cut a monochromator of (880) and (860) planes of silicon, we can get the wavelength of 0.711Å using the synchrotron radiation, thus solve the purpose of X-ray tube of (Mo $K\alpha$) source. Thus all tubes are replaced by Silicon monolithic monochromator. Now from this study, one can design the monochromator using the parameter given in Table 5 and replace the X-ray tubes according to one's need for the experiment.

REFERENCES

1. "Development of a Double Crystal Monochromator", Tom Kupp, Brasil Blank, Alex Deyhim. Eighth International Conference on Synchrotron Radiation Instrumentation, 2003, CA, USA.
2. B.D. Cullity, "Element of X-ray Diffraction", Addition-Wesley publishing company, Inc. (1967).
3. Diffraction basis, part 2, prepared by James R. Connoly, for EPS 400-002, Introduction to X-ray powder diffraction, (spring 2005).
4. Rahman M.O., Doctoral thesis; " Design, fabrication & performance of Silicon Monolithic Monochromators & its application for lattice spacing measurements of Si & GaAs single crystals with synchrotron radiation", Graduate Univ. for Advanced Studies, Japan, (2002).

Comparative study of Low Phase Noise Oscillator

[1]Soheli Farhana, [1] AHM Zahirul Alam, [1]Md. Masum Billah
[1]Faculty of Engineering, International Islamic University Malaysia (IIUM), Jalan Gombak, 53100 Kulala Lumpur, Malaysia.

Abstract: In this paper, we analyze a comparative study of low phase noise Voltage Controlled Oscillator (VCO) and propose a design of novel oscillator. Band pass filters can contain harmonics, which are integrated into a co-design with an oscillator to improve the phase's noise and harmonic rejection. The proposed oscillator/band pass filter gains a phase noise of -130.1 dBc/Hz/600 kHz and harmonic rejection of 37.94 dB and 40.85 dB for the second and third harmonics, respectively, as compared to results achieved by the oscillator before co-design of -101.6 dBc/Hz/600 kHz and 21.28 dB and 19.68 dB. Best result measures from the study of propose design.

Keywords: Co-design, oscillator, band pass filter, phase

INTRODUCTION

The design of modern RF transceiver, the carrier noise performance and harmonics rejection of the local oscillator are major consideration due to the narrow frequency spacing between communication channels. Some methods are now available to improve performance, such as adding an active feedback circuit[1], using the common-emitter configuration for the transistor[2], and employing transistors with low noise factor[3][4].

With the development of RF integrated technology, co-designs between RF circuits or between circuits and antennas have proposed and used in RF end designs which essentially changes the structure of a circuit. It combines the function of the circuits and reduces the connection between the components. In this paper, an oscillator and two band pass filters are co-designed to improve the phase noise and harmonic rejection of the oscillator. The measured results show that the relative harmonic rejections are 37.94 dB and 40.85 dB for the second and third harmonics, respectively, and the phase noise reaches up to -130.1 dBc/Hz/600 kHz.

COMPARATIVE STUDY

A lot of researchers already have done about the improvement of phase noise. Here is a comparative study of phase noise is shown bellow:

Freq (GHz)	Core Pdd (mW)	PN (DBc/Hz)	FOM	Ref
4.4	21.6	-119	178.5	[7]
5.5	5	-116	183	[8]
5.6	2	-114.6	186	[9]
5.35	7	-117@1MHz	183.1	[10]
5.8	8.1	-110@1MHz	176.2	[11]
4.39	14	-117.8@1MHz	179.6	[12]
5.8	5	-112@1MHz	180.3	[13]
5	13.75	-114 @1MHz	176.6	[14]
5	3	-120.42 @1MHz	189	[15]
1.55-1.95	16.25	-134.0 @900kHz	-187.4	[16]
1.46-1.81	10	-134.0 @900kHz	-189.8	[17]
2.80-4.55	27	-142.0 @3MHz	-183.3	[18]
3.31-4.83	10.5	-127.5 @1MHz	-187.7	[19]

CO-DESIGN AND SIMULATION

Fig. 1 shows the schematic diagram of the oscillator circuit and bandpass filters I and II. Filter I, which is used to replace the output match circuit and to

Corresponding Author: Soheli Farhana, Department of Electrical and Computer Engineering, Faculty of Engineering, International Islamic University Malaysia (IIUM), Jalan Gombak, 53100 Kuala Lumpur, Malaysia, E-mail: farhana_aub@yahoo.com.

suppress the harmonics of the output signal, is formed by C_1, C_2, C_3, L_1, L_2, and L_3. Bandpass filter II is composed of C_5, C_6, C_7, L_8, L_9, and L_{10} and is as a substitute for the oscillator resonator and to suppress the harmonics in the feedback circuit. The S_{21} of filters I and II are shown in Fig. 2. The results show that the two filters with a center frequency of 1.2 GHz can suppress the second, third, and fourth harmonics. A commercial software designer (Ansoft) [20] is used to simulate the entire circuits, and the harmonic balance simulation results are shown in Fig. 3. Before co-design, the harmonic rejections for the second and third harmonics are 20 dB and 17dB, and the phase noise is -119.0 dBc/Hz/600 kHz. After co-design, the corresponding values for harmonic rejection are 48.5 dB and 38.6 dB, and a typical phase noise level of -137.5dBc at an offset frequency of 600 kHz is observed. Obviously, the co-design suppresses the harmonics and improves the phase noise significantly.

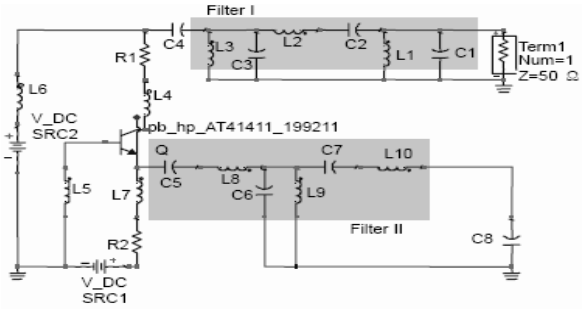

Fig. 1: schematic diagram of the oscillator circuit and bandpass filter

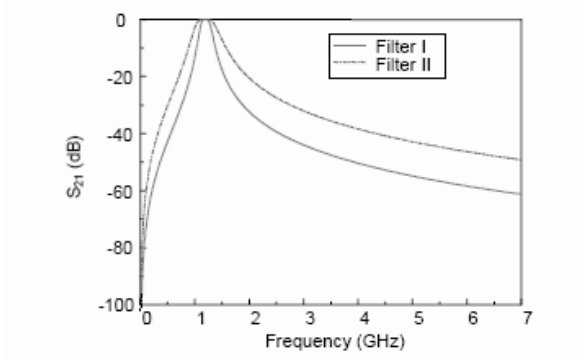

Fig.2: S_{21} of the filters I and II

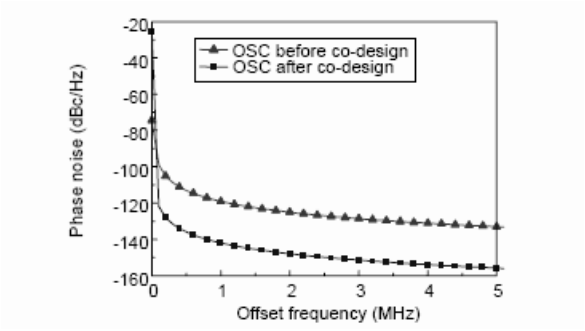

Fig.3: simulated phase noise of the oscillator except at the edge of alite phases.

EXPERIMENTAL RESULTS

The measured output spectrum and phase noise are shown in Fig. 4, respectively. Good agreement between the measurement and simulation results has been achieved. As shown in Fig.4, phase noise levels of -101.6 dBc/Hz and -130.1 dBc/Hz at an offset frequency of 600 kHz are observed for the oscillator before and after co-design respectively.

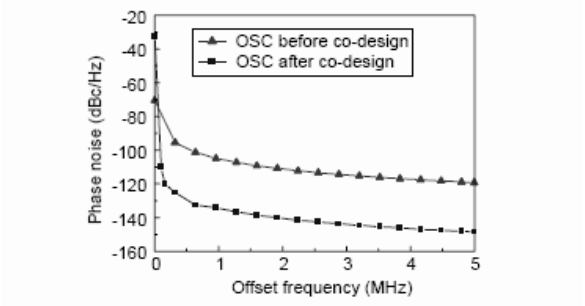

Fig.4: measured phase noise of the oscillator

CONCLUSION

In this paper, we presented an oscillator-bandpass filter design, which improves the phase noise characteristic and harmonic rejection of the oscillator. The phase noise was -130.1 dBc/Hz/600 kHz. Best result measures from this design. The results demonstrate that an oscillator-bandpass filter design can significantly improve the phase noise and the quality of the output signal.

REFERENCES

1. H.J. Kim and W.Y. Kim, "A Low Phase Noise LC VCO in 65nm CMOS Process Using Rectangular Switching Technique," *IEEE Microw. and Wirel. Compon. Lett.*, vol. 17, no. 8, Oct. 2007, pp. 610-612.
2. M.Q. Bao et al, "A 25-GHz Ultra-Low Phase Noise InGaP/GaAsHBT VCO," *IEEE Microw. and Wirel. Compon. Lett.*, vol. 15, no.11, Nov. 2005, pp. 751-753.
3. Z.Q. Cheng and Y. Cai et al, "A Low Phase-Noise X-Band MMIC VCO Using High-Linearity and Low-Noise Composite-Channel Al0.3Ga0.7N/-Al0.05 Ga0.95N/GaN HEMTs," *IEEE Trans. on Microw. Theory and Techn.*, vol. 55, no. 1, Nov. 2007, pp. 23-29.
4. S.H. Lee and W.H. Chuang et al, "Low-Phase Noise Hartley Differential CMOS Voltage Controlled Oscillator," *IEEE Microw. and Wirel. Compon. Lett.*, vol. 17, no. 2, Feb. 2007, pp. 145-147.
5. W. Wang and Y.P. Zhang, "0.18-μm CMOS Push-Pull Power Amplifier with Antenna in IC Package," *IEEE Microw. and Wirel. Compon. Lett.*, vol. 14, no. 1, Jan. 2004, pp. 13-15.
6. S. Alalusi and R. Brodersen, "Antenna-Filter-CMOS LNA Codesign Strategy," *CPD2000 (Chip-Package Co-design)*, Zurich, Switzerland, Mar. 2000.
7. M. A. Margarit, D. Shih, P. J. Sullivan, and F. Ortega, "A 5-GHz BiCMOS RFIC front-end for IEEE 802.11a/HiperLANWireless LAN," *IEEE J. Solid-State Circuits*, vol. 7, pp. 1284–1287, July 2003.
8. J. Rogers and C. Plett, "A 5-GHz radio front-end with automatically Q-tuned notch filter and VCO," *IEEE J. Solid-State Circuits*, vol. 9, no. 9, pp. 1547–1554, Sep. 2003.
9. N. Fong, J. Plouchart, N. Zamdmer, D. Liu, L. Wagner, C. Plett, and N. Tarr, "Design of wide-band CMOS VCO for multiband wireless LAN applications," *IEEE J. Solid-State Circuits*, vol. 38, no. 8, pp. 1333–1342, Aug. 2003.
10. 5.35-GHz CMOS VCOs and prescalers," *IEEE Trans. Microw. Theory Tech.*, vol. 49, no. 1, pp. 17–22, Jan. 2001.
11. Y. K. Chu and H. R. Chuang, "A fully integrated 5.8 GHz U-NII band 0.18-_m CMOS VCO," *IEEE Microw. Wireless Compon. Lett.*, vol. 13, no. 7, pp. 287–289, Jul. 2003.
12. Y. Eo, K. Kim, and B. Oh, "Low noise 5 GHz differential VCO using InGaP/GaAs HBT technology," *IEEE Microw. Wireless Compon. Lett.*, vol. 13, Jul. 2003.
13. J. B. Bhattacharjee, D. Mukherjee, S. Nuttinck, and J. Laskar, A 5.8 GHz fully integrated low power phase noise CMOS LC VCO forWLAN applications," in *IEEE MTT-S Dig.*, Jun. 2002, pp. 585–588.
14. C. Samori, S. Levantion, and V. Boccuzzi, "A 94 dBc/Hz@100 KHz fully-integrated, 5-GHz, CMOS VCO with 18% tuning range for Bluetooth applications," in *IEEE Custom Integrated Circuits Conf. Proc.*, 2001, pp. 201–204.
15. Ming-Da Tsai, Yi, Hue, "A 5-GHz low phase noise differential colpitts CMOS VCO", IEEE microwave and wireless components letter, vol. 15, No. 5, May 2005.
16. J. Oehm and D. Pham-Stabner, "Linear controlled temperature independent varactor circuitry," in *Proc. 28th Eur. Solid-State Circuits Conf.*, 2002, pp. 143–146.
17. E. Hegazi, H. Sjöland, and A. Abidi, "A filtering technique to lower LC oscillator phase noise," *IEEE J. Solid-State Circuits*, vol. 36, no. 12, pp. 1921–1930, Dec. 2001.
18.] K. Manetakis, D. Jessie, and C. Narathong, "A CMOS VCO with 48% tuning range for modern broadband systems," in *Proc. IEEE Custom Integr. Circuits Conf.*, 2004, pp. 265–268.
19. Svetorzar S., Tapio A., Nokolay, " A wideband low phase noise, -VCO with programmable Kvco", IEEE MICROWAVE AND LC WIRELESS COMPONENTS LETTERS, VOL. 17, NO. 4, APRIL 2007.
20. Ansoft Designer SV User Manual, Ansoft Ltd., available at http://www.ansoft.com.

Hexagonal Structure Hexapod Robot: Developing a Method for Omni-directional Navigation

[1]Md. Masum Billah, [2]Mohiuddin Ahmed, [1]Md. Raisuddin Khan and [1]Soheli Farhana
[1]Faculty of Engineering, International Islamic University Malaysia (IIUM), Jalan Gombak, 53100 Kulala Lumpur, Malaysia.
[2]Faculty of ICT, International Islamic University Malaysia (IIUM), Jalan Gombak, 53100 Kulala Lumpur, Malaysia.

Abstract: This paper presents an optimal gait generation algorithm for a hexapod robot with hexagonal structure. Typical body structures of hexapod robots are analyzed. Various constraints like stability, foot force, leg workspace and leg collision that affect the walk, are taken into consideration to maximize the stroke of a leg during direction phase by making it pass through the center of workspace. The gait generated extracts maximum stroke length subject to the constraints, with the legs on ground during locomotion. Finally, an algorithm is developed for omni-directional navigation for a hexapod robot.

Keywords: Optimal gait generation; walking machine; Hexapod

INTRODUCTION

The better rough terrain mobility of omni-directional walking machines over wheeled vehicles has generated a significant research interest in the development of walking robot. Control duty for a walking robot involves leading execution of a command for walking, without losing stability and continuity of motion. Due to the complexity involved, the control duty has been split into levels such as higher-level controller and lower level controller. The higher level interprets the operator commands to actuator motions for the specified body motion. These actuator motions are then converted into actual movements of legs and body by the lower level controller. In order to make the machine omni-directionally navigated, it is required to make the higher-level controller more competent. This paper presents the development of higher-level controller algorithms for omni-directional walking of a hexapod robot.

Some problems of free gait generation were identified by researchers in various ways. The geometric approach[1] of varying gait parameters like stroke, duty factor relies on the modeling capabilities thus restricted to a particular direction. A constraint based approach can be useful for the robot and its environment taken into consideration while formulating the constraints. The behavior based approach[2] integrated with planning has its capability dependent upon the reaction time of the machine, which may be critical when a heavy vehicle is moving on a highly unstructured terrain where reaction time needs to be very small. Graph search and hierarchical approach[3]-[5] rely on a rule base to trim several less promising branches at a decision making stage.

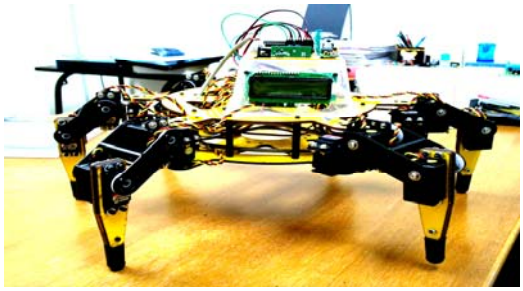

Fig. 1: The walking hexapod robot

DESCRIPTION OF THE WALKING ROBOT

The walking machine under consideration, hexapod robot, is shown in Fig. 1. The walking machine has six legs arranged axe-symmetrically

Corresponding Author: Md. Masum Billah, Department of Mechatronics Engineering, Faculty of Engineering, International Islamic University Malaysia (IIUM), Jalan Gombak, 53100 Kuala Lumpur, Malaysia, E-mail: liton_aub@yahoo.com.

around a vertical axis passing through the center of the body. It stands 6 feet tall and is having a mass of 1 kg. Each leg has three degrees of freedom vertical, horizontal, and twirl. The limits on leg movements in these directions define the three dimensional workspace in which direction the leg can be moved. Our task here is to design a higher level controller strategy for effective and efficient omni-directional walking of the hexapod robot.

The higher-level controller optimizes the way to move the feet (the servos) in order to achieve the motion of the body.

The higher level controller was developed[6] [7] which are capable of generating straight line motion along any direction motions about any point with a free gait. For maximizing stroke of the legs in each case, it determines optimal foot locations for straight line and circular motions of the body. The algorithm is also capable of generating total motions for any directional paths concatenated with hexagonal structure.

The above strategy is applicable only for two types of body orientations. One in: which the body orientation is kept fixed and the-other in which the body orientation is always in the direction of the tangent to the path traced by the body center. The more general motion of the body should allow the body orientation to change independent of the path of center of mass.

THE CENTRAL IDEA

When a tripod is to be placed on the floor to start a stance phase, we need to decide where exactly each foot of the legs has to be placed within its workspace. The importance of this decision is that some choices of the foot location lead to short strokes, forcing the tripod to be lifted very soon after it starts the stance and consequently forcing the tripod in the air to be brought down quickly. Foot placements, which maximize stroke, are useful, but difficult to determine exactly, especially when the gait is not regular. The main contribution of this work is an algorithm for determining foot placements, which lead to relatively large strokes. We do this by ensuring that each foot passes through middle of its workspace during the stance phase. Fig. 2 illustrates this idea.

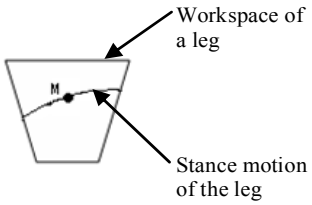

Fig. 2: Stance motion passing through mid position of workspace

The middle position of the workspace is shown as point M. We ensure that the path of the foot during stance passes through this point at all stance motions. The extent of stance motion on either side of pint of M is determined to maximize the stroke, subject to constraints like stability margin, foot force limit, workspace limits and avoiding collision amongst legs.

GAIT GENERATION

We assume that the x and y (horizontal) components of body center and the orientation, θ angle have been specified as functions of a dummy parameter. A useful dummy parameter is the distance along the curve representing body motion in the three dimensional space of x,y,θ. At each point of motion, we have to ensure that stability margin is sufficient, force on each foot is not beyond its limit, each foot is within its workspaces, and no two legs are colliding.

When starting, we assume that one tripod is in stance phase, with each foot at the mid point of its workspace. We first determine all the stance motions of the two tripods**,** and then join the adjacent stance motions with smooth transfer motions of the feet. The crucial algorithm is that of determining the touch down foot locations for a tripod for starting a stance. The basis of this algorithm is to estimate the instance at which the feet of the tripod arrive at their respective mid points, so that the touch down points can be obtained by working backwards in time. The estimate mentioned above is modified to ensure that there is sufficient overlap between two tripods. This uses the information about the instance at which the previous tripod is lifted. The algorithms for touch down and lift off are described in detail below. The dummy parameter used for specifying body motion is L. We consider discrete values of L to make the algorithm faster.

A. Algorithm for determining touchdown position

The problem of determining the touchdown position can be solved iteratively as follows.

1. Let the value of L at which the current tripod (assume 2-4-6**)** is getting lifted be Le. Let the specified overlap between the stance motions of two tripods be (in terms of number of intervals n_o of L) n_o ▲L. Then the value of L at which the next tripod has to be placed is L1 =Le – n_o ▲L.
2. Choose an estimate Lm, the instant at which the tripod to be put down (1-3-5) will reach its mid stance position.
3. Determine the motion of feet of the tripod 1-3-5 from the respective workspace midpoints at Lm, backwards in time, till the first occurrence of violation of any of the constraints (Fig. 3).

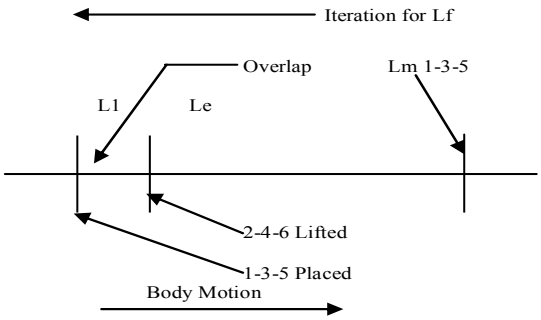

Fig. 3: Representation of hack iteration to obtain the touchdown position L1.

4. Let the earliest violation of constraints be at Lf. We calculate the correction required on the initially selected Lm as DL = Lf-L1. This is the amount by which the calculated touchdown position is different from the required value.
    - If DL is negative and less than DLT in magnitude (a tolerance), no adjustment is required on Lm and proceed to step 5
    - If DL is negative and greater than DLT in magnitude, more stride is possible than our initial guess of Lm, and we can increase Lm by DL and repeat step 4.
    - If DL is positive, new smaller Lm is calculated as Lm = Lm-DL and step 4 is repeated.

We now have the correct Lm such that when the tripod touches down at L1, no constraint is violated till Lm. The sequence of foot positions, generated from mid stance to touchdown, is stored. Note that for forward body motion, the legs move backwards in body coordinate frame, so while back iterating for Lf, the legs move forward for checking the limits.

B. Algorithm for determining the liftoff position

Here we determine how far a particular support tripod can move the body forward. Starting from mid stance position Lm, we find an instance where first violation of any of stability constraint, workspace constraint, foot force constraint or collision constraint occurs.

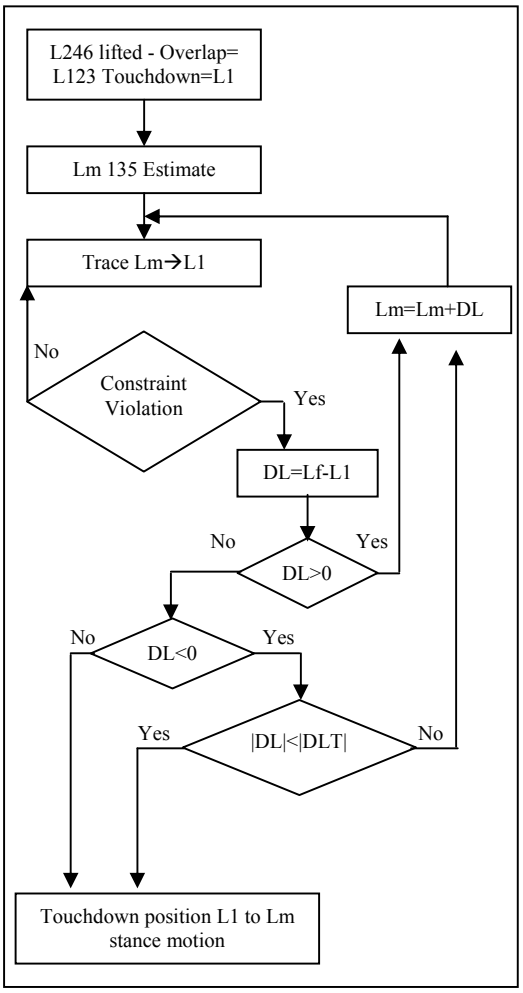

Fig. 4: Flow chart for algorithm of determining touchdown position

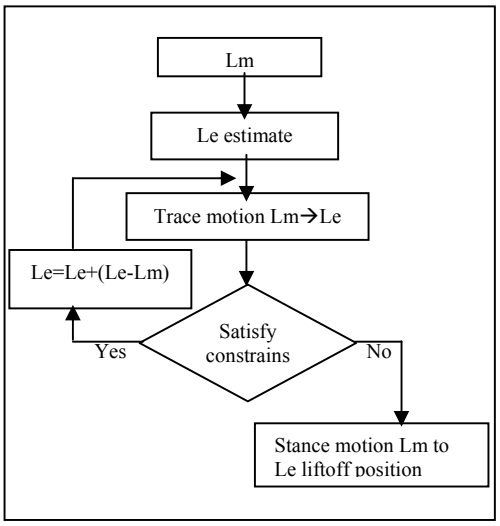

Fig. 5: Flow chart for algorithm for determining Liftoff position

This instance would be marked as a liftoff instance Le, for that support pattern. Thus this algorithm determines the value of the parameter L at which the tripod has to be lifted and the stance motion from mid stance to liftoff.

The above two algorithms provide the stance motion for the body, where each leg passes through its middle position of its workspace during the stance phase. Determination of positions of the feet of a tripod during stance is based on the known body motion and the position of the three feet in world coordinate frame at touch down. When the body undergoes a known displacement from its touch down position, the stance feet remain fixed at known positions in the global frame. Coordinate transformations are then used to obtain the positions of the stance feet in the robot's body fixed coordinate system. We now describe how the constraints are calculated.

C. Determination of stability margin

Stability margin is defined as the least distance from the vertical projection of center of mass on ground to the convex hull formed by the feet on ground. We compute the distance of center of gravity from all sides of support pattern. The minimum of the three distances is the stability margin. This should be more than a specified minimum stability margin.

D. Determination of reaction forces of stance feet

The design of the walking robot and its feet is based on the condition that a leg would be able to bear a weigh equivalent to 1kg anywhere within its workspace. Given the set of tripod positions with respect to body frame during stance motion and the mass and payload of the machine, we, calculate the reaction forces coming on the feet. A support motion remains feasible if the reaction forces of the feet are within the specified limits.

E. Checking foot workspace limits

The legs of the machine need to be in their respective workspaces during stance as well as transfer phase. We define certain workspace for each leg depending on their kinematics constraint and examine whether the leg remains within that by a margin called workspace margin. Limits are put on all three direction movements of the leg, radial, swivel and vertical. The foot position is transformed into its leg coordinate frame in radial coordinates and is examined to satisfy the limits.

F. Algorithm for determining collision among legs

This algorithm detects whether there is any collision between two neighboring legs while following a specific path with certain sequence of foot positions. For checking collision between legs, we examine some critical points of a leg. We identify the outermost points of a leg depending upon whether the leg is stretched or folded. The potential collision situation can occur when a leg is touching down and its neighbor is ready to be lifted, i.e., in the overlap portions of the motion. We follow following steps

- Find out whether a leg is folded or stretched i.e. examining the radial distance of thigh and the foot tip.
- Express the critical points of a leg in its neighbor's leg reference frame as shown in Fig. 7, for the global scene as Fig. 6.
- Check whether the critical points are outside the collision margin polygon PlP2P3P4 as shown in Fig. 7.

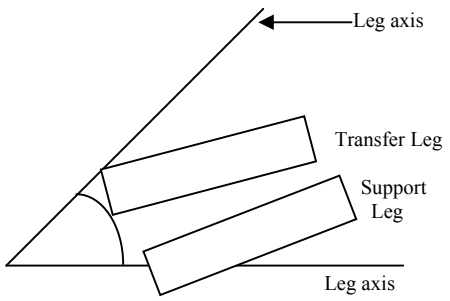

Fig. 6**:** Global scene of legs at the critical moment

Thus a touchdown position is collision free if there is no collision for all three support legs and corresponding brackets.

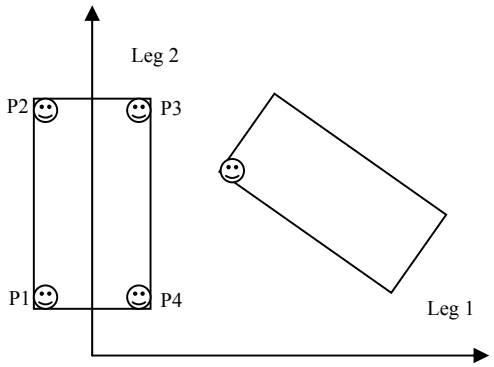

Fig. 7: Points on a leg expressed in its neighbor's leg reference frame

G. Determination of transfer motion

After determining all stance motions, transfer motions of feet are determined as smooth curves joining a liftoff to next touch down. The transfer paths of feet have to be within their respective workspaces. We have the Limits on radial, swing and vertical movements of the legs due to workspace and kinematics' constraints. We know the xyz coordinates of a leg at the time of liftoff and touchdown; we convert this position in respective radial coordinates, and fit a curve between these two radial positions, which will represent the radial leg motion in transfer phase. Similarly we fit a curve for the swing motion, keeping position and velocity continuity at liftoff and touchdown. While generating the transfer motion in vertical direction we keep an extra constraint that the leg should get lifted by a specified amount. This transfer motion generated in radial coordinates is convened to xyz coordinates and is checked motion thus we have a transfer motion with minimum of swing, radial and vertical movements. Combined motion of all the transfer legs constitutes the transfer motion for the tripod.

At the beginning and at the end of motion, we assume that the tripod in transfer phase has feet at their mid stance raised position.

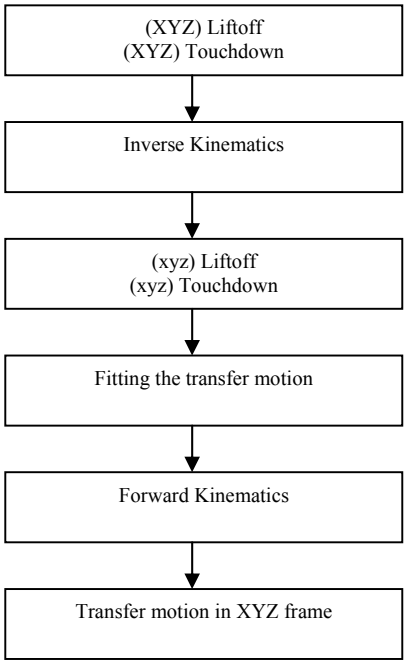

Fig. 8: Flow chart for transfer motion generation

The above sections described the planning of leg trajectories in terms of position and distance traveled. This motion is in terms of the parameter L of the walk. Now we need to convert this motion with respect to time, in order to determine terms like speed and acceleration of travel. An earlier 'developed algorithm[7] for controlling speed of motion of the machine, determines the exact variation of parameter L with respect to time so that the potentiometer limits are satisfied. Fig. 9 gives the flow chart of gait generation algorithm.

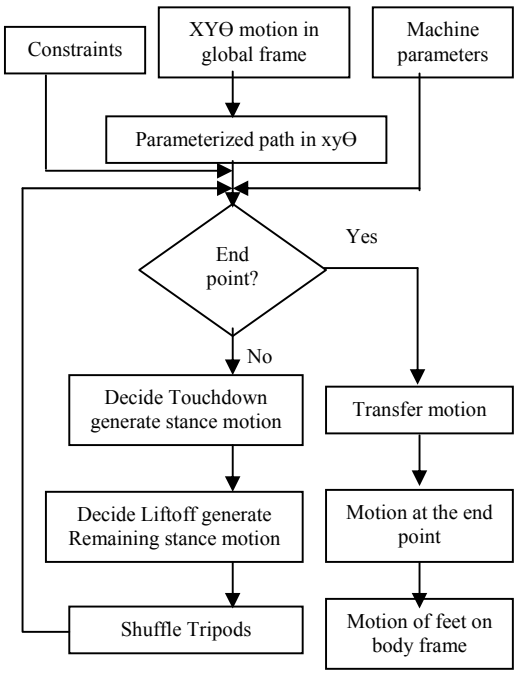

Fig. 9: Flow chart of gait generation algorithm

CONCLUSION

The problem of optimal gait generation for a six legged walking machine, hexapod, is addressed here. An algorithm, which generates near maximal stroke tripod gait, has been developed for walking on regular terrain. Limits on minimum stability margin, maximum foot force, foot motion and collision between adjacent legs are considered for generating the gait. The algorithm is capable of generating leg trajectories for complex paths with body allowed to turn while walking. The algorithm can be used with minor modifications, for generating regular gaits like wave gait and for free gaits, and also for walking on inclined planes and steps. Walking on irregular terrain would require some substantial extensions.

REFERENCES

1. Kumar V. R. and Waldron K.J., Adaptive Gait Control for a Walking Robot, Journal of Robotic Systems, pp 49-76.
2. Wettergreen D., Thorpe C., Gail generation for Legged Robots, Proceedings of the IEEE International Conference on intelligent Robots and Systems, July 1992.
3. Pal P.K. and Jayarajan K. Generation of Free Gaits- A Graph Search Approach, IEEE Transactions on Robotics and Automation, Vo17, No. 3, June 1991 pp 299-305.
4. Ching-Long Shih and Klein C.A., An Adaptive Gait for Legged Walking Machines over Rough Terrain, IEEE Transactions on Systems, man and cybernetics. Vol23, No. 4, August 1993, pp 1150-1155.
5. Mcghee R.B., lswandhi G. I. Adoptive Locomotion of Multi-legged Robot over Rough Terrain, IEEE Transactions on Systems, man and cybernetics, Vol SMC 9, No. 4, April 1979, pp 176-182.
6. Nilesh S. Brahme and K. Kurien Issac, Gait generation for LI Six legged Walking Robot, Proc. of the 10th National Conference on Machine and Mechanics, 209-216, 2001.
7. Amit P. Gabale. K. Kurien Issac, Consideration of Gait Transitions and Extended Feet in the Determination of Foot trajectories for a Six Legged Walking Robot, proceedings of the 11th World Congress in Mechanism and Machine Science, Tianjin, China, August 2003.

Turbulent Diffusion in Wave-Current-Vegetation Flow

Sandeep Patil and Xiang-gui Li
School of Engineering and IT, Charles Darwin University, NT, Australia. 0909.
Xiang-gui Li
Beijing I S & T University, Beijing 100101.

Abstract: Present study describes turbulent diffusion in the flow through flexible vegetation subject to waves and current for the cases with and without waves. For the no-wave (current-only) case, the flexibility in the stems causes lateral vibration of stems as a response to the current which increases the magnitude of turbulent diffusion over that in flow through rigid stems. In the presence of waves, the stems-scale eddies are found to be enhanced which can better be approximated by stem-spacing scale. This increase in the scale of eddies further increases the magnitude of turbulent diffusion over no-wave case. A mathematical model is proposed as an estimator of the total diffusion in wave-current-flexible vegetation in which the effects of waves and stem vibration are included in separate parameters. If wave amplitude made zero, the model predicts the non-wave diffusion and for no vibration, it predicts the diffusion in rigid vegetation.

Keywords: Turbulent diffusion, flexible vegetation, wave-current flow

INTRODUCTION

Environmental flows are often turbulent in nature with a range of sizes or scales of motion which can be conceived as an alternate cycle of expanded large-scale eddies that shrinks to small scale in time under viscous dissipation. Presence of vegetation further breaks the eddies to the scale of stem diameter but enhances the turbulence within entire canopy (Nepf, 1999). The magnitude of the vegetative turbulence depends on the flow depth and the density of vegetation (Nepf and Vivoni, 2000), the rate of growth of vegetation by incident light by sediment re-suspension (Burd and Dunton, 2000) and deposition owing to the reduced bed shear (Ward et. al., 1984; Leonard et. al., 1995). The reduced eddy scale weakens the macroscale diffusion relative to un-vegetated channel (Worcester, 1995; Ackerman and Okubo, 1993). The velocity distribution using Prandtl's mixing length approach has been derived by Carollo et al. (2002) who also proposed a relation between velocity and turbulent intensity. The vertical turbulent diffusion has been observed to be higher around interface and lower in above and below it (Shimizu et al. 1992). Apart from the rigid vegetation, the flexibility in the vegetation also affects the flow structure (Patil et al., 2006). Kouwen and Unny (1973) proposed a parameter to calculate hydraulic roughness using flexible plastic sticks. Tsujimoto and Kitamura (1998) proposed a parametric solution for the flow through flexible canopy using procedure of Shimizu and Tsujimoto (1994) for rigid vegetation. The bending increases the local frontal area, which increases effective stem density at the top of the canopy. The rubber-made flexible stems used in the present experiments show transverse vibration under unidirectional flow. Dye study is conducted to quantify additional turbulent diffusion due to this transverse vibration. Total diffusion as an addition of stem-scale diffusion, mechanical diffusion and stem-vibration generated diffusion shows agreement with the results of present experiment conduced on semi-flexible vegetative flow.

Apart from the vegetation, surface waves that often exist due to the ubiquity of wind shear, may also contribute in the turbulence (Zeidler 1976). The experiments are therefore extended to study the turbulent diffusion in wave-current-vegetation flow which generally exists in nature. A flow study on wave-current flow in vegetation (Ota et al. 2004) suggested that the drag coefficient (C_d) of current-vegetation is too large to simulate wave-current-vegetation flow. They obtained $C_d = 0.6$ to simulate the profile in flexible vegetation. Patil (2008) proposed an empirical expression for longitudinal dispersion in wave-current-vegetation. In this paper, the depth-wise velocity profiles and turbulence have been measured and by conducting dye studies, an empirical expression for turbulent diffusion coefficient for wave-current-vegetation flow is proposed. The results of this study will improve the understanding of the hydrodynamics and pollutant mixing in the combined wave-current-vegetation flow.

Corresponding Author: Sandeep Patil, School of Engineering and IT, Charles Darwin University, NT 0909, Australia, Tel: +618-89467367, Fax: +618-89466680, E-mail: sandeep.patil@cdu.edu.au, coastlab1@yahoo.com

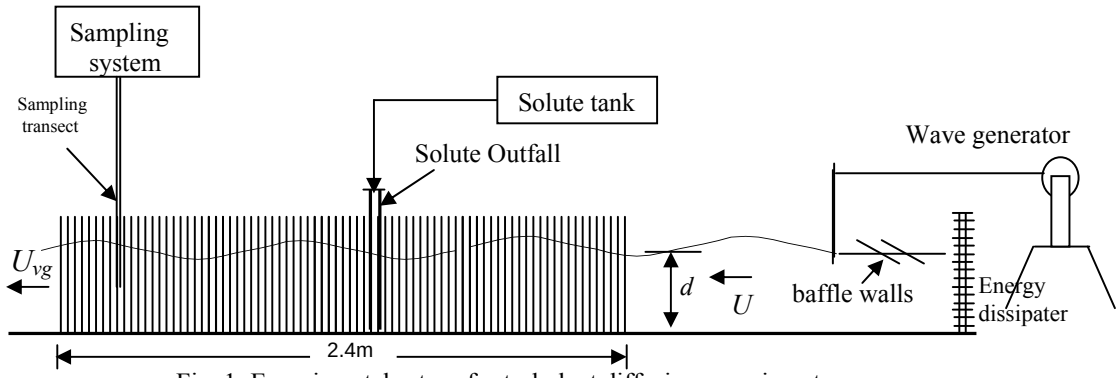

Fig. 1: Experimental set-up for turbulent diffusion experiments

EXPERIMENTS

Laboratory experiments are conducted in a 0.3 m wide self-contained tilting flume with smooth steel bottom as shown in Fig 1. Water from the upstream end is passed through the energy dissipaters to generate uniform flow which is also controlled by adjusting the tailgate at the downstream end. The surface fluctuations are absorbed by baffle walls to get a smooth water surface. Wave generator is located after these walls to generate progressive surface waves for wave-current-vegetation experiments. The wave reflection from the tail end is avoided by allowing them to pass over the tail gate without reflecting back. Temperature fluctuation during experiments is noted within 2^0C. Two vegetation models are imitated with 150mm long semi-flexible rubber rods and dimensionless densities (ad_s) = 0.04 and 0.07 ($a = nd_s = \frac{d_s}{\Delta S^2}$; n is the number of stems per unit area, stem diameters d_s = 6mm and 8mm respectively and stem spacing ΔS =30mm). These densities are on the higher side of the range observed by Gambi et. al. (1990) in salt water and Kadlec (1990) in fresh water so as to observe higher limit of possible turbulence; the lower limit will tend to the diffusion in bare-bed channel. The stems are fixed in a square grid on 2.4m long plexiglass board, extended from wall to wall to avoid elevated flow near the walls. Model is placed sufficiently away from the flume inlet to avoid the interference of initial turbulence. The drag in the beginning of vegetation reduces downstream by the wake turbulence and delays the point of separation. As a result, flow velocity becomes steady towards downstream. For the current-vegetation case, the flexible stems reveal transverse vibrations of which the amplitude and frequency of vibration increases with increase in flow velocity. However in wave-current-vegetation, these transverse vibrations are observed to be not intense because of the dominant wave-induced orbital motions in the longitudinal flow direction.

Dye study for the current-vegetation flow is conducted in the rear part of the vegetation model where the flow velocity attains steady state to avoid initial transition. The same location is used for the wave-current-vegetation cases by passing surface waves. The turbulent range of wake structure in the canopy is maintained by assuring stem Reynolds number ($R_e = Ud_s/\nu$) $\geq$ 200 (ν is the kinematic viscosity) (Tamura et. al.; 1980) in all experiments. Depth-wise velocity profiles are measured using Ultrasonic Velocity Profiler (UVP) with five transducers spaced vertically to cover the complete flow depth. In case of dowel impedance, two or three dowels are displaced to clear the optical path of the UVP. All these velocities are averaged to get a vertically averaged vegetative flow velocity

where u_1 to u_5 are the velocities measured by five transducers. The U_{vg} is related to the uniform velocity on bare-bed before entering in vegetation (U), using a vegetative parameter $(1 - ad_s)$ as

$$U_{vg} = U(1 - ad_s)^{8.137} \qquad (1)$$

where the parameter 8.137 is estimated using least square method. Eq. 1 provides the flow velocity in bare-bed channel if $d_s \rightarrow 0$. Further, for the very high density, $d_s \sim \Delta S$ reflects total blockage of flow, for which $ad_s = 1$ that provides $U_{vg} \rightarrow 0$ as expected due to total blockage of the flow. Eq. 1 shows good correlation with the observed values of the mean vegetative velocities (Fig. 2). To conduct dye study for the measurement of turbulent diffusion, a solute is prepared by adding 50ml of 100-fold 20% active Rhodamine dye in 10 liter ambient water. Solute is injected through an outlet of a 5mm vertical glass

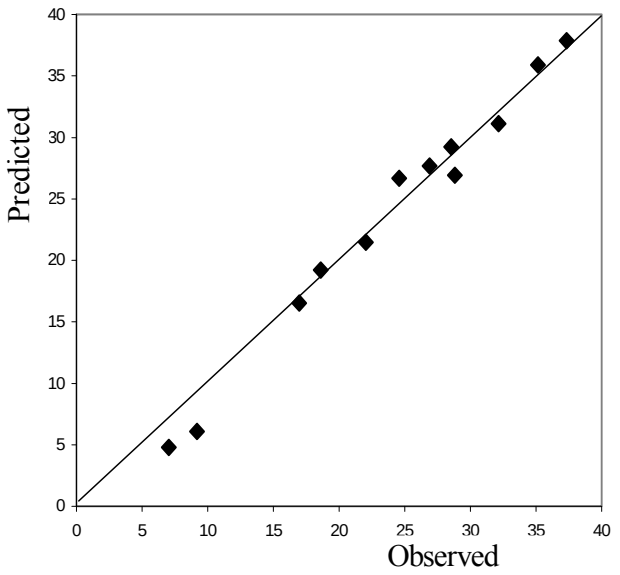

Fig. 2: Observed U_{vg} (mm/sec) v/s Eq. 1

tube perforated by 0.5mm holes in the flow direction. The outlet is placed at the mid-width and is 1.5m from the canopy front to assure it is in steady state flow field. The solute is sampled laterally for a total duration of one minute for each run from the mid-depth and measured continuously using fluorometer with data-acquisition system. The sampling transect is located sufficiently away from the outfall to ensure linear dependency of the lateral variance on x. The turbulent diffusivity is estimated by fitting the experimental data on the theoretical gaussian profile using least square technique (Fischer, 1979).

For wave-current-vegetation flow, waves of various configurations are generated on uniform flow. It is ensured that the stems are emergent at all times above wavy surface. The sampling procedure is repeated and the amplitude and period of waves in the region of the outfall and transect are measured using ruler and stopwatch respectively. The wave damping between outfall and sampling points is neglected as the distance between them is short.

TURBULENT DIFFUSION IN CURRENT-VEGETATION FLOW

For the rigid vegetation, Nepf (1999) proposed an expression for turbulent diffusion as an addition of the stem-scale turbulence and the mechanical diffusion occur in the flow paths through stems. For the flexible stems used in this study, it is observed that the current makes the stem to vibrate laterally which helps eddies to further amplify and enhance turbulence. Nepf's expression has been modified to include this vibration-generated diffusion. To begin with, the lateral equalised force per unit mass (Liu, 1991) is given as

$$P_v = X_v\left(\omega_0^2 - \omega^2\right) \qquad (2)$$

where angular frequency of the material $\omega_0 = 2\pi N_1$, $N_1 = \dfrac{0.56}{d^2}\sqrt{\dfrac{E_s I_s}{m_s}}$ in which E_s = 6.01×10^5 is the modulus of elasticity for rubber material used to simulate stems, I_s is the moment of inertia of the stem, m_s is the mass of the stem per unit length in which the total mass of the stem = 7.8 gm, all estimated in the laboratory. Further, $\omega = 2\pi N_2$ is the observed angular frequency of vibration during experiment in which $N_2 = \dfrac{1}{T_v}$. X_v and T_v are the amplitude and period of the vibration respectively, measured during the experiments.

The kinetic energy is estimated on the basis of the balance between the work input by vibration-generated wakes and the dissipation. Also it is assumed that the turbulence due to vibration is homogeneous within the canopy. Thus, the kinetic energy can be estimated based on the dissipation rate $\varepsilon = k_t^{3/2} d_s^{-1}$ (Tennekes and Lumley, 1990) as

$$\sqrt{k_t} \approx \left(d_s P_v \frac{X_v}{T_v}\right)^{1/3} \qquad (3)$$

where $(P_v\ X_v\ )/T_v$ is the work input to vibrate the dowel in which $(X_v\ /T_v)$ is the dowel velocity. The characteristic length scale of the turbulence i.e. stem diameter is assumed to remain same in vibration-generate turbulence. The resultant turbulent diffusion now can be determined by multiplying stem diameter to both side of Eq. 3 as

$$\sqrt{k_t}\, d_s \approx \left(d_s P_v \frac{X_v}{T_v}\right)^{1/3} d_s \qquad (4)$$

The left hand side quantity is the turbulent diffusion owing principally to the vibration-generated turbulence. As P_v is always positive, the kinertic energy will always more in the vegetation with flexible stems than in the rigid stems. In other words, it is independent on canopy density ad_s if the stem diameter is constant.

Finally, Eq. 4 is added to that propsed by Nepf (1999) to get the total diffusion as

$$\frac{D}{U_{vg} d_s} = \alpha\left(ad_s\right)^{1/3}\left[\overline{C}_D + \psi\ P_v\, d_s\left(\frac{X_v}{T_v}\right)^2\right]^{1/3} + \left[\frac{\beta^2}{2}\right] ad_s \qquad (5)$$

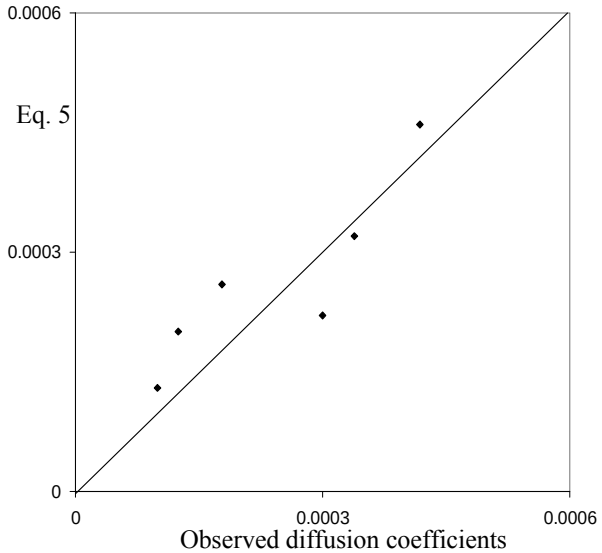

Fig 3: Observed v/s Predicted diffusion coefficients in non-wavy flow

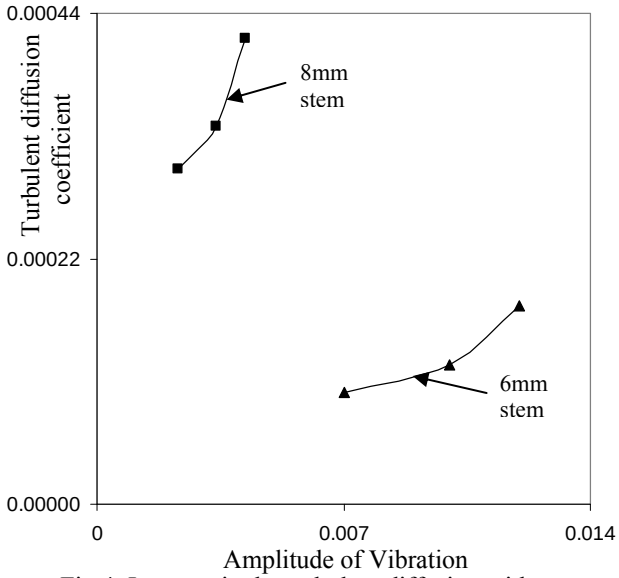

Fig 4: Increase in the turbulent diffusion with increase in amplitude of vibration of stem

where, D is the total turbulent diffusion and $\overline{C}_D$ is the bulk drag coefficient calculated from force balance equation as

$$\left(1 - ad_s\right) C_b U^2 + 0.5\, \overline{C}_D\, ad_s \frac{d}{d_s} U^2 = g\, d \frac{\partial d}{\partial x} \quad \text{where}$$

C_b is the bed drag coefficient. The second bracket on the right hand side is the mechanical diffusion analogous to the porous media. The value of $\Psi = 0.0038$ is estimated to get the best fit by maintaining original values of $\alpha = 0.81$ in Nepf's cylinder model (1999). The compatibility of Eq. 5 can be accessed in Fig. 3 which shows good correlation between the observed and the predicted values of diffusion. The diffusion in rigid canopy can be worked out by substituting $P_v = 0$ in Eq. 5. The dependency of the vibration-generated diffusion on the amplitude of vibration (displacement of the stem tip from its mean position) shown in Fig. 4. It can be revealed from the figure that the diffusion is increasing with increase in the amplitude of vibration. The clarification can be advanced on the basis of the additional mixing due to the transverse vibrations of dowels.

TURBULENT DIFFUSION IN WAVE-CURRENT-VEGETATION FLOW

In the experiments on wave-current-vegetation flow, the wave drag and the resultant wake formation are bi-directional and periodic around stems ($d_s << L$, wavelength of wave). The drag force per unit mass can be written as

$$F_{dw} = \frac{1}{2} C_{dw}\, A U_w \left|U_w\right| \qquad (6)$$

where A is the area of stem exposed to the flow and the wave drag coefficient can be $C_{dw} = 1$ for the present range of $R_{ed} = (200\text{-}700)$ (Dean and Aagaard; 1970). The transverse vibrations present in current-vegetation flow are now not important as the flow is dominated by bidirectional wave-induced motions in the flow direction. The periodic wake generated by the horizontal wave velocity U_w is stronger under the crest due to additional concurrent steady current underneath, whereas it is weaker under trough provided steady current is higher than the wave velocity. The net flow is still in the direction of flow but with the point of separation pushed ahead on the stem surface resulting significant reduction in the

drag and trapping capacity of pollutants. The alternate action of pressure and viscous drag within a wave period provides stirring effect between wakes and flow which can influence diffusion. Conversely, if the wave velocity under the trough exceeds the steady current, a temporary wake is formed upstream of stem washing out the previously formed wake downstream of stem. The flow pattern under the tough behaves as if flowing in the opposite direction with the net velocity as the difference between the steady and wave components of flow velocity. The upcoming crest again revives the original wake downstream of stem and the sequence repeats. Both the wave-current patterns cause churning of pollutants. The scale of the stem-scale eddies in current-vegetation case will be expanded in presence of wavelength-scale wave motions. However, due to the interference of stems, eddies will not be able to adapt the scale of wavelength as the expansion will be limited to the stem spacing. Thus, a scale of stem spacing can reasonably be used to approximate the eddy scale in wave-current-vegetation flow. The formulation of the wave-induced diffusion is described in the following section.

FORMULATION OF MODEL

The total diffusion in wave-current vegetation flow (D_{wT}) can be formulated by initially dividing the flow into two parts viz. the diffusion due to vegetative drag and the diffusion in bare bed region (region away from stem surfaces) and then further subdividing as

$$D_{wT} = D_b\,|_{current} + D_v\,|_{vibration} + D_v\,|_{mech} + D_v\,|_{drag} + D_v\,|_{wave} + \lambda D_b\,|_{wave} \quad (7)$$

where subscript *b* stands for bare-bed and *v* stands for vegetation. The first term on the right side ($D_b\,|_{current}$) is negligible as in current-vegetation case, the canopy is fully dominated by the diffusion due to drag $D_v\,|_{drag}$, vibration $D_v\,|_{vibration}$ and mechanical transport $D_v\,|_{mech}$ as explained by Eq. 5. For the wave-current-vegetation case, the scaling parameter λ (explained in the next section) is applied to account for the effective area occupied by the bare-bed eddies. The $D_v\,|_{wave}$ can be evaluated on the basis of dissipation theory in which the dissipation due to wave drag can be written as

$$\varepsilon_{wv} = F_{dw} U_w \quad (8)$$

Substituting Eq. 6 in Eq. 8, the period average ε_{wv} can be evaluated over the flow depth as

$$\varepsilon_{wv} = \int_{-h}^{0} \frac{1}{2} C_{dw} A U_w |U_w| U_w dz = 2\frac{a_w^3 C_{dw}}{3\pi}\frac{d_s}{k}\frac{\left(\sinh^3 kh + 3\sinh kh\right)}{3\cosh^3 kh}\left(\frac{gk}{\sigma}\right)\left(\frac{1}{\Delta S^2}\right) \quad (9)$$

where a_w is the wave amplitude, k is the wave number, σ is the wave frequency and ΔS is the stem spacing. The vortices generated by the wave drag are of stem diameter scale and therefore the corresponding turbulent intensity can be give as

$$\sqrt{k_{vt}\,|_{wave}} = \left(\varepsilon_{wv}\, d_s\right)^{1/3} = \left[2\frac{a_w^3 C_{dw}}{3\pi}\frac{d_s}{k}\frac{\left(\sinh^3 kh + 3\sinh kh\right)}{3\cosh^3 kh}\left(\frac{gk}{\sigma}\right)\left(\frac{1}{\Delta S^2}\right)(d_s)\right]^{1/3} \quad (10)$$

The diffusion $D_v\,|_{wave}$ now can be worked out similar to Eq. 4 as

$$D_v\,|_{wave} \approx \sqrt{k_{vt}\,|_{wave}}\, d_s \approx \left[2\frac{a_w^3 C_{dw}}{3\pi}\frac{d_s}{k}\frac{\left(\sinh^3 kh + 3\sinh kh\right)}{3\cosh^3 kh}\left(\frac{gk}{\sigma}\right)\left(\frac{1}{\Delta S^2}\right)(d_s)\right]^{1/3} d_s \quad (11)$$

The fifth term in Eq. 7 i.e. $D_b\,|_{wave}$ is the contribution from the flow region away from stem surfaces. Although this term does not exist in current-vegetation case, it contributes significantly in wave-current-vegetation flow through the periodic bed drag in the near boundary region and the expanded eddies of stem-spacing scale. Thus $D_b\,|_{wave}$ can be worked out by using depth- and period-averaged horizontal wave velocity $\overline{\overline{U}}_w$ as

$$D_b\,|_{wave} = \lambda\left|\overline{\overline{U}}_w\right|\Delta S \quad (12)$$

where ΔS is the characteristics length scale of the enhanced eddies and λ is the scaling parameter which reflects the effective area occupied by the enhanced eddies and is determined in the next section. The total diffusion can be expressed by adding Eq. 11 and 12 into Eq. 5 as

$$\frac{D_{wT}}{U_{vg} d_s} = \alpha\left[\overline{C}_D a d_s + \psi\frac{P_v d_s}{U_{vg}^2} + \right]^{1/3} + \left[\frac{\beta^2}{2}\right] a d_s + \left\{\left[2\frac{a_w^3 C_{dw}}{3\pi}\frac{d_s}{k}\frac{\left(\sinh^3 kh + 3\sinh kh\right)}{3\cosh^3 kh}\left(\frac{gk}{\sigma}\right)\left(\frac{1}{\Delta S^2}\right)(d_s)\right]\frac{1}{U_{vg}^3}\right\}^{1/3} + \frac{\lambda\left|\overline{\overline{U}}_w\right|\Delta S}{U_{vg} d_s} \quad (13)$$

In other words, the relative magnitude of $D_v\,|_{wave}$ and $D_b\,|_{wave}$ is governed by the magnitude

of λ. In the wave-current-vegetation flow, the flow between stems will be occupied by the stem-scale eddies in the very near vicinity of stems and ΔS-scale eddies away from the stems. A scaling parameter λ is introduced to quantify the relative contribution from these two eddies. As λ appears in the presence of waves, it can be made a function of d_s and a_w. For example; for the higher a_w and smaller d_s, larger area between stems will be occupied by ΔS-scaled eddies and the contribution of $D_b|_{wave}$ will be higher. On

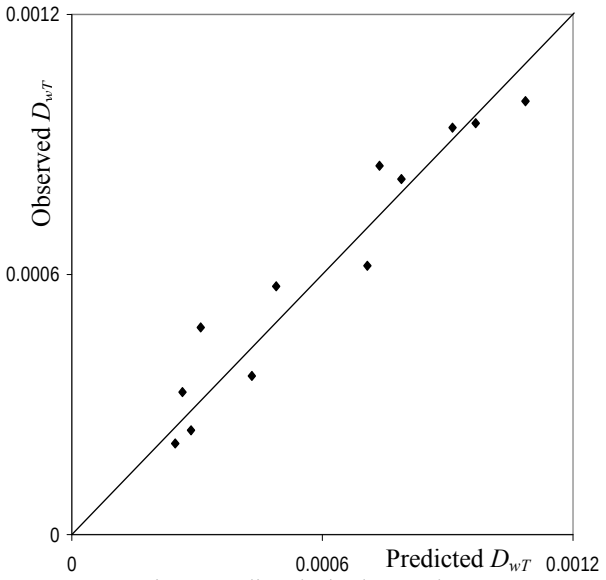

Fig 5: Predicted v/s observed diffusion in wave-current-vegetation

this basis, the dependency relationship for λ can be written as

$$\lambda \approx \left\{ a_w, \frac{1}{d_s} \right\} \qquad (14)$$

Based on Eq. 14, $\lambda = \left(\frac{a_w}{1+d_s} \right)^{\phi}$ of this form is considered for the further analysis where the index ϕ is estimated by the least square method. The λ for smaller d_s allows large scale eddies over the maximum flow area between stems whereas for the thicker stems, $\lambda \rightarrow 0$ as thicker stems reduce ΔS and therefore the magnitude of $D_b|_{wave}$. The thicker stems are also more effective in wave dissipation as explained later which further supports reduction in $D_b|_{wave}$. On the other hand, for $a_w \rightarrow 0$ in non-wavy flow, $\lambda \rightarrow 0$ so that enhanced ΔS -scale eddies disappear and the stem-scale eddies will persist all over the flow. Appearance of the surface wave increases the magnitude of λ and $D_b|_{wave}$.

EMPIRICAL EXPRESSION FOR TURBULENT DIFFUSION COEFFICIENT

The observed D_{wT} and that predicted from Eq. 13 are plotted in Fig. 5 which shows good correlation. The diffusion coefficients in wavy flow are distinctly different than non-wavy flow, the former are higher due to additional wave drag on

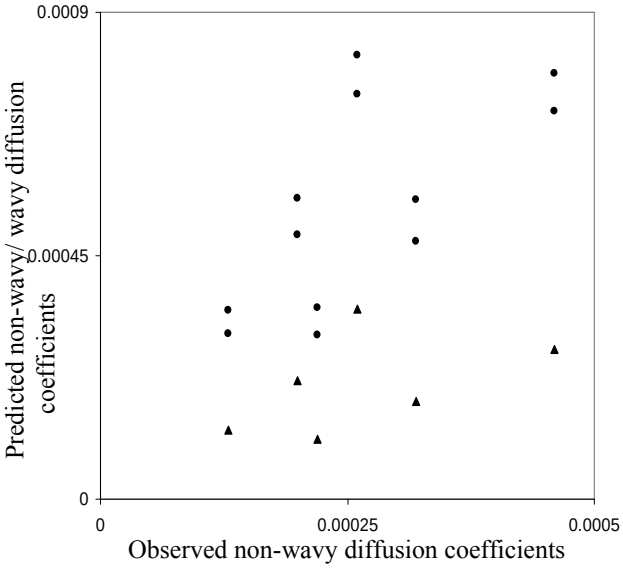

Fig 6: Increase in the diffusion due to wave superposition (▲non-wavy; ● wavy, upper circle denotes higher wave amplitude)

stems and distended eddies and increases with increase in a_w. For the rigid array in wavy flow, Eq. 13 can provide diffusion coefficient by substituting P_v = 0. However Eq. 13 is complicated to use. Therefore the work is further extended by proposing a simple empirical form as an alternative to Eq. 13. To achieve this, easily measurable independent variables for the vibration and waves are selected and dimensional analysis is applied to get an empirical model. The independent variable for the vibration and waves which can be visually measured, are their amplitudes and periods i.e. X_v, T_v and a_w, T. Thus, a non-dimensional functional relationship between turbulent diffusion coefficient and the vibration & wave variables can be written as

$$\frac{D_{wT}}{d_s U_{vg}} \approx \left\{ \frac{X_v}{T_v U_{vg}}, \frac{a_w}{T U_{vg}} \right\} \qquad (15)$$

Using Eq. 15, Eq. 13 now can be written in the simple most form as

$$\frac{D}{U_{vg} d_s} = \alpha \left[\overline{C}_D a d_s \right]^{1/3} + \left[\frac{\beta^2}{2} \right] a d_s + \left[\frac{X_v}{T_v U_{vg}} \right]^{\psi_1} + \left[\frac{a_w}{T U_{vg}} \right]^{\psi_2} \quad (16)$$

where the indices $\Psi_1 = 0.85$ and $\Psi_2 = 0.23$ are estimated by least square method. The third and the forth bracket on right side accounts for vibration-generated and wave-generated diffusion, respectively. The model is capable such that the diffusion in the rigid vegetation in non-wavy flow can be estimated by substituting $X_v = 0$ and $a_w = 0$. Fig. 6 demonstrates the suitability of Eq. 16 in which the triangle symbols are for current-vegetation flow in semi-flexible stems used in this study. The two circular symbols above each triangle are the diffusion coefficients due to additional wave activity corresponding to that triangle. The uppermost circle symbol reflects the diffusion under higher magnitude of a_w which shows increase in the turbulent diffusion.

CONCLUSION

The study quantifies the turbulent diffusion due to the transverse vibration of flexible vegetation in current-vegetation flow and extends to find additional contribution due to wave activity. For current-vegetation flow, increase in the amplitude of vibration directly increases the turbulent diffusion whereas the period of vibration reveals inverse relationship. The low frequency vibrations do not contribute to the turbulence but rather help in releasing wake-trapped pollutants in the flow. The vibration-induced turbulent diffusion with the stem-scale turbulence and mechanical diffusion found to be providing the estimate for the total diffusion in flexible vegetation. It can be stated that stem material with lower modulus of elasticity will provide higher vibration and increase the diffusion coefficient, however is not examined in this study.

For wave-current-vegetation flow, the influence of surface short waves is found to be further increasing the turbulent diffusion. The wave-induced diffusion is evaluated as a combination of two parts; diffusion due to wave drag force and wave-induced diffusion between stems. The former onsets the vortex shedding earlier than in the non-wavy case whereas the later enhances the eddy sizes in the region away from stem surfaces, thereby increases the turbulence and its scale. The transverse vibrations of stem in current-vegetation flow become longitudinal (concurrent to the flow direction) in presence of waves as wave-induce orbital motions are in longitudinal direction. Minor transverse vibrations are sometimes present at mean water depth however are in phase with the wave motion. Their contribution can be neglected compare to the contribution from dominant wave-induced orbital motions. Thus, vibration-induced diffusion can be neglected in wavy flow as far as the vibration frequency is less than or comparable to the wave frequency. The models for the current-vegetation and wave-current-vegetation flows reasonably simulate the magnitude of turbulent diffusions in respective cases. Finally, an empirical expression for diffusion coefficient using primitive, easily measurable variables provides quick and reliable estimate of turbulent diffusion in rigid as well as flexible canopy in both current-vegetation and wave-current-vegetation flow fields.

Knowledge of the combined hydrodynamics of wave-current-vegetation is practical in understanding the particulate sediment transport, exchange of vertical momentum transfer (Ikeda & Kanazawa 1996), pollutant mixing in estuaries (Valentine and Totterdell 2007) and distortion of plant morphology (Grizzle et al., 1996).

Acknowledgment: This work is partly supported by NSFC10671023 of Beijing I S & T University.

REFERENCES

1. Ackerman, J. and A. Okubo, 1993, Reducing mixing in a marine macrophyte canopy, Functional Ecol., 7, 305-309.
2. Burd and Dunton, 2000, Field verification of a light-driven model of biomass changes in the seagrass Halodule Wrightii, University of Texas, Austin.
3. Carollo, F. G., V. Ferro and D. Termini, 2002, Flow velocity measurements in vegetated channels, J. Hydrau.Eng., 128(7), 664-673.
4. Dean, R. G. and P. M. Aagaard, 1970, Wave forces, Data Analysis and Engineering Calculation Methods, J. Petrol. Technol.
5. Fischer, H. B., E. J. List, R. Koh, J. Imberger and N. Brooks, Mixing in inland and coastal waters. Academic press, Inc. New York, NY, 1979.
6. Gambi, M. A., Nowell and P. Jumars, 1990, Flume observations on dynamics in Zostera marina (eelgrass) beds. Mar. Ecol. Prog. Soc., 159-169.
7. Ghisalberti, M., and H. M. Nepf, 2002, Mixing layers and coherent structures in vegetated aquatic flows. J. Geophysical Research, 107 C2, 1-11.
8. Grizzle, R. E., F. T. Short, C. R. Newell, H. Hoven, and L. Kindblom, 1996, Hydrodynamically induced synchronous waving of seagrasses: 'monami' and its possible effects on larval mussel settlement. J. Experimental Marine Biology and Ecology, 206, 165-177.
9. Ikeda, S. and M. Kanazawa, 1996, Three-dimensional organized vortices above flexible water plants, J. Hydrau.Eng., 122(11), 634-640.

10. Kadlec, R., 1990, Overland flow in wetlands: Vegetation resistance, J. Hydraulic Engg., 116, 691-707.
11. Kouwen, N. and T. E. Unny, 1973, Flexible roughness in open channel, J. Hydraulic Div., 99, HY5, 713-728.
12. Liu, H., 1996, Wind Engineering, Prentice Hall, pp. 228.
13. Leonard, L. A. and M. E. Luther, 1995, Flow hydrodynamics in tidal marsh canopies, Limnology and Oceanography, 40(8), 1474-148.
14. Nepf H. M., 1999, Drag, turbulence and diffusion in flow through emergent vegetation, Water Resources Research, 35(2), 479-489.
15. Nepf, H. and E. R. Vironi, 2000, Depth-limited Vegetated Flow, J. Geophysical Research, 105 (C12) 28, 547-557.
16. Ota, T., N. Kobayashi, and J. T. Kirby, 2004, Wave and current interactions with vegetation., Proceedings of 29thCoastal Engineering Conference, USA, ASCE, 1, 508-520.
17. Patil S., V. P. Singh, and A. K. Rastogi, 2006, Monami wave in submerged vegetation, 6th international symposium on stratified fluid, (Perth, Western Australia , Australia), 348-353.
18. Patil Sandeep, 2008, Longitudinal Dispersion in Wave-Current-Vegetation Flow. Engineers Australia, 9th National Conference on Hydraulics in Water Engineering Darwin Convention Center, Australia.
19. Shimizu, Y., T. Tsujimoto, and H. Nakagawa, 1992, Numerical study on turbulent flow over rigid vegetationcovered bed in open channel, Proc. Japan Soc. of Civil Eng., 447(II-19), 35-44.
20. Shimizu, Y. and T. Tsujimoto, 1994, Numerical analysis of turbulent open-channel flow over a vegetation layer using a k-ε turbulence model, J. hydroscience and hydraulic engg., 11(2), 57-67
21. Tennekes, H., and J. L. Lumley, 1990, A First Course in Turbulence, MIT Press, Cambridge, Mass.
22. Tsujimoto and Kitamura (1998), A model for flow over flexible vegetation-covered bed, Proc. Int. Water Resource Engg. Conf., 556-561.
23. Valentine, E.M. and P. J. Totterdell, 2007, Effluent Dispersion in a Macro-Tidal Tropical Estuary, 32nd Congress of the International Association of Hydraulic Engineering and Research, Venice, Italy, 733.
24. Ward, L. G., W. M. Kemp, and W. R. Boynton, 1984, The influence of waves and seagrass communities on suspended particulates in an estuarine embayment, Maine Geology, 59, 85-103.
25. Worcester, S., 1995, Effects of eelgrass beds on advection and turbulent mixing in low current and low shoot density environments, Mar. Ecol. Prog. Ser., 126, 223-232.
26. Zeidler, R. B., 1976, Coastal dispersion of pollutants, J. Waterways, Harbours Coastal Eng. Div., 102, 235-254.

Design of Computer Experiment for Drawbead Design in Sheet Metal Restraint

Thaweepat Buranathiti [1,*] and Anut Kositpipat [2]
[1] Division of Materials Technology
School of Energy, Environment and Materials,
King Mongkut's University of Technology Thonburi, Bangkok 10140, Thailand
[2] Thai Summit AutoParts Industry Co. Ltd., Samut Prakan 10540, Thailand

Abstract: In automotive part manufacturers, drawbead on many sheet metal stamping dies is an important feature to control the flow of materials. Different drawbead configurations can lead to significantly different restraining forces. Also, the restraining force depends on the blank properties. This paper presents a design of computer experiment (DOCE) on drawbead restraining force so that the design process can fully utilize an analytical drawbead model. An explicit finite element method (FEM) is applied to obtain the drawbead restraining force used in the analytical or line drawbeads in forming analysis. The design was constructed by applying latin hypercube sample (LHS) design under a given parameterization. Three surrogate models, i.e., the second order polynomial model (Poly), radial basis function (RBF), and Kriging model, are applied on the restraining force obtained from finite element analysis (FEA) to the drawbead configurations. It is found that Poly cannot well represent the system while RBF and Kriging can well represent the system through evaluating the percentage of root mean square error (PRMSE).

Keywords: Drawbead, Restraining Force, Finite Element Analysis, Design of Computer Experiment

INTRODUCTION

Drawbead is an important feature on many stamping dies in automotive parts manufacturers. Typically, the industry applies drawbeads in sheet metal forming dies to control the flow of materials to the die cavity to form a product as shown an example in Fig. 1. The investigation of drawbead forces has been a research topic ranging from analytical models (e.g., Stoughton, 1988; Ludovic *et al*., 2003) to numerical models (e.g., Courvoisier *et al*., 2003; Lee *et al*., 2008; Firat, 2008).

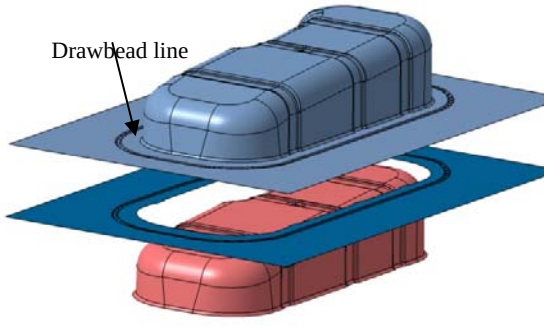

Figure 1. An example of drawbead applications.

The drawbead can have either symmetrical or unsymmetrical configuration. However, most drawbeads used in the industry are symmetrical for the sake of simplicity and practicality as shown an illustration in Fig. 2. In this research, symmetrical drawbeads are focused. A drawbead configuration is parameterized as a function of the given 4 parameters (i.e., L_1, L_2, R_1 and R_2).

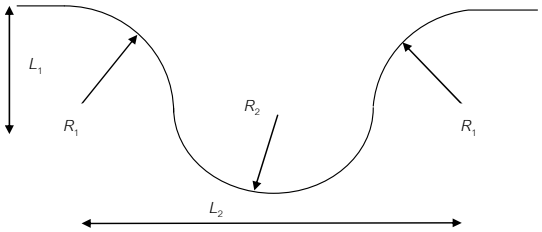

Figure 2. An illustration of a symmetrical drawbead.

In autopart manufacturing industry, drawbeads have been widely adopted on dies as shown in Figs. 3-4. Figure 3 illustrates current drawbead applications on a top lower tank forming die or a female die. Figure 4 illustrates current drawbead applications on a bottom lower tank forming die or a male die. The drawbead design has been incorporated in product development

Corresponding Author : Thaweepat Buranathiti Division of Materials Technology School of Energy, Environment and Materials, King Mongkut's University of Technology Thonburi, Bangkok 10140, Thailand

during tooling design by computational approaches in many ways (e.g., Vahdat *et al*., 2006; Sheriff and Ismail, 2008; Hu *et al*., 2008).

Figure 3. An example of a top lower tank forming die.

Figure 4. An example of a bottom lower tank forming die.

This paper presents drawbead models used in finite element analysis (FEA) and needed in an autopart forming industry. FEA has been an important tool for forming design (Buranathiti and Kositpipat, 2008). The focus is on characterizing the drawbead configurations into an analytical drawbead model, which is much less expensive than the geometrical drawbead model used in FEA for forming analysis. The design of computer experiment (DOCE) via latin hypercube sample (LHS) design and surrogate models are adopted in this work. The effectiveness of each surrogate model is presented and discussed.

DRAWBEAD MODEL

In analysis of sheet metal forming, finite element method (FEM) is a prime tool widely accepted nowadays. In finite element analysis (FEA), there are 2 main models for drawbeads: (1) geometrical or true drawbead; and (2) analytical or equivalent drawbead. The geometrical drawbead needs a CAD model that reflects the true geometry of the drawbead in the model. As a result, a fine mesh is needed at the drawbead line. The analytical drawbead does not need the true geometry in the CAD model except the central line of the drawbead line to represent the boundary effect. However, a correct set of drawbead information must be given. On computational aspects, the geometrical drawbead usually provides better prediction accuracy than the analytical drawbead. However, since drawbead is a small feature compared to the tooling system, there is a computational difficulty in applying geometrical drawbead model in FEA.

In this work, the focus is on analytical or equivalent drawbead. It is aimed to find an efficient method to have an accurate analytical drawbead model so that an industrial application can achieve a sufficient accuracy. There are many forms of analytical models from many literatures or research works in estimating the restraining force due to drawbead applications on tooling. A widely adopted equivalent drawbead model, which is a restraining force from a binder or a blank holder in a form of locking (Hallquist, 2000), is focused in this paper. The amount of restraining force to lock/resist a sheet metal to move/flow consists of 2 main components (friction and bending components) as shown in Fig. 5. It should be noted that the depth of the drawbead shown in Fig. 6 is another parameter in the analytical drawbead model.

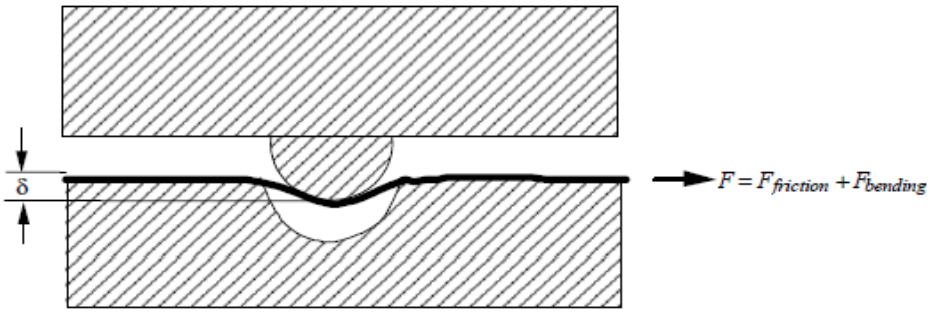

Figure 5. A deformed stage resulting the restraining force. (LSTC, 2007)

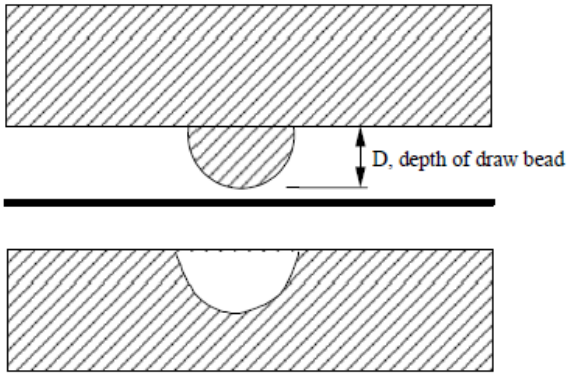

Figure 6. An illustration of the depth of drawbead at an undeformed stage. (LSTC, 2007)

The 2 main components are:

1. Bending component: This component comes from bending and unbending of a sheet metal traveling passing through drawbead. In a quantitative explanation, the quantity can be represented per the length of the drawbead in various forms, e.g., ramp shown in Fig. 7, logarithm, sine, etc.

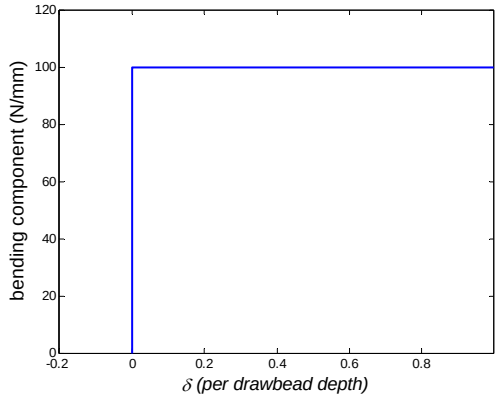

Figure 7. An illustration of bending component.

2. Normal component: This component comes from the deformed sheet metal at the drawbead while closing the binders. This normal force exists when the distance between the lower and upper binders is less than the drawbead depth. The normal component is also per drawbead length. And the function of the drawbead force vs. the displacement can be defined in various functions such as a ramp function shown in Fig. 8.

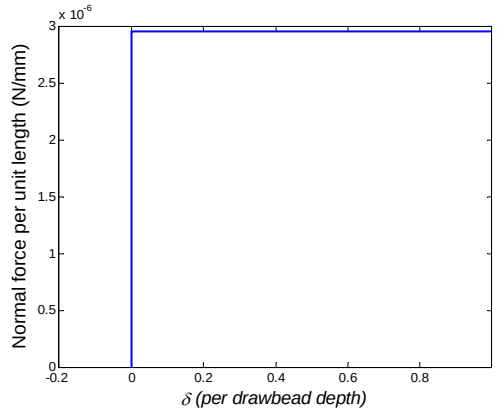

Figure 8. An illustration of normal component.

The total restraining force ($F_{restraining}$) is a summation of both bending and normal components as shown in the following equation

$$F_{restraining} = F_{bending} + F_{friction}. \quad (1)$$

In general, the bending component dominates the majority of the restraining force.

In an in-depth analysis of drawbead, this work creates numerical models through CAD and FEA models via Dynaform and LS-DYNA as shown in Fig. 9. The next step is to test the effect of different drawbead configurations on the reaction force to the sheet metal. A number of cases will be created to construct surrogate models through a design of computer experiment (DOCE).

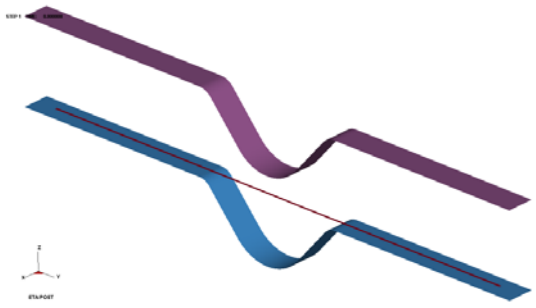

Figure 9. An example of FEA models for drawbead analysis.

DESIGN OF COMPUTER EXPERIMENT

This research focuses on symmetrical drawbeads. A drawbead configuration shawn in Fig. 2 is parameterized as a function of the given 4 parameters (i.e., L_1, L_2, R_1 and R_2). However, these 4 parameters cannot be completely independent to each other. Let

$$L_1 = R_1, \quad (2)$$
$$L_2 = 2(R_1 + R_2). \quad (3)$$

In this definition, a drawbead with $L_2 < L_1$ is not allowed since the contour will not be smooth. For $L_2 > L_1$, then L_1 can be anywhere in a range of $[0.5L_2, 1.5L_2]$

Latin Hypercube Sample (LHS) design is applied to create a design of computer experiment (DOCE). In this study, all the samples are shown in Table 1. Eighteen samples were created with the following ranges:

$R_1 = [5,15]$ in mm.
$R_2 = [5,20]$ in mm.
$L_2 = [1.0L_1, 1.5L_1]$ in mm.
$L_1 = [0.5L_2, 1.5L_2]$ in mm.

Table 1. The list of all drawbead configurations (in mm.) for constructing surrogate models.

Case #	R1	R2	L1	L2
1	14.534	13.220	21.374	55.525
2	6.351	19.157	6.478	66.902
3	9.239	6.755	6.565	36.930
4	8.498	12.334	9.735	60.761
5	12.474	18.085	17.475	87.917
6	10.864	5.282	5.624	39.789
7	7.947	8.096	9.509	38.040
8	5.210	10.442	4.467	46.122
9	11.781	9.113	15.843	58.357
10	7.246	15.844	7.222	58.479
11	9.710	11.182	12.621	57.168
12	5.000	5.000	5.000	20.000
13	4.000	4.000	4.000	16.000
14	5.000	4.000	5.000	18.000
15	4.000	5.000	4.000	18.000

FINITE ELEMENT MODELS

In this drawbead study, finite element methods have been adopted to analyze the drawbead effect. FEM is set up as shown in Fig. 9. The model consists of a lower binder, an upper binder, and a sheet metal modeled in a strip and plane strain conditions. The blank is modeled as a deformable body while tools are modeled as rigid bodies. The blank sheet is modeled by using 3D shell elements with Belytschko-Tsay scheme under plane stress assumptions and 5 integration points along the thickness direction.

In this study, if the initial position of the blank and the binders is not suitable, an initial penetration can cause a simulation error resulting a wave as shown in Fig. 10.

Figure 10. A wave created from an initial penetration.

The simulation of the drawbead effect is conducted subsequently on binder closing and sheet drawing as shown in Fig. 11.

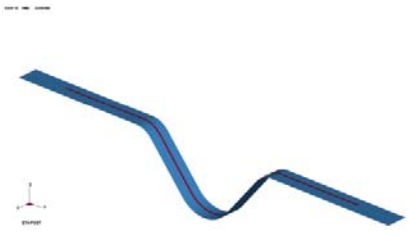

Figure 11. The binder closing step.
(a) intermediate (b) complete

The sheet is then drawn to a given drawn-in amount as shown in Fig. 12.

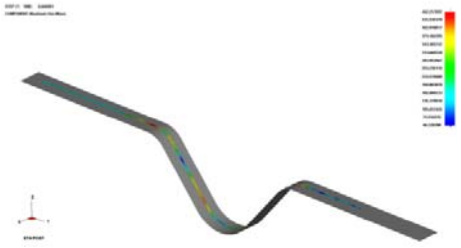

Figure 12. A representation of maximum von Mises stresses at the sheet metal

.

This study focuses on the restraining force given from a drawbead as shown in Fig. 13. The Y-axis is in x10N for a strip of sheet metal. The length of the strip is given as 1 mm. The average force of the region of interest is about 80N/1mm. The restraining force for this drawbead configuration is given as ~80N/mm.

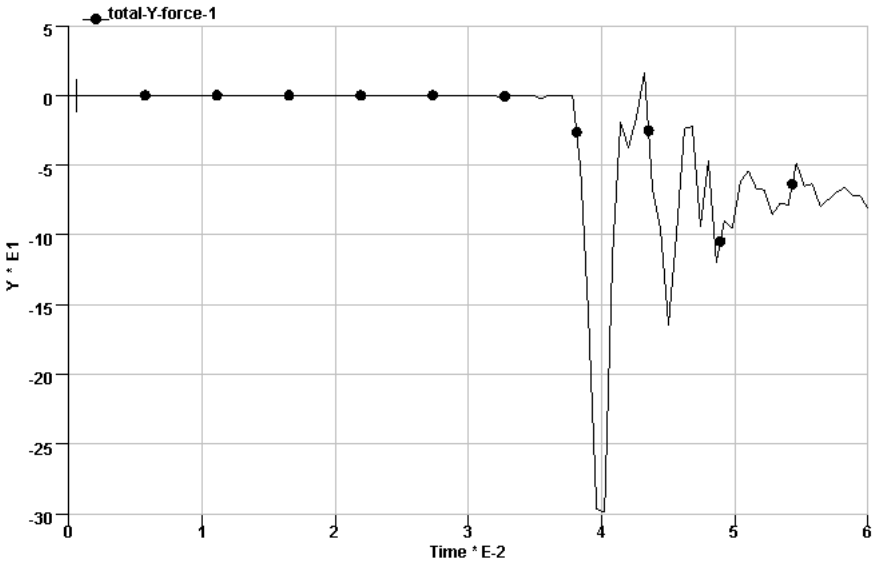

Figure 13. The restraining force given from a drawbead.

This study conducts a sensitivity study to observe whether or not the draw-in amount is an issue on getting the restraining force information. The result is shown in Fig. 14. It should be noted that this study was conducted by merely increasing the draw-in velocity without changing other parameters. It can be seen that the analysis results are about the same. There is no significant effect in the draw-in amount to the drawbead restraining force.

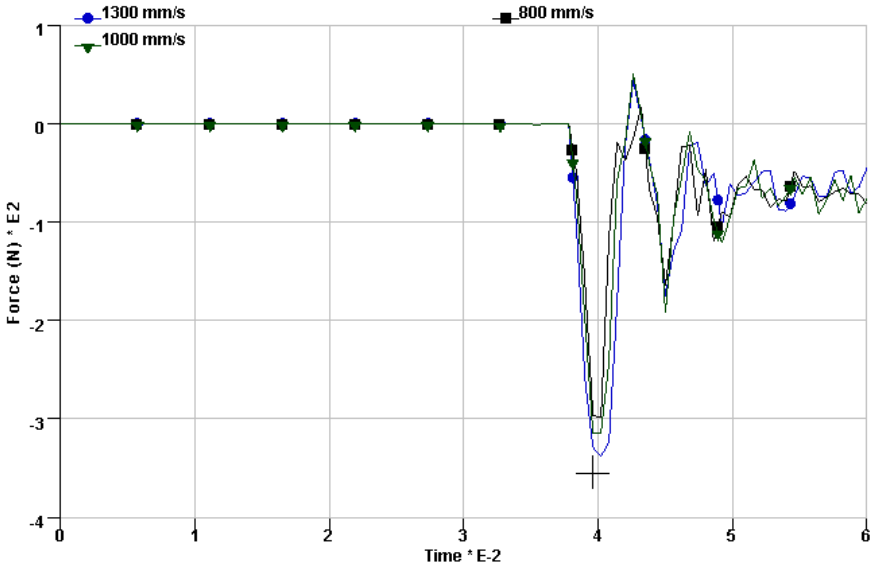

Figure 14. The restraining force from 2 different draw-in amounts (800, 1000, 1300 mm/s) through the same drawbead configuration.

Based on the drawbead configuration shown in Table 1 and FEA shown above, the restraining force of all drawbead configurations in N/mm is summarized in Table 2. The negative sign only indicates that it is opposite to the axis given in FEA models. Each value comes from an average of the pulling stage. Outliers and other noticeable fluctuations are discarded.

Table 2. The list of the restraining force to all drawbead configurations studied in this work.

Configuration #	Restraining Force (N/mm)
1	-52.107
2	-114.428
3	-102.470
4	-88.565
5	-72.061
6	-101.896
7	-100.757
8	-120.952
9	-81.315
10	-45.366
11	-81.160
12	-141.240
13	-240.397
14	-222.572
15	-221.839

SURROGATE MODELS AND COMPARISON

For different configurations of drawbeads, it is not practical to do the previous procedures for every configuration change. A concept of DOCE is adopted. A traditional design method is a full factorial design (Montgomery, 2001). This method is rather practical for conducting experiments in industry. However, the drawback is that the required sample size seems to grow exponentially with the number of parameters studied (Kalagnanam and Diwekar, 1997).

In applications involving computational simulations, the design space is continuous. The full factorial design is no longer well suited this class of applications. The Latin Hypercube sample (LHS) design is adopted in this work. LHS is one sampling method that can evenly distribute the sample points throughout the region. The details on the algorithm of LHS can be seen in Kalagnanam and Diwekar (1997), Helton and Davis (2003) and Diwekar (2003). Each configuration can be written in a function of **x** as

$$y = y(\mathbf{x}) \qquad (4)$$

where $\mathbf{x} = [x_1, x_2, x_3, x_4]^T$.

To construct an arbitrary relation, one may use 'radial basis function' (RBF) or 'Kringing' models in addition to traditional quadratic functions. In this paper, surrogate modeling techniques [Sacks *et al*., 1989; Jin *et al*., 2001; Montgomery *et al*., 2001] are utilized.

Polynomial Model

By taking advantage of a surrogate model representing the finite element simulations, the restraining force is represented by a polynomial function as follows

$$\hat{y} = a_0 + \sum_{i=1}^{N} b_i x_i + \sum_{i=1}^{N} c_i x_i^2 + \sum_{i=1}^{N}\sum_{j=i}^{N} d_{ij} x_i x_j \,, \qquad (5)$$

where $\hat{y}$ is the estimated restraining force, a, b_i, c_i and d_{ij} are the corresponding constants, and N is the number of design variables. The effectiveness of the surrogate model $\hat{y}$ is measured by evaluating the percentage of root mean square error (PRMSE) as follows

$$\text{PRMSE} = \frac{\sqrt{\sum_{i=1}^{n}(y-\hat{y})^2}}{n} \cdot \frac{100}{\bar{y}}\%, \qquad (6)$$

where n is the number of samples for the regression analysis, and y is the computational results from finite element methods. The linear regression analysis is used to create the surrogate model. For simplicity Eq. (7) is rewritten into a matrix form as follows

$$\mathbf{Y} = \mathbf{X}\mathbf{A}, \qquad (7)$$

where $\mathbf{Y}$ is the $n\times1$ vector of the dependent variable, and $\mathbf{X}$ is the $n\times m$ matrix of the independent variables. The $m\times1$ constant vector $\mathbf{A}$ in Eq. (7) is obtained by solving the normal equation as follows

$$\mathbf{A} = \left(\mathbf{X}^{\mathrm{T}}\mathbf{X}\right)^{-1}\mathbf{X}^{\mathrm{T}}\mathbf{Y}, \qquad (8)$$

where $\mathbf{X}^{\mathrm{T}}$ is a transpose of the matrix $\mathbf{X}$.

Kriging Model

A Kriging model postulates a combination of a polynomial model and a departure of the polynomial model. It can be represented as follows

$$\hat{y} = \sum_{j=1}^{k} \beta_j f_j(x) + Z(x), \quad (9)$$

where $Z(x)$ is assumed to be a realization of a stochastic process with a zero mean and a spatial correlation function given by

$$Cov[Z(x_i), Z(x_j)] = \sigma^2 R(x_i, x_j), \quad (10)$$

where σ^2 is the process variance, and R is the correlation.

Radial Basis Function

RBF uses linear combinations of a radially symmetric function based on Euclidean distance to approximate response functions. It can be represented as follows

$$\hat{y} = \sum_i a_i \left\| x - x_{0i} \right\|, \quad (11)$$

where a_i are the coefficients of the expression, and x_{0i} are the observed inputs.

These three surrogate models are implemented to observe the effectiveness of each model via evaluating PRMSE in Eq. (6) from additional 7 samples as shown in Table 3.

Table 3. PRSE for each surrogate model.

Method	PRMSE
Poly	2475.50
RBF	12.29
Kriging	4.18

CONCLUDING REMARKS

The drawbead configurations can lead to a variety of restraining force. FEA is an effective tool to investigate the influence of the drawbead configuration. Then, DOCE through LHS can be effectively implemented. In order to have a design via computation, 3 surrogate models are studied.

It can be seen that the traditional second order polynomial is not a suitable surrogate model for this system although it has been reported that it successfully worked in Koc *et al*. (2000) and Buranathiti *et al*. (2006). The system appears highly nonlinear as evident on PRMSE that the polynomial model cannot well represent the system. RBF and KM are more suitable since they can capture the nonlinearity better or they use the training data for further extrapolation.

After this relationship is established, one can apply to the forming die design to see whether or not the blank has been pulled too much or too little. If 'too little' or 'too weak drawbead', the drawbead restraint is added. If 'too much' or 'too strong drawbead', the drawbead restraint is reduced. The given guideline can be applied further to design stamping dies for optimal sheet metal flow and draw-in. An important point is how to tell which one is 'too little' or 'too much'. This conclusion can be drawn by observing the FEA of the forming process.

ACKNOWLEDGEMENTS

The authors greatly appreciate a financial support from the National Metal and Materials Technology Center (MTEC), National Science and Technology Development Agency (NSTDA) of Thailand under contract MT-B-50-ATO-20-039-G and a software package support from Engineering Technology Associates Inc. (ETA).

REFERENCES

1. Buranathiti, T., and Kositpipat, A., 2008, Analysis and Design of Body Jack Case Stamping for Fewer Production Steps, Journal of Materials Processing Technology, 205, 1-3, pp. 451-458
2. Buranathiti, T., Cao, J., Baghdasaryan, L., Chen, W., and Xia, Z.C., 2006, Approaches for Model Validation: Methodology and Illustration on a Sheet Metal Flanging Process, Journal of Manufacturing Science and Engineering, Transactions of ASME, 128, 2, pp. 588-597.
3. Courvoisier, L., Martiny, M., and Ferron, G., 2003, Analytical modeling of drawbeads in sheet metal forming, Journal of Materials Processing Technology, 133, 3, pp. 359-370.
4. Courvoisier, L., Martiny, M., Ferron, G., 2003, Analytical modelling of drawbeads in sheet metal forming, Journal of Materials Processing Technology, 133, 3, pp. 359-370.
5. Diwekar, U.M., 2003, A novel sampling approach to combinatorial optimization under uncertainty, Computational Optimization and Applications, 24, 2-3, pp. 335-371.

6. Firat, M., An analysis of sheet drawing characteristics with drawbead elements, Computational Materials Science, 41, 3, pp. 266-274.
7. Hallquist, 2006, LS-DYNA Theory Manual.
8. Helton, J.C., and Davis, F.J., 2003, Latin hypercube sampling and the propagation of uncertainty in analyses of complex systems, Reliability Engineering and System Safety, 81, pp. 23-69.
9. Hu, W., Enying, L., Yao, L.G., 2008, Optimization of drawbead design in sheet metal forming based on intelligent sampling by using response surface methodology, Journal of Materials Processing Technology. 206, 1-3, pp. 45-55.
10. Jin, R., Chen, W., Simpson, T., 2001, Comparative studies of metamodeling techniques under modeling criteria, Journal of Structural Optimization, 23, 1, pp. 1-13.
11. Kalagnanam, J.R., and Diwekar, U.M., 1997, An efficient sampling technique for off-line quality control, Technometrics, 39, 3, pp. 308-319.
12. Koc, M., Allen, T., Jiratheranat, S., and Altan, T., 2000, The use of FEA and design of experiments to establish design guidelines for simple hydroformed parts, International Journal of Machine Tools & Manufacture, 40, pp. 2249-2266.
13. Lee, M.G., Chung, K., Wagoner, R.H., Keum, Y.T., 2008, A numerical method for rapid estimation of drawbead restraining force based on non-linear, anisotropic constitutive equations, International Journal of Solids and Structures, 45, 11-12, pp. 3375-3391.
14. LSTC, 2007, LS-DYNA Keyword User's Manual.
15. Montgomery, D.C., 2001, Design and Analysis of Experiment, John Wiley & Sons, New York, 684p.
16. Montgomery, D.C., Peck, E.A., and Vining, G.G., 2001, Introduction to Linear Regression Analysis, John Wiley & Sons, Inc., New York, 641p.
17. Sack, J., Welch, W.J., Mitchell, T.J., and Wynn, H.P., 1989, Design and analysis of computer experiments, Statistical Science, 4, 4, pp. 409-435.
18. Sheriff, N. M., Ismail, M. M., 2008, Numerical design optimisation of drawbead position and experimental validation of cup drawing process, Journal of Materials Processing Technology. 206, 1-3, pp. 83-91.
19. Stoughton, T.B., 1988, Model of drawbead forces in sheet metal forming, Proceedings of 15th Biennial IDDRG Congress, Dearborn, 5, pp. 205–215.
20. Vahdat, V., Santhanam, S., Chun, Y.W., 2006, A numerical investigation on the use of drawbeads to minimize ear formation in deep drawing, Journal of Materials Processing Technology, 176, 1-3, pp. 70-76.

Spatial Pattern Analysis from High Resolution Data Using Spatial and Spectral Properties

[1]Thandar Htoon, [2]Myint Myint Khaing, [3]Minakshi Kumar
[1]Remote Sensing Department, Mandalay Technological University, Myanmar
[2]Associate Professor and Head, Remote Sensing Department,
Mandalay Technological University, Myanmar
[3]Remote Sensing and Photogrammetry Division, Indian Institute of Remote Sensing Campus,
Dehradun, India

Abstract: This paper is reported on some results by using High Resolution Imagery of IKONOS data for the analysis of the selected urban area: the south-east part of Dehradun City, located in India (Case Study I) and comparison between the pixel based classification result for IKONOS and IRS-1D (LISSIV) in Mandalay City, Myanmar (Case Study II). For Case Study I, the classification accuracy is improved by pixel-based classification using Maximum Likelihood Classifier (MLC). In addition, multiresolution segmentation and fuzzy rule based classification improved the classification accuracy to a much larger extent using multiresolution segmentation. The accuracy improved from 78.57% in spectral classification to 90.72% using the object oriented approach. For Case Study II, the result of the comparison between IKONOS and LISS IV are 82.1% and 76.6% in accuracy by pixel-based classification using MLC. The different results are due to High Spatial Resolution data by using IKONOS-Pan Sharpened (2001) and IRS-1D LISSIV (2006).

Key Words: Spatial Pattern, High Resolution Data, Spatial and Spectral Properties

1. INTRODUCTION

Land cover classification is a simple process that involves grouping an image's pixels based on the reflectance properties of the land cover feature being classified. IKONOS Pan-Sharpened and IRS-1D LISSIV satellite provide the high resolution multispectral imagery. If data processing is applied, very useful information can be derived for urban area classification.

A very important aspect of classification of this urban area image is that it consists of highly heterogeneous classes. Moreover, the urban environment possesses the identical spectral reflectance values correspond to different land uses and diverse functions. The overlapping of the spectral signature of some classes is even higher than from pure urban area since each pixel and its adjacent pixels have a relatively spatial coverage in these images. Therefore conventional pixel based approaches are not expected to produce good results for high resolution data.

The main research problem in this work is to what extent high resolution data can detect urban area structures. The other questions are when processing image analysis, which classification approach is better for interpreting urban area structures and how remote sensing techniques using pixel-based and object-based analysis can be integrated to analyze urban area benefits.

For spatially complex and spectrally mixed classes, the classification accuracy is likely to improve if the spatial properties of classes could be incorporated into the classification criteria. In case study I, the data used are IKONOS merged multispectral (4m, 4 bands)-PAN (1m). The present study aims to analyze the main problem in urban classification using Maximum Likelihood Classification (MLC). In addition multiresolution segmentation and fuzzy rule based classification improved the classification accuracy to a much larger extent. For case study II, Aung Myae Tharzan and Chan Aye Tharzan townships in Mandalay City, Mandalay District, Myanmar are analysed by Maximum Likelihood Classification (MLC) method using IKONOS Pan-Sharpened (1m, 4 bands) and LISS IV (5.8m, 3 bands) data.

Corresponding Author : Thandar Htoon Remote Sensing Department, Mandalay Technological University, Myanmar

2. METHODOLOGY (Case Study I)

The Pan and multispectral data of IKONOS were available in Geo TIFF format. The MSS data were registered to high resolution PAN data. The two data sets were fused using with the help of Gram-Schmidt Spectral sharpening in ENVI 4.2. The good result of Gram-Schmidt Spectral Sharpening method may be due to the fact that it maintains the original scene radiometry of the input IKONOS multispectral image. The Brovey and multiplicative, in ERDAS 8.7 are generally used for urban application but after segmentation this method does not give the good result compared to Gram-Schmidt sharpening.

Dehradun lies between 30°15'58"N to 30°24'16"N latitude and 78°06'05"E - 78°58'56"E longitude. The study area is as shown in Fig.1.

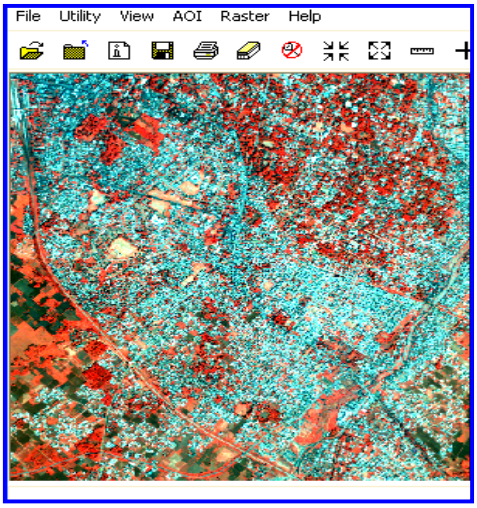

Fig.1. Study area of Dehra Dun city (IKONOS Pan-sharpened image)

For case study I, classified only Low Level for pixel-based analysis and Low and High Levels were including for object-based analysis. There are five classes for Low Level classification and nine classes for High Level.

The methodology flow chart is as follows.

3. PIXEL-BASED CLASSIFICATION

Urban areas are complicated because of the mix of man-made features and natural features. Among the cues for image-interpretation, only color can readily be extracted from the images for urban identification. However, it is difficult to determine size and shape by using per-pixel approaches. In addition, pattern and association are higher-level structural and topological information that is also difficult to extract by using pixel-based approaches, but they are useful in urban feature classification.

Nowadays, pixel-based approaches have been developed and are widely used in remote sensing image processing and classification.

With the use of high-resolution remote sensing data, the problem of mixed pixels is reduced but the internal variability and the noise within land use classes are increased. Most conventional pixel-based classifiers such as minimum distance and maximum likelihood assume parametric statistical models such as the Gaussian distribution.

METHODOLOGY FLOW CHART

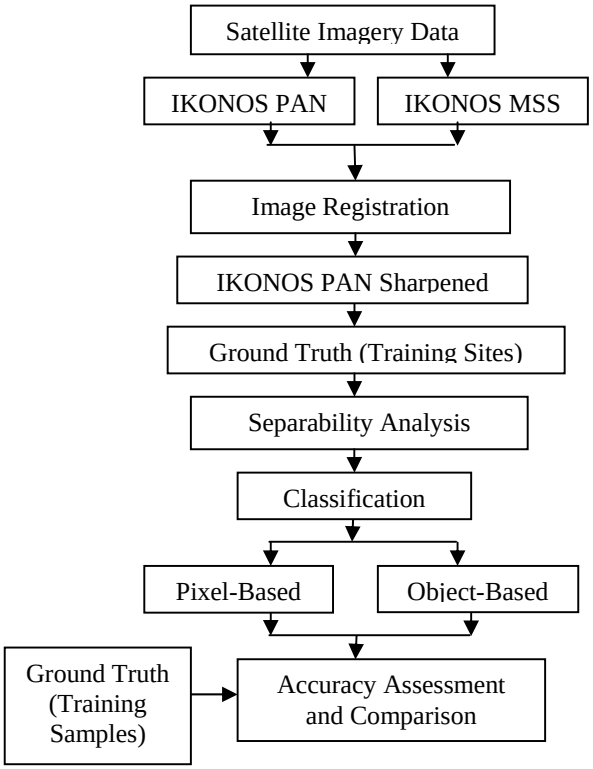

3.1 EXPERIMENTAL PIXEL-BASED CLASSIFICATION AND RESULTS

Pixel based Classification was then attempted on the fused image using Maximum Likelihood

Classifier and Accuracy was assessed. Even though High Resolution data used, High-level Classification could not be attempted because the pixel-based classification for image is heterogeneous. *Agriculture, Plantation, River Bed, Settlements and Water Body* are performed to classify for Low Level classification.

The MLC quantitatively evaluates both the variance and covariance of the category spectral response pattern when classifying an unknown pattern. An assumption made is that the distribution of the training set is Gaussian. Under this assumption, the distribution of a training set of a class can be completely described by the mean vector and covariance matrix. Given these parameters, it may be computed the statistical probability of a given pixel being a member of a particular class.

In this project, Maximum Likelihood Classification (MLC) method is used for pixel-based supervised classification and then accuracy was assessed. For this classification, the project was analyzed by Low Level classification for IKONOS- Pan sharpened image. It could not be studied by High Level Classification because pixel-based methods of image classification cannot work successfully using high-resolution satellite images (HRSI) since they have been assigned each pixel to one of the urban classes solely on the basis of its spectral properties.

The heterogeneous classes were expected to improve accuracy assessment for urban area delineation. The classification result for Low Level of IKONOS Pan-Sharpened is shown in Fig.2.

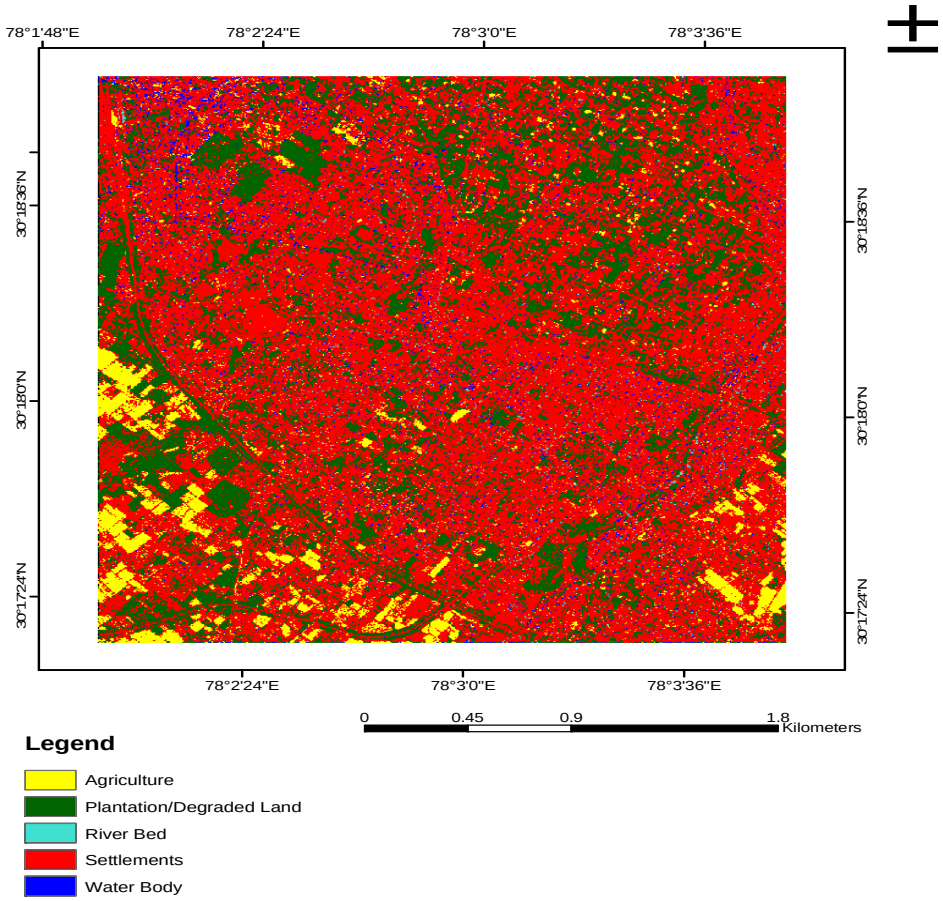

Fig.2. Low level classified result of the study area

4. MULTI-RESOLUTION SEGMENTATION

Multi-resolution segmentation is a bottom-up region-merging technique starting with one-pixel objects. In numerous subsequent steps, smaller image objects are merged into bigger ones. ECognition4.0 software supports a simultaneous raster/vector representation of image objects. After segmentation, vectorization functionally allows production of polygons for each image objects.

The purpose of multiresolution segmentation is the object-oriented image analysis for land use/ land cover classification or the extraction of object interest. These image object primitives represent image information in an abstracted serving as building blocks and information carriers for subsequent classification. Beyond purely spectral information, image objects contain a lot of additional attributes which can be used for classification.

4.1. EXPERIMENTAL OBJECT-BASED CLASSIFICATION AND RESULTS

Object-oriented image analysis is a new procedure for image classification. In contrast to traditional image processing methods, the basic processing units of object oriented image analysis are image objects or segments, and not single pixels. Even the classification acts on image objects.

One motivation for the object-oriented approach is that the expected result of many image analysis tasks is the extraction of real world objects and proper in shape and in classification. This expectation cannot be fulfilled by common pixel-based approaches.

Segmentation parameters: shape, texture and tone operating over the network, were used a whole set of relational/ contextual information. Table.1 (a) and Table.1 (b) describe the different scale parameters including the color and shape criteria used and the suitable classification rule for the study purpose. Fig.3 illustrates for False Color Composite (FCC) and segmented image of sub-portion of study area. The experimental results of low level and high level Fuzzy Classification for IKONOS Dataset are shown in Fig.4 and Fig.5.

Table.1 (a).Chosen Segmentation Parameters

Level	Scale Para-meters	Shape Factor	Compa-ctness	Smooth-ness
Low	35	0.3	0.3	0.7
High	75	0.2	0.3	0.7

Table.1 (b).Classification Rule

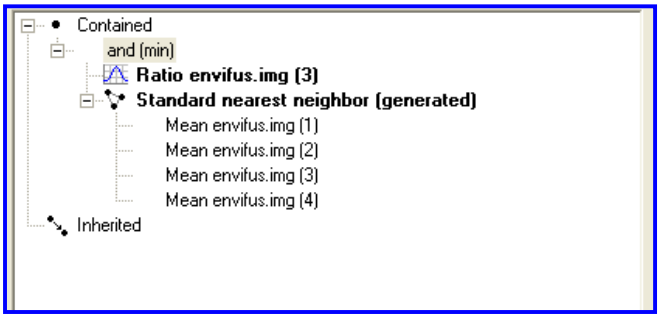

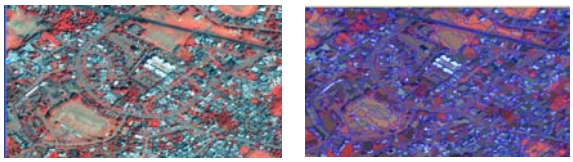

Fig.3. FCC and segmented image sub-portion

The results of the comparison between two different classification methods for study area are shown in Table.2

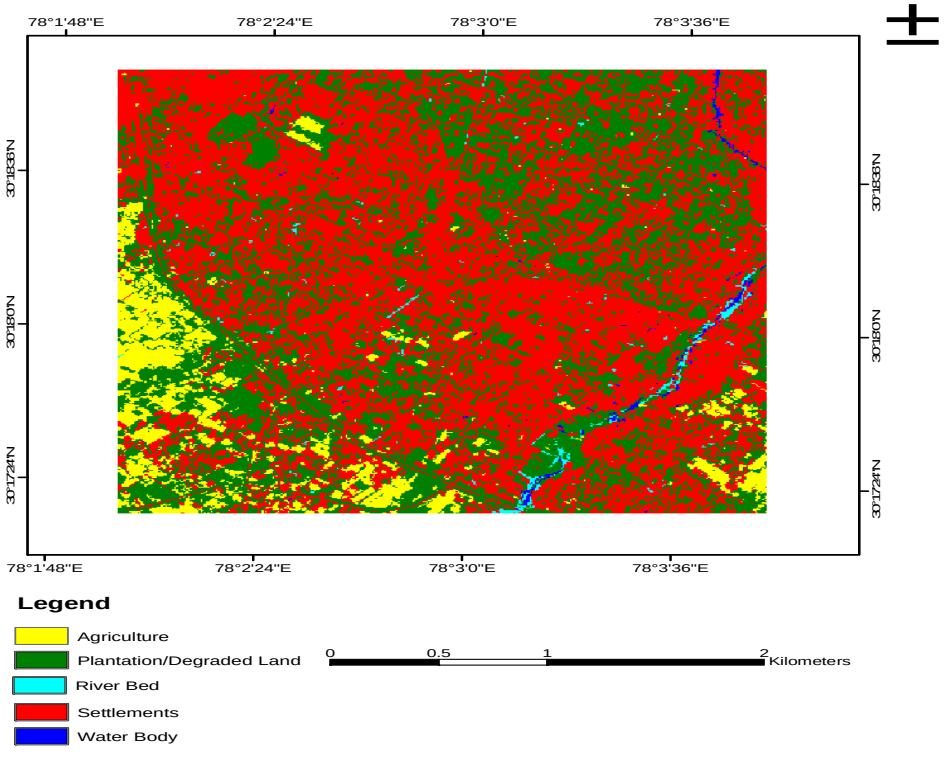

Fig.4. Low level fuzzy classification for IKONOS dataset

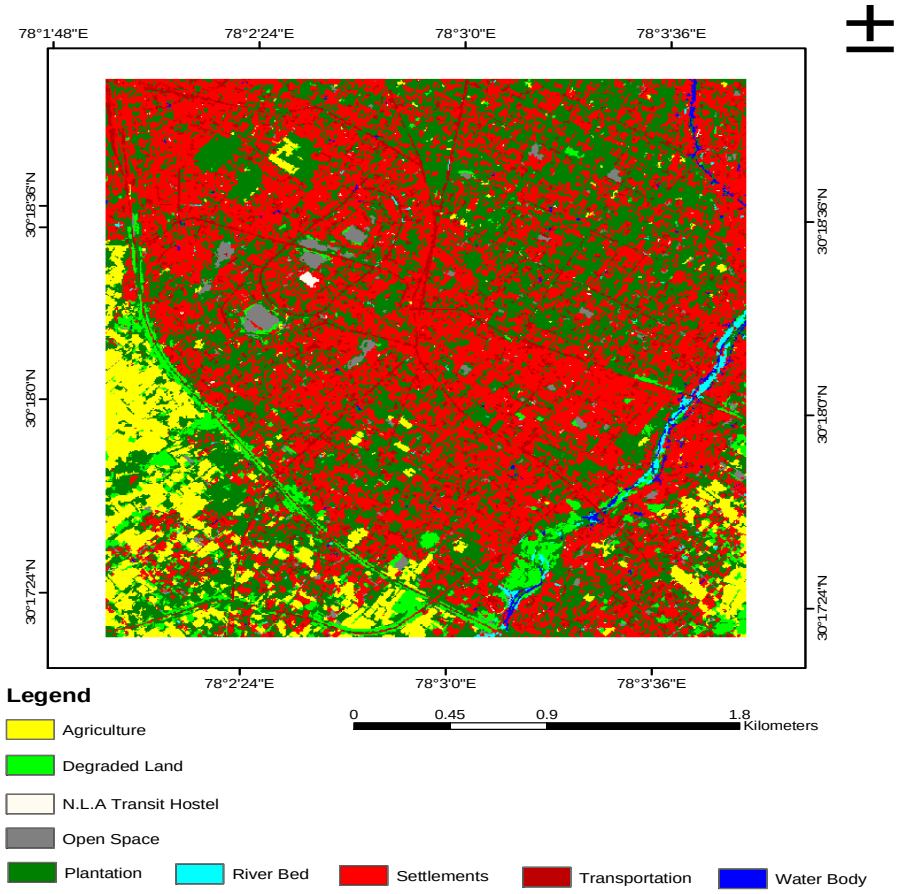

Fig.5. High level fuzzy classification for IKONOS Pan-sharpened

Table.2. Comparison results of accuracy assessment for IKONOS dataset

Classified Level	IKONOS-Pan Sharpened
Low level with pixel-based	78.57%
Low level with object-based	90.72%
High level with object-based	87.48%

4. EXPERIMENTAL PIXEL-BASED ANALYSIS AND RESULTS (Case Study II)

In the present study, for the selection of training sets and subsequently supervised classification, a preliminary classification was prepared for two satellite data products covering almost all land use/land cover categories that are typical in Mandalay, Myanmar. With regard to the present planning scenario, the pixel-based classification can be adopted. At the same time it is flexible and easy to understand.

The analysed images are used for IKONOS (2001, December) and LISSIV (2006, October) in case study of Aung Myae Tharzan and Chan Aye Tharzan townships in Mandalay City according to the data available. Aung Myae Tharzan and Chan Aye Tharzan Townships lie between 21°30'N and 21°50'24"N latitude and 96°05'E - 96°08'E longitude.

The images of the palace compound in Aung Myae Tharzan Township are compared in Fig.6. It can easily be seen that the difference spatial resolution for IKONOS and LISSIV data.

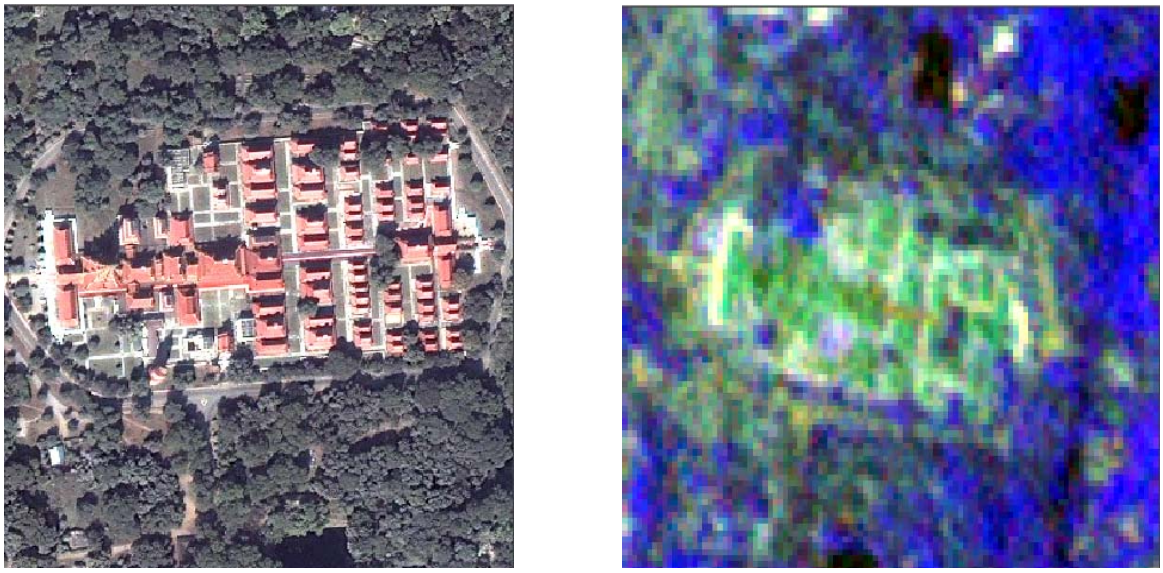

Fig.6. Zoom in portion of Palace Compound in Mandalay city (a) IKONOS (b) LISSIV data

The classified maps are dividied into five classes: including *Pagoda, Agriculture, Settlement, Water body and Ttree*s. It was analyzed by MLC method using Erdas 8.7 because of its accuracy and the variability of classes.

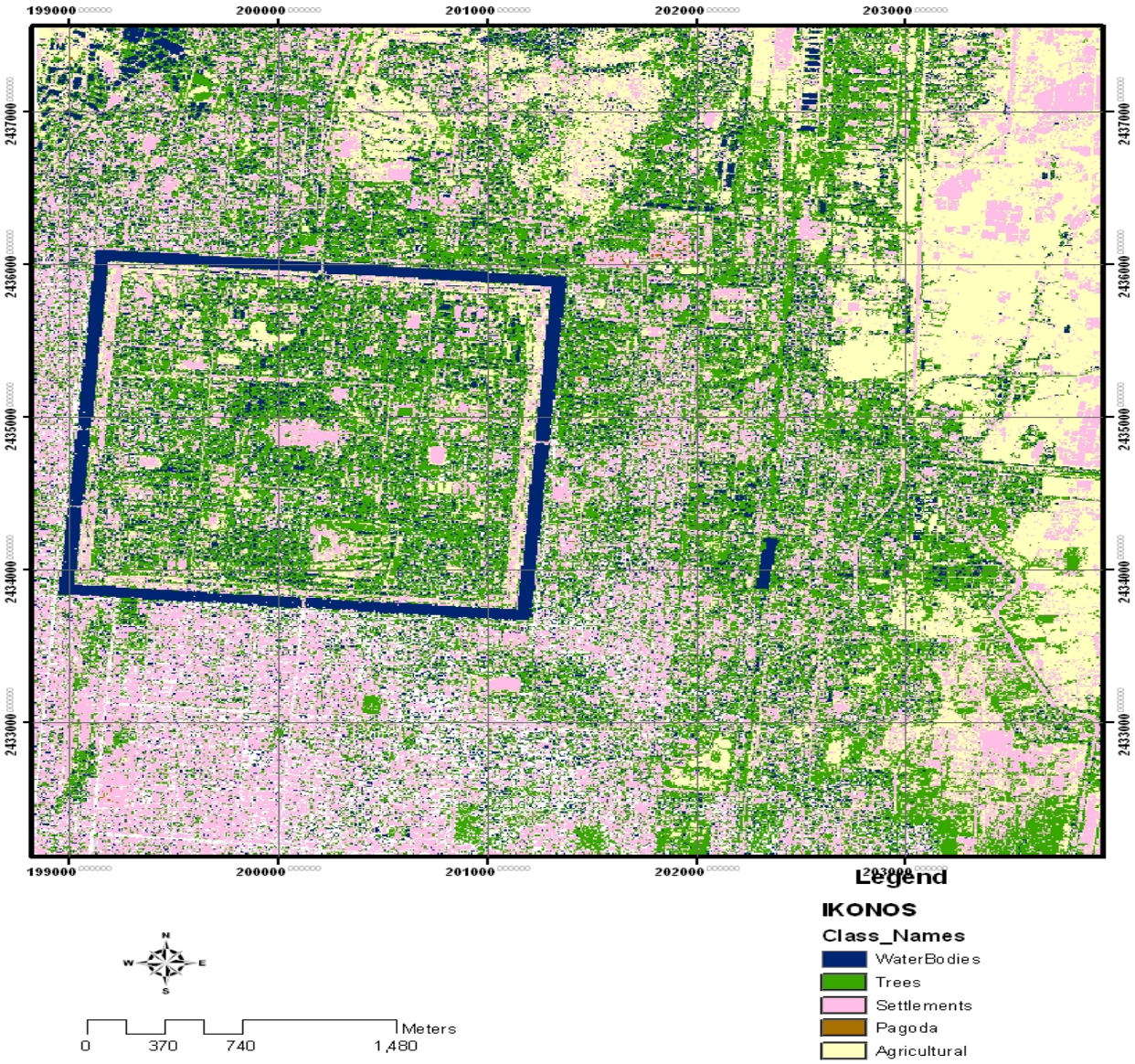

Fig.7. Pixel-based classification for IKONOS (2001)

The comparison land use classified maps are shown in Fig.7. and Fig.8. The accuracy assessment for IKONOS and LISS IV are 86% and 78.26% due to the difference spatial resolution. The land use of the city over a period from the year 2001 to 2006 showed tremendous rises in the built-up-form from agricultural area and open spaces.

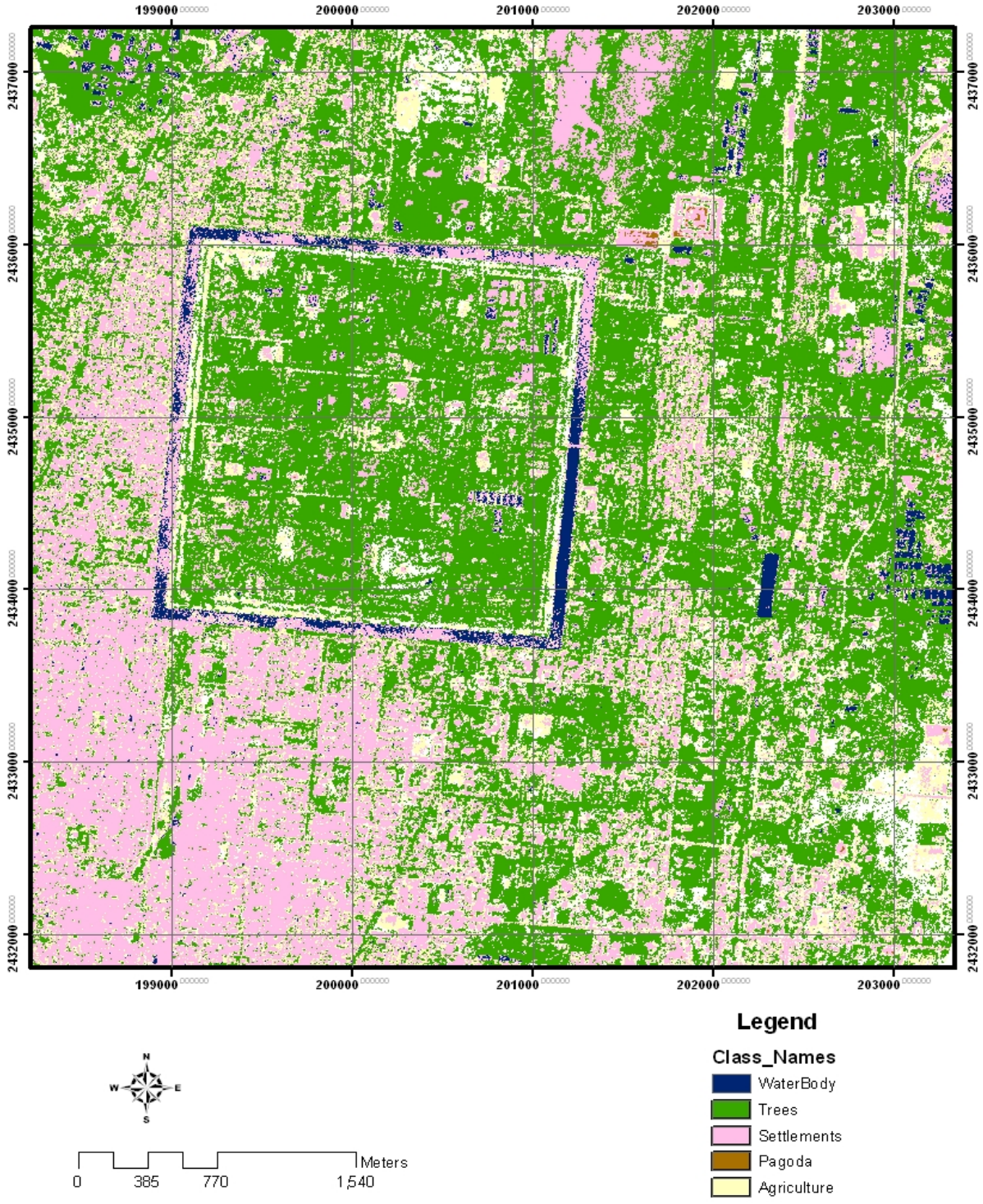

Fig.8. Pixel-based classification for LISSIV (2006)

5. CONCLUSION

The detailed land use, land cover type classes are classified by using different types of image classification techniques. For case study I, it is generally observed that the plantation of urban greenness area is always mixing with agriculture and degraded land due to relative dominance of a particular species. In this classification technique, there is a problem in Settlements with Water Body and River Bed due to same reflection of the classes. In pixel-based classification, Maximum Likelihood Classification approach is shown for better accuracy assessment results than other simple classification approach. For case study II, the MLC pixel-based classifier method is used by Erdas Imagine software 8.7. It can only be analysed by pixel-based classification for five classes due to available of software. But it cannot be performed for high level classification because of heterogeneity of urban area features and water body and settlements are a little mixed class for LISS IV data due to its lower spatial resolution than IKONOS. To be concluded, the performance for digital classification is best to assess the best accuracy by using better spatial and spectral properties included. And it is better to adopt segmentation approach classification, for more number of classes in particular.

ACKNOWLEDGEMENTS

We would like to acknowledge Indian Institute of Remote Sensing, Dehra Dun City, India for the supporting of satellite data for providing the Long-Term Grant to support this project. And also special thanks to Remote Sensing Department, Ministry of Science and Technology for providing of satellite images and other available facilities.

REFERENCES

1. John R Jensen. 1996. “Introductory Digital Image Processing: A Remote Sensing Perspective”. 2nd Edition. Englewood Cliffs, New Jersey: Prentice-Hall.
2. Lillesand and Kiefer, 2004, “Remote Sensing and Image Interpretation”, Fifth Edition, Pg. 532 – 575.
3. Congalton R.G., 1991, "A Review of Assessing the Accuracy of Classification of Remotely Sensed Data",Remote Sensing of the Environment, volume 37, Pg. 35-46.
4. Congalton R.G. and K. Green. 1999. “Assessing the Accuracy of Remotely Sensed Data: Principles and Practices”, Lewis Publishers. Pg.137.
5. William K Pratt. “Digital Image Processing” Pub Wiley. Pg.597-623
6. Zhan, A Hierarchical Object-Based Approach for Urban Land-Use Classification from Remote Sensing Data: http://www.itc.nl/library, http://www.isprs.org

http://beam.to/asimmod2009